OCS Study
MMS 2002-055

Northeastern Gulf of Mexico Chemical Oceanography and Hydrography Study

Synthesis Report

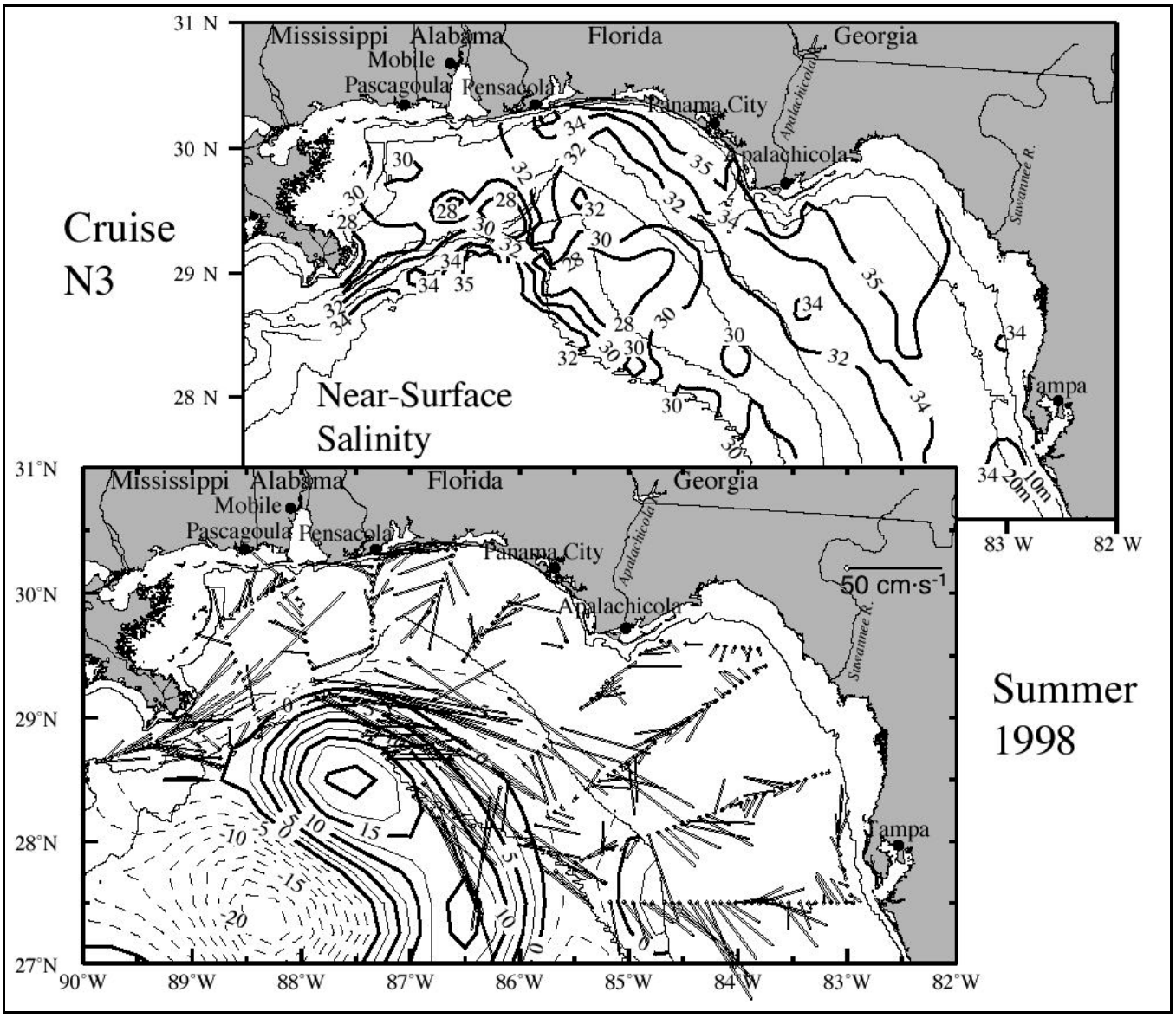

U.S. Department of the Interior
Minerals Management Service
Gulf of Mexico OCS Region

OCS Study
MMS 2002-055

Northeastern Gulf of Mexico Chemical Oceanography and Hydrography Study

Synthesis Report

Authors

Ann E. Jochens
Steven F. DiMarco
Worth D. Nowlin, Jr.
Robert O. Reid
Mahlon C. Kennicutt II

Prepared under MMS Contract
1435-01-97-CT-30851
by
Texas A&M University
Department of Oceanography
College Station, Texas 77843-3146

Published by

U.S. Department of the Interior
Minerals Management Service
Gulf of Mexico OCS Region

New Orleans
October 2002

DISCLAIMER

This report was prepared under contract between the Minerals Management Service (MMS) and the Texas A&M Research Foundation. This report has been technically reviewed by the MMS, and it has been approved for publication. Approval does not signify that the contents necessarily reflect the views and policies of the MMS, nor does mention of trade names or commercial products constitute endorsement or recommendation for use. It is, however, exempt from review and compliance with the MMS editorial standards.

REPORT AVAILABILITY

Extra copies of the report may be obtained from the Public Information Office (Mail Stop 5034) at the following address:

U.S. Department of the Interior
Minerals Management Service
Gulf of Mexico OCS Region
Public Information Office (MS 5034)
1201 Elmwood Park Boulevard
New Orleans, Louisiana 70123-2394

Telephone: (504) 736-2519 or
1-800-200-GULF

CITATION

Suggested citation:

Jochens, A. E., S. F. DiMarco, W. D. Nowlin, Jr., R. O. Reid, and Mahlon C. Kennicutt II. 2002. Northeastern Gulf of Mexico Chemical Oceanography and Hydrography Study: Synthesis Report. U.S. Dept. of the Interior, Minerals Management Service, Gulf of Mexico OCS Region, New Orleans, LA. OCS Study MMS 2002-055. 586 pp.

ABOUT THE COVER

The cover art depicts salinity at 3-m depth (upper panel) and sea surface height (SSH) from satellite altimeter data superimposed on gridded acoustic Doppler current profiler (ADCP) currents at 14-m depth (lower panel) for cruise N3 in July/August 1998. The SSH field for 1 August 1998 shows a large anticyclonic eddy stretching along the slope from just southeast of the Mississippi River delta to the eastern flank of DeSoto Canyon. The ADCP currents show strong ($\geq$ 50 $cm \cdot s^{-1}$) near-surface eastward flow along the shelf edge off the Mississippi River, caused by the anticyclone. These currents extend along the 1000-m isobath to the eastern flank of DeSoto Canyon and then turn southeastward over deeper water. They transport the low salinity water from the Mississippi River discharge along the shelf edge and slope. Note that the salinity during this cruise (and other summer cruises) increased toward shore because of this transport of low-salinity river water over the outer shelf.

ACKNOWLEDGMENTS

This report would not have been possible without the contributions of a large number of people. Each NEGOM-COH principal investigator (PI) contributed ideas to or authorship of portions of the text, many participated in the cruises and in data reduction and processing. The principal investigators, their affiliations, and their tasks are:

Worth D. Nowlin, Jr.	TAMU	Program Manager, PI for Task 3
Ann E. Jochens	TAMU	Deputy Program Manager, PI for Program Management and Task 2
Douglas C. Biggs	TAMU	Co-PI for Task 1
Norman L. Guinasso, Jr.	GERG/TAMU	Co-PI for Task 1
Matthew K. Howard	TAMU	Co-PI for Task 2
M. C. Kennicutt II	GERG/TAMU	Co-PI for Tasks 1 and 3
Robert O. Reid	TAMU	Co-PI for Task 3

Additionally, Dr. Steven F. DiMarco, Dr. Yaorong Qian, and Dr. Gary A. Wolff contributed to the authorship of this report. The assistance of Mrs. Susan Martin in preparation of this report is appreciated.

To all who participated on the nine NEGOM-COH cruises, both the crew of the *R/V Gyre* and the scientific teams, we extend our great appreciation. We also thank the voluntary contributions of the scientists and students at the University of Colorado (CU), University of South Florida (USF), University of Southern Mississippi (USM), Texas A&M University (TAMU), and TAMU-Galveston who participated in these cruises. We also greatly appreciate the cruise participation of Dr. Piers Chapman, TAMU.

Thanks go to those who helped prepare equipment and process the data on shore, including many named above, as well as Bob Albers, Woody Lee, and Ou Wang. Finally, thanks go to Dr. Joseph Yip for preparation of hourly surface wind and wind stress fields for the NEGOM field period and to Dr. Robert L. Leben, Colorado Center for Astrodynamics Research, University of Colorado, for production of the daily sea surface height anomaly fields from satellite altimeter data.

We appreciate the thoughtful comments of the outside reviewers. These were the Science Review Board members: Dr. John Bane of the University of North Carolina, Dr. Eileen Hofmann of Old Dominion University, and Dr. Stephen Macko of the University of Virgina, as well as external reviewer, Dr. William Schroeder of the University of Alabama. Their comments helped to improve this report. We also appreciate the time, effort, and advice that Science Review Board members contributed during the study.

The enthusiastic and timely support of Dr. Alexis Lugo-Fernández, the MMS Contracting Officer's Technical Representative, is greatly appreciated.

TABLE OF CONTENTS

		PAGE
List of Figures		xi
List of Tables		xxi
Acronyms		xxiii
1.	Executive Summary	1
	1.1 Introduction	1
	1.2 Field Measurements	1
	1.3 Forcing Functions	1
	1.4 Major Results	2
2.	Introduction	7
	2.1 NEGOM Program Objectives and Description	7
	2.2 Data Collected	9
	2.3 Report Organization	13
3.	Forcing Functions	15
	3.1 Long-term Averages	15
	3.1.1 Meteorological Conditions	15
	3.1.2 River Discharge Rates	30
	3.2 Other Time Series During the NEGOM-COH Program	45
	3.2.1 Coastal and Selected Offshore Winds	45
	3.2.2 Sea Surface Temperature from Offshore Buoys	45
	3.2.3 Sea Surface Height Fields	59
4.	Circulation and its Variability	99
	4.1 Current Fields Inferred from Multiple Techniques During NEGOM Cruises	99
	4.2 The Annual Cycle of Currents from Surface Drifters	115
	4.3 Space-time Patterns of Low-frequency Circulation from ADCP Currents	131
	4.4 Examination of Wind Forcing of Nearshore Currents	138
	4.5 Examination of Forcing by Off-shelf Circulation Features	145
	4.6 Conclusions	151
5.	Synthesis of Physical Properties	153
	5.1 Introduction	153
	5.2 Fall: Cruises N1, N4, and N7	154
	5.3 Spring: Cruises N2, N5, and N8	157
	5.4 Summer: Cruises N3, N6, and N9	161
6.	Particulates	165
	6.1 Introduction	165
	6.2 Distributions of Particulate Matter	170
	6.3 Distributions of Particulate Organic Carbon and Nitrogen	184

TABLE OF CONTENTS

		PAGE
7.	Dissolved Oxygen and Hypoxia	199
	7.1 Introduction	199
	7.2 Surface Oxygen Distributions	199
	7.3 Subsurface Oxygen Distributions on Selected Density Surfaces	211
	7.4 Bottom Oxygen Distributions and Incidences of Hypoxia	217
8.	Nutrients	227
	8.1 Basic Vertical Profiles of Nutrients	227
	8.2 Seasonally Averaged Nutrient Concentrations	230
	8.3 Nutrient Distributions on Selected Density Surfaces	242
9.	Phytoplankton Pigments	255
	9.1 Introduction	255
	9.2 Estimation of the Contribution of Chlorophyll *a* by Algal Group	255
	9.3 Pigment Distributions by Cruise	259
	9.4 Discussion and Summary	287
10.	Integrated Water Column Chemistry	295
	10.1 Introduction	295
	10.2 General Patterns	296
	10.3 Univariate Analysis	296
	10.4 Multivariate Analyses	300
	10.5 Properties in the Deep Water Column	304
11.	Conclusions and Retrospective	315
	11.1 Principal Conclusions	315
	11.1.1 Forcing and circulation	315
	11.1.2 Major water masses found over the slope and outer shelf	316
	11.1.3 Distributions of oxygen	317
	11.1.4 Distributions of nutrients	317
	11.1.5 Chlorophyll	318
	11.1.6 Distributions of particulate matter	319
	11.1.7 Major algal groups	320
	11.1.8 Integrated water column chemistry	321
	11.1.9 Interrelationships between the observed patterns in abiotic and biotic variables	321
	11.2 Remarks Regarding Experimental Design	324
	11.2.1 Adequacy of sampling period	324
	11.2.2 Sampling plan	324
	11.2.3 Need for simultaneous measurement program	324
	11.2.4 Need for integrating time series and synoptic surveys	325
	11.2.5 Space-time aliasing	325
12.	Literature Cited	327

TABLE OF CONTENTS

		PAGE
Appendix A:	Summary of Conditions during Cruise N1	A-1
Appendix B:	Summary of Conditions during Cruise N2	B-1
Appendix C:	Summary of Conditions during Cruise N3	C-1
Appendix D:	Summary of Conditions during Cruise N4	D-1
Appendix E:	Summary of Conditions during Cruise N5	E-1
Appendix F:	Summary of Conditions during Cruise N6	F-1
Appendix G:	Summary of Conditions during Cruise N7	G-1
Appendix H:	Summary of Conditions during Cruise N8	H-1
Appendix I:	Summary of Conditions during Cruise N9	I-1

LIST OF FIGURES

FIGURE		PAGE
2.1-1.	Study area and bathymetry of the northeastern Gulf of Mexico.	8
2.2-1.	Typical locations for hydrographic stations on NEGOM-COH cruises, November 1997 through August 2000.	11
3.1.1-1.	COADS enhanced mean wind field and principal component ellipses for January.	18
3.1.1-2.	COADS enhanced mean wind field and principal component ellipses for February.	19
3.1.1-3.	COADS enhanced mean wind field and principal component ellipses for March.	20
3.1.1-4.	COADS enhanced mean wind field and principal component ellipses for April.	21
3.1.1-5.	COADS enhanced mean wind field and principal component ellipses for May.	22
3.1.1-6.	COADS enhanced mean wind field and principal component ellipses for June.	23
3.1.1-7.	COADS enhanced mean wind field and principal component ellipses for July.	24
3.1.1-8.	COADS enhanced mean wind field and principal component ellipses for August.	25
3.1.1-9.	COADS enhanced mean wind field and principal component ellipses for September	26
3.1.1-10.	COADS enhanced mean wind field and principal component ellipses for October.	27
3.1.1-11.	COADS enhanced mean wind field and principal component ellipses for November.	28
3.1.1-12.	COADS enhanced mean wind field and principal component ellipses for December.	29
3.1.2-1.	Rivers discharging into the NEGOM study area and locations of associated gauging stations.	31
3.1.2-2.	Discharge rates in 10^6 $m^3 \cdot day^{-1}$ for the Mississippi River and Mobile Bay (Alabama+Tombigbee).	34
3.1.2-3.	Discharge rates in 10^6 $m^3 \cdot day^{-1}$ for the Alabama River (Claiborne and Millers Ferry).	35
3.1.2-4.	Discharge rates in 10^6 $m^3 \cdot day^{-1}$ for the Tombigbee River (Coffeeville) and Apalachicola River.	36
3.1.2-5.	Discharge rates in 10^6 $m^3 \cdot day^{-1}$ for the Tombigbee River (Demopolis) and Pascagoula River.	37
3.1.2-6.	Discharge rates in 10^6 $m^3 \cdot day^{-1}$ for the Escambia River (Molino) and Choctawhatchee River.	38
3.1.2-7.	Discharge rates in 10^6 $m^3 \cdot day^{-1}$ for the Suwannee River and Pearl River.	39
3.1.2-8.	Discharge rates in 10^6 $m^3 \cdot day^{-1}$ for the Escambia River (Century) and Ochlockonee River.	40
3.1.2-9.	Discharge rates in 10^6 $m^3 \cdot day^{-1}$ for the Yellow River and Perdido River.	41
3.1.2-10.	Discharge rates in 10^6 $m^3 \cdot day^{-1}$ for the Aucilla River and Blackwater River.	42

LIST OF FIGURES

FIGURE		PAGE
3.1.2-11.	Discharge rates in 10^6 $m^3 \cdot day^{-1}$ for the Steinhatchee River and Econfina River.	43
3.1.2-12.	Discharge rates in 10^6 $m^3 \cdot day^{-1}$ for the Fenholloway River.	44
3.2.1-1.	Locations of surface meteorological stations in the NEGOM region.	46
3.2.1-2.	Along-shelf (a) and cross-shelf (b) wind components for 1997.	47
3.2.1-3	Along-shelf (a) and cross-shelf (b) wind components for 1998.	49
3.2.1-4.	Along-shelf (a) and cross-shelf (b) wind components for 1999.	51
3.2.1-5.	Along-shelf (a) and cross-shelf (b) wind components for 2000.	53
3.2.2-1.	Near-surface 40-hr low-pass water temperature for NDBC stations in the NEGOM region in 1997.	55
3.2.2-2.	Near-surface 40-hr low-pass water temperature for NDBC stations in the NEGOM region in 1998.	56
3.2.2-3.	Near-surface 40-hr low-pass water temperature for NDBC stations in the NEGOM region in 1999.	57
3.2.2-4.	Near-surface 40-hr low-pass water temperature for NDBC stations in the NEGOM region in 2000.	58
3.2.3-1.	Sea surface height from satellite altimeter data for (a) 1 October 1997, (b) 8 October 1997, (c) 15 October 1997, and (d) 22 October 1997.	61
3.2.3-2.	Sea surface height from satellite altimeter data for (a) 29 October 1997, (b) 5 November 1997, (c) 12 November 1997, and (d) 19 November 1997.	62
3.2.3-3.	Sea surface height from satellite altimeter data for (a) 26 November 1997, (b) 3 December 1997, (c) 10 December 1997, and (d) 17 December 1997.	63
3.2.3-4.	Sea surface height from satellite altimeter data for (a) 24 December 1997, (b) 31 December 1997, (c) 7 January 1998, and (d) 14 January 1998.	64
3.2.3-5.	Sea surface height from satellite altimeter data for (a) 21 January 1998, (b) 28 January 1998, (c) 4 February 1998, and (d) 11 February 1998.	65
3.2.3-6.	Sea surface height from satellite altimeter data for (a) 18 February 1998, (b) 25 February 1998, (c) 4 March 1998, and (d) 11 March 1998.	66
3.2.3-7.	Sea surface height from satellite altimeter data for (a) 18 March 1998, (b) 25 March 1998, (c) 1 April 1998, and (d) 8 April 1998.	67
3.2.3-8.	Sea surface height from satellite altimeter data for (a) 15 April 1998, (b) 22 April 1998, (c) 29 April 1998 and (d) 6 May 1998.	68
3.2.3-9.	Sea surface height from satellite altimeter data for (a) 13 May 1998, (b) 20 May 1998, (c) 27 May 1998, and (d) 3 June 1998.	69
3.2.3-10.	Sea surface height from satellite altimeter data for (a) 10 June 1998, (b) 17 June 1998, (c) 24 June 1998, and (d) 1 July 1998.	70
3.2.3-11.	Sea surface height from satellite altimeter data for (a) 8 July 1998, (b) 15 July 1998, (c) 22 July 1998, and (d) 29 July 1998.	71
3.2.3-12.	Sea surface height from satellite altimeter data for (a) 5 August 1998, (b) 12 August 1998, (c) 19 August 1998, and (d) 26 August 1998.	72
3.2.3-13.	Sea surface height from satellite altimeter data for (a) 2 September 1998, (b) 9 September 1998, (c) 16 September 1998, and (d) 23 September 1998.	73

LIST OF FIGURES

FIGURE		PAGE
3.2.3-14.	Sea surface height from satellite altimeter data for (a) 30 September 1998, (b) 7 October 1998, (c) 14 October 1998, and (d) 21 October 1998.	74
3.2.3-15.	Sea surface height from satellite altimeter data for (a) 28 October 1998, (b) 4 November 1998, (c) 11 November 1998, and (d) 18 November 1998.	75
3.2.3-16.	Sea surface height from satellite altimeter data for (a) 25 November 1998, (b) 2 December 1998, (c) 9 December 1998, and (d) 16 December 1998.	76
3.2.3-17.	Sea surface height from satellite altimeter data for (a) 23 December 1998, (b) 30 December 1998, (c) 6 January 1999, and (d) 13 January 1999.	77
3.2.3-18.	Sea surface height from satellite altimeter data for (a) 20 January 1999, (b) 27 January 1999, (c) 3 February 1999, and (d) 10 February 1999.	78
3.2.3-19.	Sea surface height from satellite altimeter data for (a) 17 February 1999, (b) 26 February 1999, (c) 3 March 1999, and (d) 10 March 1999.	79
3.2.3-20.	Sea surface height from satellite altimeter data for (a) 17 March 1999, (b) 24 March 1999, (c) 31 March 1999, and (d) 7 April 1999.	80
3.2.3-21.	Sea surface height from satellite altimeter data for (a) 14 April 1999, (b) 21 April 1999, (c) 28 April 1999, and (d) 5 May 1999.	81
3.2.3-22.	Sea surface height from satellite altimeter data for (a) 12 May 1999, (b) 19 May 1999, (c) 26 May 1999, and (d) 2 June 1999.	82
3.2.3-23.	Sea surface height from satellite altimeter data for (a) 9 June 1999, (b) 16 June 1999, (c) 23 June 1999, and (d) 30 June 1999	83
3.2.3-24	Sea surface height from satellite altimeter data for (a) 7 July 1999, (b) 14 July 1999, (c) 21 July 1999, and (d) 28 July 1999.	84
3.2.3-25.	Sea surface height from satellite altimeter data for (a) 4 August 1999, (b) 11 August 1999, (c) 18 August 1999, and (d) 25 August 1999.	85
3.2.3-26.	Sea surface height from satellite altimeter data for (a) 1 September 1999, (b) 8 September 1999, (c) 15 September 1999, and (d) 22 September 1999.	86
3.2.3-27.	Sea surface height from satellite altimeter data for (a) 29 September 1999, (b) 6 October 1999, (c) 13 October 1999, and (d) 20 October 1999.	87
3.2.3-28.	Sea surface height from satellite altimeter data for (a) 27 October 1999, (b) 3 November 1999, (c) 10 November 1999, and (d) 17 November 1999.	88
3.2.3-29.	Sea surface height from satellite altimeter data for (a) 24 November 1999, (b) 1 December 1999, (c) 8 December 1999, and (d) 15 December 1999.	89
3.2.3-30.	Sea surface height from satellite altimeter data for (a) 22 December 1999, (b) 29 December 1999, (c) 5 January 2000, and (d) 12 January 2000.	90
3.2.3-31.	Sea surface height from satellite altimeter data for (a) 19 January 2000, (b) 26 January 2000, (c) 2 February 2000, and (d) 9 February 2000.	91
3.2.3-32.	Sea surface height from satellite altimeter data for (a) 16 February 2000, (b) 25 February 2000, (c) 1 March 2000, and (d) 8 March 2000.	92

LIST OF FIGURES

FIGURE		PAGE
3.2.3-33.	Sea surface height from satellite altimeter data for (a) 15 March 2000, (b) 22 March 2000, (c) 29 March 2000, and (d) 5 April 2000.	93
3.2.3-34.	Sea surface height from satellite altimeter data for (a) 12 April 2000, (b) 19 April 2000, (c) 26 April 2000, and (d) 3 May 2000.	94
3.2.3-35.	Sea surface height from satellite altimeter data for (a) 10 May 2000, (b) 17 May 2000, (c) 24 May 2000, and (d) 31 May 2000.	95
3.2.3-36.	Sea surface height from satellite altimeter data for (a) 7 June 2000, (b) 14 June 2000, (c) 21 June 2000, and (d) 28 June 2000	96
3.2.3-37.	Sea surface height from satellite altimeter data for (a) 5 July 2000, (b) 12 July 2000, (c) 19 July 2000, and (d) 26 July 2000.	97
3.2.3-38.	Sea surface height from satellite altimeter data for (a) 2 August 2000, (b) 9 August 2000, (c) 16 August 2000, and (d) 23 August 2000.	98
4.1-1.	Gridded ADCP-measured currents at 10 m and 12 m on NEGOM Cruise N1, 16-27 November 1997.	101
4.1-2.	Trajectories of NEGOM drifters (drogued in the upper meter) deployed during cruise N1.	102
4.1-3.	Gridded ADCP-measured currents at 14 m on NEGOM Cruise N2, 5-16 May 1998.	103
4.1-4.	Trajectories of NEGOM drifters (drogued in the upper meter) deployed during cruise N2.	105
4.1-5.	Gridded ADCP-measured currents at 14 m on NEGOM Cruise N3, 25 July – 7 August 1998.	106
4.1-6.	Trajectories of NEGOM drifters (drogued in the upper meter) for period from 20 July through 4 September 1998.	107
4.1-7.	Gridded ADCP-measured currents at 12 m on NEGOM Cruise N4, 13-24 November 1998.	108
4.1-8.	Trajectories of NEGOM drifters (drogued in the upper meter) deployed during cruise N4.	109
4.1-9.	Gridded ADCP-measured currents at 14 m on NEGOM Cruise N5, 15-28 May 1999.	111
4.1-10.	Gridded ADCP-measured currents at 14 m on NEGOM Cruise N6, 15-28 August 1999.	112
4.1-11.	Gridded 38 kHz ADCP-measured currents at 14 m on NEGOM Cruise N7, 13-25 November 1999.	113
4.1-12.	Trajectories of NEGOM drifters (drogued in the upper meter) deployed during cruise N7.	114
4.1-13.	Gridded 150 kHz ADCP-measured currents at 12 m on NEGOM Cruise N8, 15-26 April 2000.	116
4.1-14.	Gridded 150 kHz ADCP-measured currents at 12 m on NEGOM Cruise N9, 29 July – 8 August 2000.	117
4.2-1.	Numbers of observations from winter SCULP II drifter releases February 1996-March 1997.	118
4.2-2.	Average surface vectors for winter from SCULP II drifter releases February 1996-March 1997.	119
4.2-3.	Variance ellipses for winter from SCULP II drifter releases February 1996-March 1997.	120
4.2-4.	Numbers of observations from spring SCULP II drifter releases February 1996-March 1997.	121

LIST OF FIGURES

FIGURE		PAGE
4.2-5.	Average surface vectors for spring from SCULP II drifter releases February 1996-March 1997.	122
4.2-6.	Variance ellipses for spring from SCULP II drifter releases February 1996-March 1997.	123
4.2-7.	Numbers of observations from summer SCULP II drifter releases February 1996-March 1997.	124
4.2-8.	Average surface vectors for summer from SCULP II drifter releases February 1996-March 1997.	125
4.2-9.	Variance ellipses for summer from SCULP II drifter releases February 1996-March 1997.	126
4.2-10.	Numbers of observations from fall SCULP II drifter releases February 1996-March 1997.	127
4.2-11.	Average surface vectors for fall from SCULP II drifter releases February 1996-March 1997.	128
4.2-12.	Variance ellipses for fall from SCULP II drifter releases February 1996-March 1997.	129
4.3-1.	ADCP currents at vertical bin centered at 10-14 m.	132
4.3-2.	Pattern of EOF mode 1 for non-divergent currents at vertical bin centered at 10-14 m using ADCP data from eight NEGOM cruises.	133
4.3-3.	Pattern of EOF mode 2 for non-divergent currents at vertical bin centered at 10-14 m using ADCP data from eight NEGOM cruises.	134
4.3-4.	Pattern of EOF mode 3 for non-divergent currents at vertical bin centered at 10-14 m using ADCP data from eight NEGOM cruises.	135
4.3-5.	Pattern of EOF mode 4 for non-divergent currents at vertical bin centered at 10-14 m using ADCP data from eight NEGOM cruises.	136
4.3-6.	Amplitudes of first four EOF modes at times of NEGOM cruises.	137
4.3-7.	Amplitudes of EOF modes 5-7 at times of NEGOM cruises.	139
4.4-1.	Locations near the 20-m isobath at which time series of 10-m winds were constructed using optimal interpolation from hourly measurements over the region during the NEGOM field period.	141
4.4-2.	Time series of along-shelf components of 10-m winds at the locations shown in Figure 4.4-1.	142
4.4-3.	Plots of along-shelf components of 40-hr low-pass winds and of near-surface ADCP currents at the time of each of eight NEGOM cruises for location 4 in Figure 4.4-1.	143
4.4-4.	Correlation values between along-shelf components of wind and near-surface current calculated between gridded fields of these values using data from eight NEGOM cruises.	144
4.5-1.	Locations at which time series of SSH gradients along the four lines shown were calculated using SSH distributions prepared by R. Leben.	146
4.5-2.	Fields of correlations between SSH gradients at the locations indicated (solid square) and gridded near-surface ADCP currents for eight NEGOM cruises.	147
6.1-1.	Linear correlations between PBAC and PM for the NEGOM region hydrographic cruises.	167
6.1-2.	Depth profile of percent transmission for (upper panel) station N3L07S13 showing surface nepheloid layer and (lower panel) station N4L02S06 showing bottom nepheloid layer (BNL).	171

LIST OF FIGURES

FIGURE		PAGE
6.2-1.	PM distribution for cruise N1 in November 1997.	172
6.2-2.	PM distribution for cruise N4 in November 1998.	174
6.2-3.	PM distribution for cruise N7 in November 1999.	175
6.2-4.	PM distribution for cruise N2 in May 1998.	176
6.2-5.	PM distribution for cruise N5 in May 1999.	178
6.2-6.	PM distribution for cruise N8 in April 2000.	179
6.2-7.	PM distribution for cruise N3 in July/August 1998.	180
6.2-8.	PM distribution for cruise N6 in August 1999.	181
6.2-9.	PM distribution for cruise N9 in July/August 2000.	183
6.2-10.	Average water column PM (g) for stations on the shelf (water depth < 200 m).	185
6.2-11.	Average PM (g) in BNL for stations on the shelf (water depth < 200 m).	186
6.3-1.	Particulate organic carbon ($\mu g \cdot L^{-1}$) from the near-surface observations on fall cruises N1, N4, and N7.	189
6.3-2.	Particulate organic carbon ($\mu g \cdot L^{-1}$) from the near-surface observations on spring cruises N2, N5, and N8.	190
6.3-3.	Particulate organic carbon ($\mu g \cdot L^{-1}$) from the near-surface observations on summer cruises N3, N6, and N9.	191
6.3-4.	Particulate organic carbon ($\mu g \cdot L^{-1}$) on fall cruises N1, N4, and N7 from the near-bottom (a and b) and chlorophyll maximum (c) observations.	192
6.3-5.	Particulate organic carbon ($\mu g \cdot L^{-1}$) on spring cruises N2, N5, and N8 from the near-bottom (a and b) and chlorophyll maximum (c) observations.	193
6.3-6.	Particulate organic carbon ($\mu g \cdot L^{-1}$) on summer cruises N3, N6, and N9 from the near-bottom (a and b) and chlorophyll maximum (c) observations.	194
7.1-1.	Example oxygen profiles along the 100- (left), 500- (middle), and 1000-m (right) isobaths.	200
7.2-1.	Surface saturation (percent) of dissolved oxygen from spring cruises N2 (May 1998), N5 (May 1999), and N8 (April 2000).	201
7.2-2.	Surface salinity from spring cruises N2 (May 1998), N5 (May 1999), and N8 (April 2000).	203
7.2-3.	Surface saturation (percent) of dissolved oxygen from summer cruises N3 (July/August 1998), N6 (August 1999), and N9 (July/August 2000).	204
7.2-4.	Surface salinity from summer cruises N3 (July/August 1998), N6 (August 1999), and N9 (July/August 2000).	205
7.2-5.	Surface saturation (percent) of dissolved oxygen from fall cruises N1 (November 1997), N4 (November 1998), and N7 (November 1999).	206
7.2-6.	Surface salinity from fall cruises N1 (November 1997), N4 (November 1998), and N7 (November 1999).	207
7.2-7.	Near-surface percent dissolved oxygen saturation versus salinity for fall, spring, and summer cruises in 1997-2000.	209
7.2-8.	Near-surface dissolved oxygen saturation (percent) versus chlorophyll *a* ($ng \cdot L^{-1}$) for fall, spring, and summer cruises in 1997-2000.	210

LIST OF FIGURES

FIGURE		PAGE
7.3-1.	Mean and standard deviation of dissolved oxygen from nine cruises on an average sigma-theta level of 22 $kg \cdot m^{-3}$, which represents the average σ_θ for the near-surface samples	212
7.3-2.	Mean and standard deviation of dissolved oxygen from nine cruises on an average sigma-theta level of 25.4 $kg \cdot m^{-3}$	213
7.3-3.	Mean and standard deviation of dissolved oxygen from nine cruises on an average sigma-theta level of 26.5 $kg \cdot m^{-3}$	214
7.3-4.	Mean and standard deviation of dissolved oxygen from nine cruises on an average sigma-theta level of 27.15 $kg \cdot m^{-3}$	215
7.3-5.	Mean and standard deviation of dissolved oxygen ($mL \cdot L^{-1}$) from nine cruises at the bottom sigma-theta level for each station.	216
7.4-1.	Bottom dissolved oxygen ($mL \cdot L^{-1}$) from spring cruises N2 (May 1998), N5 (May 1999), and N8 (April 2000).	218
7.4-2.	Bottom dissolved oxygen ($mL \cdot L^{-1}$) from summer cruises N3 (July/August 1998), N6 (August 1999), and N9 (July/August 2000).	219
7.4-3.	Bottom dissolved oxygen ($mL \cdot L^{-1}$) from fall cruises N1 (November 1997), N4 (November 1998), and N7 (November 1999)	220
7.4-4.	Percent dissolved oxygen saturation versus stability ($kg \cdot m^{-4}$) near bottom over the shelf west of 87°W for fall, spring, and summer cruises.	222
7.4-5.	Percent dissolved oxygen saturation versus stability ($kg \cdot m^{-4}$) near bottom in all water depths over the shelf east of 87°W for fall, spring, and summer cruises	223
7.4-6.	Percent dissolved oxygen saturation versus nitrate (µM) near-bottom for fall, spring, and summer cruises in 1997-2000.	225
8.1-1.	Example profiles of nitrate, phosphate, and silicate showing influence of river water on surface concentrations.	228
8.1-2.	Nutrients versus salinity and nitrate-phosphate property plots for data below 150 m on all NEGOM cruises.	229
8.2-1.	Sequential numbering of stations used in presenting average nutrient concentrations.	231
8.2-2.	Seasonal average surface nitrate concentrations plotted by station number (see Figure 8.2-1) for all (a) spring, (b) summer, and (c) fall NEGOM hydrography cruises.	232
8.2-3.	Seasonal average surface nitrate concentrations for stations from lines 3 through 11 plotted by station number (see Figure 8.2-1) for all (a) spring, (b) summer, and (c) fall NEGOM hydrography cruises.	234
8.2-4.	Standard deviation of seasonal surface nitrate concentrations plotted by station number (see Figure 8.2-1) for (a) spring, (b) summer, and (c) fall for all NEGOM hydrography cruises.	235
8.2-5.	Seasonal average surface phosphate concentrations plotted by station number (see Figure 8.2-1) for all (a) spring, (b) summer, and (c) fall NEGOM hydrography cruises.	236
8.2-6.	Seasonal average surface silicate concentrations plotted by station number (see Figure 8.2-1) for all (a) spring, (b) summer, and (c) fall NEGOM hydrography cruises.	237
8.2-7.	Average concentrations of nitrate (µM) over the western and eastern NEGOM shelves.	239

LIST OF FIGURES

FIGURE		PAGE
8.2-8.	Average concentrations of phosphate (µM) over the western and eastern NEGOM shelves.	240
8.2-9.	Average concentrations of silicate (µM) over the western and eastern NEGOM shelves.	241
8.3-1.	Mean and standard deviation of nitrate from nine cruises on an average sigma-theta level of 22 $kg \cdot m^{-3}$.	244
8.3-2.	Mean and standard deviation of nitrate from nine cruises on an average sigma-theta level of 25.4 $kg \cdot m^{-3}$.	245
8.3-3.	Mean and standard deviation of nitrate from nine cruises on an average sigma-theta level of 26.5 $kg \cdot m^{-3}$.	246
8.3-4.	Mean and standard deviation of nitrate from nine cruises on an average sigma-theta level of 27.15 $kg \cdot m^{-3}$.	247
8.3-5.	Mean and standard deviation of nitrate from nine cruises on an average sigma-theta level of 27.45 $kg \cdot m^{-3}$.	248
8.3-6.	Mean and standard deviation of nitrate from nine cruises at the bottom sigma-theta level for each station.	249
8.3-7.	Mean and standard deviation of phosphate from nine cruises at the bottom sigma-theta level for each station.	251
8.3-8.	Mean and standard deviation of silicate from nine cruises on an average sigma-theta level of 22 $kg \cdot m^{-3}$.	252
8.3-9.	Mean and standard deviation of silicate from nine cruises on an average sigma-theta level of 25.4 $kg \cdot m^{-3}$.	253
8.3-10.	Mean and standard deviation of silicate from nine cruises at the bottom sigma-theta level for each station.	254
9.2-1.	Correlation of chlorophylls (sum of chlorophyll *a*, *b*, and *c*) determined by HPLC and the chlorophylls calculated from the response of *in vivo* fluorometry from surface seawater samples during cruises N1 and N3 through N9.	257
9.3-1.	Chlorophyll *a* concentrations ($\mu g \cdot L^{-1}$) from near-surface (~1-3 m depth) observations on NEGOM hydrographic cruises.	260
9.3-2.	Chlorophyll *a* concentrations ($\mu g \cdot L^{-1}$) from subsurface DCM observations on NEGOM hydrographic cruises.	261
9.3-3.	Prymnesiophyte abundance, as a percent of chlorophyll *a*, in near-surface waters on nine NEGOM cruises from November 1997 through August 2000.	263
9.3-4.	Prymnesiophytes (as a percent of chlorophyll *a*) at the deep chlorophyll maximum during NEGOM cruise N1, 16-26 November 1997.	264
9.3-5.	Pelagophytes (as a percent of chlorophyll *a*) at the deep chlorophyll maximum during NEGOM cruise N1, 16-26 November 1997.	265
9.3-6.	Cyanobacteria (as a percent of chlorophyll *a*) in near-surface waters during NEGOM cruise N1, 16-26 November 1997.	267
9.3-7.	Diatoms (as a percent of chlorophyll *a*) in near-surface waters during NEGOM cruise N1, 16-26 November 1997.	268
9.3-8.	Diatoms (as a percent of chlorophyll *a*) at the deep chlorophyll maximum during NEGOM cruise N2, 5-16 May 1998.	270
9.3-9.	Prochlorophytes (as a percent of chlorophyll *a*) in near-surface waters during NEGOM cruise N3, 26 July-6 August 1998.	273

LIST OF FIGURES

FIGURE		PAGE
9.3-10.	Prochlorophytes (as a percent of chlorophyll *a*) at the deep chlorophyll maximum during NEGOM cruise N5, 16-27 May 1999.	276
9.3-11.	Prochlorophytes (as a percent of chlorophyll *a*) at the deep chlorophyll maximum during NEGOM cruise N6, 17-28 August 1999.	279
9.3-12.	Diatoms (as a percent of chlorophyll *a*) at the deep chlorophyll maximum during NEGOM cruise N7, 13-22 November 1999.	282
9.3-13.	Pelagophytes (as a percent of chlorophyll *a*) at the deep chlorophyll maximum during NEGOM cruise N7, 13-22 November 1999.	283
9.3-14.	Prochlorophytes (as a percent of chlorophyll *a*) in near-surface waters during NEGOM cruise N9, 29 July-8 August 2000.	286
9.4-1.	Seasonal variations in chlorophyll *a* concentrations and the average relative abundance of major phytoplankton groups in the near-surface waters from November 1997 through August 2000.	289
9.4-2.	Seasonal variations in chlorophyll *a* concentrations and the average relative abundance of major phytoplankton groups in the deep chlorophyll maximum waters from November 1997 through August 2000.	290
9.4-3.	Average chlorophyll *a* concentrations in near-surface waters grouped by the station depth into inner-middle shelf ($z < 50$ m), outer shelf ($50 < z < 400$ m), and continental slope ($z > 400$ m)	291
10.2-1.	River discharges into the study area for the 30-day period preceding each cruise.	297
10.2-2.	Geographic sub-regions within the study area.	298
10.4-1.	Data classified by time of year to detect seasonal trends.	303
10.4-2.	Data classified by geographic location to detect variability due to distance from the Mississippi River.	305
10.4-3.	Data classified by depth in the water column to detect vertical variability in the data.	306
10.4-4.	Data for May cruises classified by depth in the water column.	307
10.4-5.	Data for May classified by water depth.	308
10.4-6.	Data from May cruises classified by year of sampling.	309
10.4-7.	Data for August classified by year of sampling.	310
10.4-8.	Data from November cruises classified by year of sampling.	311
10.5-1.	Representative vertical profiles of NEGOM nutrients, dissolved oxygen, salinity, and potential temperature.	312

LIST OF TABLES

TABLE		PAGE
2.1-1.	NEGOM-COH program tasks.	9
2.2-1.	Cruise identifiers and dates	10
2.2-2.	Summary of data collection and scientific participation on NEGOM-COH cruises.	12
3.1.1-1.	Number of frontal passages over the NEGOM study area during each field year and resulting averages of cold front passages	16
3.1.1-2.	Average interval between fronts (days), where "n" means no meaningful interval.	16
3.1.1-3.	Available monthly COADs data at 167 grid points in the Gulf of Mexico.	30
3.1.1-4.	Monthly mean ocean heat storage rates for NEGOM region adopted from Etter.	30
3.1.2-1.	Record-length mean daily discharge rate for rivers discharging into the NEGOM region.	32
3.1.2-2.	Mean river discharges associated with the 30-day period prior to each cruise for selected rivers.	33
3.2.1-1.	Along-shelf directions at meteorological stations relative to local bathymetry	45
4.3-1.	Variance associated with modes resulting from EOF analysis of residual 10-14 m current fields for NEGOM cruises N1-N3 and N5-N9.	138
4.4-1.	Correlations between along-shelf components of 40-hr low-pass wind and near-surface ADCP currents at each location based on measurements from all NEGOM cruises.	145
6.1-1.	Coefficients of linear regressions of measured particulate matter (PM) against the particle beam attenuation coefficient (PBAC), where PM = A + B * PBAC.	166
6.2-1.	Basic statistics for particulate matter observations	187
6.3-1.	Basic statistics for observations of particulate organic carbon and particulate organic nitrogen and ratio of POC to PON.	195
6.3-2.	Ratio of POC to PM from near-surface observations.	196
6.3-3.	Ratio of POC to PM from near-bottom observations (N1 through N6) or chlorophyll maximum observations (N7 through N9).	197
7.2-1.	Correlation coefficients for percent of surface oxygen saturation with surface salinity and surface chlorophyll *a* values over the Mississippi-Alabama shelf west of 87°W.	211
7.4-1.	Bottom bottle dissolved oxygen measurements.	221
7.4-2.	Correlation coefficients for percent bottom oxygen saturation with bottom nitrate concentrations over the shelf west of 87°W.	226
8.2-1.	Ratio of average concentrations on NEGOM cruises of the western to the eastern study area.	238
8.3-1.	Basic statistics for nutrient concentrations on selected sigma-theta surfaces	243
9.1-1.	Summary of major photosynthetic pigments present in marine phytoplankton groups.	256
9.2-1.	Pigment algorithms used to partition chlorophyll *a* biomass among major phytoplankton groups (Letelier et al. 1993; Mackey et al. 1996; Write and van den Enden 2000).	258

LIST OF TABLES

TABLE		PAGE
9.3-1.	Percent of chlorophyll *a* contributed by individual algal groups in near-surface, deep chlorophyll maximum (DCM), and below DCM (BDCM) waters on cruise N1 (November 1997).	262
9.3-2.	Percent of chlorophyll *a* contributed by individual algal groups in near surface, deep chlorophyll maximum (DCM), and below DCM (BDCM) waters on cruise N2 (May 1998).	269
9.3-3.	Percent of chlorophyll *a* contributed by individual algal groups in near-surface, deep chlorophyll maximum layer (DCM), and below DCM (BDCM) waters on cruise N3 (July-August 1998).	271
9.3-4.	Percent of chlorophyll *a* contributed by individual algal groups in near-surface, deep chlorophyll maximum layer (DCM), and below DCM (BDCM) waters on cruise N4 (November 1999).	274
9.3-5.	Percent of chlorophyll *a* contributed by individual algal groups in near-surface, deep chlorophyll maximum layer (DCM), and below DCM (BDCM) waters on cruise N5 (May 1999).	275
9.3-6.	Percent of chlorophyll *a* contributed by individual algal groups in near-surface, deep chlorophyll maximum layer (DCM), and below DCM (BDCM) waters on cruise N6 (August 1999).	278
9.3-7.	Percent of chlorophyll *a* contributed by individual algal groups in near-surface, deep chlorophyll maximum layer (DCM), and below DCM (BDCM) waters on cruise N7 (November 1999).	280
9.3-8.	Percent of chlorophyll *a* contributed by individual algal groups in near-surface, deep chlorophyll maximum layer (DCM), and below DCM (BDCM) waters on cruise N8 (April 2000).	284
9.3-9.	Percent of chlorophyll *a* contributed by individual algal groups in near-surface, deep chlorophyll maximum layer (DCM), and below DCM (BDCM) waters on cruise N9 (July-August 2000).	285
10.3-1.	Correlations of NEGOM data.	299
10.4-1.	Variances from PCA.	301
10.4-2.	Principal component loadings.	301

ACRONYMS

AAIW	Antarctic Intermediate Water
ADCP	Acoustic Doppler current profiler
AVHRR	Advanced Very High Resolution Radiometer
BB150	broadband 150 kHz ADCP
BNL	bottom nepheloid layer
CCAR	Colorado Center for Astrodynamics Research, University of Colorado
COADS	Comprehensive Ocean-Atmosphere Data Set
COH	NEGOM Chemical Oceanography and Hydrography Study
CTD	conductivity-temperature-depth sensor
CU	University of Colorado
DCM	deep chlorophyll maximum
EIS	NEGOM DeSoto Canyon Eddy Intrusion Study
EOF	empirical orthogonal function analysis
GERG	Geochemical and Environmental Research Group at TAMU
GPS	global positioning system
HPLC	high performance liquid chromatography
ID	identifier for cruises
INL	intermediate-depth nepheloid layer
LATEX	Louisiana-Texas Shelf Physical Oceanography Program
LC	Loop Current
LCE	Loop Current eddy
MBT	mechanical bathythermograph
MMS	Minerals Management Service, U.S. Department of the Interior
MSL	mean sea level
NASA	National Aeronautics and Space Administration??
NEGOM	Northeastern Gulf of Mexico Physical Oceanography Program
NOAA	National Oceanic and Atmospheric Administration
N/P	nitrogen/phosphorus ratio
OSU	Ohio State University
PBAC	particle beam attenuation coefficient
PCA	principal component analysis
PM	particulate matter
POC	particulate organic carbon
PON	particulate organic nitrogen
QA/QC	quality assurance/quality control
R/V	research vessel
SAIC	Science Applications International Corporation
SCULP II	Surface Current Lagrangian Program II (over the northeastern Gulf shelves)
SeaWiFS	Sea-viewing Wide Field-of-view Sensor
SSH	sea surface height
SSHA	sea surface height anomaly
SST	sea surface temperature
SUW	Subtropical Underwater
TACW	Tropical Atlantic Central Water
TAMU	Texas A&M University
USF	University of South Florida
USM	University of Southern Mississippi
UTC	Universal Coordinated Time
XBT	expendable bathythermograph probe

1 EXECUTIVE SUMMARY

1.1 Introduction

The Minerals Management Service (MMS) of the U. S. Department of the Interior awarded the contract for the Northeastern Gulf of Mexico Physical Oceanography Program (NEGOM): Chemical Oceanography and Hydrography Study (NEGOM-COH) to the Texas A&M Research Foundation in September 1997. Under the contract, scientists at Texas A&M University (TAMU) conducted the study. The basic study area was between the 10- and 1000-m isobaths from the Mississippi Delta along 89°W to off Tampa Bay along 27.5°N. Vertically the study area extended from the sea surface to sea floor.

MMS had three objectives for the study. First was to develop an oceanographic experimental design of research cruises covering the NEGOM study area with sufficient frequency to resolve seasonal variations of chemical oceanography and hydrographic parameters. Second was to collect the ancillary data needed to complement and analyze the chemical oceanographic and hydrographic measurements. Third was to analyze the data to describe the vertical and horizontal spatial distributions and temporal variability of water properties and to describe the processes that contribute to the production of the observed distributions. Study results will assist MMS in its management of the nation's Outer Continental Shelf Leasing Program, including oil and gas leases in federal waters of the northeast Gulf shelves and upper slope.

1.2 Field Measurements

Nine oceanographic research cruises were conducted aboard the *R/V Gyre* over three field years from November 1997 to August 2000. During a field year, one cruise was conducted in each of the spring (April/May), summer (July/August), and fall (November) seasons. Continuous profiles were made of temperature, salinity, dissolved oxygen, light transmission, fluorescence, downwelling irradiance, and optical backscatterance. A total of 883 conductivity-temperature-depth (CTD) stations were occupied. Discrete water samples were drawn at each CTD station for analyses of nutrients (nitrate, phosphate, silicate, nitrite, ammonium, and urea), pigments, particulate matter, and particulate organic carbon. Four to twelve discrete samples per station were taken, totaling over 8000 oxygen and 8000 nutrient samples, over 1500 pigment and particulate matter samples, and over 1000 particulate organic carbon samples. Over 800 expendable bathythermograph (XBT) measurements were made. Acoustic Doppler current profiler (ADCP) observations and underway flow-through measurements of near-surface temperature, salinity, fluorescence, and calculated chlorophyll were made continuously along track. Nearly 1000 near-surface chlorophyll samples were taken to calibrate the underway, near-surface fluorescence data. Ancillary data sets, such as river discharge, sea surface height fields from satellite altimeter, and meteorological measurements, were assembled to support the data analysis and interpretation.

1.3 Forcing Functions

The three major forcing functions are winds, river discharge, and energetic off-shelf features. Winds were examined by time series of meteorological data at offshore buoys and coastal land stations. These winds were gridded to provide hourly wind fields over the NEGOM study area. Over the Gulf of Mexico, mean winds are generally toward the southwest from October through February; toward the northwest from April through August; and westward in March and September. Conditions during the NEGOM cruises followed this general

pattern with some variability. River discharge data were assembled for 18 rivers discharging into the NEGOM bays and estuaries or directly into the Gulf. These included the Mississippi River, the Tombigbee and Alabama Rivers that empty into Mobile Bay, the Apalachicola River, and the Suwannee River. Off-shelf features that can impinge on the study area include small diameter cyclonic or anticyclonic slope eddies, Loop Current eddies or filaments, and the Loop Current. The presence of these features was determined through the use of sea surface height fields from satellite altimeter data. During NEGOM, neither the Loop Current nor Loop Current eddies impinged on the study area; however, there were a number of anticyclonic and cyclonic eddies and a Loop Current filament that occurred over the slope of the study area.

1.4 Major Results

Circulation. The circulation over the NEGOM region is described principally using shipboard 150 kHz ADCP measurements made along the track of each survey cruise. Comparison of the ADCP currents in the upper bin (centered ~12-14 m) with the surface geopotential anomaly relative to 800 m, as extrapolated onto the shelf, shows generally good agreement between the 1000-m isobath and mid-shelf (approximately 50-m isobath). Over the inner shelf there was less agreement, and frequently the relative geostrophic flow indicated onshore-offshore flow in regions of along shelf ADCP currents. We attribute such lack of agreement to the lack of representation in the geopotential anomaly of pycnobathic current components generated when isobaths and bottom isopycnals are non-coincident. Fields of sea surface height (SSH) were used to describe and study the surface geostrophic flow off the shelf. The SSH patterns agreed well with those from ADCP measurements inshore as far as the upper slope. In water depths less than approximately 500 m, agreement lessened and we discounted the SSH fields.

Using a combination of ADCP measurements, geopotential anomaly fields, SSH fields, conservative property distributions, surface drifters, and moored current measurements (as available), the circulation regime over the NEGOM area was described for the period of each of the nine cruises.

A general result of our study is the conclusion that interannual variability overshadows seasonal signals. We attribute this principally to two factors. First, the offshelf circulation, consisting of both cyclonic and anticyclonic eddies as well as the Loop Current and filaments thereof, is very energetic, highly variable, and greatly affects the shelf circulation—even over the inner shelf in the regions of narrow shelf (e.g., Mississippi Delta) and near DeSoto Canyon. Second, the seasonal cycle of wind forcing over the inner shelf is neither so strong nor so regular as that needed to ensure a strongly seasonal coastal current regime.

Realizing the large interannual variability and the fact that only three realizations of the circulation for each season were available, we nevertheless sought space-time patterns over the area applying empirical orthogonal function (EOF) analysis to surface ADCP currents. First we combined measurements from 38 kHz ADCP with 150 kHz to obtain eight fields of near surface currents covering the entire NEGOM region. Each field was gridded and an overall mean obtained and removed from each individual field. Then, to remove the considerable noise known to be associated with divergence, the divergent component was removed from each residual field before applying an EOF analysis. The first four resulting EOF modes contained 84% of the variance. Mode 1, with 34% of the variance, is essentially along shelf circulation pattern with maximum speeds over the outer shelf and slope. Mode 2 appears to result from offshelf eddies driving cyclonic-anticyclonic flow regimes over the outer NEGOM region and accounts for 22% of the variance. The third mode, with 18% of

the variance, focuses most of the energy in an eddy centered over the apex of DeSoto Canyon. The fourth and higher modes are all associated principally with nearshore currents, that are apparently wind and river induced. Examination of amplitudes shows no clear seasonal patterns, as discussed earlier.

Nutrient, dissolved oxygen, and pigment property distributions. The distributions, inventories, and variability were examined for the variables: dissolved oxygen, nutrients, and pigments. Then univariate and multivariate analyses were applied to these variables in relation to conservative variables and forcing functions.

The distributions of dissolved oxygen and nutrients were described and discussed in relation to the circulation for each NEGOM cruise. Further analysis of surface distributions of dissolved oxygen was based on oxygen saturation. Most values fell between 95 and 100% saturation. However, there were numerous cases of extreme supersaturation (>110%) and some values exceeding 150%; there were considerably fewer values between 70 and 95%. The relationship of enhanced oxygen solubility with decreasing temperatures and salinity was clearly demonstrated; the effect of river discharge is clear through salinity. It also was seen that most stations with high chlorophyll *a* were also highly supersaturated in oxygen, illustrating the potential effect of primary production on dissolved oxygen.

Bottom dissolved oxygen concentrations are greatest in fall because of cooler air temperatures that result in higher saturation oxygen values in surface waters and deep mixing by energetic wind events. Values are lowest in summer due to increased vertical stability that inhibits renewal of oxygen in bottom waters and to oxygen utilization during oxidation of organic material. Over the inner shelf there were significant correlations between high hydrostatic stability and low bottom oxygen in summer but not in other seasons. Over the western NEGOM region, where nutrient input and primary production are relatively high, bottom oxygen saturation was positively correlated with high bottom detrital material as represented by nitrate on every NEGOM cruise. No hypoxic conditions, as defined by dissolved oxygen concentrations below 1.4 $mL \cdot L^{-1}$, were observed during NEGOM. However, very low (~2 $mL \cdot L^{-1}$) concentrations were observed on two spring and one summer cruise off Chandeleur Sound and in one summer cruise near the 30-m isobath south of the Florida-Alabama border.

Stations on all nine NEGOM cruises were co-located. Average values and standard deviations for oxygen and nutrients were calculated at each station representative of a series of density (sigma-theta) surfaces corresponding approximately to the salinity maximum of the Subtropical Underwater, the oxygen maximum of the 18°C Sargasso Sea Water, the oxygen minima of the Tropical Atlantic Central Water, and the salinity minimum (and nutrient maxima) of the Antarctic Intermediate Water remnant. Bottom distributions were examined also. Variability in the western study area (Mississippi-Alabama shelf) was greatest on the upper surfaces. Deeper surfaces sometimes evidenced greater variability on the west Florida shelf. No relative dissolved oxygen maximum associated with the 18°C Sargasso Sea Water was found. However, a relative oxygen minimum associated with the Tropical Atlantic Central Water near 425 m and relative nutrient maxima (nitrate, phosphate) associated with the Antarctic Intermediate Water near 750 m were observed.

At each NEGOM station, nutrient concentrations were averaged for summer, fall and spring seasons, for the surface observations, over the upper 5 m, and over the upper 60 m. (Sixty meters being a first approximation to the depth of the photic zone.) Results show elevated concentrations in areas of enhanced river water and of uplift of density surfaces by dynamic processes, bringing high nutrient levels into the photic zone. Such processes can include the

presence of cyclones near the shelf edge, divergence between cyclone-anticyclone pairs, and wind or bottom-induced upwelling.

Temporal and spatial variations in phytoplankton communities are described using analyses of photosynthetic pigment composition and concentrations. Chlorophyll *a* concentrations indicate how much of the particulate matter, and specifically particulate organic carbon, is living. Identification and quantification of the major algal groups is carried out by analyzing the types and amounts of photosynthetic and photoprotective pigments in particulate matter. Many pigments (so-called marker pigments) are restricted principally to one or two taxa and, therefore, can be used as indicators of the presence of specific taxa.

At each station on each NEGOM cruise, chlorophyll and carotenoid pigment concentrations were measured in near-surface (2-3 m) waters, the core of the deep chlorophyll maximum (DCM) as indicated by in situ fluorometry, and just below the highest fluorescence region (close to the base of the euphotic zone). Marker pigments were then used to identify the presence of 10 major phytoplankton groups. Algorithms relating chlorophyll *a* to marker pigments enabled analysis for the percentage of chlorophyll accounted for by each of the 10 phytoplankton groups.

The four major algal groups present in the NEGOM area were prymnesiophytes (haptophytes), prochlorophytes, pelagophytes (chrosophytes), and cyanobacteria (blue-green algae), although locally high abundances of other groups were detected. Prymnesiophytes were the dominant group on each cruise, accounting for between 31% and 46% of the chlorophyll present at the DCM. Prochlorophytes, pelagophytes, and cyanobacteria were the second most abundant groups in the DCM on 4, 3, and 2 cruises, respectively, accounting for 13-23%, 6-18%, and 0-21% of the chlorophyll *a*.

The highest chlorophyll *a* concentrations in near-surface water as well as waters at the DCM were consistently found between lines 1-4 and lines 7-8 during the nine cruises (see Figure 2.2 for location of lines). The high concentrations in these areas resulted from discharges of the Mississippi and Apalachicola rivers. Chlorophyll *a* concentrations in low-salinity, greenish waters from these rivers varied from 0.5 $\mu g \cdot L^{-1}$ to > 5 $\mu g \cdot L^{-1}$. Offshore waters generally had concentrations below 0.4 $\mu g \cdot L^{-1}$.

For the study region as a whole, the average surface and DCM chlorophyll concentrations were lower in fall-winter (November–March) than in spring-summer (April–October). This was a consequence of (1) the fact that most stations were over the shelf rather than offshore, (2) summer transport into the region of low-salinity Mississippi River water with enhanced nutrient levels, and (3) the presence of various offshelf eddies that contributed enhanced nutrient levels to the photic zone during summer by uplift of density surfaces. In contrast, average surface chlorophyll *a* values in waters of depth greater than 400 m were several times higher in fall than in spring. This is because the spring phytoplankton bloom depletes available nutrients leading to low chlorophyll concentrations in summer, whereas wind mixing and reduced stability in fall leads to an increase in nutrients in the euphotic zone and a secondary (fall) plankton bloom with increased chlorophyll concentrations.

Spatial distributions of chlorophyll *a* were similar for cruises in the same seasons. Likewise, seasonal variations among relative abundance of the major phytoplankton groups generally were similar in each year. The average abundances of prochlorophytes and pelagophytes in near-surface waters were higher in November and August than in May; at DCM depths, there was little seasonal difference for prochlorophytes while pelagophytes were more abundant in November than in May and August. In both near-surface and DCM waters, cyanobacteria

were in greatest abundance during May and least in November. Prymnesiophytes showed little seasonal variation in abundance.

General patterns within the integrated water column chemistry were examined using both univariate and multivariate analyses. Factors considered included discharge rates of three drainage basins (Mississippi, Mobile (including both Alabama and Tombigbee rivers), and Apalachicola), water column nutrients, chlorophyll *a*, fluorescence, salinity, particulate organic carbon and nitrogen, suspended particulate matter, and percent light transmission. Univariate analyses between these factors showed the expected relationships, such as: negative correlation between percent transmission and particulate matter, indicating particulates decrease light transmission; chlorophyll *a* correlates positively with dissolved oxygen signifying that oxygen is a product of photosynthesis; or nutrients correlate among themselves demonstrating that they are removed from the water column in a relatively constant ratio as they are fixed into biomass.

For multivariate analyses the factors first were subjected to Principal Component Analyses (PCA) to detect the principal components of structure between the factors (data) considered and to reduce the number of factors important within each structure component. Sixty-five percent of the variability in water column properties can be explained by the first three principal components. Component one indicates that 41% of the variability is related to particle dynamics and river water inputs as indicated by relationships between chlorophyll *a*, fluorescence, particulate matter, particulate organic carbon, and salinity. It also indicates that phytoplankton biomass is a major source of variability, suggesting that phytoplankton dynamics exert strong control on water column properties in the NEGOM area. The second component accounts for almost 14% of water column property variability and indicates nutrient variability is closely coupled to variability in particulate matter properties because nutrients are consumed during photosynthetic production of biomass. Finally, river discharge accounts for almost 17% of the variability (10% in the third principal component; 7% in the fourth) in water column properties reflecting the regional influence of river discharges on a range of water column properties both directly and indirectly.

Finer multivariate analyses were performed by dividing the NEGOM region into four sub-areas (east-west and offshore-onshore) and considering factors from three distinct seasons (summer, spring, and fall).

Light transmission and particulate matter Particulate matter distributions in the study area were described in terms of concentrations of particulate matter (PM), particulate organic carbon (POC), particulate organic nitrogen (PON), and light transmission. Vertically continuous profiles of transmissometry were used to calculate particle beam attenuation coefficients (PBAC) as functions of depth for each station. PBAC values then were calibrated using discrete PM samples from near surface, near bottom, and a clear, mid-water depth at each station. Correlations between PM and PBAC were obtained for upper and lower portions of the water column. Excellent correlations were obtained for each cruise. The resulting relationships were used to calculate vertical profiles of PM at each station.

For each cruise, distributions of PM were considered using three types of contoured fields: PM concentration, total PM mass per unit surface area, and percent of total PM mass in the bottom nepheloid layer (BNL). The study area was limited to the continental shelf (water depth < 200 m) where potential influences of sediments carried in river plumes or re-suspended by currents and waves can be more clearly identified.

The average water column PM mass within the eastern shelf, defined as east of 87°W, versus the western shelf was calculated for each cruise. Over the eastern shelf, the averages varied only between 14 and 19 $g \cdot m^{-2}$, but over the western shelf cruise averages were much larger and more variable, ranging from 27 to 50 $g \cdot m^{-2}$. Similarly, the cruise average PM per unit surface area contained in BNLs over the shelf was much lower and less variable over the eastern than the western shelf. This is evidence for the effects of the Mississippi and other rivers on PM and light transmission, as well as suggestive of more re-suspension, on the western shelf.

Comparing PM observations from near-surface and near-bottom samples showed lower mean near-surface concentrations in fall and most variability in spring. Near-bottom means were similar for the three seasons, though the smallest variability was observed in summer.

Both POC and PON were measured near surface and at one sub-surface depth (near-bottom or the chlorophyll maximum) on all stations. The highest POC levels in all seasons generally were associated with high PM plumes near river mouths. As expected, near-surface POC concentrations are greater and evidence more variability than sub-surface concentrations. The larger variability in near-surface concentrations was seen in spring and summer associated with distributions of river discharge; sub-surface POC concentrations showed no clear seasonal variability. Ratios of POC to PON are near 6 with high correlation, evidence that the behavior of PON generally mirrors that of POC. On average POC in near-surface waters accounted for 28% of the PM, but only 12% in near-bottom waters. Indicative of phytoplankton productivity in the photic zone, and remineralization of organic carbon in the water column, the quantity of POC accounting for PM was more variable near surface than within the water column. Near-bottom particulates also may have a contribution from re-suspended sediments relatively poor in organic carbon.

2 INTRODUCTION

2.1 NEGOM Program Objectives and Description

The Northeastern Gulf of Mexico Physical Oceanography Program (NEGOM) was supported by the Minerals Management Service (MMS) of the U.S. Department of the Interior. NEGOM was divided into six observational components of which one is the NEGOM Chemical Oceanography and Hydrography study (NEGOM-COH). Other NEGOM components were the inner shelf study, DeSoto Canyon eddy intrusion study, operational remote sensing study, NEGOM remote sensing study, and meteorology study. Additionally, there was a modeling study component. This report summarizes the findings of the NEGOM-COH component, which was conducted by scientists at Texas A&M University.

The study area, shown in Figure 2.1-1, encompassed the region of the northeastern Gulf shelves and upper slope from the Mississippi River delta to Tampa Bay in water depths of 10 to 1000 m. Data collection in NEGOM-COH consisted of nine cruises conducted over three field years and assembly of historical and collateral data. This was followed by data analysis and synthesis. Continuous profiles were made of temperature, salinity, dissolved oxygen, light transmission, fluorescence, downwelling irradiance, and optical backscatterance. Discrete water samples were drawn for analyses of nutrients, pigments, particulate matter, and particulate organic carbon. Acoustic Doppler current profiler (ADCP) observations and underway flow-through measurements of near-surface temperature, salinity, fluorescence, and calculated chlorophyll were made continuously along track. Ancillary data sets, such as river discharge, sea surface height fields from satellite altimeter, and meteorological measurements, were assembled to support the data analysis and interpretation. In this report, the observations are synthesized, interpreted, and reported to provide a better understanding of the circulation and property distributions over the shelf and upper slope, their spatial and temporal variability, and causal factors.

The motivation for the NEGOM program comes from the responsibilities of MMS in management of the nation's Outer Continental Shelf Leasing Program, including oil and gas leases in federal waters of the northeast Gulf shelves and upper slope. MMS seeks to understand the physical processes and circulation of the shelf and upper slope waters that influence the stability of structures, the transport of pollutants, and the evolution of the ecosystems of regions that may be affected by oil and gas operations. Additionally, knowledge of the circulation supports MMS oil spill risk analysis models. It was to further the base of knowledge in these areas that MMS sponsored NEGOM.

The three objectives for the NEGOM-COH study were:

(1) Develop an oceanographic experimental design of research cruises covering the NEGOM study area with sufficient frequency to resolve seasonal variations of chemical oceanography and hydrographic parameters.

(2) Collect the ancillary data needed to complement and analyze the measurements collected in objective 1.

(3) Analyze the data collected in objectives 1 and 2 to describe spatial fields and distributions in the vertical and horizontal planes, temporal variations, and processes (physical, biological, or chemical) which contribute to the production of the observed fields and distributions.

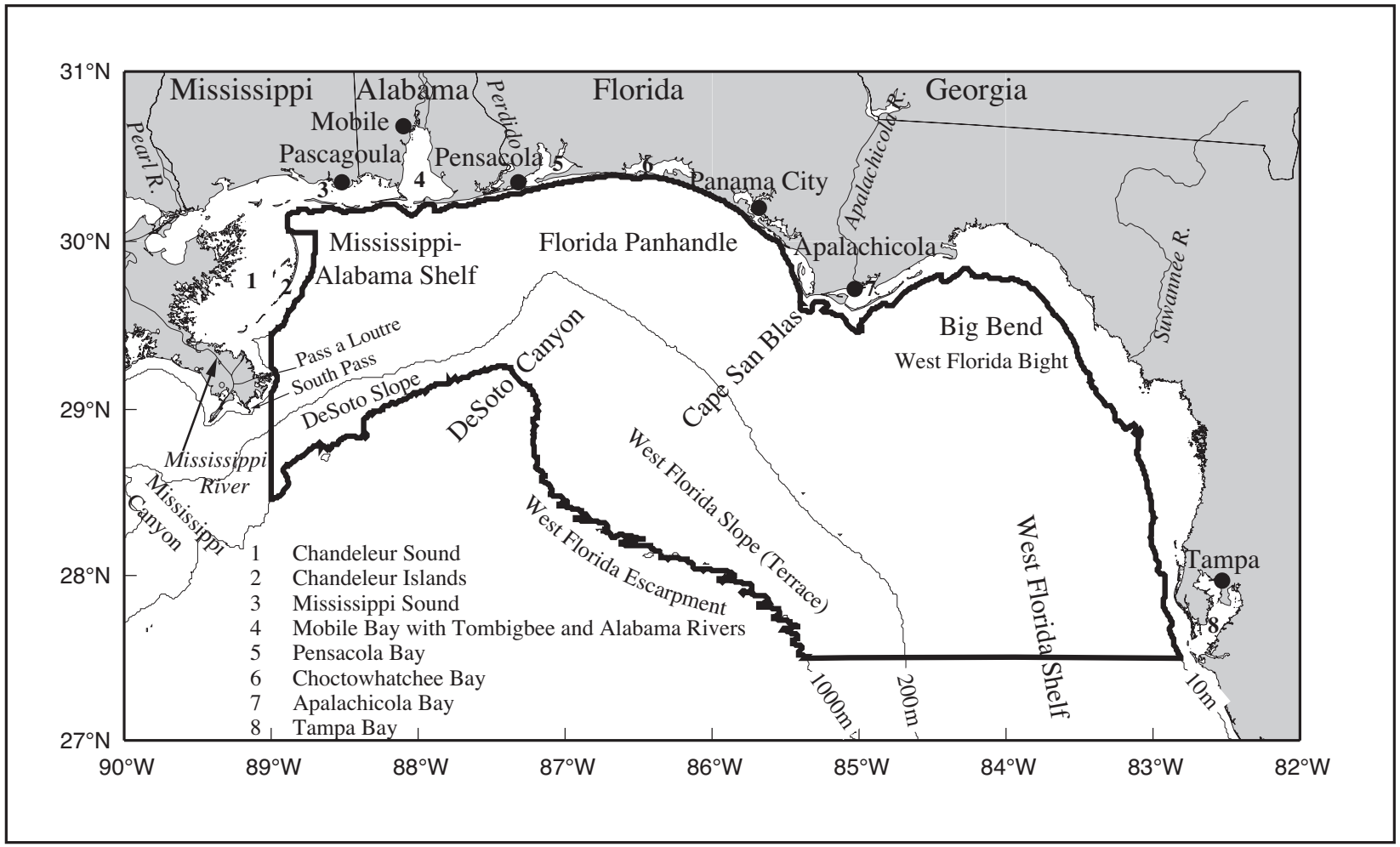

Figure 2.1-1. Study area and bathymetry of the northeastern Gulf of Mexico. Hydrography stations were located over the shelf and upper slope region within the area encompassed by the bold line. Geographical names are provided.

Objectives 1 and 2 were met through the completion of the three-year field program of observations over the northeastern Gulf of Mexico continental shelf and upper slope. This is discussed further in Section 2.2. Objective 3 is met in this synthesis report.

The NEGOM-COH study area encompassed the Mississippi-Alabama-West Florida shelves and northeastern Gulf upper slope from the 10-m isobath out to the 1000-m isobath. The study had four tasks: a field task, a data processing task, a data synthesis task, and program management. The tasks, Principal Investigators, and brief task descriptions are given in Table 2.1-1. All Principal Investigators are affiliated with Texas A&M University (TAMU). Each of the tasks is fully described in Jochens and Nowlin (1998).

Table 2.1-1. NEGOM-COH program tasks.

Task	Task Name	Description	Principal Investigators
	Program Management	Management of all aspects of the program, including scientific, operational, and fiscal	W. D. Nowlin, Jr., Program Manager A. E. Jochens, Deputy Program Manager
1	Field Work and Data Collection	Cruise logistics and completion of data collection in the field	D. C. Biggs, co-PI N. L. Guinasso, Jr. , co-PI M. C. Kennicutt II, co-PI
2	Data Reduction/Analysis and Synthesis	Data quality control and management; assembly of ancillary data sets	A. E. Jochens, PI M. K. Howard, co-PI
3	Information/Data Synthesis and Technical Reports	Report preparation	W. D. Nowlin, Jr., PI R. O. Reid, co-PI M. C. Kennicutt II, co-PI

2.2 Data Collected

The NEGOM-COH field program was undertaken from November 1997 through August 2000. Nine cruises were conducted; three each in spring, summer, and fall. All were aboard the *R/V Gyre*, operated by the TAMU Department of Oceanography. A listing of these cruises, their various identifiers, and their start and end dates is given in Table 2.2-1. The NEGOM ID is the shorthand identifier used in this report. The cruise ID number is the standard cruise identifier in wide use in the oceanographic community. The first two characters give the year of the cruise, the third character gives the ship identifier, G for *Gyre*, and the last two characters give the number of that ship's cruise for that year.

The cruises were designed to characterize the spatial and temporal distribution and variation of patterns of circulation and water properties and the processes that contribute to them. Cruise N1 covered the region between the 20- and 1000-m isobaths. The other eight cruises covered the region between the 10- and 1000-m isobaths to better observe the extent and possible sources of relatively low salinity water over the inner shelf. Conductivity-Temperature-Depth (CTD) stations, with rosette water bottle sampling, were occupied on each cruise at nearly identical station locations. Expendable bathythermograph (XBT) probes

Table 2.2-1. Cruise identifiers and dates.

Survey No.	Start Date	End Date	NEGOM ID	Cruise ID
1	16 November 1997	26 November 1997	N1	97G14
2	5 May 1998	16 May 1998	N2	98G05
3	25 July 1998	6 August 1998	N3	98G10
4	13 November 1998	24 November 1998	N4	98G15
5	15 May 1999	28 May 1999	N5	99G07
6	15 August 1999	28 August 1999	N6	99G08
7	13 November 1999	25 November 1999	N7	99G12
8	15 April 2000	26 April 2000	N8	00G04
9	28 July 2000	8 August 2000	N9	00G08

were launched between CTD stations. A 150 kHz ADCP, a thermosalinograph, and a flow-through fluorometer were operated continuously along the cruise track. Navigation data and station locations were determined using differential Global Positioning System (GPS).

Each survey covered 11 cross-shelf lines. Approximately 95-100 CTD stations were occupied on each cruise, with stations typically at the 10-, 20-, 100-, 200-, 500-, 1000-m and selected other isobaths. To enhance the resolution of temperature observations to ~10 km, approximately 70-80 XBT drops were made between the CTD stations. Figure 2.2-1 shows a typical station location pattern for the NEGOM cruises.

The surveys consisted of continuous vertical profiling using a Sea-Bird 911+ CTD system and discrete water sampling using a General Oceanics 12-place rosette with 10-liter Niskin bottles. Continuous vertical profiles were taken of seawater conductivity/salinity, temperature, pressure/depth, fluorescence, light transmission, optical backscatterance, downwelling irradiance, and dissolved oxygen. Discrete water samples were taken for analysis of dissolved oxygen and nutrients (phosphate, silicate, nitrate, nitrite, ammonium, and urea) at every station, and phytoplankton pigments, particulate matter, particulate organic carbon, and salinity at selected stations. ADCP data were collected continuously along the cruise track using either a narrow-band 150 kHz ADCP (N1, N4, N9) or a broad-band 150 kHz ADCP (N2, N3, N5-N8). Additionally, a 38 kHz ADCP was operated on N7-N9. The thermosalinograph and flow-through fluorometer provided near-surface (~3-m depth) measurements of temperature, salinity, and fluorescence at approximately 2-minute intervals along the cruise track. The fluorescence data were calibrated with approximately 100 filters analyzed for chlorophyll concentrations to produce a 2-minute, near-surface chlorophyll data set. Table 2.2-2 summarizes the data collection by cruise. Numbers represent the total number of data points remaining after quality assurance/quality control (QA/QC) procedures were applied. Specifics of cruise tracks and station locations, instrumentation and methods, data processing, and additional cruise information are provided in the three NEGOM annual reports by Jochens and Nowlin (1998, 1999, 2000).

QA/QC procedures were applied to all data collected. This consisted mainly of wild point editing of continuous profiles and discrete measurements. Additional information is in the

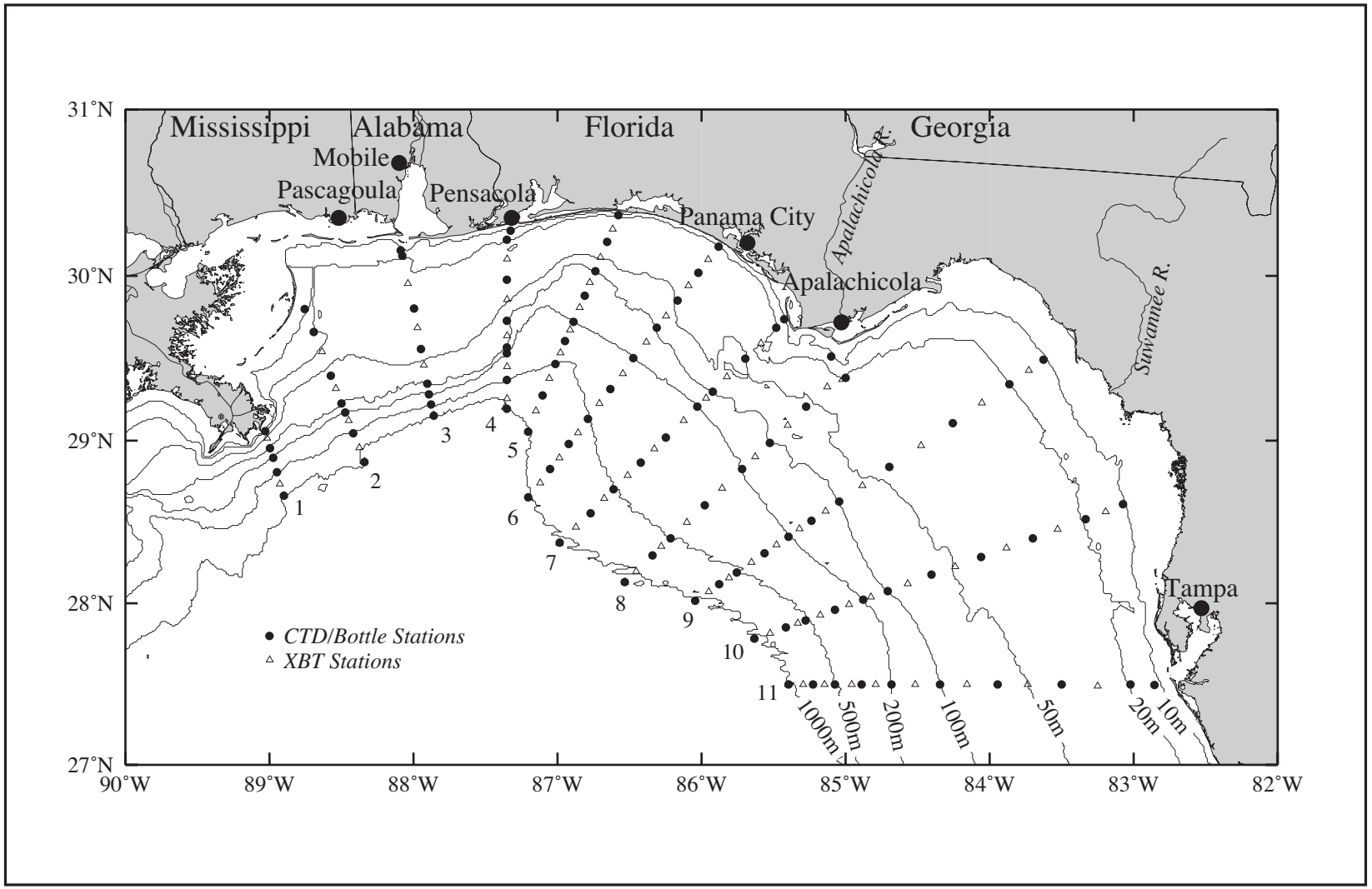

Figure 2.2-1. Typical locations for hydrographic stations on NEGOM-COH cruises, November 1997 through August 2000. The line number is given at the seaward end of each cross-shelf transect.

Table 2.2-2. Summary of data collection and scientific participation on NEGOM-COH cruises.

Description	N1 Nov. 1997	N2 May 1998	N3 Aug. 1998	N4 Nov. 1998	N5 May 1999	N6 Aug. 1999	N7 Nov. 1999	N8 Apr. 2000	N9 Aug. 2000
Cruise Duration (days)	11	11	13	12	14	13	13	12	11
Cruise Track* (km)	3283	3380	3817	3815	4497	3743	3659	2825	3195
Total Hydrographic Stations	94	98	98	98	102	98	98	101	98
CTD Stations	94	98	98	98	100	98	98	101	98
Nutrient Stations	95[a]	98	98	98	100	98	98	101[a]	98
Oxygen Stations	94	98	98	98	100	98	98	101	98
Salinity Stations	94	22	22	22	48	23	22	27	24
Pigment Stations	51	61	58	59	61	60	59	60	60
Particulate Matter Stations	60	60	60	60	61	60	52	59	60
Particulate Organic Carbon Stations	60	60	60	60	61	61	52	60	60
Successful XBT Drops	80	97	101	112	96	89	84	78	75
Nutrient Samples	794	850	883	901	925	913	899	959	912
Oxygen Samples	782	854	883	900	925	913	901	936	912
Salinity Samples	782	179	180	167	357	175	176	195	188
Pigment Samples	183	191	169	163	182	175	170	163	158
Particulate Matter Samples	180	188	181	178	174	180	156	174	178
Particulate Organic Carbon Samples	118	120	118	120	115	126	100	118	104
Surface Bucket Salinity Samples	0	0	0	0	33	57	81	68	95
Surface Chlorophyll Samples	181	71	101	108	102	101	99	99	101
150kHz narrow-band ADCP Measurements	√			√			√		√
150kHz broad-band ADCP Measurements		√	√		√	√	√	√	
38 kHz ADCP Measurements							√	√	√
Thermosalinograph 2-min Logging	√	√	√	√	√	√	√	√	√
Flow-through Fluorescence 2-min Logging	√	√	√	√	√	√	√	√	√
Total Scientific Party	23	24	23	22	23	23	18	24	23
NEGOM-COH Scientists	15	15	13	15	15	13	14	13	15
Guest Investigators	4	7	10	6	8	6	3	7	5
Students (Graduate and Undergraduate)	10	10	12	9	10	10	7	12	11
Complementary Studies	4	6	7	5	4	7	5	10	4

* N1, N2: Pascagoula, MS, to Pascagoula, MS
N3, N4: Gulfport, MS, to Galveston, TX
N5: Galveston, TX, to Galveston, TX
N6: Galveston, TX, to Panama City, FL
N7: Gulfport, MS, to ST. Petersburg, FL; excludes 1000-m isobath ADCP run
N8: St. Petersburg, FL, to Pascagoula, MS
N9: Pascagoula, MS, to Panama City, FL

[a] N1: nutrients were frozen at 12 stations, for 110 frozen samples
N8: duplicate nutrient samples from 2 stations were frozen, for 24 frozen samples

annual reports (Jochens and Nowlin 1998, 1999, 2000). All times are reported in Universal Coordinated Time (UTC) unless stated otherwise.

Major sets of ancillary data assembled to aid in interpretations are briefly summarized here.

Those associated with forcing functions are described in Section 3; others are included in the synthesis as applicable. Concurrent meteorological measurements were obtained from coastal airports, weather stations, and the offshore buoys of the National Data Buoy Center. Historical meteorological information and mean fields were obtained from a number of sources including the historical review of meteorology by Florida A&M University (1988) and the mean fields of the Comprehensive Ocean-Atmosphere Data Set (COADS). Record-length river discharge rates were assembled from the U.S. Geological Survey and the U.S. Army Corps of Engineers for selected rivers in eastern Louisiana, Mississippi, Alabama, and west Florida that discharge into the NEGOM region. Sea surface height fields, produced from a blend of TOPEX/Poseidon and ERS-2 satellite altimeter data, were obtained from the Colorado Center for Astrodynamics Research, University of Colorado. Satellite Advanced Very High Resolution Radiometer (AVHRR) images of sea surface temperature were obtained from various sources including the NEGOM operational remote sensing study with the U.S. Geological Survey, the NOAA COASTWATCH program, and the Ocean Remote Sensing Group of The Johns Hopkins University Applied Research Lab. Composite ocean color images derived from the satellite Sea-viewing Wide Field-of-view Sensor (SeaWiFS) for the periods of cruises N1 through N9 were provided through the NEGOM remote sensing study by the Remote Sensing Laboratory at the University of South Florida. Hydrographic data and current measurements, collected from March 1997 through April 1999 under the NEGOM DeSoto Canyon Eddy Intrusion Study (EIS), were provided to NEGOM-COH by Science Applications International Corporation. Drifting buoy data, which were from drifters deployed on NEGOM-COH cruises N1, N2, N3, N4, and N7 as part of the internal MMS program on Collection of Environmental Data for Oil Spill Risk Analysis Model Verification, were obtained from MMS.

2.3 Report Organization

This report synthesizes the data collected during the NEGOM field program and provides a scientific presentation of the results. Section 1 is the executive summary. Section 3 describes the forcing fields present during the field program. Section 4 describes the circulation and its variability as observed during NEGOM. Section 5 presents a seasonal synthesis of the physical properties. Sections 6 through 9 describe particulates (6), dissolved oxygen and hypoxia (7), nutrients (8), and pigments (9). An integrated synthesis of the water column chemistry is provided in Section 10. Recommendations for consideration of future studies and a summary of the main results of this report are given in Section 11. References are provided in Section 12. Appendices A through I summarize the forcing functions, evidence of circulation, and water properties during the N1 through N9 NEGOM cruises.

3 FORCING FUNCTIONS

3.1 Long-term Averages

3.1.1 Meteorological Conditions

The northeastern Gulf of Mexico (north of 26°N and east of 89°W) experiences two distinct weather patterns, winter (December-March) and summer (May-October), with quite brief transitions between. Most of the year the region is dominated by moist, warm maritime tropical air masses. In winter, however, cold, dry continental polar air masses intrude into the region. This is one mechanism that can result in formation of extratropical cyclones. In summer, the region is influenced by the northeast trade winds, with the northward migration of the North Atlantic ("Bermuda") subtropical high and the polar jet stream. This leads to fewer frontal passages in summer than winter, but also results in the northeastern Gulf experiencing tropical storm systems. An in-depth review of the meteorological data base and climatology of the Gulf of Mexico is given by Florida A&M University (1988). A recent review of meteorological conditions over the northeastern Gulf is given by Hamilton et al. (1997).

Frequent frontal passages and the occurrence of extratropical cyclones characterize winter conditions over the northeastern Gulf of Mexico. Cold air outbreaks and frontal passages occur at 3- to 10-day intervals between October and March (Fernandez-Partegas and Mooers 1975). Based on observations, DiMego et al. (1976) calculated that some 8-9 frontal passages per month occurred over the region during winter. While extreme cold air outbreaks can lead to freezing conditions over the coastal region (occurring approximately every five years according to Mortimer et al., 1988), significant effects of such events normally are limited to the region north of Tampa (28°N). The frequency of extratropical cyclone development in the northeastern Gulf is estimated (Hayden 1981) as 2 to 3 per winter season (December-March). This represents only about 20% of the number of such cyclones developed in the Gulf (Johnson et al. 1986), the preponderance (order of 10 per year) occur over the Texas-Louisiana shelf (Hsu 1988; Nowlin et al. 1998b).

By contrast with winter, summer is characterized by light and variable wind conditions. However, those conditions are punctuated with tropical cyclone activity. The nominal hurricane season is from June 1 through November 30. Hamilton et al. (1997) summarized tropical cyclone occurrence over the northeastern Gulf for the past 100 years by decade. They found an average of 10-12 cyclones per decade with a decreasing trend from 14 to order 10 per decade. Moreover, they also noted a tendency for the frequency of occurrence west of Cape San Blas to be out of phase (and different by as much as 7 storms per decade) with that for the shelf region between Cape San Blas and Tampa.

To determine the frequency of cold front passage during the period of the NEGOM study, the *Daily Weather Maps* of the Climate Analysis Center of NOAA were examined for the passage of cold fronts over the NEGOM study area. The maps for 1 November 1997 through 31 August 2000 were examined. The appearance of cold front symbols over all or part of the NEGOM study area were counted as frontal passages. Table 3.1.1-1 shows the number of frontal passages by month and includes the average number for periods in the 1960s and 1970s as given by DiMego et al. (1976) for the NEGOM study area and Henry (1979) for the whole Gulf.

The average number of passages was used to determine the typical number of days between fronts. These are given in Table 3.1.1-2. During fall cruises, fronts passed over the NEGOM

Table 3.1.1-1. Number of frontal passages over the NEGOM study area during each field year and resulting averages of cold front passages. "—" means not a NEGOM field period.

Month	1997	1998	1999	2000	Total	Average	DiMego[1]	Henry[2]
Jan	—	7	6	6	19	6.3	8.5	5.5
Feb	—	6	5	5	16	5.3	9.0	5.7
Mar	—	2	6	7	15	5.0	8.0	6.2
Apr	—	5	5	7	17	5.7	6.5	4.5
May	—	4	4	2	10	3.3	4.5	3.0
Jun	—	1	1	2	4	1.3	2.5	2.0
Jul	—	0	1	1	2	0.7	2.0	0.8
Aug	—	2	2	0	4	1.3	3.0	0.9
Sep	—	2	4	—	6	3.0	3.0	2.4
Oct	—	2	5	—	7	3.5	5.5	3.7
Nov	7	5	4	—	16	5.3	6.5	5.2
Dec	5	7	7	—	19	6.3	7.5	6.6

[1] DiMego et al. (1976) considered the years 1965-1972; values interpreted for the NEGOM study area from their Figure 1.
[2] Henry (1979) considered the years 1967-1977; values given are from his Table 1 for the whole Gulf.

Table 3.1.1-2. Average interval between fronts (days), where "n" means no meaningful interval.

Month	NEGOM	DiMego	Henry
Jan	4.9	3.6	5.6
Feb	5.3	3.1	4.9
Mar	6.2	3.9	5.0
Apr	5.3	4.6	6.7
May	9.3	6.9	10.3
Jun	22.5	12.0	15.0
Jul	n	15.5	n
Aug	23.3	10.3	n
Sep	15.0	10.0	12.5
Oct	13.3	5.6	8.4
Nov	5.6	4.6	5.8
Dec	4.9	4.1	4.7

study area at intervals of 5-6 d on average. During the spring cruises, the average period between frontal passages increased from 5 d in April to 9 d in May. During the summer cruises, fronts rarely passed over the NEGOM study area.

For mean background wind fields, we used the COADSPACS Enhanced 1960-1997 data. The Comprehensive Ocean-Atmosphere Data Set (COADS) is the most extensive collection of surface marine data available for the world ocean. Monthly summaries on a 1-degree latitude by 1-degree longitude grid were completed in support of the Pan-American Climate Studies (PACS) Program, based on COADS Release 1b and 1a data for 1960-1997. The Enhanced data set is based on data from ships plus other in situ platforms and employs wide sigma limits

(4.5) to accommodate more extreme climate events. COADSPACS Enhanced data are provided by the NOAA-CIRES Climate Diagnostics Center, Boulder, Colorado, from their Web site at http://www.cdc.noaa.gov. For more information refer to Woodruff et al. (1987).

In determining the monthly mean wind climatology for the Gulf of Mexico, the average mean wind velocity components were computed for each month based on the total values available at each grid location. The mean vector was then assembled from the mean u and v components. In Figures 3.1.1-1 through 3.1.1-12 are shown long-term mean monthly COADS wind fields. Winds at grid locations having less than 6 years of data are not shown. Also shown are ellipses of the principal axes of variance of monthly means for that month. For each of the 167 grid points in the Gulf of Mexico we examined the number of individual monthly means available to produce our long-term mean winds for all months. The percent of long term monthly means versus number of years of individual monthly mean values on which they were based is given in Table 3.1.1-3. As an example, data were available for 36 years for 44% of the calculated long-term monthly means.

Over the Gulf of Mexico, mean winds are generally toward the southwest from October through February; toward the northwest from April through August; and westward in March and September. Mean winds over the northeast Gulf of Mexico have a westward component in every month. Beginning in October and continuing through February, there are southward components to the monthly mean winds. This is especially true over the inner shelf near Florida, where mean southward components are seen also in March at some locations. The mean winds are stronger during mid-winter. Winds with southward components along the west coast of Florida (October-March) are favorable for coastal upwelling.

From April through August mean monthly winds at most northeast Gulf locations have a component toward the north. This is also true for March and September with some exceptions, such as near Tampa for March. During June and July the winds along the northern Gulf shelf from the Mississippi River to Florida are onshore with some eastward alongshore components; such winds should be favorable for producing coastal upwelling in that area. Winds over the northeastern Gulf are generally weaker than over the northwestern region except during September through December.

In a study of the heat and freshwater budgets of the Gulf of Mexico, Etter (1983) estimated the rate of ocean heat storage in the upper 200 m of the water column. Using MBT and XBT data from 1941-1980, he estimated the mean monthly heat storage for 23 gridded areas. The three areas representing the NEGOM region are: 1° latitude x 2° longitude centered on 29.5°N, 86°W and 29.5°N, 88°W; 2° latitude x 2° longitude centered on 28°N, 84°W. We have averaged the monthly rates of heat storage for these three areas to obtain the rates shown in Table 3.1.1-4.

The majority of heat loss occurs in the months October through February with a clear maximum in November. Oceanic heat gain occurs from April through September with a clear maximum in May and relatively smaller values in August and September.

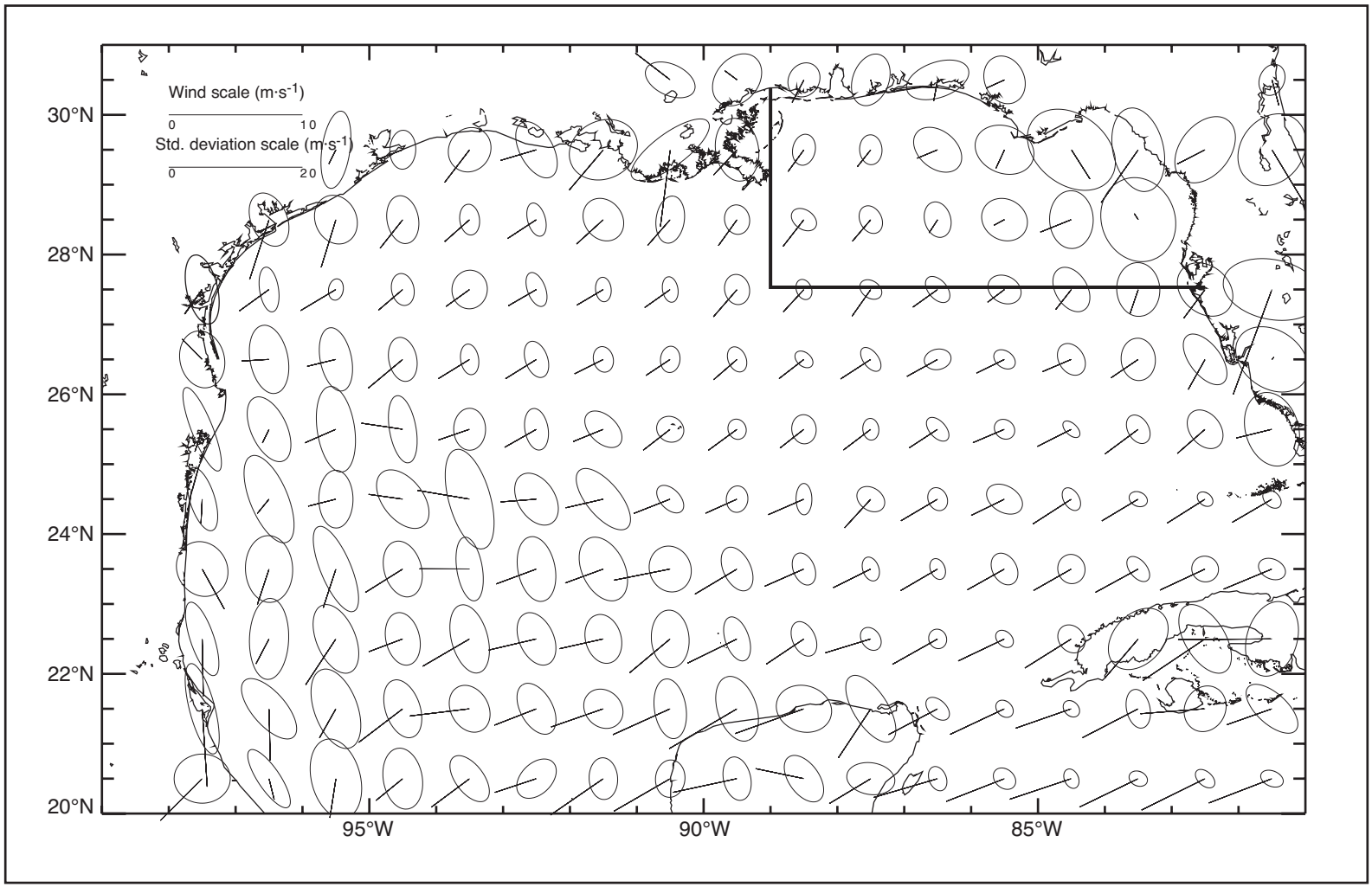

Figure 3.1.1-1. COADS enhanced mean wind field and principal component ellipses for January. Data averaged over the period 1960-1997. NEGOM study area is indicated.

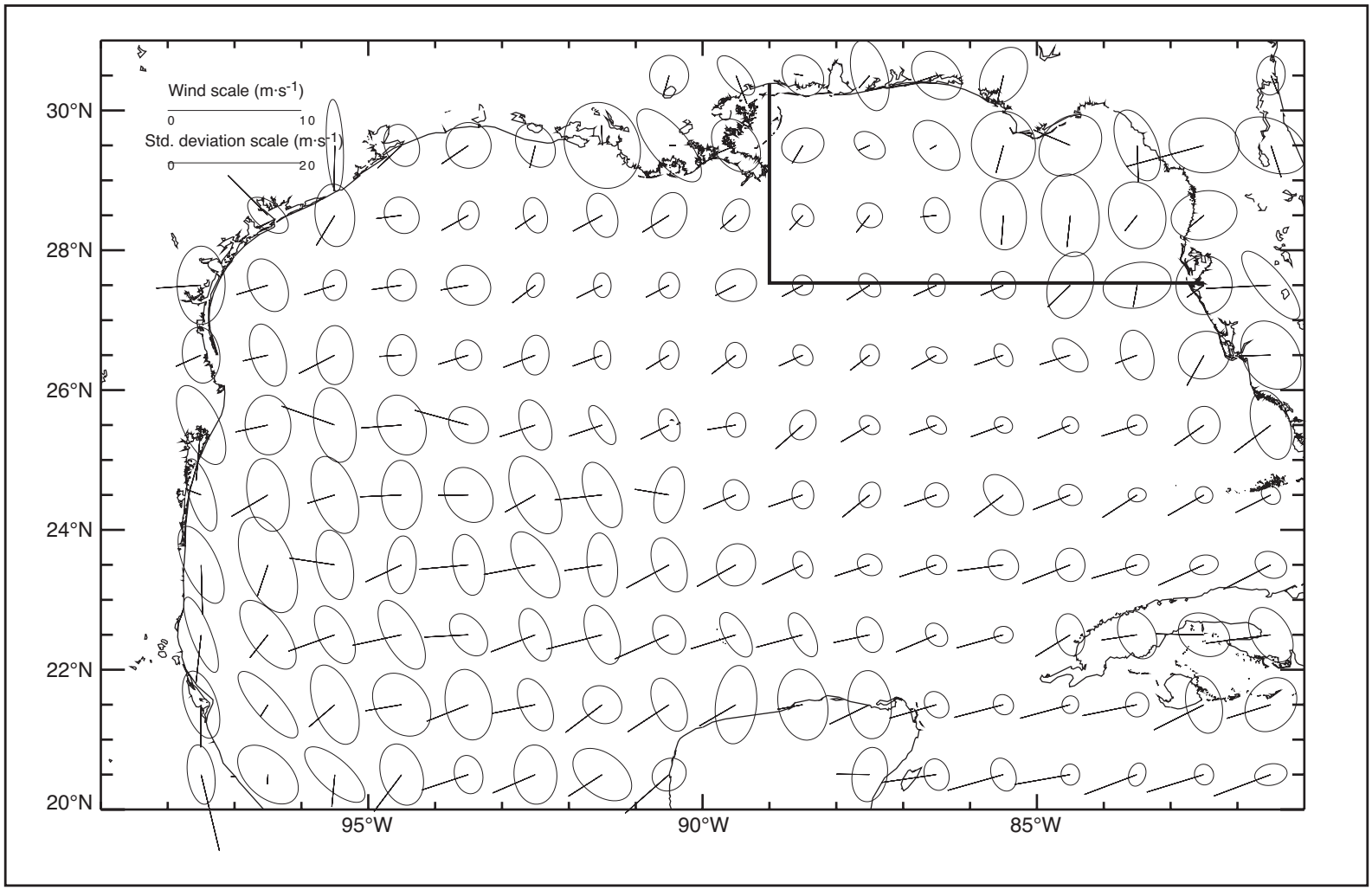

Figure 3.1.1-2. COADS enhanced mean wind field and principal component ellipses for February. Data averaged over the period 1960-1997. NEGOM study area is indicated.

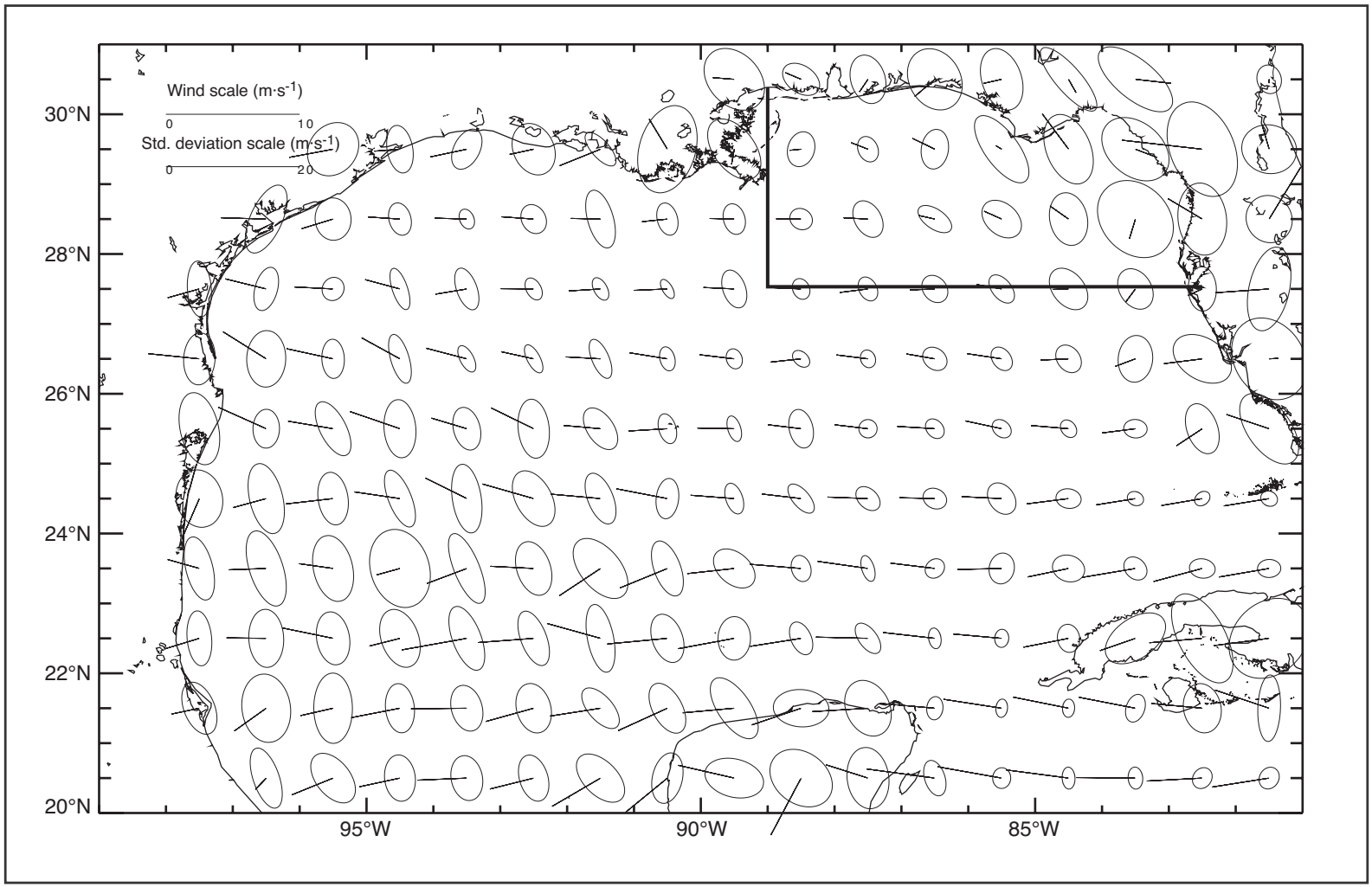

Figure 3.1.1-3. COADS enhanced mean wind field and principal component ellipses for March. Data averaged over the period 1960-1997. NEGOM study area is indicated.

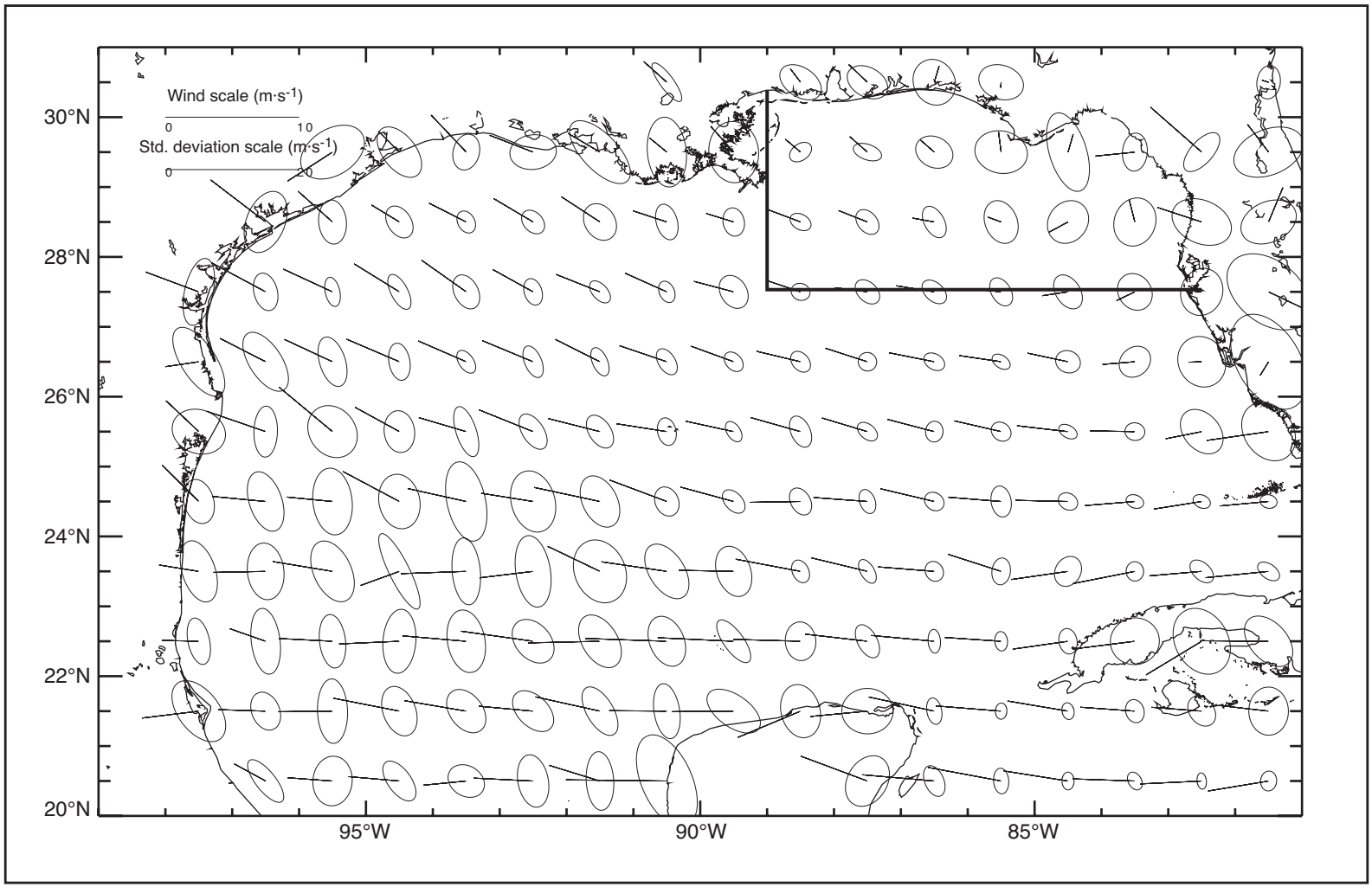

Figure 3.1.1-4. COADS enhanced mean wind field and principal component ellipses for April. Data averaged over the period 1960-1997. NEGOM study area is indicated.

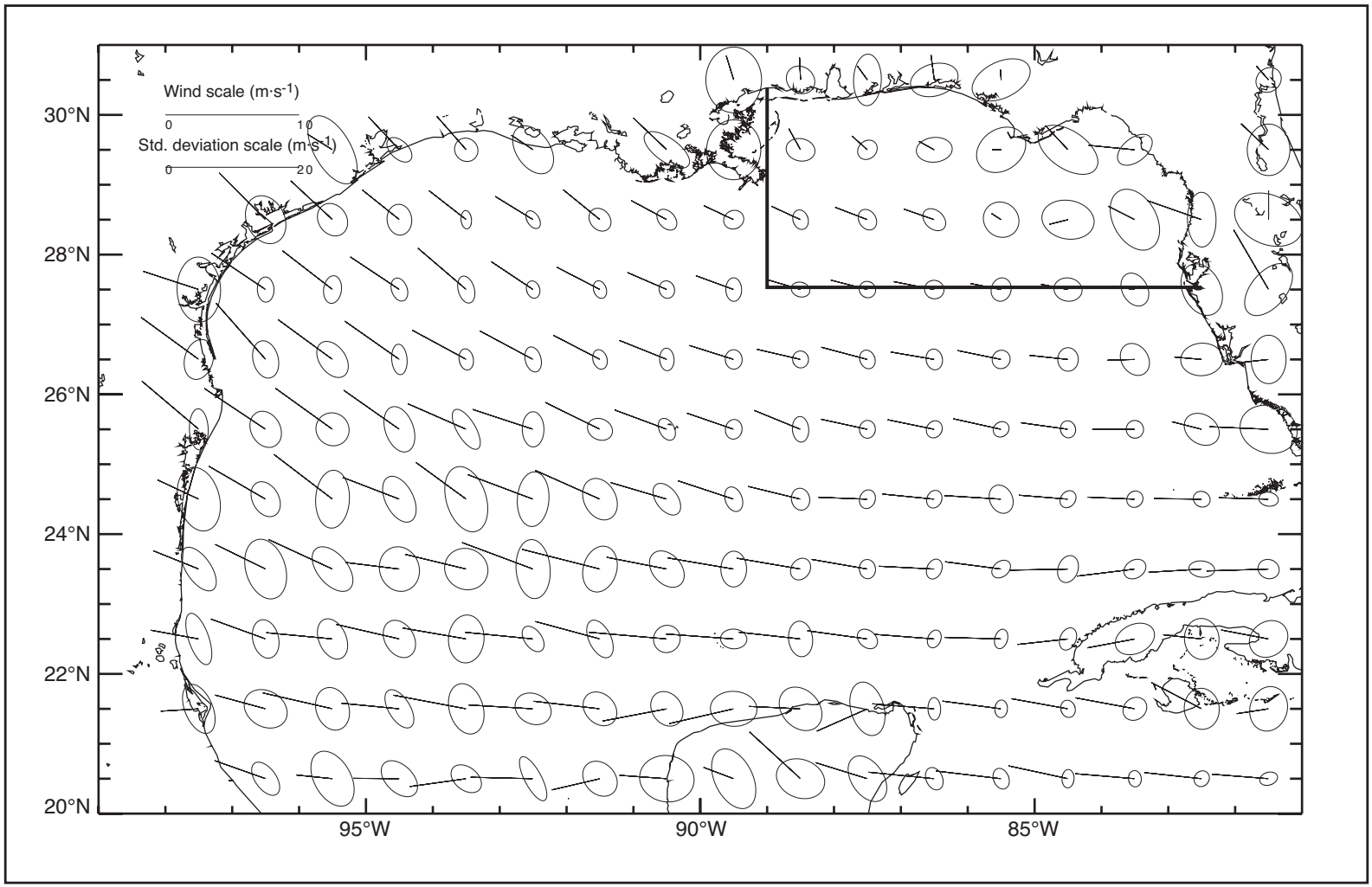

Figure 3.1.1-5. COADS enhanced mean wind field and principal component ellipses for May. Data averaged over the period 1960-1997. NEGOM study area is indicated.

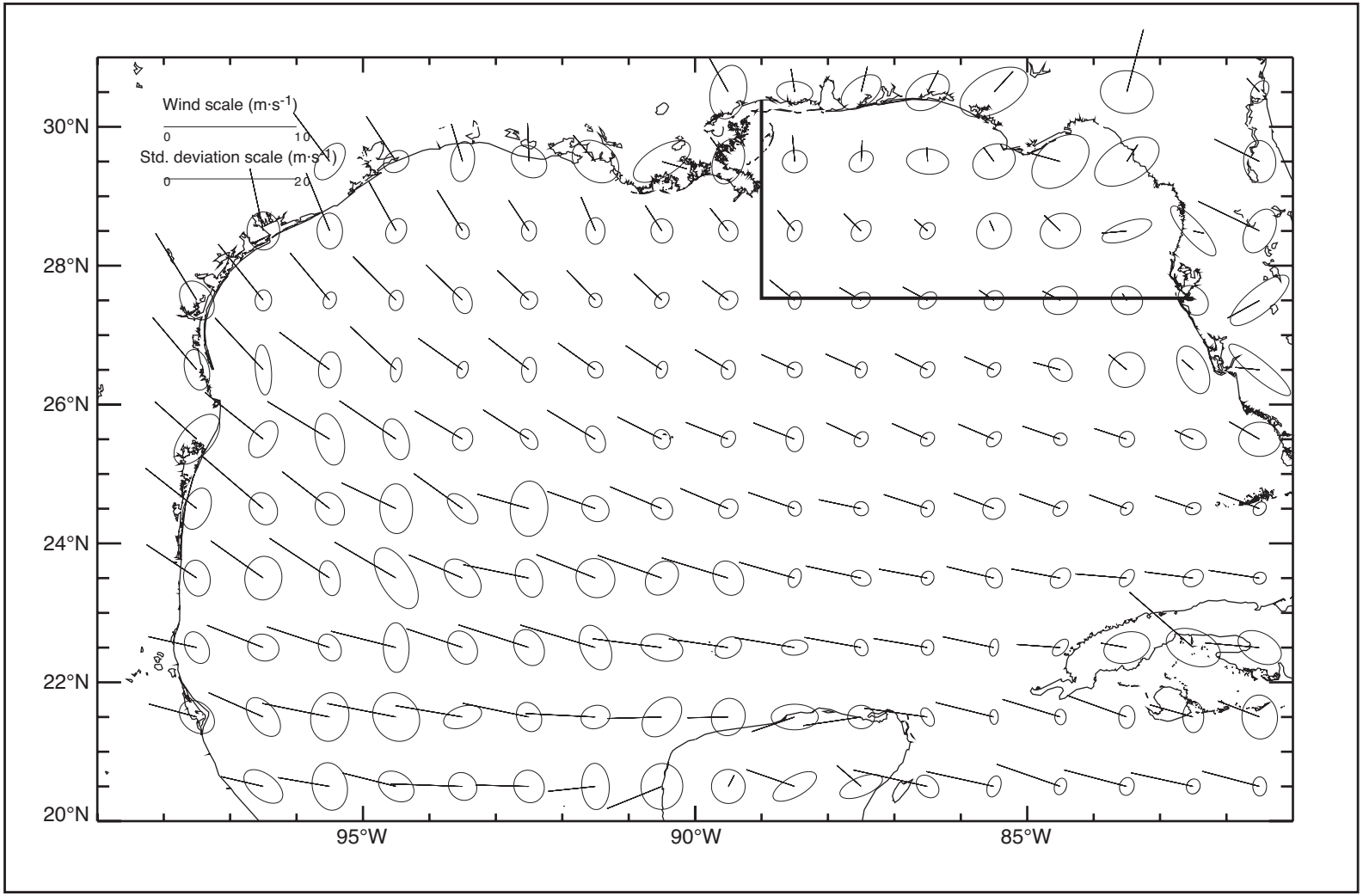

Figure 3.1.1-6. COADS enhanced mean wind field and principal component ellipses for June. Data averaged over the period 1960-1997. NEGOM study area is indicated.

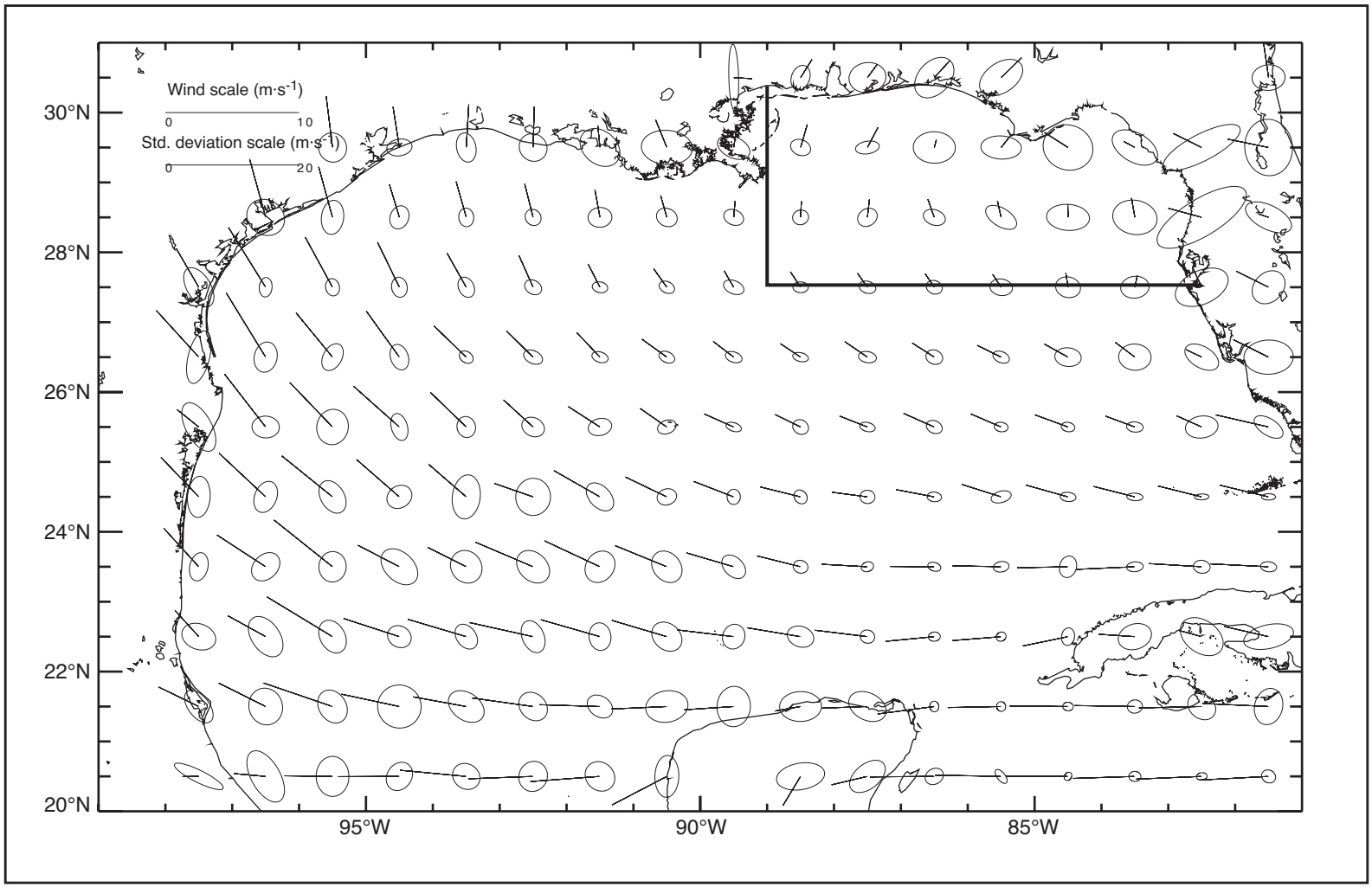

Figure 3.1.1-7. COADS enhanced mean wind field and principal component ellipses for July. Data averaged over the period 1960-1997. NEGOM study area is indicated.

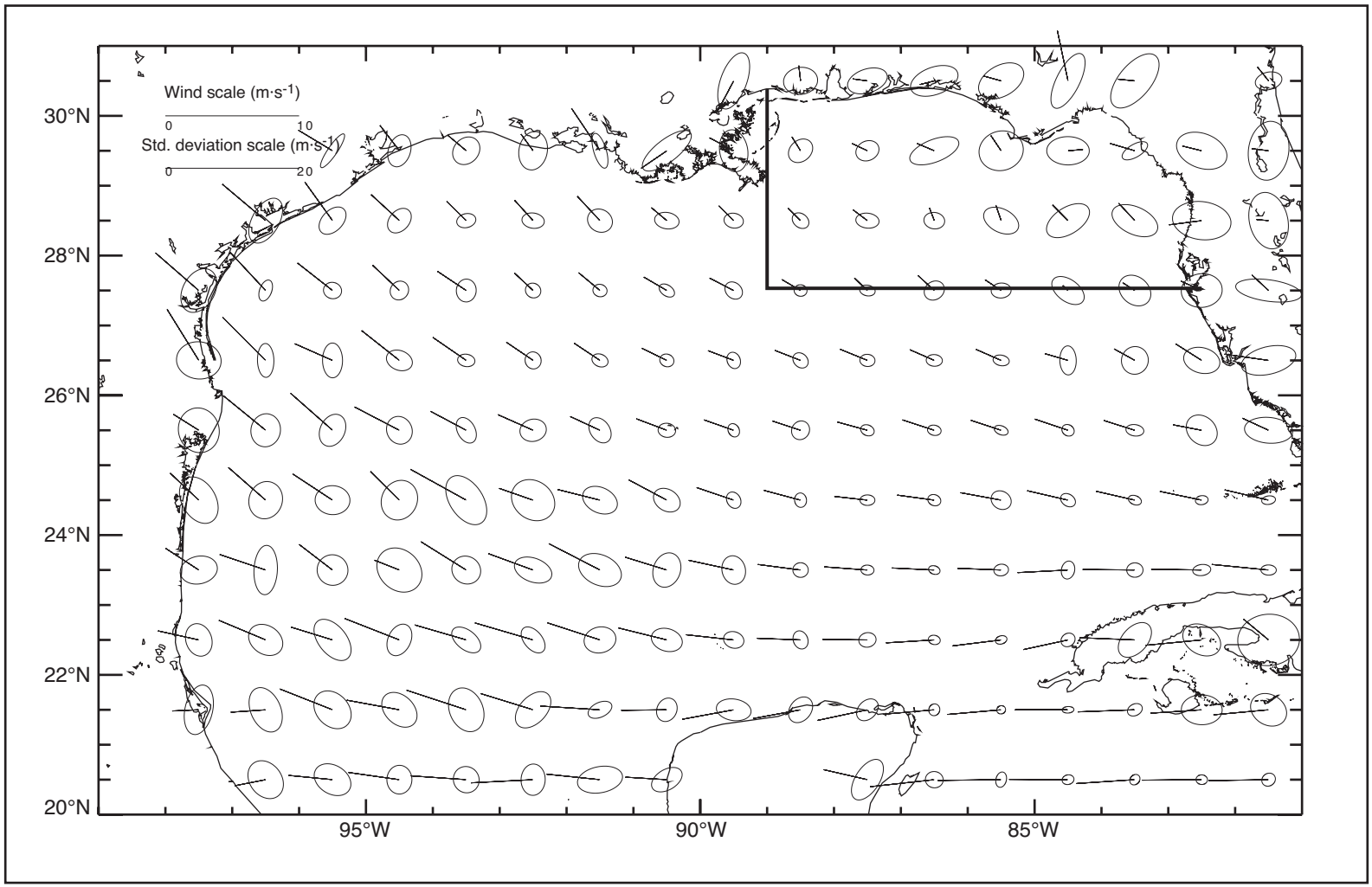

Figure 3.1.1-8. COADS enhanced mean wind field and principal component ellipses for August. Data averaged over the period 1960-1997. NEGOM study area is indicated.

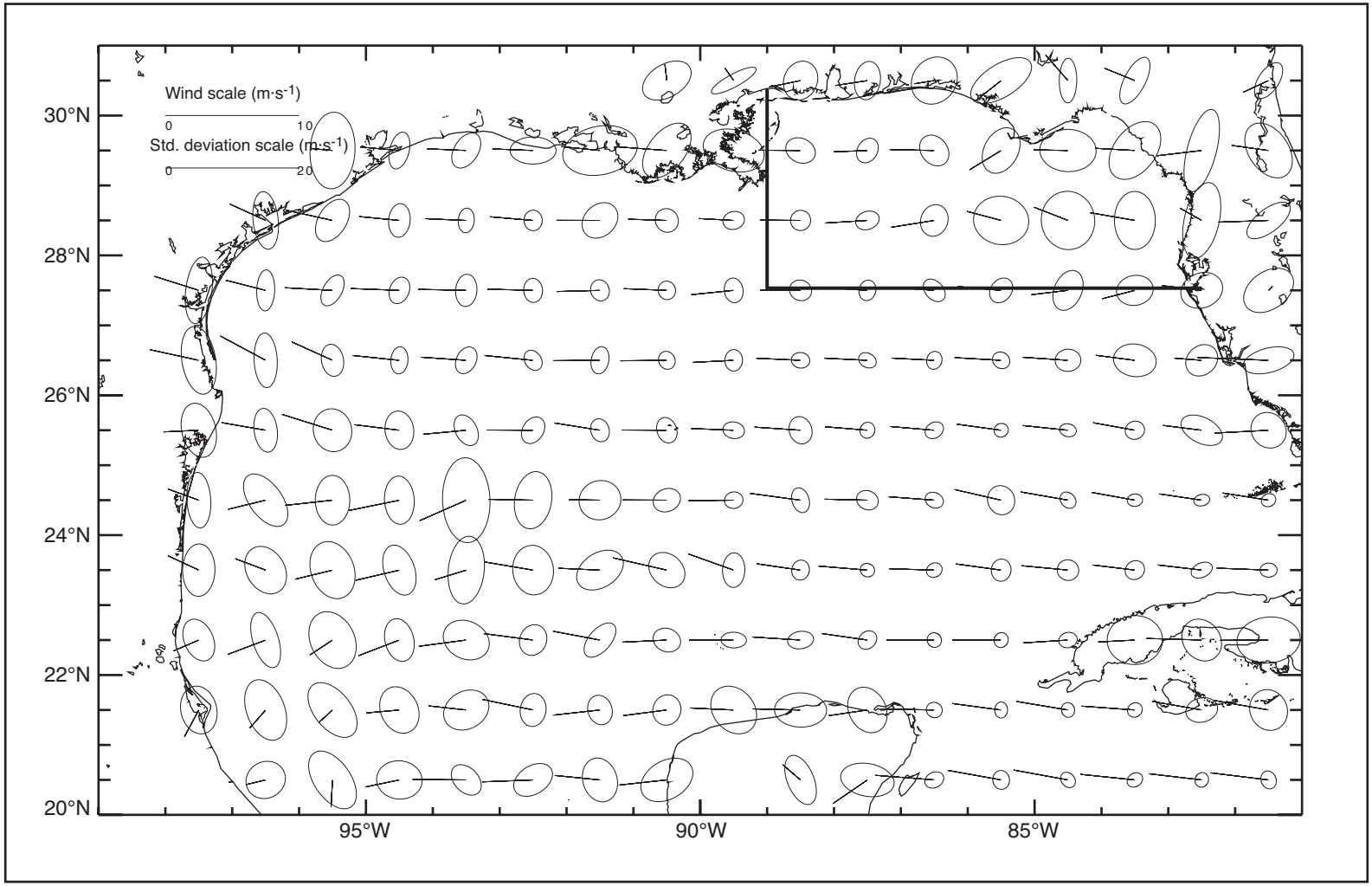

Figure 3.1.1-9. COADS enhanced mean wind field and principal component ellipses for September. Data averaged over the period 1960-1997. NEGOM study area is indicated.

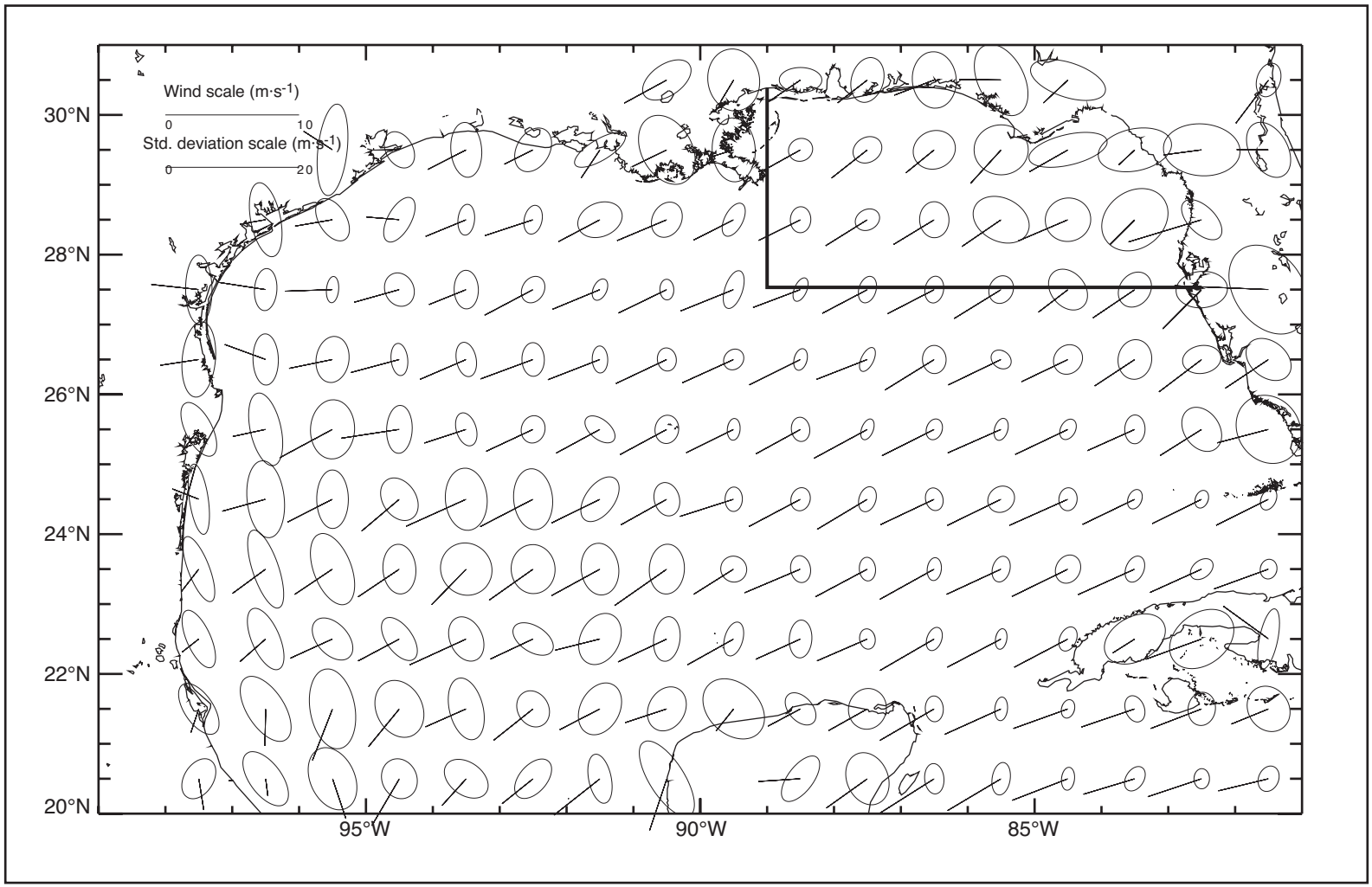

Figure 3.1.1-10. COADS enhanced mean wind field and principal component ellipses for October. Data averaged over the period 1960-1997. NEGOM study area is indicated.

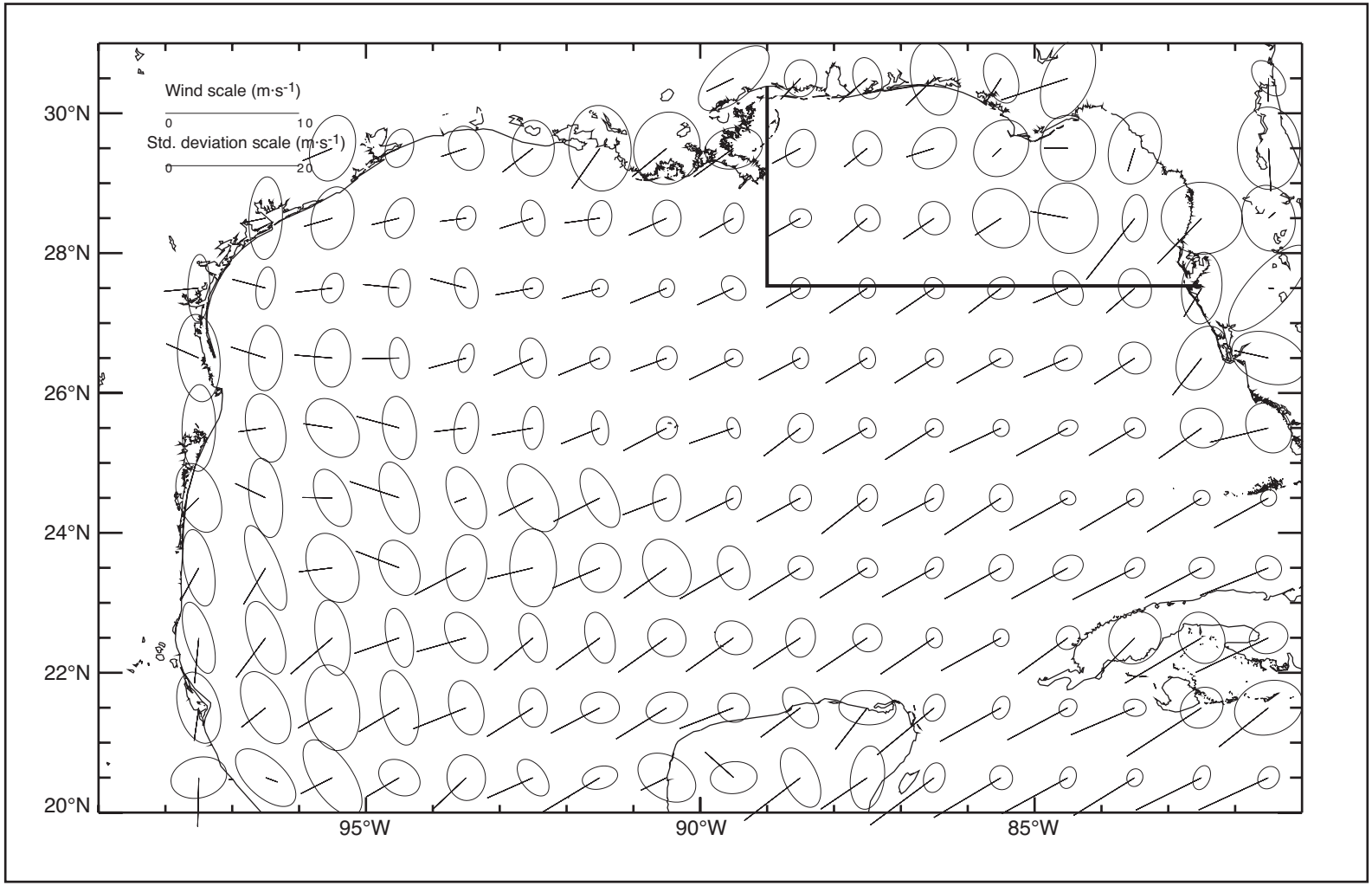

Figure 3.1.1-11. COADS enhanced mean wind field and principal component ellipses for November. Data averaged over the period 1960-1997. NEGOM study area is indicated.

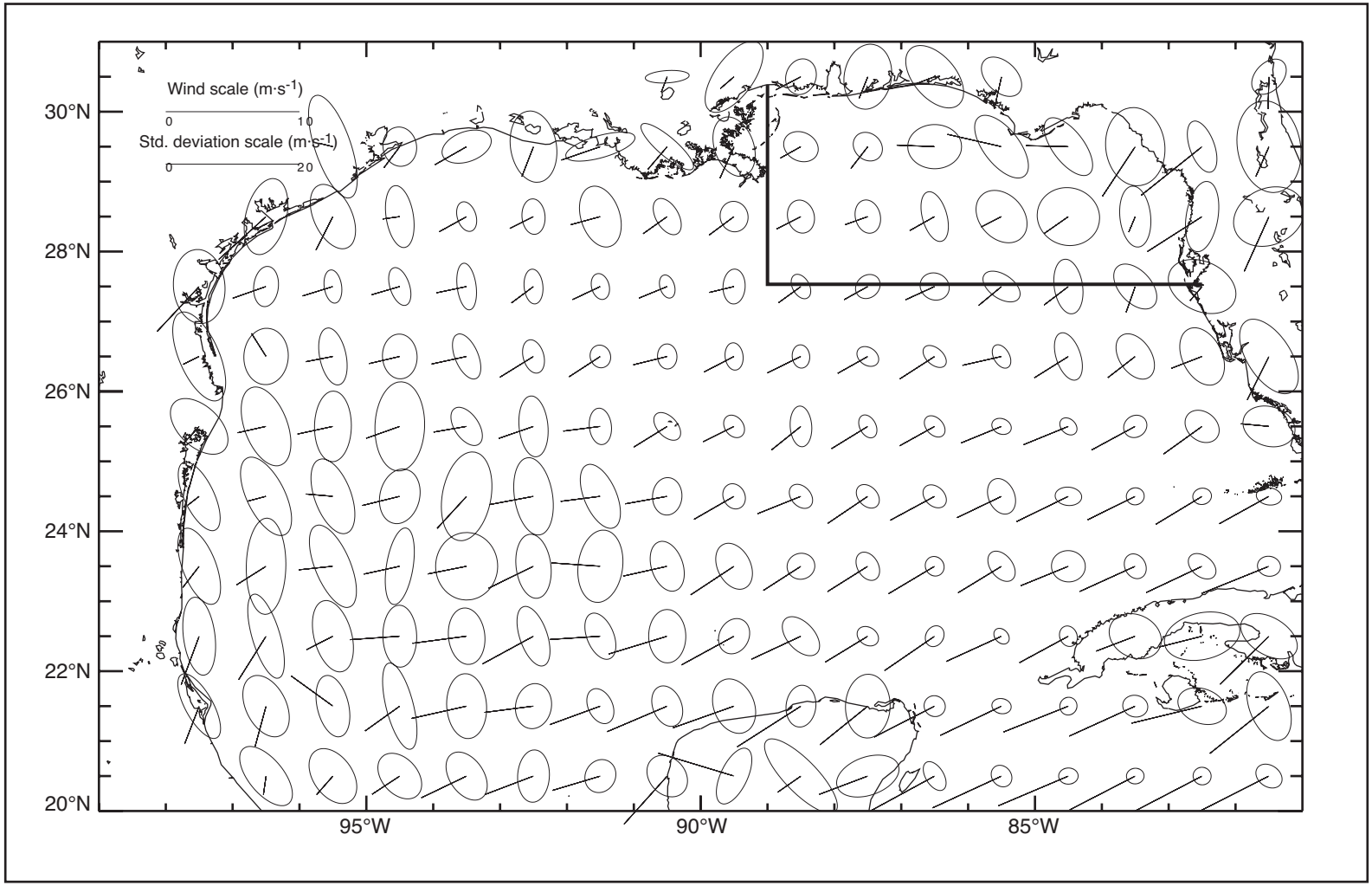

Figure 3.1.1-12. COADS enhanced mean wind field and principal component ellipses for December. Data averaged over the period 1960-1997. NEGOM study area is indicated.

Table 3.1.1-3. Available monthly COADS data at 167 grid points in the Gulf of Mexico.

Minimum percent of long-term monthly means	Years of available data
44	36
66	30
84	20
90	13
96	6

Table 3.1.1-4. Monthly mean ocean heat storage rates for NEGOM region adopted from Etter (1983; personal communication 1999). Positive indicates oceanic gain of heat.

Month	Rate of ocean heat storage ($W \cdot m^{-2}$)
Jan	-214
Feb	-162
Mar	-11
Apr	198
May	294
Jun	200
Jul	142
Aug	83
Sep	59
Oct	-203
Nov	-270
Dec	-216

3.1.2 River Discharge Rates

Locations of gauging stations of the principal rivers discharging into the NEGOM region are given in Figure 3.1.2-1. Table 3.1.2-1 shows the record-length mean daily discharge rate of these rivers arranged in descending order of discharge. The mean daily discharge rates bracketed by one standard deviation for these rivers are shown in Figures 3.1.2-2 through 3.1.2-12. These are based on the entire available record with the number of years of record length (N) shown. If N is less than four, no standard deviation is shown. Also shown are the daily discharge rates, as available, for 1997, 1998, 1999, and 2000 through August. Scales are variable.

Maximum mean discharge for these rivers generally occurs between early March and mid-April. The Mississippi River peak is in mid-April. Minimum mean discharge occurs between early September and late November, with rivers in the west typically reaching their minimum discharges before those in the east. The minimum in mean Mississippi River discharge is in mid-September. River discharge conditions during each cruise are discussed in the respective cruise summaries in appendices A through I.

To compare the river discharge conditions preceding each cruise with the mean conditions, the mean discharge and its standard deviation for the 30 days preceding each cruise were calculated for selected major rivers and the record-length mean discharges for the same periods were determined. Table 3.1.2-2 shows the mean river discharges associated with the 30-day period prior to each cruise. In comparing the record-length mean with the cruise mean, the cruise mean

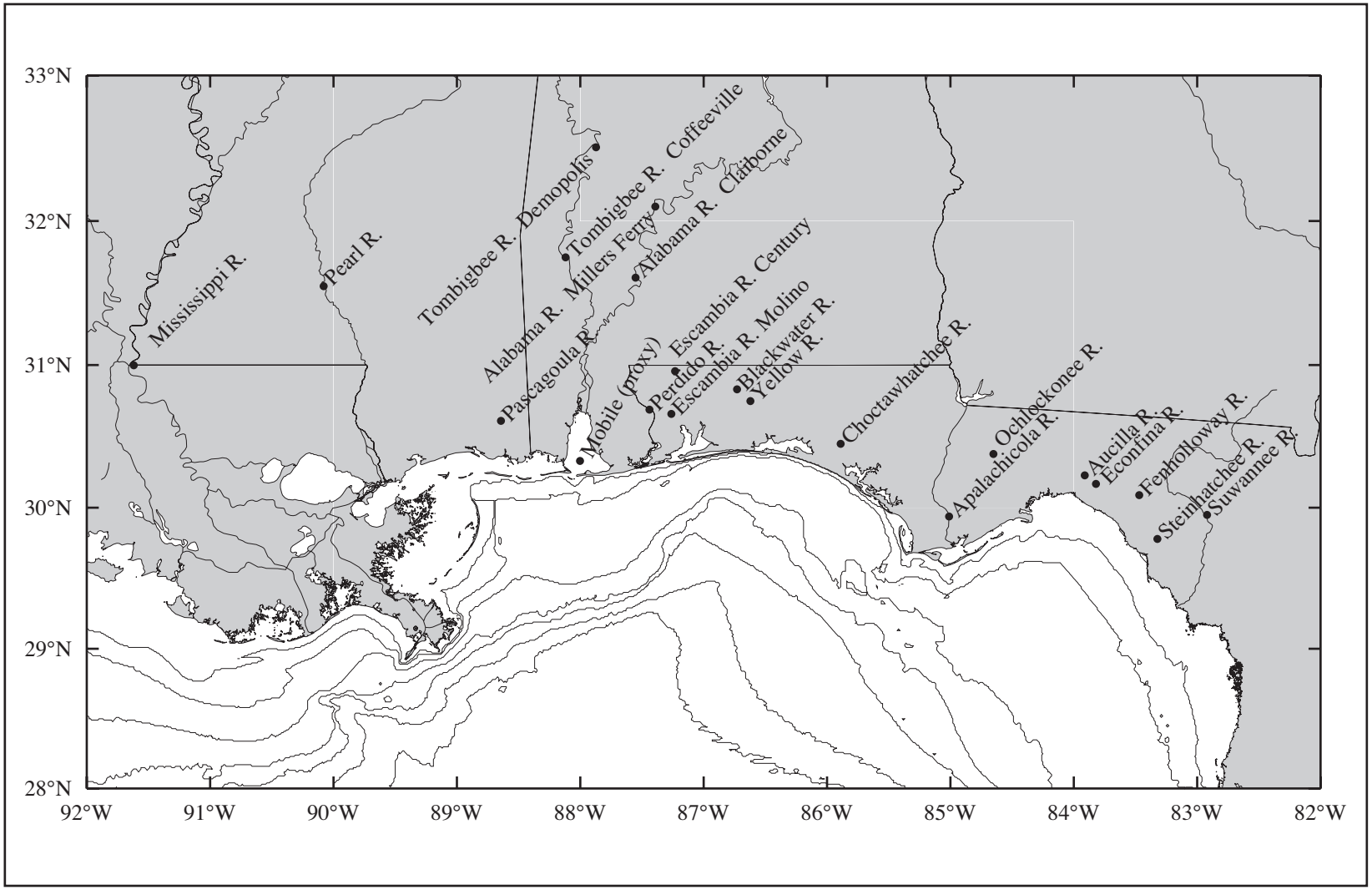

Figure 3.1.2-1. Rivers discharging into the NEGOM study area and locations of associated gauging stations. Bathymetric contours shown are 10, 20, 50, 100, 200, 500, and 1000 m.

Table 3.1.2-1. Record-length mean daily discharge rate for rivers discharging into the NEGOM region.

River name and gauging station location	Mean daily discharge ($m^3 \cdot d^{-1}$)	Period of record (mm/dd/yyyy)
Mississippi River at Tarbert Landing, LA	1179905152	01/02/1930 to 11/14/2000
Alabama River at Claiborne L&D, AL	80300248	10/01/1975 to 09/30/2000
Alabama River at Millers Ferry L&D, AL	78841648	05/01/1970 to 09/30/2000
Tombigbee River at Coffeeville L&D, AL	72714752	10/01/1960 to 09/30/2000
Apalachicola River near Sumatra, FL	63376308	10/01/1977 to 04/05/2001
Tombigbee River at Demopolis L&D, AL	57965020	08/01/1928 to 04/05/2001
Pascagoula River at Graham Ferry, MS	25858540	10/01/1993 to 04/05/2001
Escambia River near Molino, FL	18489804	11/20/1983 to 03/14/2000
Choctawatchee River near Bruce, FL	17389676	10/01/1930 to 04/05/2001
Suwannee River at Branford, FL	16984920	07/01/1931 to 04/05/2001
Pearl River near Monticello, MS	16549406	10/01/1938 to 04/05/2001
Escambia River near Century, FL	15352452	10/01/1934 to 04/05/2001
Ochlockonee River near Bloxham, FL	4200082	07/01/1926 to 04/05/2001
Yellow River at Milligan, FL	2826336	08/01/1938 to 04/05/2001
Perdido River at Barrineau Park, FL	1925047	06/09/1941 to 09/30/2000
Aucilla near Scanlon, FL	1340322	09/03/1976 to 10/07/1997
Blackwater River near Baker, FL	857140	04/01/1950 to 04/05/2001
Steinhatchee River near Cross City, FL	769451	03/01/1950 to 01/30/2000
Econfina River near Perry, FL	344564	02/01/1950 to 09/30/2000
Fenholloway River near Foley, FL	130394	10/01/1955 to 09/30/1999

was considered to be similar to the record-length mean if the range of the cruise mean plus or minus the standard deviation encompassed the value of the record-length mean. Cases where the cruise mean substantially exceeded the record-length mean indicate wet years; cases where the cruise mean was substantially below the record-length mean indicate dry years. During all cruises in 1998, the discharge from the Mississippi River preceding the cruises was substantially above the record-length mean, indicating that there likely was an above average amount of fresh water over the western part of the study area during those cruises. In fall 1999 and spring 2000, however, the discharge before the cruises was substantially less than the mean, suggesting there was a below average amount of fresh water over the western part of the study area during those cruises. For the other rivers, only the Apalachicola River (spring 1998) and Suwannee River (spring and fall 1998) had cruises preceded by discharges that were substantially higher than the record-length mean. A number of rivers had discharges substantially below the record-length means, particularly in spring 1999 and spring and summer 2000. Note that the variability of the Mississippi River discharge is greater in spring and summer than fall. Other rivers do not show a discernible seasonal pattern in variability.

A strong El Niño beginning April 1997 and ending July 1998 overlapped cruises N1 and N2. This event strengthened quickly during the summer of 1997, as evidenced by the multivariate El Niño - Southern Oscillation (ENSO) index (Wolter and Timlin 1998) and remained strong until May 1998 when it diminished rapidly. Over the last 50 years, the 1997-98 El Niño was second in strength only to the 1982-83 El Niño. Cruises N3 through N9 were conducted during a moderate La Niña which followed the 1997-98 El Niño. Review of precipitation data and the Palmer Drought Severity Index (PDSI) during the NEGOM study period shows that the coastal regions of the northeast Gulf of Mexico were relatively wet during El Niño and dry during La Niña events. This is reflected further in the non-Mississippi River discharge data

Table 3.1.2-2. Mean river discharges (in million $m^3 \cdot d^{-1}$) associated with the 30-day period prior to each cruise for selected rivers. Given are the individual means and standard deviations for the 30-days prior to each cruise (CM: cruise mean; SD: cruise standard deviation) and the record-length mean for that same 30-day period (RM: record mean). The Mobile Bay discharge rate is a combination of discharges for the Tombigbee and Alabama rivers. Values in bold indicate CM is substantially greater than RM; italics indicate CM is substantially less than RM.

	N1	N2	N3	N4	N5	N6	N7	N8	N9
Mississippi River									
RM	611.8	1901.7	1100.0	602.2	1871.6	845.5	602.2	1868.1	1061.3
CM	560.2	**2262.0**	**1754.7**	**850.0**	1813.0	973.4	*399.5*	*1213.7*	**1286.2**
SD	52.2	97.9	110.9	124.4	245.9	212.1	35.1	259.2	261.3
Mobile Bay									
RM	75.3	268.7	82.1	70.6	214.5	63.5	70.6	323.2	79.2
CM	115.0	248.9	*50.5*	*27.6*	*107.3*	52.7	*28.1*	305.3	*24.8*
SD	75.0	80.0	21.8	5.2	53.4	26.4	8.6	160.0	4.0
Apalachicola River									
RM	34.5	84.9	52.0	34.1	73.0	50.4	34.1	108.4	52.5
CM	45.3	**117.8**	40.0	40.1	*26.3*	45.9	*19.3*	*62.4*	*13.8*
SD	11.0	18.9	8.2	15.3	2.7	4.6	1.6	18.3	0.8
Pascagoula River									
RM	9.3	39.1	14.4	8.9	37.3	12.6	8.9	48.2	14.2
CM	9.3	32.9	9.5	9.1	*10.1*	*7.1*	10.2	*24.3*	*3.4*
SD	3.2	11.6	3.8	2.5	2.4	2.3	10.0	10.0	1.1
Choctawhatchee River									
RM	9.1	25.2	13.5	9.1	20.1	14.4	9.1	29.8	13.7
CM	10.1	24.7	*7.3*	17.8	*9.9*	15.2	7.3	*11.6*	*3.6*
SD	4.5	6.5	1.8	13.5	2.9	5.3	1.4	2.8	0.5
Suwannee River									
RM	11.8	27.8	12.6	12.2	24.0	13.6	12.2	30.0	12.7
CM	14.6	**44.2**	*9.7*	**23.4**	*6.2*	*5.5*	*5.1*	*7.2*	*4.0*
SD	8.4	13.1	0.4	8.7	0.4	0.1	0.1	1.3	0.1
Pearl River									
RM	4.0	33.3	6.3	3.7	28.5	5.9	3.7	35.2	6.3
CM	4.8	20.4	4.5	1.6	*5.2*	*2.1*	2.3	29.7	*1.6*
SD	2.1	13.6	3.0	0.3	3.7	0.5	1.8	25.9	0.2
Escambia River (Century)									
RM	6.1	24.9	9.7	5.8	18.7	10.7	5.8	32.4	9.7
CM	7.1	22.9	6.0	10.6	*9.2*	11.8	5.2	*8.9*	*1.9*
SD	4.6	8.1	2.2	4.3	4.9	6.3	1.6	3.3	0.8

shown in Figures 3.1.2-2 through 3.1.2-12, where larger than normal river output is seen from April 1997 through May 1998 and low output from July 1998 through December 2001.

It is more difficult to interpret the Mississippi River discharge as measured at Tarbert Landing (Figure 3.1.2-2, top panel) because of the influence of the many different climatic zones of the central and northern United States that make up the Mississippi River drainage basins. However, one can see that the Mississippi River discharge tends to be above normal during 1997-98 and at or below normal during 1999-2000. Quantifying the interannual variability that is solely attributable to ENSO phenomena or a combination of ENSO with decadal scale climate indicators such the North Atlantic Oscillation or the Pacific Decadal Anomaly is not possible from the available data sets.

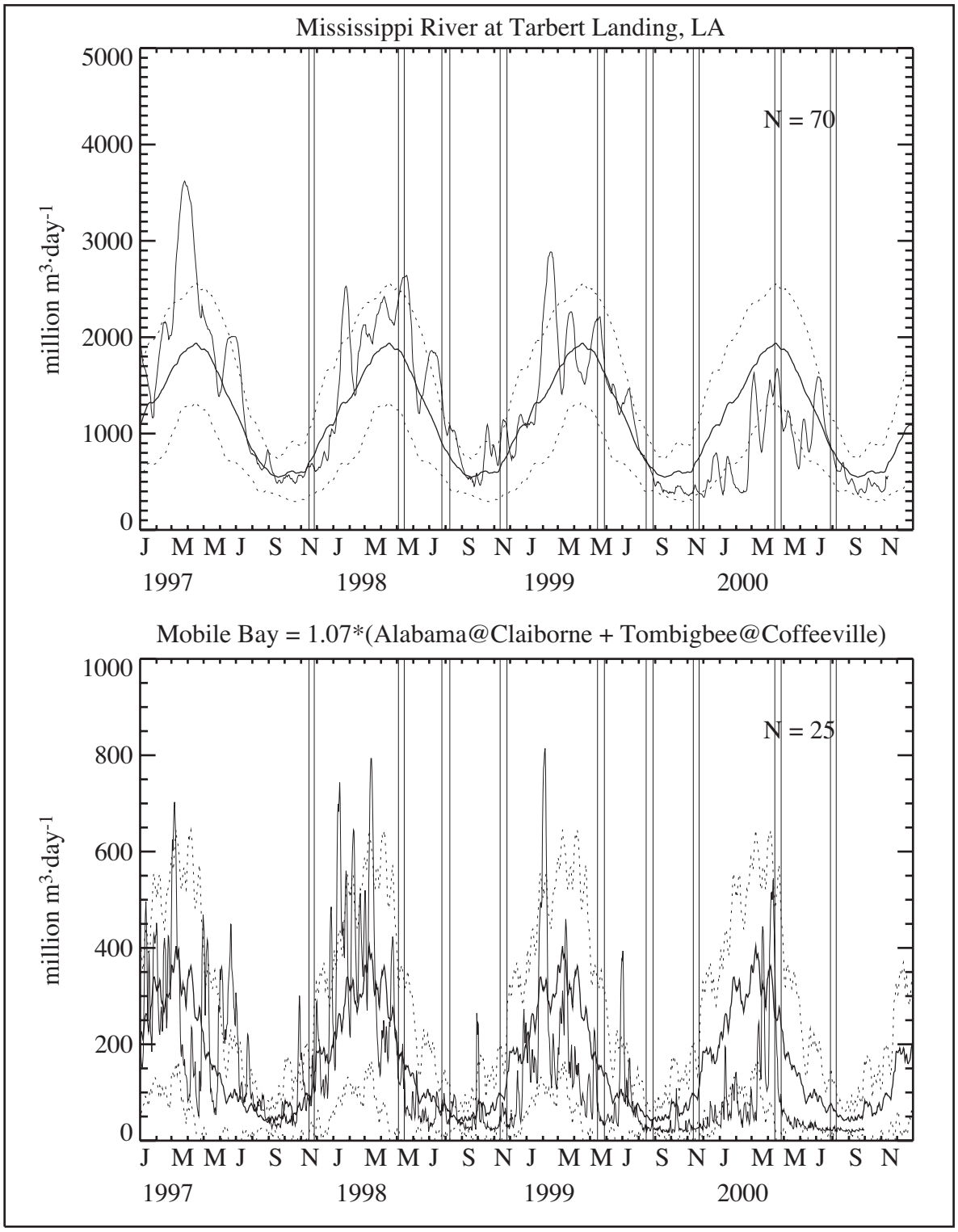

Figure 3.1.2-2. Discharge rates in 10^6 $m^3 \cdot day^{-1}$ for the Mississippi River and Mobile Bay (Alabama+Tombigbee). (thin line) daily discharge for 1997–2000, (thick line) mean daily discharge averaged over N years, (dashed line) mean ± one standard deviation. Vertical lines show start and end dates of the cruises.

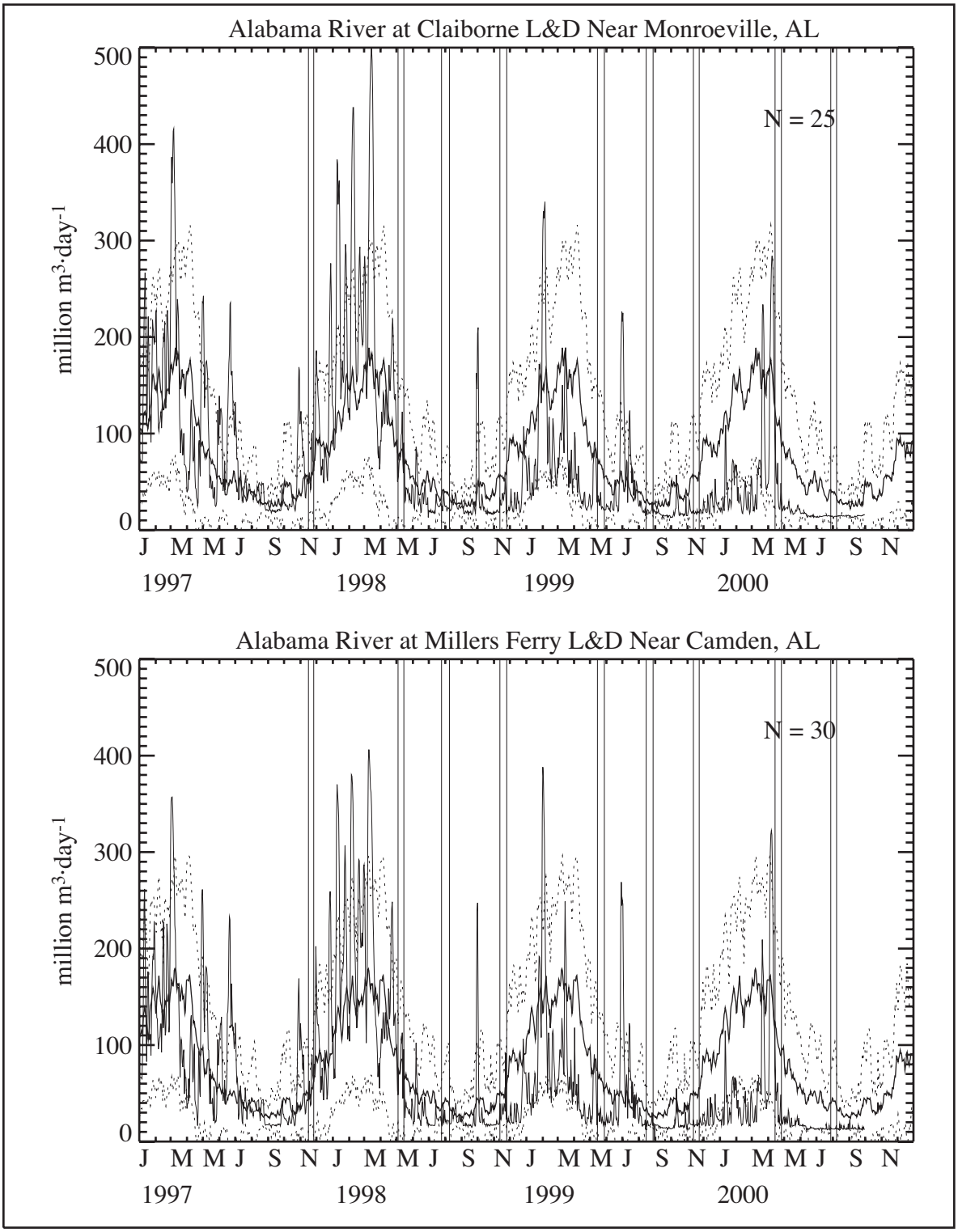

Figure 3.1.2-3. Discharge rates in 10^6 $m^3 \cdot day^{-1}$ for the Alabama River (Claiborne and Millers Ferry). (thin line) daily discharge for 1997-2000, (thick line) mean daily discharge averaged over N years, (dashed line) mean ± one standard deviation. Vertical lines show start and end dates of cruises.

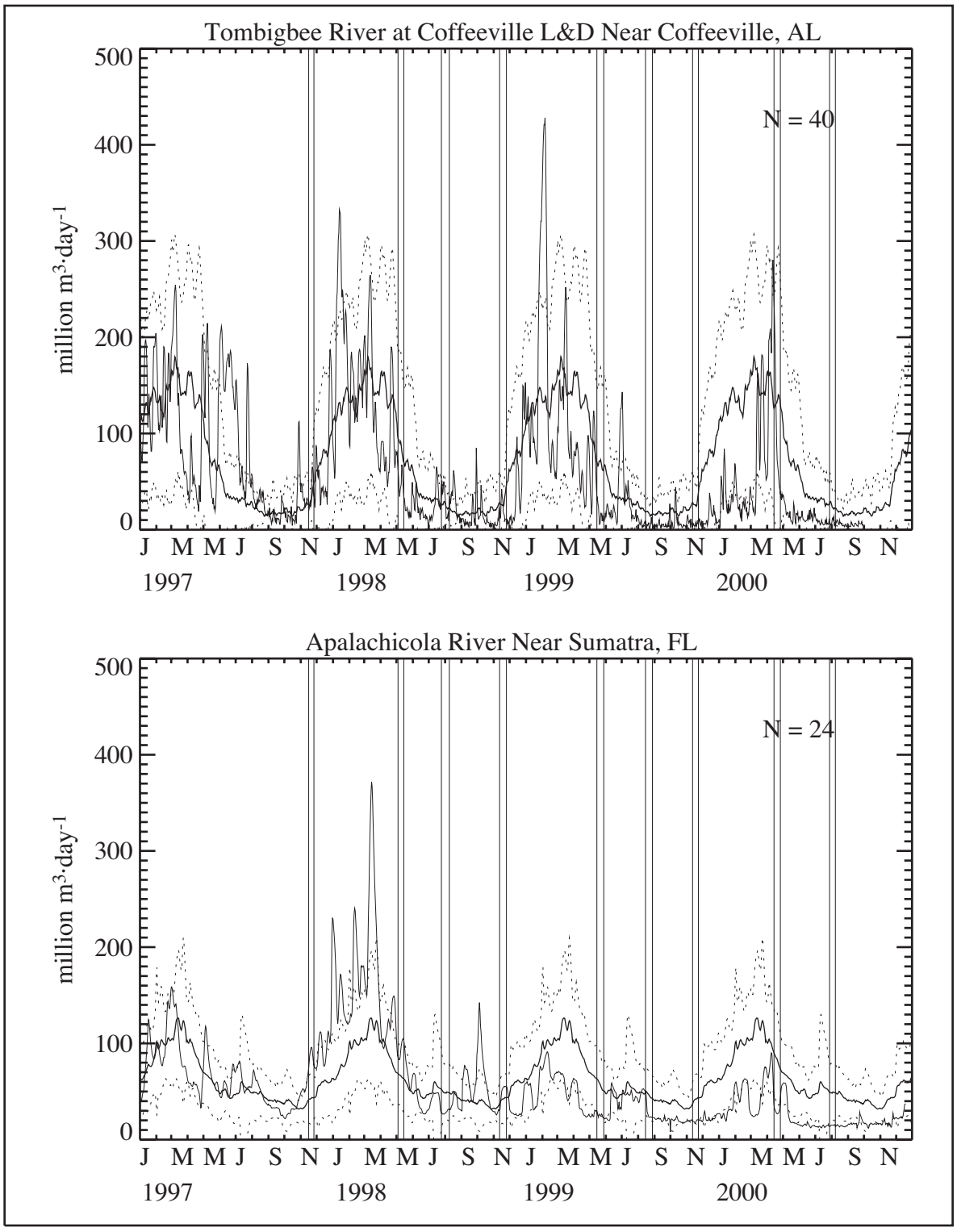

Figure 3.1.2-4. Discharge rates in 10^6 $m^3 \cdot day^{-1}$ for the Tombigbee River (Coffeeville) and Apalachicola River. (thin line) daily discharge for 1997-2000, (thick line) mean daily discharge averaged over N years, (dashed line) mean ± one standard deviation. Vertical lines show start and end dates of cruises.

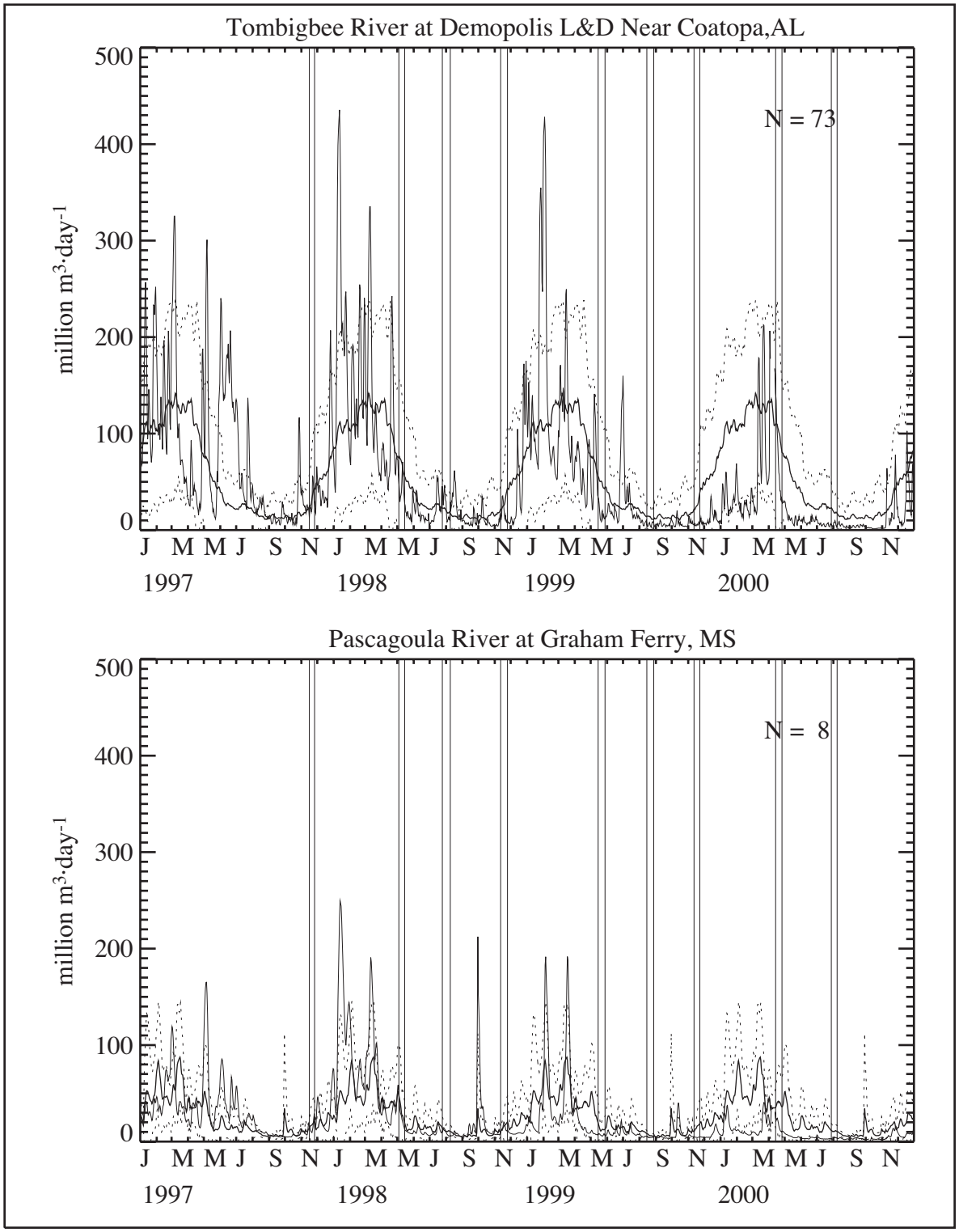

Figure 3.1.2-5. Discharge rate in 10^6 $m^3 \cdot day^{-1}$ for the Tombigbee River (Demopolis) and Pascagoula River. (thin line) daily discharge for 1997-2000, (thick line) mean daily discharge averaged over N years, (dashed line) mean ± one standard deviation. Vertical lines show start and end dates of cruises.

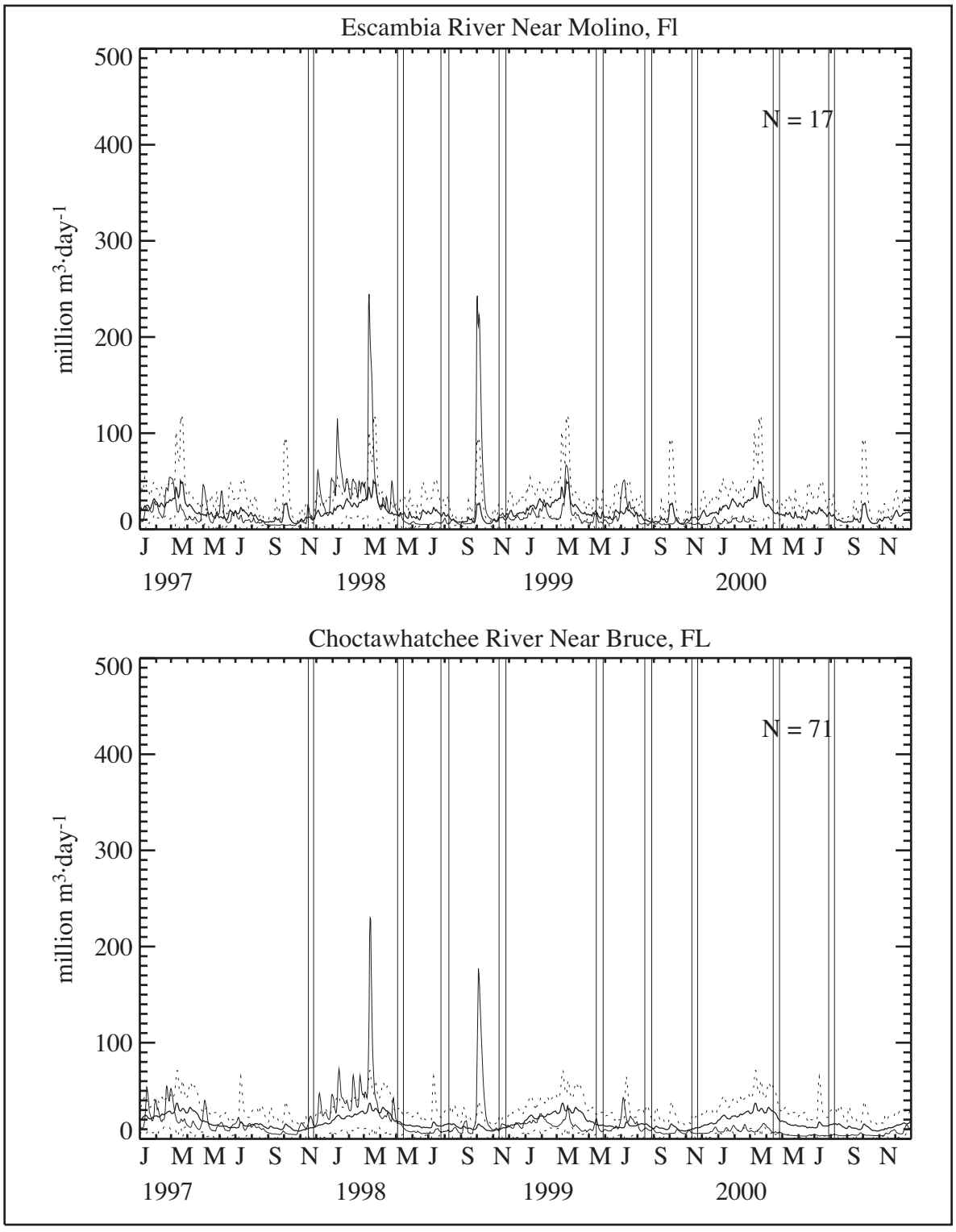

Figure 3.1.2-6. Discharge rate in 10^6 $m^3 \cdot day^{-1}$ for the Escambia River (Molino) and Choctawhatchee River. (thin line) daily discharge for 1997-2000, (thick line) mean daily discharge averaged over N years, (dashed line) mean ± one standard deviation. Vertical lines show start and end dates of cruises.

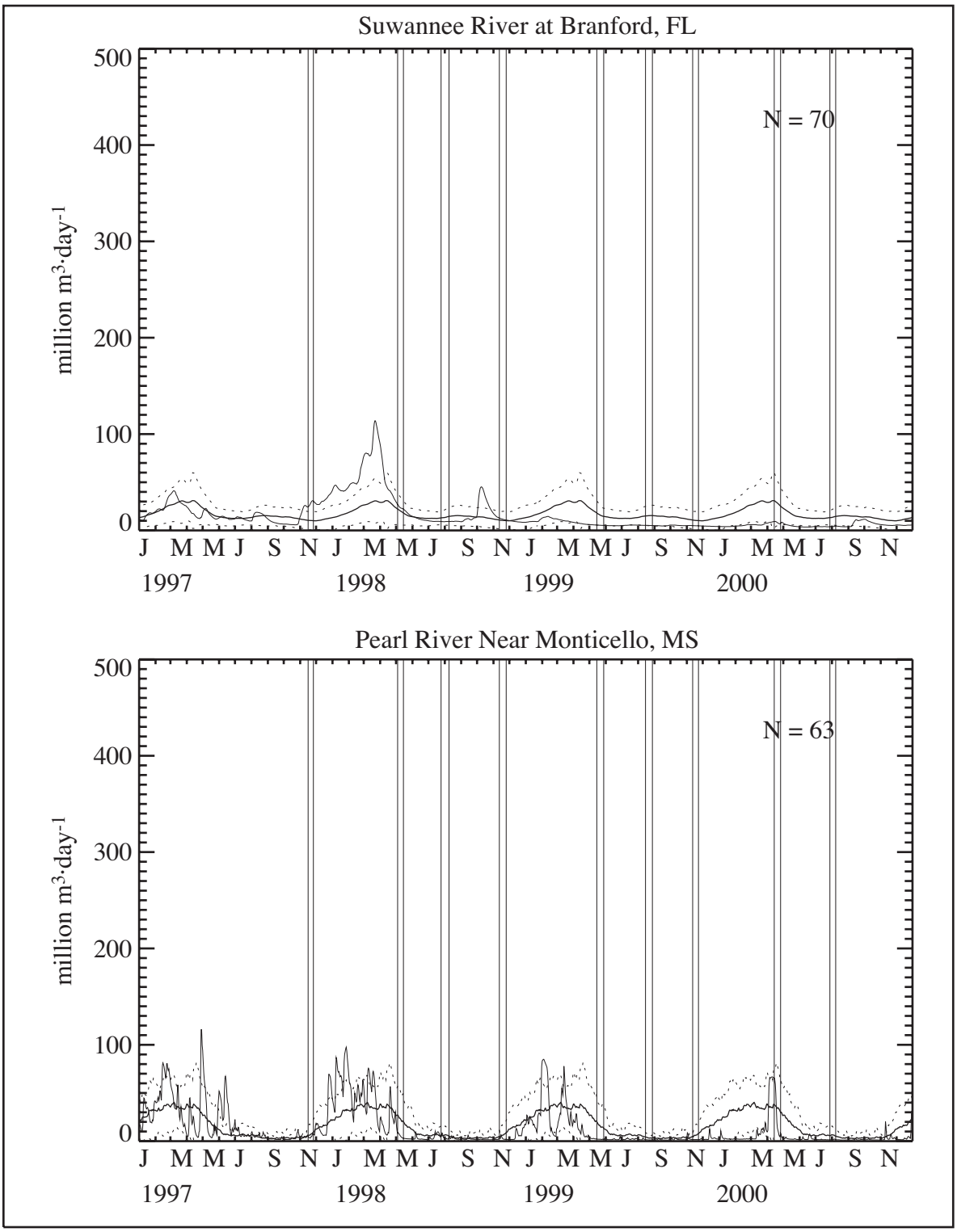

Figure 3.1.2-7. Discharge rate in 10^6 $m^3 \cdot day^{-1}$ for the Suwannee River and Pearl River. (thin line) daily discharge for 1997-2000, (thick line) mean daily discharge averaged over N years, (dashed line) mean ± one standard deviation. Vertical lines show start and end dates of cruises.

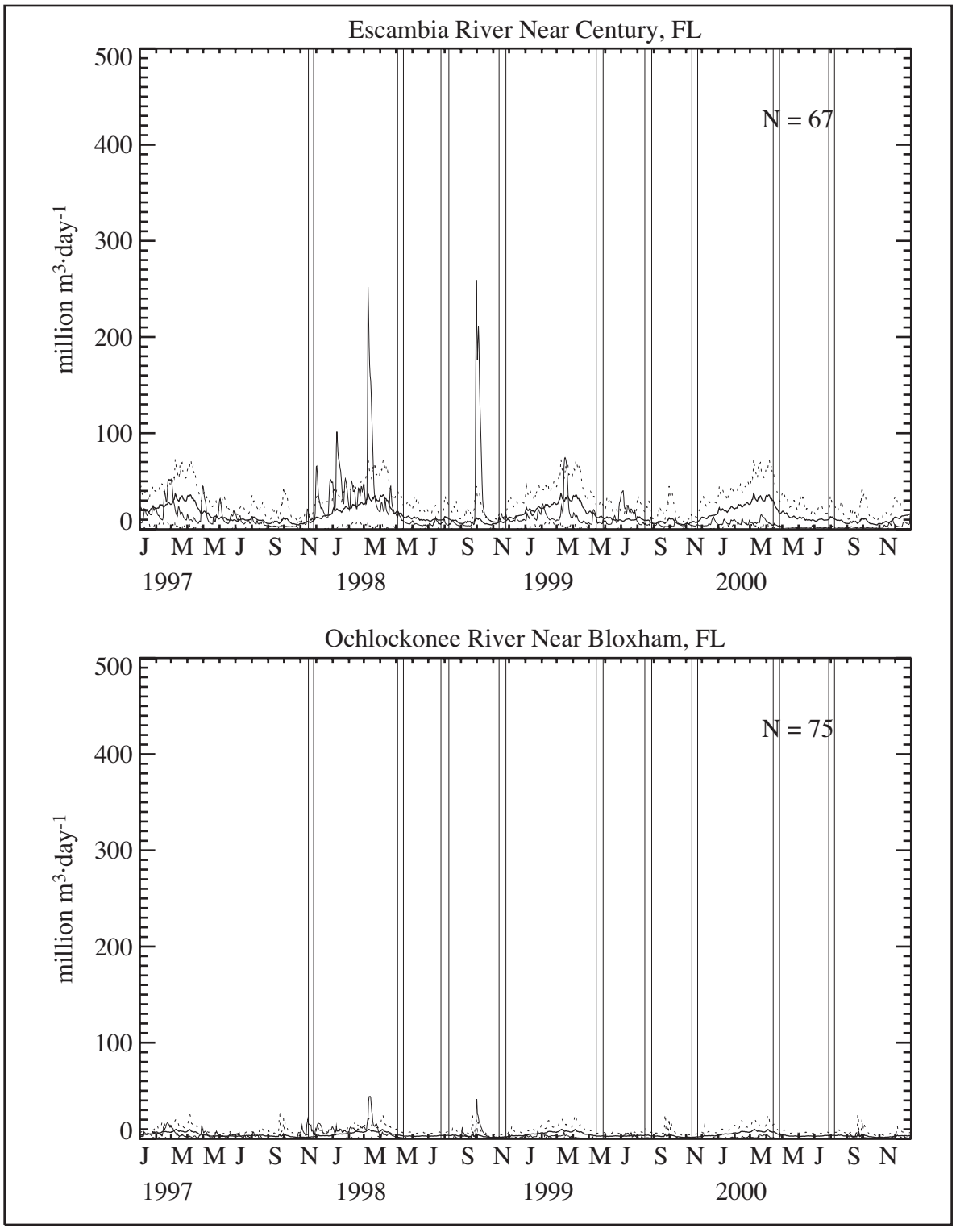

Figure 3.1.2-8. Discharge rate in 10^6 $m^3 \cdot day^{-1}$ for the Escambia River (Century) and Ochlockonee River. (thin line) daily discharge for 1997-2000, (thick line) mean daily discharge averaged over N years, (dashed line) mean ± one standard deviation. Vertical lines show start and end dates of cruises.

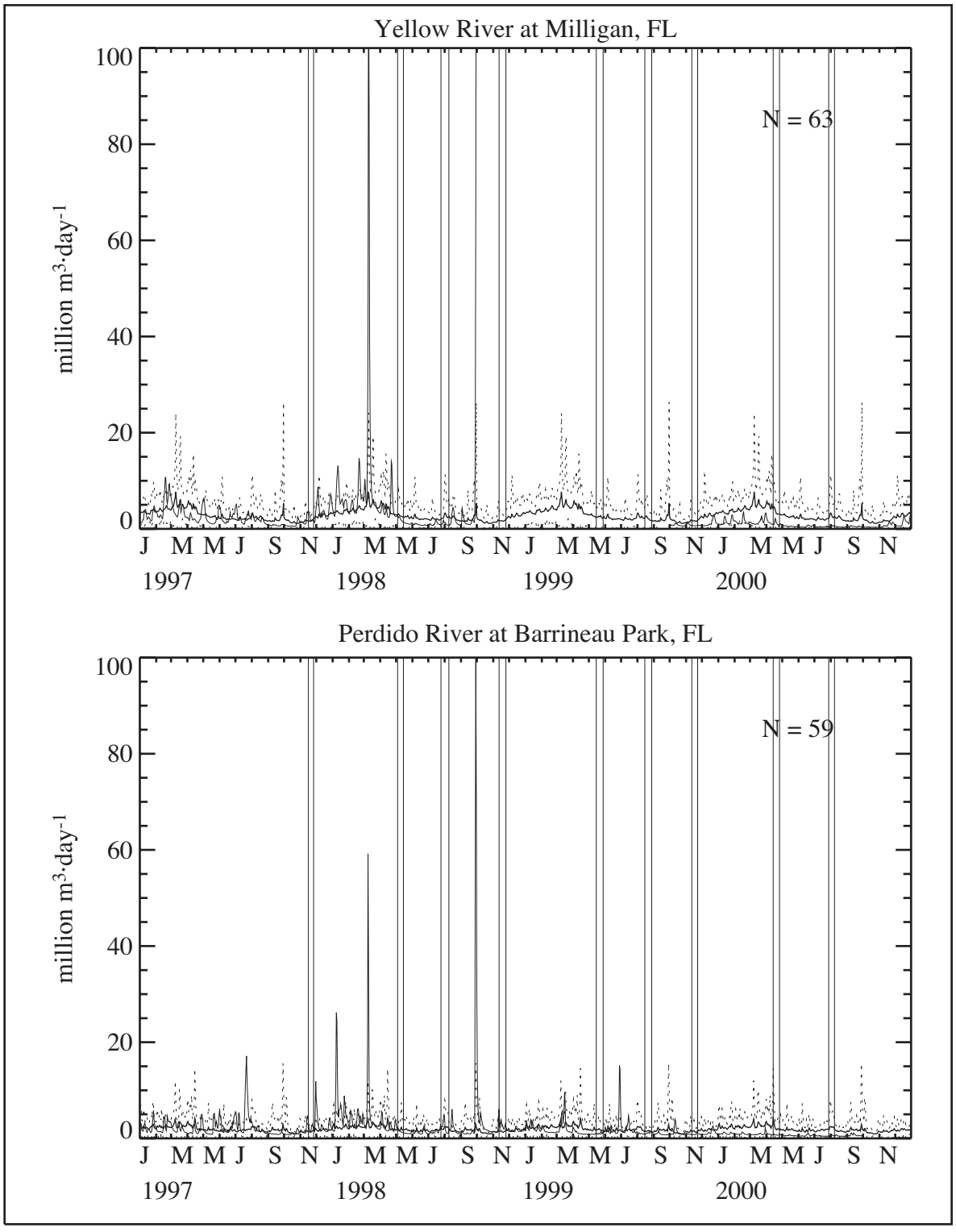

Figure 3.1.2-9. Discharge rate in 10^6 $m^3 \cdot day^{-1}$ for the Yellow River and Perdido River. (thin line) daily discharge for 1997-2000, (thick line) mean daily discharge averaged over N years, (dashed line) mean ± one standard deviation. Vertical lines show start and end dates of cruises.

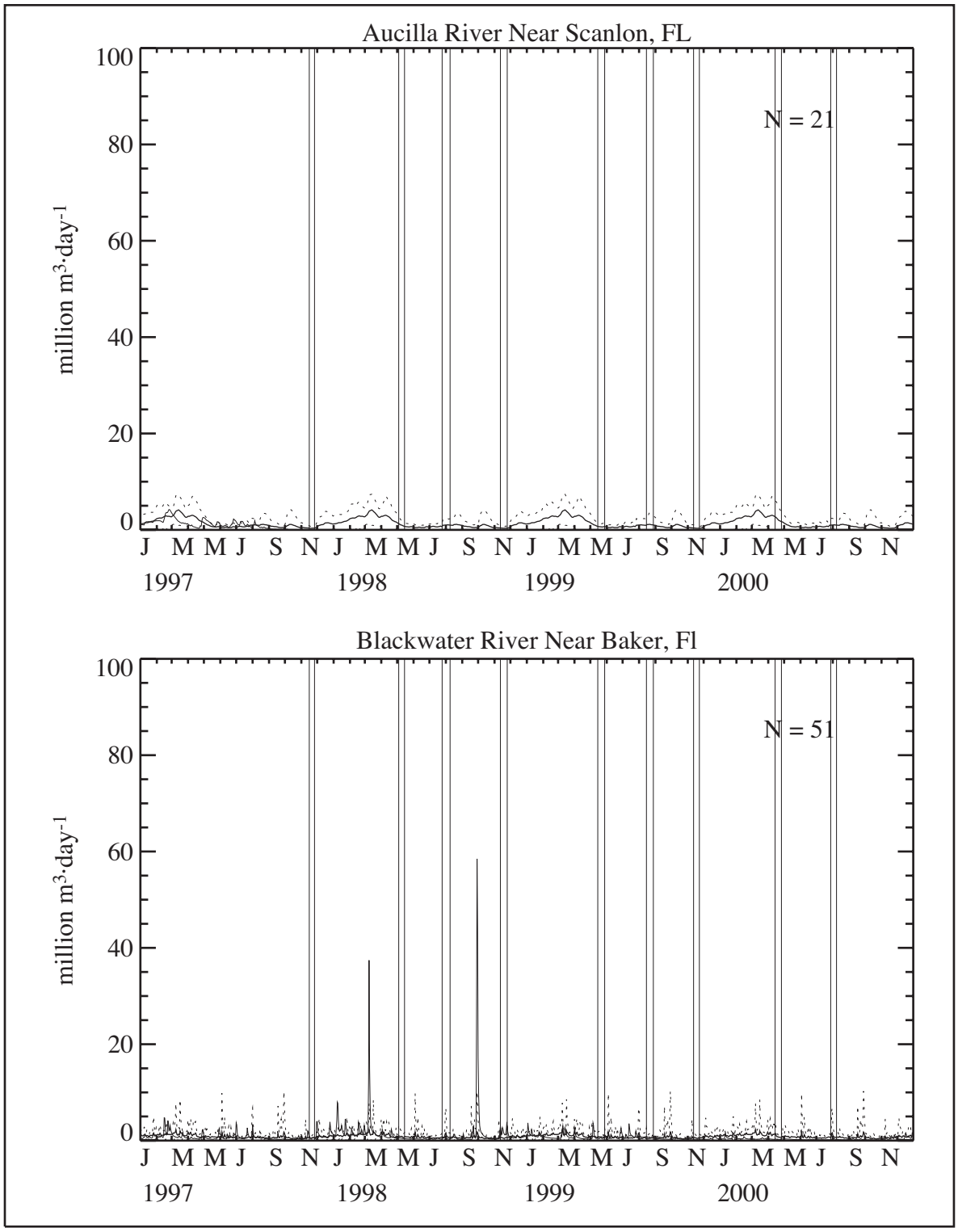

Figure 3.1.2-10. Discharge rate in 10^6 $m^3 \cdot day^{-1}$ for the Aucilla River and Blackwater River. (thin line) daily discharge for 1997-2000, (thick line) mean daily discharge averaged over N years, (dashed line) mean ± one standard deviation. Vertical lines show start and end dates of cruises.

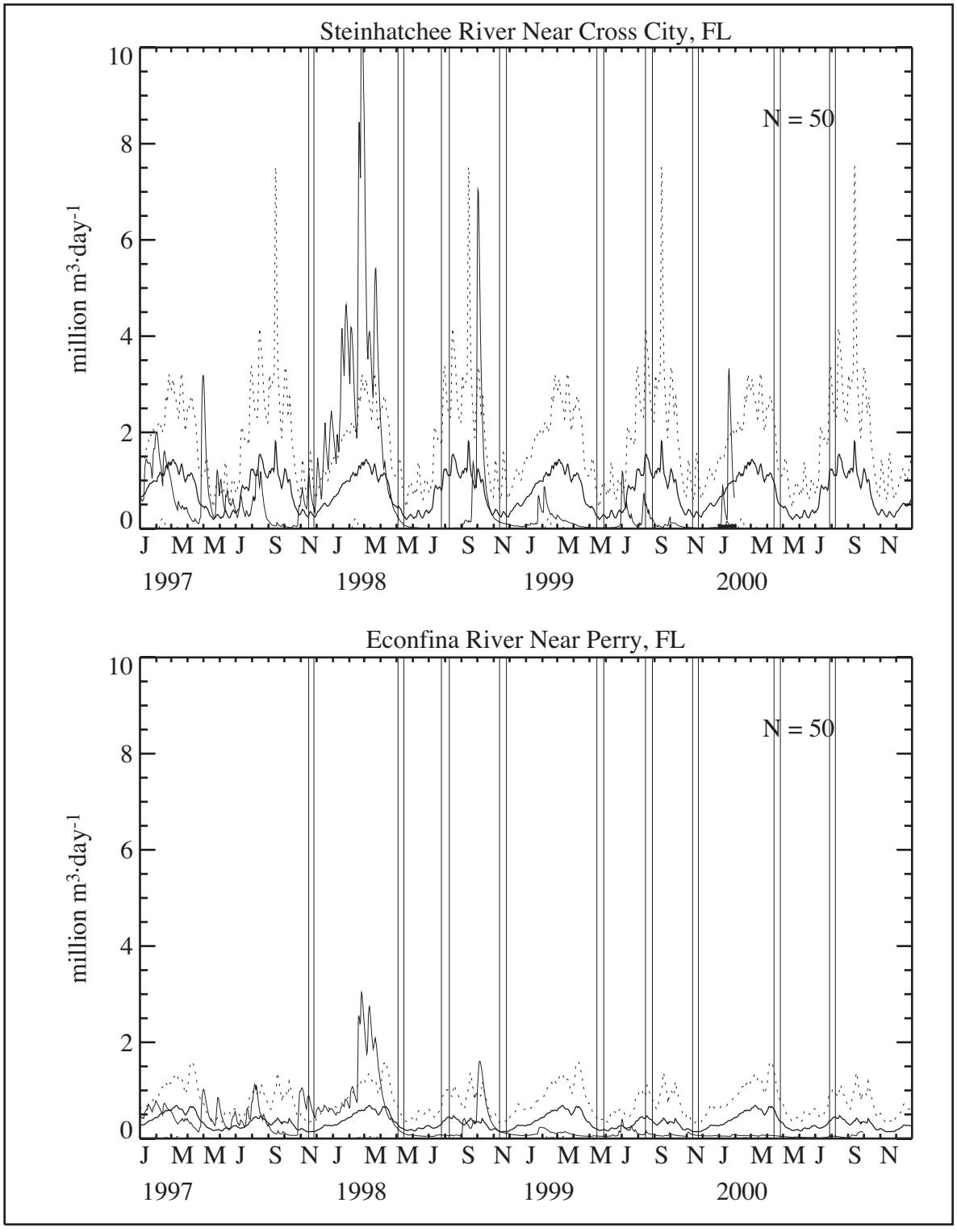

Figure 3.1.2-11. Discharge rate in 10^6 $m^3 \cdot day^{-1}$ for the Steinhatchee River and Econfina River. (thin line) daily discharge for 1997-2000, (thick line) mean daily discharge averaged over N years, (dashed line) mean ± one standard deviation. Vertical lines show start and end dates of cruises.

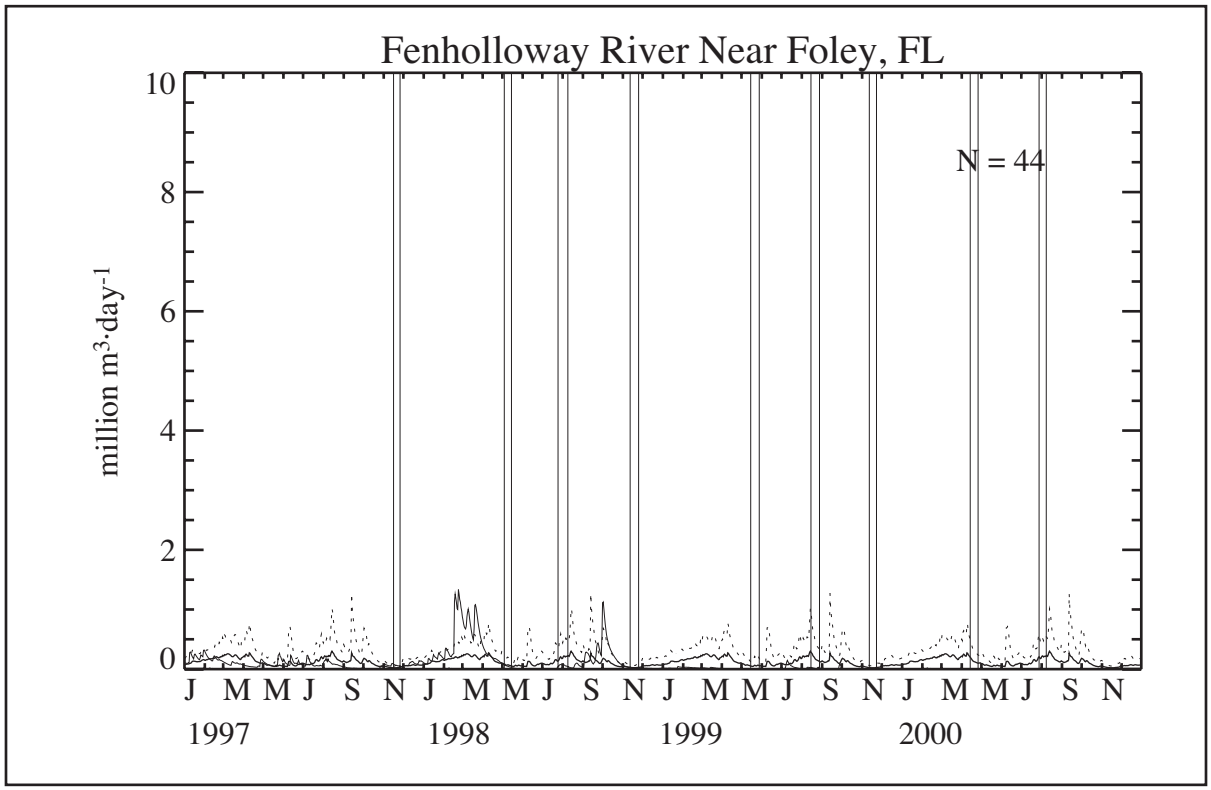

Figure 3.1.2-12. Discharge rate in 10^6 $m^3 \cdot day^{-1}$ for the Fenholloway River. (thin line) daily discharge for 1997-2000, (thick line) mean daily discharge averaged over N years, (dashed line) mean ± one standard deviation. Vertical lines show start and end dates of cruises.

3.2 Other Time Series During the NEGOM-COH Program

3.2.1 Coastal and Selected Offshore Winds

The locations of surface meteorological stations from which long time series of winds were observed is shown in Figure 3.2.1-1. For 1997-2000, the 40-hr low-passed wind components for the stations indicated by solid triangles are shown in Figures 3.2.1-2 through 3.2.1-5. Along-shelf components are positive upcoast (Mississippi to Tampa); cross-shelf components are positive onshore. Table 3.2.1-1 gives the rotation angle relative to local bathymetry used to convert earth coordinates to along- and cross-shelf coordinates. A cursory inspection shows considerable coherence between winds measured at stations in three sets: those shore stations west of Cape San Blas, those shore stations southeast of Cape San Blas, and the offshore buoy stations 42036, 42039, and 42040. The frequency of shifts in wind directions as well as wind speeds are notably greater in non summer than in summer.

3.2.2 Sea Surface Temperature from Offshore Buoys

Sea surface temperature (SST) was measured at six of the meteorological stations: buoys 42007, 42040, 42039, and 42036, and stations DPIA1 and VENF1. Locations are shown in Figure 3.2.1-1. The 40-hr low-passed SST for each of these stations are given in Figures 3.2.2-1 through 3.2.2-4. The most notable pattern is the annual cycle of heating and cooling.

Table 3.2.1-1. Along-shelf directions at meteorological stations relative to local bathymetry. Angles are given relative to degrees true north. Cross-shelf direction is to the left of the along-shelf.

Station	Along-shelf angle (° true N)
BURL1	55
42007	45
DPIA1	90
CSFB1	120
KTNF1	135
CDRF1	147
VENF1	160
42040	65
42039	125
42036	140

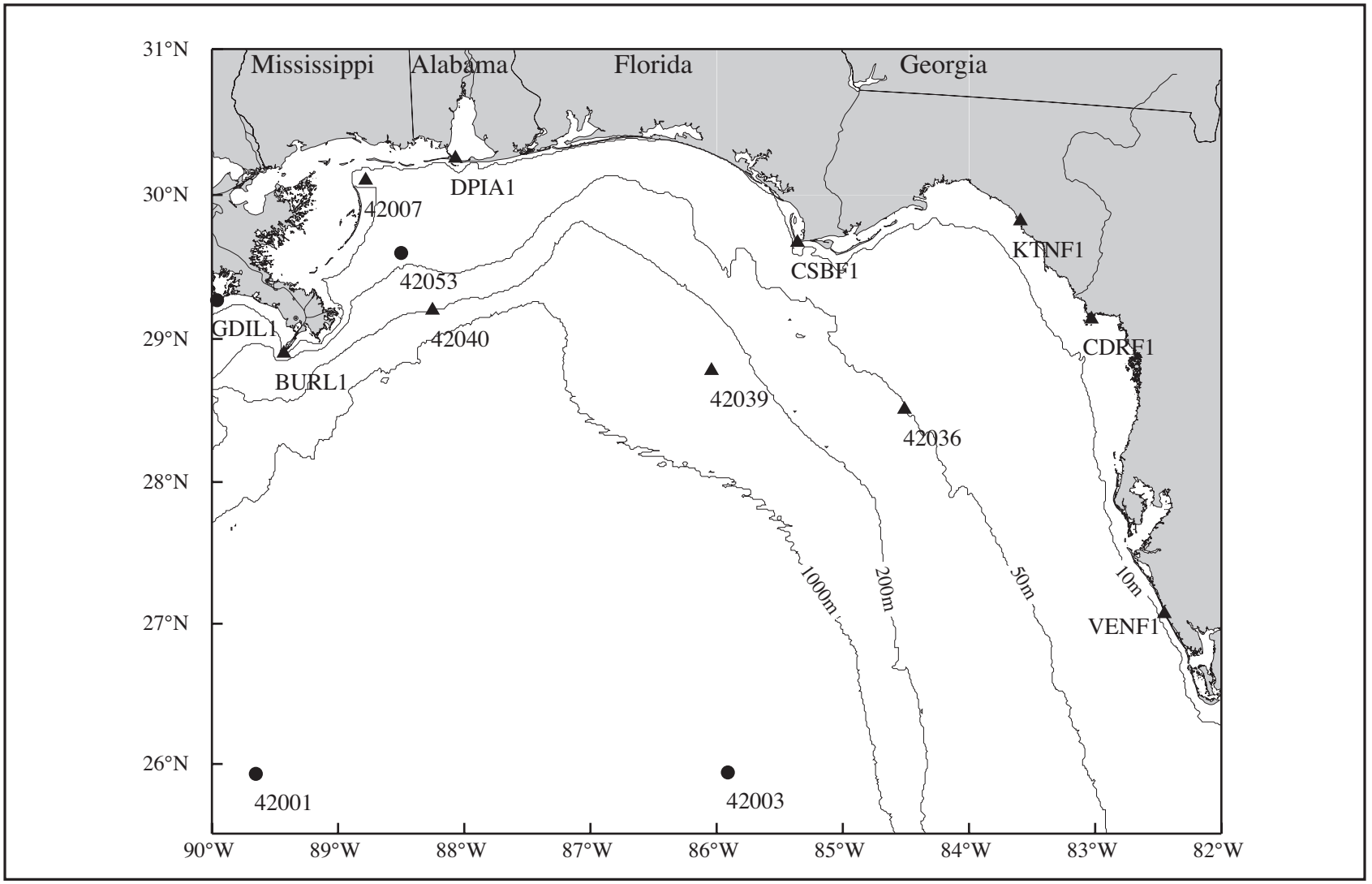

Figure 3.2.1-1. Locations of surface meteorological stations in the NEGOM region. Triangles denote wind component time series stations in Figures 3.2.1-2 through 3.2.1-5. Except for buoy 42053, all stations were used for computation of the gridded wind field.

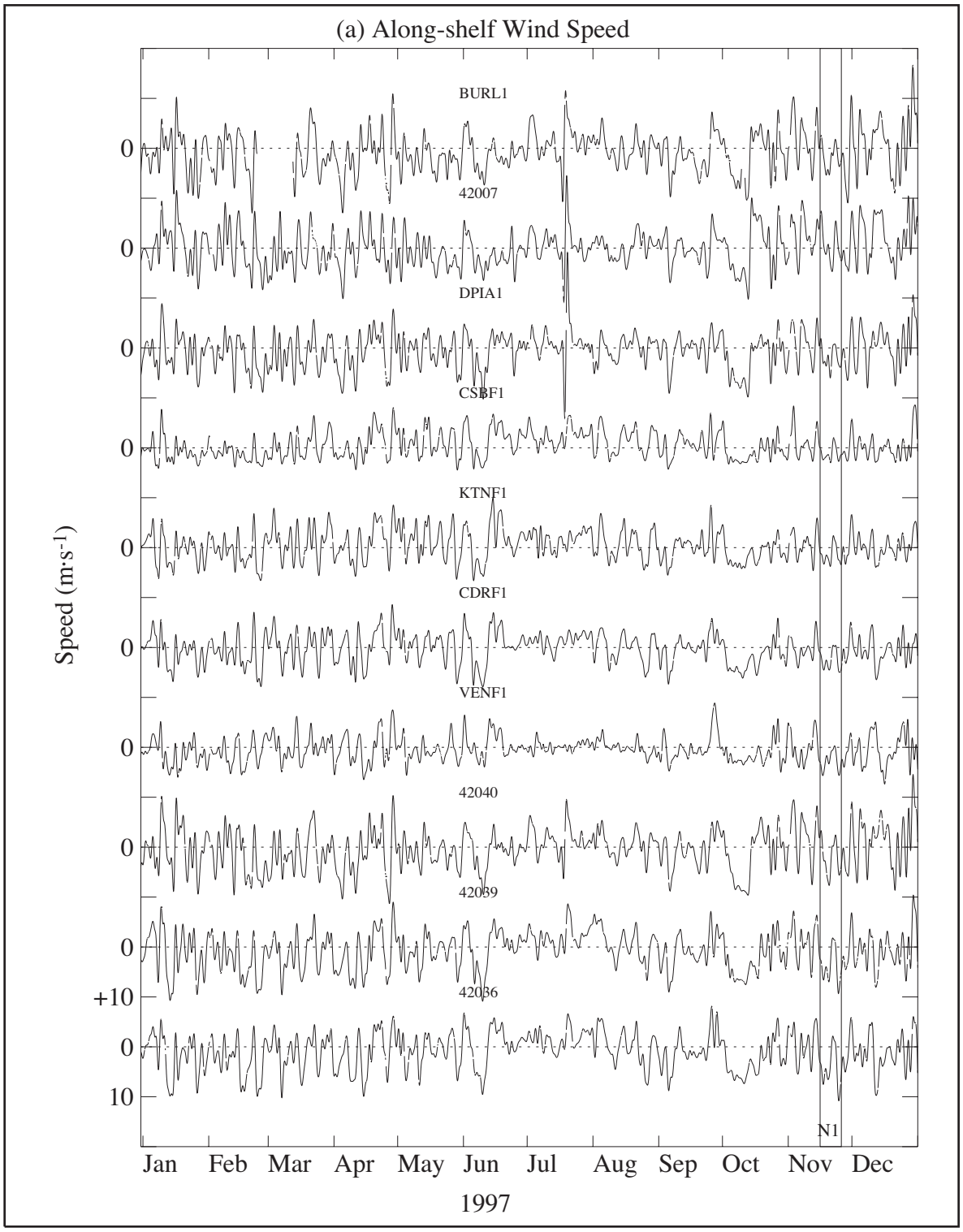

Figure 3.2.1-2. Along-shelf (a) and cross-shelf (b) wind components for 1997.

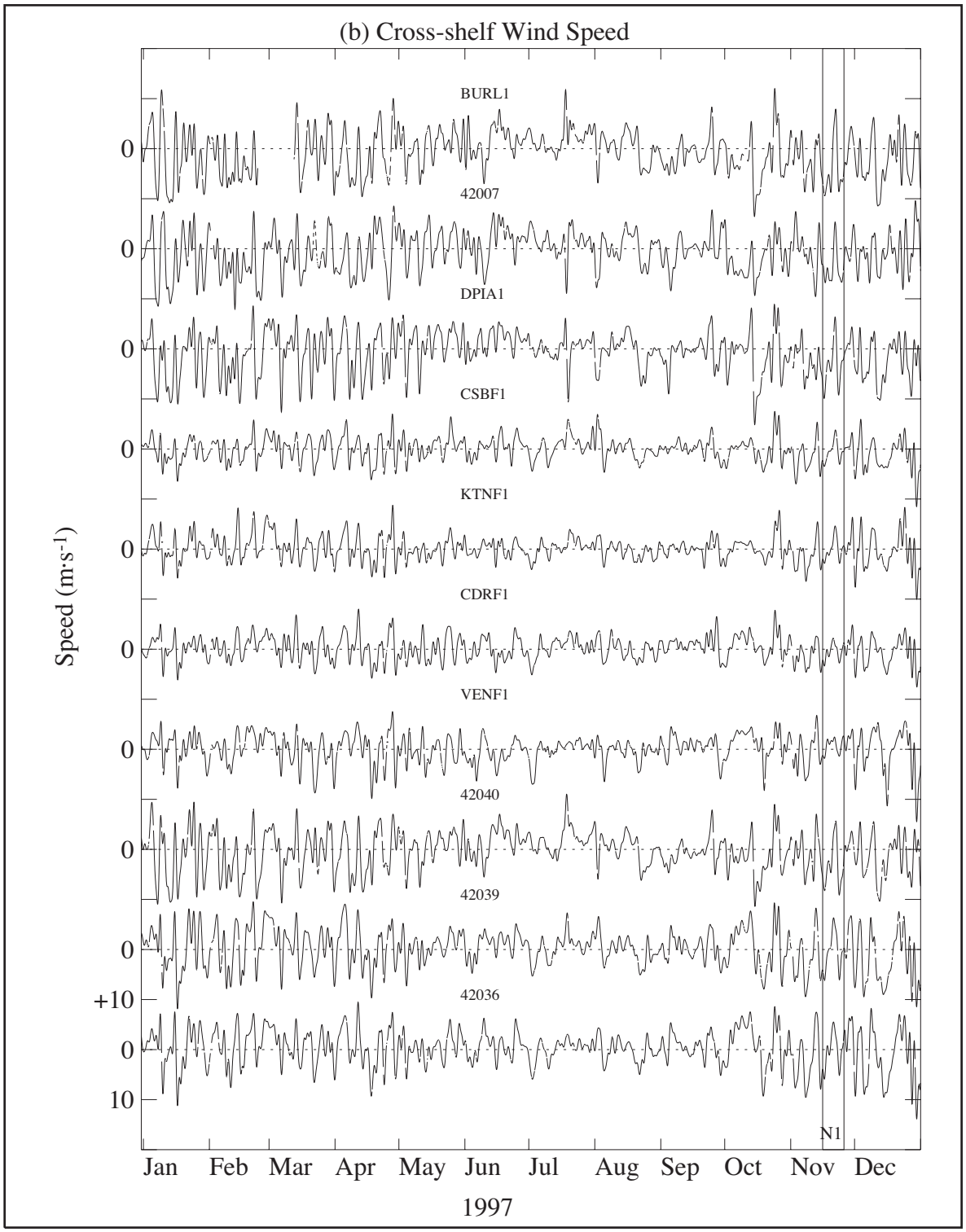

Figure 3.2.1-2. Along-shelf (a) and cross-shelf (b) wind components for 1997. (continued)

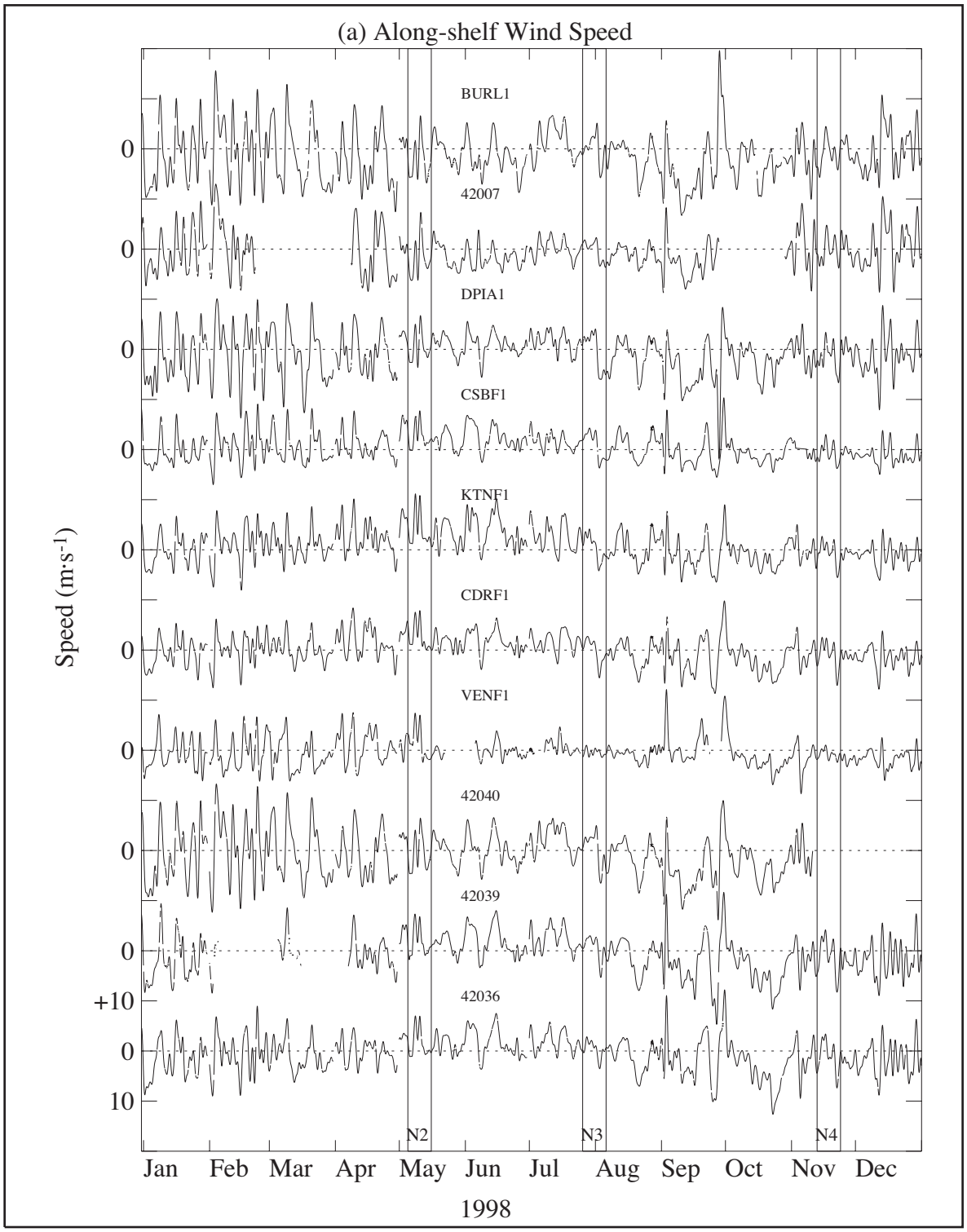

Figure 3.2.1-3. Along-shelf (a) and cross-shelf (b) wind components for 1998.

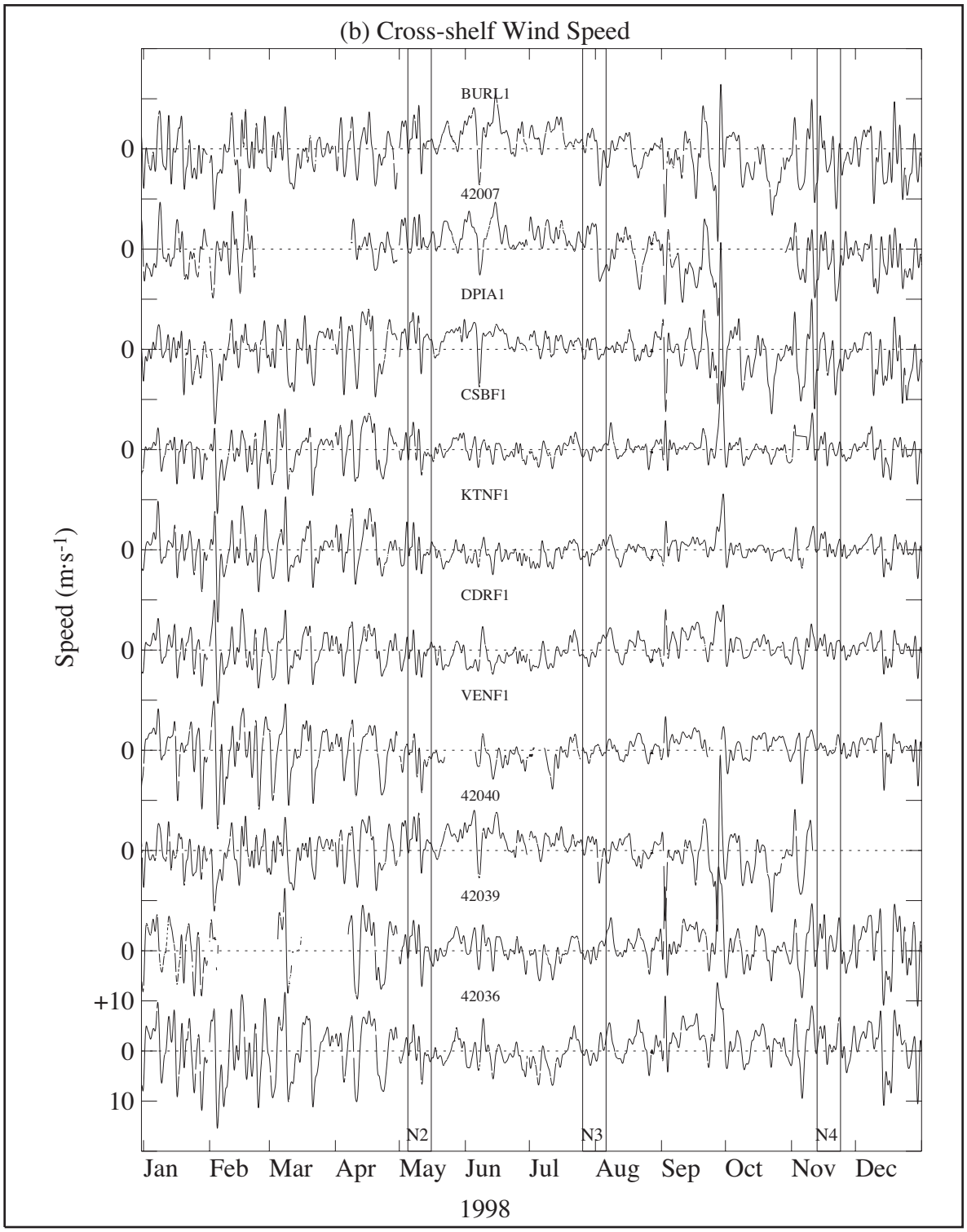

Figure 3.2.1-3. Along-shelf (a) and cross-shelf (b) wind components for 1998. (continued)

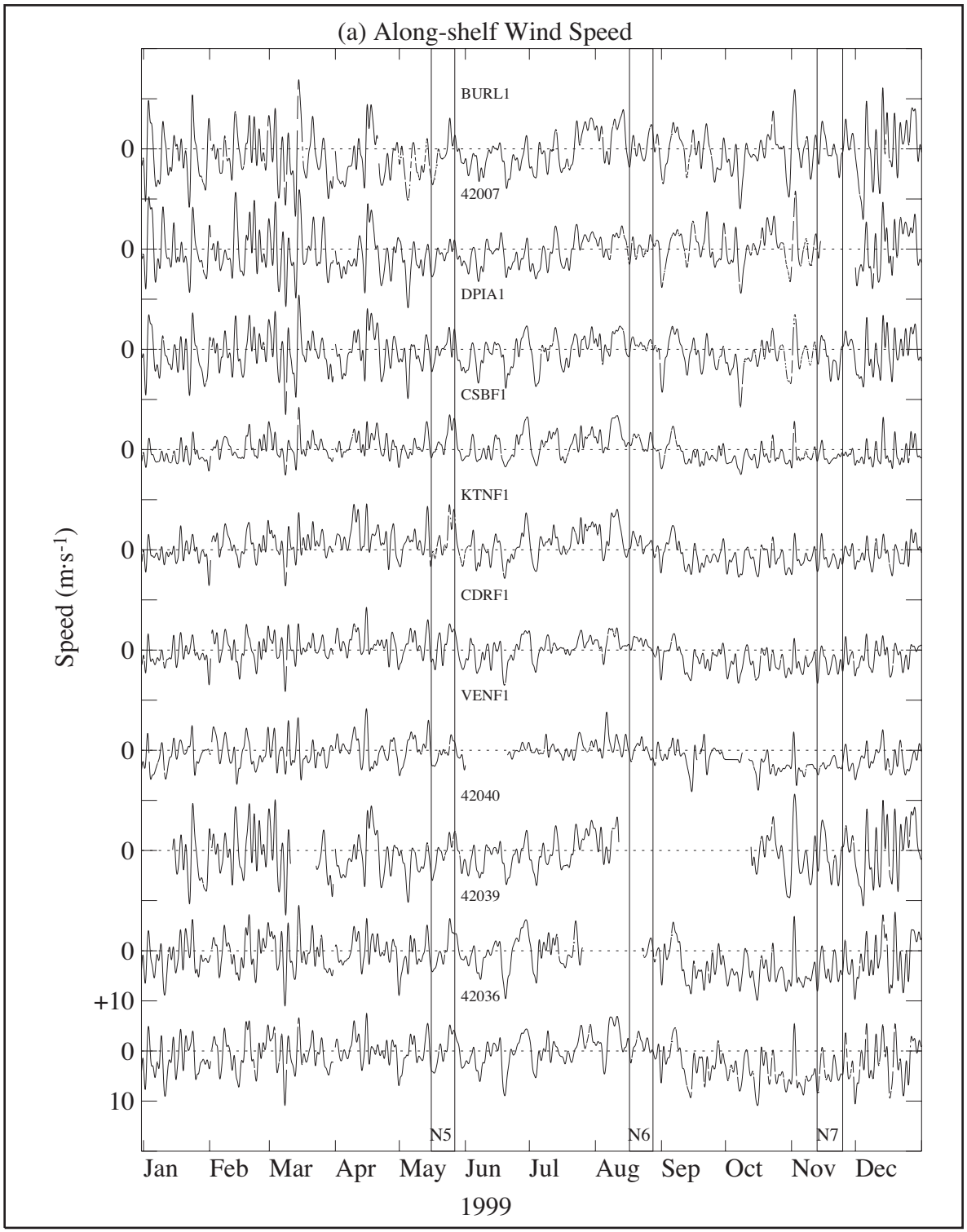

Figure 3.2.1-4. Along-shelf (a) and cross-shelf (b) wind components for 1999.

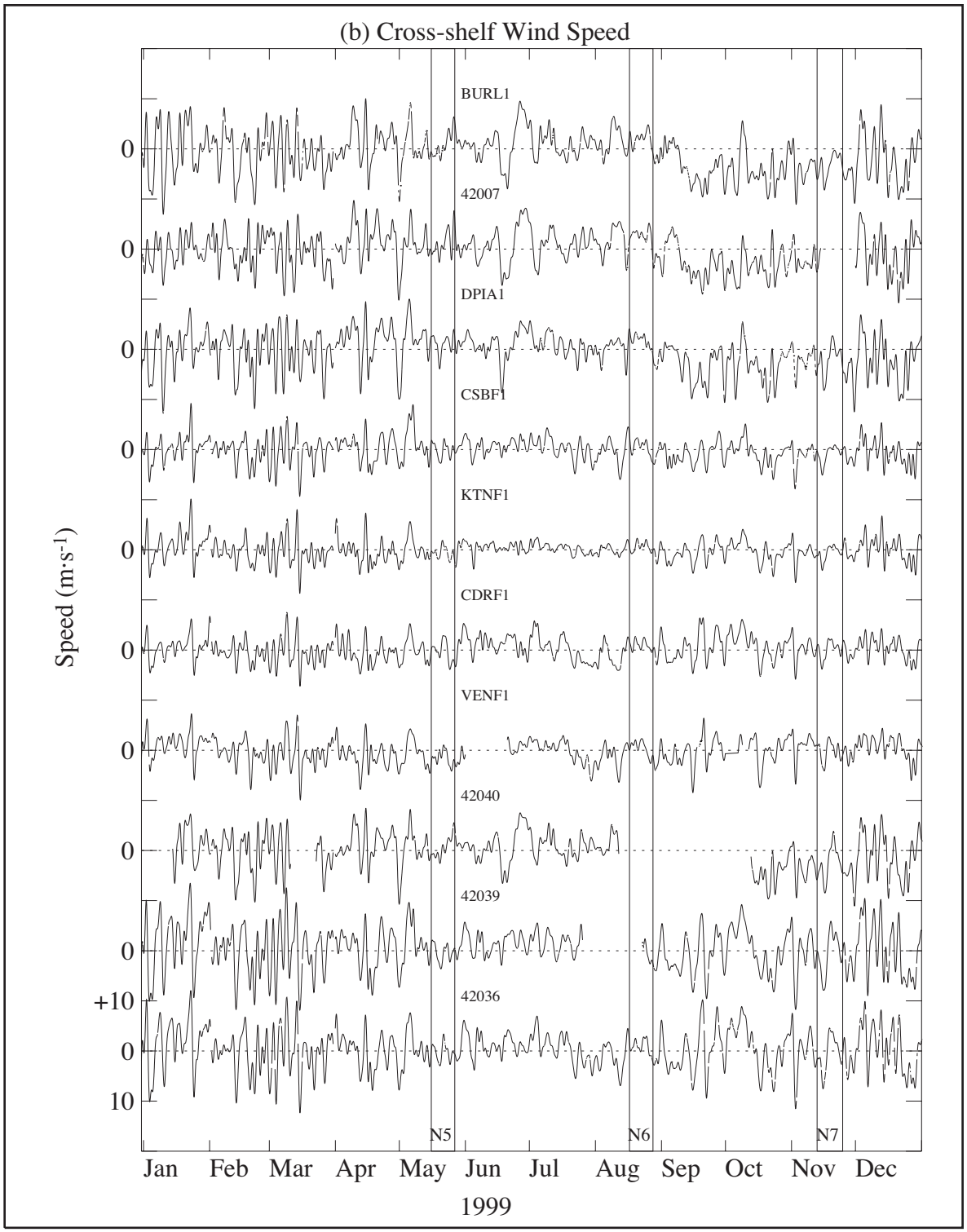

Figure 3.2.1-4. Along-shelf (a) and cross-shelf (b) wind components for 1999. (continued)

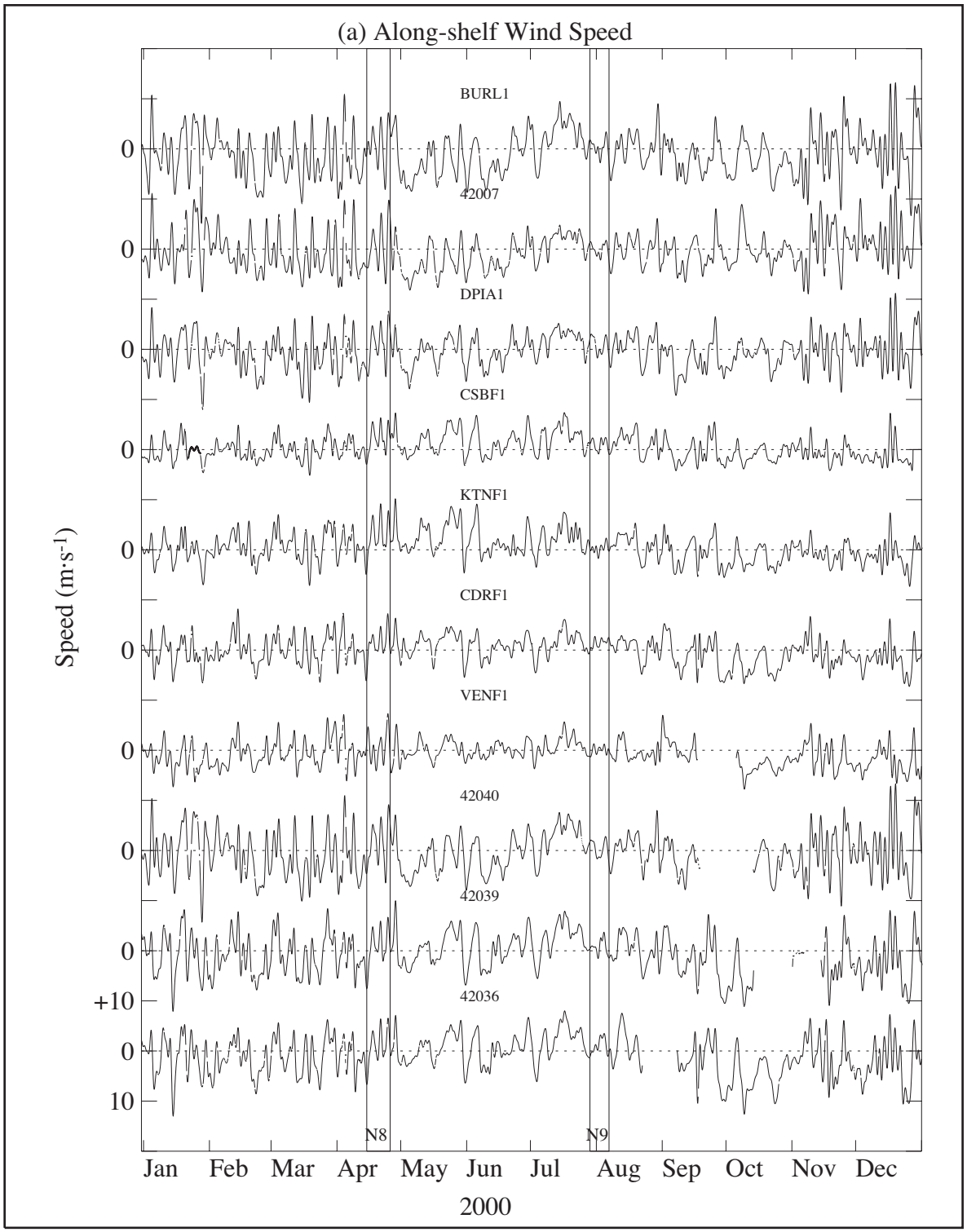

Figure 3.2.1-5. Along-shelf (a) and cross-shelf (b) wind components for 2000.

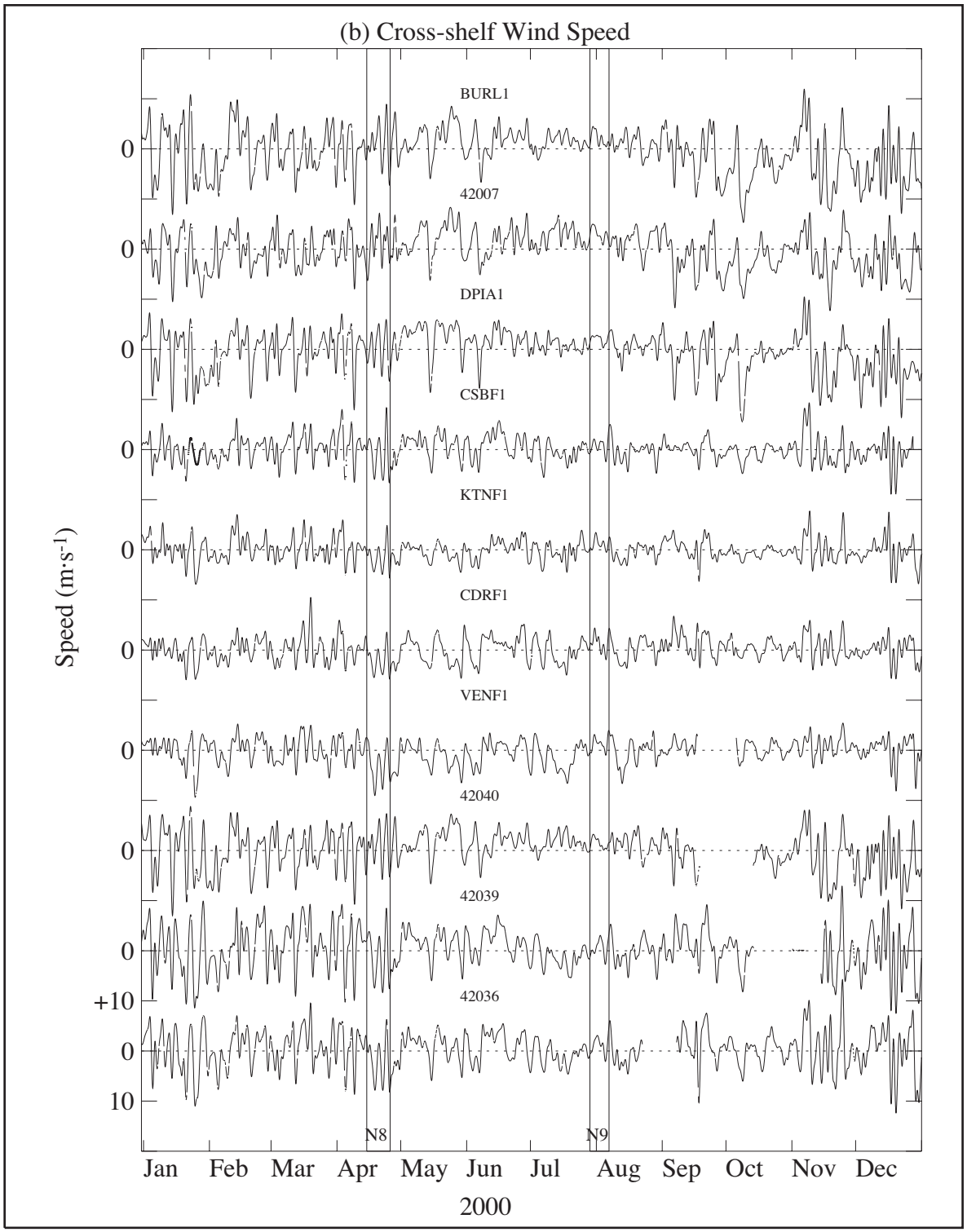

Figure 3.2.1-5. Along-shelf (a) and cross-shelf (b) wind components for 2000. (continued)

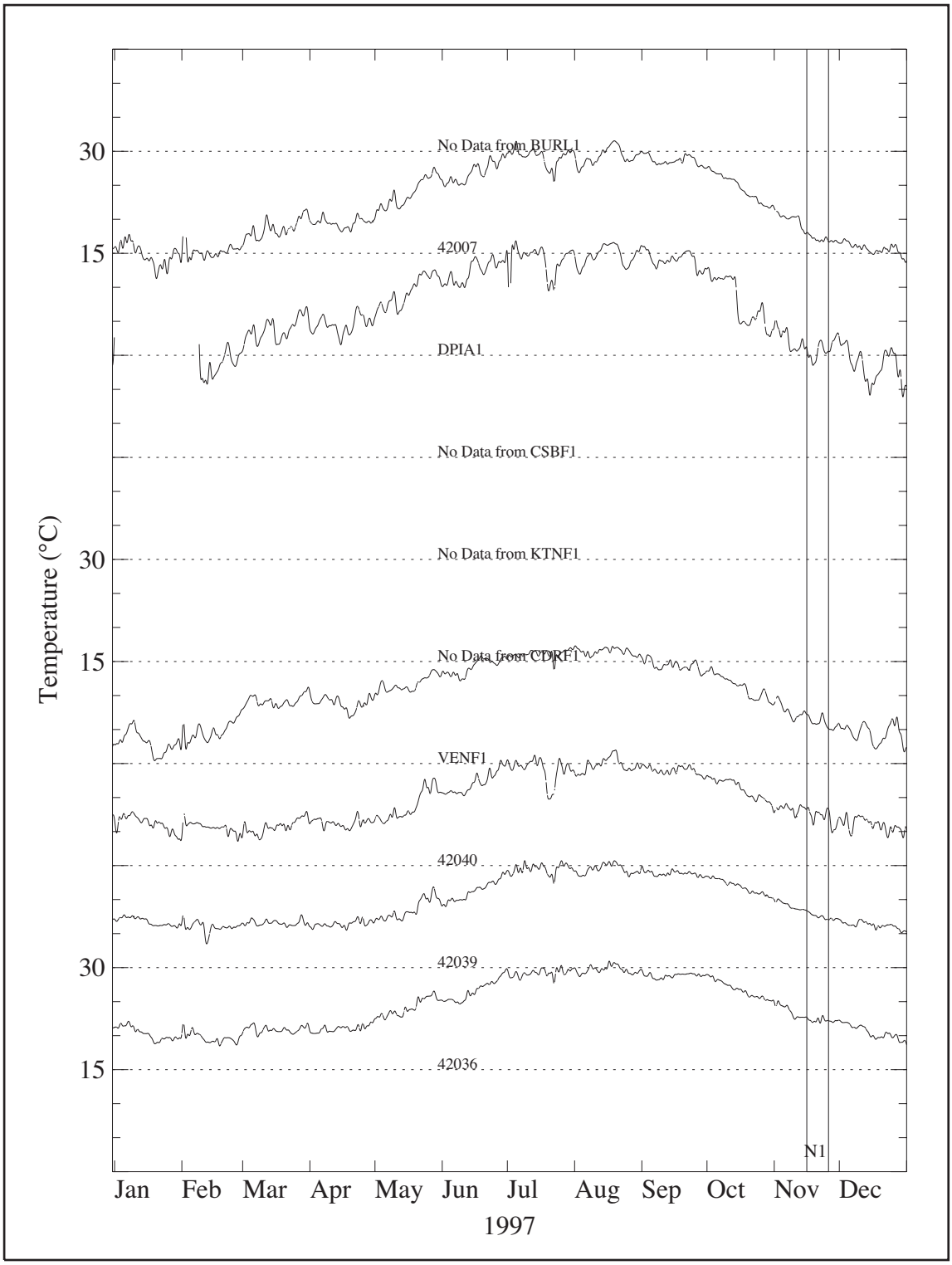

Figure 3.2.2-1. Near-surface 40-hr low-pass water temperature for NDBC stations in the NEGOM region in 1997. The baseline (dashed) for each record starts at 15°C.

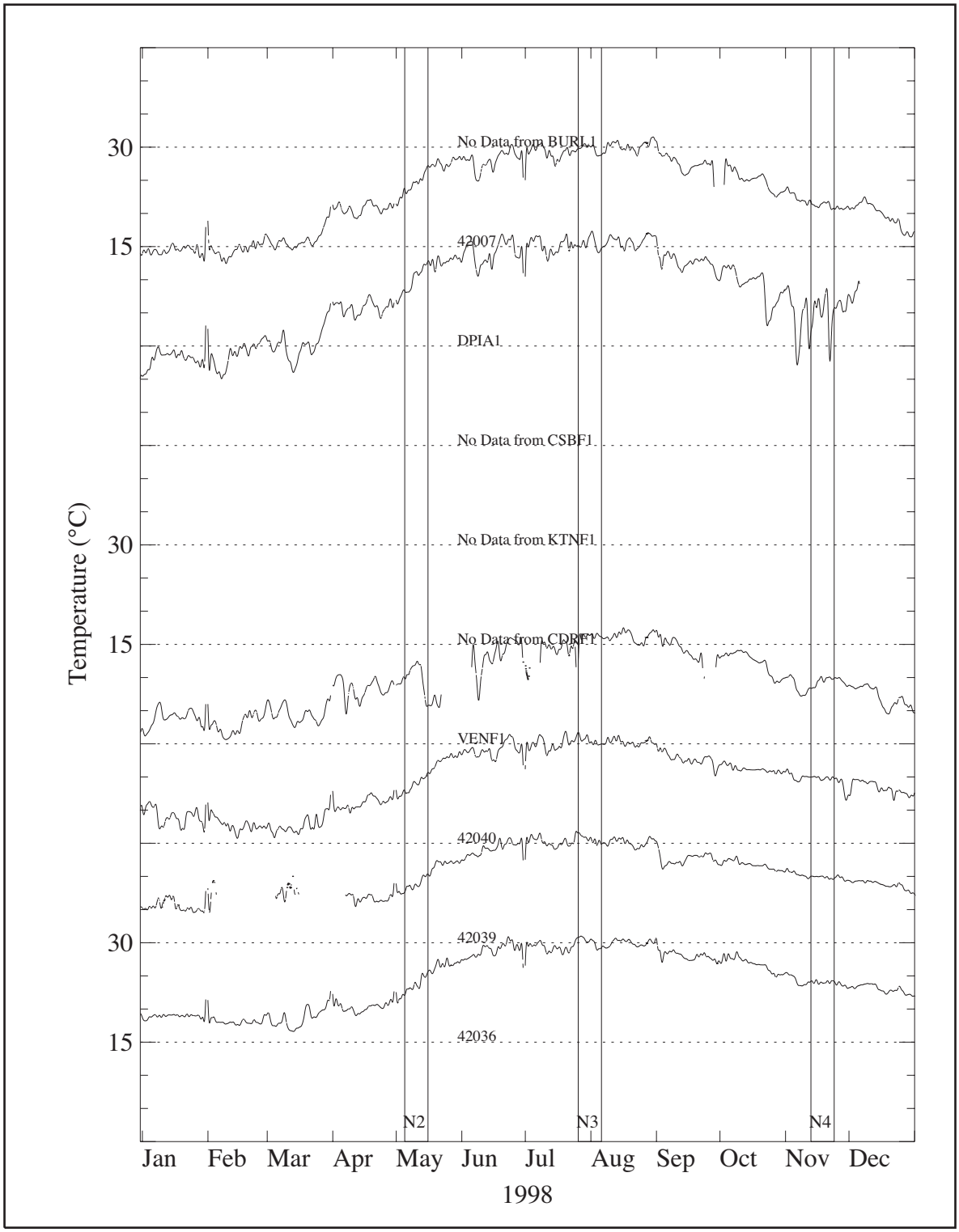

Figure 3.2.2-2. Near-surface 40-hr low-pass water temperature for NDBC stations in the NEGOM region in 1998. The baseline (dashed) for each record starts at 15°C.

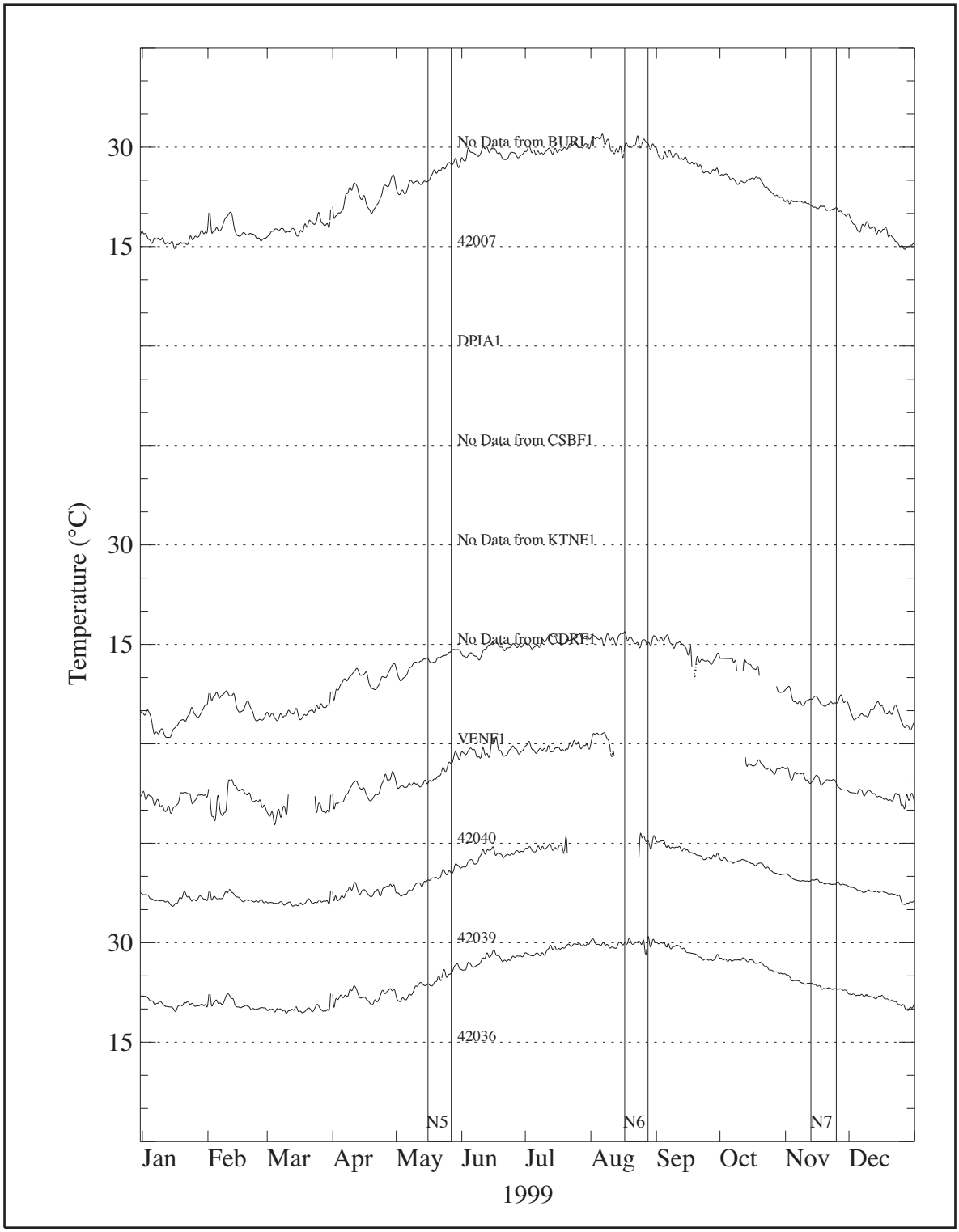

Figure 3.2.2-3. Near-surface 40-hr low-pass water temperature for NDBC stations in the NEGOM region in 1999. The baseline (dashed) for each record starts at 15°C.

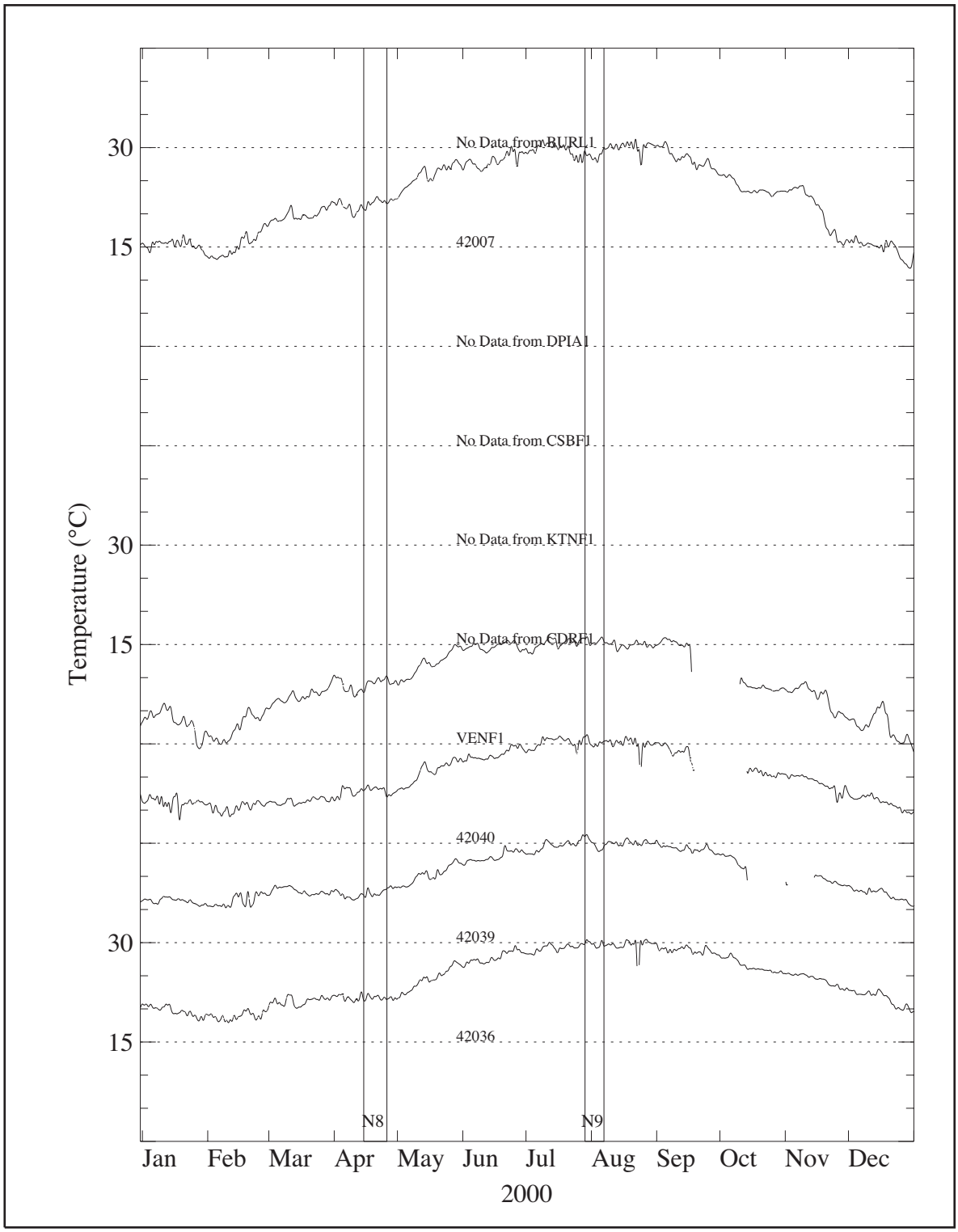

Figure 3.2.2-4. Near-surface 40-hr low-pass water temperature for NDBC stations in the NEGOM region in 2000. The baseline (dashed) for each record starts at 15°C.

3.2.3 Sea Surface Height Fields

Sea surface topography derived from satellite altimeter data can be a valuable tool for interpretation of the off-shelf forcing functions from mesoscale eddies and similar features (e.g., see Jochens 1997). Weekly distributions of sea surface height (SSH) for the Gulf of Mexico north of 25°N and east of 90°W are presented in the figures of this section for the period of the NEGOM-COH field program.

The SSH fields are based on a product prepared by Dr. Robert Leben of the University of Colorado (CU) using a combination of altimeter data from the TOPEX/Poseidon and ERS-2 satellites with 10-day and 35-day repeat orbits, respectively. Sea surface height anomaly (SSHA) values from the two altimeters are combined by objective analysis to produce SSHA daily fields at the mid-point of the cycle using temporal and spatial decorrelation scales of approximately 12 days and 100 km (Sturges and Leben 2000; Hamilton et al. 2000; Lillibridge et al. 1997; Leben et al. 2002). This processing includes the removal of the Ohio State University Mean Sea Level (OSU MSL; Yi 1995). The OSU MSL is an estimate of the geoid plus an unknown mean sea level departure from the geoid due to ocean circulation. An estimate of the mean sea surface height associated with ocean circulation was computed by averaging the sea surface height output of the high-resolution hindcast implementation of the CU Princeton Ocean Model for the period 1993-1999 (see Nowlin et al. 2001 for additional information on the model). The mean departure of the non-geoid portion of the OSU MSL from the mean sea level for the period 1993-1999 can be estimated from the residual obtained by averaging the daily SSHA fields for that period. To obtain a best estimate of the SSH due to ocean circulation for a given day, the residual mean SSHA for 1993-1999 is subtracted from the SSHA for the day of interest and then the model mean sea surface height for 1993-1999 is added to the result.

In this synthesis, near-surface velocity fields prepared from shipboard ADCP measurements, fields of surface geopotential anomaly relative to a subsurface reference, and fields of SSH based on satellite altimetry measurements are compared. Often the comparisons are favorable, but sometimes they are not. We should note and remember that there are various reasons why the comparisons might not be favorable. First, the ADCP-derived fields are based on direct measurements that include not only geostrophic but other current components as well, while the interpretations of surface currents based on SSH or geopotential anomaly fields assume geostrophic flow only. Moreover, the ADCP measurements begin at a subsurface level (perhaps 12-15 m deep), not the surface.

Then, there are the aliasing problems to be considered. Because of the repeat cycles of the altimetric satellites (10 and 35 d) and the spatial and temporal averaging (100 km and 12 d) applied in producing the SSH fields, the SSH fields are not expected to capture accurately fast moving or quite small current features. Moreover, the fact that each cruise took some 8-10 days to complete means that the ADCP-measured currents and the density profiles used for geopotential anomalies are aliased as well. Finally, it should be noted that geopotential anomaly fields are relative to a selected deeper reference level. Their computations require the application of interpolation techniques which, if extended onto the shelf, may result in estimated geostrophic currents with undetermined errors.

Therefore, we have attempted to keep these problems in mind when interpreting surface current fields based on these techniques. When there were differences, we have tried to ascertain why and which representation might be more faithful to reality. A key technique in such determinations is to examine the distributions of observed properties and the timing (order) in which the cruise track (stations) was (were) carried out.

Figures 3.2.3-1 through 3.2.3-38 show one SSH field per week from 1 October 1997 through 23 August 2000. Given the temporal decorrelation scale, one SSH field per week provides the information on the off-shelf eddy forcing conditions necessary for data interpretations. It should be noted that, because of the spatial and temporal smoothing, features may appear weaker than they actually were and small scale features may not be resolved. Contours for regions with water depths less than 200 m have been removed because Jochens (1997) has shown that the correlation between SSHA and geopotential anomaly constructed from in situ data deteriorate with decreasing water depth on the Texas-Louisiana continental shelf.

The SSH fields reveal several general features associated with the off-shelf eddies forcing field. The Loop Current and Loop Current eddies (LCE) generally were located south of 27.5°N and did not directly influence the NEGOM study area. Neither the Loop Current nor an LCE were present in the study area during the cruises. The region most influenced directly by these features was located in the southeast part of the NEGOM study area over the west Florida Slope off Tampa. An example occurred from late February through early April 1998 when LCE Fourchon was breaking off the Loop Current and was adjacent to the shelf edge and slope off Tampa (Figures 3.2.3-5 through 3.2.3-7).

Cyclonic eddies often were located north and/or east of the Loop Current or LCEs (e.g., Figure 3.2.3-1). Some of these influenced the NEGOM slope and shelf edge regions (e.g., Figure 3.2.3-25). Development of small (~100 km diameter) anticyclonic slope features occurred, particularly adjacent to the Mississippi-Alabama shelf over the DeSoto Slope. These anticyclonic features sometimes developed the ring-like characteristic of eddies and intensified when a Loop Current Eddy moved westward and separated from the Loop Current. For example, in fall 1999 an anticyclonic slope eddy, located over the DeSoto Slope, intensified and then weakened as Loop Current Eddy Juggernaut moved westward, after separation from the Loop Current, and then out of the eastern Gulf (Figures 3.2.3-29 and 3.2.3-31; in Figure 3.2.3-29a, Juggernaut is the feature with center about 89.5°W 26°N and the Loop Current is the feature with center about 86°W south of 25°N). Details on the SSH fields associated with each NEGOM cruise are provided in the sections describing those cruises.

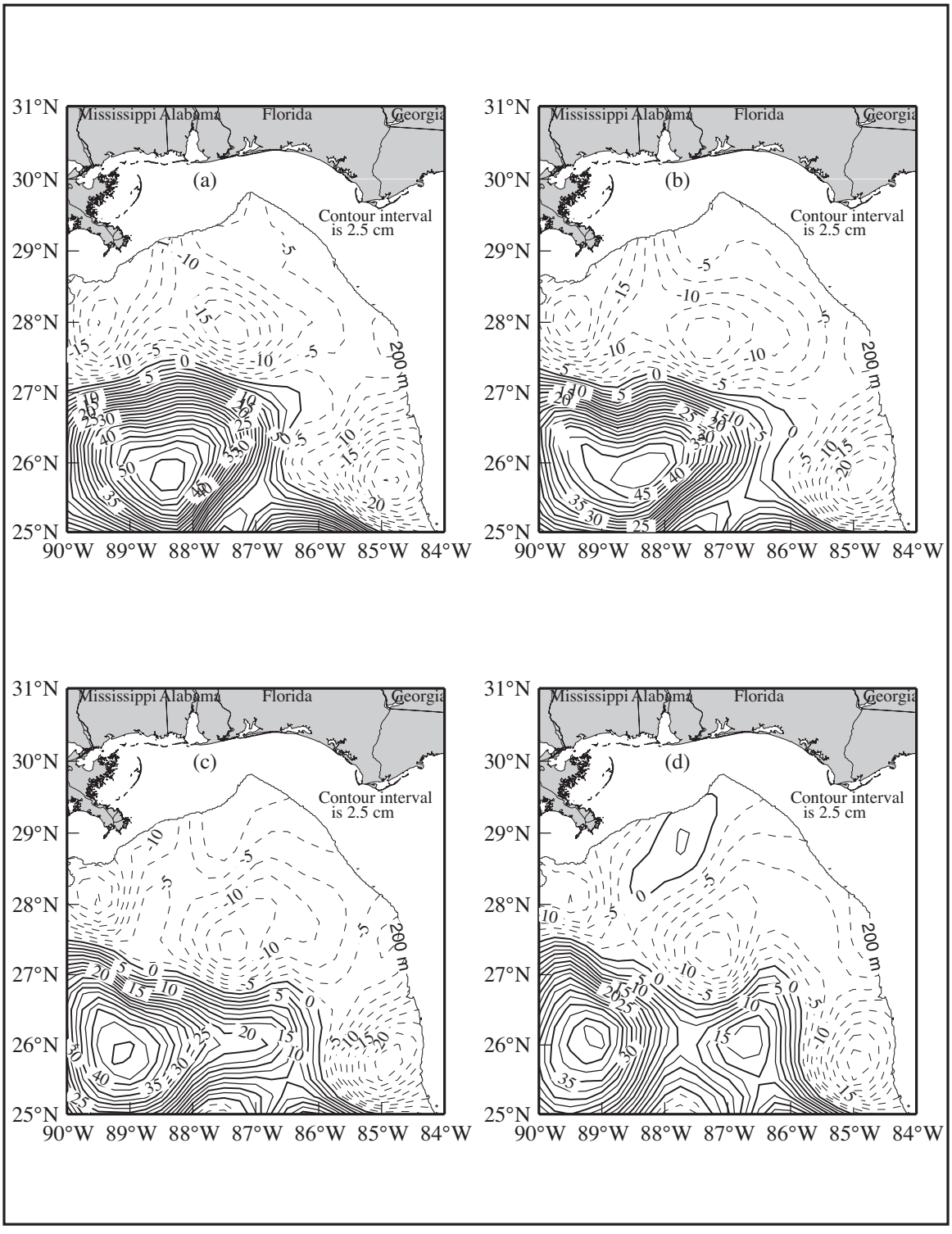

Figure 3.2.3-1. Sea surface height from satellite altimeter data for (a) 1 October 1997, (b) 8 October 1997, (c) 15 October 1997, and (d) 22 October 1997.

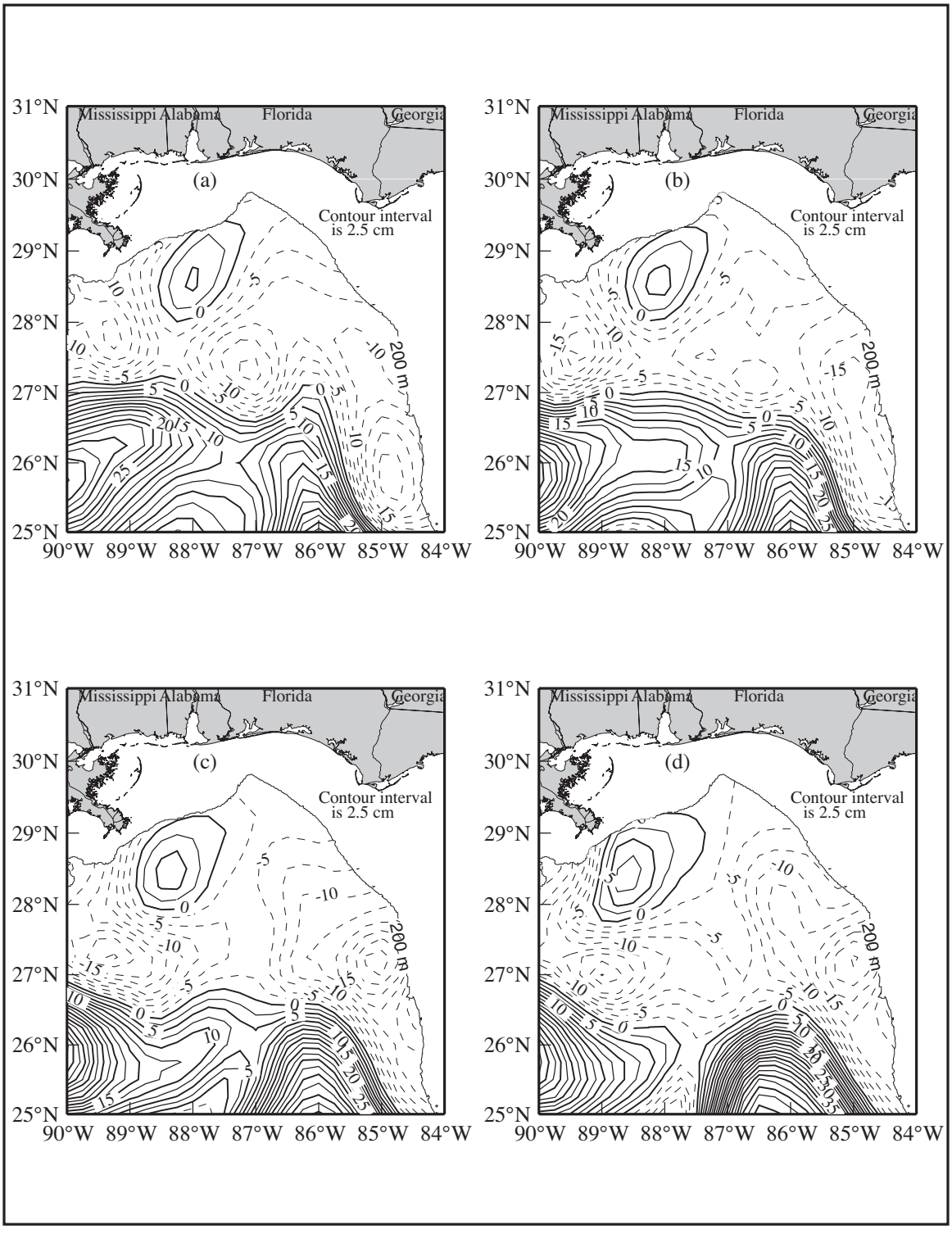

Figure 3.2.3-2. Sea surface height from satellite altimeter data for (a) 29 October 1997, (b) 5 November 1997, (c) 12 November 1997, and (d) 19 November 1997.

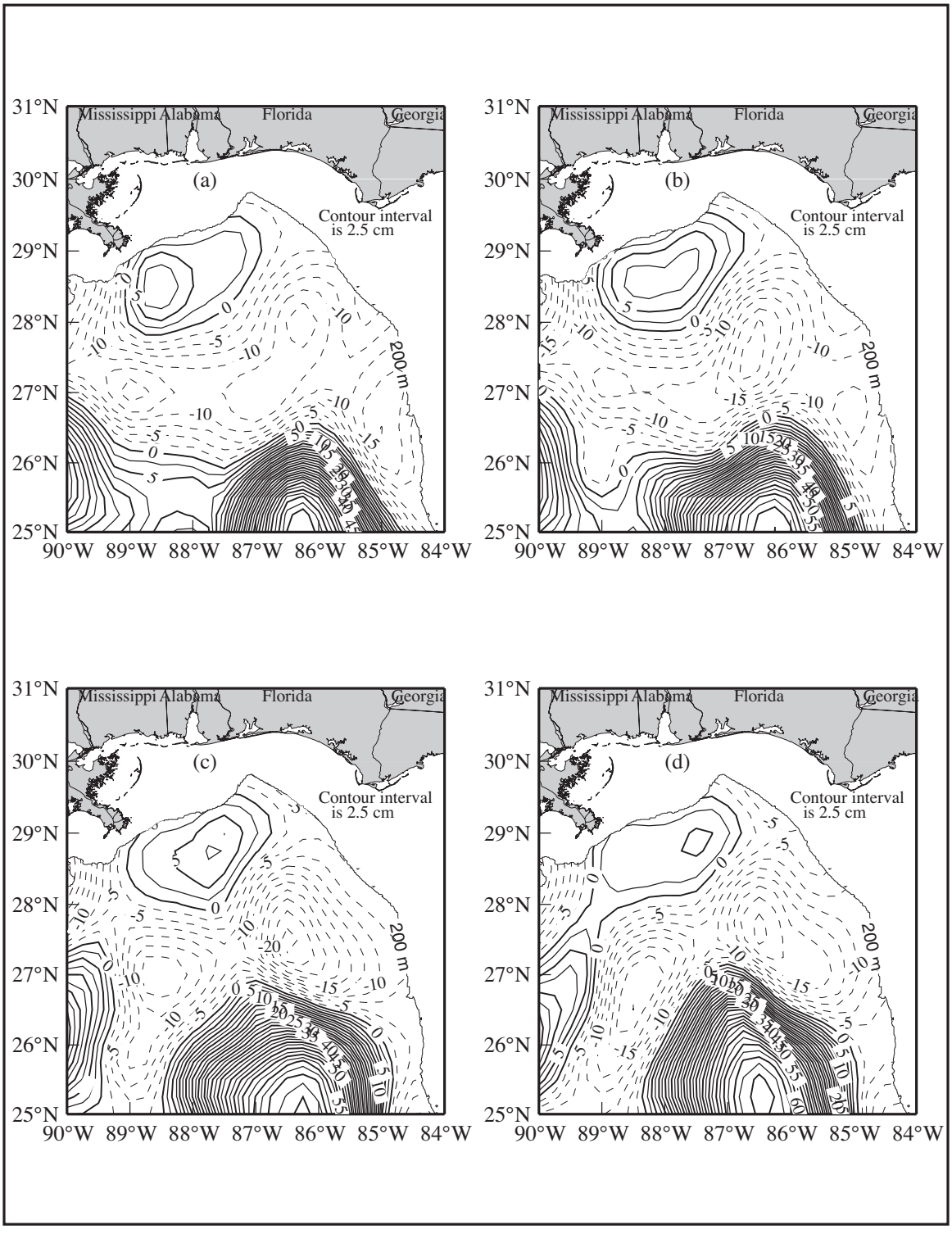

Figure 3.2.3-3. Sea surface height from satellite altimeter data for (a) 26 November 1997, (b) 3 December 1997, (c) 10 December 1997, and (d) 17 December 1997.

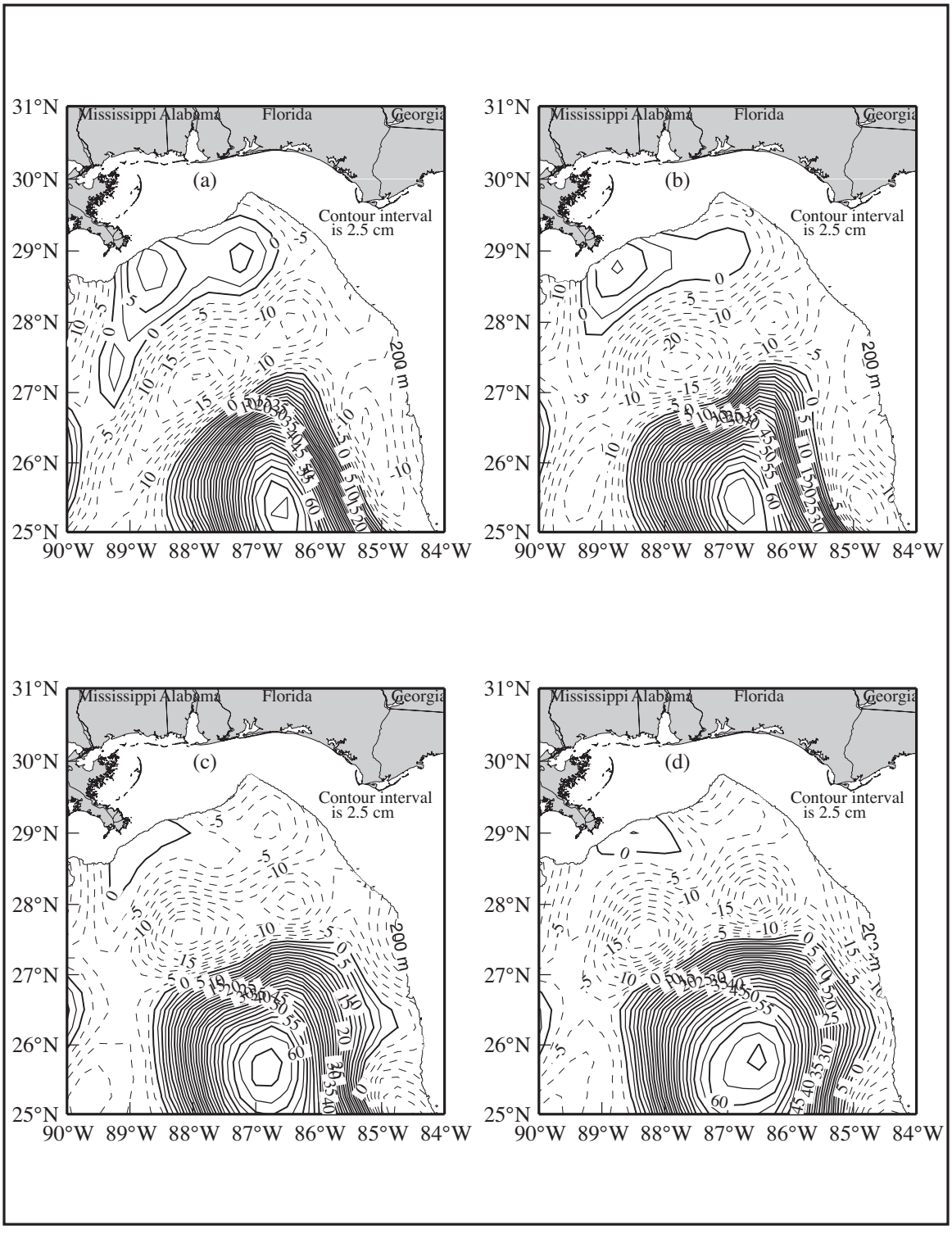

Figure 3.2.3-4. Sea surface height from satellite altimeter data for (a) 24 December 1997, (b) 31 December 1997, (c) 7 January 1998, and (d) 14 January 1998.

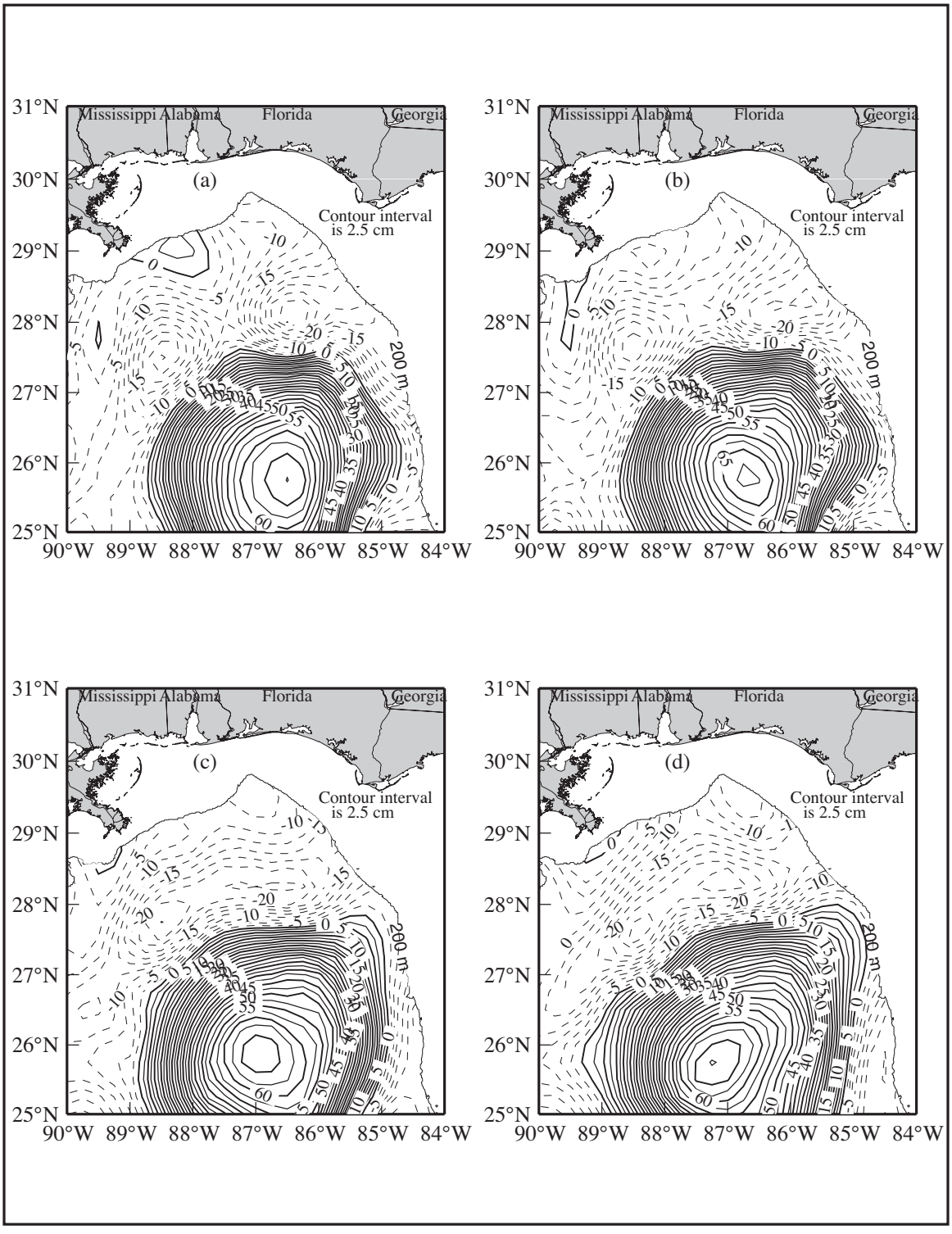

Figure 3.2.3-5. Sea surface height from satellite altimeter data for (a) 21 January 1998, (b) 28 January 1998, (c) 4 February 1998, and (d) 11 February 1998.

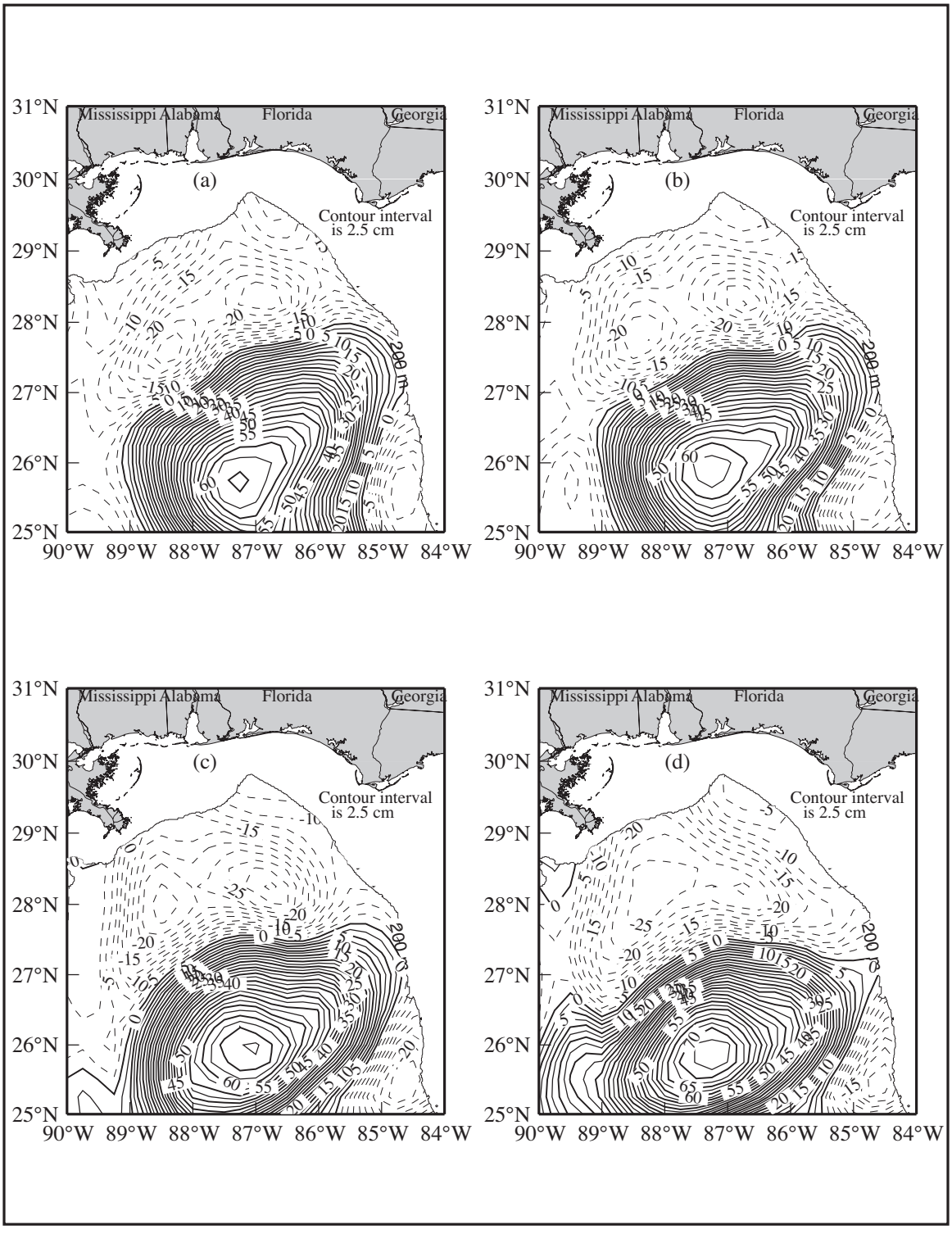

Figure 3.2.3-6. Sea surface height from satellite altimeter data for (a) 18 February 1998, (b) 25 February 1998, (c) 4 March 1998, and (d) 11 March 1998.

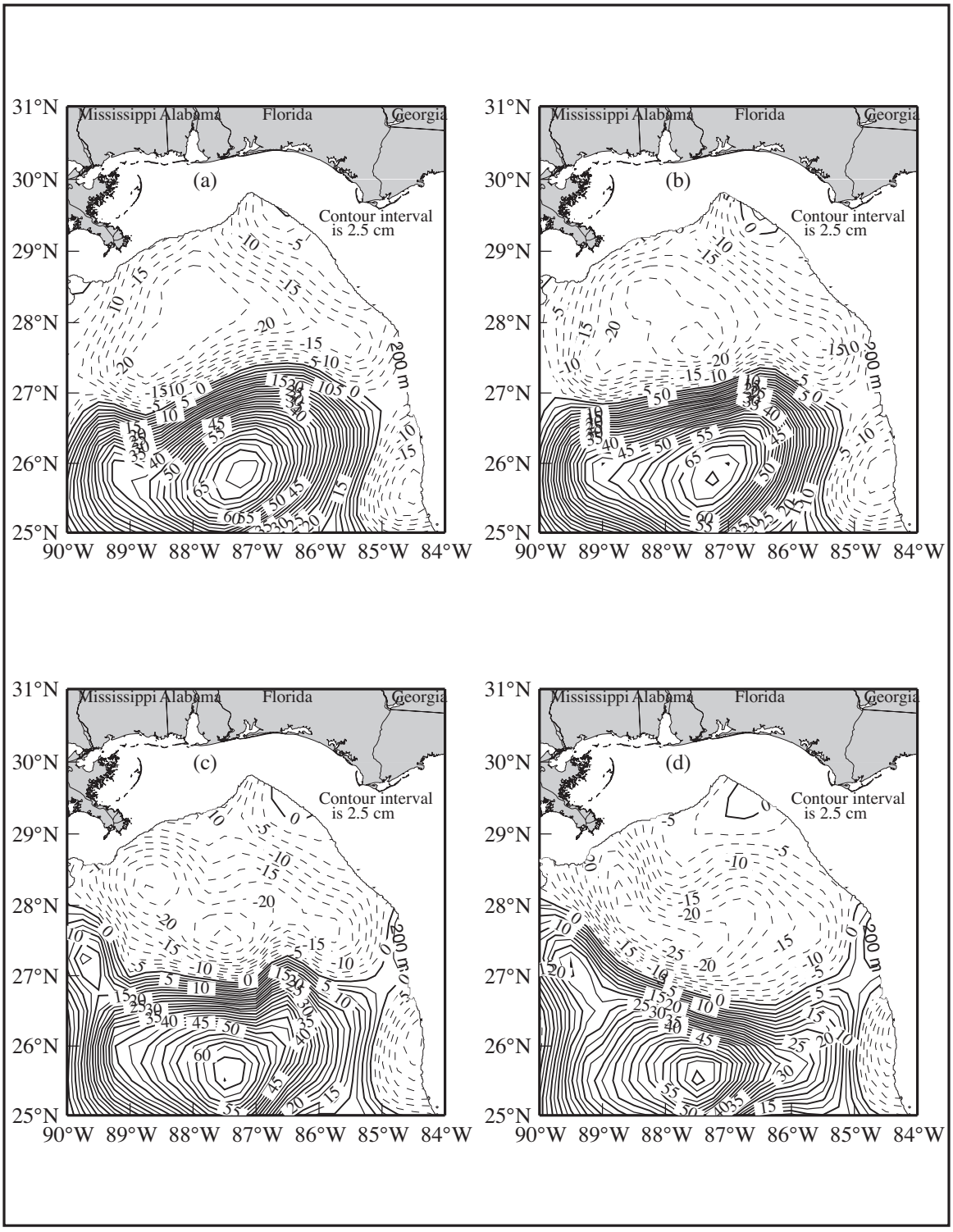

Figure 3.2.3-7. Sea surface height from satellite altimeter data for (a) 18 March 1998, (b) 25 March 1998, (c) 1 April 1998, and (d) 8 April 1998.

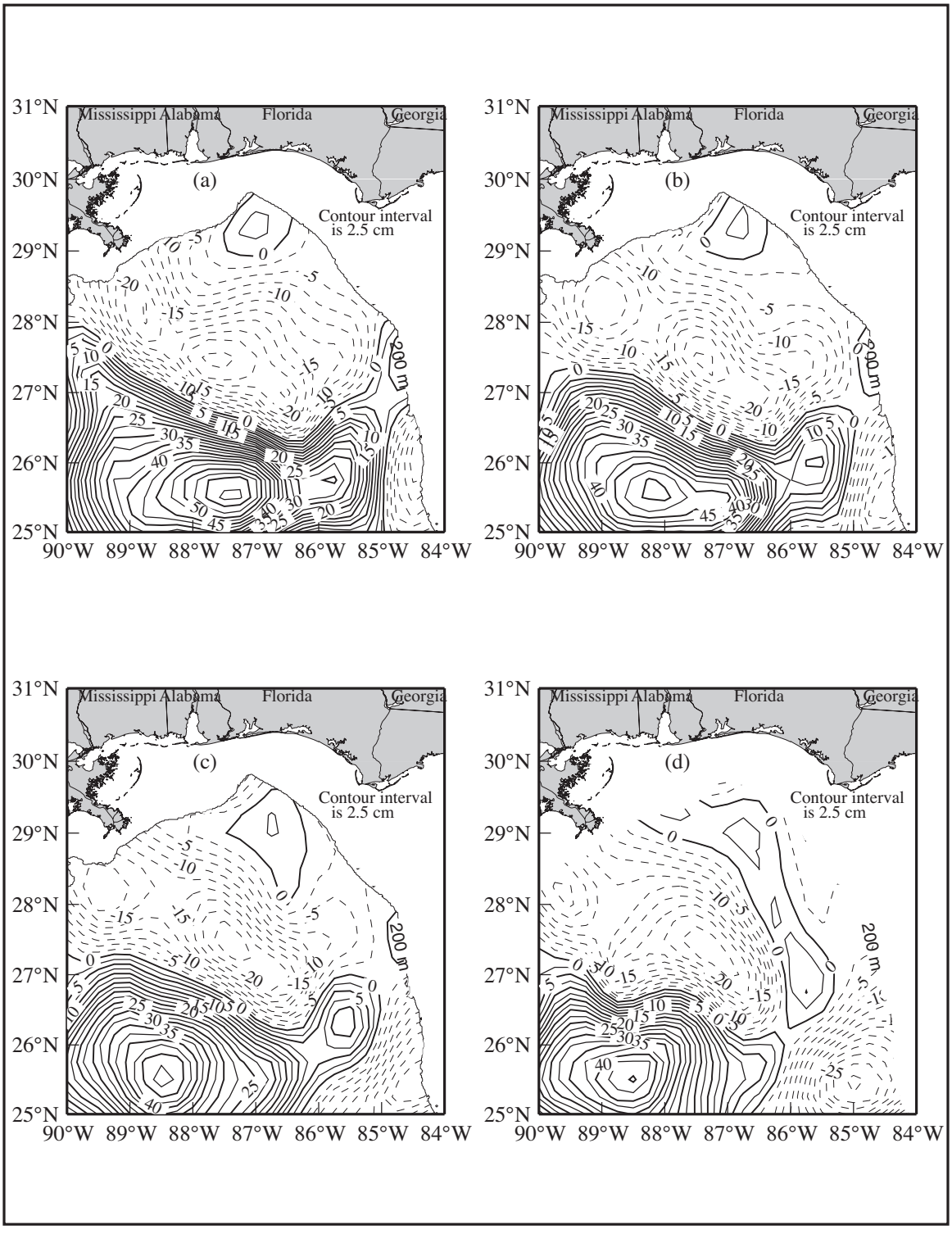

Figure 3.2.3-8. Sea surface height from satellite altimeter data for (a) 15 April 1998, (b) 22 April 1998, (c) 29 April 1998, and (d) 6 May 1998.

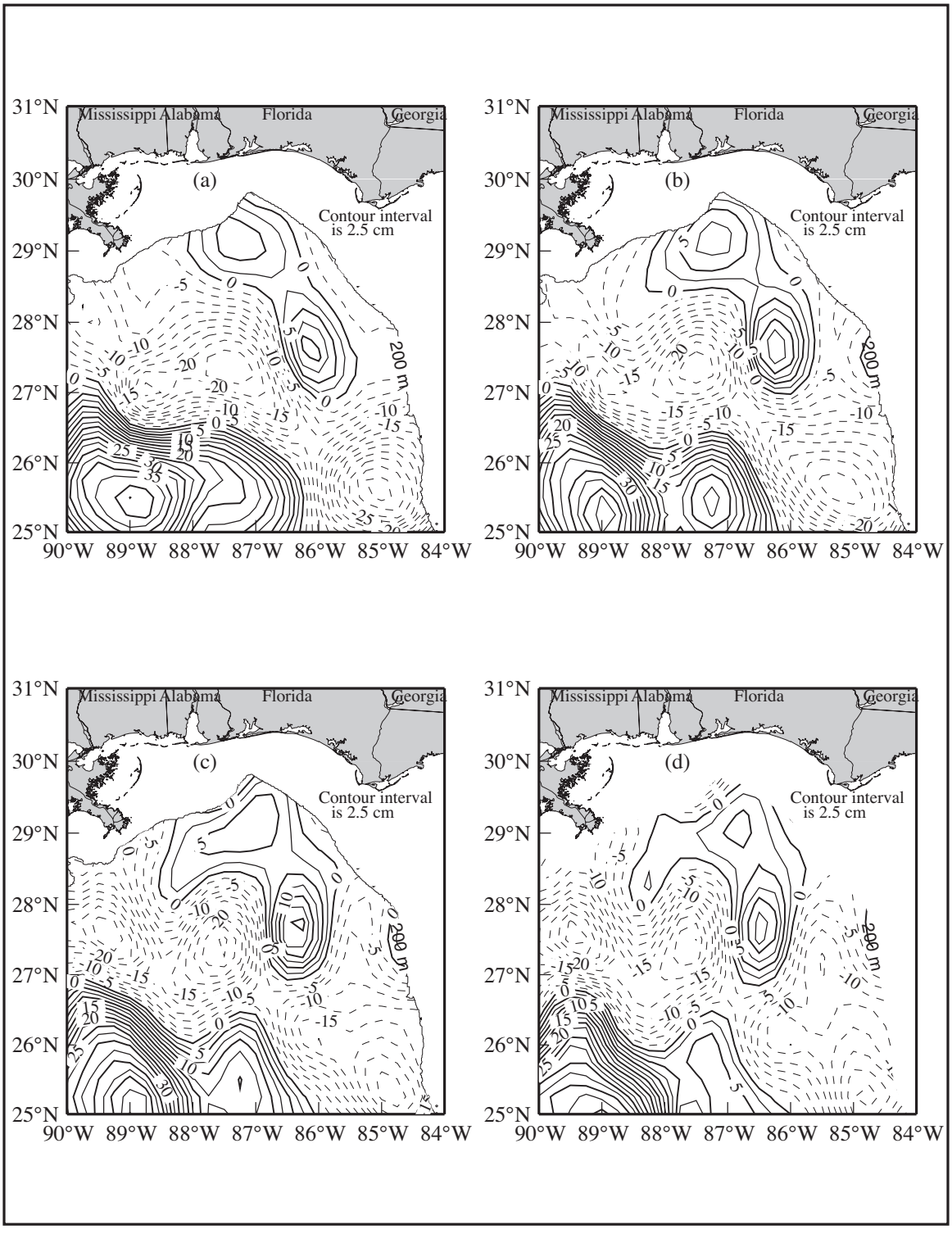

Figure 3.2.3-9. Sea surface height from satellite altimeter data for (a) 13 May 1998, (b) 20 May 1998, (c) 27 May 1998, and (d) 3 June 1998.

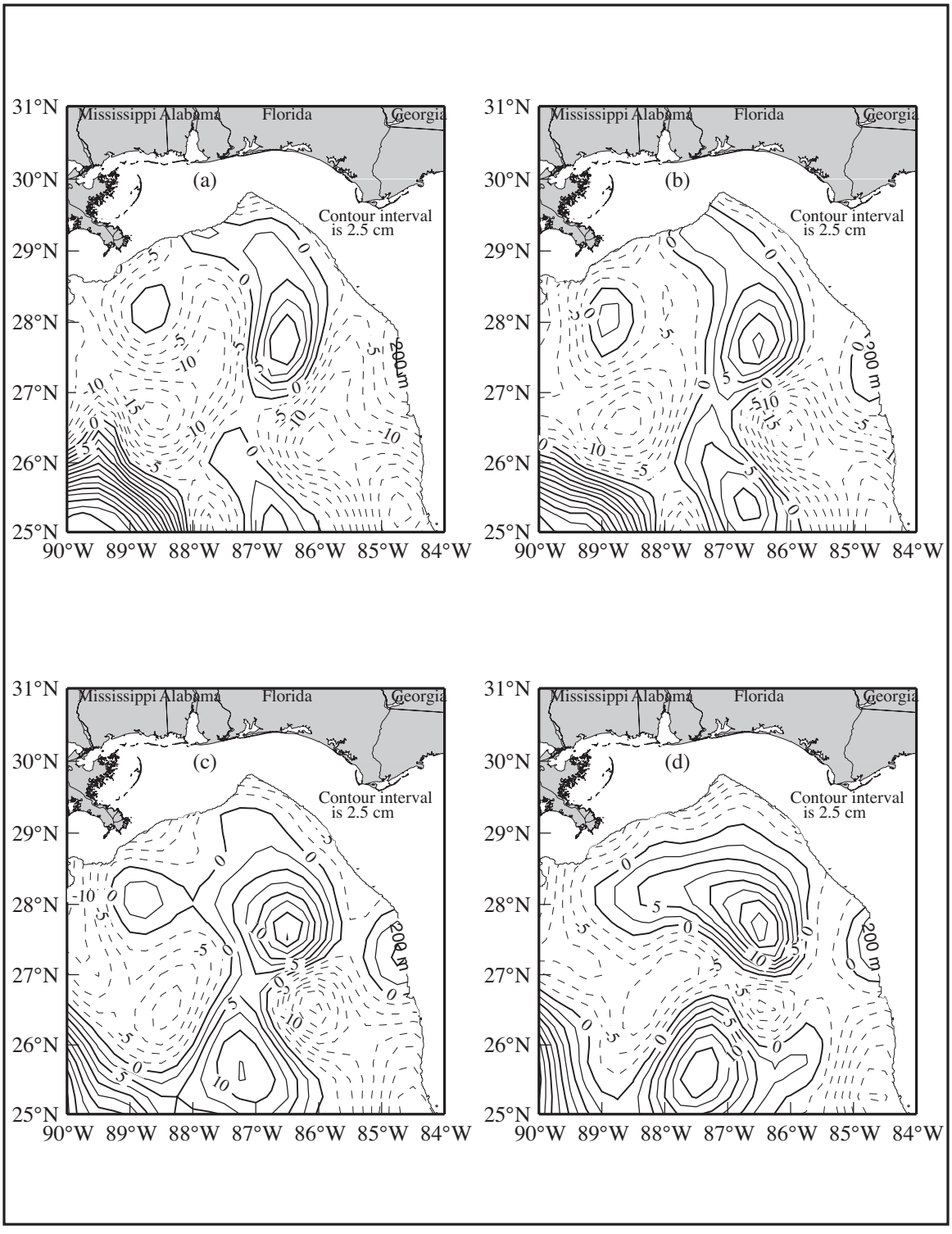

Figure 3.2.3-10. Sea surface height from satellite altimeter data for (a) 10 June 1998, (b) 17 June 1998, (c) 24 June 1998, and (d) 1 July 1998.

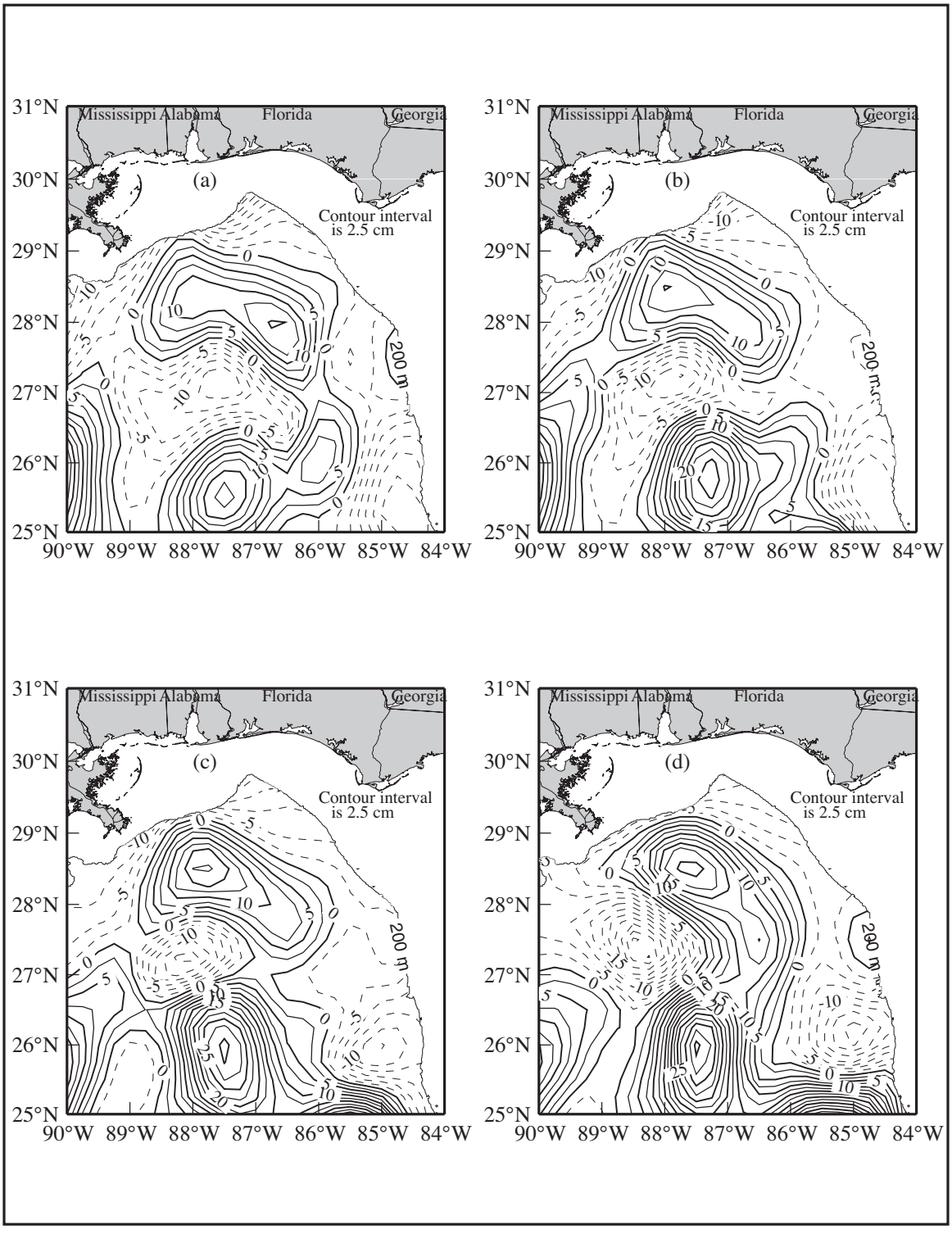

Figure 3.2.3-11. Sea surface height from satellite altimeter data for (a) 8 July 1998, (b) 15 July 1998, (c) 22 July 1998, and (d) 29 July 1998.

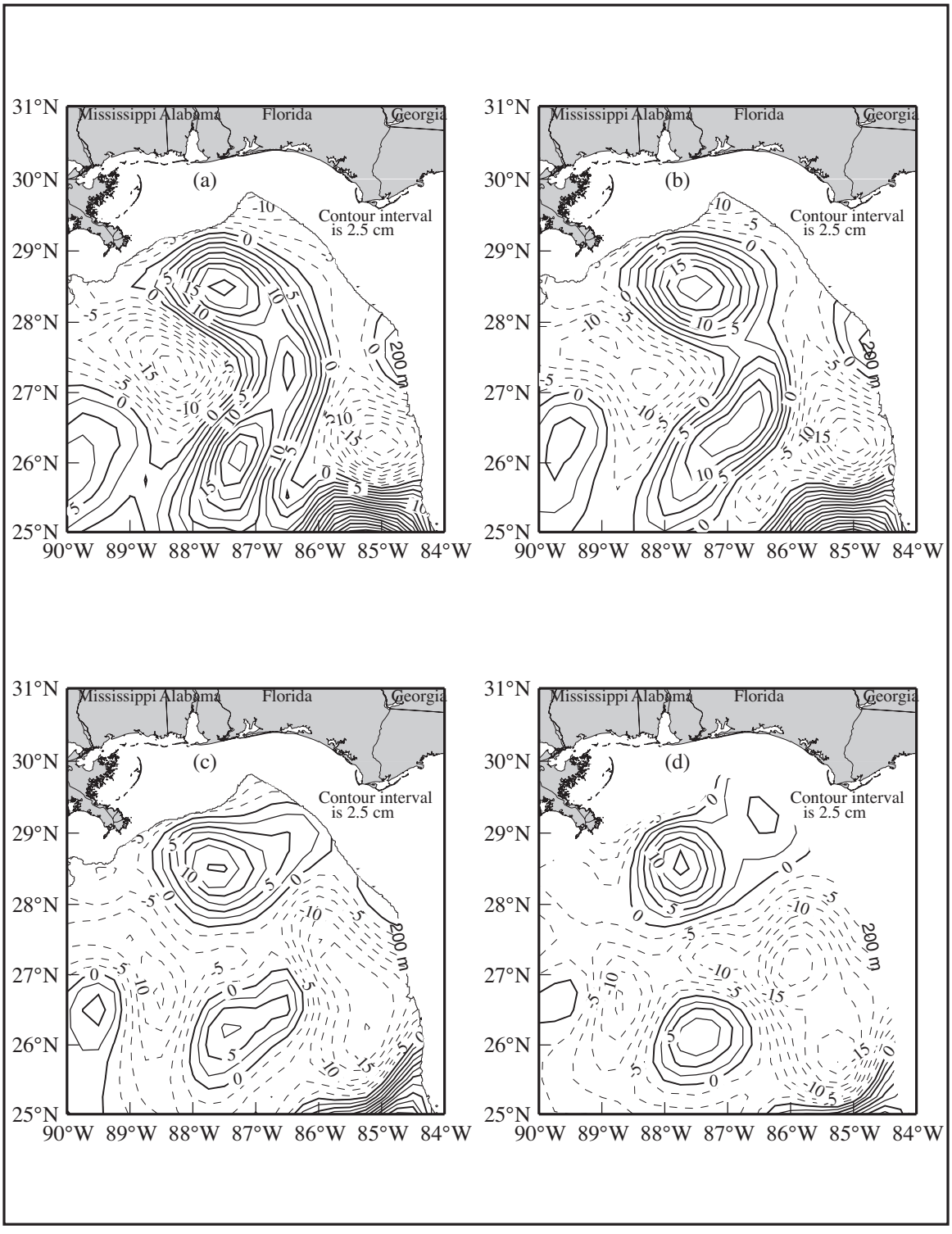

Figure 3.2.3-12. Sea surface height from satellite altimeter data for (a) 5 August 1998, (b) 12 August 1998, (c) 19 August 1998, and (d) 26 August 1998.

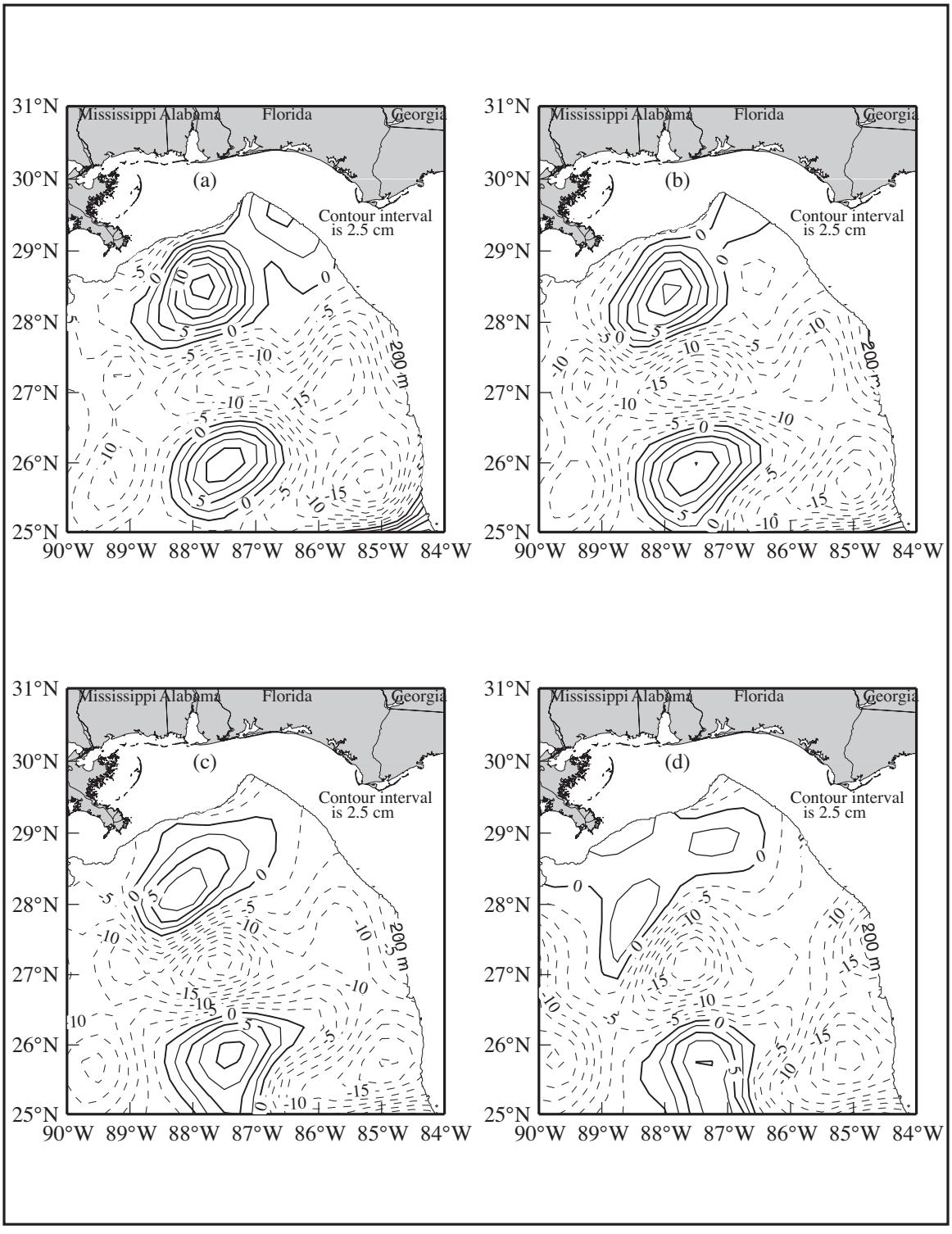

Figure 3.2.3-13. Sea surface height from satellite altimeter data for (a) 2 September 1998, (b) 9 September 1998, (c) 16 Setpember 1998, and (d) 23 September 1998.

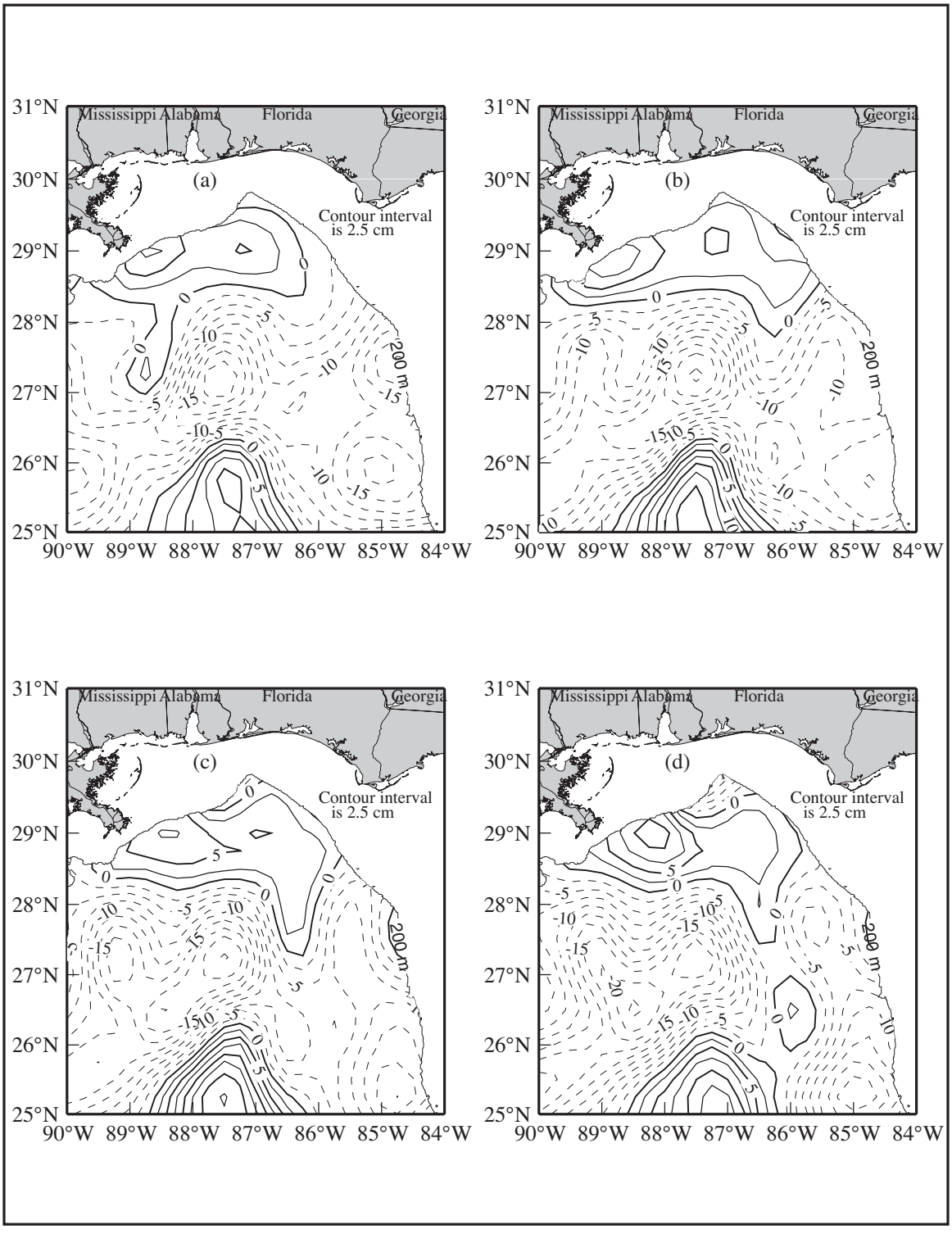

Figure 3.2.3-14. Sea surface height from satellite altimeter data for (a) 30 September 1998, (b) 7 October 1998, (c) 14 October 1998, and (d) 21 October 1998.

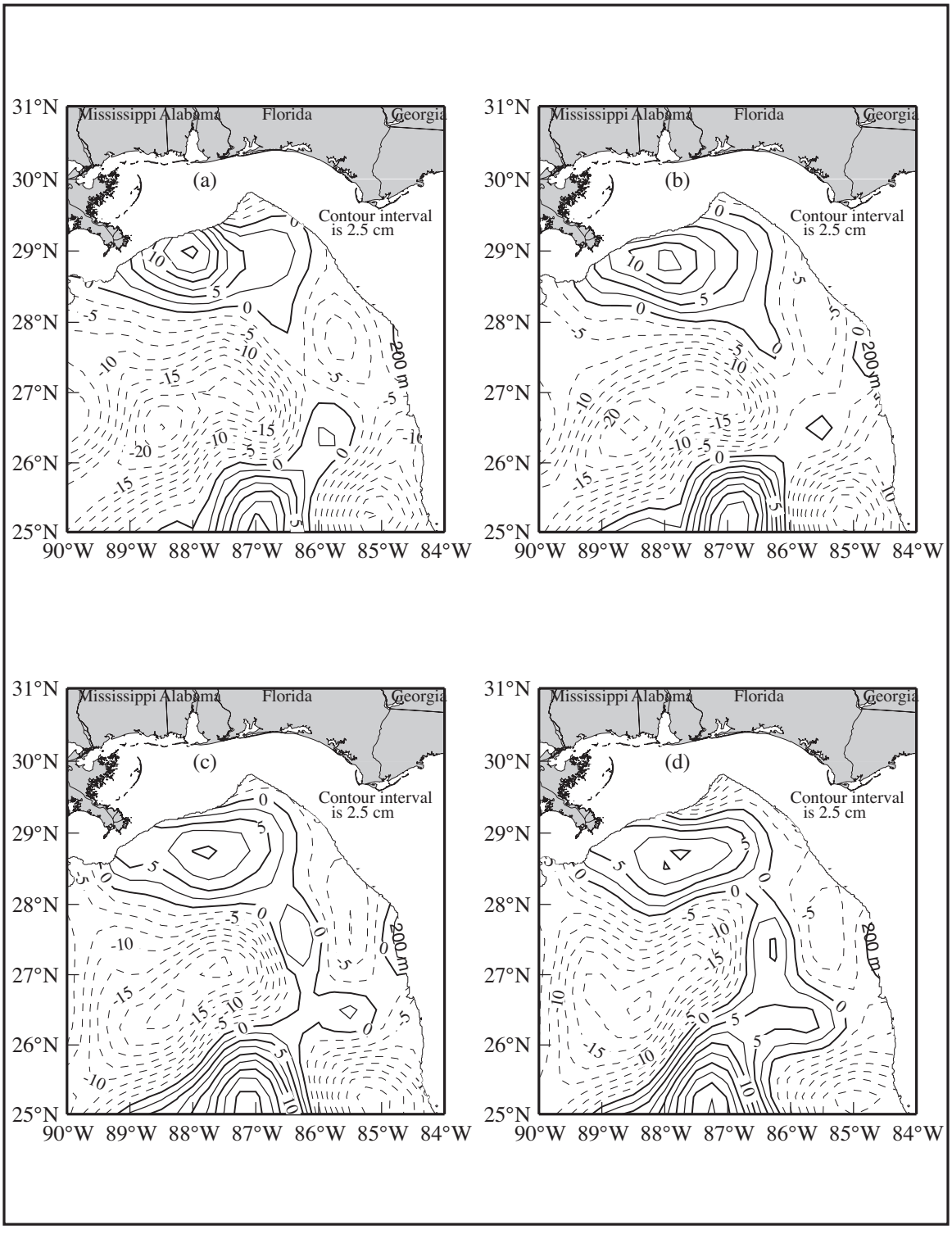

Figure 3.2.3-15. Sea surface height from satellite altimeter data for (a) 28 October 1998, (b) 4 November 1998, (c) 11 November 1998, and (d) 18 November 1998.

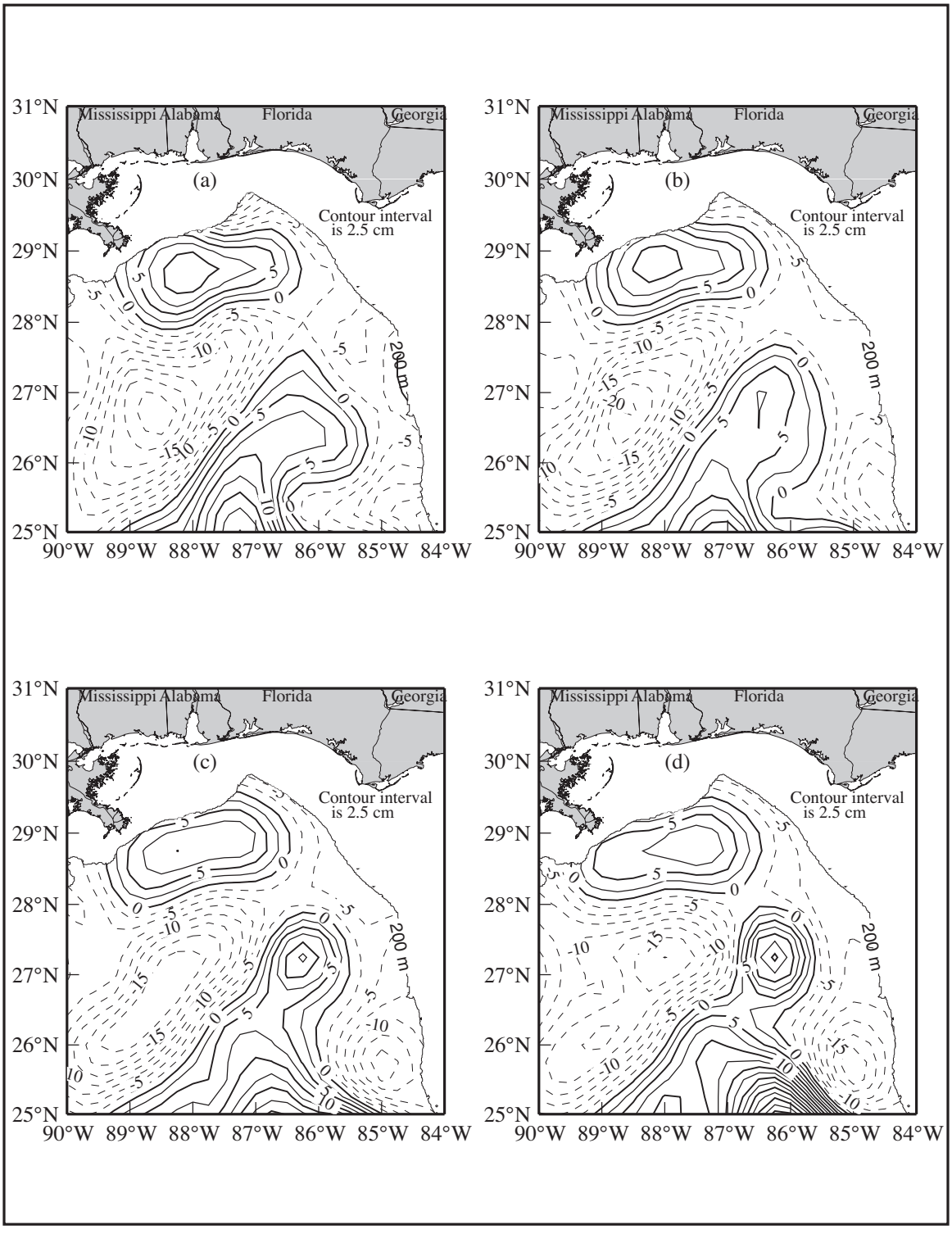

Figure 3.2.3-16. Sea surface height from satellite altimeter data for (a) 25 November 1998, (b) 2 December 1998, (c) 9 December 1998, and (d) 16 December 1998.

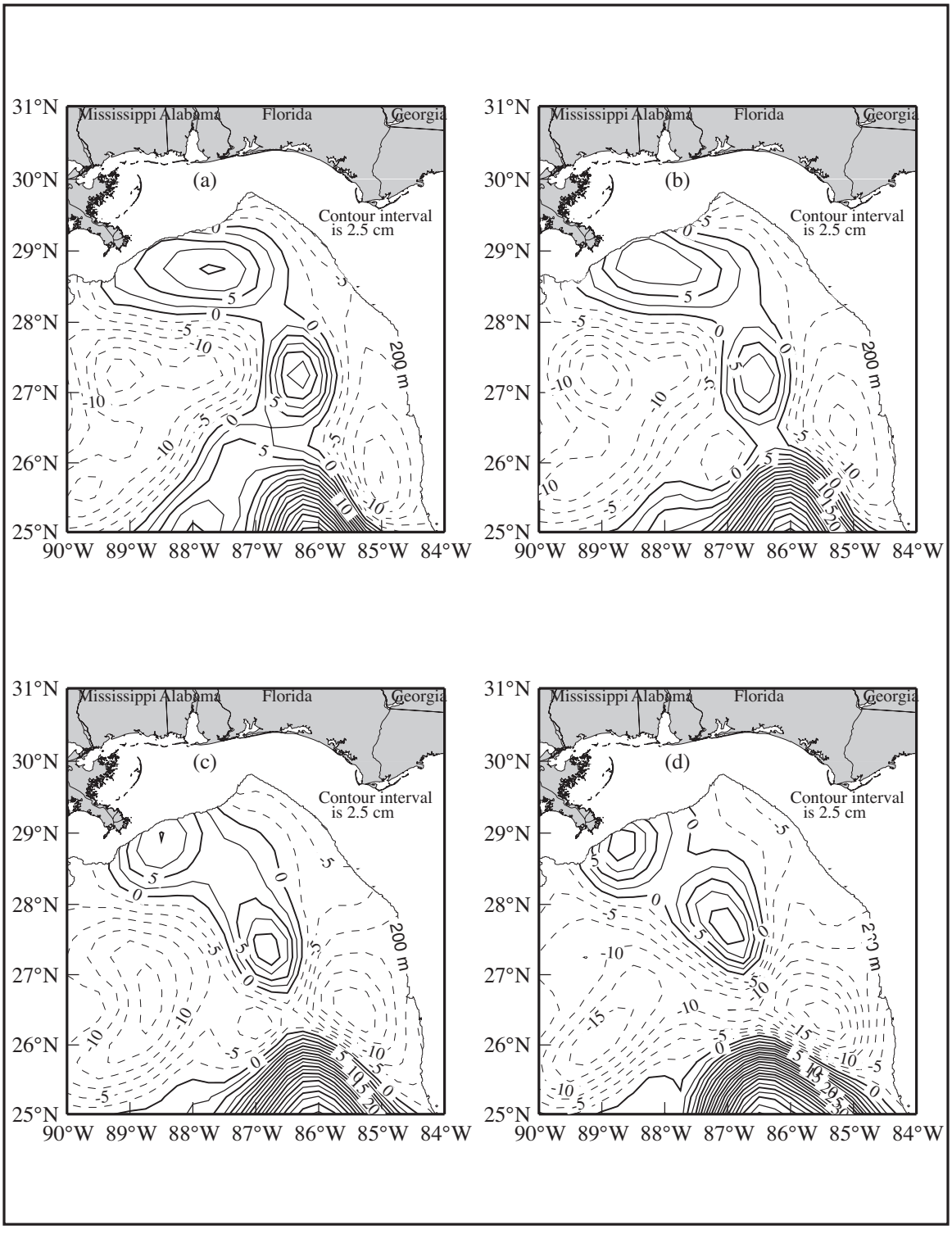

Figure 3.2.3-17. Sea surface height from satellite altimeter data for (a) 23 December 1998, (b) 30 December 1998, (c) 6 January 1999, and (d) 13 January 1999.

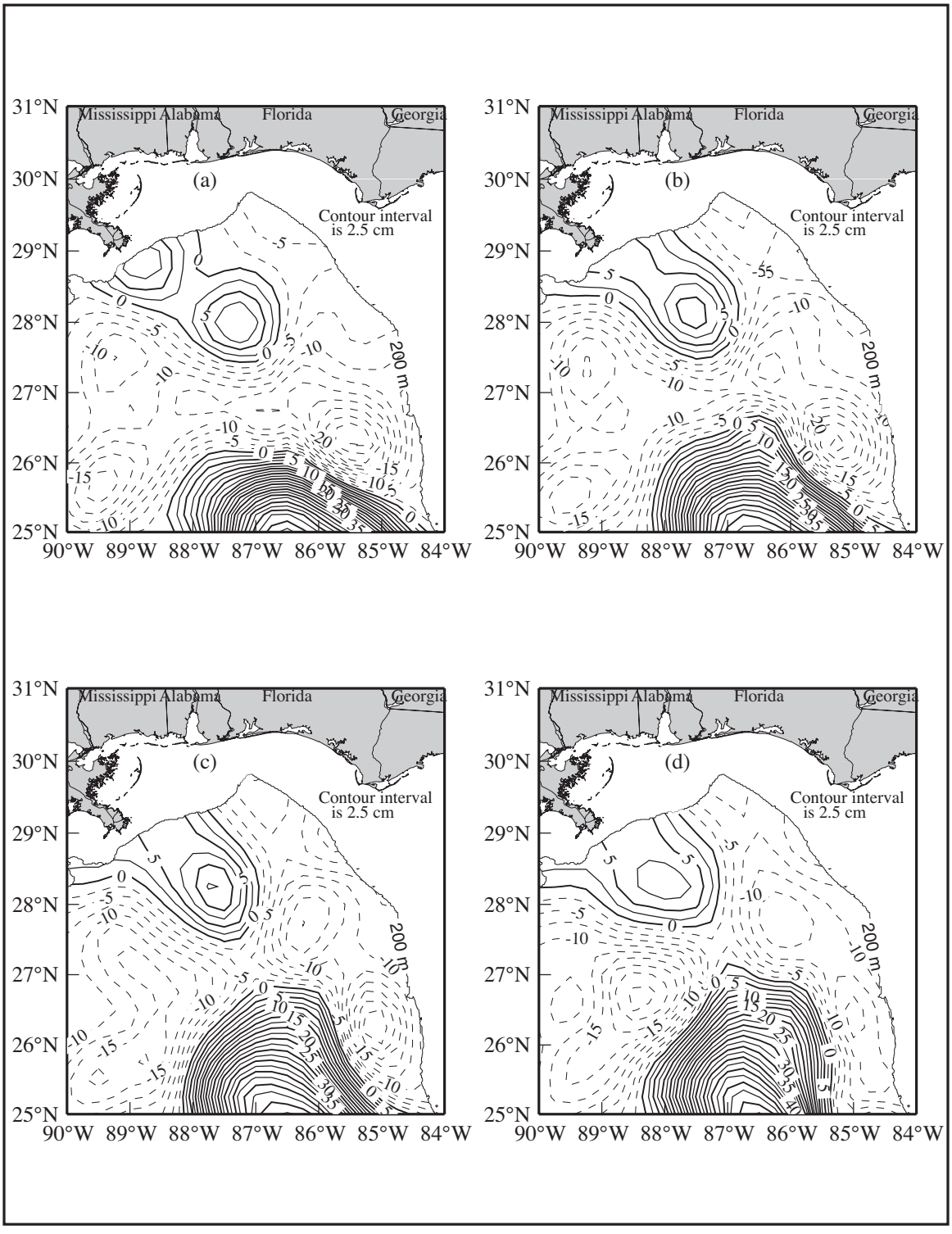

Figure 3.2.3-18. Sea surface height from satellite altimeter data for (a) 20 January 1999, (b) 27 January 1999, (c) 3 February 1999, and (d) 10 February 1999.

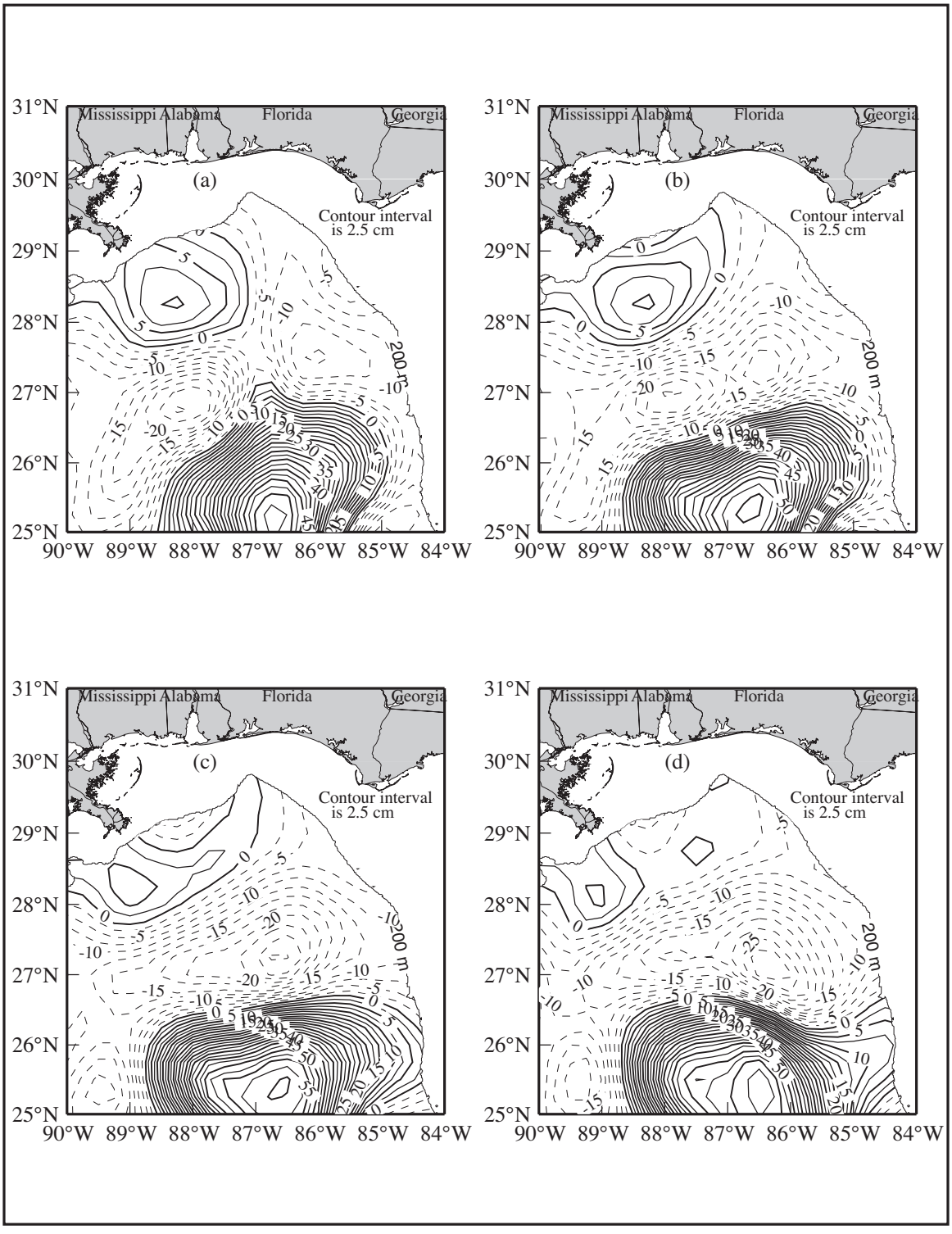

Figure 3.2.3-19. Sea surface height from satellite altimeter data for (a) 17 February 1999, (b) 26 February 1999, (c) 3 March 1999, and (d) 10 March 1999.

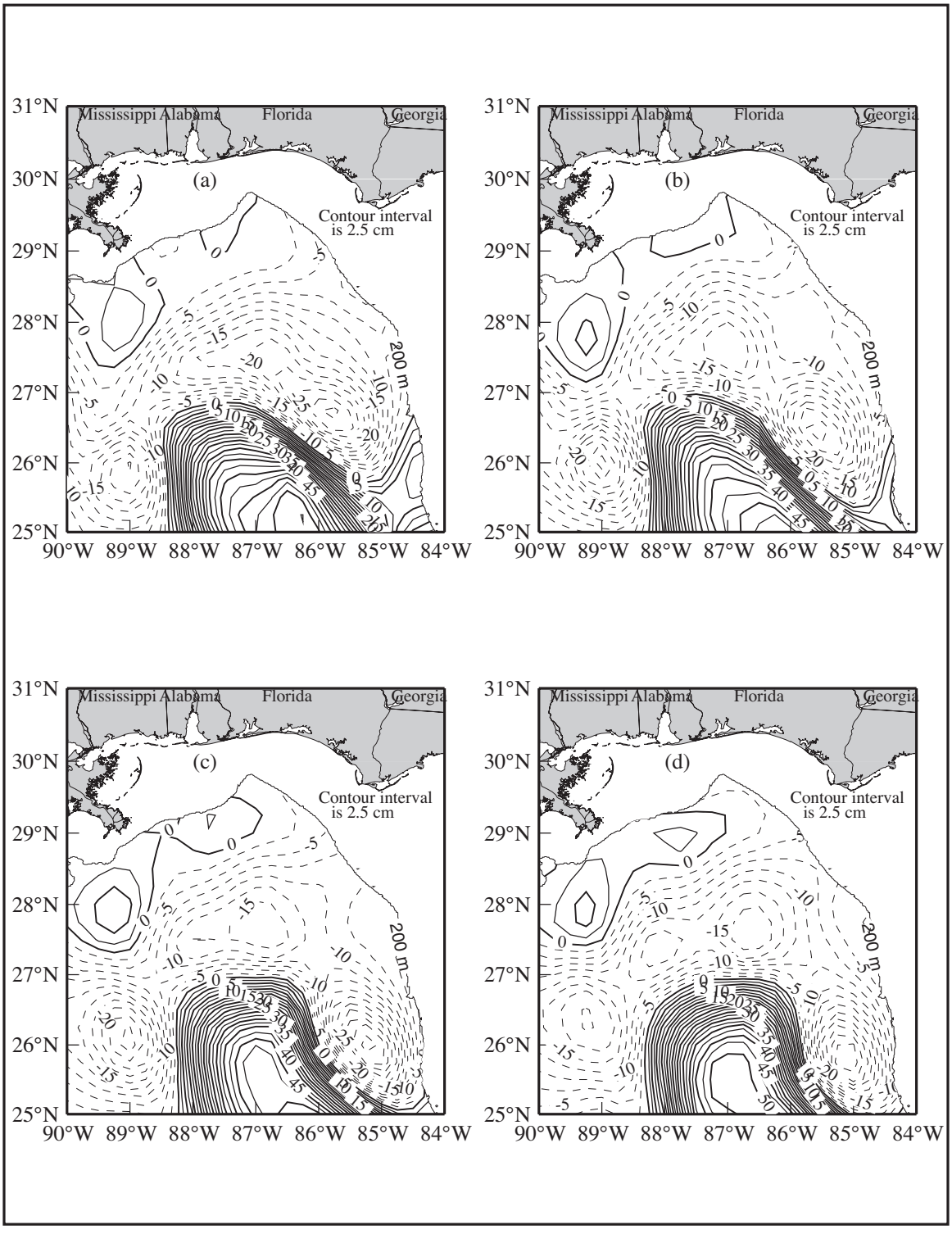

Figure 3.2.3-20. Sea surface height from satellite altimeter data for (a) 17 March 1999, (b) 24 March 1999, (c) 31 March 1999, and (d) 7 April 1999.

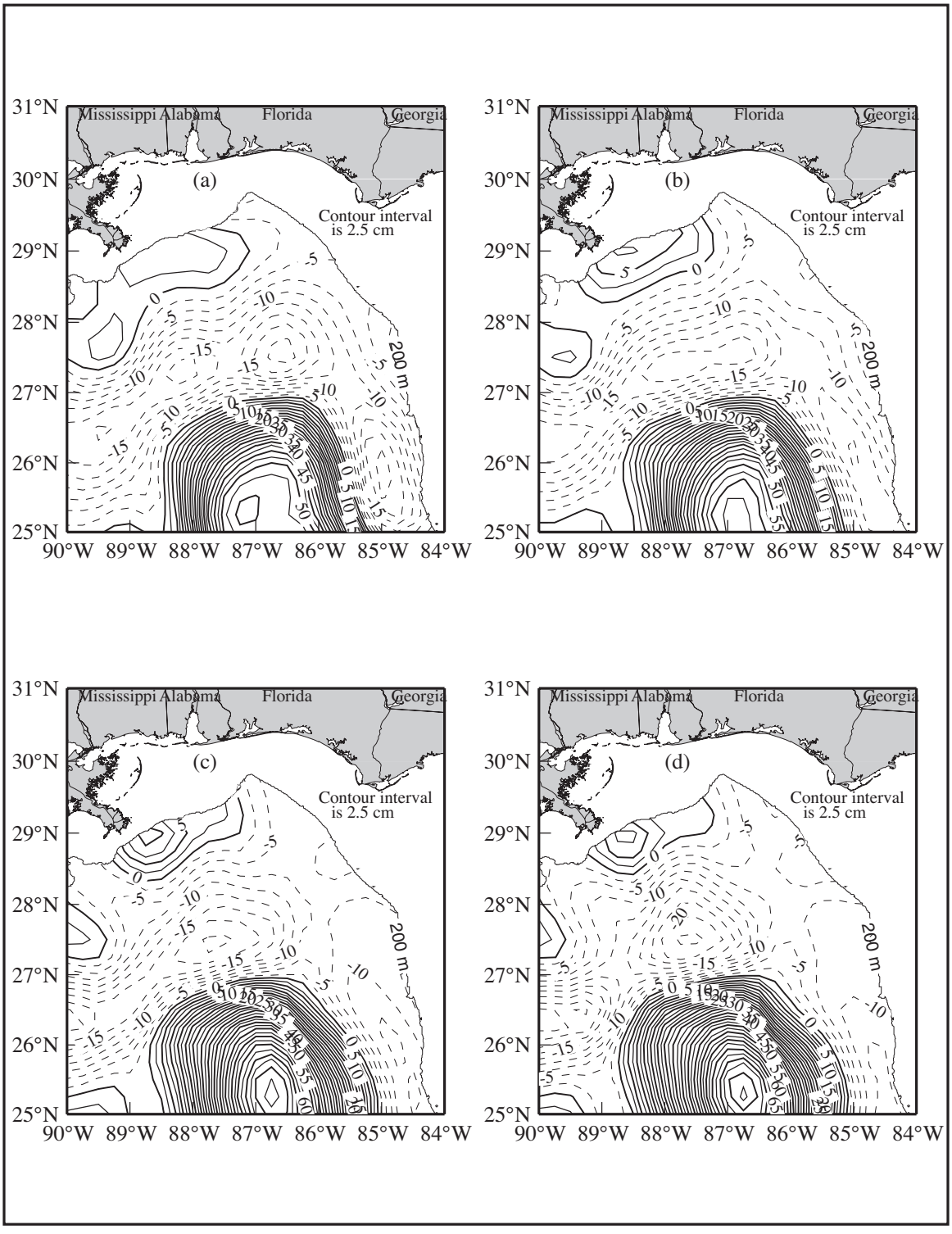

Figure 3.2.3-21. Sea surface height from satellite altimeter data for (a) 14 April 1999, (b) 21 April 1999, (c) 28 April 1999, and (d) 5 May 1999.

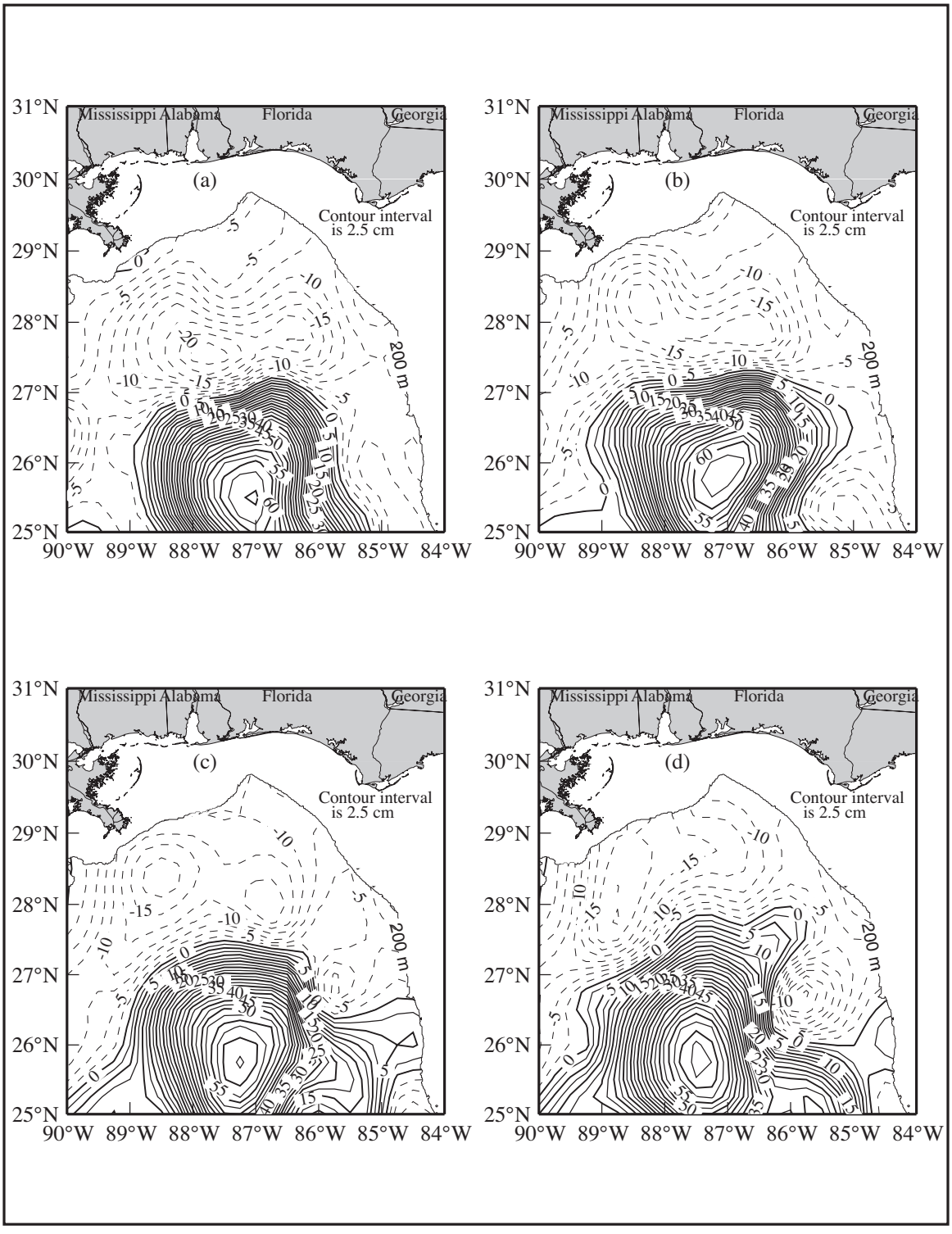

Figure 3.2.3-22. Sea surface height from satellite altimeter data for (a) 12 May 1999, (b) 19 May 1999, (c) 26 May 1999, and (d) 2 June 1999.

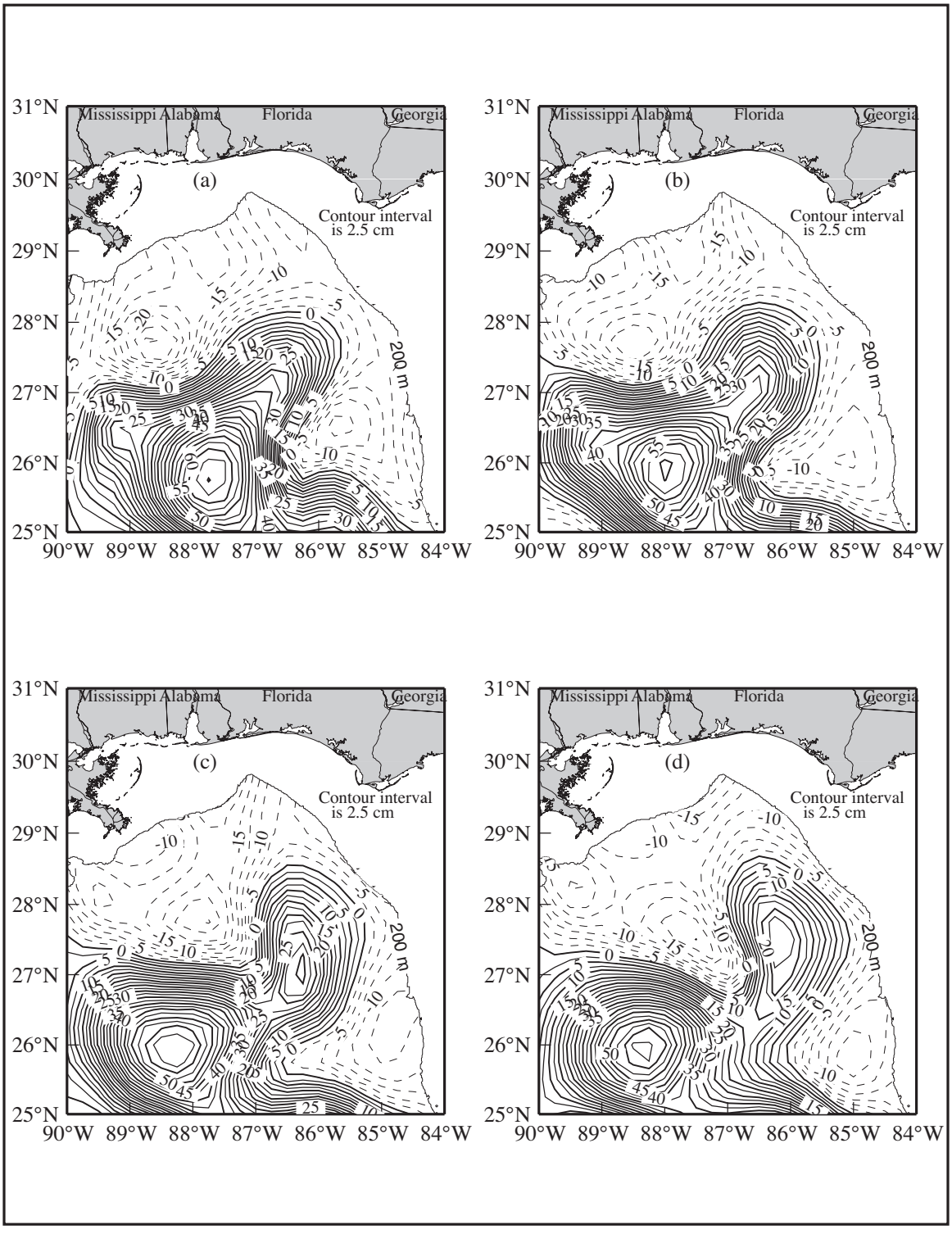

Figure 3.2.3-23. Sea surface height from satellite altimeter data for (a) 9 June 1999, (b) 16 June 1999, (c) 23 June 1999, and (d) 30 June 1999.

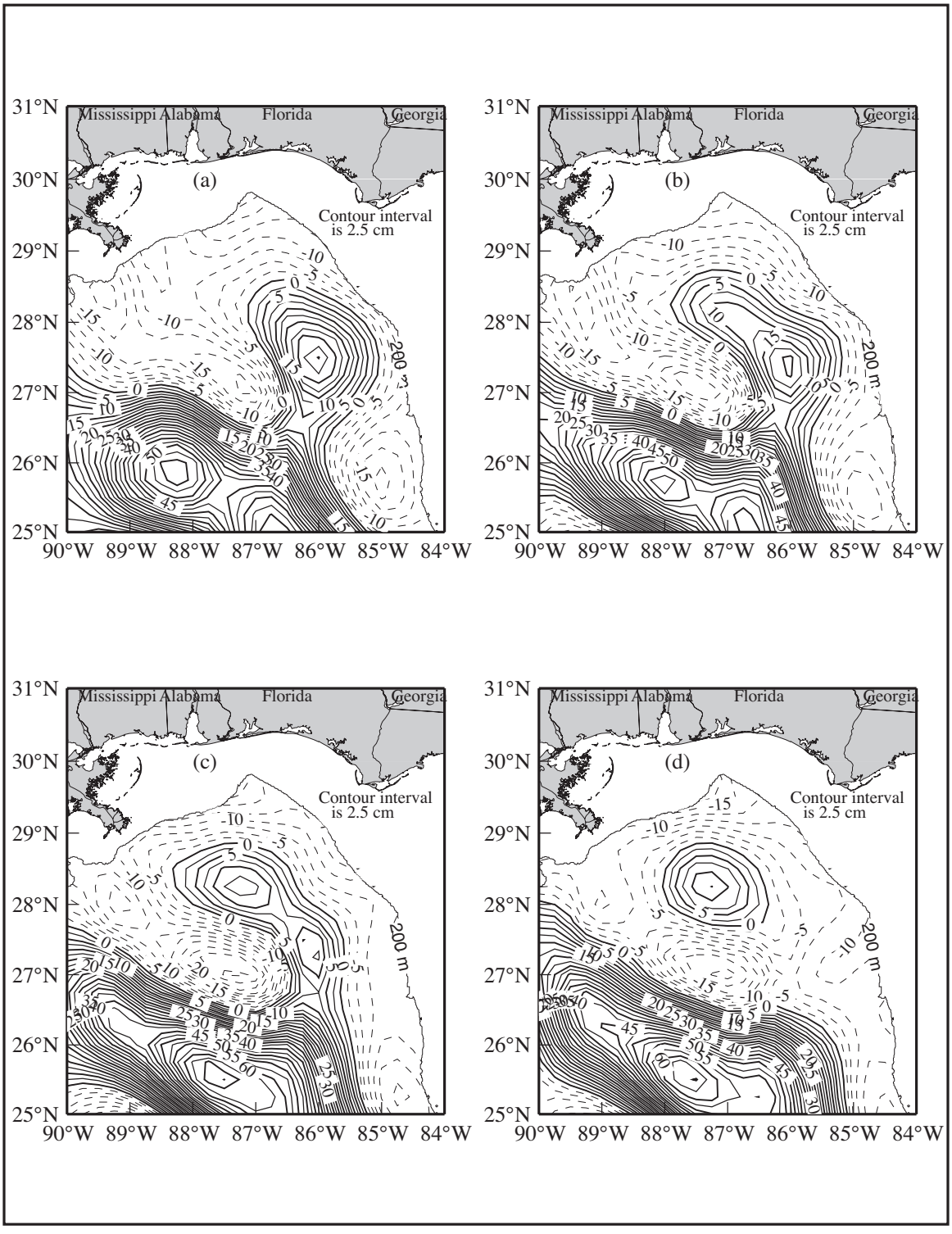

Figure 3.2.3-24. Sea surface height from satellite altimeter data for (a) 7 July 1999, (b) 14 July 1999, (c) 21 July 1999, and (d) 28 July 1999.

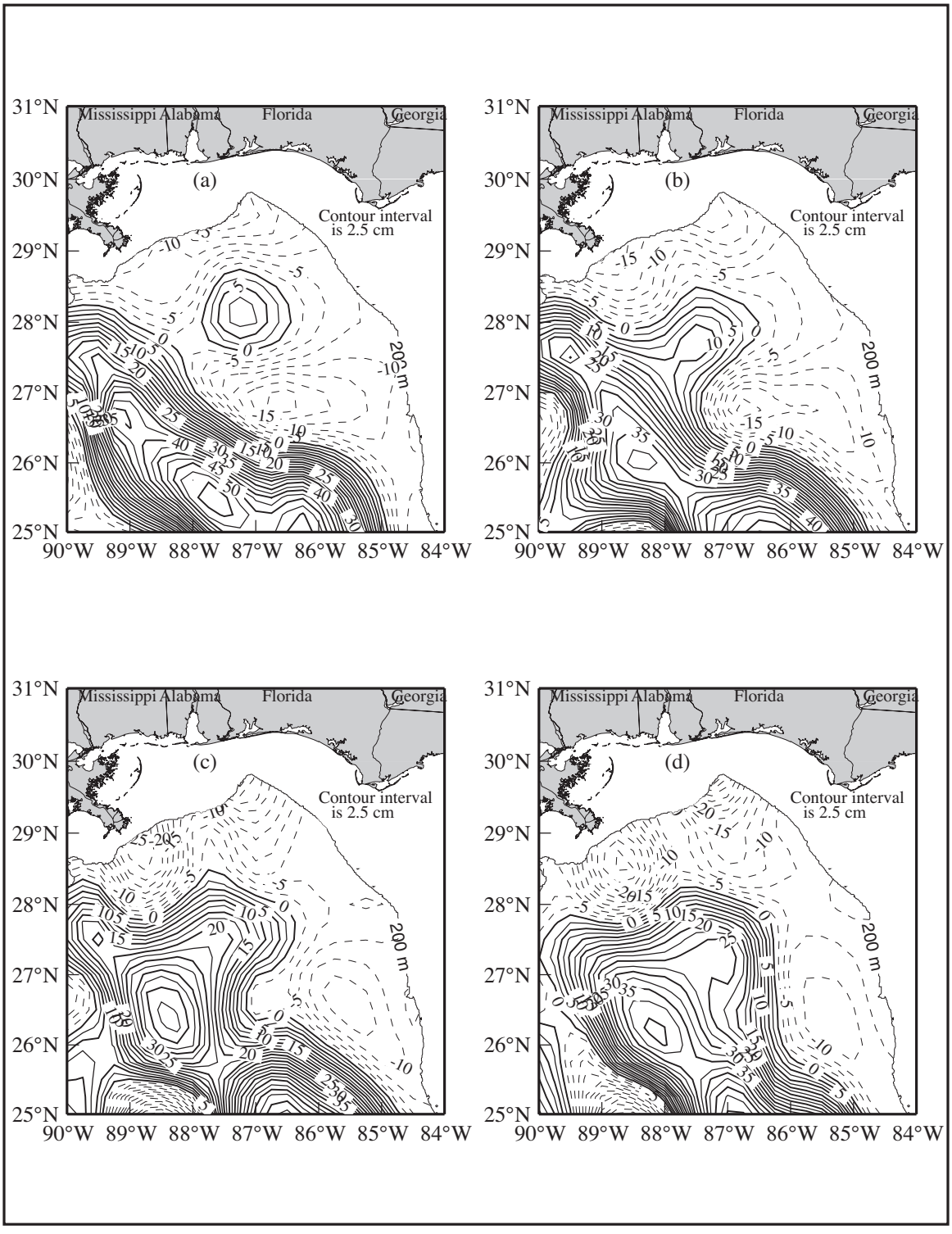

Figure 3.2.3-25. Sea surface height from satellite altimeter data for (a) 4 August 1999, (b) 11 August 1999, (c) 18 August 1999, and (d) 25 August 1999.

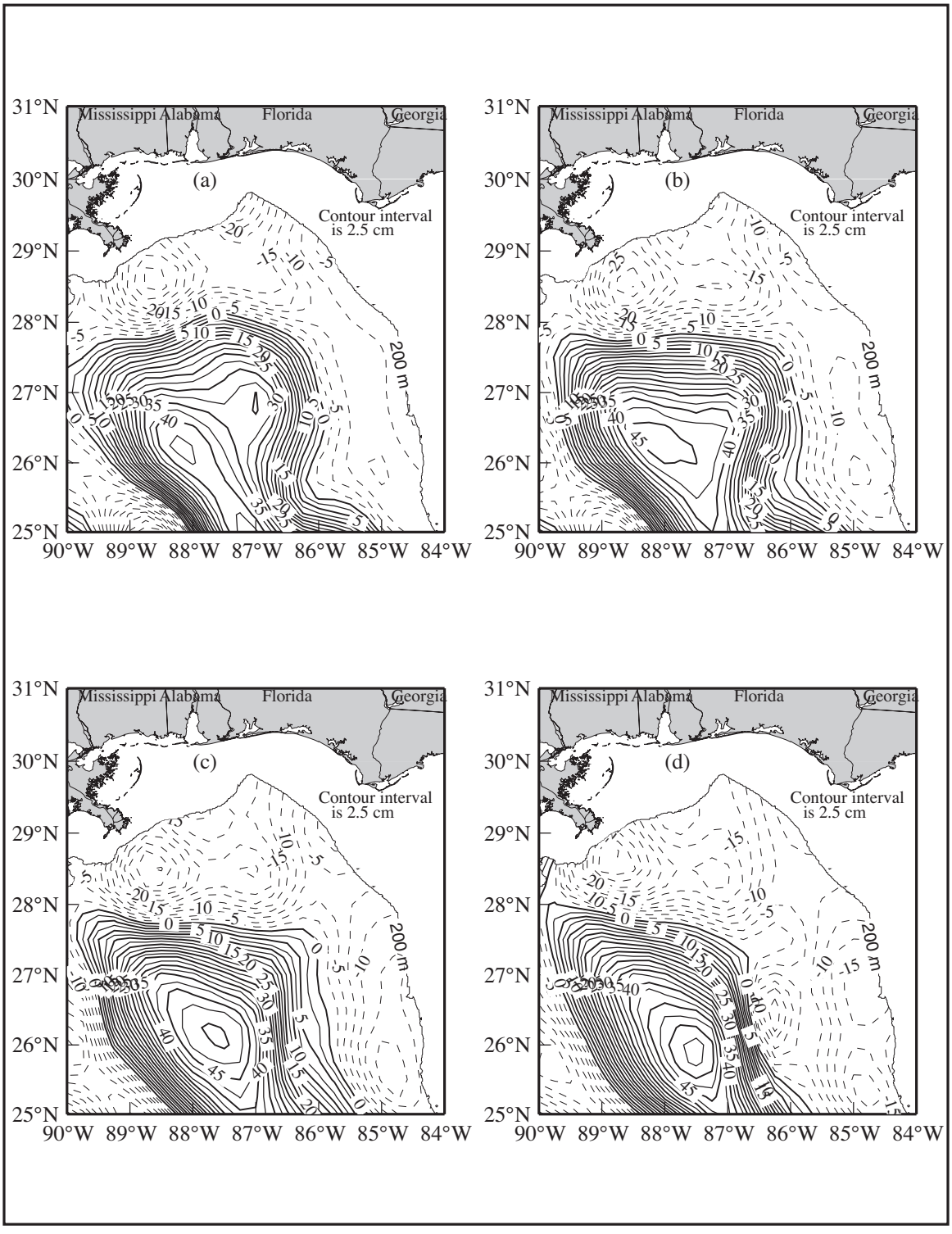

Figure 3.2.3-26. Sea surface height from satellite altimeter data for (a) 1 September 1999, (b) 8 September 1999, (c) 15 September 1999, and (d) 22 September 1999.

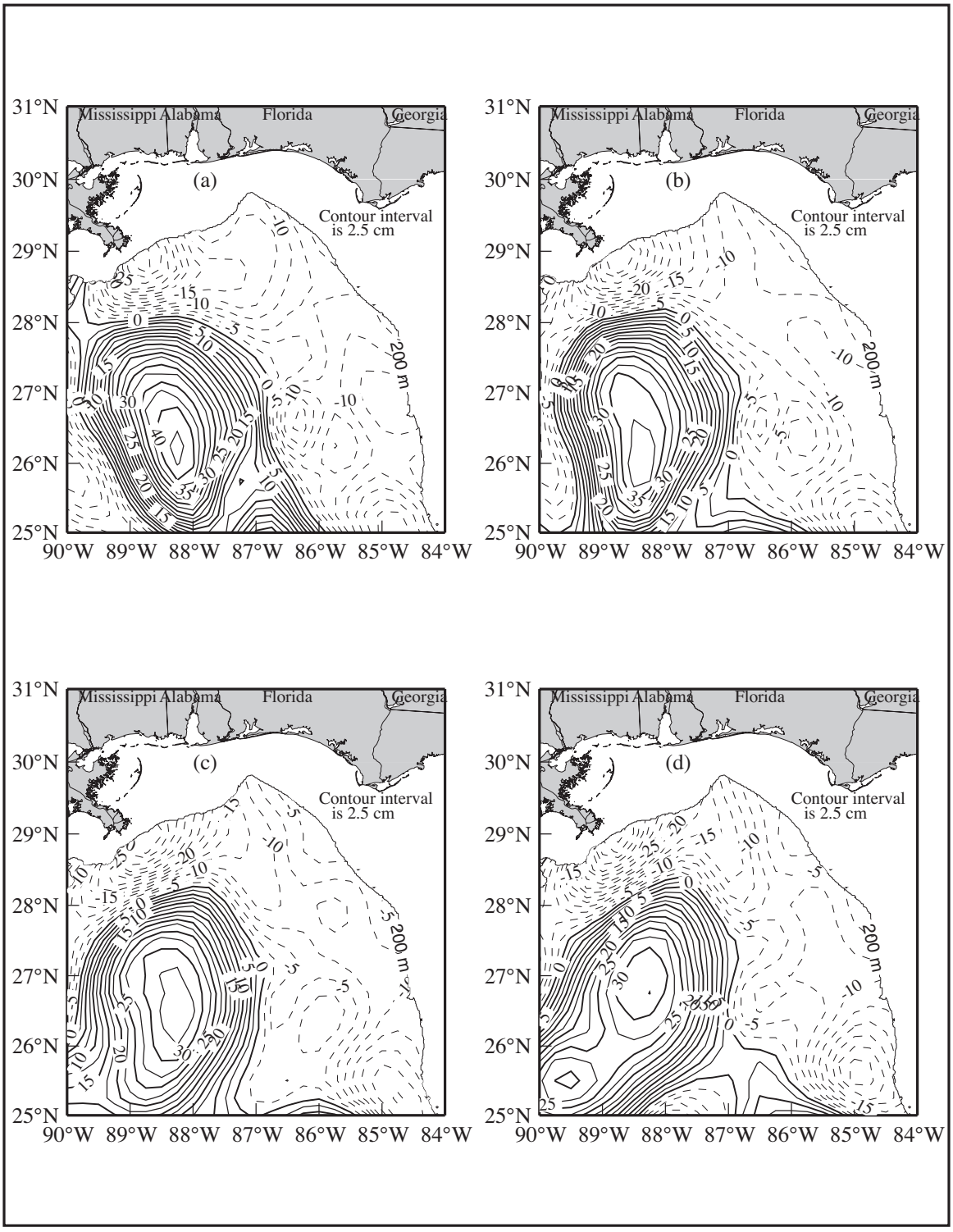

Figure 3.2.3-27. Sea surface height from satellite altimeter data for (a) 29 September 1999, (b) 6 October 1999, (c) 13 October 1999, and (d) 20 October 1999.

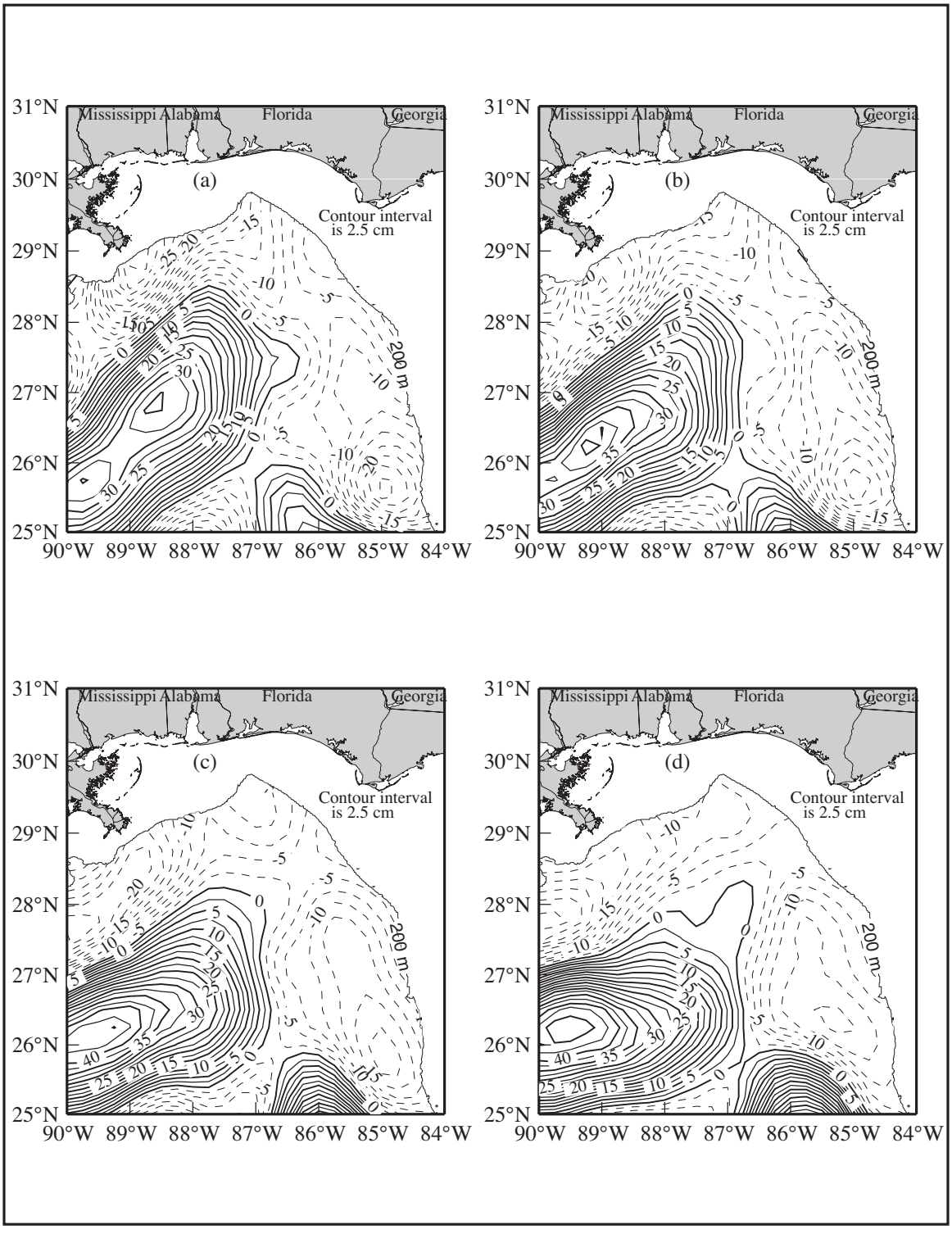

Figure 3.2.3-28. Sea surface height from satellite altimeter data for (a) 27 October 1999, (b) 3 November 1999, (c) 10 November 1999, and (d) 17 November 1999.

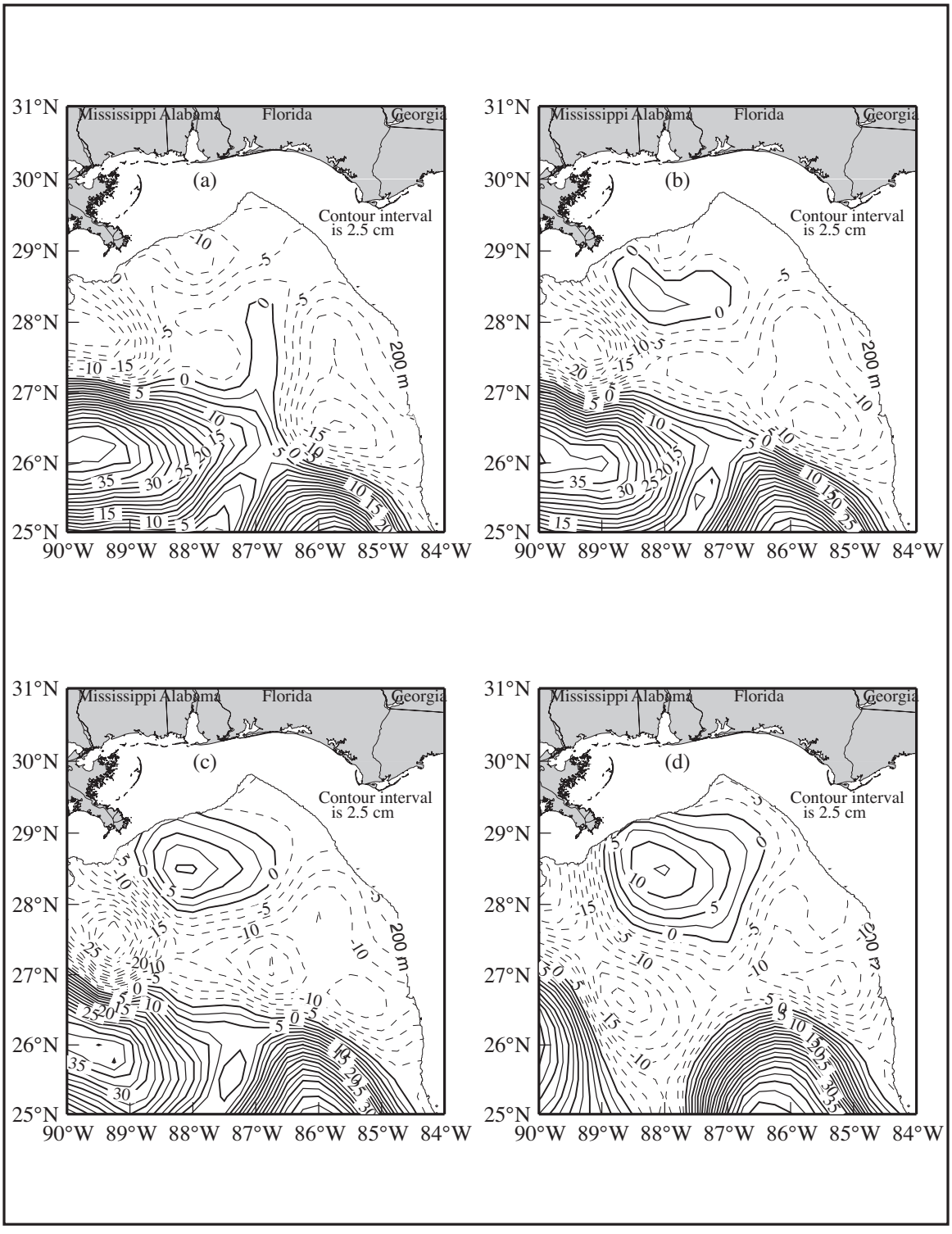

Figure 3.2.3-29. Sea surface height from satellite altimeter data for (a) 24 November 1999, (b) 1 December 1999, (c) 8 December 1999, and (d) 15 December 1999.

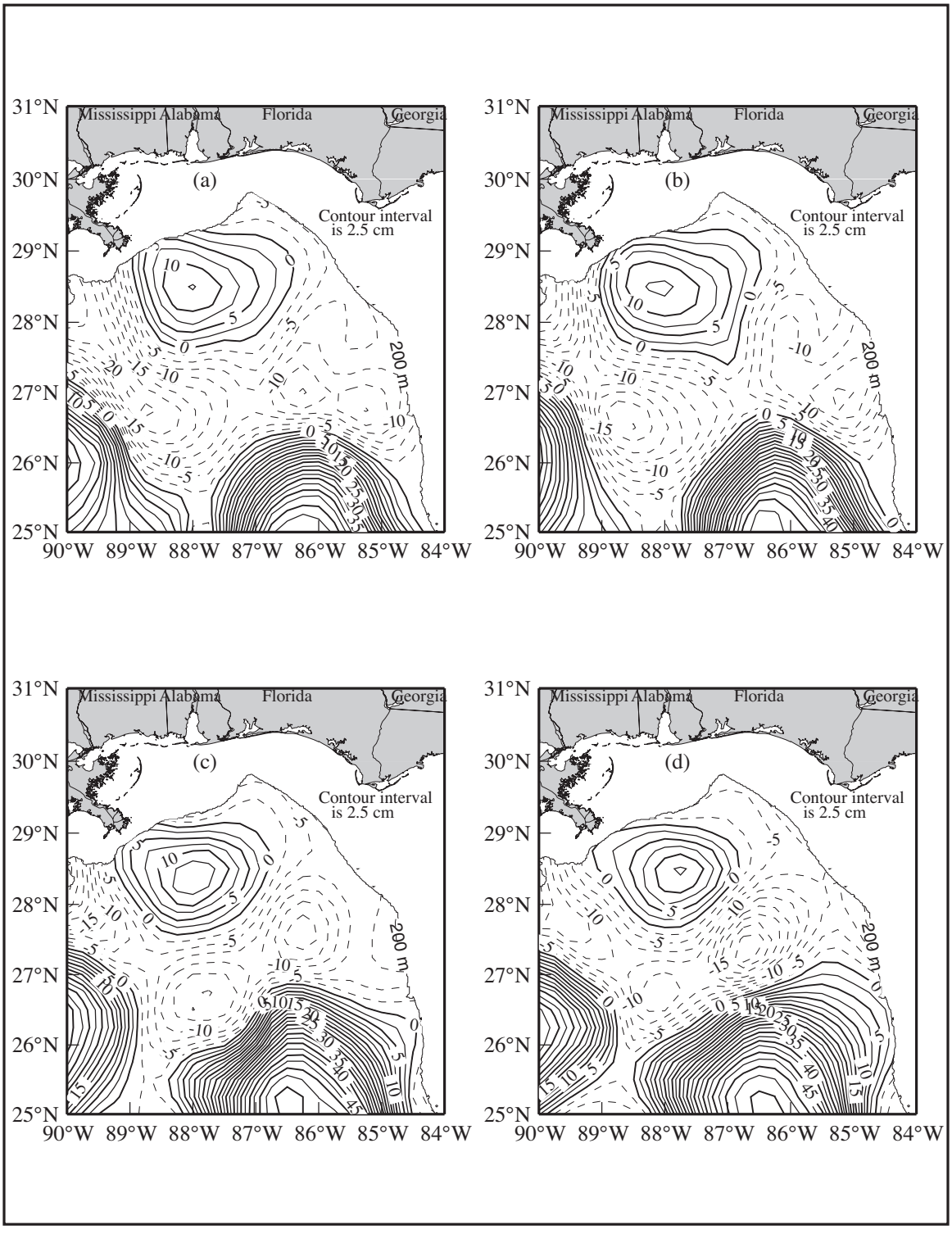

Figure 3.2.3-30. Sea surface height from satellite altimeter data for (a) 22 December 1999, (b) 29 December 1999, (c) 5 January 2000, and (d) 12 January 2000.

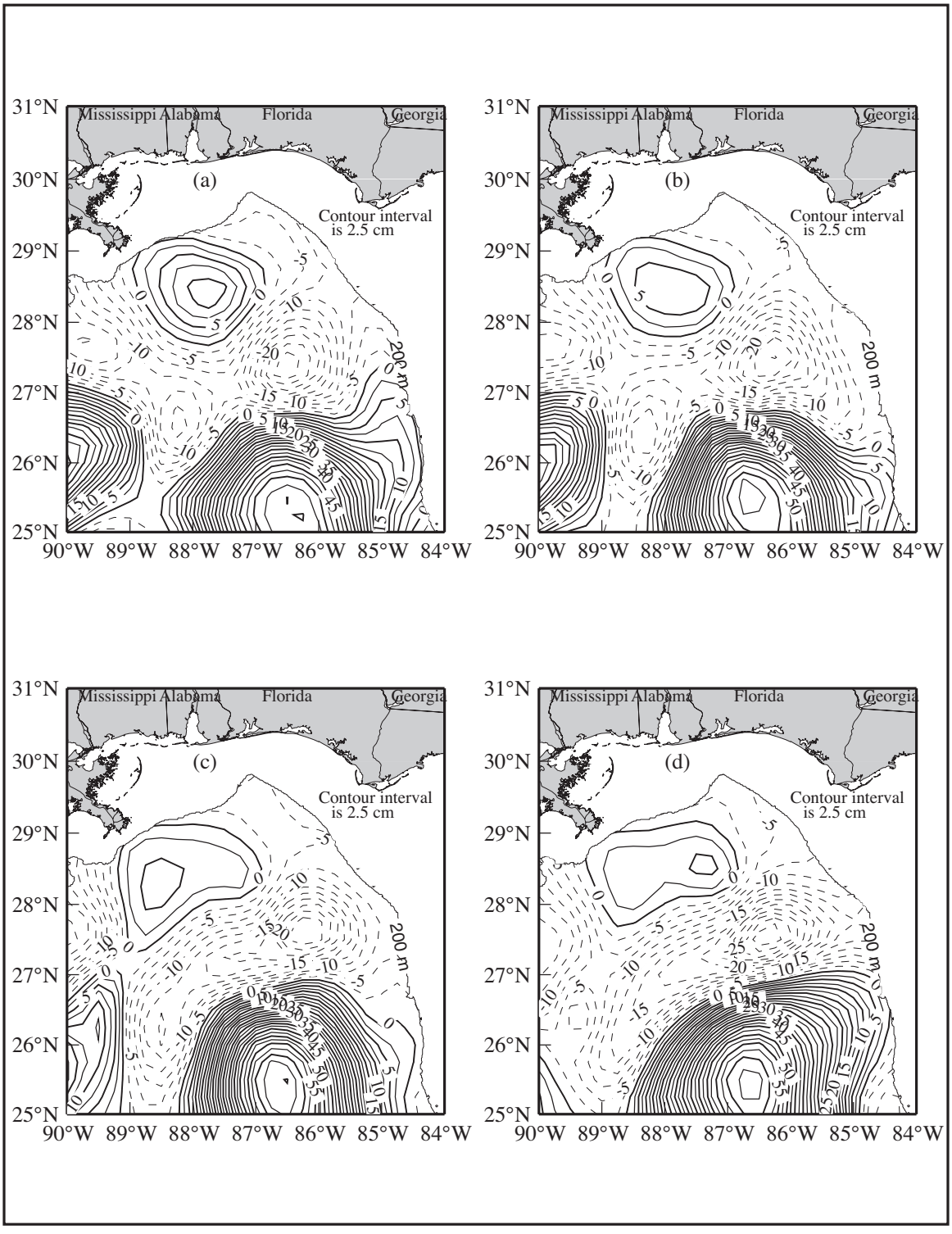

Figure 3.2.3-31. Sea surface height from satellite altimeter data for (a) 19 January 2000, (b) 26 January 2000, (c) 2 February 2000, and (d) 9 February 2000.

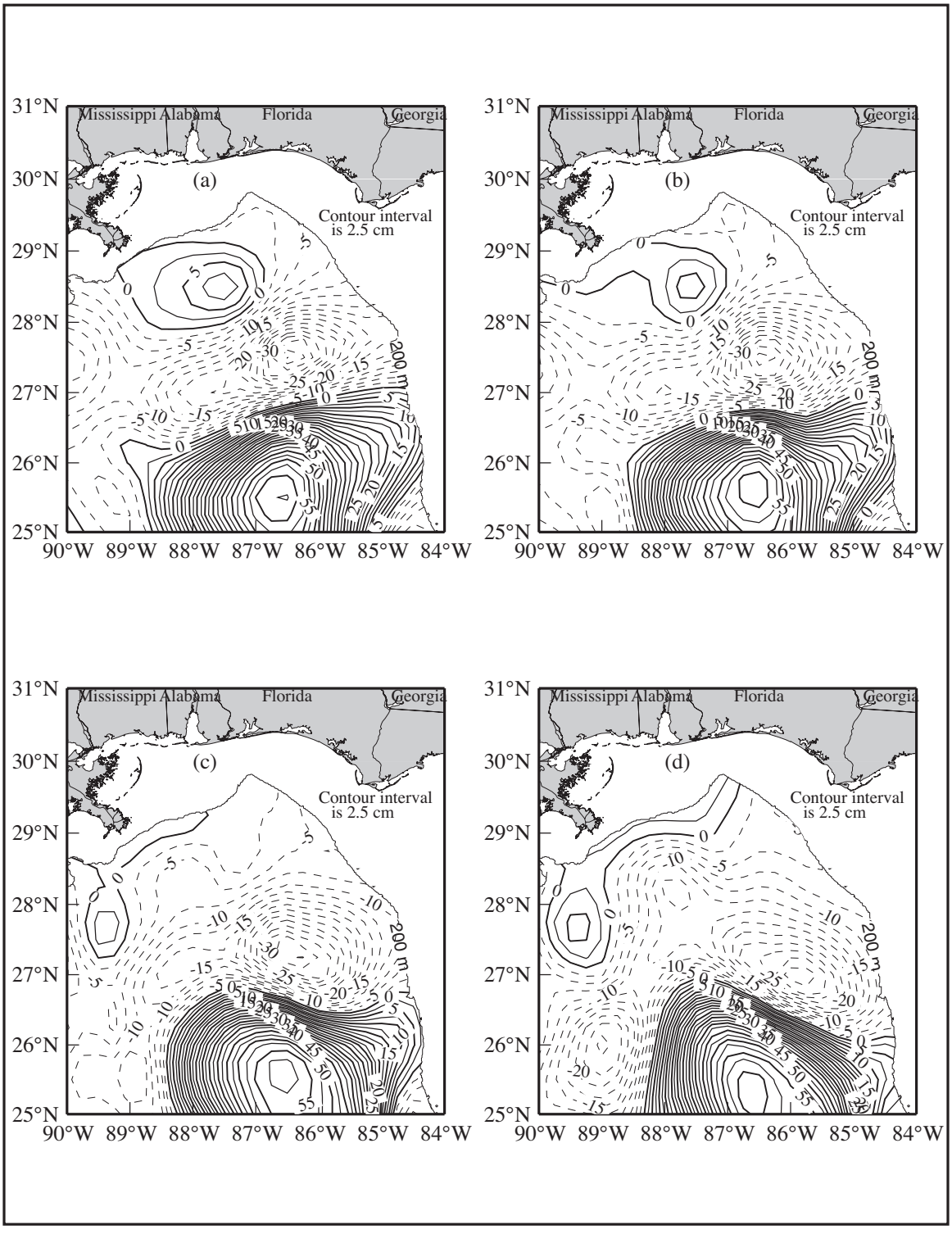

Figure 3.2.3-32. Sea surface height from satellite altimeter data for (a) 16 February 2000, (b) 25 February 2000, (c) 1 March 2000, and (d) 8 March 2000.

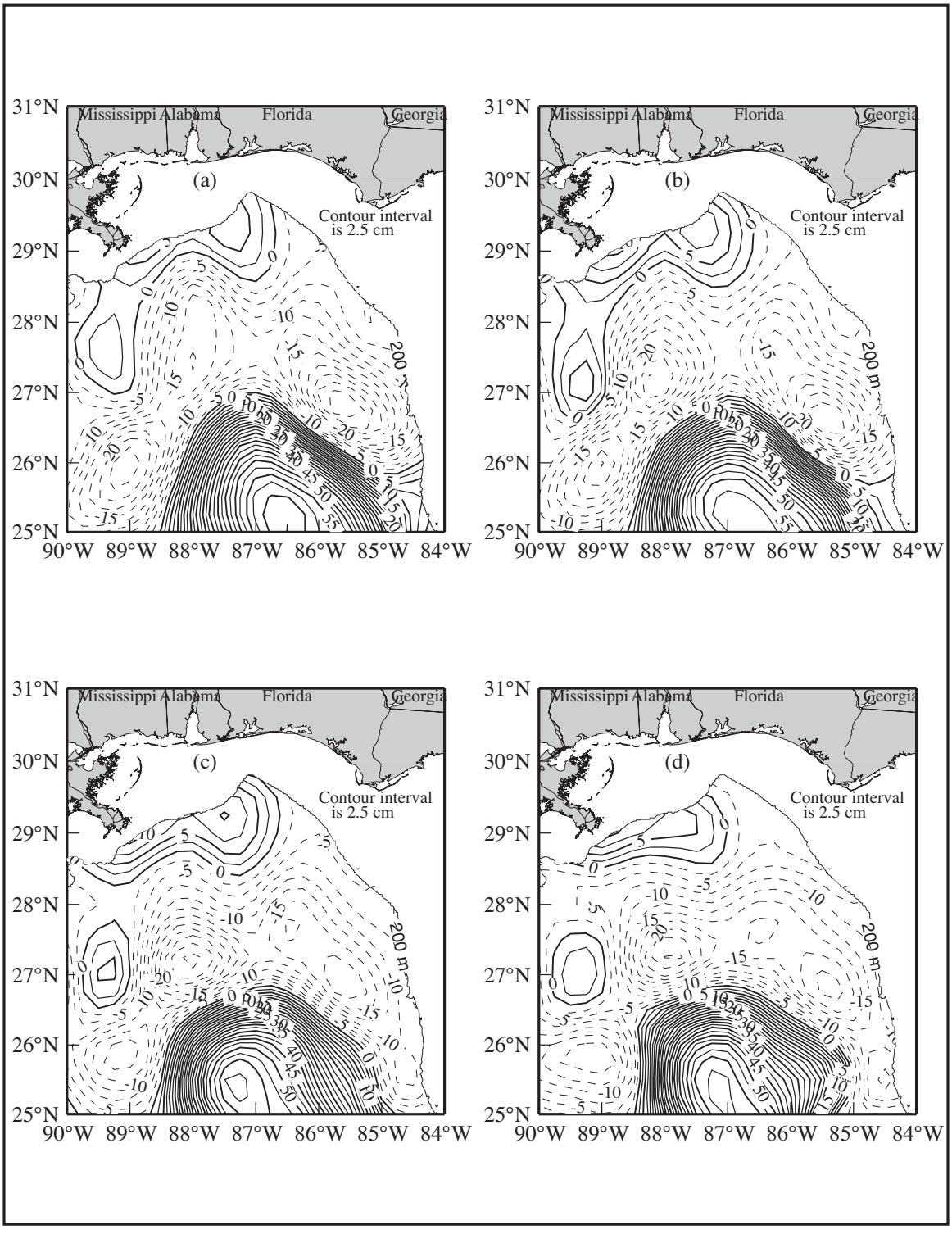

Figure 3.2.3-33. Sea surface height from satellite altimeter data for (a) 15 March 2000, (b) 22 March 2000, (c) 29 March 2000, and (d) 5 April 2000.

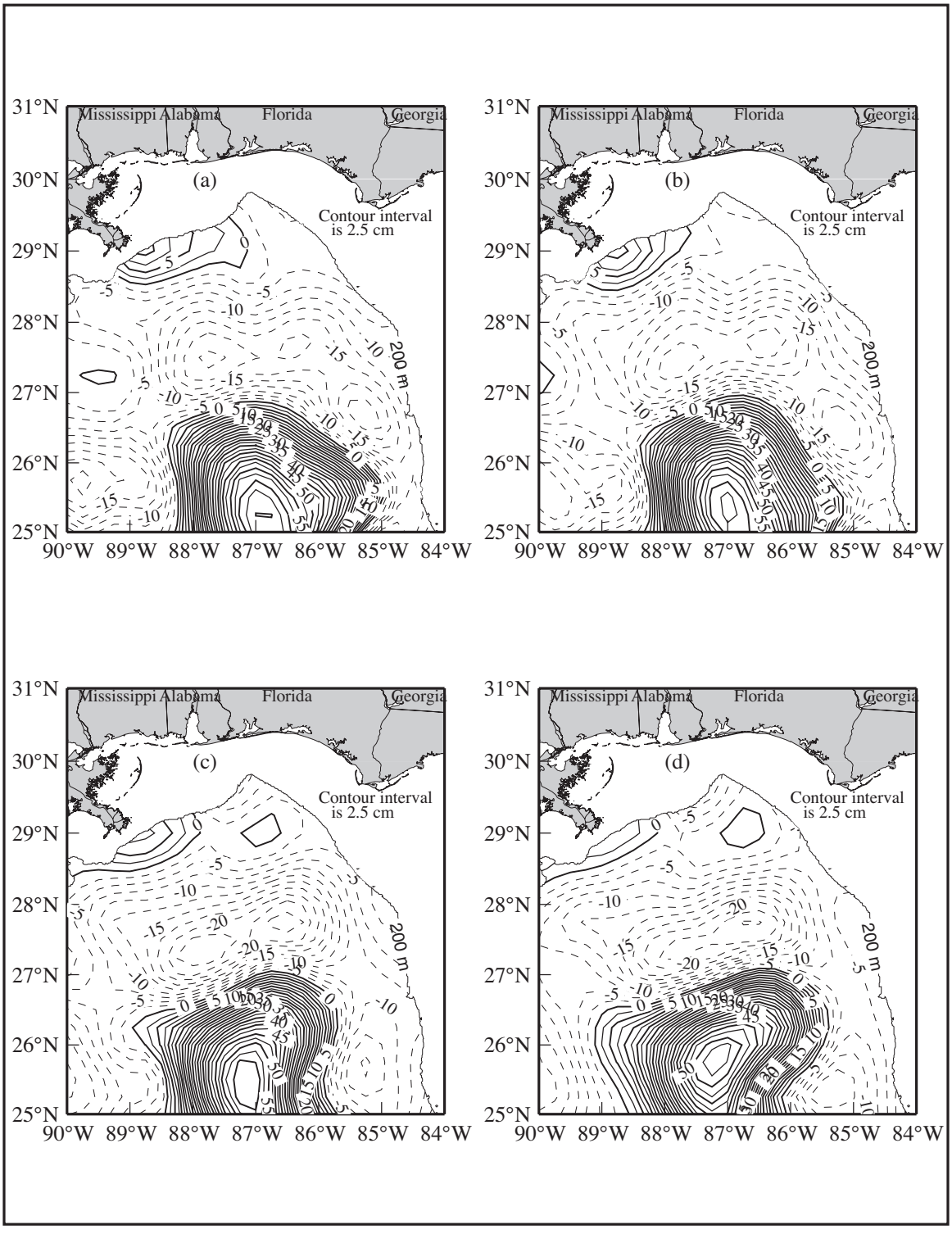

Figure 3.2.3-34. Sea surface height from satellite altimeter data for (a) 12 April 2000, (b) 19 April 2000, (c) 26 April 2000, and (d) 3 May 2000.

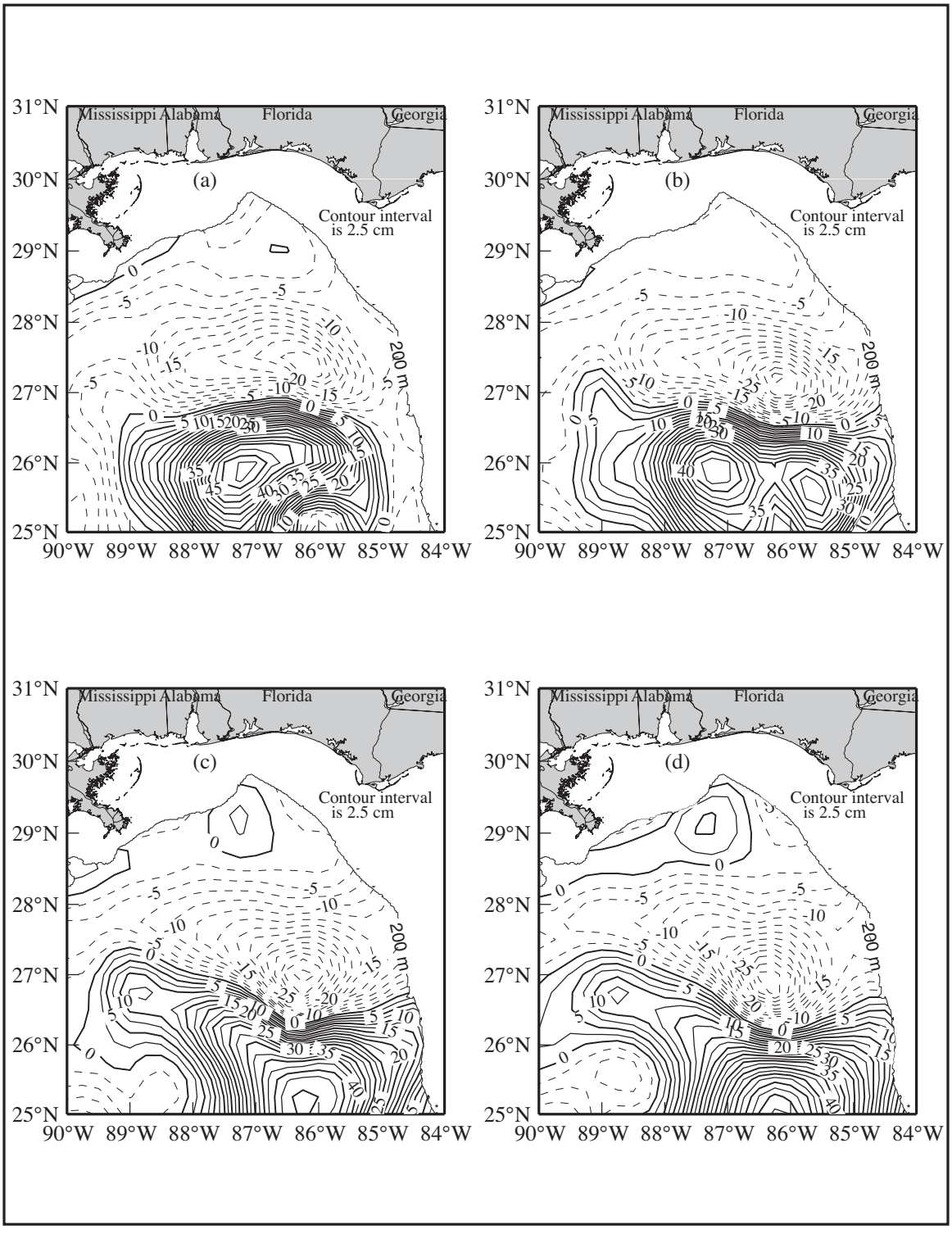

Figure 3.2.3-35. Sea surface height from satellite altimeter data for (a) 10 May 2000, (b) 17 May 2000, (c) 24 May 2000, and (d) 31 May 2000.

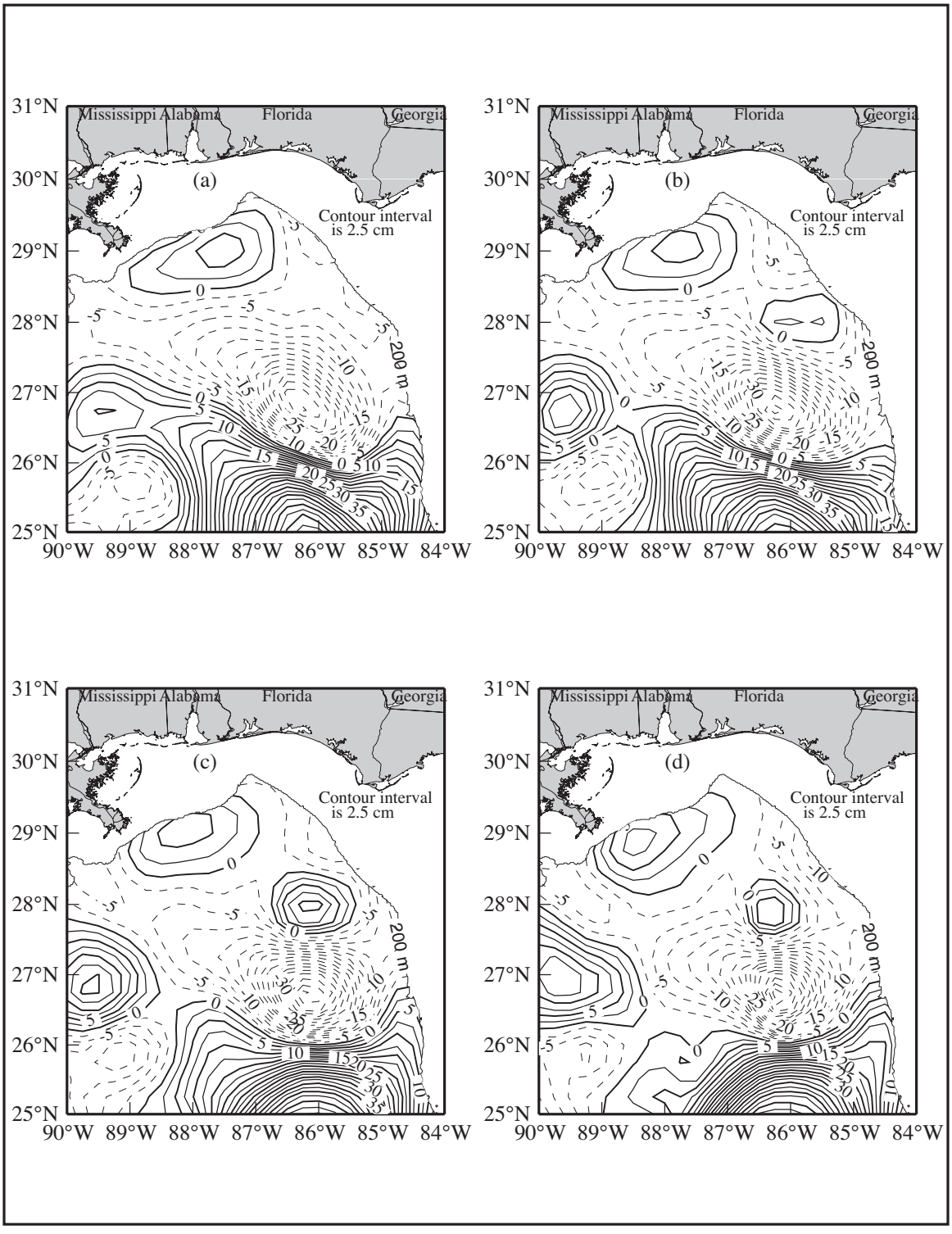

Figure 3.2.3-36. Sea surface height from satellite altimeter data for (a) 7 June 2000, (b) 14 June 2000, (c) 21 June 2000, and (d) 28 June 2000.

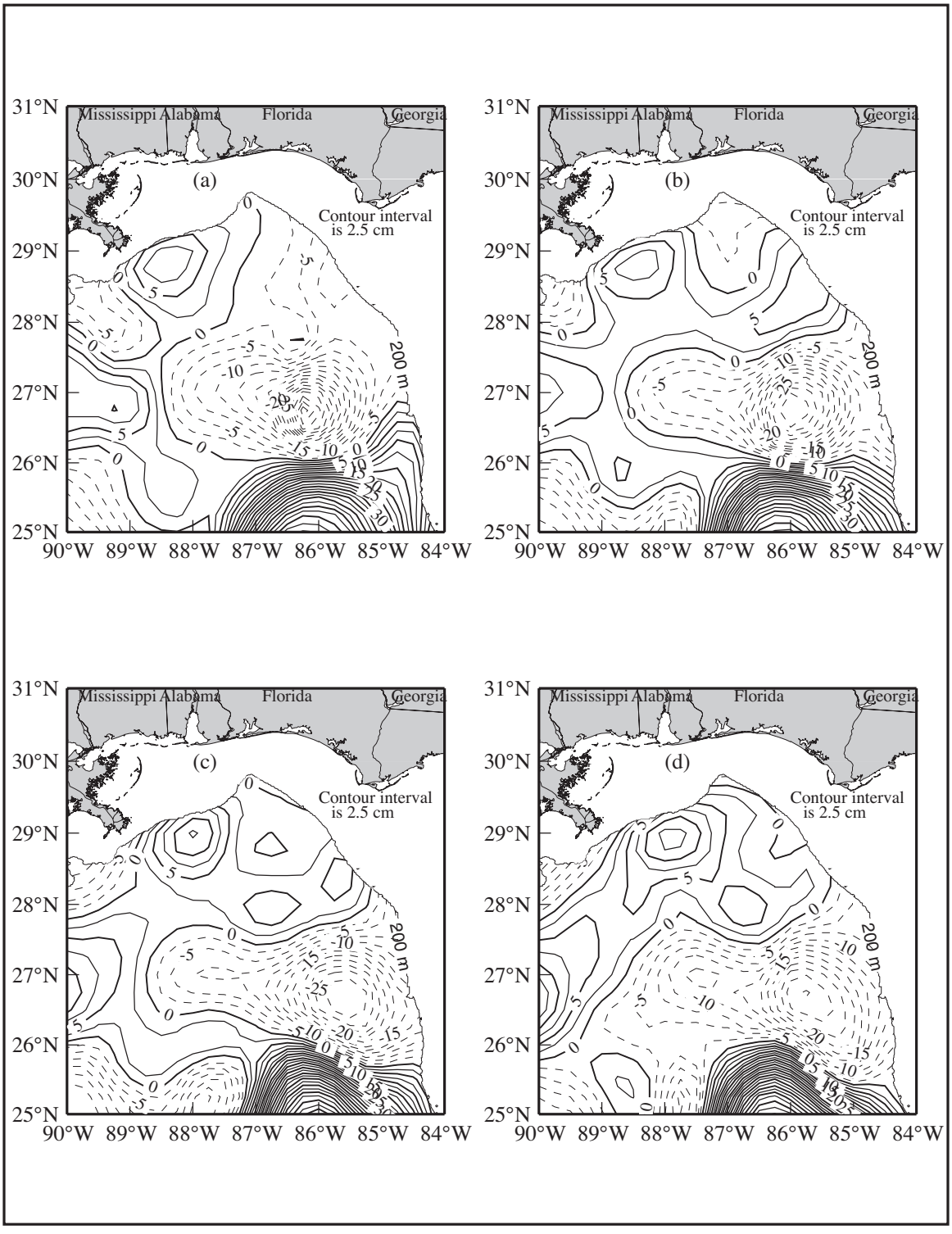

Figure 3.2.3-37. Sea surface height from satellite altimeter data for (a) 5 July 2000, (b) 12 July 2000, (c) 19 July 2000, and (d) 26 July 2000.

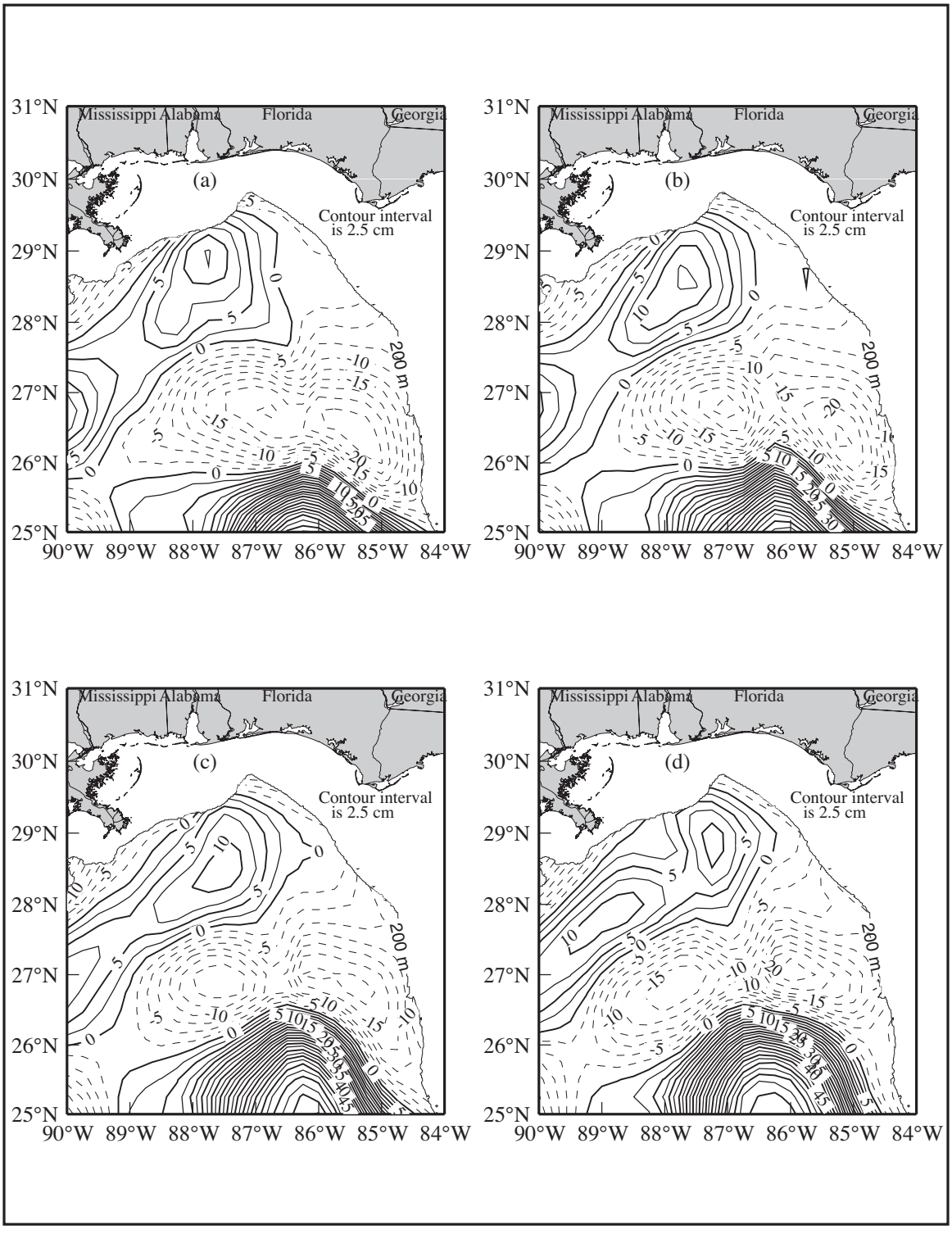

Figure 3.2.3-38. Sea surface height from satellite altimeter data for (a) 2 August 2000, (b) 9 August 2000, (c) 16 August 2000, and (d) 23 August 2000.

4 CIRCULATION AND ITS VARIABILITY

Presented in this section are interpretations of the circulation and its variability as based on observations collected during the study period and from selected data analyses. In Section 4.1 are presented our inferences regarding surface currents at the time of each cruise based on multiple measurement techniques. Then, the annual cycle of surface currents from surface drifters is presented in Section 4.2. It should be noted that the time series is too short to establish this cycle with any great degree of certainty. The space-time pattern of low frequency currents, based on EOF analysis of ADCP measurements is given in Section 4.3. Section 4.4 gives an examination of wind fields as potential forcing of nearshore coastal currents and the observed response. The potential for forcing on-shelf circulation by off-shelf circulation features is estimated in Section 4.5, and an attempt is made to relate such forcing to currents over the outer shelf. Finally, in Section 4.6 we give some conclusions.

Throughout this report we refer to currents with upcoast and downcoast components. These terms are used in the sense of how a Kelvin wave would propagate on this shelf, with downcoast having land on the right in the direction of propagation.

4.1 Current Fields Inferred from Multiple Techniques During NEGOM Cruises

In this section gridded fields of currents measured in vertical bins centered between 10 and 14 m are presented for each cruise as indicators of the circulation patterns during the times of the cruises. They are compared with appropriate off-shelf fields of SSH (presented in Section 3) and with fields of vector winds averaged over the cruise periods and of geopotential anomaly of 3 m relative to 800 m (presented by cruise in Appendices A through I). Drifters were released during five of the cruises. Trajectories are presented and compared with other indicators of near-surface circulation. In considering these comparisons, the reader is advised to keep in mind the implications of the aliasing of the fields of SSH, ADCP, and geopotential anomaly discussed in Section 3.2.3.

In preparing the gridded fields of ADCP current vectors, repeated ADCP measurements over the same area during individual cruises have been removed; this may have removed some of the variability that might be seen in the ADCP vectors along cruise tracks shown in Appendices A through I describing the individual cruises. Then, gridded fields were produced using GMT. This may have reduced the effects of inertial oscillations and variability in general, but the ADCP measurements still contain high frequency motions such as tides and internal waves.

Current measurements using the shipboard ADCP were not detided prior to analysis for this report. Tides and inertial motions present in the ocean at the time of the measurements may introduce unwanted variability and, therefore, may be a source of noise in some of the calculations. Prior current meter studies from the west Florida shelf indicate that the percentage of total kinetic energy resulting from tidal motions in water depths greater than 50 m is low. Koblinsky (1979) reports that less than 10% of the total kinetic energy between 50 and 200 m on the west Florida shelf is due to semi-diurnal tides; thirty-two percent is contained in the diurnal band. A considerable portion of the diurnal energy, however, is incoherent with the tidal potential and presumably is related to local wind forcing and inertial motions. Marmorino (1983b) reports that 95% of the total kinetic energy off Cape San Blas (where the shelf narrows and tidal current ellipses diminish) is in the low (sub-inertial/tidal) frequencies. Inshore of the 20-m isobath on the west Florida shelf, tides can account for up to 85% of the observed kinetic energy (Marmorino 1983a). Because most of the study was in water depths greater than 20 m and because tidal current amplitudes decrease both offshore and to the west of the west Florida

shelf, we consider 20% to be an upper bound for the percentage of total kinetic energy attributable to tides.

If it is desired in future studies to remove tidal motions contained in shipboard ADCP measurements, we recommend using the ADCIRC tidal model for the Gulf of Mexico, which is driven at the open boundaries using a global model of the form of Tiernay et al. (2001). Inertial motions will continue to be a source of unwanted variability; however, estimates for the percentage of kinetic energy due to inertial motions in the shipboard measurements may be obtained if nearby long-term fixed or moored observations are available.

To estimate geopotential anomaly values at stations shallower than 800 m, the geopotential anomaly relative to 800 m was calculated first for an off-shelf station deeper than 800 m. Then, following the method of Montgomery (1941), the specific volume anomaly values along the bottom were extrapolated to obtain contributions of geopotential anomaly to the deepest sample depth of successively shallower stations. The implications of this method were discussed by Csanady (1985). To the extent that the bottom potential density is not uniform along isobaths, the estimation will not be independent of path of integration and caution is advised in interpreting results.

The drifter measurements presented here are from water-following drifters deployed on behalf of the MMS during selected NEGOM cruises. They are designed so they should follow the water of the upper meter of the water column. Thus, their trajectories are expected to display more Ekman effect than the ADCP measurements.

Cruise N1, 16-27 November 1997. The gridded ADCP currents at 10-12 meters observed on cruise N1 are shown in Figure 4.1-1. During this period an anticyclone was located over the western slope with center near 28.5°N, 88°W and moving eastward; a cyclone was off-shelf to the southeast centered near 28°N, 86.5°W (Figure 3.2.3-3a). The influence of both these features is clear in the geopotential anomaly field at 3 m relative to 800 m (Figure A.2-5) where the anticyclonic feature appeared to extend onto the eastern flank of DeSoto Canyon. The effect of the anticyclone likewise is clear in the ADCP field at the shelf edge south of Mississippi-Alabama; the cyclone is not seen. In both the ADCP and geopotential anomaly fields there is evidence of another anticyclonic feature over the slope south of about 28°N.

Winds during this period (Figure A.1.1-1) were downcoast west of about 84°W and there is some indication of downcoast nearshore flow in the ADCP field. West of Cape San Blas, the geopotential anomaly inshore of the 50-m isobath does not agree well with ADCP measured currents—indicating instead cross-isobath flow. Over the west Florida shelf in the Big Bend region both dynamics and ADCP show a cyclonic circulation centered on line 10. The inshore closure is not so clear in the ADCP field with indications of upcoast flow on the inshore portion of this line, which would agree with an upcoast component of along-coast wind in the area.

Trajectories of the four drifters deployed during cruise N1 (Figure 4.1-2) appear to follow reasonably well the geopotential anomaly pattern over the outer shelf and slope. The drifter deployed over the inner shelf between Pensacola and Panama City first moved up and downcoast, probably in a varying coastal current, and then moved southeast.

Cruise N2, 5-16 May 1998. The 14-m ADCP current field is shown in Figure 4.1-3. The principal features over the outer shelf and slope are a region of apparent divergence centered near 28.7°N, 86.5°W and three regions of anticyclonic flow: a small feature centered near 88.5°W, a closed feature over DeSoto Canyon (centered near 29.4°N, 87°W), and part of a

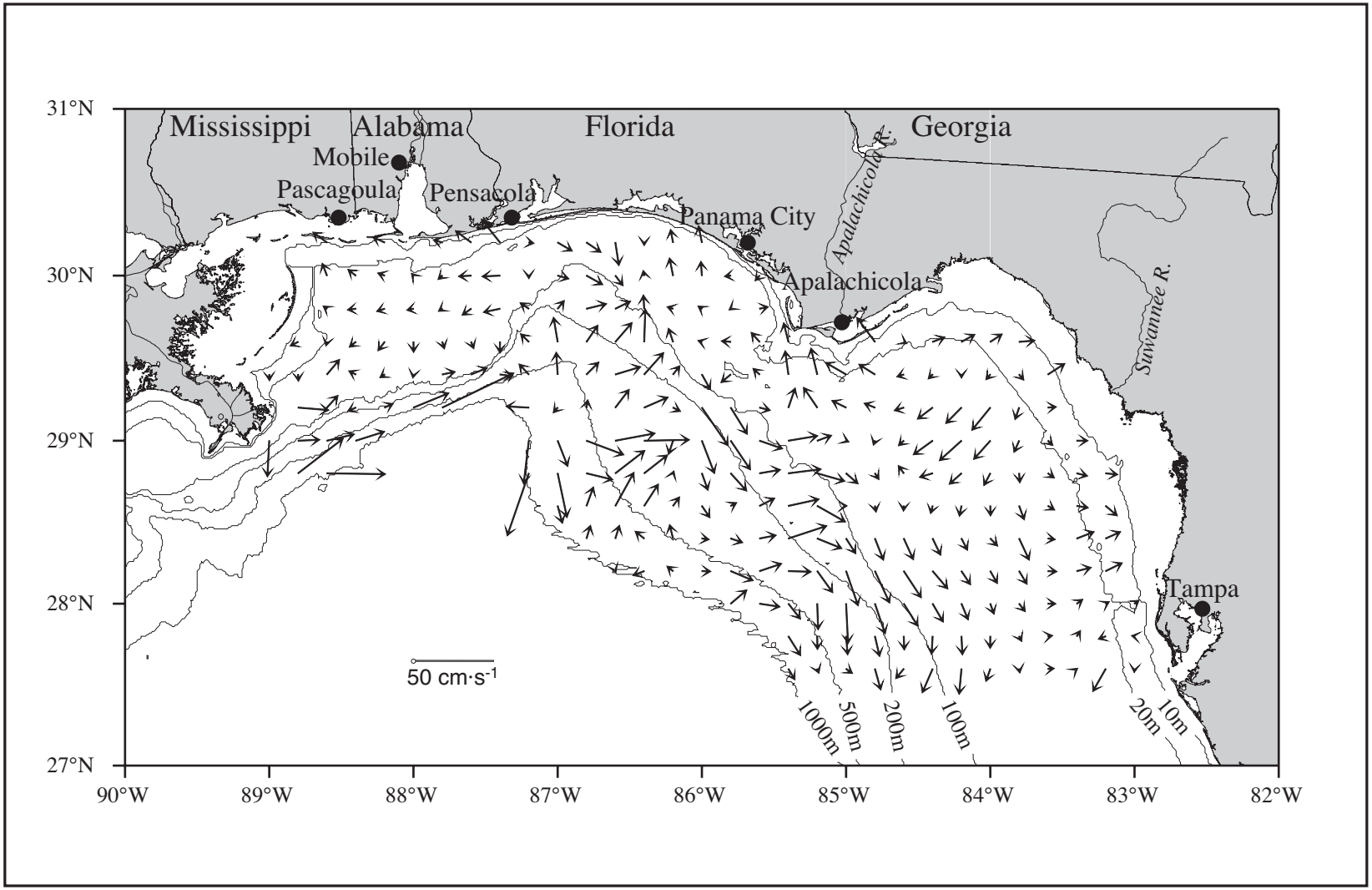

Figure 4.1-1. Gridded ADCP-measured currents at 10 m and 12 m on NEGOM Cruise N1, 16-27 November 1997.

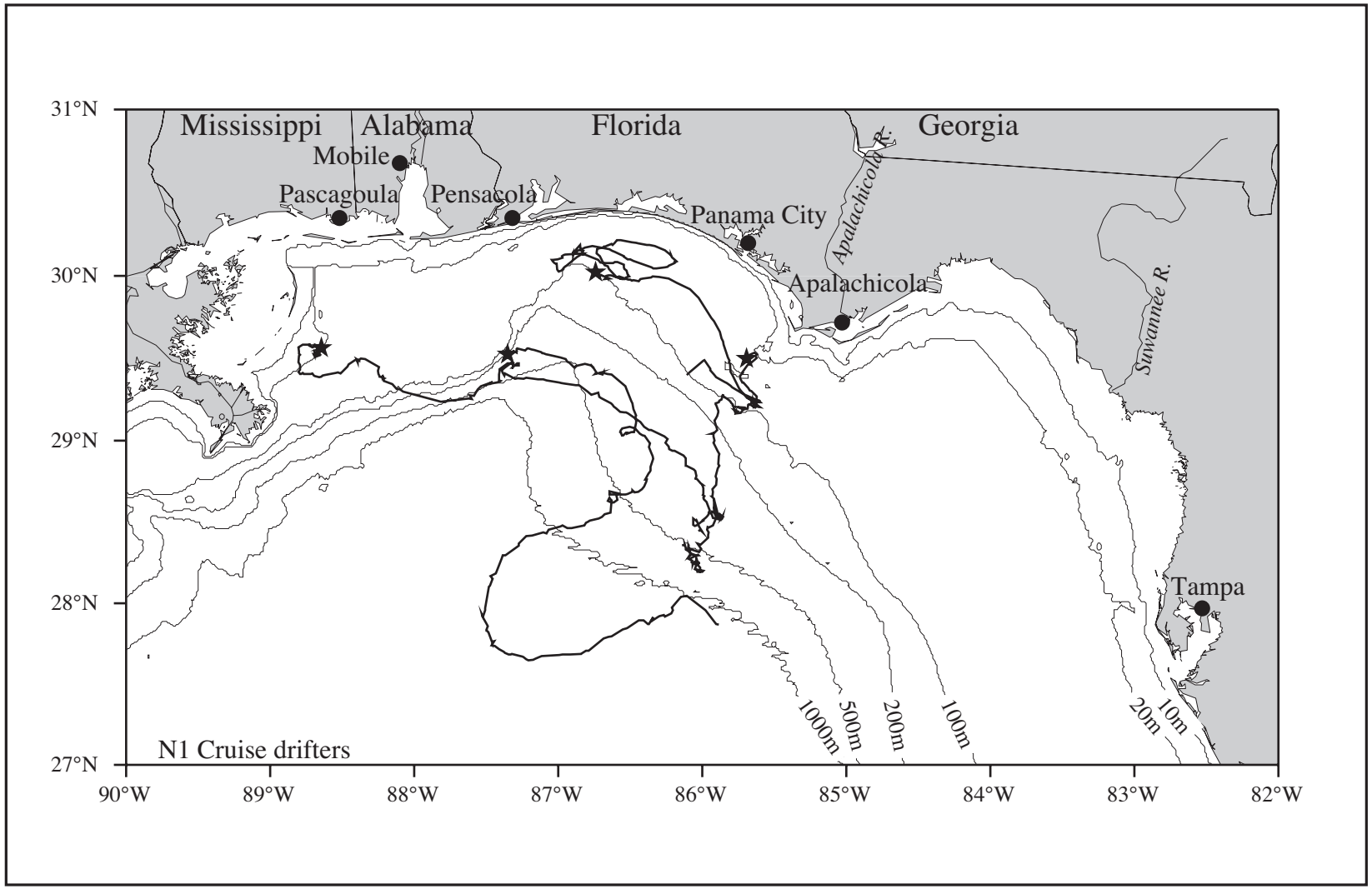

Figure 4.1-2. Trajectories of NEGOM drifters (drogued in the upper meter) deployed during cruise N1. Trajectories are continued for one month (26 December 1997) past the cruise period. Stars denote drifter deployment location.

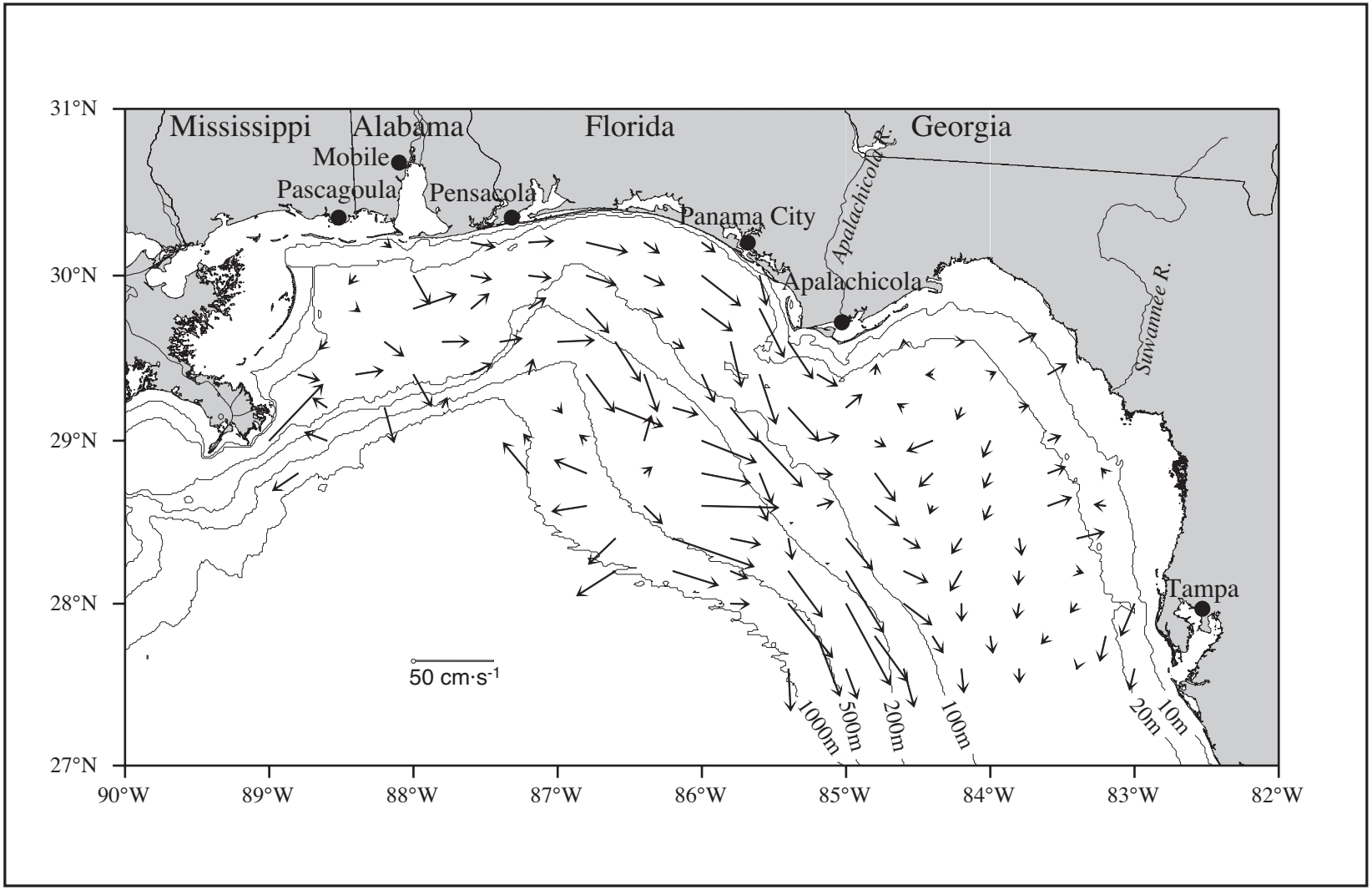

Figure 4.1-3. Gridded ADCP-measured currents at 14 m on NEGOM Cruise N2, 5-16 May 1998.

strong feature with center somewhere off-shelf near 27.5°N. These anticyclonic features are clearly seen in the geopotential anomaly of 3 m relative to 800 m (Figure B.2-1). The surface divergence region was located between the central and eastern anticyclones. These two off-shelf anticyclones are seen in the SSH field (Figure B.1.3-1).

Over the inner shelf from Mobile Bay to somewhat past Cape San Blas both geopotential anomaly and ADCP fields show strong upcoast flow. This might be attributed to a combination of the effect of the anticyclone over DeSoto Canyon and a wind regime slightly favorable for upcoast flow in that same area for the period of the cruise (Figure B.1.1-1). Over the inner shelf in the Big Bend area the dynamics and ADCP results generally indicate onshore drift north of Tampa and upcoast flow off Tampa and to the south.

The trajectories for surface drifters released on cruise N2 are shown in Figure 4.1-4. We examined the beginning portions of individual trajectories and found them to be in reasonably good agreement with circulation indicated by other fields.

Cruise N3, 25 July–7 August 1998. The gridded 14-m ADCP currents are shown in Figure 4.1-5. Shown here and in the 3 m relative to 800 m geopotential anomaly field (Figure C.2-4) is the strong effect over the outer shelf and slope of an off-shelf anticyclone. That feature was elongated northwest-southeast with a center approximately at 28.5°N, 87.5°W during the cruise period (Figures 3.2.3-11 and 3.2.3-12a). The closed circulation in that feature as well as the strong upcoast flow over the outer shelf and slope are confirmed also by surface drifter trajectories (Figure 4.1-6).

Over the inner shelf there is evidence in the ADCP field of a cyclone centered over the apex of DeSoto Canyon but extending over much of the Alabama-Mississippi shelf as well, and probably associated with the northward flow over the Mississippi shelf. A cyclone was over the inner shelf in the Florida Big Bend centered about line 10 according to ADCP vectors. The inshore closure of that feature by northward flow is seen in several of the drifter trajectories. Winds were weak during cruise N3 (Figure C.1.1-1) but were consistent with downcoast flow west of Cape San Blas. The geopotential anomaly field (Figure C.2-4) agrees rather well with the ADCP field over the inner shelf west of Cape San Blas; the cyclone pictured on the west Florida shelf in the geopotential anomaly field is displaced northwestward to give a center between lines 8 and 9, rather than on line 10.

Cruise N4, 13-24 November 1998. For this cruise period, the SSH fields (Figures 3.2.3-15c, d, and 3.2.3-16a) showed a weak anticyclone centered about 28.5°N, 88°W and a continued lowering of sea level into DeSoto Canyon. The ADCP 12-m vectors for cruise N4 (Figure 4.1-7) exist only for the region offshore and west of Pensacola. Shown in that pattern is strong downcoast inshore flow and weak upcoast flow over the shelf edge and slope. This is consonant with strong downcoast wind components west of the Suwannee River during the cruise period (Figure D.1.1-1) and a weak off-shelf anticyclone.

That pattern of inner shelf flow west of DeSoto Canyon is greatly at odds with the geopotential anomaly at 3 m relative to 800 m (Figure D.2-4) which shows cross-shelf contours over the entire inner shelf. The drifter trajectories over the Alabama shelf (Figure 4.1-8) showed along-shelf currents, also at odds with the dynamics. Drifter trajectories east of DeSoto Canyon give evidence of upcoast flow for three trajectories located over the mid-shelf to slope. According to the dynamics, a large, if weak, cyclone extended across the entire west Florida shelf southeast of Cape San Blas.

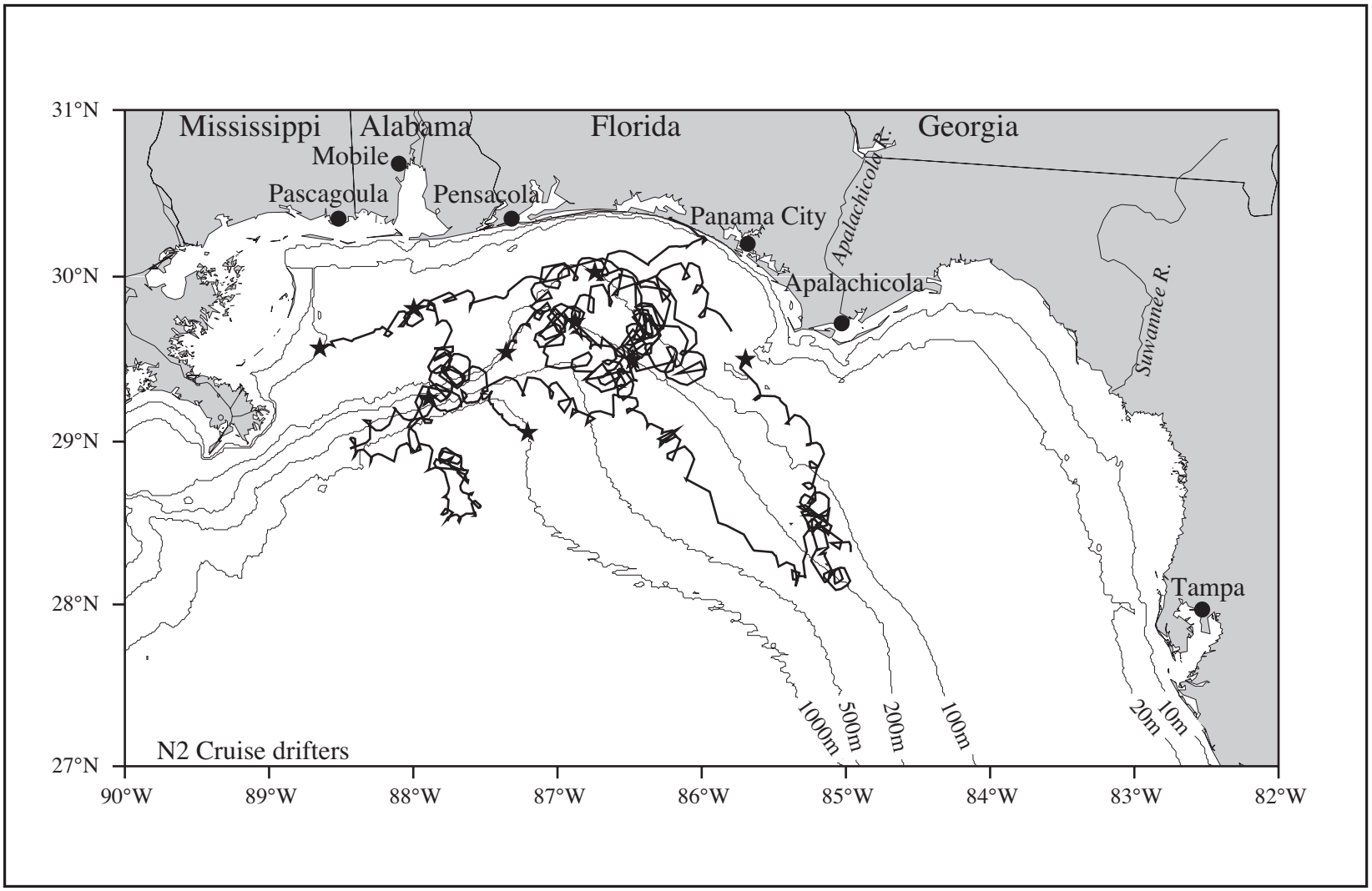

Figure 4.1-4. Trajectories of NEGOM drifters (drogued in the upper meter) deployed during cruise N2. Trajectories are continued until 31 May 1998. Stars denote drifter deployment location.

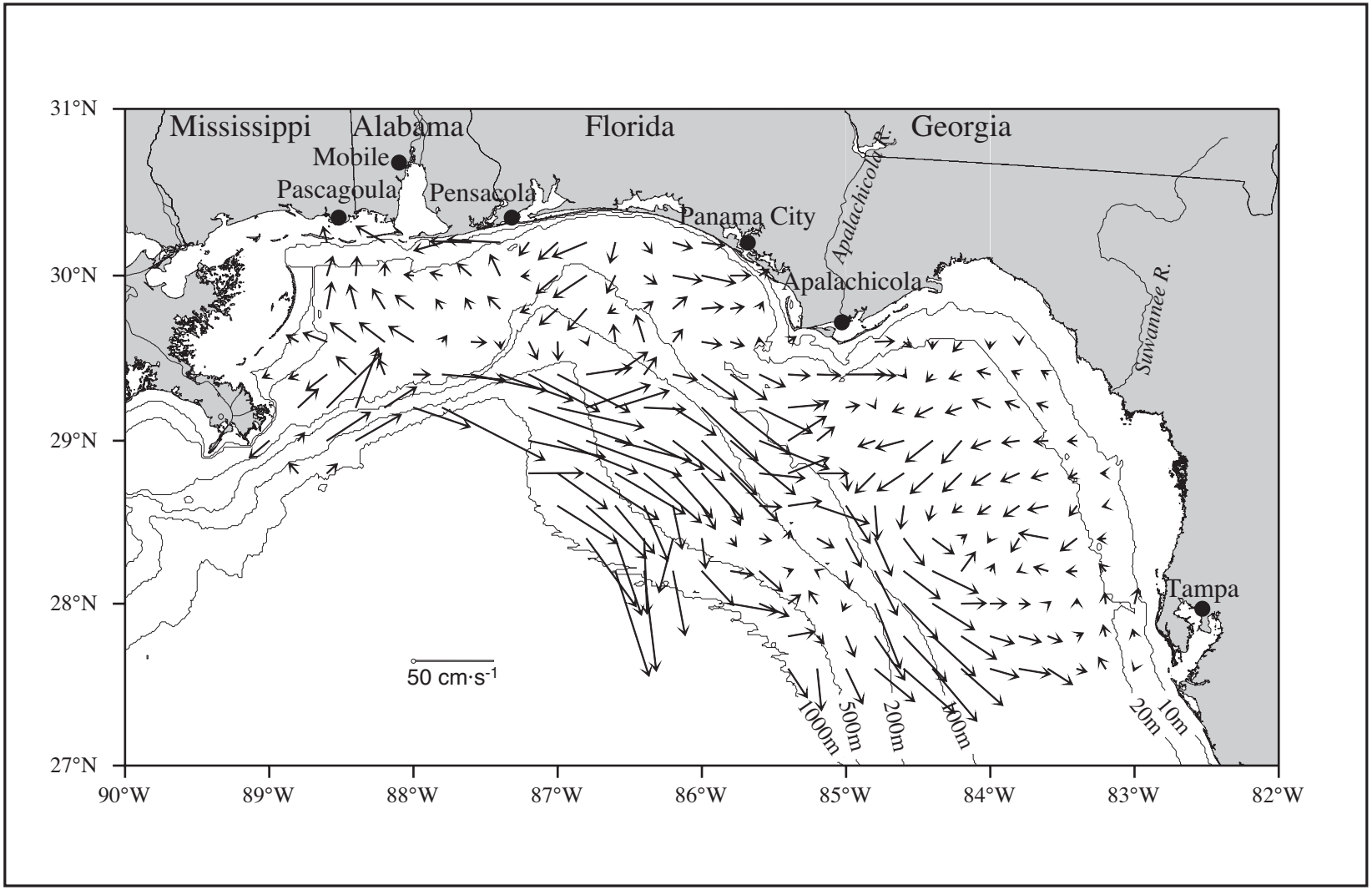

Figure 4.1-5. Gridded ADCP-measured currents at 14 m on NEGOM Cruise N3, 25 July - 7 August 1998.

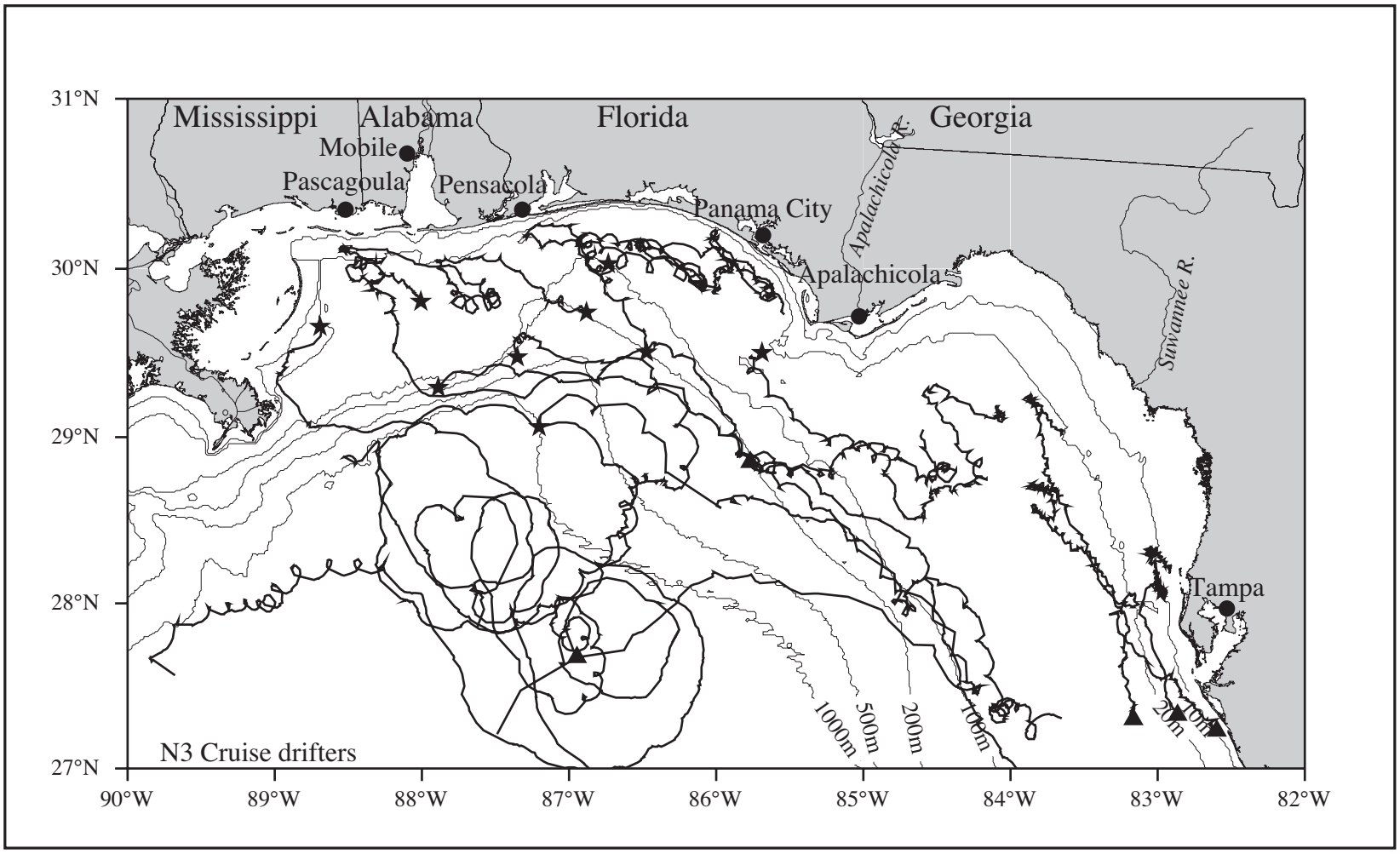

Figure 4.1-6. Trajectories of NEGOM drifters (drogued in the upper meter) for period from 20 July through 4 September 1998. Stars denote drifter deployment locations; triangles denote drifter locations on 20 July 1998 for drifters deployed prior to the period covered here.

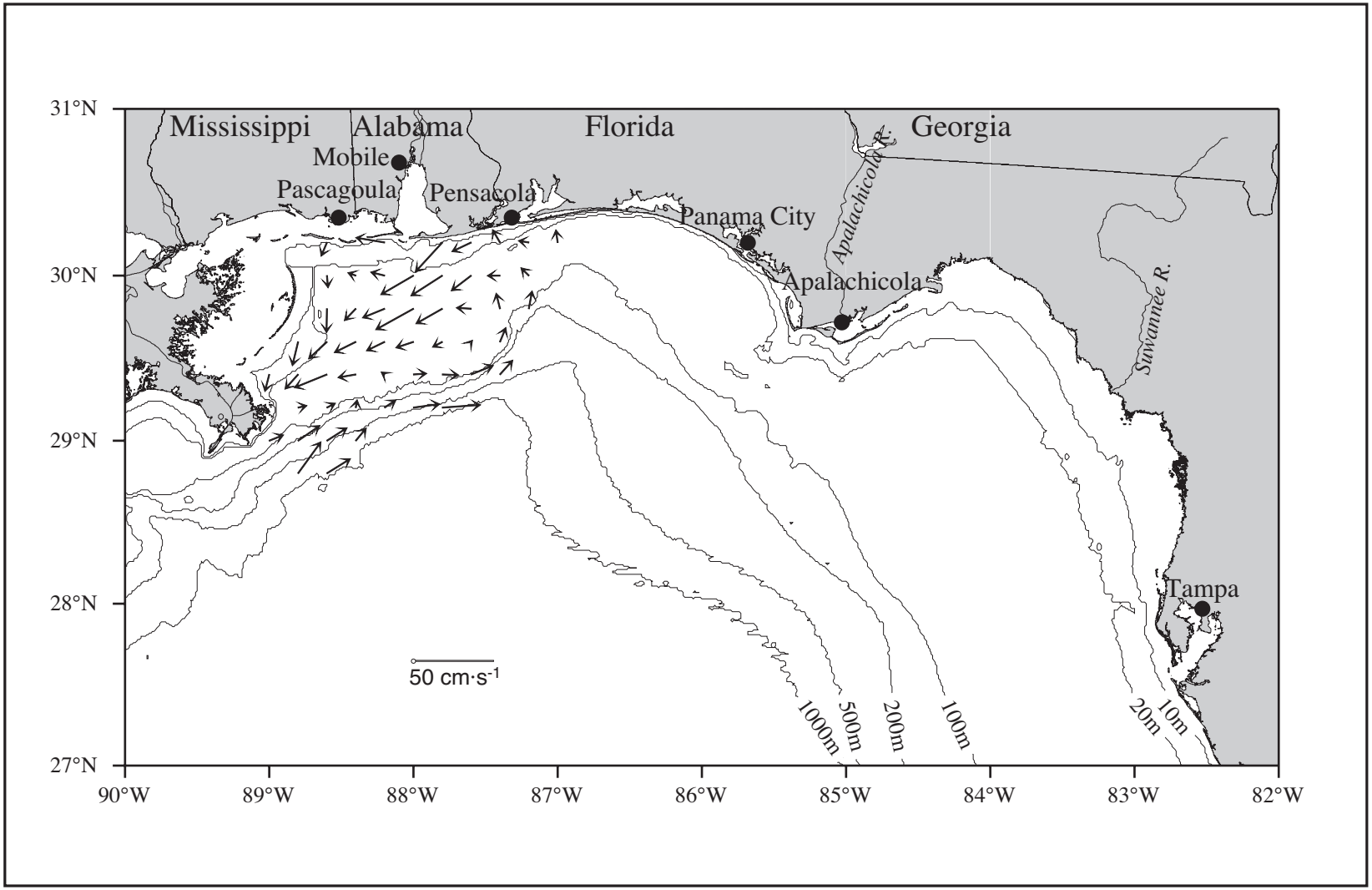

Figure 4.1-7. Gridded ADCP-measured currents at 12 m on NEGOM Cruise N4, 13 - 24 November 1998.

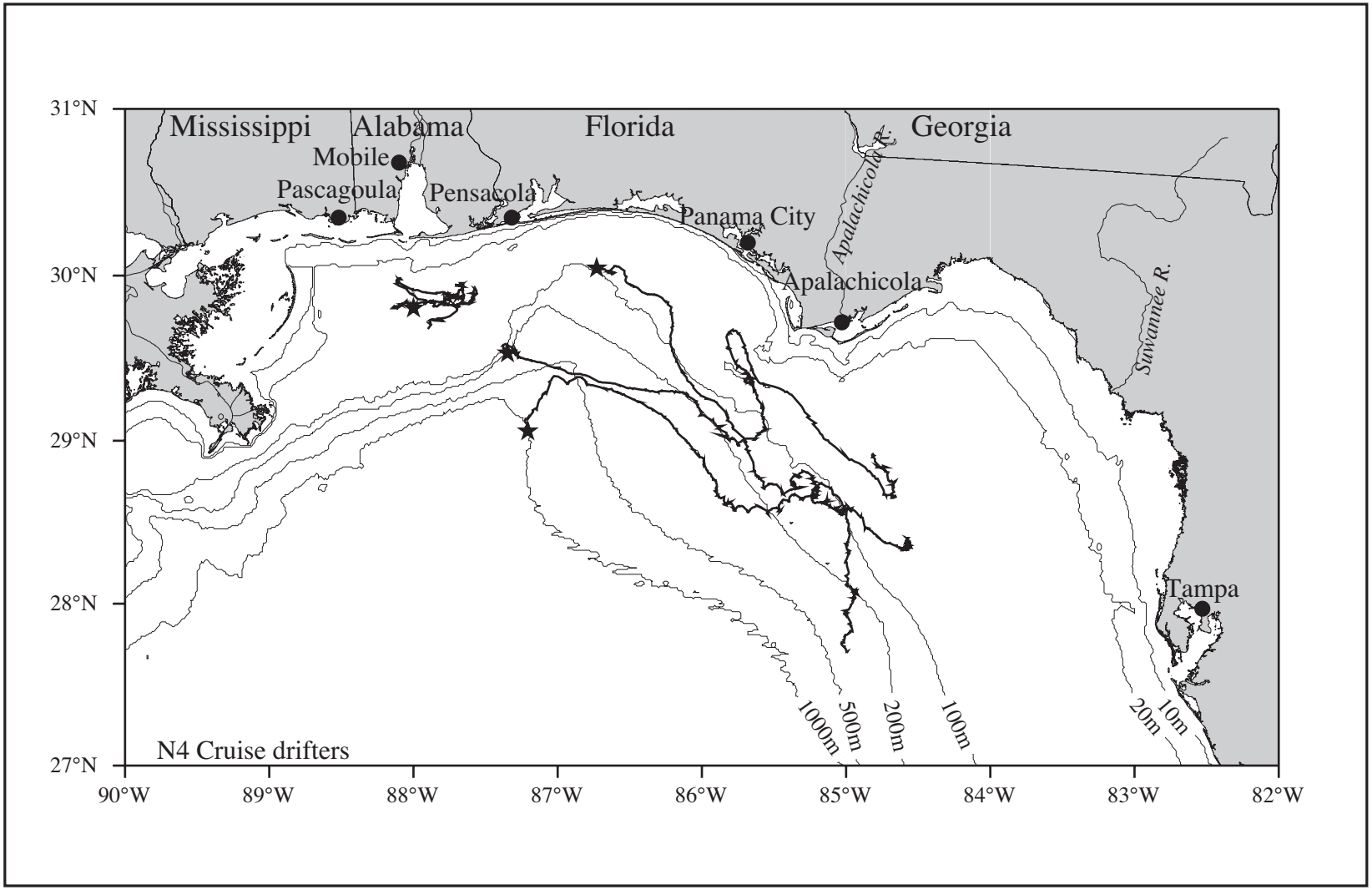

Figure 4.1-8. Trajectories of NEGOM drifters (drogued in the upper meter) deployed during cruise N4. Trajectories are continued for one month (24 December 1998) past the cruise period. Stars denote drifter deployment locations.

Cruise N5, 15-28 May 1999. During this cruise period a low in SSH was located south of the region (Figures 3.2.3-22a-c). It was elongated with its center stretching from about 28.2°N, 88.5°W to 28°N, 86.5°W. It was relatively weak, with center depressions of 15-20 cm, and extended to the shelf edge only south of the Mississippi Delta. No evidence of that feature is seen in the gridded ADCP field (Figure 4.1-9) or the geopotential anomaly field at 3 m relative to 800 m (Figure E.2-2). Both of the latter fields agree well over the outer shelf showing a low around the mouth of the Mississippi, a small closed cyclone over the shelf edge near 88.5°W, a weak cyclone over DeSoto Canyon centered near 29.2°N, 86.8°W, and a quite strong anticyclonic feature off-shelf west of Tampa.

Over the inner shelf, the geopotential anomaly field is consistent with upcoast coastal flow west of Cape San Blas, with a closed clockwise circulation centered south of Pensacola. The ADCP field shows upcoast flow over the entire shelf (inner and outer) west of Cape San Blas. In the Big Bend region the geopotential anomaly was essentially flat while the ADCP field showed a large-scale cyclonic circulation with strong cross-shelf components (20 $cm \cdot s^{-1}$) but no closure nearshore was measured. Winds during the cruise (Figure E.1.1-1) were quite variable, especially over the western shelf, with mean along-shelf components upcoast east of Pensacola.

Cruise N6, 15-28 August 1999. Before and during the cruise period, SSH analyses (Figures 3.2.3-25a-d) showed development of an anticyclonic feature centered near 28°N, 87°W as an extension of a much stronger anticyclonic feature to the south. SSH was shown to decrease onshore to the 200-m isobath. That is in rather good agreement with the geopotential anomaly of 3 m relative to 800 m (Figure F.2-1) and the gridded ADCP field (Figure 4.1-10). The geopotential anomaly field shows strong upcoast currents over the outer shelf and slope with an anticyclonic extension into the DeSoto Canyon; the ADCP field shows mixed directions south of Mississippi-Alabama.

Over the inner west Florida shelf, there is some evidence of a clockwise flow pattern in the ADCP fields, but the geopotential anomaly shows a cyclone. Both patterns are very weak and likely unreliable indicators of the actual flow regime at the time. Wind fields during the cruise period were weakly downcoast in this area and upcoast west of Cape San Blas with small to moderate variability (Figure F.1.1-1) in agreement with the field of geopotential anomaly.

Cruise N7, 13-25 November 1999. The gridded ADCP field (Figure 4.1-11) shows for the slope: downcoast flow west of DeSoto Canyon, upcoast flow from the canyon axis to about 86.5°W, and evidence of an off-shelf cyclone southeast thereof. This is in agreement with currents indicated by the SSH fields during the cruise (Figures 3.2.3-28d and 3.2.3-29a). Those fields show cyclones off-shelf along the study area west of DeSoto Canyon and to the southeast with upcoast flow along the slope in between. Drifter trajectories also give evidence of an off-shelf cyclone in the western study area and upcoast flow over the slope east of DeSoto Canyon (Figure 4.1-12). Both ADCP and geopotential anomaly fields (Figure G.2-2) show a low over the southeastern flank of DeSoto Canyon, the cyclonic flow over the slope off Tampa, and upcoast flow over the slope in between. Otherwise, the geopotential anomaly field generally is not in agreement with the ADCP field.

Winds during the cruise (Figure G.1.1-1) were rather strong with moderate variability over the inner shelf. They had upcoast along-shelf components from Tampa to somewhat northwest of the Suwannee River mouth; farther westward they were favorable for driving downcoast currents. This is in good agreement with the ADCP field over the Big Bend region. However, west of Cape San Blas the measured nearshore currents were upcoast. Surface drifters in that nearshore region generally moved downcoast, presumably in response to the wind forced coastal current.

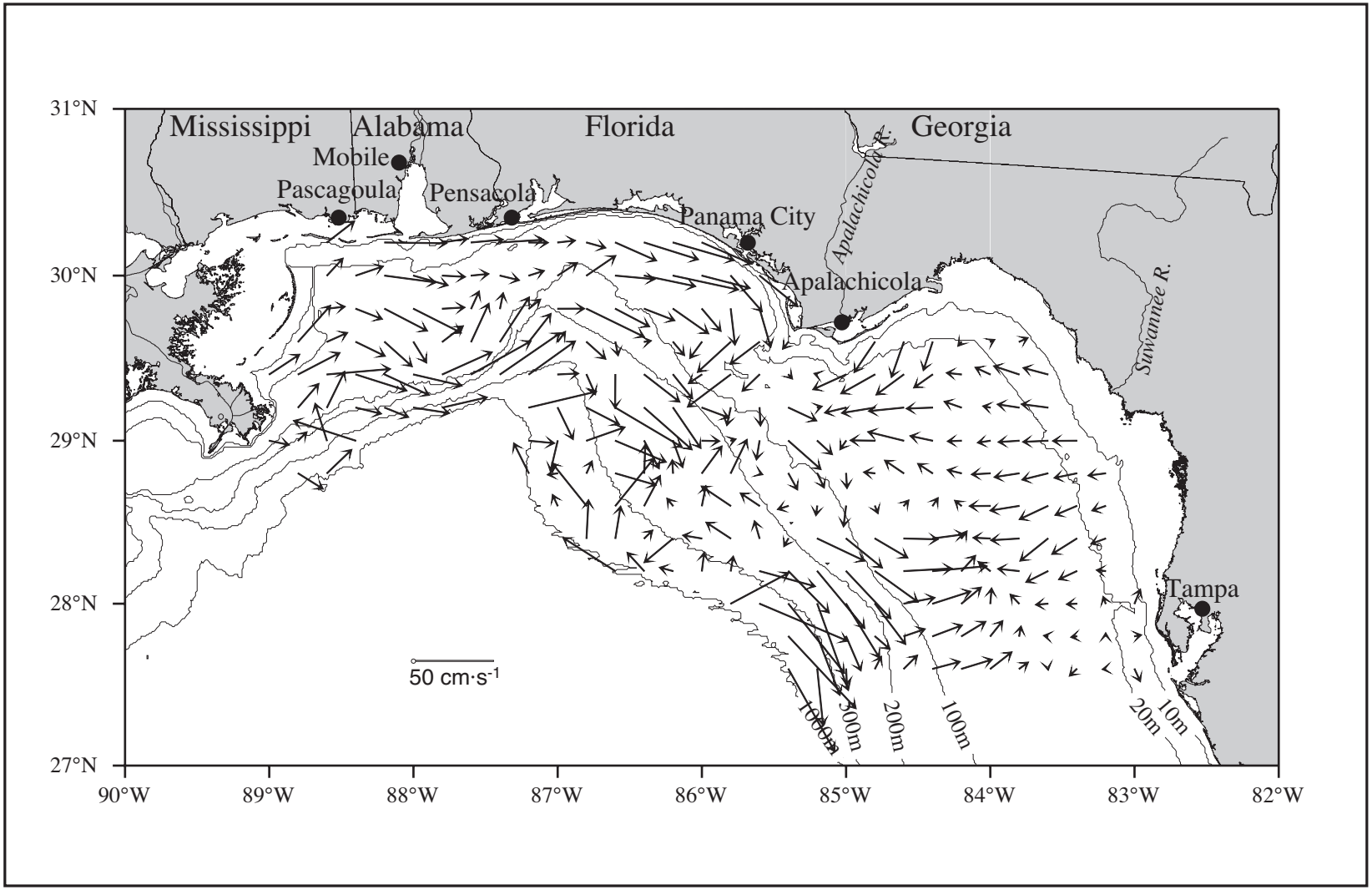

Figure 4.1-9. Gridded ADCP-measured currents at 14 m on NEGOM Cruise N5, 15-28 May 1999.

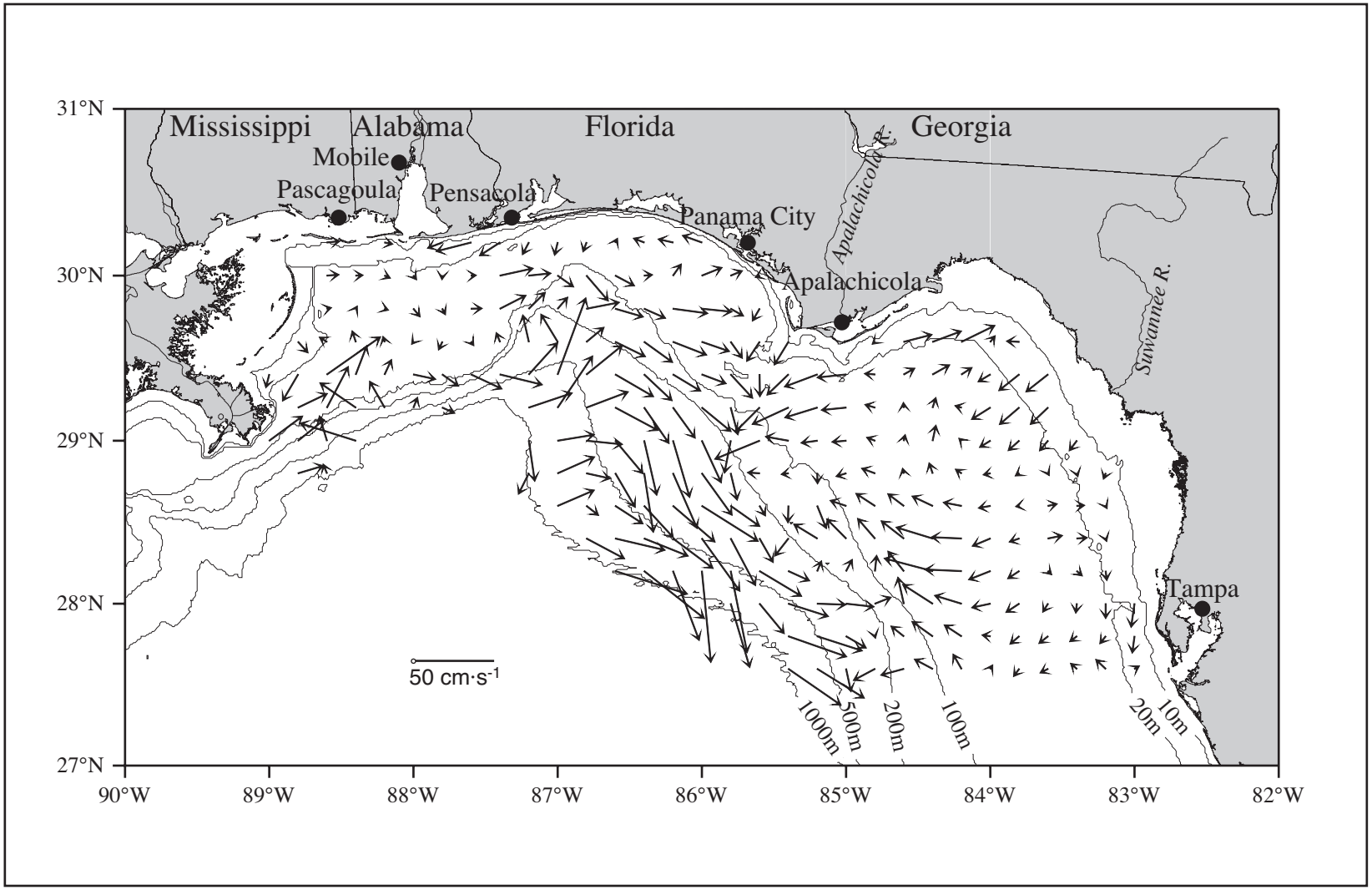

Figure 4.1-10. Gridded ADCP-measured currents at 14 m on NEGOM Cruise N6, 15-28 August 1999.

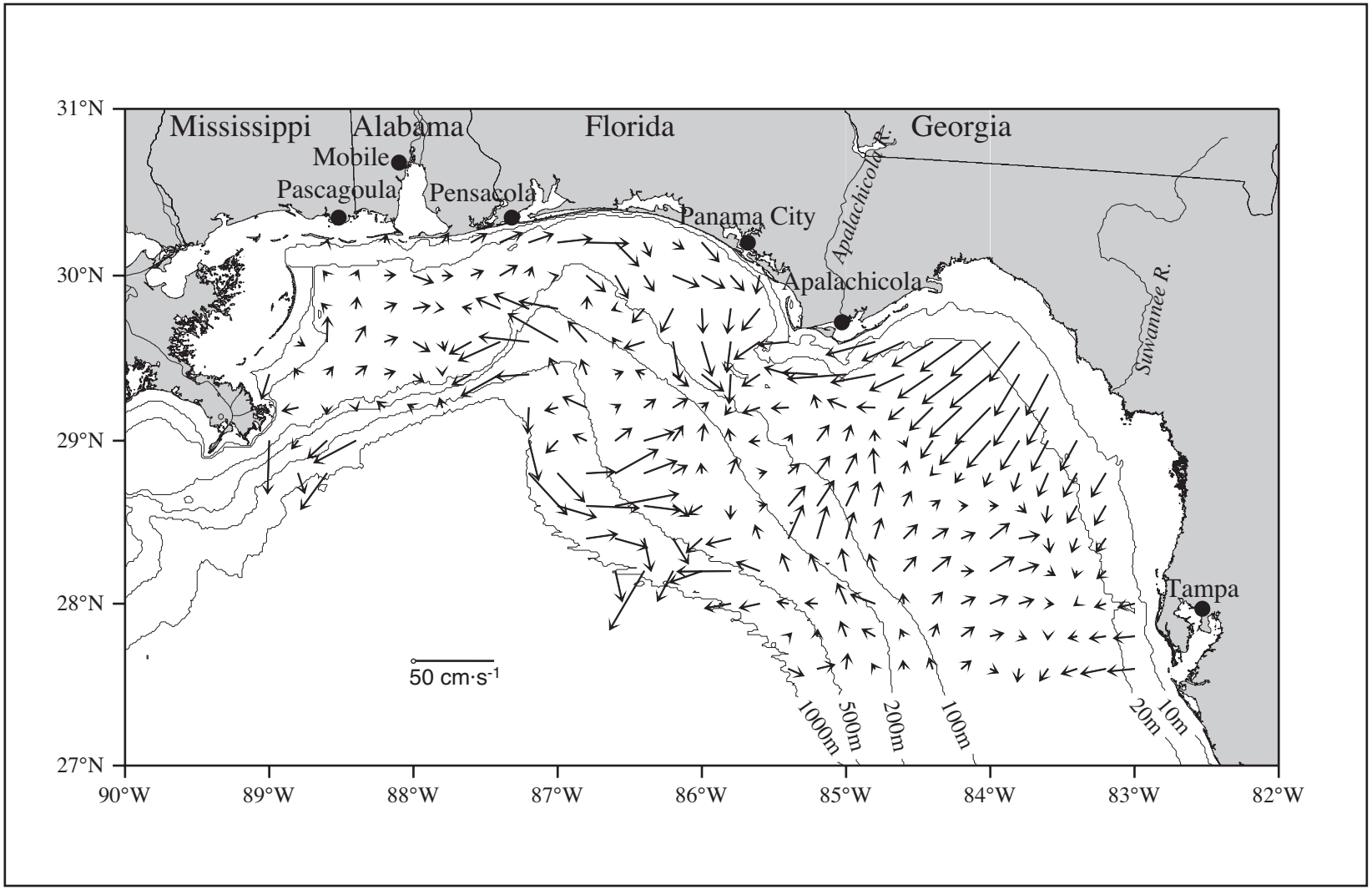

Figure 4.1-11. Gridded 38kHz ADCP-measured currents at 14 m on NEGOM Cruise N7, 13-25 November 1999.

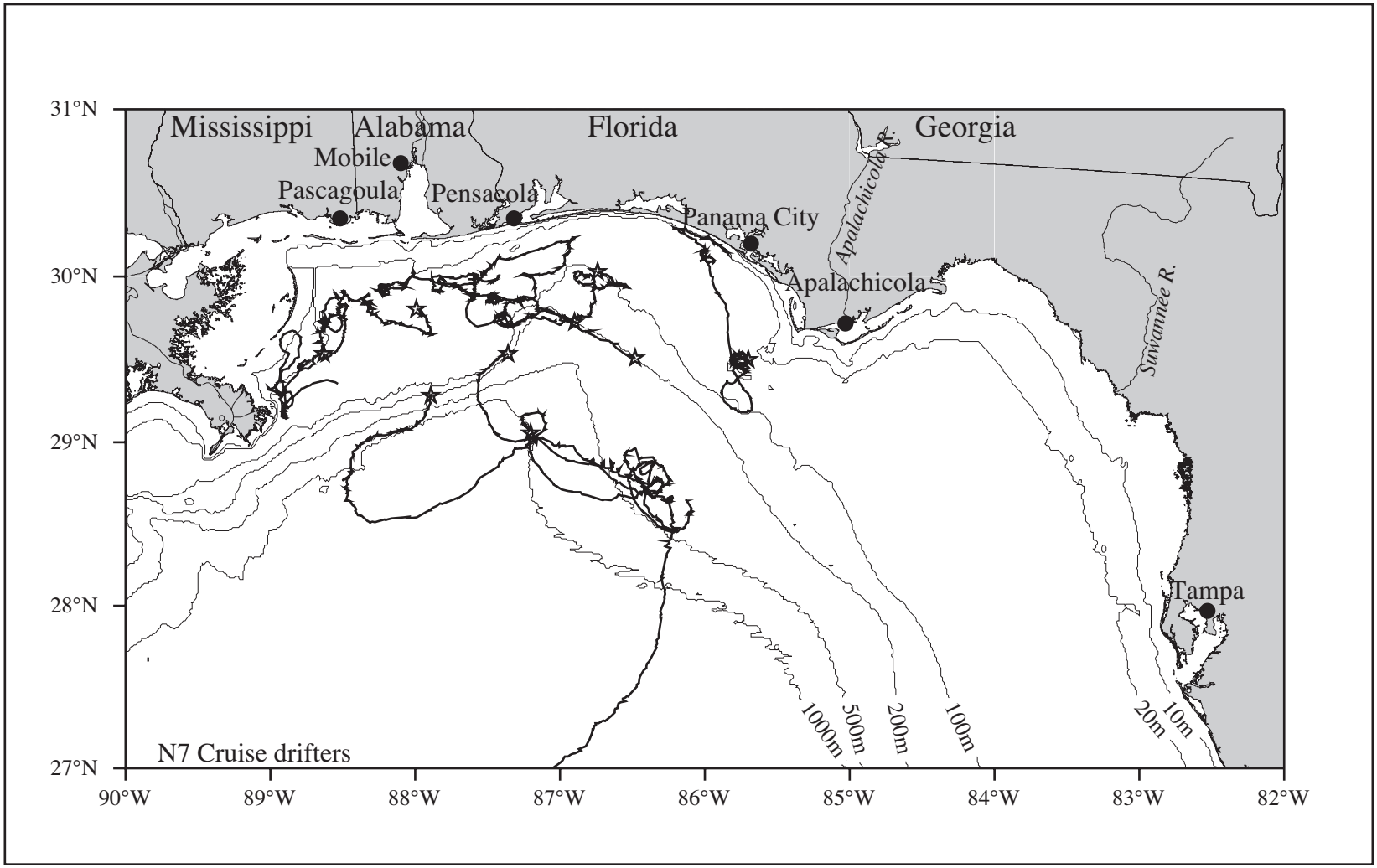

Figure 4.1-12. Trajectories of NEGOM drifters (drogued in the upper meter) deployed during cruise N7. Trajectories are continued for about one month (18 December 1999) past the cruise period. Stars denote drifter deployment locations.

Cruise N8, 15-26 April 2000. SSH fields during the cruise period (Figures 3.2.3-34a-c) showed an anticyclone centered over the shelf break near 88.5°W, a weak anticyclone centered near 29°N, 86.5°W, and a cyclonic system further off-shelf and to the southeast. This is in agreement with the geopotential anomaly of 3 m relative to 800 m dynamic (Figure H.2-3). The gridded ADCP field (Figure 4.1-13) shows a similar pattern south of the Louisiana-Mississippi, but the ADCP currents are not coherent over the DeSoto Canyon region. The geopotential anomaly field is in poor agreement with ADCP currents over the inner shelf. Winds during cruise N8 (Figure H.1.1-1) were upcoast favorable at all locations though quite variable during the cruise period. However, they were quite weak along the Mississippi and Alabama coast, strongest in the central study area, and almost onshore closer to Tampa Bay. The nearshore ADCP currents show good agreement with the expected pattern of wind-driven coastal currents.

Cruise N9, 29 July–8 August 2000. According to SSH fields, a relatively strong anticyclone was located over the slope extending from just southeast of the Mississippi Delta to near 86.5°W during the cruise period (Figures 3.2.3-38a-b). This is seen in both the geopotential anomaly for 3 m relative to 800 m (Figure I.2-2) and the gridded ADCP field (Figure 4.1-14). Another large anticyclonic feature is seen in both fields centered near 28.5°N, 86.6°W and dominating the outer shelf and slope circulation. In general, the ADCP currents and geopotential anomaly field agree rather well for this cruise with two exceptions. From Cape San Blas to Pensacola, ADCP currents nearshore were westward but isopleths of geopotential anomaly were cross-shelf over most of this region. In the Big Bend area, both fields give evidence of a large cyclonic feature centered near the 50-m isobath; ADCP vectors do not show inshore closure (i.e., downcoast flow) although the winds were downcoast favorable over that area during the cruise (Figure I.1.1-1).

4.2 The Annual Cycle of Currents from Surface Drifters

Prior to the beginning of the NEGOM Chemical Oceanography and Hydrography study, MMS supported the release of surface water following drifters (called SCULP II for the Surface Current Lagrangian Program) over the study area. Releases were carried out at two-week intervals from February 1996 until March 1997. The positions of these drifters were tracked via System Argos until they left the area of interest.

Although this release of SCULP drifters occurred over a time interval too short to establish meaningful measures of seasonal variability or to give indications of interannual variability, the resulting patterns of surface currents still seem worthy of examination. It should be noted that these drifters are expected to have large local Ekman effects compared with the ADCP measurements discussed.

We received the drifter locations from the MMS. Raw position fixes were converted to 1.5 hour intervals prior to our reception. Velocities were calculated by estimating the distance between successive fixes and dividing by the time interval (1.5 hours). For each 1/5° latitude x 1/5° longitude box in the region north of 27°N and east of 90°W vector velocities were averaged and variance ellipses prepared for all observations and by season. Examination showed that the currents over deeper water showed wildly varying velocities and quite large variances because of the limited number of observations. We limited our examinations to grid boxes having at least 100 observations.

The resulting numbers of observations, fields of vector mean surface currents, and variance ellipses are shown in Figures 4.2-1 through 4.2-12 for winter (December - February), spring (March - May), summer (June - August), and fall (September - November) seasons.

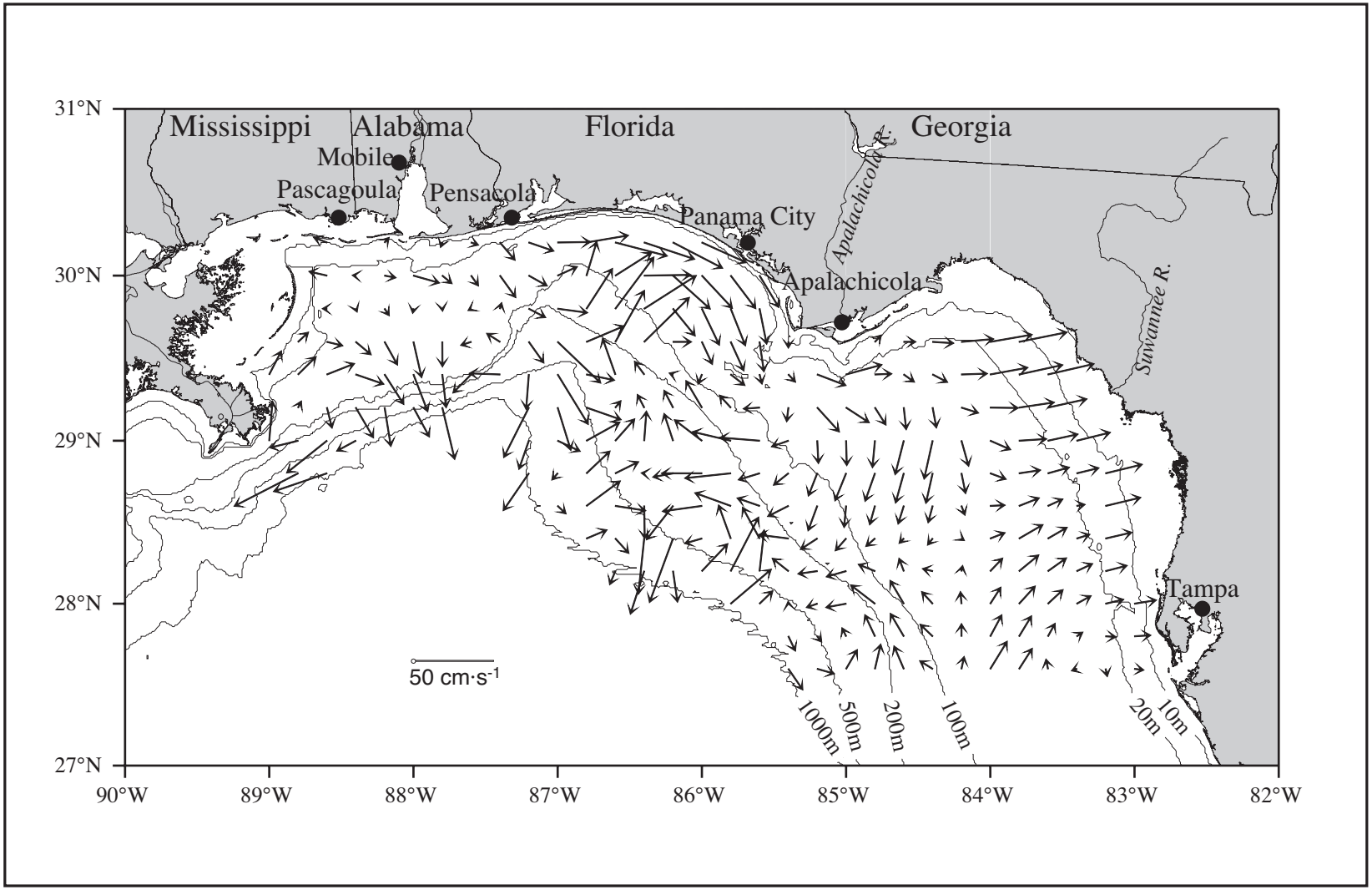

Figure 4.1-13. Gridded 150 kHz ADCP-measured currents at 12 m on NEGOM Cruise N8, 15-26 April 2000.

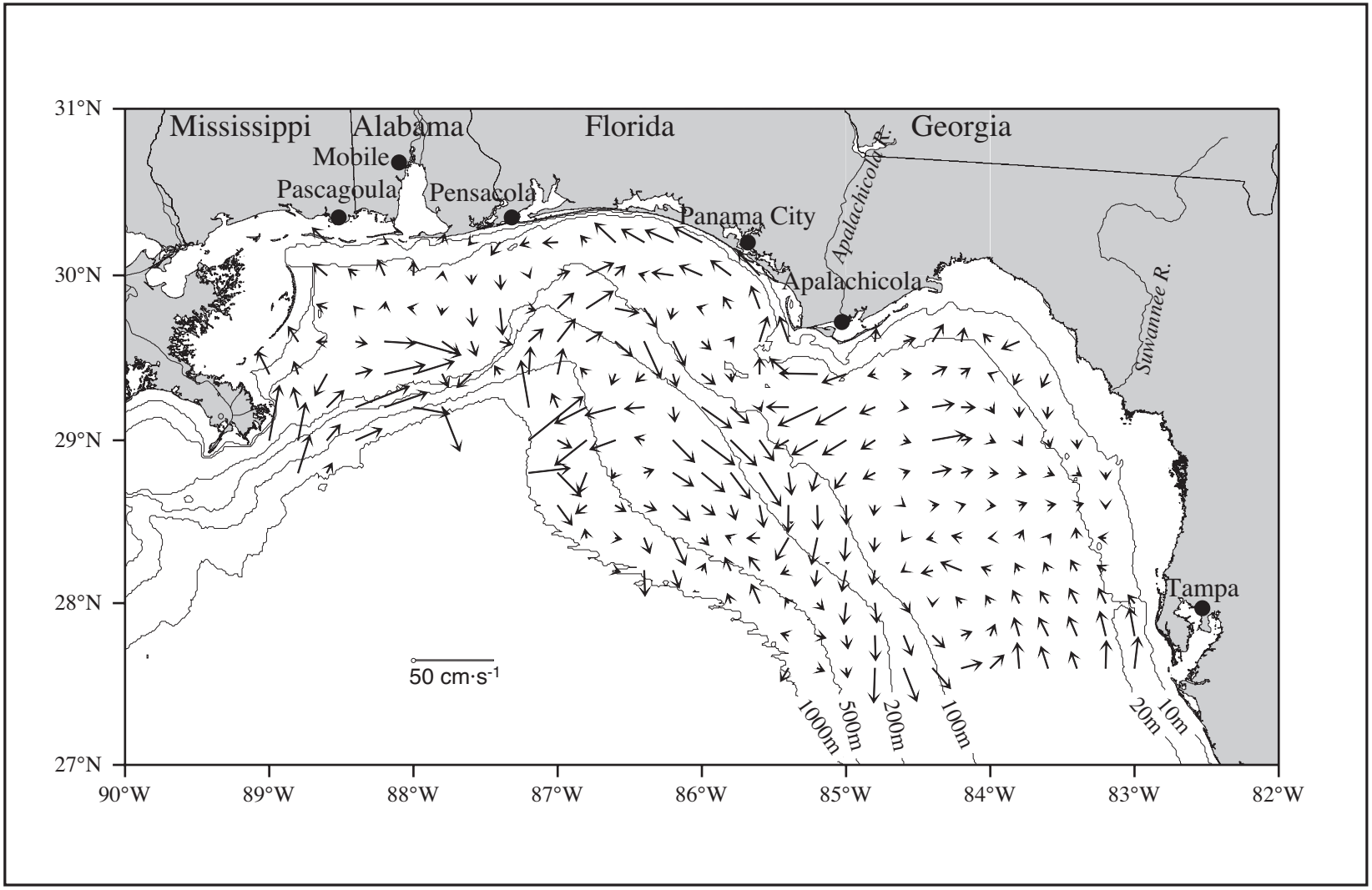

Figure 4.1-14. Gridded 150 kHz ADCP-measured currents at 12 m on NEGOM Cruise N9, 29 July - 8 August 2000.

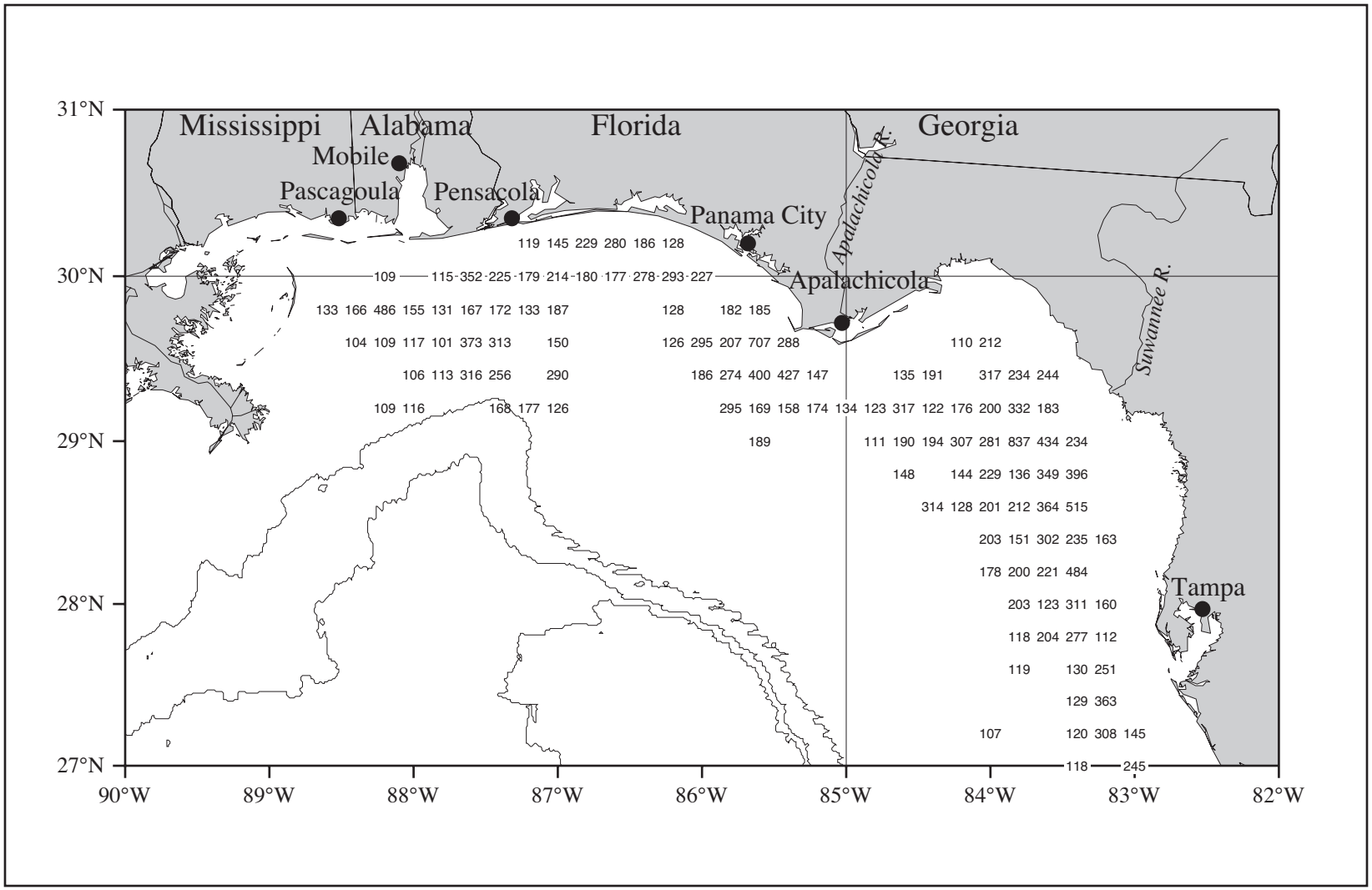

Figure 4.2-1. Numbers of observations from winter SCULP II drifter releases February 1996-March 1997. Shown are the 1000-, 2000-, and 3000-m isobaths.

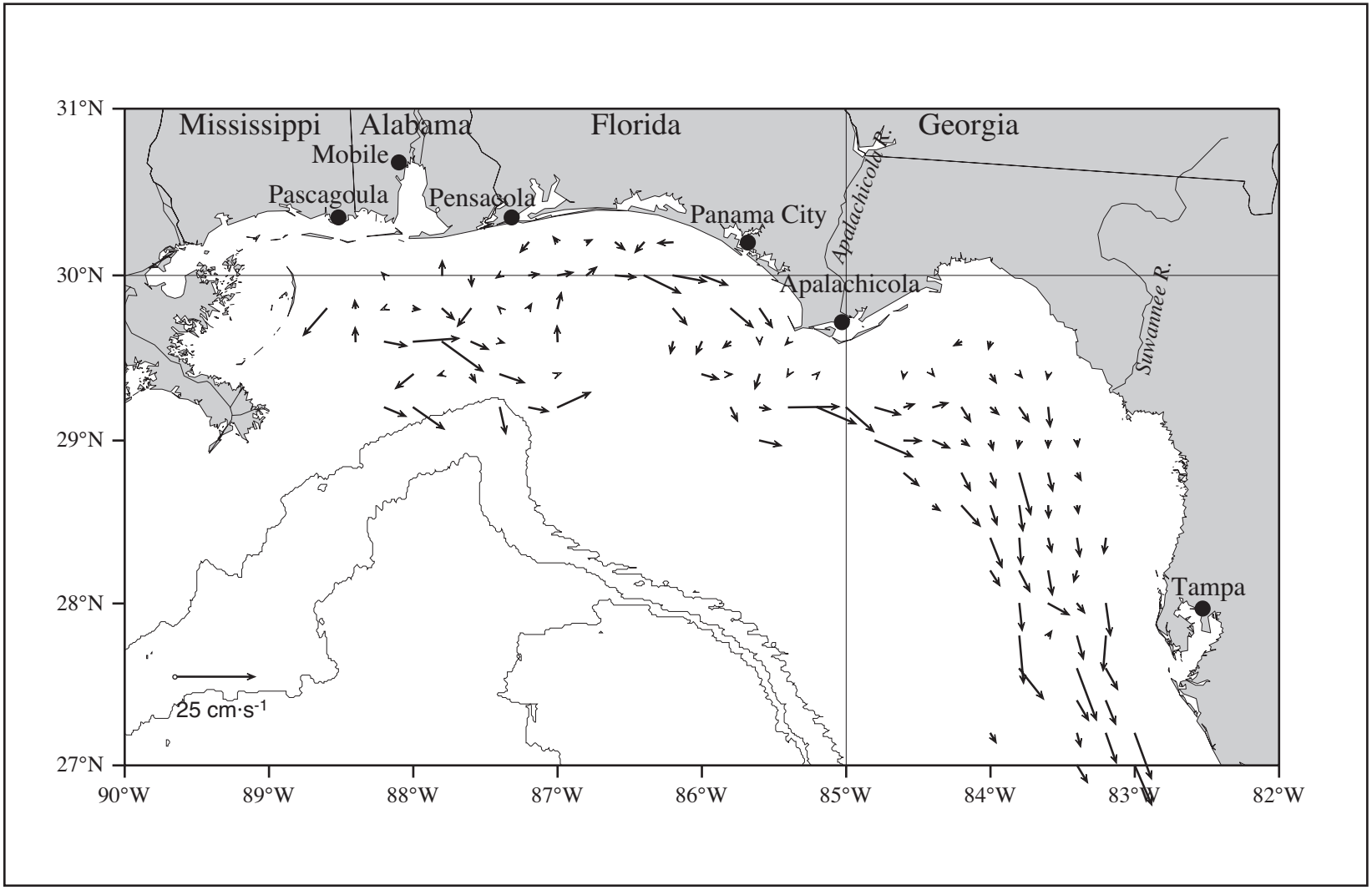

Figure 4.2-2. Average surface vectors for winter from SCULP II drifter releases February 1996-March 1997. Shown are the 1000-, 2000-, and 3000-m isobaths.

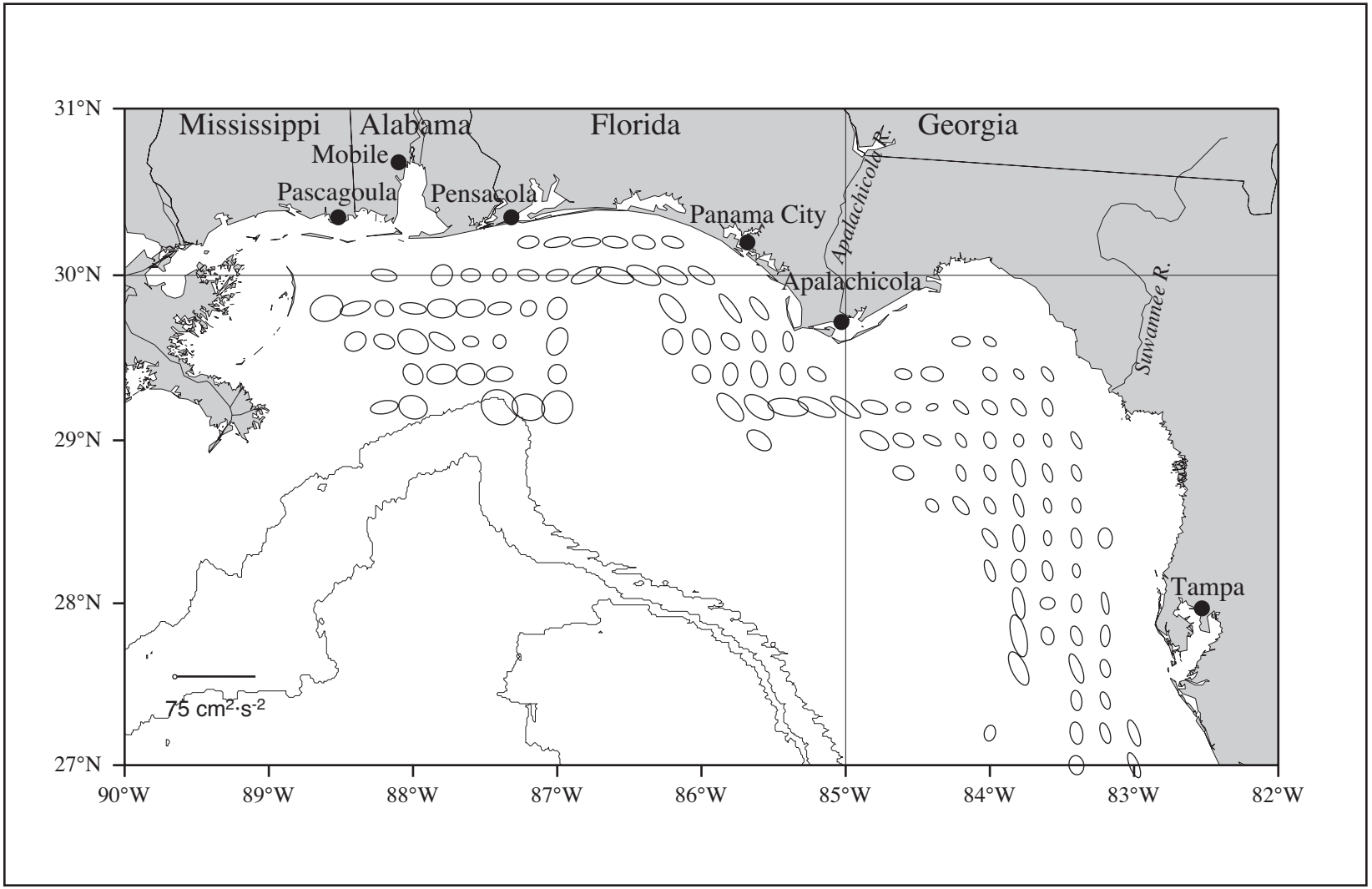

Figure 4.2-3. Variance ellipses for winter from SCULP II drifter releases February 1996-March 1997. Shown are the 1000-, 2000-, and 3000-m isobaths.

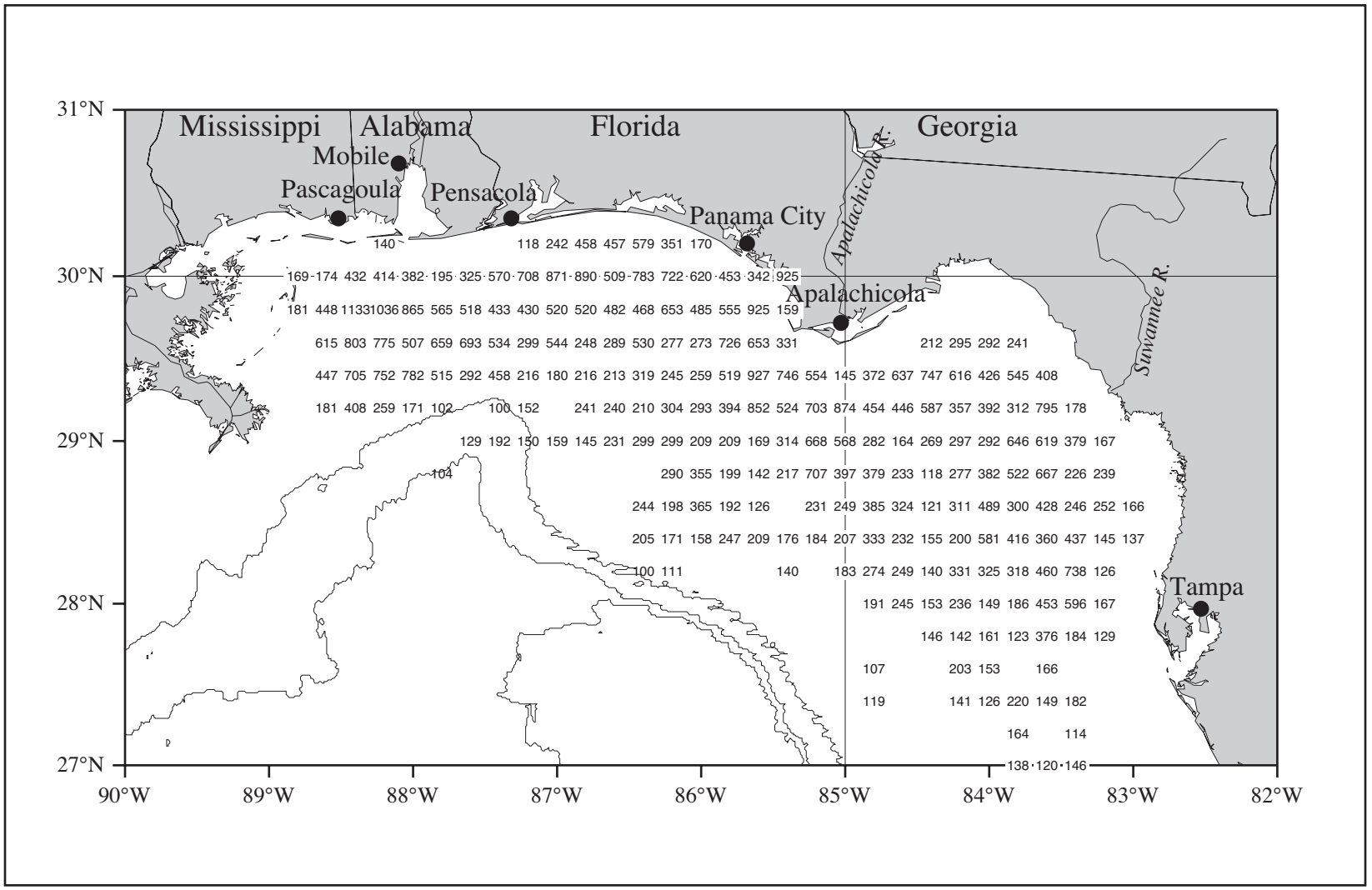

Figure 4.2-4. Numbers of observations from spring SCULP II drifter releases February 1996-March 1997. Shown are the 1000-, 2000-, and 3000-m isobaths.

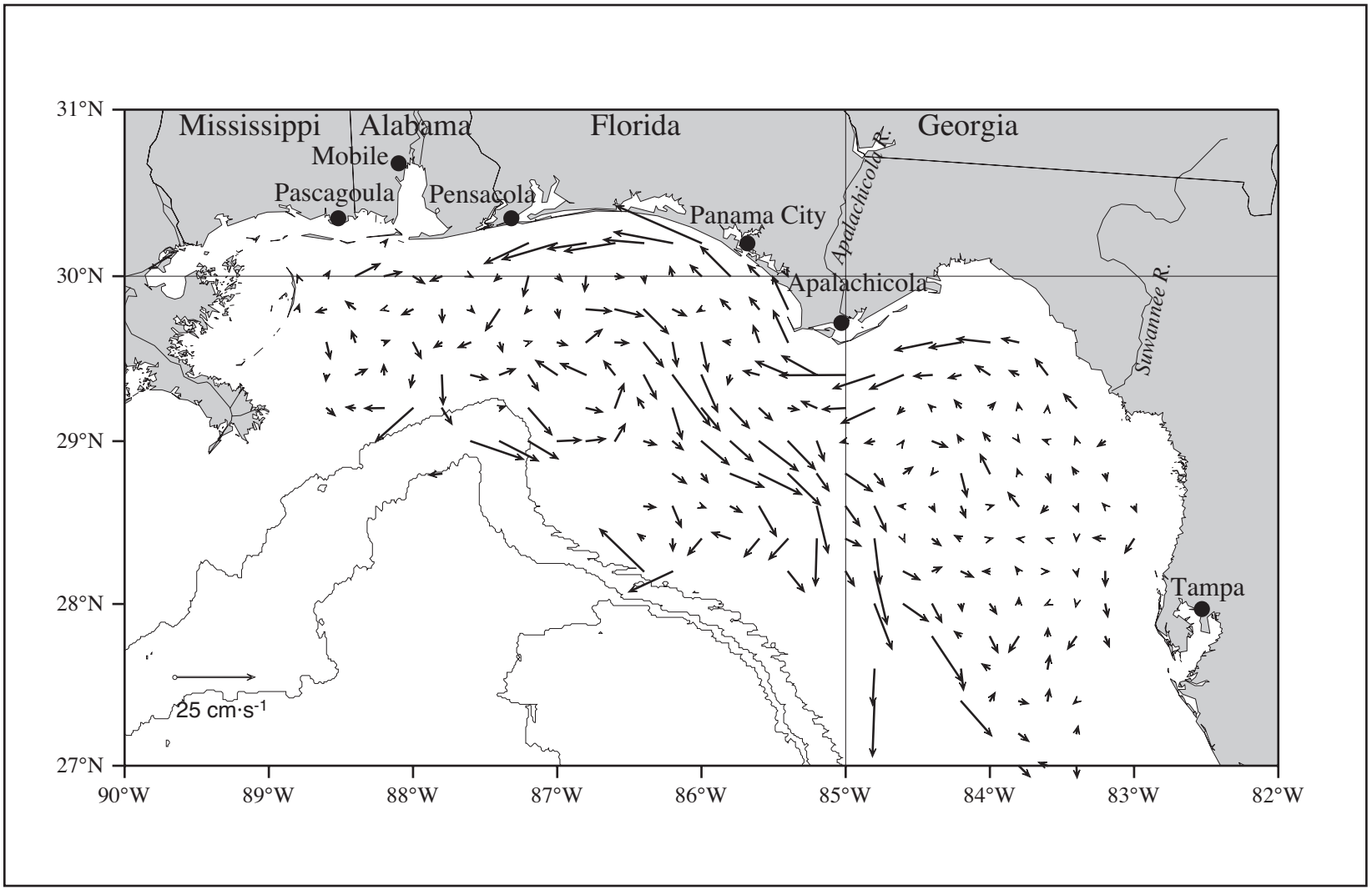

Figure 4.2-5. Average surface vectors for spring from SCULP II drifter releases February 1996-March 1997. Shown are the 1000-, 2000-, and 3000-m isobaths.

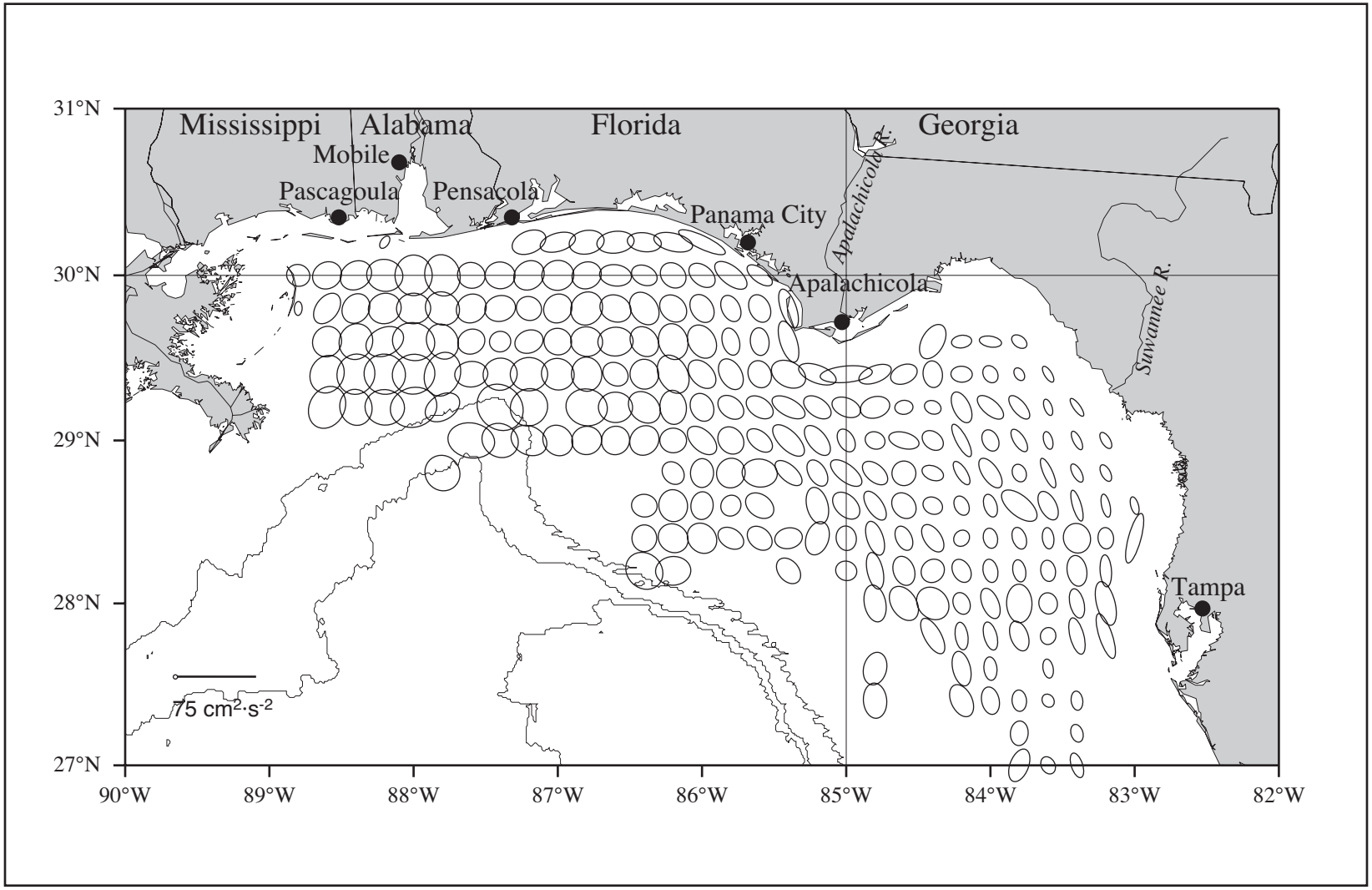

Figure 4.2-6. Variance ellipses for spring from SCULP II drifter releases February 1996-March 1997. Shown are the 1000-, 2000-, and 3000-m isobaths.

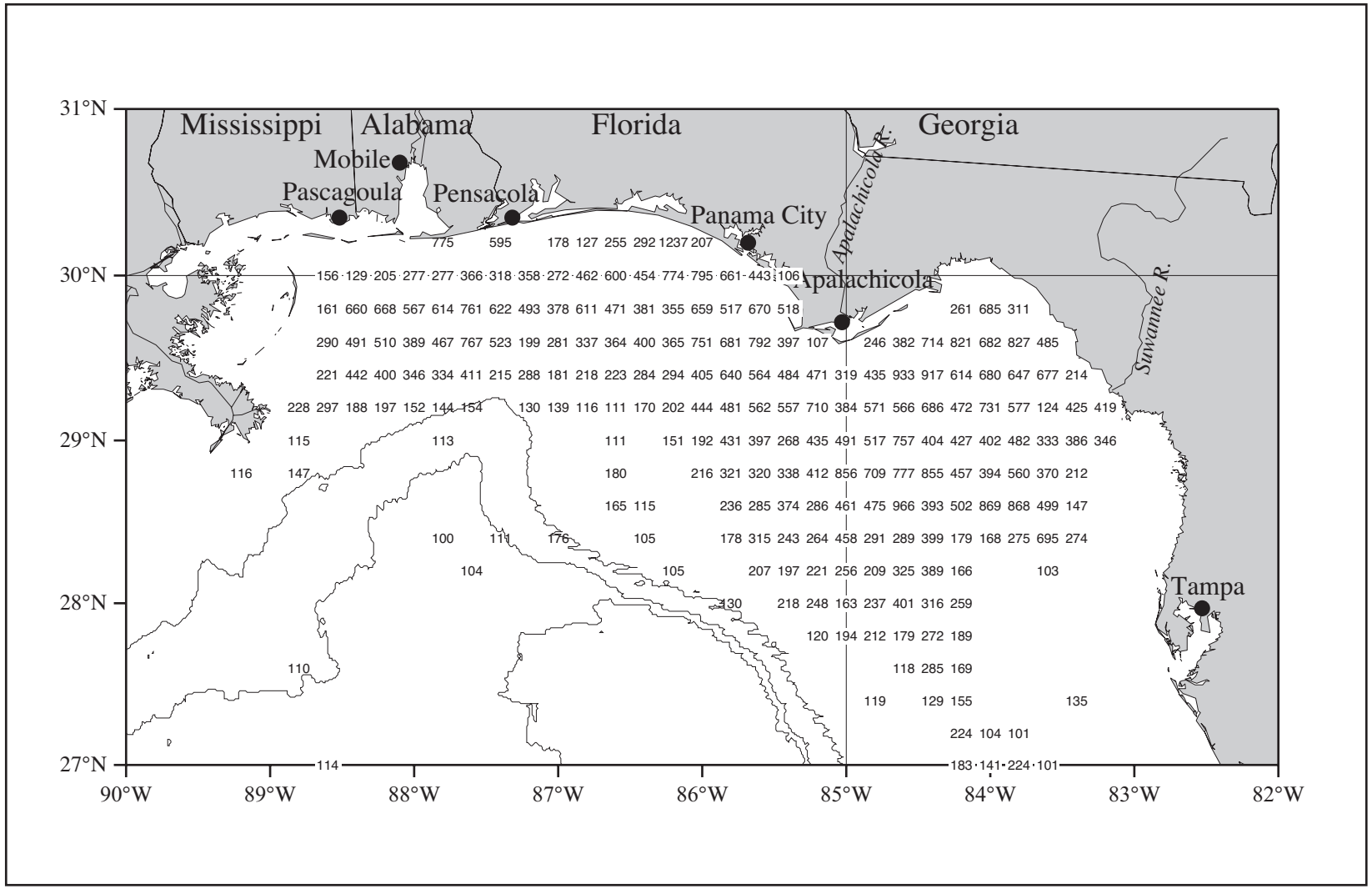

Figure 4.2-7. Numbers of observations from summer SCULP II drifter releases February 1996-March 1997. Shown are the 1000-, 2000-, and 3000-m isobaths.

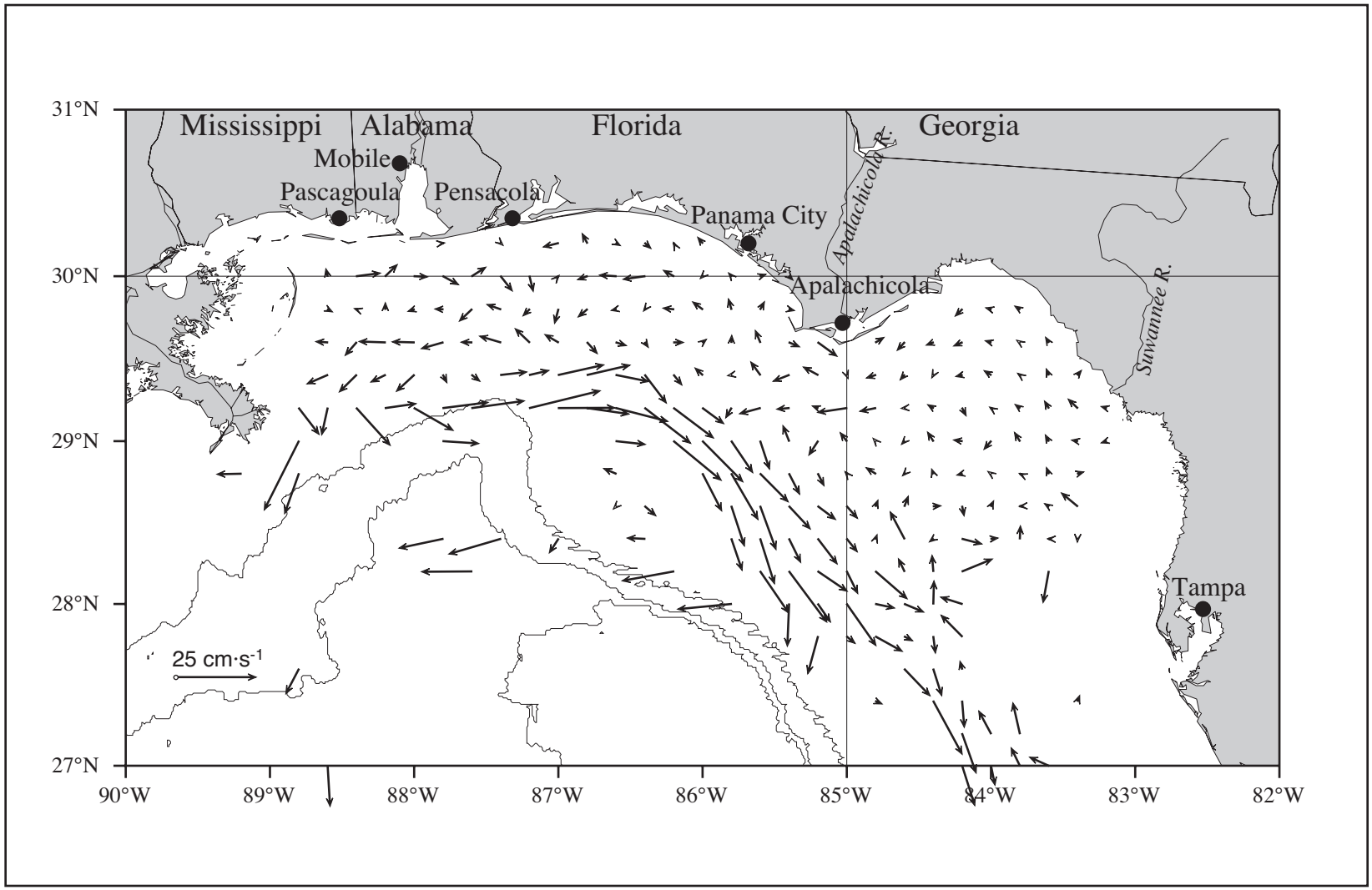

Figure 4.2-8. Average surface vectors for summer from SCULP II drifter releases February 1996-March 1997. Shown are the 1000-, 2000-, and 3000-m isobaths.

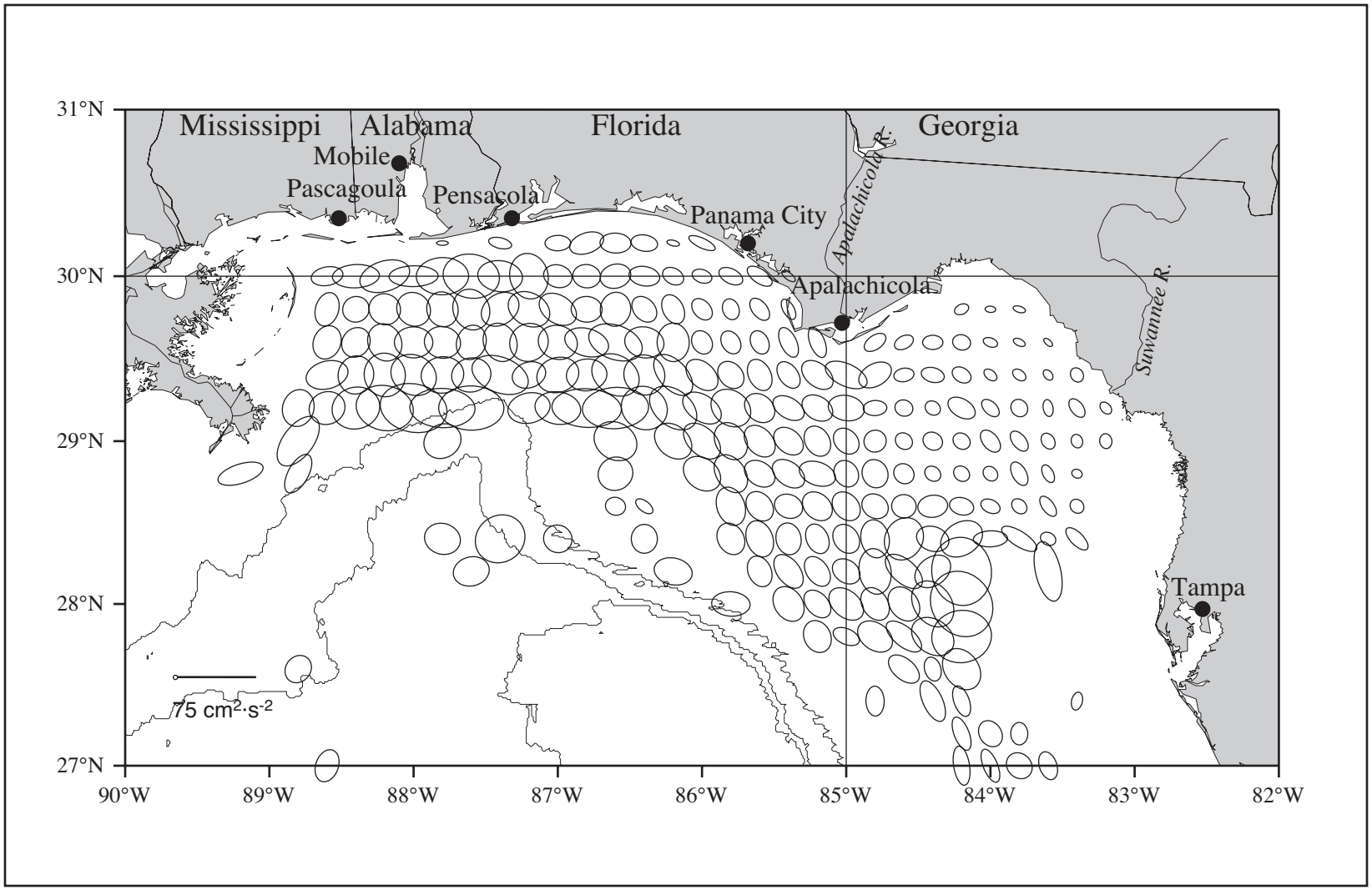

Figure 4.2-9. Variance ellipses for summer from SCULP II drifter releases February 1996-March 1997. Shown are the 1000-, 2000-, and 3000-m isobaths.

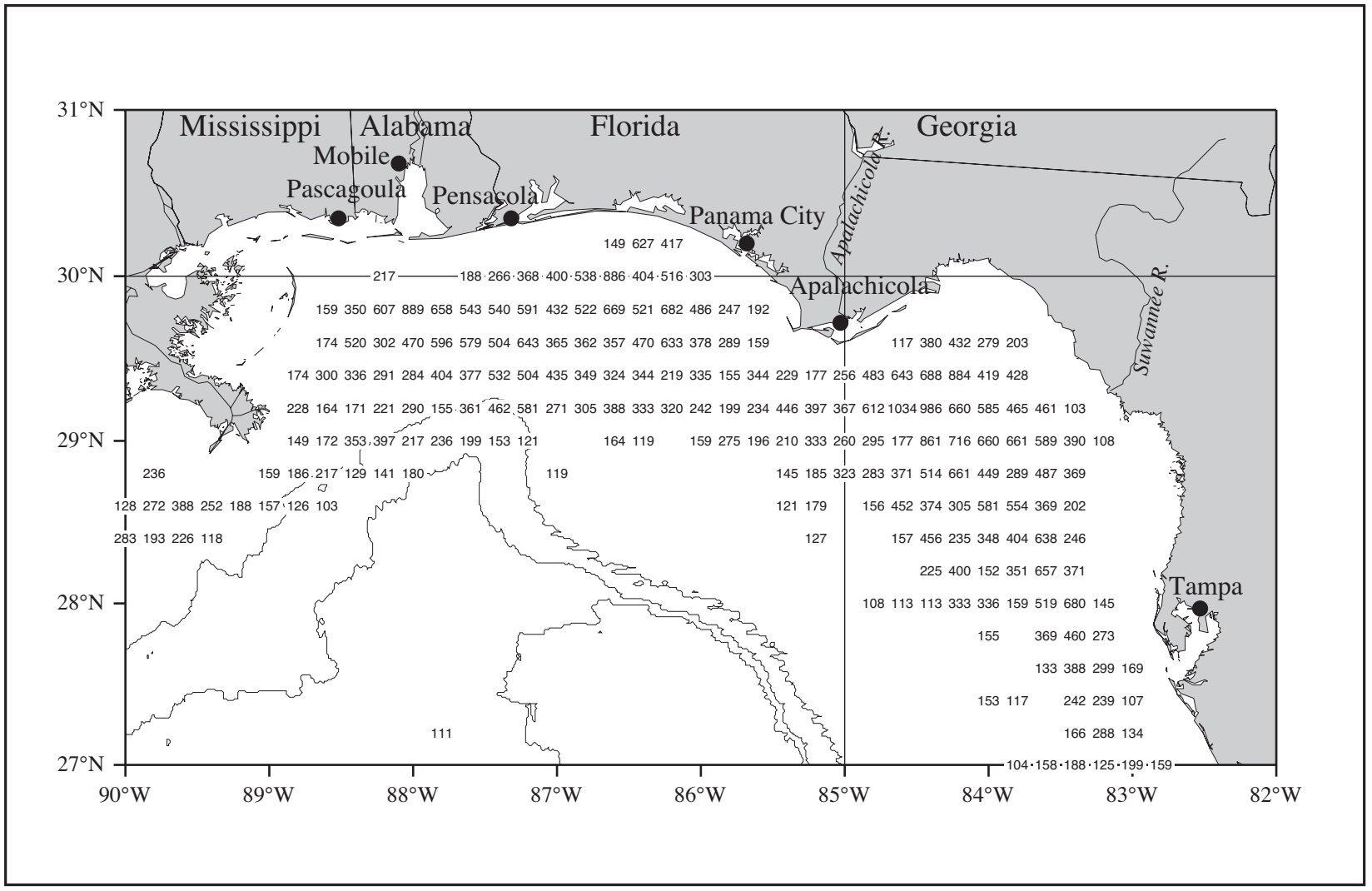

Figure 4.2-10. Numbers of observations from fall SCULP II drifter releases February 1996-March 1997. Shown are the 1000-, 2000-, and 3000-m isobaths.

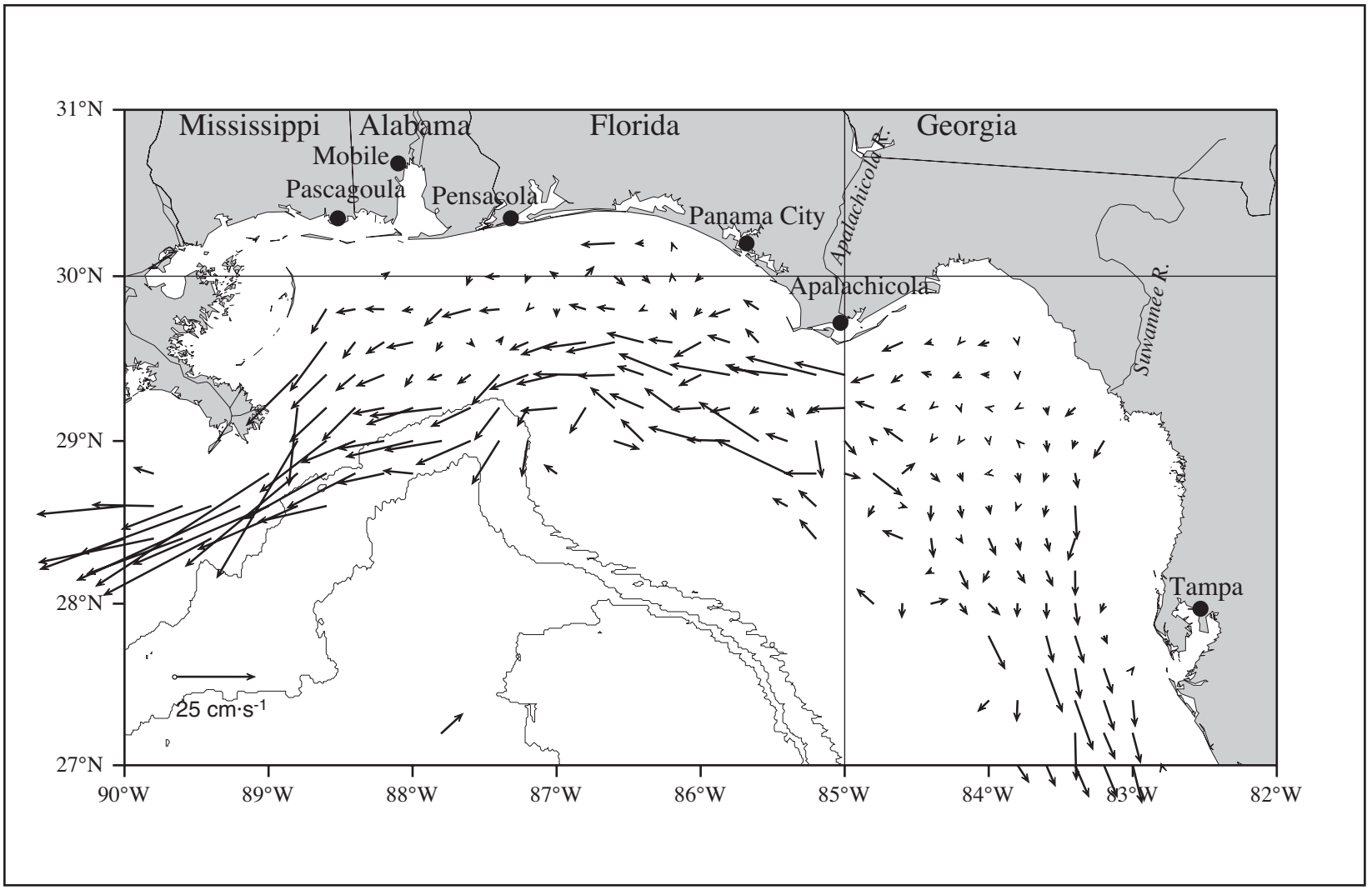

Figure 4.2-11. Average surface vectors for fall from SCULP II drifter releases February 1996-March 1997. Shown are the 1000-, 2000-, and 3000-m isobaths.

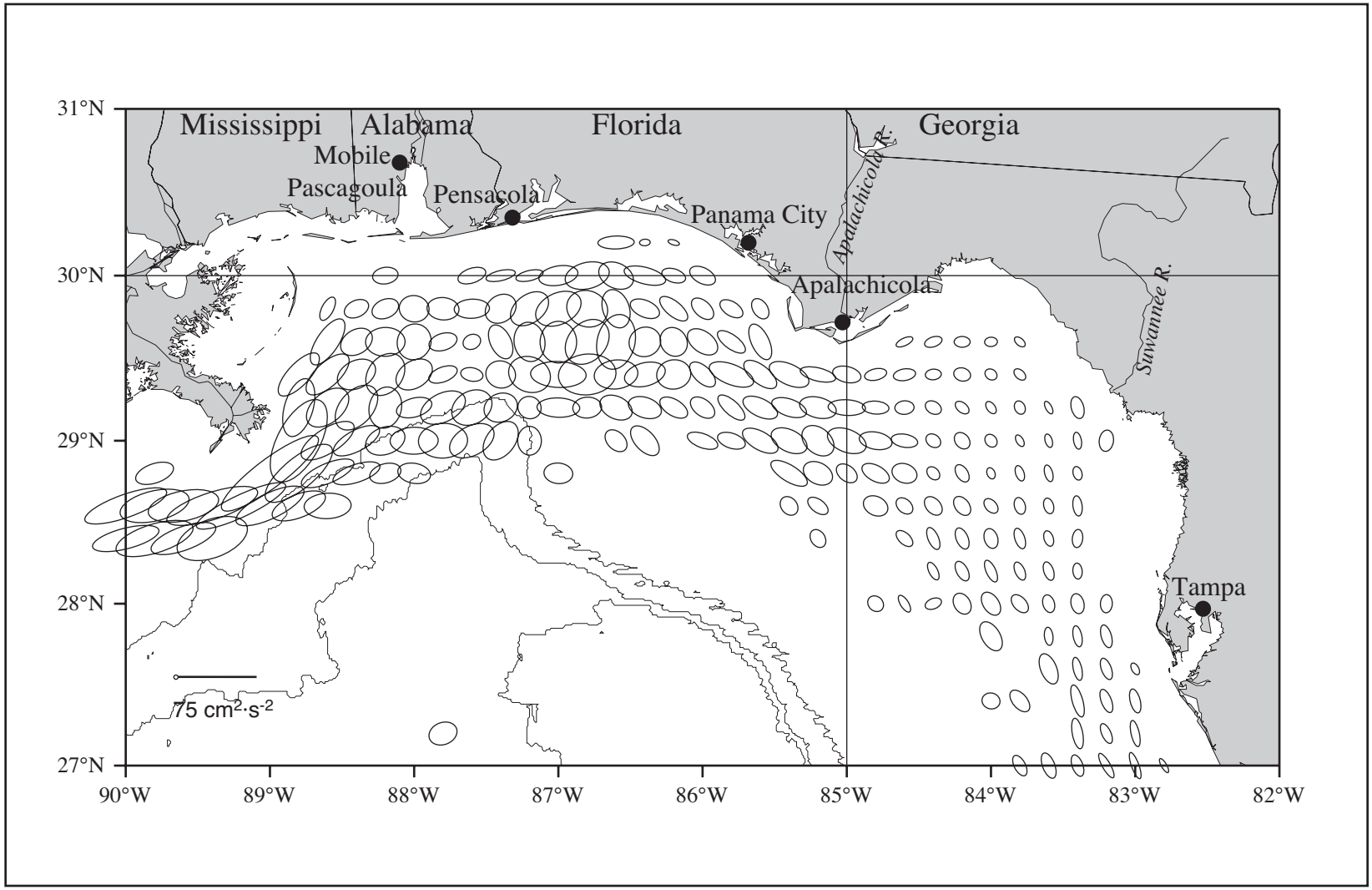

Figure 4.2-12. Variance ellipses for fall from SCULP II drifter releases February 1996-March 1997. Shown are the 1000-, 2000-, and 3000-m isobaths.

The numbers of winter observations (Figure 4.2-1) generally ranged between 100 and 300 per grid box and, with the exception of the region south of Alabama, were limited to the inner shelf. In the latter region, the pattern over the outer shelf shows a poorly organized flow regime with relatively large variability (Figures 4.2-2 and 4.2-3). Over the inner shelf just west of Cape San Blas and upcoast from about 85.4°W, winter surface currents were generally upcoast with variance ellipses oriented in the average flow direction. Both magnitude and variance appear to increase offshore toward near mid shelf. The nearshore flow direction is consistent with generally upcoast components for climatological (COADS) winds over the Big Bend area of the west Florida shelf in October—February and downcoast components for March/April—September (Figures 3.1.1-1 to 3.1.1-12).

Examination of the mean wind fields and variance ellipses for December 1996 and January and February 1997 show patterns that generally agree with the dominant patterns seen from climatology. Mean winds during the winter of 1996-1997 are 2-4 $m \cdot s^{-1}$ and to the southwest and west-southwest over the NEGOM region with large variance ellipses relative to the mean. Variance ellipses and magnitude of winds generally increase with distance from shore. Variance ellipses are also larger in the western NEGOM region than in the east.

Many more observations were available for spring and grid boxes with 100 or more observations covered most of the shelf but not all out to the 1000-m isobath (Figure 4.2-4). A strong downcoast coastal current was present from the middle of the Big Bend area (~26.25°N) to the Perdido River (near 87°W). Again this is consistent with the COADS climatology which shows downcoast favorable winds over the northern west Florida shelf beginning in March (Figure 3.1.1-3) and westward components over west of Cape San Blas for spring (Figures 3.1.1-3 to 3.1.1-5). Currents over most of the west Florida shelf were weak and poorly organized. Spring surface currents over the outer shelf were generally upcoast and stronger at the shelf edge, but both numbers of observations and variance ellipses increased toward the shelf edge. Cyclonic flow appears over the apex of DeSoto Canyon.

Coverage by observations during the summer was somewhat better than for spring in the far western part of the study area but not so good in the southeast (Figure 4.2-7). Over the inner shelf currents were weak and variable in direction, consistent with typical summer wind patterns. Near coast variance was small on the west Florida shelf but increased to a maximum near Mobile Bay. In that region inner shelf currents were generally larger than elsewhere and may have been organized into an anticyclonic circulation cell, though closure at its western end was not confirmed by these measurements. The summer pattern was of strong upcoast flow along the shelf edge, except off the Mississippi Delta where flow was south-southwestward. The eastward and southeastward flow along the shelf edge is in agreement with summer observations during NEGOM and was likely driven by off-shelf eddies.

Fall coverage was quite good over the southwestern region—even extending southwest of the delta (Figure 4.2-10). However, coverage generally was reduced relative to spring and summer over the outer shelf and near the coasts. The most striking feature seen in the fall surface currents for 1996 (Figure 4.2-11) was strong westward flow extending from the central shelf off Cape San Blas across the apex of DeSoto Canyon and along the shelf edge as far as observations are shown (90°W). That flow was joined by strong southwestward surface currents from the mid to inner shelf east of the Mississippi Delta. Average currents were largest south of the delta. Variance ellipses there (Figure 4.2-12) appear to be larger than in other areas with larger mean speeds and oriented in the mean current direction. An exception is the region of large, nearly circular variance ellipses over the head of DeSoto Canyon. Strong southward flow also was seen leaving the study region west of Tampa.

4.3 Space-time Patterns of Low-frequency Circulation from ADCP Currents

The patterns of low-frequency circulation over the NEGOM study area were examined using shipboard ADCP current measurements obtained during the NEGOM cruises. Near-surface current measurements were gridded, the mean and divergent components were removed, and the residual fields examined using an empirical orthogonal function (EOF) analysis to obtain the most energetic spatial patterns and their amplitudes at the time of each cruise.

ADCP measurements were available from 8 of the 9 cruises over the entire NEGOM study area; for cruise N4, good ADCP measures were obtained only west of 87°W. The ADCP currents were from vertical bins centered at 10-14 m. For each cruise the gridded current field was analyzed to remove divergent components (Wang et al. 2002a), and so to correspond more closely to geostrophic current fields. This procedure likely also removed part of the inertial and tidal signals. The fraction of variance remaining in the non-divergent flow was 68% relative to the measured variance averaged over all cruises.

A gridded vector average field was obtained using the 8 fields and is shown in Figure 4.3-1. The current regime west of about 87.5°W is weakly southeastward. That between about 87°W and Cape San Blas and over the shelf outside the 100-m isobath is upcoast with larger speeds (10-15 $cm \cdot s^{-1}$). Average currents inshore of the 100-m isobath on the west Florida shelf are quite weak with an indication of cyclonic flow.

The average field was removed from each of the eight individual fields. An EOF analysis was performed on the residual fields. The percentage of variance associated with each of the seven EOF modes is given in Table 4.3-1. The first four modes contained 84% of the variance. The patterns of the first four modes are shown in Figures 4.3-2 through 4.3-5.

Mode 1, with 34% of the variance, is essentially an along-shelf circulation pattern above the outer shelf and slope east of 87.5°W (Figure 4.3-2). There also is some evidence of closed circulation over the MS-AL-FL shelf as well as a partially closed circulation over the inner shelf centered off Tampa.

Mode 2 (Figure 4.3-3) shows strong northeast (or southwest) flow over the Mississippi-Alabama shelf and a large energetic eddy centered near the 200-m isobath and 28.5°N. This mode contains 22% of the variance. The third mode, accounting for almost an equivalent fraction of the variance (18%), consists of an eddy centered over the upper DeSoto Canyon. Flow is strongly on- or off-shelf on the eastern and western limbs of this eddy (Figure 4.3-4). Another off-shelf eddy appears to be forcing the currents over the upper slope and outer shelf off the Big Bend region.

Modes 1, 2, and 3 evidence no clear seasonal patterns (Figure 4.3-6). We speculate that modes 1, 2, and 3 are driven principally by the off-shelf circulation features.

EOF Mode 4 shows a pattern with the largest currents generally over the inner shelf (Figure 4.3-5). This mode, with 10% of the variance, appears principally related to coastal circulation and may be wind driven. It is the only mode with some apparent seasonality. The amplitudes are positive for both fall NEGOM cruises, N1 and N7 (Figure 4.3-6). The wind fields for those cruise periods (Figures A.1.1-1 and G.1.1-1) show winds over the inner shelf with downcoast components from the upper Big Bend area westward, consonant with downcoast flow in that region shown in Figure 4.3-5 for positive amplitude. One might also note that the downcoast winds were quite weak for cruise N1 and strong for cruise N7, corresponding to the relative amplitudes of mode 4 for fall. The mode 4 amplitudes for times of the three spring cruises are

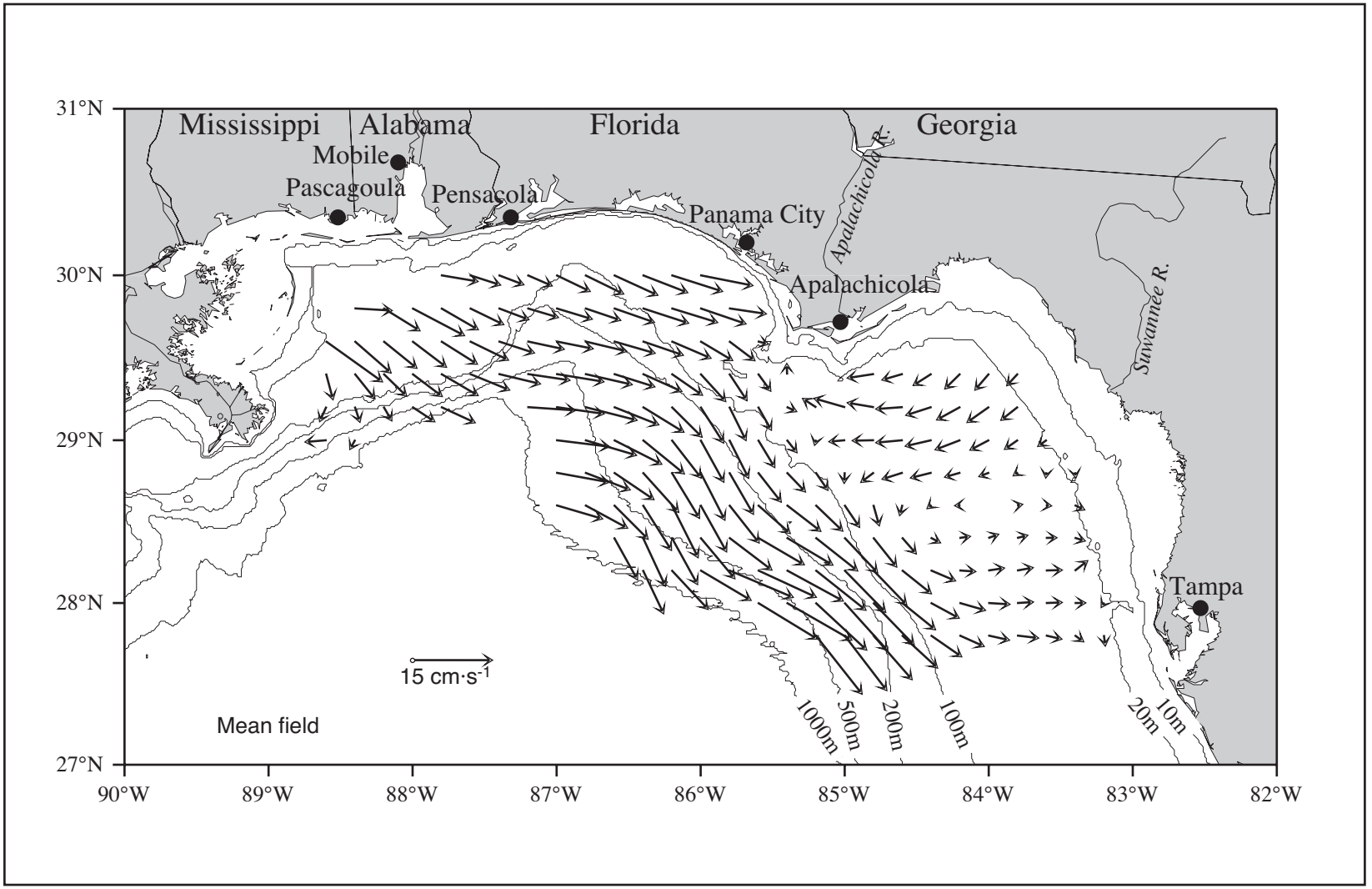

Figure 4.3-1. ADCP currents at vertical bin centered at 10-14 m. Vector average of results from cruises N1-N3 and N5-N9.

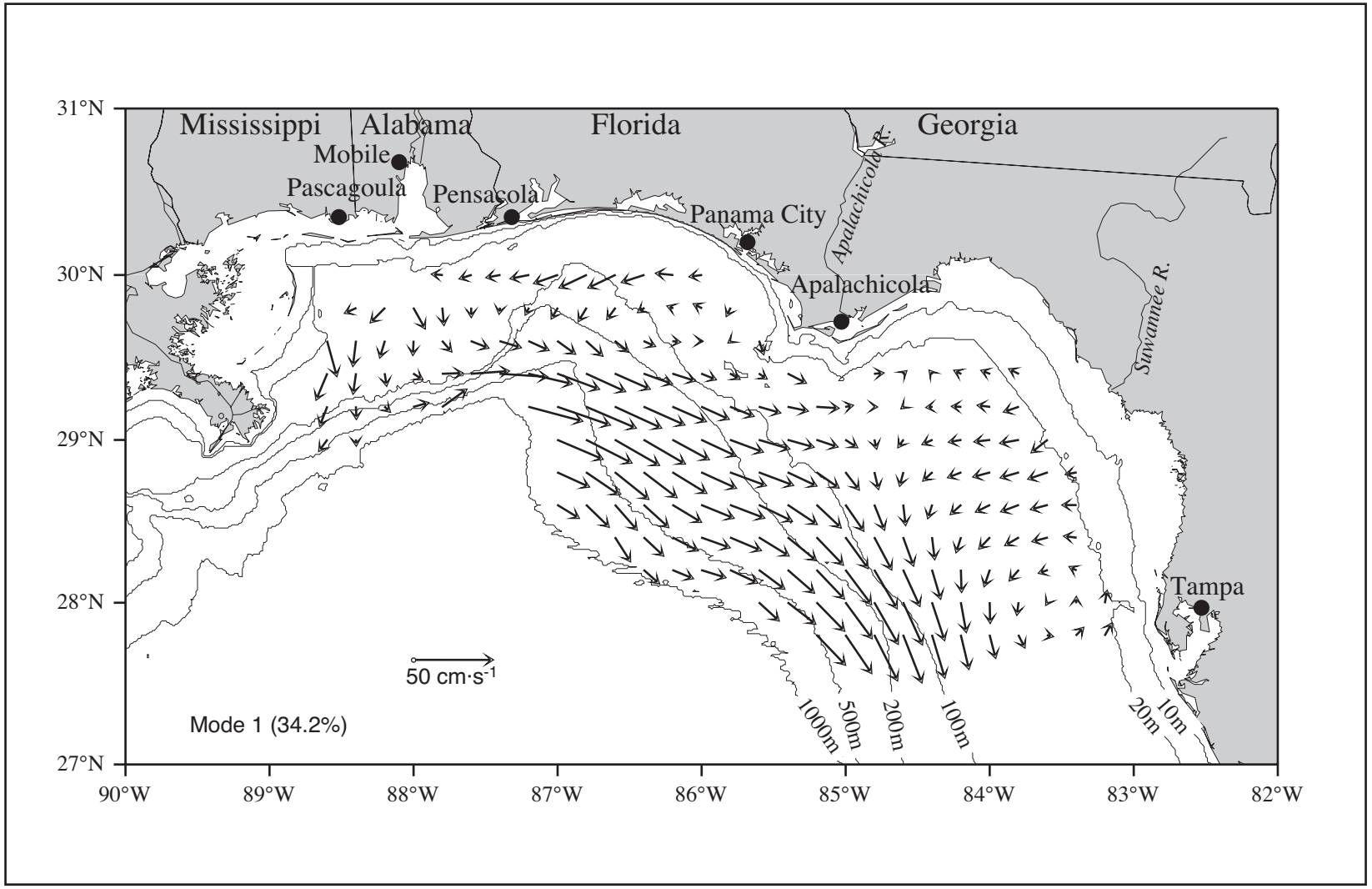

Figure 4.3-2. Pattern of EOF mode 1 for non-divergent currents at vertical bin centered at 10-14 m using ADCP data from eight NEGOM cruises.

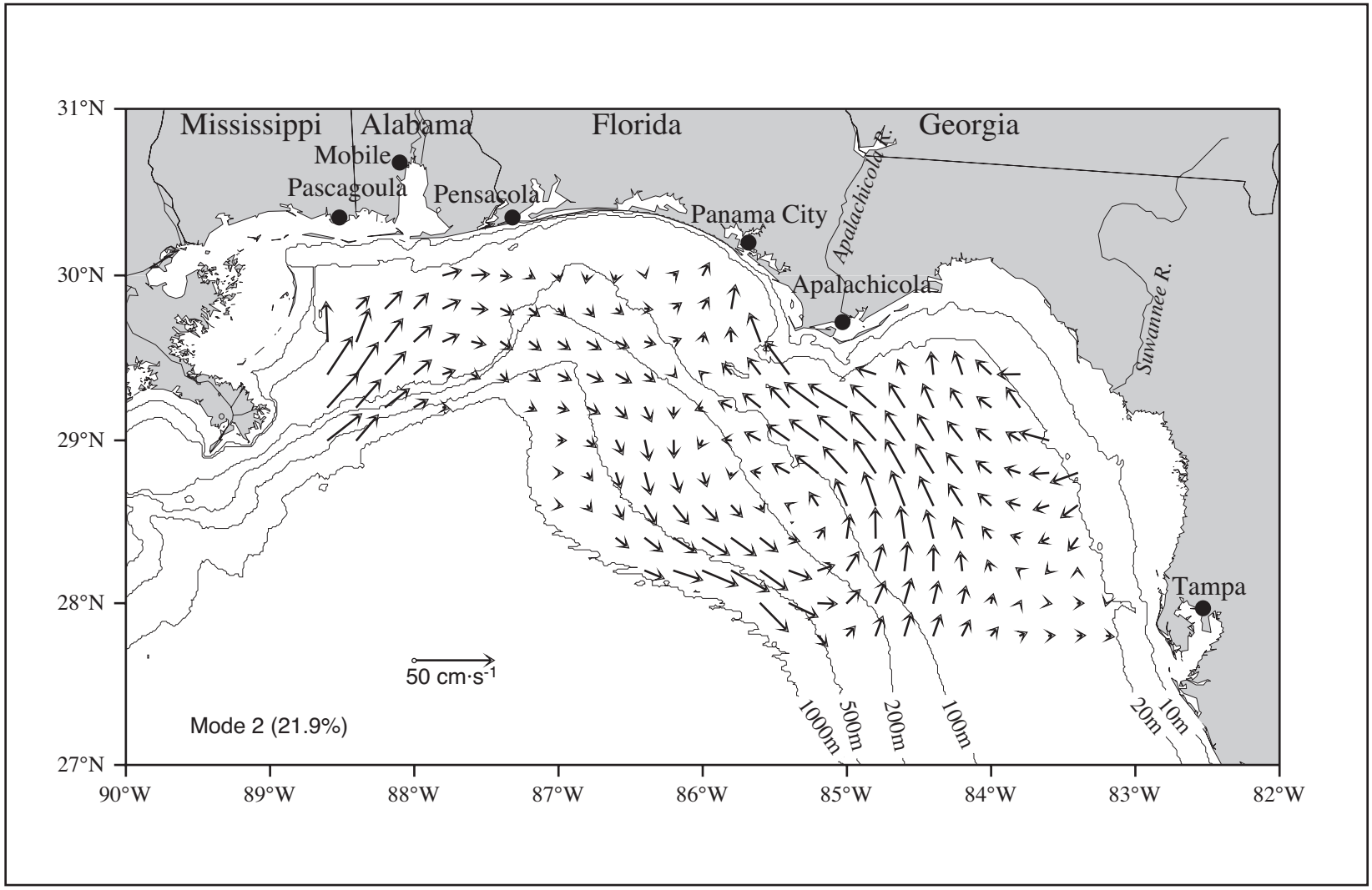

Figure 4.3-3. Pattern of EOF mode 2 for non-divergent currents at vertical bin centered at 10-14 m using ADCP data from eight NEGOM cruises.

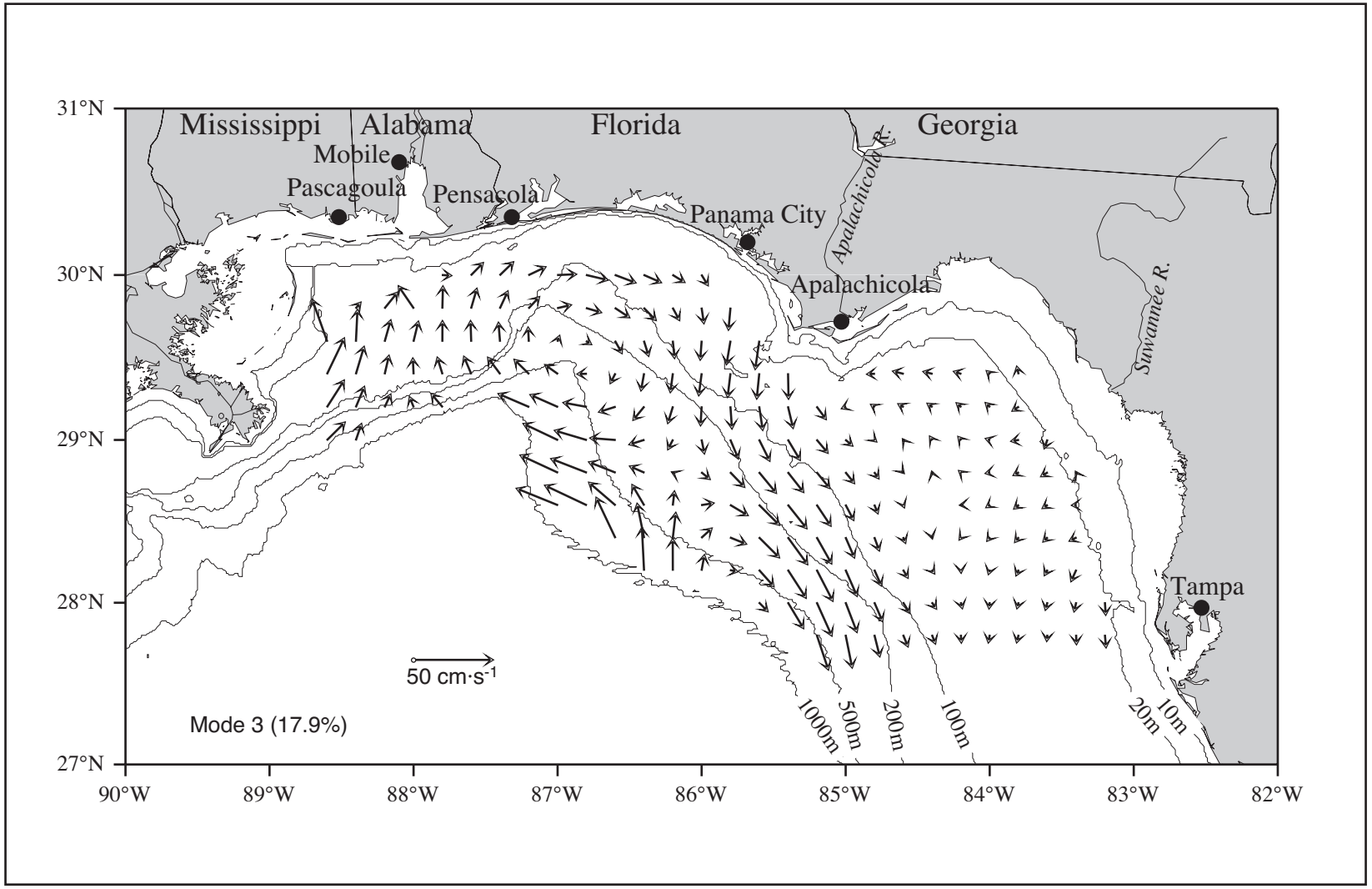

Figure 4.3-4. Pattern of EOF mode 3 for non-divergent currents at vertical bin centered at 10-14 m using ADCP data from eight NEGOM cruises.

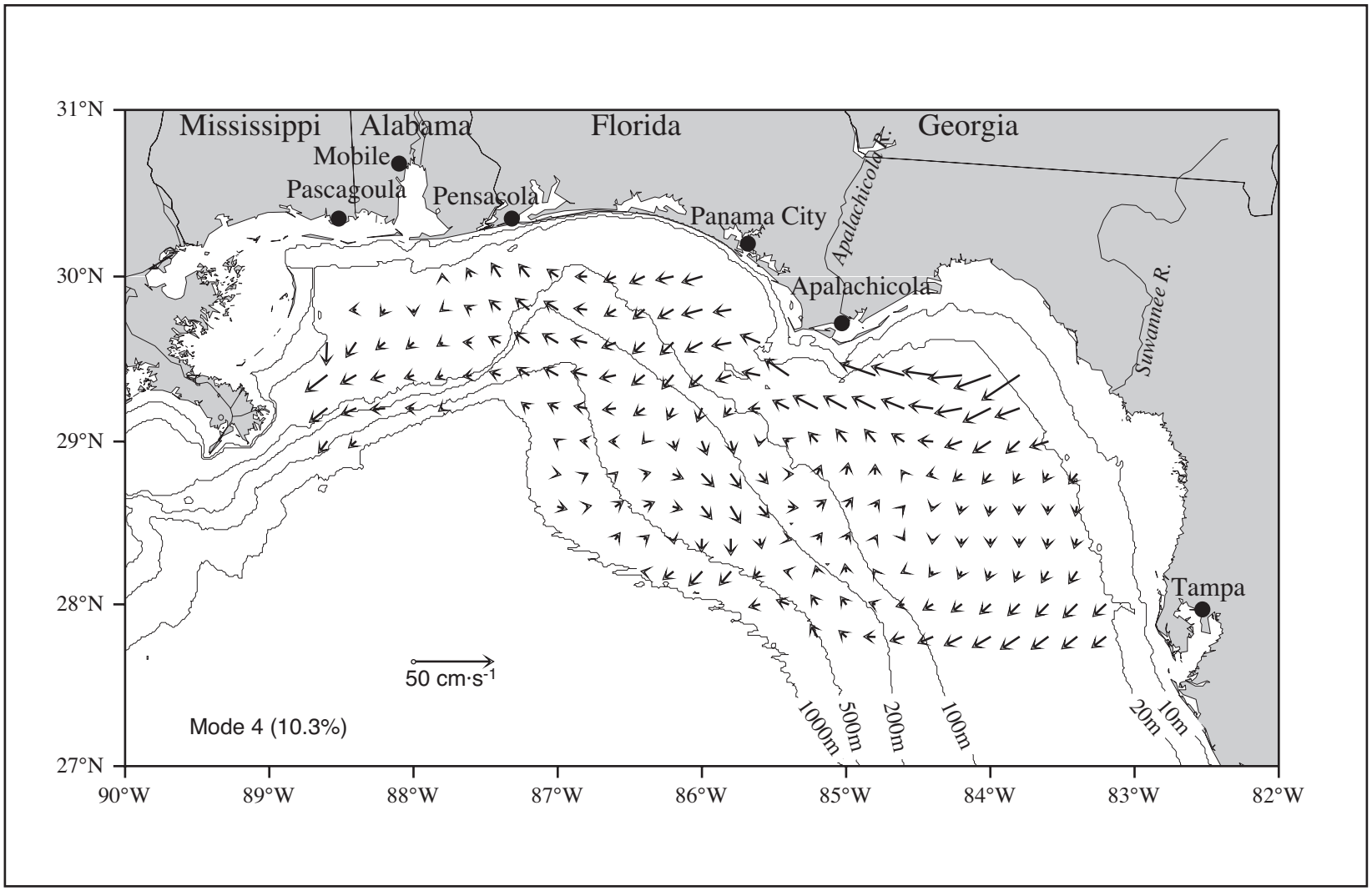

Figure 4.3-5. Pattern of EOF mode 4 for non-divergent currents at vertical bin centered at 10-14 m using ADCP data from eight NEGOM cruises.

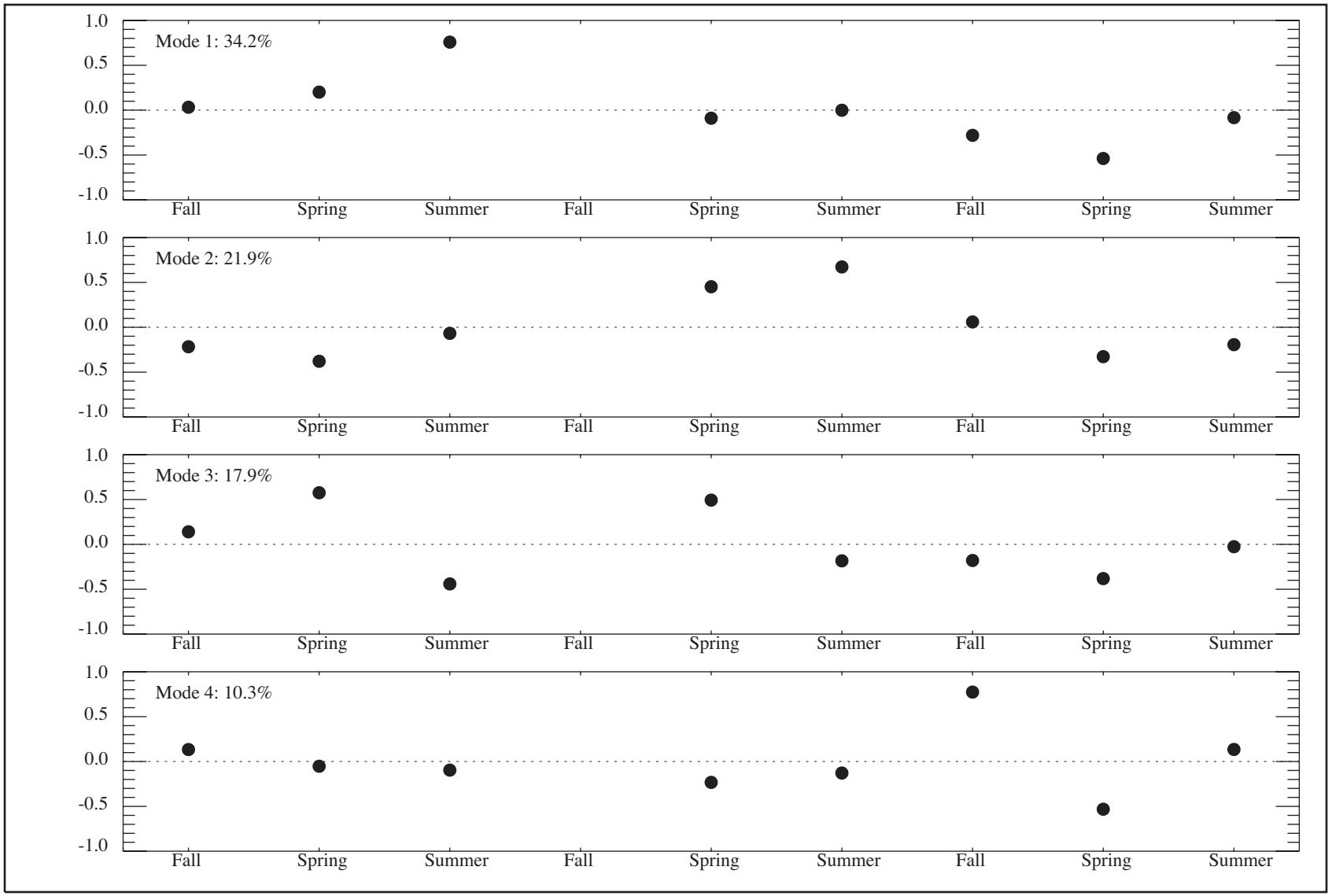

Figure 4.3-6. Amplitudes of first four EOF modes at times of NEGOM cruises

negative indicating upcoast coastal flow; amplitudes increase from N2 to N5 to N8. This agrees with the upcoast components of along-shore winds observed during the spring cruises N2, N5, and N8 (Figures B.1.1-1, E.1.1-1, and H.1.1-1). Amplitudes for mode 4 during the three summer cruises were near zero in agreement with expectations based on the weak and generally onshore winds observed during the summer cruise periods (Figures C.1.1-1, F.1.1-1, and I.1.1-1).

Table 4.3-1. Variance associated with modes resulting from EOF analysis of residual 10-14 m current fields for NEGOM cruises N1-N3 and N5-N9.

Mode	Associated variance
1	34%
2	22%
3	18%
4	10%
5	7%
6	5%
7	3%

The spatial patterns for modes 5-7 are not shown; together these modes contain only 15% of the variance. Suffice to say that the currents on all three modes are weak, but strongest over the inner shelf or near the Mississippi River mouth. We believe they are associated with local forcing by winds and river discharge. However, their amplitudes show no clear seasonal patterns (Figure 4.3-7).

For comparison, we may consider the results of an EOF analysis of near-surface currents measured at a fixed grid for 32 months over the Texas-Louisiana continental shelf (Cho et al. 1998). Monthly averaged currents were used to produce horizontal EOFs. The first two modes accounted for 92% of the variance, in striking contrast to our analysis for the NEGOM region. However, the circulation over the Texas-Louisiana shelf was shown to have a dominant seasonal pattern (depicted by mode 1 with 89.2% of the variance) and modified by off-shelf eddy interactions (depicted by mode 2 with 3.4% of the variance). Based on this analysis, the circulation in the NEGOM region has no such dominant seasonal pattern.

4.4 Examination of Wind Forcing of Nearshore Currents

We note that the nearshore currents by season given by drifter patterns in Section 4.2 were in rather good agreement with the expected along-shelf direction as inferred from climatology of wind fields. Also, there was some indication of such seasonal forcing in the pattern and amplitudes of mode 4 of the low-frequency EOF analysis of near-surface, ADCP-measured currents, described in Section 4.3.

However, we wished to examine the relationship of along-shelf winds to currents over the inner shelf based on measurements during the NEGOM field period. First, we examined the character of the nearshore wind fields as functions of time and location. To do so, we selected eight

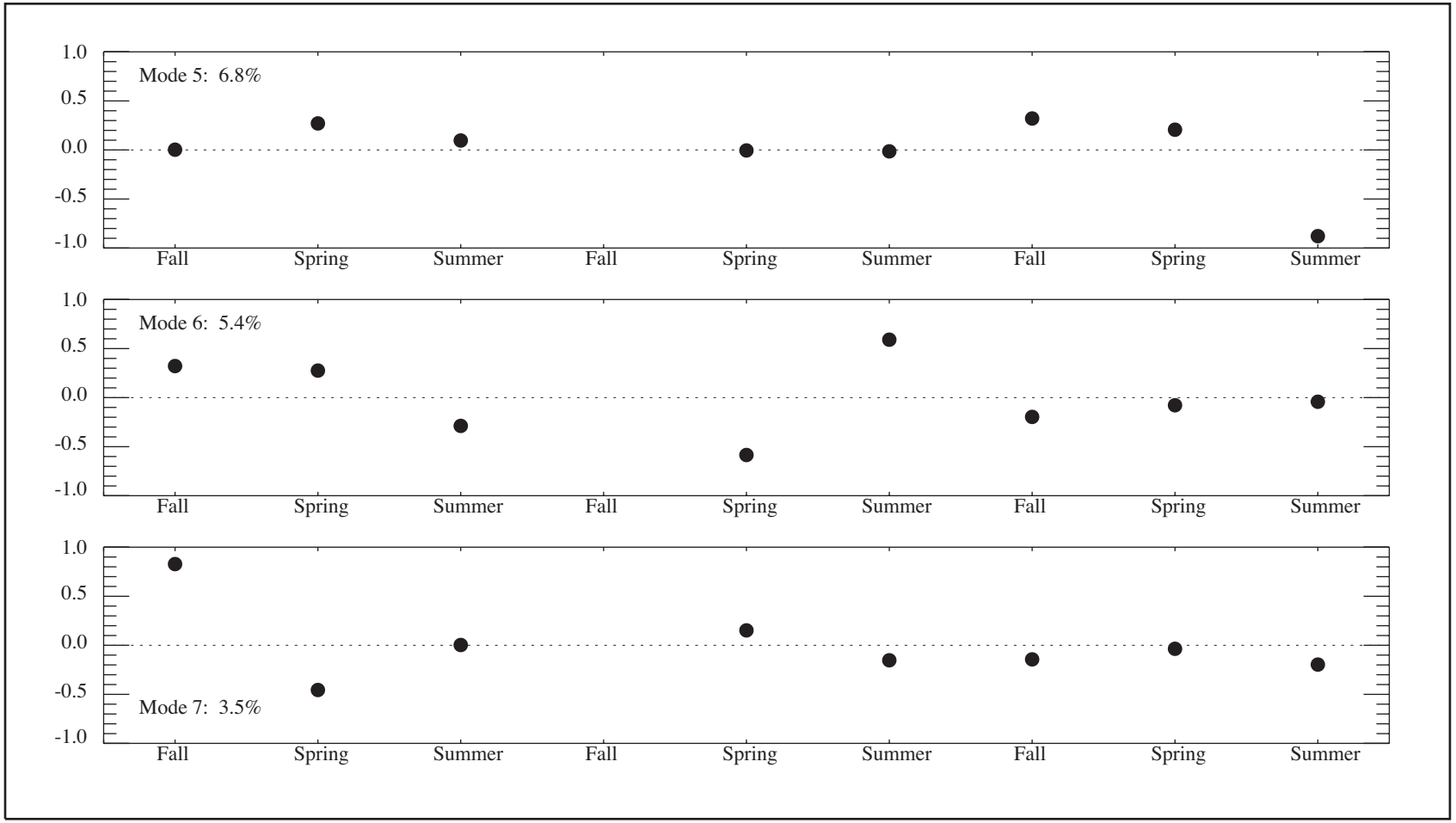

Figure 4.3-7. Amplitudes of EOF modes 5-7 at times of NEGOM cruises.

locations near the 20-m isobath along the inner shelf (Figure 4.4-1). Four locations were between Mobile Bay and Apalachicola, representing the upper coast, and four were located between Apalachicola and Tampa Bay, representing the lower coast. Based on hourly wind fields for the NEGOM region constructed from measurements by optimum interpolation techniques (described in Section 3), we constructed 40-hr low-passed time series at each of these locations. Then, plots were made and examined of along- and cross-shelf wind components at each location. Because of the visual difference in character of the variability at lower and upper coast locations, we averaged the daily values from 40-hr low-passed series at the four upper (lower) coast locations and then averaged over the entire period to form an annualized mean time series of daily wind components for the upper and lower coast. The resulting along-shelf components for the upper and lower coast are shown in Figure 4.4-2. Also plotted are daily values from the averaged 40-hr time series smoothed using a 14-d low-pass filter.

For the upper and lower coast regions it is clear that variability in the magnitude and direction of the along-shelf wind component is greatest during the period from mid-December into early spring, less during the period from August into December, and least during the period from mid-May through about July. Also clear is the difference in the level of variability between the upper and lower coast. Particularly in summer, but also to lesser extent from August into winter, the variability is greater along the upper coast. The temporal patterns of up- and downcoast wind components are less pronounced than are the clear temporal patterns of different wind intensity. Nevertheless, it is seen that the smoothed along-shelf winds are generally downcoast in spring, becoming near zero in May and June. Then, for the upper coast, winds shift to upcoast for late June, July and most of August; while over the lower coast they remained nearly zero for this period. In both regions there was a pronounced shift to downcoast wind components beginning in late August to early September, and this trend continued into or through October. This pattern would give rise to coastal currents over the upper and lower coast with large directional variability through the winter and much of spring. Coastal currents should be weak over the lower coast during the summer and over the upper coast during the early summer, shifting to upcoast in June and continuing into August. In both regions there should be a pronounced period of downcoast coastal flow beginning in September and continuing through most of the fall season.

At each of the eight locations, we examined the along-shelf components of near-surface ADCP currents measured at the time during each cruise when the ship was nearest the location. We plotted these values on the same plot with the along-shelf component of the 40-hr low-pass wind at that time and location. For the upper coast locations these plots showed fair correspondence (the result for location 4 is shown in Figure 4.4-3); agreement between wind and current is less good for the lower coast locations. The correlations between along-shelf components of wind and of near-surface current at each location are given in Table 4.4-1. There are few realizations, and thus high confidence levels correspond only to large correlations. At only one location (4) is the correlation significant at the 95% level. Nevertheless, the values do indicate that there is some correlation between along-shelf wind and current over the inner shelf at all locations excepting the two southern locations on the lower coast.

As a final effort to assign some quantitative estimate to the correlation between along-shelf components of wind and near-surface current, correlations were calculated between gridded fields of these values using data from eight NEGOM cruises. Of course this is just an extension of the calculations described above but it does delineate the spatial distribution of the correlation values. The result is shown in Figure 4.4-4. Shading indicates regions where the

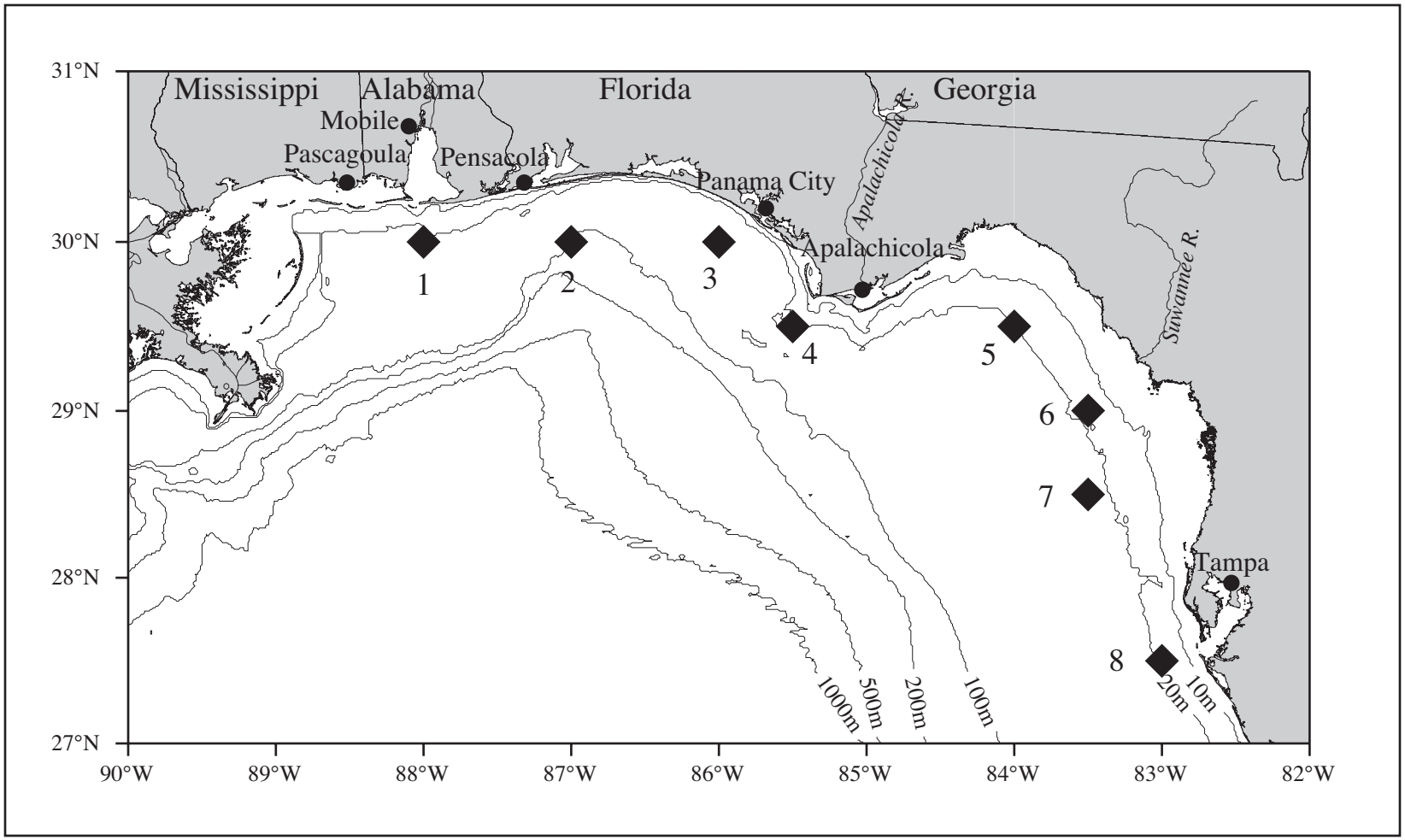

Figure 4.4-1. Locations near the 20-m isobath at which time series of 10-m winds were constructed using optimal interpolation from hourly measurements over the region during the NEGOM field period. The four locations between Mobile Bay and Apalachicola were selected to represent the upper coast, the four between Apalachicola and Tampa Bay to represent the lower coast.

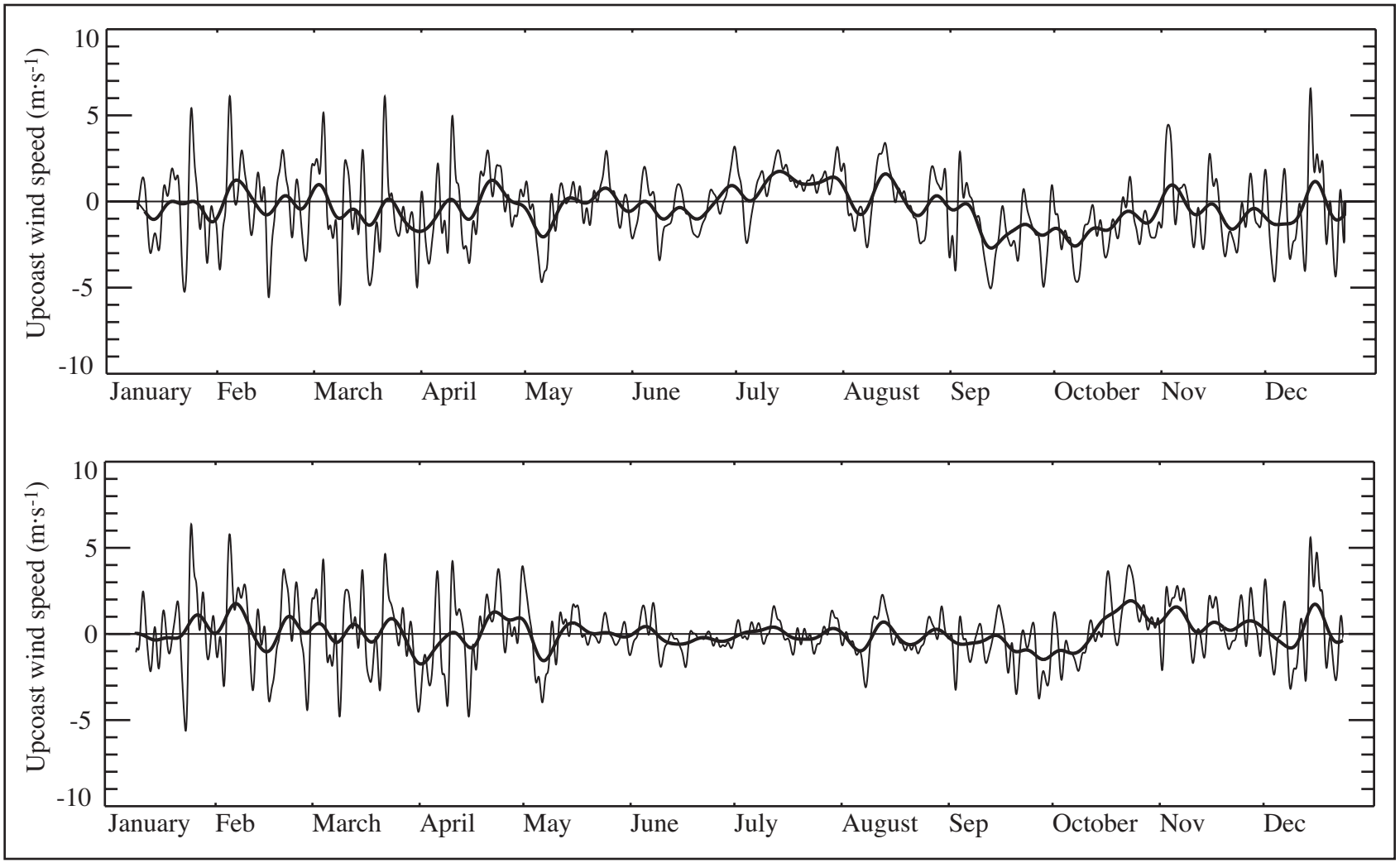

Figure 4.4-2. Time series of along-shelf components of 10-m winds at the locations shown in Figure 4.4-1. At each location the time series were 40-hr low-passed and daily values were averaged to produce an annual time series. Then the results for the four upper (lower) coast locations were averaged to produce the upper (lower) panel. The resulting records were smoothed with a 14-day filter.

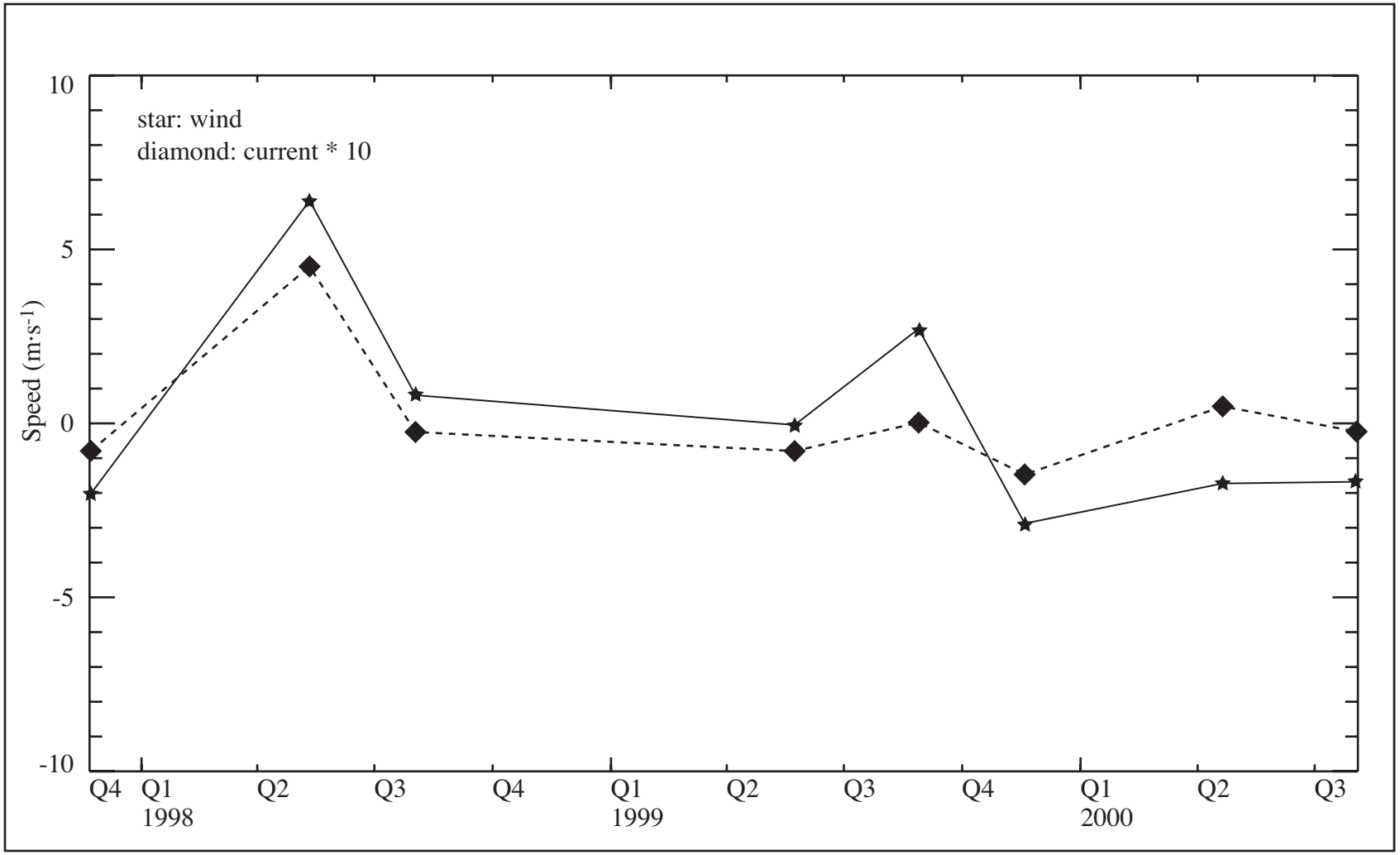

Figure 4.4-3. Plots of along-shelf components of 40-hr low-pass winds and of near-surface ADCP currents at the time of each of eight NEGOM cruises for location 4 in Figure 4.4-1.

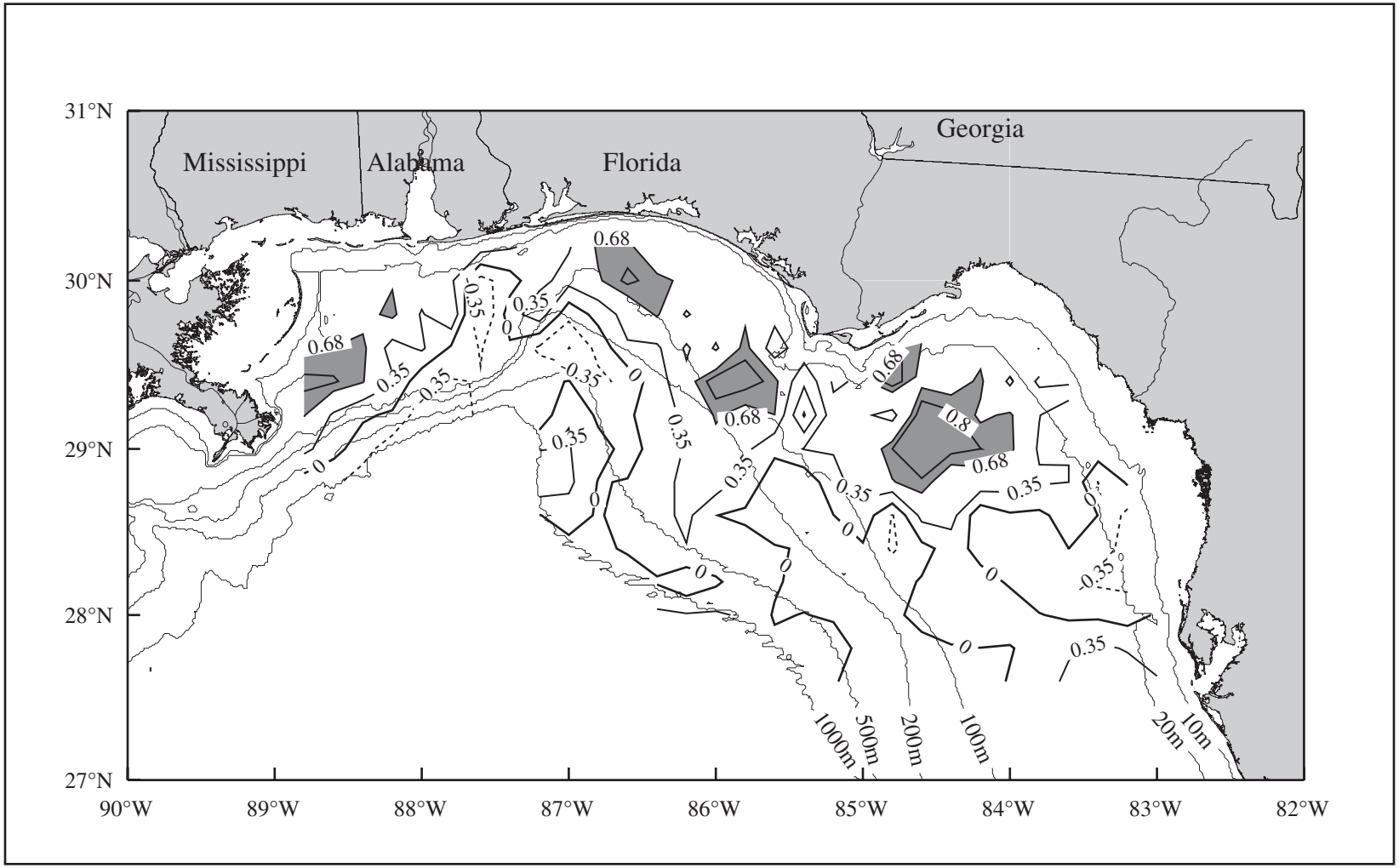

Figure 4.4-4. Correlation values between along-shelf components of wind and near-surface current calculated between gridded fields of these values using data from eight NEGOM cruises. Shading indicates regions where the correlation is greater than 0.68, which indicates the 90% confidence level.

correlation is greater than 0.68, which indicates the 90% confidence level. This seems clear evidence of the fact that, based on this limited data set, there was wind forcing of currents over the inner shelf, perhaps with the exception of the southeastern part of the study area.

Table 4.4-1. Correlations between along-shelf components of 40-hr low-pass wind and near-surface ADCP currents at each location based on measurements from all NEGOM cruises. The locations are shown in Figure 4.4-1. A value of 0.76 (0.68) corresponds to the 95% (90%) confidence level.

Location	Correlation
1	0.62
2	0.57
3	0.68
4	0.85
5	0.53
6	0.65
7	0.31
8	0.39

4.5 Examination of Forcing by Off-shelf Circulation Features

Using the SSH fields of R. Leben, we constructed time series of SSH gradients at three locations along the four lines shown in Figure 4.5-1. The locations were between the 200-m and ~2000-m isobaths. We plotted each of these time series, overlaid the times of the NEGOM cruises, and visually compared the gradients at and just before the time of each cruise to the near-surface ADCP currents over the slope and outer shelf. As one would expect the agreement seemed reasonable. We even noted reversals of near-along-isobath currents with reversals in sign of the SSH gradients along the lines. In summary, however, this exercise did not produce any new, unexpected information.

To obtain more quantitative relations between along-shelf currents and cross-isobath SSH gradients we performed a number of correlations between the two. We averaged the SSH gradients at each of the 12 locations described above over the time of each NEGOM cruise (except N4, for which we did not have complete ADCP measurements). Then these average SSH gradients were correlated for the 8 cruises with the gridded near-surface ADCP current components normal to the SSH gradient. The resulting correlations likely have little meaning when considering currents and gradients separated widely, e.g., SSH on line 1 with currents normal to that line south of Cape San Blas. For the locations on each line nearest 1000 m depth the correlation maps are shown in Figures 4.5-2 a-d. Correlations generally are high for the regions of the slope and outer shelf near the four locations.

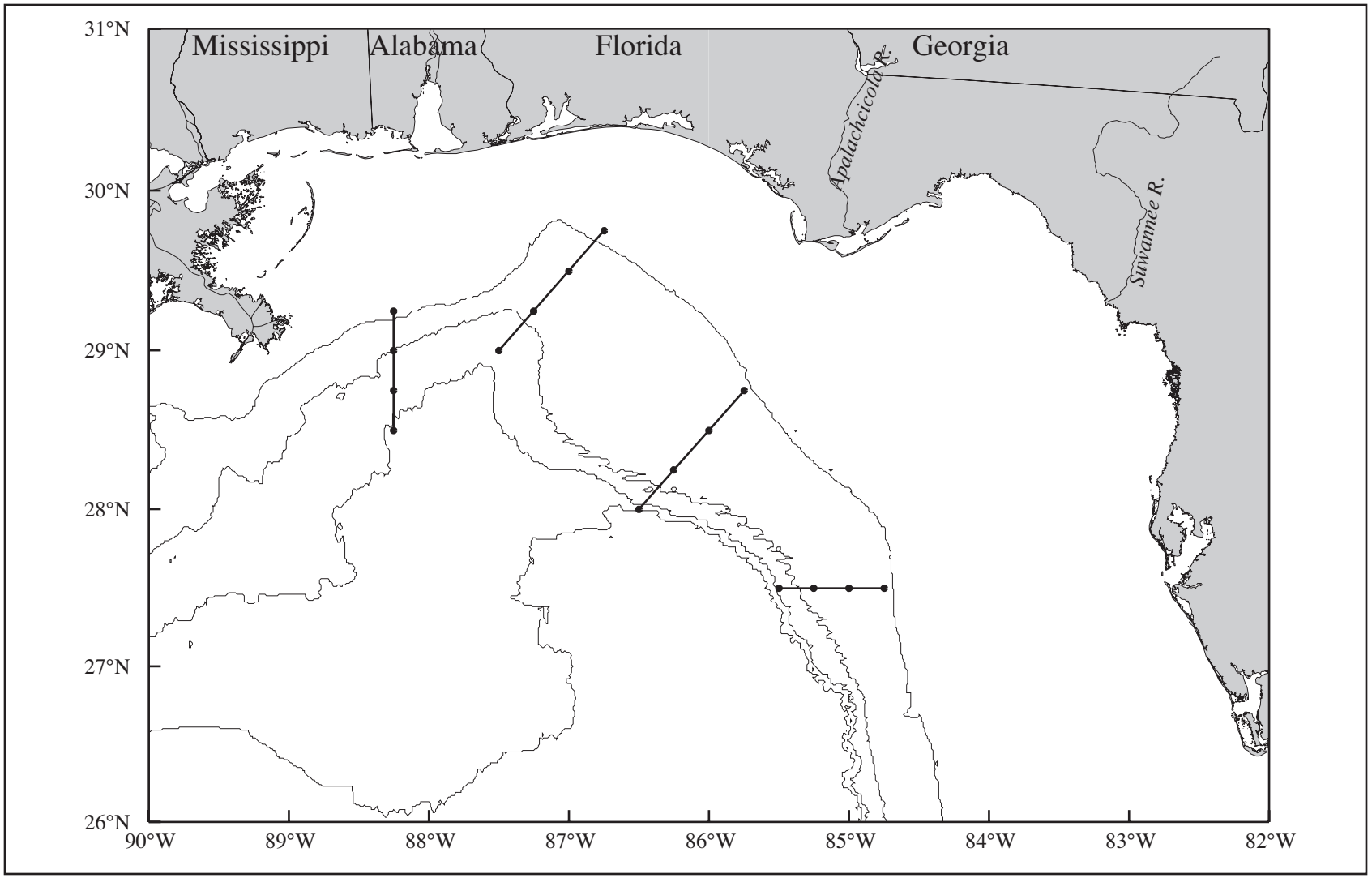

Figure 4.5-1. Locations at which time series of SSH gradients along the four lines shown were calculated using SSH distributions prepared by R. Leben. Bathymetric contours are the 200-,. 1000-, 2000-, and 3000-m isobaths.

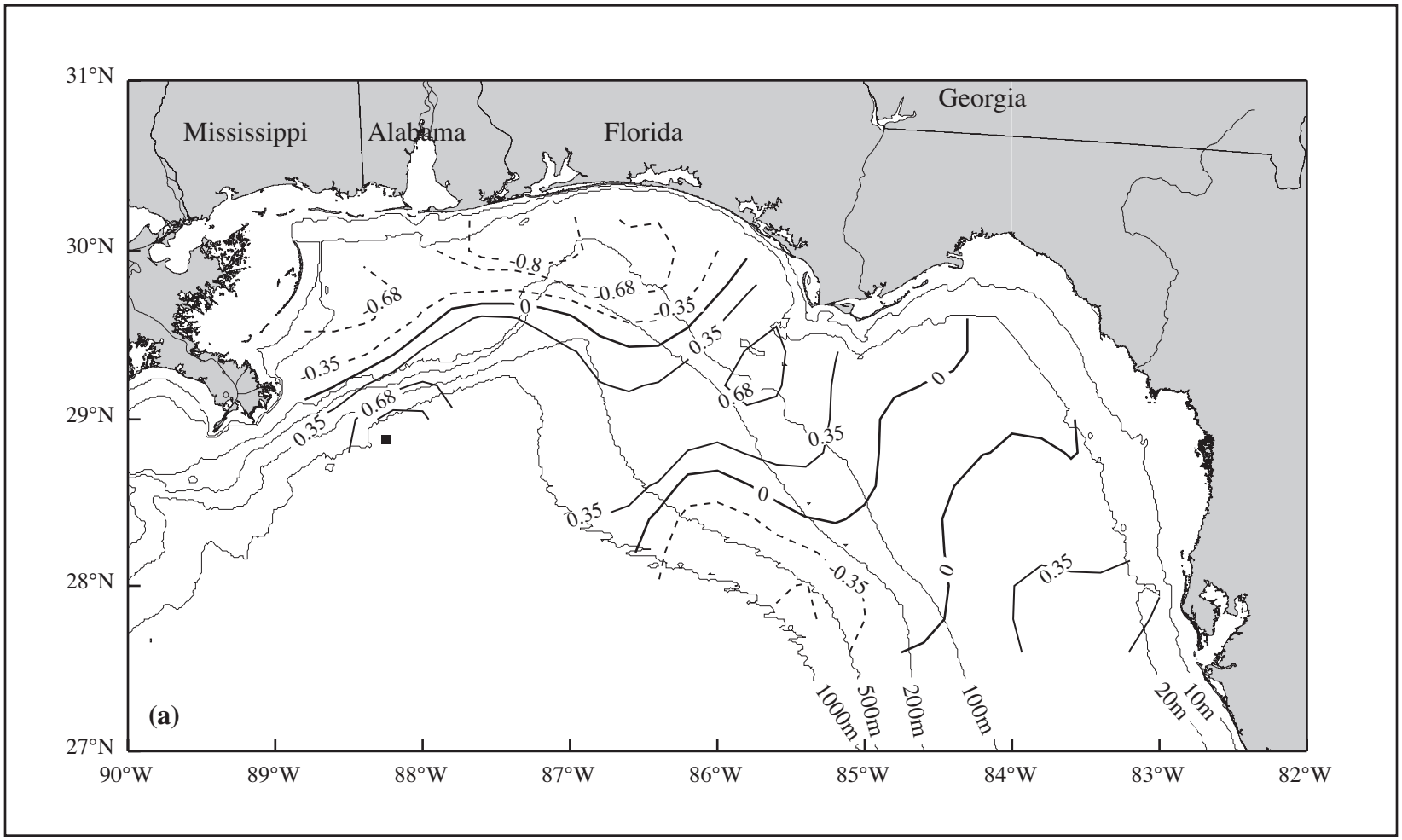

Figure 4.5-2. Fields of correlations between SSH gradients at the locations indicated (solid square) and gridded near-surface ADCP currents for eight NEGOM cruises. The gradients were along the lines shown in Figure 4.5-1 and were averaged over the period of each cruise. The correlations were with the current components normal to the lines. A correlation of 0.68 is significant at the 90% confidence level.

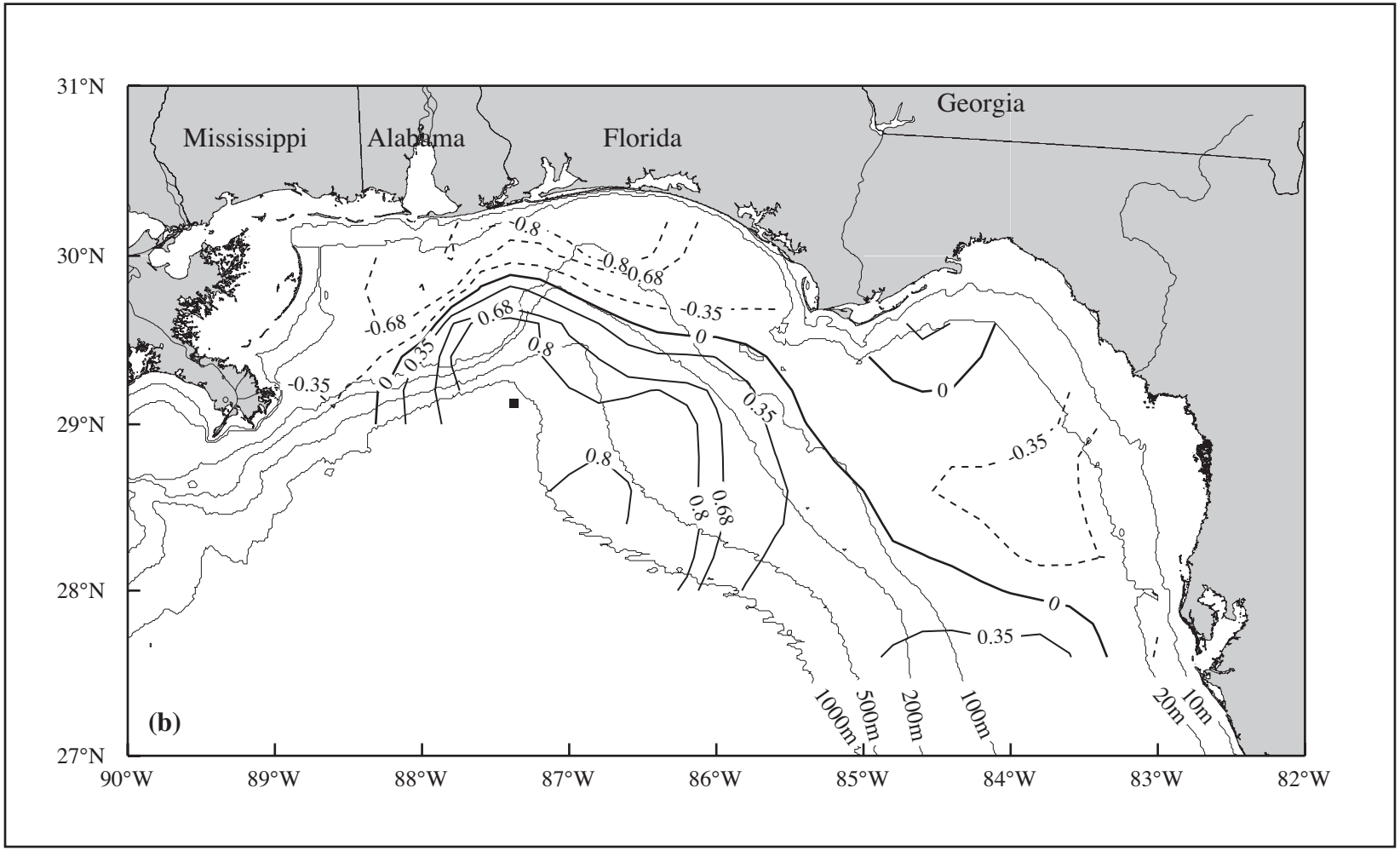

Figure 4.5-2. Fields of correlations between SSH gradients at the locations indicated (solid square) and gridded near-surface ADCP currents for eight NEGOM cruises. (continued)

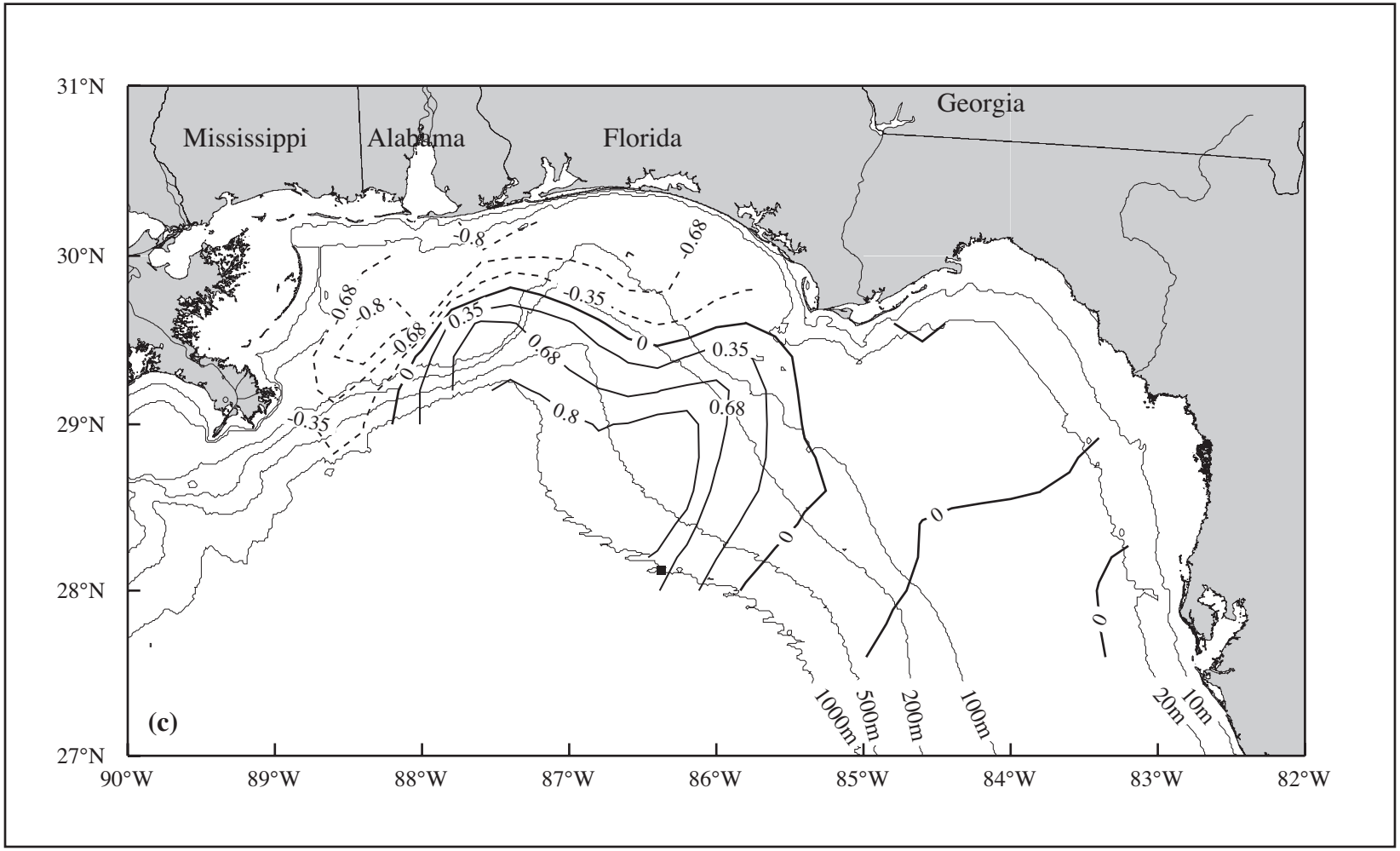

Figure 4.5-2. Fields of correlations between SSH gradients at the locations indicated (solid square) and gridded near-surface ADCP currents for eight NEGOM cruises. (continued)

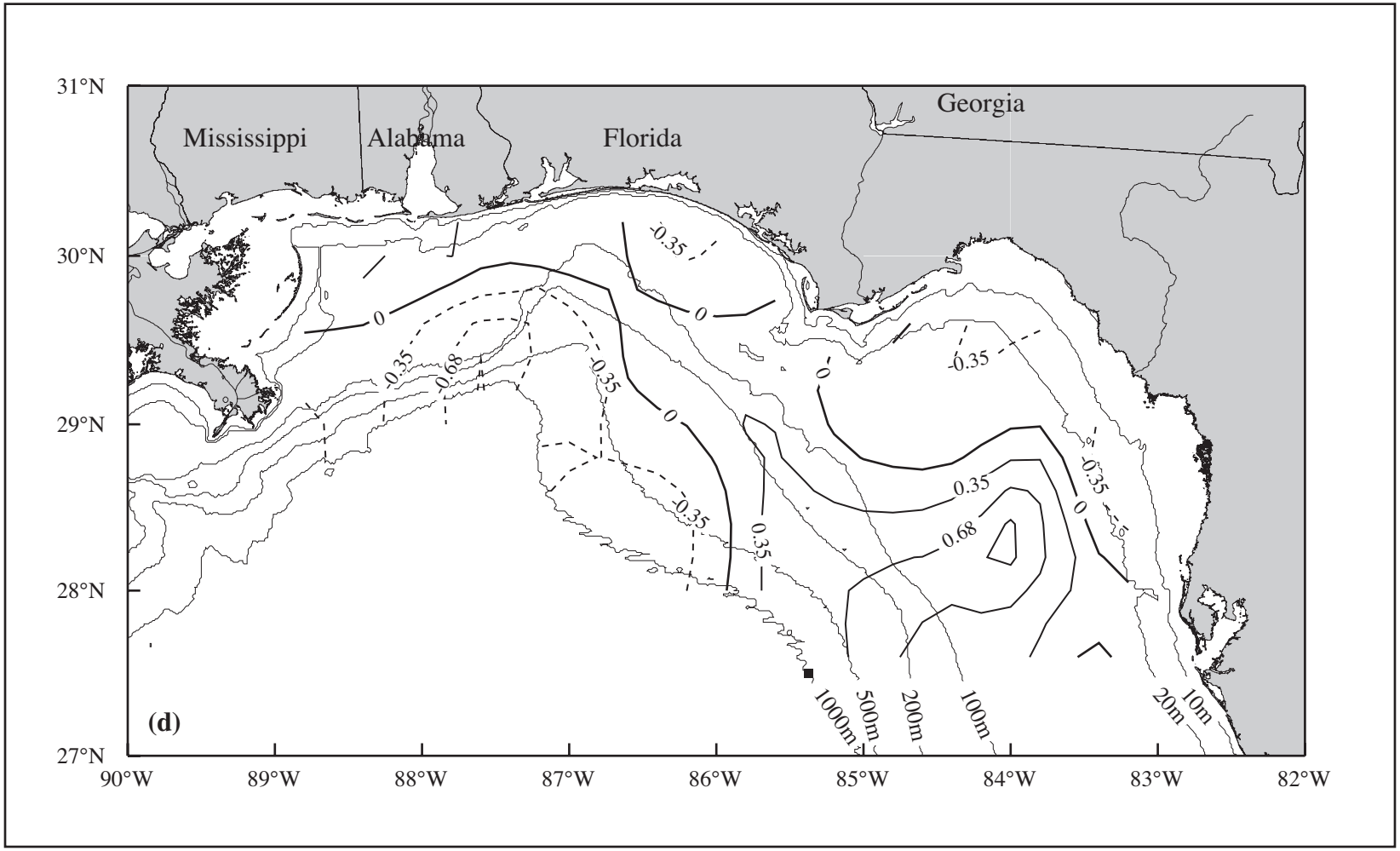

Figure 4.5-2. Fields of correlations between SSH gradients at the locations indicated (solid square) and gridded near-surface ADCP currents for eight NEGOM cruises. (continued)

4.6 Conclusions

The circulation over the NEGOM study area is very complicated, and cannot be fully characterized on a seasonal basis. This is due to a number of factors. First, the region is strongly influenced by the presence of eddies over the continental slope, and these features are not seasonal or deterministic in occurrence. Second, although there is a clear seasonal pattern in the climatological winds over the study area, we have observed much interannual variability. Moreover, the variability in direction from downcoast to upcoast occurs with great frequency, leading to rapid shifts in direction of the wind-driven coastal current. Finally, the discharge of rivers to this area follows a complicated pattern, as compared to the northwestern Gulf shelves. The dominant river is the Mississippi and its discharge is often carried eastward along the outer continental shelf or over the slope, leading to a pattern of decreasing offshore salinity over the mid to outer shelf and consequent buoyancy effects.

Key points regarding the circulation:

- Eddies, and at times the Loop Current and associated surface filaments, are present over the continental slope off the study area. They exert very strong influences on the shelf circulation, especially over the Mississippi-Alabama shelf and around the DeSoto Canyon. These off-shelf circulation features appear to account for about three-quarters of the variance of the near-surface circulation of the study area.

- Nearshore currents may be driven by along-shelf winds. Along-shelf coastal currents related to the along-shelf wind components appear to exist over much of the region, perhaps with the exception of the southeastern most area. However, the wind regime in the study area is quite variable on both short and interannual time scales, rendering climatological predictions of diminished value. Only some ten percent of the variance of the near-surface circulation observed during the NEGOM study showed a seasonal pattern associated with the wind regime.

- Approximately an additional 15% of the variability of near-surface circulation in the study region is associated mainly with currents over the inner shelf and may be attributed to the effects of local winds and river discharge.

- Variability in both circulation and property distributions is judged considerably greater in the western than in the eastern study region.

Some notes regarding methodology to be used in the study area:

- The Montgomery method (Montgomery 1941) of extrapolating measurements of geopotential anomaly into shallow water and the approach of Sheng and Thompson (1996) both gave gross errors in estimating the surface geostrophic currents in the study area (Wang et al. 2002a; Wang et al. 2002b in preparation). They should be used only with caution over the inner shelf (depths < 50-100 m) in this area. Over the outer shelf, comparisons between ADCP fields and geopotential anomaly calculated using the Montgomery method agreed fairly well. In contrast, the Montgomery method performed quite well over the Texas-Louisiana shelf (Nowlin et al. 1998a).

- The SSH fields used gave excellent indications of currents near the 1000-m isobath, but the agreement with the ADCP fields diminished with decreasing water depths.

- As is usually the case in oceanography, the distribution of conservative properties is a prudent and accurate method of describing the circulation.

5 SYNTHESIS OF PHYSICAL PROPERTIES

5.1 Introduction

A discussion of the circulation within the NEGOM study area and its observed variability is found in the preceding section (4). That discussion considers the general relationships between forcing functions and circulation. However, it does not consider the details of the circulation and related distributions of physical properties for each cruise. Those connections are explored in Appendices A through I, each of which describes the conditions observed during one of the NEGOM cruises N1 through N9.

In this section we give an overview of those observed conditions. For fall, spring, and summer, we summarize the major physical conditions observed on the three cruises conducted during that season. This serves to highlight the observed seasonality and contrast seasonal differences.

The discussion of cruises in the fall, spring, and summer seasons generally explores the following issues in the order given here: cruise dates, general vertical stratification, climatological wind regime, winds during the cruises, nearshore flow regimes in relationship to along-shelf winds, inner shelf circulation in the Big Bend area, climatological river discharges, river discharges prior to cruises, surface salinity distributions, off-shelf circulation features and effects over the outer shelf and slope, general features of property distributions, and small-scale eddies observed.

The overview presented here does not include references to specific figures. It is assumed that the interested reader will refer to Section 4 and especially to the appendices for details. Distributions of geopotential anomaly referred to here are for 3 m relative to 800 m. Surface distributions of salinity, oxygen, nutrients, chlorophyll *a*, and temperature are in reality based on observations taken from approximately 3-m depth. Near-surface, shipboard ADCP currents are from the shallowest bin available for the data set referred to. The geopotential anomaly distributions generally agree well with the SSH distributions and ADCP currents over the slope and shelf edge. Further inshore over the shelf the geopotential anomaly distributions have complicated patterns and often are not in agreement with ADCP currents. They should be viewed with suspicion and not be taken to represent surface geostrophic currents relative to the reference depth, for reasons given in Section 4.6.

From this overview, it should be clear that some physical oceanographic characteristics of the study area were common for the three cruises of a season and were different from those in other seasons. One such example is general vertical stratification resulting in large measure from the annual cycles of heating/cooling and of surface winds. Another example is the upcoast circulation over the inner shelf (driven by surface winds) observed during the spring cruises and the associated along-coast eastward advection of river discharge. However, it should be remembered that we have only three samples in each season and that interannual variability of most forcing functions (surface winds and river discharge included) do occur.

Other physical characteristics were very similar for the three cruises in a given season, but resulted from phenomena which are not necessarily expected to occur on a regular seasonal basis. An example is the eastward distribution along the outer shelf and slope of Mississippi River discharge observed on the three summer cruises. This distribution was due to off-shelf circulation features which may not occur regularly in summer.

Finally, it will be clear that many of the physical patterns observed during the three cruises in a given season were quite different. This clearly results from the large interannual variability of: wind fields forcing mainly the circulation over the inner shelf, off-shelf circulation features forcing slope and outer shelf circulation, and river discharge patterns which affect vertical stratification and buoyancy forcing of currents as well as help determine the surface distributions of many properties, including salinity, light transmission, nutrient levels, and sometimes temperature.

5.2 Fall: Cruises N1, N4, and N7

The three fall cruises (N1, N4, and N7) were carried out during the early second half of Novembers; they began on November 16, 13, and 13, in 1997, 1998, and 1999, respectively.

The stratification observed during the three fall cruises was very similar, with relatively deep mixed layers, indicating the effects of wind mixing and the beginning of winter cooling. Excepting areas influenced by river water discharge (and so creating a shallow pycnocline), the inner shelf was mixed to the bottom, often to water depths of 50 m or more. Over the outer shelf and slope mixed layers extended to 60 or 70 m and the seasonal pycnocline was found in the range of 60 to 100 m, unless disturbed by circulation features.

The climatological surface mean winds during November in the NEGOM area are principally toward the west to southwest. Variance ellipses are almost circular and indicative of very high variability over the inner shelf east of Pensacola and over the entire eastern study area. Winds during the fall cruises generally followed this pattern.

Average winds during cruise N1 were to the southwest at less than 5 $m \cdot s^{-1}$, with variances of the same magnitude oriented east-west and having semi-major axes of 20-50 $m^2 \cdot s^{-2}$, increasing to the west and offshore. During cruise N4 average winds were westward except off Mississippi and Alabama where they were to the southwest; variances ellipses were oriented N-S with semi-major axes ranging from 12-30 $m^2 \cdot s^{-2}$ and again increasing to the west and offshore. Average winds during cruise N7 were everywhere southwestward at about 5 $m \cdot s^{-1}$ with variances oriented west-northwest to east-southeast with semi-major axes in the range of 10-25 $m^2 \cdot s^{-2}$ and increasing to the west and offshore. Two frontal passages occurred during N1 and N4, and winds shifted toward the northeast one time during N7. This illustrates the large amount of variability in magnitude and direction of winds during the fall season.

Near-surface currents observed by shipboard ADCP showed weak nearshore flow during cruise N1; it was generally downcoast west of Cape San Blas but indeterminate regarding dominant direction over the Big Bend region. ADCP measurements during cruise N4 (made only over the Mississippi-Alabama shelf) showed downcoast nearshore flow. Those patterns would be expected to occur for surface winds with downcoast components over the western study region. For cruise N7, the nearshore ADCP currents were upcoast west of Cape San Blas and downcoast just south of Cape San Blas, leading to some convergence and cross-isobath flow over the inner shelf southwest of the cape. This clearly seems due to the fact that the winds had upcoast components west of Cape San Blas when the survey worked in that region and downcoast components when measurements were made on the west Florida shelf.

The west Florida shelf is rather wide; the inner shelf (water depths less than 100 m) is somewhat protected from the influence of off-shelf circulation features and is considerably wider than the nearshore coastal flow regime. Thus, the circulation over the inner shelf in the Big Bend area deserves separate note. During cruise N1, no clear closed circulation pattern was observed in this area. On cruise N4, no useful ADCP data were obtained over the eastern study

area and the circulation pattern based on property distributions is not clear. There was some evidence in both ADCP currents and property distributions for a cyclonic circulation feature over the northern part of the Big Bend area (mostly north of 28.3°N) during cruise N7. In summary, we did not see a consistent pattern on the two fall cruises for which data were available.

Climatological river discharges into the study area are at minima in the September to November period. During the summer before cruise N1, the flow rates of the Mississippi River and others flowing into the area west of Cape San Blas were at or above record-length means, but were below means during fall. Discharges of the Apalachicola and Suwannee rivers exceeded mean rates by one standard deviation during the period from October through November of 1997. The resulting pattern of surface salinity observed during cruise N1 showed a tongue of low-salinity water extending eastward along the shelf break from the Mississippi. Salinity values below 34 extended to 88.5°W, and such values were present around the Chandeleur Islands and along the coast as far east as Pensacola. Except for the low-salinity tongue extending eastward from the Mississippi River, the overall pattern was of surface salinity increasing from the coast offshore.

In October and November of 1998, discharge rates were slightly above their long-term means for the Mississippi and Suwannee rivers and slightly below their means for other rivers discharging into the region. The resulting surface salinity pattern for cruise N4 was very similar to that for cruise N1, with two exceptions: (1) the Mississippi River low-salinity tongue contained considerably lower salinity water and did not extend quite so far eastward along the outer shelf, but rather seemed to extend northward into the Mississippi Sound; (2) surface waters with salinities below 34 were found also off Cape San Blas resulting from the Apalachicola River and offshore from the Suwannee River extending to the southern boundary of the study area. Again the overall pattern was of surface salinity increasing from the coast offshore.

The Mississippi and other major rivers discharging into the study area had discharge rates nearly one standard deviation below their long-term means for September through December of 1999. This resulted in a surface salinity pattern for cruise N7 quite different from the other fall cruises. With the exception of the Mississippi-Alabama shelf, surface salinity did not generally increase from the coast offshore; instead, surface salinity values were nearly uniform at values around 35.5 to 36. The Mississippi River influence was limited to an area very near its mouth and nearshore along the Chandeleur Islands to the north. Values less than 34 were limited to the mouth of the Mississippi and off Mobile Bay; nearshore values less than 35 were found from the Mississippi to just east of Pensacola and in a small area near the mouth of the Apalachicola River. South of the Suwannee River was found a nearshore band of surface waters with values less than 36, in contrast to slightly further offshore.

Chlorophyll *a* and percent light transmission in surface waters also reflect river influence and so correspond reasonably well with surface salinity distributions. For cruise N1 there was much greater influence by the Apalachicola and Suwannee rivers on chlorophyll *a* and light transmission than on salinity. Nearshore chlorophyll values south of the Suwannee were greater than those off Pass a Loutre and high chlorophyll values were seen south and southwest of the Apalachicola River mouth out to the 50-m isobath. Decreased light transmission mirrored this distribution. The surface distribution of chlorophyll *a* during cruise N4 was very similar to that on N1; the surface pattern of percent light transmission was also similar except that values were not noticeably diminished by the Suwannee River discharge. The surface chlorophyll *a* distribution for cruise N7 reflected the surface salinity distribution, except that the influence of the Apalachicola River was to be seen out to the 50-m isobath south and southwest of Cape San

Blas (as was the case for N1), and the influence of the Suwannee River on enhanced chlorophyll along the coast southward to Tampa could not have been predicted from the slight freshening of this band of water.

Fields of SSH from satellite altimetry provide evidence of off-shelf circulation features. Confirmation of these features over the slope and their influence on the shelf circulation was provided by shipboard ADCP measurements of near-surface currents. The influence of these circulation features also is reflected in distributions of surface temperature and salinity. The SSH field for 19 November 1997, during cruise N1, shows a weak anticyclone centered near 28.5°N, 88.5°W, impinging on the outer shelf edge, and a somewhat stronger cyclone with elongated center outside the 1000-m isobath extending from 27°N, 85°W to 28°N, 86°W. The near-surface ADCP currents substantiate this pattern. Eastward currents were measured over the slope and outer shelf from off the Mississippi Delta to about 87.5°W, and southwestward currents were measured over the slope around 87°W between the cyclone and anticyclone. The surface temperature distribution confirms this pattern; seen is an intrusion of warm (>23C) water along the northwestern flank of the DeSoto Canyon to 29.6°N, 87°W and cooler water carried across and off the outer shelf in the region between the two offshore circulation features. Warm (>23°C) water was seen covering the outer west Florida shelf along the northeastern side of the cyclone.

As was the case for cruise N1, there was an anticyclone off the shelf in the western study region during N4. The SSH field for N4 showed a relatively large, but weak, anticyclone along the continental slope extending eastward from 89°W to about 86°W. A weak low was located over the slope in the eastern study region. The anticyclone was substantiated by moored current measurements at 20-m depth from the DeSoto Canyon Eddy Intrusion Study and from the shipboard ADCP measurements from N4 (unfortunately made only in the western study region). The anticyclone advected warm (approximately 25°C or greater) offshore water east-northeastward along the northwest flank of DeSoto Canyon onto the shelf edge, similar to the situation observed during cruise N1. Again on N4 there was a warm water intrusion (slight in extent) along the eastern edge of the Mississippi River tongue of low salinity surface. As during the time of cruise N1, warm (>25°C) water extended onshore over the outer west Florida shelf during cruise N4.

SSH for 18 November 1999 during cruise N7 showed the extremely strong anticyclonic Loop Current Eddy Juggernaut located south of 27°N and generally west of 88°W. One protrusion of positive SSH from that eddy extended just to the 1000-m isobath near 28°N, 86,7°W, and the resulting clockwise circulation over the neighboring slope outside of the 500-m isobath is clearly seen in the geopotential anomaly distribution for N7. Between that anticyclonic feature and the shelf edge the SSH distribution showed lows south of the Mississippi River delta extending into the DeSoto Canyon and to the west of Tampa. The effects of those features was seen in the surface temperature field. The cyclone south of the delta caused advection of warmer surface water onto the shelf around the eastern end of the Mississippi River influence; the anticyclonic intrusion also brought warmer surface water over the upper slope; and the eastern cyclone appeared to draw cooler water from the shelf over the slope. In consequence, the surface property distributions over the outer shelf during N7 looked much like those for the other two fall cruises.

Bottom temperatures are expected to decrease with increasing depth, with isotherms generally paralleling isobaths, because water temperatures generally decrease with depth. Indeed this is the pattern for the spring and summer cruises. However, for the fall cruises (N1, N4, and to lesser extent N7) the pattern is different with the bottom waters nearest shore being colder than those further offshore out to approximately the 50-m isobath. This reflects the fact that the fall

cooling reaches the bottom in shallow nearshore waters before cooling the entire water column further offshore.

Small scale eddies and other circulation features that affect the distribution of physical, chemical, and biological properties are found over the outer shelf and slope. During cruise N1, such a small cyclonic feature, with diameter of approximately 60 km was centered near 29.2°N, 88.5°W, which was just within the eastern end of the Mississippi River tongue extending along the shelf edge and may account for the northward flow of low-salinity water and termination of that tongue. Another small-scale feature in property distributions seen during cruise N1 as a doming of isopleths extending from the outer shelf onto the slope was associated with the off-shelf flow between the cyclone and anticyclone mentioned above. In the case of these two features, the upward doming of isopleths resulted in additional nutrients being available in the upper ocean, perhaps to be used by plankton in the photic zone. Two cyclonic eddies, with diameters on the order of 50 km, were observed on N4 centered near 28.4°N, 86°W and 29.3°N, 87.2°W. The doming effects within both were confined to depths greater than 250 m. Likewise on cruise N7 a cyclonic feature with center near 29°N, 87°W with diameter about 50 km was observed by the upward doming of isopleths of temperature, nutrients, and other properties. Bottom observations of temperature and nutrients at the four cruise N7 lines nearest the apex of DeSoto Canyon gave indications of on-shelf bottom flow across the 100-m isobath, which could be attributed to a bottom Ekman layer driven by anticyclonic flow near the bottom.

5.3 Spring: Cruises N2, N5, and N8

The spring cruises N2, N5, and N8 were offset by about two weeks in time of year; they began on 5 May 1998, 15 May, 1999, and 15 April 2000, respectively. So conditions during cruise N8 were less advanced toward summer than during N2 and even more so relative to N5.

As a result of very large river discharge and movement of the resulting low-salinity surface waters over all of the shelf west of Cape San Blas, on cruise N2 there was a very strong pycnocline within the upper 10-15 m in that area. In the eastern part of the study area nearshore isopycnals were nearly vertical as a result of the low salinity water being confined to the coastal regime. Over the outer west Florida shelf the seasonal pycnocline was relatively weak and confined to the upper 150 m with maximum strength near 80-100 m. The stratification on cruise N5 was similar to that on N2 although the areal extent affected by very low-salinity surface waters was confined to the inner shelf west of Panama City and the outer shelf west of about 87.5°W. The effects of very low salinity surface waters were confined on cruise N8 to an even smaller area in the northwest of the study region than on N5; otherwise the general stratification was similar. For none of the spring cruises was there a pronounced surface mixed layer. In the regions having strong near-surface pycnoclines due to river water, the replenishment of oxygen to the bottom waters, where it was being consumed, was precluded. Several areas with low bottom oxygen values were noted.

Climatological surface winds over the study area are quite similar for April and May, although historically May represents a transition between westward mean wintertime winds and northward mean summertime winds. Over the outer shelf and slope they are essentially westward with speeds less than 5 $m \cdot s^{-1}$ and standard deviations smaller than the means with little preferred direction. Over the inner shelf mean directions generally are toward the north or northwest with standard deviations commonly at least as large as the means. Over the inner shelf region of the Big Bend means may exceed 5 $m \cdot s^{-1}$ and variances are the largest in the study area.

The mean winds during cruise N2 were generally weak (≤ 5 m·s^{-1}) with variances of comparable magnitudes. They were directed onshore over the Mississippi-Alabama shelf, but had slight upcoast components from off Pensacola to the Suwannee River and downcoast components from there southward to off Tampa. Mean wind speeds for the period of cruise N5 were small (1-3 m·s^{-1}). Mean directions were northward over the Mississippi-Alabama shelf but were rotated clockwise with increasing distance upcoast, giving upcoast along-shelf components over all of the Florida shelf. Variances during the cruise period were large in relation to means, with semi-major axes of variance ellipses of order 20 m^2·s^{-2} in the western study decreasing to 10 m^2·s^{-2} in the east. This variability resulted from frontal passages on May 19 and 24. Mean wind directions during cruise N8 were to the east and east-southeast, so they were favorable for coastal upwelling everywhere. However, though mean wind speeds were small (1-4 m·s^{-1}), the instantaneous wind speeds produced during the passage of three fronts during the cruise exceeded 10 m·s^{-1}, giving variance ellipses for the cruise oriented northwest-southeast with semi major axes of 20-40 m^2·s^{-2}.

There were two upwelling favorable periods of rather weak winds on cruise N2. Nearshore ADCP currents were variable in direction offshore from Mississippi but eastward (upcoast) from there throughout the study area. They increased in magnitude eastward to Cape San Blas and were weak in the Big Bend area. Vertical sections of properties gave some indication, by upward slope of isopleths toward shore, of coastal upwelling in the region between Pensacola and Apalachicola. Currents observed with shipboard ADCP during cruise N5 were upcoast and relatively large over the inner shelf west of Cape San Blas. This situation was substantiated by the surface salinity distribution which resulted from eastward advection of river discharges with the strongest effects (lowest salinities) near to shore. Vertical sections of properties in the western study area showed indications of coastal upwelling. Nearshore currents over the west Florida shelf were indeterminate from the cruise data with the exception of a region south of Apalachicola from about 84.5°W to 85.5°W where ADCP currents were downcoast. The convergence of nearshore currents off Cape San Blas resulted in offshore flow across isobaths to the shelf edge. East of Pensacola to Apalachicola the nearshore currents observed on cruise N8 were upcoast, consistent with the wind direction, with speeds of 20-40 cm·s^{-1}. Nearshore upcoast current speeds were smaller west of Cape San Blas, and south of the Suwannee River nearshore currents were weak and directionally variable. The surface temperature distribution as well as the slope of isopleths nearshore on cross-shelf sections gives some evidence that coastal upwelling had occurred from near Pensacola to about 83.5°W. This was confirmed by high chlorophyll *a* estimates in this region. Nearshore surface currents were weakly northward off the mouth of the Mississippi River. Over the Mississippi shelf nearshore currents were weak and of mixed direction, but between the 20-to 100-m isobaths they were strongly northeastward. In summary, there was evidence for eastward transport of nearshore waters from the Mississippi and other rivers in two of the spring cruises. For all spring cruises the surface salinities tended to increase offshore, and for all there was some evidence of coastal upwelling, principally in the study area west of Cape San Blas.

During cruise N2, gridded near-surface ADCP currents indicated a weak cyclonic flow regime over the inner shelf of the Big Bend area. ADCP currents in that area during cruise N5 were weakly divergent with no closed circulation pattern. Note that data coverage from cruise N5 was rather sparse. Surface flow over the inner Big Bend area had a quite complicated pattern during cruise N8. Upcoast (downcoast) current components dominated over the northern (southern) part of the area and onshore (offshore) current components dominated over the inner (outer) part of the area. Thus, we could confirm little similarity between the patterns seen over the inner shelf for the Big Bend area on the three spring cruises.

Long-term discharge rates for the Mississippi River reach their maximum in April. Those from other rivers discharging into the area reach near peak values beginning in February and continuing into the March-April time frame.

During winter-spring 1997-98, the Mississippi River considerably exceeded its 70-yr average discharge rates, except during April when discharge was about average. Rivers between the Mississippi River delta to Apalachicola exceeded long-term average discharge rates during spring 1998, in some cases by significantly more than one standard deviation. Mississippi River discharge rates during February, March, and May of 1999 were marked by a series of pulses which exceeded the 70-yr mean by about one standard deviation. Other rivers discharging into the study area were marked by spring 1999 discharge rates significantly under their long-term averages except for a very high discharge peak from the Tombigbee River at the beginning of May. Thus, much low-salinity surface water was observed on both cruises N2 and N5, but more limited to the west and with higher salinity values on N5 than on N2. River discharge into the study area generally was low in 2000. Mississippi River discharge rates were below their 70-yr average for January through April. Except for pulses of higher than normal discharge, rivers west of Pensacola also were below their average discharge rates for January through April, and those rivers to the east of Pensacola generally were well below their average discharge rates for this period. Thus, much less river water was available over the study area during cruise N8 than for cruises N2 and N5.

On cruise N2 there was widespread influence of rivers. Values less than 34 extended at least to the 1000-m isobath off Mississippi and Alabama, over the entire shelf as far east as 86°W, and over the west Florida shelf inshore of about the 50-m isobath. Values over the inner shelf west of Cape San Blas generally were less than 32, with regional minima of less than 24 near Mobile Bay and 31-32 off the Suwannee River. During cruise N5 the effects of the Mississippi River were seen to dominate surface waters of the western study area. Salinities less than 34 extended at least to the 1000-m isobath off Mississippi and Alabama, over the western flank of the DeSoto Canyon, and to the coast east of Panama City. Salinities as low as 26 were seen east of the Mississippi River delta and were associated with the highest observed chlorophyll *a* concentrations, as well as enhanced oxygen and nutrient concentrations. Surface salinities over the slope east of 87°W and over most of the west Florida Shelf exceeded 35.5–36 over much of the area. Localized freshening near Mobile Bay may be attributed to the Tombigbee River discharge. On cruise N8, the effects of the river discharge on the near-surface salinity distribution was most clearly seen in the western study area, but also was somewhat evident in the vicinity of Cape San Blas and Apalachicola Bay. In the west, a triangle of low salinity (< 35.5) water extended from the Mississippi River delta to east of Pensacola. This low salinity region was due mostly to the influx of fresh water from Mobile Bay and the estuarine areas south of Pascagoula and east of the Chandeleur Islands. The ADCP currents measured off the mouth of the Mississippi River were generally to the southwest transporting the discharge from that river out of the study area. The effects of river water also can be seen in the distribution of chlorophyll *a* for which high concentrations were seen near the coast with highest concentrations near the mouth of Mobile Bay and Apalachicola Bay.

During April 1998, a small anticyclone began to develop in the vicinity of DeSoto Canyon. During cruise N2, an anticyclonic system, oriented northwest-southeast along the DeSoto Canyon and west Florida shelf with two regions of high SSH, was intensifying. One high was located near the slope apex of DeSoto Canyon and the other was encroaching over the slope and outer shelf west of Tampa. A cyclonic system was shown in the SSH field west of the anticyclonic system, but with weak gradients near the study area southeast of the Mississippi River delta.

The SSH field for 20 May 1999 shows an elongated cyclone with center near 28°N extending from about 86.5°W to 88.5°W . The Loop Current penetrated northward only to about 27°N during May 1999, but a small bulge from its northeastern limb was seen to extend onto the slope near 27.5°N and 85.5°W by the beginning of June. It is believed that this intrusion was dynamic during cruise N5, and it may have briefly intruded into the study region during the cruise.

Based on SSH fields the Loop Current remained south of 27°N during March and April 2000. A peanut shaped low oriented east-west with center about 27.5°N is shown in the SSH field for April 20, midway through cruise N8. That cyclonic feature was seen to encroach onto the edge of the west Florida shelf. Between that cyclone and the Mississippi-Alabama shelf was an anticyclonic circulation feature.

The distribution of geopotential anomaly and shipboard ADCP currents for cruise N2 confirms the anticyclonic feature located over the DeSoto Canyon and that encroaching over the outer shelf edge west of Tampa (both seen in the SSH field). The currents associated with the DeSoto Canyon eddy were < 40 $cm \cdot s^{-1}$; currents near the shelf break west of Tampa reached ~75 $cm \cdot s^{-1}$. The anticyclonic features also were seen in the 50- and 102-m depth currents. Vertical distributions of properties did not clearly exhibit the dipping isolines characteristic of anticyclonic eddies, though there was some depression of isopycnals in waters deeper than 500 m. This is consistent with the fact that the eddies were relatively weak—perhaps they were spinning up just prior to and during the cruise.

There was a large divergence of flow at the 14-m depth seaward of about the 200-m isobath between the two anticyclones seen on cruise N2. This divergence weakened with depth, but still was present in currents at 100-m depth. There was evidence in the SSH field for an intense cyclone located adjacent to the 1000-m isobath on the west side of the saddle point between the two anticyclones. This cyclone likely would have induced flow out of the study area from the region of apparent divergence. Examination of silicate along the 1000- and 500-m isobaths suggests possible upwelling, which may have replaced fluids removed by the divergent flows, though other properties show this less clearly if at all.

Observed on cruise N2 were effects of upwelling of cool bottom waters near the head of DeSoto Canyon. Vertical sections of hydrographic properties provide clear evidence that onshore, near-bottom flow, extending in most cases to the innermost stations (10-m isobath), had occurred prior to cruise N2. There is evidence from ADCP and moored current measurements for along-isobath flow along the northern reaches of the canyon and cross-isobath flow directed inshore on the west side of the anticyclone and near the canyon axis. Such flow would lead to transport in a bottom Ekman layer directed to the left of the flow—leading to more penetration of bottom waters toward shallower depths.

Geopotential anomaly based on N5 data shows a pattern of one major high and several relatively weak features. Most prevalent is the high encroaching onto the outer shelf at 28°N, 85°W, which is likely associated with a tongue protruding from the Loop Current, as mentioned. Warm surface temperatures (> 27°C) can be seen over the outer west Florida as warm off-shelf oceanic waters are advected onto the slope around this anticyclone. Warm surface temperatures (>27°C) also can be seen over the Mississippi-Alabama shelf and roughly correspond to the low salinity and high productivity areas resulting from river waters.

A weak high is seen in the N5 geopotential anomaly over the apex of DeSoto Canyon close to shore and between Pensacola and Panama City; another is centered at the 200-m isobath and 88.6°W east of the mouth of the Mississippi River. Lows in dynamic height are present directly

south of the Mississippi River delta, over the eastern flank of the DeSoto Canyon at 87°W, and inshore of the 500-m isobath south of the strong anticyclone. Because good ADCP data on cruise N5 were limited to water depths of less than 100 m, these features in dynamic height cannot be confirmed with direct measurements. However, at depths below 50 m along the 100-m isobath, the oscillations in the isopycnals can be matched to the major features seen in dynamic height.

Geopotential anomaly based on cruise N8 data shows a series of three highs and two lows along the outer shelf and slope. Indeed, there is some correspondence between these and the vertical distribution of properties along isobaths 200-m and 1000-m isobaths. The ADCP currents are in general agreement with the geopotential anomaly distribution. A 50-km diameter anticyclone was seen east of the Mississippi River over the slope; this is confirmed also by the SSH field. A cyclone was located over the DeSoto Canyon. An anticyclone was centered near 28.5°N, 86.8°W. A cyclone was seen centered at 86°W, 28.3°N with a diameter of roughly 50 km and speeds of 20-30 $cm \cdot s^{-1}$. This cyclone can be seen in currents measured at 100-m depth with slightly diminished speeds. A weak anticyclone was seen at the southern line of the study area. Effects of the two stronger anticyclones were seen as cross-isobath transport of properties.

No evidence was found for small eddies over the outer shelf and upper slope during cruise N2. Weak cyclonic features were indicated in property distributions from cruise N5. One was centered between the 500- and 200-m isobaths at the southeast end of the study area and another on the eastern flank of DeSoto Canyon. A third was directly south of the Mississippi River delta at the western end of the study area. They affected property distributions principally below 50 m. Sizes are difficult to estimate for those at the extreme ends of the region of study; the low over the DeSoto Canyon might have had a semi-major axis as large as 50 km. Two small cyclonic and three small anticyclonic eddies were seen over the outer shelf and upper slope during cruise N8. All appeared to have diameters of order 50 km.

5.4 Summer: Cruises N3, N6, and N9

The 1998 and 2000 summer cruises N3 and N9 were carried out in late July and early August, beginning on July 25 and 28, respectively. Cruise N6 began about two weeks later in the season, on August 15, 1999.

During these summer cruises there was strong vertical stratification in the upper 100 m, with the strongest pycnoclines occurring just below thin mixed layers. During cruises N3 and N6 the strongest pycnoclines were found in the depth range 10-20 m. For cruise N9 this range extended to 30 m. This strong near-surface stratification in summer resulted from a combination of summer heating and low surface salinity. More low-salinity water at the surface resulted in the strongest vertical stratification being nearer the sea surface; cruise N9 had the least amount of relatively low salinity surface water and consequently a deeper range of maximum vertical stratification. The strong vertical stratification may preclude renewal of oxygen to bottom waters depleted by oxygen consumption processes. Near hypoxic bottom conditions were found on several occasions.

The climatological winds for July are mainly northward over the outer shelf. Over the inner shelf they have slight upcoast components west of Cape San Blas but downcoast components in the Big Bend area. Average speeds are weak (1-5 $m \cdot s^{-1}$) and standard deviations vary from about 2 to 6 $m \cdot s^{-1}$ from west to east across the study area. August mean speeds over the area are 1-3 $m \cdot s^{-1}$ with standard deviations of 2-4 $m \cdot s^{-1}$, increasing slightly from west to east. Mean along-shelf wind components generally are directed downcoast in August.

The average winds during cruise N3 were quite weak (2-3 $m \cdot s^{-1}$) with slight downcoast components and principally east-west variance ellipses. Four days prior to the cruise's end (on August 2) winds increased to speeds reaching 10 $m \cdot s^{-1}$ directed toward the west. During cruise N6 average winds were northeastward from the Mississippi Delta to just east of Cape San Blas and northward over the rest of the west Florida shelf. Average speeds were only 2-5 $m \cdot s^{-1}$ with small but dominantly east-west variances. Instantaneous winds generally were less than 7 $m \cdot s^{-1}$ and northward, but there were several periods of directional changes to east or west. Average winds during cruise N9 were northward with slight upcoast components over the Mississippi-Alabama shelf and downcoast components east of Cape San Blas. As during the other summer cruises, wind speeds were weak (with strongest instantaneous wind speeds generally <10 $m \cdot s^{-1}$) and variance ellipses oriented east-west. In summary, the regional winds were quite similar during each summer cruise and consonant with the climatological fields for August.

Nearshore near-surface currents as measured by shipboard ADCP during cruise N3 were northward off Tampa, but from there to past Cape San Blas were generally small in magnitude and variable in direction. There was some evidence of a cyclone inshore of the 100-m isobath in the Big Bend area. West of Panama City nearshore currents had downcoast components, reversing to strong northeastward flow off the mouth of the Mississippi River. This pattern was consonant with the surface distributions of salinity, chlorophyll *a*, and silicate, all of which showed the effects of strong northeastward movement of Mississippi River discharge just off the river's mouth and rather strong east-west gradients over the inner shelves of Mississippi and Alabama. During cruise N6, near-surface ADCP currents were upcoast over the inner shelf in the Big Bend, downcoast from Cape San Blas to Pensacola, and had directions varying from survey line to survey line further west. This is in contrast to expectations from mean winds during the cruise, and probably resulted from east-west variability in wind direction during the cruise. With the exception of salinity, surface property distributions provided little help in confirming the pattern of near-surface ADCP currents observed during cruise N6. The surface salinity field did show the effects of upcoast flow of the outflow from Mobile Bay and downcoast movement of the discharge from the Suwannee River. Nearshore currents during cruise N9 were northward off Tampa, indeterminate in the Big Bend, downcoast from Cape San Blas, and northeastward off the Mississippi River mouth. This pattern was quite similar to that observed during cruise N3, but different from the situation during cruise N6.

Over the inner shelf (water depths $\leq$ 100m) in the Big Bend area, there was a cyclonic circulation pattern in the near-surface ADCP currents measured on cruise N3. No clear closed pattern of circulation was seen in this area during cruises N6 and N9. As was the case for the fall and spring cruises, no seasonal pattern was detected. Overall, we saw evidence for cyclonic circulation over the inner shelf of the Big Bend area for one cruise in each season and no closed circulation patterns for the other cruises.

The SSH distribution on 5 August 1998, at the end of summer cruise N3, showed a large anticyclonic eddy stretching along the slope from just southeast of the Mississippi River delta to the eastern flank of DeSoto Canyon. Also shown was cyclonic flow over the apex of the canyon and a smaller anticyclonic flow centered over the 200-m isobath west of Tampa. This pattern is confirmed by geopotential anomaly calculations from N3 as well as by ADCP currents. Eastward near-surface currents with speeds of 50 $cm \cdot s^{-1}$ or more were measured along the shelf edge off the Mississippi River mouth, extending along the 1000-m isobath to the eastern flank of DeSoto Canyon, and there turning southeastward over deeper water.

The SSH field for 18 August 1999, taken as representative for cruise N6, shows that the slope and outer shelf of the western study area were dominated by two areas of cyclonic flow, one centered near 88.6°W and the other near 87.1°W. South of these features was a large, strong

(center height in excess of 30 cm) anticyclone, and so eastward flow continued over the outer slope. The geopotential anomaly pattern also showed strong eastward flow along the shelf edge into DeSoto Canyon, but without the on- and off-shelf flow implied by two cyclones in the SSH field. The geopotential anomaly field and measured currents both showed the flow turning southeastward in the DeSoto Canyon and continuing along the along the slope out of the study region.

On 2 August 2000 the SSH field showed a weak anticyclone (center height ~13 cm) impinging on the continental shelf from about 88.5° to 87°W. Fields of near-surface ADCP currents and geopotential anomaly from cruise N9 agree quite well over the outer shelf and slope. They indicate strong along-isobath flow along the shelf and outer slope from off the Mississippi River delta to near 87.7°W. Centered at about 28.7°N, 87.5°W on the shelf edge was a small cyclone; it separated the anticyclonic flow to the west from another anticyclonic (not seen in the SSH field) farther to its east. Indicated was strong eastward flow onto the eastern flank of DeSoto Canyon between about 85° to 86°W. Slope currents were weaker over the eastern than the western study region.

Long-term river discharge rates for the Mississippi River are at a minimum in September-October and thus are falling and already low in July and August. The long-term maximum discharge rates for the Mississippi are in April. For most other rivers discharging into the region, the period of maximum discharges are somewhat earlier, during February-April, and the distributions are more peaked than for the Mississippi River, leaving a long period of relatively small discharge. Our summer cruises were within that period of minimum average discharge.

Mississippi River discharge rates exceeded long-term mean values for January-August of 1998; they exceeded the mean by more than one standard deviation during most of July. Most other rivers discharging into the study area also exceeded their mean flow rates early in 1998 but were at or near mean rates during July and August. The Apalachicola River, however, exceeded its long-term mean discharge during most of March through May, often by one standard deviation, and the Suwannee River exceeded its mean flow rate from October 1997 through May 1998 by as much as 150%. In 1999, Mississippi River discharge exceeded its 70-yr mean in May, was average in June, exceeded the mean in July, and was nearly one standard deviation below its mean in August. Except for the Tombigbee River, which had a pulse of high discharge in July, other rivers discharged at or below their long-term means during spring and summer 1999. During the first 8 months of 2000, river discharge rates were generally low relative to their long-term means, though there were pulses of high flow rates for Mississippi and Alabama rivers during April and/or May.

In response to the large Mississippi discharge rates, surface salinities during cruise N3 were <34 over the entire region except for the inner Florida shelf. The lowest values were found (1) near the river mouth (<27), with values <32 extending northeast over the shelf past Mobile Bay, and (2) over the outer shelf and slope along the east flank of DeSoto Canyon (<27), with values <32 extending inshore to the 100-m isobath around the canyon and along the west Florida shelf. East of Pensacola (i.e., over most of the study region) surface salinity generally decreased with distance offshore from the coast. An exception was slightly less salty water near the coast from the mouth of the Suwannee River southward, probably resulting from the relatively high Suwannee River discharge. The pattern of low salinity near the Mississippi River mouth and along the outer shelf and slope is consistent with the indicated circulation. Currents along the slope were strongly eastward from the Mississippi River delta to and into outer DeSoto Canyon, accounting for the low salinity water over the eastern flank of the canyon. Northward currents east of the delta might have aided movement of river water upcoast over the inner shelf. Surface distribution of chlorophyll *a* was very similar to that of surface salinity. The surface

distribution of silicate also was similar to that of salinity with two notable exceptions. Regions of high silicate were found over the inner shelf from Mobile Bay eastward past Pensacola and in a tongue extending southeastward from off Apalachicola to mid shelf.

The result of river discharge rates prior to cruise N6 and the eastward flow along the shelf edge was that low salinity waters generally were seen only over the Mississippi shelf and along the outer shelf and slope eastward from the mouth of the Mississippi River. Consequently, with the exceptions of somewhat lower salinity off the Suwannee River and from Mobile Bay to just east of Pensacola, the pattern of surface salinity seen on N6 was of surface salinity over the shelf decreasing offshore, similar to the situation during N3. The cyclone centered near the head of DeSoto Canyon near 29.5°N, 87.1°W greatly affected observed property distributions. Waters with surface salinities greater than 32 were drawn from the inner shelf over the slope on its western (southward flowing) flank; low-salinity water (<30) was advected onto the shelf up the DeSoto Canyon along its eastern flank. The anticyclone further to the south impinged on the upper slope near 86.5°W. This resulted in the transport of waters with surface salinities between 33 and 36 onto the slope between the 500- and 1000-m isobaths. With that exception all surface waters over the slope in the study area were influenced by the Mississippi River discharge, as evidenced by their relatively low salinities.

As for cruises N3 and N6, low salinity waters were found on cruise N9 over the outer shelf and slope, with salinity increasing eastward from the mouth of the Mississippi River. As a result of this distribution and of low discharge rates from the minor rivers, the surface salinity during N9 decreased offshore without the exceptions seen on N3 and N6 near the mouths of minor rivers. Overall, observed surface salinities were greater, and by inference the influence of rivers less, during cruise N9 than during N3 and N6. For all of the summer cruises, nutrients were enhanced in the upper 15 m of the water column in regions of low salinity caused by river discharges, but concentrations decreased with distance from the discharge points because of uptake by plankton. Nutrients in the lower portion of the photic zone were enhanced by upward doming of isopleths related to circulation features such as small cyclones.

On cruise N3, a small (diameter about 50 km) cyclonic circulation feature was seen in uplifted property distributions centered near 29.4°N, 87.4°W. A somewhat larger (diameter near 100 km) anticyclone was centered over the apex of DeSoto Canyon near 29.7°N, 86.9°W as seen in the SSH field, ADCP currents, geopotential anomaly, and distributions of nutrients and other properties. The former feature may have been a satellite to the latter. Uplift of isopleths in the larger cyclone was limited to depths greater than about 15 m. During N6 a small cyclone was centered near 28.7°N, 85.5°W between the 100- and 200-m isobaths as indicated by the patterns of geopotential anomaly, ADCP currents, and the doming of nutrient-rich waters into the upper 50 m of the water column. Its diameter appeared to be about 75 km. A second small cyclone (diameter of 50 km) was seen in ADCP currents and property distributions off the mouth of the Mississippi River during N6. That cyclone was centered near 28.7°N, 88.6°W between the 500- and 1000-m isobaths and had near-surface speeds to 50 $cm \cdot s^{-1}$. During cruise N9 one small cyclone (diameter of order 50-75 km) was detected, centered over the upper slope at about 28.7°N, 87.5°W. Surface currents exceeded 50 $cm \cdot s^{-1}$ and extended at least to 150 m in depth. In summary, cyclones over the outer shelf and slope with diameter scales of order 50-75 km were seen on all of the cruises made during this study with the exception of spring cruise N2.

6 PARTICULATES

6.1 Introduction

Particulate matter in the world oceans is derived from a variety of sources including river discharges, living phytoplankton and bacteria, atmospheric deposition, and detrital remains of organisms. Particulate matter is organic as well as inorganic and contains living biological organisms resulting in a complex biogeochemical cycle. The living portion of particulate matter interacts with water column chemistry through the uptake of nutrients to form biomass, production of oxygen during photosynthesis, and chemical reactions related to excretion of waste products and decay of organic detritus. Water column chemical and particulate matter concentrations and distributions are the end results of these interactions.

Particulate matter distributions in the study area were described in terms of particulate matter (PM), particulate organic carbon (POC), particulate organic nitrogen (PON), and light transmission. Vertically continuous estimates of particulate concentrations are provided by transmissometry calibrated with the discrete particulate samples. This provides a rapid determination of the horizontal and vertical distribution of particles and an assessment of temporal (seasonal and interannual) variability over the three-year observation period.

In the open ocean most particles are biological organisms and associated detritus. However in near-shore regions, riverine sources of inorganic materials and terrestrial sources of organic matter can be significant. In the open ocean, particulates detected via beam attenuation (c_p), are believed to be primarily due to particle sizes less than 20 microns in diameter (Chung et al. 1996) and represent a range of organisms including heterotrophic bacteria, prokaryotic prochlorophytes, cyanobacteria, eukaryotic picoplankton and smaller nanoplankton. Beam transmission is converted to a total beam attenuation coefficient (c), where $c = c_w+c_p+c_y$ (w=seawater, y=yellow dissolved organic matter, and p=particles). Seawater attenuation is constant and the contribution of yellow dissolved organic matter at the light wavelengths utilized is generally considered to be minimal (e.g., Pak et al. 1988; Chung et al. 1996). In coastal waters, this second assumption may or may not be true. Based on these assumptions, particle concentrations can be estimated from transmissometry readings. These water column properties can be used to understand the origins of cloudy, turbid layers in the water column, called nepheloid layers. Particulate distributions and temporal variations are to be evaluated in the context of the physical processes that operate within the study area. Particulate matter concentrations, distributions, and temporal variations are evaluated in the context of water column stability, river discharge, wind fields, and circulation patterns.

Methods: After quality control processing of the transmissometer data was completed, the particle beam attenuation coefficient (PBAC) was computed as

$$PBAC = -4.0 * \ln\left(\frac{\%T}{T_{\max}}\right)$$

where %T is the measured percent transmission and T_{max} is the maximum percent transmission observed on the cruise (e.g., see Emery and Thomson 1998). The particulate matter data were collected from near-surface, near-bottom, and mid-depth, "clear" water samples at selected stations. The water sample was filtered through a filter that had been weighed prior to the cruise to determine the filter's weight; the filter then was dried and re-

weighed. The PM data then were determined by the differential between the pre-cruise and post-cruise weight of the filter divided by the volume of water filtered (Jochens and Nowlin 1998). These PM data were used to calibrate the PBAC data to estimate the PM concentrations throughout the water column.

Varying sources of particulates result in different particle environments in the surface and bottom waters. Resuspension of particulates from the sea floor is the major source of particulates in waters near bottom. In surface waters, however, there are several major sources of particulates. These include sediments carried in discharges from rivers, bays, and estuaries, production of detritus and fecal matter from biological activity, and wind-borne dust. There can be exchanges between the surface and bottom sediments as particles settle through the water column or, in shallow water, as currents cause mixing of re-suspended material into upper waters. Because the major sources are different, independent correlations between PBAC and PM concentrations were determined for the surface and bottom waters.

Correlations were determined for the surface and bottom data sets from all cruises. These are shown in Figure 6.1-1. All the correlations are positive, indicating that the PBAC increases (light transmission decreases) as particle loading increases. The squared correlations are all better than 0.75 and significant at the 99% level. This indicates excellent correlations between the PM concentrations and associated PBAC values in both surface and bottom waters for each of the nine cruises.

The resulting linear equations were used to calculate PM from the continuous PBAC data. Table 6.1-1 shows the coefficients, A and B, used for the equations with the form

$$PM = A + B * PBAC.$$

There were two equations per cruise; one for the surface and one for the bottom. The water column was divided into upper and lower parts, with the surface equation applied to the upper part and the bottom equation to the lower. To determine where the boundary between the upper and lower parts was, the vertical transmissometer profiles were examined for the

Table 6.1-1. Coefficients of linear regressions of measured particulate matter (PM) against the particle beam attenuation coefficient (PBAC), where PM = A + B * PBAC. BNL refers to the bottom nepheloid layer.

Season	Cruise	Above BNL		In the BNL	
		A	B	A	B
Fall	N1	0.02	1.46	0.01	1.75
Fall	N4	0.12	1.49	0.13	1.38
Fall	N7	0.06	1.70	0.10	1.30
Spring	N2	0.12	1.07	0.00	1.67
Spring	N5	0.09	1.46	0.01	1.66
Spring	N8	0.11	1.28	0.05	1.55
Summer	N3	0.10	1.36	0.03	1.49
Summer	N6	0.09	1.63	0.02	1.52
Summer	N9	0.13	1.16	0.03	1.35

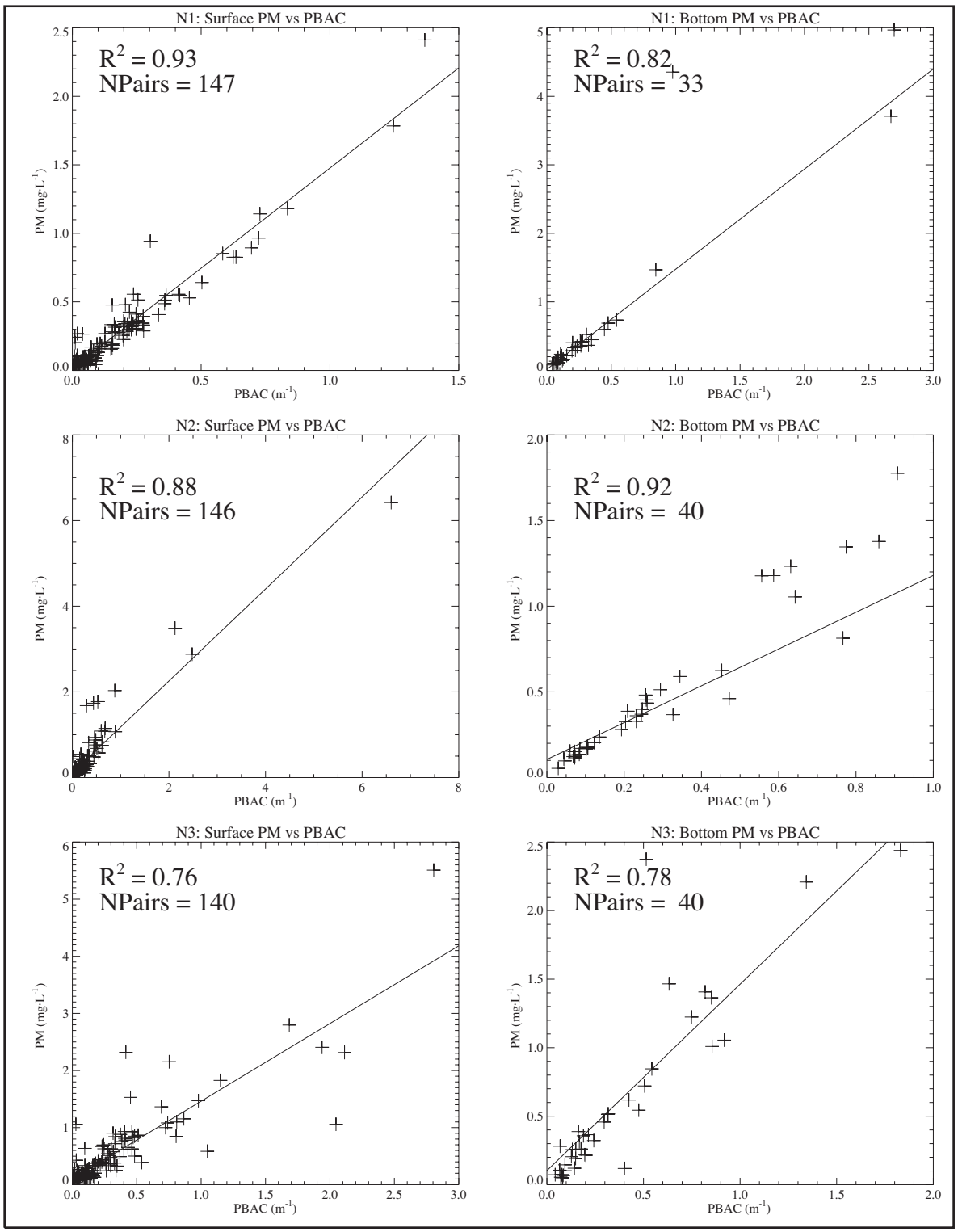

Figure 6.1-1. Linear correlations between PBAC and PM for the NEGOM region hydrographic cruises. Crosses represent the data points. Separate correlations were obtained for surface and bottom waters.

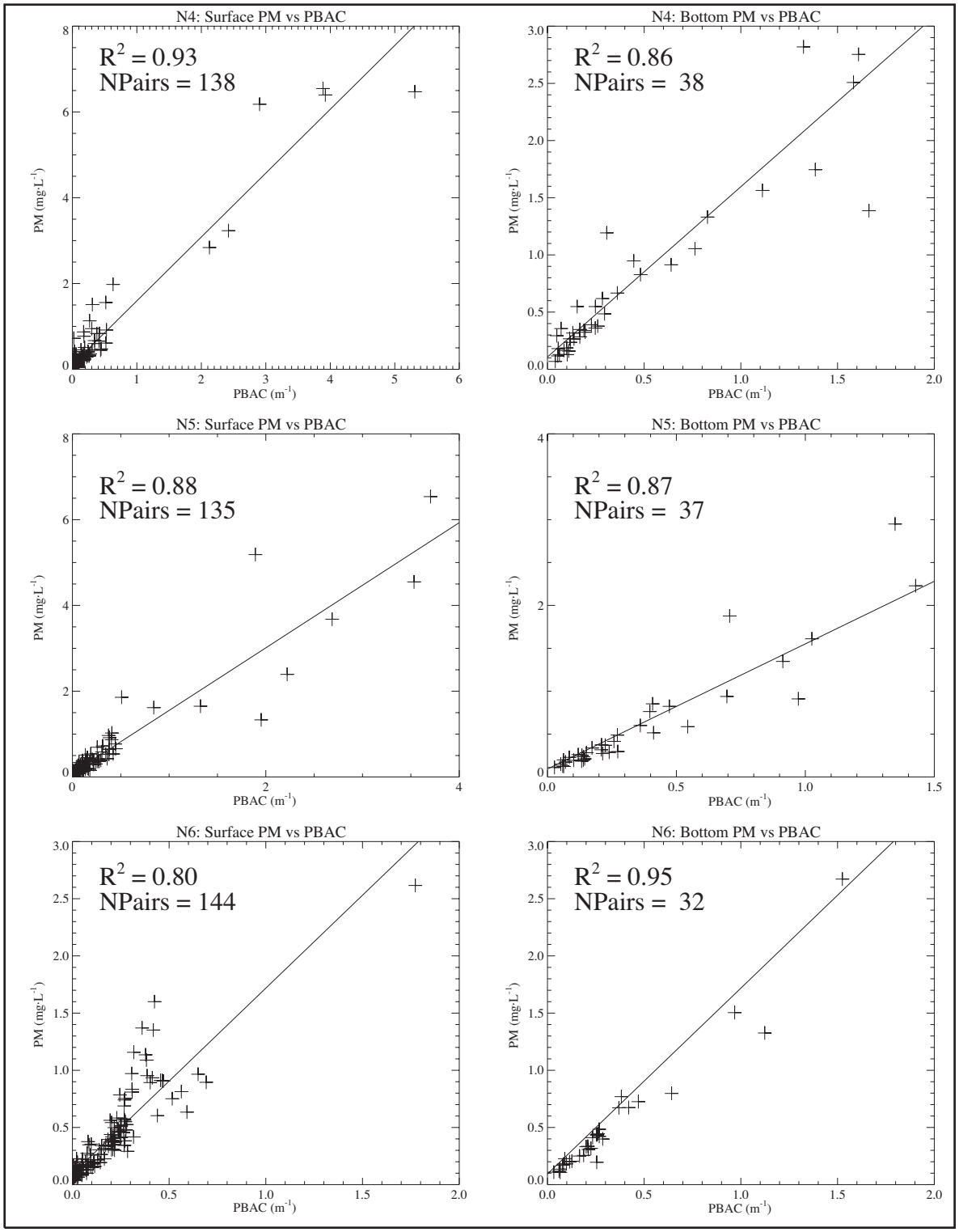

Figure 6.1-1. Linear correlations between PBAC and PM for the NEGOM region hydrographic cruises. (continued)

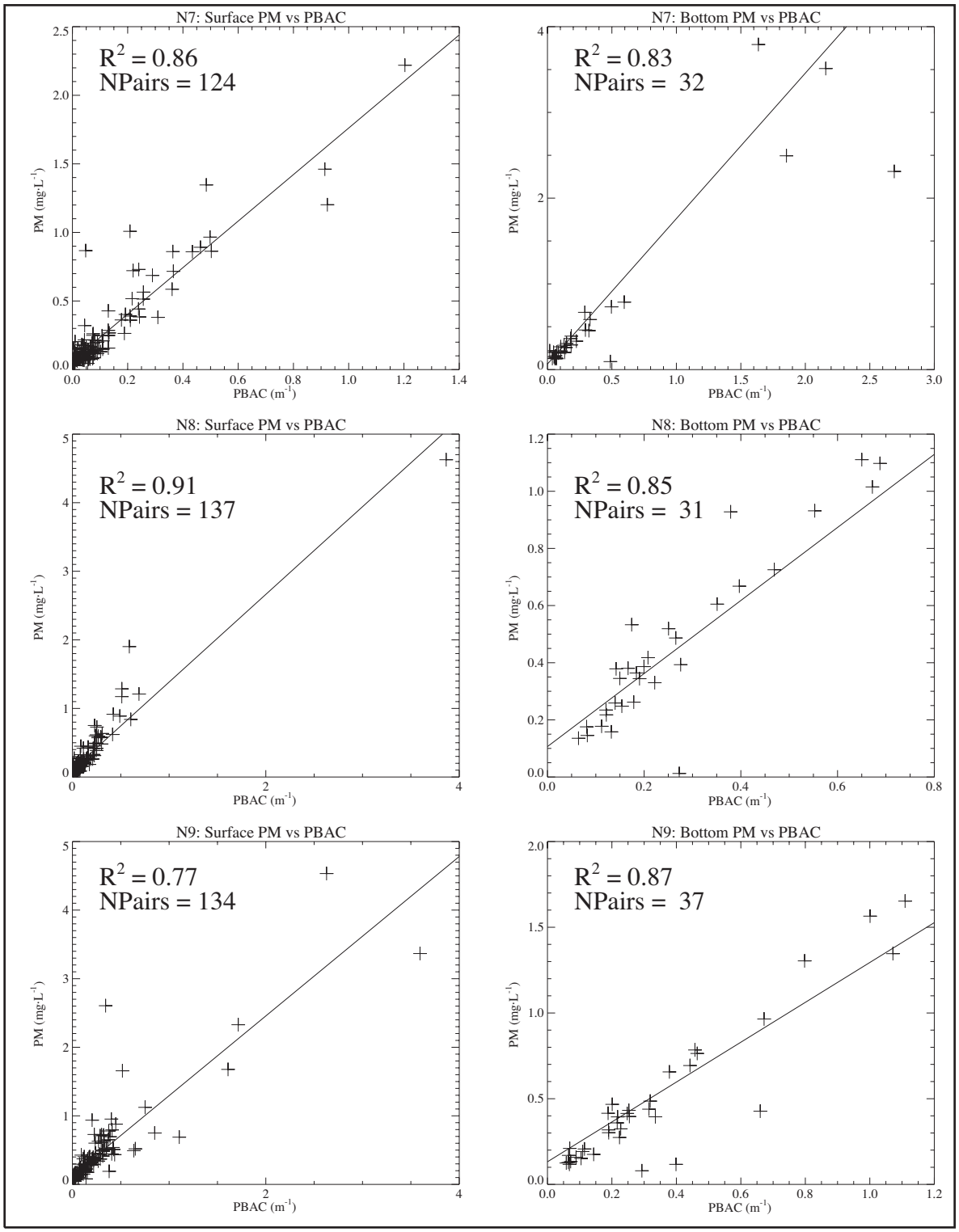

Figure 6.1-1 . Linear correlations between PBAC and PM for the NEGOM region hydrographic cruises. (continued)

presence of bottom nepheloid layers (BNLs). The bottom correlation was applied to water in the BNL, and the surface equation was applied to the rest of the water column. At stations where intermediate-depth nepheloid layers (INLs) were present above the BNL, the bottom equation was used for the waters within the INL if there was no water of surface optical properties separating the layers.

Figure 6.1-2 gives examples of nepheloid layers in the transmissometer data showing a surface layer strongly influenced by river discharge (upper panel; ~500-m water depth) and a BNL (lower panel; ~200-m water depth). For cases where profiles of transmissometry data indicated differences between upper and lower waters, the depth at which the optical properties changed was chosen to divide the water column. For cases with no obvious difference, the mid-depth was chosen for the division.

General vertical profiles of particulate matter: Rivers, most notably the Mississippi River, supply sediments to the NEGOM shelf that are suspended in low-density river plumes. The sediment in the river plume creates a surface nepheloid layer (Figure 6.1-2, upper panel). As particles settle out, they are deposited on the sea floor and later may be re-suspended and transported by the action of currents and waves. Particles traveling close to the sea floor while in resuspension create a turbid layer just above the bottom that is called a bottom nepheloid layer (Figure 6.1-2, lower panel).

6.2 Distributions of Particulate Matter

Distributions of particulate matter (PM) are discussed by cruise using three presentation types. First, the distribution of the surface (~3 m) particulate matter (PM) concentration is examined. For each station the PM concentration was calculated from the optical data using the surface equation; these data then were contoured and examined for patterns. Second, distributions of the total mass of PM in the water column are described. The total mass of PM was calculated at each station as the total mass under one square meter of sea surface. Third, distributions of the percent of the total PM mass in the water column that is contained in bottom nepheloid layer is examined. Note that the total mass is a function of the water depth; the total mass offshore of the 200-m isobath reflects this fact by the relatively large totals seen in the off-shelf region. Therefore, the discussion of the total mass and percent in BNL will focus on the results found over the continental shelf, where the potential influence of sediments carried in river plumes or re-suspended by currents and waves can be more clearly identified. Descriptions of the PM distributions are given by cruise in the three seasonal groups: fall, spring, and summer.

Fall Cruise N1 (16 November 1997 – 26 November 1997): Cruise N1 was the first fall cruise. Low surface salinities (< 32), indicative of possible river plumes, were confined to the regions immediately adjacent to the Mississippi River at Pass a Loutre and Mobile Bay (Figure A.1.2-1). Surface particulate matter concentrations were highest ($\geq$ 1 mg·L^{-1}) near the coast in three regions associated with river discharges: off the mouths of the Mississippi River and Mobile Bay in the west, off the Apalachicola River near Cape San Blas, and south of the Suwannee River in the east (Figure 6.2-1). Offshore of approximately the 50-m isobath surface concentrations were low, being generally $\leq$ 0.2 mg·L^{-1}. Total mass of PM over the shelf generally was low (< 25 g·m^{-2}), except immediately adjacent to the Mississippi River, where values in excess of 50 g·m^{-2} were present. Over much of the inner shelf ($\leq$ 50-m water depths), 50% or more of the total mass was contained in the bottom nepheloid layer, even immediately adjacent to the Mississippi River.

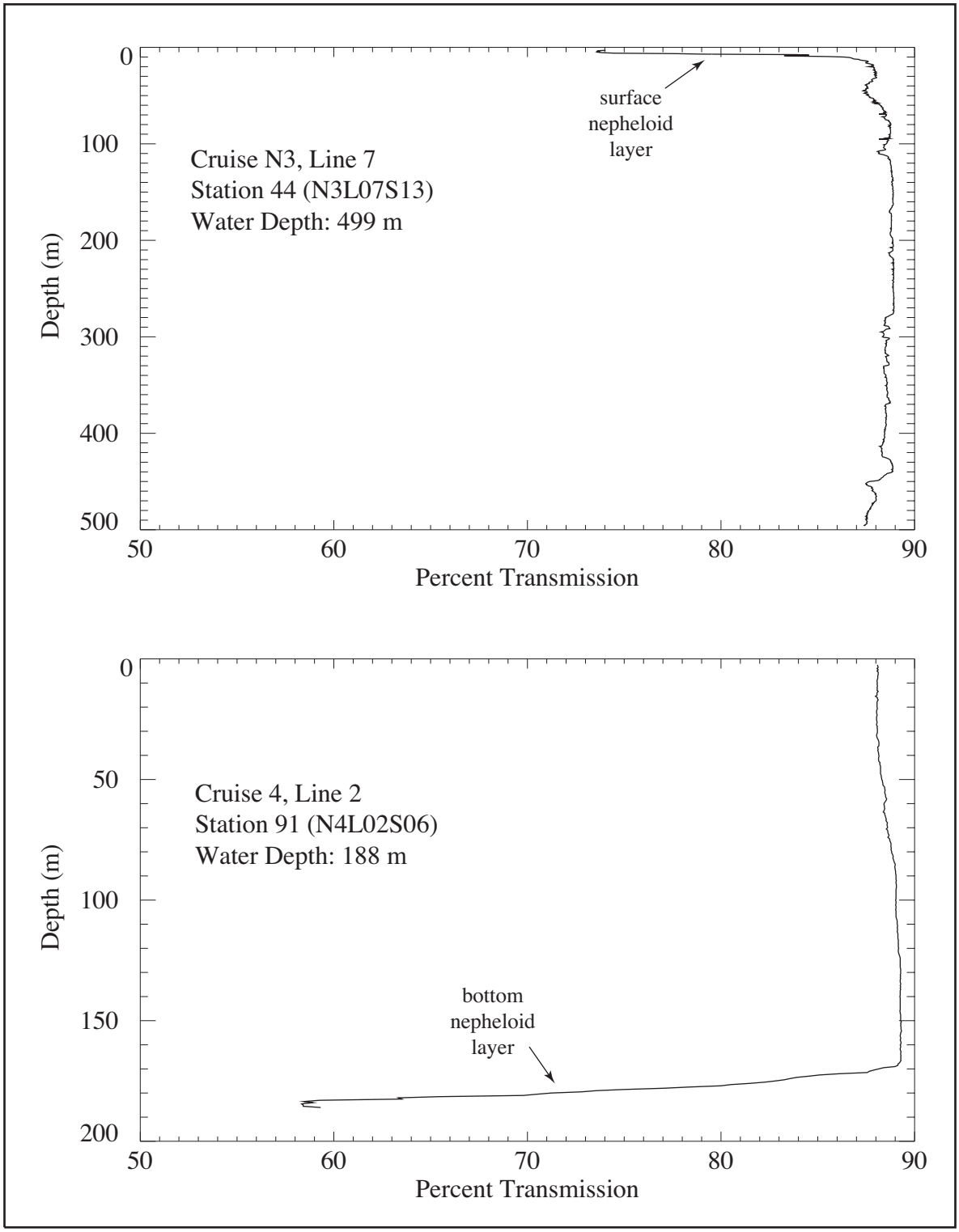

Figure 6.1-2. Depth profile of percent transmission for (upper panel) station N3L07S13 showing surface nepheloid layer and (lower panel) station N4L02S06 showing bottom nepheloid layer (BNL).

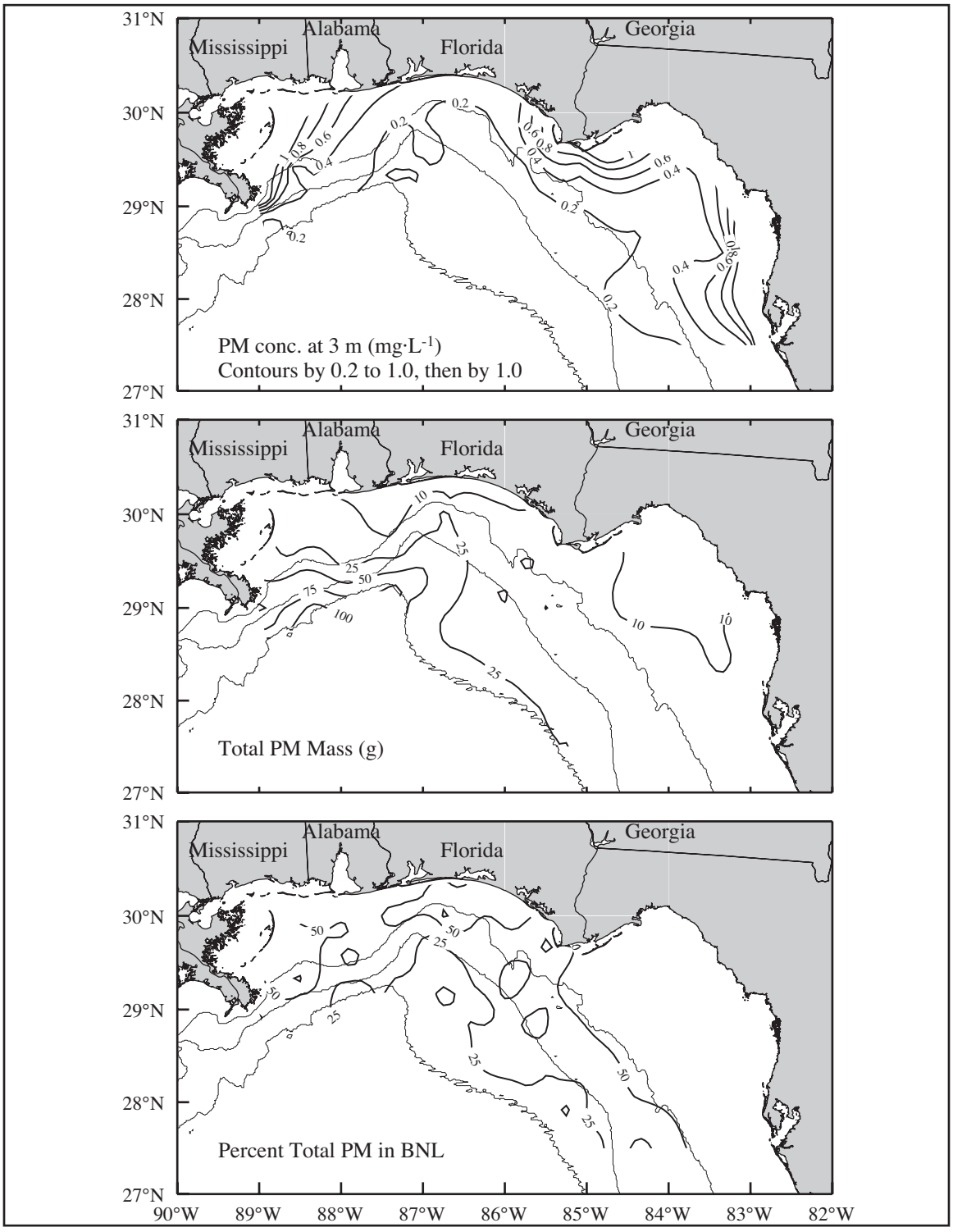

Figure 6.2-1. PM distribution for cruise N1 in November 1997. (Upper) Near-surface (3 m) concentration (mg·L^{-1}). (Middle) Total mass of PM under one square meter of sea surface (g). (Lower) Percent of total PM mass located in BNL. Bathymetric contours shown are 50, 200, and 1000 m.

Fall Cruise N4 (13 November 1998 – 24 November 1998): The second fall cruise, N4, was conducted at a time when surface salinities of less than 32 were located only west of 88.5°W. There was a definite plume from the Mississippi River, with salinities lower than 25 occurring immediately adjacent to Pass a Loutre (Figure D.1.2-1). Near-surface PM concentrations exceeded 5 $mg \cdot L^{-1}$ in this plume, and concentrations greater than 1 $mg \cdot L^{-1}$ extended along the inner shelf from this plume to just east of Mobile Bay (Figure 6.2-2). Elevated concentrations ($\geq$ 0.6 $mg \cdot L^{-1}$) occurred nearshore all along the Mississippi-Alabama shelf to off the mouth of the Apalachicola River east of Cape San Blas. High total PM values of 50 $g \cdot m^{-2}$ or more were associated with the Mississippi River plume and extended inshore to Mobile Bay. Elsewhere over the inner shelf, the total mass was < 25 $g \cdot m^{-2}$, with lowest values over the west Florida shelf. There were substantial regions over the inner shelf, even in the plume, in which resuspension of particulates near bottom was important, as indicated by those regions where 50% or more of the total mass was in bottom nepheloid layers.

Fall Cruise N7 (13 November 1999 – 25 November 1999): Near-surface salinities were higher on the third fall cruise, N7, than the other fall cruises. Lowest salinities were located in close proximity to the Mississippi River mouth, with the innermost observation on line 1 having a salinity of ~31 (Figure G.1.2-1). Low salinities of ~32 also were present south of Mobile Bay. Salinities elsewhere generally were higher and were over 34. Highest near-surface PM concentrations were in the region just east of the Mississippi River, reaching 5 $mg \cdot L^{-1}$ off the Pass a Loutre mouth of the Mississippi River (Figure 6.2-3). Elevated concentrations of more than 0.6 $mg \cdot L^{-1}$ extended eastward and inshore from the Mississippi River mouth to just east of Mobile Bay. There also were elevated near-surface PM concentrations in the nearshore region off Cape San Blas. The outer shelf had generally low near-surface PM concentrations of < 0.2 $mg \cdot L^{-1}$. Associated with the high near-surface PM concentrations on the shelf off the mouth of the Mississippi was a high total PM mass of > 50 $g \cdot m^{-2}$. The region of the high mass did not extend to Mobile Bay. It was a region where the percent of mass in the BNL was < 50%, suggesting surface transport of particles was important in this region. Elsewhere over the inner shelf the BNL contained 50% or more of the total mass.

Spring Cruise N2 (5 May 1998 – 16 May 1998): Cruise N2 was the first of the three spring cruises. It was conducted at a time when low-salinity surface water was widespread over the study area (Figure B.1.2-1). Waters with salinity < 32 covered most of the shelf from the Mississippi River to Cape San Blas and also inshore of the 20-m isobath on the west Florida shelf. High near-surface PM concentrations, exceeding 1 $mg \cdot L^{-1}$, were located from the mouth of the Mississippi River eastward and inshore to ~87°W, offshore of Pensacola Bay (Figure 6.2-4). Concentrations of $\geq$ 5 $mg \cdot L^{-1}$ occurred immediately off the mouth of the Mississippi. Elevated concentrations of $\geq$ 0.6 $mg \cdot L^{-1}$ also were located along the nearshore east of 87°W to ~83.5°W. Unlike the fall season, the concentrations over the outer shelf generally exceeded 0.2 $mg \cdot L^{-1}$. In the shelf region with high near-surface PM concentration, the total PM mass exceeded 25 $g \cdot m^{-2}$, but was less elsewhere over most of the rest of the shelf. In spite of the widespread low-salinity water, the total PM mass on the shelf was not high, except immediately adjacent to the discharge point of the river, where the mass was ~50 $g \cdot m^{-2}$. Fifty percent or more of the mass over most of the inner shelf was in the BNL, even in the region associated with the elevated near-surface concentrations.

Spring Cruise N5 (15 May 1999 – 28 May 1999): The second spring cruise was N5. During this cruise, low-salinity surface water extended over the entire shelf from the Mississippi River to offshore of Choctawhatchee Bay (Figure E.1.2-1). There was no low-salinity surface water over the west Florida shelf. Near-surface waters with high PM concentrations, exceeding 1 $mg \cdot L^{-1}$, were located over the shelf and slope from the mouth of

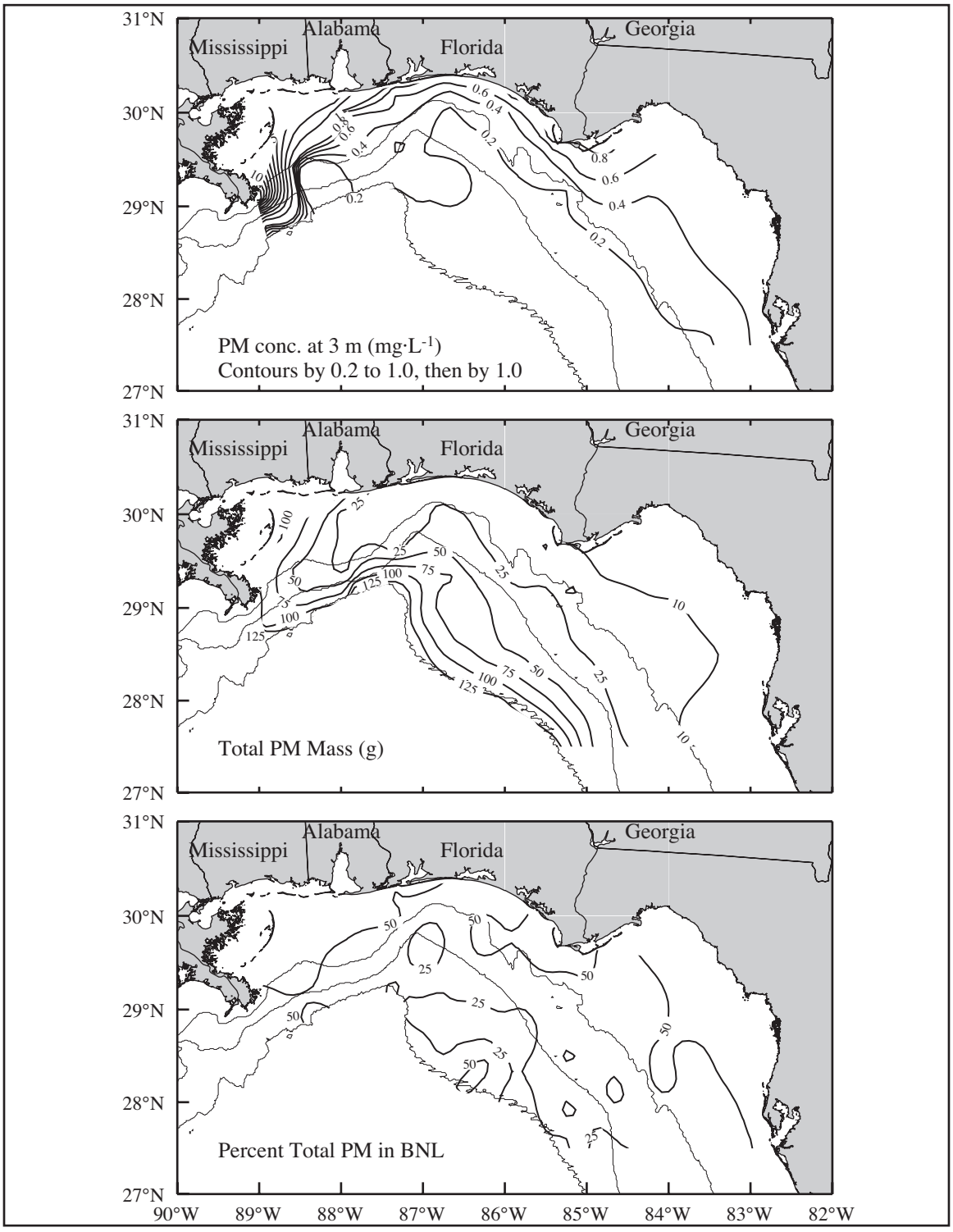

Figure 6.2-2. PM distribution for cruise N4 in November 1998. (Upper) Near-surface (3 m) concentration (mg·L^{-1}). (Middle) Total mass of PM under one square meter of sea surface (g). (Lower) Percent of total PM mass located in BNL. Bathymetric contours shown are 50, 200, and 1000 m.

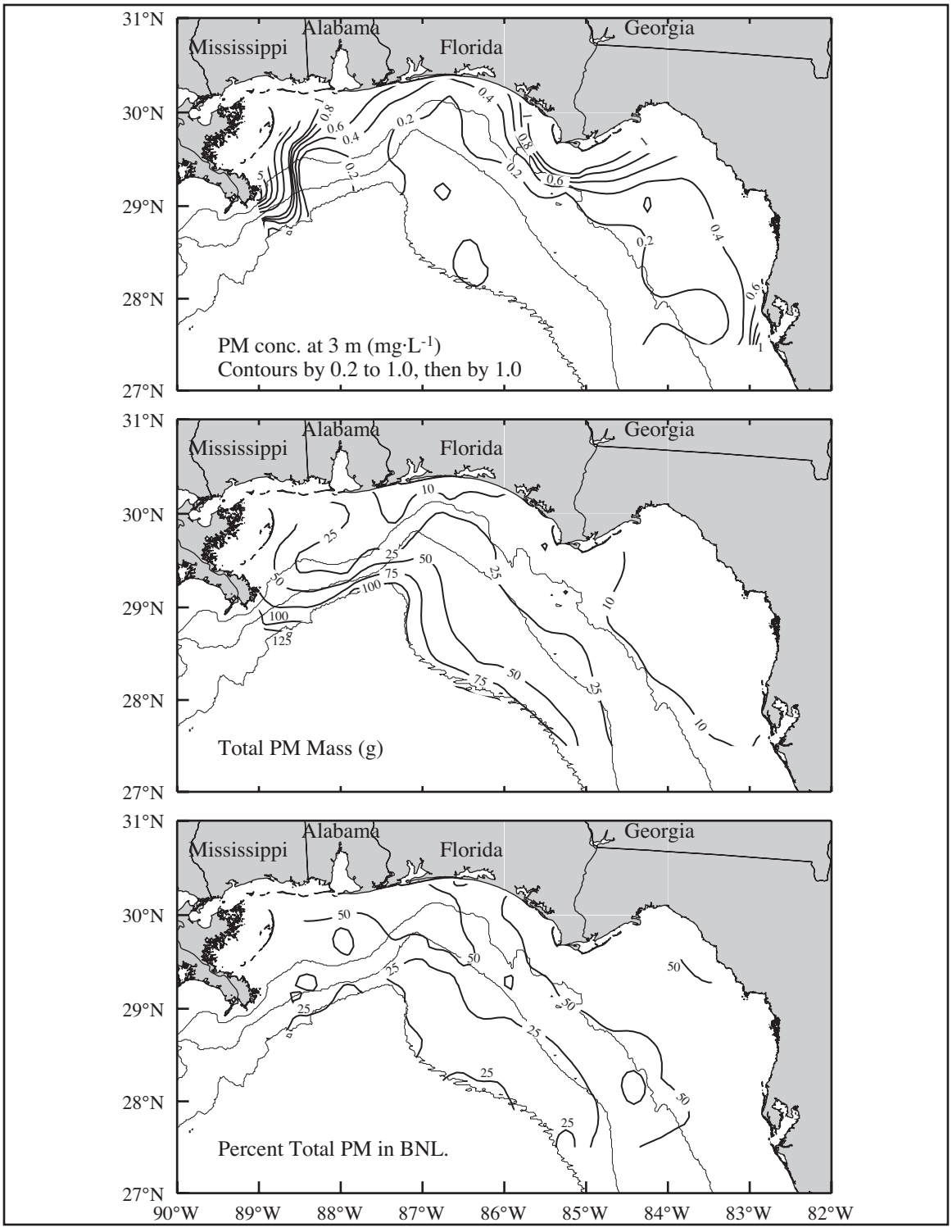

Figure 6.2-3. PM distribution for cruise N7 in November 1999. (Upper) Near-surface (3 m) concentration (mg·L^{-1}). (Middle) Total mass of PM under one square meter of sea surface (g). (Lower) Percent of total PM mass located in BNL. Bathymetric contours shown are 50, 200, and 1000 m.

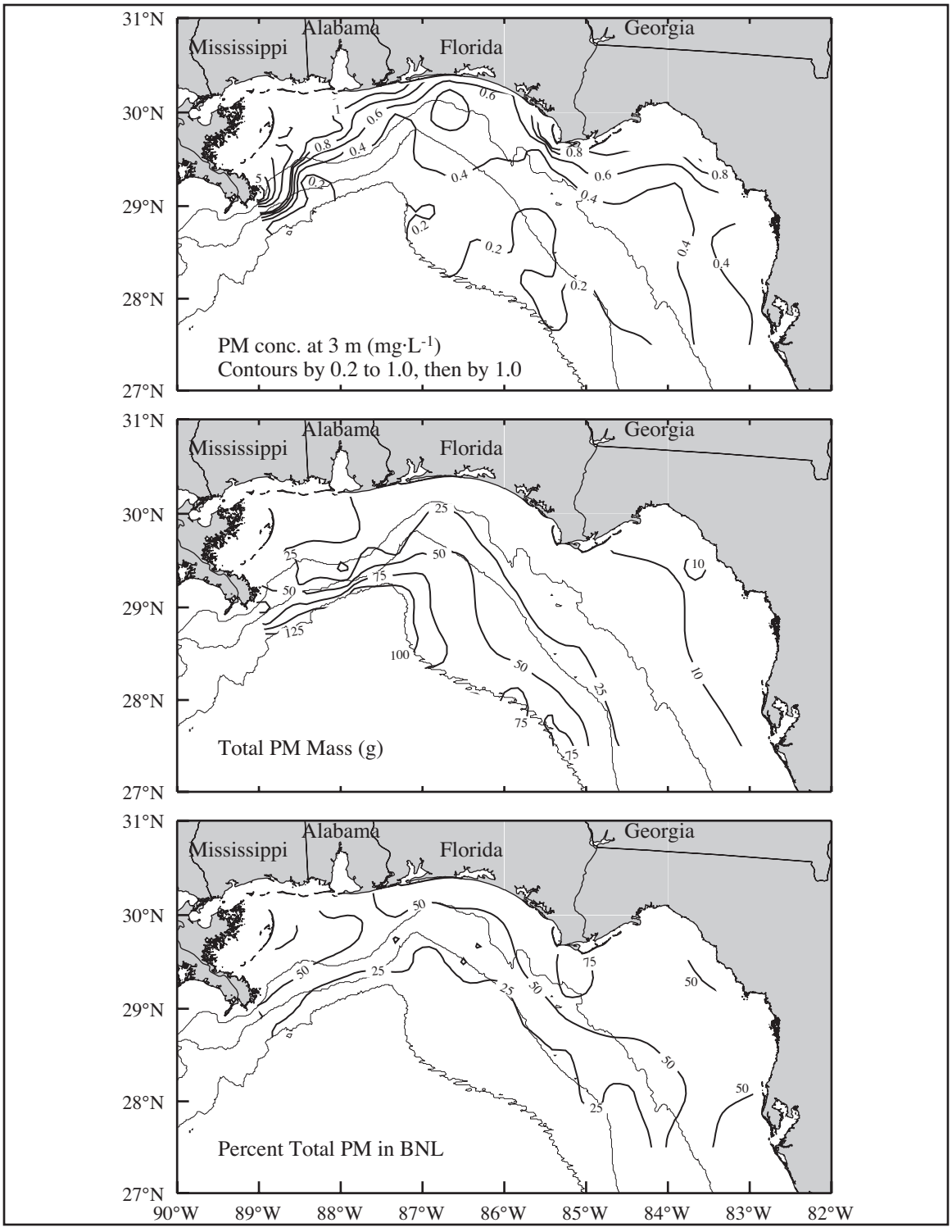

Figure 6.2-4. PM distribution for cruise N2 in May 1998. (Upper) Near-surface (3 m) concentration (mg·L^{-1}). (Middle) Total mass of PM under one square meter of sea surface (g). (Lower) Percent of total PM mass located in BNL. Bathymetric contours shown are 50, 200, and 1000 m.

the Mississippi River to ~88°W offshore of Mobile Bay (Figure 6.2-5). As with cruise N2, most of the remainder of the shelf had PM concentrations that exceeded 0.2 $mg \cdot L^{-1}$. Total PM mass over the shelf was generally < 50 $g \cdot m^{-2}$, and over the nearshore of the Florida shelf, the mass was < 10 $g \cdot m^{-2}$. The mass in the BNL exceeded 50% on the inner shelf between the Mississippi River and Mobile Bay and from Cape San Blas to off Tampa Bay.

Spring Cruise N8 (15 April 2000 – 26 April 2000): N8 was the third and final spring cruise. It was conducted earlier in the season than the two previous spring cruises, and consequently, there was much less low-salinity surface water present over the shelf (Figure H.1.2-1). Only off Mobile Bay was the surface salinity < 32. There were two areas with high near-surface PM concentrations. One was off the Mississippi River, and the other was offshore of Mobile Bay (Figure 6.2-6). PM concentrations over the remainder of the inner shelf generally were more than 0.2 $mg \cdot L^{-1}$ but less than 1 $mg \cdot L^{-1}$. Unlike the other spring cruises, however, most of the outer shelf had PM concentrations of < 0.2 $mg \cdot L^{-1}$; this was similar to the pattern on the fall cruises. Total mass was < 25 $g \cdot m^{-2}$ over the inner shelf except in the nearshore off Mobile Bay where the lowest salinities were seen. Over the inner shelf and part of the outer shelf, the mass in the BNL was 50% or more of the total mass in the water column.

Summer Cruise N3 (25 July 1998 – 6 August 1998): The first summer cruise was N3. During this summer cruise, there were two regions with low-salinity surface water: over the shelf from Mobile Bay west and over the outer shelf and slope from the apex of DeSoto Canyon southeast to the boundary of the study area (Figure C.1.2-1). In the region with this low-salinity water, the near-surface PM concentrations exceeded 0.6 $mg \cdot L^{-1}$ (Figure 6.2-7). In addition to the nearshore off the Mississippi River, Mobile Bay, and the Suwannee River mouths, there was a broad area over the slope southwest of Cape San Blas where the concentrations exceeded 1 $mg \cdot L^{-1}$. The chlorophyll concentrations in this slope region also were relatively high (Figure C.1.2-3), suggesting that most of the particles were biological in nature, as opposed to being associated with sediment discharged from a river. In contrast to the fall and spring cruises, PM concentrations were greater than 0.2 $mg \cdot L^{-1}$ everywhere in the study area. Over the shelf, the total PM mass in the water column under a square meter of the sea surface exceeded 50 $g \cdot m^{-2}$ only off the mouth of the Mississippi River. The total mass over the eastern inner shelf generally was less than that in comparable water depths over the western inner shelf. The BNL constituted over 50% of the total mass nearshore from the Mississippi River to Tampa Bay.

Summer Cruise N6 (15 August 1999 – 28 August 1999): The second summer cruise, N6, was conducted during a time when the low-salinity surface water (< 32) extended over the outer shelf and slope of most of the study area (Figure F.1.2-1). In only a small area over the slope southwest of Cape San Blas were there salinities > 32 on the outer shelf and slope. Inshore, salinities were higher than offshore. Near-surface PM concentrations were elevated (≥ 0.6 $mg \cdot L^{-1}$) over the Mississippi-Alabama shelf and over the slope of the western side of DeSoto Canyon (Figure 6.2-8). The chlorophyll concentrations in this region (not shown) were relatively high, suggesting that many of the particles were biological in nature. The concentrations in the nearshore off and north of Tampa Bay also were elevated. As with cruise N3, PM concentrations were greater than 0.2 $mg \cdot L^{-1}$ everywhere in the study area. Associated with the small area, with the relatively high salinities, over the slope southwest of Cape San Blas were near-surface PM concentrations that were relatively low compared to those in adjacent waters. Total PM mass was generally less than 50 $g \cdot m^{-2}$ over the shelf, with the mass over the eastern inner shelf being less than that of the western inner shelf at comparable water depths. BNLs carried the majority of the mass in the region off the Mississippi River and in the nearshore north of Tampa Bay.

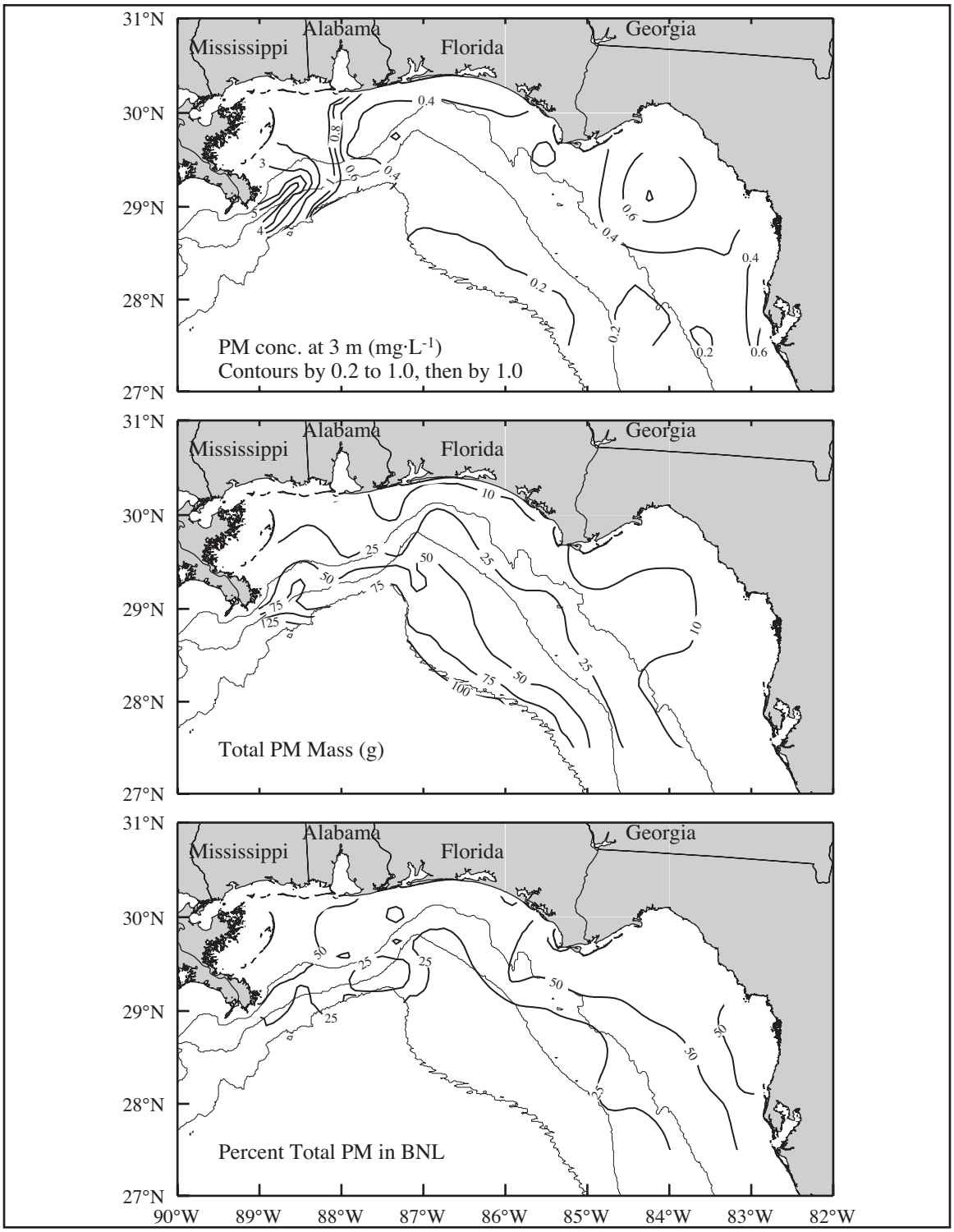

Figure 6.2-5. PM distribution for cruise N5 in May 1999. (Upper) Near-surface (3 m) concentration (mg·L^{-1}). (Middle) Total mass of PM under one square meter of sea surface (g). (Lower) Percent of total PM mass located in BNL. Bathymetric contours shown are 50, 200, and 1000 m.

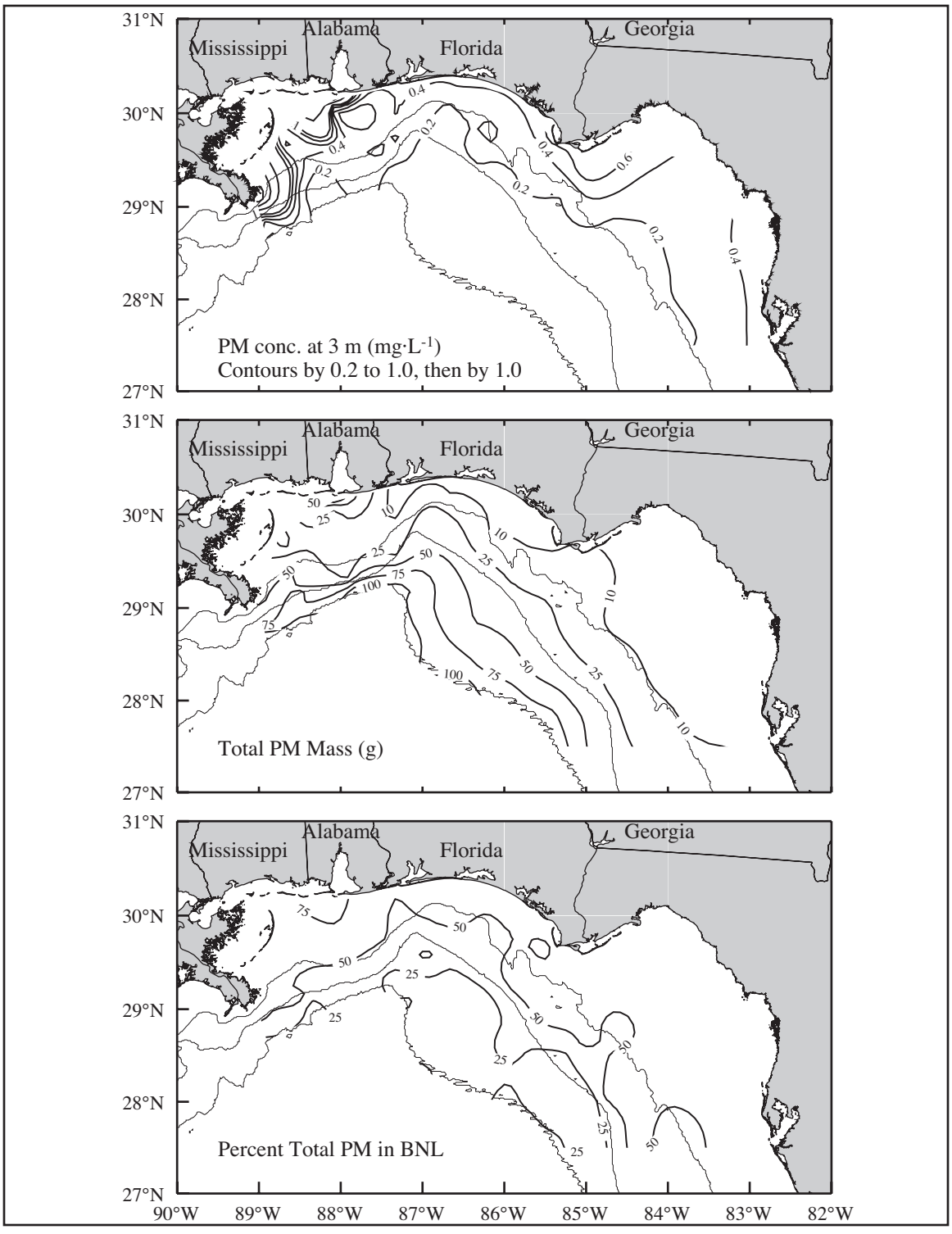

Figure 6.2-6. PM distribution for cruise N8 in April 2000. (Upper) Near-surface (3 m) concentration (mg·L^{-1}). (Middle) Total mass of PM under one square meter of sea surface (g). (Lower) Percent of total PM mass located in BNL. Bathymetric contours shown are 50, 200, and 1000 m.

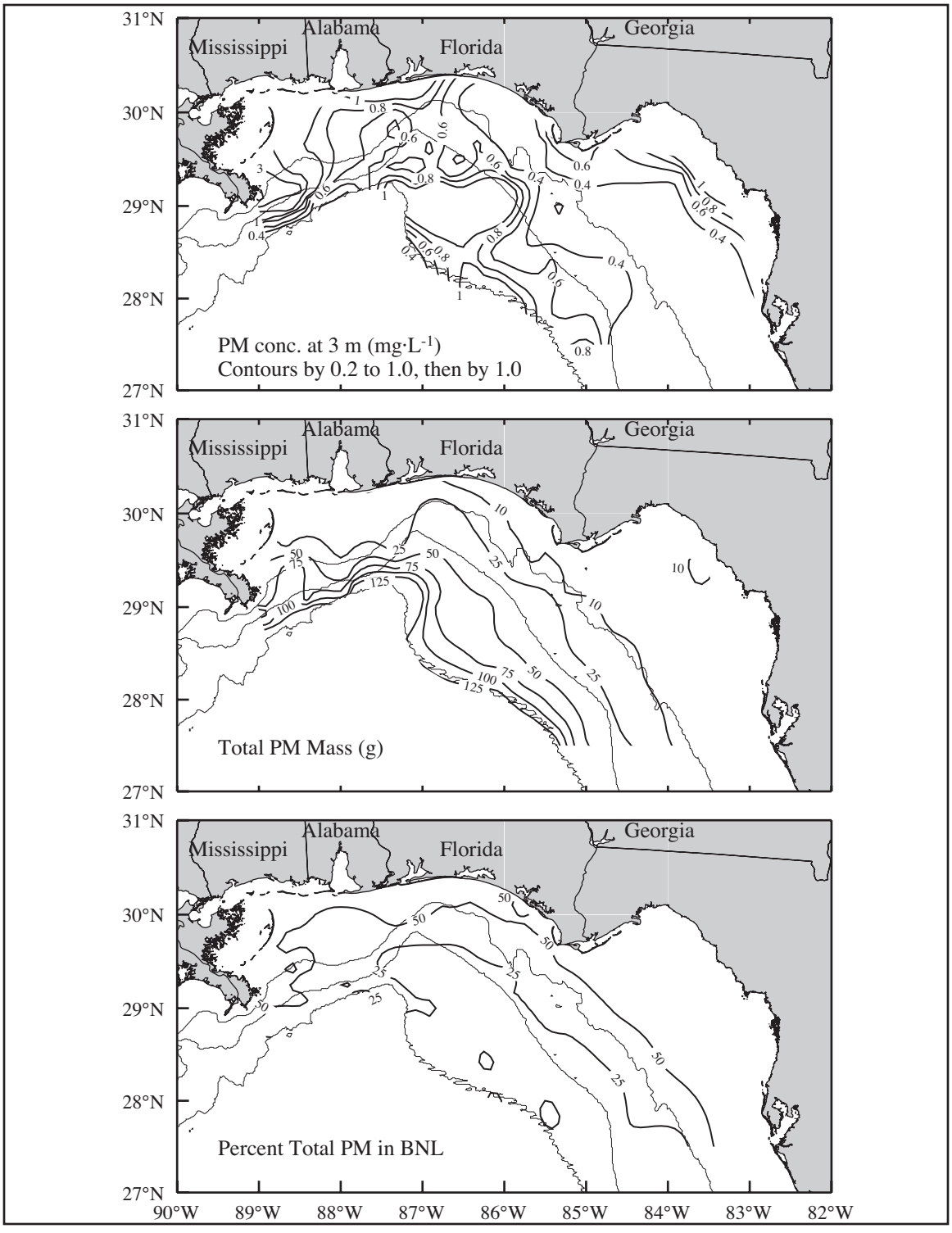

Figure 6.2-7. PM distribution for cruise N3 in July/August 1998. (Upper) Near-surface (3 m) concentration (mg·L^{-1}). (Middle) Total mass of PM under one square meter of sea surface (g). (Lower) Percent of total PM mass located in BNL. Bathymetric contours shown are 50, 200, and 1000 m.

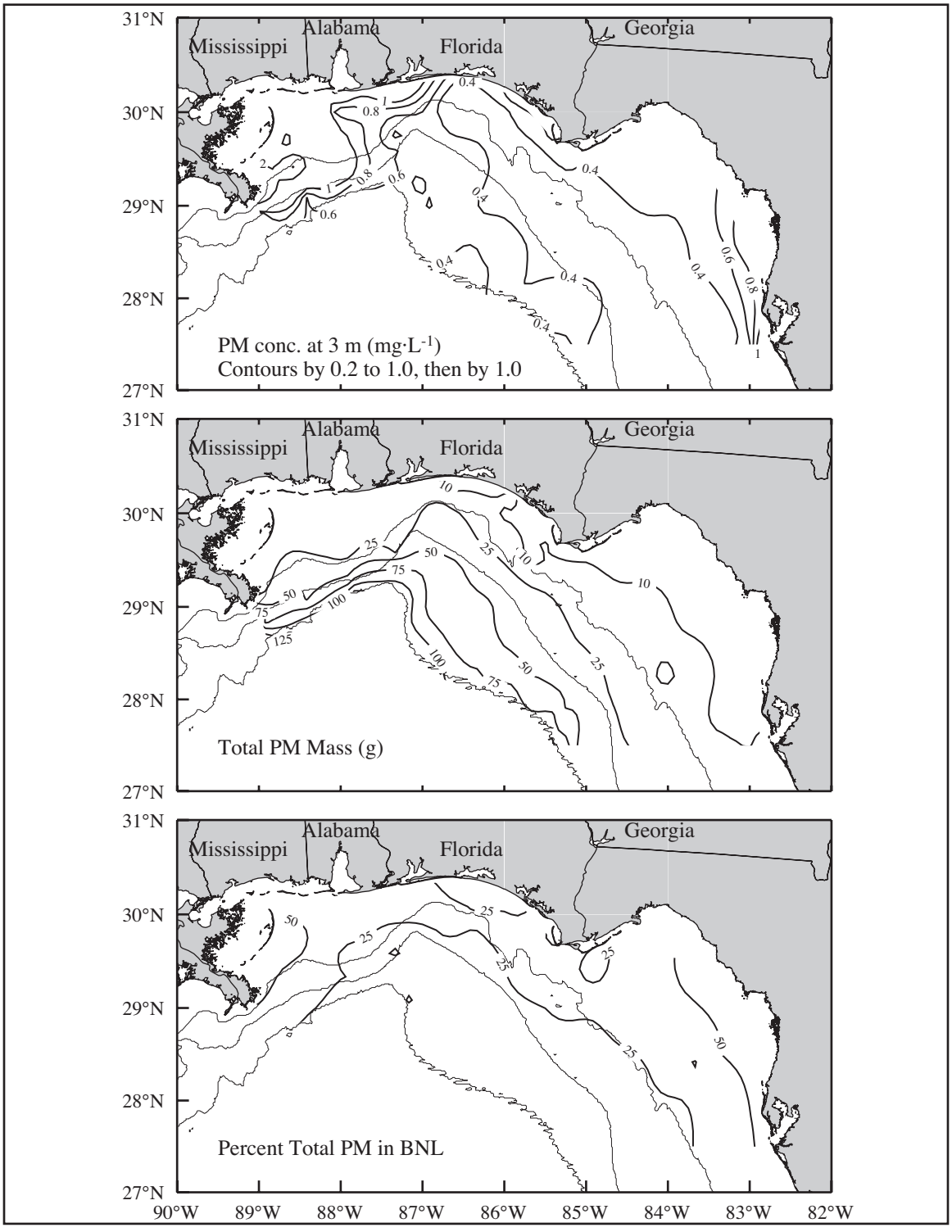

Figure 6.2-8. PM distribution for cruise N6 in August 1999. (Upper) Near-surface (3 m) concentration (mg·L^{-1}). (Middle) Total mass of PM under one square meter of sea surface (g). (Lower) Percent of total PM mass located in BNL. Bathymetric contours shown are 50, 200, and 1000 m.

Summer Cruise N9 (28 July 2000 – 8 August 2000): N9 was the third summer cruise. Low-salinity water (< 32) was present on the outer shelf and slope from the Mississippi River to southwest of Cape San Blas (Figure I.1.2-1). Inner shelf waters were more saline. Associated with the low-salinity waters were near-surface PM concentrations that were 0.6 $mg \cdot L^{-1}$ or more (Figure 6.2-9). Highest values were in the waters extending over the outer shelf and slope eastward from the Mississippi River to ~87.5°W. The chlorophyll concentrations in this region were relatively high (Figure I.1.2-2), again suggesting that many of the particles were biological in origin. There were elevated concentrations south of the Suwannee River mouth to just north of Tampa Bay. Total PM mass values were relatively low ($\leq$ 10 $g \cdot m^{-2}$) over much of the inner shelf except that part of the inner shelf offshore and west of Mobile Bay. Highest total PM mass over the shelf was located east of the Mississippi River, with values exceeding 50 $g \cdot m^{-2}$. Much of the mass over the inner shelf was contained in BNLs, even in the region of highest near-surface PM concentrations.

Summary of Seasonal Particulate Distributions: Near-surface particulate concentrations were highly and negatively correlated with low salinity values associated with discharges of fresh water from rivers, bays, and estuaries (see Section 10). This was reflected in the patterns of particulate distributions. In all seasons, high near-surface particulate concentrations ($\geq$ 1 $mg \cdot L^{-1}$) over the shelf (water depths of 200 m or less) were located adjacent to the Mississippi River. This is consistent with the high terrestrial sediment discharge associated with that river. The region of high concentration generally extended northeast to Mobile Bay. High concentrations also were located adjacent to the discharge sources for other rivers, bays, and estuaries; however, these did not occur consistently in a season off any particular discharge source, likely reflecting the influence of the interannual variability of localized river discharge on the particulate concentrations adjacent to such discharge sources. Low concentrations ($\leq$ 0.2 $mg \cdot L^{-1}$) over the shelf were most extensive in fall and were located mainly over the west Florida shelf. The N8 cruise in April 2000 exhibited distributions similar to those of fall, most likely because the cruise was conducted before the peak spring river runoff occurred. Away from the mouths of the rivers, bays, and estuaries, concentrations over the shelf in summer were generally higher than those in spring.

In all three seasons sampled, high concentrations ($\geq$ 1 $mg \cdot L^{-1}$) over the slope (water depths of > 200 m) could occur adjacent to the Mississippi River. This varied between years in fall and spring. However, only in summer was the pattern consistent between years, with high concentrations located off-shelf of the Mississippi River and over the slope to the southeast. Further, the region of high concentration over the slope was more extensive in summer than fall or spring and occurred even off the west Florida shelf. The summer off-shelf pattern generally reflected the pattern of high chlorophyll concentrations, suggesting particulate concentrations in these regions were related to biological productivity. The summer concentrations over the slope were related to the presence of anticyclonic/cyclonic circulation features that transported the Mississippi River water and associated increased phytoplankton abundances southeastward along the shelf edge.

The percent of the total particulate mass of the water column that was contained in the bottom nepheloid layer was lowest off the shelf (> 200 m) regardless of season. The percent was highest, often exceeding 50%, over the inner shelf (approximately $\leq$ 50 m water depth). This was particularly true of the west Florida shelf in all three seasons sampled. Over the western part of the study area, the extent of the region where the bottom nepheloid layer contained 50% or more of the total particulate mass was variable in all seasons, likely reflecting the variability of river discharge which could increase the near-surface contribution to the total particulate mass, thus reducing the percent that was in the bottom nepheloid layer.

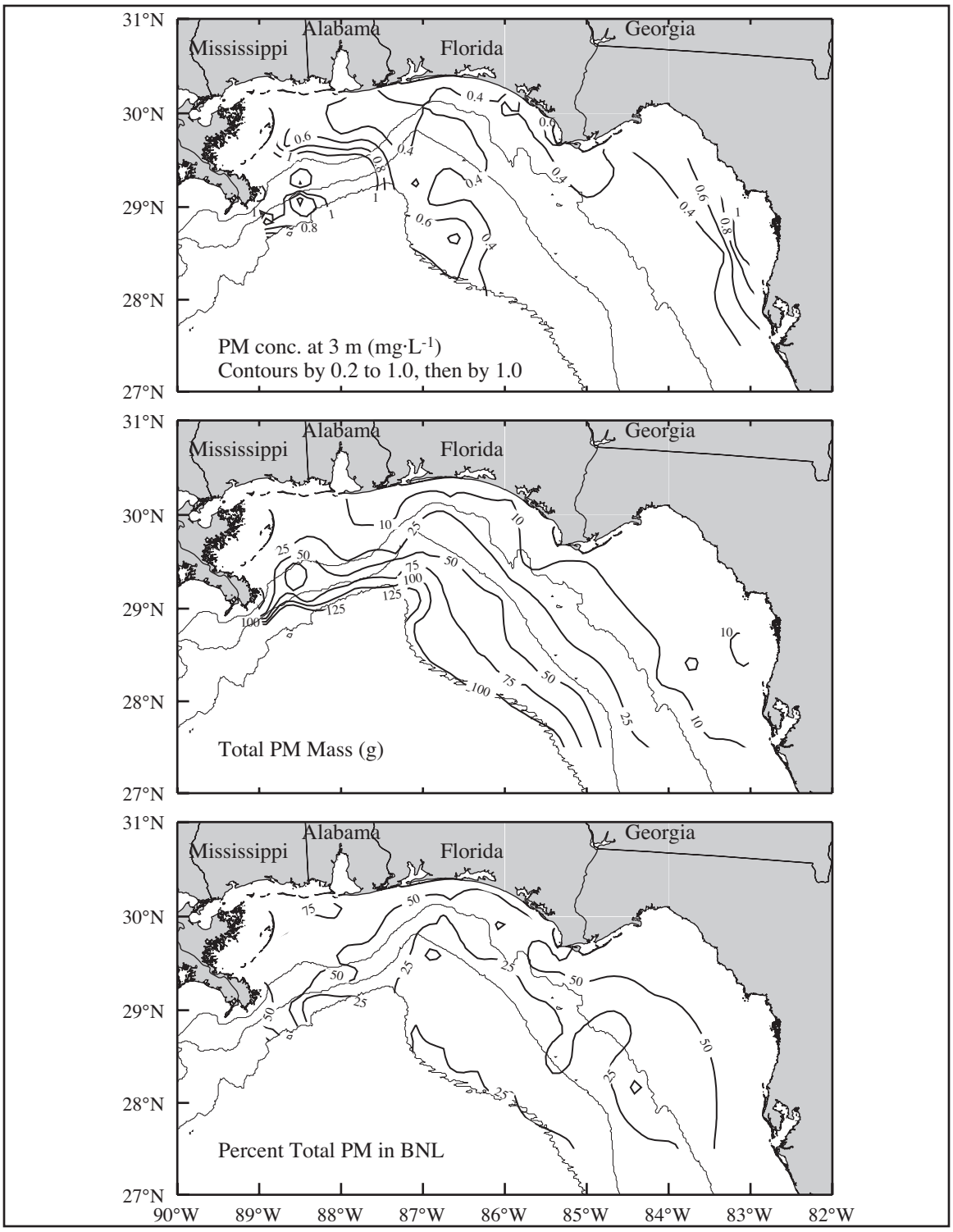

Figure 6.2-9. PM distribution for cruise N9 in July/August 2000. (Upper) Near-surface (3 m) concentration (mg·L^{-1}). (Middle) Total mass of PM under one square meter of sea surface (g). (Lower) Percent of total PM mass located in BNL. Bathymetric contours shown are 50, 200, and 1000 m.

Basic statistics: The average water column PM mass under a square meter of sea surface is shown in Figure 6.2-10 for each cruise by east and west shelf, using 87°W as the division. Note that these averages do not include data offshore of the 200-m water depth. Over the eastern shelf (represented by pluses), the average has little variability between cruises, ranging from 14 to 19 g. Cruise N1 has the lowest average over the eastern shelf. The averages for all cruises are higher over the western shelf (represented by triangles) than over the eastern by 10 g or more. There is significant variability between cruises, but there is no clear seasonal pattern to the highest or lowest values. Cruise N4 had the highest value of any cruise. This cruise had the highest near-surface particulate concentrations off the Mississippi River and extending inshore toward the Mississippi Sound. The associated total PM mass in this region also was higher than on other cruises. Examination of the near-surface salinity on cruise N4 (Figure D.1.2-1) shows relatively low salinity water (< 30) in a strong gradient in the region of the high particulates. This suggests that the Mississippi River plume was present in this region, resulting in the high particulate mass over the western shelf.

Similarly, the mean PM mass under a square meter of sea surface for the BNLs over the shelf (Figure 6.2-11) is lower and less variable between cruises over the eastern shelf (pluses) than over the western shelf (triangles). Fall values over the eastern shelf are relatively constant near ~7 g, and, ranging from 5 to 8 g, spring values are slightly more variable than the other seasons. Summer values are less than those of the preceding or following season. Over the western shelf, the mean PM mass in the BNL is variable between cruises and even between cruises within the same season. Comparing the average PM in the BNL from the western half of the NEGOM shelf (Figure 6.2-11) with that from the eastern half of the LATEX shelf (see Figure 5.1-17 in Nowlin et al. 1998) suggests the values on the western NEGOM shelf are higher in summer, comparable in fall, and slightly lower and less variable in spring.

Basic statistics for the particulate matter observations from near-surface and near-bottom water samples are given in Table 6.2-1. On average the fall season had lower mean near-surface PM concentrations. The spring season had more variability as suggested by the larger standard deviation and the wider range of near-surface PM concentrations. Near-bottom means were similar for the three seasons. The lowest standard deviation and the smallest range for the near-bottom observations were in the summer season, suggesting near-bottom particulate concentrations were less variable in summer than fall or spring. Statistical relationships between particulates and other parameters, such as salinity, chlorophyll, nutrients, and oxygen, are presented in Section 10.

6.3 Distributions of Particulate Organic Carbon and Nitrogen

Particulate matter can be organic or inorganic in origin and living or dead. As a first indication of the origins of PM, the particulate organic carbon (POC) content was measured near-surface on all cruises. On cruises N1 through N6, it was measured also in near-bottom waters. Because POC values near the bottom had little or no correlation with the near-bottom PM concentrations, POC was measured at the chlorophyll maximum, rather than near bottom, on cruises N7 through N9.

The general pattern of both near-surface and subsurface POC concentration is of decreasing concentration with increasing distance offshore, which coincides with increasing water depth. Static measurement of POC concentrations reflects the end result of a dynamic process between *in situ* production of particles, advective horizontal transport of particles either from river discharges or shallow resuspension events, and consumption due to *in situ* microbial reworking. The observed decreases are probably a result of several factors acting

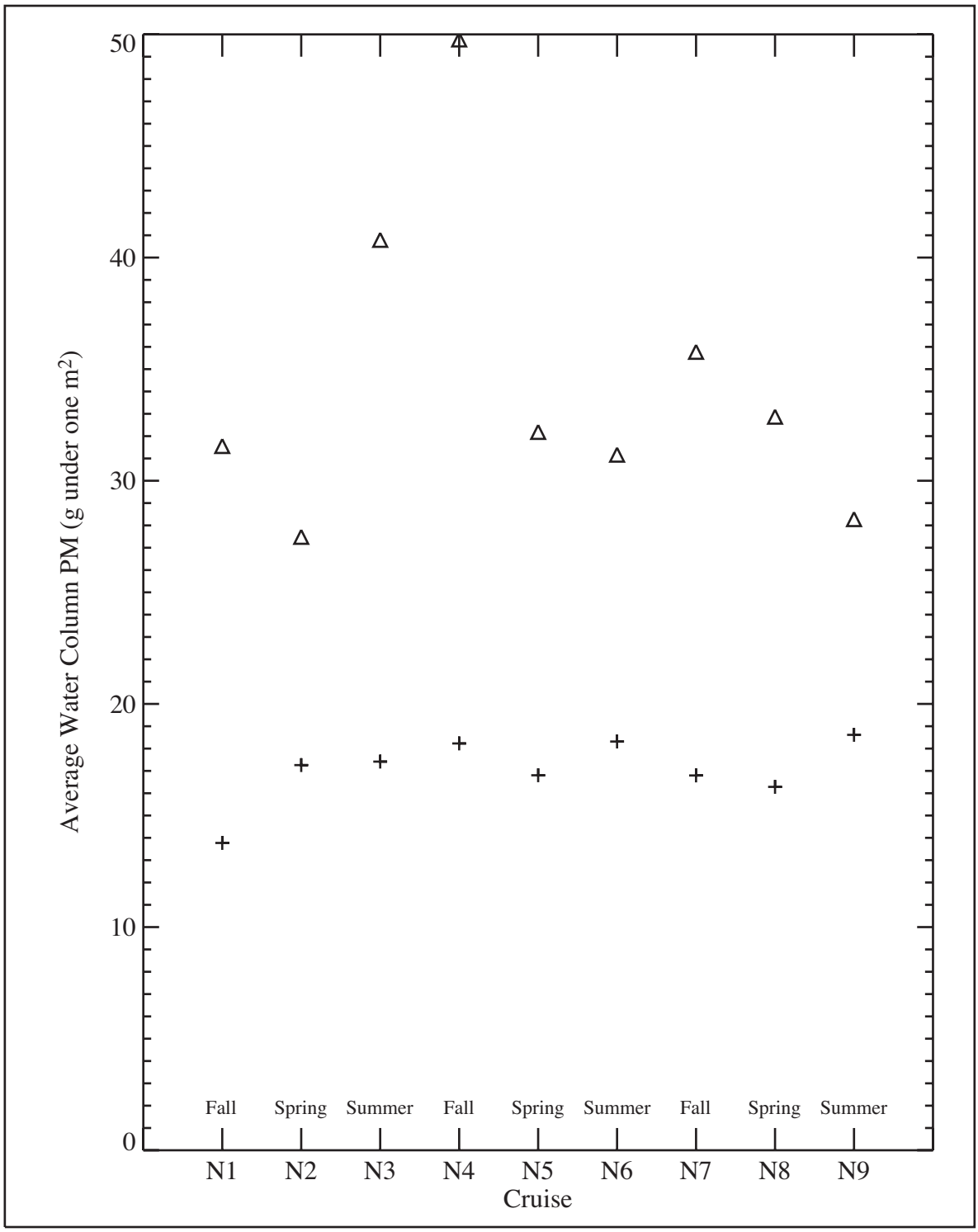

Figure 6.2-10. Average water colum PM (g) for stations on the shelf (water depth < 200 m). Pluses represent average values over the eastern shelf (east of 87°W). Triangles represent average values over the western shelf (west of and including 87°W).

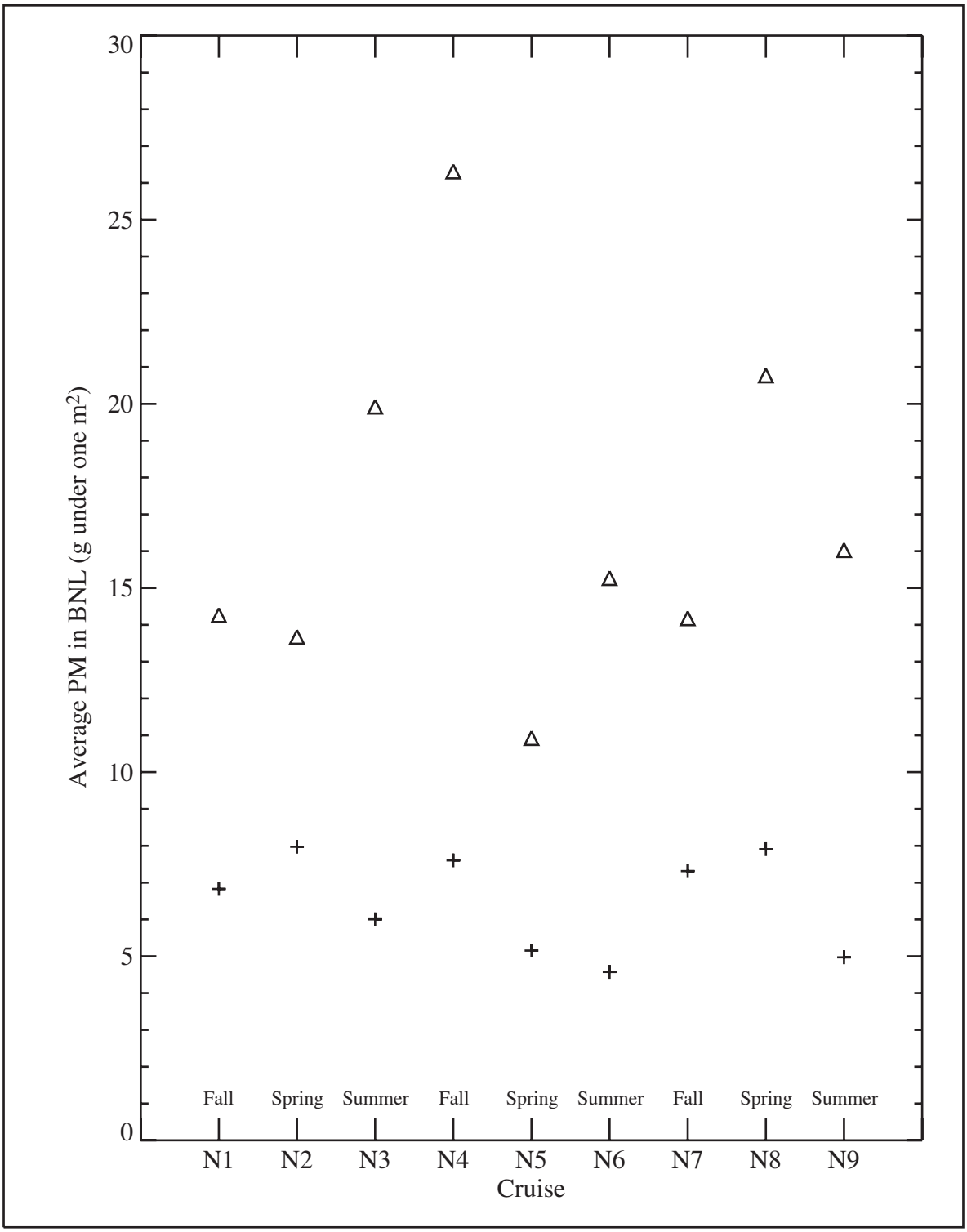

Figure 6.2-11. Average PM (g) in BNL for stations on the shelf (water depth < 200 m). Pluses represent average values over the eastern shelf (east of 87°W). Triangles represent average values over the western shelf (west of and including 87°W).

Table 6.2-1. Basic statistics for particulate matter observations.

Type	Mean ($\mu g \cdot L^{-1}$)	Standard Deviation ($\mu g \cdot L^{-1}$)	Maximum ($\mu g \cdot L^{-1}$)	Minimum ($\mu g \cdot L^{-1}$)
Surface				
All	566	1187	15462	40
Fall	393	999	10368	40
N1	287	359	2411	40
N4	607	1601	10368	41
N7	269	384	2219	45
Spring	617	1507	15462	56
N2	482	942	6420	56
N5	1070	2346	15462	59
N8	323	623	4627	56
Summer	685	961	9200	87
N3	787	1254	9200	87
N6	568	424	2616	99
N9	702	1013	5648	99
Near-bottom				
All	533	877	9849	5
Fall	596	1011	6471	21
N1	498	933	4967	21
N4	776	1229	6471	59
N7	502	785	3792	70
Spring	525	962	9849	5
N2	471	658	4207	5
N5	459	539	2949	35
N8	650	1457	9849	13
Summer	481	611	3708	37
N3	510	635	2797	44
N6	500	716	3708	37
N9	433	461	2606	51

in concert. First as we move offshore, we are farther from nearshore sources of particles and the particles advected laterally through the water column will decrease in concentration because the larger particles have settled out of the water column during the transport, i.e., particulate matter is preferentially deposited near shore. Further offshore also equates to a longer water column and thus longer settling times; therefore sinking particles are subject to more reworking by bacteria. Bacterial reworking generally decreases particle size (as opposed to large animal fecalization processes), disaggregates particles, and converts particulate forms to dissolved forms all decreasing the concentrations of particles. Thus increased distance from shore equates to increased water depth and in combination equates to reduced particulate loads.

In fall, near-surface POC concentrations decreased with increasing distance offshore (Figure 6.3-1). Only on cruise N1 did high POC concentrations ($\geq 100\ \mu g \cdot L^{-1}$) extend beyond the shelf; this occurred off the mouth of the Mississippi River. In spring, near-surface POC concentrations also decreased with increasing distance offshore (Figure 6.3-2). However, the region of high POC concentrations was more extensive than in fall, except for cruise N8, which occurred early in the spring season. The near-surface POC concentrations of summer were high across the western shelf and slope in all three years sampled (Figure 6.3-3). On N3, high POC was seen over the slope of the eastern shelf, reversing the pattern of decreasing concentrations with increasing distance offshore seen in the fall and spring cruises. The highest POC levels in all seasons generally were associated with high PM plumes near river mouths (e.g., compare the region of PM $\geq 0.6\ mg \cdot L^{-1}$ in Figure 6.2-6, upper panel, with the region of POC $\geq 100\ \mu g \cdot L^{-1}$ in Figure 6.3-2, lower panel). In many instances, high POC values were broadly distributed across the shelf, indicative of an *in situ* phytoplankton origin (e.g., Figure 6.3-3, upper panel).

The general pattern of subsurface POC concentrations also is of decreasing concentrations with increasing distance offshore. Highest values ($\geq 100\ \mu g \cdot L^{-1}$) tend to occur mainly off the Mississippi and Apalachicola Rivers and the Mobile and Choctawhatchee Bays (Figures 6.3-4, 6.3-5, and 6.3-6). This is the case even on summer cruise N3 when the near-surface POC concentrations were widespread across the shelf and slope (compare upper panels of Figures 6.3-3 and 6.3-6). Near-bottom POC concentrations were measured on cruises N1 through N6. At stations in depths of more than 100 m, the near-bottom POC concentrations generally were significantly less than near-surface water POC concentrations as a result of remineralization of organic matter during transport through the water column. In shallow depths, near-bottom water POC could exceed POC in near-surface waters, probably due to the primary productivity maxima being below the near-surface water depth of collection. At some locations, resuspension of organic-rich sediments may be occurring. The third year of sampling measured POC at the chlorophyll maximum, rather than near bottom as in the first two years. The pattern of regions of high POC concentrations at the chlorophyll maximum generally mirrored that at the near-surface (compare the bottom panels of Figures 6.3-1, 6.3-2, and 6.3-3 with those for Figures 6.3-4, 6.3-5, and 6.3-6).

Basics statistics were calculated for the observations of particulate organic carbon and particulate organic nitrogen (Table 6.3-1). On average, the near-surface POC concentrations are greater than those sub-surface. There also is more variability in the near-surface. The fall season has generally smaller near-surface POC concentrations than the other seasons, and the summer has larger. Note that the near-surface statistics for cruise N8, which was conducted prior to the time when the spring discharge from the Mississippi River reached the ocean, are more like those of the fall cruises than the other spring cruises. There is more variability in spring and summer near-surface POC concentrations, as evidenced by larger standard deviations and greater ranges, than in fall. Sub-surface concentrations do not seem to have

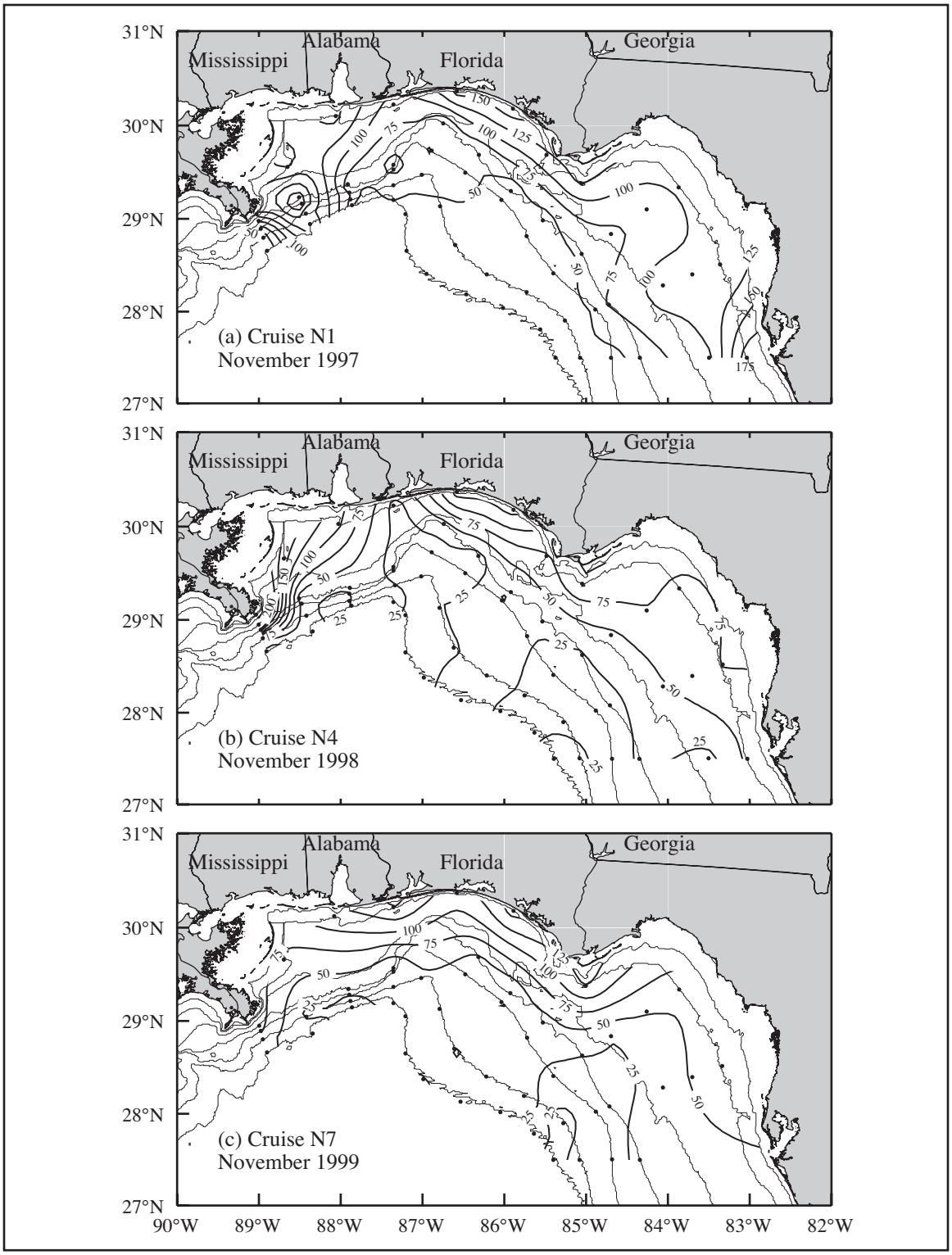

Figure 6.3-1. Particulate organic carbon ($\mu g \cdot L^{-1}$) from the near-surface observations on fall cruises N1, N4, and N7. Bathymetric contours shown are 10, 20, 50, 100, 200, 500, and 1000 m.

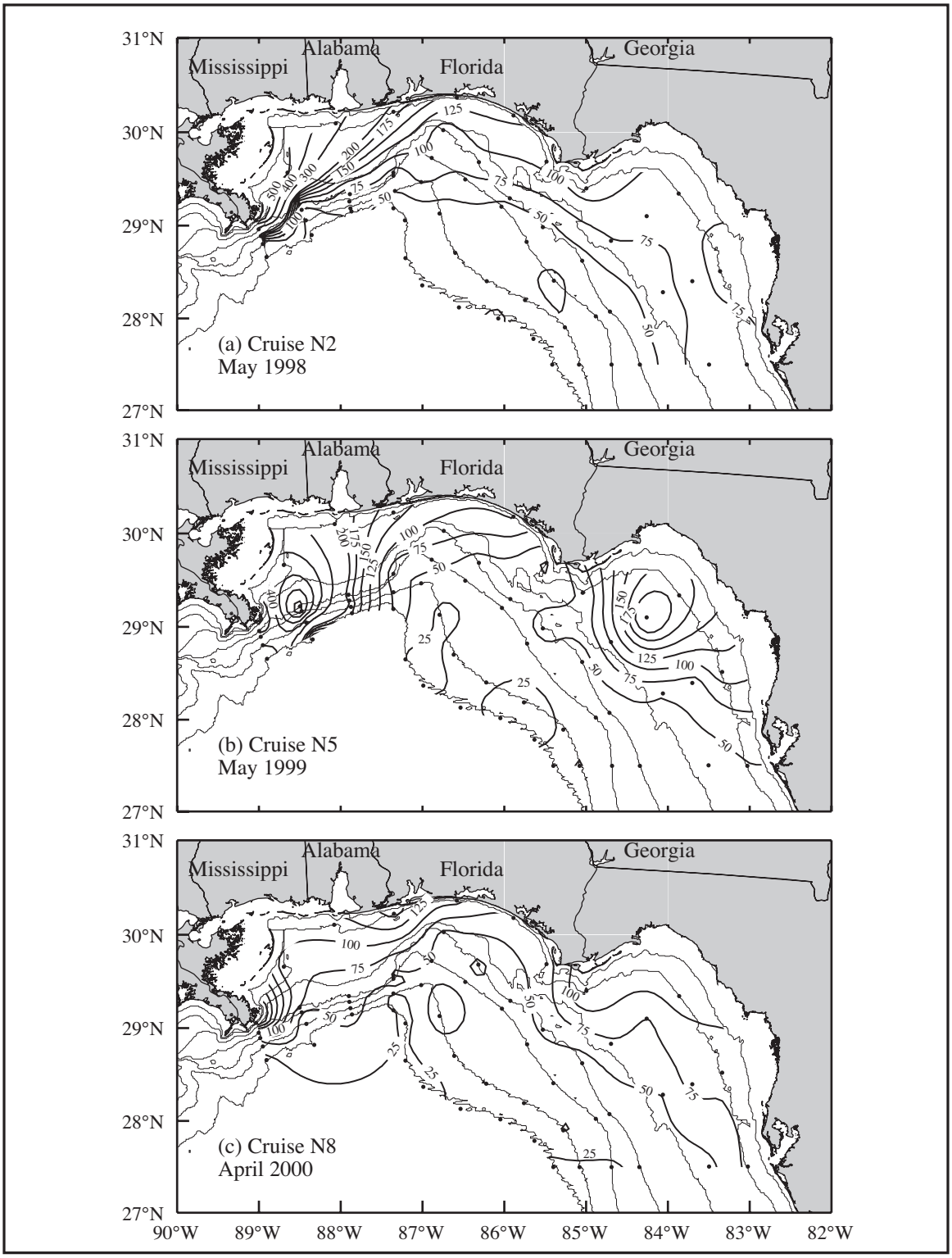

Figure 6.3-2. Particulate organic carbon ($\mu g \cdot L^{-1}$) from the near-surface observations on spring cruises N2, N5, and N8. Bathymetric contours shown are 10, 20, 50, 100, 200, 500, and 1000 m.

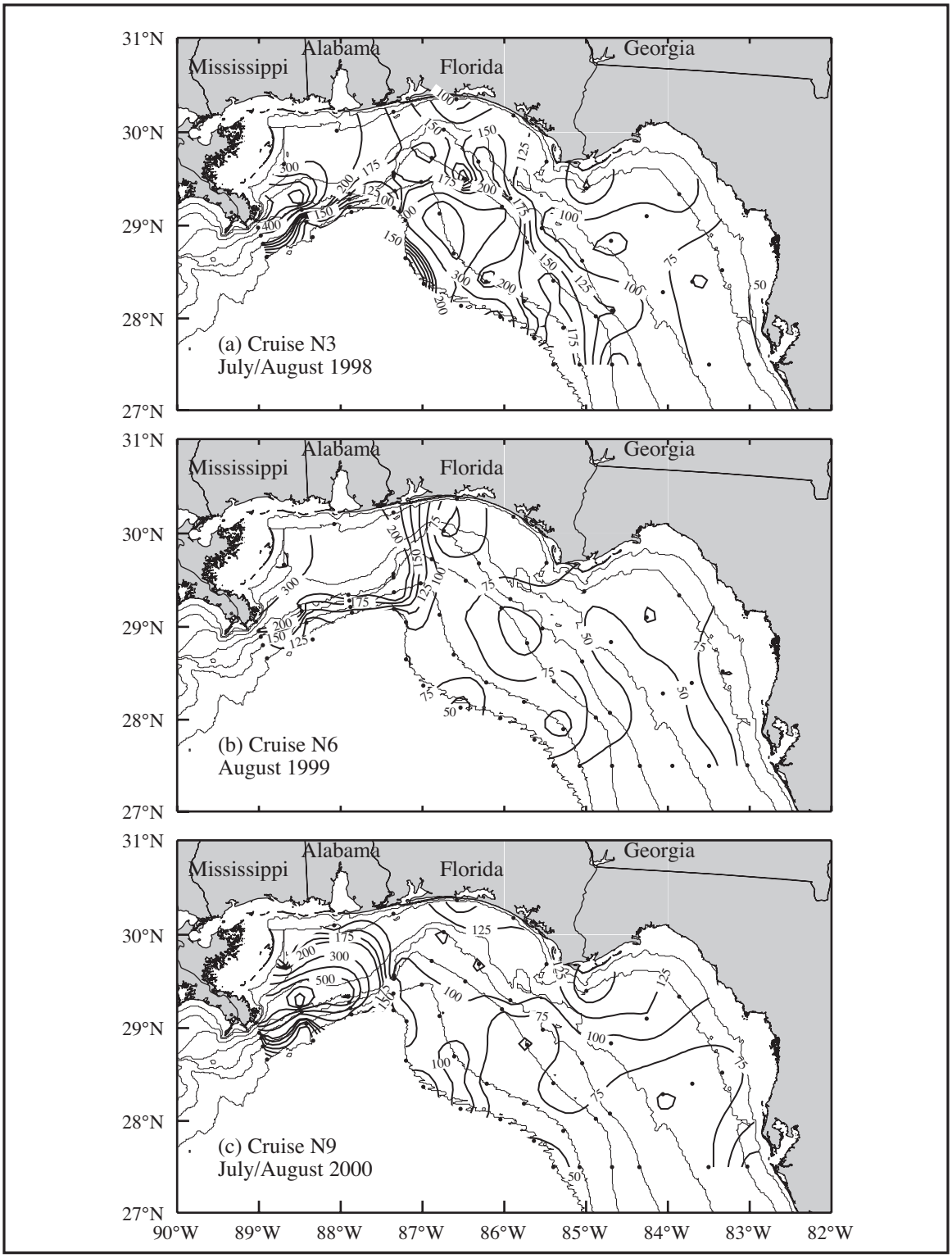

Figure 6.3-3. Particulate organic carbon ($\mu g \cdot L^{-1}$) from the near-surface observations on summer cruises N3, N6, and N9. Bathymetric contours shown are 10, 20, 50, 100, 200, 500, and 1000 m.

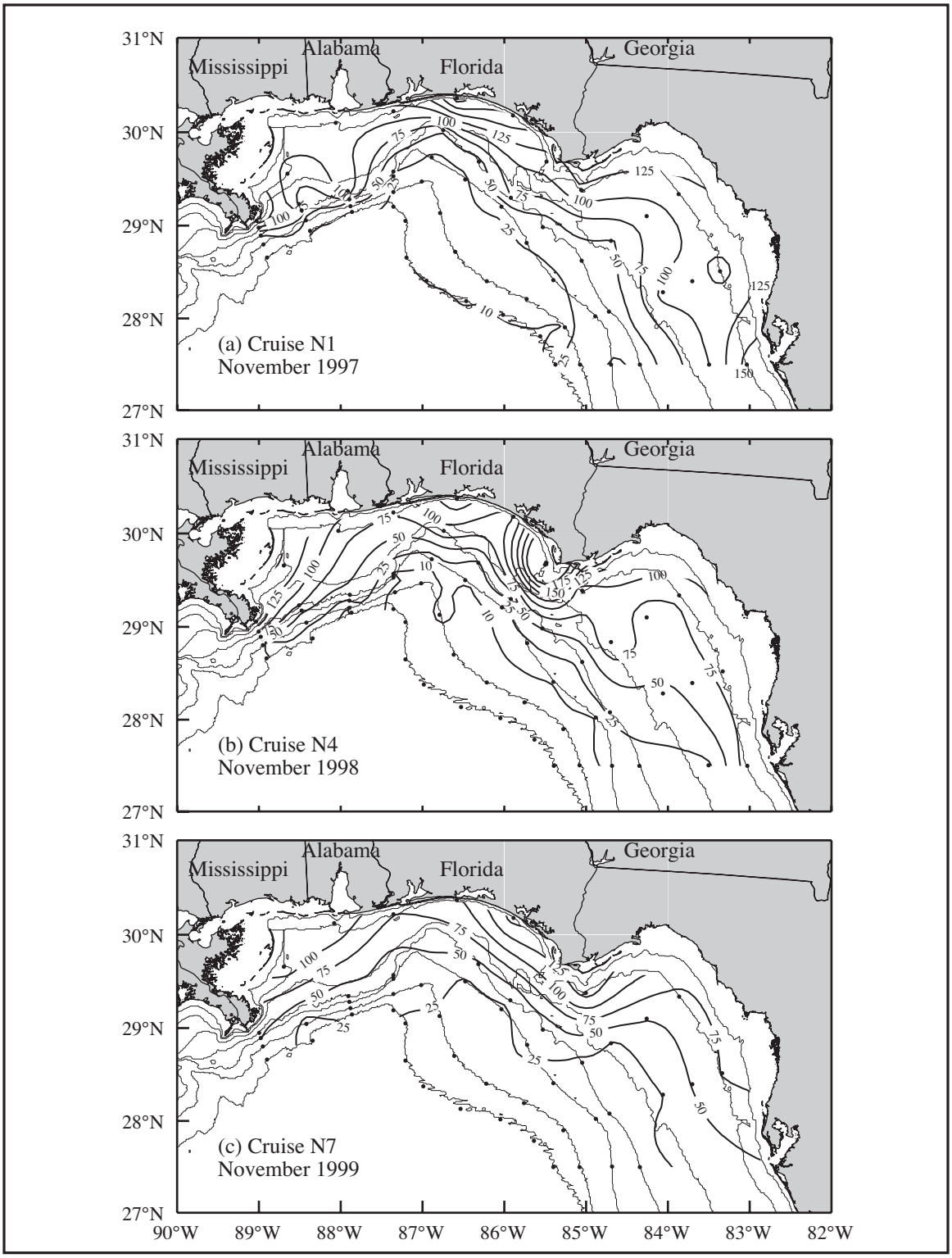

Figure 6.3-4. Particulate organic carbon ($\mu g \cdot L^{-1}$) on fall cruises N1, N4, and N7 from the near-bottom (a and b) and chlorophyll maximum (c) observations. Bathymetric contours shown are 10, 20, 50, 100, 200, 500, and 1000 m.

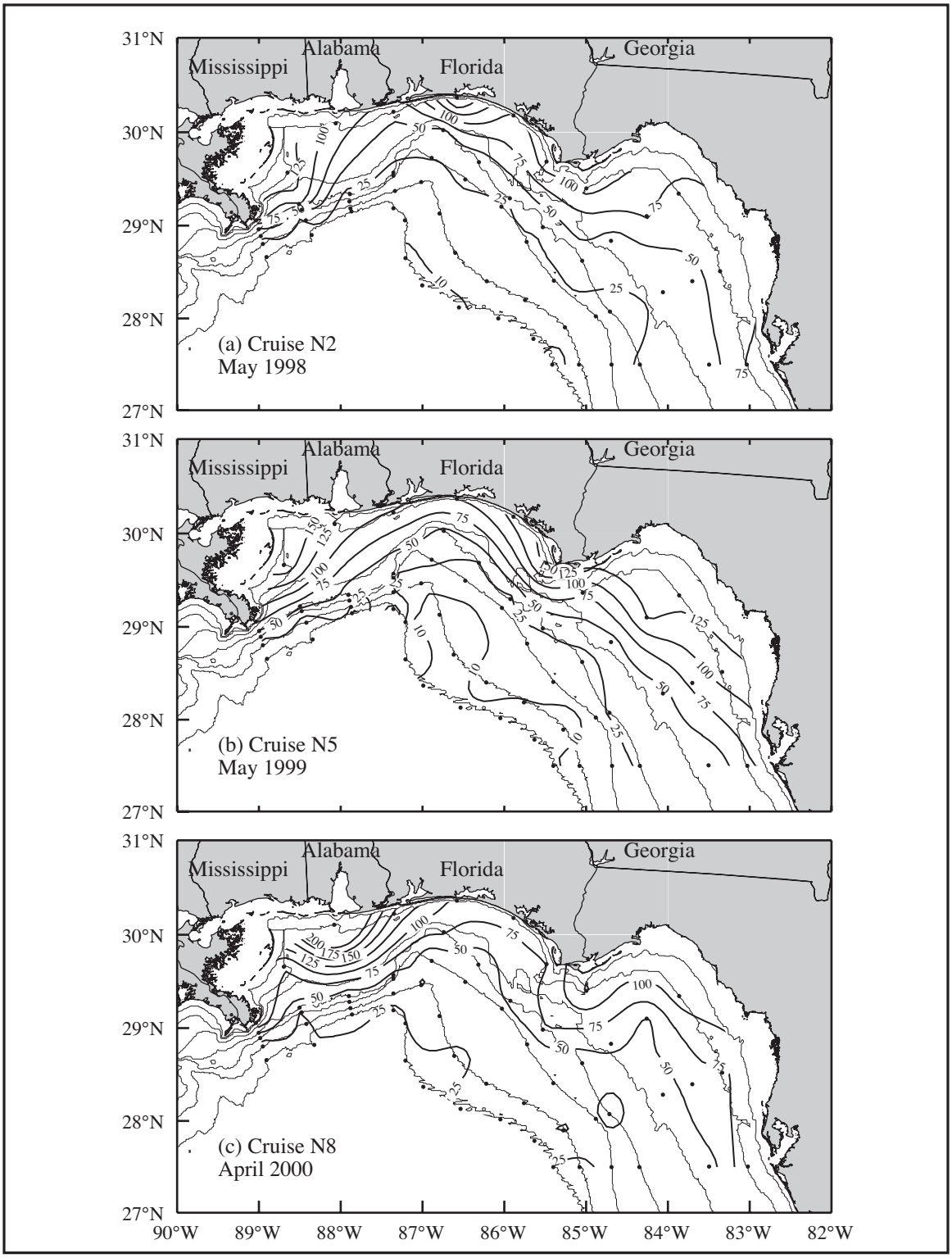

Figure 6.3-5. Particulate organic carbon ($\mu g \cdot L^{-1}$) on spring cruises N2, N5, and N8 from the near-bottom (a and b) and chlorophyll maximum (c) observations. Bathymetric contours shown are 10, 20, 50, 100, 200, 500, and 1000 m.

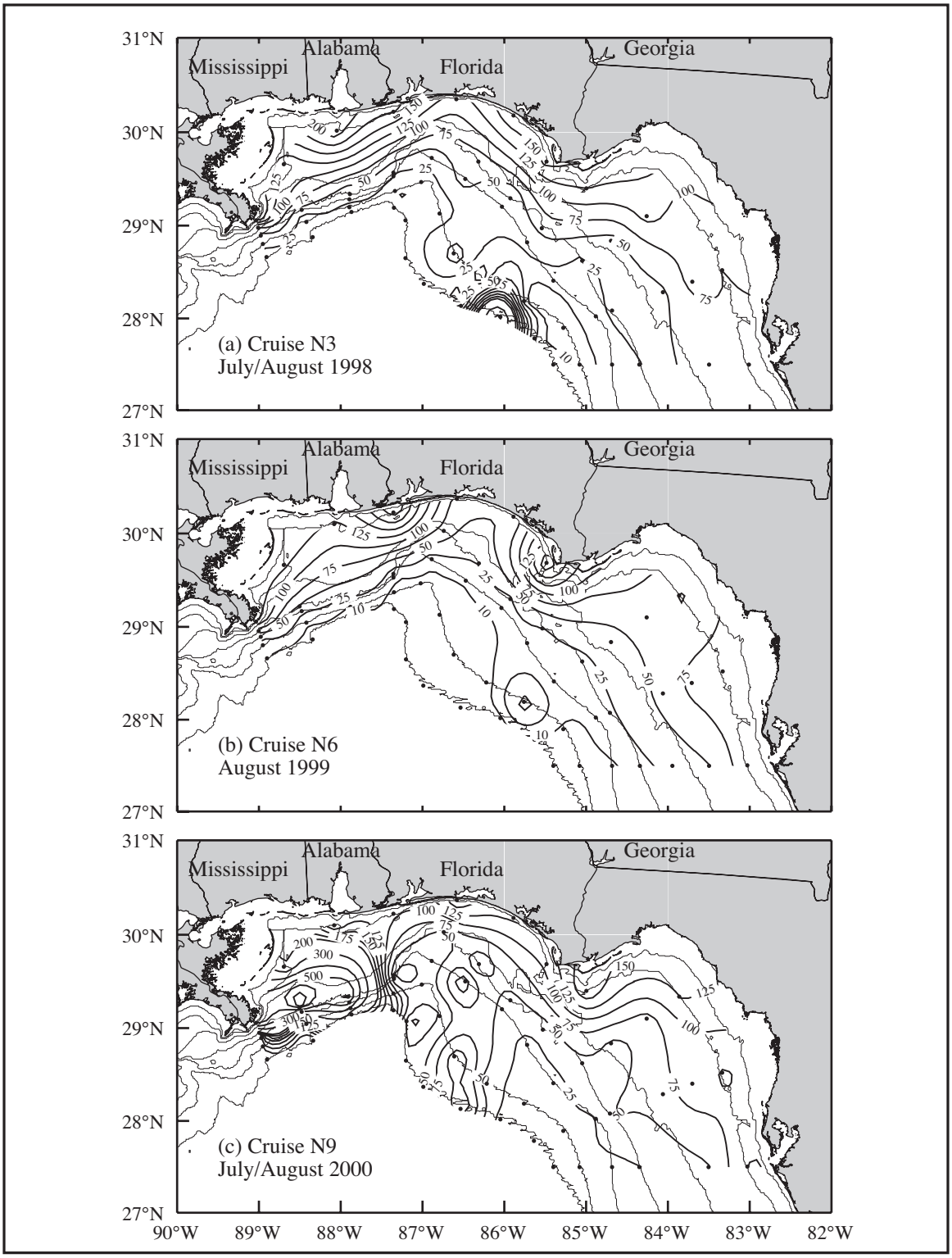

Figure 6.3-6. Particulate organic carbon ($\mu g \cdot L^{-1}$) on summer cruises N3, N6, and N9 from the near-bottom (a and b) and chlorophyll maximum (c) observations. Bathymetric contours shown are 10, 20, 50, 100, 200, 500, and 1000 m.

Table 6.3-1. Basic statistics for observations of particulate organic carbon and particulate organic nitrogen and ratio of POC to PON. The units for the mean, standard deviation, maximum, and minimum are $\mu g \cdot L^{-1}$. Sub-surface observations from cruises N1 through N6 were near-bottom; those from cruises N7 through N9 were from the chlorophyll maximum. The Redfield ratio of C:N is 7:1.

Type	Particulate Organic Carbon				Particulate Organic Nitrogen				Ratio
	Mean	Stand. Dev.	Maxi-mum	Mini-mum	Mean	Stand. Dev.	Maxi-mum	Mini-mum	POC to PON
Near-Surface									
All	98.10	113.99	771.25	11.68	17.56	21.53	147.61	0.18	5.91
Fall	59.60	55.27	403.26	12.78	10.81	10.23	78.14	2.12	5.59
N1	79.51	49.98	235.46	26.54	14.24	8.88	39.53	5.07	5.62
N4	51.56	68.58	403.26	12.78	10.00	13.36	78.14	2.12	5.26
N7	45.91	34.32	160.69	15.03	7.77	5.39	27.53	2.44	5.93
Spring	89.42	121.91	771.25	11.68	16.40	23.41	140.84	0.18	6.27
N2	86.70	109.56	666.85	20.59	15.12	18.23	108.50	3.38	5.75
N5	127.65	172.59	771.25	15.31	25.28	34.47	140.84	2.28	5.61
N8	55.91	39.58	252.33	11.68	9.28	7.10	42.90	0.18	7.42
Summer	144.09	131.53	751.97	26.27	25.26	25.08	147.61	4.48	5.88
N3	178.12	144.46	730.26	47.21	31.64	27.23	144.02	8.22	5.67
N6	111.44	76.46	415.43	26.27	17.51	12.00	64.70	4.48	6.38
N9	142.64	154.40	751.97	30.12	26.70	30.55	147.61	5.86	5.57
Sub-surface									
All	47.90	49.54	320.83	0.49	8.64	8.91	49.55	0.12	6.00
Fall	50.35	51.65	320.83	3.74	8.27	8.27	48.97	0.48	6.18
N1	56.06	49.87	211.86	9.41	9.01	8.22	28.89	1.60	6.53
N4	43.05	53.58	320.83	3.74	7.38	8.48	48.97	0.48	5.77
N7	68.13	44.71	138.26	22.27	9.97	6.54	20.97	3.73	6.81
Spring	46.05	46.36	301.43	3.97	8.65	8.71	49.55	0.12	6.20
N2	38.79	36.58	180.98	6.08	7.08	6.63	31.77	1.38	5.52
N5	41.35	42.62	169.45	3.97	8.41	9.08	38.39	0.12	6.91
N8	96.95	67.18	301.43	25.79	16.41	11.23	49.55	3.56	6.16
Summer	47.45	50.95	219.07	0.49	9.01	9.74	41.05	0.43	5.61
N3	50.53	51.22	218.63	7.04	9.58	9.74	38.10	1.28	5.35
N6	36.97	46.33	219.07	0.49	6.94	8.72	37.10	0.43	5.91
N9	103.70	47.47	205.29	60.39	20.36	9.75	41.05	10.27	5.16

any seasonality to them. However, the average POC concentrations at the chlorophyll maximum (cruises N7 through N9) are greater than those from near-bottom (cruises N1 through N6).

The ratios of POC to PON also are shown in Table 6.3-1. The average ratio is approximately 6 as compared to a C:N Redfield ration of 7:1. The correlation coefficient was 0.95 or better for all cruises. Thus, the behavior of PON generally tends to mirror that of POC.

Basic statistics of the ratio of POC to PM were calculated for pairs of observations in the near-surface (Table 6.3-2) and sub-surface (Table 6.3-3). On average, POC in near-surface waters accounted for 28% of the PM while in near-bottom water POC was only about 12% of the PM. In general, the quantity of POC accounting for PM was more variable in near-surface waters than in sub-surface waters, as evidenced both by the wider range of ratios and the larger standard deviations of the near-surface compared to the sub-surface data. This is indicative of phytoplankton productivity in the shallow water photic zone and remineralization of organic carbon in the water column. Near-bottom particulates also may have a contribution from re-suspended sediments relatively poor in organic carbon. The wide range of ratios in the near-surface observations suggests a mixed origin of inorganic detritus and phytoplankton biomass or remains. Section 10 presents correlations of POC with other parameters including salinity and nutrients.

Table 6.3-2. Ratio of POC to PM from near-surface observations.

Type	Mean	Standard Deviation	Maximum	Minimum
All	0.28	0.15	0.99	0.01
Fall	0.31	0.20	0.99	0.01
N1	0.40	0.20	0.95	0.06
N4	0.24	0.20	0.79	0.01
N7	0.27	0.16	0.99	0.02
Spring	0.25	0.13	0.71	0.04
N2	0.29	0.13	0.65	0.05
N5	0.19	0.09	0.46	0.04
N8	0.28	0.14	0.71	0.05
Summer	0.27	0.11	0.69	0.02
N3	0.33	0.13	0.69	0.08
N6	0.21	0.05	0.34	0.10
N9	0.26	0.11	0.68	0.02

Table 6.3-3. Ratio of POC to PM from near-bottom observations (N1 through N6) or chlorophyll maximum observations (N7 through N9).

Type	Mean	Standard Deviation	Maximum	Minimum
All	0.12	0.10	0.93	0.01
Fall	0.13	0.11	0.54	0.02
N1	0.20	0.13	0.54	0.03
N4	0.07	0.05	0.23	0.02
N7	0.16	0.04	0.21	0.10
Spring	0.12	0.07	0.32	0.02
N2	0.12	0.07	0.32	0.03
N5	0.10	0.07	0.30	0.02
N8	0.16	0.06	0.25	0.06
Summer	0.12	0.11	0.93	0.01
N3	0.15	0.10	0.45	0.03
N6	0.09	0.12	0.93	0.01
N9	0.16	0.05	0.22	0.08

7 DISSOLVED OXYGEN AND HYPOXIA

7.1 Introduction

The main source of dissolved oxygen in the ocean is the atmosphere. Surface waters are generally near saturation, and, in the upper few tens of meters, often are supersaturated by a few percent, in part from entrainment of air bubbles as well as photosynthesis (Broecker and Peng 1982). Subsurface waters generally are undersaturated due to oxidation of detritus and to oxygen consumption by animals and bacteria. As will be shown in this section, this pattern of saturation is true for the NEGOM shelf. In vertical profile, oxygen concentrations are high near surface, decrease to a minimum near 400 m depth, and increase with increasing depth (e.g., Figure 7.1-1). In summer (shown here) and spring, the upper 150 m are quite variable; in fall, the variability is substantially less because the water column is well-mixed by the action of the wind.

The distribution and variability of dissolved oxygen is examined by consideration of the percent of oxygen saturation relative to atmospheric concentration in the NEGOM water samples. Temperature and salinity observations were used with the equation and coefficients for $mL \cdot L^{-1}$ given in Weiss (1970) to compute oxygen saturation values. Oxygen concentrations then were divided by the computed oxygen saturation value for the potential temperature and salinity of the water sample and converted to percent saturation. The solubility of oxygen in water decreases as either temperature or salinity increase. The relationship of oxygen saturation in surface waters to surface salinity and chlorophyll *a* is examined. The relationships of bottom oxygen saturation to water column stability and bottom nitrate concentrations are considered. In this report waters with saturation greater than or equal to 110% will be referred to as "highly supersaturated".

An important aspect of the distribution of dissolved oxygen over the Gulf shelves has been the observed occurrence of hypoxia. Waters with dissolved oxygen concentrations less than 1.4 $mL \cdot L^{-1}$ are classified as hypoxic. Hypoxic waters contain too little oxygen to sustain healthy animal communities (e.g., Rabalais et al. 1999). As found during the LATEX study (Nowlin et al. 1998a; Murray 1998), one of the factors contributing to hypoxia over the Texas-Louisiana shelf is the discharge of the Mississippi River. This discharge adds a layer of fresh water to the surface, increasing the stratification of the water column. Strong stratification, in turn, can decrease oxygen replenishment below the pycnocline. The discharge also contributes significant nutrients to the marine environment, allowing production of greater biomass in the upper waters. Greater biomass production then can increase oxygen consumption through larger quantities of detritus being oxidized below the pycnocline. Because a significant portion of the Mississippi River discharge extends onto the NEGOM shelf, the possibility of hypoxic conditions within the NEGOM study area is examined in this section for the period of the cruises in November 1997 through August 2000.

7.2 Surface Oxygen Distributions

Distributions of the percent oxygen saturation for near-surface samples on the NEGOM cruises are examined. Near-surface samples are considered to be those taken within the upper 6 m of the water column. The distributions for the three spring cruises, N2, N5, and N8, are shown in Figure 7.2-1. During these cruises, most of the NEGOM study area was supersaturated by at least a few percent, with much of the area being at approximately 105% saturation. Highly supersaturated surface waters were present over the Mississippi-Alabama

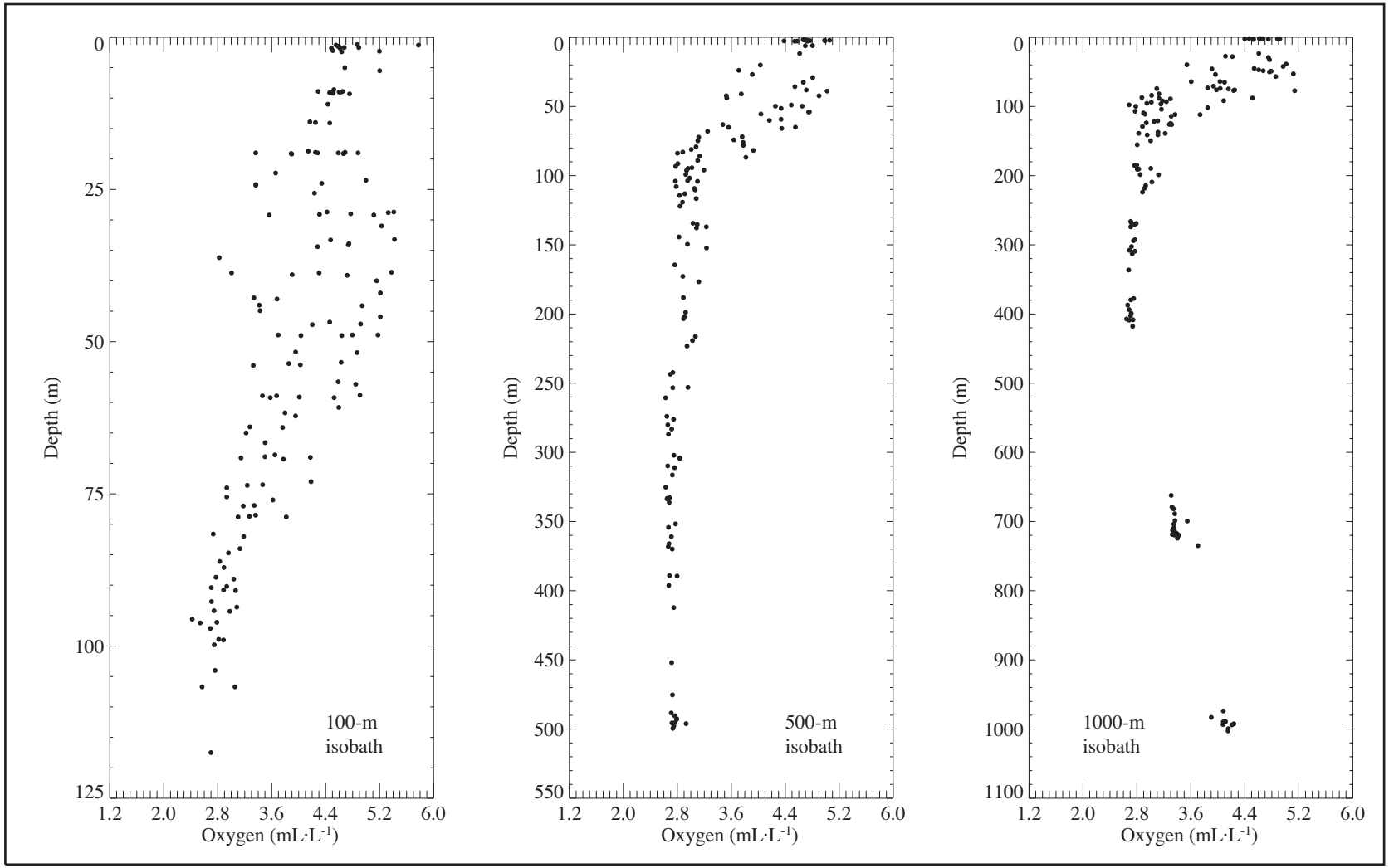

Figure 7.1-1. Example oxygen profiles along the 100- (left), 500- (middle), and 1000-m (right) isobaths. Data are from cruise N6 in August 1999.

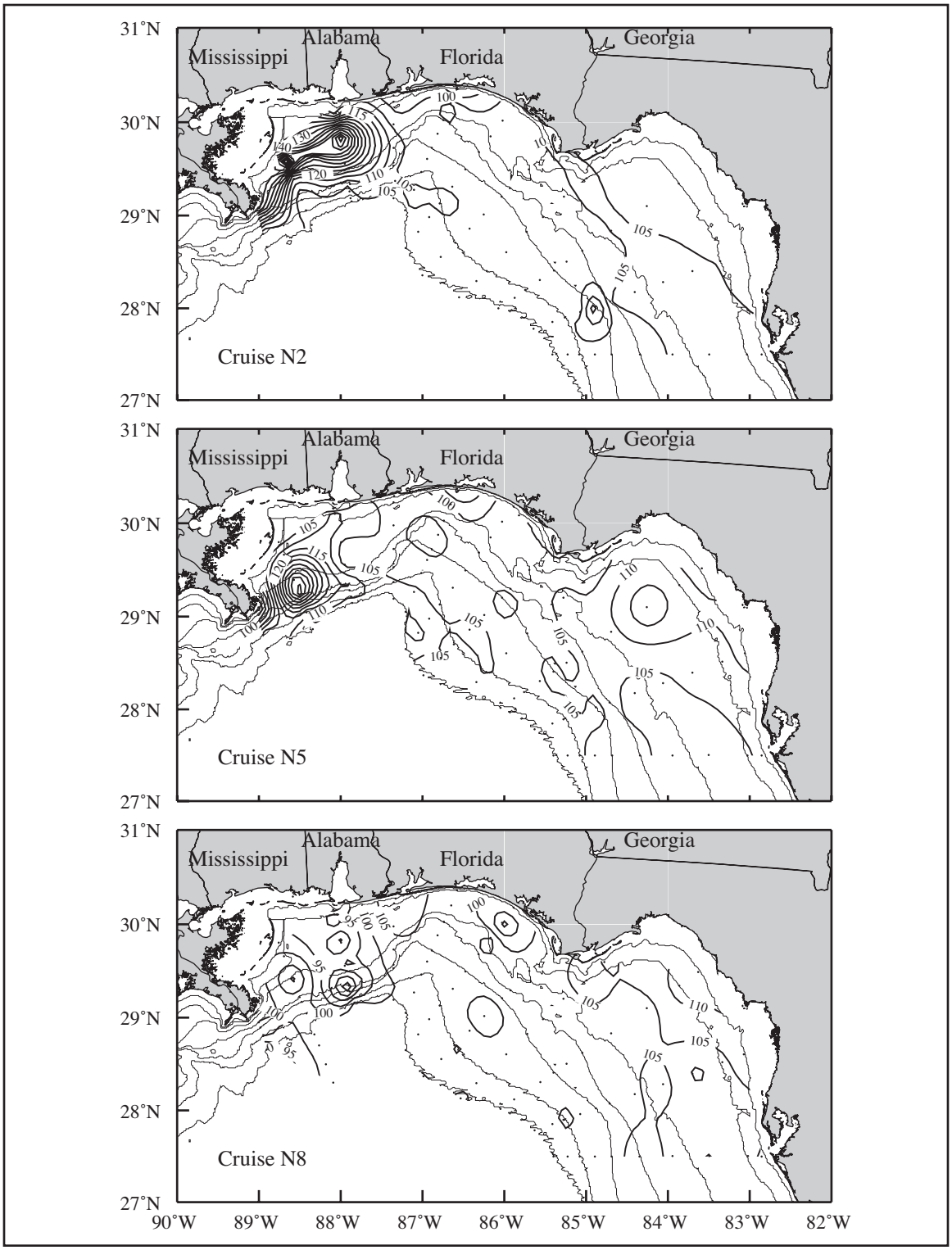

Figure 7.2-1. Surface saturation (percent) of dissolved oxygen from spring cruises N2 (May 1998), N5 (May 1999), and N8 (April 2000). Bathymetric contours shown are 10, 20, 50, 100, 200, 500, and 1000 m.

shelf on cruises N2 in 1998 and N5 in 1999. In contrast, on cruise N8 in 2000, the surface waters were near saturated or undersaturated. These regions of highly supersaturated and under-saturated oxygen levels likely are related to the discharge of fresh water from the rivers and the presence of circulation features at the shelf edge.

Cruises N2 and N5 occurred in May, approximately 1-1.5 months after peak pulses in discharge from the Mississippi River that exceeded the 70-year record-length mean. In 1998, the discharge of relatively low salinity water from Mobile Bay also was high due to large flows in the Tombigbee and Alabama Rivers, with peak discharges in April that exceeded one standard deviation from the mean. The region of highly supersaturated waters coincided well with the region of lowest salinity waters (< 30) for those two years (Figure 7.2-2). The region during cruise N2 was more extensive than that during N5, reflecting the larger flows from Mobile Bay in 1998 than in 1999.

The distribution of oxygen saturation over the Mississippi-Alabama shelf on cruise N8 differed considerably from that of the other two spring cruises. This region had surface waters that mainly were near saturation (100% ± 5%), rather than being highly supersaturated as on cruises N2 and N5. There are several likely reasons for this difference. First, being conducted in the second half of April 2000, it was completed earlier in the year when river discharge into the Gulf was lower and the salinity of the area was higher than in May (compare Figure 7.2-1 with Figure 7.2-2). Any effect of the cooler temperatures during N8, in comparison to N2 and N5, did not act preferentially over the Mississippi-Alabama shelf and did not compensate for the effect there of saltier water on the oxygen solubility. Second, the river water discharge 1-1.5 months prior to the cruise was below the record-length mean for the Mississippi River, but had peak pulses that exceeded the mean for the Tombigbee and Alabama Rivers. Third, there was a cyclonic feature at the shelf edge that moved Mississippi waters to the west, away from the NEGOM shelf (see Figure H.1.3-1).

Distributions of the percent oxygen saturation for the surface samples on the three summer NEGOM cruises, N3, N6, and N9, are shown in Figure 7.2-3. On cruise N3 in 1998, the percent saturation generally was near 105% ± 5% over the study area. There was considerable water of relatively low salinity over the outer shelf and slope (Figure 7.2-4), but surface temperatures there were generally warm, exceeding 30°C. During cruise N6 in 1999, the surface waters generally had greater than 100% saturation in oxygen. The region extending from the Mississippi River delta east to about 87°W was highly supersaturated. This region contained relatively low salinity water associated with Mississippi River discharge (compare Figure 7.2-3 with Figure 7.2-4). As on cruise N3, the region of relatively low salinity water extended over the outer shelf and slope and was much more extensive in area than the highly supersaturated oxygen waters. Again, surface temperatures exceeded 30°C over the study area. The distribution of percent oxygen saturation for cruise N9 in 2000 consisted of oxygen saturation levels that were near 100% ± 5%, except in a small region east of the Mississippi River mouth (Figure 7.2-3). This region coincides reasonably well with a region of relatively low salinity water (Figure 7.2-4). Surface water temperatures were 29-31°C throughout the study area. On both cruise N6 and N9, there was an area in the Big Bend of the west Florida shelf that had saturation percents of less than 100. In these areas, the salinity was greater than 35.5.

Distributions of the percent oxygen saturation for the surface samples on the three fall NEGOM cruises, N1, N4, and N7, are shown in Figure 7.2-5. These patterns show an indication of the effect of temperature on oxygen saturation levels, in part because the river discharge was low prior to these cruises so the effects of salinity were damped (Figure 7.2-6). During cruise N1 the surface temperatures were colder over the whole shelf than those during

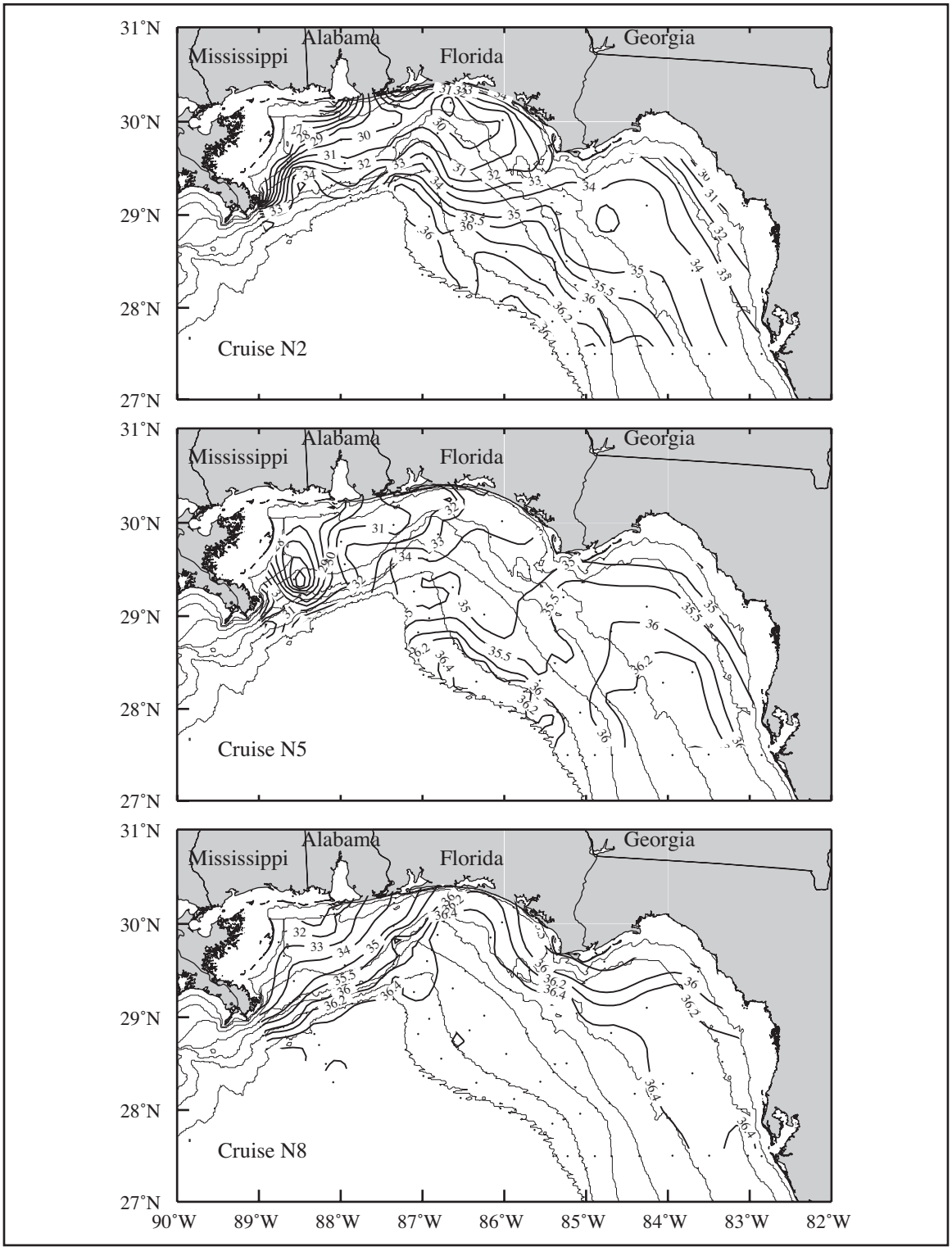

Figure 7.2-2. Surface salinity from spring cruises N2 (May 1998), N5 (May 1999), and N8 (April 2000). Bathymetric contours shown are 10, 20, 50, 100, 200, 500, and 1000 m.

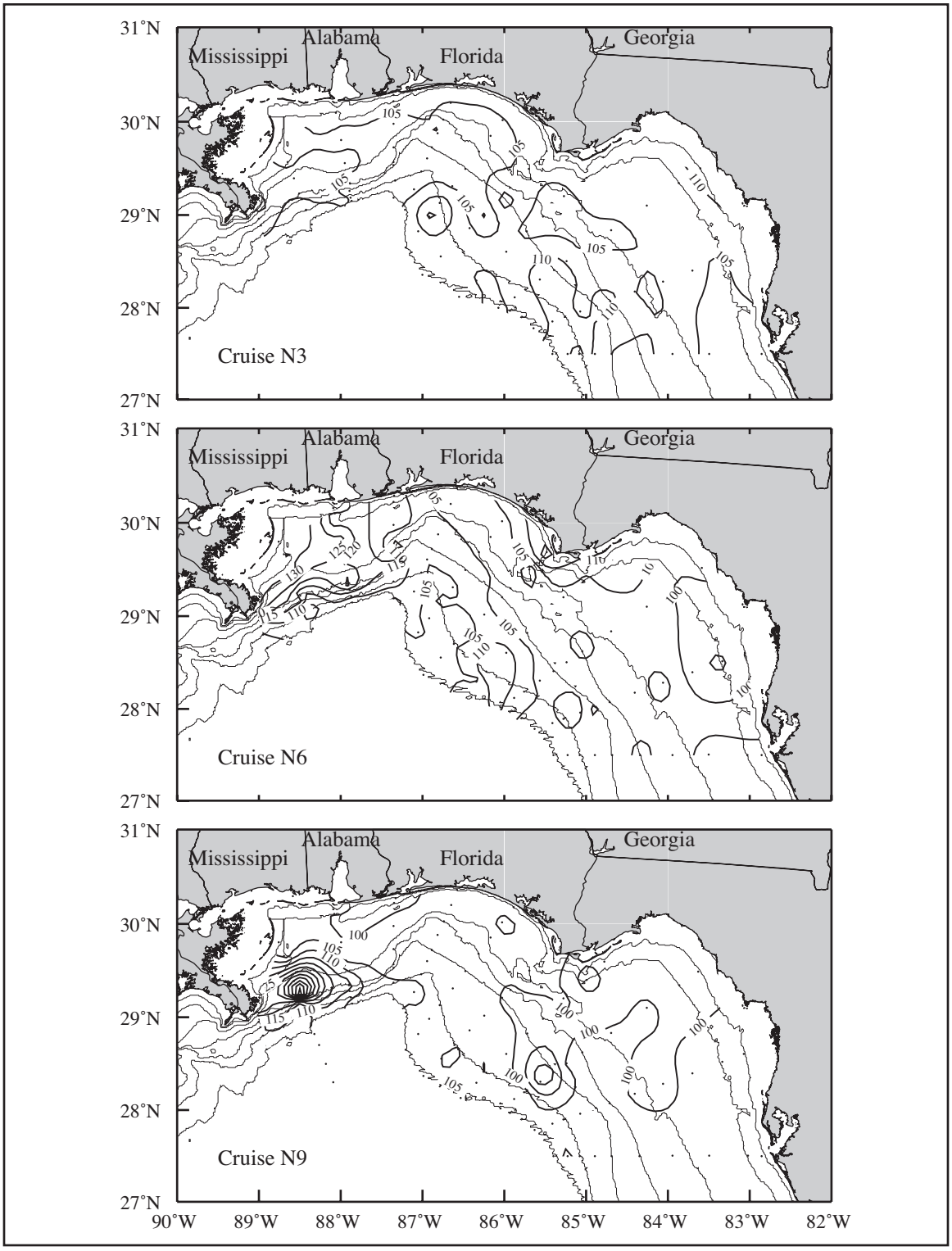

Figure 7.2-3. Surface saturation (percent) of dissolved oxygen from summer cruises N3 (July/August 1998), N6 (August 1999), and N9 (July/August 2000). Bathymetric contours shown are 10, 20, 50, 100, 200, 500, and 1000 m.

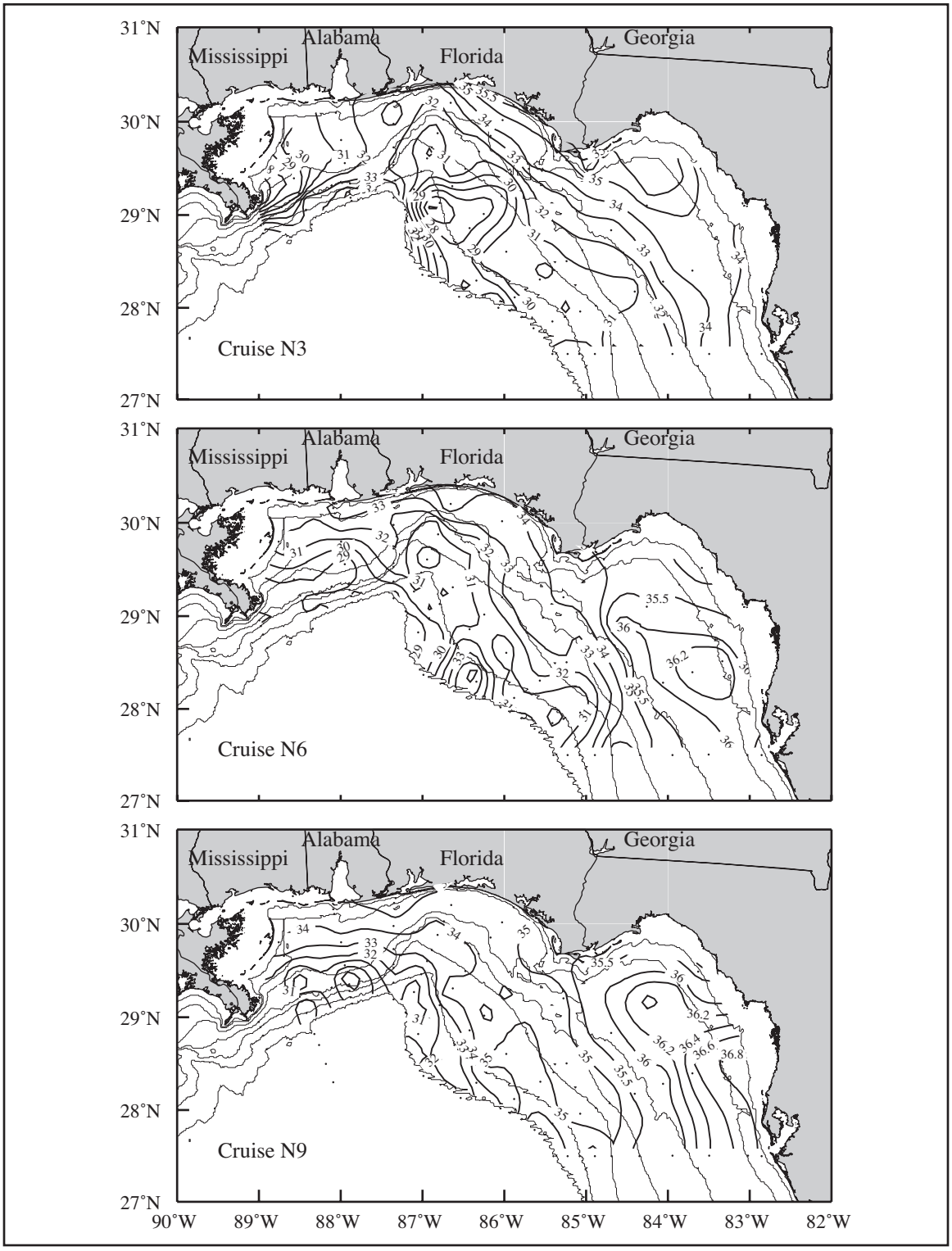

Figure 7.2-4. Surface salinity from summer cruises N3 (July/August 1998), N6 (August 1999), and N9 (July/August 2000). Bathymetric contours shown are 10, 20, 50, 100, 200, 500, and 1000 m.

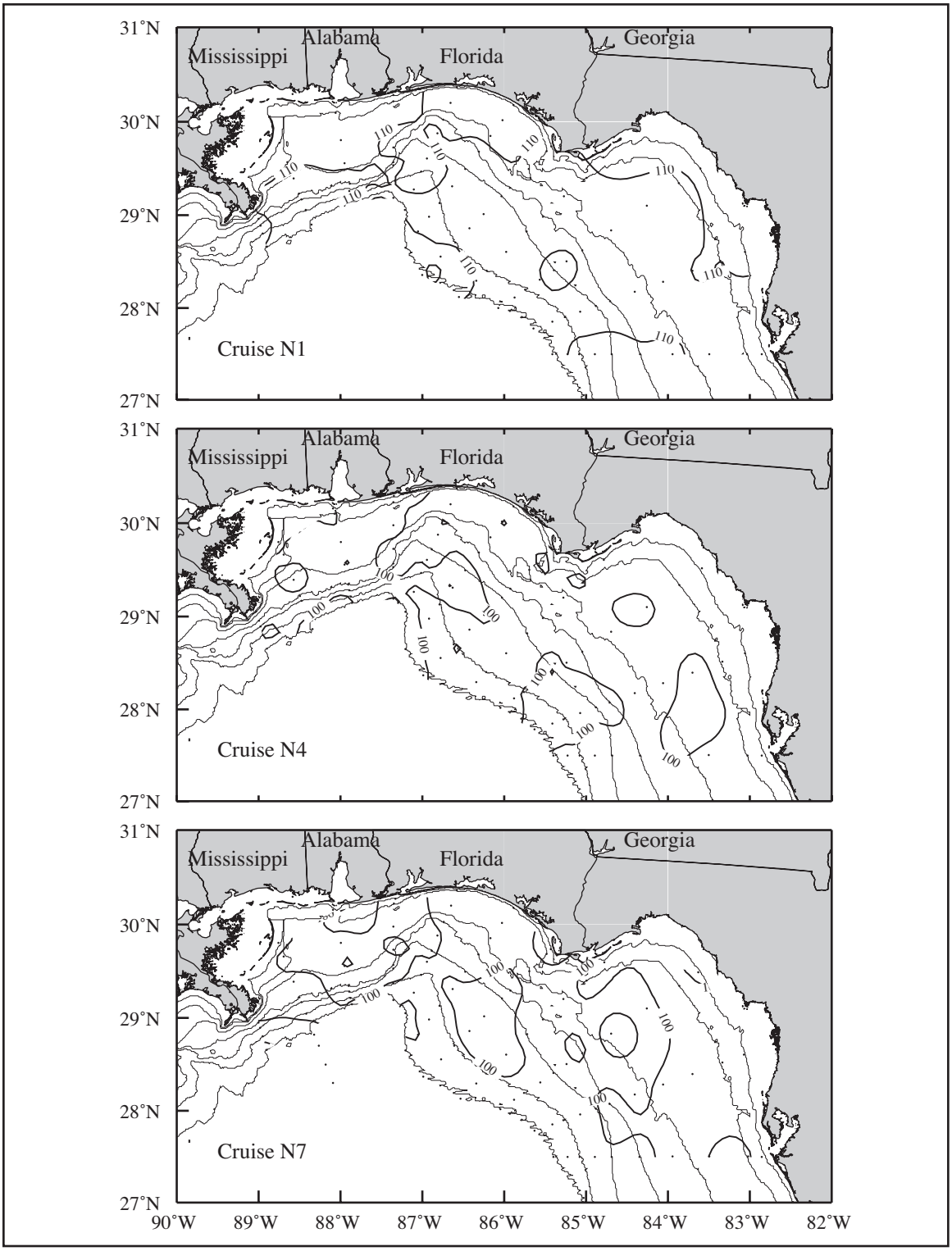

Figure 7.2-5. Surface saturation (percent) of dissolved oxygen from fall cruises N1 (November 1997), N4 (November 1998), and N7 (November 1999). Bathymetric contours shown are 10, 20, 50, 100, 200, 500, and 1000 m.

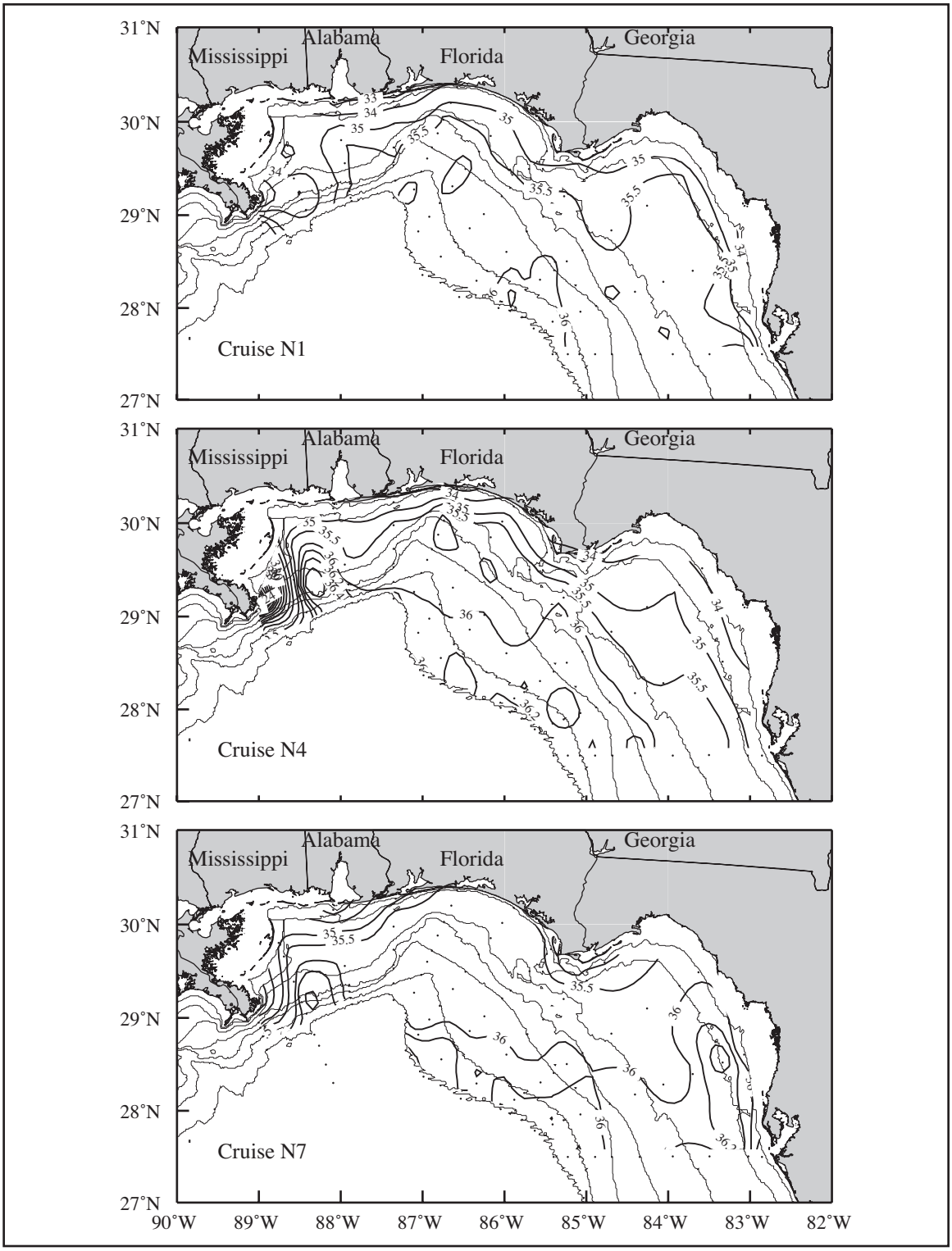

Figure 7.2-6. Surface salinity from fall cruises N1 (November 1997), N4 (November 1998), and N7 (November 1999). Bathymetric contours shown are 10, 20, 50, 100, 200, 500, and 1000 m.

cruises N4 and N7. On N1 temperatures were generally 23°C or less. On N4 and N7, surface waters with temperatures ≤ 23°C were limited generally to the inshore of the 50-m isobath. The percent oxygen saturation on N1 was generally 110% ± 5%, while those on N4 and N7 were 100% ± 5%.

The relationship of surface dissolved oxygen saturation to surface salinity for the fall, spring and summer seasons is shown in Figure 7.2-7. Most of the oxygen saturation values are a few percent above saturation, being near 105% saturation (±5%). Saturated or supersaturated values occur over the full range of high to low salinity waters in all three seasons. The lowest percent saturation is 75%, occurring on spring cruises N5 and N8. Stations with highly supersaturated values occur on all spring and summer cruises, but only on fall cruise N1 in 1997. In general, the spring season has the highest oxygen saturation levels. In 2000, however, the summer cruise had higher saturation levels than the spring cruise. This may be associated with the low river discharge from the Mississippi River preceding the spring cruise N8, which also was earlier in the season than the other two spring cruises, and the occurrence of a relatively high discharge peak, which was near one standard deviation above the record-length mean in early July, preceding the summer cruise N9. High oxygen saturation generally seems associated with low salinity, although fall cruises N4 and N7 and spring cruise N8 are somewhat exceptional (but those three cases had few highly supersaturated waters). This suggests that highly supersaturated waters are related to river discharge. However, the highly supersaturated surface waters on fall cruise N1 clearly were not associated with low salinity, but rather with low surface temperatures. The correlation coefficients for surface oxygen saturation and surface salinity for stations located over the Mississippi-Alabama shelf west of 87°W are given in Table 7.2-1. The associated squared correlation coefficients are less than 0.5 except for the summer cruise N9, which is at 0.53. The correlations on one spring cruise and two summer cruises are significant at the 95% level. These correlations are negative, indicating that low surface salinities are correlated with high surface oxygen saturation.

Phytoplankton adds oxygen to the water during photosynthesis, and chlorophyll *a* is an indicator of phytoplankton biomass. The relationship between surface oxygen saturation levels and surface chlorophyll *a* concentrations is examined for the fall, spring, and summer cruises. As shown in Figure 7.2-8, waters near or above saturation have a wide range of chlorophyll *a* concentrations in all three seasons. This is consistent with the major source of the oxygen being the atmosphere. For the cruises on which there was substantial low salinity over the shelf and/or slope, there were a number of stations with chlorophyll *a* concentrations in excess of 1000 $ng \cdot L^{-1}$. These cruises are the two spring cruises, N2 and N5, and all three summer cruises. Significantly, the spring cruise, N8, that was conducted earlier in spring than the other two, had no such high chlorophyll *a* concentrations. Most of the stations with high chlorophyll *a* concentrations also were highly supersaturated in oxygen. This suggests that the phytoplankton blooms can contribute locally to the oxygen concentrations in the surface waters. However, there are a few stations with high chlorophyll *a* concentrations that have percent oxygen saturation levels that are under-saturated. This suggests that high oxygen levels do not always accompany high phytoplankton activity. Because river water carries a high nutrient content that enhances phytoplankton growth, the correlation between the percent oxygen saturation and chlorophyll *a* concentrations was examined for the Mississippi-Alabama shelf west of 87°W. The squared correlation coefficients were less that 0.50 for all cruises. However, the correlations for one spring and all three summer cruises were significant at the 95% level (Table 7.2-1). These significant correlations were positive, which indicates that high surface chlorophyll *a* concentrations are correlated with high surface oxygen saturation.

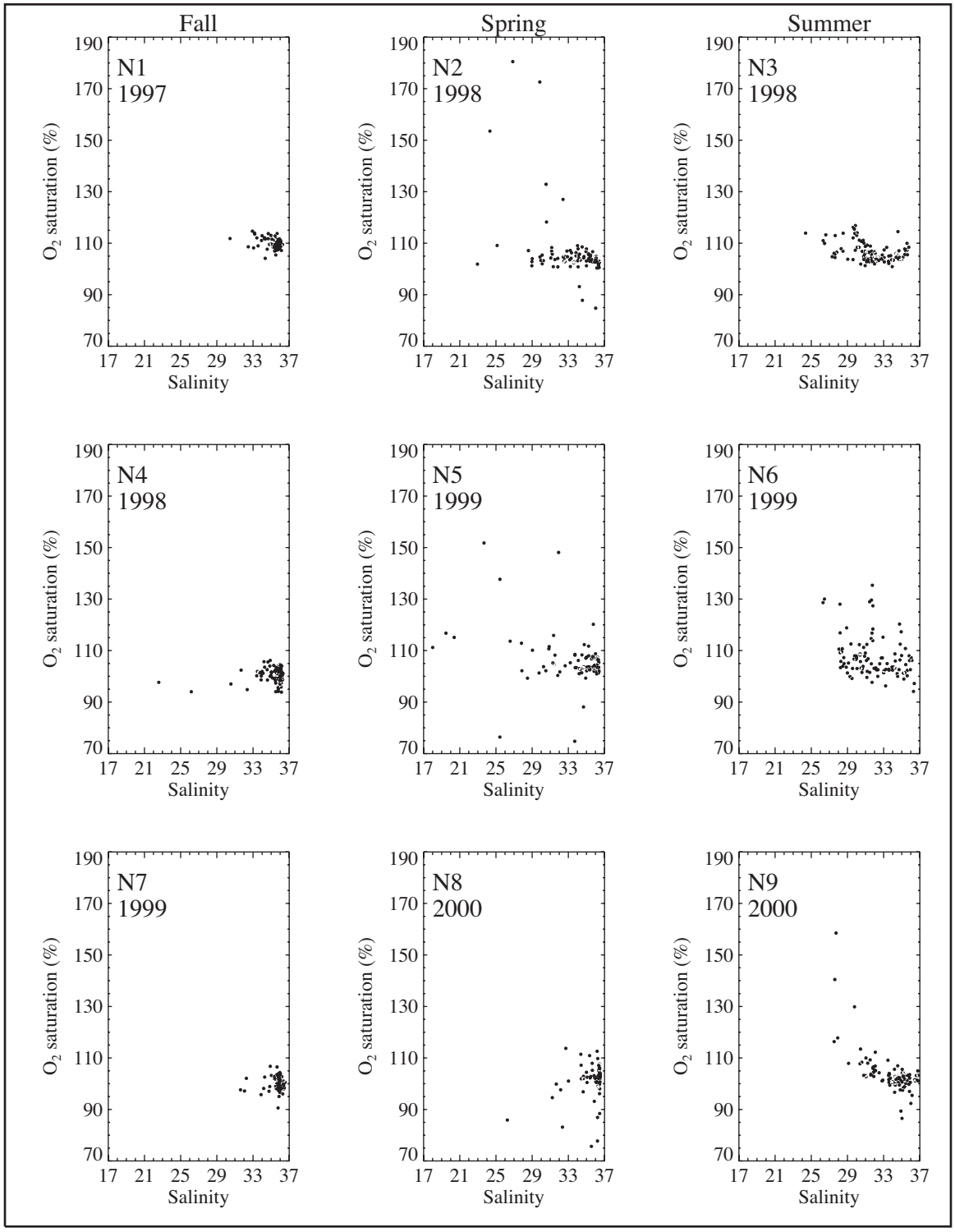

Figure 7.2-7. Near-surface percent dissolved oxygen saturation versus salinity for fall, spring, and summer cruises in 1997-2000.

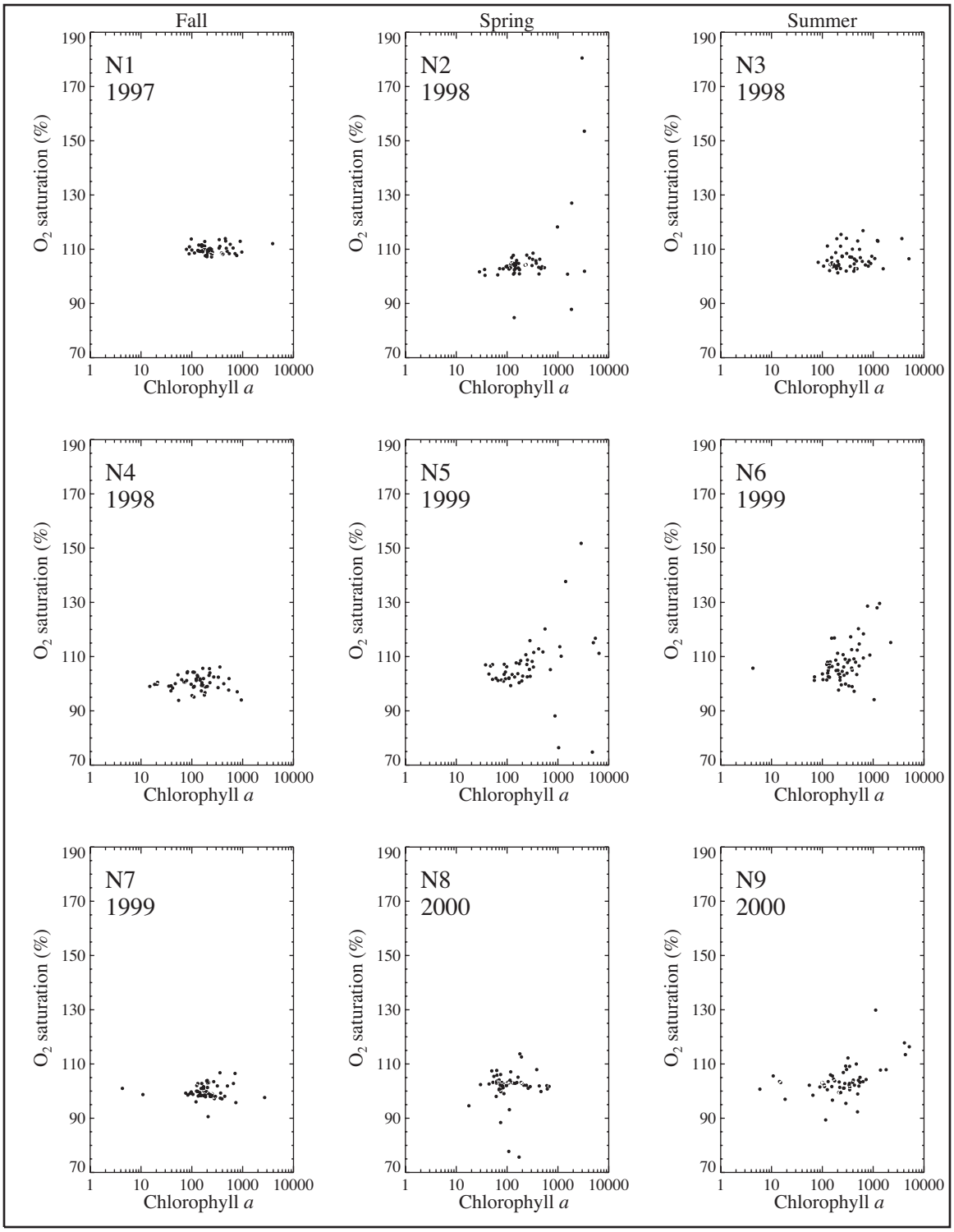

Figure 7.2-8. Near surface dissolved oxygen saturation (percent) versus chlorophyll *a* ($ng \cdot L^{-1}$) for fall, spring, and summer cruises in 1997-2000.

Table 7.2-1. Correlation coefficients for percent of surface oxygen saturation with surface salinity and surface chlorophyll *a* values over the Mississippi-Alabama shelf west of 87°W.

Cruise	Correlation coefficient	Significance level (%)
Percent surface oxygen saturation with surface salinity		
N1	-0.31	90
N2	-0.50	99.5
N3	-0.62	99.9
N4	0.32	90
N5	-0.30	90
N6	0.09	<50
N7	0.16	60
N8	0.21	70
N9	-0.73	99.9
Percent surface oxygen saturation with surface chlorophyll		
N1	-0.11	<50
N2	0.70	99.9
N3	0.60	99.5
N4	-0.38	90
N5	0.07	<50
N6	0.55	99
N7	-0.19	60
N8	0.13	<50
N9	0.54	99

7.3 Subsurface Oxygen Distributions on Selected Density Surfaces

On all the NEGOM cruises, sampling stations were co-located to provide repeat measurements, and water samples were taken on selected sigma-theta surfaces. The sigma-theta surfaces were, in $kg \cdot m^{-3}$: 24.6, 25.4 (associated with the salinity maximum of the Subtropical Underwater), 25.9, 26.2, 26.5 (associated with the oxygen maximum of the 18°C Sargasso Sea Water), 26.8, 27.0, 27.15 or 27.10 (associated with the oxygen minimum of the Tropical Atlantic Central Water), and 27.45 (associated with the salinity minimum of Antarctic Intermediate Water). To examine the general subsurface distributions of oxygen, measurements at each station made within bins centered on these sigma-theta surfaces were averaged over the nine cruises. The bin boundaries were set at the half-way point between adjacent sigma-theta surfaces (for example, the boundaries for σ_θ = 26.8 are 26.65 and 26.9). Standard deviations were determined. In Figures 7.3-1 through 7.3-5 are shown horizontal fields of the average (upper panel) and standard deviation (middle panel) on the near-surface, 25.4, 26.5, 27.15, and bottom sigma-theta surfaces; the number of data points for each station also are shown (lower panel).

Samples taken near-surface were on sigma-theta surfaces ranging from 23.4 to ~10 $kg \cdot m^{-3}$, with an average of 21.9 $kg \cdot m^{-3}$. On average, the near-surface oxygen values are high, 4.5 $mL \cdot L^{-1}$ or greater (Figure 7.3-1). The largest variability was over the Mississippi-Alabama shelf and likely

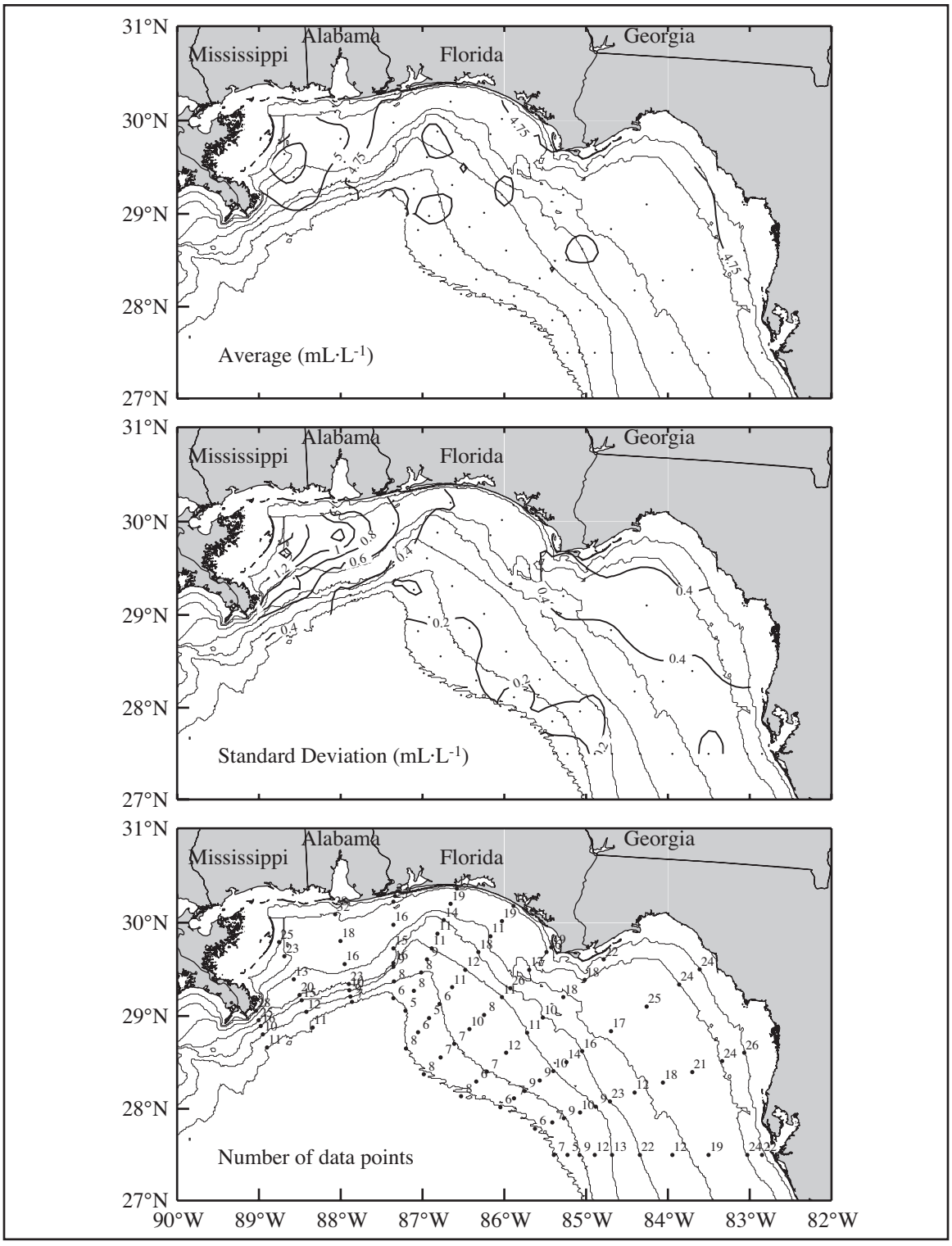

Figure 7.3-1. Mean and standard deviation of dissolved oxygen from nine cruises on an average sigma-theta of 22 kg·m^{-3}, which represents the average σ_θ for the near-surface samples. Number of observations are shown. Bathymetric contours given are 10, 20, 50, 100, 200, 500, and 1000 m.

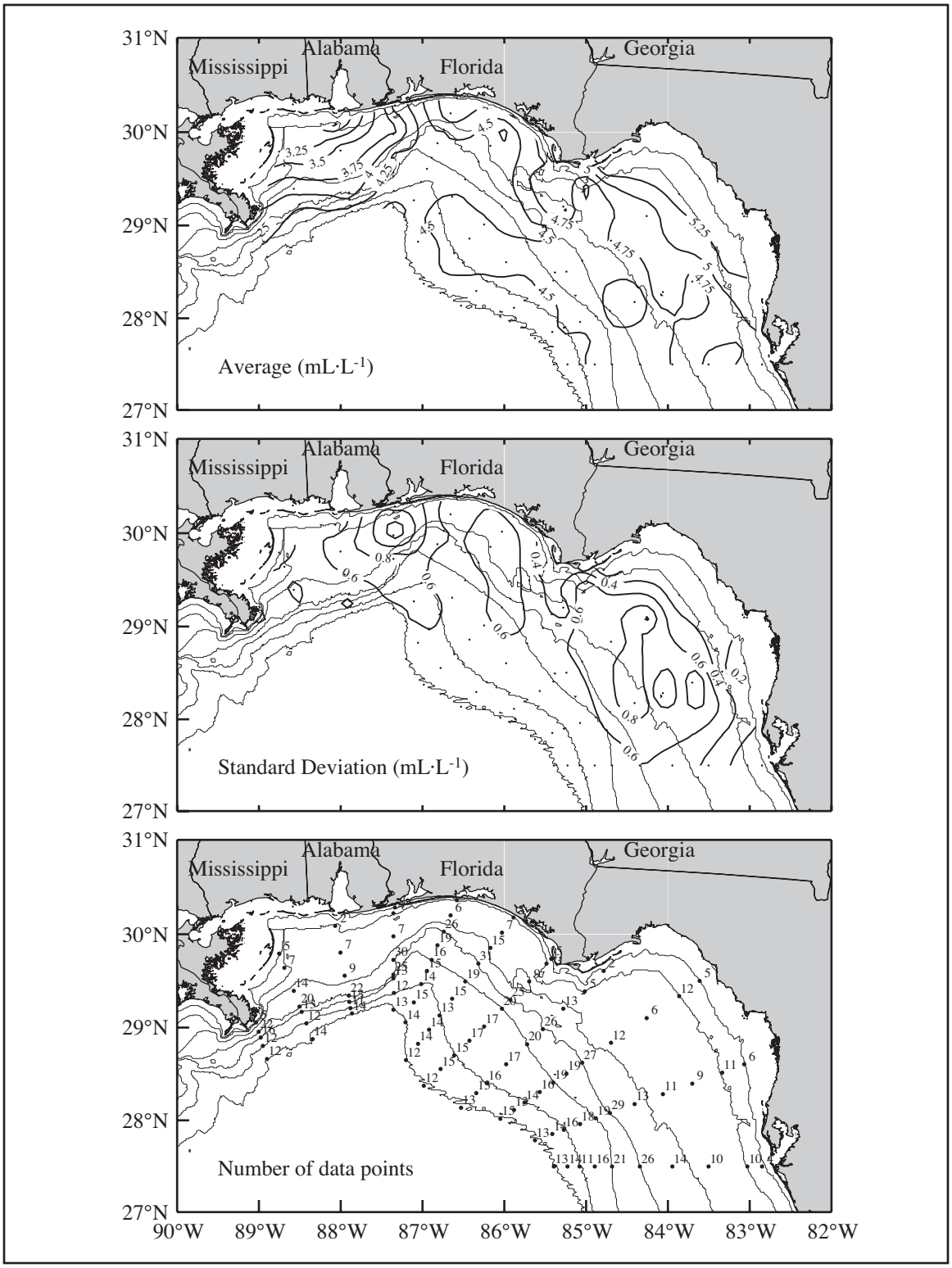

Figure 7.3-2. Mean and standard deviation of dissolved oxygen from nine cruises on an average sigma-theta level of 25.4 kg·m^{-3}. Number of observations are shown. Bathymetric contours given are 10, 20, 50, 100, 200, 500, and 1000 m.

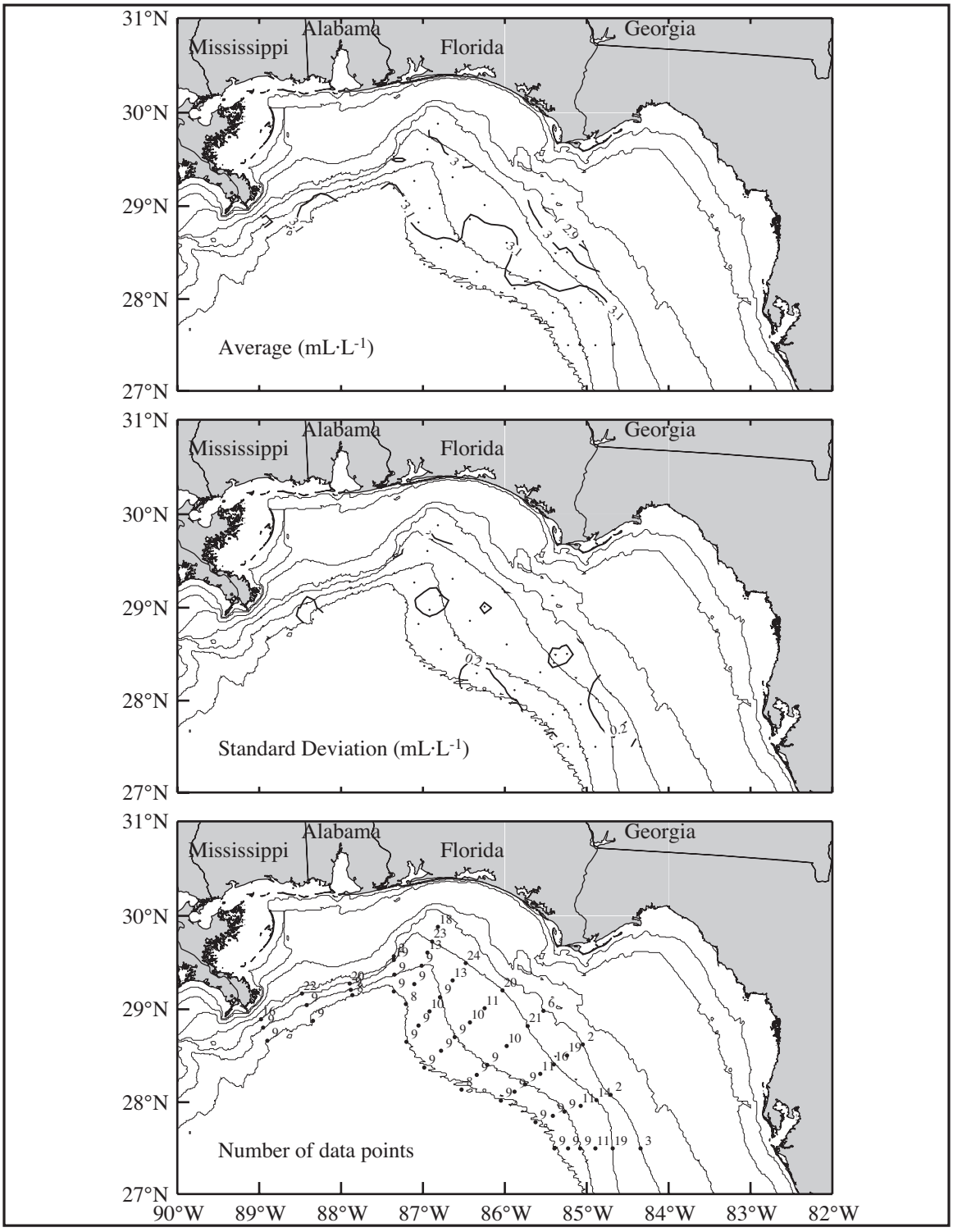

Figure 7.3-3. Mean and standard deviation of dissolved oxygen from nine cruises on an average sigma-theta level of 26.5 kg·m^{-3}. Number of observations are shown. Bathymetric contours given are 10, 20, 50, 100, 200, 500, and 1000 m.

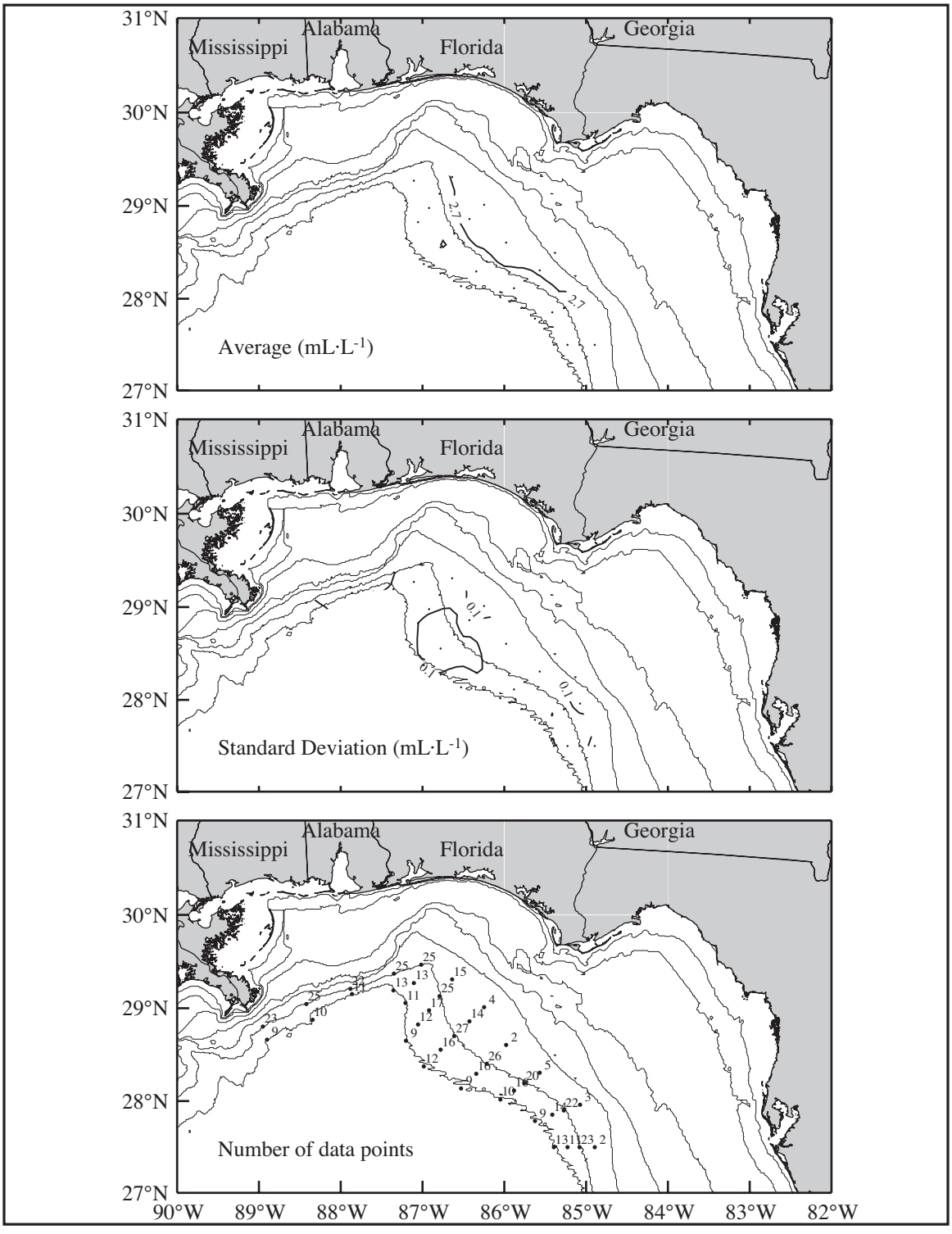

Figure 7.3-4. Mean and standard deviation of dissolved oxygen from nine cruises on an average sigma-theta level of 27.15 kg·m^{-3}. Number of observations are shown. Bathymetric contours given are 10, 20, 50, 100, 200, 500, and 1000 m.

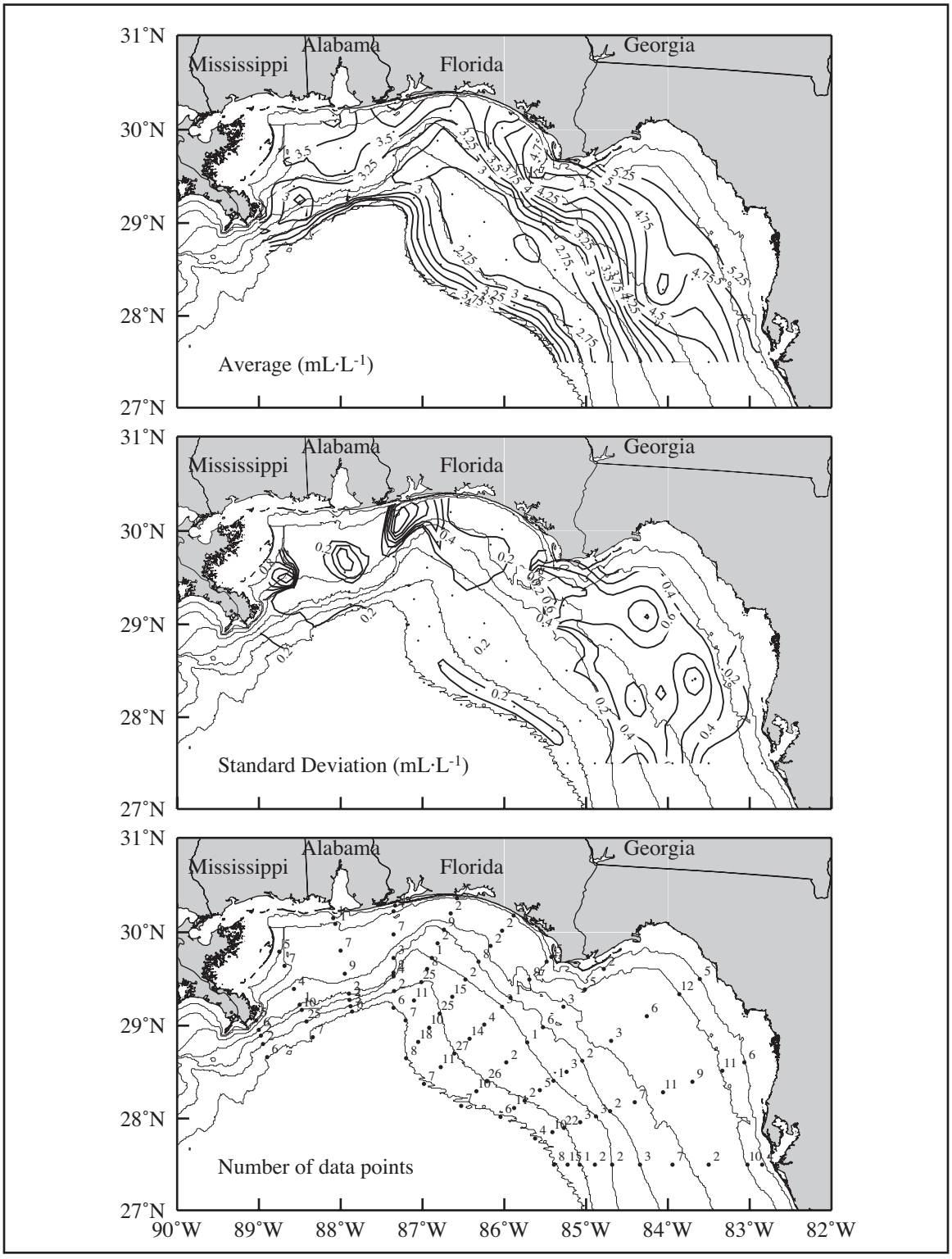

Figure 7.3-5. Mean and standard deviation of dissolved oxygen (mL·L^{-1}) from nine cruises at the bottom sigma-theta level for each station. Number of observations are shown. Bathymetry contours are 10, 20, 50, 100, 200, 500, and 1000 m.

due to variability in river discharge, which not only affects the oxygen solubility of the surface water, but also results in the wide range of near-surface sigma-theta values. Off shelf the standard deviation was approximately 0.2 $mL \cdot L^{-1}$.

The 25.4 $kg \cdot m^{-3}$ sigma-theta surface associated with the Subtropical Underwater has higher oxygen concentrations over the west Florida shelf than over the Mississippi-Alabama shelf (Figure 7.3-2). Inshore over the Big Bend region, oxygen concentrations on this sigma-theta surface exceed 5 $mL \cdot L^{-1}$ on average and decrease going offshore to the slope. Inshore off Mississippi and Chandeleur Sounds, oxygen concentrations are approximately 3.5 $mL \cdot L^{-1}$ on average and increase going offshore. In the vicinity of DeSoto Canyon average oxygen concentrations are fairly uniform across the shelf. Variability is approximately 0.6 $mL \cdot L^{-1}$ over most of the study area. On the 25.9 surface (not shown), the oxygen concentrations are 3-4 $mL \cdot L^{-1}$, less than those at the 25.4 surface, with typical standard deviations of 0.4-0.6 $mL \cdot L^{-1}$.

There is no relative maximum in vertical distribution of oxygen at the 26.5 sigma-theta surface associated with the 18°C Sargasso Sea Water. The oxygen concentrations on that surface are approximately 2.9-3.1 $mL \cdot L^{-1}$, being less near the 100-m isobath and more over the slope, with standard deviation of ~0.2 $mL \cdot L^{-1}$ (Figure 7.3-3). Although the oxygen concentrations on the 26.8 surface are generally lower, being ~2.8-2.9 $mL \cdot L^{-1}$, than those on the 26.5 surface, those on the 26.2 surface above are higher being ~3.1-3.2 $mL \cdot L^{-1}$ (not shown). The standard deviations on these surfaces decrease with depth.

There is an indication of a relative minimum in the vertical distribution of oxygen at the 27.15 sigma-theta surface associated with the Tropical Atlantic Central Water. Oxygen concentrations on that surface are ~2.7 $mL \cdot L^{-1}$ with standard deviation of 0.1 $mL \cdot L^{-1}$ (Figure 7.3-4). Concentrations on the 27.0 surface above are slightly higher at ~2.8-2.9 $mL \cdot L^{-1}$, and those on the 27.45 surface below also are higher at > 3.2 $mL \cdot L^{-1}$ (not shown).

Average oxygen concentrations of the bottom-most samples are shown in Figure 7.3-5. There is an oxygen minimum approximately between the 200- and 500-m isobaths. Oxygen concentrations at the bottom in the Big Bend region are higher than concentrations at comparable depths on the Mississippi-Alabama shelf. This likely reflects the greater oxygen concentrations of that region in the surface waters. Variability is highest in the shallow waters and low off the shelf, with the exception of the region southeast of the Mississippi Delta.

7.4 Bottom Oxygen Distributions and Incidences of Hypoxia

Bottom distributions of dissolved oxygen were examined using the deepest bottle oxygen measurement at each station. The distributions for spring, summer, and fall cruises are shown in Figures 7.4-1, 7.4-2, and 7.4-3, respectively. Evident in all seasons is the oxygen minimum associated with the Tropical Atlantic Central Water located generally between the 200- and 500-m isobaths and the increase in oxygen concentration below 500 m. Over the shelf, the spring cruises are characterized by higher bottom oxygen concentrations on cruises with less overlying low salinity water (Figure 7.4-1). Cruise N2, which has more overlying low salinity water than the other spring cruises (Figure 7.2-2), has the lowest oxygen values. In general, the concentrations over the west Florida shelf are higher than over the Mississippi-Alabama shelf. Cruise N8, which not only has the least overlying low salinity water but also is earlier in the season, has the highest concentrations over the shelf, with the isolines approximately paralleling the isobaths over the entire shelf. This distribution is similar to the distribution in fall (Figure 7.4-3). The bottom oxygen concentrations over the shelf on the summer cruises are generally lower than those of the spring cruises (Figure 7.4-2). Values over the west Florida shelf typically are higher than over the Mississippi-Alabama shelf at comparable isobaths.

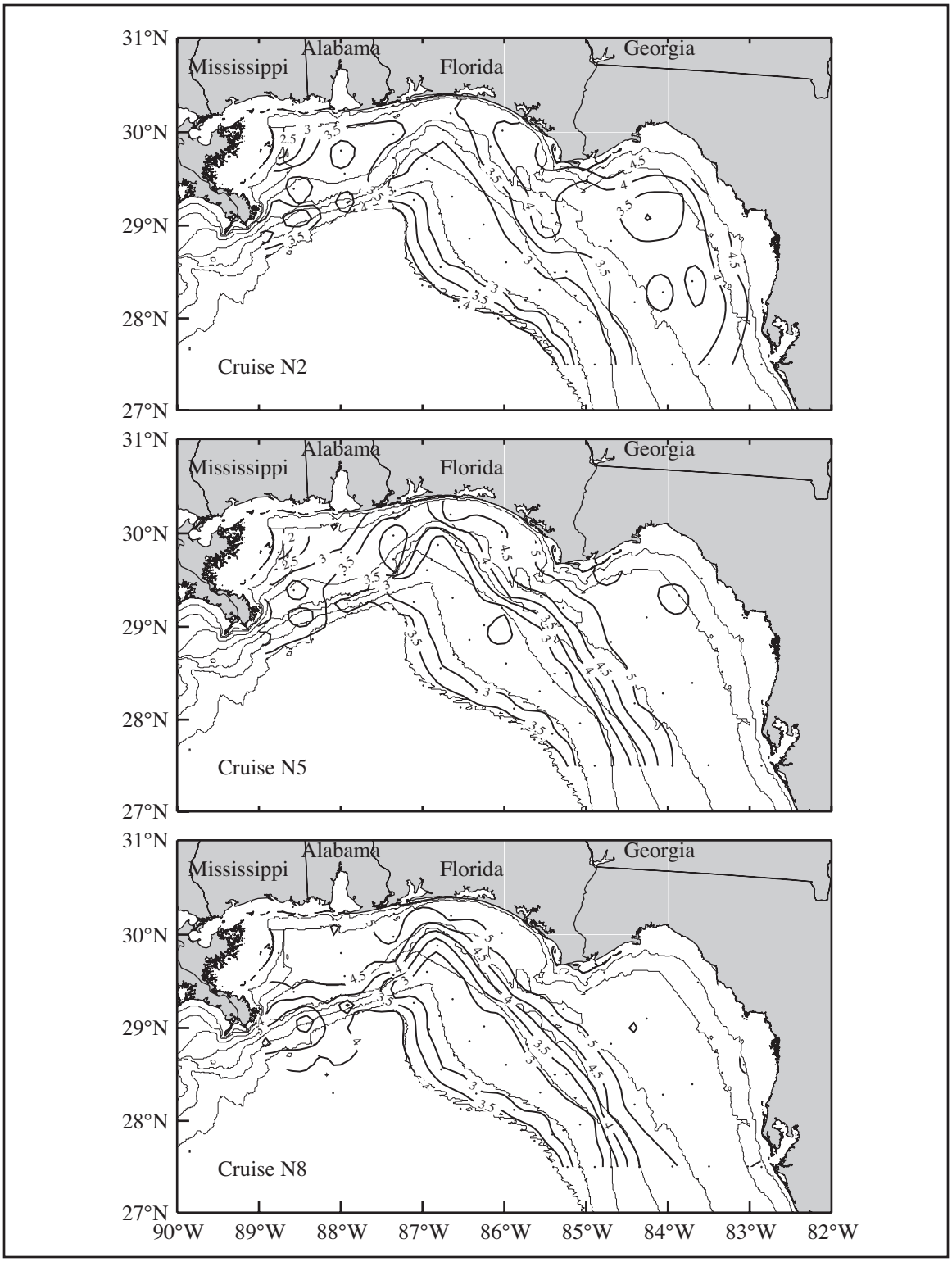

Figure 7.4-1. Bottom dissolved oxygen ($mL \cdot L^{-1}$) from spring cruises N2 (May 1998), N5 (May 1999), and N8 (April 2000). Bathymetric contours shown are 10, 20, 50, 100, 200, 500, and 1000 m.

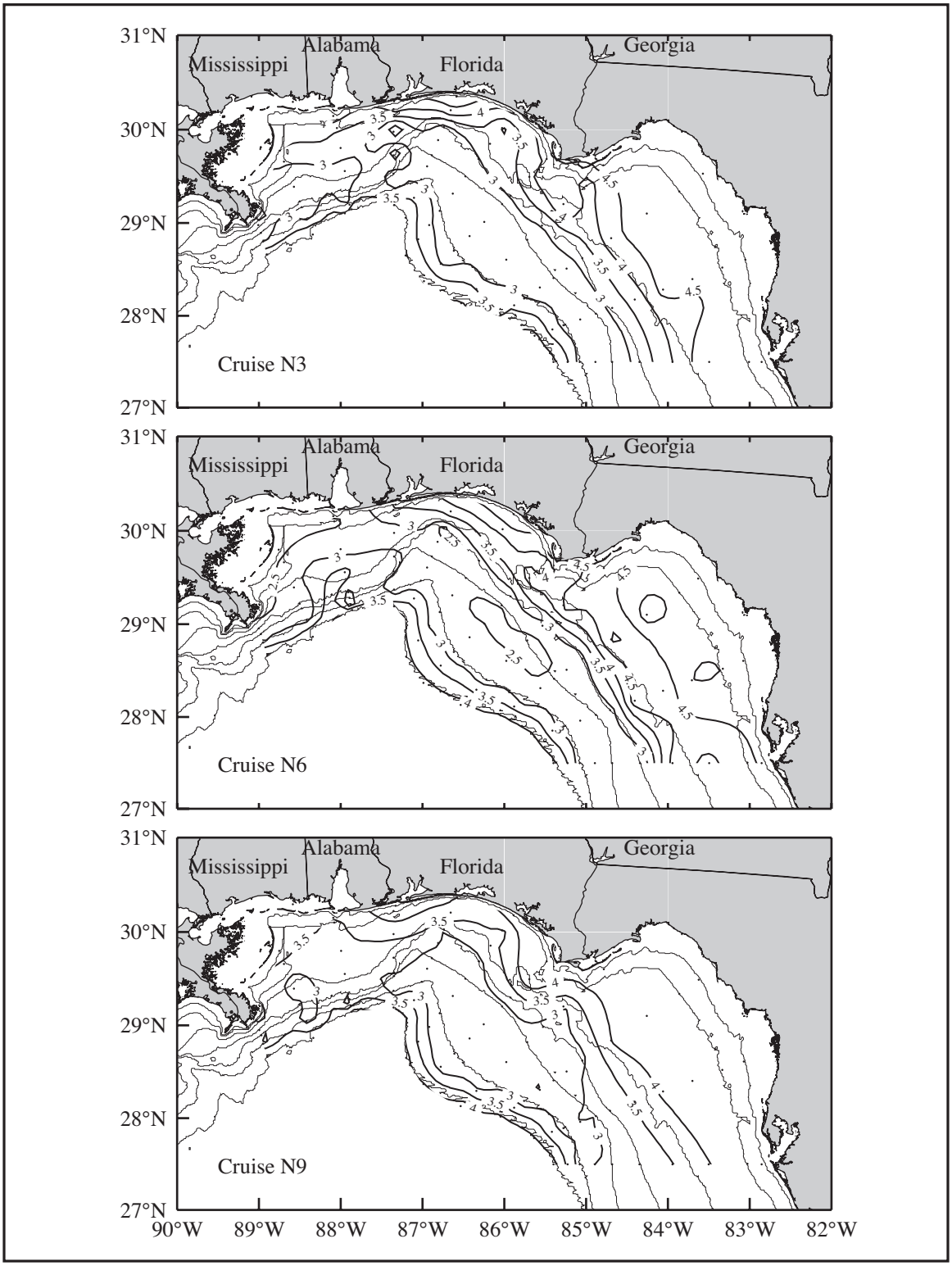

Figure 7.4-2. Bottom dissolved oxygen ($mL \cdot L^{-1}$) from summer cruises N3 (July/August 1998), N6 (August 1999), and N9 (July/August 2000). Bathymetric contours shown are 10, 20, 50, 100, 200, 500, and 1000 m.

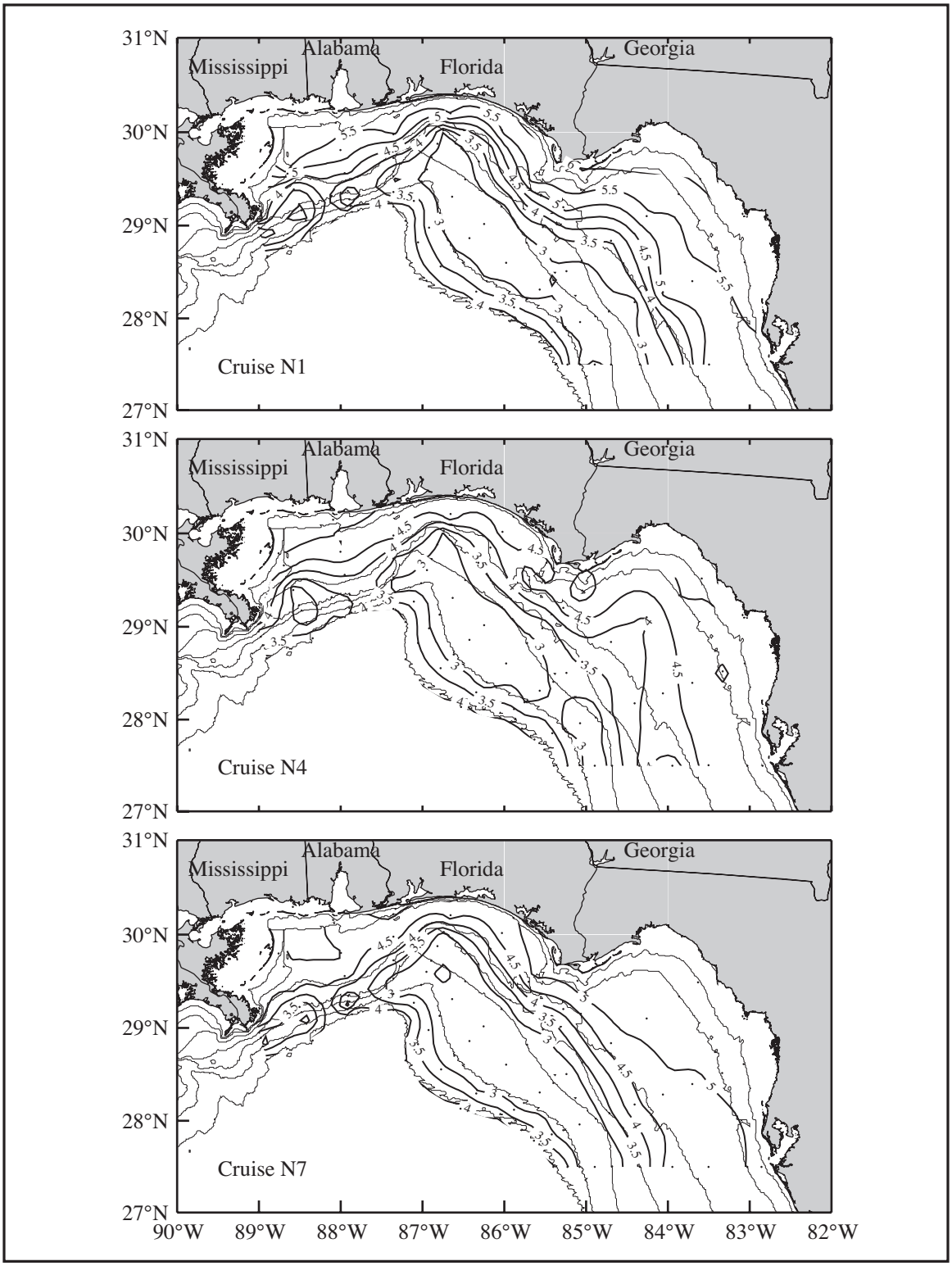

Figure 7.4-3. Bottom dissolved oxygen ($mL \cdot L^{-1}$) from fall cruises N1 (November 1997), N4 (November 1998), and N7 (November 1999). Bathymetric contours shown are 10, 20, 50, 100, 200, 500, and 1000 m.

Unlike the Louisiana shelf, incidences of hypoxia over the NEGOM study area are not well-documented, although Schroeder (1977) noted that in 1973 bottom oxygen concentrations off Mobile Bay decreased as flooding of the Mobile Bay river system progressed, reaching saturation levels as low as 30%. To examine the possible occurrence of hypoxia in the study area, the bottom distributions of dissolved oxygen were examined. The ranges and spatial means of dissolved oxygen measurements for the cruises are given in Table 7.4-1. Hypoxic waters are considered to be those with oxygen concentrations of 1.4 $mL \cdot L^{-1}$ (2 $mg \cdot L^{-1}$) or less (Nowlin et al. 1998a; Rabalais et al. 1999). By this definition, no hypoxic waters were observed during the NEGOM cruises, although near hypoxic water (1.5 $mL \cdot L^{-1}$) was seen at the innermost station of Line 2 off Chandeleur Sound on spring cruise N5. Minimum oxygen concentrations (2.1-2.3 $mL \cdot L^{-1}$) also were located there during spring cruise N2 and summer cruise N6. The minimum on summer cruise N3 (1.9 $mL \cdot L^{-1}$) was near the 30-m isobath on Line 3. All other minima were in deeper water.

Because stratification can affect the re-supply of oxygen from the surface to depth, it can facilitate the formation of hypoxia. In summer, the stability is expected to be higher than in other seasons because of reduction in wind stress and the seasonal thermocline. Additionally, high river discharge can add to increased stratification. The relationship between water column stratification and bottom oxygen values is examined using stability computed by

$$Stability = \frac{\sigma_{\theta_{bottom}} - \sigma_{\theta_{surface}}}{water\ \ depth},$$

where values were not normalized by density. Figures 7.4-4 and 7.4-5 show the percent bottom oxygen saturation versus stability for the fall, spring, and summer cruises in 1997-2000. Data are presented as west and east regions relative to the 87°W longitude line, with stations west of and including 87°W being the west region (Figure 7.4-4).

The distributions indicate three basic patterns. The first consists of a hook-shaped distribution with stability values centered near 0.01 $kg \cdot m^{-4}$ and oxygen saturation values centered near 50%. This pattern occurs at the deeper stations on the outer shelf and slope. It

Table 7.4-1. Bottom bottle dissolved oxygen measurements.

Cruise, Year	**Range of bottom values** ($mL \cdot L^{-1}$)	**Spatial average** ($mL \cdot L^{-1}$)
Spring cruises		
N2, 1998	2.116 to 5.286	3.493
N5, 1999	1.495 to 5.449	3.610
N8, 2000	2.436 to 5.602	3.952
Summer cruises		
N3, 1998	1.895 to 5.003	3.441
N6, 1999	2.296 to 5.174	3.346
N9, 2000	2.472 to 4.502	3.418
Fall cruises		
N1, 1997	2.699 to 6.134	3.938
N4, 1998	2.575 to 5.313	3.720
N7, 1999	2.538 to 5.310	3.765

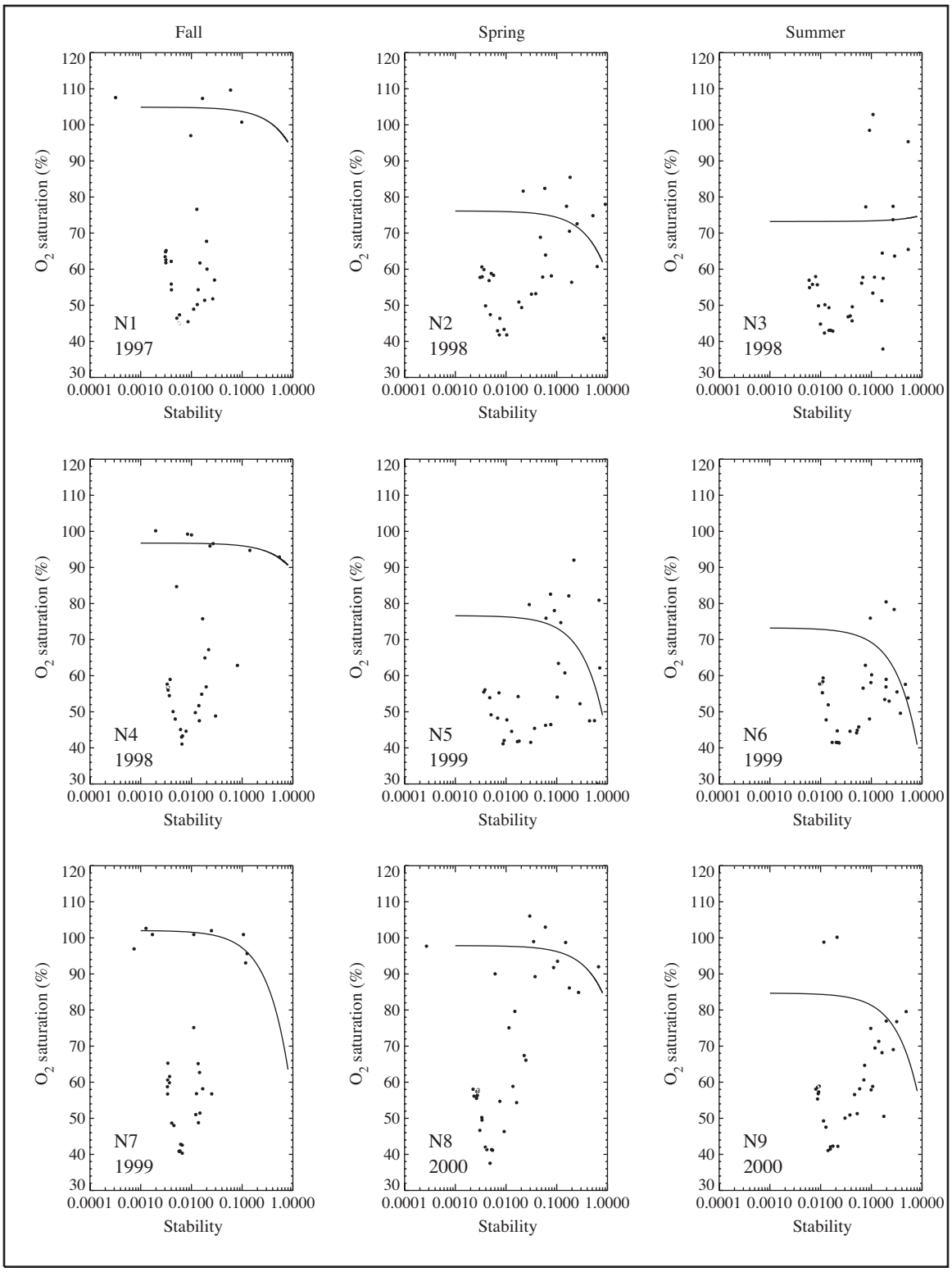

Figure 7.4-4. Percent dissolved oxygen saturation versus stability ($kg \cdot m^{-4}$) near bottom over the shelf west of 87°W for fall, spring, and summer cruises. A linear fit is drawn through stations in water depths of 50 m or less.

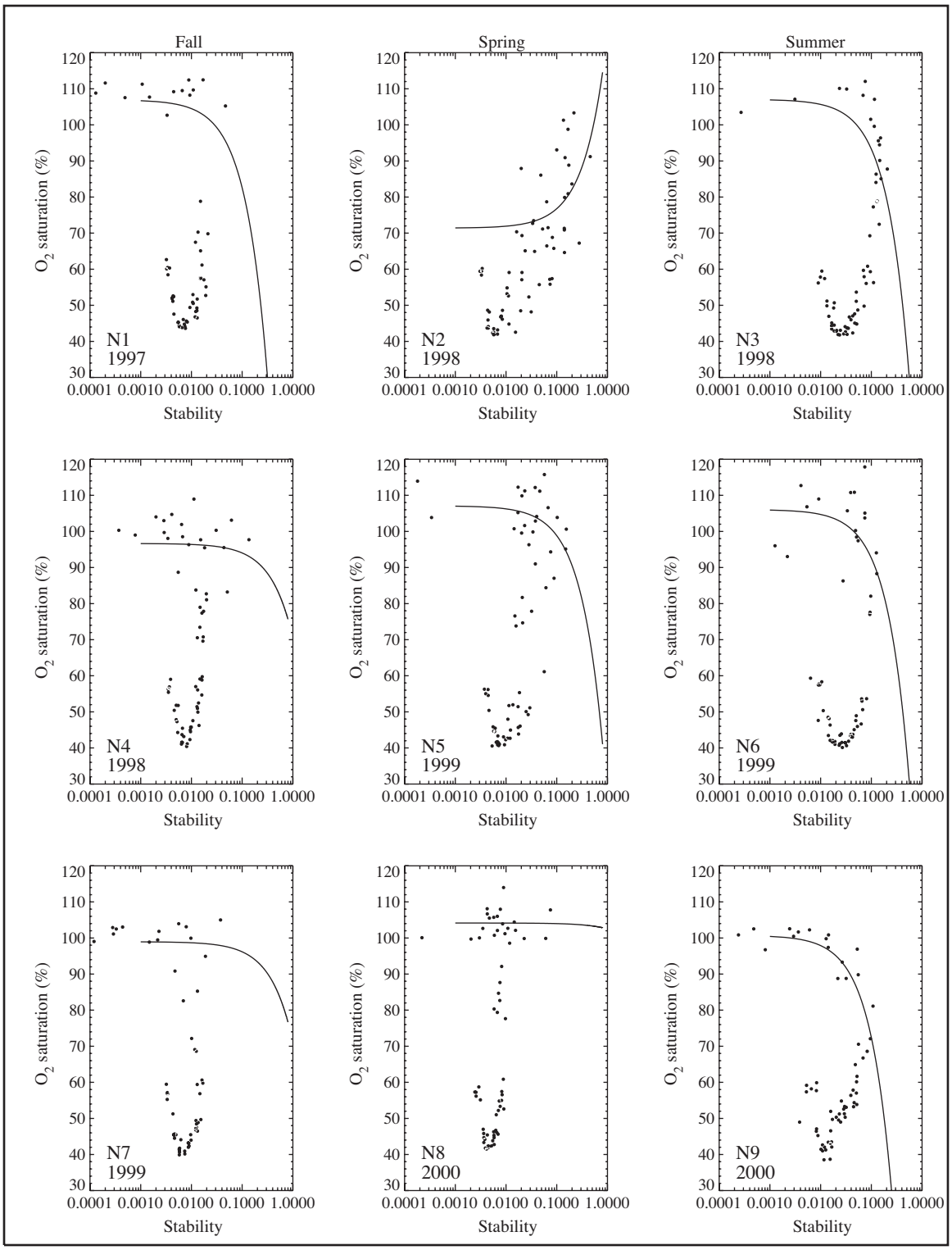

Figure 7.4-5. Percent dissolved oxygen saturation versus stability ($kg \cdot m^{-4}$) near bottom in all water depths over the shelf east of 87°W for fall, spring, and summer cruises. A linear fit is drawn through stations in water depths of 50 m or less.

is seen in both the east and west regions and in all three seasons. It is very similar to the pattern seen over the outer shelf and slope in the northwestern Gulf during LATEX (Nowlin et al. 1998a).

The second pattern, which also occurred in the northwestern Gulf, is best seen in the fall cruises, which had very little highly stratified water. It consists of stability values ranging from low (<0.001 $kg \cdot m^{-4}$) to high (>0.1 $kg \cdot m^{-4}$) and near bottom oxygen saturation values centered about 100%. This pattern occurs at stations located over the inner shelf. In fall, the waters at these shallow depths are relatively well-oxygenated by the wind-driven mixing that occurs to near bottom. This pattern is less apparent or absent in the spring and summer cruises, when mixing to near bottom is reduced. It is more apparent in the region east of 87°W during both spring and summer, than in the region west of 87°W. Indeed in the western region it is only the 2000 spring cruise, which occurred early in the spring season and had less influence from river discharge, that shows the second pattern. The difference in the prevalence of this second pattern between east and west is indicative of the influence of the larger quantities of river water over the western region during spring and summer.

The third pattern consists of high stability values, defined here as a stability of ≥0.1 $kg \cdot m^{-4}$, over a wide range of bottom oxygen saturation values (30-110%). This pattern occurs during spring and summer cruises over both the eastern and western regions. The saturation values of this pattern in the eastern region range from approximately 65% to 110%, while those in the western region are lower. In general, the stations with high stability were located in water depths of 50 m or less.

The linear fit of stability with saturation percentage for stations in water depths of 50 m or less are shown on the figures (note: this fit does not include the stations deeper than 50 m that are shown on the figures and are part of the "hook" feature). Associated with these fits are correlations, which are negative except for summer cruise N3 in the west and spring cruise N2 in the east. With three exceptions, the squared correlations are not significant at the 95% level. In the east, the only significant correlations were the summer cruises N3, with an R^2 of 0.24, and N9, with an R^2 of 0.64. In the west, the only significant correlation was the fall cruise N7 with an R^2 of 0.63. These results are consistent with the wide range of saturation values associated with the high stability values in spring and summer and with the well-mixed waters in fall.

To examine whether there was an enhanced flux of organic material to the bottom that resulted in oxygen depletion from decomposition, the nitrate versus bottom oxygen saturation percents were considered. Figure 7.4-6 shows this relationship for all bottom stations over the study area in the fall, spring, and summer cruises of 1997-2000. The basic pattern is of an increase in bottom nitrate concentrations from shallow stations (nearly 100% saturation) to deep stations (40-50% saturation) and then a decrease in nitrate associated with the increased saturation of the waters below 500 m. The correlation coefficients between bottom nitrate concentration and percent bottom oxygen saturation over the shelf west of 87°W are shown in Table 7.4-2. They are negative, reflecting the general increase of nitrate as saturation decreases. All are significant at the 95% level and all have an R^2 greater than 0.5. The correlations over the east shelf (not shown) are similarly high, negative, and significant.

At some shallow stations, there was enhanced nitrate concentration (2-10 μM) with reduced saturation (40-60%). This is most prevalent on the spring cruises conducted in May (N2 and N5), but not that conducted in April (N8); it is less prevalent on summer cruises. Note that it is in spring, not summer, that the fresh water from the Mississippi and other rivers is spread most broadly over the inner shelf and thereby more greatly contributes to the stability. In

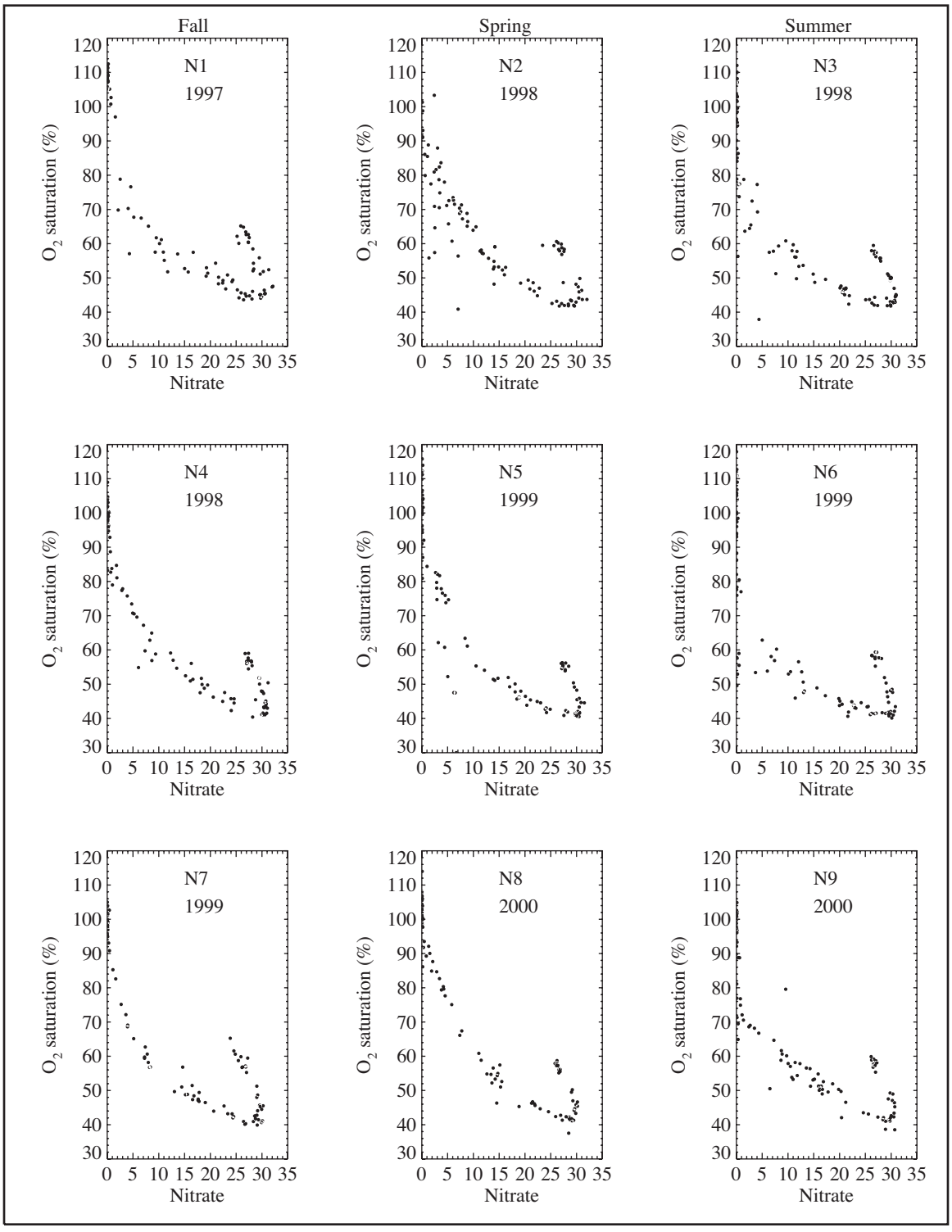

Figure 7.4-6. Percent dissolved oxygen saturation versus nitrate (μM) near-bottom for fall, spring, and summer cruises in 1997-2000.

contrast, over the northwest (Texas-Louisiana) shelf, the enhanced nitrate associated with reduced oxygen saturation at shallow stations was most prevalent on the three summer cruises (as well as one of three spring cruises) when the low salinity water associated with the Mississippi-Atchafalaya Rivers was pooled over the Louisiana shelf and hypoxia occurred. This difference between the northwest and northeast Gulf shelves suggests that the opportunity for occurrence of hypoxia over the northeast shelf is less than that of the northwest shelf because of the different timing of the greatest presence of the freshwater from river discharge over the shelf.

Table 7.4-2. Correlation coefficients for percent bottom oxygen saturation with bottom nitrate concentrations over the shelf west of 87°W.

Cruise	Correlation coefficient	Significance level (%)
N1	-0.85	99.9
N2	-0.74	99.9
N3	-0.69	99.9
N4	-0.88	99.9
N5	-0.68	99.9
N6	-0.59	99.9
N7	-0.87	99.9
N8	-0.91	99.9
N9	-0.77	99.9

8 NUTRIENTS

The distributions and variability of the nutrients, as well as processes affecting them, on each of the NEGOM cruises are discussed in Appendices A through I. In this section, a description of the basic vertical distribution and the average seasonal inventories and variability of nitrate, phosphate, and silicate will be examined.

8.1 Basic Vertical Profiles of Nutrients

The vertical distributions of nutrients in the Gulf of Mexico follow the general pattern of very low concentrations in the upper tens of meters, associated with the euphotic zone and the efficient utilization of nutrients there by phytoplankton, and gradually increasing values with increasing depth, associated with oxidation of detritus. Off the shelf, where water depths exceed 600 m, there is a maximum in nitrate and phosphate at depths of 600-900 m that is associated with the Antarctic Intermediate Water, which enters the Gulf with the Loop Current. A silicate maximum may occur deeper than 800 m. The basic pattern in the euphotic zone can be altered if the sampling station is in close proximity to the source of river discharge into the ocean, or if dynamic processes cause uplift of isopycnals bringing nutrients into the photic zone. In such situations, nutrient concentrations can be non-negligible in near-surface waters.

Figure 8.1-1 gives example vertical profiles of nitrate, phosphate, and silicate from two stations sampled on cruise N5 in May 1999. Station 49 is on line 7 and station 98 is on line 1; both are located along the 1000-m isobath (see also Figure E.3-4). The nutrient data from these stations show the general pattern of increasing nutrient concentrations with increasing depth and the maximum in nitrate and phosphate at about 750 m. In the upper 75 m, however, the patterns of the two stations are different, with that at station 49 reflecting the usual very low nutrient concentrations in the euphotic zone. Station 98, however, is in close proximity to the mouth of the Mississippi River, which in 1999 had relatively high levels of discharge prior to the cruise. This station shows the strong influence of river discharge in the form of very high nutrient concentrations at the surface. This example is unusual in that the concentrations were extremely high and wide-spread over the western two lines (see Figures E.3-4, E.3-7, and E.3-8).

Nutrients are non-conservative in the upper water column due to biological activity. Below 150 m, however, there is no light for photosynthesis, and nutrients are not consumed. Although nutrient increases can result from microbial decomposition of organic material, property-property plots of nutrients versus salinity show the generally conservative nutrient behavior below the photic zone. This is seen in Figure 8.1-2 which shows the property-property plots of nitrate, phosphate, and silicate versus salinity for all water samples taken on NEGOM cruises at or below 150 m depth. The squared correlation coefficients, shown on each plot, are high, exceeding 0.85. The correlations, all of which are significant at 99.9%, are negative indicating that generally as salinity decreases, nutrient concentration increases. Note, however, that although the relationship is approximately linear for salinities greater than 35, it is not linear over the entire range of salinities measured. Linear fits are shown for the nitrate and phosphate versus salinity plots, and the slopes of these fits are given. A cubic fit is shown for the silicate-salinity plot, although the linear correlation coefficient is given. The banding seen in the plots reflects the strategy of sampling on density surfaces. The squared correlations for samples above 150 m are less than 0.1, which is consistent with the non-conservative nature of nutrients in the euphotic zone.

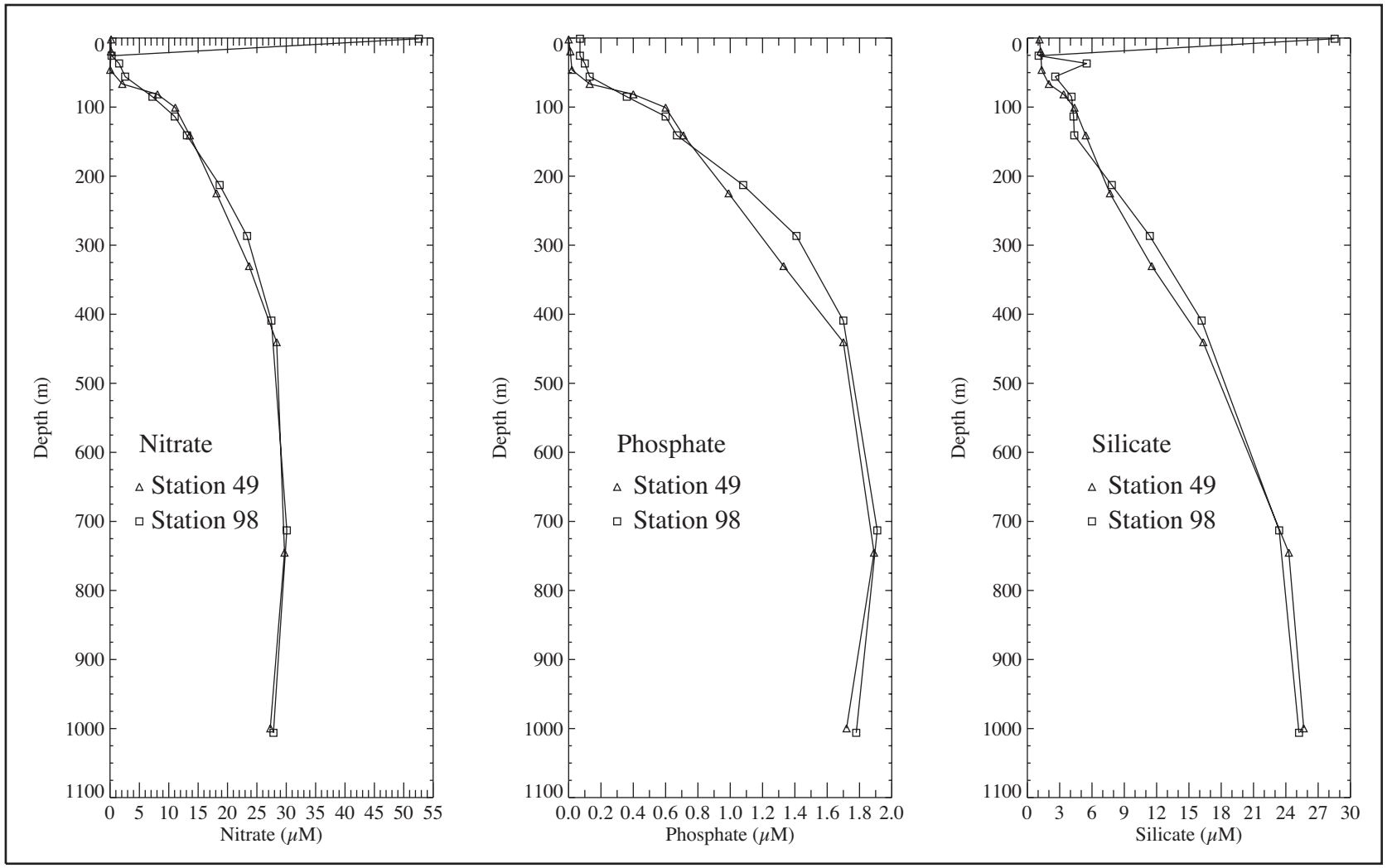

Figure 8.1-1. Example profiles of nitrate, phosphate, and silicate showing influence of river water on surface concentrations. Data are from stations 49 (triangle) and 98 (square) on cruise N5 in May 1999, along the 1000-m isobath on lines 7 and 1, respectively. Station 98 shows the influence of river water.

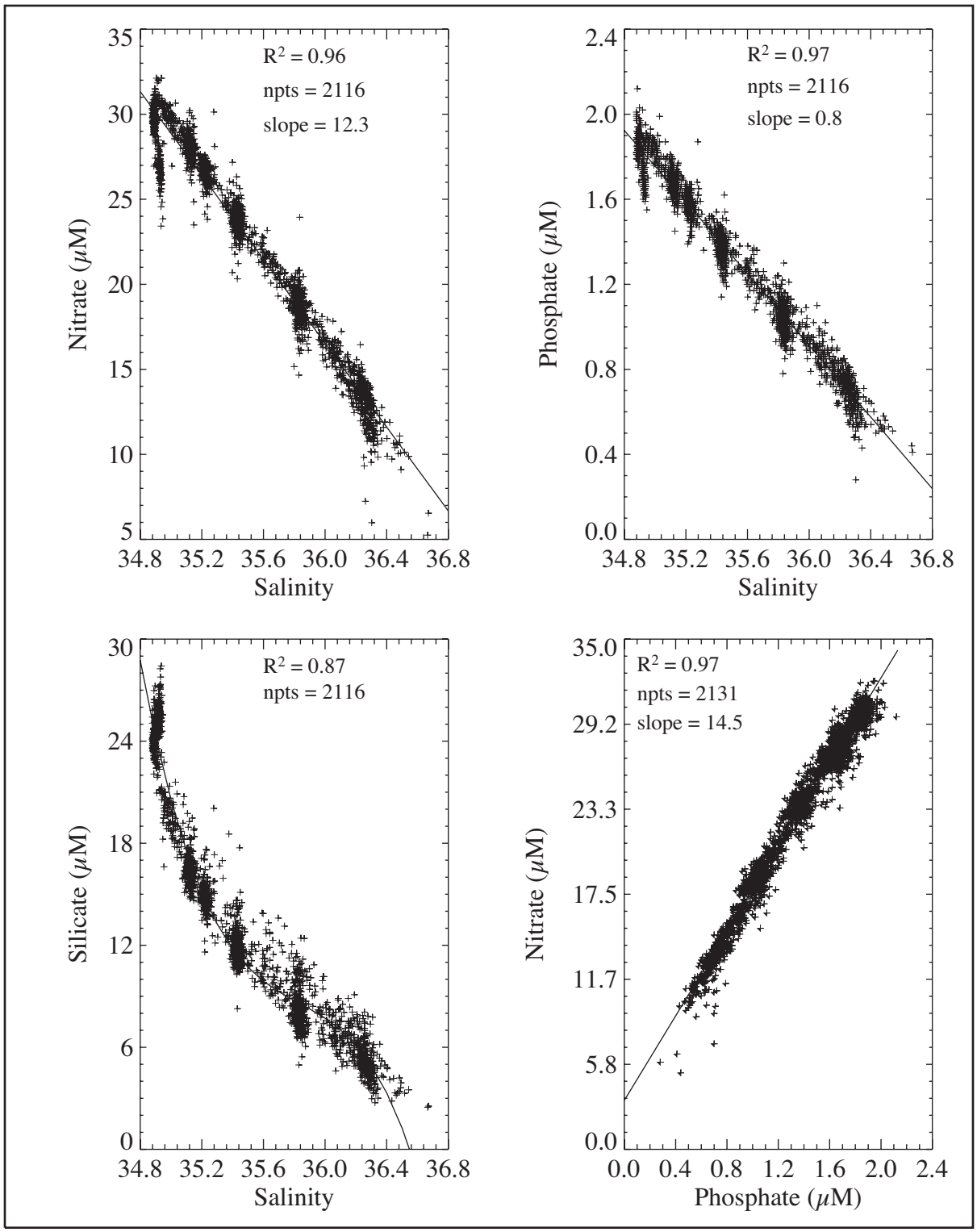

Figure 8.1-2. Nutrients versus salinity and nitrate-phosphate property plots for data below 150 m on all NEGOM cruises. The linear fits and associated slopes are shown for nitrate and phosphate; a cubic fit is shown for silicate.

The nitrate-phosphate relationship is approximately linear throughout the water column below 150 m (Figure 8.1-2, lower right). The squared correlation coefficient is 0.97 and significant at the 99.9% level. The correlation is positive, indicating that phosphate increases as nitrate increases. The slope of the linear equation for these data is 14.5, which is close to the classical N:P Redfield ratio of ~16 for marine organic material. This suggests that the nutrient data are of high quality. For the waters above 150 m, the squared correlation coefficient is 0.87, and the correlation also is positive.

8.2 Seasonally Averaged Nutrient Concentrations

Because phytoplankton growth is dependent on nutrient availability, average concentrations of nitrate, phosphate, and silicate near surface were examined by season. Each cruise repeated the stations on the eleven cross-shelf lines and sampled from the same available sigma-theta surfaces, as well as at the top, bottom, and chlorophyll maximum. Thus, there generally are three realizations at every station for the spring, summer, and fall seasons. One caveat to bear in mind is that this sample size of three per season is extremely small, and so patterns based on this sample size likely reflect the interannual variability more than the seasonal patterns.

As discussed in section 8.3, below a σ_θ surface of approximately 26.2 $kg \cdot m^{-3}$ (corresponding to an average depth of ~120 m), the seasonally averaged subsurface nutrient concentrations typically have variances that are less than 20% of the mean. Thus, if the density surface of the subsurface sample is known, a reasonable estimate of the nutrient concentration is known. Higher in the water column, however, the variance tends to be equal to or greater than the mean.

The variability is greatest near-surface. So, to examine seasonal averages and variability, we considered the data within the upper 5 m. The stations for the nine cruises first were grouped for display of the results. This was done by numbering the standard stations sequentially inshore to offshore from line 1 to line 11, beginning with the inner station on line 1. Figure 8.2-1 shows the numbering scheme. For each station, data within the upper 5 m were averaged over the three cruises of each of season. Typically, there were 3-4 data points at each station for computation of the seasonal mean in the upper 5 m. Data from cruises N1, N4, and N7 were used for the fall season; data from cruises N2, N5, and N8 for the spring; and data from cruises N3, N6, and N9 for the summer. Plots then were made of the seasonal mean nutrient concentrations versus the station numbers. Stations that were at or inshore of the 50-m isobath are marked on the figures by a solid circle enclosed by an open square.

Nitrate seasonal mean concentrations are highest on lines 1 and 2 (stations 1 through 12) and low on lines 3-11 in all three seasons (Figure 8.2-2; spring is the top panel, summer the middle, and fall the bottom). Lines 1 and 2 are in closest proximity to the mouth of the Mississippi River, which is the major source of nitrate to the Gulf. In spring on lines 1 and 2 and in fall on line 1, the variability between years is high, with standard deviations ranging from 4 to 46 μM in spring and 4 to 18 μM in fall at the inner three stations. For the majority of stations on lines 1-3, the standard deviation exceeds the mean in spring. This high variability is due in part to the unusually high nitrate concentrations observed on cruise N5. These concentrations were given particular scrutiny during the QA/QC process because of their unusual levels. Rabalais et al. (1999) summarized nearly 40 years of nitrate data for the lower Mississippi in their figure 18-6; they showed nitrate concentrations in the 1990s of order 100 μM. Thus, it is likely that cruise N5 fortuitously occurred when a pulse of high river discharge first reached the NEGOM shelf and nitrate had not yet all been consumed by

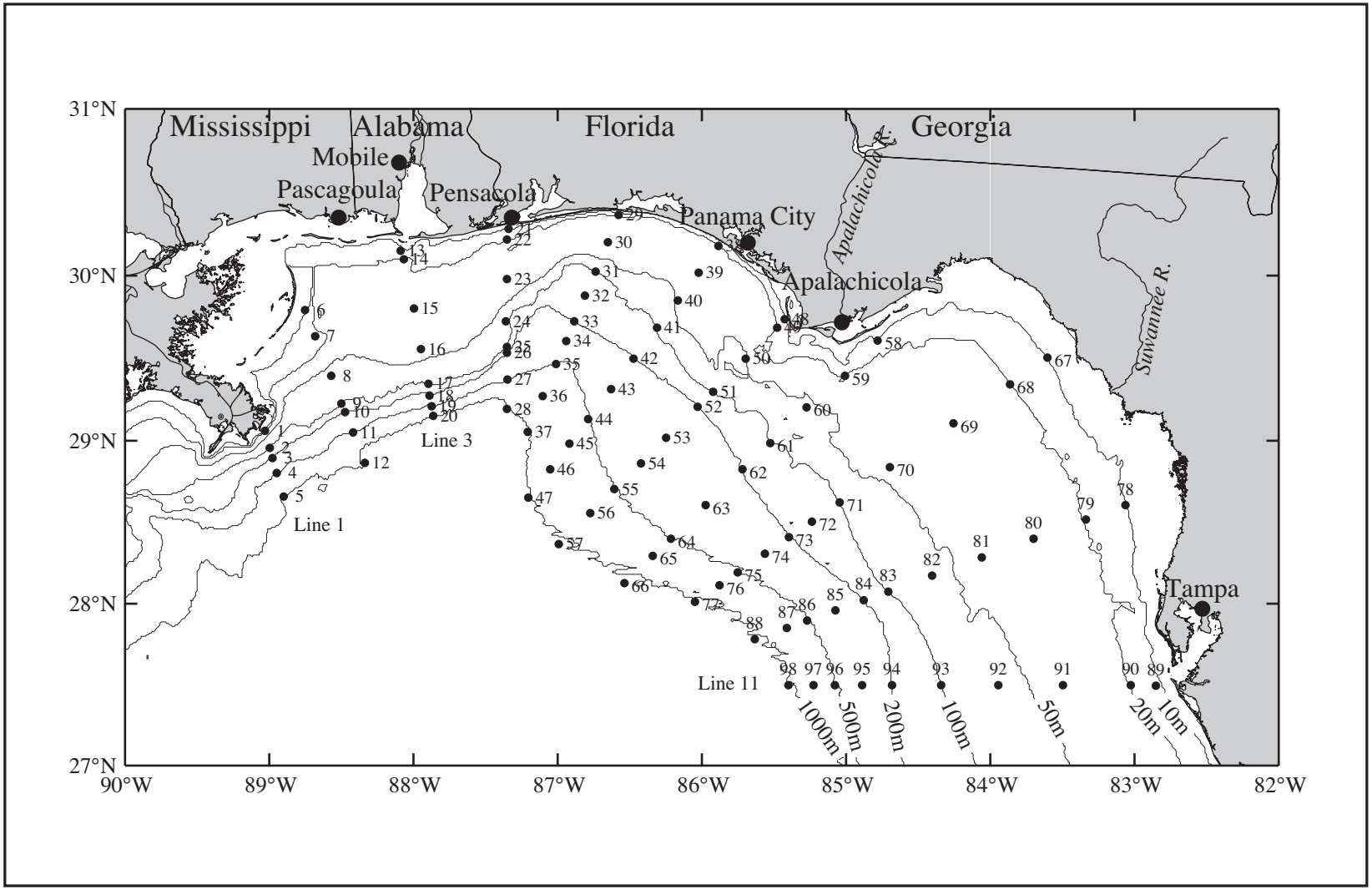

Figure 8.2-1. Sequential numbering of stations used in presenting average nutrient concentrations.

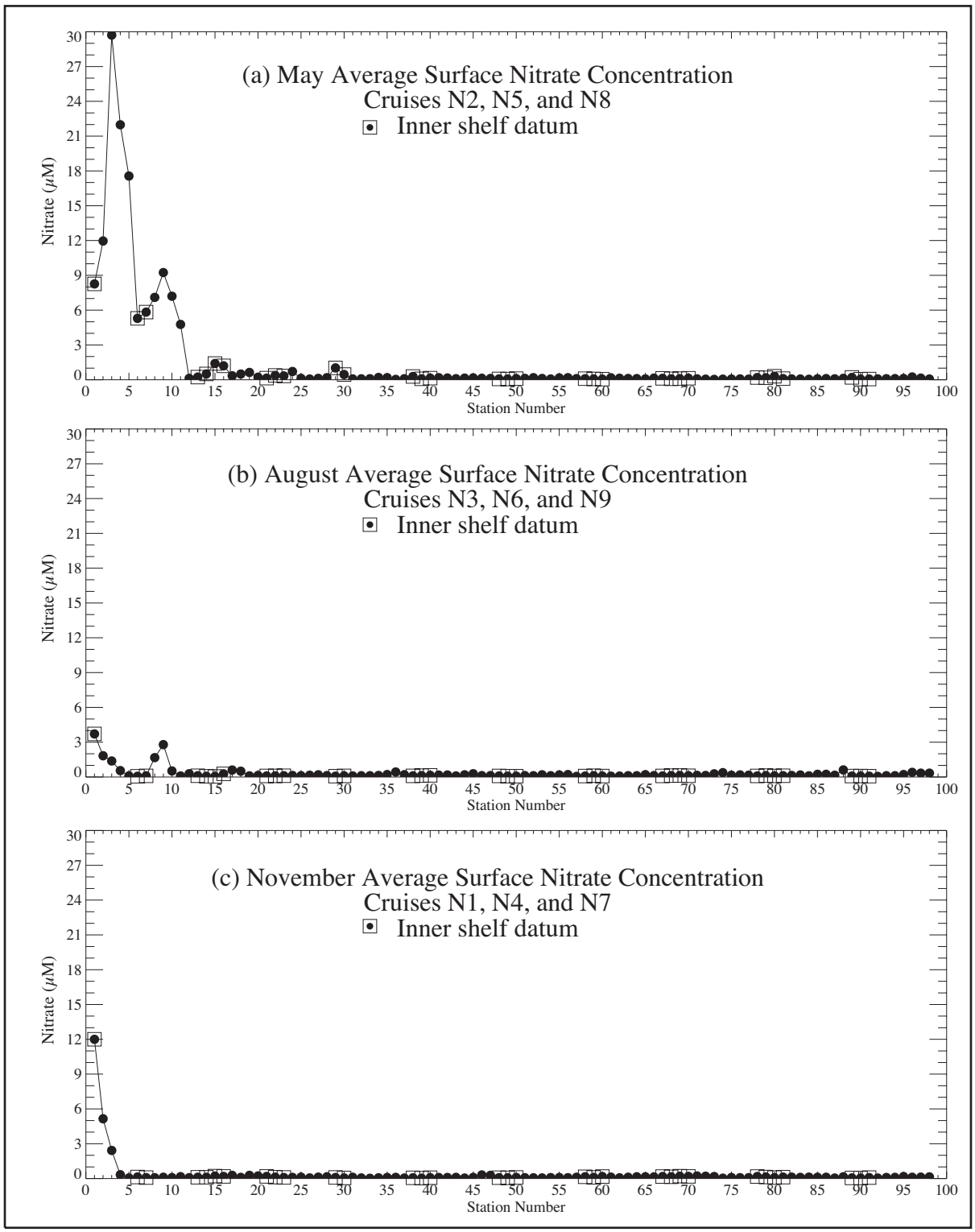

Figure 8.2-2. Seasonal average surface nitrate concentrations plotted by station number (see Figure 8.2-1) for all (a) spring, (b) summer, and (c) fall NEGOM hydrography cruises.

the phytoplankton. Variability in summer on lines 1 and 2 is less than in spring or fall, with highest standard deviation being ~4 μM at the innermost station on line 1.

In spring, stations on lines 3-4 have elevated mean nitrate concentrations relative to lines 6 through 11, which have low mean concentrations of less than approximately 0.3 μM (Figure 8.2-3). Mean summer nitrate concentrations on lines 3-11 are less than ~0.6 μM, and mean fall concentrations are less than ~0.3 μM. In all seasons, variability on lines 3-11 is highest where the means are highest. In general, the standard deviations are less than the means on lines 3-11, with spring exhibiting more exceptions (Figure 8.2-4).

Seasonal mean phosphate concentrations also exhibit the pattern seen with nitrate of highest values on line 1 in all three seasons (Figure 8.2-5). Values on that line are smaller in summer than in spring or fall. On lines 2-11 mean values are generally less than 0.1 μM. Except for line 1 in spring, standard deviations are generally less than or equal to the means. This reflects the low phosphate concentrations that are everywhere over the shelf except near the mouth of the Mississippi River.

Seasonal mean silicate concentrations are highest on lines 1-3 in spring, lines 1-2 in summer, and line 1 in fall (Figure 8.2-6). In spring over the shelf on lines 2-8, stations with the highest values along the line are located over the inner shelf and concentrations tend to decrease offshore to the outer shelf where values are low (<2 μM). The peak concentrations over the inner shelf on lines 3-8 decrease to the east. The summer and fall patterns of distribution of silicate have similarity to the spring pattern of high values inshore and lower values offshore. In addition to the higher values located near the mouth of the Mississippi River, however, summer and fall silicate concentrations have two regions with locally high means. One is on the inner shelf off line 4 (e.g., station 21 in Figure 8.2-6), and likely is related to discharge from Pensacola Bay or advection of waters with relatively high silicate concentrations from Mobile Bay. The other is a local high over the outer shelf and slope off lines 6-9 (e.g., stations 46 on line 7 and 55 on line 8 in Figure 8.2-6). This is consistent with the presence of river water over the outer shelf and slope observed there during the three summers sampled. In fall, the mean silicate concentrations were less than 2 μM everywhere except on line 1 and over the inner shelf of lines 2 through 5. As with nitrate and phosphate, variability of silicate concentrations is greatest where the mean concentrations are greatest. For the majority of the stations, the standard deviations are less than the means. The major exceptions are clusters of 2-3 stations on lines 1 and 2 in spring and on lines 6 through 9 in summer over the outer shelf/slope region.

The general surface nutrient distributions in all seasons consist of higher concentrations adjacent to the mouth of the Mississippi River, resulting in non-negligible concentrations over the Mississippi-Alabama shelf and slope, and very low concentrations over the remainder of the NEGOM study area. In contrast to the LATEX shelf, there is no clear pattern of nutrient concentrations decreasing offshore on the majority of the cross-shelf lines. This likely reflects the difference in how Mississippi River water spreads over the NEGOM and LATEX shelves. Over the LATEX shelf, there is a nearshore coastal current that carries the Mississippi-Atchafalaya River water downcoast toward Mexico in non-summer seasons. Thus, the influence of nutrients associated with river water is greatest inshore and decreases to negligible amounts over the outer shelf (Nowlin et al. 1998a, 1998b). Over the NEGOM shelf, the Mississippi River water can be carried inshore onto the Mississippi-Alabama shelf by wind-driven currents or eastward along the outer shelf edge and slope by the action of off-shelf cyclones and anticyclones. Thus, the influence of nutrients associated with river water is greatest over both the inner western shelf and the outer shelf/slope of the NEGOM study area.

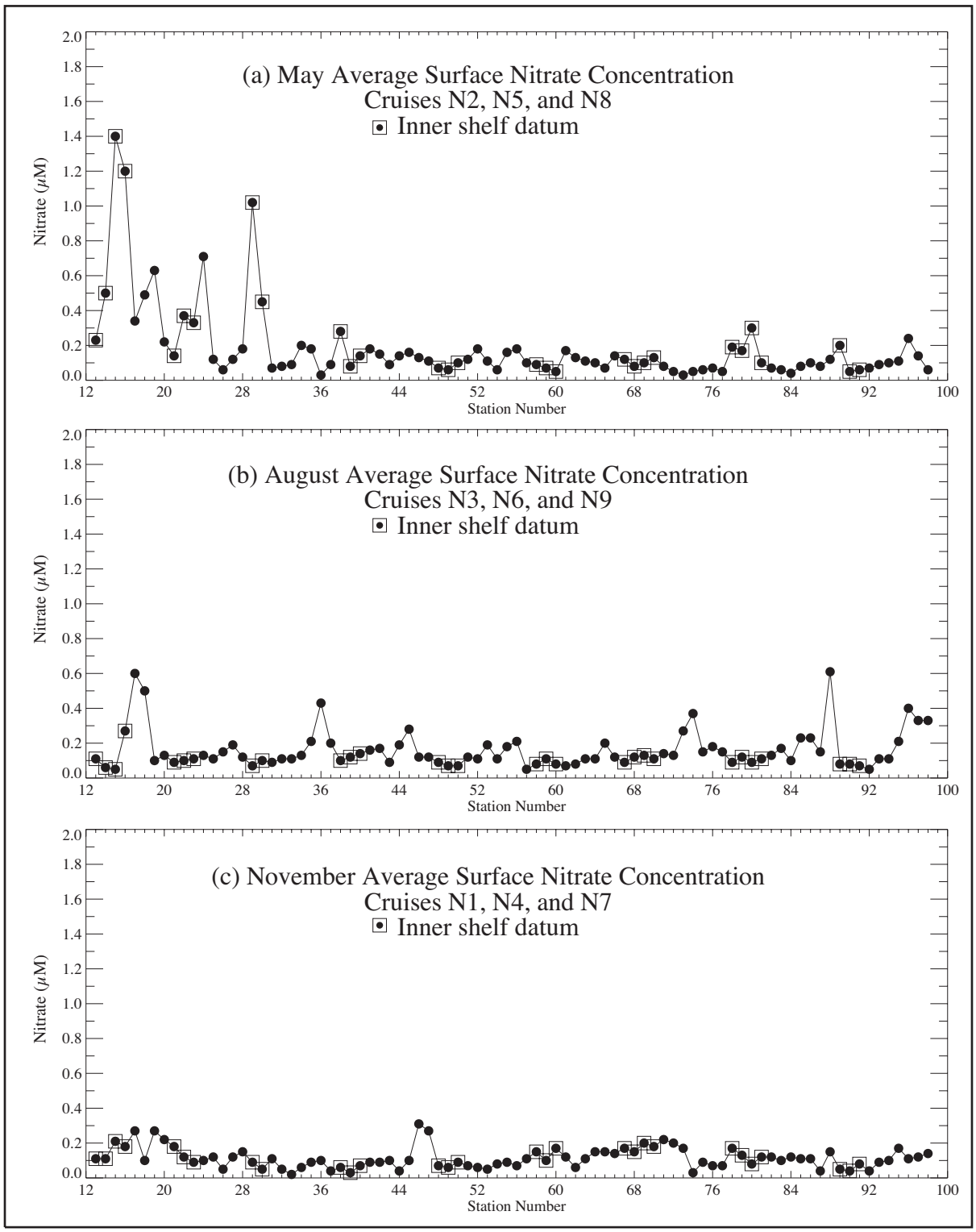

Figure 8.2-3. Seasonal average surface nitrate concentrations for stations from lines 3 through 11 plotted by station number (see Figure 8.2-1) for all (a) spring, (b) summer, and (c) fall NEGOM hydrography cruises.

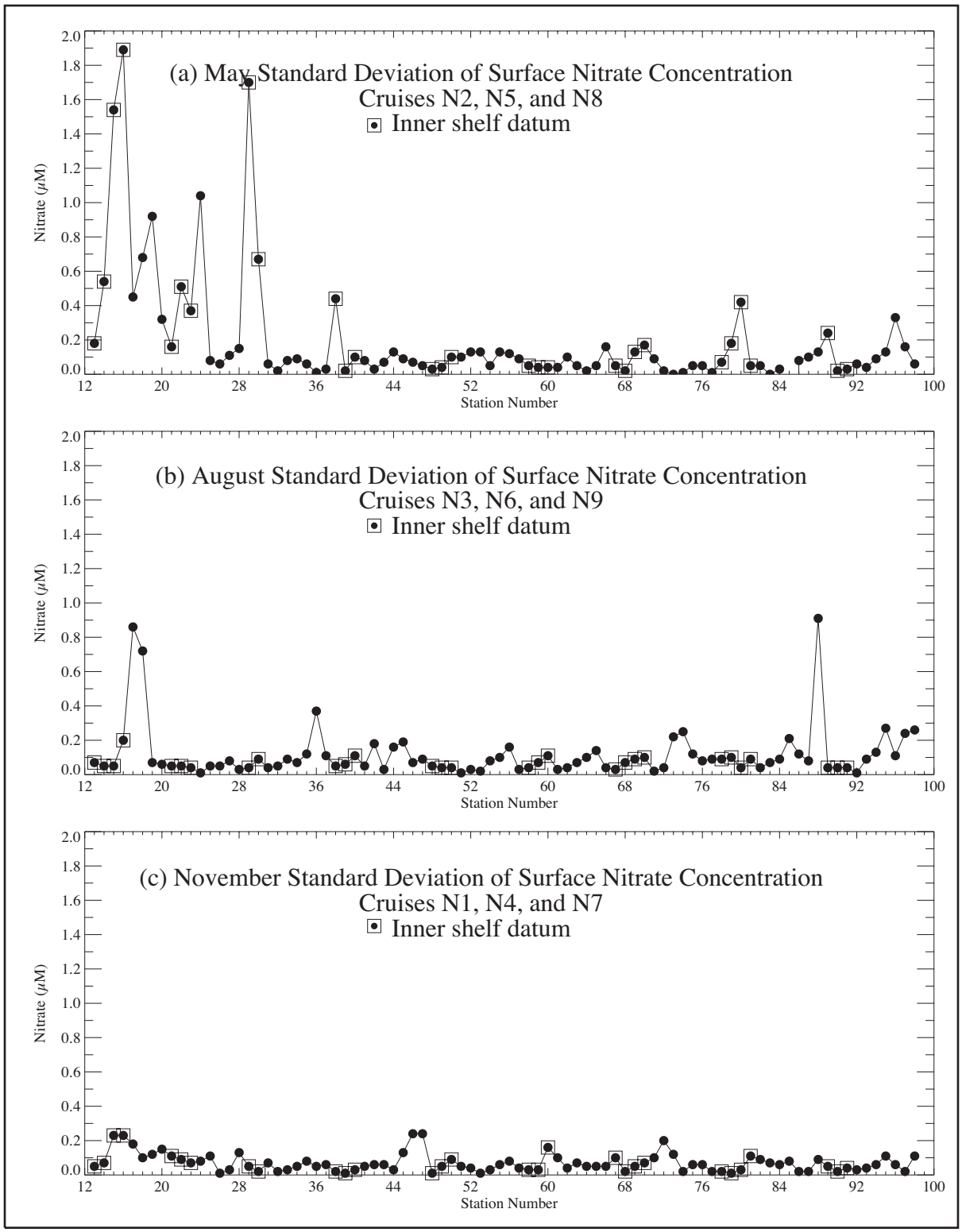

Figure 8.2-4. Standard deviation of seasonal surface nitrate concentrations plotted by station number (see Figure 8.2-1) for (a) spring, (b) summer, and (c) fall for all NEGOM hydrography cruises. Shown are stations from lines 3 through 11.

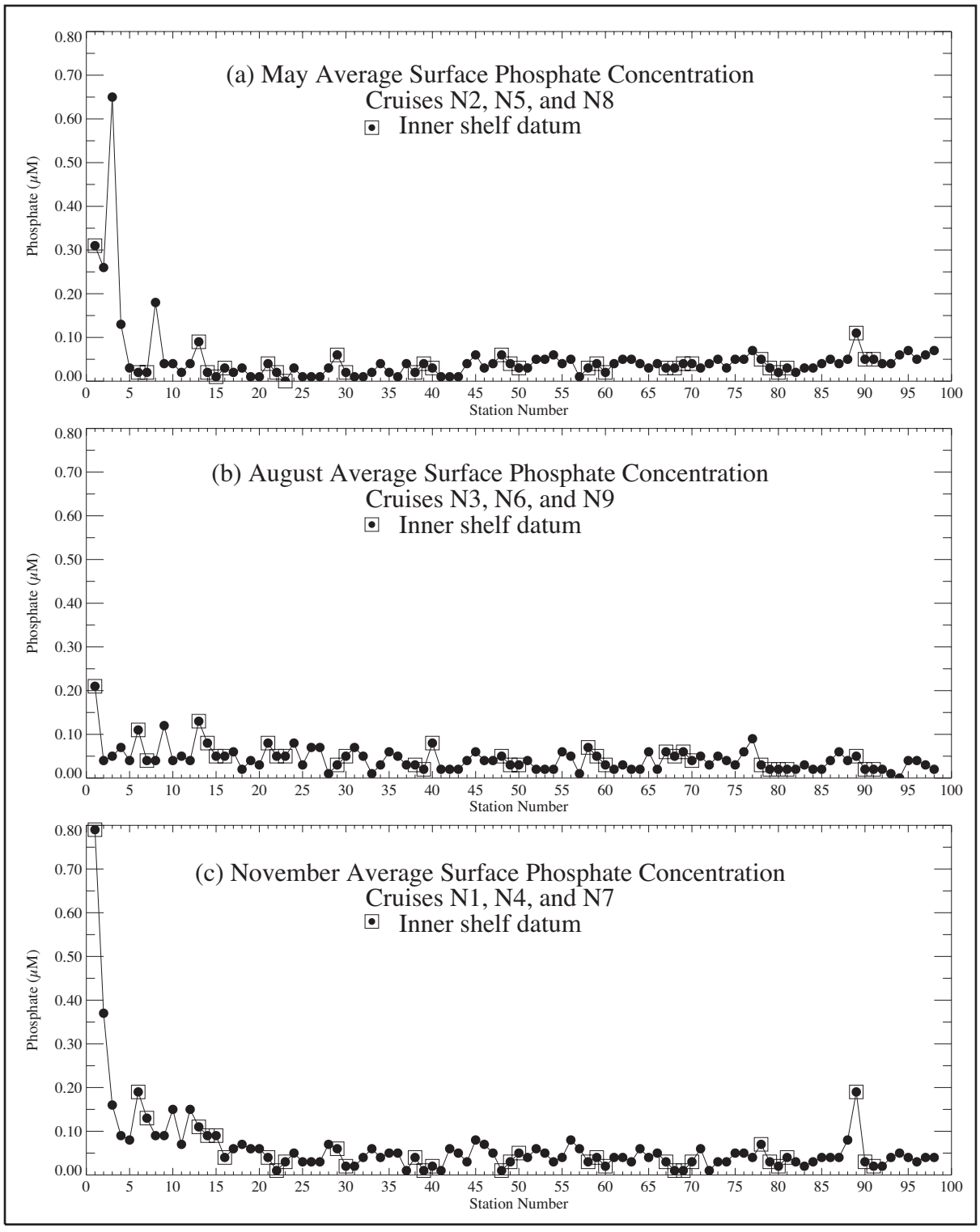

Figure 8.2-5. Seasonal average surface phosphate concentrations plotted by station number (see Figure 8.2-1) for all (a) spring, (b) summer, and (c) fall NEGOM hydrography cruises.

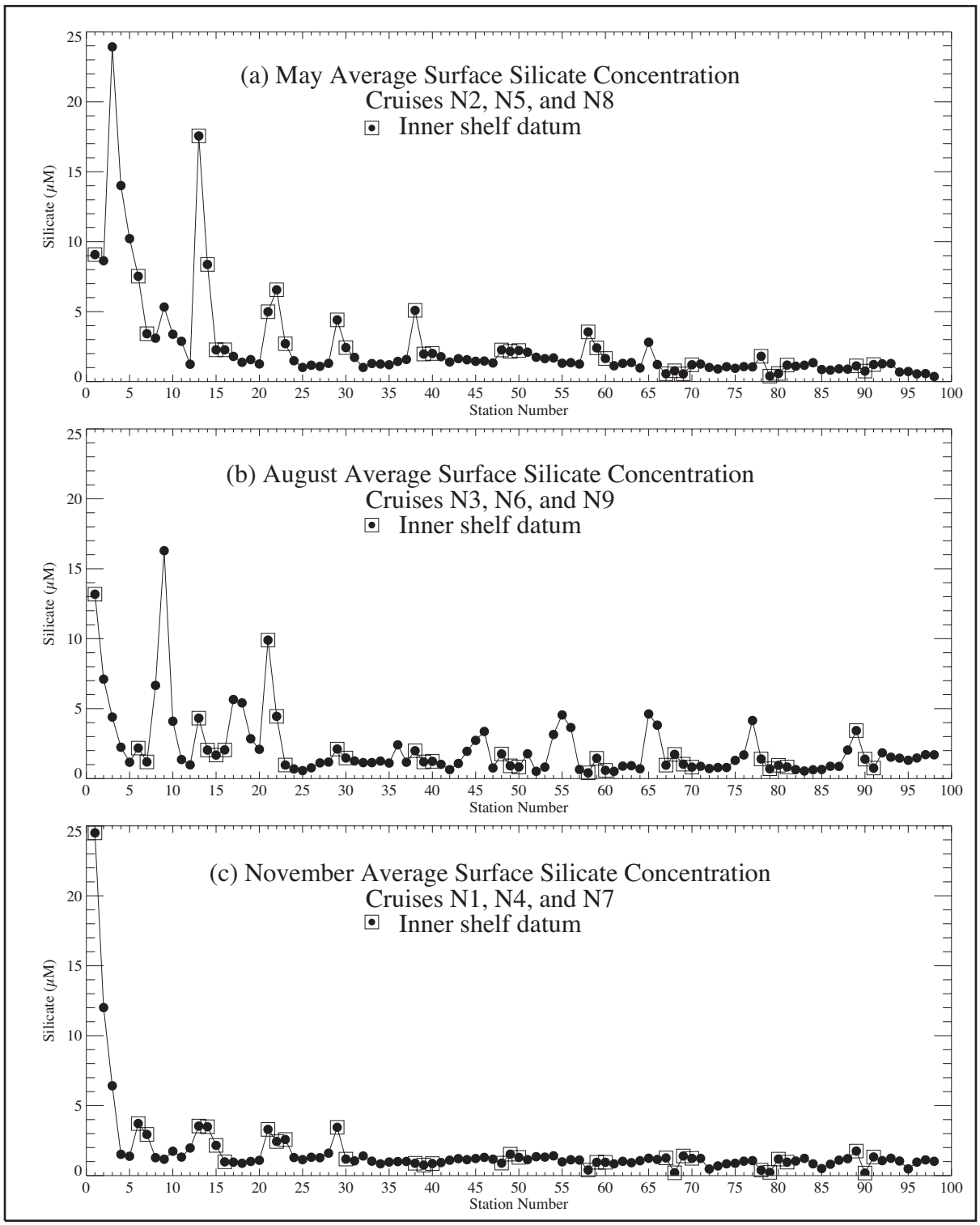

Figure 8.2-6. Seasonal average surface silicate concentrations plotted by station number (see Figure 8.2-1) for all (a) spring, (b) summer, and (c) fall NEGOM hydrography cruises.

The NEGOM stations were divided into two regions: stations west of and including the 87°W longitude line for the western region and stations east of 87°W for the eastern region. For each cruise, the mean concentration for each region was calculated as the average of all nutrient values in the upper 5 m, representing a measure of the surface inventory, and in the upper 60 m, representing a measure of the photic zone inventory. The results are given in Figure 8.2-7 for nitrate, Figure 8.2-8 for phosphate, and Figure 8.2-9 for silicate.

The cruise average nutrient concentrations in both the surface and photic zones are larger over the western region than the eastern, except for cruise N2 in surface phosphate, as seen in the ratios of west to east given in Table 8.2-1. The higher nutrients over the western shelf reflect inputs from the Mississippi River. The surface nitrate was of order 10 times higher in the west than the east during the spring cruises; the ratios for nitrate in the photic zone also tended to be higher in spring than summer or fall. These reflect the large input of nitrate to the western NEGOM shelf from the large, springtime Mississippi River discharge. In contrast, the ratios for phosphate and silicate tended to be similar in all three seasons. The effects of interannual variability can be seen be comparing the ratios for the spring cruises. The ratios for all nutrients on cruise N5 in May 1999 were substantially higher than those for cruise N2 in May 1998 or cruise N8 in April 2000. This reflects the fact that the sampling during cruise N5 occurred during a time when higher than average spring discharge from the Mississippi River had reached the shelf waters.

Average surface nitrate concentrations on spring cruises are higher over the western region than the preceding fall and following summer cruises, while the average surface concentrations on fall cruises are lower than on the cruises in the preceding or following seasons. This also is true for the photic zone, except for cruise N8, which may have occurred too early in the spring to have measured the impact of the springtime Mississippi River discharge. Over the eastern shelf, no one season is consistently higher or lower than the others over the three years of sampling. In phosphate, there is a seasonal trend only in the

Table 8.2-1. Ratio of average concentrations on NEGOM cruises of the western to the eastern study area. The 87°W longitude line was used to separate east from west. Shown are the ratios for the average data in the upper 5 m, representing the surface water, and in the upper 60 m, representing the photic zone. Cruises N1, N2, and N4 were in the fall; N2, N5, and N8 in spring; N3, N6, and N9 in summer.

Cruise	Upper 5 m			Upper 60 m		
	Nitrate	Phosphate	Silicate	Nitrate	Phosphate	Silicate
N1	1.8	2.0	2.2	1.6	1.7	1.9
N4	15.3	5.5	3.5	4.0	2.7	2.4
N7	2.1	1.8	2.1	1.4	1.8	1.6
N2	11.9	0.8	2.2	2.4	1.3	1.9
N5	70.5	2.4	5.2	21.0	2.0	2.8
N8	10.5	1.5	2.6	6.8	1.3	1.8
N3	5.7	1.2	2.5	3.1	1.7	2.1
N6	1.5	2.3	2.1	2.7	2.8	2.2
N9	4.4	1.7	3.4	1.9	1.4	2.1

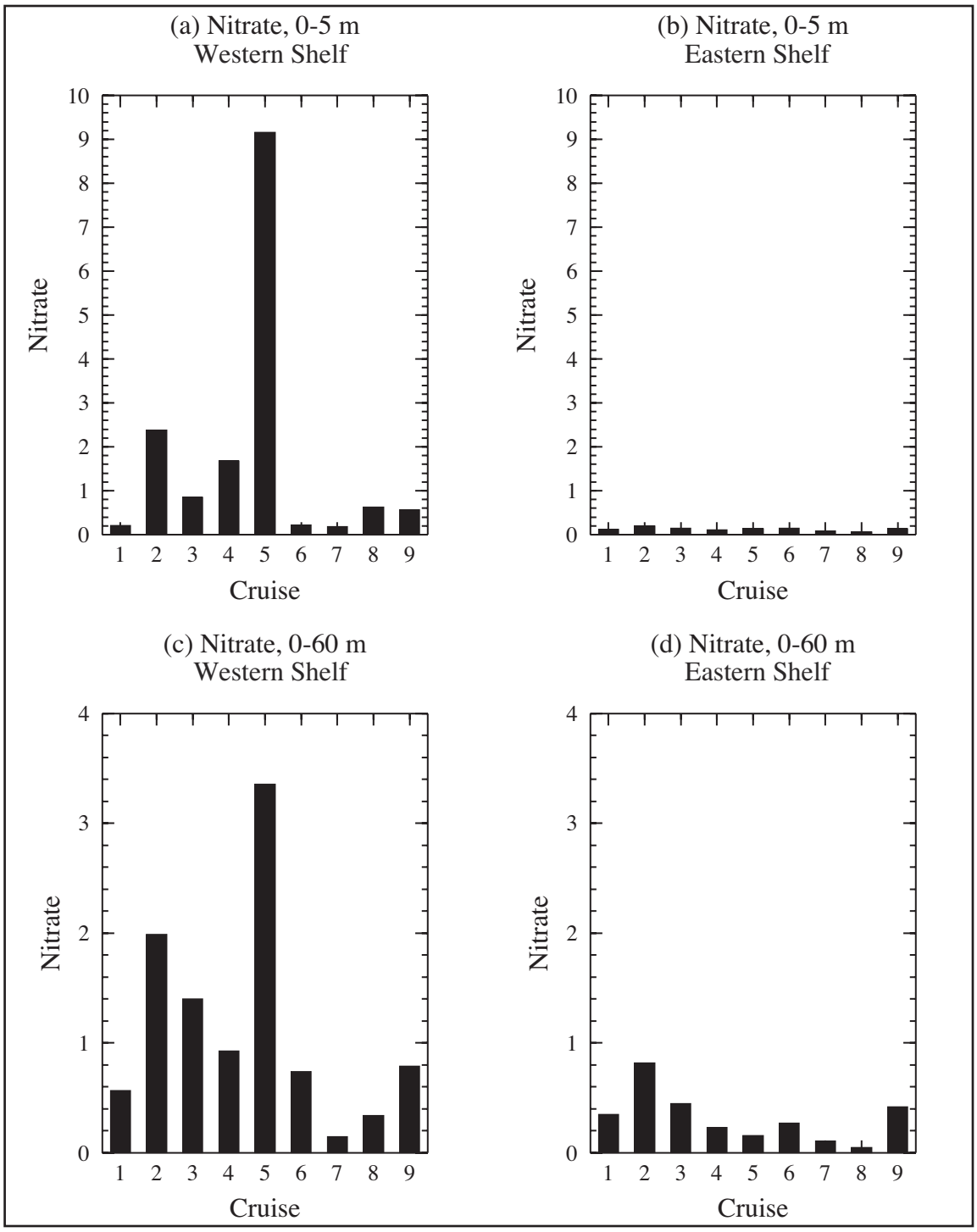

Figure 8.2-7. Average concentrations of nitrate (μM) over the western and eastern NEGOM shelves. Averages were computed for all samples taken in the upper 5 m and 60 m. The 87°W longitude line was used to demark the west (including 87°W) from east shelf. Fall cruises are numbers 1, 4, and 7; spring are 2, 5, and 8; and summer are 3, 6, and 9.

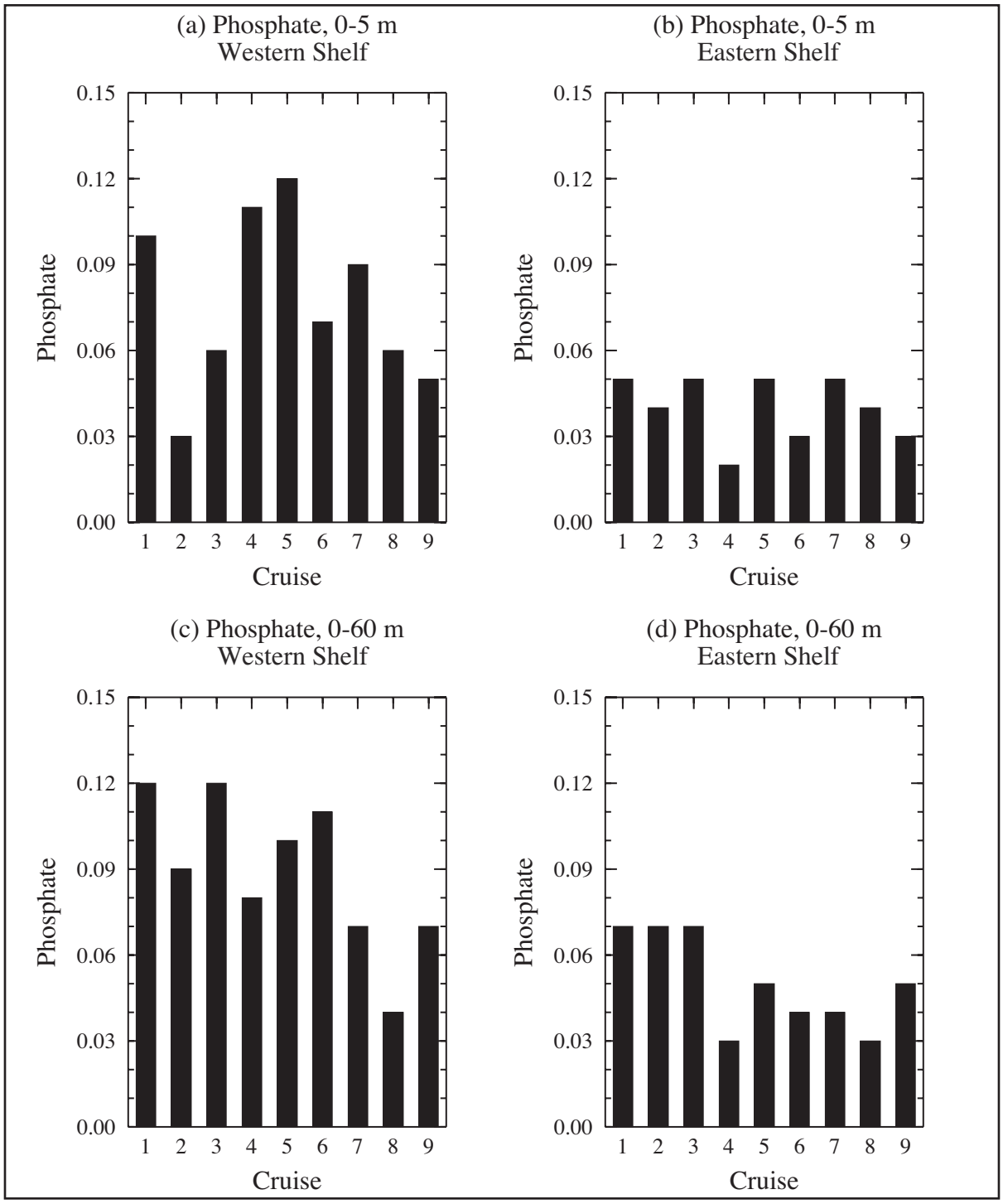

Figure 8.2-8. Average concentrations of phosphate (μM) over the western and eastern NEGOM shelves. Averages were computed for all samples taken in the upper 5 m and 60 m. The 87°W longitude line was used to demark the west (including 87°W) from east shelf. Fall cruises are numbers 1, 4, and 7; spring are 2, 5, and 8; and summer are 3, 6, and 9.

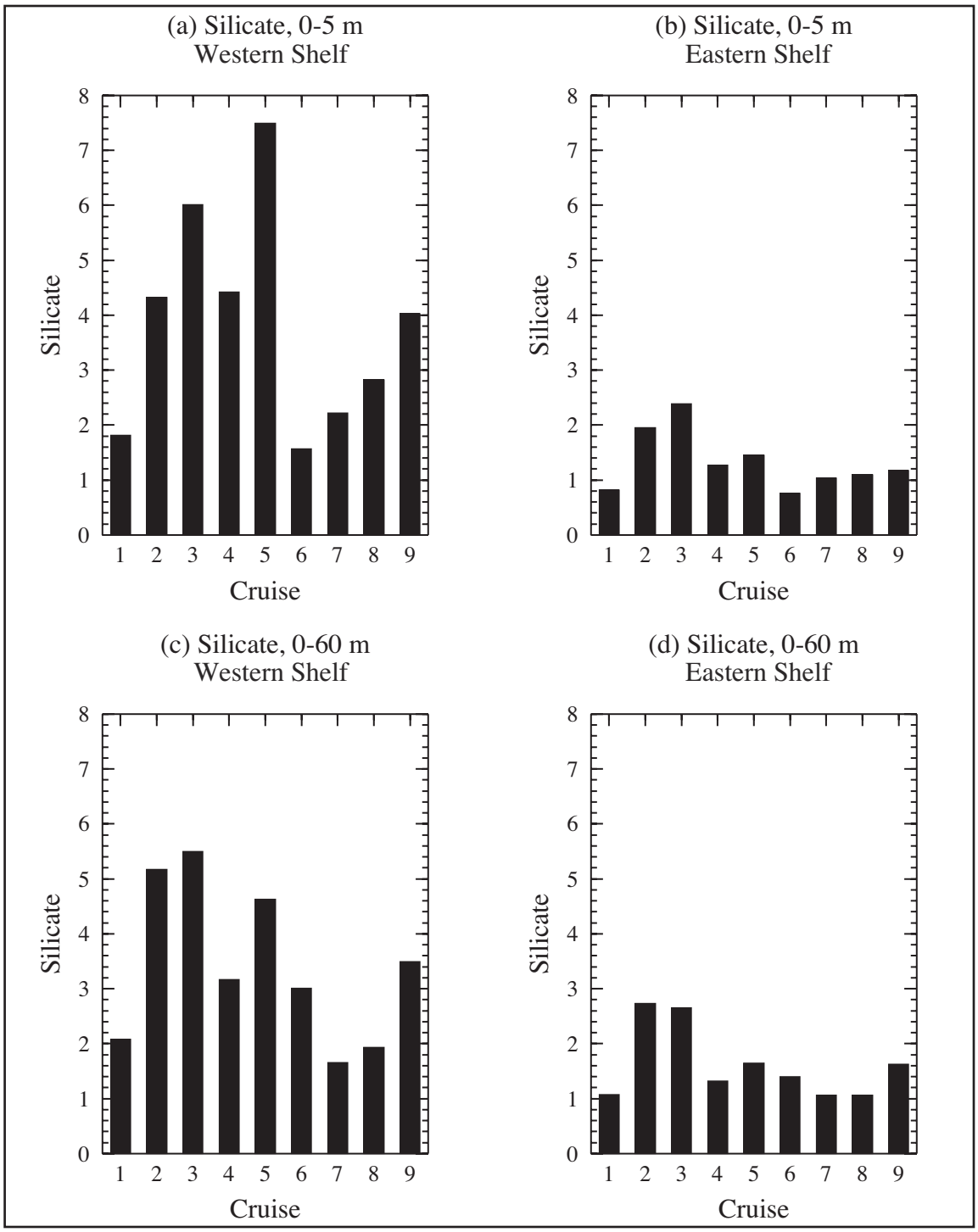

Figure 8.2-9. Average concentrations of silicate (μM) over the western and eastern NEGOM shelves. Averages were computed for all samples taken in the upper 5 m and 60 m. The 87°W longitude line was used to demark the west (including 87°W) from east shelf. Fall cruises are numbers 1, 4, and 7; spring are 2, 5, and 8; and summer are 3, 6, and 9.

western shelf photic zone values. The summer cruises have higher values than the preceding spring or following fall seasons. In silicate, the fall photic zone average over the western region tends to be less than the bounding summer or spring averages.

8.3 Nutrient Distributions on Selected Density Surfaces

Water samples were taken for nutrients at all stations on selected density surfaces. These were sigma-theta surfaces 24.6, 25.4, 25.9, 26.2, 26.5, 26.8, 27.0, 27.15, and 27.45 $kg \cdot m^{-3}$. Additionally, samples were taken near-surface (~3 m depth), at bottom (1 to 5 m off the sea floor), and at the chlorophyll maximum. Data were grouped into bins centered on each of the nine sigma-theta surfaces plus a near-bottom bin with $\sigma_\theta \geq 27.60$ $kg \cdot m^{-3}$ (average 27.63) and a near-surface bin with $\sigma_\theta < 23.8$ $kg \cdot m^{-3}$ (average 22.0).

Basic statistics for all nitrate, phosphate, and silicate data were computed for each σ_θ surface (Table 8.3-1). The general vertical profile for the nutrients is present in the averages, with low values near surface and increasing values with increasing density. At the 27.45 σ_θ surface, there is a maximum in nitrate and phosphate as expected in waters associated with the Antarctic Intermediate Water (bold numbers in Table 8.3-1). The associated silicate maximum occurs lower in the water column. Variability is highest relative to the mean for σ_θ surfaces of 25.4 $kg \cdot m^{-3}$ or less and tends to decrease with greater density. The range is greatest near-surface and generally tends to decrease with increasing density.

The horizontal distribution of nutrients is examined in a series of contour plots on specific sigma-theta surfaces. In each of the figures, the upper panel will show contours of the average concentration for the indicated σ_θ bin. The middle panel will show contours of the standard deviation on that surface, and the lower panel will give the number of data points used to form the statistics on that surface for each station.

Distributions of nitrate concentrations are considered first. The average nitrate concentration in the upper σ_θ bin, which averaged 22 $kg \cdot m^{-3}$ and had an average depth of 10 m, is shown in Figure 8.3-1. The nitrate is very low over all the NEGOM study area except west of 88°W. Note that relatively high values extend to the outer shelf and slope in the region adjacent to the mouth of the Mississippi River. Variability is highest there, with the standard deviations generally exceeding the mean. The pattern seen in this figure is representative of the pattern from the top water samples. At the σ_θ surface of 25.4 $kg \cdot m^{-3}$ associated with the Subtropical Underwater, at an average depth of approximately 54 m, a nitrate distribution pattern different from the near-surface pattern emerges (Figure 8.3-2). The lowest mean values are located over the inner west Florida shelf, and highest values are at and inshore of the shelf break over the Mississippi-Alabama shelf. Means over the outer west Florida shelf and in the DeSoto Canyon region are nominally 1 µM. The 25.9 and 26.2 sigma-theta surfaces have a pattern of low means inshore and high means offshore (not shown). The σ_θ surface of 26.5 $kg \cdot m^{-3}$ is associated with the 18°C Sargasso Sea water; the average depth of this surface is 153 m. The pattern of mean nitrate distribution is of lowest values (<13 µM) west off Tampa Bay and highest values (> 13.6 µM) in the DeSoto Canyon region, particularly near its apex (Figure 8.3-3). The standard deviations generally are less than 10% of the mean. Deeper sigma-theta surfaces have a pattern of lower mean values inshore and higher values offshore, as seen in the 27.15 kg·m-3 surface (Figure 8.3-4). This surface is associated with the Tropical Atlantic Central Water and has an average depth of 416 m. The standard deviation is low. The maximum in nitrate associated with the Antarctic Intermediate Water (mean depth of 721 m) can been seen by comparing Figure 8.3-5, showing the 27.45 σ_θ surface, with Figure 8.3-4, representing waters above, and Figure 8.3-6, representing waters below. The bottom values shown in Figure 8.3-6 reflect the low mean values that occur throughout the

water column over the inner shelf and the increasing values with increasing depth. Note also that the contours tend to follow isobaths.

Table 8.3-1. Basic statistics for nutrient concentrations on selected sigma-theta surfaces. Surfaces associated with the Subtropical Underwater (SUW), 18°C Sargasso Seawater (18°C), Tropical Atlantic Central Water (TACW), and Antarctic Intermediate Water (AAIW) are indicated. The numbers in bold in the average column indicate the highest average for the sub-surface sigma-theta surfaces shown.

σ_θ surface ($kg \cdot m^{-3}$)	Average (µM)	Standard Deviation	Maximum (µM)	Minimum (µM)
	Nitrate			
22.0	0.58	3.74	82.97	0.00
24.6	0.32	0.68	7.59	0.00
25.4 (SUW)	1.36	1.70	9.20	0.00
25.9	6.10	2.48	11.92	0.02
26.2	10.37	1.52	13.68	4.53
26.50(18°C)	13.32	1.35	17.22	7.24
26.8	18.42	1.33	23.94	13.88
27.0	23.56	1.01	27.17	20.07
27.15 (TACW)	27.81	1.29	30.92	23.49
27.45 (AAIW)	**29.67**	1.05	32.12	25.52
27.63	26.59	0.81	28.15	23.42
	Phosphate			
22.0	0.05	0.09	1.80	0.00
24.6	0.05	0.05	0.49	0.00
25.4 (SUW)	0.10	0.10	0.61	0.00
25.9	0.32	0.13	0.73	0.01
26.2	0.54	0.09	0.84	0.24
26.5 (18°C)	0.72	0.09	1.02	0.43
26.8	1.04	0.09	1.36	0.73
27.0	1.37	0.07	1.62	1.08
27.15 (TACW)	1.66	0.10	1.99	1.36
27.45 (AAIW)	**1.85**	0.06	2.12	1.68
27.63	1.69	0.05	1.83	1.55
	Silicate			
22.0	2.42	3.98	66.02	0.01
24.6	1.71	1.87	16.34	0.00
25.4 (SUW)	2.34	2.43	21.31	0.00
25.9	3.33	1.57	13.61	0.14
26.2	4.34	1.27	11.70	1.75
26.5 (18°C)	5.42	1.13	9.54	2.74
26.8	8.21	1.29	13.60	4.61
27.0	11.81	1.10	18.54	8.27
27.15 (TACW)	16.37	1.85	22.76	11.60
27.45 (AAIW)	24.17	1.05	27.25	20.56
27.63	**25.77**	0.89	28.42	23.07

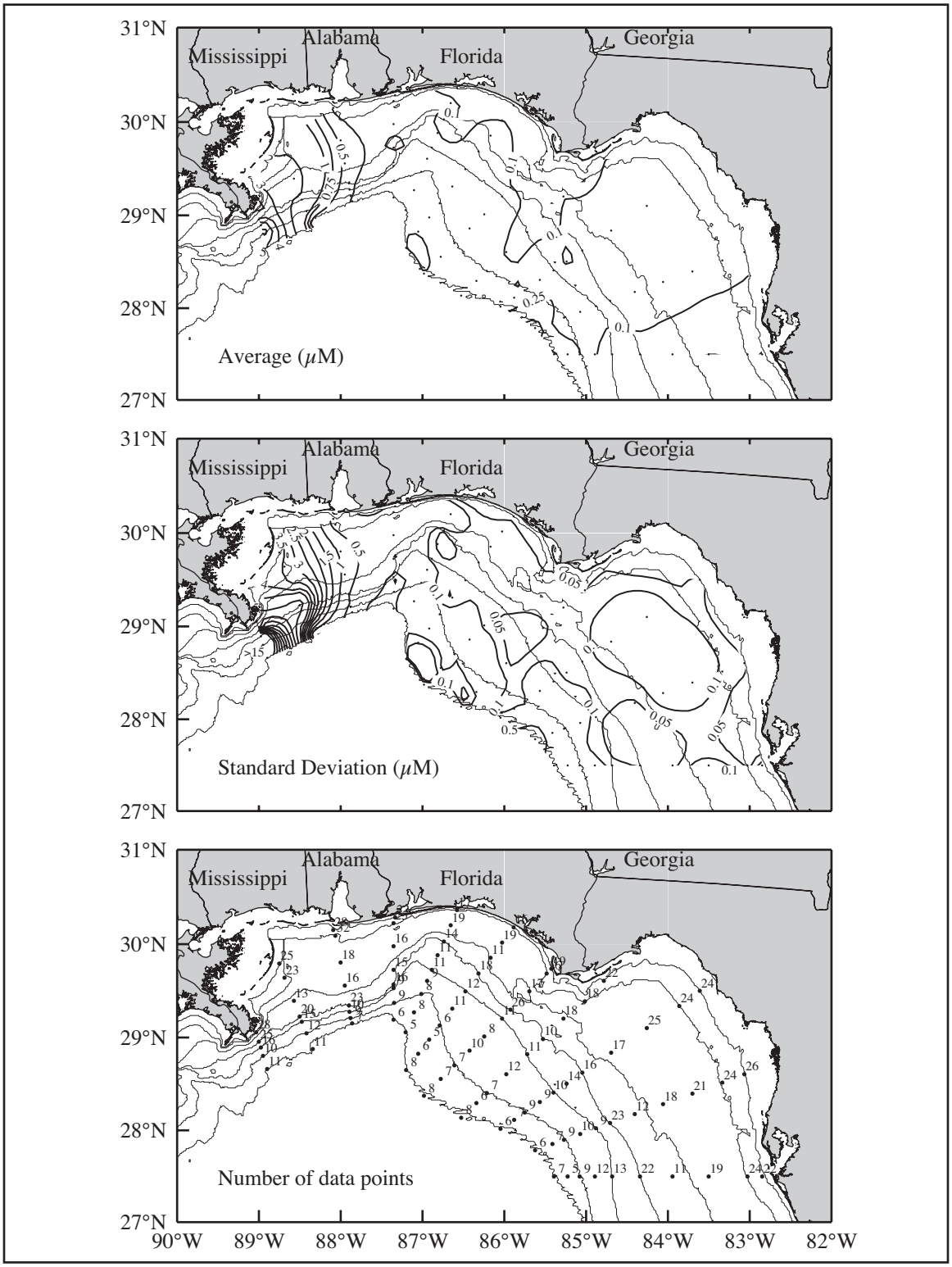

Figure 8.3-1. Mean and standard deviation of nitrate from nine cruises on an average sigma-theta level of 22 kg·m^{-3}. Number of observations are shown. Bathymetry contours are 10, 20, 50, 100, 200, 500, and 1000 m.

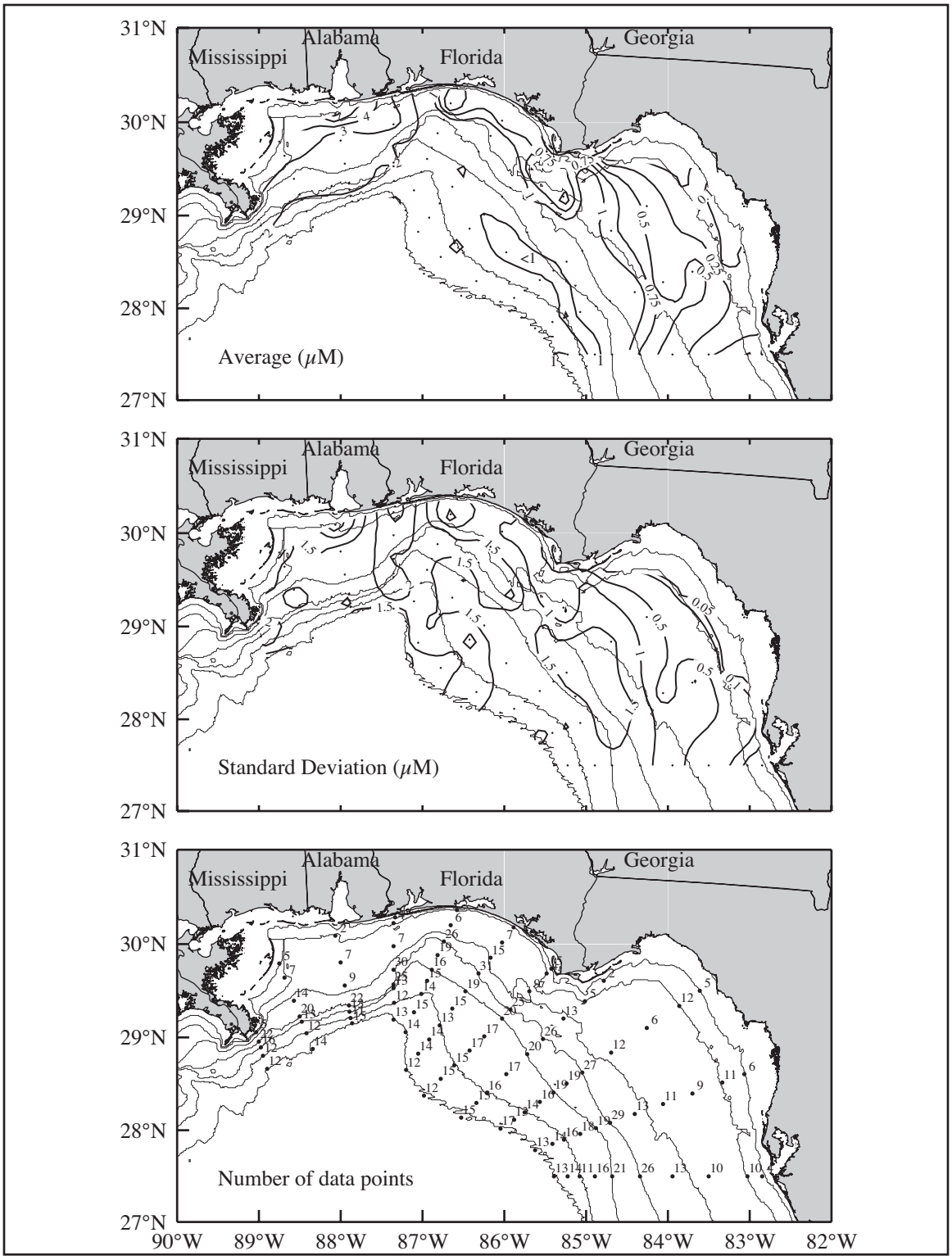

Figure 8.3-2. Mean and standard deviation of nitrate from nine cruises on an average sigma-theta level of 25.4 kg·m^{-3}. Number of observations are shown. Bathymetry contours are 10, 20, 50, 100, 200, 500, and 1000 m.

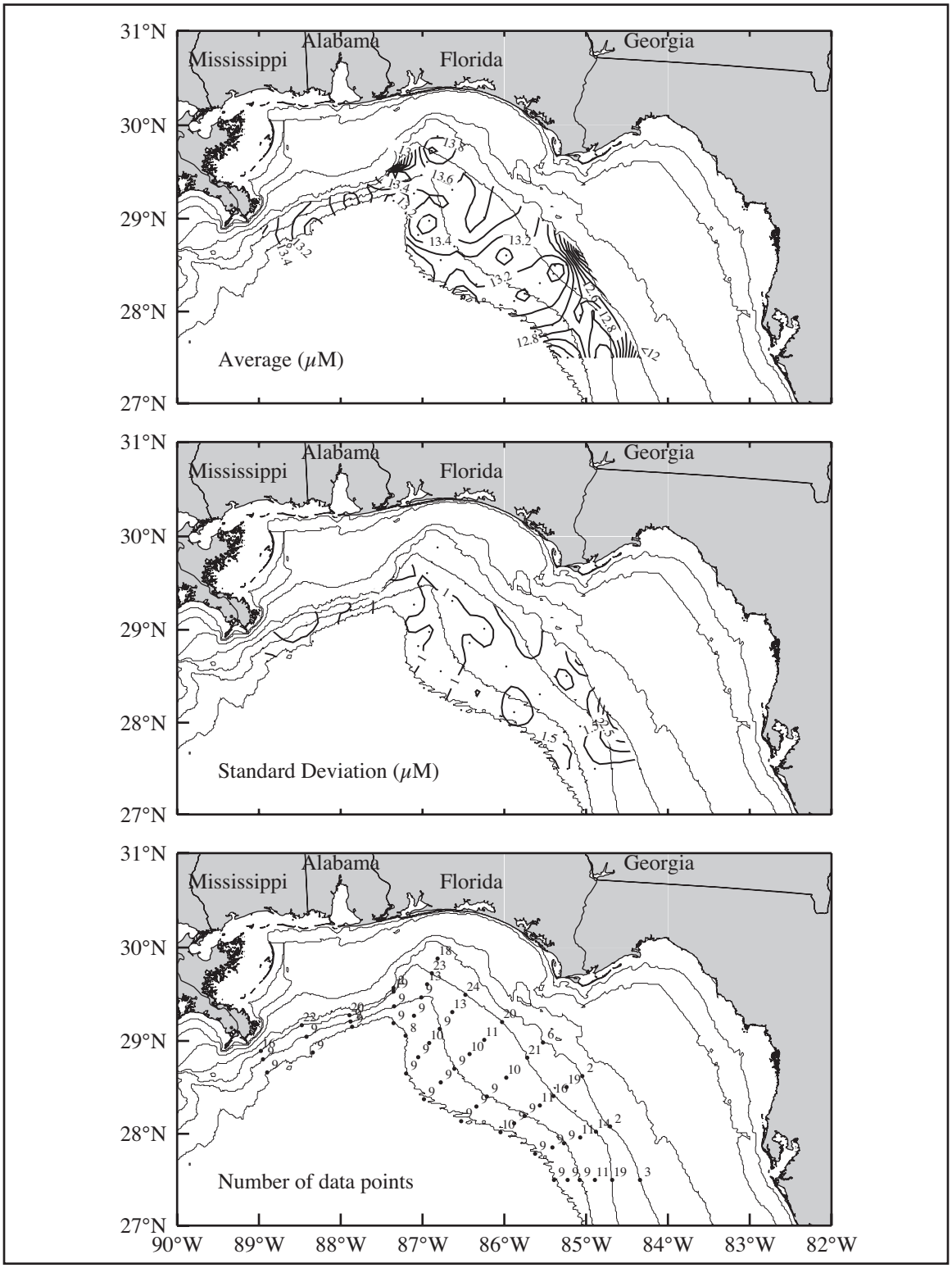

Figure 8.3-3. Mean and standard deviation of nitrate from nine cruises on an average sigma-theta level of 26.5 kg·m^{-3}. Number of observations are shown. Bathymetry contours are 10, 20, 50, 100, 200, 500, and 1000 m.

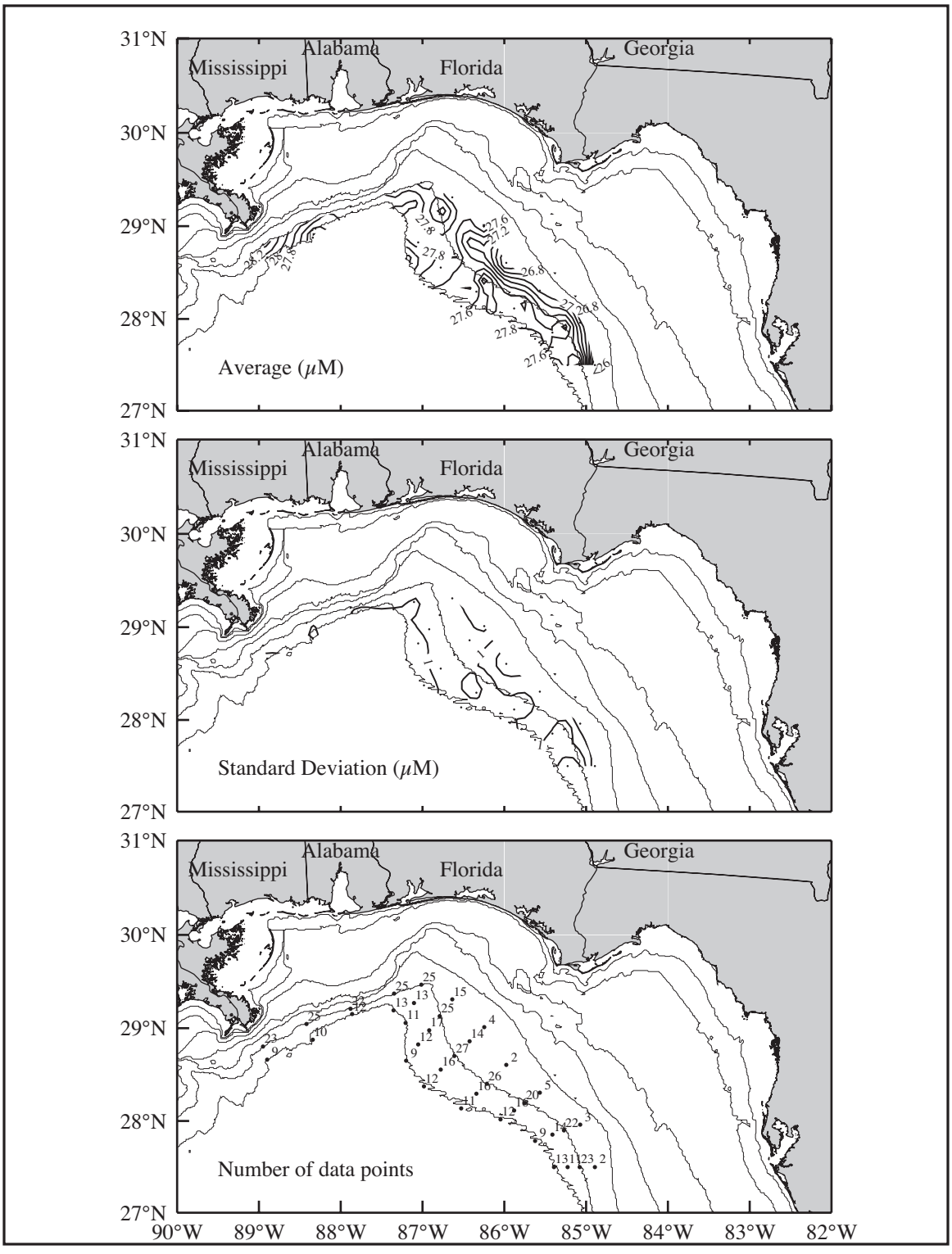

Figure 8.3-4. Mean and standard deviation of nitrate from nine cruises on an average sigma-theta level of 27.15 kg·m^{-3}. Number of observations are shown. Bathymetry contours are 10, 20, 50, 100, 200, 500, and 1000 m.

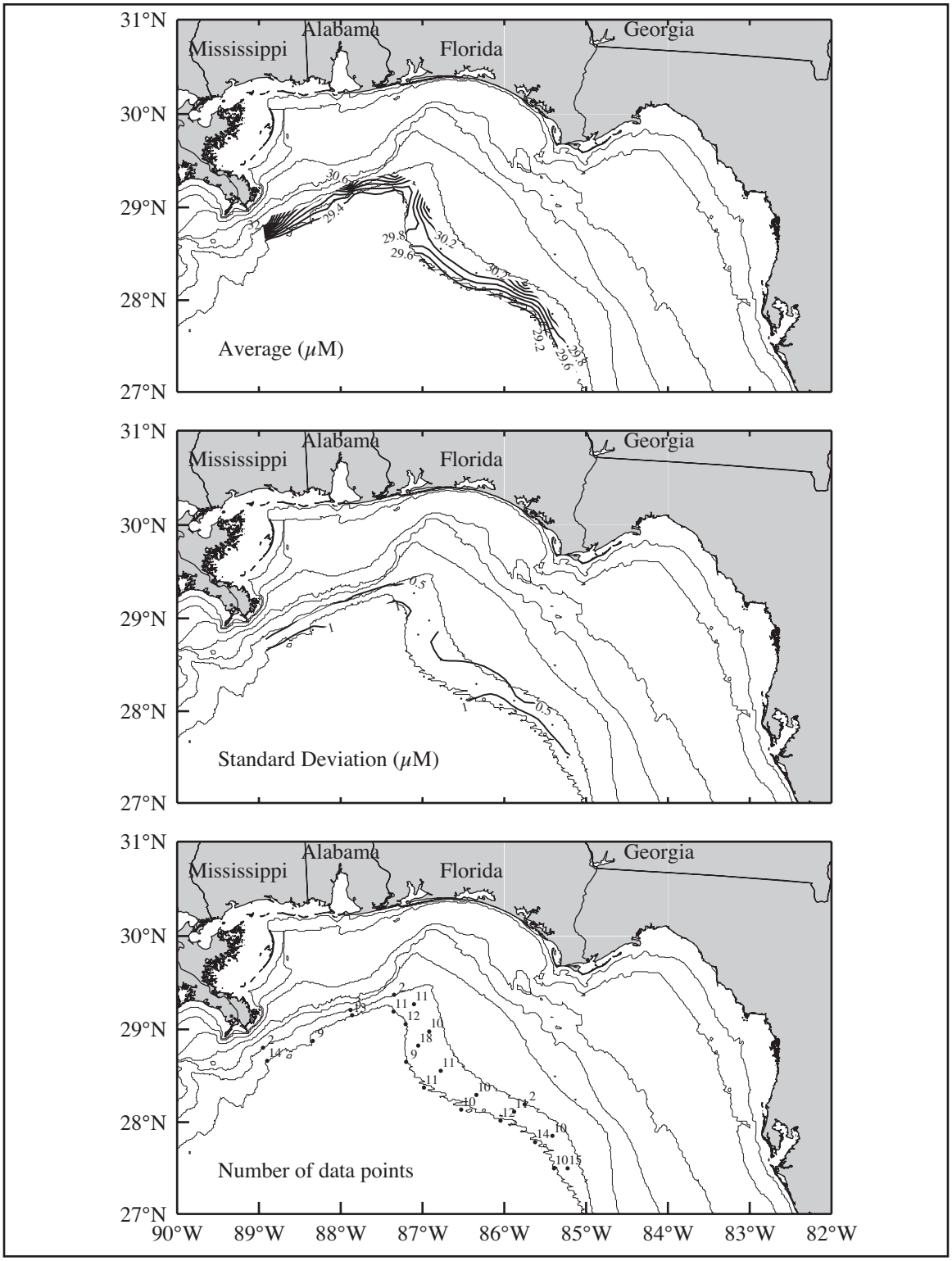

Figure 8.3-5. Mean and standard deviation of nitrate from nine cruises on an average sigma-theta level of 27.45 kg·m^{-3}. Number of observations are shown. Bathymetry contours are 10, 20, 50, 100, 200, 500, and 1000 m.

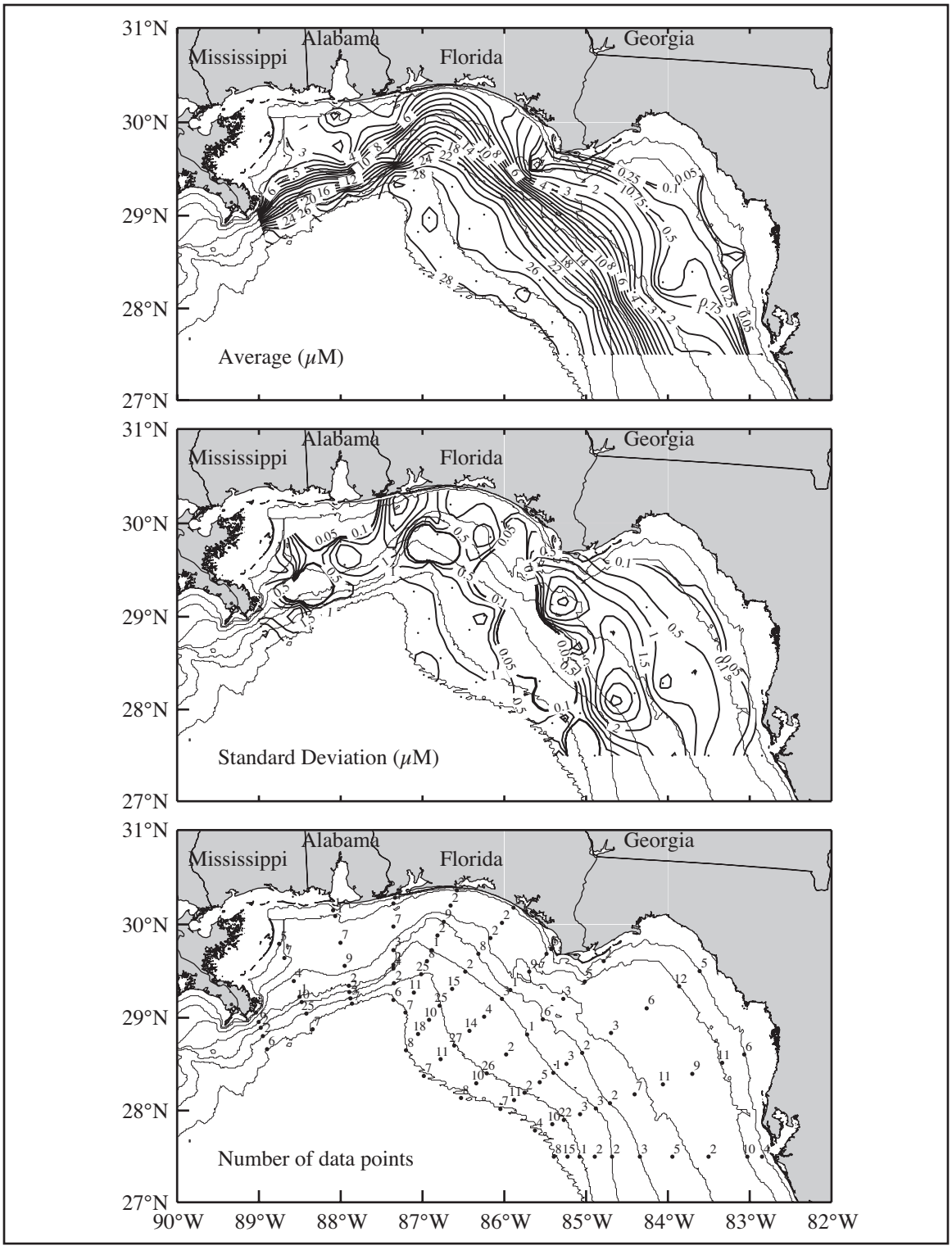

Figure 8.3-6. Mean and standard deviation of nitrate from nine cruises at the bottom sigma-theta level for each station. Number of observations are shown. Bathymetry contours are 10, 20, 50, 100, 200, 500, and 1000 m.

The distributions of phosphate follow patterns that are similar to those of nitrate. The average from the bottom samples is shown in Figure 8.3-7. The phosphate throughout the water column over the inner shelf is low, indicating consumption of this nutrient by photosynthesis. Note however that the mean concentration over the inner Mississippi-Alabama shelf is generally higher that those over the inner west Florida shelf. This reflects the high nutrient inputs from the Mississippi River as compared to other rivers, such as the Apalachicola and Suwannee, discharging to the west Florida shelf. As with nitrate, the phosphate concentrations increase with depth and isolines of phosphate tend to follow isobaths. The phosphate maximum associated with the Antarctic Intermediate Water is seen in the pattern of 1.8 μM concentration between the 500 and 1000-m isobaths.

Distributions of silicate also follow the general patterns exhibited in the nitrate distributions. The near-surface (σ_θ of 22 $kg \cdot m^{-3}$) mean silicate distribution is shown in Figure 8.3-8. The major difference between the nitrate pattern and the silicate pattern seen here is that the relatively high silicate values extend over the entire Mississippi-Alabama shelf to the western Florida Panhandle shelf. Additionally, there is a local high in average silicate over the slope on lines 6 through 8. This also is a region with relatively high variability as indicated by the standard deviation of 2.5-3 μM, reflecting the presence of low-salinity water that carries high silicate concentrations that are not used up by photosynthesis.

The silicate distribution deeper in the upper water column also has differences from the nitrate pattern. At the 25.4 $kg \cdot m^{-3}$ surface (Figure 8.3-9), the highest average silicate values are inshore over the Mississippi-Alabama shelf. There also is a local high off Cape San Blas. Patterns of average silicate near the bottom show the characteristics of the nitrate patterns in the low values throughout the water column over the inner west Florida shelf, increasing values with increasing depth, and silicate isolines generally following isobaths. The average near-bottom silicate value over the inner Mississippi-Alabama shelf, however, is relatively high (Figure 8.3-10). A minimum is seen at about the 100-m isobath on that shelf, with values increasing inshore in shallower water and offshore in deeper water. Additionally, there is no silicate maximum between the 500 and 1000-m isobath as seen in nitrate and phosphate.

Several major characteristics of the nutrient distributions have been discussed here; these characteristics are well-known. Except as associated with regions of large river water discharge, values of nutrients within the photic zone are generally low, with very low to negligible values in the near surface, indicating efficient biological uptake of any nutrients that reach the shelf. Highest near-surface values are adjacent to the Mississippi River. Near-surface values over the west Florida shelf are low even adjacent to rivers, but sampling did not extend inshore of the 10-m isobath. Relatively high silicate concentrations in the photic zone show the silicate either is not fully utilized in photosynthesis or additional processes that re-suspend particulates are at work, particularly in the nearshore environment (see Section 6). Nutrient concentrations increase with depth to about 700-800 m, at the level associated with the Antarctic Intermediate Water, below which they decrease with increasing depth.

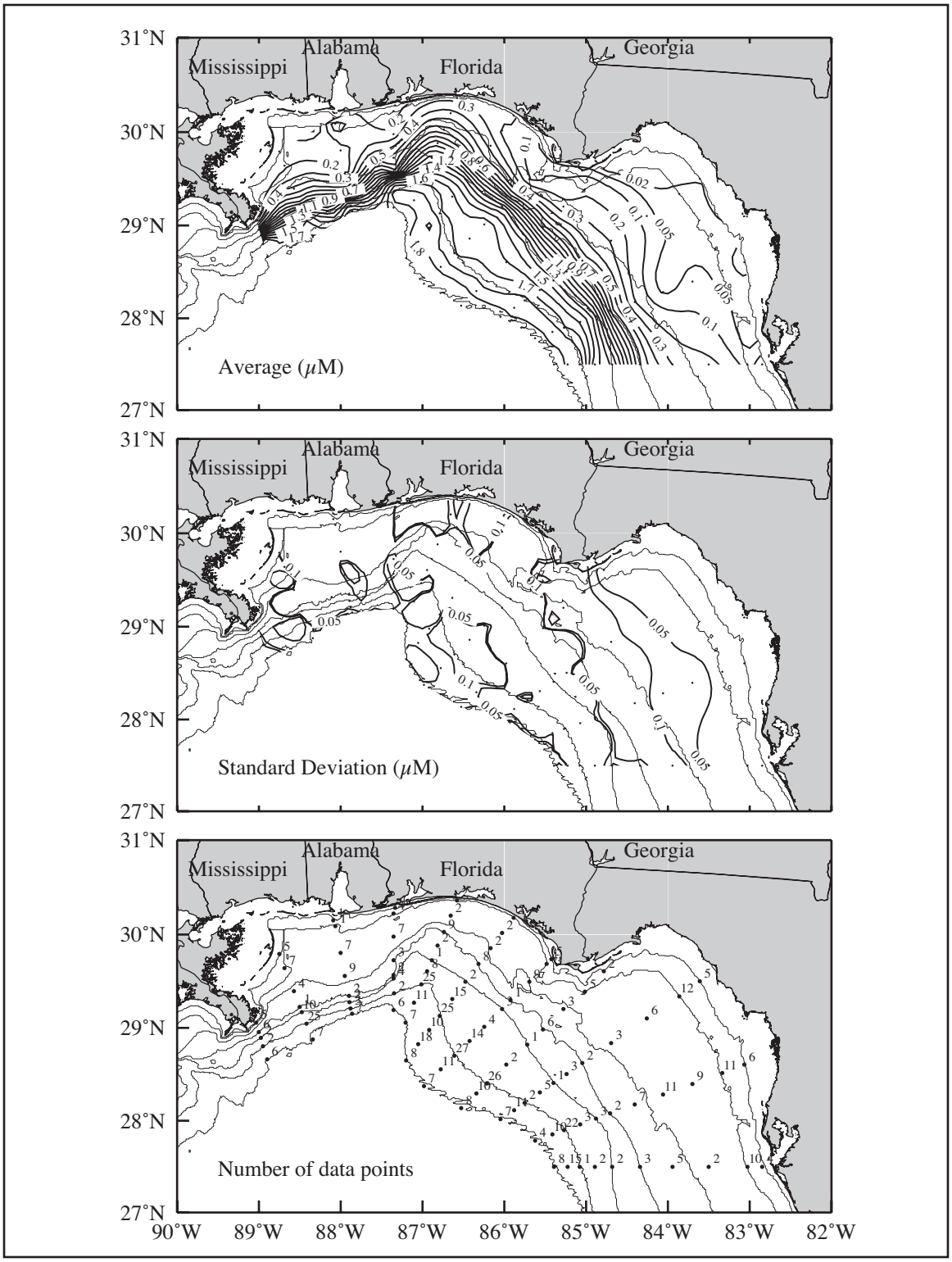

Figure 8.3-7. Mean and standard deviation of phosphate from nine cruises at the bottom sigma-theta level for each station. Number of observations are shown. Bathymetry contours are 10, 20, 50, 100, 200, 500, and 1000 m.

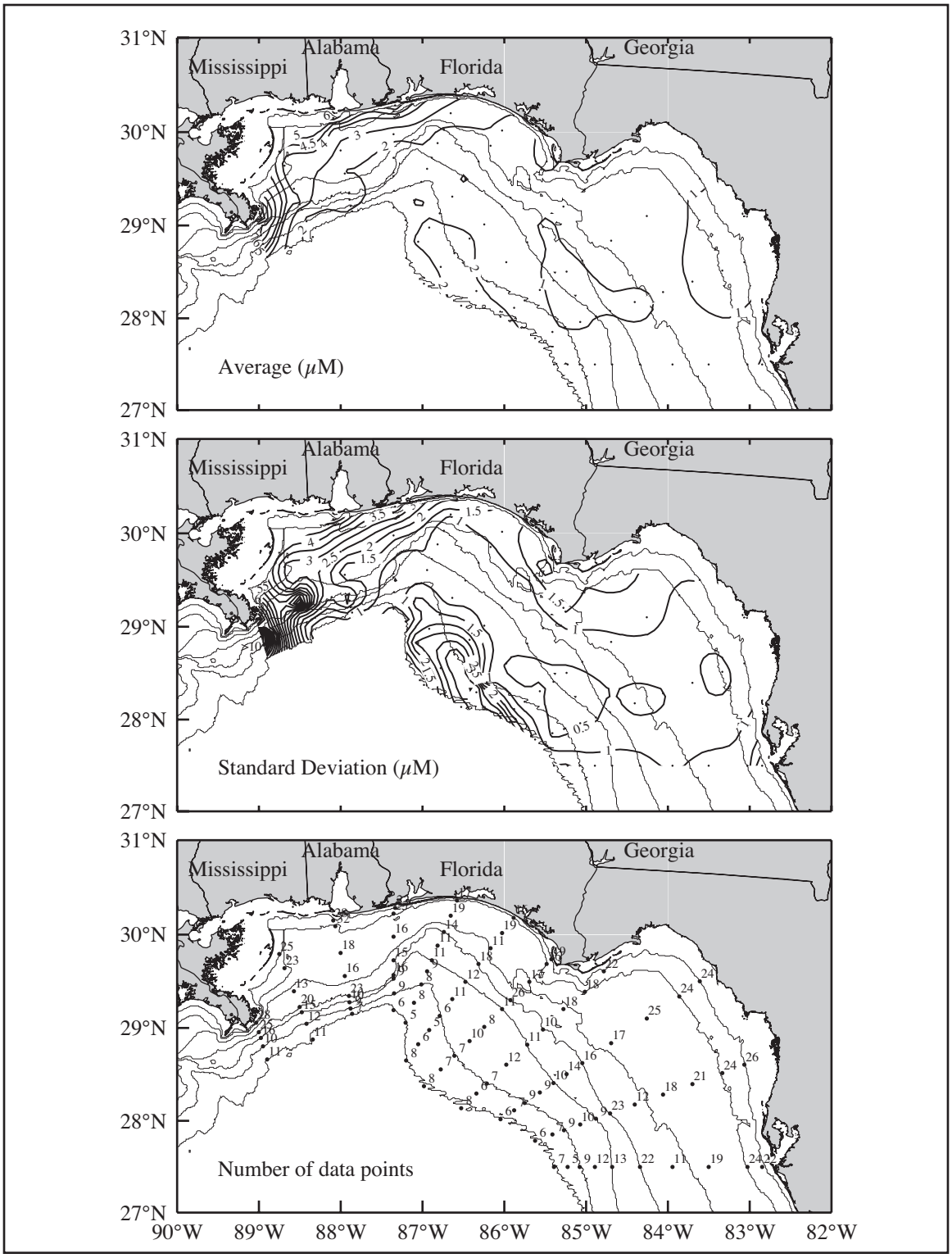

Figure 8.3-8. Mean and standard deviation of silicate from nine cruises on an average sigma-theta level of 22 kg·m^{-3}. Number of observations are shown. Bathymetry contours are 10, 20, 50, 100, 200, 500, and 1000 m.

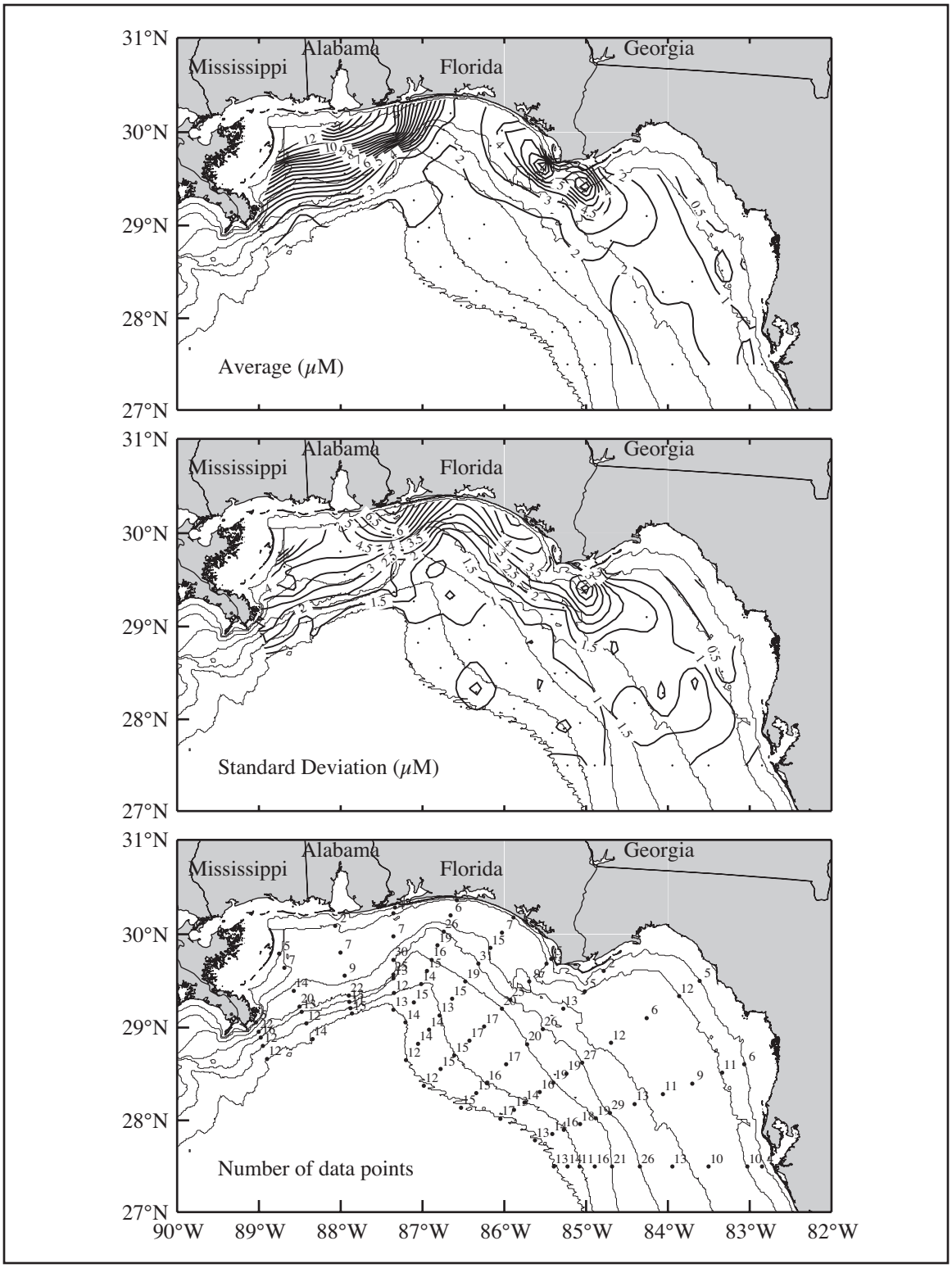

Figure 8.3-9. Mean and standard deviation of silicate from nine cruises on an average sigma-theta level of 25.4 kg·m^{-3}. Number of observations are shown. Bathymetry contours are 10, 20, 50, 100, 200, 500, and 1000 m.

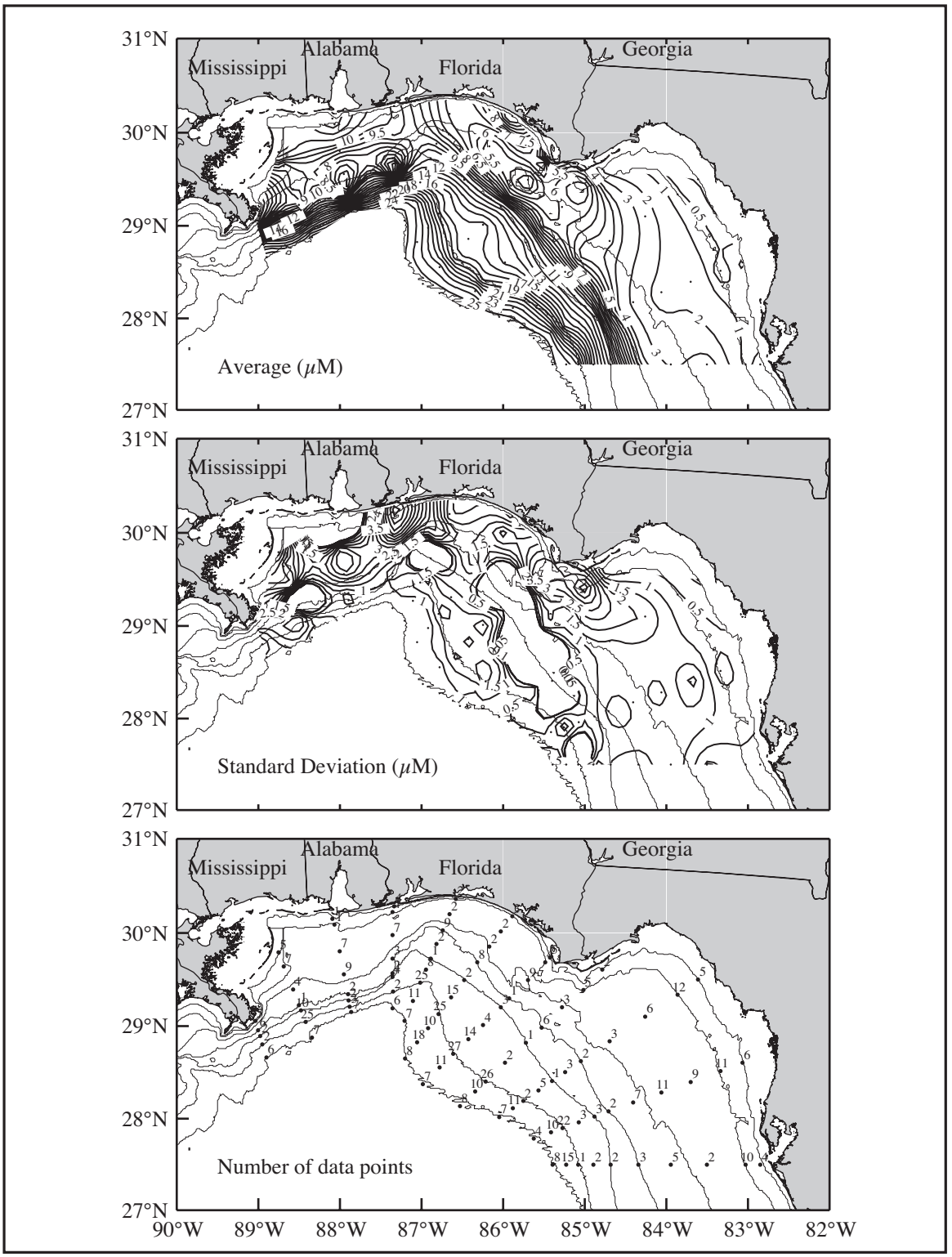

Figure 8.3-10. Mean and standard deviation of silicate from nine cruises at the bottom sigma-theta level for each station. Number of observations are shown. Bathymetry contours are 10, 20, 50, 100, 200, 500, and 1000 m.

9 PHYTOPLANKTON PIGMENTS

9.1 Introduction

As evidenced by the high chlorophyll concentrations observed in the photic zone, NEGOM shelf waters are highly productive. This productivity is due to a combination of freshwater input from rivers that drain into the study area and outflows from adjacent estuaries. Periodic onshore flow of deep nutrient-rich seawater mediated by shelf circulation and eddy patterns has been implicated as an additional factor in high productivity in the study area. Shelf circulation and riverine input of nutrients exert a strong influence on the distribution of water column properties over the shelf including phytoplankton composition and distribution. (See Section 10 for a detailed discussion of these relationships.)

Phytoplankton exert major control on the chemical properties of near-surface water, especially within the photic zone. Phytoplankton are an important source of particulate matter, produce oxygen during photosynthesis, and fix water column nutrients into biomass.

Temporal and spatial variations in phytoplankton communities can be described based on photosynthetic pigment composition and their relative concentrations in particulate matter. Chlorophyll *a* concentrations can be used to estimate how much of the particulate matter, and specifically particulate organic carbon, is living. Particulate pigment compositions can be used to estimate the relative abundances of major algal groups.

Identification and quantification of phytoplankton assemblages is performed by analyzing the types and amounts of photosynthetic and photoprotective pigments in particulate matter. Many pigments (the so-called marker pigments) are restricted to one or two taxa and are used as indicators of the presence or absence of specific taxa in the water column (Table 9.1-1). The use of marker pigments in the identification of phytoplankton classes in seawater, so-called chemotaxonomy, has greatly increased in the past decade, mainly due to the development of high performance liquid chromatographic (HPLC) analytical techniques and algorithms that quantitatively assess the presence of various algal types (e.g., Gieskes and Kraay 1983; Letelier et al. 1993; Mackey et al. 1996; Wright and van den Eden 2000; Gibb et at. 2001). These methods have provided a more rapid alternative indication of taxonomic identity than traditional labor and time intensive microscopic counting methods.

Chlorophyll and carotenoid pigment distributions were used to infer phytoplankton taxonomic composition and document spatial and temporal variations in phytoplankton biomass in the northeastern Gulf of Mexico during the sampling period. Phytoplankton pigment concentrations and compositions were measured in near-surface waters (generally at 2-3 m), in the core of the subsurface chlorophyll maximum (here called the deep chlorophyll maximum or DCM) as indicated by *in situ* fluorometry, and just below the highest fluorescence region of the DCM (and so at or close to the base of the euphotic zone). In the discussion below, the term near-shore denotes regions where the water depth is less than approximately 100 m and offshore denotes regions where water depth is more than 100 m.

9.2 Estimation of the Contribution of Chlorophyll *a* by Algal Group

Sample collection and analysis methods for phytoplankton pigments were described in Jochens and Nowlin (1998). Preliminary comparisons between on-board fluorometric measurements and post-cruise HPLC measurements of chlorophyll concentrations also briefly were described. To summarize, at most of the CTD stations a calibration sample was drawn from the seawater line to the shipboard fluorometer when, or shortly after, the CTD

Table 9.1-1. Summary of major photosynthetic pigments present in marine phytoplankton groups. Chlorophyll and carotenoid pigments in bold are diagnostic markers (Andersen et al. 1996).

Algal Group	Major Pigments Present
Prochlorophytes	**Divinyl chlorophylls *a*** and ***b***, monovinyl chlorophyll *b*, zeaxanthin, α-carotene, chlorophyll *c*-like pigment
Cyanobacteria	Monovinyl chlorophyll *a*, zeaxanthin, β-carotene, phycoerythrin, phycocyanin, allophycocyanin
Diatoms	Monovinyl chlorophyll *a*, chlorophyll c_1 and c_2, **fucoxanthin + diadinoxanthin**, diatoxanthin, β-carotene
Prymnesiophytes	Monovinyl chlorophyll *a*, chlorophyll c_1 and $c_2$or c_2 and c_3, **19'-hexanoyloxyfucoxanthin**, fucoxanthin, diadinoxanthin, diatoxanthin, β-carotene
Pelagophytes	Monovinyl chlorophyll *a*, chlorophyll c_2 and c_3, **19'-butanoyloxyfucoxanthin**, fucoxanthin, diadinoxanthin, diatoxanthin, β-carotene
Chrysophytes	Monovinyl chlorophyll *a*, chlorophyll c_1 and c_2, **fucoxanthin + violaxanthin**, β-carotene
Chryptophytes	Monovinyl chlorophyll *a*, chlorophyll c_2, **alloxanthin**, phycoerythrin or phycocyanin, crocoxanthin, monadoxanthin, α-carotene
Dinoflagellates	Monovinyl chlorophylls *a*, chlorophyll c_2, **peridinin***, dinoxanthin, diadinoxanthin, diatoxanthin, β-carotene
Prasinophytes	Monovinyl chlorophylls *a* and *b*, **prasinoxanthin‡**, chlorophyll *c*-like pigment (Mg 3,8 $DVPa_5$), zeaxanthin, neoxanthin, violaxanthin, α- and β-carotene
Chlorophytes	Monovinyl chlorophylls *a* and *b*, **lutein**, neoxanthin, violaxanthin, antheraxanthin, zeaxanthin, α- and β-carotene

* some species possess fucoxanthin-related pigments instead of peridinin.
‡ Some species possess lutein (e.g., *Pyramimonas*), siphonaxanthin instead of prasinoxanthin.

started down. The sample was filtered, and after 12 to 24 hours of extraction in 90% acetone, the amount of chlorophyll was determined fluorometrically aboard ship following the standard procedure of Parsons et al. (1985). These quick-look, fluorometric analyses of chlorophyll generally agreed well with the quantitative analyses of chlorophylls *a, b*, and *c* performed after the cruise in a land-based laboratory using HPLC methods. HPLC samples were taken from Niskin bottles tripped on the upcast of the CTD. Depending on the water depth at the station, the time difference between when samples were drawn for onboard fluorometric analysis and for post-cruise HPLC analysis ranged from 5 to 60 minutes. During the time on station, the ship sometimes drifted tens to hundreds of meters, depending on local wind and current. In general though, differences between calibration samples drawn from the flow-through seawater system and the near-surface Niskin bottle at the same station were generally less than 10%, although some paired samples varied by more than 50%. Greatest variability occurred at stations with turbid water near river plumes indicating a relatively heterogeneous water column (see Hu et al. 2001).

The relationship between shipboard flow-through fluorescence and HPLC-derived chlorophyll values is illustrated in Figure 9.2-1. Data from each of the cruises were evaluated for intra-cruise and inter-cruise variability. The overall slope of the linear correlation of chlorophylls in near-surface waters between the shipboard fluorometric measurements and laboratory HPLC analyses was 0.84, with a correlation coefficient (R^2) of 0.72 for eight of nine cruises. This was significant at better than a 99.9% confidence limit using the Student's t-distribution test. Comparisons of results from cruise N2 were not included because most of the fluorometric data were not co-collected with the bottle stations, thus confounding direct comparisons.

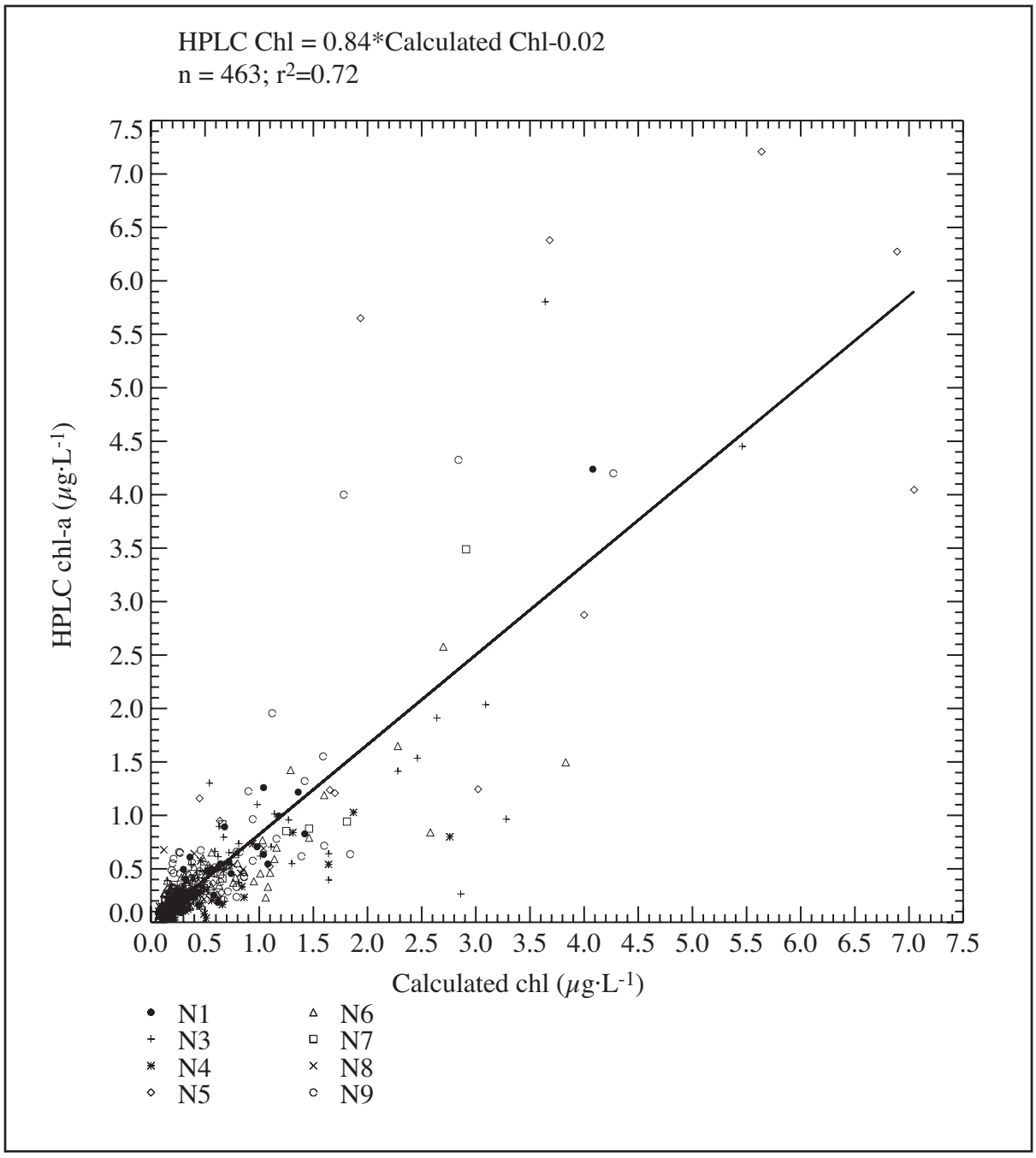

Figure 9.2-1. Correlation of chlorophylls (sum of cholorophyll *a*, *b*, and *c*) determined by HPLC and the cholorophylls calculated from the response of *in vivo* fluorometry from surface seawater samples during cruises N1 and N3 through N9. Correlation was significant at better than 99.9% confidence limit.

The ratios of accessory pigments to chlorophyll *a* characteristic of each algal group were obtained from previous studies and the analysis of phytoplankton cultures (Table 9.2-1). These ratios were further refined by inverse methods to determine the least-squares best solution to the equation following the approach of Letelier et al. (1993). Using these algorithms, biomass can be assigned to specific taxa. This approach assumes that (1) the species of the taxonomic groups present in the study area produce pigments in approximately the same ratios as those in culture, and (2) any unknown algal groups in the sample do not significantly contribute to total phytoplankton biomass. These assumptions have been confirmed by Anderson et al. (1996). Therefore the error associated with the use of culture derived algorithms is expected to be small.

The equations of Letelier et al. (1993) were used to calculate the contribution of individual algal groups to chlorophyll *a* concentrations in the near-surface, DCM, and below DCM waters. The accessory pigment to chlorophyll *a* ratios of Mackey et al. (1996) and Wright and van den Enden (2000) were similar to those used by Letelier et al. (1993). Equations for chlorophytes and chryptophytes were derived from Mackey et al. (1996) and Wright and van den Enden (2000). In cases of negative values and/or overestimates (sum of contributions to chlorophyll *a* by all algal groups greater than 120%), a least square regression was used to optimize the solutions of these algorithms by varying the ratios of accessory pigments to chlorophyll *a* per Mackay et al. (1996).

It is well known that the cellular content and ratios of carotenoid and chlorophyll pigments can vary with physiological state, which, in turn, is dependent on factors such as nutrient concentrations, light intensity and spectral quality. Estimates of phytoplankton community structure using pigment compositions and mathematical equations have additional intrinsic limitations. The algorithm solutions from one study may not be directly applicable to another

Table 9.2-1. Pigment algorithms used to partition chlorophyll *a* biomass among major phytoplankton groups (Letelier et al. 1993; Mackey et al. 1996; Wright and van den Enden 2000).

Algal Groups	Chl *a*/pigment seed values	Equations
Prochlorophytes	Chl *a*:Chl *b* 0.87 Zea:Chl *b* 0.29	$[\text{Chl } a]_{pro} = 0.91([\text{Chl } b]-2.5[\text{prasino}])$
Cyanobacteria	Chl *a*:Zea 2.5	$[\text{Chl } a]_{cyano} = 2.1\{[\text{xeax}]-0.07([\text{Chl b}]-2.5[\text{prasino}])\}$
Prymnesiophytes	Chl *a*:19'-hex 1.6 Fuco:19'-hex 0.05 19'-hex:19'-but 54.27	$[\text{Chl } a]_{prymn} = 1.3[19'\text{-hex}]$
Pelagophytes	Chl *a*:19'-but 3.82 Fuco:19'-but 1.39 19'-hex:19'-but 0.14	$[\text{Chl } a]_{pela} = 0.9\ [19'\text{-but}]$
Dinoflagellates	Chl *a*:perid 1.55	$[\text{Chl } a]_{dino} = 1.5[\text{perid}]$
Diatoms	Chl *a*:fuco 0.8	$[\text{Chl } a]_{diat} = 0.8\{[\text{focu}]-(0.02[19'\text{-hex}]+0.14[19'\text{-but}])\}$
Chlorophytes	Chl *a*:viol 9.2	$[\text{Chl } a]_{chlor} = 9.2[\text{viol}]$
Chryptophytes	Chl *a*:allox 4.3	$[\text{Chl } a]_{chryp} = 4.3[\text{allox}]$
Prasinophytes	Chl *a*:prasino 2.54 Chl *b*:prasino 2.62	$[\text{Chl } a]_{pras} = 2.1[\text{prasino}]$

environment. Optimization of the algorithms to calculate the biomass contributions of different algal types is required for each environment.

The major groups of phytoplankton in the NEGOM area were cyanobacteria (blue-green algae), pelagophytes (chrysophytes), prymnesiophytes (haptophytes), and prochlorophytes. In general, chlorophytes, chryptophytes, diatoms (bacillariophytes), dinoflagellates and prasinophytes were minor contributors to living biomass, although locally high abundances of some of these groups were detected. Because not all algal species can be identified with this approach, the resulting sum of the contributions to chlorophyll *a* by all groups of phytoplankton identified by phytoplankton pigment analyses varied from 30% to 120% of chlorophyll *a* with the majority of the samples between 60% and 100%.

9.3 Pigment Distributions by Cruise

Distributions of chlorophyll, major accessory pigments, and, by inference, major phytoplankton species present, are discussed first on a cruise by cruise basis. As the cruises constitute a time series of observations, these general distributions also indicate changes over time in the study area including seasonal variations.

Cruise N1: In November 1997, chlorophyll *a* concentrations varied from 0.08 to 3.9 $\mu g \cdot L^{-1}$ for near-surface waters and from 0.09 to 2.8 $\mu g \cdot L^{-1}$ at the deep chlorophyll maximum (DCM) with most samples having concentrations ≤ 0.9 $\mu g \cdot L^{-1}$. The spatial distribution of chlorophyll *a* in near-surface waters (Figure 9.3-1, top left panel) was similar to that for the DCM (Figure 9.3-2, top left panel). Chlorophyll *a* concentrations were highest for samples collected near-shore and off river mouths, particularly in near-shore waters between Tampa Bay and the Suwannee River (between lines 9 and 11), near the mouth of the Apalachicola River (between lines 6 and 9), and close to the Mississippi River Delta (lines 1 and 2). Chlorophyll *a* concentrations were lowest along the outer continental shelf between lines 6 and 10.

The major accessory pigments detected were chlorophylls *b*, c_2, and c_3 and β-carotene, fucoxanthin, 19'-butanoyloxyfucoxanthin, 19'-hexanoyloxyfucoxanthin, and zeaxanthin. Concentrations of these accessory pigments (the fucoxanthins, zeaxanthin, and chlorophylls *b*, c_2 and c_3) were low, ranging from 0.3 $\mu g \cdot L^{-1}$ to less than 0.01 $\mu g \cdot L^{-1}$. Peridinin, violaxanthin, diadinoxanthin, diatoxanthin, and alloxanthin were detected in trace amounts, generally < 0.01 $\mu g \cdot L^{-1}$, in only a few samples.

Major phytoplankton species inferred from the accessory pigment compositions were cyanobacteria, prymnesiophytes, prochlorophytes, and pelagophytes. These four types of phytoplankton accounted for over 70% of the chlorophyll *a* detected. The average relative proportions of these four algal groups were, respectively, 30%, 24%, 16%, and 6% in near-surface waters and 16%, 31%, 21%, and 10% in DCM waters (Table 9.3-1). Diatoms accounted, on average, for about 7% of chlorophyll *a* in both near-surface and DCM waters. Other types of phytoplankton, such as chlorophytes, chryptophytes, dinoflagellates, and prasinophytes were minor contributors to biomass during cruise N1 (Table 9.3-1).

The spatial distribution of each algal group was patchy. Prymnesiophytes, which accounted for 20-50% of chlorophyll *a* in near-surface (Figure 9.3-3, top left panel) and DCM (Figure 9.3-4) waters across the study area, were highest between lines 2 and 9. Prymnesiophytes were relatively low in near-shore waters and in waters influenced by riverine outflows. Pelagophytes and cyanobacteria were found mostly in offshore regions (Figures 9.3-5 and

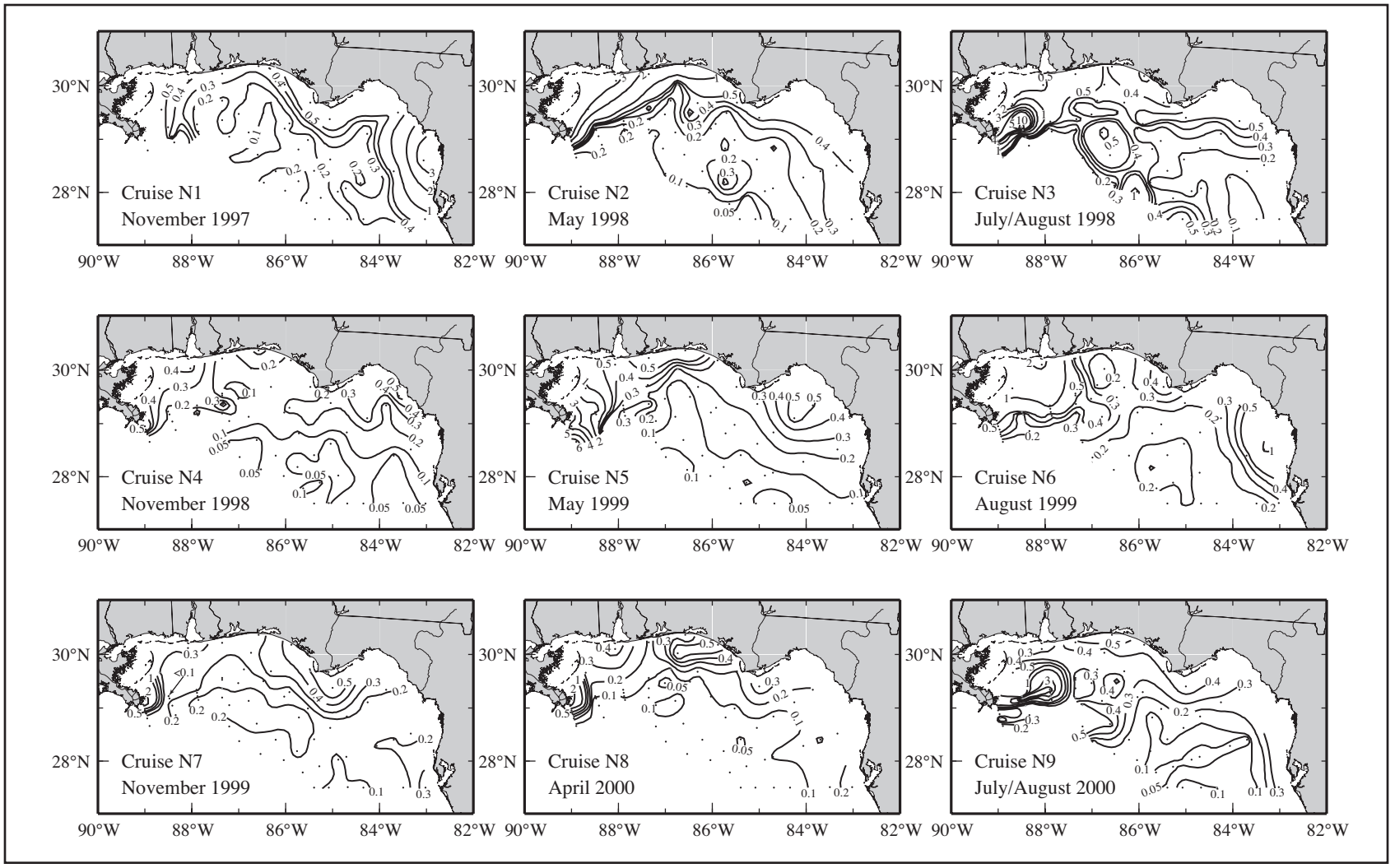

Figure 9.3-1. Chlorophyll *a* concentrations ($\mu g \cdot L^{-1}$) from near-surface (~1-3 m depth) observations on NEGOM hydrographic cruises. Dots show station locations. Due to the large range of chlorophyll *a* concentrations, the contour scale is not linear. Left panels show the fall cruises; middle the spring cruises; and right the summer cruises.

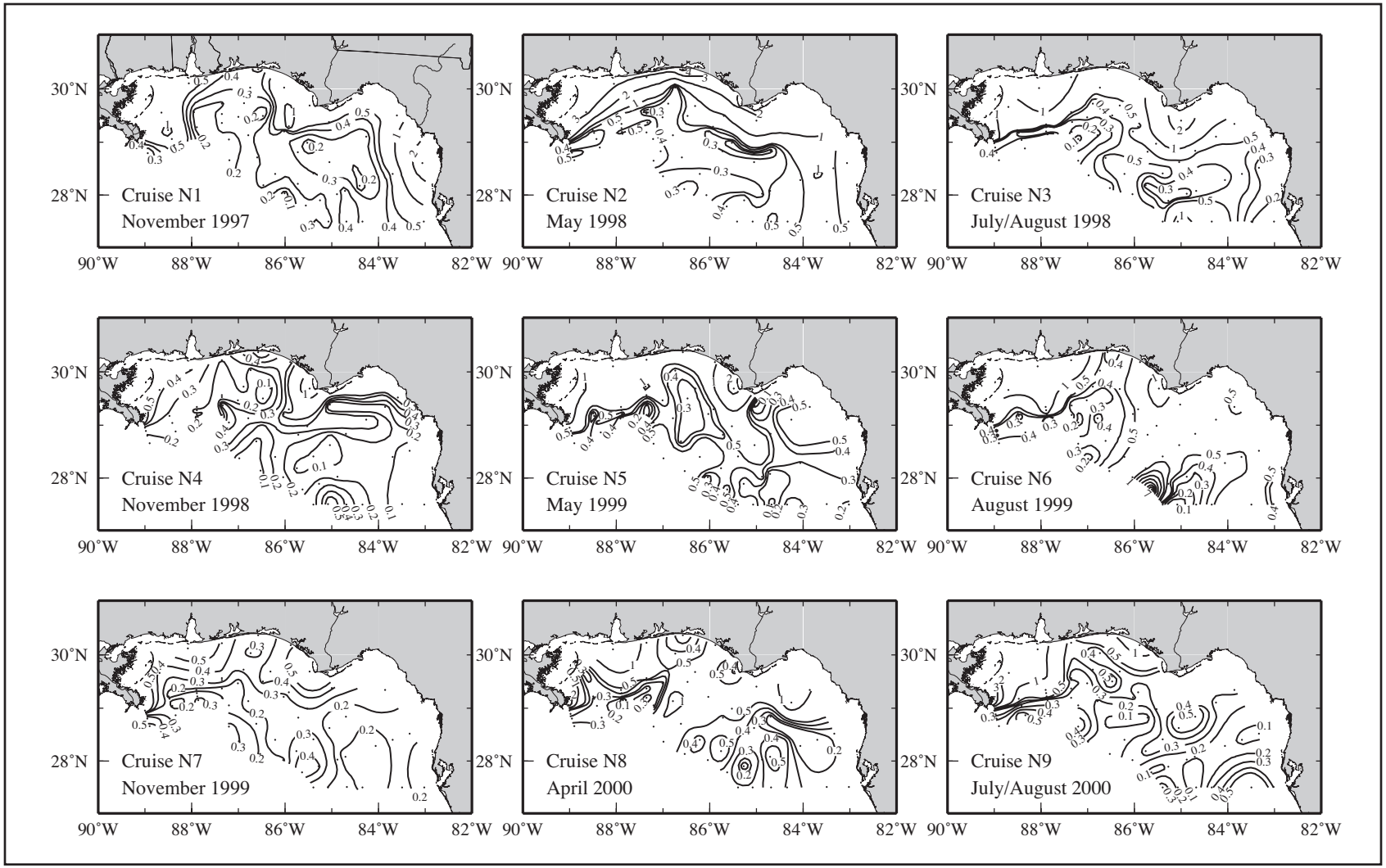

Figure 9.3-2. Chlorophyll *a* concentrations ($\mu g \cdot L^{-1}$) from subsurface DCM observations on NEGOM hydrographic cruises. Dots show station locations. Due to the large range of chlorophyll *a* concentrations, the contour scale is not linear. Left panels show the fall cruises; middle the spring cruises; and right the summer cruises.

Table 9.3-1. Percent of chlorophyll *a* contributed by individual algal groups in near-surface, deep chlorophyll maximum (DCM), and below DCM (BDCM) waters on cruise N1 (November 1997). Chlorophyll *a* concentration is in $\mu g \cdot L^{-1}$.

Algal Groups	Water Depth	Average (%)	Standard Deviation	Minimum (%)	Maximum (%)
Prochlorophytes	Surface	16	7	0	30
	DCM	21	11	0	40
	BDCM	24	17	0	45
Cyanobacteria	Surface	30	14	0	46
	DCM	16	9	0	40
	BDCM	7	8	0	25
Chlorophytes	Surface	2	7	0	28
	DCM	2	7	0	34
	BDCM	0	1	0	7
Chryptophytes	Surface	2	5	0	19
	DCM	1	3	0	15
	BDCM	1	3	0	18
Chlorophytes	Surface	2	7	0	28
	DCM	2	7	0	34
	BDCM	0	1	0	7
Pelagophytes	Surface	6	5	0	20
	DCM	10	7	0	26
	BDCM	15	10	0	30
Dinoflagellates	Surface	2	6	0	30
	DCM	4	8	0	36
	BDCM	1	6	0	40
Diatoms	Surface	6	6	0	24
	DCM	7	7	0	24
	BDCM	8	6	0	22
Prymnesiophytes	Surface	24	12	0	51
	DCM	31	16	0	66
	BDCM	28	15	0	60
Prasinophytes	Surface	0	0	0	0
	DCM	0	0	0	0
	BDCM	0	0	0	0
Chlorophyll *a*	Surface	0.37	0.54	0.08	3.89
	DCM	0.41	0.40	0.09	2.77
	BDCM	0.23	0.44	0.01	3.16

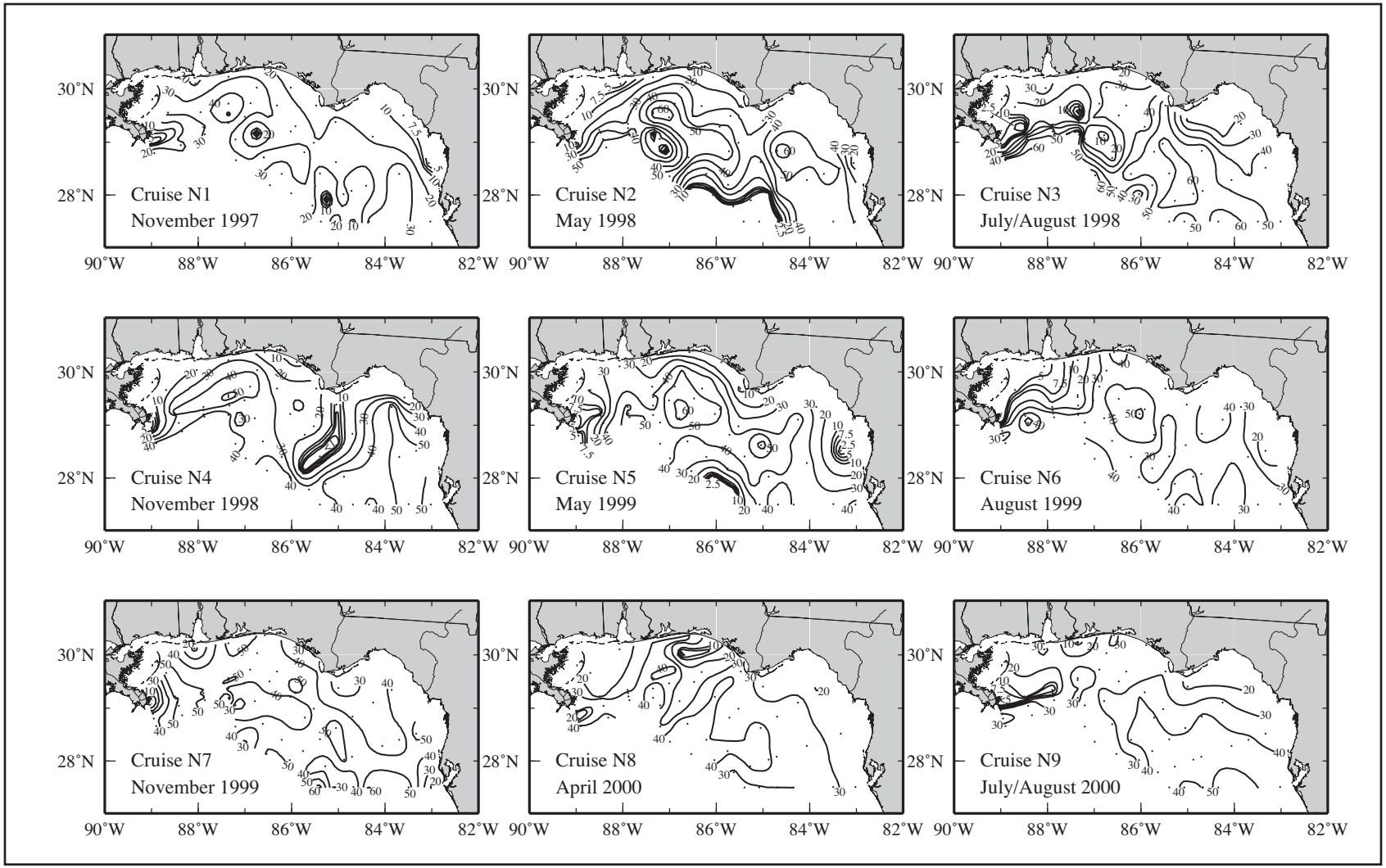

Figure 9.3-3. Prymnesiophyte abundance, as percent of chlorophyll *a*, in near-surface waters on nine NEGOM cruises from November 1997 through August 2000. Left panels show the fall cruises; middle the spring cruises; and right the summer cruises.

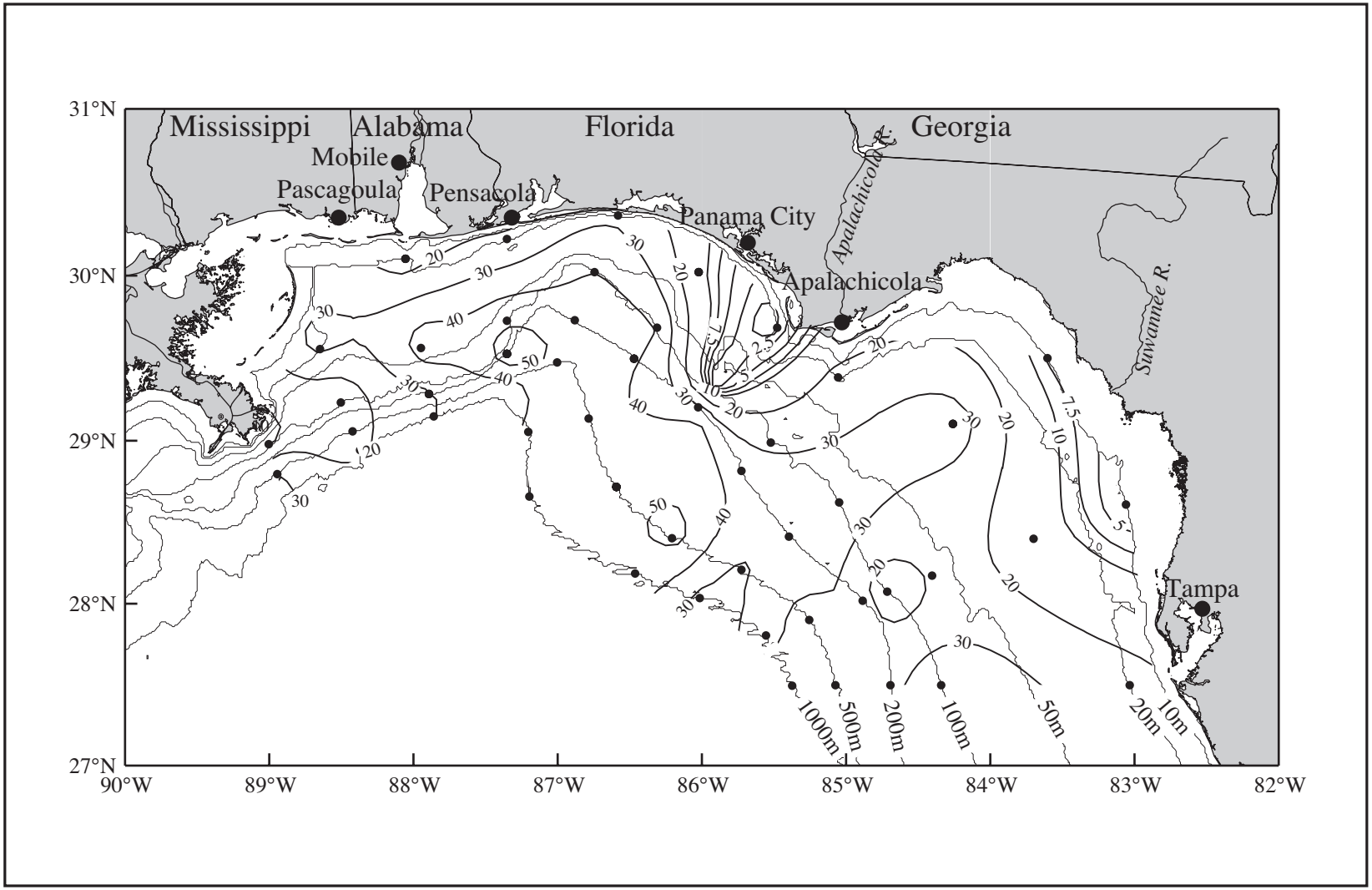

Figure 9.3-4. Prymnesiophytes (as a percent of chlorophyll *a*) at the deep chlorophyll maximum during NEGOM cruise N1, 16-26 November 1997.

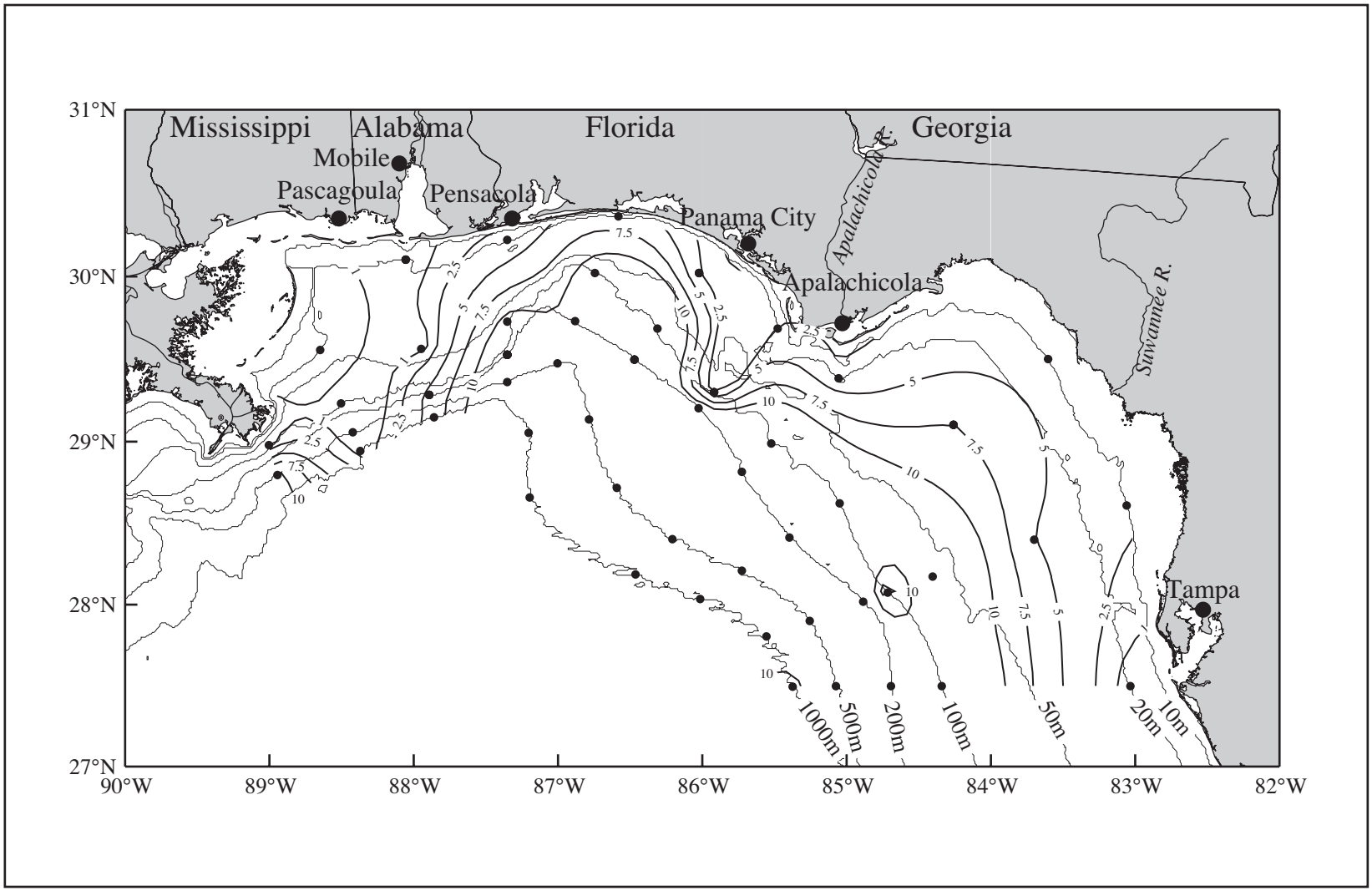

Figure 9.3-5. Pelagophytes (as a percent of chlorophyll *a*) at the deep chlorophyll maximum during NEGOM cruise N1, 16-26 November 1997.

9.3-6). Diatoms, although a minor contributor to chlorophyll *a*, were found primarily in near-shore waters (Figure 9.3-7), particularly west of Cape San Blas.

Cruise N2: In May 1998, chlorophyll *a* concentrations ranged from 0.03 to 3.33 $\mu g \cdot L^{-1}$ in near-surface water samples and from 0.12 to 4.18 $\mu g \cdot L^{-1}$ in DCM water samples with most chlorophyll *a* concentrations ≤ 1.0 $\mu g \cdot L^{-1}$. Highest chlorophyll *a* concentrations (ranging from 0.4 to 3.3 $\mu g \cdot L^{-1}$) were encountered in the near-shore waters between lines 1 and 5 in both the near-surface and DCM waters. Chlorophyll *a* concentrations were lower in the rest of the study area, ranging from 0.03 to 0.6 $\mu \cdot L^{-1}$ (Figure 9.3-1, top center panel).

Major pigments that were commonly detected included chlorophylls *b*, c_2, and c_3 and β-carotene, fucoxanthin, 19'-butanoyloxyfucoxanthin, 19'-hexanoyloxyfucoxanthin, diadinoxanthin, and zeaxanthin. Concentrations of these major accessory pigments (the fucoxanthins, diadinoxanthin, zeaxanthin, and chlorophylls *b*, c_2, and c_3) ranged from 1.2 $\mu g \cdot L^{-1}$ to less than 0.01 $\mu g \cdot L^{-1}$. Peridinin, violaxanthin, diatoxanthin, and alloxanthin were detected in trace amounts, generally < 0.01 $\mu g \cdot L^{-1}$, in only a few samples.

The major algal species inferred from the accessory pigment compositions were prymnesiophytes and cyanobacteria, with minor (<10% each) contributions from diatoms and prochlorophytes. These four types of phytoplankton accounted for over 70% of the chlorophyll *a* detected. The average relative proportions of these four algal groups were, respectively, 31%, 28%, 8%, and 4% in near-surface waters and 36%, 20%, 8%, and 22% in DCM waters (Table 9.3-2). In contrast to the algal communities encountered on cruise N1, pelagophytes were present in trace amounts in near-surface waters and at slightly higher abundances in DCM waters during N2 (Table 9.3-2). As on cruise N1, other types of phytoplankton, such as chlorophytes, chryptophytes, dinoflagellates, and prasinophytes, were minor contributors to the living biomass during cruise N2.

Prochlorophytes were lowest in near-surface waters and highest in DCM waters. The highest abundances of prochlorophytes were along the offshore shelf between lines 1 and 9 in DCM waters. Cyanobacteria were relatively abundant throughout the region with patches of high abundance on the offshore shelf as well. High relative abundances of diatoms were present in near-shore waters (Figure 9.3-8). The occurrence of prymnesiophytes was widespread and the highest abundances of prymnesiophytes were located offshore (Figure 9.3-3, top center panel).

Cruise N3: In August 1998, chlorophyll *a* concentrations ranged from 0.08 to 12.23 $\mu g \cdot L^{-1}$ in near-surface water samples and from 0.07 to 2.67 $\mu g \cdot L^{-1}$ in DCM water samples with most chlorophyll *a* concentrations ≤ 1.0 $\mu g \cdot L^{-1}$. The highest chlorophyll *a* concentrations were in near-surface waters close to the Mississippi River Delta along lines 1 and 2 (Figure 9.3-1, top right panel). Also relatively high concentrations are seen over the outer shelf and slope at 86° to 87°W. High chlorophyll *a* concentrations in DCM waters occurred in near-shore waters between lines 1 and 3 and near Apalachicola (Figure 9.3-2, top right panel). Chlorophyll *a* concentrations in near-shore waters were lower across the remaining study area and ranged from 0.08 to 0.6 $\mu g \cdot L^{-1}$. Over the outer shelf and slope, the highest chlorophyll *a* concentrations in the DCM were at the shelf edge near 85°W along line 11.

Commonly detected pigments included chlorophylls *b* and c_2, and β-carotene, fucoxanthin, 19'-butanoyloxyfucoxanthin, 19'-hexanoyloxyfucoxanthin, peridinin, diadinoxanthin, and zeaxanthin. Concentrations of major accessory pigments (the fucoxanthins, diadinoxanthin,

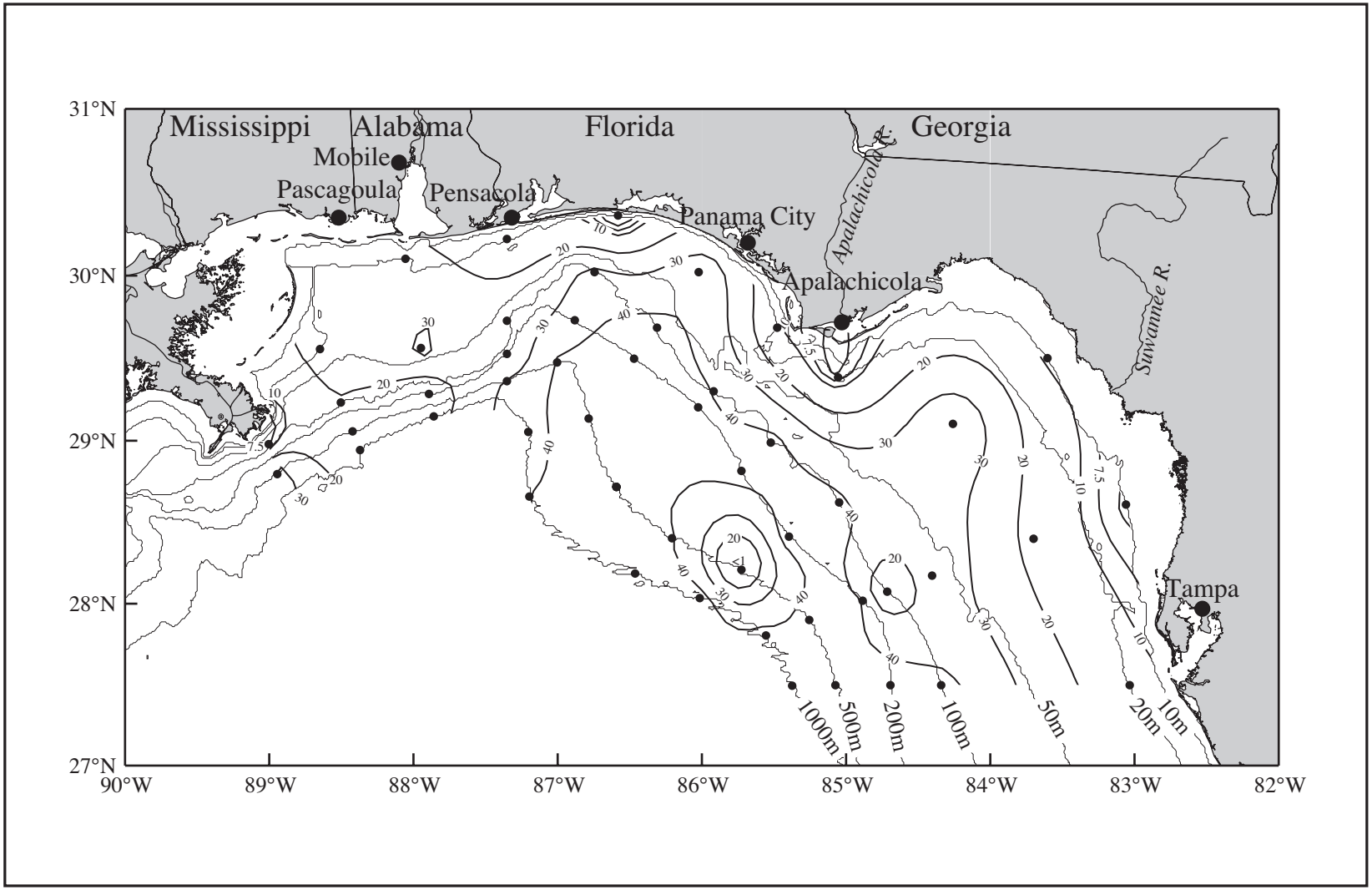

Figure 9.3-6. Cyanobacteria (as a percent of chlorophyll *a*) in near-surface waters during NEGOM cruise N1, 16-26 November 1997.

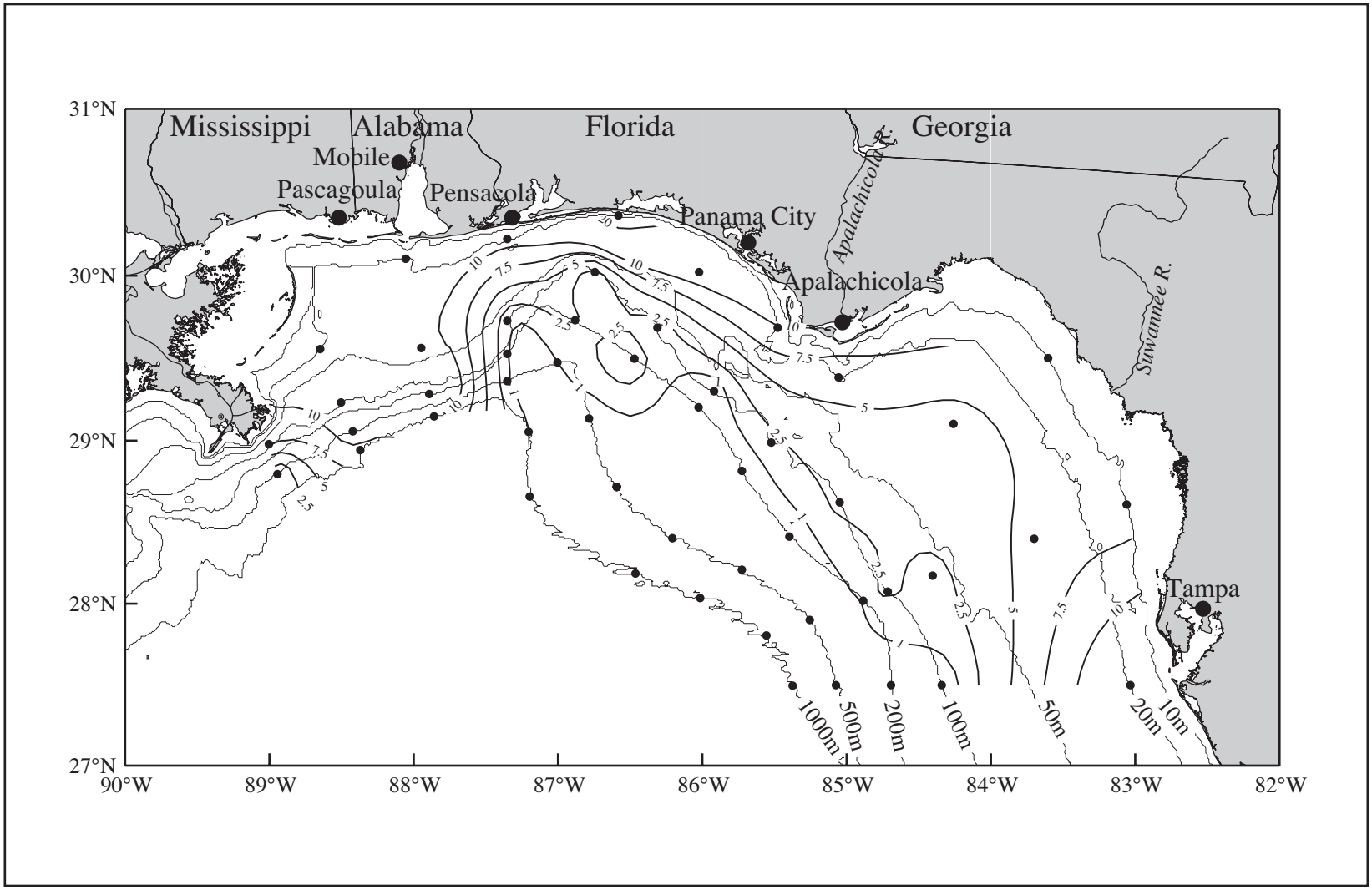

Figure 9.3-7. Diatoms (as a percent of chlorophyll *a*) in near-surface waters during NEGOM cruise N1, 16-26 November 1997.

Table 9.3-2. Percent of chlorophyll *a* contributed by individual algal groups in near surface, deep chlorophyll maximum (DCM), and below DCM (BDCM) waters on cruise N2 (May 1998). Chlorophyll *a* concentration is in $\mu g \cdot L^{-1}$.

Algal Groups	Water Depth	Average (%)	Standard Deviation	Minimum (%)	Maximum (%)
Prochlorophytes	Surface	4	6	0	18
	DCM	22	14	0	43
	BDCM	8	13	0	43
Cyanobacteria	Surface	28	17	0	43
	DCM	20	13	0	44
	BDCM	4	8	0	34
Chlorophytes	Surface	1	5	0	21
	DCM	3	7	0	26
	BDCM	2	7	0	25
Chryptophytes	Surface	2	5	0	20
	DCM	3	6	0	31
	BDCM	2	5	0	22
Pelagophytes	Surface	1	2	0	15
	DCM	7	7	0	22
	BDCM	10	15	0	43
Dinoflagellates	Surface	2	6	0	28
	DCM	1	3	0	17
	BDCM	2	6	0	36
Diatoms	Surface	8	8	0	36
	DCM	8	7	0	30
	BDCM	9	8	0	24
Prymnesiophytes	Surface	31	21	0	66
	DCM	36	17	0	60
	BDCM	31	23	0	61
Prasinophytes	Surface	0	1	0	8
	DCM	1	2	0	14
	BDCM	0	1	0	7
Chlorophyll *a* ($\mu g \cdot L^{-1}$)	Surface	0.44	0.75	0.03	3.33
	DCM	0.67	0.80	0.12	4.18
	BDCM	0.29	0.43	0.01	1.84

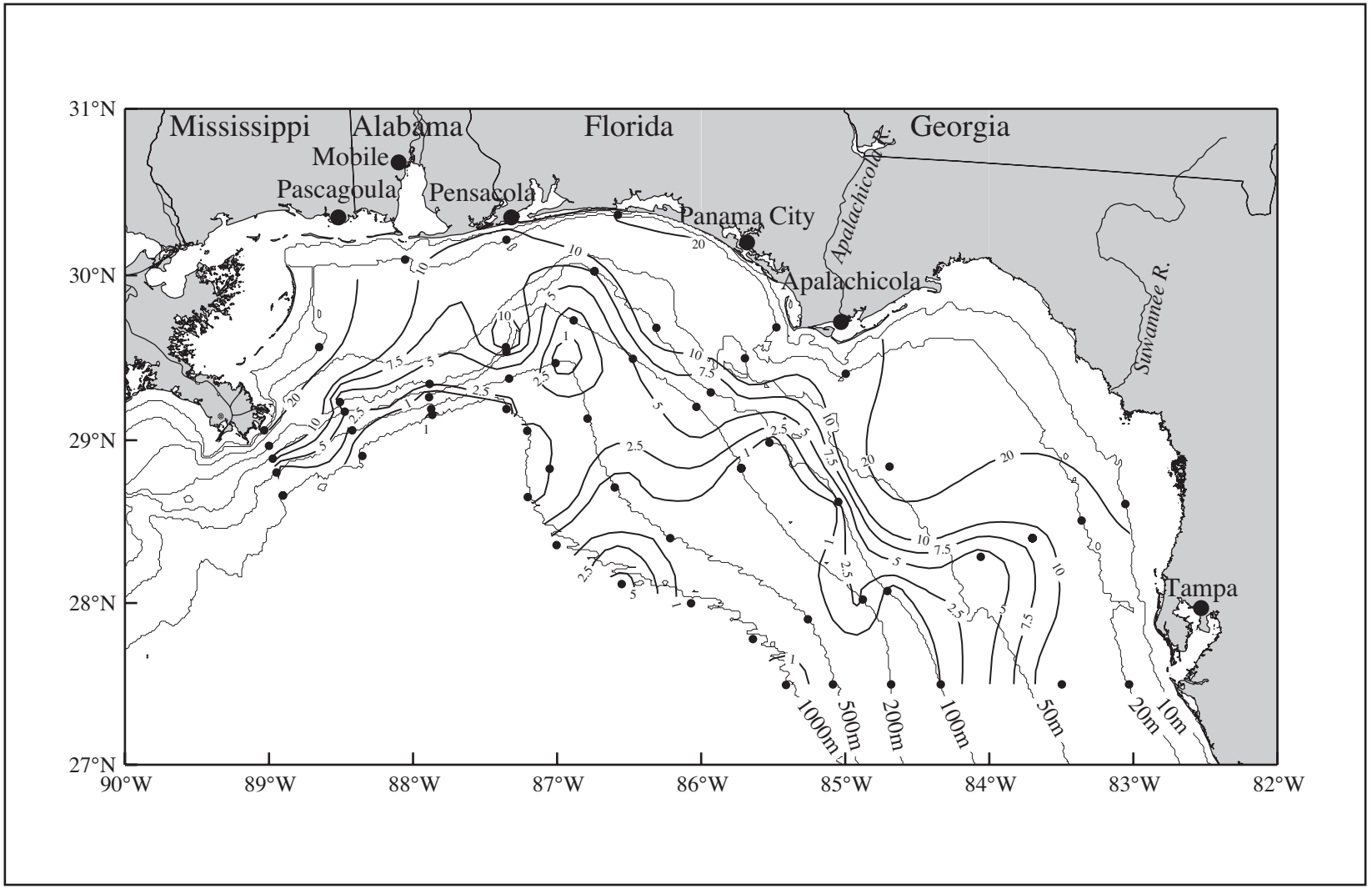

Figure 9.3-8. Diatoms (as a percent of chlorophyll *a*) at the deep chlorophyll maximum during NEGOM cruise N2, 5-16 May 1998.

zeaxanthin, and chlorophyll c_2) ranged from 0.5 $\mu g \cdot L^{-1}$ to less than 0.01 $\mu g \cdot L^{-1}$. Chlorophyll c_3, violaxanthin, diatoxanthin, and alloxanthin were detected in trace amounts, generally < 0.02 $\mu g \cdot L^{-1}$, in only a few samples.

The dominant species inferred from the accessory pigment compositions were prymnesiophytes, cyanobacteria, prochlorophytes, and diatoms. These four types of phytoplankton accounted for over 90% of the chlorophyll *a* detected. The average relative proportions of these four algal groups were, respectively, 37%, 27%, 17%, and 12% in near-surface waters and 34%, 21%, 23%, and 10% in DCM waters (Table 9.3-3). Pelagophytes and dinoflagellates accounted for 7%-10% of total chlorophyll *a* in both near-surface and DCM waters (Table 9.3-3). Other types of phytoplankton, such as chlorophytes, chryptophytes, and prasinophytes, were minor contributors to the living biomass during N3.

Table 9.3-3. Percent of chlorophyll *a* contributed by individual algal groups in near-surface, deep chlorophyll maximum layer (DCM), and below DCM (BDCM) waters on cruise N3 (July-August 1998). Chlorophyll *a* concentration is in $\mu g \cdot L^{-1}$.

Algal Groups	Water Depth	Average (%)	Standard Deviation	Minimum (%)	Maximum (%)
Prochlorophytes	Surface	17	12	0	44
	DCM	23	13	0	48
	BDCM	19	13	0	44
Cyanobacteria	Surface	27	14	0	48
	DCM	21	12	0	43
	BDCM	12	11	0	38
Chlorophytes	Surface	1	4	0	20
	DCM	2	6	0	29
	BDCM	2	5	0	28
Chryptophytes	Surface	1	3	0	14
	DCM	2	5	0	19
	BDCM	2	5	0	17
Pelagophytes	Surface	3	5	0	20
	DCM	6	5	0	20
	BDCM	10	10	0	35
Dinoflagellates	Surface	4	5	0	17
	DCM	2	3	0	16
	BDCM	1	4	0	24
Diatoms	Surface	12	10	2	40
	DCM	10	8	0	36
	BDCM	12	8	0	32
Prymnesiophytes	Surface	37	21	0	68
	DCM	34	16	0	60
	BDCM	32	19	0	58
Prasinophytes	Surface	1	3	0	14
	DCM	2	5	0	18
	BDCM	1	3	0	18
Chlorophyll *a* ($\mu g \cdot L^{-1}$)	Surface	0.74	1.73	0.08	12.23
	DCM	0.55	0.44	0.07	2.67
	BDCM	0.41	0.78	0.04	5.38

The spatial distribution of individual algal groups was different for each algal type at different water depths. High relative abundances of prochlorophytes were distributed between lines 1 and 5 in near-surface and DCM waters (Figure 9.3-9). Cyanobacteria generally were higher in near-surface waters than in DCM waters and exhibited a patchy distribution. Prymnesiophytes were generally high across the study area in both near-surface and DCM waters, except in the near-shore areas between lines 1 and 4 where their abundance typically was relatively lower than the rest of the study region (Figure 9.3-3, top right panel).

Cruise N4: In November 1998, chlorophyll *a* concentrations ranged from 0.01 to 0.94 $\mu g \cdot L^{-1}$ in near-surface water samples and from 0.03 to 1.35 $\mu g \cdot L^{-1}$ in DCM water samples with most chlorophyll *a* concentrations ≤ 0.5 $\mu g \cdot L^{-1}$. Chlorophyll *a* concentrations were low compared to previous cruises. Highest chlorophyll *a* concentrations were present in near-surface waters close to the Mississippi River Delta on lines 1 and 2 (Figure 9.3-1, middle left panel). High chlorophyll *a* concentrations were distributed in the near-shore DCM waters off Apalachicola between lines 7 and 9 in DCM waters (Figure 9.3-2, middle left panel). Chlorophyll *a* concentrations were lower in the remaining study area, ranging from 0.01 to 0.5 $\mu g \cdot L^{-1}$.

Commonly detected accessory pigments included chlorophyll *b*, β-carotene, fucoxanthin, 19'-butanoyloxyfucoxanthin, and 19'-hexanoyloxyfucoxanthin. Concentrations of major accessory pigments (the fucoxanthins) ranged from 0.35 $\mu g \cdot L^{-1}$ to below the detection limit of the analysis method. Chlorophylls c_2 and c_3, peridinin, violaxanthin, diadinoxanthin, diatoxanthin, alloxanthin, and zeaxanthin were detected in trace amounts, generally < 0.1 $\mu g \cdot L^{-1}$, in limited samples.

The dominant species inferred from the accessory pigment compositions were prymnesiophytes, pelagophytes, diatoms, and prochlorophytes. These four types of phytoplankton accounted for about 50% of the chlorophyll *a* detected in near-surface waters and about 90% in DCM waters. The average relative proportions of these four algal groups were 32%, 6%, 4%, and 6% in near-surface waters and 36%, 18%, 9%, and 15% in DCM waters, respectively (Table 9.3-4). Cyanobacteria and chryptophytes each accounted for 1%-3% of total chlorophyll *a* in near-surface and DCM waters (Table 9.3-4). Other types of phytoplankton, such as chlorophytes, dinoflagellates, and prasinophytes, were minor contributors to the living biomass during cruise N4.

The spatial distribution of individual algal groups was different for each algal type. Prymnesiophytes were generally high in both near-surface and DCM waters across the study area, except near-shore and in the region between lines 8 and 10 (e.g., Figure 9.3-3, middle left panel). Diatoms were primarily present in near-shore waters, particularly near Apalachicola and the area between lines 1 and 4 (not shown).

Cruise N5: In May 1999, chlorophyll *a* concentrations ranged from 0.04 to 6.43 $\mu g \cdot L^{-1}$ in near-surface water samples and from 0.05 to 2.40 $\mu g \cdot L^{-1}$ in DCM water samples with most chlorophyll *a* concentrations ≤ 1.0 $\mu g \cdot L^{-1}$. The highest chlorophyll *a* concentrations were present in near-surface waters close to the Mississippi River Delta on lines 1 and 2 (Figure 9.3-1, middle center panel). Chlorophyll *a* concentrations in the remainder of the study area were low, generally below 0.4 $\mu g \cdot L^{-1}$. Distribution of chlorophyll *a* in DCM waters differed from that of near-surface waters. Highest chlorophyll *a* concentrations were present in the near-shore DCM waters near Apalachicola between lines 7 and 9 (Figure 9.3-2, middle center panel). The DCM waters on lines 1 and 2 also had high chlorophyll *a* concentrations.

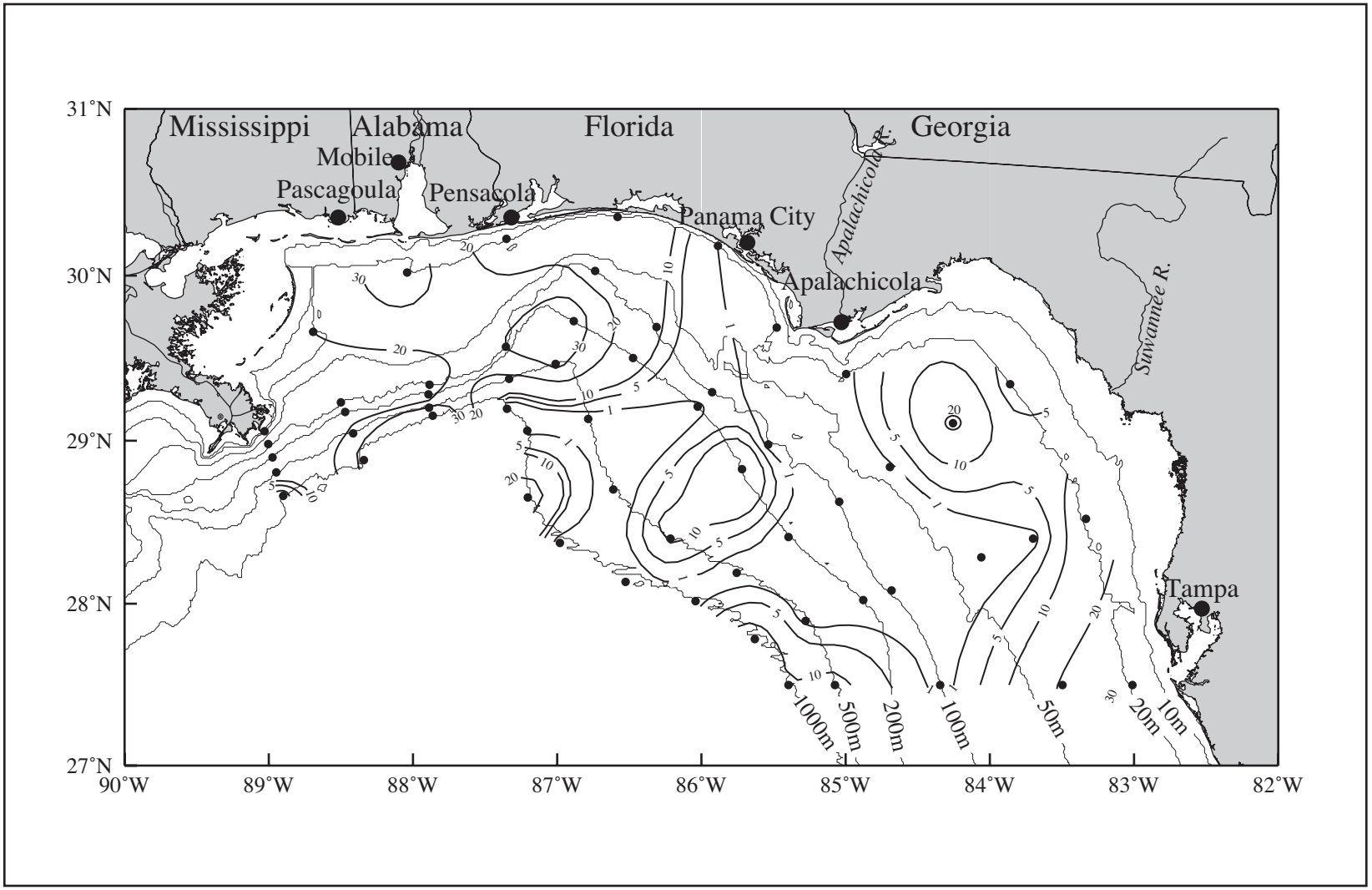

Figure 9.3-9. Prochlorophytes (as a percent of chlorophyll *a*) in near-surface waters during NEGOM cruise N3, 26 July-6 August 1998.

Table 9.3-4. Percent of chlorophyll *a* contributed by individual algal groups in near-surface, deep chlorophyll maximum layer (DCM), and below DCM (BDCM) waters on cruise N4 (November 1999). Chlorophyll *a* concentration is in $\mu g \cdot L^{-1}$.

Algal Groups	Water Depth	Average (%)	Standard Deviation	Minimum (%)	Maximum (%)
Prochlorophytes	Surface	6	10	0	32
	DCM	15	13	0	35
	BDCM	19	13	0	37
Cyanobacteria	Surface	4	7	0	23
	DCM	0	2	0	8
	BDCM	0	1	0	5
Chlorophytes	Surface	0	3	0	20
	DCM	1	4	0	20
	BDCM	1	2	0	12
Chryptophytes	Surface	3	6	0	25
	DCM	2	5	0	21
	BDCM	1	4	0	21
Pelagophytes	Surface	6	7	0	23
	DCM	18	11	0	38
	BDCM	24	10	0	46
Dinoflagellates	Surface	0	0	0	0
	DCM	0	1	0	6
	BDCM	0	1	0	7
Diatoms	Surface	4	8	0	28
	DCM	9	13	0	42
	BDCM	10	13	0	33
Prymnesiophytes	Surface	32	17	0	55
	DCM	36	14	0	50
	BDCM	42	11	0	58
Prasinophytes	Surface	0	0	0	0
	DCM	0	0	0	0
	BDCM	0	0	0	0
Chlorophyll *a* ($\mu g \cdot L^{-1}$)	Surface	0.18	0.18	0.01	0.94
	DCM	0.26	0.21	0.03	1.35
	BDCM	0.16	0.12	0.02	0.64

Commonly detected pigments included chlorophylls *b* and c_2 and β-carotene, fucoxanthin, 19'-butanoyloxyfucoxanthin, 19'-hexanoyloxyfucoxanthin, diadinoxanthin, and zeaxanthin. Concentrations of major accessory pigments (the fucoxanthins, diadinoxanthin, zeaxanthin) ranged from 1.8 $\mu g \cdot L^{-1}$ to below the method's detection limit. Chlorophyll c_3, peridinin, violaxanthin, diatoxanthin, and alloxanthin were detected in trace amounts, generally < 0.1 $\mu g \cdot L^{-1}$, in only a few samples.

The dominant species inferred from accessory pigments were prymnesiophytes, pelagophytes, cyanobacteria, and prochlorophytes. These four types of phytoplankton account for, on average, over 70% of chlorophyll *a* detected. Average relative proportions of these four algal groups were, 34%, 3%, 28%, and 5% in near-surface waters and 37%, 10%, 21%, and 17% in DCM waters, respectively (Table 9.3-5). Cyanobacteria, prymnesiophytes,

Table 9.3-5. Percent of chlorophyll *a* contributed by individual algal groups in near-surface, deep chlorophyll maximum layer (DCM), and below DCM (BDCM) waters on cruise N5 (May 1999). Chlorophyll *a* concentration is in $\mu g \cdot L^{-1}$.

Algal Groups	Water Depth	Average (%)	Standard Deviation	Minimum (%)	Maximum (%)
Prochlorophytes	Surface	5	7	0	30
	DCM	17	10	0	40
	BDCM	17	12	0	32
Cyanobacteria	Surface	28	10	0	43
	DCM	21	12	0	50
	BDCM	10	9	0	31
Chlorophytes	Surface	3	6	0	20
	DCM	4	6	0	24
	BDCM	0	2	0	13
Chryptophytes	Surface	2	5	0	20
	DCM	3	4	0	20
	BDCM	1	2	0	12
Pelagophytes	Surface	3	5	0	21
	DCM	10	8	0	34
	BDCM	19	10	0	36
Dinoflagellates	Surface	3	6	0	30
	DCM	2	4	0	22
	BDCM	1	3	0	13
Diatoms	Surface	5	6	0	21
	DCM	6	9	0	34
	BDCM	5	8	0	28
Prymnesiophytes	Surface	34	17	0	64
	DCM	37	16	0	71
	BDCM	34	12	0	48
Prasinophytes	Surface	1	2	0	11
	DCM	1	2	0	10
	BDCM	0	1	0	5
Chlorophyll *a* ($\mu g \cdot L^{-1}$)	Surface	0.64	1.36	0.04	6.43
	DCM	0.50	0.36	0.05	2.40
	BDCM	0.21	0.15	0.02	0.66

and prochlorophytes accounted for over 60% of the total chlorophyll *a* concentration in near-surface and DCM waters. Pelagophytes, chlorophytes, dinoflagellates, and diatoms constituted the majority of the remaining chlorophyll *a*. The average relative proportions of each of the species are given in Table 9.3-5.

The spatial distribution of individual algal groups varied for each algal type and with water depth. The contribution of prochlorophytes to chlorophyll *a* was low in near-surface waters but high in DCM waters. Relatively high abundances of prochlorophytes were present in offshore shelf DCM waters (Figure 9.3-10). Cyanobacteria were generally high in both near-surface and DCM waters. Prymnesiophytes were high across the study area, particularly on the offshore shelf in near-surface and DCM waters (Figure 9.3-3, middle center panel).

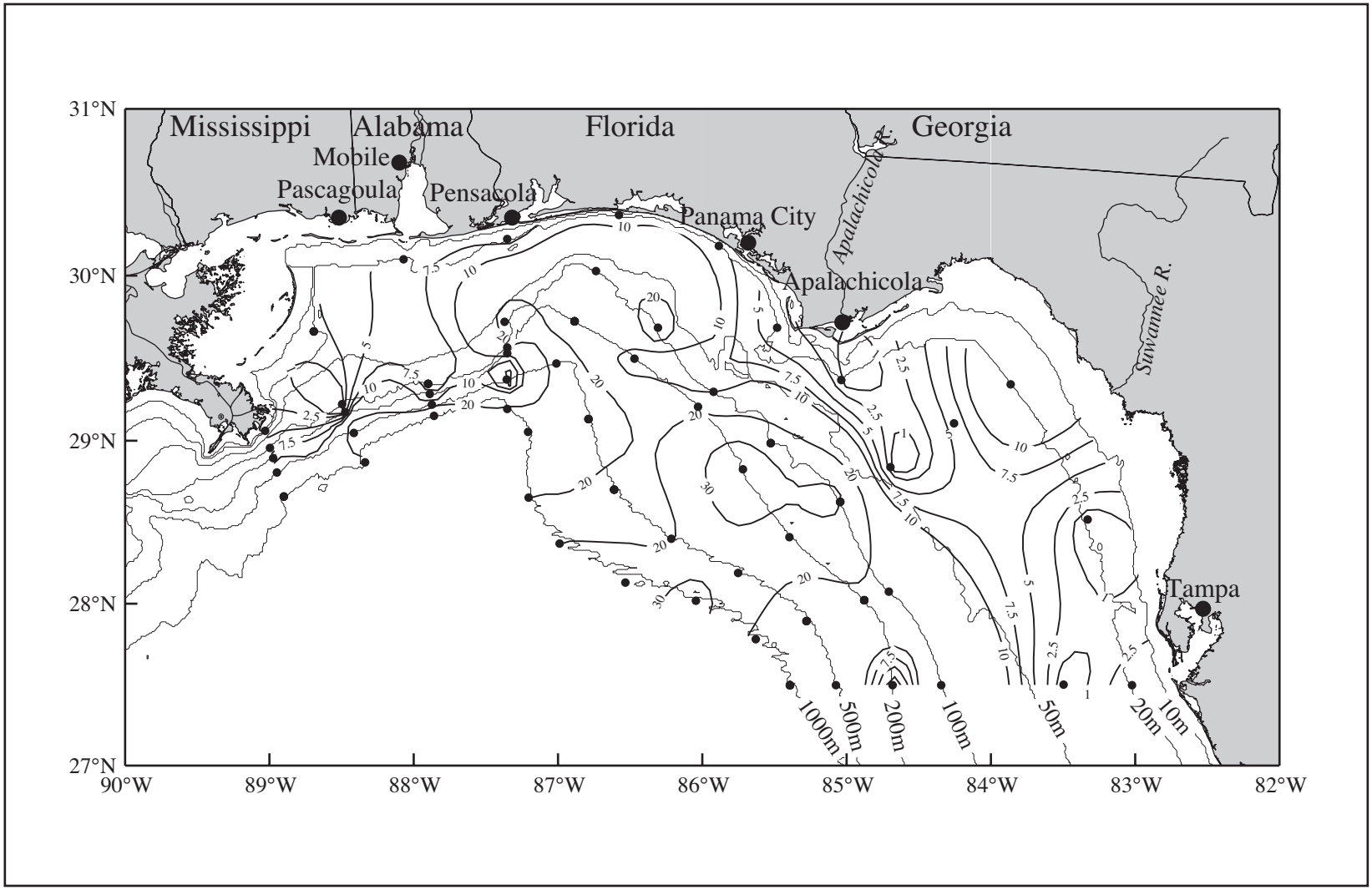

Figure 9.3-10. Prochlorophytes (as a percent of chlorophyll *a*) at the deep chlorophyll maximum during NEGOM cruise N5, 16-27 May 1999.

Cruise N6: In August 1999, chlorophyll *a* concentrations ranged from 0.01 to 2.21 $\mu g \cdot L^{-1}$ in near-surface water samples and from 0.07 to 7.74 $\mu g \cdot L^{-1}$ in DCM water samples with most chlorophyll *a* concentrations ≤ 0.8 $\mu g \cdot L^{-1}$. Highest chlorophyll *a* concentrations were encountered in near-shore near-surface waters south of Mississippi and Alabama between lines 1 and 4 (Figure 9.3-1, middle right panel). Chlorophyll *a* concentrations in near-shore waters north of Tampa Bay between lines 10 and 11 were also high. Chlorophyll *a* concentrations in the remainder of the study area were low, generally below 0.4 $\mu g \cdot L^{-1}$. The distribution of chlorophyll *a* in DCM waters was similar to that in near-surface waters (Figure 9.3-2, middle right panel), except that values off Cape San Blas were relatively larger and there were very high values over the slope between lines 9 and 11.

Commonly detected pigments included chlorophylls *b* and c_2 and β-carotene, fucoxanthin, 19'-butanoyloxyfucoxanthin, 19'-hexanoyloxyfucoxanthin, diadinoxanthin, and zeaxanthin. Concentrations of major accessory pigments (the fucoxanthins, diadinoxanthin, zeaxanthin) ranged from 0.3 $\mu g \cdot L^{-1}$ to below the method's detection limit. Chlorophyll c_3, peridinin, violaxanthin, diatoxanthin, prasinoxanthin, and alloxanthin were detected in trace amounts, generally < 0.1 $\mu g \cdot L^{-1}$, in only a few samples.

Many types of algal groups were present in high abundance in near-surface and DCM waters. The major species inferred from the accessory pigment compositions were prymnesiophytes, pelagophytes, cyanobacteria, diatoms, dinoflagellates, chlorophytes, and prochlorophytes. Prasinophytes were not detected. Prymnesiophytes were the dominant algal groups. Other types of phytoplankton species were present in low abundances (Table 9.3-6).

The spatial distribution of individual algal groups varied by algal type. Relatively high abundances of prochlorophytes in near-surface and DCM waters occurred over the offshore shelf (Figure 9.3-11), particularly in the eastern region. Cyanobacteria were high in near-surface waters except in the areas between lines 1 and 3 and lines 6 and 7. Cyanobacteria abundance was lower in DCM waters than in near-surface waters. Prymnesiophytes were high across the study area in both near-surface and DCM waters, particularly over the offshore shelf and slope (Figure 9.3-3, middle right panel). Prymnesiophytes were relatively low in near-shore waters between lines 1 and 3. Diatoms were present in highest abundances in near-shore waters.

Cruise N7: In November 1999, chlorophyll *a* concentrations ranged from 0.07 to 2.7 $__ \cdot L^{-1}$ in near-surface water samples and from 0.12 to 0.86 $__ \cdot L^{-1}$ in DCM water samples with most chlorophyll *a* concentrations ≤ 0.6 $__ \cdot L^{-1}$. Highest chlorophyll *a* concentrations were present in near-shore near-surface waters close to the Mississippi River Delta on line 1 (Figure 9.3-1, bottom left panel). Chlorophyll *a* concentrations in near-shore waters near Apalachicola between lines 7 and 8 were also high. Chlorophyll *a* concentrations in the remainder of the study area were low, generally below 0.4 $__ \cdot L^{-1}$.

The distribution of chlorophyll *a* in DCM waters was similar to that in near-surface waters. Highest chlorophyll *a* concentrations were present in near-shore waters between lines 1 and 4 and near Cape San Blas between lines 7 and 8 in DCM waters (Figure 9.3-2, bottom left panel).

Commonly detected pigments included chlorophylls *b* and c_2 and β-carotene, fucoxanthin, 19'-butanoyloxyfucoxanthin, 19'-hexanoyloxyfucoxanthin, diadinoxanthin, and diatoxanthin. Concentrations of major accessory pigments (the fucoxanthins, diadinoxanthin,

Table 9.3-6. Percent of chlorophyll *a* contributed by individual algal groups in near-surface, deep chlorophyll maximum layer (DCM), and below DCM (BDCM) waters on cruise N6 (August 1999). Chlorophyll *a* concentration is in $\mu g \cdot L^{-1}$.

Algal Groups	Water Depth	Average (%)	Standard Deviation	Minimum (%)	Maximum (%)
Prochlorophytes	Surface	15	10	0	35
	DCM	19	9	0	34
	BDCM	21	8	0	31
Cyanobacteria	Surface	17	11	0	38
	DCM	11	8	0	30
	BDCM	10	5	0	20
Chlorophytes	Surface	8	8	0	34
	DCM	8	7	0	30
	BDCM	4	7	0	31
Chryptophytes	Surface	2	3	0	12
	DCM	5	4	0	16
	BDCM	3	4	0	12
Pelagophytes	Surface	5	4	0	17
	DCM	9	6	0	24
	BDCM	14	6	0	25
Dinoflagellates	Surface	13	9	0	40
	DCM	10	9	0	40
	BDCM	6	7	0	29
Diatoms	Surface	10	6	0	29
	DCM	10	8	0	31
	BDCM	7	6	0	24
Prymnesiophytes	Surface	33	12	3	56
	DCM	32	13	4	56
	BDCM	28	10	4	49
Prasinophytes	Surface	0	0	0	0
	DCM	0	0	0	0
	BDCM	0	0	0	0
Chlorophyll *a* ($\mu g \cdot L^{-1}$)	Surface	0.38	0.35	0.10	2.21
	DCM	0.65	0.93	0.07	7.74
	BDCM	0.24	0.25	0.00	1.27

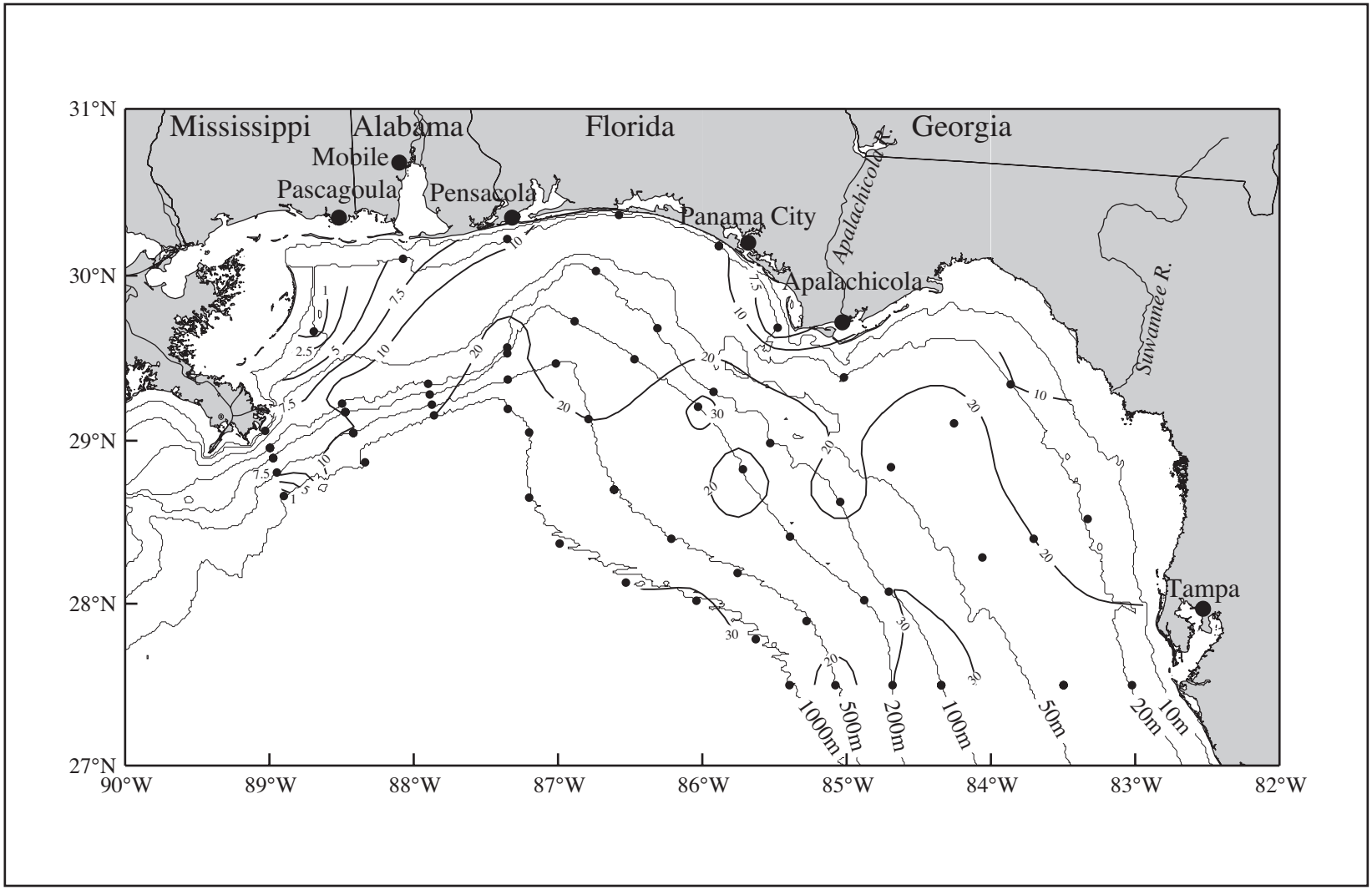

Figure 9.3-11. Prochlorophytes (as a percent of chlorophyll *a*) at the deep chlorophyll maximum during NEGOM cruise N6, 17-28 August 1999.

diatoxanthin) ranged from 0.3 __·L^{-1} to below the detection limit of the method. Chlorophyll c_3, peridinin, violaxanthin, prasinoxanthin, zeaxanthin, and alloxanthin were detected in trace amounts, generally < 0.1 __·L^{-1}, in only a few samples.

Many types of algal groups were present in high abundance in both near-surface and DCM waters. Major species inferred from accessory pigment compositions were prymnesiophytes, pelagophytes, chlorophytes, and prochlorophytes. Diatoms, dinoflagellates, cyanobacteria, chryptophytes and prasinophytes were detected in low abundances in both near-surface and DCM waters (Table 9.3-7).

Table 9.3-7. Percent of chlorophyll *a* contributed by individual algal groups in near-surface, deep chlorophyll maximum layer (DCM), and below DCM (BDCM) waters on cruise N7 (November 1999). Chlorophyll *a* concentration is in __·L^{-1}.

Algal Groups	Water Depth	Average (%)	Standard Deviation	Minimum (%)	Maximum (%)
Prochlorophytes	Surface	11	4	0	23
	DCM	15	8	0	36
	BDCM	19	8	2	30
Cyanobacteria	Surface	4	8	0	40
	DCM	3	4	0	19
	BDCM	6	7	0	20
Chlorophytes	Surface	12	6	0	32
	DCM	9	6	0	25
	BDCM	3	5	0	15
Chryptophytes	Surface	3	4	0	12
	DCM	6	3	0	12
	BDCM	5	4	0	20
Pelagophytes	Surface	9	5	0	28
	DCM	18	10	1	31
	BDCM	20	9	1	38
Dinoflagellates	Surface	4	2	1	10
	DCM	4	3	1	12
	BDCM	3	3	0	10
Diatoms	Surface	4	6	0	24
	DCM	7	7	0	29
	BDCM	4	7	0	20
Prymnesiophytes	Surface	42	11	7	64
	DCM	46	12	10	65
	BDCM	34	11	0	63
Prasinophytes	Surface	1	2	0	7
	DCM	2	2	0	7
	BDCM	1	3	0	18
Chlorophyll *a* (µg·L^{-1})	Surface	0.27	0.35	0.07	2.70
	DCM	0.31	0.16	0.12	0.86
	BDCM	0.20	0.14	0.02	0.72

The spatial distribution of individual algal groups was different for each algal type. Relatively high abundances of prochlorophytes were present in offshore DCM waters. Prymnesiophytes were high across the study area (Figure 9.3-3, bottom left panel), particularly in the offshore near-surface and DCM waters. Prymnesiophytes were relatively low in near-shore waters associated with river inflow. Diatoms occurred in relatively high abundance in near-shore waters (Figure 9.3-12). Pelagophytes were present in higher abundance in offshore waters (Figure 9.3-13).

Cruise N8: In April 2000, chlorophyll *a* concentrations ranged from 0.03 to 2.48 $\mu g \cdot L^{-1}$ in near-surface water samples and from 0.08 to 2.52 $\mu g \cdot L^{-1}$ in DCM water samples with most chlorophyll *a* concentrations ≤ 0.6 $\mu g \cdot L^{-1}$. Chlorophyll *a* spatial distributions in near-surface waters were similar to those on cruise N7, with highest chlorophyll *a* concentrations present in near-shore near-surface waters close to the Mississippi River Delta along line 1 (Figure 9.3-1, bottom center panel). Chlorophyll *a* concentrations in the remaining study area were low, generally below 0.4 $\mu g \cdot L^{-1}$.

The distribution of chlorophyll *a* in DCM waters differed from that in near-surface waters. Highest chlorophyll *a* concentrations were present in near-shore waters between lines 1 and 4 and in the Big Bend between lines 8 and 9 in DCM waters (Figure 9.3-2, bottom center panel). Patchy, high chlorophyll *a* concentrations also were observed in offshore DCM waters between lines 5 and 7.

Commonly detected pigments included chlorophylls *b* and c_2 and β-carotene, fucoxanthin, 19'-butanoyloxyfucoxanthin, 19'-hexanoyloxyfucoxanthin, diadinoxanthin, and zeaxanthin. Concentrations of major accessory pigments (the fucoxanthins, diadinoxanthin, diatoxanthin) ranged from 0.3 $\mu g \cdot L^{-1}$ to below detection. Chlorophyll c_3, peridinin, violaxanthin, prasinoxanthin, and alloxanthin were detected in trace amounts, generally < 0.1 $\mu g \cdot L^{-1}$, in only a few samples.

Many types of algal groups were present in high abundance in both near-surface and DCM waters. The major algal species inferred from the accessory pigment compositions were prymnesiophytes, pelagophytes, cyanobacteria, and prochlorophytes. Diatoms, dinoflagellates, chlorophytes, chryptophytes and prasinophytes were detected in low abundances in near-surface and DCM waters (Table 9.3-8).

The spatial distribution of individual algal groups was different for each algal type. Relatively high abundances of prochlorophytes were present in offshore near-surface and DCM waters. Prymnesiophytes were generally high across the study area, particularly in near-surface and DCM waters of the offshore shelf (e.g., Figure 9.3-3, bottom center panel). Prymnesiophytes were relatively low in near-shore waters influenced by river inflow. Diatoms were present in higher abundance in near-shore waters and in areas affected by freshwater input.

Cruise N9: In August 2000, chlorophyll *a* concentrations ranged from 0.03 to 5.13 $\mu g \cdot L^{-1}$ in near-surface water samples and from 0.04 to 3.24 $\mu g \cdot L^{-1}$ for DCM water samples with most chlorophyll *a* concentrations ≤ 0.6 $\mu g \cdot L^{-1}$. Chlorophyll *a* spatial distributions in near-surface waters were similar to those from cruise N7, with highest chlorophyll *a* concentrations present in near-shore near-surface waters close to the Mississippi River Delta along lines 1 to 4 (Figure 9.3-1, bottom right panel). Chlorophyll *a* concentrations in the remainder of the study area were low, generally below 0.4 $\mu g \cdot L^{-1}$.

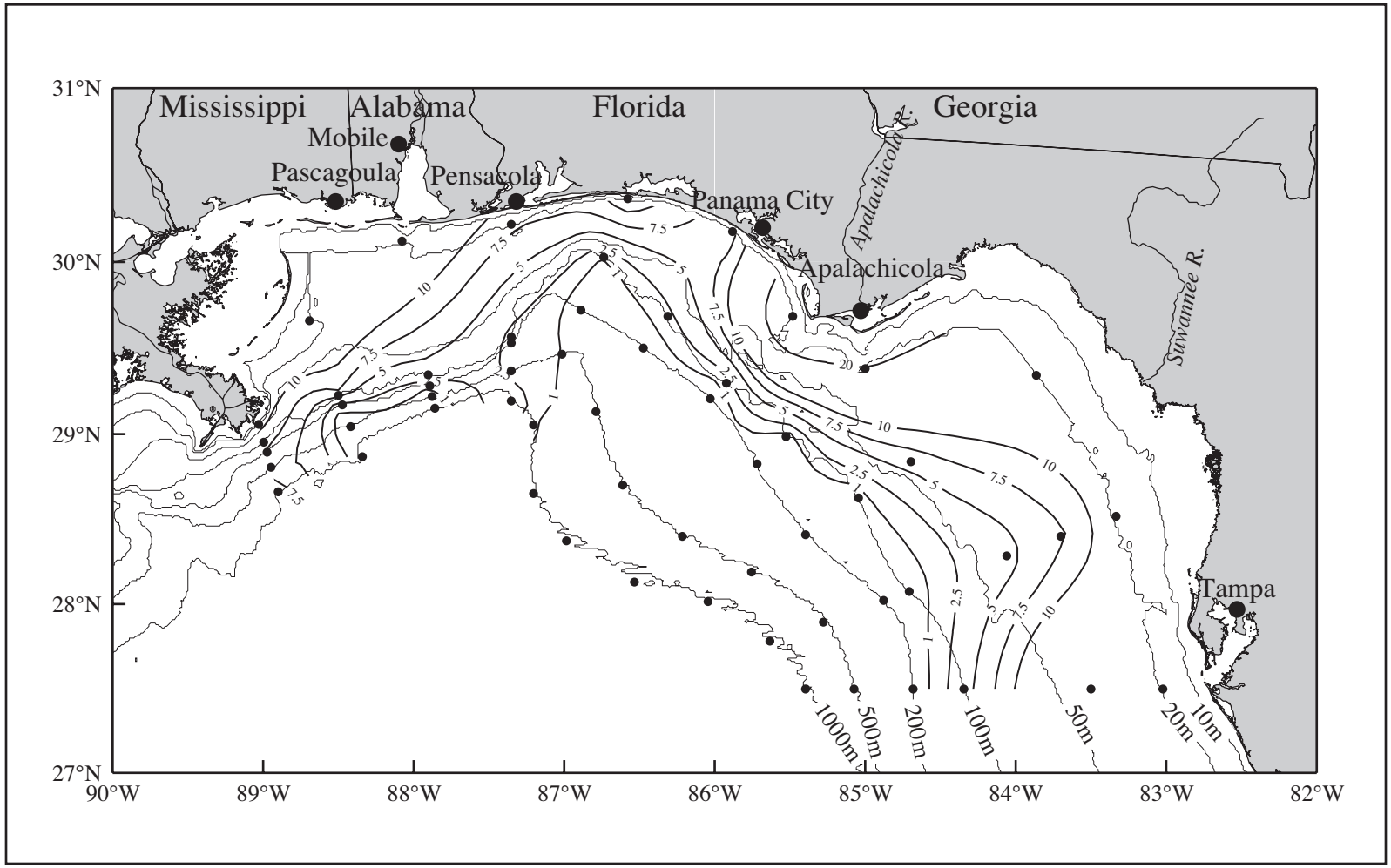

Figure 9.3-12. Diatoms (as a percent of chlorophyll *a*) at the deep chlorophyll maximum during NEGOM cruise N7, 13-22 November 1999.

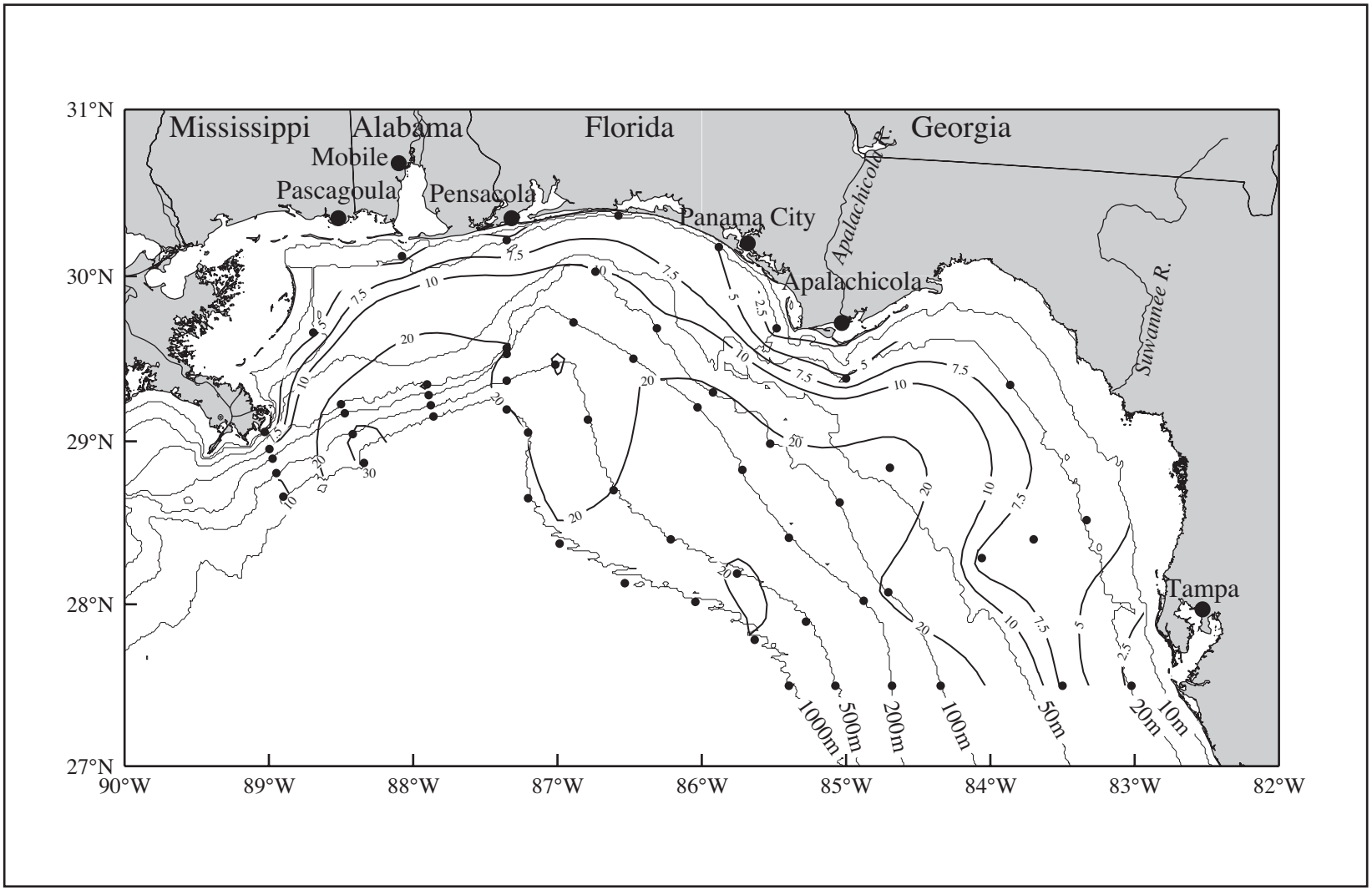

Figure 9.3-13. Pelagophytes (as a percent of chlorophyll *a*) at the deep chlorophyll maximum during NEGOM cruise N7, 13-22 November 1999.

Table 9.3-8. Percent of chlorophyll *a* contributed by individual algal groups in near-surface, deep chlorophyll maximum layer (DCM), and below DCM (BDCM) waters on cruise N8 (April 2000). Chlorophyll *a* concentration is in $\mu g \cdot L^{-1}$.

Algal Groups	Water Depth	Average (%)	Standard Deviation	Minimum (%)	Maximum (%)
Prochlorophytes	Surface	5	4	0	14
	DCM	16	7	0	29
	BDCM	23	9	5	41
Cyanobacteria	Surface	20	5	1	29
	DCM	17	5	5	30
	BDCM	10	6	2	27
Chlorophytes	Surface	3	5	0	15
	DCM	10	5	0	24
	BDCM	4	5	0	13
Chryptophytes	Surface	1	2	0	8
	DCM	4	3	0	12
	BDCM	2	3	0	10
Pelagophytes	Surface	6	4	0	20
	DCM	13	6	1	35
	BDCM	19	7	3	30
Dinoflagellates	Surface	4	7	0	26
	DCM	7	8	0	26
	BDCM	3	5	0	16
Diatoms	Surface	6	7	0	26
	DCM	6	6	0	23
	BDCM	4	5	0	13
Prymnesiophytes	Surface	32	11	0	50
	DCM	34	11	0	48
	BDCM	35	5	0	44
Prasinophytes	Surface	1	2	0	12
	DCM	3	3	0	10
	BDCM	1	2	0	7
Chlorophyll *a* ($\mu g \cdot L^{-1}$)	Surface	0.19	0.34	0.03	2.48
	DCM	0.51	0.45	0.08	2.52
	BDCM	0.27	0.15	0.05	0.72

Commonly detected pigments included chlorophylls *b* and c_2 and β-carotene, fucoxanthin, 19'-butanoyloxyfucoxanthin, 19'-hexanoyloxyfucoxanthin, peridinin, diadinoxanthin, and zeaxanthin. Concentrations of major accessory pigments (the fucoxanthins, diadinoxanthin, diatoxanthin) ranged from 0.3 $\mu g \cdot L^{-1}$ to below the detection limit. Chlorophyll c_3, violaxanthin, prasinoxanthin, and alloxanthin were detected in trace amounts, generally < 0.1 $\mu g \cdot L^{-1}$, in many samples.

Many algal groups were present in high abundances in near-surface and DCM waters. The major species inferred from the accessory pigment compositions were prymnesiophytes, pelagophytes, dinoflagellates, and prochlorophytes. Diatoms, cyanobacteria, chlorophytes, and chryptophytes were detected at low abundances in both near-surface and DCM waters (Table 9.3-9).

Table 9.3-9. Percent of chlorophyll *a* contributed by individual algal groups in near-surface, deep chlorophyll maximum layer (DCM), and below DCM (BDCM) waters on cruise N9 (July-August 2000). Chlorophyll *a* concentration is in $\mu g \cdot L^{-1}$.

Algal Groups	Water Depth	Average (%)	Standard Deviation	Minimum (%)	Maximum (%)
Prochlorophytes	Surface	11	7	0	25
	DCM	13	7	0	26
	BDCM	19	8	0	32
Cyanobacteria	Surface	8	3	0	12
	DCM	7	3	5	15
	BDCM	10	6	0	20
Chlorophytes	Surface	7	4	0	25
	DCM	5	4	0	12
	BDCM	3	4	0	12
Chryptophytes	Surface	1	2	0	5
	DCM	3	3	0	10
	BDCM	3	4	0	12
Pelagophytes	Surface	10	9	0	30
	DCM	15	9	0	32
	BDCM	20	10	2	40
Dinoflagellates	Surface	15	9	0	32
	DCM	13	6	0	26
	BDCM	9	7	0	21
Diatoms	Surface	11	8	0	30
	DCM	9	6	0	28
	BDCM	7	5	0	26
Prymnesiophytes	Surface	32	12	2	56
	DCM	33	11	0	50
	BDCM	35	7	18	47
Prasinophytes	Surface	0	1	0	5
	DCM	0	1	0	8
	BDCM	0	2	0	7
Chlorophyll *a* ($\mu g \cdot L^{-1}$)	Surface	0.54	0.97	0.03	5.13
	DCM	0.44	0.49	0.04	3.24
	BDCM	0.22	0.17	0.01	0.89

The spatial distribution of individual algal groups was different for each algal type. Highest abundances of prochlorophytes were found across the shelf in the Big Bend region between lines 7 and 10 (Figure 9.3-14). Patches of high abundance of prochlorophytes also occurred in offshore near-surface and DCM waters. Prymnesiophytes were generally high across the entire study area, particularly in the near-surface and DCM waters of the offshore shelf (e.g., Figure 9.3-3, bottom right panel). Prymnesiophytes were relatively low in near-shore waters influenced by river outflows (Figure 9.3-3, bottom right panel). Dinoflagellates were highest between lines 4 and 8 in near-surface and DCM waters. Diatoms were present in highest abundances in near-shore waters.

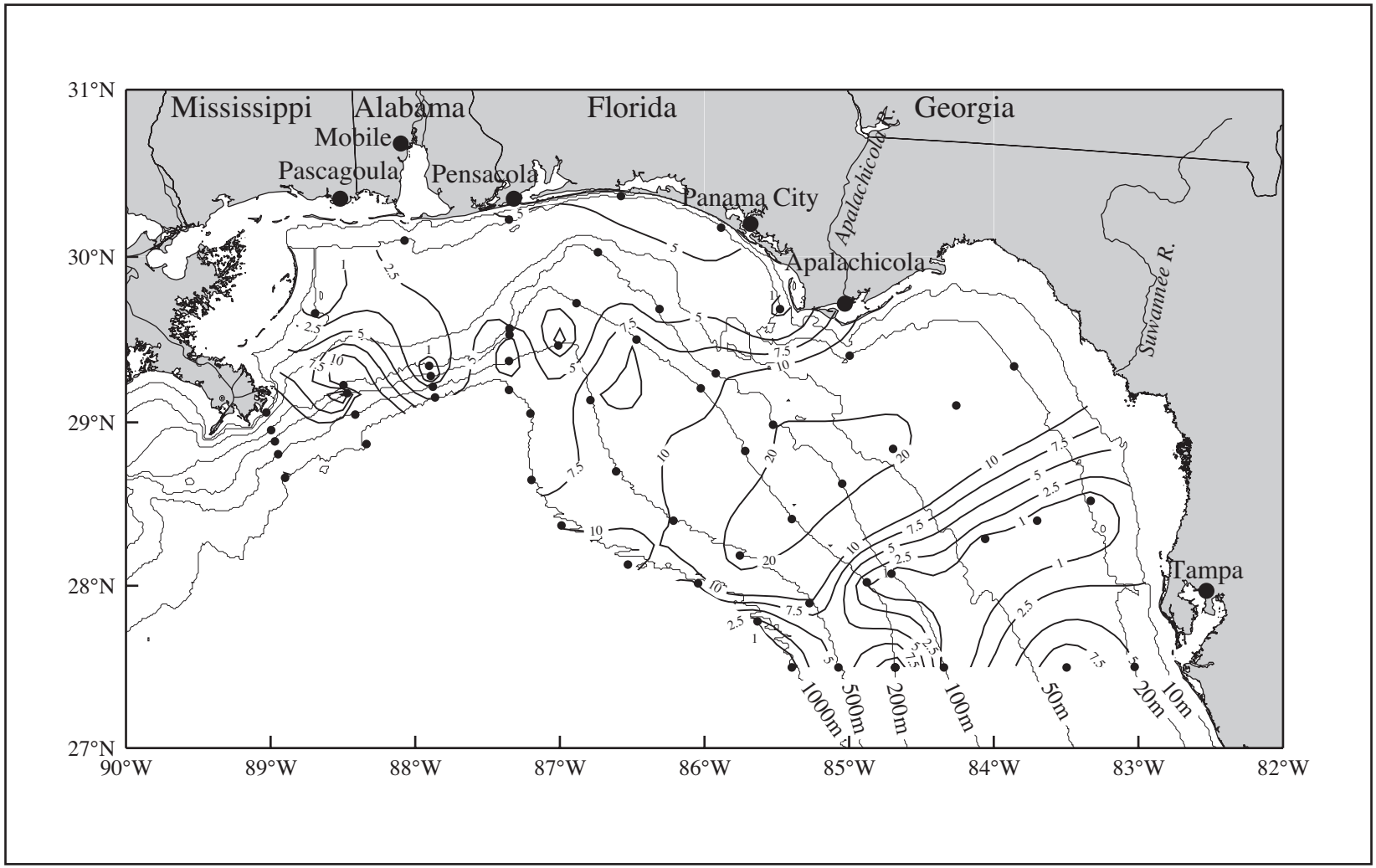

Figure 9.3-14. Prochlorophytes (as a percent of chlorophyll *a*) in near-surface waters during NEGOM cruise N9, 29 July-8 August 2000.

9.4 Discussion and Summary

Examination of the spatial distribution pattern of chlorophyll *a* in the NEGOM area in near surface waters suggests that freshwater discharge from rivers and estuaries is an important controlling factor dictating the distribution of phytoplankton standing biomass over the shelf. Highest chlorophyll *a* concentrations were generally located near river and estuary outflow areas in near-surface waters. Chlorophyll *a* values of < 0.1 $\mu g \cdot L^{-1}$ generally were found more extensively east of 86°W than to the west. They also occurred more frequently over the outer shelf and slope than over the inner shelf.

Near-surface water as well as water at DCM depths between lines 1 and 4 and between lines 7 and 8 consistently had the highest chlorophyll *a* concentrations during the nine cruises. The high chlorophyll *a* concentrations in these two areas are a consequence of freshwater outflow from rivers discharging into the study area. The major rivers in these two areas are, of course, the Mississippi River and the Apalachicola River. Total chlorophyll *a* concentrations in the low salinity, greenish water from these two rivers varied from 0.5 $\mu g \cdot L^{-1}$ to over 5 $\mu g \cdot L^{-1}$.

The influence of fresh water on chlorophyll *a* concentrations is further demonstrated by the strong correlation between chlorophyll *a* and salinity in near-surface waters despite the large variations in chlorophyll *a* concentrations (from less than 0.1 $\mu g \cdot L^{-1}$ to over 10 $\mu g \cdot L^{-1}$). The negative correlation between chlorophyll *a* and salinity in near-surface waters (Table 10.3-1) implies that fresh water inflow into the region was either importing chlorophyll generated upstream or promoting the growth of phytoplankton biomass downstream by advecting nutrients into the region, or both.

The large discharge of the Mississippi River resulted in a pattern not seen elsewhere in the study region. High concentrations of chlorophyll *a* can extend from the Mississippi River mouth to the outer shelf and slope. This was most intense in the spring and summer. The summertime extension of relatively high chlorophyll *a* waters southeastward off the shelf from the Mississippi River mouth and the patches of relatively high chlorophyll water over the outer shelf and slope of the study area tracked the extension of relatively low salinity, near-surface waters over a large portion of the study area. The chlorophyll *a* concentration in near-surface water over the outer shelf and slope southeast of the Mississippi River Delta generally was higher in summer compared to the other seasons. This elevated chlorophyll likely was caused by the off-shelf entrainment of relatively low salinity shelf water by one or more anticyclonic slope eddies located adjacent to that area during the summers sampled. Such entrainment may transport phytoplankton, nutrients, dissolved organic matter and suspended sediments from the northern to central and southern region of the study area.

In the eastern portion of the NEGOM region, two areas of high chlorophyll concentrations were consistently found to be associated with outflow from the Apalachicola River and adjacent bays and estuaries near Cape San Blas and outflow from the Suwannee River. Highest chlorophyll *a* concentrations east of 86°W along the west Florida coast occurred in November 1997 (cruise N1) and August 1999 (cruise N6), where chlorophyll *a* values south of the Suwannee River outflow exceeded 3 and 1 $\mu g \cdot L^{-1}$, respectively. The November 1997 high might be attributed to an extended large pulse of freshwater discharged to the inner shelf prior to the cruise in late October or November. This pulse of river water was near or exceeded one standard deviation from the record-length mean discharge for rivers in the region, including the Apalachicola and Suwannee Rivers, which have the largest discharge rates in the region. As a result of this large input of freshwater, there was a band of relatively low salinity water, with salinities between 30 and 35, on cruise N1 that extended all along

the coast inshore of approximately the 20-m isobath. However, the August 1999 high chlorophyll off the Suwannee River cannot be directly related to river discharge, because this and other rivers were discharging during the summer of 1999 at rates below their record-length mean for the time and salinities over the inner shelf were greater than 35 and yet a chlorophyll high was observed.

Spatial distributions of chlorophyll *a* were similar among all three fall cruises N1, N4, and N7 when discharges of all rivers were near minimum values. Near-shore waters between the Mississippi River Delta and Apalachicola River had relatively high chlorophyll *a* concentrations and the other areas had relatively low chlorophyll *a* concentrations. In contrast, in spring (cruises N2, N5, and N8), when river discharge typically is near maximum, high chlorophyll water extended over much of the inner shelf from the Mississippi River to Choctawhatchee Bay. An exception was April 2000 (cruise N8) when the distribution of high chlorophyll water was less extended. The limited spatial distribution of high chlorophyll waters during Cruise N8 was likely caused by the low river flow that preceded the cruise. Chlorophyll *a* distributions were also similar among all three summer cruises N3, N6, and N9, when waters between lines 1 and 4 had consistently high chlorophyll *a* concentrations, in addition to high chlorophyll waters on the outer shelf caused by the transport of low salinity water by warm slope eddies. The waters near Apalachicola also had high chlorophyll *a* concentrations, especially in the summer. Freshwater input from rivers and estuaries had a major influence on chlorophyll *a* concentrations during the summer months.

Although it is a semi-enclosed, subtropical ocean basin, the offshelf Gulf of Mexico undergoes pronounced seasonal variation in phytoplankton standing stock. This is now well-known from the analysis of monthly and tri-monthly averages of Coastal Zone Color Scanner satellite data during 1978-1986 (Muller-Karger et al. 1991; Melo-Gonzalez et al. 2000) and from animations of the first three years of SeaWiFS data during 1997-2000 (Behrenfield et al. 2001; see also http://www.gsgc.nasa.gov/gsfc/earth/environ/carbon/carbon/htm). This seasonality approximates a simple step-function which is driven by the high stability of the water column, with low pigment concentrations, in spring-summer (April-October) and by convective cooling and stronger winds, with high pigment concentrations, during fall-winter (November-March). Because cruises N1, N4, and N7 were fielded in the fall, it was expected that stations over the continental slope would have chlorophyll concentrations that were about two times higher than those at the same stations during spring-summer (cruises N2, N3, N5, N6, N8, and N9).

For the study region as a whole, however, the average surface and DCM chlorophyll concentrations at all stations were lower in fall than in spring or summer (Figures 9.4-1 and 9.4-2). There are two possible reasons for this. First, more than half of all stations sampled for pigments were on the continental shelf, rather than in the open ocean so that the near-shore surface waters, which had high chlorophyll *a* concentrations in summer, contributed to the high summer averages. However, the average chlorophyll concentrations in near-surface waters on the continental slope (taken for this purpose to be at the 400-m isobath or deeper) were 2-3 times higher in November than that in April-May (Figure 9.4-3), supporting the model of higher chlorophyll concentrations in fall than in spring or summer. Second, the entrainment and transport offshelf of low salinity Mississippi River water, with its high chlorophyll concentrations, by one or more warm slope eddies that generally were present during the July-August cruises also contributed to higher than expected surface chlorophyll concentrations over the slope during summer. Such off-shelf eddies also could create uplift

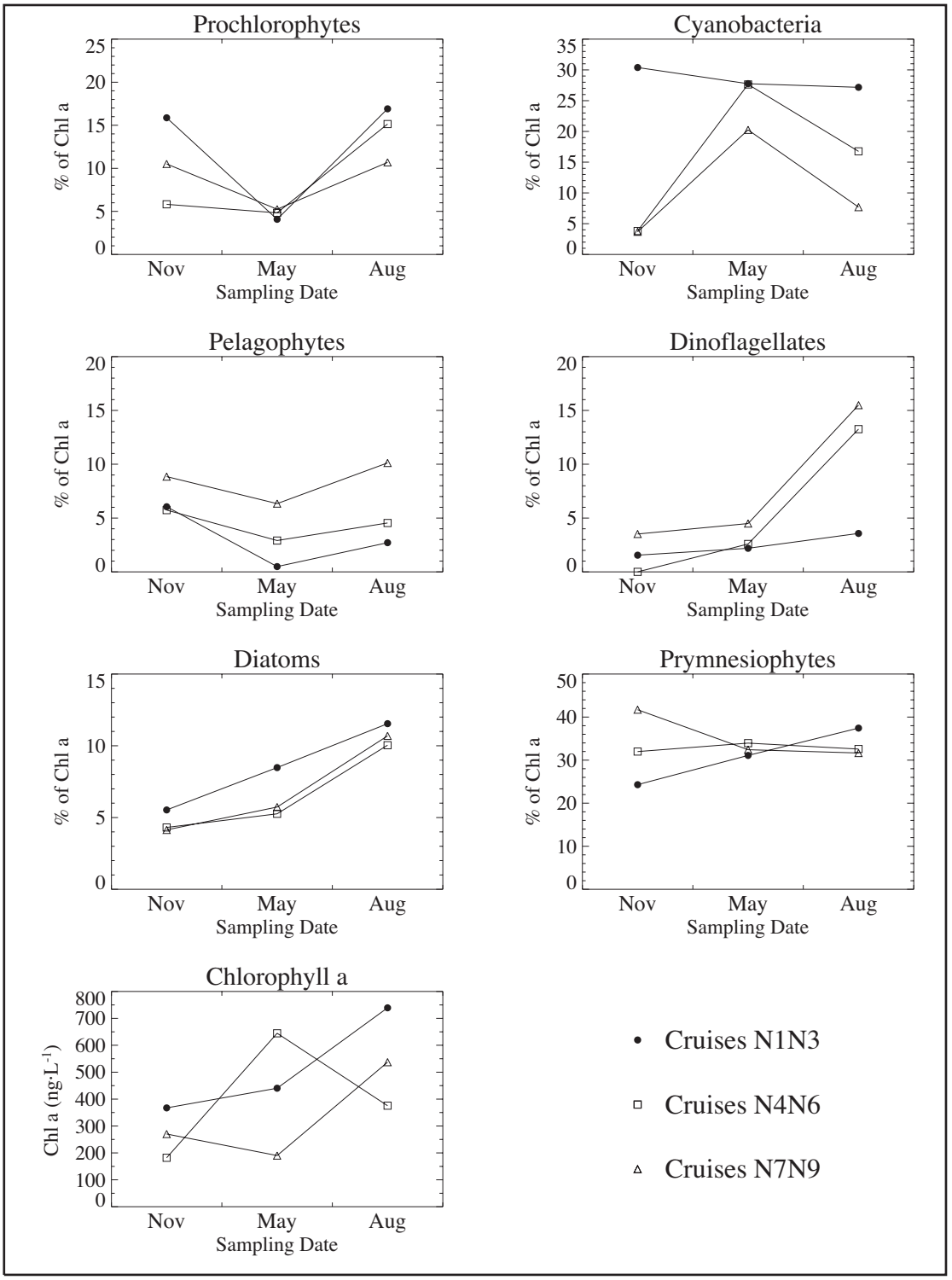

Figure 9.4-1. Seasonal variations in chlorophyll *a* concentrations and the average relative abundance on major phytoplankton groups in near-surface waters from November 1997 through August 2000.

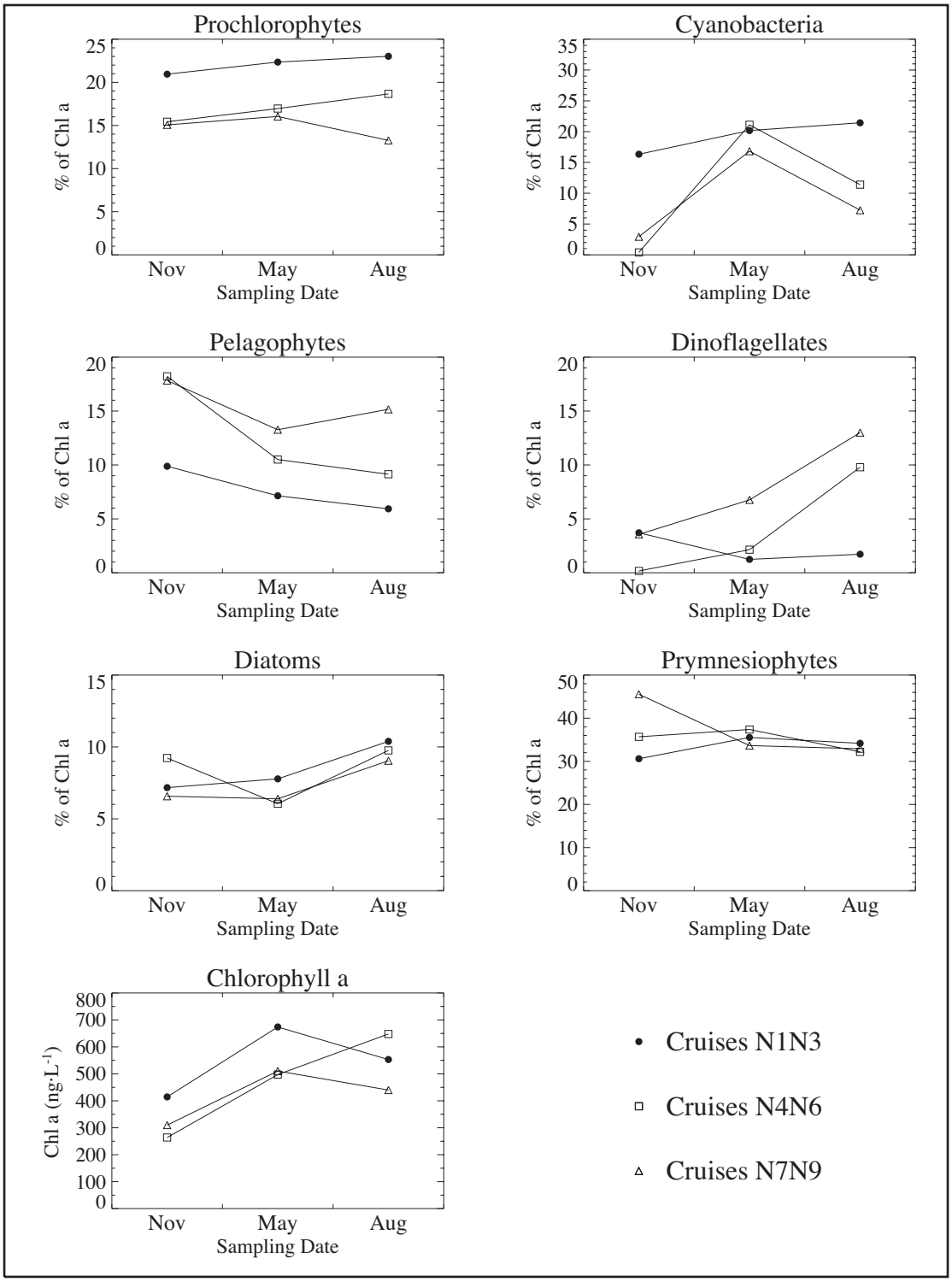

Figure 9.4-2. Seasonal variations in chlorophyll *a* concentrations and the average relative abundance of major phytoplankton groups in deep chlorophyll maximum waters from November 1997 through August 2000.

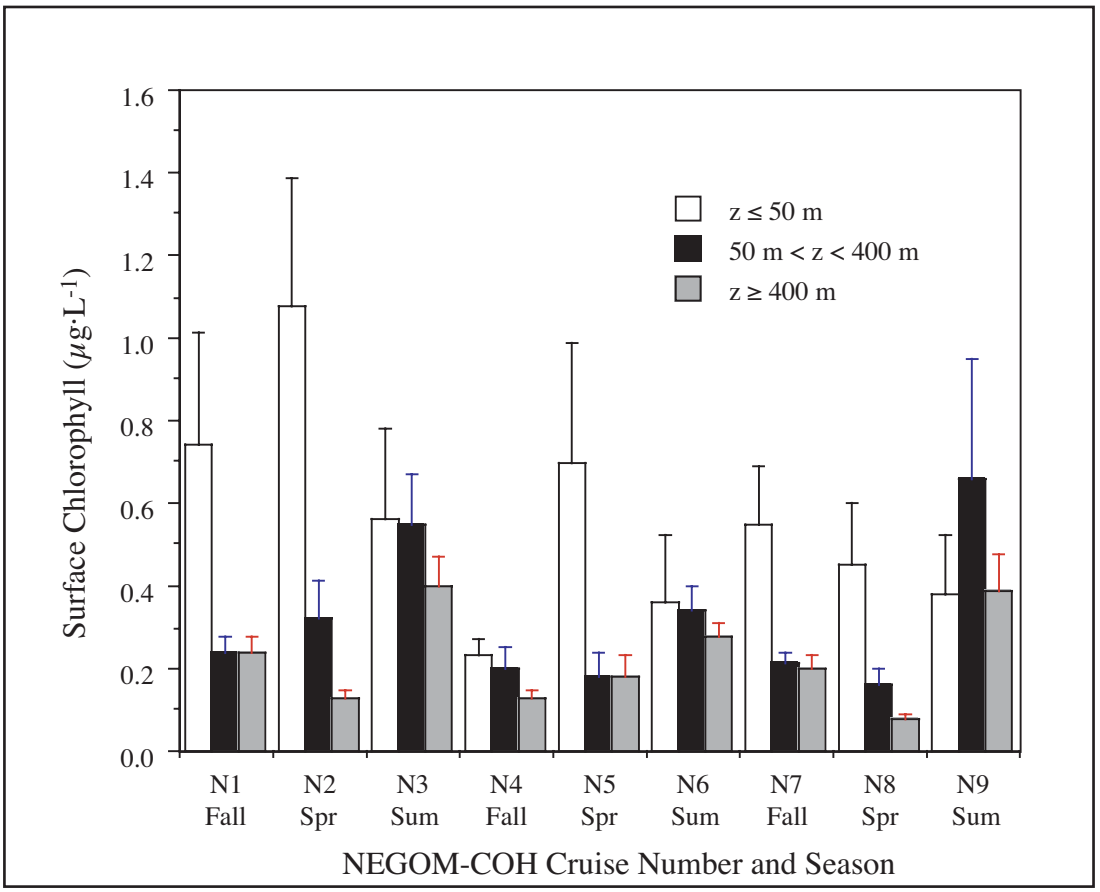

Figure 9.4-3. Average chlorophyll *a* concentrations in near-surface waters grouped by the station depth into inner-middle shelf (z < 50 m), outer shelf (50 < z < 400 m), and continental slope (z > 400 m). The standard error for each mean is indicated by the "T" over each box.

of nutrient rich waters that contributed to the creation of higher chlorophyll concentrations. In each of the three field years (1997-1998, 1998-1999, and 1999-2000), surface chlorophyll over the middle and outer shelf (61 m < z < 276 m) and over the continental slope (z > 400 m) was higher in summer than in either fall (November) or spring (April-May). This is shown graphically by Figure 9.4-3. Entrainment and transport of low salinity, high chlorophyll water to the offshelf region is evidenced by the negative correlation (R = -0.60; see Table 10.3-1) between the salinity of surface water and the chlorophyll concentration in near-surface waters.

Major accessory pigments detected during the nine cruises were chlorophyll *b* and c_2 and 19'-butanoyloxyfucoxanthin, fucoxanthin, 19'-hexanoyloxyfucoxanthin, diadinoxanthin, zeaxanthin, and β-carotene. Other pigments, such as chlorophyll c_3, peridinin, violaxanthin, alloxanthin, prasinoxanthin, diatoxanthin, antheraxanthin, usually were detected in only a few samples at low concentrations. Based on the pigment compositions, the major phytoplankton species in the study region were prymnesiophytes, prochlorophytes, cyanobacteria, pelagophytes, and diatoms. In general, prymnesiophytes, prochlorophytes, and cyanobacteria accounted for, respectively, 20-40%, 10-40%, and 10-40% of chlorophyll *a*.

Prymnesiophytes, prochlorophytes, and cyanobacteria were widespread over the entire study area with patchy higher abundances in some areas. However, not all of them were equally abundant over all water depths. High abundance of prymnesiophytes, where prymnesiophytes contributed 40% or more to the total chlorophyll *a*, was found over the outer shelf and slope. The west Florida shelf had the most stations with high abundances, which often extended from the inner shelf off Tampa Bay to the offshelf region. In contrast, the abundance of prymnesiophytes was generally low, contributing less than 20% of chlorophyll, in waters off the mouth of the Mississippi River (Figure 9.3-3). In addition, the abundance of prymnesiophytes was generally less than 30% in waters off areas influenced by other river, bay, and estuary outflows. An exception was observed during the fall cruise N7, when the abundance of prymnesiophytes was high (≥40%) in waters between Pensacola and Choctawhatchee Bays and from the Suwannee River south to Tampa Bay.

Cyanobacteria abundance in near-surface waters generally was low (<10% of chlorophyll) in the vicinity of fresh water outflow regions. However, high abundances of cyanobacteria, of 40% or more, occurred in patches over the study area, the most extensive of which was on fall cruise N1 over portions of the outer shelf and slope between 84°W and 87°W. Pelagophytes were present in high abundance (10-30% of chlorophyll) mainly in patches over the outer shelf and slope in the near-surface waters. Diatoms were primarily present in near-shore waters, especially in waters associated with freshwater outflows. Dinoflagellates, chlorophytes, and chryptophytes were generally low in abundance (below 10% of total phytoplankton), although higher abundances were observed at some locations during some cruises.

The structure of the phytoplankton communities exhibited consistent changes in vertical distributions in the water column. The vertical distribution profiles of different algal groups are believed to be determined by their size, pigment compositions (presence of photoprotective pigments), photoadaption, and nutrient availability. Prochlorophyte abundance in near-surface waters during the nine cruises was consistently lower than that in DCM waters. The average proportions of prochlorophytes relative to chlorophyll *a* in near-surface waters were 4-12% lower than those in DCM waters. Prochlorophyte abundance below the DCM waters also was high relative to near-surface water. In contrast, the abundance of cyanobacteria in near-surface waters was consistently higher than that in

deeper waters, such as DCM waters and below DCM waters. Similar to prochlorophytes, the vertical profiles of pelagophytes on the nine cruises showed low abundance in the near-surface waters but higher abundances in subsurface DCM depths. The relative proportions of prymnesiophytes, the most abundant taxon in the NEGOM region, did not change significantly with depth.

Seasonal variations in relative abundances of the major phytoplankton groups generally were similar each year (Figures 9.4-1 and 9.4-2). For the NEGOM region as a whole, average abundances of prochlorophytes and pelagophytes in near-surface waters were higher in November and August than in May. In contrast, at DCM depths, the average abundance of pelagophytes was high in November and lower in May and August, while the average abundance of prochlorophytes was similar among the three seasons. Although interannual variability was present for the average abundances of all algal groups, seasonal variability was in general larger than interannual variability. The seasonal variability was likely attributed to the fact that the primary controlling factors of phytoplankton standing stock, namely temperature, salinity, and light, to a lesser extent, nutrients were largely seasonal.

The relative abundances of both diatoms and dinoflagellates were lowest in November and highest in August for both near-surface water and water at DCM depths, except during cruise N3 (August 1998) where dinoflagellates exhibited low relative abundances in both near-surface and DCM waters. The increase in relative abundance of diatoms and dinoflagellates in summer probably was caused by the input of fresh nutrients associated with low salinity water in the spring and summer. In both near-surface and DCM waters, cyanobacteria were highest in abundance in May and lowest in November. This might be attributed to the transport of the spring blooms of cyanobacteria that occur frequently in the estuaries adjacent to the NEGOM shelf (Gilbes et al., 1996; Lavrentyev et al., 1998). Prymnesiophytes showed little seasonal variation in abundance. The abundances of prymnesiophytes were similar during all nine cruises in near-surface and DCM waters (Figures 9.4-1 and 9.4-2).

10 INTEGRATED WATER COLUMN CHEMISTRY

10.1 Introduction

The chemistry of marine water columns associated with continental shelves is determined by the dynamic interplay of water movements and biogeochemical cycles. Bioactive compounds, such as nutrients, are fixed into biomass by photosynthetic organisms in the photic zone, producing particulate matter which is laterally and vertically advected by currents as it settles through the water column into the underlying sediments. The process of photosynthesis produces oxygen that dissolves in the water. The particulate matter is reactive and can be remineralized to nutrients by microbiota in a process that consumes oxygen. Particulates, both living and non-living, can pass through the guts of larger organisms, where they are altered by digestive and assimilative reactions while residual materials are repackaged and released to the water column. Biological organisms exude dissolved organic matter and generate fecal pellets. Inorganic materials are subject to dissolution/precipitation depending on the physical/chemical environment. Once deposited in sediments, particulate matter is subject to continuing biological and chemical alteration and occasional resuspension and redistribution by bottom currents. In isolation, the balance between these processes reaches a stasis that establishes the distribution or profile of chemicals within water columns. However, on many continental shelves significant external inputs of energy and materials originate from the outflow of rivers, wet and dry atmospheric deposition, and exchange with near shore estuaries. Outflows of riverine dissolved and particulate materials onto the continental shelf are subject to the same biogeochemical and physical processes described above. Influxes of nutrient-rich, low salinity water and particulates are often important in determining the distribution of chemicals and particles in near-shore water columns. The dynamics of the water column chemistry of the northeastern Gulf of Mexico can only be understood through an integrated assessment of the effects of biogeochemical and physical redistribution and transformation processes on water column properties. It is these properties that are expected to control or force the distribution of the biotic elements of the region.

A description of water column properties has been provided, including circulation patterns and the distributions of salinity, temperature, nutrients, particulates, phytoplankton pigments, and dissolved oxygen. These data demonstrate that outflow from river systems along the northeastern Gulf of Mexico exerts an important influence on upper water column chemistry. Riverine discharges directly and indirectly influence chemical and particulate matter distributions through the introduction of dissolved and particulate inorganic and organic matter. River water introduces dissolved nutrients that provide the elements needed to support photosynthetic production of biomass by phytoplankton. Excessive particulate loads from rivers can decrease the intensity, penetration, and quality of light that penetrates the photic zone, thus limiting primary production. However, this generally occurs only in very limited near shore areas near river mouths. Wet and dry atmospheric deposition and exchange between shelf waters and coastal estuaries are more subtle processes that may be important in establishing water column chemistries, especially in areas less affected by major river systems. Climatic and weather conditions create annual cycles in water column properties as a result of seasonal variability in river discharges and available sunlight for primary productivity. Uplift of isopleths (whether wind-induced, current-induced as bottom Ekman layers, or doming associated with mesoscale, horizontal circulation features) across the region is also important in redistributing the chemicals from deep waters into the photic zone were they can be utilized by biotic components during photosynthesis. To more clearly

define the relative importance of these complex interactions, the data collected on nine survey cruises are integrated by using univariate and multivariate statistical techniques.

10.2 General Patterns

River discharge from the three major river basins that flow into the study area exhibited significant seasonality, with river discharge being greatest before May cruises and lowest before November cruises during the study period (Figure 10.2-1). Discharge data were examined for the three most significant river systems that flow into the study area: Mississippi, Apalachicola and Mobile (Tombigbee and Alabama combined). Data were converted to $m^3 \cdot d^{-1}$ and averaged for the 30 days prior to each cruise. For the Mississippi River, the total thirty-day average discharge varied by a factor of 2 to 3 over the course of a year. As expected the discharge of the Mississippi River basin was by far the largest source of riverine material to the study area. However, distant from the Mississippi River, other river basin discharges and exchanges with coastal estuaries represent significant inputs of dissolved and particulate matter.

As a first order attempt to determine the relative importance of various processes in controlling water column chemistry, the data were stratified in two ways: by time of year and by geographic location (Figure 10.2-2). The location categorization was based on ADCP characterization of four quadrants in the NEGOM area: Mississippi-Alabama shelf; DeSoto slope; west Florida shelf; and west Florida slope. The shelf break (~200-m isobath) separates these regions. The 1000-m isobath is the offshore boundary. Each seasonal sampling is represented by three cruises over a three-year period: fall—November sampling during cruises N1, N4, and N7; spring—April/May sampling during cruises N2, N5, and N8; and summer—July/August sampling during cruises N3, N6, and N9. An important observation is that water column parameters related to the influx of riverine material (e.g., particulates or nutrients) exhibit variability that far exceeds seasonal variations or temporal variations observed in areas remote from river inputs. Near-shore waters are enhanced in primary productivity over the more offshore portions of the cruise tracks, as expressed in increased water column particulate matter concentrations. In shallow water areas where the photic zone intersects the sediment surface, significant benthic productivity also may affect the overlying water column. Another observation is that nutrient concentrations at the bottom of the photic zone are highly variable, reflecting the variable depth of the mixed layer, and may indicate uplift of nutrients into the lower photic zone. In summary, water column chemical properties in the northeastern Gulf of Mexico are a function of distance from riverine inputs (geographic location), distance from shore (water depth), time of the year, prior river discharge rates, and the extent of uplift of deeper waters. To assess the relative importance of these factors univariate and multivariate statistical analyses of the data were performed.

10.3 Univariate Analysis

To perform univariate analysis the data were normalized by natural log transformations. After transformation, correlations among the variables were examined to determine what proportion of the variation in each parameter could be related to other diagnostic parameters. Examination of the resulting correlation matrix confirms previous explanations of the relationships between variables (Table 10.3-1).

While these relationships may seem trivial because they are as expected, they do confirm that the processes normally encountered in coastal marine settings are at work in the NEGOM study area. Most relationships can be explained by well-studied biotic and abiotic

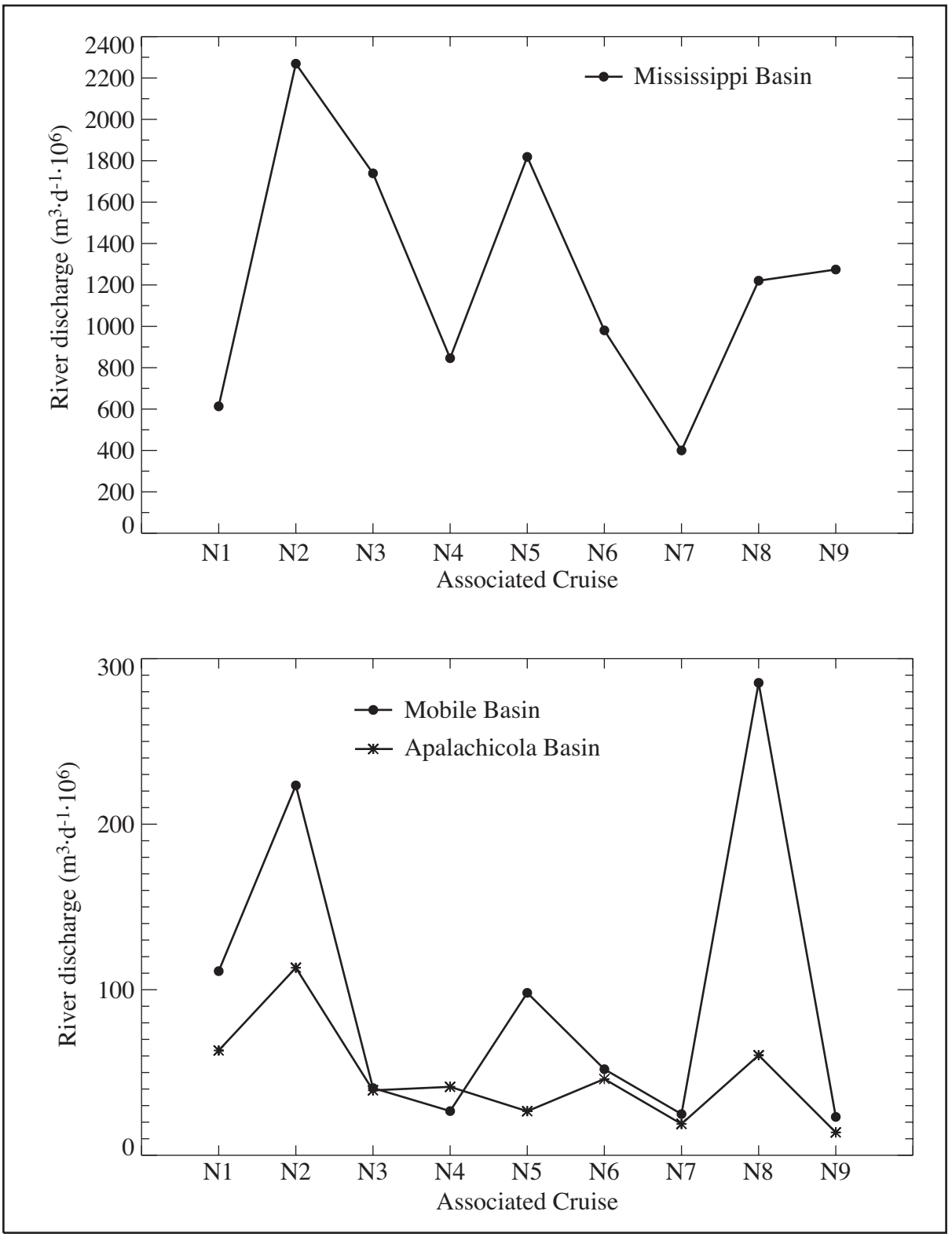

Figure 10.2-1. River discharges into the study area for the 30-day period preceding each cruise. The Mobile basin includes the Tombigbee and Alabama rivers.

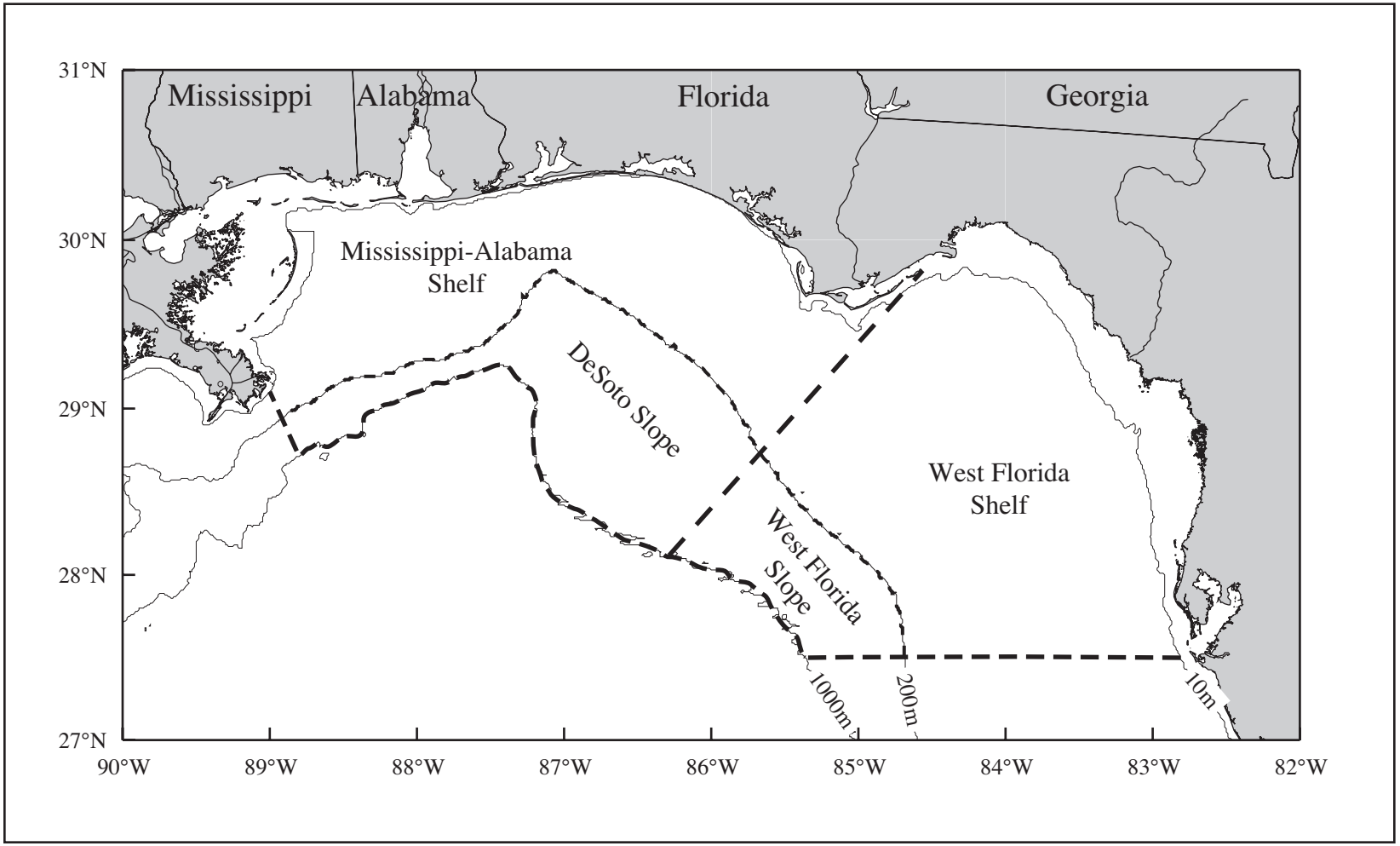

Figure 10.2-2. Geographic sub-regions within the study area.

Table 10.3-1. Correlations of NEGOM data. Highlighted area shows high correlations among the particulates, nutrients, and biomass.

	APALA	MOBIL	MISS	NH_4	UREA	NO_2	SIO_3	NO_3	TOTCHL	VFLU	CTDSAL	O_2MLL	PO_4	PM	POC	PON	XMISS
APALA	1.00																
MOBIL	.77	1.00															
MISS	.26	.37	1.00														
NH_4	.07	-.01	.19	1.00													
UREA	-.03	.01	.33	.32	1.00												
NO_2	.07	.13	.21	.41	.35	1.00											
SiO_3	-.06	-.03	.32	.43	.32	.57	1.00										
NO_3	.09	.10	.32	.35	.40	.64	.57	1.00									
TOTCHL	-.14	-.12	.15	.45	.30	.51	.52	.44	1.00								
VFLU	-.01	-.12	.07	.44	.17	.47	.36	.38	.75	1.00							
CTDSAL	.08	.07	-.19	-.36	-.30	-.38	-.48	-.50	-.60	-.53	1.00						
O_2MLL	.09	.15	-.23	.02	-.14	-.21	-.26	-.18	.01	.10	-.23	1.00					
PO_4	.08	.06	-.02	.36	.26	.47	.43	.52	.30	.22	-.19	-.27	1.00				
PM	-.14	-.11	.24	.47	.32	.52	.51	.51	.73	.70	-.59	-.00	.31	1.00			
POC	-.12	-.10	.23	.43	.21	.36	.34	.33	.74	.71	-.62	.23	.12	.79	1.00		
PON	-.13	-.12	.26	.44	.23	.37	.39	.35	.74	.70	-.62	.20	.13	.78	.97	1.00	
XMISS	.01	.00	-.16	-.48	-.40	-.59	-.56	-.60	-.55	-.52	.69	-.08	-.41	-.66	-.54	-.55	1.00

APALA = Apalachicola River discharge
MOBIL = River discharge to Mobile Bay
MISS = Mississippi River discharge
TOTCHL = chlorophyll a
VFLU = Fluorescence voltage from upcast at time of bottle trip
CTDSAL = Salinity from upcast CTD at time of bottle trip
PM = Particulate matter
POC = Particulate organic carbon
PON = Particulate organic nitrogen
XMISS = percent transmission from upcast at time of bottle trip

phenomena. The first conclusion is that the NEGOM area does not appear to be subject to any extraordinary events or processes and is rather typical of near coastal areas influenced by major river systems. Other conclusions are that properties across the area are highly spatially and temporally variable, that the presence of biological organisms is important in redistributing chemicals vertically and horizontally in the study area, and that physical movements of water both supply the necessary chemicals for growth and modify biologically generated patterns in chemical and particulate distributions.

As examples, percent of light transmission correlates negatively with all particulate parameters, i.e., particulates in water decrease light transmission. Fluorescence intensity positively correlates with chlorophyll a concentrations and particulate matter properties, indicating that living biomass is a significant source of water column particulates (see shaded area in Table 10.3-1). Chlorophyll a concentrations correlate with dissolved oxygen signifying that oxygen is a product of photosynthesis. Nutrients correlate among themselves demonstrating that they are removed from the water column in a relatively constant ratio (the so called Redfield ratio) as they are fixed into biomass. Chlorophyll a correlates weakly with nutrients suggesting that input as well as removal processes are important in controlling nutrient concentrations.

These correlations confirm well documented relationships. Most water column properties are subject to multiple processes, occurring at the same time, that can be supplying as well consumptive in nature. To better define the relative importance of these processes in determining water column property distributions, multivariate analyses of the data were performed.

10.4 Multivariate Analyses

The data were first subjected to Principal Component Analysis (PCA) to reduce the number of variables and to detect structure in the relationships among the variables (Cooley and Lohnes 1971; Stevens 1986). A varimax rotation of the normalized factor loadings (raw factor loadings divided by the square roots of the respective commonalties) was applied to the data. The rotation is aimed at developing factor loadings (or "components") that can be ascribed to processes that have a "real world" meaning. PCA analysis indicated that 40.6% of the variance was removed by the first factor, 13.6% by the second, and 10.6% by the third for a total of 65%. The factor loadings for the first four components are summarized in Table 10.4-1. Component (or "Factor") one loads positively for chlorophyll a, fluorescence intensity, particulate matter, and particulate organic carbon and negatively for salinity. Component two has positive loadings for nitrite, nitrate, phosphate and silicate. Components three and four, together totaling over 17% of the variance, have positive loadings for river discharge volumes.

Principal component analysis (PCA) indicates that sixty-five (65) percent of the variability in the upper water column properties can be explained by the first three principal components. Just over 40% of the variability in the data is related to particle dynamics and riverine water inputs as indicated by the positive and negative loadings for the diagnostic variables (Table 10.4-2; note the variables in bold). PCA also indicates that phytoplankton biomass is a major source of variability in water column properties, suggesting that phytoplankton dynamics exert a control over these variables in the study area. Close correlation among POC, PM, and chlorophyll *a* concentrations in the upper water column indicates that a large proportion of the particulate matter is living phytoplankton. The exception is in areas close to river outlets where abiotic particles can be a significant part of the particulate load. The dynamics of photosynthetic production of phytoplankton biomass (which is influenced by nutrient

Table 10.4-1. Variances from PCA.

Factor	Eigenval	% Total Variance	Cumul. %
1	6.91	40.63	40.63
2	2.31	13.57	54.21
3	1.81	10.62	64.82
4	1.12	6.60	71.42

Table 10.4-2. Principal component loadings. Major loadings are indicated in bold.

	Factor 1	Factor 2	Factor 3	Factor 4
APALA	-0.10	0.07	**0.91**	0.05
MOBIL	-0.10	0.03	**0.92**	0.15
MISS	0.20	-0.01	0.31	**0.87**
NH4	0.47	0.43	0.08	0.04
UREA	0.22	0.37	-0.05	0.48
NO_2	0.35	**0.72**	0.11	0.14
SIO_3	0.36	**0.63**	-0.09	0.32
NO_3	0.34	**0.70**	0.11	0.24
TOTCHL	**0.78**	0.32	-0.13	0.07
VFLU	**0.78**	0.24	-0.03	-0.09
CTDSAL	**-0.74**	-0.25	-0.01	-0.04
O_2MLL	0.38	-0.42	0.33	-0.52
PO_4	0.04	**0.84**	0.05	-0.12
PM	**0.80**	0.33	-0.11	0.15
POC	**0.94**	0.02	-0.04	0.08
PON	**0.93**	0.04	-0.06	0.12
XMISS	-0.62	-0.55	-0.06	-0.02
Expl.Var	5.41	3.24	1.96	1.53
Prp.Totl	0.32	0.19	0.11	0.09

Expl. Var = Explained variance: The proportion of the variability in the data accounted for by the model.
Prop. Totl = Proportionate total of the variance for each factor.

availability, light intensity and spectral properties, and temperature) accounts for most of the variance exhibited by the first component. Nutrient availability, in turn, is largely tied to riverine water inflow to the area, as suggested by the negative correlation between salinity and chlorophyll (Table 10.3-1).

Region-wide, it is difficult to assess the relative importance of uplift of isopleths as a source of nutrients from the NEGOM data set, because the process is diffuse and could occur over a very large area and is dependent on particular wind, current, and/or eddy events for its occurrence. Point source delivery of nutrients from rivers is seasonally restricted and only occasionally results in discharge of large volumes. Therefore, on an annual basis it may be less important than the low level introduction of nutrients occurring pervasively across the entire region from processes causing uplift of isopleths. The relative importance of these sources of nutrients is difficult to assess based on survey data, but much of the variability in phytoplankton biomass is correlated with variables indicative of riverine influence.

The second component loads heavily for the nutrient variables (Table 10.4-2) and accounts for 13.6% of the variability in water column properties. Nutrient variability is closely coupled to variability in particulate matter properties since nutrients are consumed during photosynthetic production of biomass by phytoplankton. The combination of low surface water nutrient concentrations, which are the result of phytoplankton consumption, and the continuous input of nutrient-rich riverine water and uplift of nutrient-rich deep water from below the photic zone, explains the variability in nutrient concentrations.

Finally, river discharge accounts for over 17% of variability in water column properties (Table 10.4-1), reflecting the regional influence of river discharges on a range of water column properties both directly and indirectly (Table 10.4-2). This influence can be of two types. First, the direct input of river water can physically displace water masses. Secondly, river water can extensively mix with in situ waters providing the critical elements needed for phytoplankton growth. Biological response in this case probably results from the in situ seed populations that are operating at some stasis level until critical changes in limiting abiotic factors occur, i.e., infusion of nutrients. This indicates mixing is an important process in contrast to water mass transport alone. The riverine water does not contain plankton, it simply provides the needed growth limiting factors, i.e., the "fertilizer". Productivity in the water column will be redistributed by the ambient current structure in the area, and local redistribution of living particles would be expected. The exact interaction of these two processes, in situ production and physical transport, will depend on the time constants of the two processes; these can be highly variable. If the current is slow compared to the phytoplankton growth rate, the bloom could occur and subside with little transport away from the source area. On the other hand if current speed is high the bloom might well occur as it is being transported along the flow field. Mixing is key to delivering the needed growth elements to the phytoplankton and the rate of delivery of nutrients to a particular location may be a limiting factor if the rate of consumption outstrips the infusion rate.

Using these reduced expressions of variability in the data, correlations between salinity/particulates/biomass, nutrient cycling, and river discharge can be explored. Classifying the data by month of the year in which sampling occurred distinguishes among the cruises (Figure 10.4-1). Riverine influences on nutrients and particulates/biomass are seasonally variable.

Geographic classification of data gives only broad resolution, with the more western sites being higher in nutrients, particulates, and biomass and lower in salinity than eastern sites

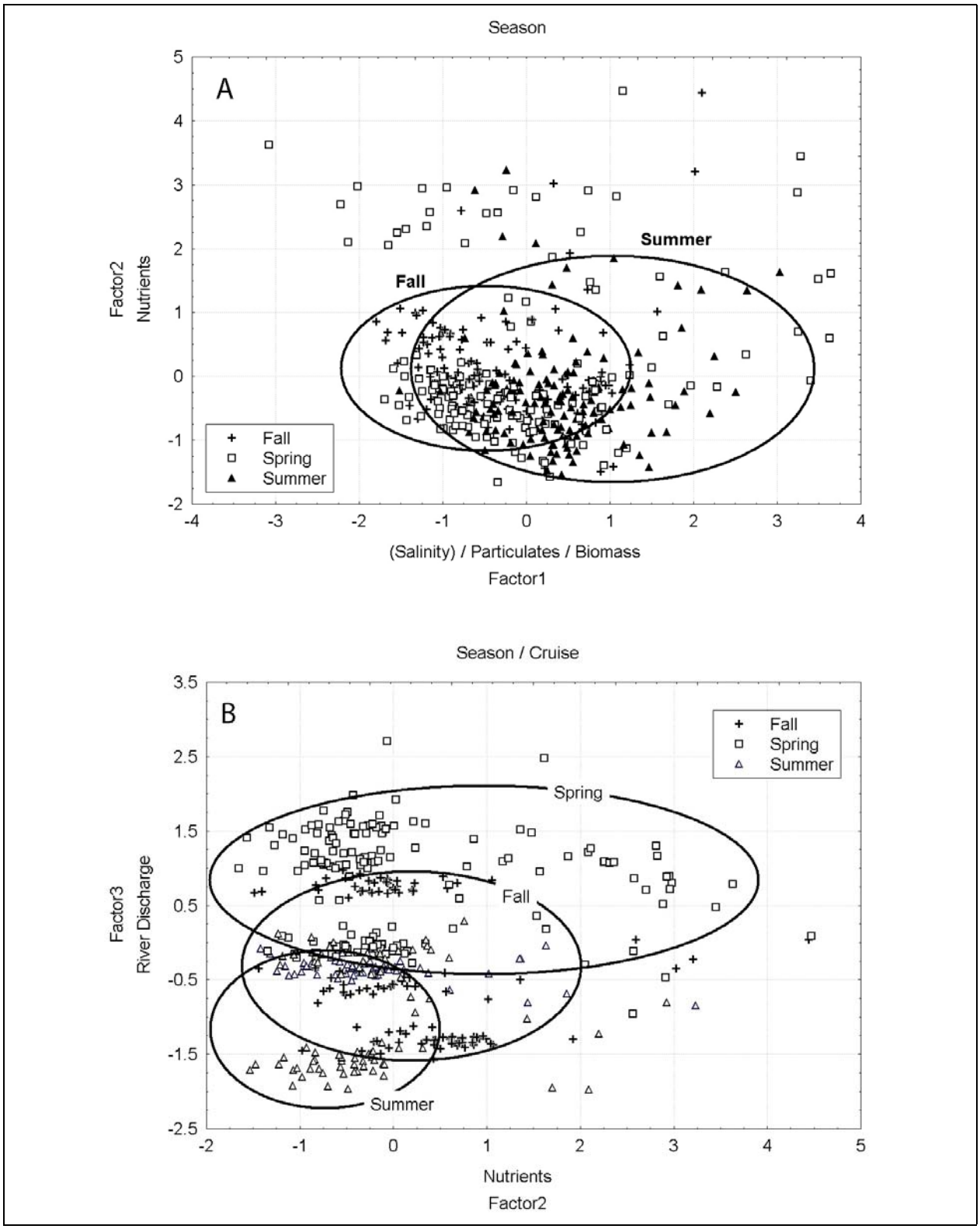

Figure 10.4-1. Data classified by time of year to detect seasonal trends.

(Figure 10.4-2). The lack of greater spatial differentiation is likely due to seasonal effects, which are responsible for the variability observed at any single location.

Classification of the data by depth in the water column confirms that, in surface waters, low nutrient concentrations correspond with increased particulates and living phytoplankton (Figure 10.4-3). It also reflects the increased nutrient levels encountered as the available light decreases with depth in the water column. Nutrient concentrations correlate with increased river discharge and the associated enhancement in phytoplankton productivity that consumes nutrients.

To filter out seasonal effects, it is informative to analyze the data binned by the time of year to detect more subtle relationships between water column chemistry and particulate matter distributions. The same PCA and rotation were applied to the data binned by season. Particulates, river discharge, and nutrients were once again the primary sources of variability in the data. However, salinity exhibited high loadings for the spring and summer cruises, and oxygen levels had high loadings for the spring and fall cruises.

The trends in the data, however, were similar during the different times of the year. The spring (May) data illustrate these trends. Higher nutrients correlated with higher particulate loads in the surface waters, and both decreased with increasing depth in the water column (Figure 10.4-4). Classifying the data by depth in the water column illustrates that nutrients and particulates are highest nearshore (Figure 10.4-5). The first principal component also strongly negatively correlated with salinity, suggesting the major source of the nutrients is river water.

River discharge and nutrient levels were different depending on the year of the sampling (Figures 10.4-6, 10.4-7, and 10.4-8). Therefore, not only is there a seasonal signal, there is also an interannual signal reflecting variability in river discharges. This interannual variability is strongest near the Mississippi River, but also is important across the study area, suggesting that the input from the adjacent bays and other river systems are important in establishing chemical distributions throughout the northeastern Gulf of Mexico. During low flow periods, such as August and November, the interannual variability is greatly reduced. However, each year of sampling is distinguishable, suggesting that area wide changes in the water column chemistry occur on an annual basis (Figures 10.4-7 and 10.4-8).

10.5 Properties in the Deep Water Column

In contrast to the dynamic variations of the water properties in the photic zone and upper mixed layer (approximately depths less than 150 m), water properties in deeper waters remain largely stratified. Below 150 m, concentrations of nutrients increase rapidly with depth in the water column. Oxygen content drops sharply below the mixing zone reaching an "oxygen minimum" before beginning to increase again. Variations in other parameters, such as temperature, salinity, and density, reach relatively constant values at the similar water depths across the study area. Figure 10.5-1 illustrates the pattern in the vertical profiles of these parameters. The lateral uniformity in the water properties indicates that the water masses below the mixed layer are stratified and stable, as expected for regions with limited vertical mixing. Seasonal and interannual variations in deep water properties are minimal, suggesting little direct influence by the dynamic processes affecting water properties in the upper layer.

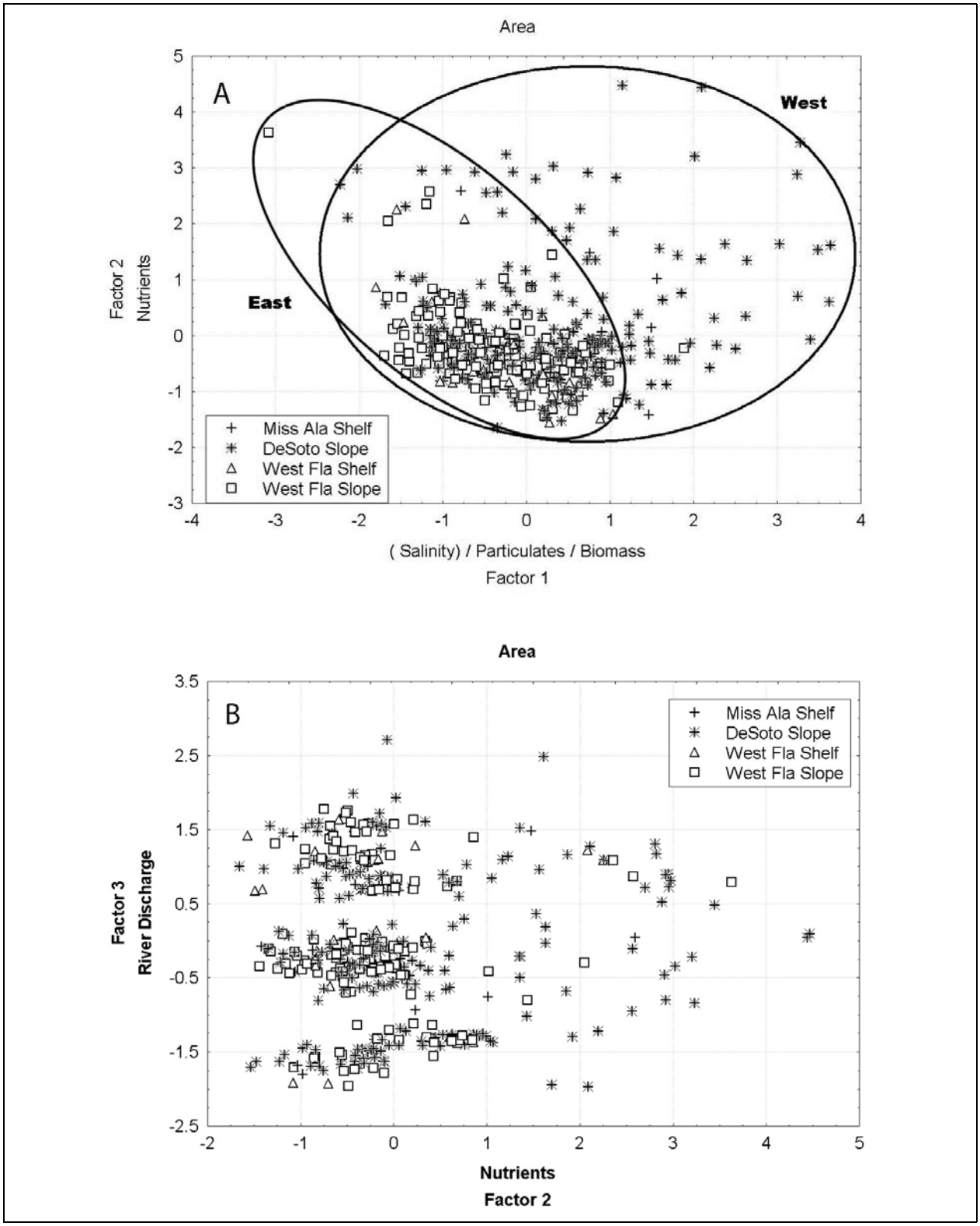

Figure 10.4-2. Data classified by geographic location to detect variability due to distance from the Mississippi River.

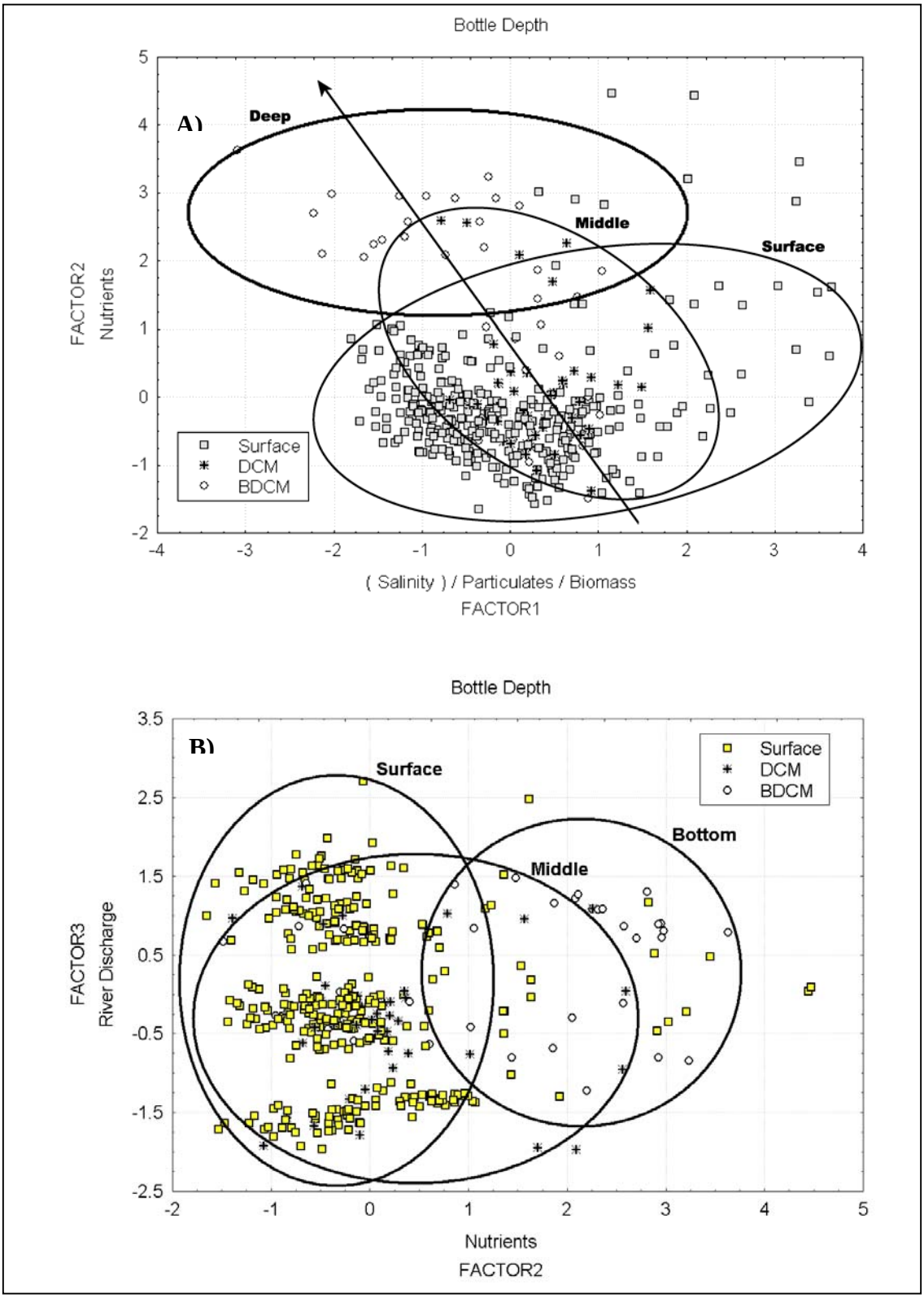

Figure 10.4-3. Data classified by depth in the water column to detect vertical variability in the data.

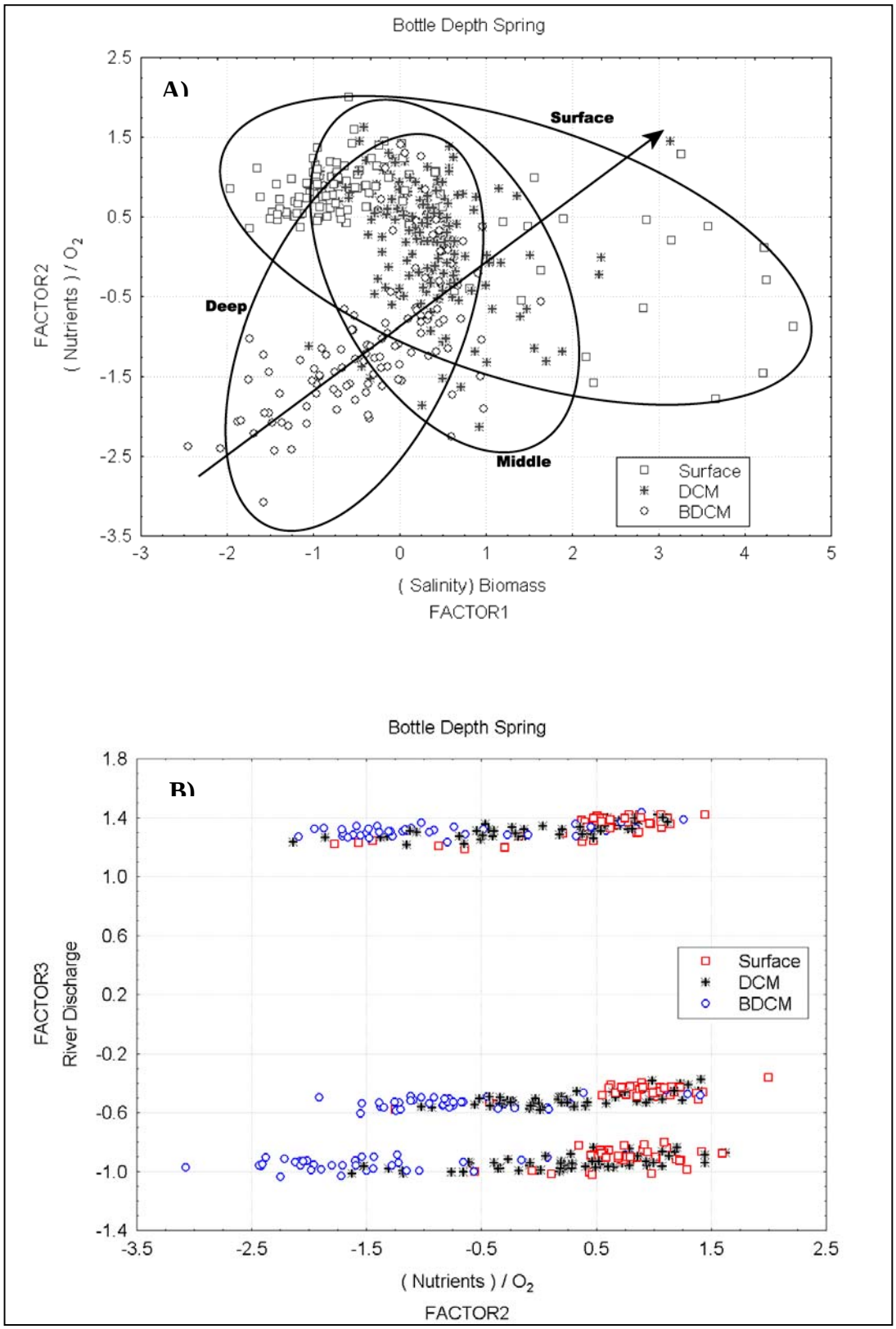

Figure 10.4-4. Data for May cruises classified by depth in the water column.

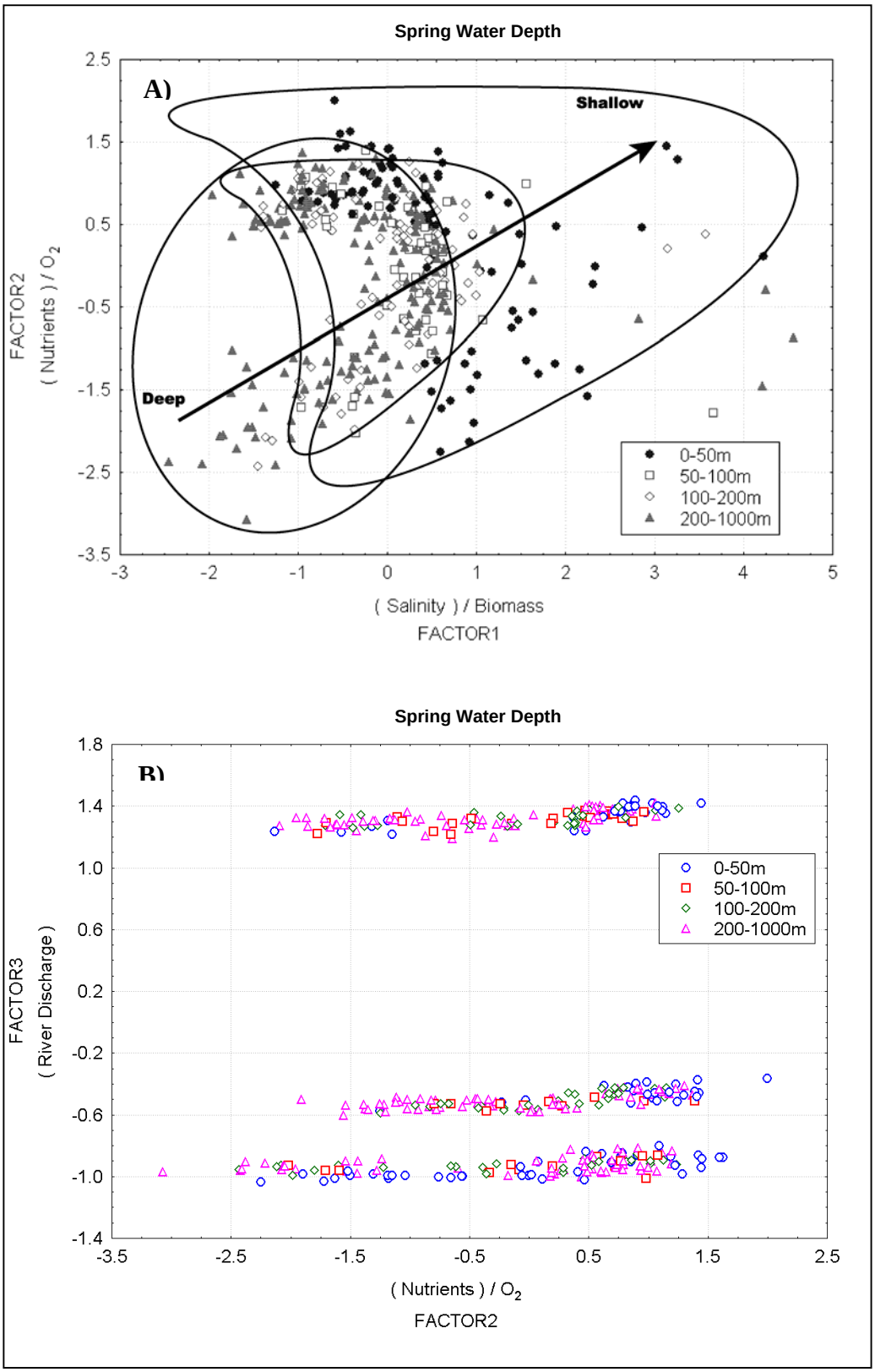

Figure 10.4-5. Data for May classified by water depth.

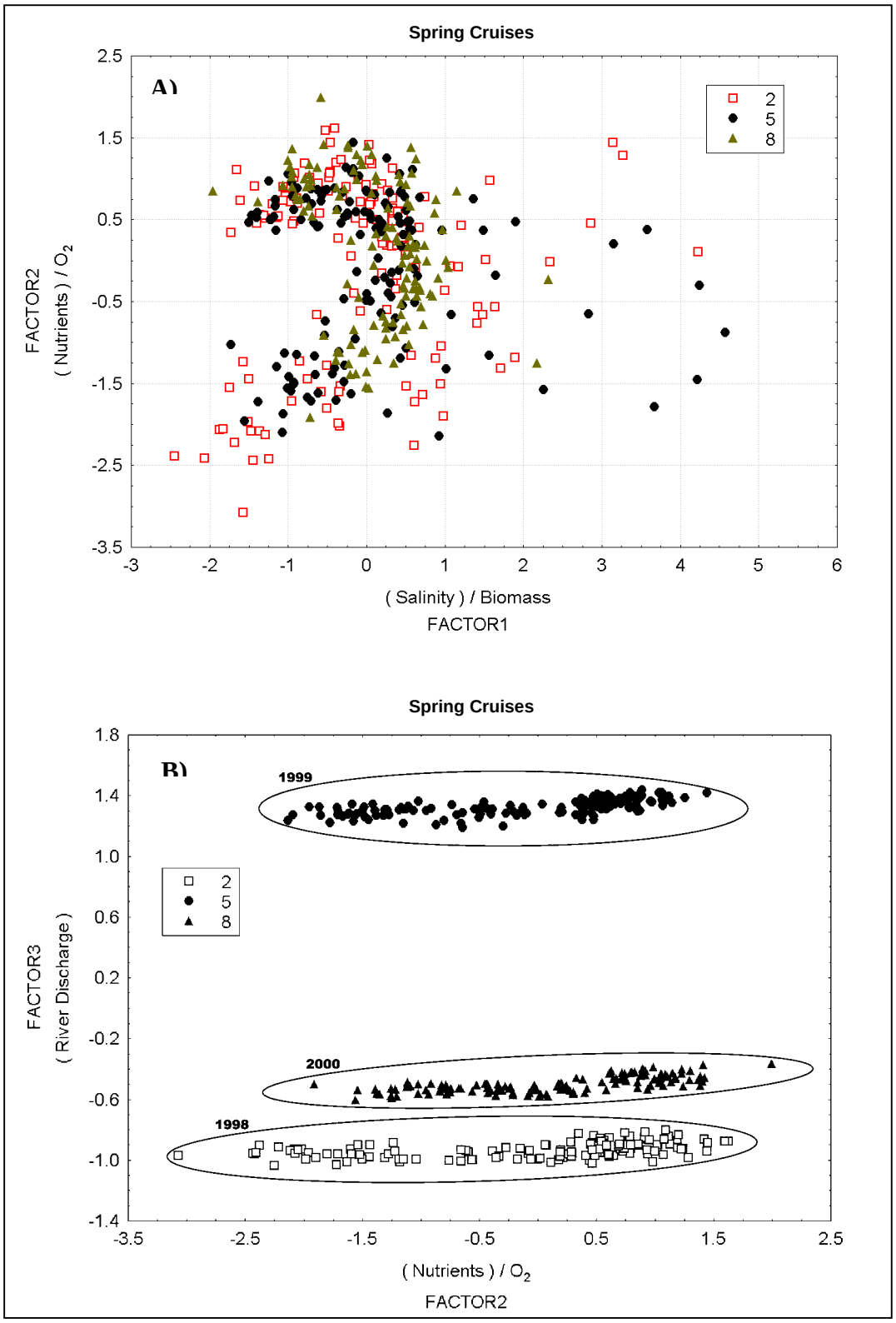

Figure 10.4-6. Data from May cruises classified by year of sampling. The symbol legend gives the cruise number.

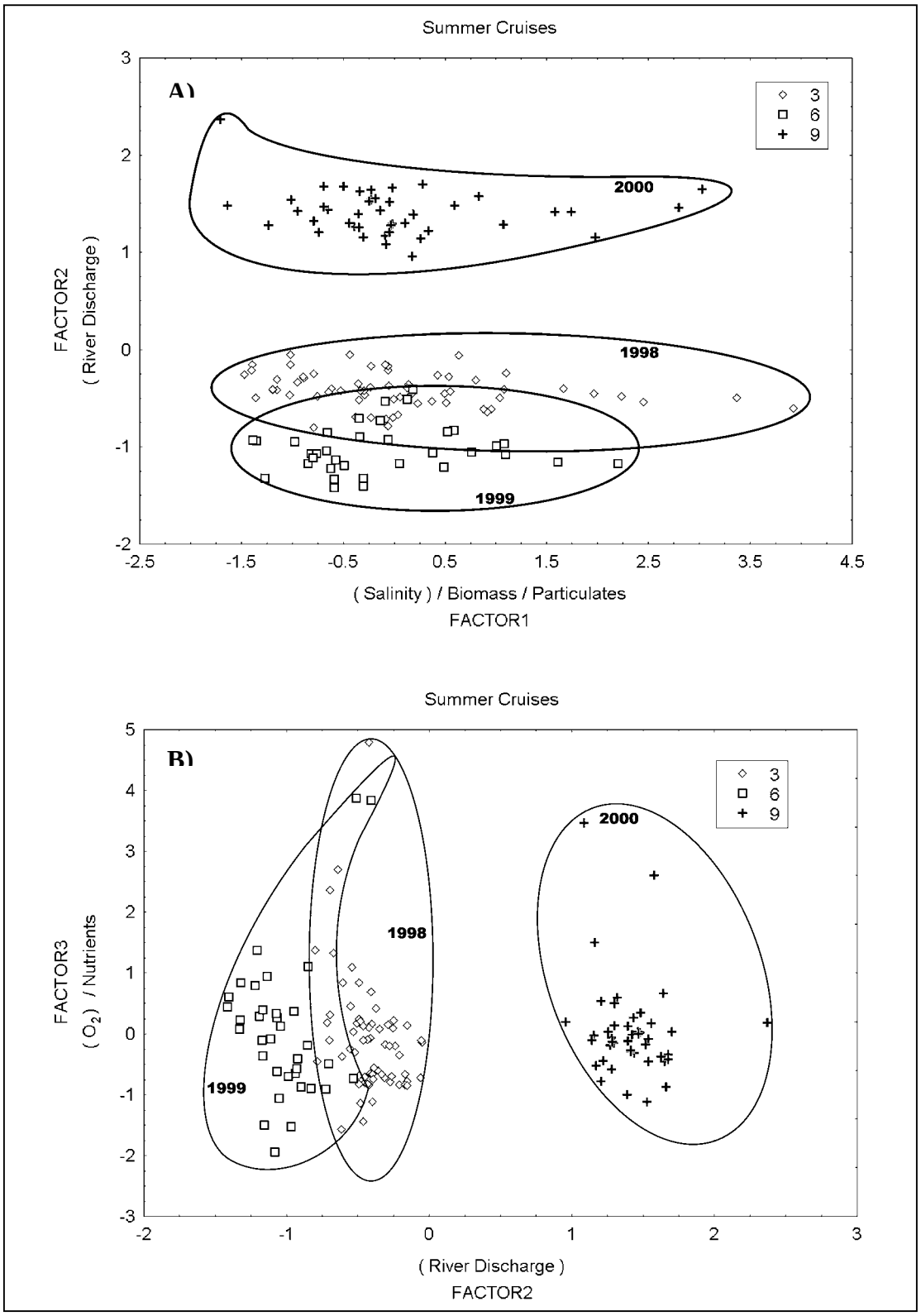

Figure 10.4-7. Data for August classified by year of sampling. The symbol legend gives the cruise number.

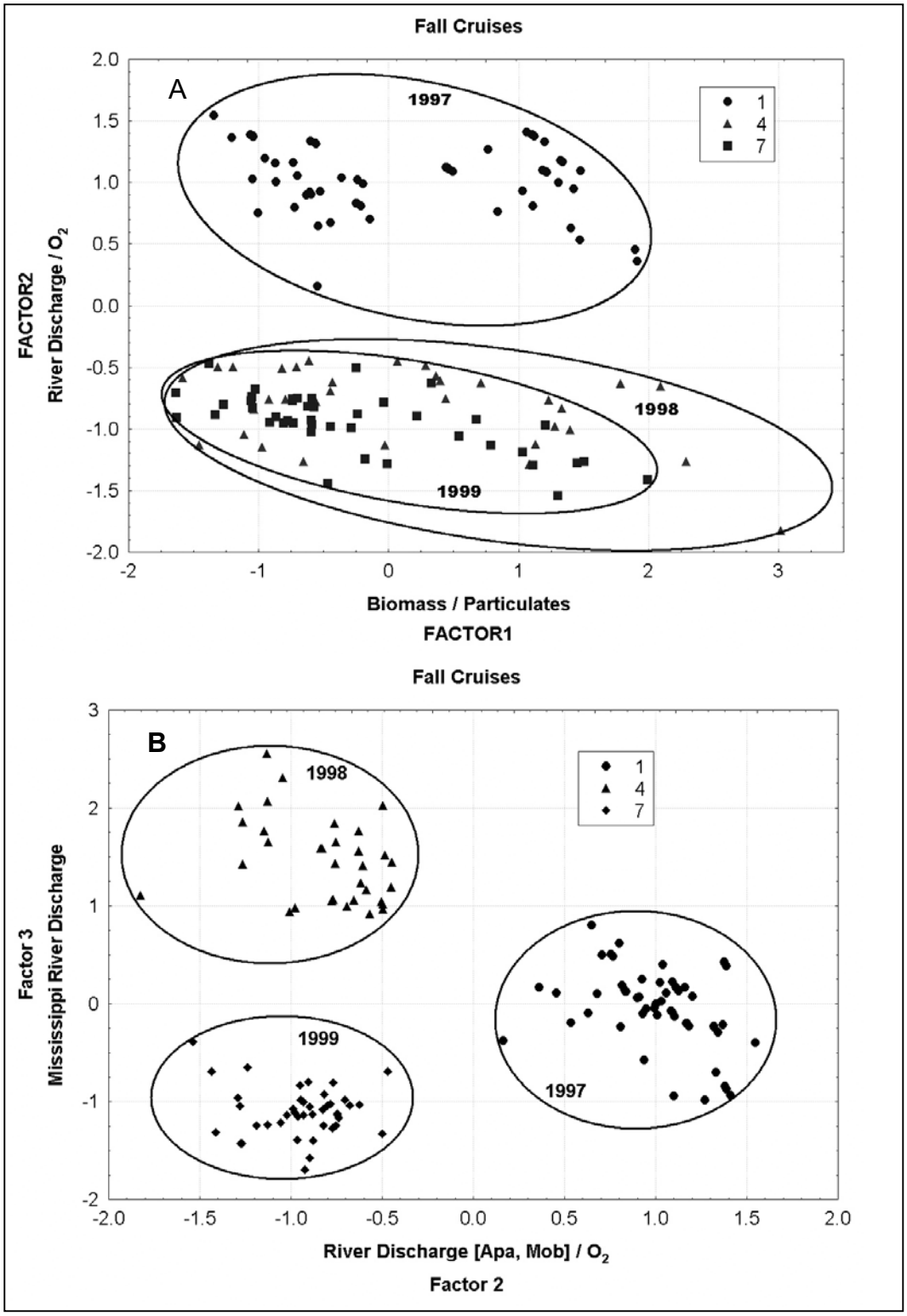

Figure 10.4-8. Data from November cruises classified by year of sampling. The symbol legend gives the cruise number.

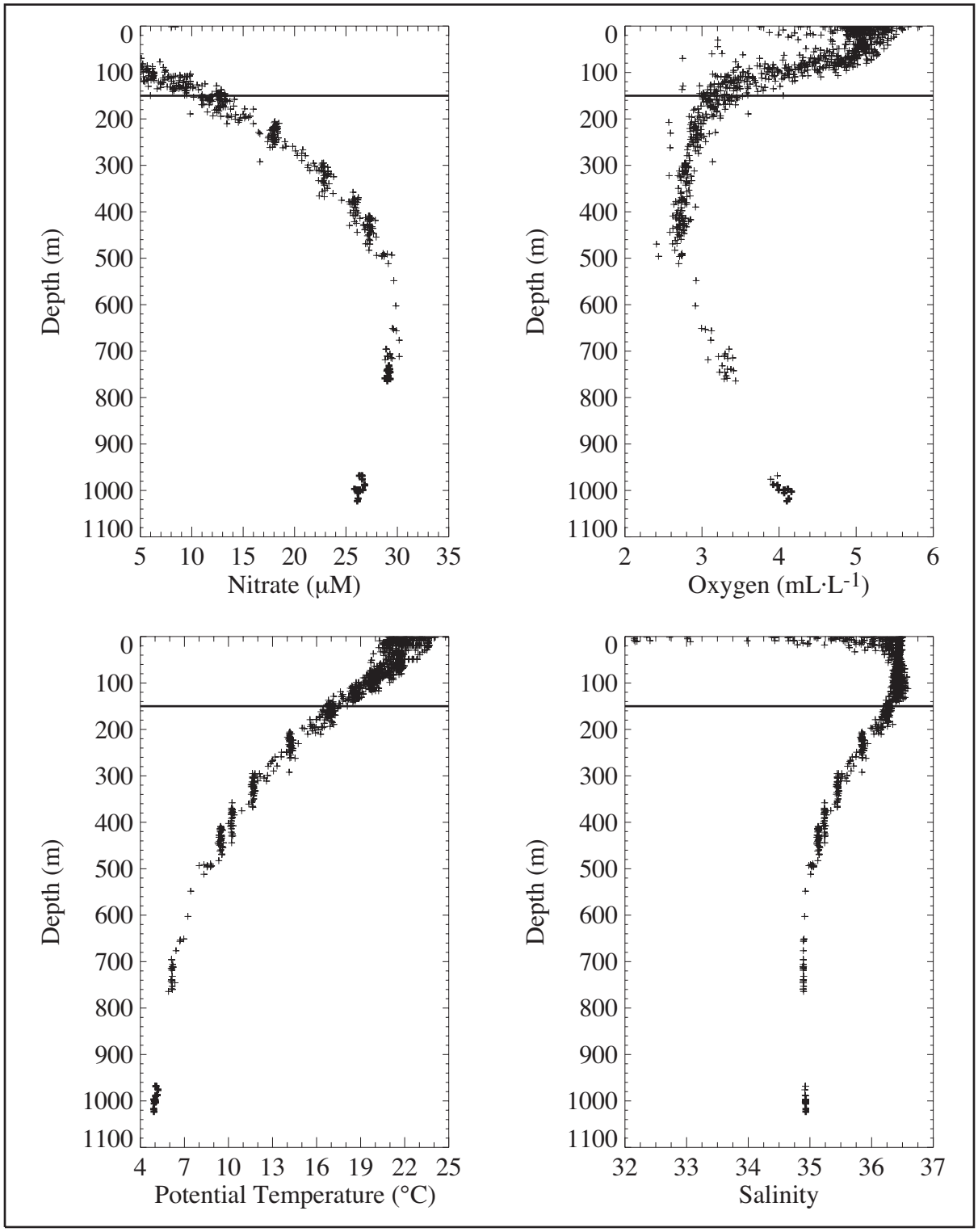

Figure 10.5-1. Representative vertical profiles of NEGOM nutrients, dissolved oxygen, salinity, and potential temperature. These data are from cruise N8 in May 2000. The range for the parameters is that for data below 150 m (horizontal line).

Deep water column POC decreases with increasing distance offshore coinciding with increasing water depth. Static measurement of POC concentrations reflects the end result of a dynamic interaction between in situ production of particles, advective horizontal transport of particles either from river discharges or shallower water resuspension events, and consumption due to in situ microbial reworking. The observed decreases are probably a result of several factors acting in concert. First, as one moves offshore, near-shore sources of particles are more distant and the particles advected laterally through the water column will decrease in concentration because the larger particles will settle out during the transport process, i.e., particulate matter is preferentially deposited near shore. Second, being farther offshore also equates to longer water columns and thus longer settling times. Therefore, sinking particles are subject to longer times of, and hence more, reworking by bacteria. Bacterial reworking generally decreases particle size, disaggregates particles, and converts particulate forms to dissolved forms, all decreasing the concentrations of particles. Thus, increased distance from shore equates to increased water depth, which in combination with settling and bacterial reworking, produces reduced levels of particulates.

11 CONCLUSIONS AND RETROSPECTIVE

11.1 Principal Conclusions

11.1.1 Forcing and circulation

- There are three expected major forcing functions for the circulation over the region: wind, off-shelf circulation features, and river discharge. As feasible, we have examined the effects of all three. The effects of river discharge other than for the Mississippi River were largely confined to near shore on the inner shelf. Although our sampling did not continue inside the 10-m isobath, the effects of the discharge of lesser rivers, as well as of the Mississippi, were clearly seen in property distributions. However, data were not taken that would have allowed us to assess the buoyancy effects of low salinity water on the circulation.

- The shelf circulation patterns west of Cape San Blas seem dominated by off-shelf circulation features; this likewise is true for the circulation over the outer shelf between Cape San Blas and Tampa. Because those features are not seasonal, interannual variability appears to overshadow seasonal signals of circulation in these regions.

  The patterns of low-frequency circulation over the NEGOM study area were examined using shipboard ADCP current measurements from vertical bins centered at 10-14 m. For 8 of the 9 cruises (cruise N4 did not cover the entire region), the gridded current fields were analyzed to remove divergent components, and so to correspond more closely to geostrophic current fields. Then the overall mean was removed from each field and the residual fields examined using an empirical orthogonal function (EOF) analysis to obtain the most energetic spatial patterns and their amplitudes at the time of each cruise. The gridded vector average field showed weak southeastward flow west of about 87.5°W, upcoast flow (10-15 $cm \cdot s^{-1}$) between about 87°W and Cape San Blas and over the shelf outside the 100-m isobath, and weak currents with an indication of cyclonic flow inshore of the 100-m isobath on the west Florida shelf.

  The first four EOF modes (Table 4.5-1) contained 84% of the variance. Mode 1, with 34% of the variance, is essentially an along-shelf circulation pattern over the outer shelf and slope east of 87.5°W. There also is some evidence of closed circulation over the shelf west of Cape San Blas as well as a partially closed circulation over the inner shelf centered off Tampa. Mode 2 with 22% of the variance shows strong northeast (or southwest) flow over the Mississippi-Alabama shelf and a large energetic eddy centered near the 200-m isobath and 28.5°N. The third mode, accounting for almost an equivalent fraction of the variance (18%), consists of an eddy centered over the upper DeSoto Canyon. Flow is strongly on- or off-shelf on the eastern and western limbs of this eddy. Another off-shelf eddy appears to be forcing the currents over the upper slope and outer shelf off the Big Bend region. Modes 1, 2, and 3 evidence no clear seasonal patterns in their amplitudes; we speculate that they are driven principally by the off-shelf circulation features.

  With 10% of the variance, EOF mode 4 generally shows largest currents over the inner shelf, appears principally related to coastal circulation, and may be wind driven. It is the only mode with some apparent seasonality. The amplitudes indicate downcoast flow to the west of Cape San Blas for both fall cruises in agreement with along-shelf wind directions over the inner shelf during those cruise periods. The mode 4 amplitudes for the three spring cruises indicate upcoast coastal flow, in agreement with along-shore winds observed during the cruises. Amplitudes during the three summer cruises were near zero in agreement with

expectations based on the weak and generally onshore winds observed during the summer cruise periods. Together modes 5-7 contain only 15% of the variance. Currents for all are weak, but strongest over the inner shelf or near the Mississippi River mouth. They likely are associated with local forcing by winds and river discharge, though their amplitudes show no clear seasonal patterns.

- Wind effects on the circulation appear to be confined to the inner shelf. One might expect the along-shelf wind component to be associated with forcing of either up- or down-coast coastal currents. There was some indication of such seasonal forcing in the pattern and amplitudes of mode 4 of the low-frequency EOF analysis of near-surface ADCP-measured currents (mentioned in the previous paragraph).

  The along-shelf wind components over the inner shelf (near the 20-m isobath) during the NEGOM field period showed some clear patterns. Variability in speed and direction were greatest from mid-December into early spring, less during the period from August into December, and least during the period from mid-May through about July. The upper coast (west of Cape San Blas) showed greater variability than the lower coast, particularly in summer, but also to lesser extent from August into winter. Temporal patterns of up- and downcoast wind components are less pronounced, but the smoothed along-shelf winds are generally downcoast in spring, becoming near zero in May and June. Along the upper coast, winds shifted to upcoast for the period late June through most of August; along the lower coast they remained nearly zero for this period. In both regions there was a pronounced shift to downcoast wind components beginning in late August to early September, and this trend continued into or through October. The resulting pattern of coastal currents should have large directional variability through the winter and much of spring. Coastal currents should be weak over the lower coast during the summer and over the upper coast during the early summer, shifting to upcoast in June and continuing into August. In both regions there should be a pronounced period of downcoast coastal currents beginning in September and continuing through most of the fall season.

  Correlation between gridded fields of along-shelf components of wind and near-surface current from all NEGOM cruises shows correlations significant at the 90% level or above only for the inner shelf. The distribution and values of the correlations seems to provide evidence that, based on this limited data set, there was wind forcing of currents over the inner shelf, perhaps with the exception of the southeastern part of the study area.

11.1.2 Major water masses found over the slope and outer shelf

- The vertical stratification of water masses off the NEGOM shelf consists of remnants of waters from various sources with well known extrema in identifying properties. Beneath the surface waters with a core near the σ_θ surface of 25.4 $kg \cdot m^{-3}$ is the Subtropical Underwater characterized by a salinity maximum. With increasing depth, the next recognizable water mass is the 18°C Sargasso Sea Water characterized by a maximum in dissolved oxygen near the σ_θ surface of 26.5 $kg \cdot m^{-3}$. A minimum in dissolved oxygen marks the core of the Tropical Atlantic Central Water found near the 27.15 $kg \cdot m^{-3}$. At the 27.45 σ_θ surface, there are maxima in nitrate and phosphate and a minimum in salinity as expected for remnants of the Antarctic Intermediate Water. An associated silicate maximum occurs lower in the water column. Of course, many of these density surfaces intersect the bottom as one moves up the slope and onto the NEGOM shelf. Those that do extend onto the shelf were found at shallower depths there than in the open water of the eastern Gulf. Over the NEGOM study area the average depths for the 25.4 $kg \cdot m^{-3}$, 26.5 $kg \cdot m^{-3}$, 27.15 $kg \cdot m^{-3}$, and 27.15 $kg \cdot m^{-3}$. surfaces are, respectively, 54, 153, 416, and 721 m. As expected, the variability of property

values on density surfaces generally decreases with increasing depth. Beneath the Subtropical Underwater, standard deviations on density surfaces range between about 5% to 29% of the mean values, depending on the property considered.

11.1.3 Distributions of oxygen

- Oxygen concentrations in the upper 6 m of the water column were examined in terms of the percent saturation of the water. In general, most values fell between 95 and 105% saturation, with numerous cases of high supersaturation (> 110%) and only a few cases with saturation lower than 95%. The magnitude and variability of saturation values was greater over the Mississippi-Alabama shelf than the west Florida shelf with more occurrences of highly supersaturated waters. Highly supersaturated values over the west Florida shelf generally occurred only nearshore in localized areas associated with river discharge.

  The saturation values generally were found to depend on the amount of fresh water discharged to the region, the sea surface temperature, and/or the biological productivity. The highly supersaturated values over the Mississippi-Alabama shelf coincided with the region of lowest salinity water (< 30). Most, but not all, stations with high chlorophyll *a* also were highly supersaturated in oxygen, illustrating the potential effect of primary production on dissolved oxygen. Highest saturation values and greatest variability occurred in spring. There was less variability in fall than in spring or summer.

- The subsurface oxygen concentrations for the nine cruises were found to have variances that were approximately 5-20% of the mean. Thus, if the density surface of the subsurface sample is known, a fair estimate of the oxygen concentration is known. Seasonal effects below approximately 100 m were limited.

- Inshore of about the 100-m isobath, the bottom dissolved oxygen concentrations were greatest in fall because of cooler air temperatures that result in higher saturation oxygen values in surface waters and deep mixing by energetic wind events. Values are lowest in summer due to increased vertical stability that inhibits renewal of oxygen in bottom waters and to oxygen utilization during oxidation of organic material. Over the inner shelf there were significant correlations between high hydrostatic stability and low bottom oxygen in summer but not in other seasons. Over the western NEGOM region, where nutrient input and primary production are relatively high, bottom oxygen saturation was positively correlated with high bottom detrital material as represented by nitrate on every NEGOM cruise. No hypoxic conditions, as defined by dissolved oxygen concentrations below 1.4 $mL \cdot L^{-1}$, were observed. However, very low (~2 $mL \cdot L^{-1}$) concentrations were observed on two spring and one summer cruise off Chandeleur Sound and on one summer cruise near the 30-m isobath south of the Florida-Alabama border.

11.1.4 Distributions of nutrients

- Nutrients are utilized during photosynthesis and regenerated when detrital material decays. The vertical distributions of nutrients reflect these processes. In the photic zone, represented approximately by the upper 60 m of the water column, nutrients generally are depleted, except where there is a source. The major source in the NEGOM study area is the Mississippi River. The nutrient input from this river results in near-surface nutrient concentrations that are substantially higher over the Mississippi-Alabama shelf than over the west Florida shelf. The distributions in the region impacted by the Mississippi River discharge have a seasonal signal with high concentrations in spring, when river discharge is at a peak, and lower concentrations during the remaining seasons. The variability of near-

surface nutrient concentrations in the region is high, as evidenced by standard deviations which exceed the means. Variability is greatest in spring and lower in fall. In summer there is some enhancement of silicate concentrations along much of the NEGOM slope; this likely is related to eastward transport of Mississippi River waters along the shelf edge and slope by circulation features located off the shelf.

Additionally, the discharges from other rivers, bays, and estuaries in the NEGOM study area can cause localized near-shore regions of higher near-surface nutrient concentrations when discharges are highest. However, at least three factors mask any resulting seasonal signal in associated nutrient concentrations that may be present. These factors are: the interannual variability of such discharges, the small number of seasonal samples available for this study (only three per season), and the distance of the innermost stations from the discharge source (no samples shallower than ~10 m isobath). Localized enhancements to nutrient concentrations in the photic zone also occur in association with dynamic processes that uplift density surfaces, bringing nutrient-rich waters from mid-depth upward into the photic zone. Such processes include the presence of cyclones, divergence between cyclone and anticyclone pairs near the shelf edge, interaction of eddies with bathymetry, and wind or bottom-induced upwelling. During the summers sampled, these processes and eastward advection of Mississippi River discharge by off-shelf anticyclones supplied nutrients to the photic zone over the outer shelf edge and upper slope. This resulted in continued primary productivity (and we suggest secondary production as well) in this region past the expected spring season.

- Below approximately 120 m, the standard deviation of a nutrient concentration on a given density surface is less than 20% of the mean, and so, if the density surface is known, a fair estimate of the nutrient concentration is known as well. The distributions of nutrients at depth tend to have little seasonal variability, at least that can be measured by the sampling program of this study. Rather, the processes that effect nutrient distributions at depth are related to the water masses that may be transported into the area (see discussion above) and the rates of decay of detrital material sinking through the water column. The general patterns of distribution are two-fold: on a given subsurface density surface, mean nutrient concentrations tend to increase with distance off shore and, in the vertical, mean concentrations increase with increasing depth to approximately 700-800 m depth, below which they decrease with depth.

11.1.5 Chlorophyll

- Examination of the spatial distribution pattern of chlorophyll *a* in the NEGOM area in near surface waters suggests that freshwater discharge from rivers and estuaries is an important controlling factor dictating the distribution of phytoplankton standing biomass over the shelf. Highest chlorophyll *a* concentrations generally were located over the inner shelf, particularly near river and estuary outflows. Chlorophyll *a* values < 0.1 $\mu g.L^{-1}$ generally were found more often east than west of 86°W. For both near-surface and chlorophyll maximum depths, the highest concentrations were observed between lines 1 and 4 and between lines 7 and 8, as a consequence of freshwater discharge from the Mississippi and the Apalachicola and Suwanee rivers, respectively. The clear negative correlation between chlorophyll *a* and salinity in near-surface waters implies that fresh water inflow into the region was exporting chlorophyll produced upstream and/or promoting the growth of phytoplankton biomass by advecting nutrients.

  Spatial distributions of chlorophyll *a* were similar among all three fall cruises (N1, N4, and N7) when discharges of all rivers were near minimum values; waters in the near shore area

between the Mississippi and Apalachicola rivers had the highest concentrations, while other areas had relatively low concentrations. In contrast, in spring (cruises N2, N5, and N8), when river discharge was near the maximum, high chlorophyll water extended over much of the inner shelf from the Mississippi River to Choctawhatchee Bay. (An exception was April 2000 likely due to the relatively (for spring) low river flow that preceded the cruise.) Distributions also were similar among all three summer cruises (N3, N6, and N9), and evidenced a pattern of high concentrations over the inner shelf associated with river discharge, particularly west of 87°W. In addition, the summertime chlorophyll *a* concentrations, were high over the outer shelf and slope; this was caused by the transport of Mississippi River discharge and uplift of mid-depth nutrient rich waters by off-shelf circulation features.

11.1.6 Distributions of particulate matter

- Particulate matter distributions in the study area were described in terms of concentrations of particulate matter (PM), particulate organic carbon (POC), particulate organic nitrogen (PON), and light transmission. Excellent correlations were obtained between PM measured at discrete depths on stations and particle beam attenuation coefficients, estimated from measurements of light transmission. These correlations were used to estimate vertical profiles of PM at each station.

- Near-surface concentrations of PM were found to correlate well with salinity (negatively) and chlorophyll (positively). The particulate distributions generally were highest near the low salinity discharge sources (rivers, bays, and estuaries) and were high in regions with high chlorophyll. In all seasons, high near-surface particulate concentrations ($\geq$ 1 mg·L^{-1}) over the shelf were located adjacent to the Mississippi River and generally extended northeast to Mobile Bay. High concentrations also were located adjacent to the other discharge sources, but with no clear seasonal pattern, likely due to the interannual variability of the discharge and the low number of synoptic data sets (three) for each season. Low concentrations ($\leq$ 0.2 mg·L^{-1}) over the shelf were most extensive in fall and located mainly over the west Florida shelf. Away from discharge sources summer concentrations over the shelf generally were higher than those in spring. Near-surface mean PM concentrations generally were lower in fall with most variability in spring. Near-bottom means were similar for the three seasons; the smallest variability was observed in summer.

  In all three seasons, high concentrations ($\geq$ 1 mg·L^{-1}) over the slope could occur adjacent to the Mississippi River. For fall and spring, the presence of such occurrences varied between years; only in summer was the pattern consistent in all three years. Further, the region of high concentration over the slope was more extensive in summer, extending from the Mississippi River to off the west Florida shelf. The summer concentrations over the slope were caused by the presence of anticyclonic/cyclonic circulation features that advected the Mississippi River discharge southeastward along the shelf edge.

  The average water column PM mass was smaller and less variable over the eastern shelf (east of 87°W) than over the western shelf. Also, the percentages of cruise average PM per unit surface area that was contained in bottom nepheloid layers over was much lower and less variable over the eastern than the western shelf. This is evidence for the effects of the Mississippi and other rivers on PM and light transmission, and it is suggestive of more re-suspension on the western shelf than on the eastern shelf. The percent was highest, often exceeding 50%, over the inner shelf (approximately $\leq$ 50 m water depth). This was particularly true of the west Florida shelf in all seasons.

- Both POC and PON were measured near surface and at one sub-surface depth (either near-bottom or the chlorophyll maximum) on all stations. The highest POC levels in all seasons generally were associated with high PM plumes near river mouths. As expected, near-surface POC concentrations are greater and more variable than sub-surface concentrations. The largest variability in near-surface concentrations was seen in spring and summer associated with distributions of river discharge; sub-surface POC concentrations showed no clear seasonal variability.

11.1.7 Major algal groups

- Chlorophyll *a* and carotenoid pigment distributions were used to infer phytoplankton taxonomic composition, and time/space variations over the NEGOM region. On each cruise, ten major algal groups were characterized as to their percentage contribution to the total measured chlorophyll *a* on the basis of HPLC measurements of accessory pigments. Major accessory pigments detected during the nine cruises were chlorophyll *b* and c_2 and 19'-butanoyloxyfucoxanthin, fucoxanthin, 19'-hexanoyloxyfucoxanthin, diadinoxanthin, zeaxanthin, and β-carotene. Other pigments, such as chlorophyll c_3, peridinin, violaxanthin, alloxanthin, prasinoxanthin, diatoxanthin, and antheraxanthin, usually were detected in only a few samples at low concentrations. Based on the pigment compositions, the major phytoplankton species in the study region were prymnesiophytes, prochlorophytes, cyanobacteria, pelagophytes, and diatoms. In general, prymnesiophytes, prochlorophytes, and cyanobacteria accounted for, respectively, 20-40%, 10-40%, and 10-40% of chlorophyll *a*.

  Prymnesiophytes, prochlorophytes, and cyanobacteria were widespread over the entire study area with patchy higher abundances in some areas. However, not all of them were equally abundant over all water depths. When in abundances of 40% or more of the total chlorophyll *a*, prymnesiophytes were found over the outer shelf and slope; the west Florida shelf had most stations with high abundances, often extending from the inner shelf off Tampa Bay to the slope. In contrast, the abundance of prymnesiophytes abundance was generally low (less than 20% of chlorophyll) in waters off the mouth of the Mississippi River and generally less than 30% in areas influenced by other river, bay, and estuary outflows. An exception was observed during the fall cruise N7, when the abundance of prymnesiophytes was high (≥40%) in waters between Pensacola and Choctawhatchee Bays and from the Suwannee River south to Tampa Bay. Cyanobacteria abundance in near-surface waters generally was low (<10% of chlorophyll) in regions of fresh water outflow. However, high abundances of cyanobacteria (40% or more) occurred in patches—the most extensive of which was during fall cruise N1 over portions of the outer shelf and slope between 84° and 87°W. Pelagophytes were present in high abundance (10-30% of chlorophyll) mainly in patches over the outer shelf and slope in the near-surface waters. Diatoms were primarily present in near-shore waters, especially in waters associated with freshwater outflows. Dinoflagellates, chlorophytes, and chryptophytes were generally low in abundance (below 10% of total phytoplankton), although higher abundances were observed at some locations during some cruises.

  The structure of the phytoplankton communities exhibited consistent changes in vertical distributions in the water column. Abundances of prochlorophytes and pelagophytes in near-surface waters during the nine cruises were consistently lower than those in DCM waters or below DCM waters. In contrast, the abundance of cyanobacteria in near-surface waters was consistently higher than that in the deeper waters. The relative proportions of prymnesiophytes, the most abundant taxon in the NEGOM region, did not change significantly with depth.

Although interannual variability was present for the average abundances of all algal groups, seasonal variability was in general larger than interannual variability. The large seasonal variability likely can be attributed to the fact that the primary controlling factors of phytoplankton standing stock, namely nutrient, temperature, and light are largely seasonal. For the study region as a whole, average abundances of prochlorophytes and pelagophytes in near-surface waters were higher in November and August than in May. In contrast, at DCM depths, the average abundance of pelagophytes was high in November and lower in May and August, while the average abundance of prochlorophytes was similar among the three seasons. The relative abundances of both diatoms and dinoflagellates were lowest in November and highest in August for both near-surface water and water at DCM depths (except during cruise N3). Increased relative abundance of diatoms and dinoflagellates in summer was probably caused by the input of fresh nutrients associated with low salinity water in the spring and summer. In both near-surface and DCM waters, cyanobacteria were highest in abundance in May and lowest in November, perhaps due to the transport of the spring blooms of cyanobacteria that occur frequently in the estuaries adjacent to the NEGOM shelf. Unlike other algal groups, abundances of prymnesiophytes were similar during all nine cruises in both near-surface and DCM waters.

11.1.8 Integrated water column chemistry

- The univariate analyses confirmed that the processes normally encountered in coastal marine settings are at work in the NEGOM area. Most resulting relationships are explainable by well-studied biotic and abiotic phenomena. Thus, our first conclusion is that the NEGOM area does not seem subject to any extraordinary events or processes and is generally typical of near-coastal regimes influenced by major river systems. Other conclusions are: that properties across the area are highly variable in time and space, that the presence of biological organisms is important in redistributing chemicals vertically and horizontally within the study area, and that physical movements of water both supply the necessary chemicals for growth and modify biologically-generated patterns in chemical and particulate distributions.

- Multivariate analyses were applied to the following suite of physical, chemical and biological data: five nutrients, dissolved oxygen, discharges from the Apalachicola River, Mississippi River and Mobile Bay, total chlorophyll, salinity, fluorescence, particulate matter, particulate organic carbon, and particulate organic nitrogen. Principal Component Analysis was used to determine which groups of related variables accounted for most of the variance in these data sets and so also are strongly related. The first component, accounting for 41% of the variance, showed positive loading for the factors chlorophyll *a*, fluorescence intensity, particulate matter, and particulate organic carbon, but negatively for salinity. The second component accounted for 14% of the variance and had positive loadings for nitrate, nitrite, phosphate, and silicate. Component 3 accounted for 10% of the variance and had positive loadings for the discharge volumes.

11.1.9 Interrelationships between the observed patterns in abiotic and biotic variables

While the primary goal of this program was to survey water column properties in the study area, it is also desirable to determine, within the limits of the data collected, interrelationships between the observed patterns in abiotic and biotic variables. To this end, we posed and answered a series of questions.

- *What are the processes that couple physical and chemical/biological variables?* In the most general sense this is the fundamental question that must be addressed if one is to develop a capability for predicting system response to possible external events, such as oil and gas development. First and foremost, the present study is primarily descriptive in nature and it was restricted to the water column. At a minimum to fully explore and understand the inner workings of the northeastern Gulf of Mexico, survey studies need to be supplemented by process studies. The entire ecosystem must be considered as well as the benthos in order to fully understand how the biology alters the chemical fields, how the chemical fields support the ecosystem, and how the air, water and benthic systems are coupled. These are complex considerations. A fundamental physical forcing is the seasonal cycle of solar radiation causing changes in temperature and light levels in upper ocean waters and thus enabling primary production and biochemical reactions. Another fundamental physical forcing is that of the seasonal cycle of wind mixing of the upper ocean that supplies nutrients and other materials from mid-depths to the waters of the photic zone in fall and winter by vertical mixing. Superimposed on these seasonal physical forcings of chemical/biological parameters are, at forefront, river inputs which change the dynamics of production through such introduced materials as nutrients and particulates. Juxtaposed on this are additional inputs from outflows of adjacent bays and the uplift of nutrients from below. These nutrient and particulate matter inputs to the near-surface waters are distributed by patterns of currents, and often affect regions far from their entry into the photic zone. In the study region, wind effects on the current regime seem principally important in the near-coastal region, while the outer shelf and slope currents are dominated by off-shelf circulation features. Quantitative assessment of the influence and the dynamics of these events at specific locations is not possible with the data collected so far.

- *How do the interannual variability of the physical parameters and the seasonal variability of the biological parameters interact*? There is significant seasonal and interannual variability in water column properties in the study area. The two influences are inseparable and complimentary. The seasonal cycles of solar radiation and wind mixing together with the overall discharge pattern for the rivers set the preconditions for how the phytoplankton react to changes in growth limiting factors. The amount and distribution of the inputs of nutrients and particulates predetermine how extensive and how intense the phytoplankton response will be. The quality of the response is most likely the same each year, but intensity and location vary. However, the seasonal signals are modified by weather and climate variations that set the stage for the dynamics of riverine discharge. Seasonal variations are inextricably linked with variations in the hydrologic cycle, which may have cycles that span years or even decades. Year-to-year variability is expected, and the multivariate analyses clearly separates the datasets by year. While not directly measured in this study, the setting of the intensity of the physical/chemical fields in the area will ultimately exert controls and limits on the productivity. In most cases productivity will be directly regulated by the delivery of nutrients to the phytoplankton. However, it is unlikely that nutrients are delivered in the exact ratios needed for biosynthesis. Thus, any one of a number of other growth limiting factors may be exhausted as the phytoplankton bloom progresses. It is also likely that these secondary limiting conditions are variable across the region and may exert differing controls on the maximum productivity that can be realized in any given subregion. The secondary supply of nutritive micronutrients such as iron may have independent, dynamical patterns across the region.

- *What do the differing patterns of algal assemblages say about phytoplankton ecology*? The compositions of phytoplankton assemblages are dynamic responses to growth conditions at each location. Coastal margins are characterized by spatial and temporal patchiness and heterogeneity over a range of scales. Each species can have differing strategies for

sustainability, and the availability of the appropriate growth conditions will determine their presence or absence and their success relative to other algal groups. The development of growth limiting conditions can stop further growth of certain species depending on their nutritional and light requirements. The role of micronutrients and other growth factors (including exudates and dissolved organic compounds) are not well understood for phytoplankton. Many algal groups appear related to a particular oceanographic setting (coastal, temperate, open ocean) and time of year. Geographic and temporal variability in growth conditions results in variable phytoplankton assemblage composition. For example:

cyanophyta fix nitrogen and grow when nutrient concentrations are low;
chrysophyta have requirements for silicon and calcium for skeletal parts, but can be phototrophic, heterotrophic or phagotrophic;
chlorophyta are mostly phototrophic;
cryptophyta appear to flourish in warmer waters; and
pyrrophyta often produce toxins or growth inhibitors.

Variations in phytoplankton assemblages result from variations in abiotic conditions and biotic interactions. However, knowledge of the critical factors that control phytoplankton ecology is limited and prediction of compositions *a priori* based on chemical/physical fields are difficult at best. Detailed process and manipulative studies are needed to quantitatively predict phytoplankton ecology based on physical/chemical forcings.

- *Why aren't the phytoplankton coupled more closely to the interannual variations in the physical fields?* The coupling of physical changes and resultant biotic responses is a complex issue in natural systems. Apparent decoupling can be explained by several factors including: process rates that are different or variable, non-linear responses, thresholds, and secondary alterations that attenuate the intensity of the response. The time constant of the physical system can be quite different from the time constants for complex biological systems. If the biological system is slow to respond to rapid changes in physical parameters, then the observed biological assemblage may have been caused by a physical change that happened some time before the actual time of sampling. Such decoupling may often be observed when sampling at separate stations as a function of time. An event (e.g., some change) may cause a cascade of responses in the affected systems that could be disconnected in time from the triggering event. Also, biological responses are not necessarily linear; for example, exponential growth will reach a maximum growth asymptote regardless of continued stimulus. In other cases, the oversupply of one nutrient may rapidly deplete another essential element that was in good supply until the onset of rapid growth; this was found in the case of iron fertilization when an iron-induced bloom reached maximum biomass as factors other than iron became growth limiting. Also biotic responses may be triggered by thresholds, where the changes in physical forcings must reach a threshold value before a response is caused, in which case no correlation between parameters would be expected until the threshold is reached. Finally, biota (e.g., phytoplankton standing crop) may be affected by non-physical factors (e.g., grazing). Because of this complex interplay of abiotic and biotic factors, related processes may appear unrelated and vice versa.

- Many questions still remain regarding the dynamics of water column properties and the associated biology in the northeastern Gulf of Mexico. This program has produced extensive descriptive data that delimit the range of what we might expect to see in water column properties. The program has also identified the relative importance of many forcing factors in the region. A better understanding of the spatial and temporal scales of variability in the system is developing. However, we are not yet positioned to predict what responses will occur given a scenario of external events. The system is complex and a static sampling

approach, such as conducted in this study, does not lend itself to predictive modeling. Surveys and process studies need to be combined to provide a quantitative description of the system and the processes that operate within it, particularly of rates. In addition, coupling with higher trophic levels and benthic processes will be needed to understand the boundary conditions at the interfaces of the system.

11.2 Remarks Regarding Experimental Design

During the review and consideration of this report, a number of issues regarding the design of the field program surfaced. It seems appropriate to end this report with a brief discussion of these issues, with the hope that the designers of future programs might benefit from their consideration.

11.2.1 Adequacy of sampling period

Because of the non-seasonal forcing by off-shelf current features, the interannual variability of river discharge forcing, and (to some extent) the interannual variability of the winds in the nearshore region, the indication is that a real seasonal signal probably does not exist for the distributions of shelf circulation and physical properties. If seasonal *averages* are sought, measurements must be sustained over a very long period to beat down the effects of the aforementioned variability of forcings.

11.2.2 Sampling plan

The sampling plan chosen for the NEGOM study consisted of cross-isobath lines of stations from ~10 m to 1000 m water depth. This was based on the fact that the cross-shelf scales of circulation and distribution of associated physical properties are shorter than the along-shelf scales. This design is very good for the situation of reasonably straight isobaths and coastline. However, with a arcuate coastline such as that in the western NEGOM region, this design leads to undersampling of the inner shelf in the along-shelf sense.

The cross-shelf scales, as obtained from analyses of surface thermosalinograph and ADCP measurements, are approximately 10-12 km for the western shelf and 21-25 km for the west Florida shelf. The cross-shelf station separations for the two regions were 13-28 km and 20-48 km, respectively. Thus, the cross-shelf sampling was likely just slightly greater than the correlation scales. Along the shelf edge, the along-shelf scales of variability based on ADCP and thermosalinograph measurements were 33-44 km, and the along-shelf station spacing was 40-60 km, longer than the likely mesoscales of variability. Along-shelf station separations over the inner shelf were much greater: ~75 km in the west and 90-120 km over the west Florida shelf. Thus, seasonal signals in along-shelf circulation, especially over the inner shelf, may actually be present with some strength, but not be determinable based on the data set collected. This is especially true, of course, if such signals are of small spatial scales.

11.2.3 Need for simultaneous measurement program

The most critical unknown for the oceanography of the shelves of the northeastern Gulf of Mexico is the lack of quantitative knowledge regarding the exchanges of mass, momentum, and properties between slope and shelf. The Northeastern Gulf of Mexico Physical Oceanography Program consisted of current meter, drifter, and hydrographic (physical, chemical, and ecosystem sampling) studies. These should have been conducted during the same sampling period, rather than at different times. These separate studies also should have been integrated and guided by some key hypotheses or phenomena (e.g., quantitative estimates of shelf-slope

exchanges associated with off-shelf circulation features; quantitative estimates of coastal currents associated with wind events; etc).

11.2.4 Need for integrating time series and synoptic surveys

Seasonal shipboard surveys give quasi-synoptic coverage of a region of limited size such as the NEGOM region (but see 11.2.5). However, with the exception of what may be inferred from atmospheric forcing, satellite observations, or occasional collateral data sets, developments in the region between such cruises are not known. Integrating the measurements suites of the Northeastern Gulf of Mexico Physical Oceanography Program would have resulted in continuous observations of key time series between hydrographic surveys to be used to tie the cruise data to conditions before and after cruises. (How could we construct long histories of fresh water movements when moored measurements did not even include near-surface salinity measures?)

11.2.5 Space-time aliasing

In this synthesis, near-surface velocity fields prepared from shipboard ADCP measurements, fields of surface dynamic height relative to a subsurface reference, and fields of SSH based on satellite altimetry measurements are compared. Often the comparisons are favorable, but sometimes they are not. We should note and remember that there are various reasons why the comparisons might not be favorable. First, the ADCP-derived fields are based on direct measurements that include not only geostrophic but other current components as well, while the interpretations of surface currents based on SSH or dynamic height fields assume geostrophic flow only. Moreover, the ADCP measurements begin at a subsurface level (perhaps 12-15 m deep), not the surface.

Then, there are the aliasing problems to be considered. Because of the repeat cycles of the altimetric satellites (10 and 35 d) and the spatial and temporal averaging (100 km and 12 d) applied in producing the SSH fields, the SSH fields are not expected to capture accurately fast moving or quite small current features. Moreover, the fact that each cruise took some 8-10 days to complete means that the ADCP-measured currents and the density profiles used for dynamic heights are aliased as well. Finally, it should be noted that dynamic height fields are relative to a selected deeper reference level. Their computations require the application of interpolation techniques which, if extended onto the shelf, may result in estimated geostrophic currents with undetermined errors.

Therefore, we have attempted to keep these problems in mind when interpreting surface current fields based on these techniques. When there were differences, we have tried to ascertain why and which representation might be more faithful to reality. A key technique in such determinations is to examine the distributions of observed properties and the timing (order) in which the cruse track (stations) was (were) carried out.

12 LITERATURE CITED

Andersen, R.A., R.R. Bidigare, M.D. Keller, and M. Latasa. 1996. A comparison of HPLC pigment signatures and electron microscopic observations for oligotrophic waters of the North Atlantic and Pacific Oceans. *Deep-Sea Res. II*, **43**, 517-537.

Behrenfeld, M.J., J.T. Randerson, C.R. McClain, G.C. Feldman, S.O. Los, C.J. Tucker, P.G. Falkowski, C.B. Field, R. Frouin, W.E. Esaias, D.D. Dolber, and N.H. Pollack. 2001. Biospheric primary production during an ENSO transition. *Science*, **291**, 2594-2597.

Broecker, W. S., and T-H Peng. 1982. *Tracers in the Sea*. Eldigio Press, Palisades, NY. 690 pp.

Cho, K., R. O. Reid, and W. D. Nowlin, Jr. 1998. Objectively mapped stream function fields on the Texas-Louisiana shelf based on 32 months of moored current meter data. *J. Geophys. Res.*, **103** (C5), 10,377-10,390.

Chung, S. P., W. D. Gardner, M. J. Richardson, I. D. Walsh, and M. R. Landry. 1996. Beam attenuation and micro-organisms: spatial and temporal variations in small particles along 140°W during the 1992 JGOFS EqPac transects. *Deep Sea Res.*, **43**, 1205-1226.

Cooley, W.W., and P.R. Lohnes. 1971. *Multivariate data analysis*. New York:Wiley.

Csanady, G. T. 1985. "Pycnobathic" currents over the upper continental slope, *J. Phys. Oceanogr.*, **15**, 306-315.

DiMego, G. J., L. F. Bosart, and G. W. Endersen. 1976. An examination of the frequency and mean conditions surrounding frontal incursions into the Gulf of Mexico and Caribbean Sea. *Mon. Wea. Rev.*, **104** (6), 709-718.

Emery, W. J., and R. E. Thomson. 1998. *Data Analysis Methods in Physical Oceanography*. Pergamon Press, UK, 650 pp.

Etter, P. C. 1983. Heat and freshwater budgets of the Gulf of Mexico, *J. Phys. Oceanogr.*, **13**, 2058-2069.

Fernandez-Partegas, J. and C. N. K. Mooers. 1975. A subsynoptic study of winter cold fronts in Florida. *Mon. Wea. Rev.*, **103**, 742-744.

Florida A&M University. 1988. *Meteorological database and synthesis for the Gulf of Mexico*, OCS Study MMS-88-0064. U.S. Department of the Interior, Minerals Management Service, Gulf of Mexico OCS Regional Office, New Orleans, LA. 486 pp.

Gibb, S.W., D.G. Cummings, X. Irigoien, R.G. Barlow, R. Fauzi, and C. Mantoura. 2001. Phytoplankton pigment chemotaxonomy of the northeastern Atlantic. *Deep-Sea Res. II*, **48**, 795-823.

Gieskes, W.W., and G.W. Kraay. 1983. Dominance of Chryptophyceae during the phytoplankton spring bloom in the central North Sea detected by HPLC analysis of pigments. *Mar. Biol.*, **75**, 179-185.

Hamilton, P., E. Waddell, and R. Wayland. 1997. Chapter 2 - The Physical Environment. In *Northeastern Gulf of Mexico Coastal and Marine Ecosystem Program, Data Search and Synthesis; Synthesis Report*, SAIC. U.S. Department of the Interior, USGS, Biological Resources Division, USGS/BRD/CR-1997-0005 and Minerals Management Service, Gulf of Mexico OCS Region, New Orleans, LA, OCS Study MMS 96-0014. 313 pp.

Hamilton, P., T.J. Berger, J.J. Singer, E. Waddell, J.H. Churchill, R.R. Leben, T.N. Lee, and W. Sturges. 2000. DeSoto Canyon Eddy Intrusion Study, Final Report, Volume II: Technical Report. OCS Study MMS 2000-080. U.S. Department of the Interior, Minerals Management Service, Gulf of Mexico OCS Region, New Orleans, LA. 275 pp.

Hayden, B. P. 1981. Secular variation in Atlantic coast extratropical cyclones. *Mon. Wea. Rev.*, **109** (1), 159-167.

Hsu, S. A. 1988. *Coastal Meteorology*. Academic Press. San Diego, CA. 260 pp.

Hu, C., B. Nababan, D.C. Biggs, and F.E. Muller-Karger. 2001. Variability of bio-optical properties at sampling stations in the NE Gulf of Mexico. Abstract OS71E-12, AGU 2000 Fall Meeting, San Francisco CA. Supplement to *EOS, Transactions, AGU* **81** *(48)*, F678.

Jochens, A. E. 1997. Circulation over the Texas-Louisiana slope based on sea surface elevation and current velocity fields. Ph.D. Dissertation, Department of Oceanography, Texas A&M University, College Station, TX, 159 pp.

Jochens, A. E., and W. D. Nowlin, Jr. 1998. Northeastern Gulf of Mexico Chemical Oceanography and Hydrography Study between the Mississippi Delta and Tampa Bay, Annual Report: Year 1. OCS Study MMS 98-0060. U. S. Department of the Interior, Minerals Management Service, Gulf of Mexico OCS Region, New Orleans, LA. 126 pp.

Jochens, A. E., and W. D. Nowlin, Jr. 1999. Northeastern Gulf of Mexico Chemical Oceanography and Hydrography Study, Annual Report: Year 2. OCS Study MMS 99-0054. U. S. Department of the Interior, Minerals Management Service, Gulf of Mexico OCS Region, New Orleans, LA. 123 pp.

Jochens, A. E., and W. D. Nowlin, Jr. 2000. Northeastern Gulf of Mexico Chemical Oceanography and Hydrography Study, Annual Report: Year 3. OCS Study MMS 2000-078. U. S. Department of the Interior, Minerals Management Service, Gulf of Mexico OCS Region, New Orleans, LA. 89 pp.

Johnson, G. A., E. A. Meindl, E. B. Mortimer, M. C. Koziara, W. L. Read, and J. S. Lynch. 1986. Winter cyclogenesis over the Gulf of Mexico. NOAA/NWSFO. Slidell, LA. 7 pp.

Koblinsky, C. J. 1979. Tides on the West Florida Shelf. School of Oceanography, Oregon State University, Ph.D. dissertation. 110 pp.

Leben, R. R., G. H. Born, and B. R. Engebreth. 2002. Operational altimeter data processing for mesoscale monitoring. *Mar. Geodesy*, **25**, 3-18.

Letelier, R.M., R.R. Bidigare, D.V. Hebel, M. Ondrusek, C.D. Winn, and D.M. Karl. 1993. Temporal variability of phytoplankton community structure based on pigment analysis. *Limnol. Oceanogr.*, **38**, 1420-1437.

Lillibridge, J., R. Leben, and F. Vossepoel. 1997. Real-time processing from ERS-2. *Proc. Third ERS Symp.*, Vol. 3, Florence, Italy, European Space Agency, SP414, 1449–1453

Liss, P. S. 1976. Chapter 4, Conservative and non-conservative behavior of dissolved constituents during estuarine mixing. pp. 93-130. In *Estuarine Chemistry*, J. D. Burton and P. S. Liss, Academic Press, London.

Mackey, M.D., D.J. Mackey, H.W. Higgins, and S.W. Wright. 1996. CHEMTAX-a program for estimating class abundances from chemical markers: Application to HPLC measurements of phytoplankton. *Mar. Ecol. Prog. Ser.*, **144**, 265-283.

Marmarino, G. O. 1983a. Summertime coastal currents in the Northeast Gulf of Mexico. *J. Phys. Ocean.*, **13**, 65-77.

Marmarino, G. O. 1983b. Variability of current, temperature, and bottom pressure across the West Florida Shelf, Winter 1981-1982. *J. Geophys. Res.*, **88**(C7), 4439-4457.

Melo-Gonzalez, N., F.E. Muller-Karger, S. Cerderira-Estrada, R. Perez de los Reyes, I. Victoria del Rio, P. Cardenas-Perez, and I. Mitrani-Arenal. 2000. Near-surface phytoplankton distribution in the western Intra-Americas Sea: The influence of El Nino and weather events. *J. Geophys. Res.*, **105**, 14,029-14,043.

Montgomery, R. B. 1941. Transport of the Florida Current off Havana, *J. Mar. Res.*, **4**, 198-219.

Mortimer, E. B., G. A. Johnson, and H. W. N. Lau. 1988. Major arctic outbreaks affecting Louisiana. *Nat. Wat. Dig.*, **13** (1), 5-13.

Muller-Karger, F.E., J.J. Walsh, R.H. Evans, and M.B. Meyers. 1991. On the seasonal phytoplankton concentration and sea surface temperature cycles of the Gulf of Mexico as determined by satellites. *J. Geophys. Res.*, **96**, 12,645-12,665.

Murray, S. P., ed. 1998. *An observational study of the Mississippi-Atchafalaya coastal plume.* OCS Study MMS 98-0040. U. S. Department of the Interior, Minerals Management Service, Gulf of Mexico OCS Region, New Orleans, LA. 513 pp.

Nowlin, W. D., Jr., and H. McLellan. 1967. A characterization of the Gulf of Mexico waters in winter. *J. Mar. Res.*, **25** (1), 29-59.

Nowlin, W. D., Jr., A. E. Jochens, R. O. Reid, and S. F. DiMarco, 1998a. *Texas-Louisiana Shelf Circulation and Transport Processes Study: Synthesis Report, Volume I: Technical Report*, OCS Study MMS 98-0035. U.S. Department of the Interior, Minerals Management Service, Gulf of Mexico OCS Region, New Orleans, LA, 502 pp.

Nowlin, W. D., Jr., A. E. Jochens, R. O. Reid, and S. F. DiMarco, 1998b. *Texas-Louisiana Shelf Circulation and Transport Processes Study: Synthesis Report, Volume II: Appendices*, OCS Study MMS 98-0036. U.S. Department of the Interior, Minerals Management Service, Gulf of Mexico OCS Region, New Orleans, LA. 288 pp.

Nowlin, W. D., Jr., A. E. Jochens, S. F. DiMarco, and R. O. Reid. 2000a. Chapter 4: Physical Oceanography, in Continental Shelf Associates, Inc., *Deepwater Gulf of Mexico Environmental and Socioeconomic Data Search and Literature Synthesis. Volume I:*

Narrative Report. U.S. Department of the Interior, Minerals Management Service, Gulf of Mexico OCS Region, New Orleans, LA, OCS Study MMS 2000-049. 340 pp.

Nowlin, W. D., Jr., A. E. Jochens, M. K. Howard, S. F. DiMarco, and W. W. Schroeder. 2000b. Hydrographic properties and inferred circulation over the northeastern shelves of the Gulf of Mexico during Spring to midsummer of 1998. *Gulf of Mexico Science*, **23** (1), 40-54.

Nowlin, W. D., Jr., A. E. Jochens, S. F. DiMarco, R. O. Reid, and M. K. Howard. 2001. Deepwater Physical Oceanography Reanalysis and Synthesis of Historical Data: Synthesis Report. OCS Study MMS 2001-xxx. U. S. Dept. of the Interior, Minerals Management Service, Gulf of Mexico OCS Region, New Orleans, LA. 530 pp.

Pak, H., D. A. Kiefer, and J. C. Kitchen. 1988. Meridional variations in the concentration of chlorophyll and microparticles in the North Pacific Ocean. *Deep Sea Res.*, **35**, 1151-1171.

Parsons, T.R., Y. Maita, and C.M. Lalli. 1985. *A Manual of Chemical and Biological Methods for Seawater Analysis*. Pergamon, Elmsford, New York, 173 pp.

Rabalais, N. N., R. E. Turner, and W. J. Wiseman, Jr. 1999. Hypoxia in the northern Gulf of Mexico: linkages with the Mississippi River. In H. Kumpf, K. Steidinger, and K. Sherman, *The Gulf of Mexico Large Marine Ecosystem*, Blackwell Science, Malden, MA. pp. 297-322.

Ressler, P. H. 2001. Acoustic estimates of zooplankton and micronekton biomass in cyclones and anticyclones of the northeastern Gulf of Mexico. Ph.D. dissertation, Department of Oceanography, Texas A&M University, College Station, TX.

Ressler, P. H., and A. E. Jochens. 2001. Acoustic volume backscatter evidence for locally enhanced stocks of zooplankton and micronekton in a cyclone located near the mouth of the Mississippi River. *Cont. Shelf Res.* Accepted, in revision.

Schroeder, W. 1977. The impact of the 1973 flooding of the Mobile River System on the hydrography of Mobile Bay and east Mississippi Sound. *Northeast Gulf Science*. **1** (2), 68-76.

Science Applications International Corporation (SAIC). 1998. DeSoto Canyon Eddy Intrusion Study; Data products: Set 4, April 1998—August 1998. SAIC, 615 Oberlin Rd., Suite 300, Raleigh, NC 27606.

Sheng J., and K. R. Thompson. 1996. A robust method for diagnosing regional shelf circulation from scattered density profiles, *J. Geophys. Res.*, **101** (C11), 25,647-25,659.

Stevens, J. 1986. *Applied multivariate statistics for the social sciences*. Hillsdale, NJ: Erlbaum.

Sturges, W., and R. Leben. 2000. Frequency of ring separations from the Loop Current in the Gulf of Mexico: a revised estimate. *J. Phys. Oceanogr.*, **30**, 1814-1819.

Tierney, C. C, L. H. Kantha, and G. H. Born, 2000. Shallow and deep water global ocean tides from altimetry and numerical modeling. *J. Geophys. Rev.*, **105**(C5) 11259-11277.

Wang, O., R. O. Reid, S. F. DiMarco, and W. D. Nowlin, Jr. 2002a. Diagnostic calculations of circulation over the northeastern Gulf of Mexico. TAMU Oceanography Tech Rpt. No. 02-1-D.

Wang, O., R. O. Reid, S. F. DiMarco, and W. D. Nowlin, Jr. 2002b. Estimation of geostrophic circulation in coastal regions from CTD and/or ADCP data: application to the northeastern Gulf of Mexico. *In preparation.*

Wang, W., W. D. Nowlin, Jr., and R. O. Reid. 1998. Analyzed surface meteorological fields over the northwestern Gulf of Mexico for 1992-1994: mean, seasonal, and monthly patterns. *Mon. Wea. Rev.*, **126** (11), 2864-2883.

Weiss, R. F. 1970. The solubility of nitrogen, oxygen and argon in water and seawater. *Deep-Sea Res.*, **17** (4), 721-735.

Wiseman, W. J., Jr., N. N. Rabalais, R. E. Turner, S. P. Dinnel, and A. MacNaughton. 1997. Seasonal and interannual variability within the Louisiana coastal current: stratification and hypoxia. *J. Mar. Syst.*, **12**, 237-248.

Wolter, K., and M.S. Timlin. 1998. Measuring the strength of ENSO - how does 1997/98 rank? *Weather*, **53**, 315-324.

Woodruff, S. D., R. J. Slutz, R. L. Jenne, and P. M. Steurer. 1987. A comprehensive ocean-atmosphere data set. *Bull. Amer. Meteor. Soc.*, **68**, 1239-1250.

Wright, S.W. and R.L. van den Eden. 2000. Phytoplankton community structure and stocks in the East Antarctic marginal ice zone (BROKE survey, January-March 1996) determined by CHEMTAX analysis of HPLC pigment signatures. *Deep-Sea Res. II*, **47**, 2363-2400.

Yi, Y. 1995. Determination of gridded mean sea surface from altimeter data of TOPEX, *ERS-1*, and GEOSAT. Ph.D. Thesis, Department of Geodetic Science and Surveying, The Ohio State University, Columbus, OH, 140 pp.

APPENDIX A
SUMMARY OF CONDITIONS DURING CRUISE N1

Cruise N1 was a fall cruise conducted 16-26 November 1997. Stations began with the most seaward station on line 11 and ended with the most inshore station on line 1. Figure A-1 shows the station locations and gives the CTD station numbers, which are sequential by sampling order.

A.1 Forcing Functions

A.1.1 Winds

The mean gridded wind field and principal axes of variance for the period of cruise N1 are shown in Figure A.1.1-1. Hourly winds from 14 sites within and bounding the study area were used to compute the gridded hourly winds at 1/2° x 1/2° resolution (Figure 3.2.1-1). Hourly fields of wind components were estimated at each grid point by a statistical optimal interpolation method, using the methodology of Wang et al. (1998). The mean field then was computed by averaging hourly data at each grid point for the duration of the cruise.

Throughout most of the N1 cruise, winds were directed to the southwest, in response to the presence, during much of the cruise, of high pressure over the continent to the north. This is in comparison to the climatological winds which are directed to the southwest or west (Figure 3.1.1-11). Mean winds were weak and generally 5 $m \cdot s^{-1}$ or less. The variance ellipses indicate the winds were variable principally in the east-west direction at about ± 5 $m \cdot s^{-1}$. The western shelf had stronger winds than the eastern shelf, and winds were stronger offshore than nearshore.

Review of the *Daily Weather Maps* of NOAA's Climate Prediction Center identified one frontal passage through the NEGOM study area during the cruise. From November 21-23, low pressure was located over the adjacent continent and, on November 22, a front passed over the study area. The cruise was conducting measurements along line 7 at this time. The winds in the study area responded mainly by changing their direction to the north and northeast during the event; speeds generally were < 10 $m \cdot s^{-1}$ (Figure A.1.1-2).

A.1.2 River Discharge

Daily discharge rates for the Mississippi River were generally at or above the 70-yr record-length mean in summer 1997 and at or below the mean in fall 1997 (Figure 3.1.2-2). Other rivers tended to follow this general pattern. A number of rivers exhibited pulses of high discharge in late October and mid-November. During late October through November, the discharges from the Apalachicola and Suwannee Rivers exceeded flow at one standard deviation from the mean (Figures 3.1.2-4 and 3.1.2-6, respectively).

The effect of the river discharge on the near-surface (~3 m) salinity distribution was to freshen the waters near the mouths of rivers and bays (Figure A.1.2-1). The Mississippi River discharge had the greatest effect, with relatively low salinity water (≤ 34) extending approximately 75 km offshore of the delta and eastward over the shelf edge and along the slope. Low near-surface salinity values (< 30) were located nearshore off Pascagoula and east of Pass a Loutre. Other than the area impacted by extension of Mississippi River water, near-surface salinity values increased with distance offshore. The nearshore waters west of Pensacola generally were fresher than the nearshore waters to the east.

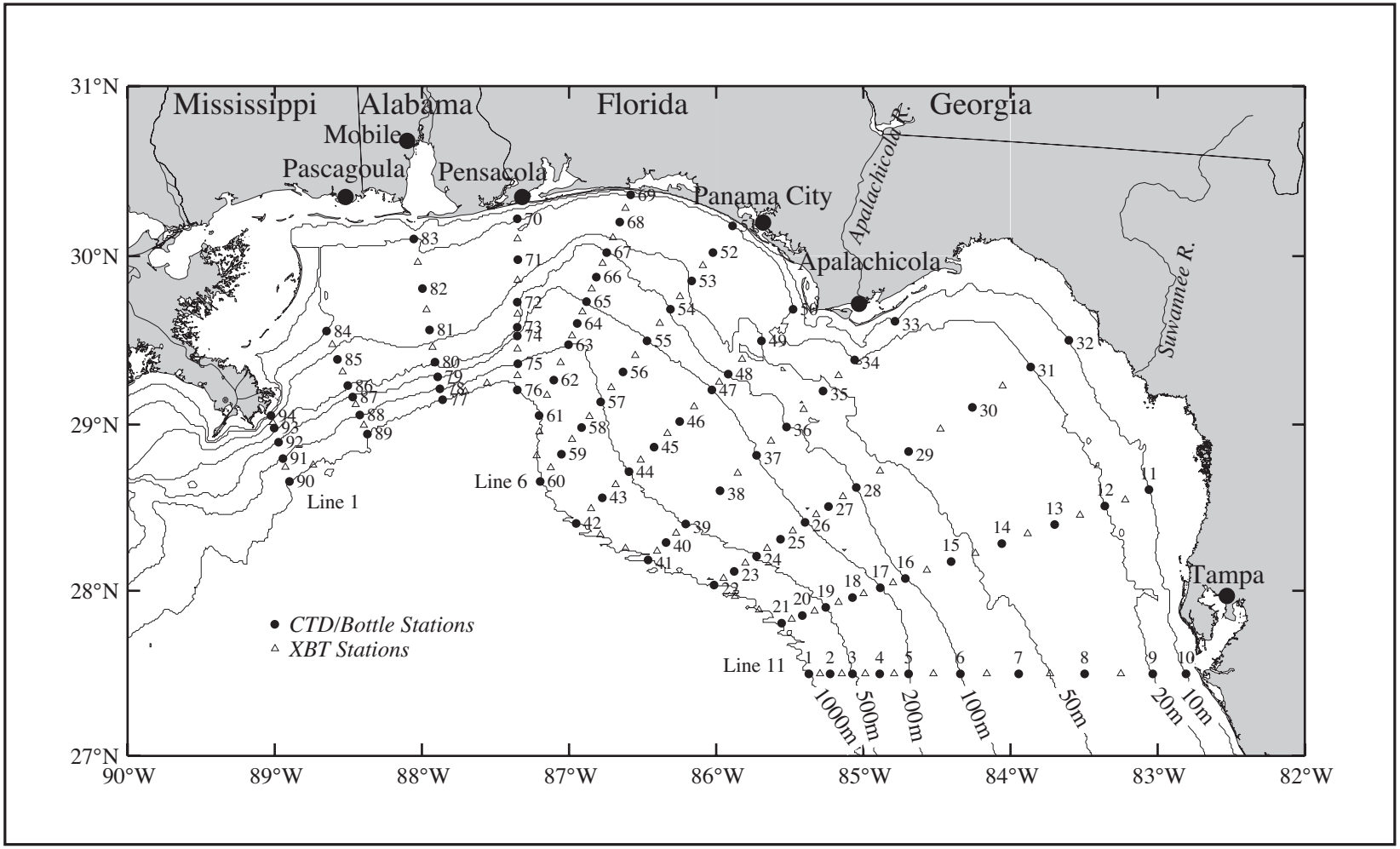

Figure A-1. Station locations for cruise N1 conducted on 16-26 November 1997. CTD stations (solid circles) are numbered; XBT stations (open triangles) are not.

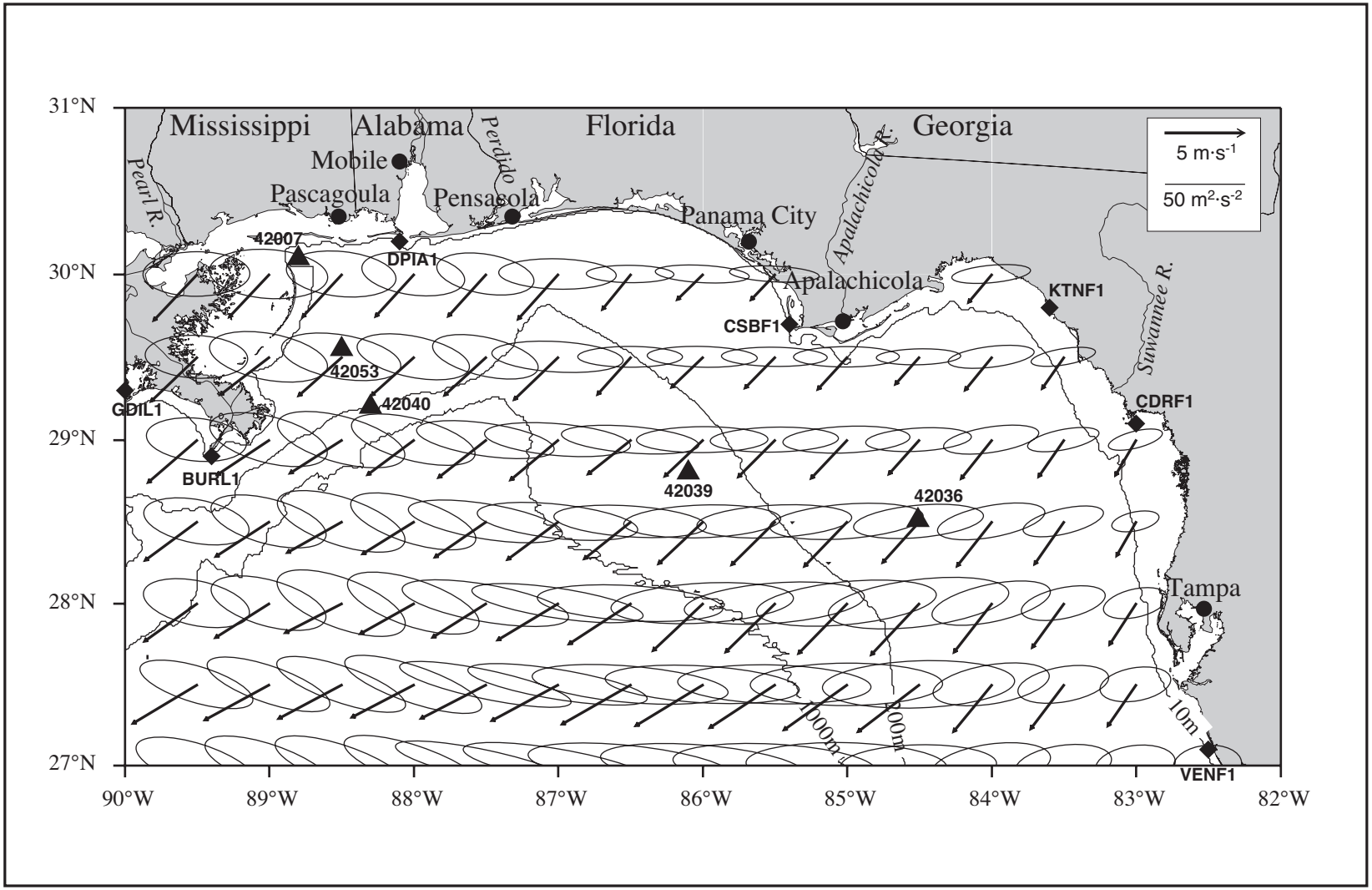

Figure A.1.1-1. Vector mean winds and variance ellipses for cruise N1 in November 1997.

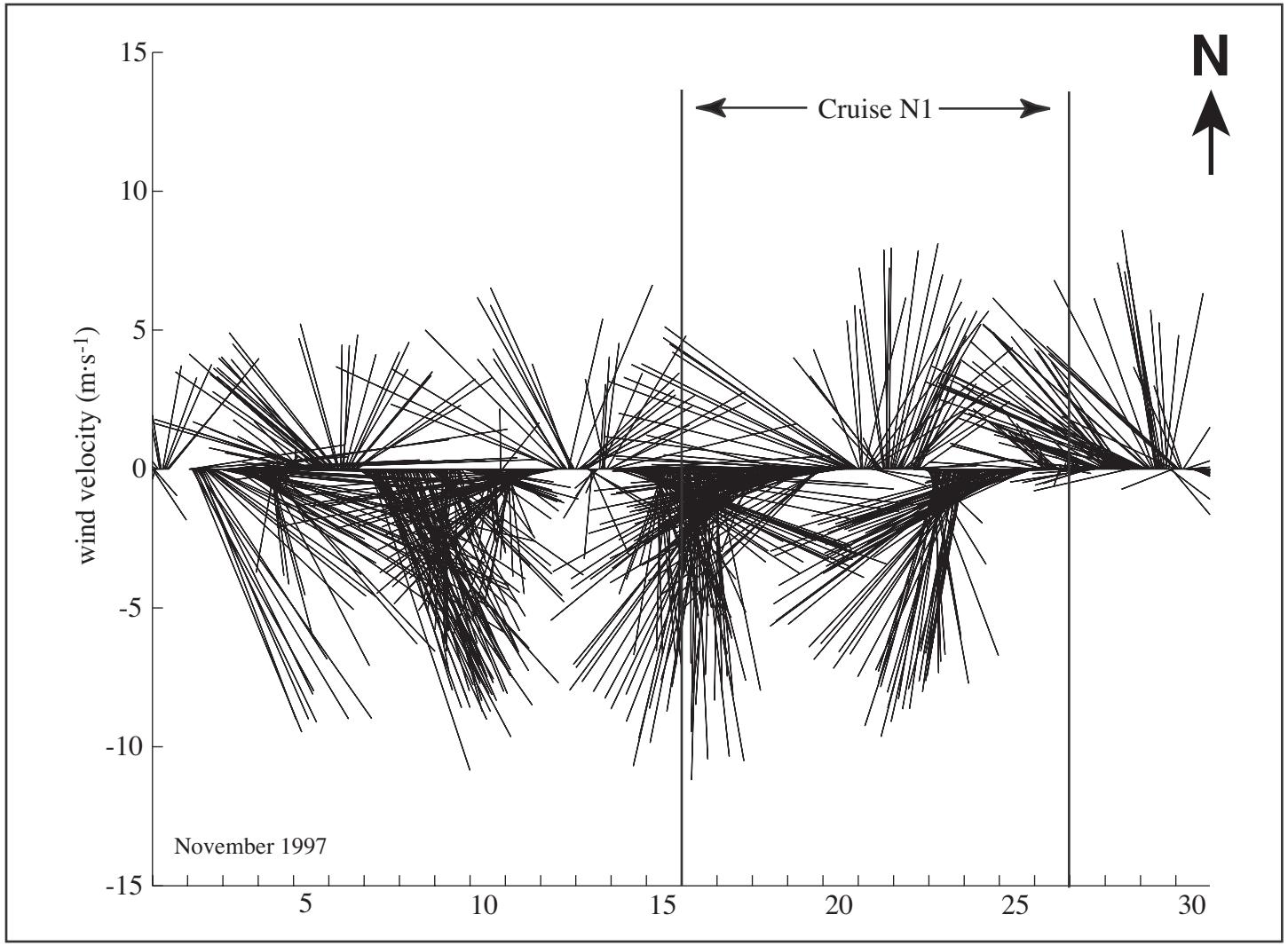

Figure A.1.1-2. Vector stick plot of wind at meteorological buoy 42040 for November 1997. Gauge height is 10 m.

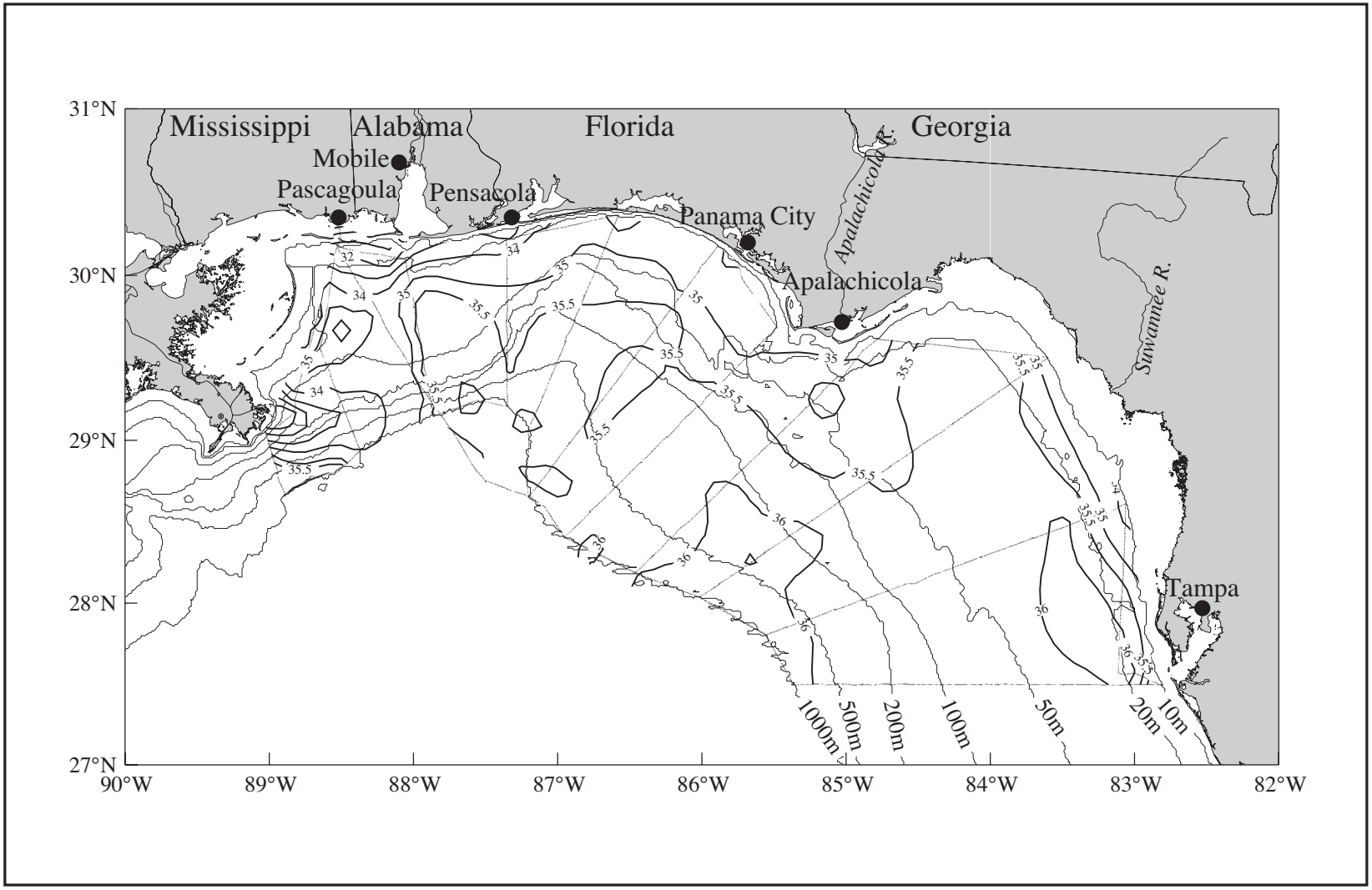

Figure A.1.2-1. Salinity at ~3m from thermosalinograph observations on cruise N1 in November 1997.

The influence of the river water distribution can be seen in the distributions of near-surface chlorophyll *a* (Figure A.1.2-2) and percent transmission (Figure A.1.2-3). The chlorophyll *a* shown here was calculated from the underway, flow-through fluorescence. It shows higher concentrations near the Mississippi River, following a pattern that extends eastward over the shelf edge and along the slope. Chlorophyll *a* values greater than 1 $\mu g \cdot L^{-1}$ also are evident in the northwest corner of the study area near Mobile Bay, off Cape San Blas and adjacent to the Apalachicola River, and west and south of the Suwannee River. The percent transmission at ~3.5 m depth has three major regions of low light transmission (< 80%), which are indicative of higher levels of particulates that are in river water. These are (1) east of the Pass a Loutre discharge mouth of the Mississippi River and northwards nearshore to Mobile Bay, (2) off Cape San Blas influenced by the Apalachicola River discharge, and (3) off and south of the Suwannee River. Highest particulate concentrations (Figure 6.2-1) occurred in the region between the Mississippi River and Mobile Bay and off Cape San Blas.

A.1.3 SSH Fields Adjacent to the Shelf

The time series of SSH fields for 1 October through 26 November 1997 (Figures 3.2.3-1, 3.2.3-2, and 3.2.3-3) show the presence of Loop Current Eddy El Dorado more than 100 km to the south of the study area as it moved westward. It extended to approximately 27°N, but did not directly impact the study area. This LCE separated from the Loop Current about 11 October 1997 (Sturges and Leben 2000). As it moved westward, a small, weak anticyclone was spun up adjacent to the western shelf edge of the NEGOM study area (Figure A.1.3-1). This anticyclonic eddy was centered southeast of South Pass, was elongated east-west, and extended into DeSoto Canyon. The SSH field indicates eastward flow would be at the shelf edge and along the upper slope off Mississippi and Alabama.

A.2 *In Situ* Evidence of Circulation

ADCP measurements were made continuously on cruise N1 using a 150 kHz narrow-band ADCP. Resulting current vectors at the depth bins centered on 10 m and 12 m are shown in Figure A.2-1. Strongest flows are seen at the shelf edge and slope on the west and east sides of DeSoto Canyon and south-southeast of the Mississippi River delta. Following the bathymetric contours, the flow is eastward along the western shelf edge and slope and, on the east side of DeSoto Canyon, southward along the slope. This flow pattern is indicative of forcing by the anticyclone seen in Figure A.1.3-1. Maximum ADCP speeds at 10-12 m in this region are in excess of 50 $cm \cdot s^{-1}$, particularly in the eastward flows off South Pass where the anticyclone most closely abutted the study region. Anticyclonic flow extended to depths of 300 to 500 m (Hamilton et al. 2000), also most prevalently in the western part of the study area. The along-isobath flows associated with DeSoto Canyon are present in the ADCP currents that extend to 150-m depth (Figures A.2-2, A.2-3, and A.2-4).

Over the slope southwest of Cape San Blas, at approximately 86.5°W 28°N, the currents are directed shoreward. These shoreward currents extend to the 150 m depth measured by the ADCP, with some clockwise turning in direction relative to the currents at 10 m and with speeds generally diminishing with depth (Figures A.2-1 through A.2-4). To the southeast, the slope currents are directed southward; this also is the case throughout the water column measured by the ADCP. The onshore flow between lines 8 and 9 and the southward flows between lines 9 and 11 have an anticyclonic characteristic extending to the measured depth.

Near the Mississippi River mouth the currents are directed southeastward and thereby can move relatively low salinity water to the shelf edge and upper slope, as seen in the salinity

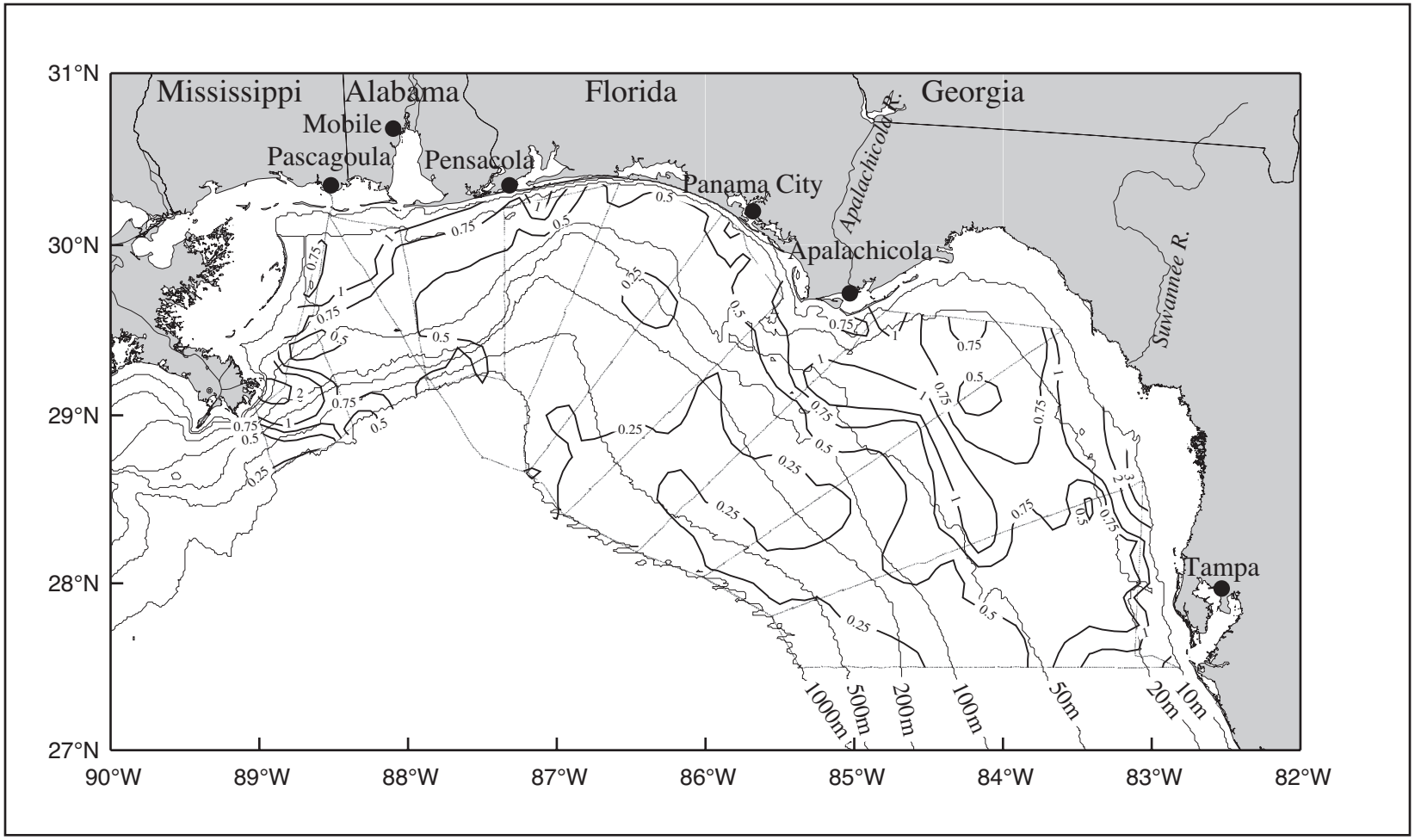

Figure A.1.2-2. Chlorophyll ($\mu g \cdot L^{-1}$) at ~3 m calculated from flow-through fluorescence on cruise N1 in November 1997.

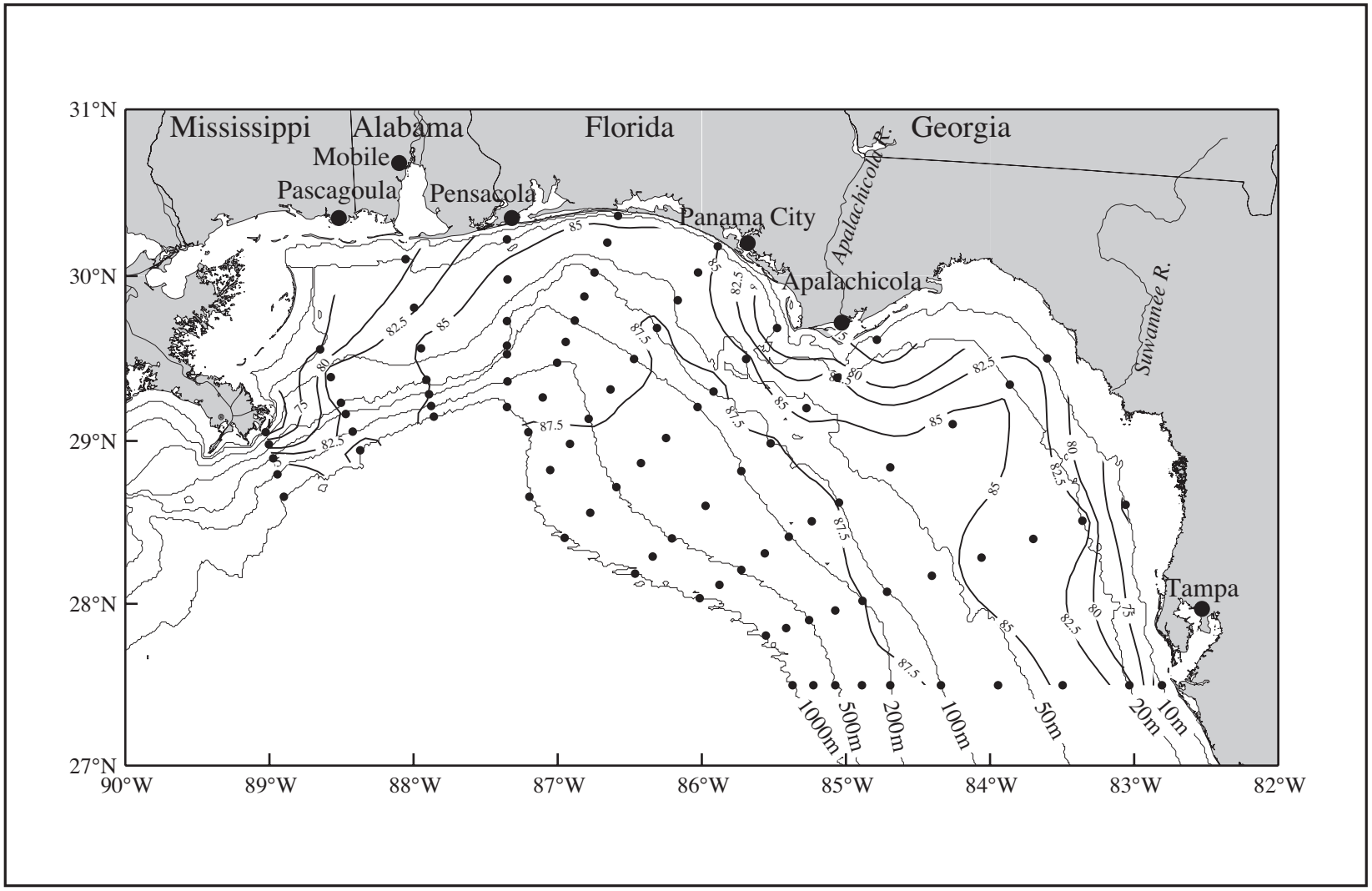

Figure A.1.2-3. Percent transmission from the near-surface (~3.5 m) observations on cruise N1 in November 1997. The transmissometer had a 25-cm path length and used a 660 nm wave length light source.

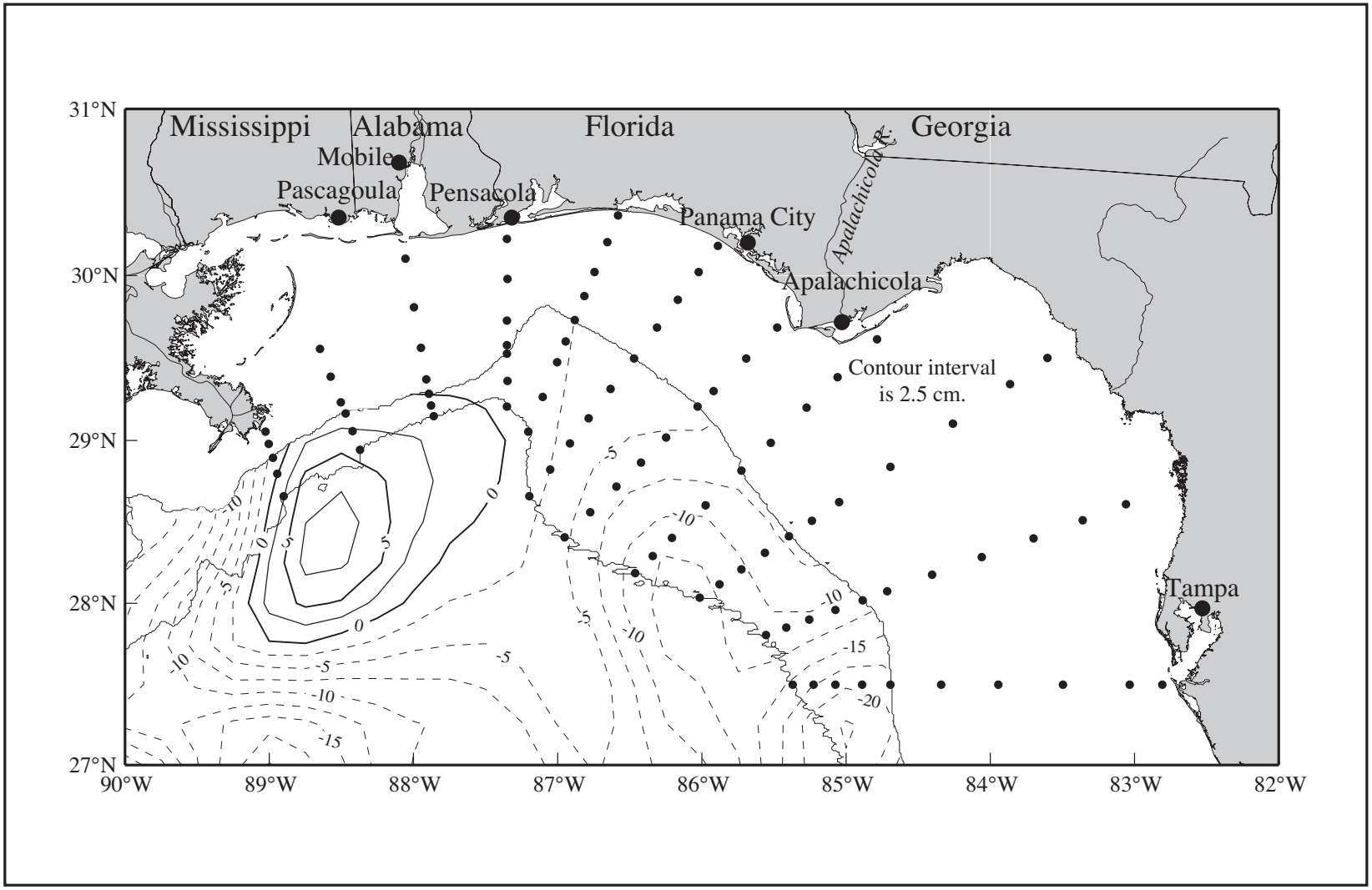

Figure A.1.3-1. Sea surface height field from satellite altimeter data for 19 November 1997 during N1. The 200 and 1000-m isobath contours and CTD stations (dots) are shown. [Data provided by Robert R. Leben, University of Colorado]

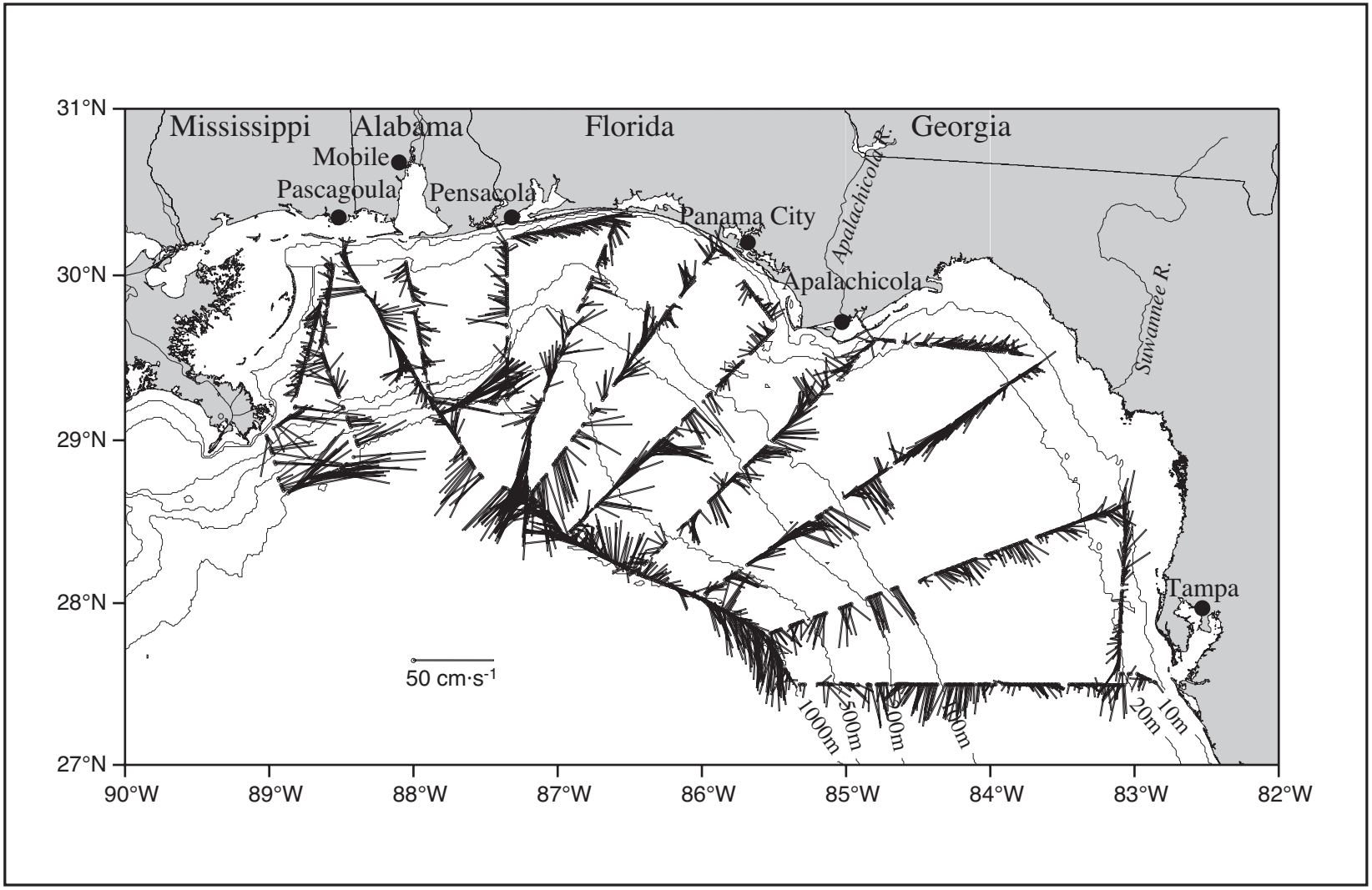

Figure A.2-1. ADCP-measured currents for the 4-m bin centered at 10 m or 12 m on cruise N1 in November 1997.

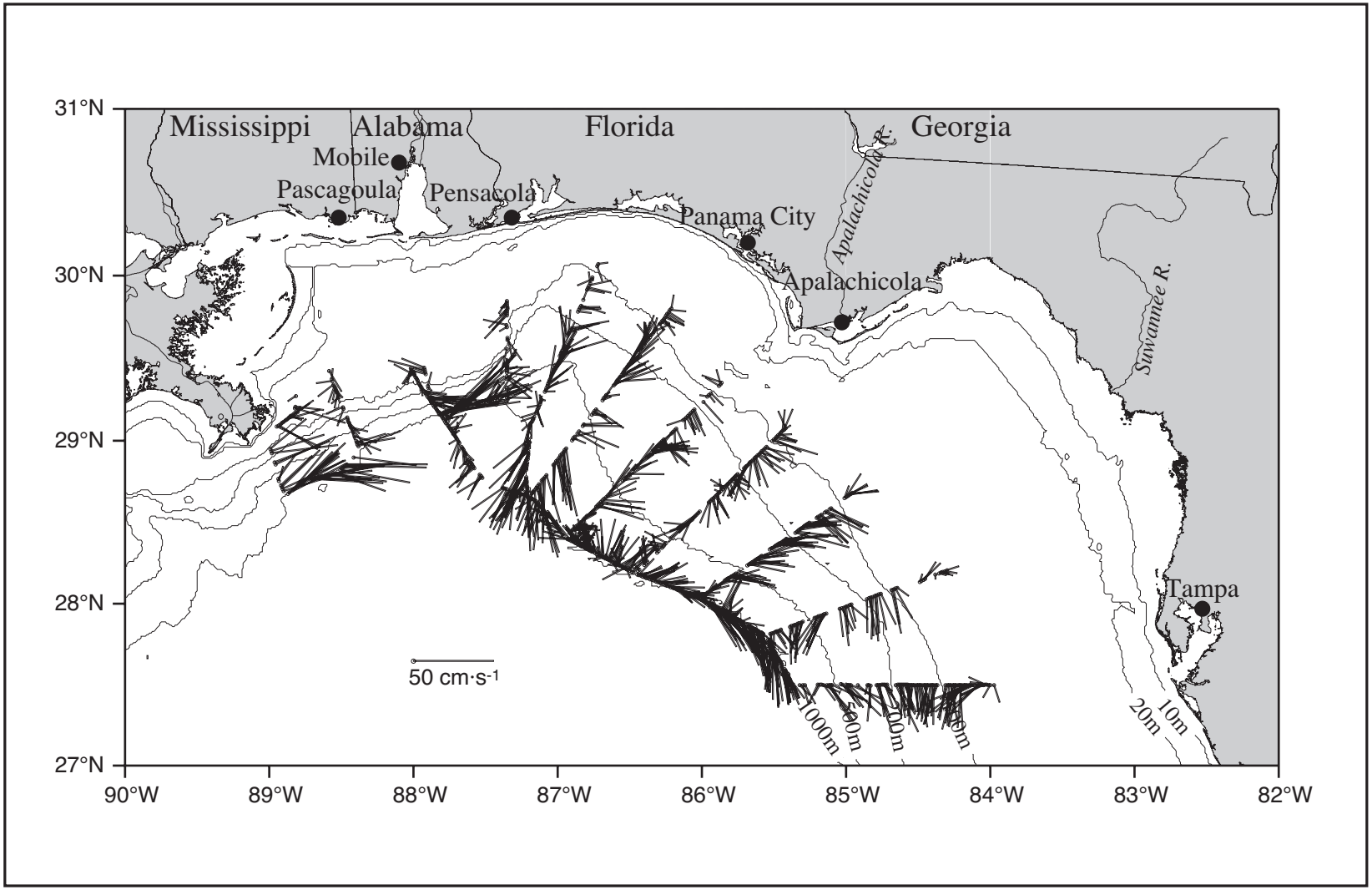

Figure A.2-2. ADCP-measured currents for the 4-m bin centered at 50 m or 52 m on cruise N1 in November 1997.

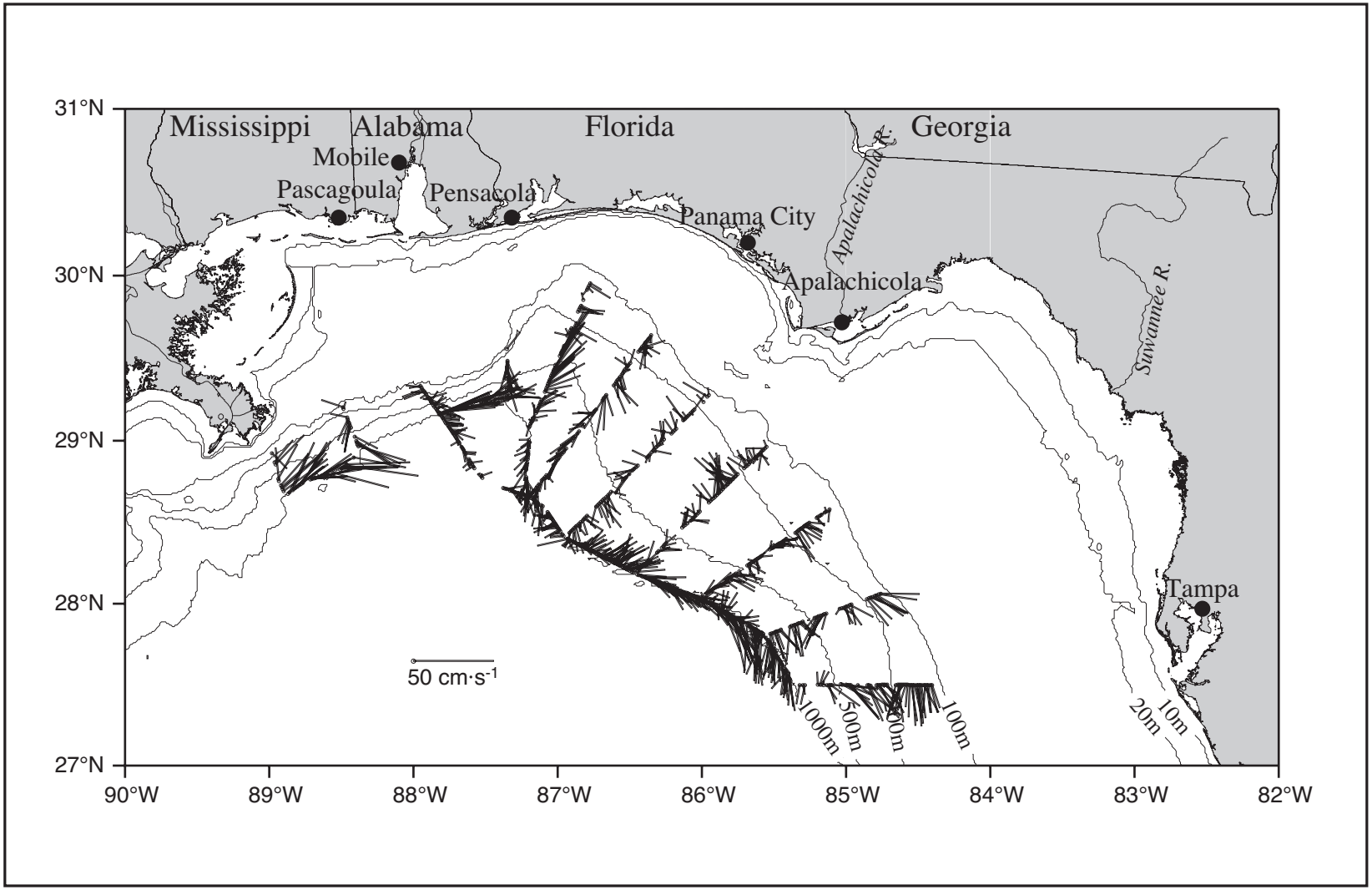

Figure A.2-3. ADCP-measured currents for the 4-m bin centered at 100 m or 102 m on cruise N1 in November 1997.

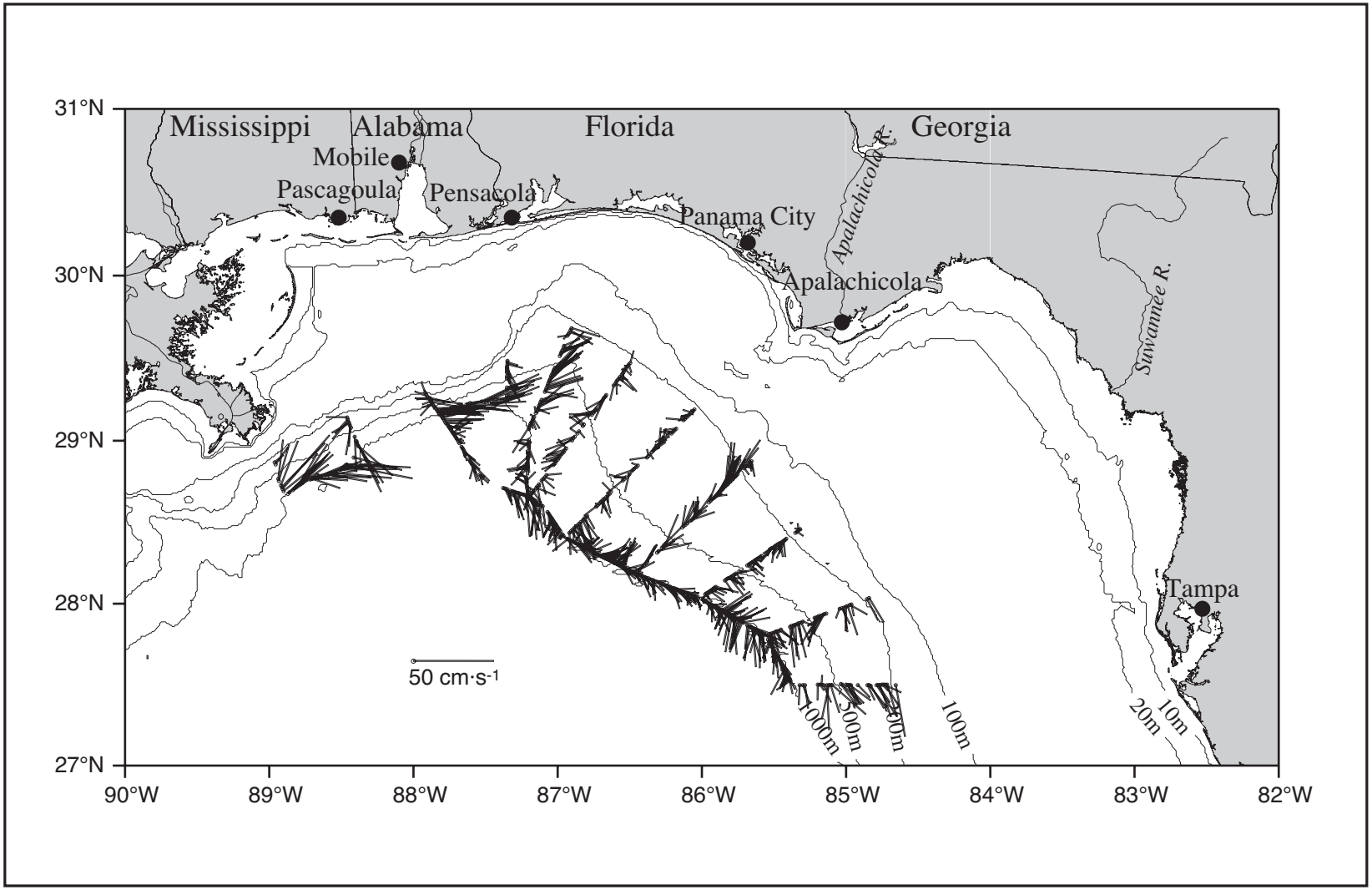

Figure A.2-4. ADCP-measured currents for the 4-m bin centered at 150 m or 152 m on cruise N1 in November 1997.

field in Figure A.1.2-1. The relatively low salinity water then is swept eastward along the shelf edge and slope by the anticyclone.

Near-surface currents over the Mississippi-Alabama shelf are variable, but with an indication of possible shelfwide cyclonic circulation centered about 88°W 29.75°N (Figure A.2-1). Over the inner shelf between Panama City and Cape San Blas, the nearshore currents are directed generally northwestward, while those near the 100-m water isobath are directed southeastward. This is suggestive of a possible cyclonic circulation over the inner and middle shelf in this region. In the Big Bend area, flows have shoreward components in shallow water (≤ 20 m) and offshore on line 9. Coupled with the northward flow near the 20-m isobath just north of Tampa, these flows suggest the presence of cyclonic flow centered over the inner shelf in this region; but the evidence is unclear. Flows over the remainder of the west Florida shelf are mainly southward, with most intense currents of 25-30 $cm \cdot s^{-1}$ approximately between the 100 and 200-m isobaths. This pattern of southward flow extends to 150-m depth, but with diminished magnitude (Figures A.2-2, A.2-3, and A.2-4).

The distribution of geopotential anomaly for the sea surface (3 m) relative to 800 m is shown in Figure A.2-5. The most prominent feature in the geopotential anomaly field is associated with the strong eastward and anticyclonic flows seen in the surface ADCP measurements along the outer shelf and slope of the Mississippi-Alabama shelf and into DeSoto Canyon. There is a high in geopotential anomaly at the outer shelf and slope off Tampa Bay. A weak cyclonic feature is seen between the two anticyclonic features. A large cyclonic feature is present over the shelf north of Tampa Bay; its center is over the inner shelf. This feature is present in the ADCP currents. There is indication of a large cyclone over the inner and middle shelf of the Mississippi-Alabama shelf and east to Cape San Blas. This cyclone appears to have two low centers; this is in contrast to the ADCP currents, which do not.

The combination of offshore anticyclonic circulation and inner shelf cyclones results in maximum alongshelf currents in a downcoast (Mississippi to Tampa) direction located over the 100- to 200-m isobaths at many cross-shelf lines. The degree to which this near "shelf edge" current is dependent on the offshore existence of anticyclones versus the observed cyclonic gyre circulation over the mid and inner shelf is yet to be determined.

A.3 Property Distributions

The temperature field at 3-m depth observed on N1 during 16-27 November 1997 is shown in Figure A.3-1. Offshelf of the South Pass of the Mississippi River is seen a warm feature (≥ 23°C) that appears to extend continuously to the east into DeSoto Canyon to just inshore of the 200-m isobath. Immediately east of the delta, a less extensive cooler tongue of water appears to be advecting south-southeastward from the shelf into this warm intrusion. The small patch of warmer water seen along line 2 between the 200- and 500-m isobaths appears to be related to a small cyclone of diameter < 50 km that was located in this region (see below). Another intrusion of warm water over the slope and onto the west Florida shelf appears near 28°N 86°W. Cooler, nearshore water extends southeastward from Cape San Blas into the warmer waters west of Tampa. This tongue of cooler water reaches the 100-m isobath off Tampa. It is in the region of southward flow over the inner shelf of the west Florida shelf. There is a marked cross-shelf temperature gradient over the inner shelf with inshore temperatures less than 18°C.

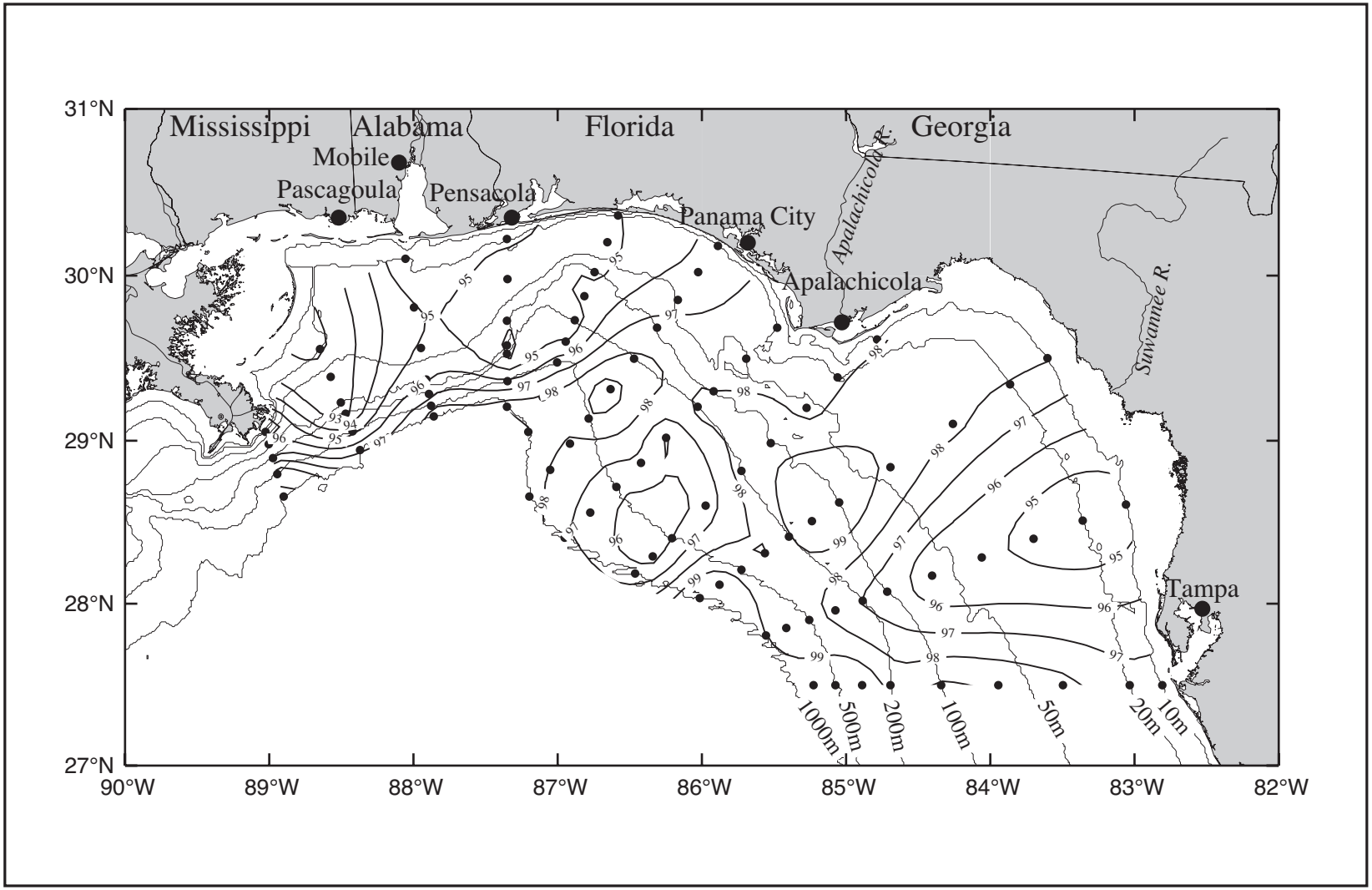

Figure A.2-5. Geopotential anomaly (dyn cm; 3 m relative to 800 m) for cruise N1 conducted 16-26 November 1997. CTD station locations are shown.

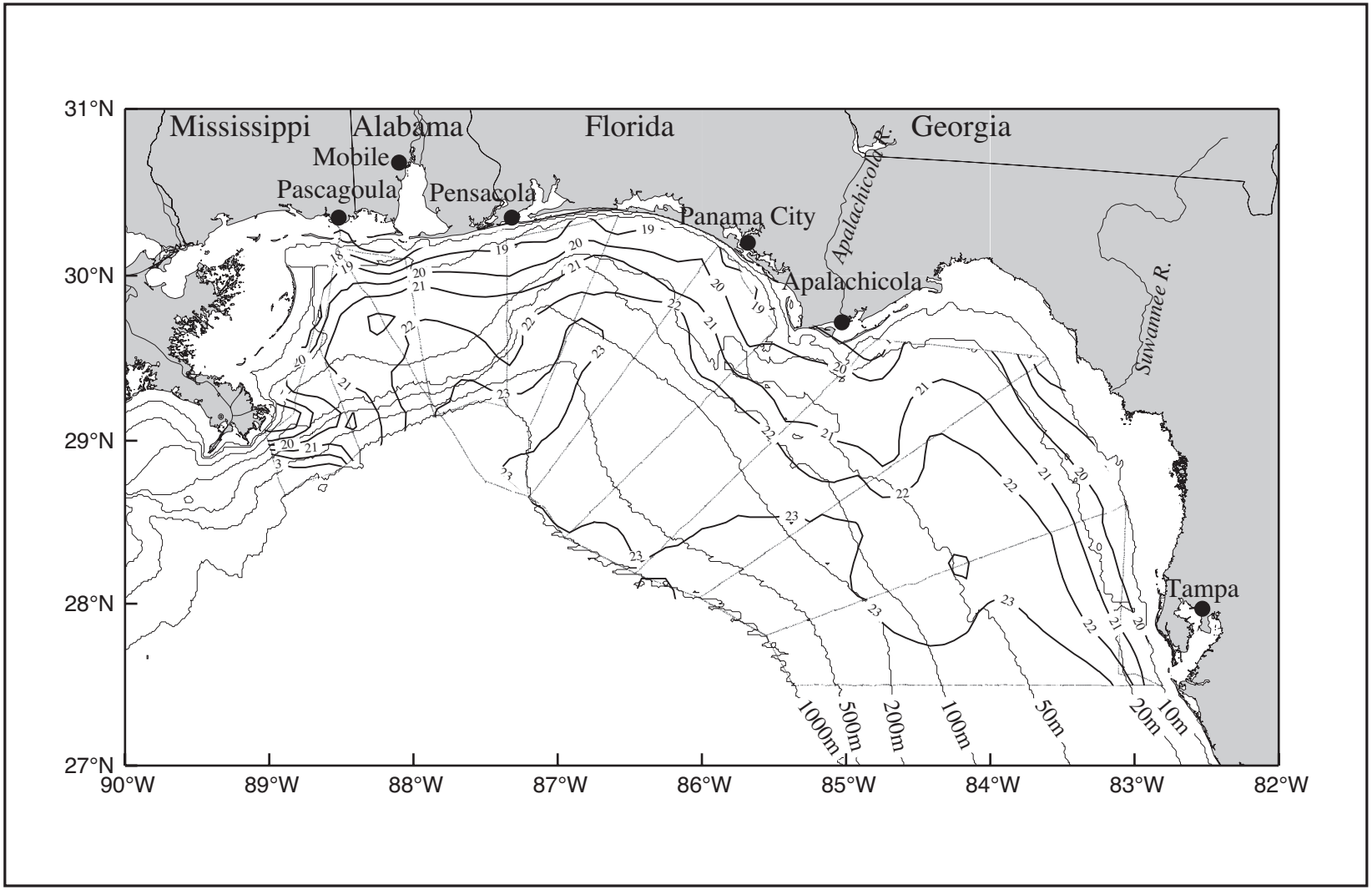

Figure A.3-1. Temperature (°C) at ~3m from thermosalinograph observations on cruise N1 in November 1997.

In the isohalines of Figure A.1.2-1, the warm water intrusions off South Pass and over the shelf of DeSoto Canyon appear as regions of relatively high salinity. Spreading eastward from Pass a Loutre, centered about 29.2°N and 88.5°W, is a distinct low salinity tongue with values less than 33. This tongue corresponds to the cooler water advecting offshore along the eastern edge of the delta. The warm water at and south of 28°N on the west Florida shelf also is relatively salty. The warm intrusion onto the slope and shelf near 28°N, 86°W is clearly seen in the salinity pattern as being relatively saline.

Because water temperatures generally decrease with depth, it is expected that a horizontal plot of bottom temperatures would show values in shallow water to be warmer than in slightly deeper water, with isotherms generally paralleling the isobaths. This general pattern prevails in the data from the spring and summer cruises. For the fall cruises (N1, N7, and to lesser extent N4), however, the pattern is different on the west Florida shelf where the bottom waters nearest shore were cooler than those farther offshore out to approximately the 50-m isobath (Figure A.3-2). This reflects the fall cooling and mixing that reaches bottom in the nearshore region before cooling all waters farther offshore to depths of 50 to 100 m (Figure A.3-3). The density, potential temperature, and salinity fields along the 1000-m isobath, shown in Figures A.3-4 through A.3-6, indicate the water column is relatively well-mixed down to about 50 m depth. Generally, the other vertical sections confirm the basic pattern of a well-mixed upper 50 m. Nearshore stations adjacent to rivers have more stratification than offshore.

The density field along the 1000-m isobath, given as σ_θ in Figure A.3-4, shows little influence from the small anticyclone located over the slope of the western part of the study area. There is, however, a small uplift in properties at 200-500 m centered near station 89 that likely is induced by a small cyclone centered about the 200-m isobath on line 2. The potential temperature field along the 1000-m isobath more clearly shows the doming isolines about this station (Figure A.3-5).

Consideration of the property extrema in vertical sections of salinity, nutrients, and oxygen along the 1000-m isobath can identify whether any water masses found in the open ocean of the Gulf of Mexico are present in the NEGOM study area. A salinity maximum of 36.4 and higher found in the upper 250 m of the water column is indicative of the presence of Subtropical Underwater, which originates in the Atlantic Ocean and enters the Gulf with the Loop Current system (Nowlin et al. 2000a). Values of 36.7 to 36.8 indicate the waters are directly of Loop Current origin, with minimal mixing with other Gulf waters. The salinity contours (Figure A.3-6) show the salinity maxima are located about 100-m depth. The maximum at line 1 is less than 36.4, possibly due to freshening from mixing of oceanic with Mississippi River waters. The maxima are greater than 36.4 between lines 2 and 8 and greater than 36.5 at lines 9 through 11; all are less than 36.6. The maximum salinity for the cruise was 36.5907 at station 1 on line 11. These are relatively low salinity values compared to waters that might come directly from the Loop Current or Loop Current eddies, and confirm that these features were not directly within the NEGOM study area during this cruise. The waters with the salinity maximum extend onto the shelf, with slight shoaling, as a continuous layer to around the 100-m isobath.

Another water mass that enters the Gulf with the Loop Current system is 18°C water. This water is characterized by an oxygen maximum of 3.6-3.8 $mL \cdot L^{-1}$ in water depths of 200-400 m in the eastern Gulf (Nowlin and McLellan 1967). This water mass is not present in the slope waters of the NEGOM study area during cruise N1 (Figure A.3-7). However, the oxygen minimum of less than 3 $mL \cdot L^{-1}$, seen at depths of 300-400 m, is located at a σ_θ of approximately 27.15, which is indicative of Tropical Atlantic Central Water. This water

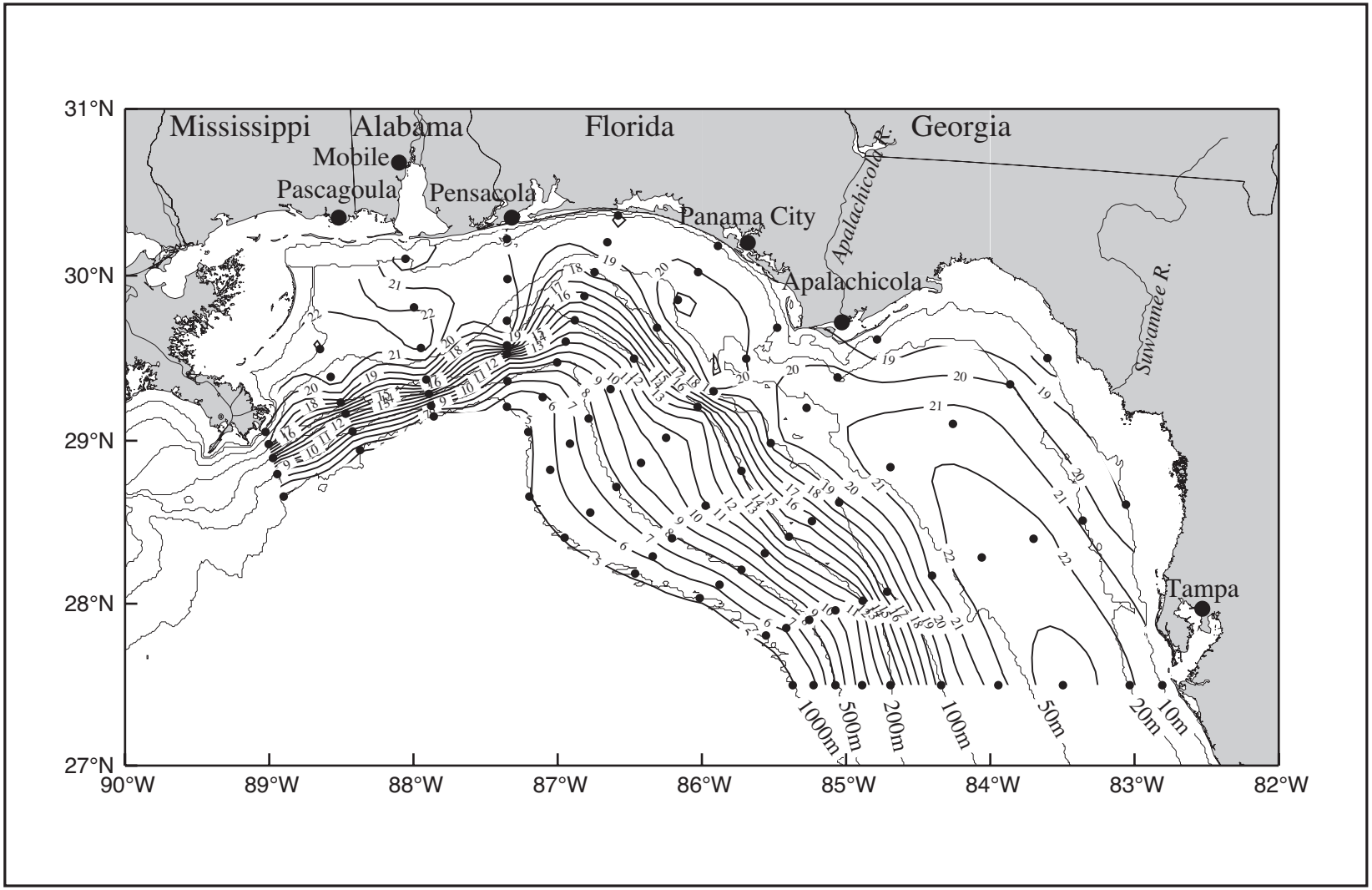

Figure A.3-2. Potential temperature (°C) from the near-bottom observations on cruise N1 in November 1997.

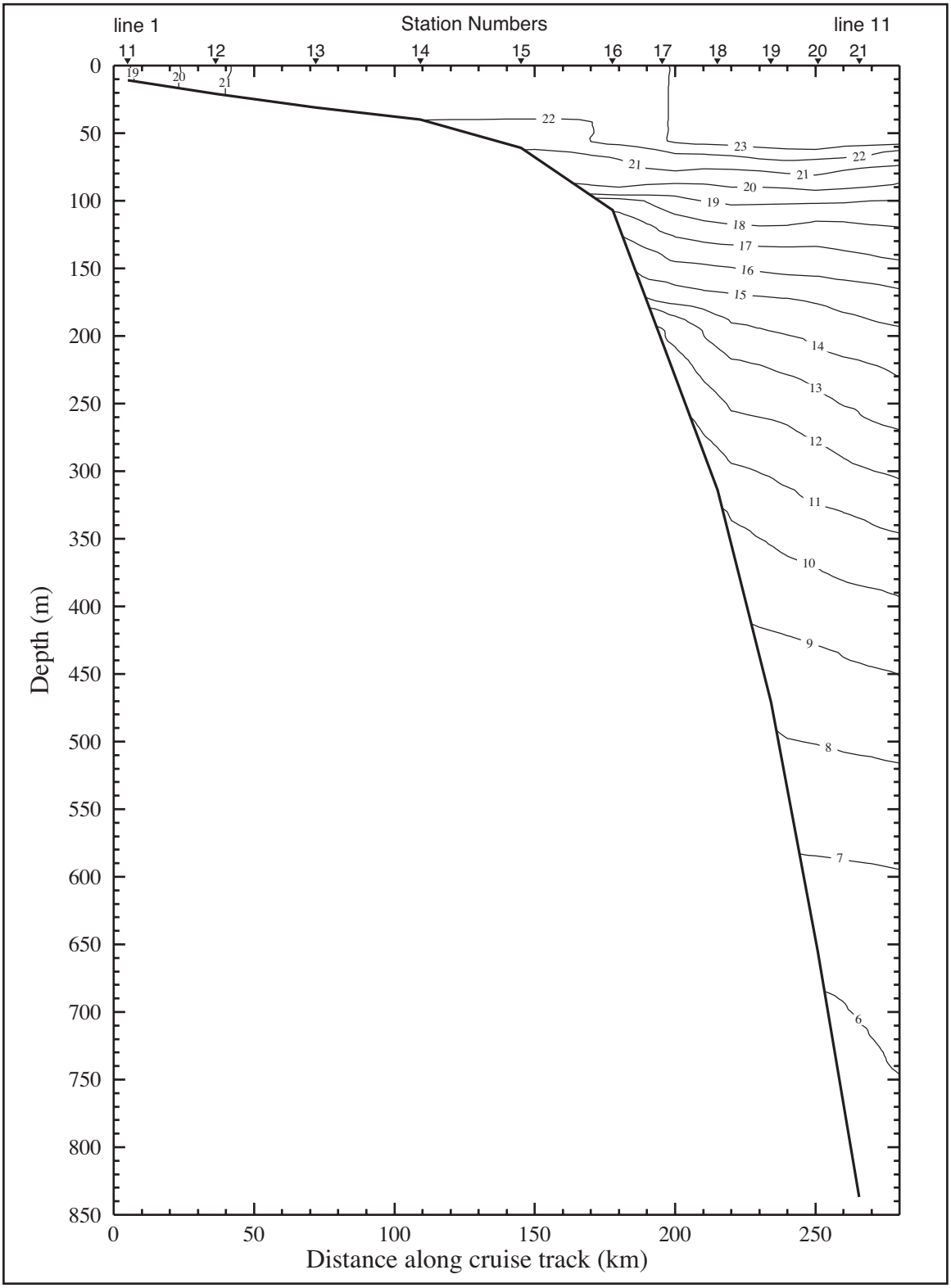

Figure A.3-3. Potential temperatures (°C) on line 10 of cruise N1, 16-26 November 1997.

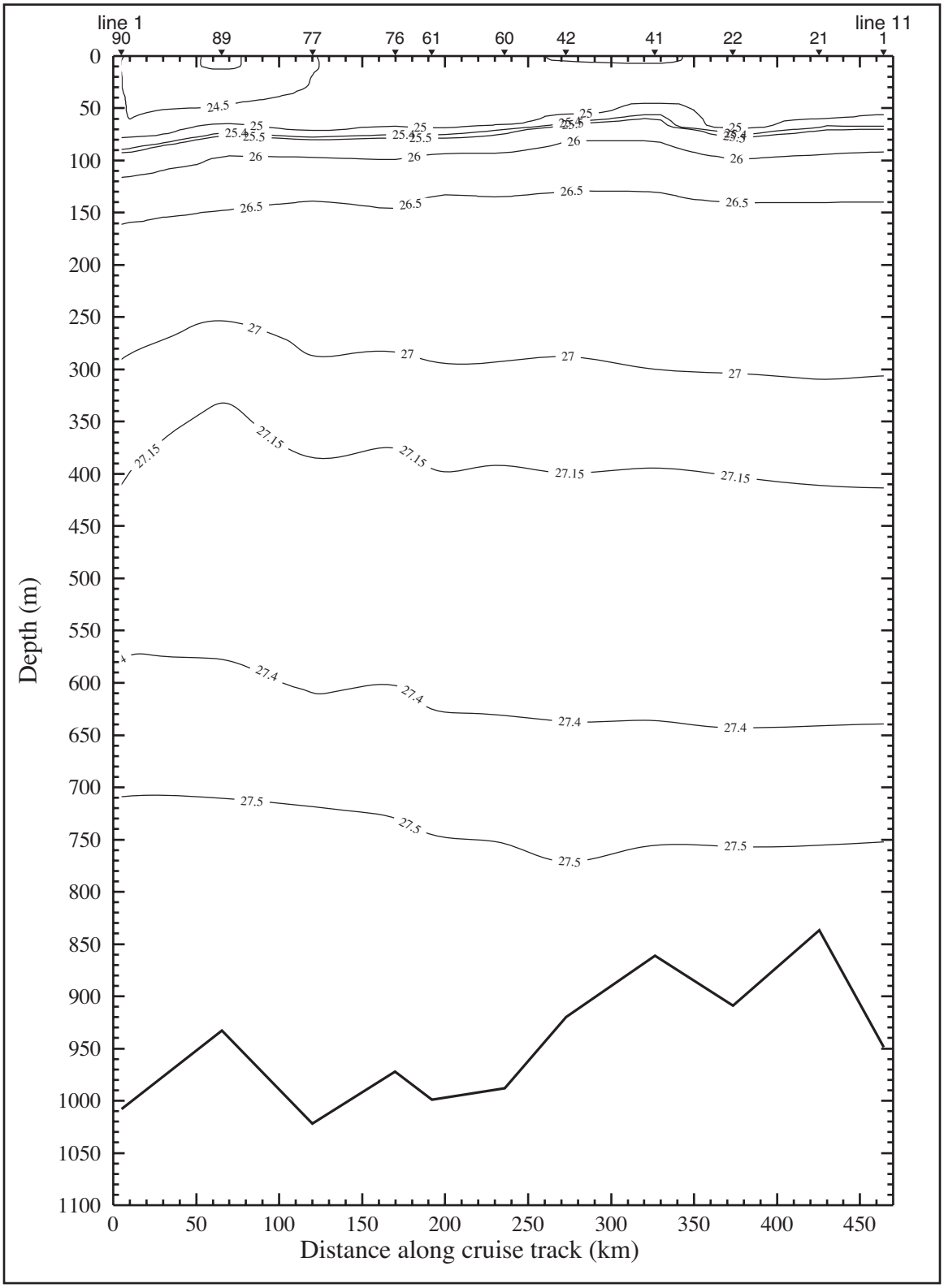

Figure A.3-4. Density anomaly (σ_θ in kg·m^{-3}) along the 1000-m isobath on cruise N1 in November 1997. Station numbers are shown on top axis.

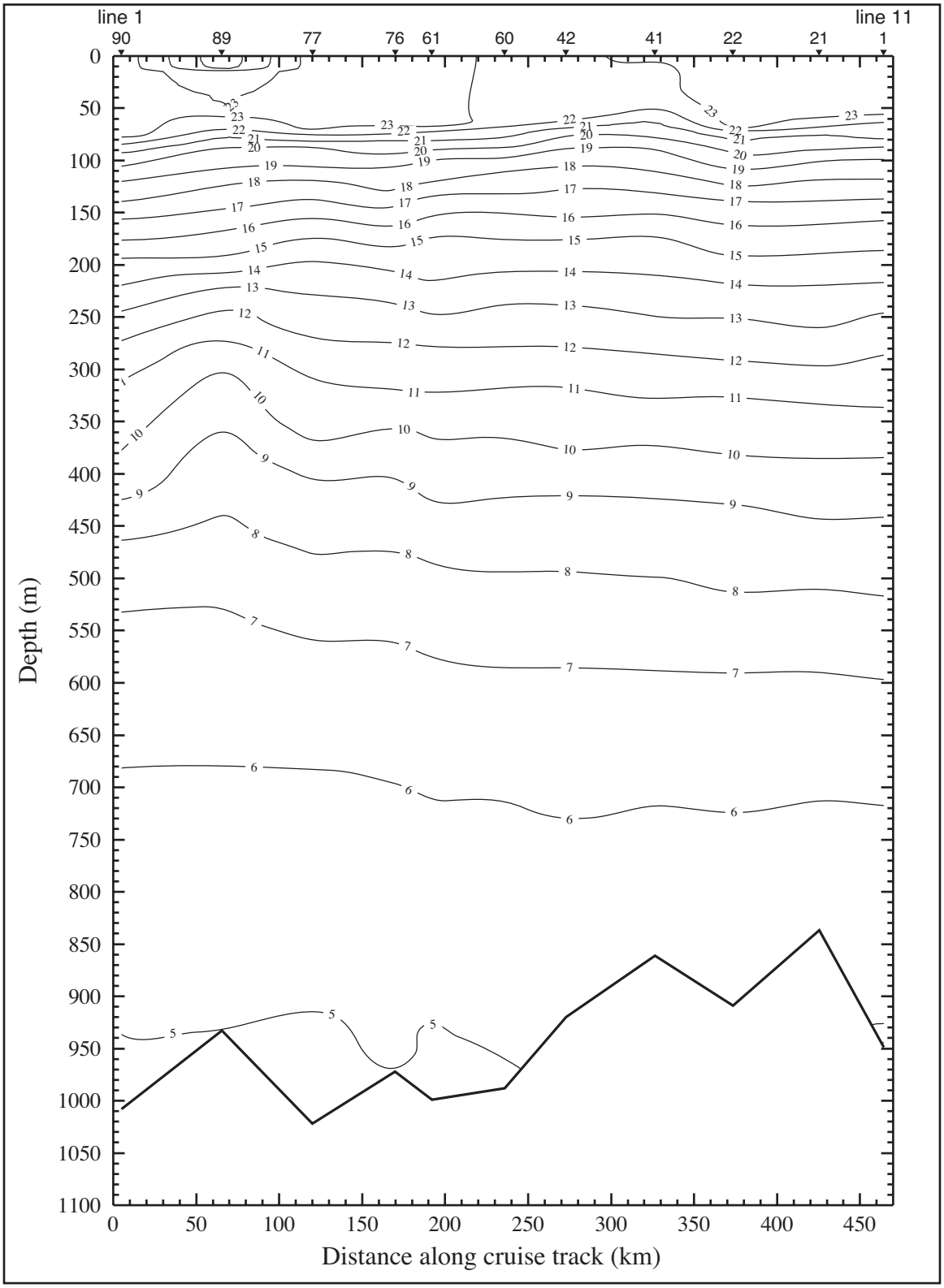

Figure A.3-5. Potential temperature (°C) along the 1000-m isobath on cruise N1 in November 1997. Station numbers are shown on top axis.

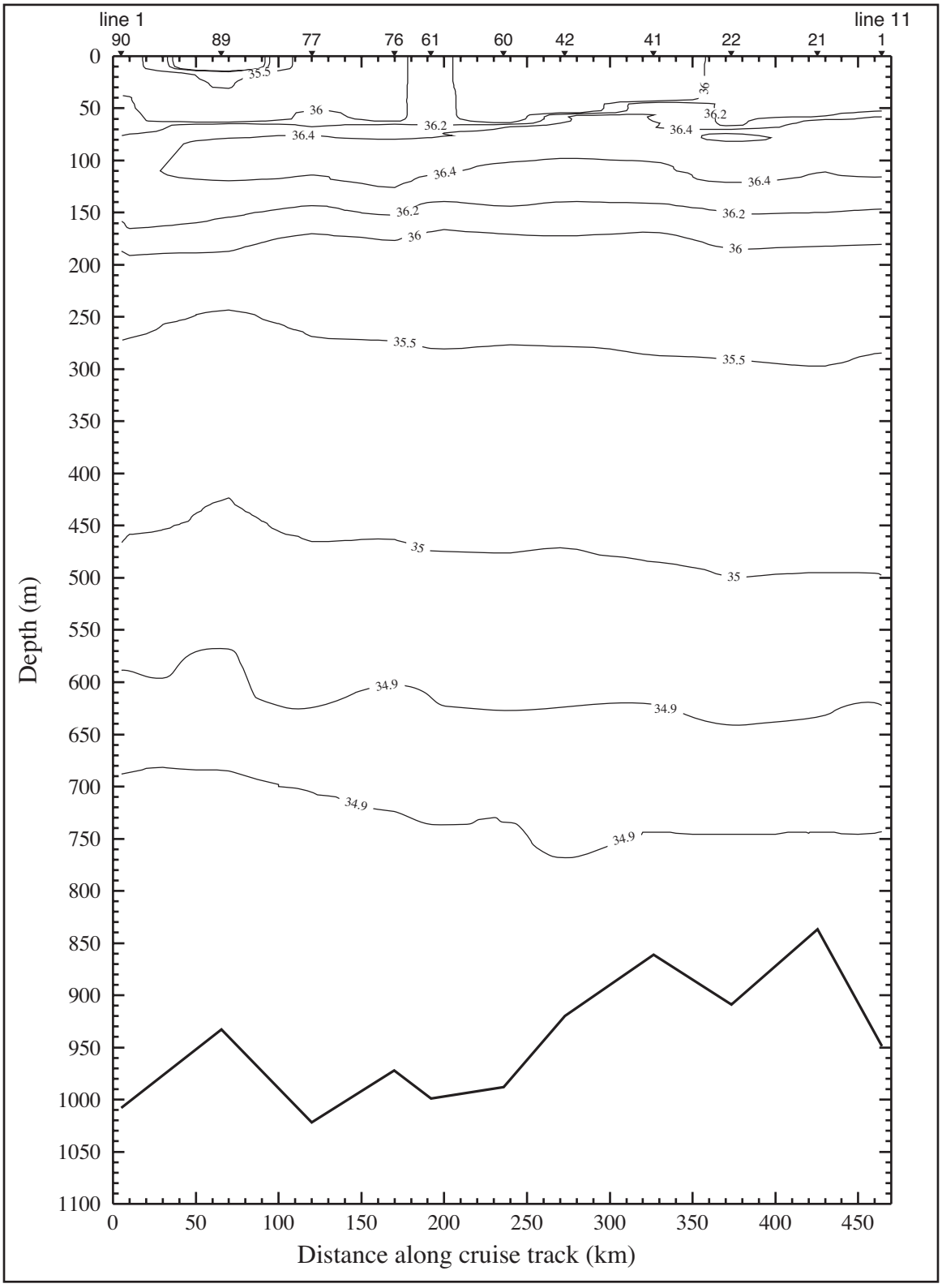

Figure A.3-6. Salinity along the 1000-m isobath on cruise N1 in November 1997. Station numbers are shown on top axis.

mass extends onto the shelf as a continuous layer to the 500-m isobath and, east of the apex of DeSoto Canyon, to the 200-m isobath. At a few stations, there are intermittent lenses of this water mass at bottom near the 100-m isobath. The final water mass found in the upper 1000-m is Antarctic Intermediate Water, which typically is identified by a salinity minimum on the 27.5 σ_θ surface. As seen in Figure A.3-6, the salinity minimum is located at a depth of approximately 650 m; the minima are between 34.89 and 34.9 and occur mainly on the 27.45 σ_θ surface. Phosphate maxima of 1.83-2.03 μM, associated with the Antarctic Intermediate Water, also are present in the 1000-m sections (not shown) at about 650-m depth. Antarctic Intermediate Water does not extend farther up the slope or onto the shelf.

Two regions along the 1000-m isobath have doming isopycnals (Figure A.3-4). These are centered at station 41 on line 8 and station 89 on line 2. The first is associated with the onshore flow located between lines 7 and 9 (Figure A.2-1). The salinity maximum along the 1000-m isobath is shallowest where this onshore flow occurs (Figure A.3-6). The effects seem limited to the upper 100-150m. The ADCP velocity vectors indicate that there is a divergence of the flow at the 1000-m isobath on line 8 between the surface and ~100m, with the onshore flow between lines 7 and 8 having a counterclockwise characteristic and that between lines 8 and 9 having a clockwise characteristic (Figures A.2-1 through A.2-3). At and below 100 m, the onshore flow is clockwise and there is no divergence.

The second doming isopycnal along the 1000-m isobath is associated with a small cyclone centered at about the 200-m isobath near line 2. The surface waters within the cyclone are cooler and fresher than adjacent waters. Salinity (left panel) and temperature (right panel) fields from the 3-m thermosalinograph data are shown in Figure A.3-8. The cruise track and CTD stations are also shown. The temperature field shows warm waters along the slope of the western part of the study area. Cooler waters extend from the mouth of the Mississippi River eastward to the 200-m isobath of line 2. The warm slope water is being drawn cyclonically onto the shelf at about 88.25°W, and is wrapping around the east end of the cool water and extending westward into shallow water near the 50-m isobath of line 2. The 3-m salinity field indicates that the waters in the cyclone have relatively low salinity compared to waters to the north, east, and south, and that the low salinity water is influenced by water coming from the Mississippi River.

The cross-transect ADCP velocity along lines 1, 2, and 3 are presented in Figure A.3-9. Examination of the cross-transect currents on line 2 (middle panel) shows a cyclonic pattern, centered near-surface about station 87 (~200-m isobath). There, flow in the upper water column is eastward over the slope offshore of the 200-m isobath and generally westward over the outer shelf inshore of that isobath. Note also that the cyclone is tilted toward the shelf. This is evidenced by the broadening region of westward flow between stations 87 and 89 as depth increases. The cyclonic flow pattern is consistent with the flows along line 2 shown in Figures A.2-1 through A.2-3. In contrast, the cross-transect ADCP velocity along line 1 is generally eastward and that along line 3 is predominantly eastward, with some westward flow near the 10- and 50-m isobaths. Thus, the region of most organized cyclonic flow is situated near line 2.

The data collected along line 2 together with data from adjacent lines 1 and 3 show the effects of this small cyclone on the water properties. The density anomaly, σ_θ, calculated from the CTD data, for the upper 200 m along lines 1, 2, and 3 is shown in Figure A.3-10. The σ_θ contours for line 1 (left panel) show no evidence of the small cyclone; however, the effects of Mississippi River discharge are seen in the lower densities (< 24 kg·m^{-3}) associated with stations 93 and 94. Along line 2, the σ_θ contours show the clear presence of the cyclone, with denser waters doming in the center at stations 86 and 87 (middle panel).

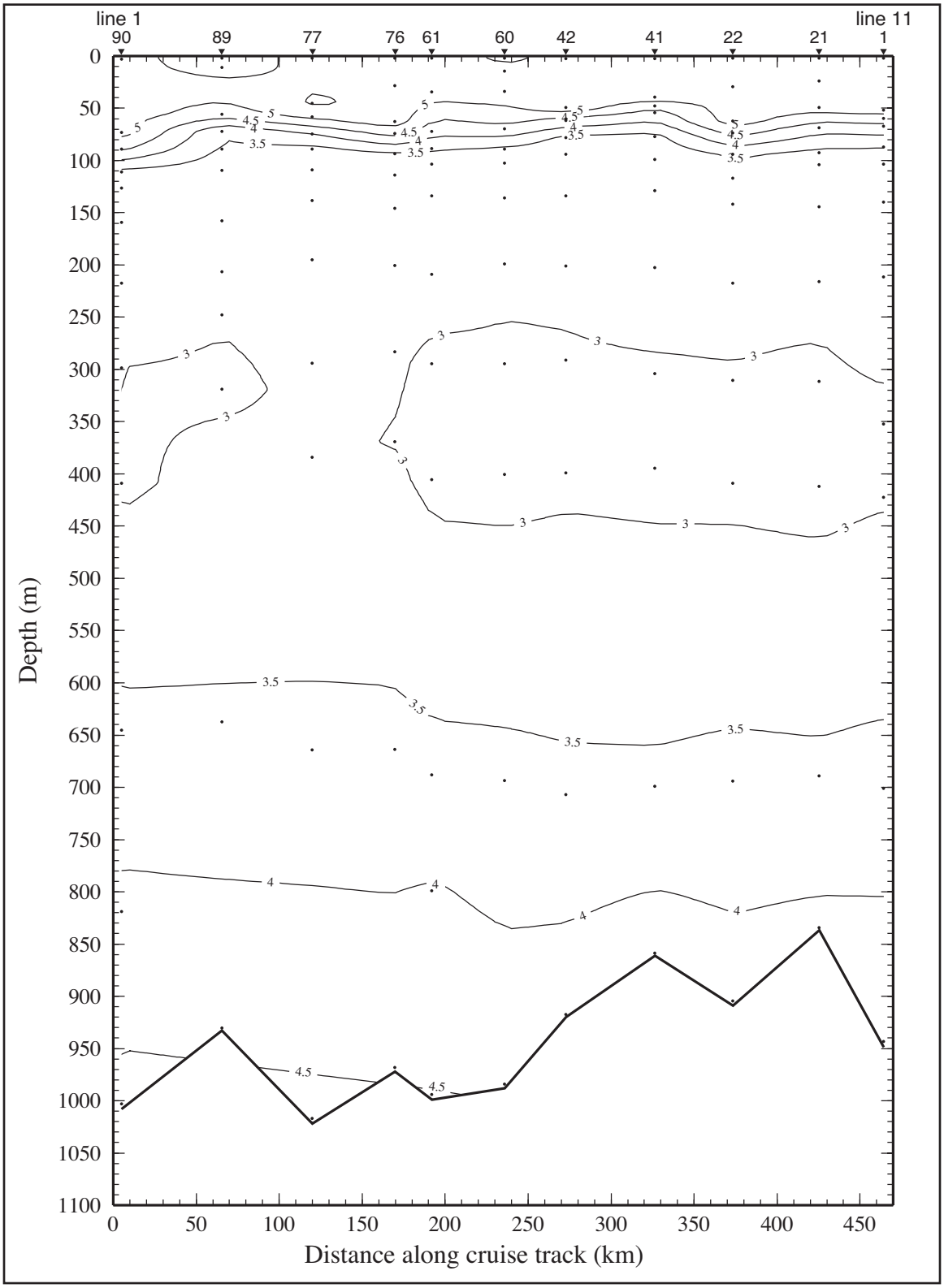

Figure A.3-7. Dissolved oxygen ($mL \cdot L^{-1}$) along the 1000-m isobath on cruise N1 in November 1997. Station numbers are shown on top axis.

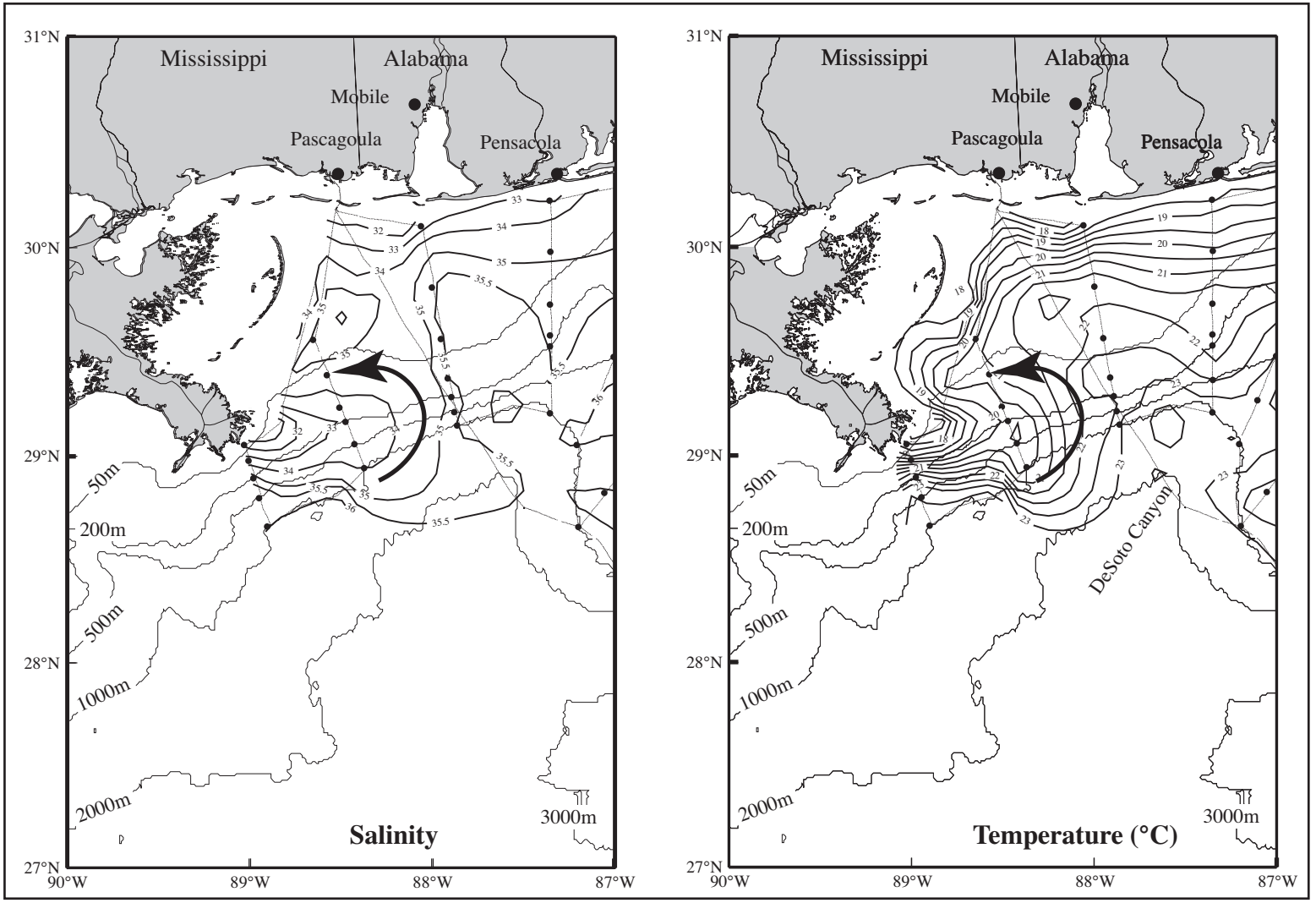

Figure A.3-8. Salinity (left panel) and temperature (°C; right panel) from the continuous thermosalinograph at ~3-m depth on cruise N1 in November 1997. CTD station locations are shown (dots). The arrows schematically show the surface flow.

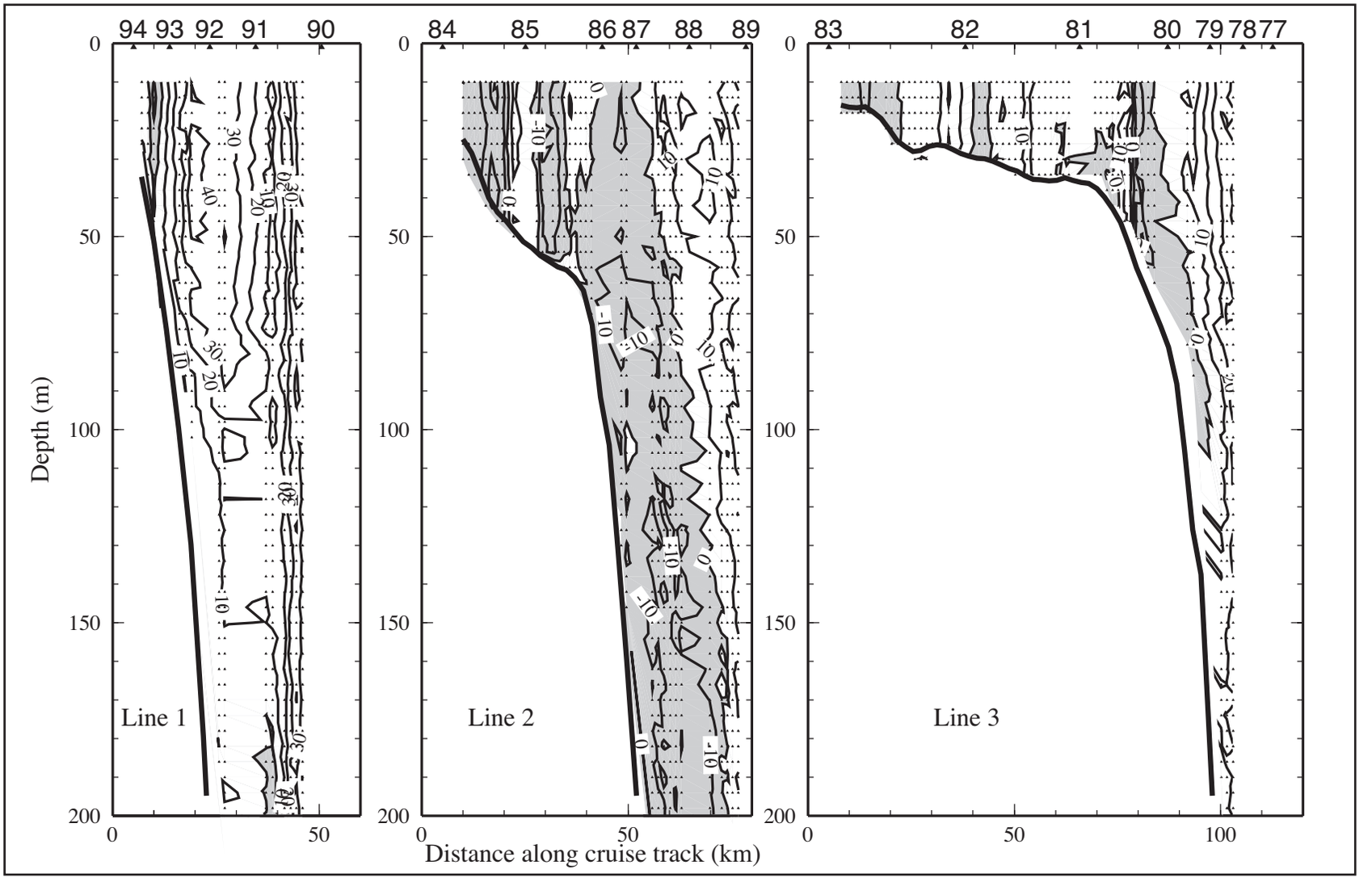

Figure A.3-9. Cross-transect ADCP velocity (cm·s^{-1}) on lines 1, 2, and 3 on cruise N1 in November 1997. Shaded areas indicate westward flow. Stations are shown along top axis.

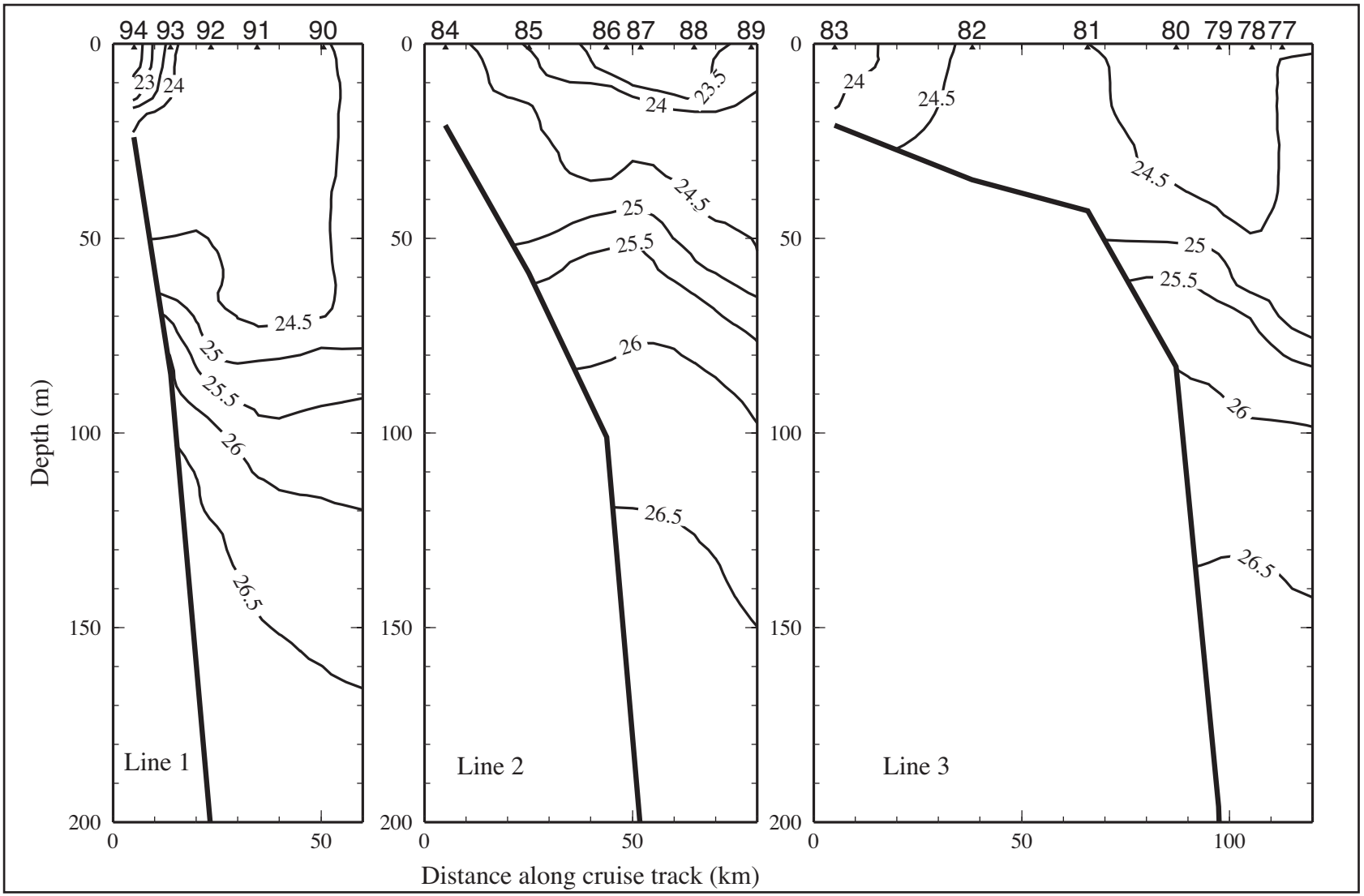

Figure A.3-10. Density anomaly (σ_θ, kg·m^{-3}) on lines 1, 2, and 3 of cruise N1 in November 1997. Stations are shown along top axis.

The effects of the cyclone extend below 100 m There is evidence of the tilting of the cyclone toward the shelf in the offset of the domes of the isopycnals. The pooling of fresher, less dense water in the center of the cyclone can be seen above the 20-m depth and is related to the relatively low salinity water, influenced by the river discharge, being pooled in the center of the cyclone. On line 3 (right panel), the σ_θ contours show very little influence from the cyclone, although there are indications of possible spin up of cyclonic flow associated with the bathymetry and the anticyclone at the edge of the study area.

The potential temperature and salinity in the upper 200 m from the CTD data along lines 1 and 2 are given in Figure A.3-11. The properties along line 1 exhibit characteristic strong gradients in temperature and salinity in the upper 30-40 m, with cooler and fresher waters nearshore, that are associated with the discharge of Mississippi River water. However, on line 2, which is farther from river discharge sources, there is no such cross-shelf gradient. On line 1, the potential temperature and salinity profiles exhibit no evidence of cyclonic circulation. The potential temperature and salinity profiles on line 2, however, exhibit the characteristic doming of isolines that is associated with cyclonic circulation. The tilt toward the shelf in these properties is indicative of the tilt in the cyclone. The potential temperature contours (upper right panel of Figure A.3-11) show cooler water being upwelled from depth. The contours in the upper 50 m show interleaving of warmer water from offshelf with cooler water from nearshore. Salinity contours on line 2 (lower right panel of Figure A.3-11) show uplift of saltier deep waters in the center of the cyclonic circulation at stations 86 and 87. Salinities in the upper 30-40 m show a patch of relatively low salinity water centered within the cyclone, indicating saltier, offshelf water has been wrapped around the cyclone onto the inner shelf.

Within cyclones, nutrient and oxygen property isolines show characteristic uplift of nutrient-rich and oxygen-poor deep waters. Shown in Figure A.3-12 are the nitrate and silicate concentrations along lines 1 and 2 for cruise N1. For nitrate, concentrations for a given depth at stations 86 and 87, in the center of the cyclone, are higher than those of adjacent stations. This enrichment at these stations is from the upward doming of isopleths. The tilt of the cyclone is also evidenced by the tilt in the doming nitrate isolines with depth. Oxygen contours on line 2 show uplifted oxygen-poor deep water in the cyclone center (not shown).

On line 2, the region of the most intense uplift occurs below 30 m in the density anomaly section (Figure A.3-10). The potential temperature and salinity sections (Figure A.3-11) also show this uplift, but the patchiness of these data suggest vertical mixing is occurring in the upper 50 m. The oxygen and nutrient sections (Figure A.3-12) do not evidence the vertical mixing. The resolution of the temperature and salinity data is 0.5 m, whereas that of the bottle data is much coarser. If the bottle data were sampled at closer spacing, they might have shown evidence of the vertical mixing. This is an example of how the differing resolutions of various data sets can result in differing interpretations.

The pattern of silicate concentration on line 2 is similar to that of nitrate in the upper 50 m and below 125 m, but is confounded by the presence of a nepheloid layer at approximately 75 m depth. In this region, the percent transmission is relatively low (< 70%) compared to adjacent waters (80%). The along-transect ADCP velocity (not shown) indicates offshelf flow at just above 75 m depth and onshelf flow just below.

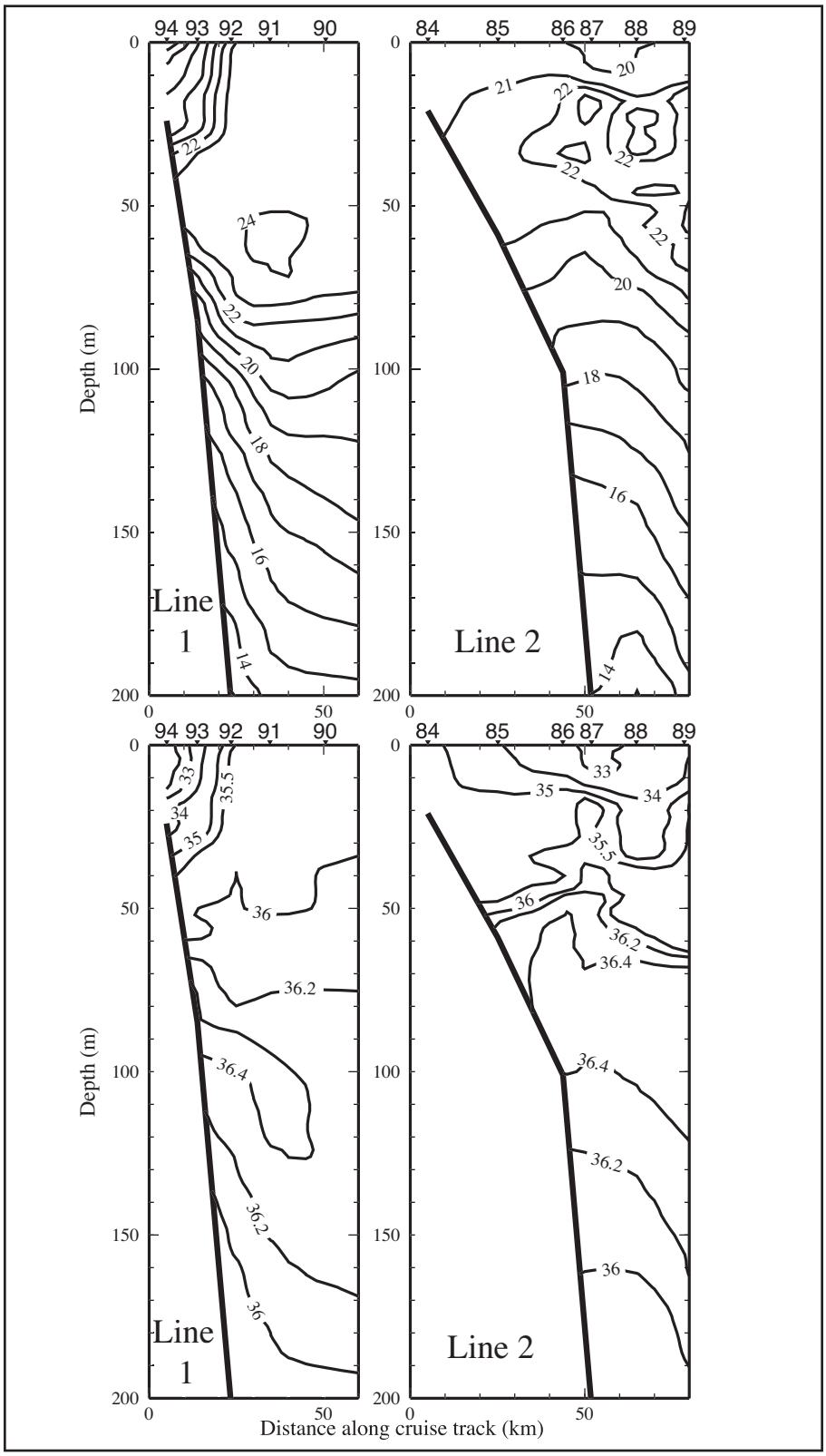

Figure A.3-11. Potential temperature (°C; upper panels) and salinity (lower panels) on lines 1 and 2 on cruise N1 in November 1997. Stations are shown on top axis.

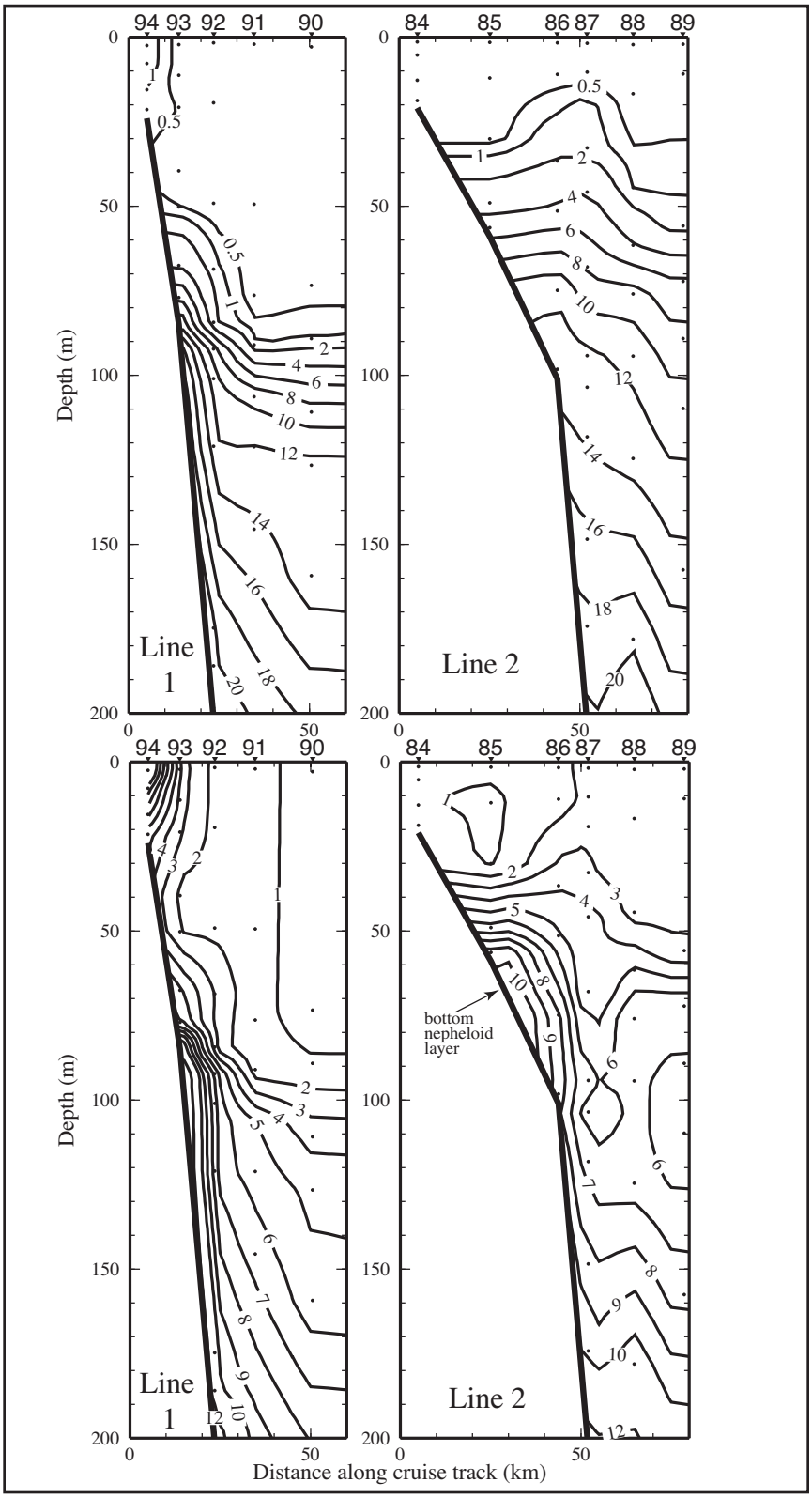

Figure 4.3-12. Nitrate (μM; upper panels) and silicate (μM; lower panels) on lines 1 and 2 on cruise N1 in November 1997. Stations are shown on top axis.

Along line 1, there is no evidence for uplifted nitrate isopleths (left panels in Figure A.3-12). The waters in the upper 100 m over the outer shelf (stations 90-92) are poor in nutrients, while those in the upper 30-50 m over the inner shelf (stations 93 and 94) exhibit nutrient enrichment associated with river discharge. This pattern of enhanced nutrient levels was a common feature at the mouths of rivers. Waters as deep as 70 m tended to be nutrient-poor, with nutrient concentrations far below those of deep waters. An abrupt increase in nutrient concentration (particularly for phosphate, nitrate, and silicate) occurred typically between 70 and 100 m water depth. This vertical structure develops as a result of fixation of nutrients into biomass by phytoplankton in the euphotic zone and remineralization of organic matter in deeper waters and sediments.

Small cyclones are biologically important in that they bring nutrients into the photic zone where they can be utilized by the plankton. The relative fluorescence is an indicator of such biological activity. In the upper 60 m of the water column, the relative fluorescence for lines 1 and 2 (not shown) is higher in those regions with the higher nutrient concentrations. The contours reflect the two different nutrient source regions: a doming of high fluorescence in the cyclone for line 2 (e.g., stations 86 and 87) and a high-to-low gradient of fluorescence from nearshore to offshore in the region under the riverine influence for line 1 (e.g., stations 92-94). Below the photic zone, the relative fluorescence is minimal, as expected. Ressler (2001) found the acoustic backscatter, which is an indicator of standing stocks of zooplankton and micronekton biomass, was higher within the region of the cyclone than outside. He concluded that the cyclone resulted in enhanced epipelagic nutrient concentrations that increased zooplankton and micronekton biomass (see also Ressler and Jochens 2001).

APPENDIX B
SUMMARY OF CONDITIONS DURING CRUISE N2

Cruise N2 was a spring cruise conducted 5-16 May 1998. Data collection began with ADCP sampling along the 1000-m isobath between lines 4 and 11. CTD/bottle stations began with the most seaward station on line 11 and ran from lines 11 through 4, and finally lines 1 through 3. Stations ended with the most inshore station on line 3. Figure B-1 shows the station locations and gives the CTD station numbers, which are sequential by sampling order. Station 1 is excluded because it was the test station.

B.1 Forcing Functions

B.1.1 Winds

Mean gridded wind field and principal axes of variance for the period of cruise N2 are shown in Figure B.1.1-1. The same gridding and averaging methods discussed in Section A.1.1 were used to produce this field (Wang et al. 1998). During cruise N2, mean winds generally were weak (< 5 $m \cdot s^{-1}$) and directed to the north over the Mississippi-Alabama shelf and to the northeast over the Florida shelf. In the first part of the cruise, winds were usually 5-10 $m \cdot s^{-1}$ with a northward component of flow. During May 10-11, a frontal passage went through the area, with the winds changing from southerly to northerly with magnitudes ~8-10 $m \cdot s^{-1}$ (Figure B.1.1-2). After passage of this front, winds were ≤ 5 $m \cdot s^{-1}$. Directions varied with eastward flow over the entire shelf after passage of the front, followed by several days of generally anticyclonic flow around a center located near the shelf break and slope to the southwest of Cape San Blas. This anticyclonic flow resulted in generally northward flow over the Mississippi-Alabama shelf, eastward, weak flow in the vicinity of Cape San Blas, and southward flow over the west Florida shelf. There were two periods with upwelling-favorable, though weak, westerly winds, particularly near-shore.

B.1.2 River Discharge

In winter 1998, the river discharges exceeded the long-term mean discharge rates by significant amounts. By spring, the Mississippi River continued to discharge at a rate well above its 70-year record-length mean, as shown in Figure 3.1.2-2. Other rivers had flows below their means with the exception of one time period. In late April, rivers from the Pearl to Apalachicola exhibited a brief pulse of much greater than average discharge—in some cases significantly exceeding the mean plus one standard deviation. This pattern is illustrated in Figure 3.1.2-3 that shows daily discharge rates for the Tombigbee River, which discharges into Mobile Bay. During winter and spring 1998, major rivers east of Cape San Blas generally had only one episode, in March, of very high discharge relative to the mean.

Greater than average river discharge into the Gulf from Mississippi Sound to Cape San Blas during early 1998 is consistent with the extensive surface expression of low salinity water observed in that region during cruise N2 in May 1998. This can be seen in the near-surface (~3 m) salinity distribution (Figure B.1.2-1). On lines 1-3, the freshest surface waters (< 28) are inshore. This is evidence of mixing with the local river waters. A tongue of relatively low salinity water (< 32), centered over mid-shelf, extends from the Mississippi Sound to Cape San Blas. Note that, from line 4 to line 7, the inshore waters generally are slightly saltier than the waters at the 100-m isobath. East of Cape San Blas, water with salinity < 32 occurs only nearshore off the mouth of the Suwannee River. There is much less low salinity water over the west Florida shelf than over the Mississippi-Alabama-Florida panhandle shelves.

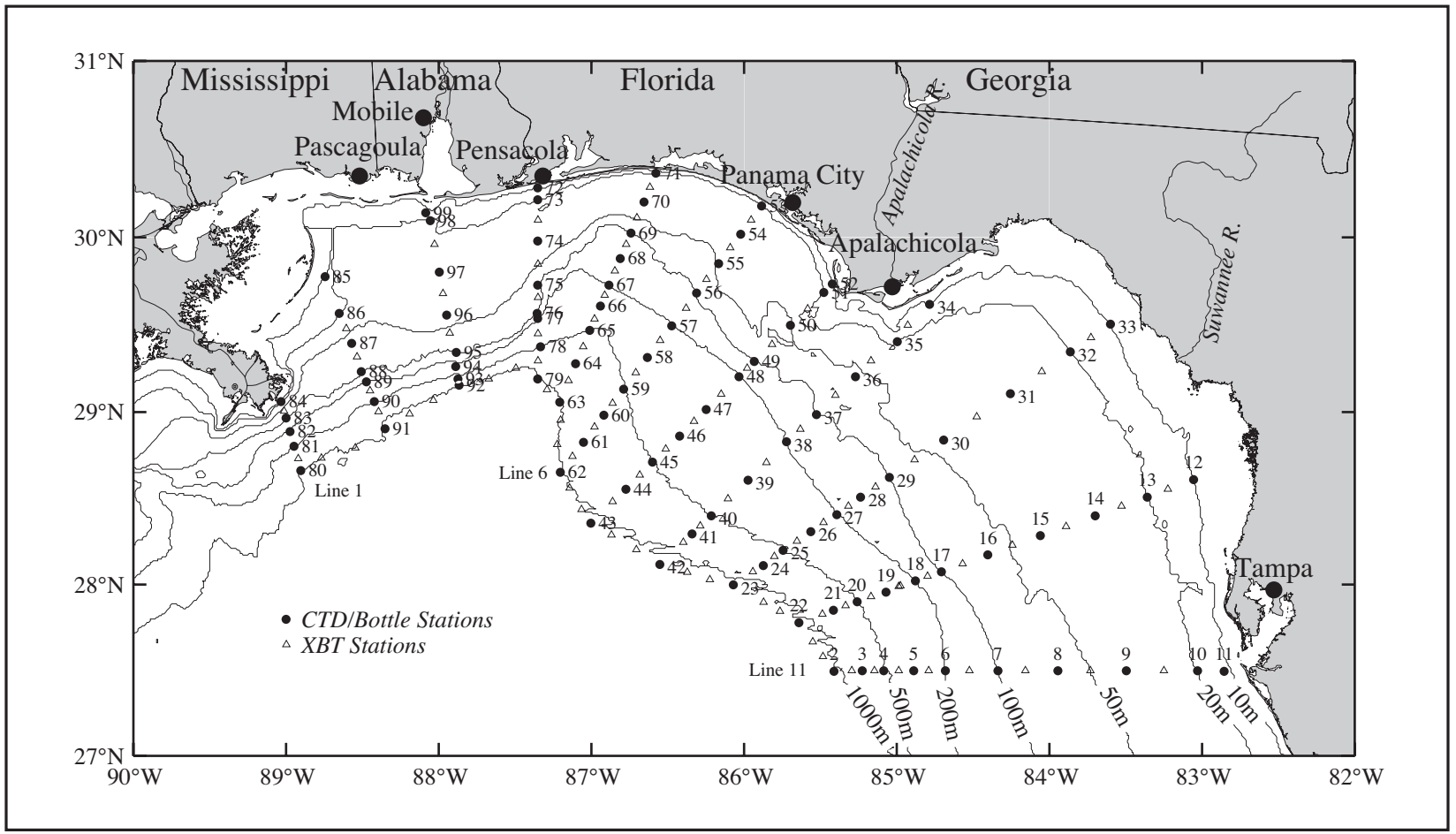

Figure B-1. Station locations for cruise N2 conducted on 5-16 May 1998. CTD stations (solid circles) are numbered; XBT stations (open triaangles) are not). Station 1 (not shown) was the test station on N2.

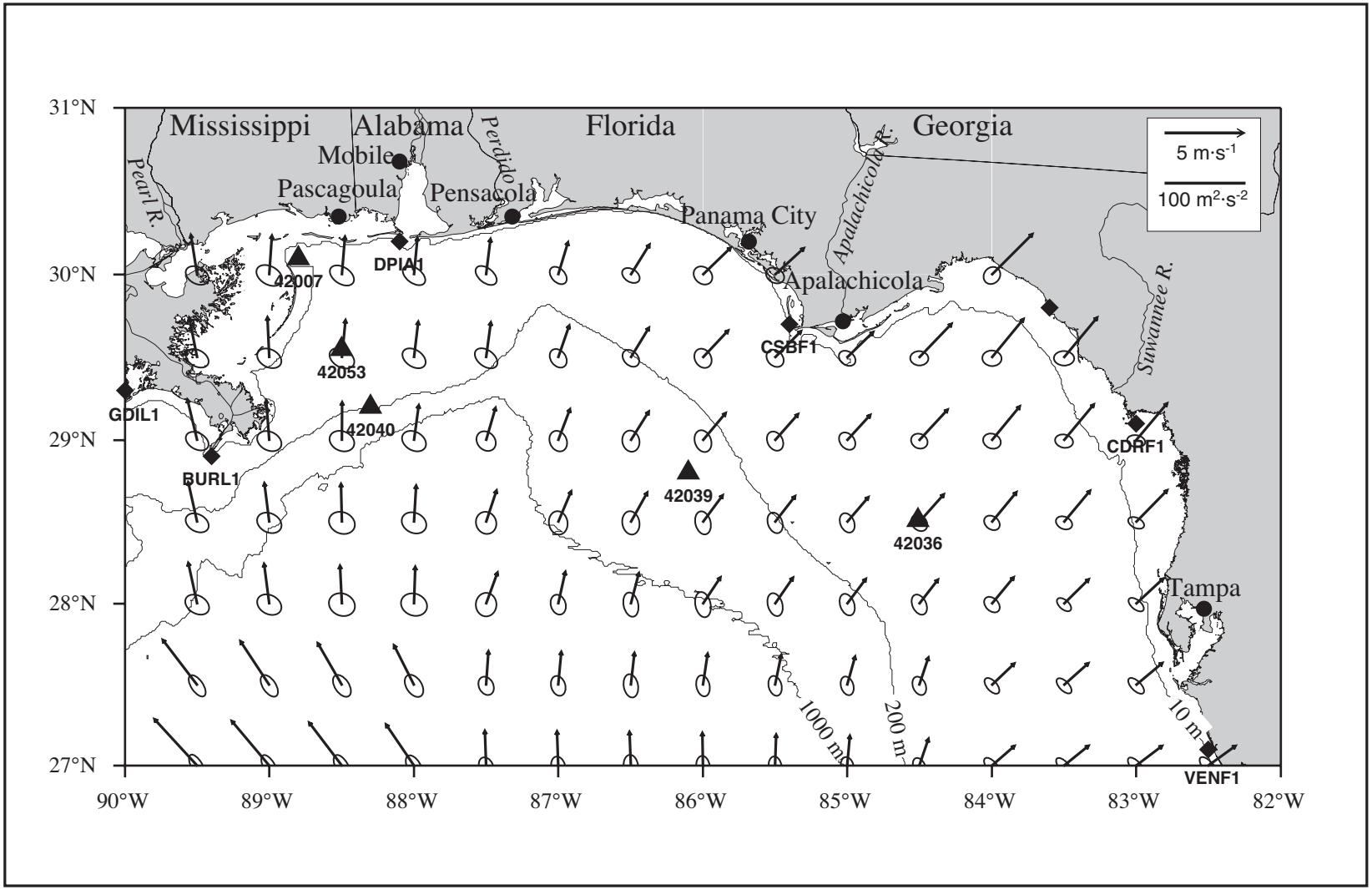

Figure B.1.1-1. Vector mean winds and variance ellipses for cruise N2 in May 1998.

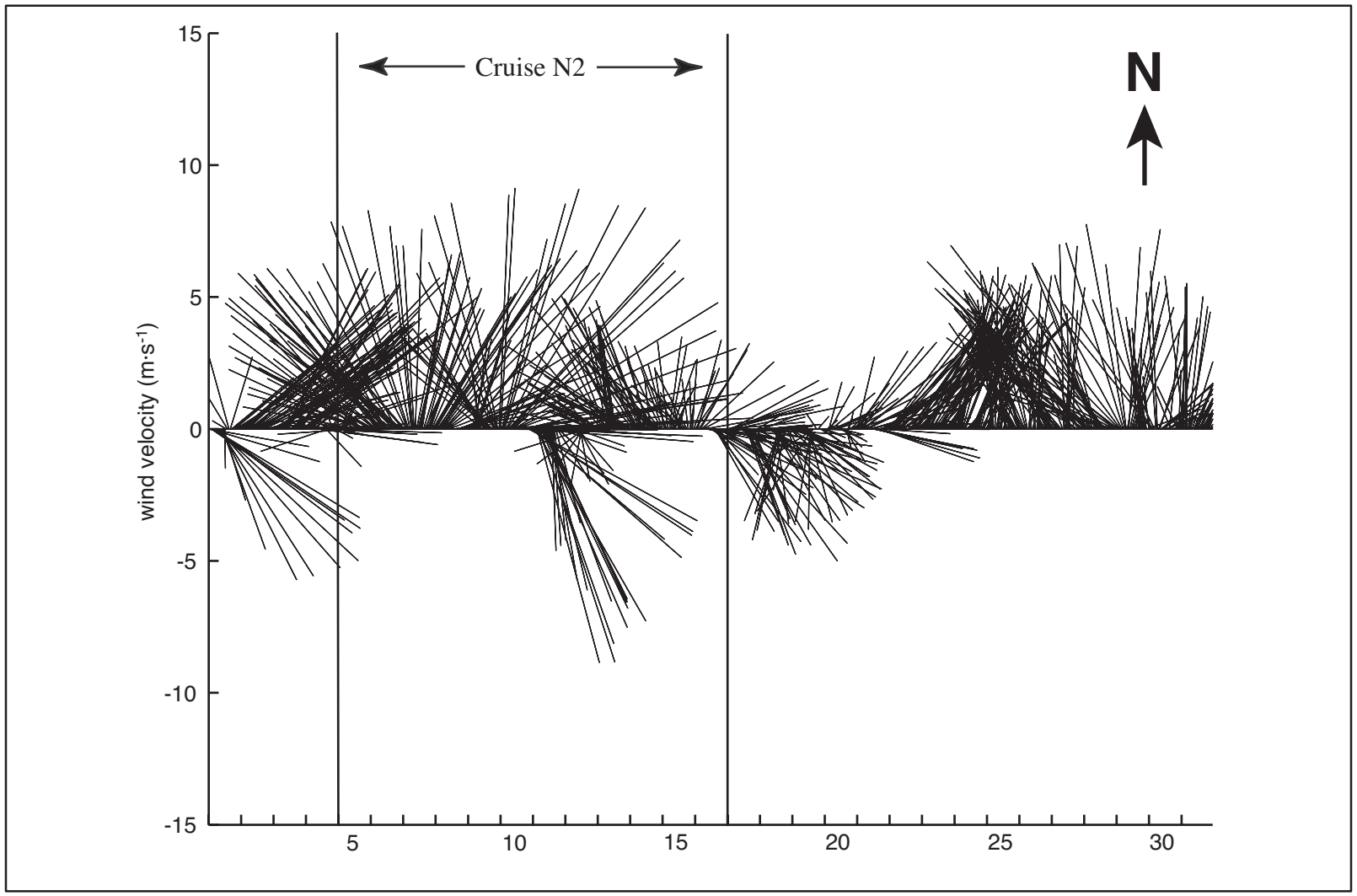

Figure B.1.1-2. Vector stick plot of wind at meteorological buoy 42040 for May 1998. Gauge height is 10 m.

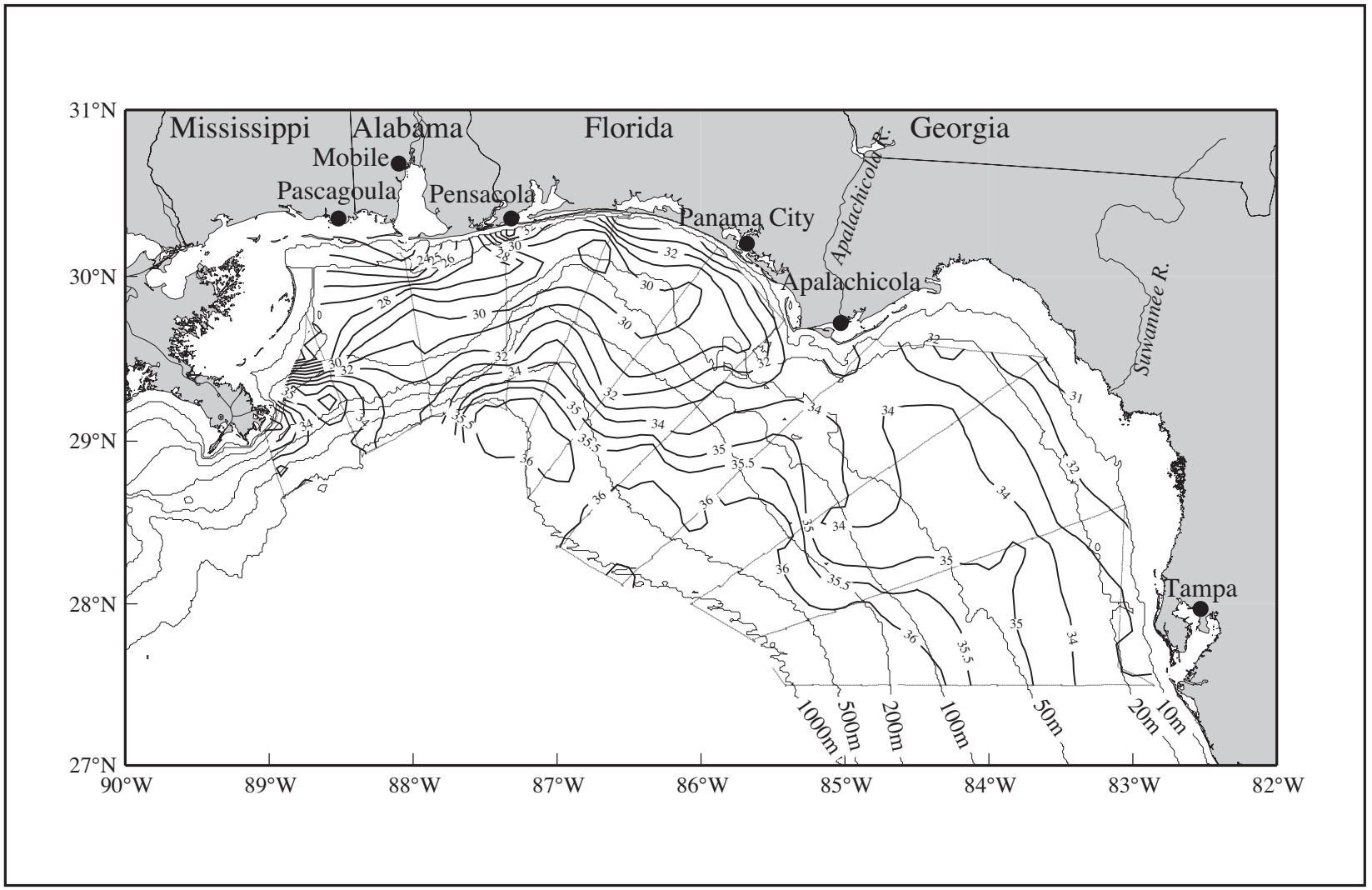

Figure B.1.2-1. Salinity at ~3m from thermosalinograph observations on cruise N2 in May 1998.

B.1.3 SSH Fields Adjacent to the Shelf

In early April 1998, the off-shelf area, with water depths or 200 m or more, was under the influence of cyclonic flow. As April progressed, a small anticyclone began to develop in the vicinity of DeSoto Canyon. During the N2 cruise, an anticyclonic system, which was oriented northwest-southeast with two regions of high SSH, was intensifying. One high was located near the slope apex of DeSoto Canyon and the other was encroaching over the slope and outer shelf west of Tampa (Figure B.1.3-1).

B.2 *In Situ* Evidence of Circulation

The distribution of geopotential anomaly for the sea surface (3 m) relative to 800 m shows an anticyclonic feature over the DeSoto Canyon and a second anticyclone encroaching over the outer shelf edge west of Tampa (Figure B.2-1). These features are associated with the two highs seen in the SSH field (Figure B.1.3-1). The circulation indicated by these features is corroborated by shipboard ADCP measurements taken along the cruise track using a broadband 150 kHz ADCP. Currents from the 4-m bin centered at the 14-m depth are shown in Figure B.2-2. The currents associated with the DeSoto Canyon eddy and the eddy over the slope off Tampa are < 40 $cm \cdot s^{-1}$. The currents in both anticyclones are relatively weak compared to those of other slope eddies, which can exceed 50-75 $cm \cdot s^{-1}$. This is evidence that these features were not well developed during cruise N2. The anticyclonic features also are seen in the 50- and 102-m depth currents (Figures B.2-3 and B.2-4). Currents over the outer shelf west of Tampa reach ~75 $cm \cdot s^{-1}$ near the shelf break. It is unclear to what extent these currents are due to the anticyclone that was spinning up offshore or are associated with the southward currents that were moving along the shelf break between lines 8 and 11.

There is a large divergence of flow at the 14-m depth seaward of about the 200-m isobath between lines 7 and 8 (Figure B.2-2). This divergence weakens with depth, but is still present in the 102-m depth currents (Figure B.2-4). Although at the time of sampling of the off-shelf stations on lines 7 and 8 there was a front that passed through, examination of the direction of oceanic currents relative to the direction of the winds shows it did not cause the divergence. During sampling on line 8, when currents were approximately southeastward, the winds were directed approximately northward or were turning southward. During sampling on line 7, however, when currents were northwestward, the winds were toward the southeast.

The SSH field provides information on the likely cause of the divergence (Figure B.1.3-1). The anticyclonic eddy west of Tampa likely would induce currents in the southeast direction over the off-shelf region of line 8, while the anticyclonic eddy over DeSoto Canyon would induce currents in the west to northwest direction over the off-shelf region of line 7. Further, there is an intense cyclone located adjacent to the 1000-m isobath on the west side of the saddle point between the two anticyclones. This cyclone likely would induce flows out of the study area between lines 7 and 8. The pattern of ADCP currents approximates the flow patterns expected from the SSH field (Figure B.2-2). Examination of silicate along the 1000- and 500-m isobaths suggests possible uplift of waters to replace the fluids removed by the divergent flows, near line 8 (Figure B.2-5); other properties show this less clearly if at all.

There is evidence for along-isobath flow along the northern reaches of the canyon and cross-isobath flow directed inshore on the west side of the anticyclone and near the canyon axis (see also Figures B.2-3 and B.2-4 showing the currents at the 50- and 102-m depths). Such flow will lead to transport in a bottom Ekman layer that is to the left of the flow—leading to more penetration of bottom waters toward shallower depths.

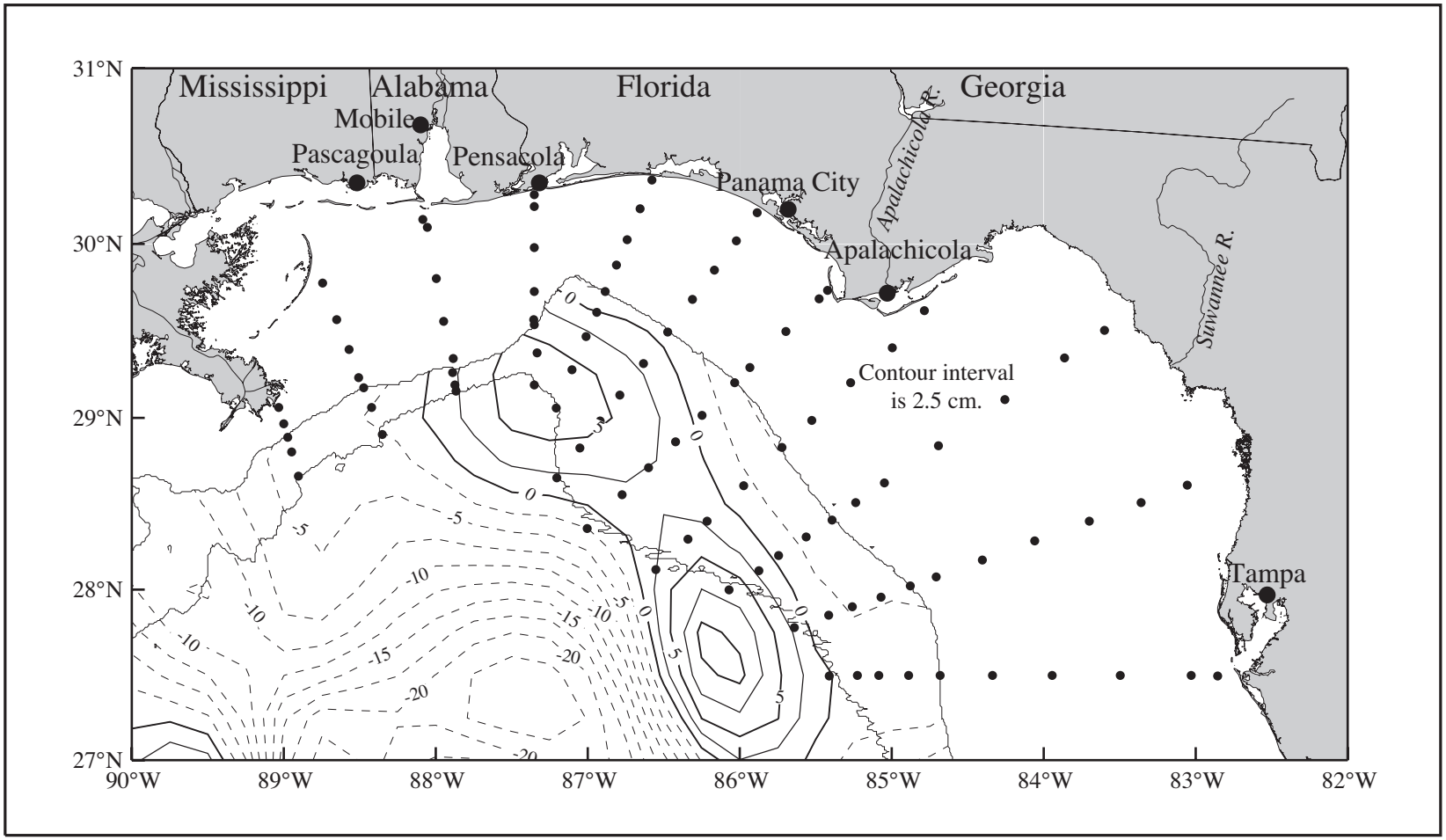

Figure B.1.3-1. Sea surface height field from satellite altimeter data for 13 May 1998 during N2. The 200- and 1000-m isobath contours and CTD stations (dots) are shown. [Data provided by Robert R. Leben, University of Colorado.]

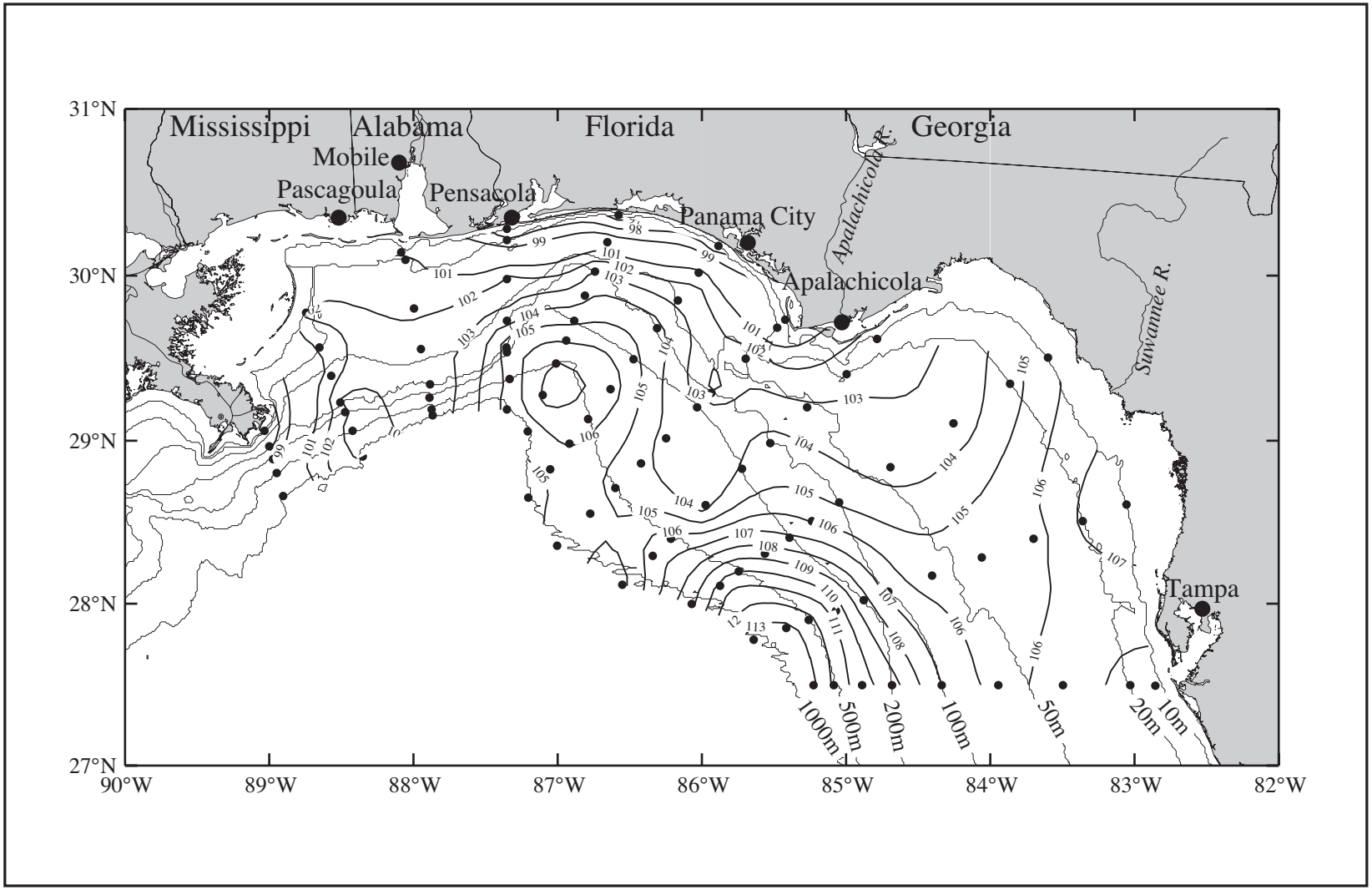

Figure B.2-1. Geopotential anomaly (dyn cm; 3 m relative to 800 m) for cruise N2 conducted 5-16 May 1998. CTD station locations are shown.

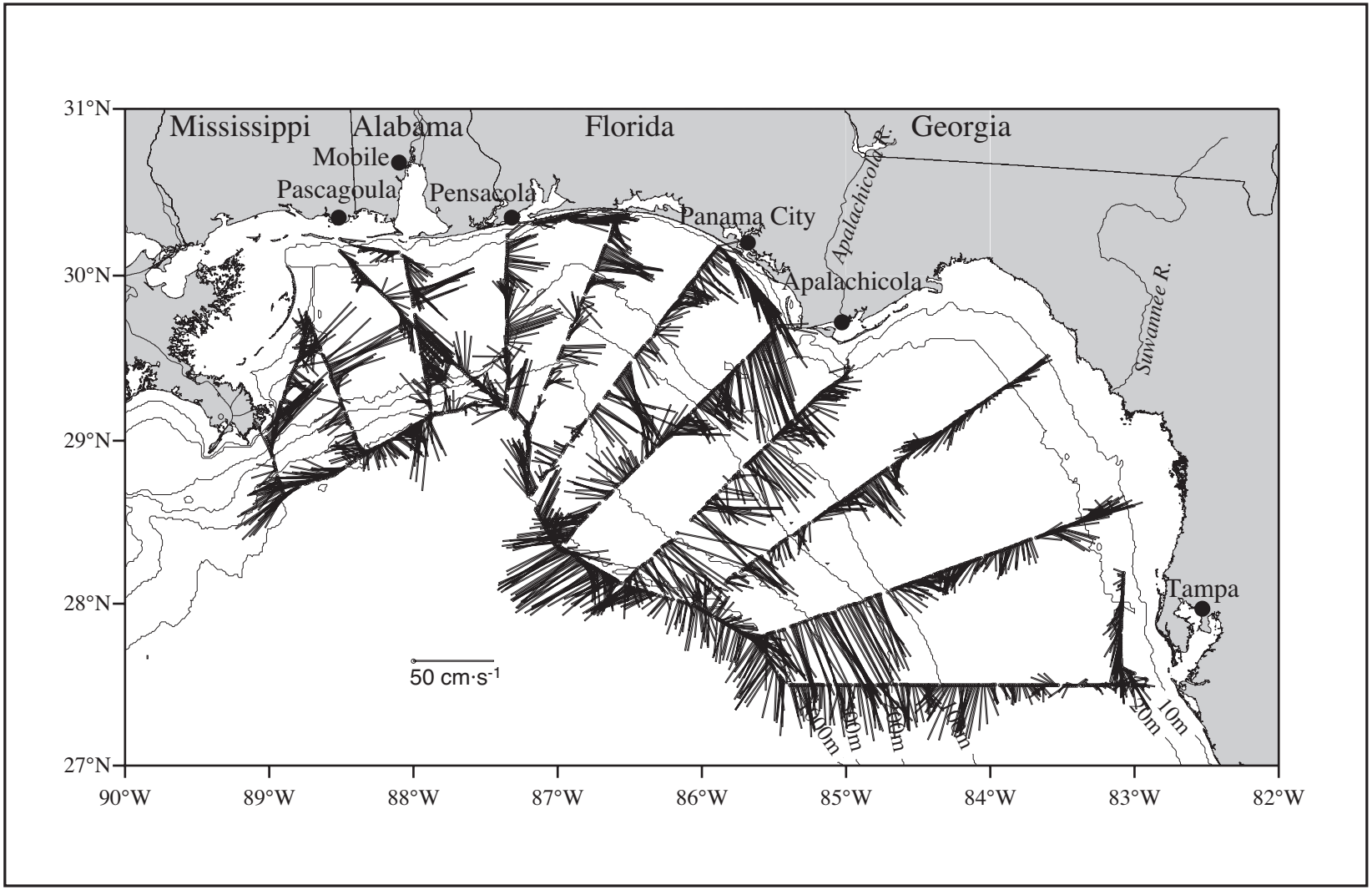

Figure B.2-2. ADCP-measured currents for the 4-m bin centered at 14 m on cruise N2 in May 1998.

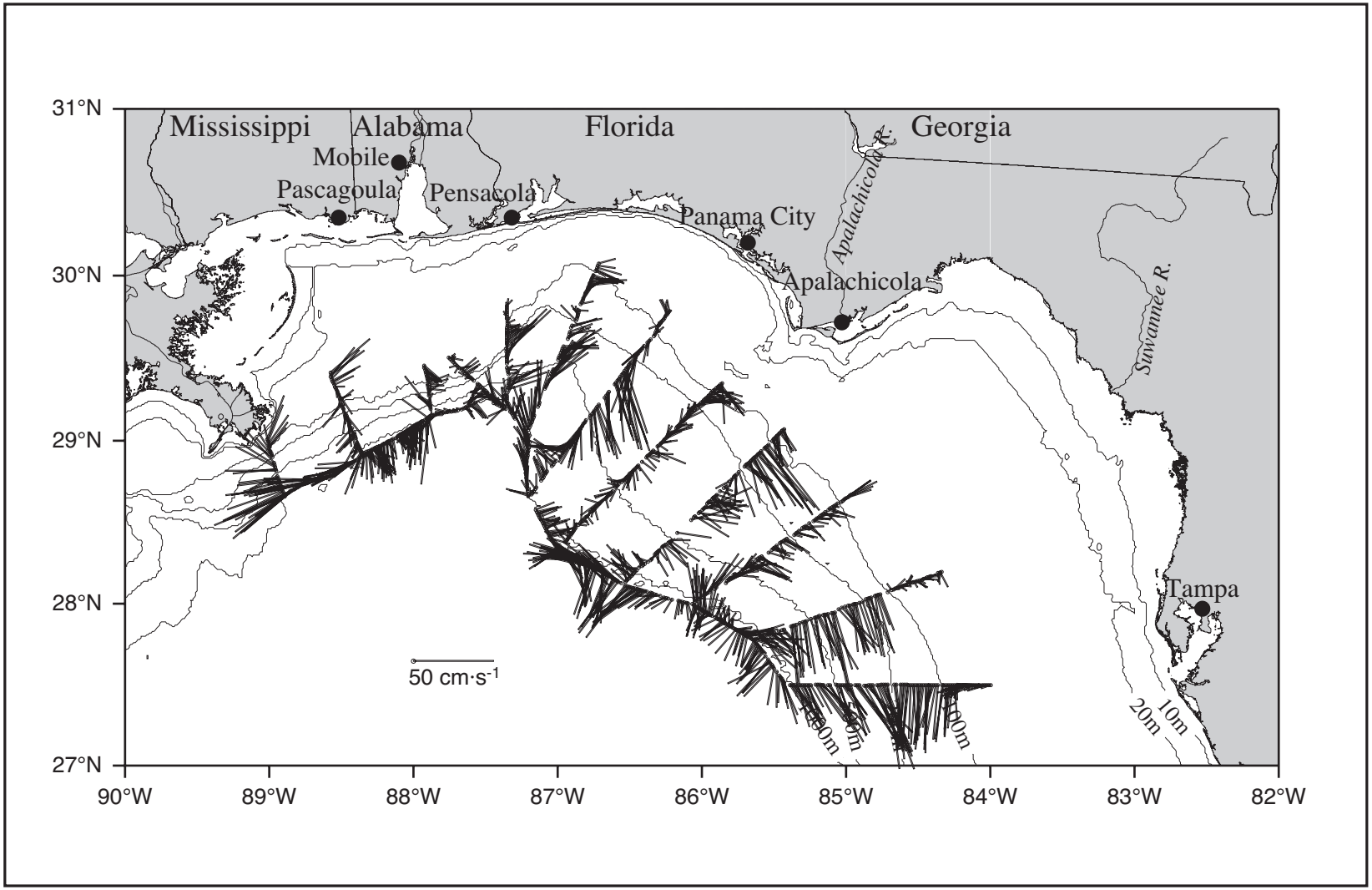

Figure B.2-3. ADCP-measured currents for the 4-m bin centered at 50 m on cruise N2 in May 1998.

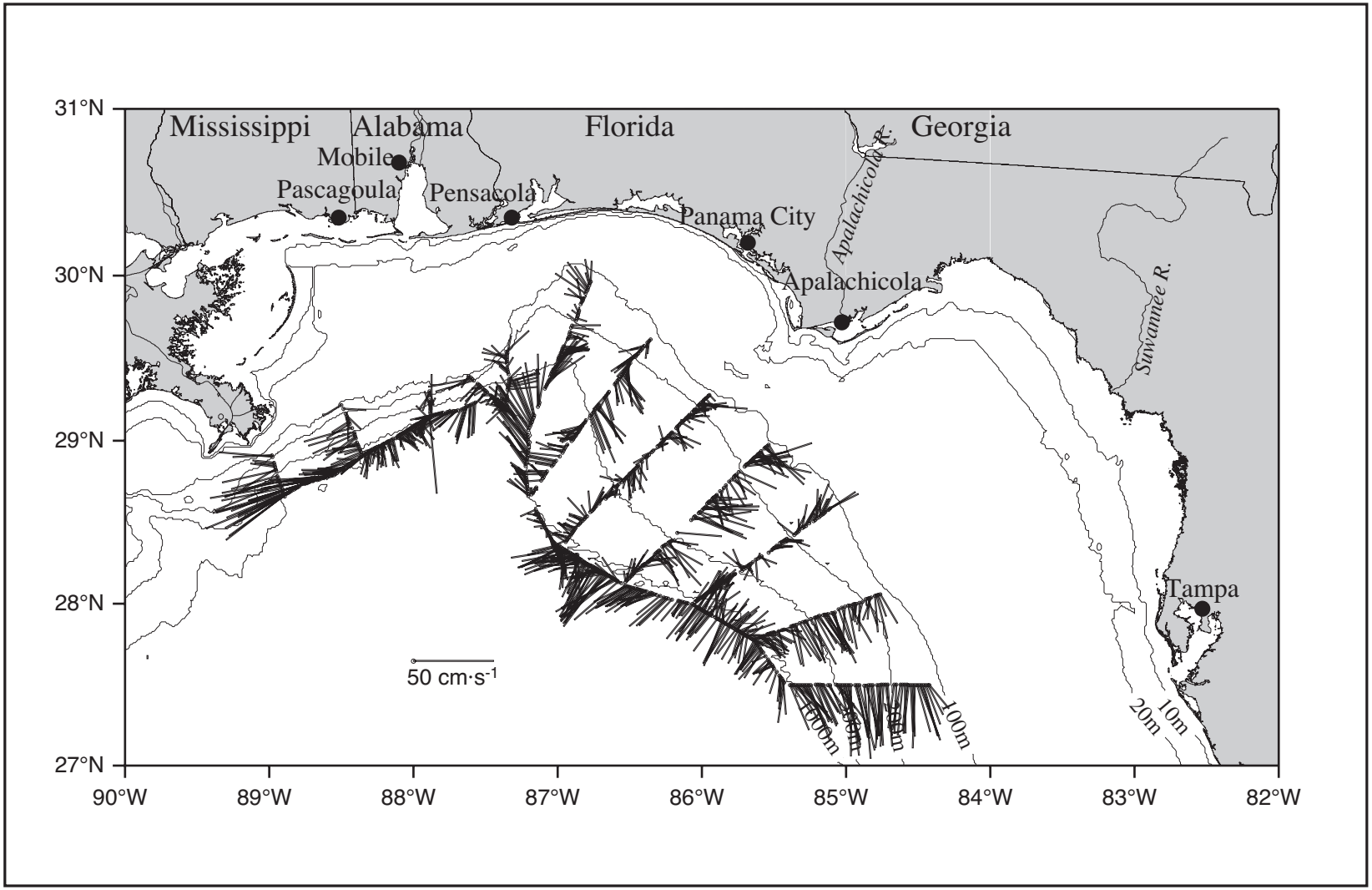

Figure B.2-4. ADCP-measured currents for the 4-m bin centered at 102 m on cruise N2 in May 1998.

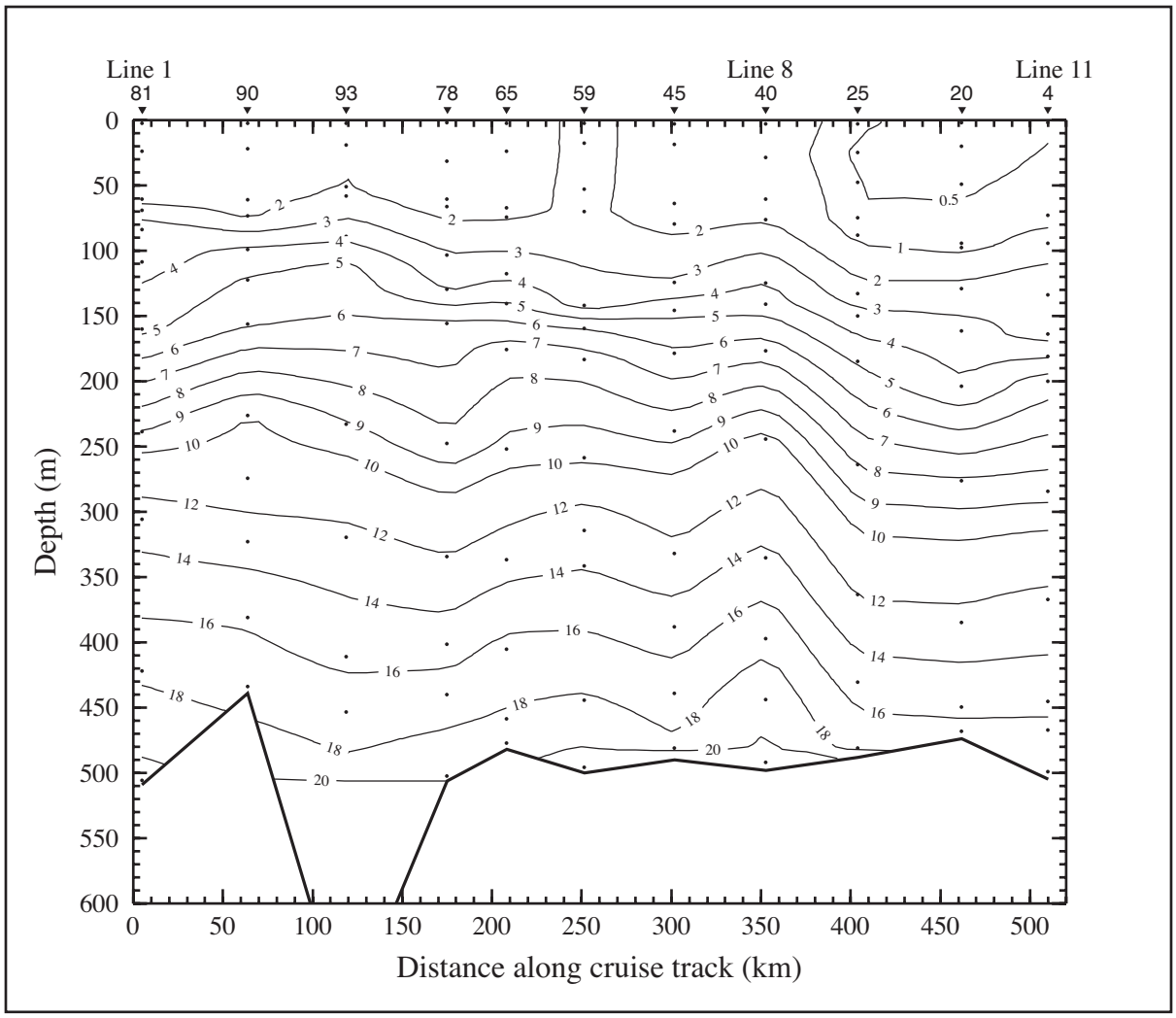

Figure B.2-5. Silicate (μM) along the 500-m isobath during cruise N2 in May 1998. Stations are shown on top axis.

Currents over the Mississippi-Alabama shelf tend to be upcoast (Louisiana to Florida), particularly along the 50-m isobath, with magnitudes reaching 50 $cm \cdot s^{-1}$ (Figure B.2-2). This upcoast flow turns somewhat offshore east of Cape San Blas and then runs just inshore of the 100-m isobath, with magnitudes < 50 $cm \cdot s^{-1}$. Flows in the nearshore of Big Bend are very weak.

B.3 Property Distributions

The conditions at the offshore boundary of the study area are shown in the potential temperature, salinity, and σ_θ vertical sections along the 1000-m isobath shown in Figures B.3-1 through B.3-3. In the vicinity of the two anticyclonic features observed in the SSH, ADCP, and geopotential anomaly maps, these vertical distributions do not clearly exhibit the dipping isolines, which are characteristic of many surface anticyclonic eddies. There is, however, a down dip in the σ_θ isopleths in deeper waters (> 500 m) at both stations 4 and 5 and near station 10. This suggests that, consistent with the fact that they were spinning up just prior to and during the cruise, the eddies are relatively weak. Little deep water appears to be reaching the shelf, as evidenced by the discontinuous lenses of 36.4 salinity water near 100 m and the small lens of 36.6 salinity water at stations 22 and 2. The influence of river water can be seen in the relatively low density waters of the upper 20 m between stations 80 and 79, associated with lines 1 through 4, respectively.

The high river discharge onto the Mississippi-Alabama shelf resulted in a large region of low-salinity surface water. The horizontal extent, core, and possible sources of the low salinity water lens may be deduced from the surface (3 m) salinity distribution shown in Figure B.1.2-1. Note the tongue of freshest water extending eastward from the Mississippi Sound/Mobile Bay area. The vertical extent of the relatively low salinity water also varies. West of Mobile Bay, the relativity low salinity water (≤ 34) is limited to the upper 10 m or less, with the freshest waters observed at the inshore stations—evidence of local river sources for this water (Figure B.3-4, upper). East of Cape San Blas on lines 8-11, the freshest water in the surface layers also was found mainly at the inshore stations (Figure B.3-4, lower), but with vertical extents of 10-20 m. On lines 4-7, the low-salinity surface water was to up to 20 m thick over the middle shelf; the lowest salinity surface waters were found in a longshore lens some 50 km offshore near the 100-m isobath (Figure B.3-4, middle). This could have been caused by nearshore upwelling moving surface water offshore. Advection from the west due to the anticyclonic circulation over DeSoto Canyon is an unlikely cause because the anticyclone was not well-developed before the cruise. The vertical distributions of salinity exhibit a strong halocline in the upper 20 m over the region west of Cape San Blas.

In addition to the strong near-surface salinity gradient over the shelf west of Cape San Blas, there is indication of upwelling of cool bottom waters near the head of DeSoto Canyon. The bottom distribution of temperature (Figure B.3-5) shows a maximum inshore penetration of cool bottom water near the head of DeSoto Canyon (line 5). The spread of cool water onto the shelf is clearly seen by noting the area covered between the 18° and 19° isotherms at the bottom. Waters offshore of Alabama are warmer by as much as 2° to 3° C than those off west Florida. Vertical sections of hydrographic properties provide clear evidence that onshore, near-bottom flow, extending in most cases to the innermost stations (10-m isobath), had occurred prior to cruise N2. The vertical distributions of temperature on line 5 and along the 100-m isobath are shown in Figure B.3-6. The distribution on line 5, which is characteristic of the distributions for lines 4-7, shows cooler (18° to 19°C) water at the bottom at the innermost stations. This suggests that upwelling had been strong prior to the time of the cruise. Southeast of Cape San Blas (lines 8-11) this onshore movement generally

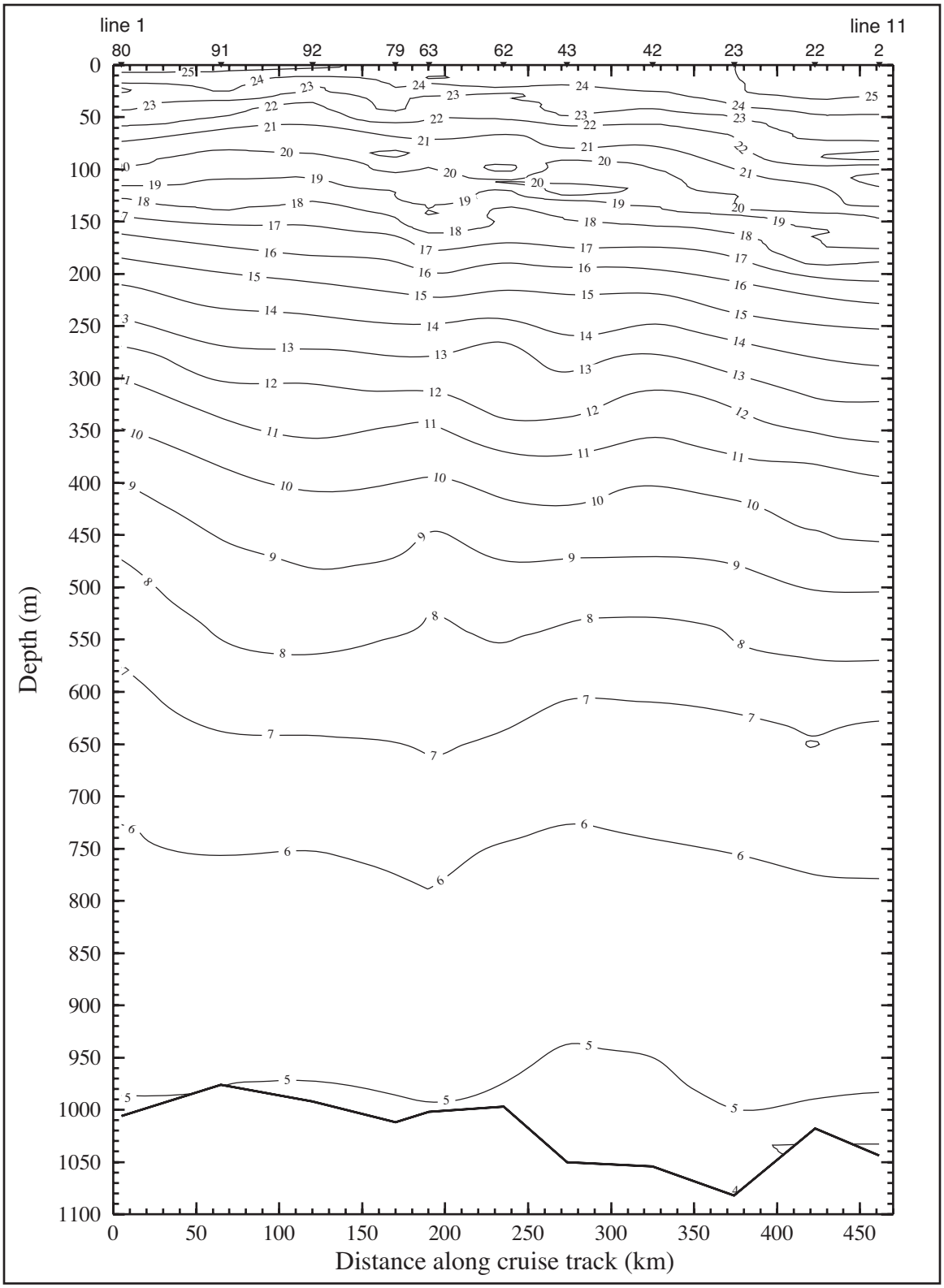

Figure B.3-1. Potential temperature (°C) along the 1000-m isobath of cruise N2, 5-16 May 1990. Stations are shown on top axis.

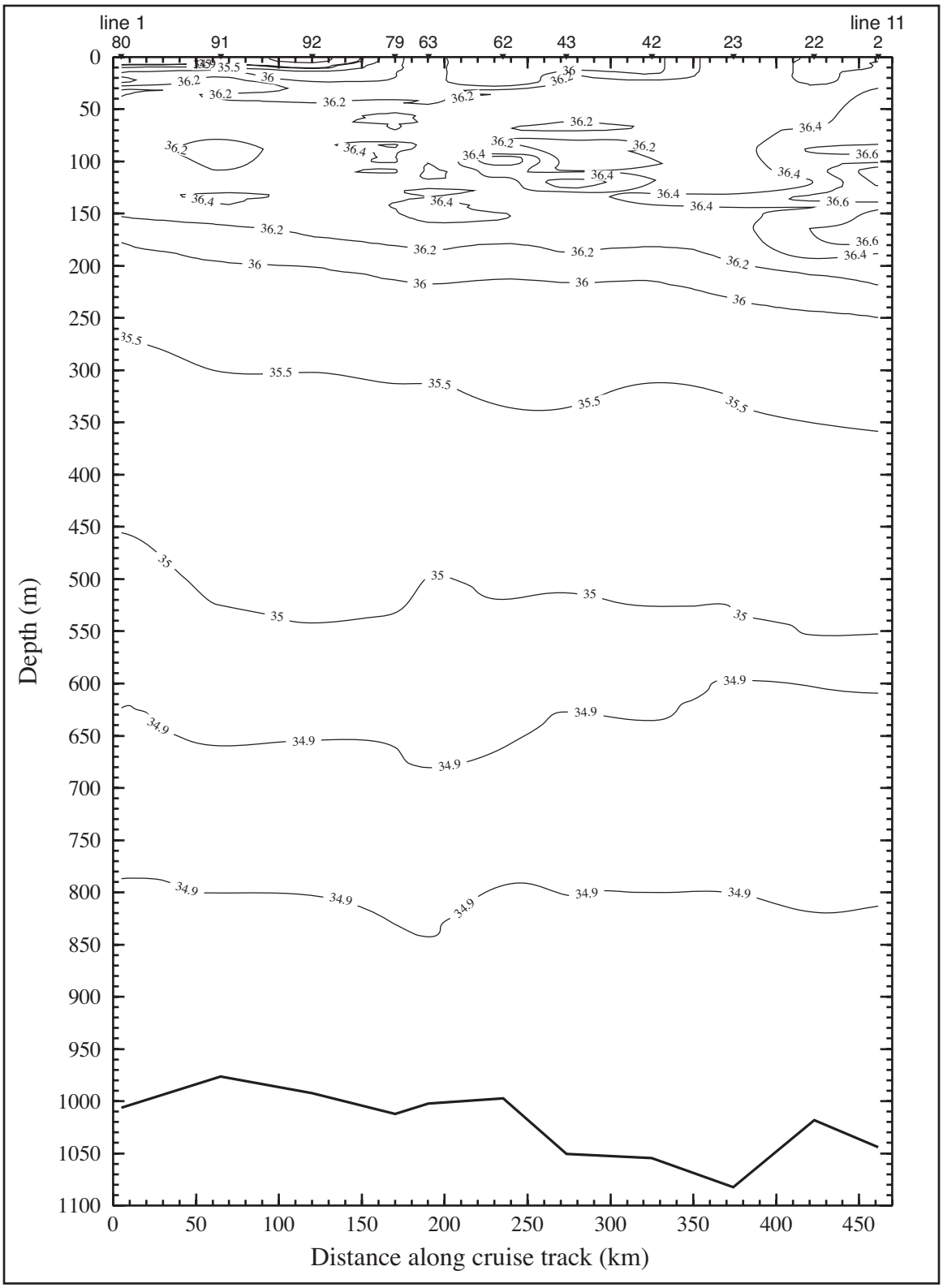

Figure B.3-2. Salinity along the 1000-m isobath of cruise N2 in May 1998. Stations are shown on top axis.

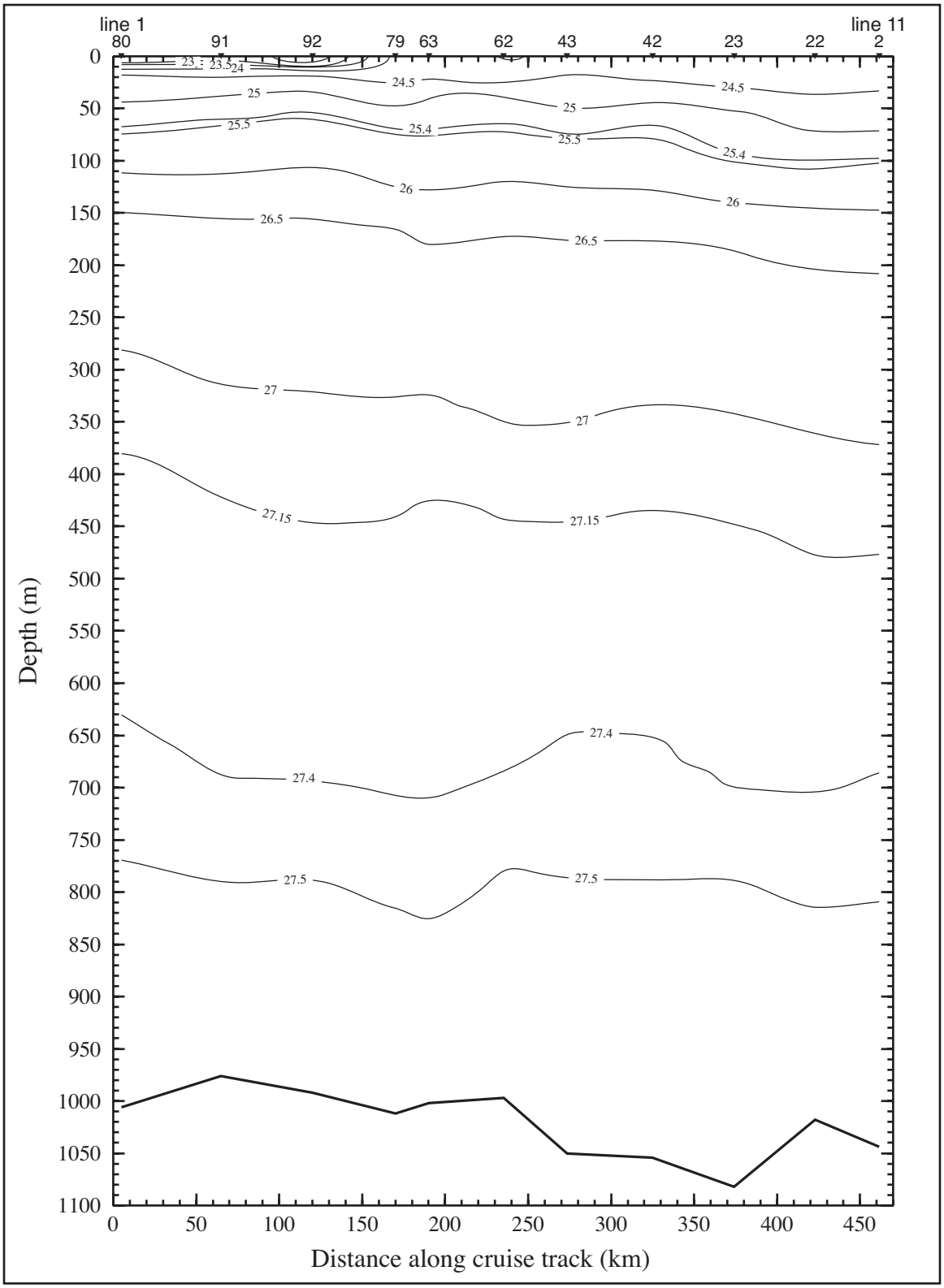

Figure B.3-3. Density anomaly (σ_θ in kg·m^{-3}) along the 1000-m isobath of cruise N2 in May 1998. Stations are shown on top axis.

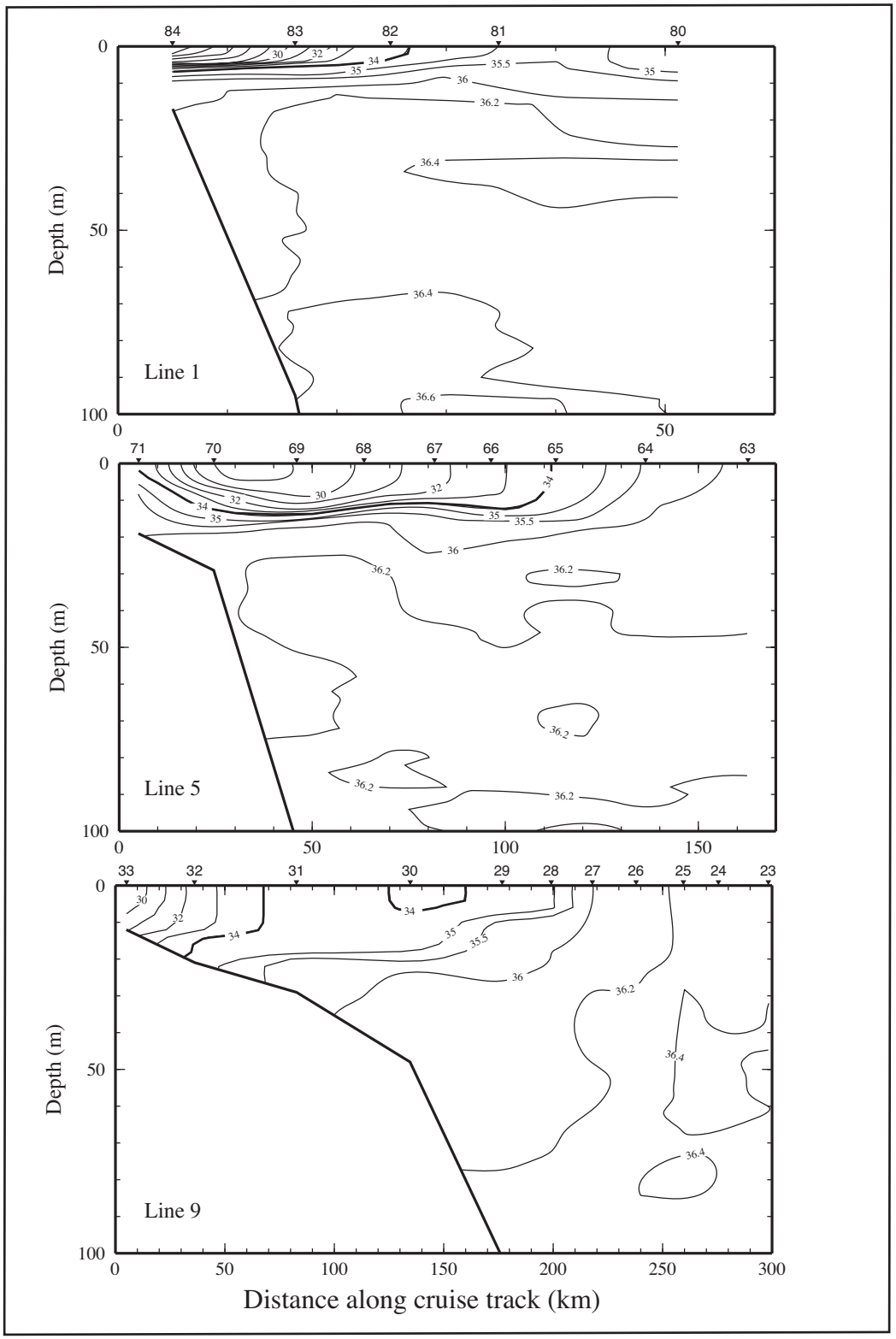

Figure B.3-4. Salinity on lines 1, 5, and 9 during cruise N2 in May 1998. Stations are shown on top axis.

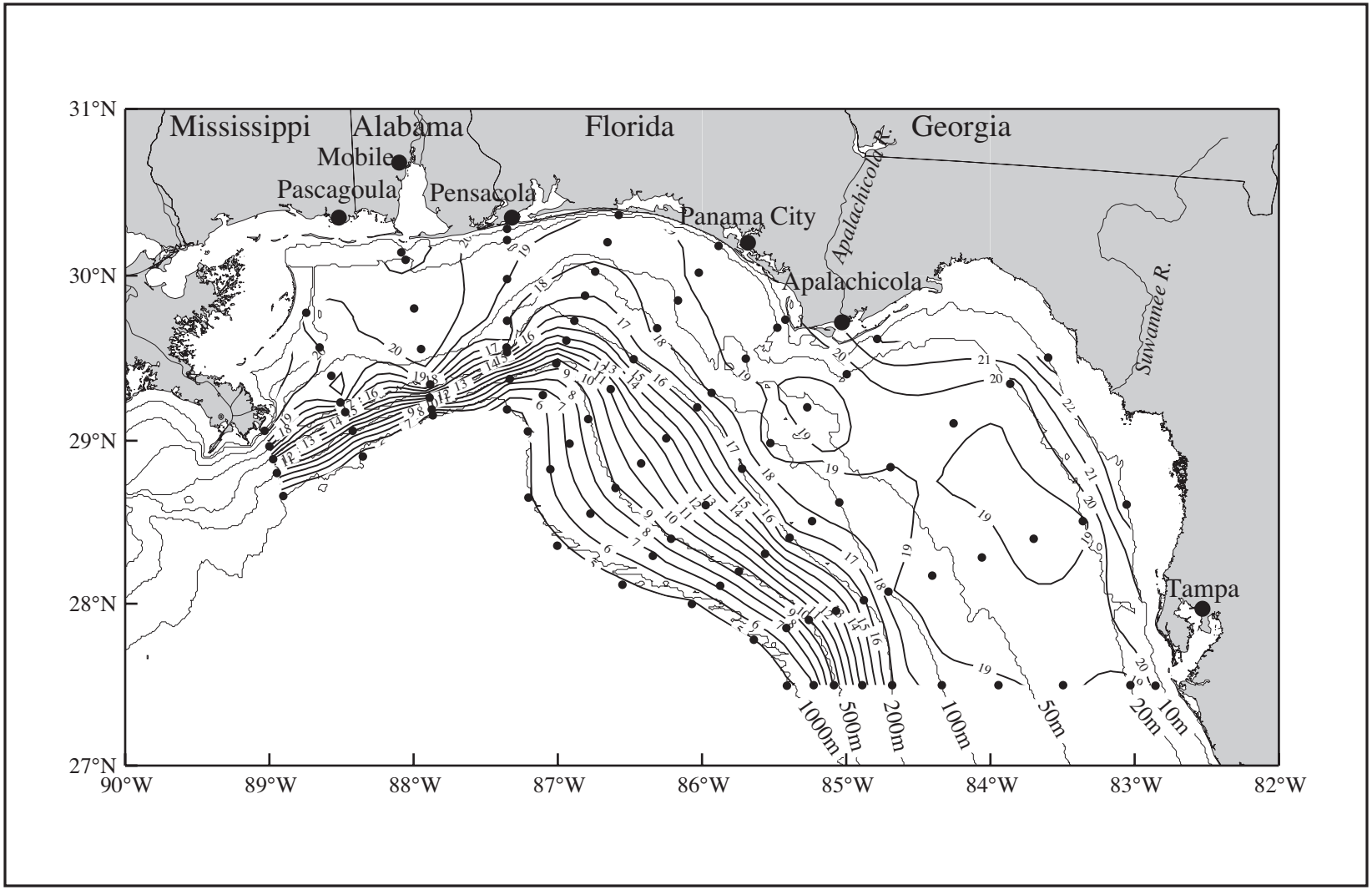

Figure B.3-5. Potential temperature (°C) from the near-bottom observations on cruse N2 in May 1998.

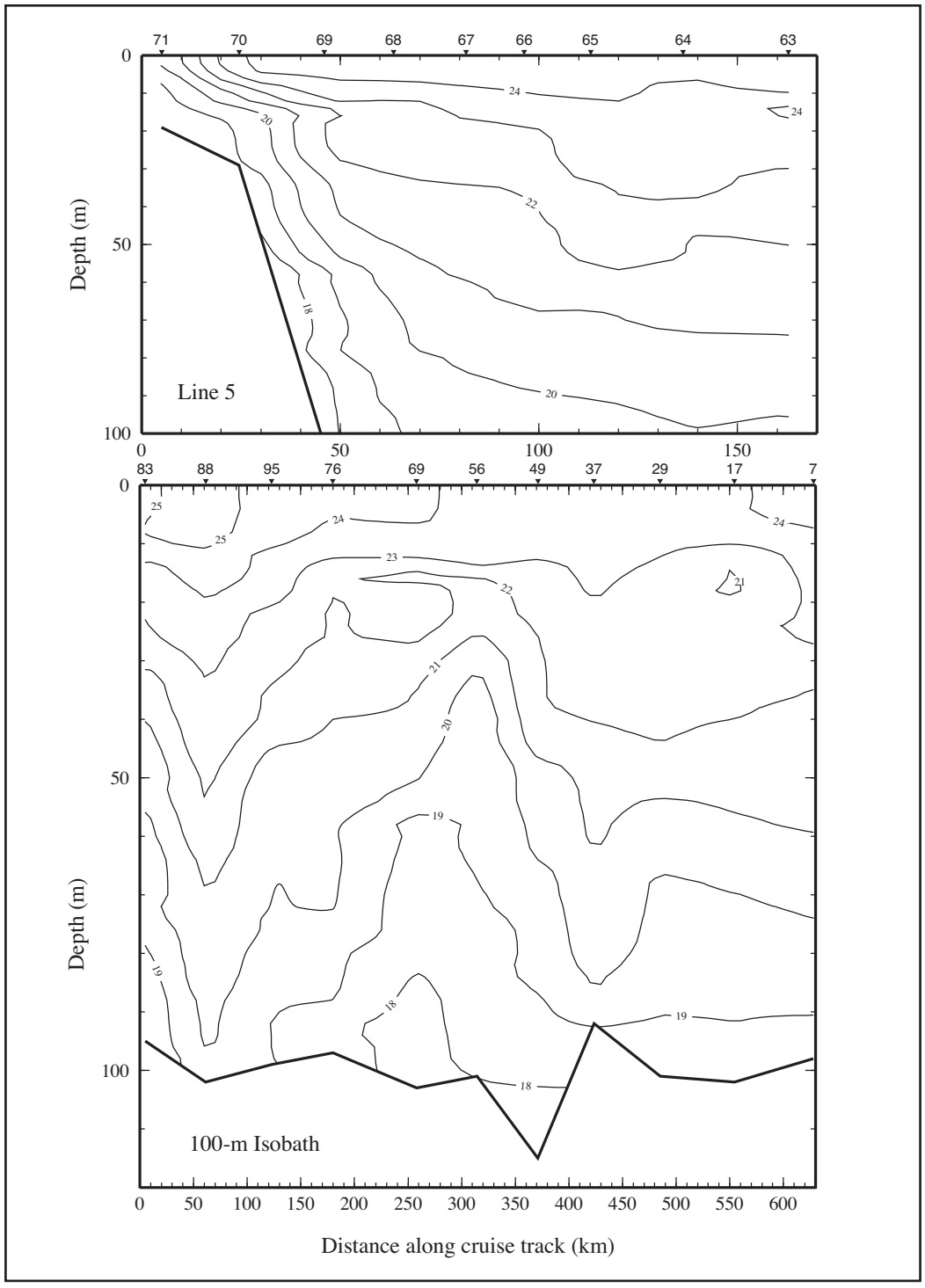

Figure B.3-6. Potential temperature (°C) on line 5 (top) and along the 100-m isobath (bottom) on cruise N2 in May 1998. Stations are shown on top axes. On the 100-m isobath, line 1 is at the left station and line 11 is at the right.

did not extend to the shallowest stations. The distribution along the 100-m isobath shows upwelling of the cool water at the apex of DeSoto Canyon. Nowlin et al. (2000b) examined time series of temperatures and currents from moorings set and recovered by Science Applications International Corporation (SAIC; 1998) in the DeSoto Canyon from early April to early August 1998. They found two pulses with near-bottom temperatures lower by several degrees than before or afterwards were recorded in mid and late April near the bottom over the 100-m isobath. They also found that the cool pulses were usually associated with flows directed toward the head of the canyon and toward shallower depths. They concluded these intrusions likely set the stage for the cool bottom water observed over the outer west Florida shelf during cruise N2.

The combination of cool bottom water, seasonal warming of surface waters, and the lens of lower salinity surface water produced a very strong pycnocline over the inner and mid shelf regions. West of Cape San Blas the pycnocline was much stronger than to the east; compare the distribution for lines 3 and 5 with that for line 9 (Figure B.3-7). It is likely that this stability would have inhibited vertical mixing.

Stratification due to low salinity surface waters and seasonal heating, lack of mixing, and enhanced primary production is well known to lead to hypoxia (dissolved oxygen concentrations of ≤ 1.4 mL·L^{-1}) or near-hypoxic conditions on the Louisiana shelf (Wiseman et al. 1997; Nowlin et al. 1998a). During cruise N2 many bottom dissolved oxygen values were near 3 mL·L^{-1}, and values approached 2 mL·L^{-1} near Chandeleur Sound (Figure B.3-8). Dissolved oxygen values at the bottom were not particularly low east of Cape San Blas. That could have been due to the difference in stratification in the two regions, with stronger pycnoclines observed west of Cape San Blas. The band of relatively low bottom dissolved oxygen seen centered around the 500-m isobath reflects the intersection of the core of Tropical Atlantic Central Water with the bottom.

The distributions of near-surface (3.5 m) nutrients on cruise N2 show a high loading in relatively low salinity surface waters associated with river discharge. The near-surface distribution of nitrate is highest on lines 1, 2, and 3 (Figure B.3-9). The near-surface distributions of silicate and phosphate (not shown) show good correspondence with that for nitrate. Bottom nutrient distributions observed over the mid and inner shelf appear elevated at locations corresponding to the cooler upwelled waters. As an example, higher nitrate values at the bottom (Figure B.3-10) correspond well with cooler bottom waters (Figure B.3-5). The bottom distribution shows the effects of onshore movement of nutrient rich bottom waters. Comparison of the bottom nitrate distribution (Figure B.3-10) with the bottom oxygen distribution (Figure B.3-8) show lower values of dissolved oxygen correspond with higher values of nitrate. In general distributions of phosphate and silicate mirror those of nitrate with the notable exception that quite elevated silicate values were observed at the bottom, as well as near surface, on the inshore portion of the westernmost region (Figure B.3-11, top panel shows nitrate, middle panel shows silicate). Such high values are not unexpected, since quite high dissolved silicon is associated with low salinity river waters in general, and the Mississippi in particular (Liss 1976), and the inshore waters of the westernmost portion of the study area were characterized by low salinity river waters during cruise N2. Associated with these elevated bottom silicates are lower percent transmission values indicative of higher particulate concentrations in the water (Figure B.3-11, lower panel).

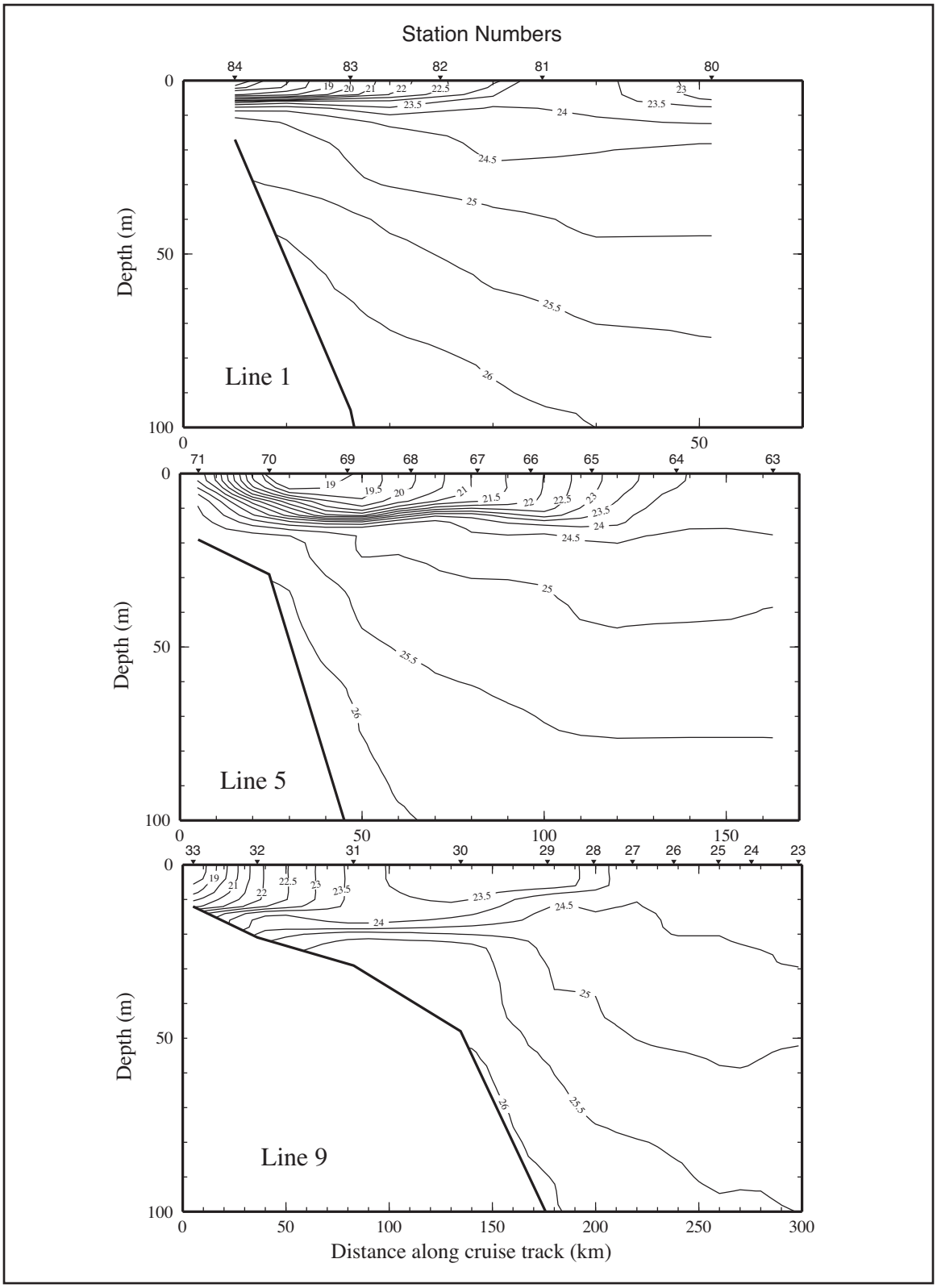

Figure B.3-7. Density anomaly (σ_θ in kg·m^{-3}) on lines 1, 5, and 9 on cruise N2 in May 1998.

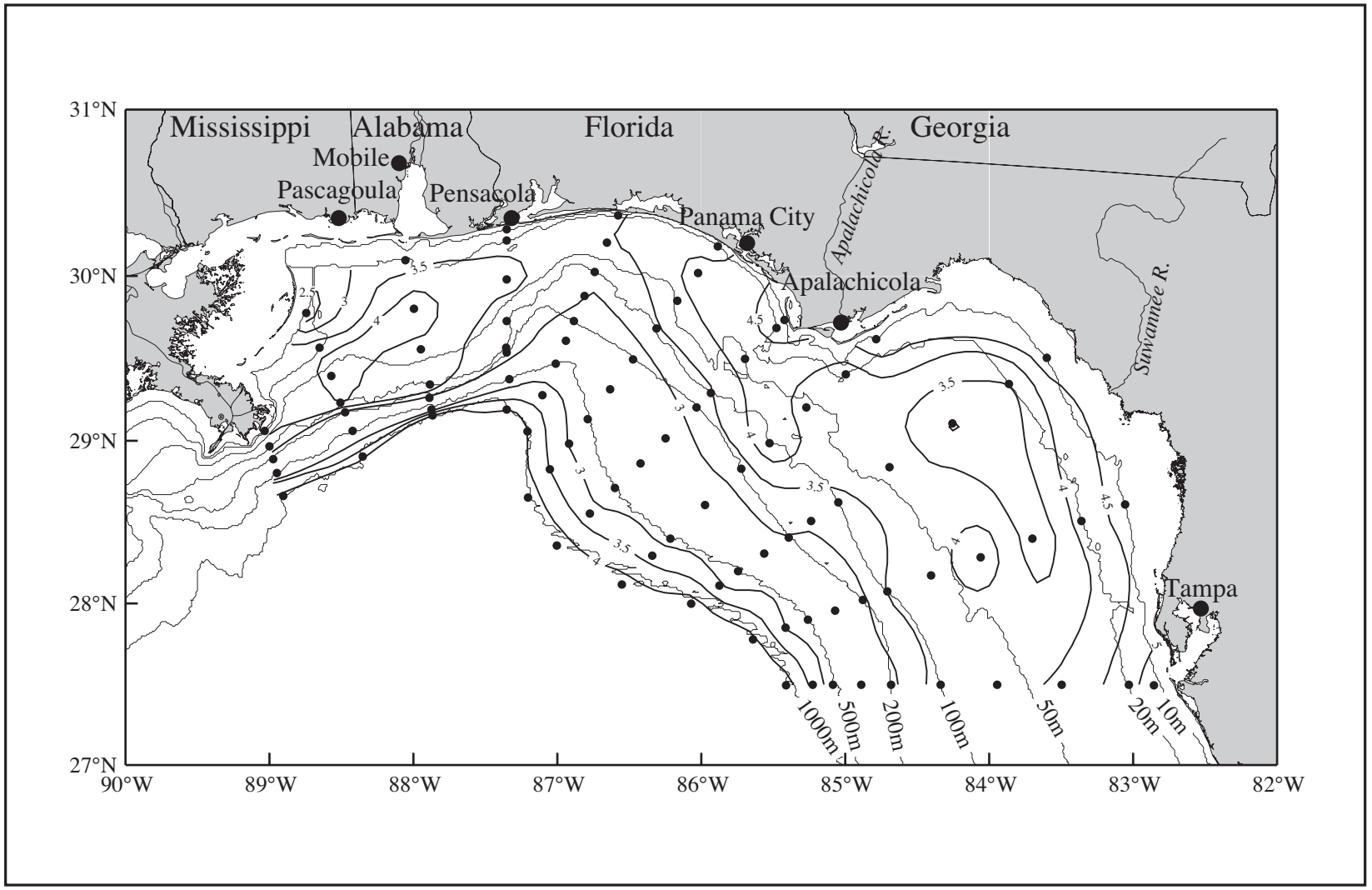

Figure B.3-8. Dissolved oxygen ($mL \cdot l^{-1}$) from the near-bottom observations on cruise N2 in May 1998.

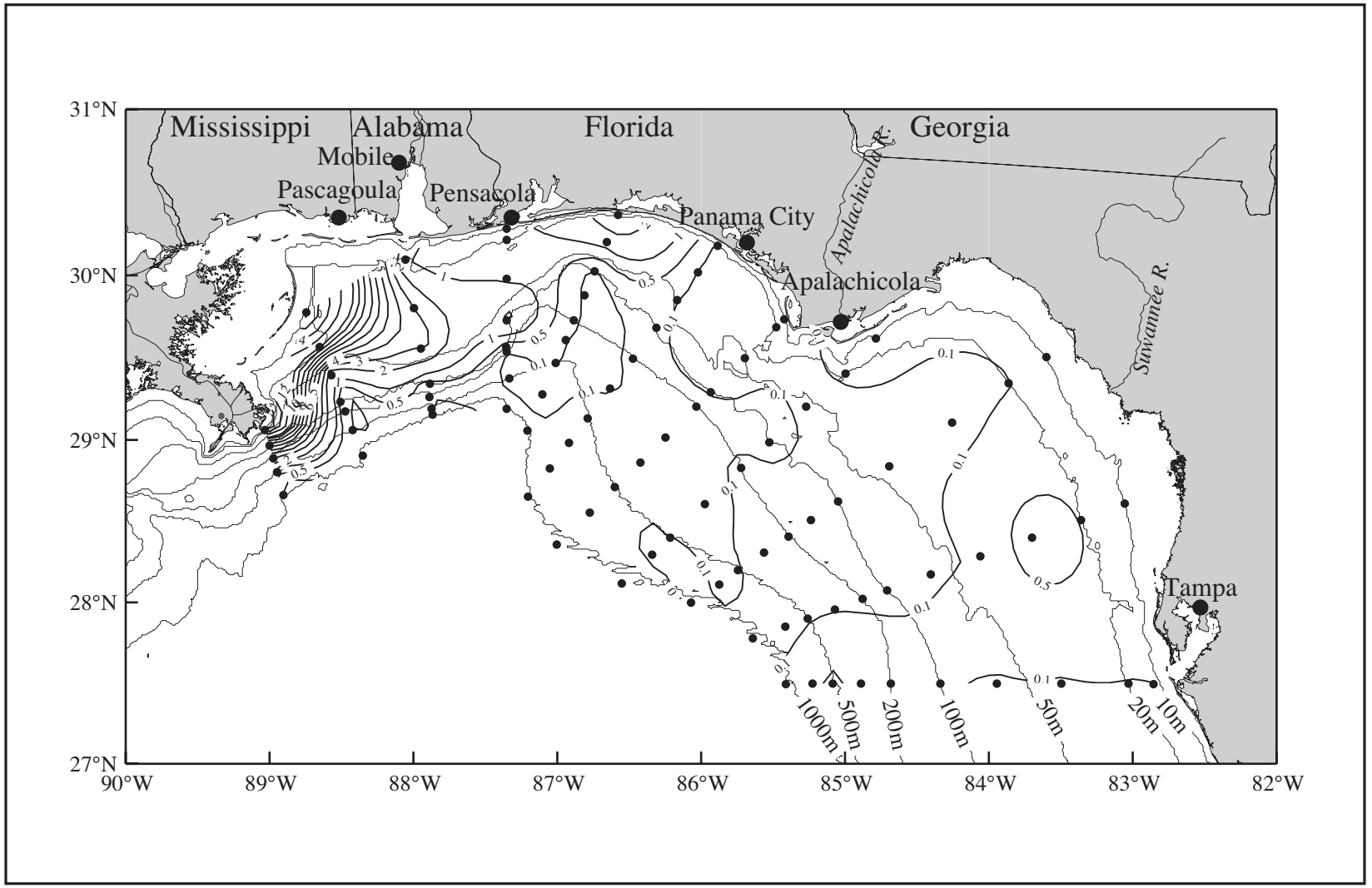

Figure B.3-9. Nitrate (μM) from the near-surface (~3.5 m) observations on cruise N2 in May 1998

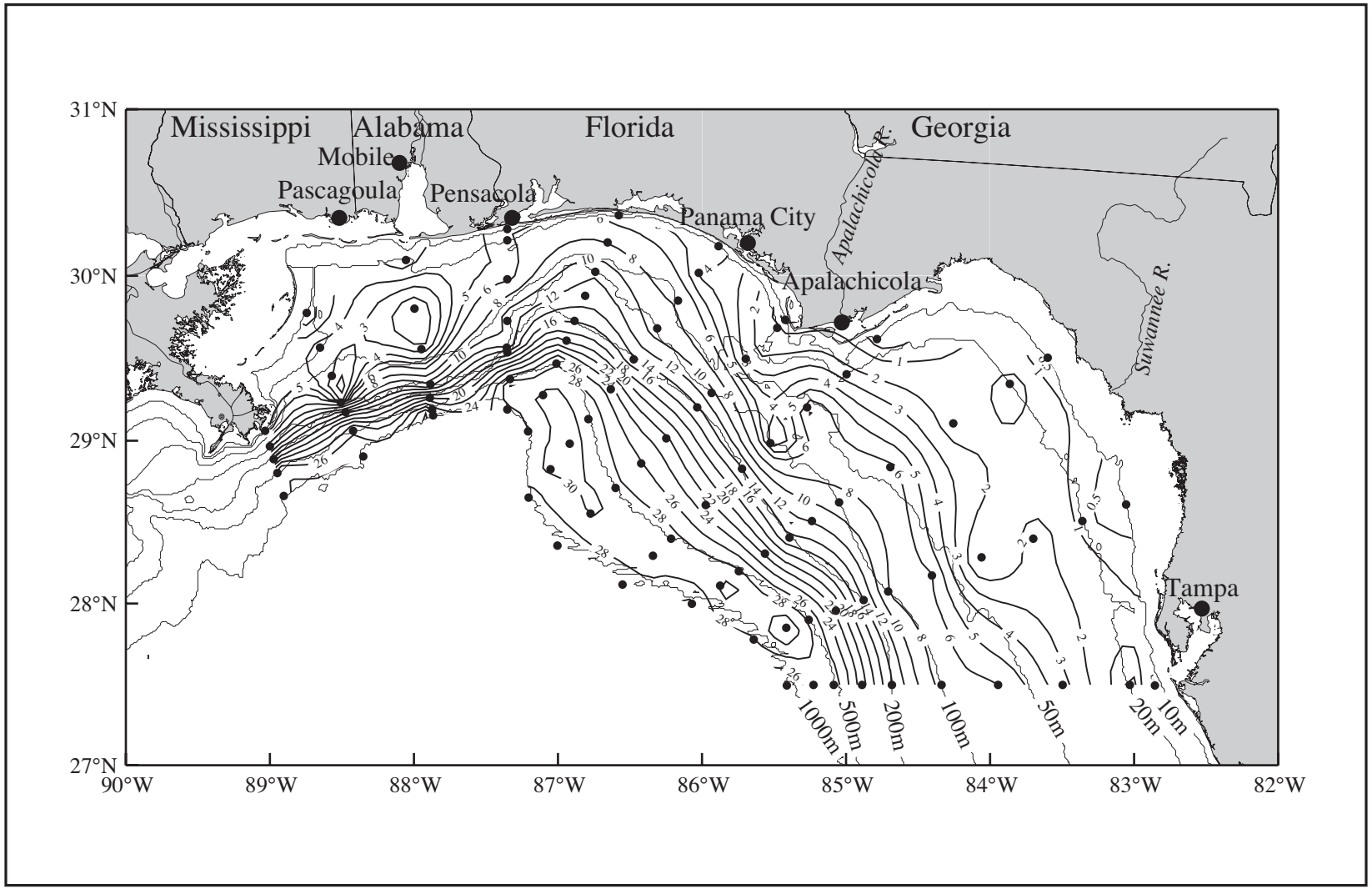

Figure B.3-10. Nitrate (μM) from the near-bottom observations on cruise N2 in May 1998.

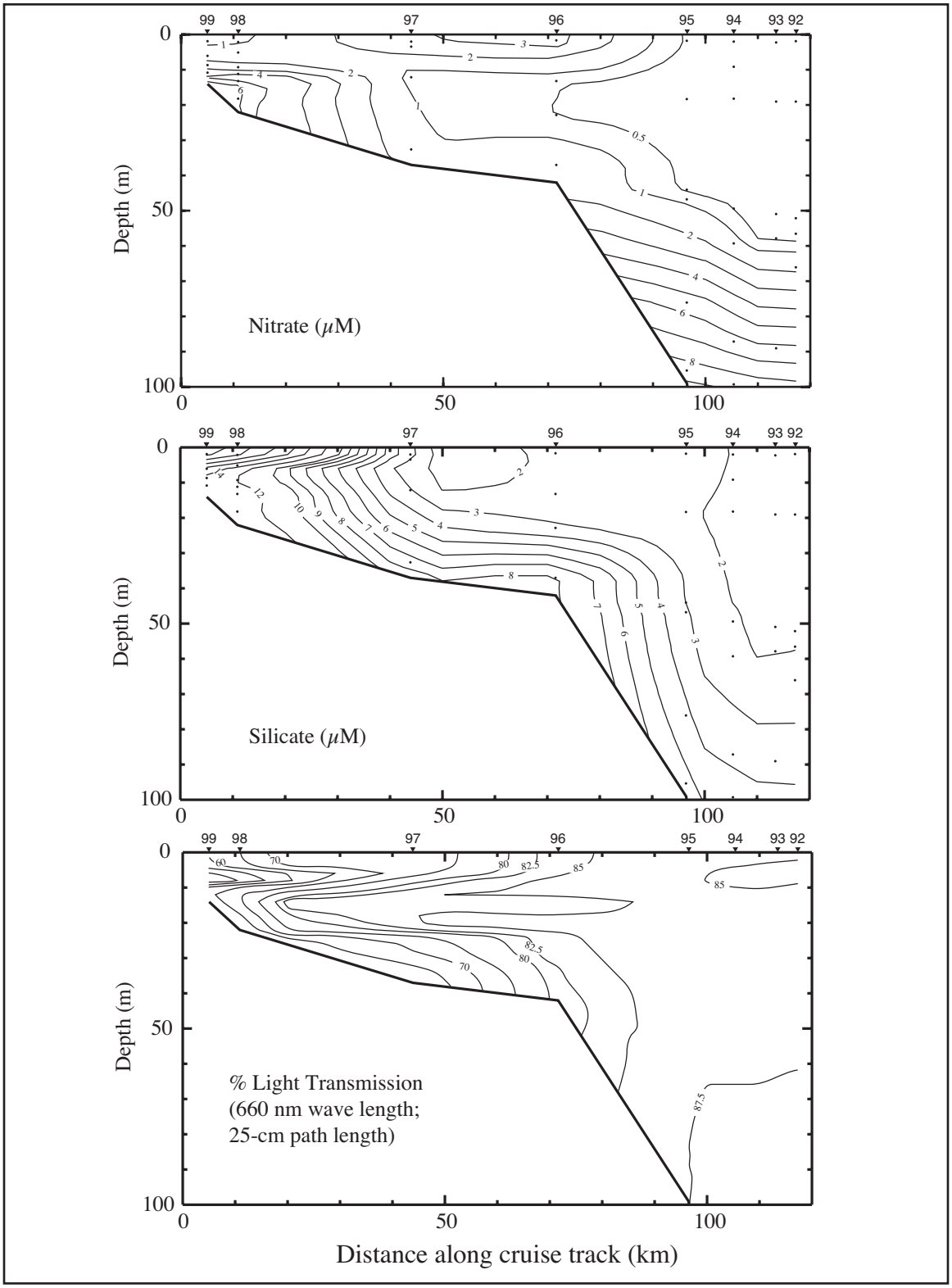

Figure B.3-11. Nitrate, silicate, and percent transmission on line 3 on cruise N2 in May 1998. Stations are shown on top axes.

APPENDIX C
SUMMARY OF CONDITIONS DURING CRUISE N3

Cruise N3 was a summer cruise conducted 25 July to 6 August 1998. Stations began with the most seaward station on line 11 and ended with the most inshore station on line 1. Figure C-1 shows the station locations and gives the CTD station numbers, which are sequential by sampling order.

C.1 Forcing Functions

C.1.1 Winds

The mean wind field and principal axes of variance for the period of cruise N3 are shown in Figure C.1.1-1. The methodology used is that of Wang et al. (1998) applied to hourly observations at meteorological stations located as shown in the figure. During cruise N3, mean winds were weak (< 2-3 $m \cdot s^{-1}$). Directions generally were to the west over the Mississippi-Alabama shelf and to the north or northwest over the west Florida shelf. The variance ellipses indicate the winds were variable principally in the east-west direction at about ± 5 $m \cdot s^{-1}$ or less. From 25 July through 1 August, there was a high over the northern Gulf, and winds in the NEGOM study area were generally < 5 $m \cdot s^{-1}$ and varied directionally in response to the movement of the high (e.g., Figure C.1.1-2). On August 2 there was a wind shift in the NEGOM study area to strong easterlies, in response to passage of a low in pressure into the region, that continued through the N3 cruise. Wind speeds reached 10 $m \cdot s^{-1}$.

C.1.2 River Discharge

Daily discharge rates for the Mississippi River were above the long-term mean for January-August 1998; they exceeded the mean by more than one standard deviation during most of July (Figure 3.1.2-2, upper panel). Other major rivers entering the region discharged at rates below their long-term means for June-August (see Section 3.1.2).

The effects of these discharge rates are seen in the surface (3 m) salinity distributions observed during cruise N3 (Figure C.1.2-1). Lowest values were observed nearshore east of Pass a Loutre and in a mesoscale feature located over the 500-m isobath on the east side (wall) of DeSoto Canyon. Eastward from Pensacola, surface salinity values generally decreased offshore, with minimum observed values over the 500- to 1000-m isobaths.

The distribution of relatively low salinity water is seen clearly also in the near-surface (3.5 m) patterns of silicate and chlorophyll *a* observed on cruise N3 (Figures C.1.2-2 and C.1.2-3). This pattern is confirmed by the SeaWIFs-derived chlorophyll *a* distribution averaged for 28 July–6 August, 1998 (not shown). High silicates are associated with less saline waters, e.g., east of the Mississippi Delta and over the outer shelf and slope southwest of Cape San Blas. Highest chlorophyll *a* values are seen just east of the Mississippi Delta.

C.1.3 SSH Fields Adjacent to the Shelf

From 1-15 July 1998, SSH fields show an anticyclone having double highs with its axis elongated NW-SE from the 200-m isobath southeast of the Mississippi River Delta (near 29°N, 88.5°W) to the west Florida terrace (near 27.5°N, 86.5°W). See Figures 3.2.3-10 and 3.2.3-11. Between 15 July and 8 August, the feature strengthened (the two highs coalesced) and its southeastern edge moved somewhat westward to about 86°W (Figures 3.2.3-11 and 3.2.3-12).

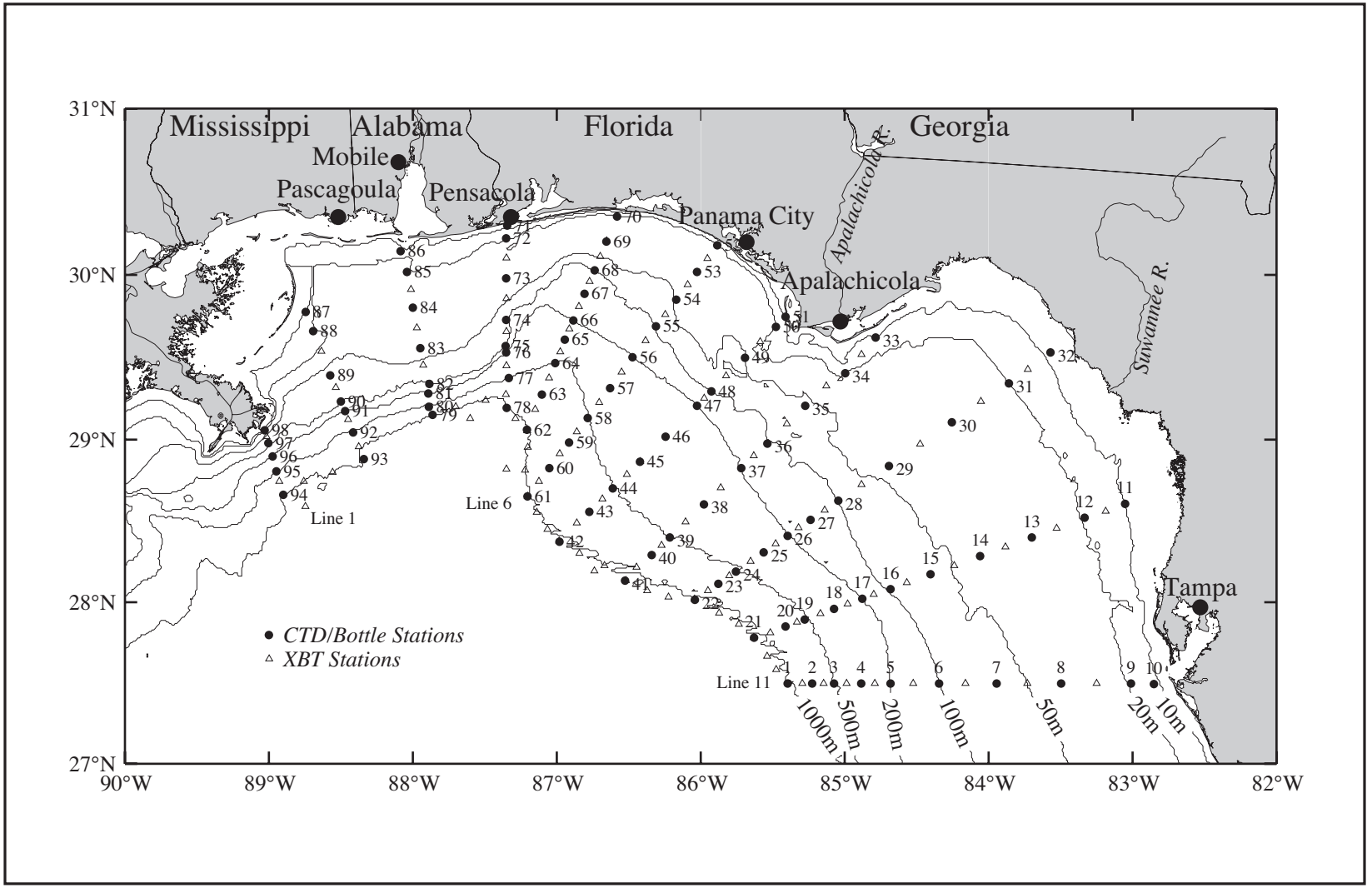

Figure C-1. Station locations for cruise N3 conducted on 25 July - 6 August 1998. CTD stations (solid circles) are numbered; XBT stations (open triangles) are not.

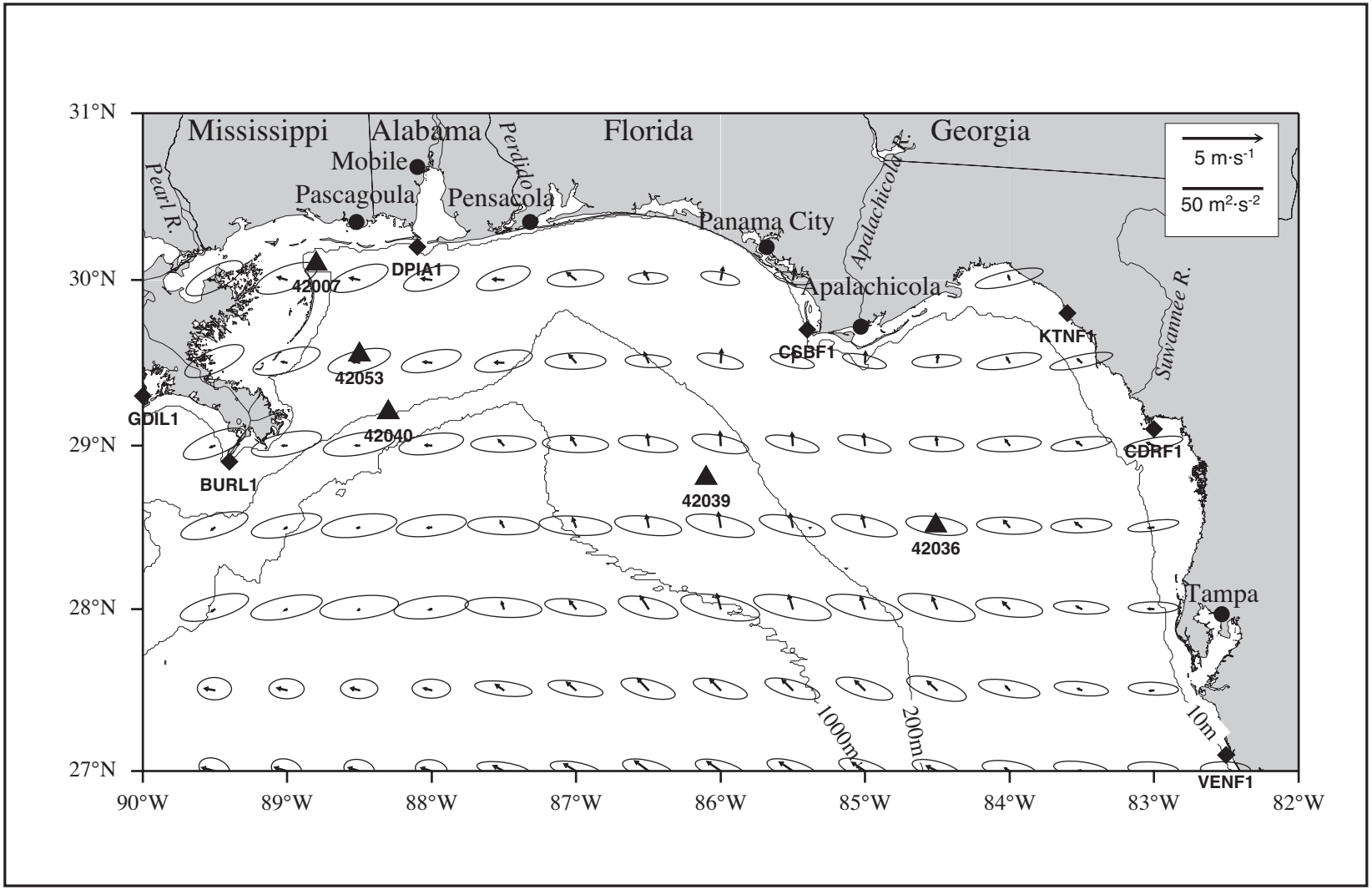

Figure C.1.1-1. Vector mean winds and variance ellipses for cruise N3 from 25 July to 6 August 1998.

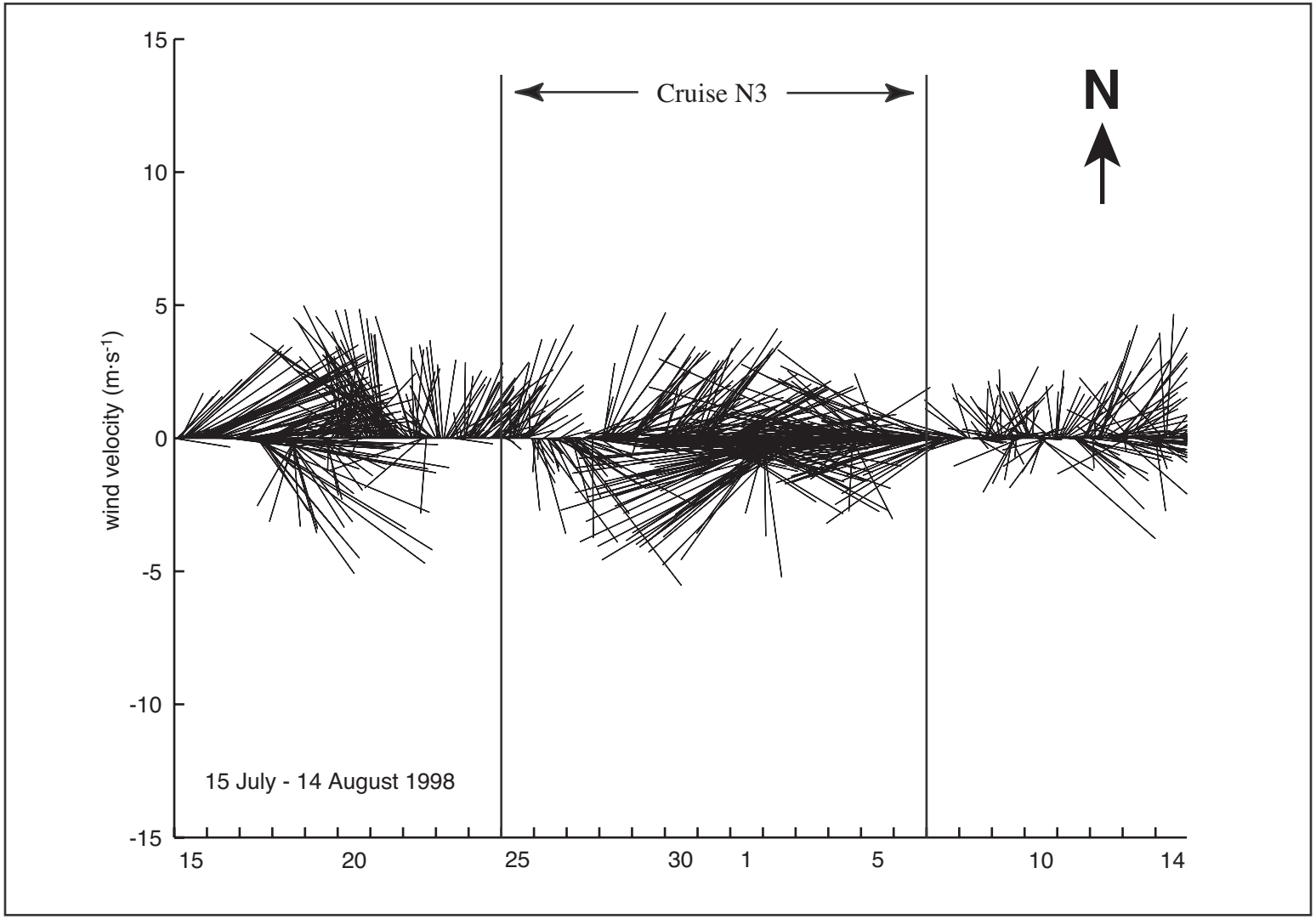

Figure C.1.1-2. Vector stick plot of wind at meteorological buoy 42040 for July/August 1998. Gauge height is 10 m.

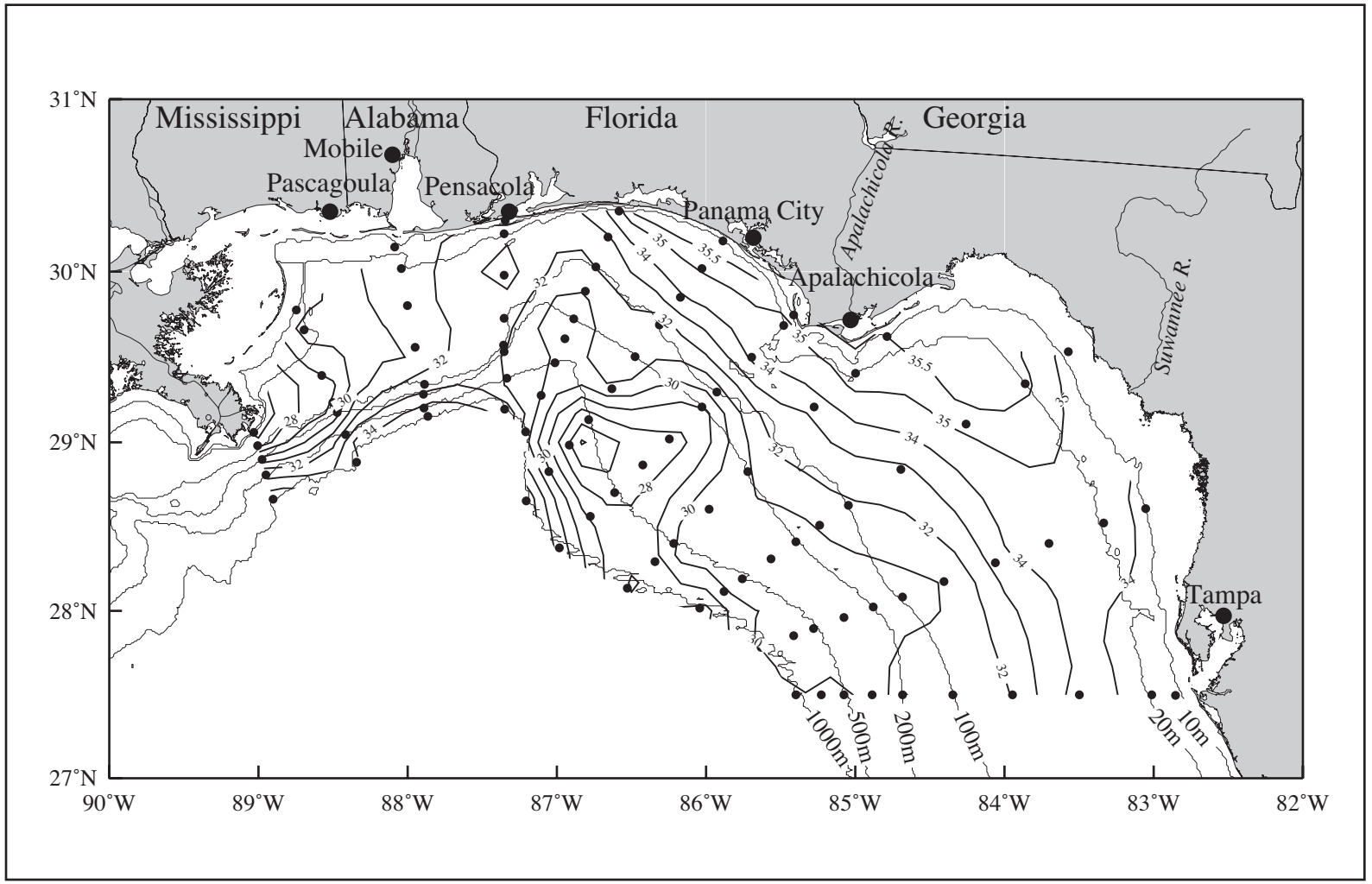

Figure C.1.2-1. Salinity, derived from CTD data, at 3.5 m on cruise N3, 25 July - 6 August 1998.

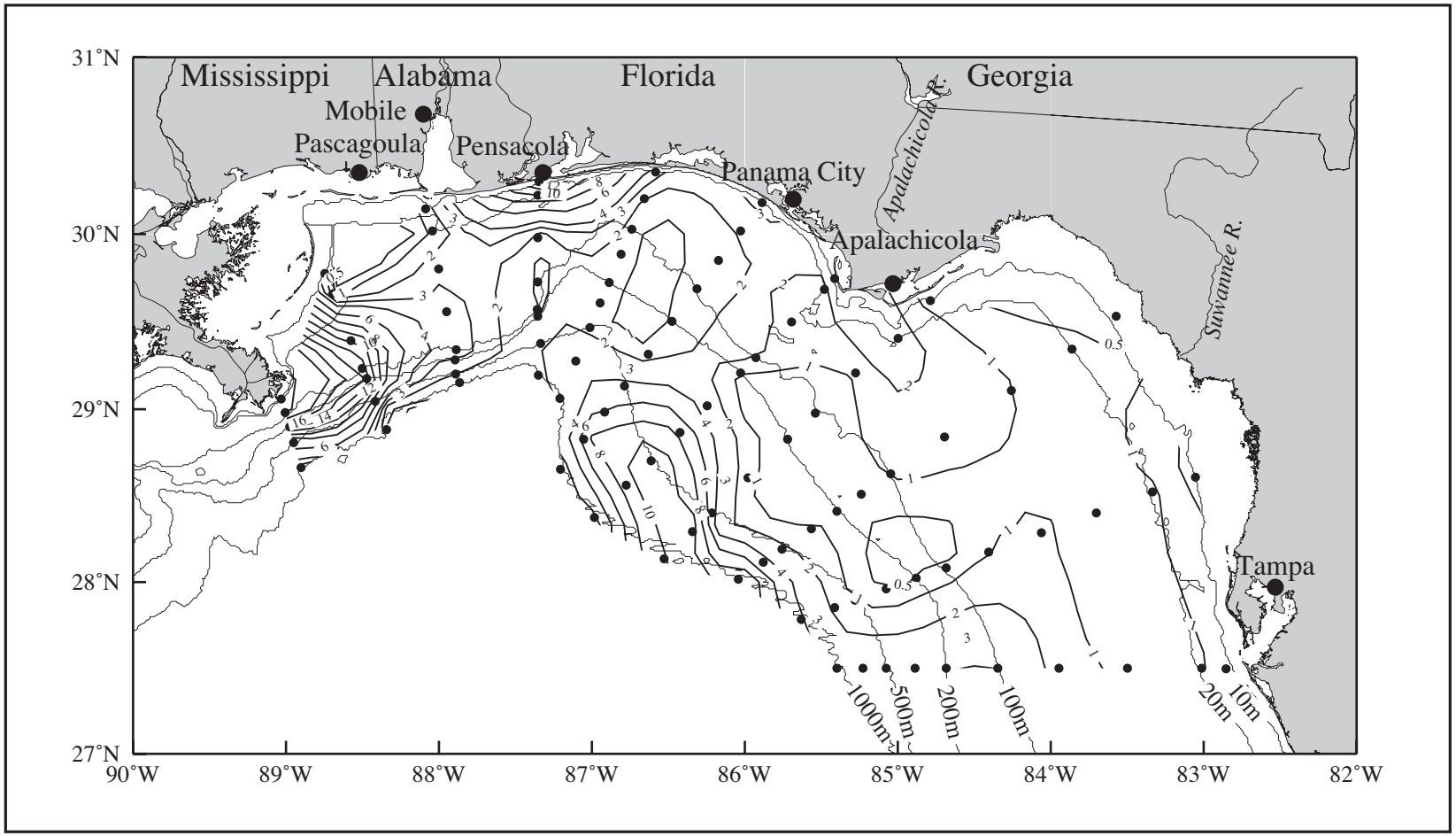

Figure C.1.2-2. Silicate (μM) at 3.5 m on cruise N3, 26 July - 6 August 1998.

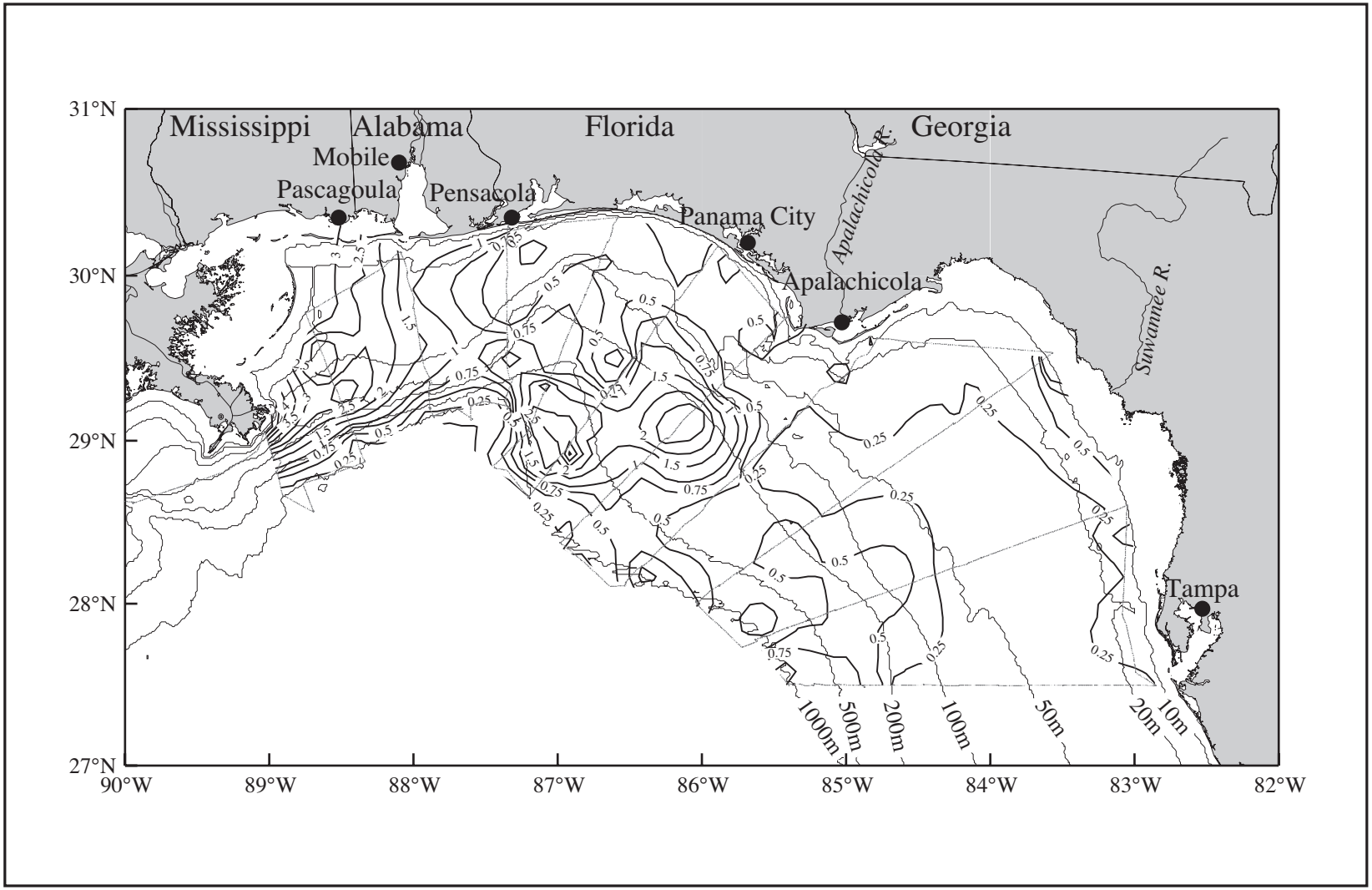

Figure C.1.2-3. Chlorophyll *a* ($\mu g \cdot L^{-1}$) at ~3 m calculated from flow-through fluorescence on cruise N3 in July-August 1998.

During this period its northwestern limb seemed to encroach on the shelf southeast of the delta while its center strengthened near 28.5°N, 87.5°W.

The SSH field for 5 August 1998 is shown in Figure C.1.3-1. This would indicate strong eastward flow over the slope (and perhaps the outer shelf) off Mississippi and Alabama as well as strong southeastward flow over the west Florida slope southeast of DeSoto Canyon. This results in transport of relatively low salinity water associated with the Mississippi River to the outer shelf and slope. To the southwest and south southeast of the anticyclone are seen closed cyclonic circulation features. The latter cyclone impinges on the edge of the west Florida shelf between 26° and 26.5°N.

6.2 *In Situ* Evidence of Circulation

The ADCP measurements made during cruise N3 can be considered as indicative of the circulation features present. ADCP vectors at the depth bin centered on 14 m are shown in Figure C.2-1. Clearly seen over the slope and shelf edge in the western part of the region is strong anticyclonic flow. With maximum speeds in excess of 50 $cm \cdot s^{-1}$ east of the DeSoto Canyon axis, the location of this flow corresponds well with the northern limb of the offshelf anticyclone seen in SSH fields for the time of cruise N3. Much of that flow turns clockwise across the bathymetry, generally being to the south by 86°W. However, there is a band of strong southeast currents near the 100-m isobath which continues to the southern edge of our study region. Between the southward flow of the anticyclonic eddy and the along-shelf-edge band there is indication of weak cyclonic flow over the west Florida slope. That cyclonic flow seems to divide the upstream flow into offshelf and along-shelf components.

Inshore of the 100-m isobath most of the Big Bend area is filled with a well organized cyclone. The exception is that some southeastward flow is seen rounding Cape San Blas and entering the region.

Over the inner shelf west of Cape San Blas, the flow field at 14 m is less well organized, although some cyclonic tendency is seen off Mississippi and Alabama as well as near the head of DeSoto Canyon. These patterns, as well as the cyclonic flow over the Big Bend area, are seen deeper in the water column as well. The ADCP fields for 50 m and 102 m are shown in Figures C.2-2 and C.2-3.

Geopotential anomaly at 3 db relative to 800 db based on cruise N3 data (Figure C.2-4) corresponds reasonably well with the major circulation features over the outer shelf and slope noted in discussion of the ADCP data. This includes a low centered over the 200-m isobath at the head of the DeSoto Canyon. Even the turning of isopleths of dynamic topography on line 8 between the 200- and 500-m isobath matches the flow in the ADCP field in Figure C.2-1. Over the inner shelf the cyclonic flow indicated in Figure C.2-4 south of Cape San Blas is offset northward relative to the near-surface ADCP field; the hint of cyclonic flow seen over the Mississippi-Alabama inner shelf in the ADCP field is absent in the geopotential anomaly; and there is no inshore southeastward flow past Cape San Blas. These discrepancies may be attributed to the fact that the geopotential field probably does not reflect the full geostrophic flow field over the inner shelf; the isobaths and bottom isopycnals do not coincide, giving rise to pycnobathic currents (Csanady 1985).

Tracks of drifters deployed on cruises N2 and N3 are shown during the time of the latter cruise in Figure C.2-5. Inside the 1000-m isobath agreement with the ADCP and geopotential anomaly fields shown is excellent with two exceptions: the drifters deployed over the inner shelf

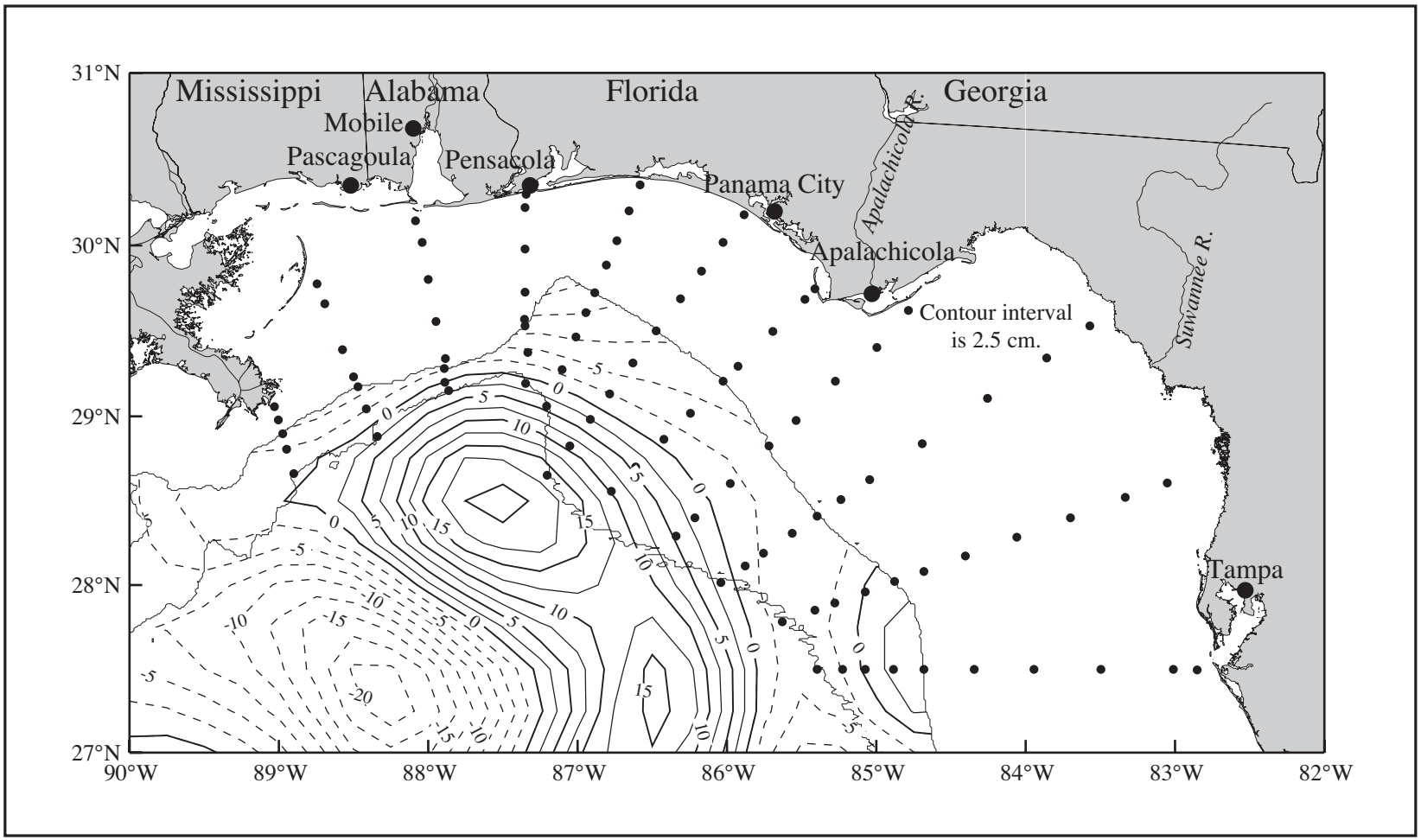

Figure C.1.3-1. Sea surface height field from satellite altimeter data for 5 August 1998 during N3. The 200 and 1000-m isobath contours and CTD stations (dots) are shown. [Data provided by Robert R. Leben, University of Colorado]

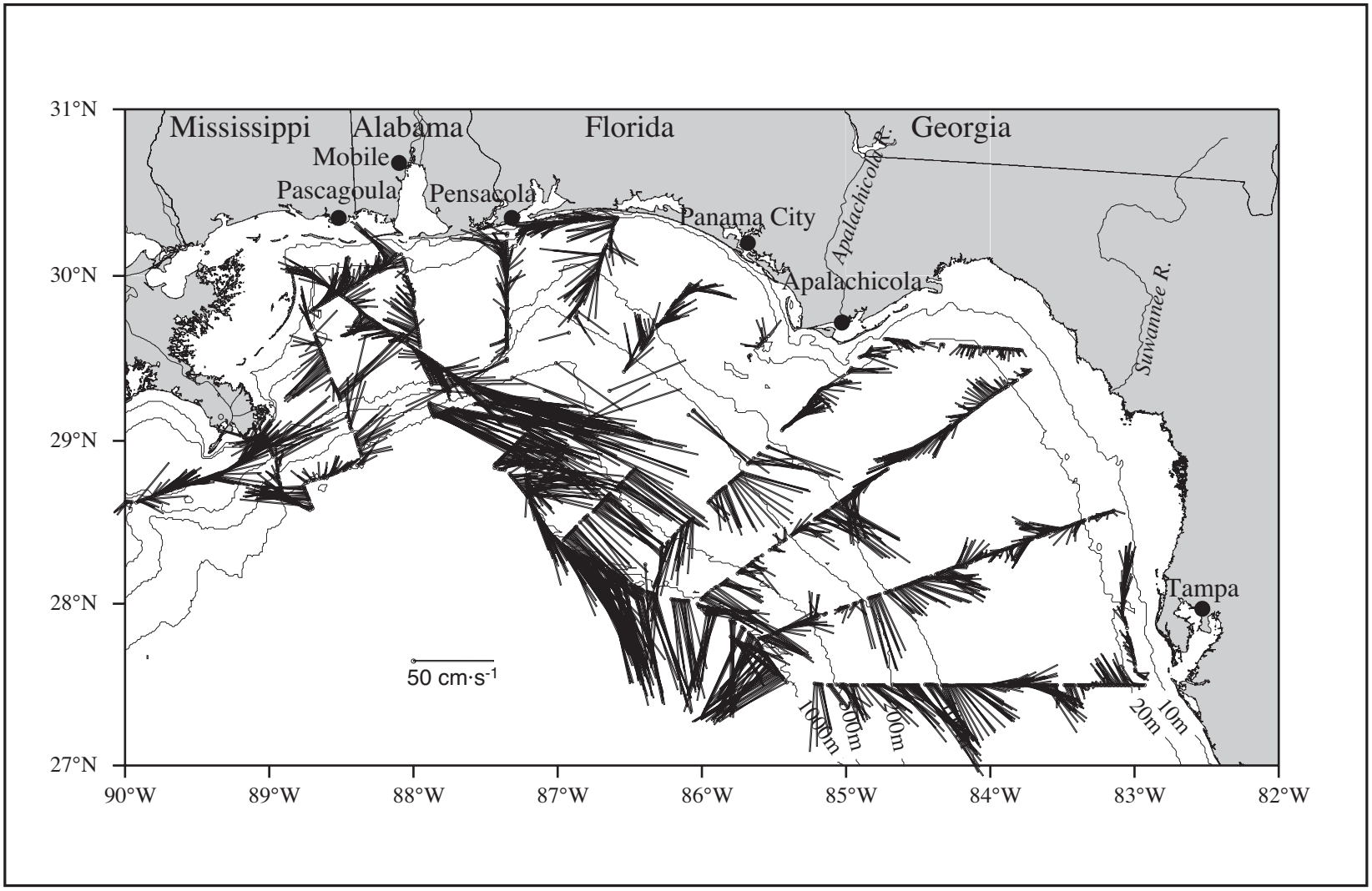

Figure C.2-1. ADCP-measured currents for the 4-m bin centered at 14 m on cruise N3 in July-August 1998.

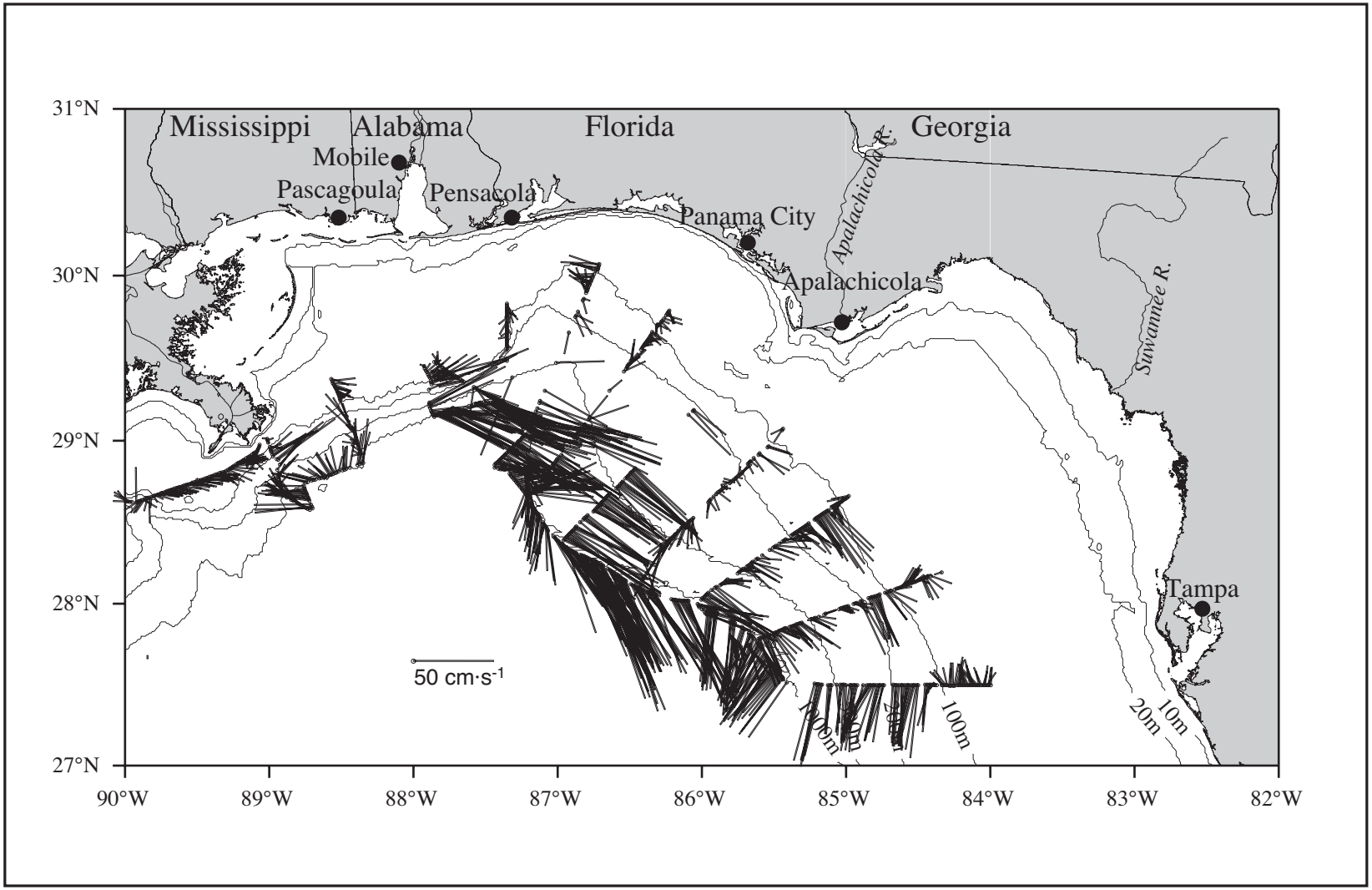

Figure C.2-2. ADCP-measured currents for the 4-m bin centered at 50 m on cruise N3 in July-August 1998.

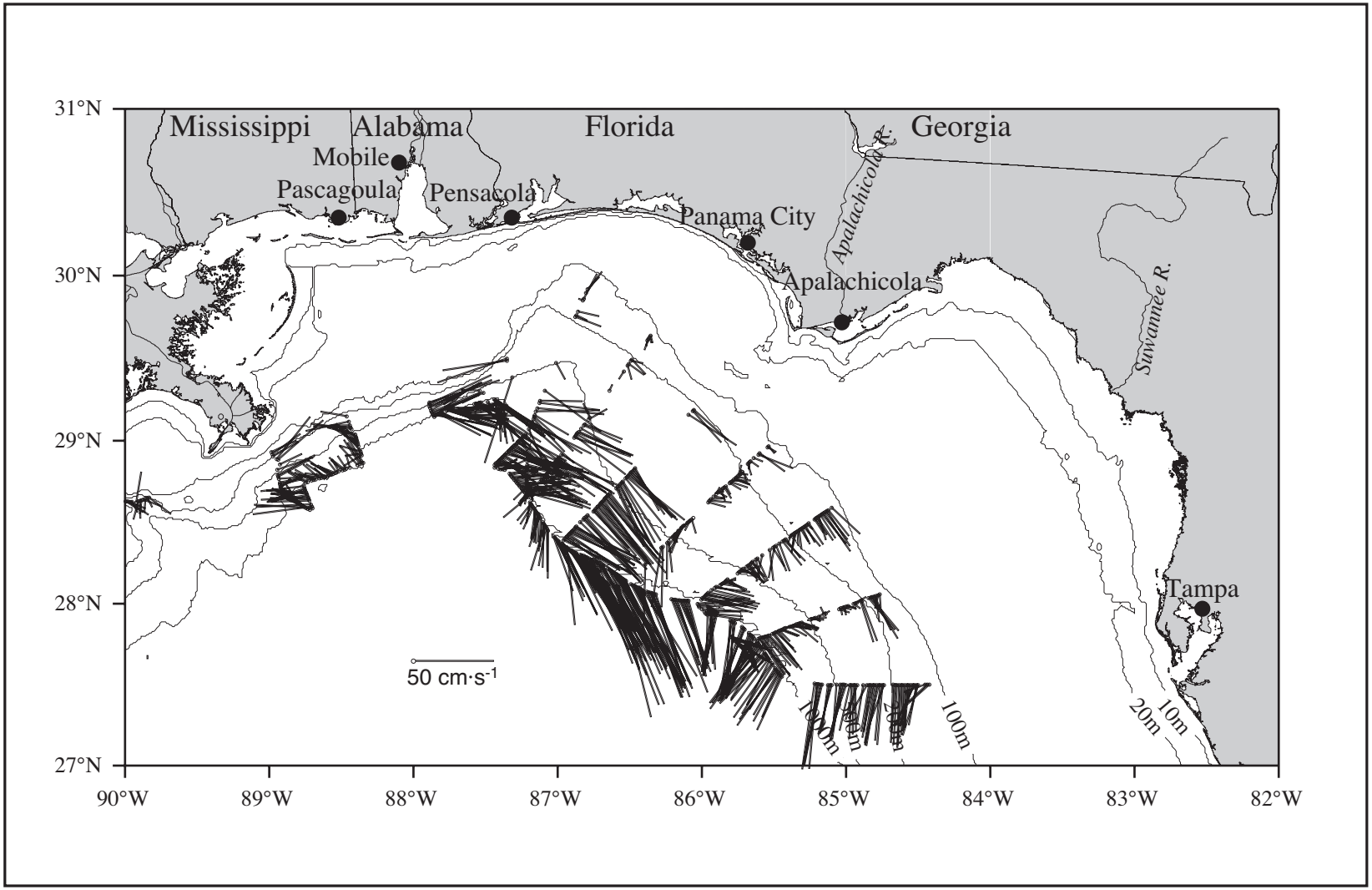

Figure C.2-3. ADCP-measured currents for the 4-m bin centered at 102 m on cruise N3 in July-August 1998.

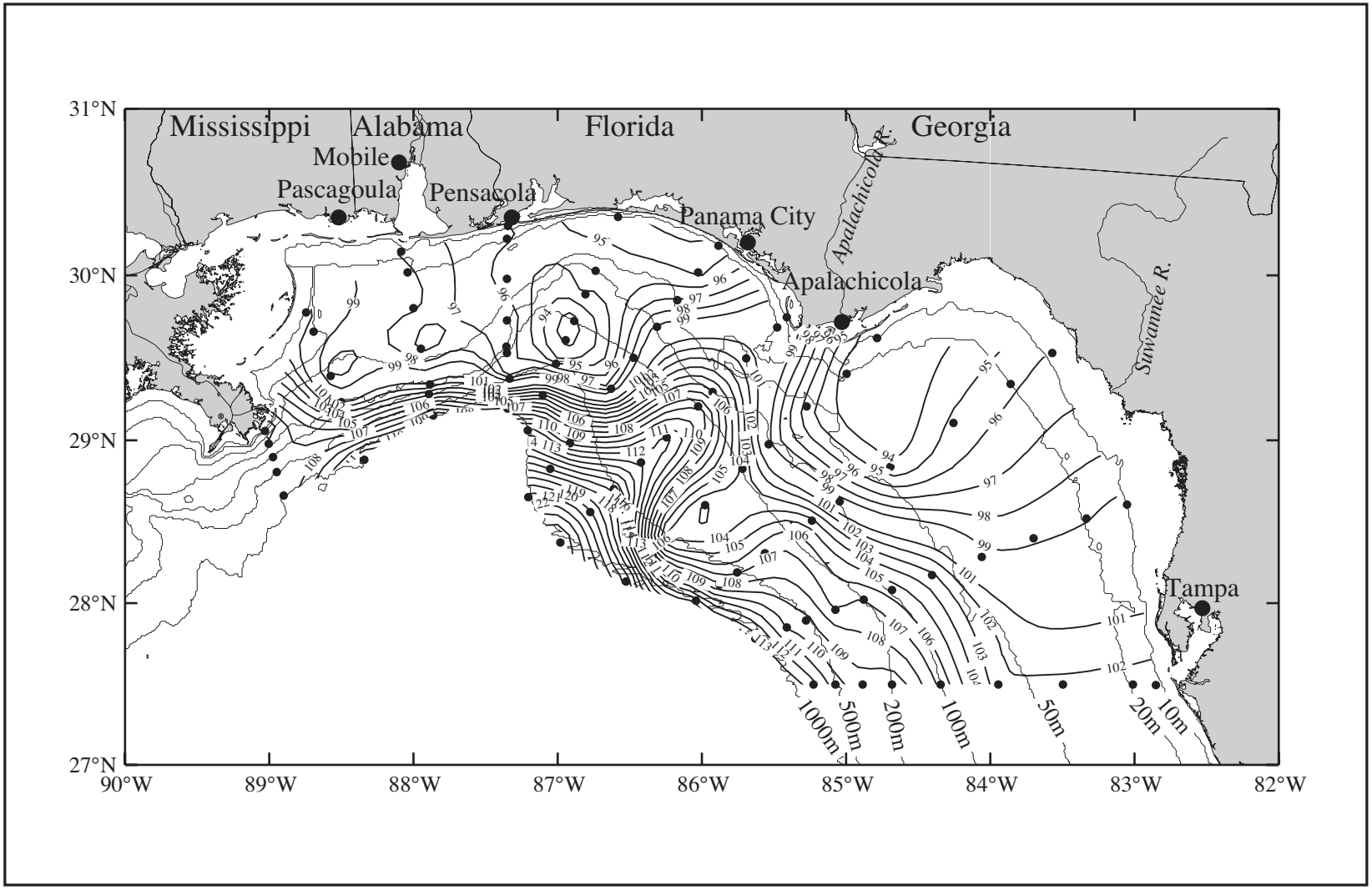

Figure C.2-4. Geopotential anomaly (dyn cm; 3 m relative to 800 m) for cruise N3 conducted 25 July - 6 August 1998. CTD station locations are shown.

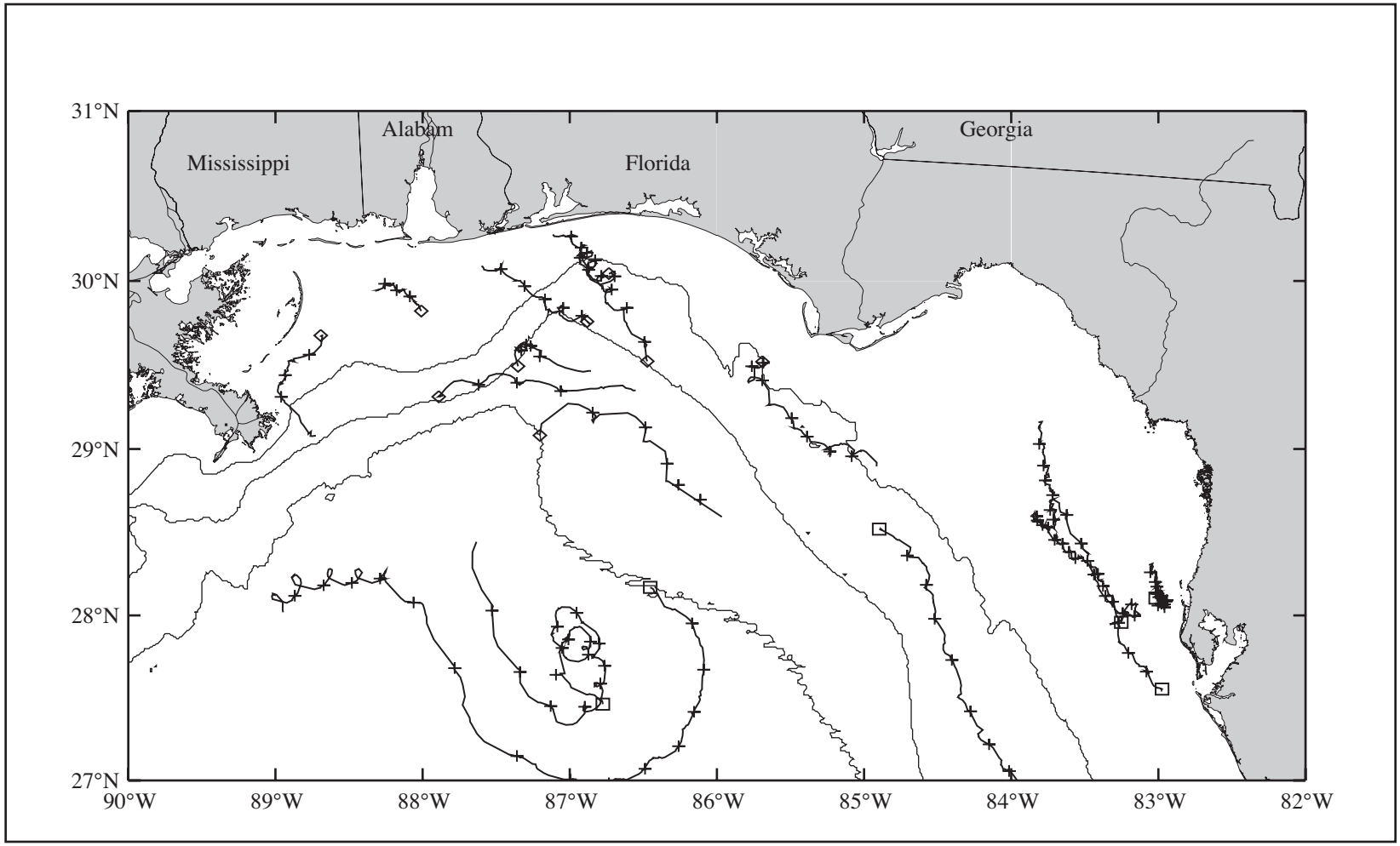

Figure C.2-5. Drifter trajectories for drifters deployed during N2 (squares) for the period 25 July - 9 August 1998 and on N3 (diamonds) for the period 1-9 August 1998. Plus signs mark 00Z each day. Bathymetric contours shown are 50, 200, and 1000 m.

south of Mobile Bay and just southwest of Cape San Blas moved in good agreement with the ADCP field but not the geopotential anomaly.

The two drifters shown offshore of the 1000-m isobath were moving in an anticyclonic pattern very consistent with the position and shape of the anticyclone shown in the SSH field for the same period. Shown in Figure C.2-6 are the tracks of all drifters operating in the study region during the period 1-8 August 1998. These tracks are consistent with and add weight to the circulation patterns previously discussed. In addition, these drifter tracks confirm the existence of a cyclone southwest of the anticyclone, although they indicate its center to be about 27.7°N, 88.3°W, which is somewhat north of the center shown by SSH in Figure C.1.3-1. The drifter tracks showing currents moving to the southeast in the region 27°-28°N, 84°-86°W are consistent with the existence of a cyclone east of the anticyclone.

Near the end of cruise N3, on 4 August 1998, SAIC began a cruise aboard the *R/V Pelican* that covered the region of DeSoto Canyon ending 13 August 1998. CTD stations were taken along the 100-m isobath from approximately 86°W to 89°W and extending offshore to approximately 28.5°N (SAIC 1998). Shown in Figures C.2-7 and C.2-8, respectively, are the depth of the 20°-isothermal surface and 6-m geostrophic velocities relative to 1000 m constructed by SAIC from that cruise. The upper circulation inferred from these figures agrees very well with that seen on cruise N3 (see Figures C.2-1, C.2-4), from SSH (Figure C.1.3-1), or drifters (Figure C.2-6).

C.3 Property Distributions

Potential temperature, salinity, and sigma-θ as observed during cruise N3 are shown in vertical section along the 1000-m isobath in Figures C.3-1, C.3-2, and C.3-3. Clear in these distributions is the effect of the offshelf anticyclone that depressed the depths of isotherms, isohalines, and isopycnals most noticeably near stations 93 east of the Mississippi Delta and 43 over the eastern flank of DeSoto Canyon. The distributions clearly coincide with the circulation described in Section C.2.

The salinity maxima seen near 100-150 m depth at stations 94-79 and 61-42 have maximum values of approximately 36.5 between 160-180 m at station 42 and between 115-135 m at station 93. Such values at the expected core of the Subtropical Underwater indicate the anticyclone was likely the remnant of a Loop Current eddy, though our sampling did not reach into any Caribbean Water remaining in the ring.

A number of relatively high salinity lenses are seen along the 1000-m isobath at depths shallower than 100 m. Salinity in a number of lenses examined exceeds 36.5, some have values greater than 36.56. Examination of cross-shelf sections of properties (e.g., see Figure C.3-4 showing salinity in vertical section along line 7) indicates there are multiple lenses of high salinity that are located along isopycnal surfaces and that there is interleaving. This is evidence for vigorous mixing in the shoreward limb of the anticyclone, likely associated with encroachment of the anticyclone on the shelf edge.

Distributions of potential temperature and density along the 500-m isobath (not shown) reflect the presence of strong anticyclonic flow off-shelf as along the 1000-m isobath (Figures C.3-1 and C.3-3), Salinity along the 500-m isobath (Figure C.3-5) shows greater shoreward penetration of salty waters near 100 m along lines 1 and 2 than elsewhere.

In Figure C.3-6 are shown vertical sections of potential temperature, salinity, and sigma-θ along the 100-m isobath. Waters with salinity greater than 36.4 are absent on lines 1 and 2, except at the bottom at station 90. However, near bottom waters at stations 48, 36, and 28 on lines 7, 8,

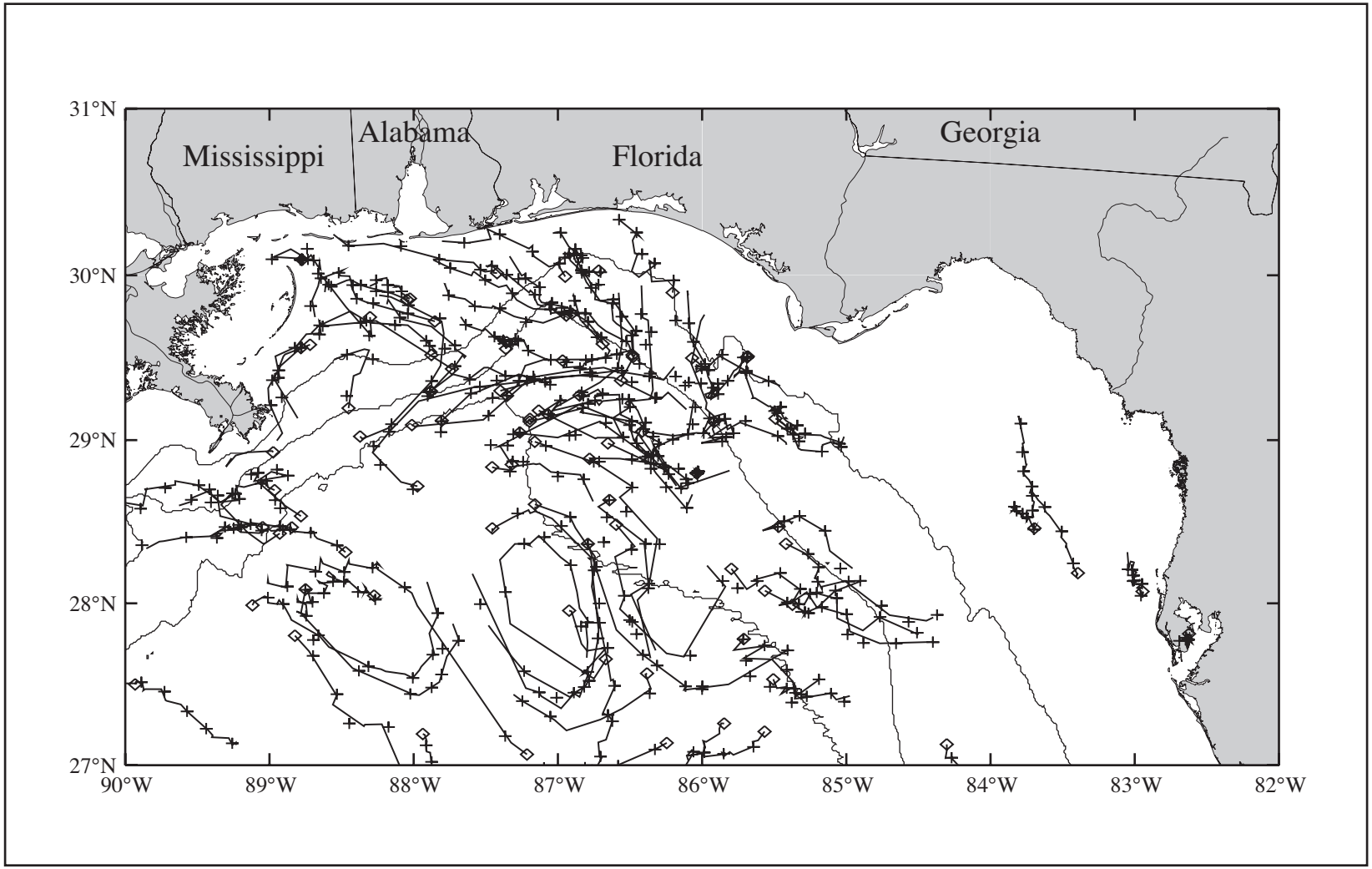

Figure C.2-6. All drifting buoys reporting from the NEGOM region from 1 to 8 August 1998. Bathymetric contours shown are 50, 200, and 1000 m.

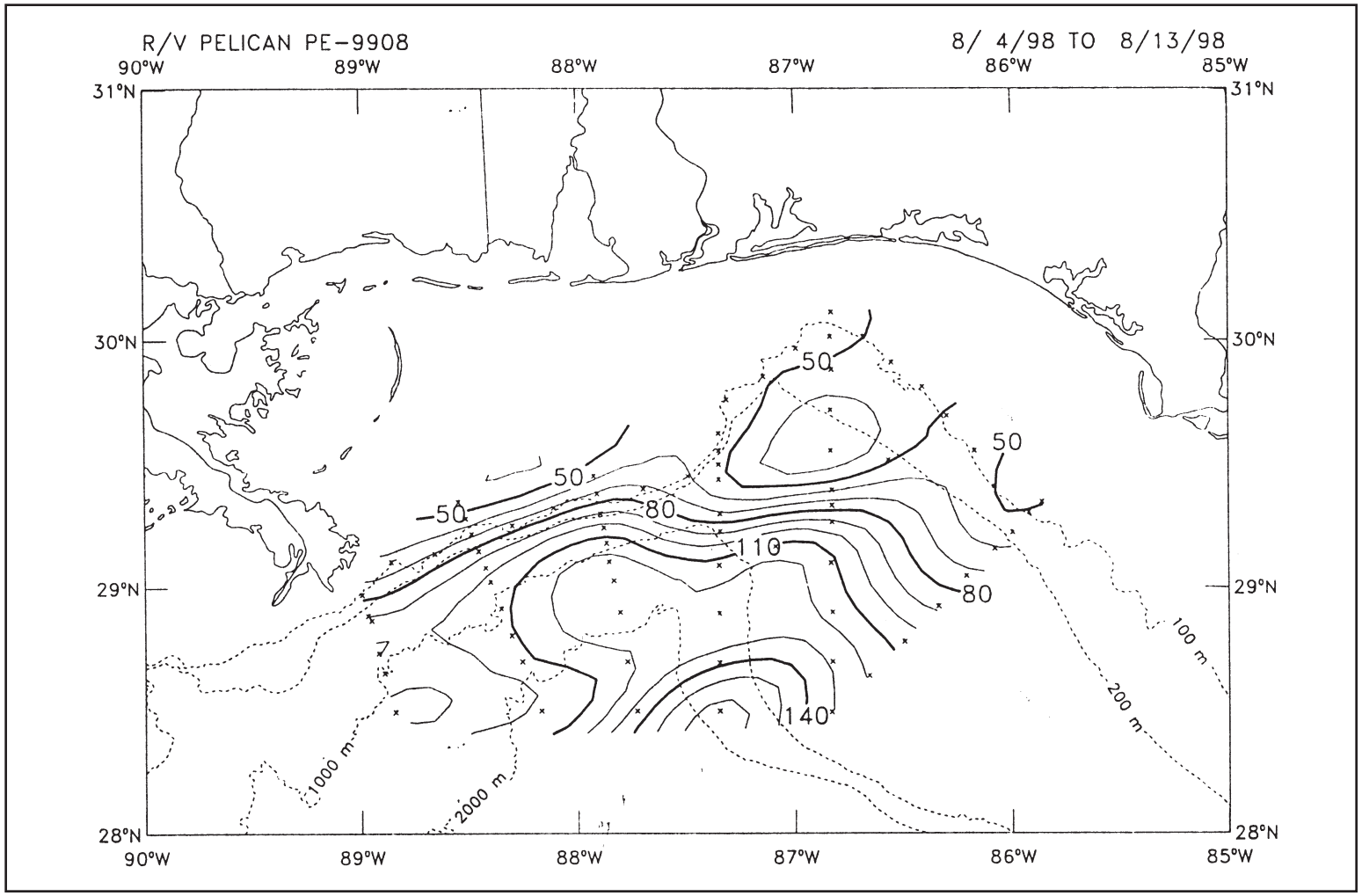

Figure C.2-7. Depth of the 20°C isotherm surface for 4-13 August 1998 (from Science Applications International Corporation, 1998).

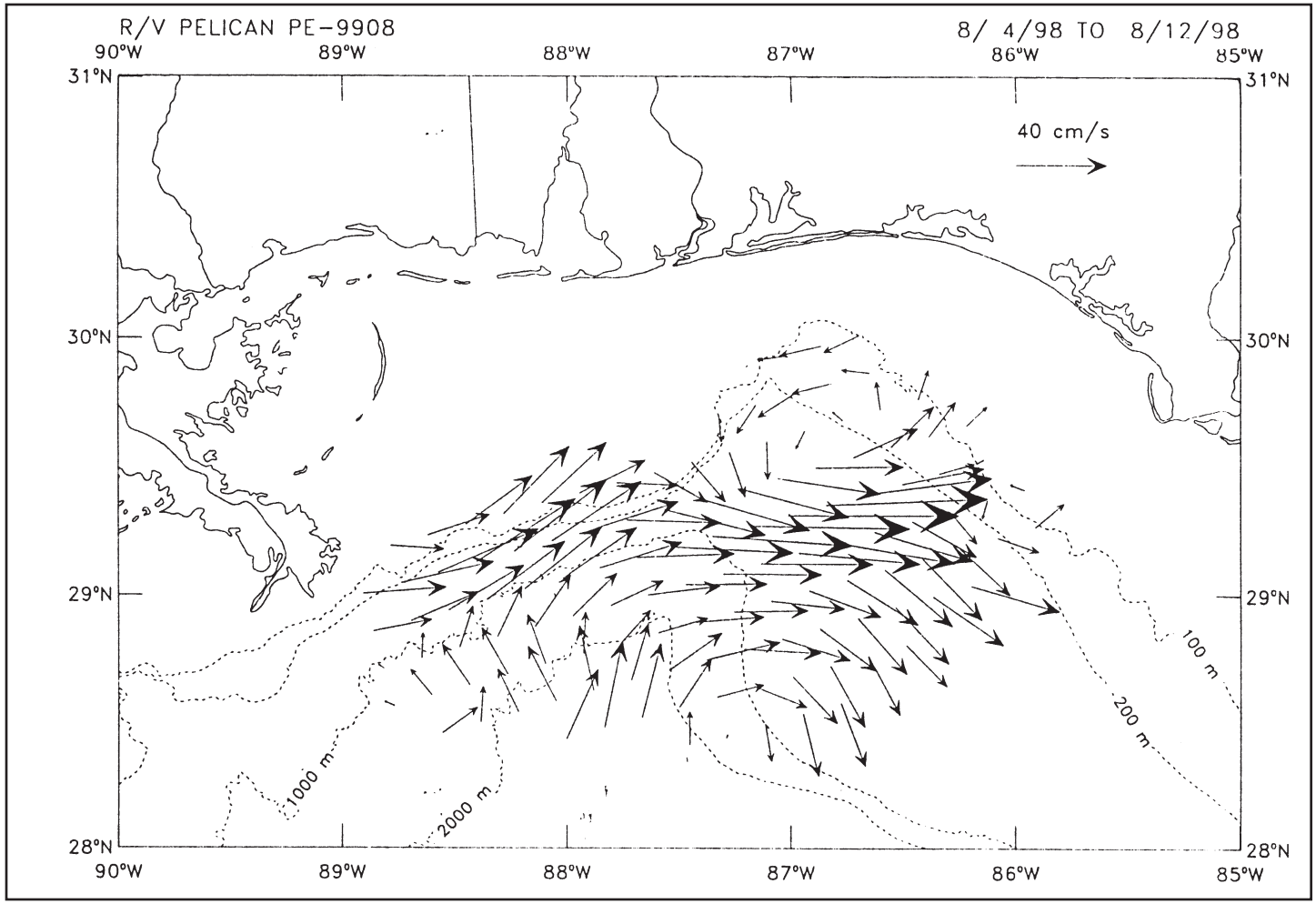

Figure C.2-8. Geostrophic velocity of 6 m relative to 1000-m flow for 4-12 August 1998 (from Science Applications International Corporation, 1998).

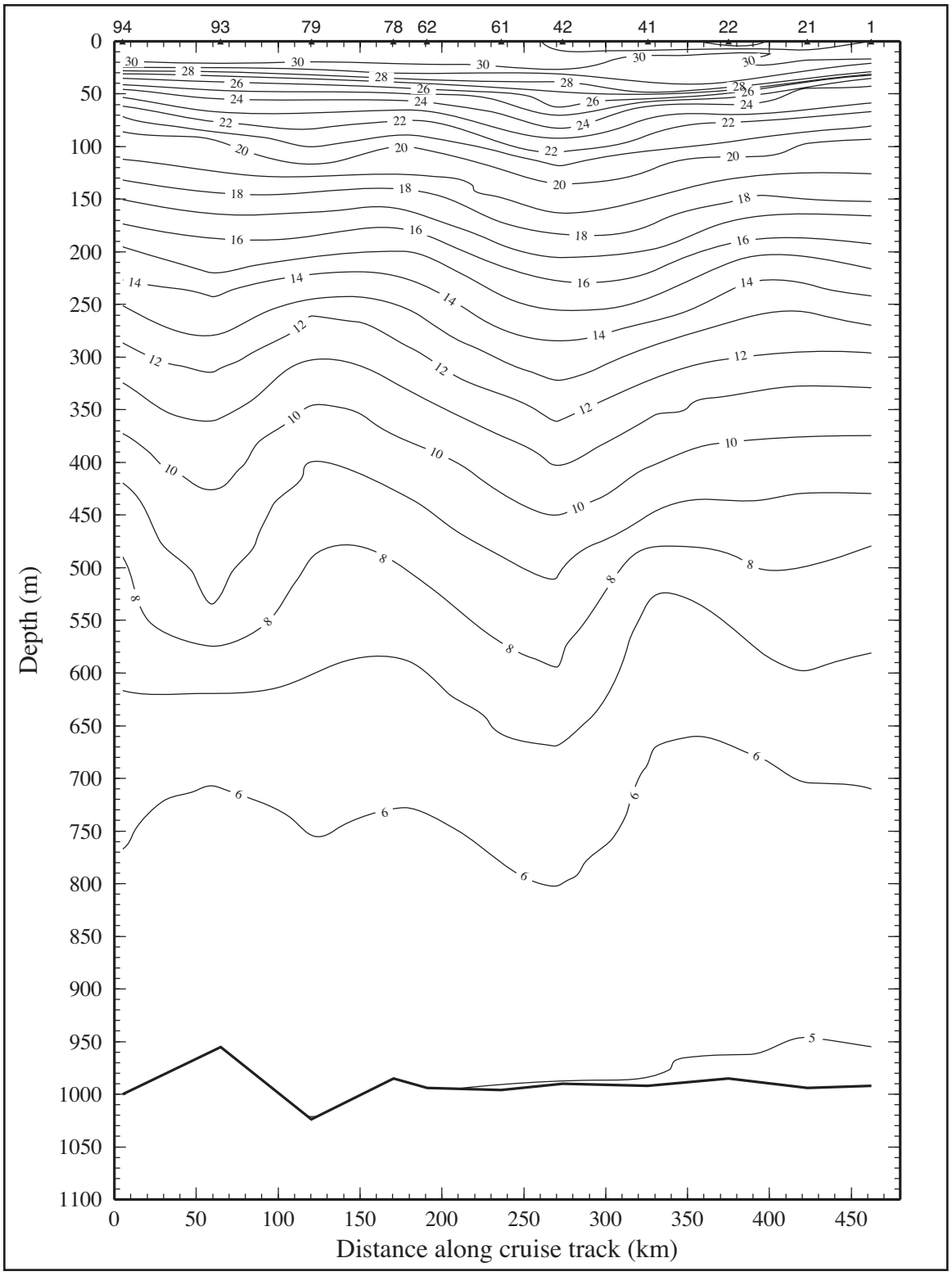

Figure C.3-1. Potential temperature (˚C) along the 1000-m isobath of cruise N3 in July/ August 1998. Stations are shown on top axis. Line 1 is at the left station; line 11 is at the right.

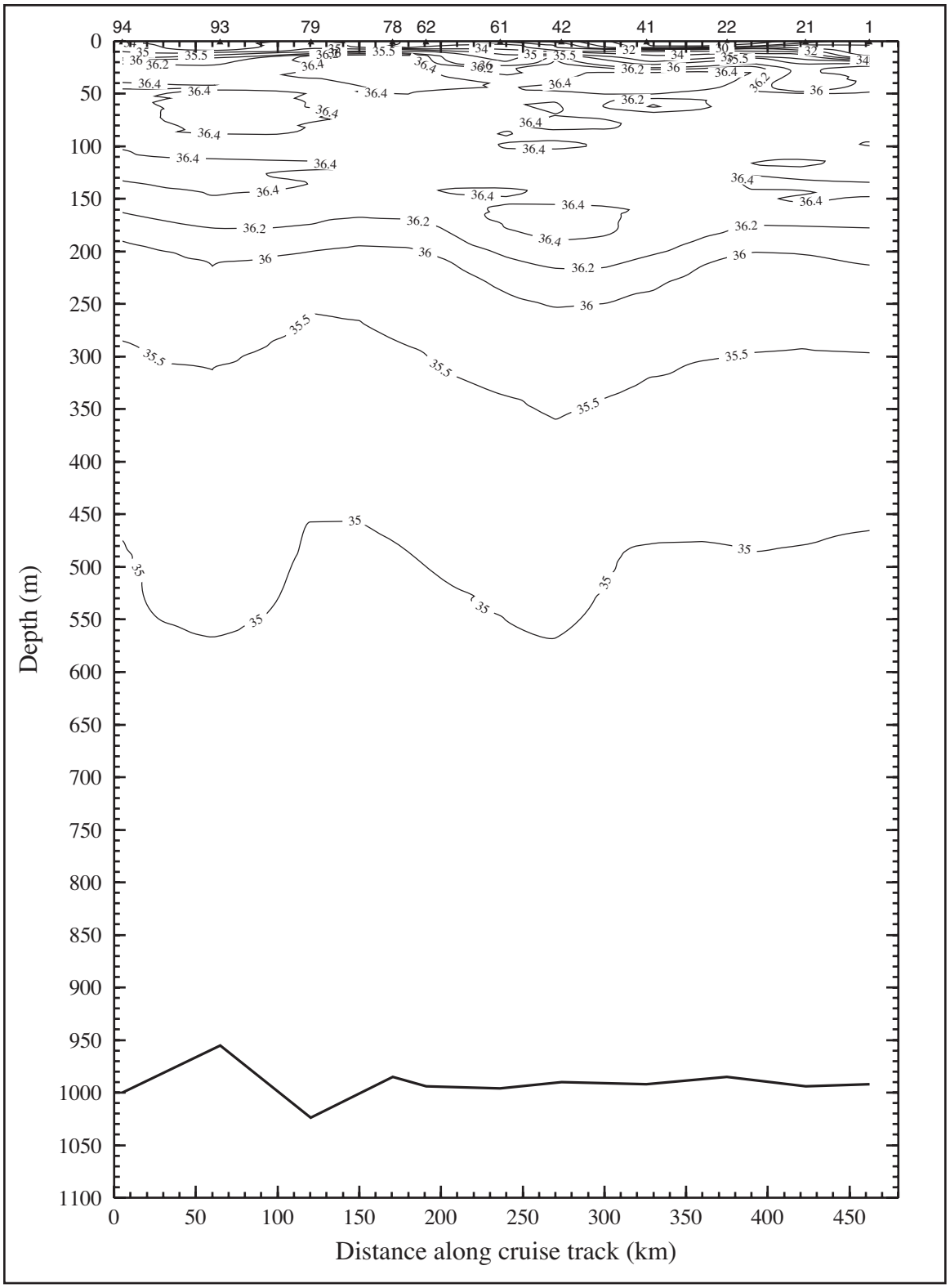

Figure C.3-2. Salinity along the 1000-m isobath of cruise N3 in July-August 1998. Stations are shown on top axis. Line 1 is at the left station; line 11 is at the right.

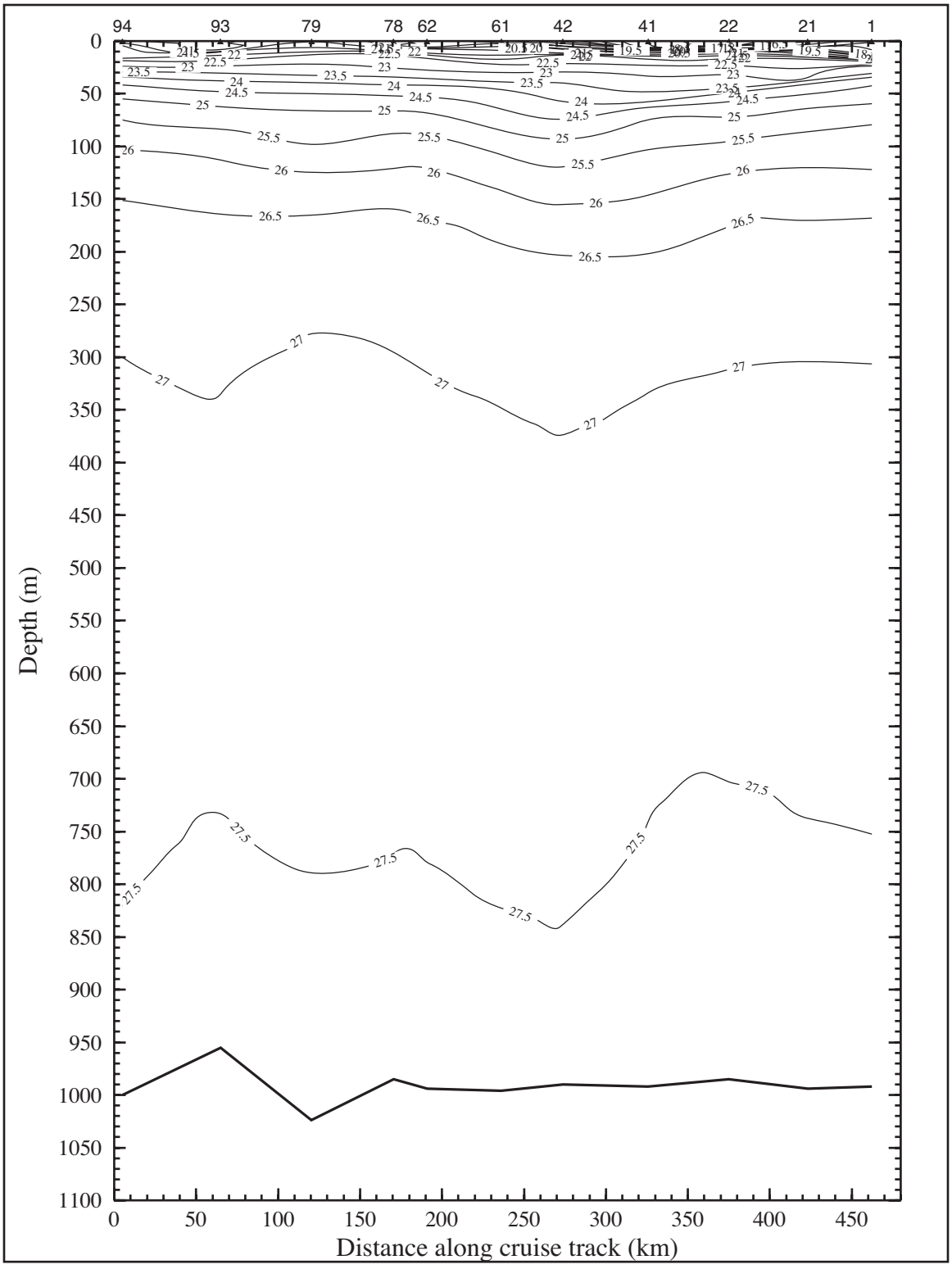

Figure C.3-3. Density anomaly (σ_θ in kg·m^{-3}) on the 1000-m isobath of cruise N3 in July-August 1998. Stations are shown on top axis. Line 1 is at the left station; line 11 is at the right.

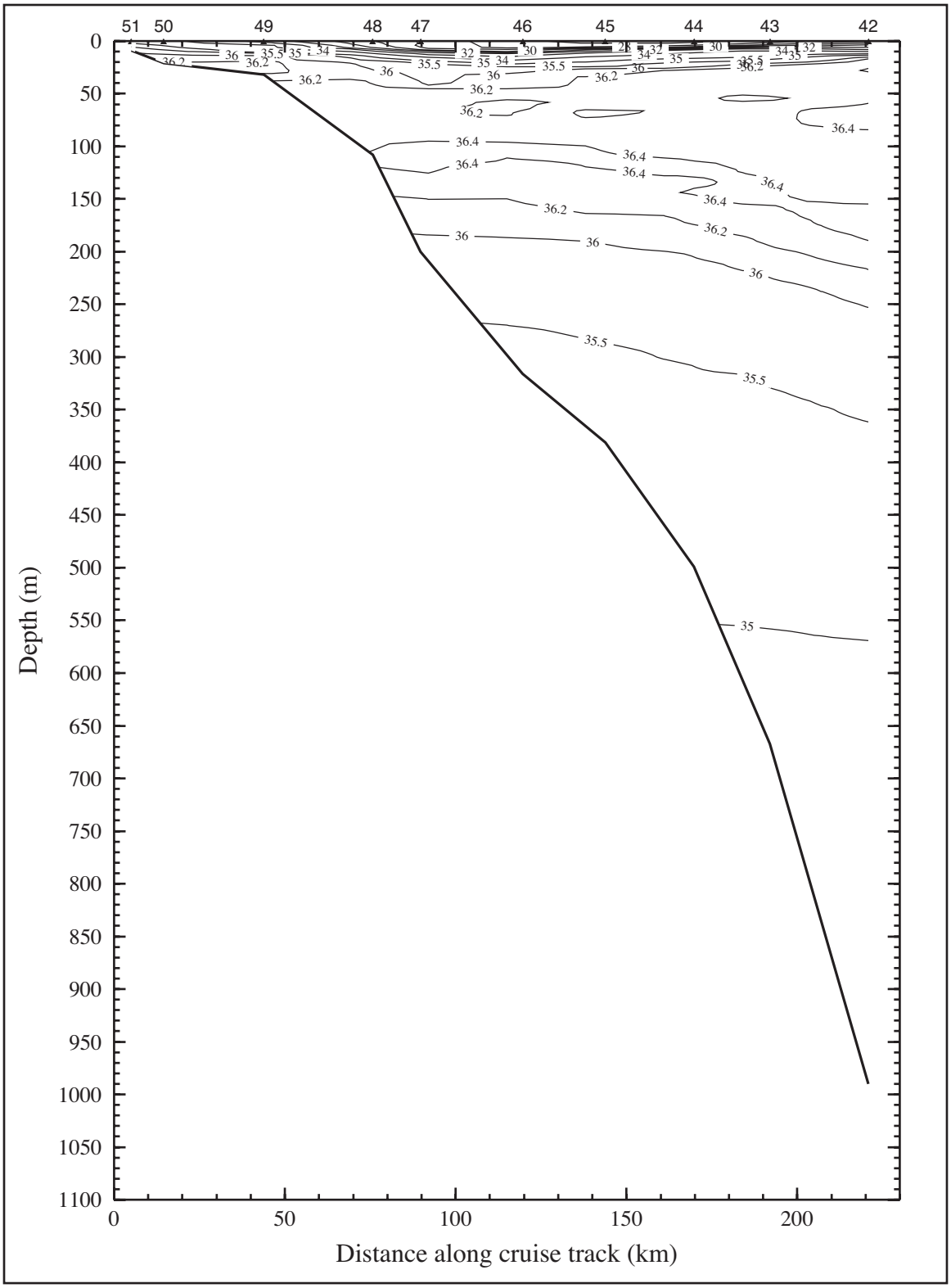

Figure C.3-4. Salinity on line 7 of cruise N3 in July-August 1998. Stations are shown on top axis.

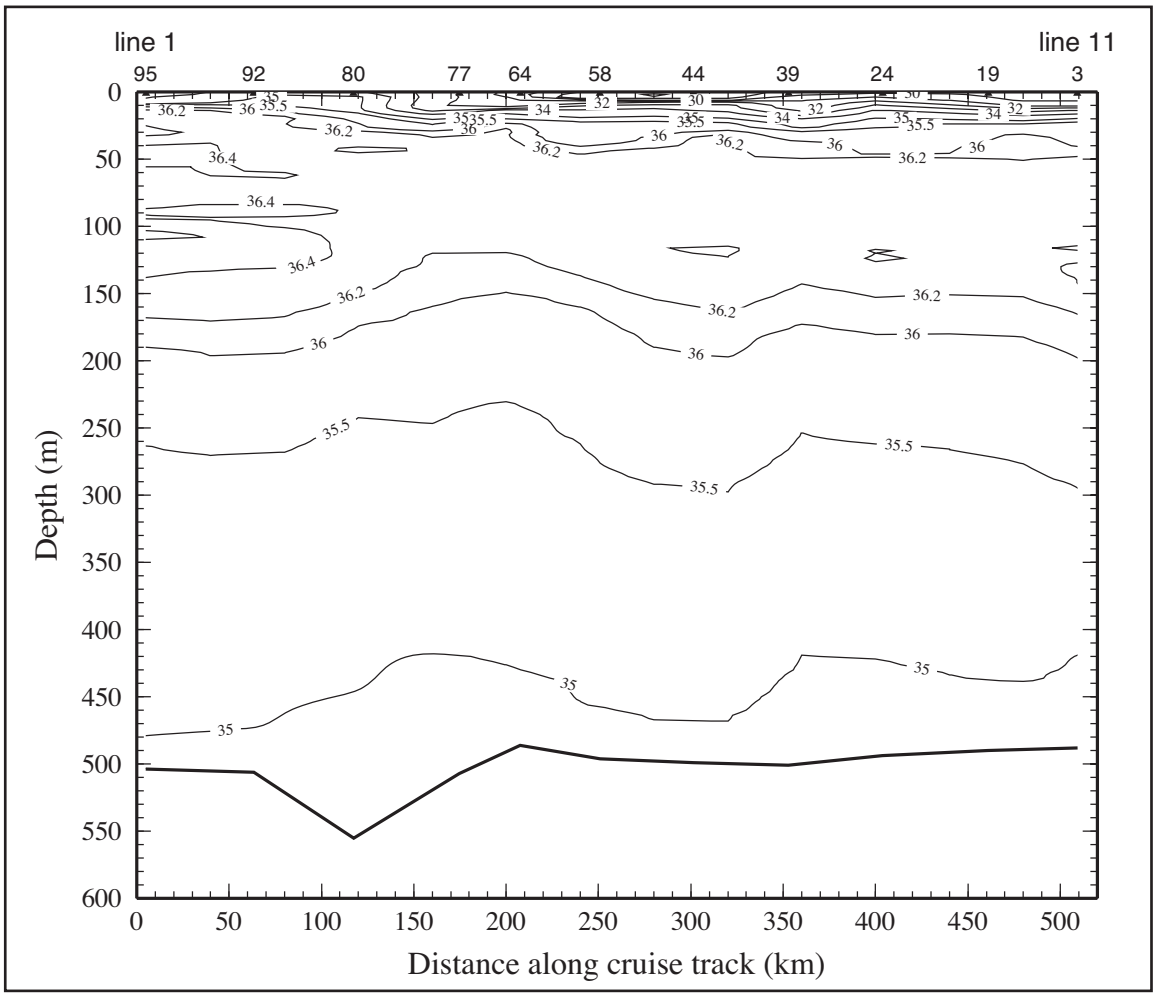

Figure C.3-5. Salinity on the 500-m isobath of cruise N3 in July-August 1998. Stations are shown on the top axis.

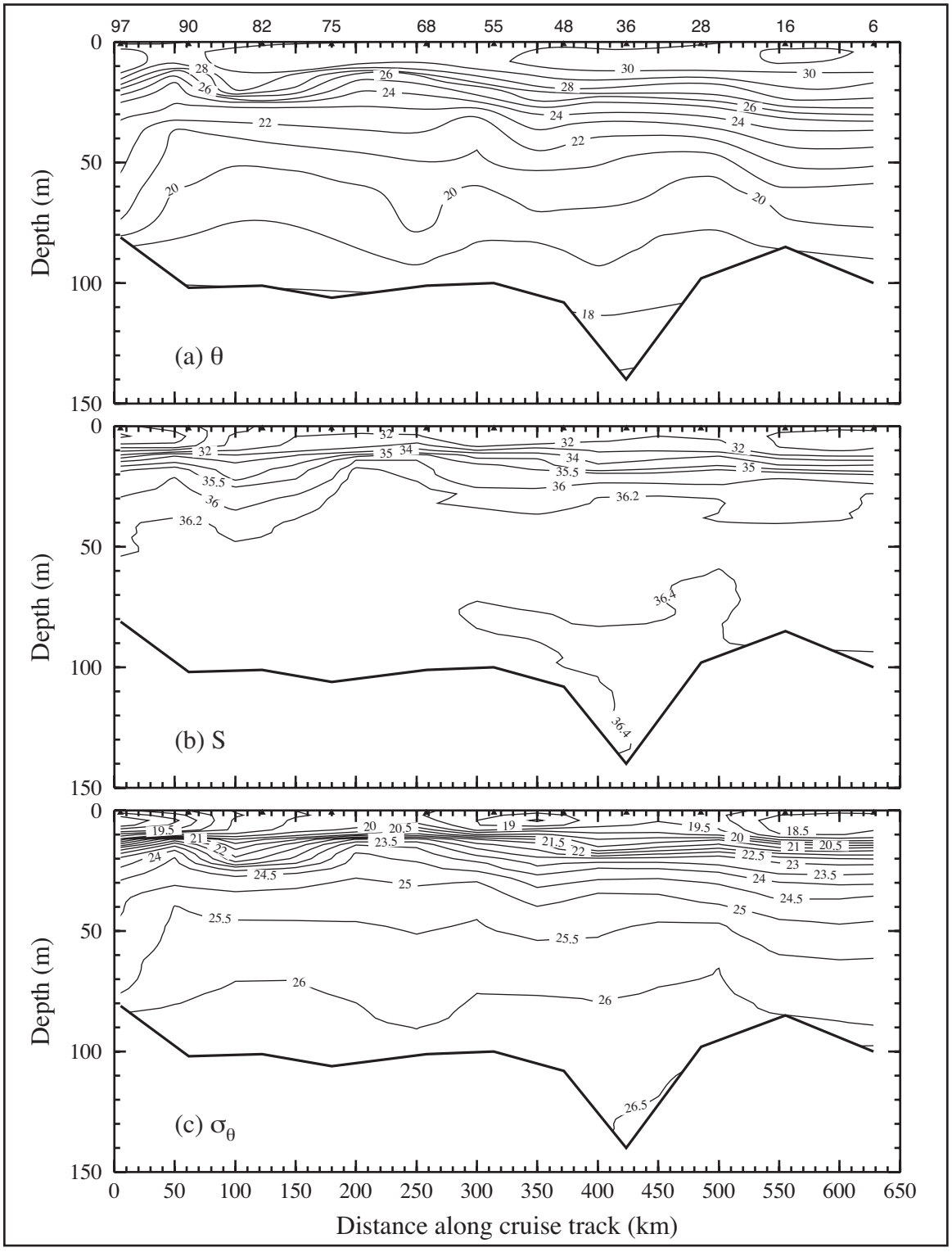

Figure C.3-6. (a) Potential temperature (°C), (b) salinity, and (c) density anomaly (σ_θ in kg·m^{-3}) on the 100-m isobath for cruise N3 in July-August 1998. Stations are shown on top axis. Line 1 is at the left station; line 11 at the right.

and 9 respectively, are saltier than 36.4. Returning to Figure C.3-5, only a very small lens of water saltier than 36.4 was present near 100-m depth on line 7 and 9 (none on line 8). What is the source of the salty waters seen on lines 7-9 along 100-m isobath?

In the vertical distribution of salinity on line 7 (Figure C.3-4) a continuous layer of waters with S > 36.4 is shown. Examination of ADCP velocities near 100 m (Figure C.2-3) shown nearly onshelf flow extending from water depths greater than 200 m to 100 m along line 7. Between water depths of 100 and 200 m southeastward along isobath flow is seen crossing lines 8 and 9 but opposing flow (to the north northwest) is seen crossing lines 8 and 9 somewhat further offshore (water depths near 300 m). It is postulated that the lens of near-bottom salty water seen along the 100-m isobath is carried onshore near the line 7 and then spreads southeastward across lines 8 and 9. Relatively low salinity water is transported northwestward offshore of the 200-m isobath, leading to cross-isobath salinity distributions such as seen in line 8 of Figure C.3-7.

From the thermosalinograph, with intake water depth of approximately 3 m, the salinity field shown in Figure C.3-8 was constructed. Of course, this field coincides with that shown from 3.5 m CTD values (Figure C.1-2), but considerably more detail is shown and control is better—as is apparent from consideration of the track lines (shown) along which sampling was carried out. The surface layer of low salinity over the southeast flank of DeSoto Canyon is seen to be fresher and somewhat more extensive based on the thermosalinograph data. (Of course, this might also be attributed to the somewhat (0.5 m) shallower sampling depth in the presence of a thin layer of relatively low salinity water.)

Bottom salinity (not shown) generally evidences highest values just inshore of the 100-m isobath where remnants of the relatively salty Subtropical Underwater contacts the bottom.

Dissolved oxygen at the surface (3.5 m) was essentially uniform with values near 5 $mL \cdot L^{-1}$ and so is not shown. Figure C.3-9 pictures the near-bottom distribution of dissolved oxygen. Only on line 4 is there any indication of reduced oxygen at the bottom. There measured oxygen was 1.89 $mL \cdot L^{-1}$ at 26.5 m, approximately 5 m above the bottom (see Figure C.3-10). Vertical stability at base of the surface mixed layer (~15 m) was quite strong on line 4, especially at stations 73-77. As seen in Figure C.3-10, there is apparent uplift of isopleths at station 77. This is seen in isopleths of density and other nutrients as well. Similar pronounced uplift of isopleths is seen on lines 5 and 6 over the 200 to 250-m isobaths. Sigma-θ and nitrate for the upper waters on line 5 are shown in Figure C.3-11. Near-surface ADCP currents (Figure C.2-1) and geopotential anomaly (Figure C.2-4) indicate the region of uplift to be the center of a cyclonic circulation. Further evidence for uplift of isopleths at the center is offered by the relative density of the uplifted waters at the center of this cyclone (see percent transmission on line 5 in Figure C.3-12).

Nitrate distributes at 3.5 m and near bottom are shown in Figures C.3-13 and C.3-14. It appears that biological activity has depleted surface nitrate except in the region of continuing Mississippi River water outflow east of the delta. Near-bottom values are depleted over inner shelf (depths less than 50 m) in the Big Bend region southeast of Cape San Blas. West of Cape San Blas nitrate is depleted only very near shore. Elsewhere the isopleths tend to follow isobaths with increasing values offshore—this is characteristic of the bottom distributions of phosphate and silicate distributions as well.

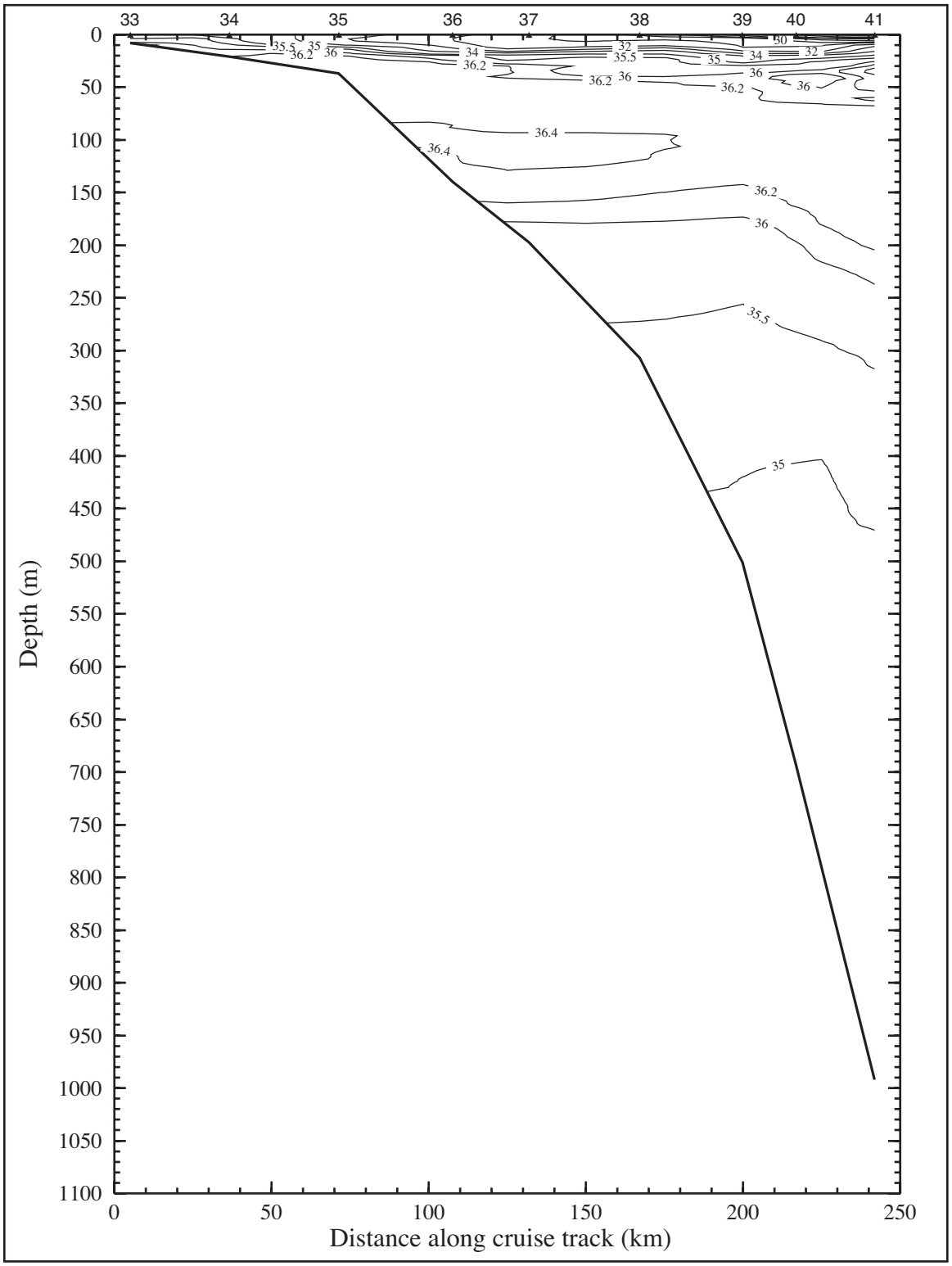

Figure C.3-7. Salinity, from CTD data, on line 8 of cruise N3 in July-August 1998. Stations are shown on top axis.

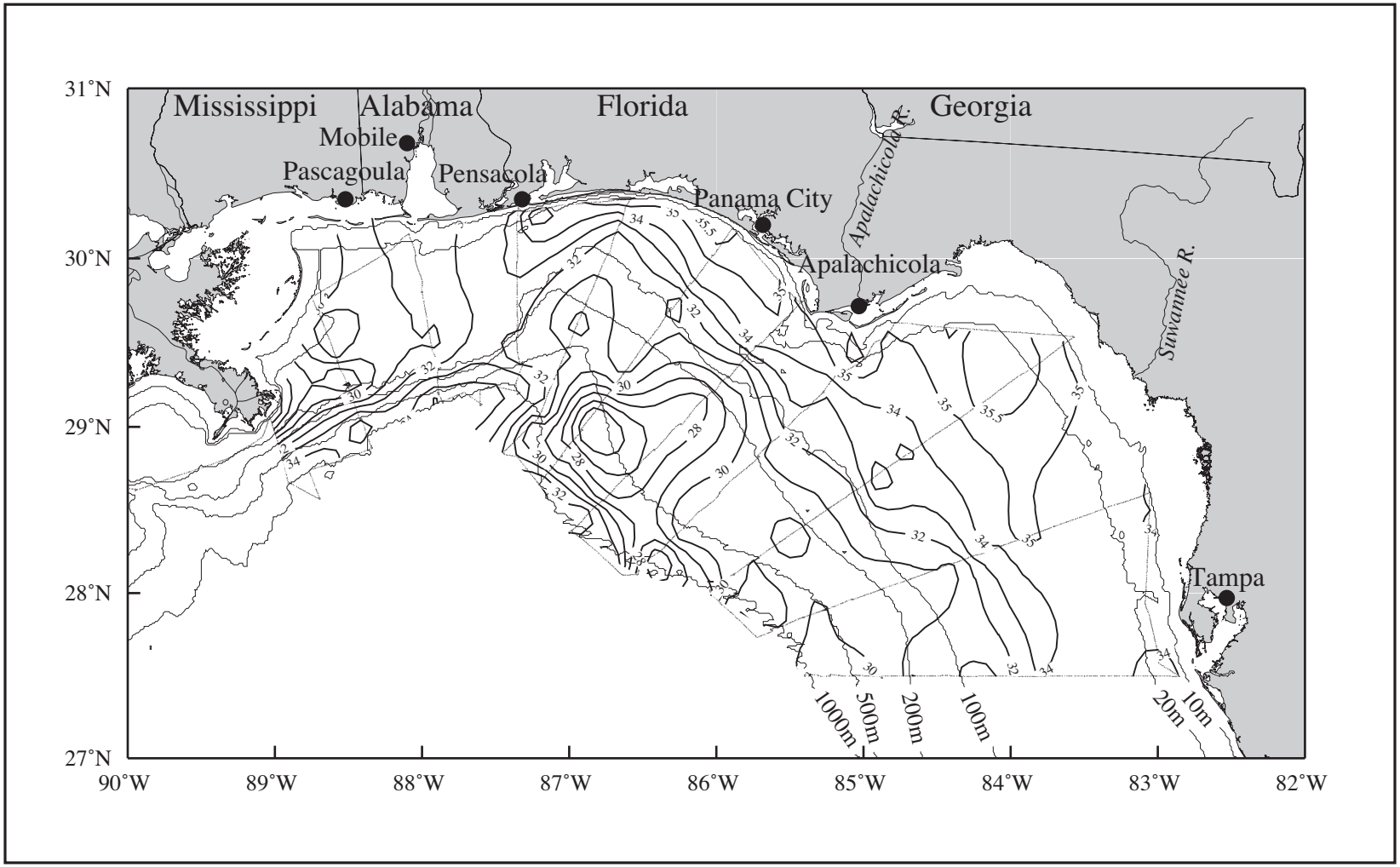

Figure C.3-8. Salinity at ~3 m from thermosalinograph observations on cruise N3 during 26 July - 6 August 1998.

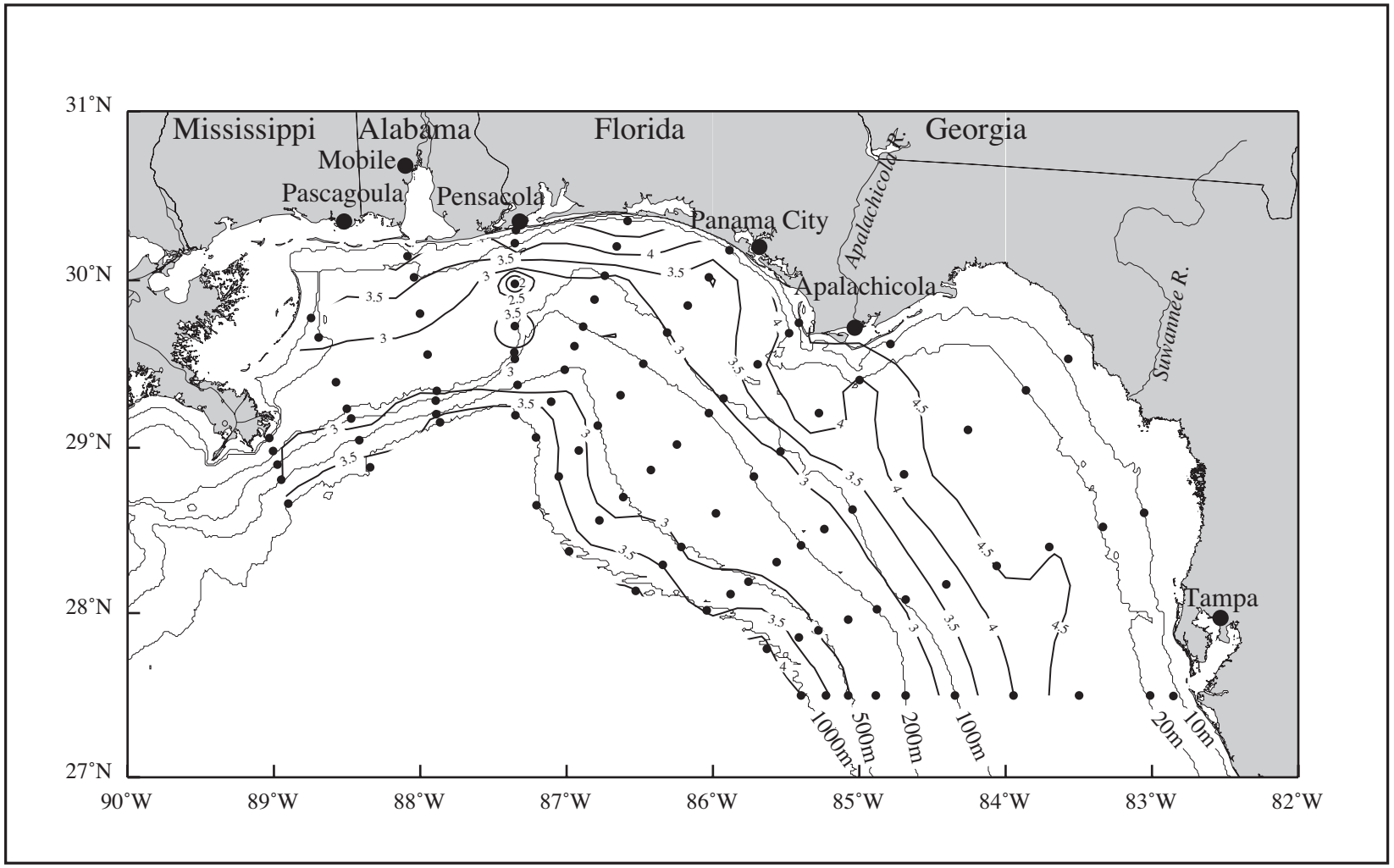

Figure C.3-9. Dissolved oxygen (mL·L^{-1}) near bottom on cruise N3 during 26 July-6 August 1998.

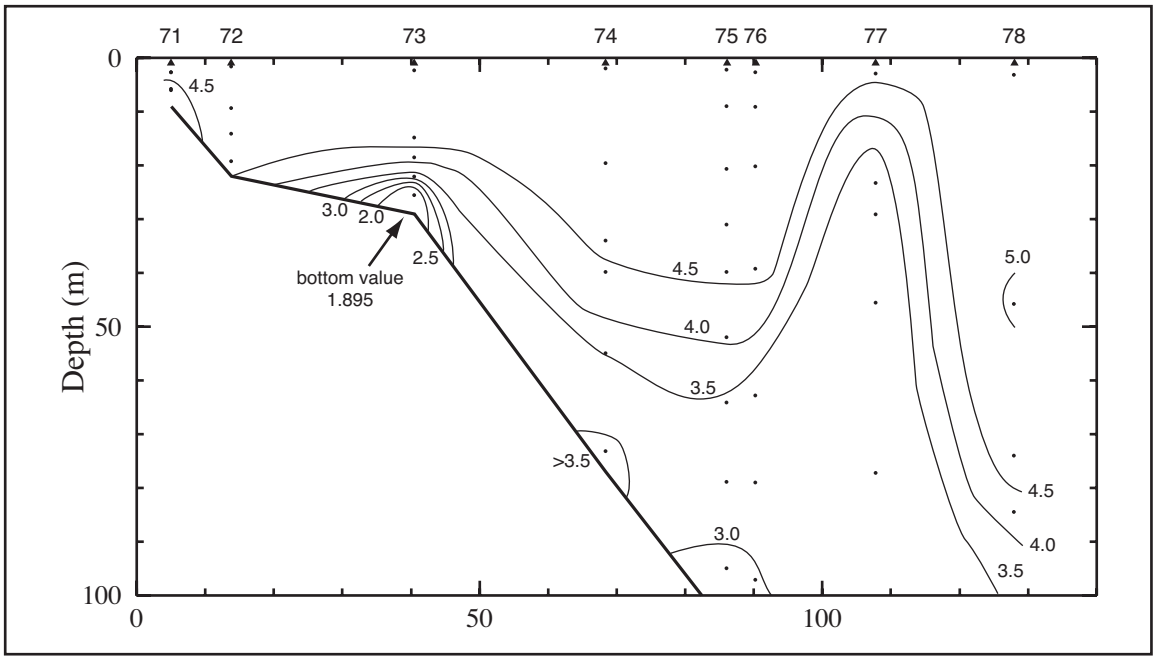

Figure C.3-10. Dissolved oxygen ($mL \cdot L^{-1}$) on line 4 of cruise N3 in July-August 1998. Stations are shown on top axis.

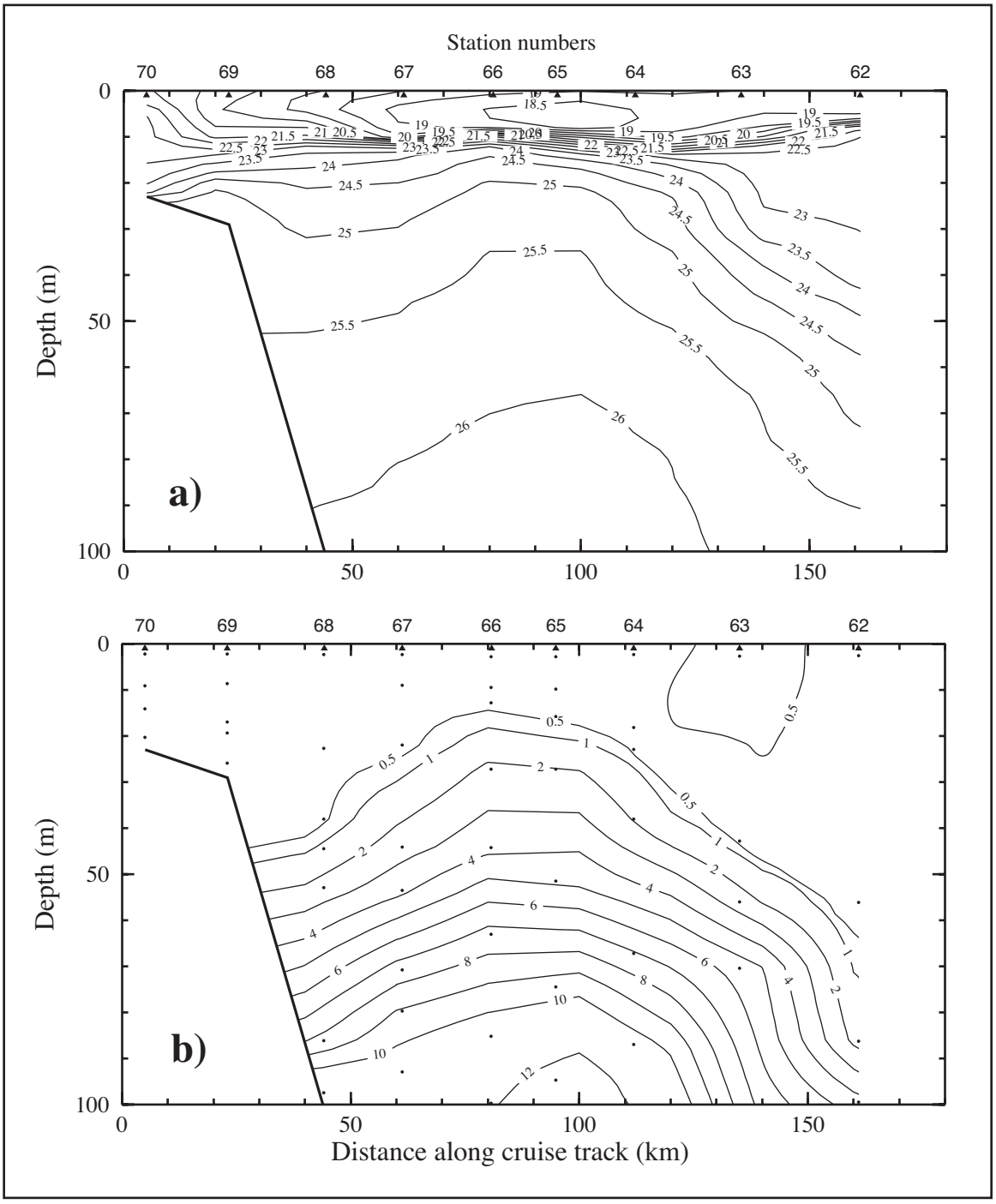

Figure C.3-11. (a) Density anomaly (σ_θ in kg·m^{-3}) and (b) nitrate (μM) on line 5 of cruise N3, 26 July–6 August 1998.

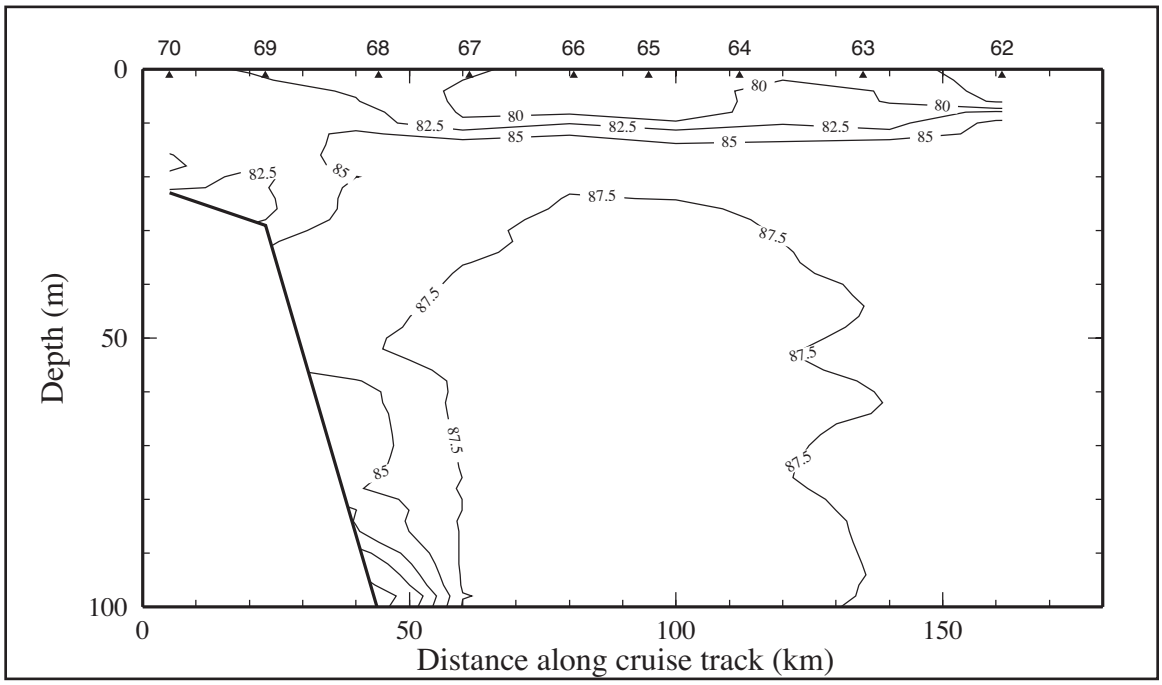

Figure C.3-12. Percent transmission (660 nm wave length; 25-cm path length) on line 5 of cruise N3 in July-August 1998. Stations are shown on top axis.

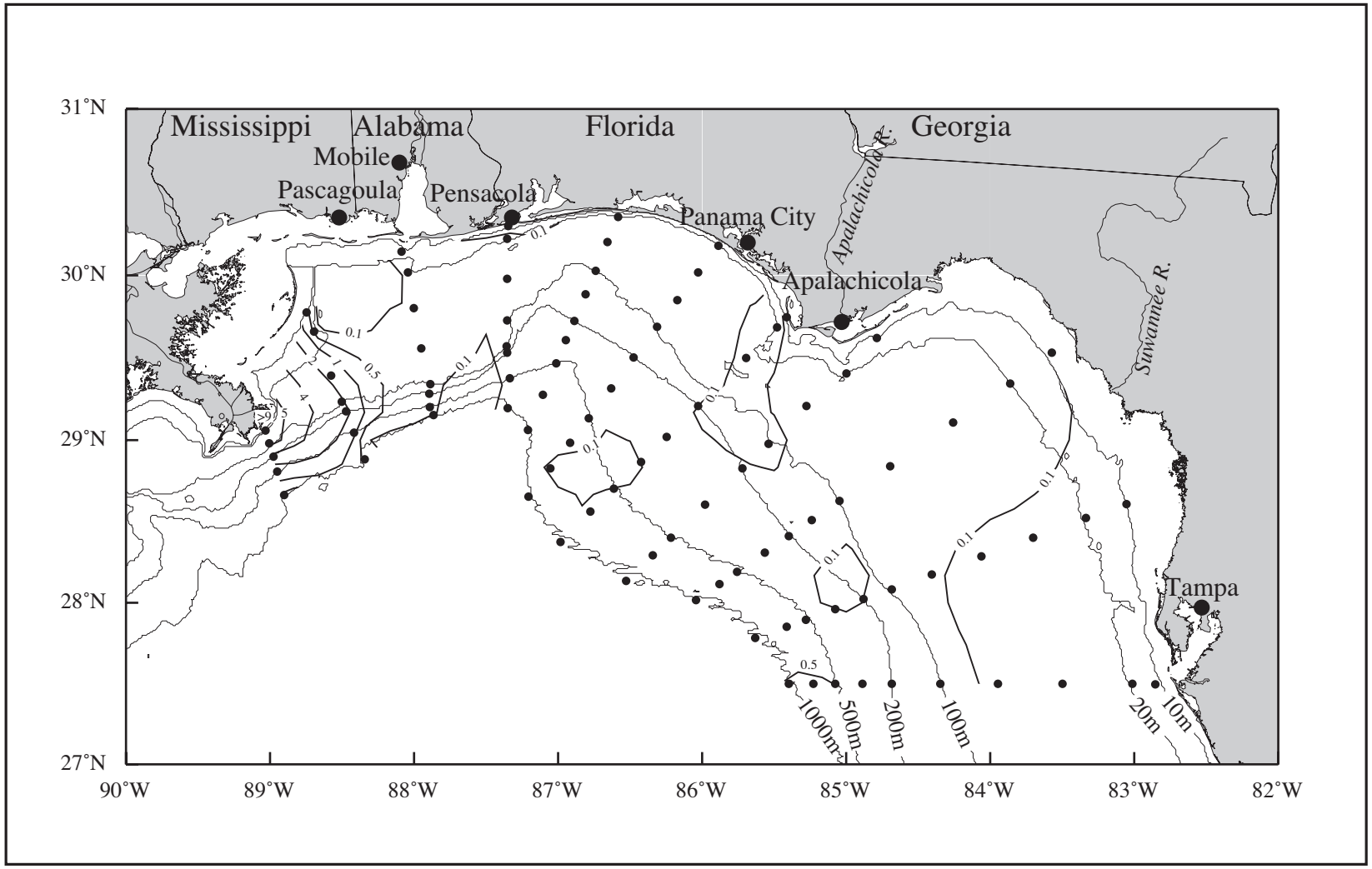

Figure C.3-13. Nitrate (μM) at 3.5 m on cruise N3 during 26 July–6 August 1998.

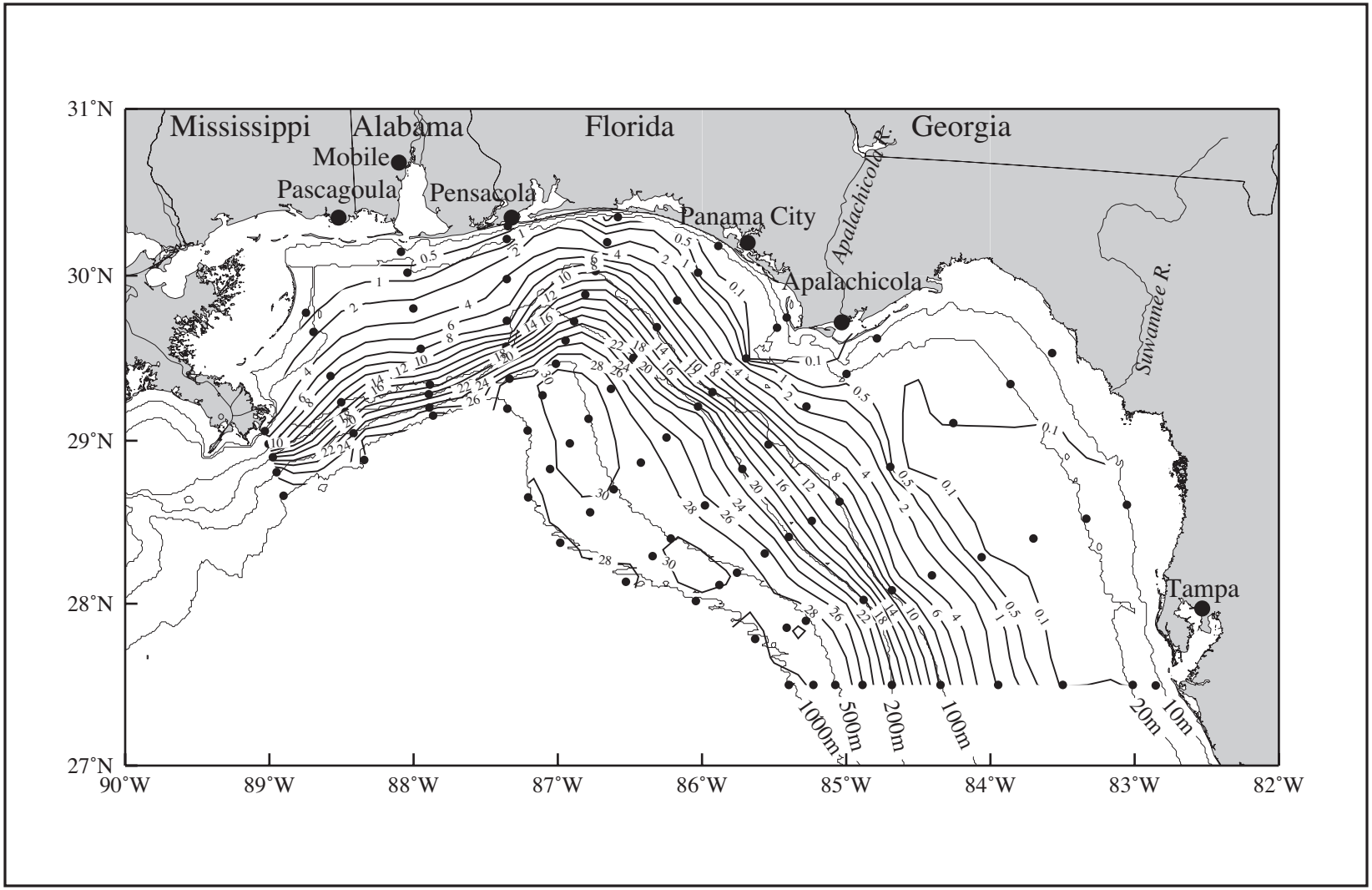

Figure C.3-14. Nitrate (μM) near bottom on cruise N3 during 26 July–6 August 1998.

APPENDIX D
SUMMARY OF CONDITIONS DURING CRUISE N4

Cruise N4 was a fall cruise conducted 13-24 November 1998. The cruise commenced from Gulfport, MS. A test station was performed near the offshore end of line 5 at the 1000-m isobath. The cruise track then followed the 1000-m isobath to the seaward station on line 11 and ended with the most inshore station on line 1. In this way, the station sequence was identical to that of the prior fall cruise, N1. Figure D-1 shows the station locations and gives the CTD station numbers, which are sequential by sampling order.

D.1 Forcing Functions

D.1.1 Winds

The mean wind field for the period of cruise N4 (13-24 November 1998) is shown in Figure D.1.1-1. The methodology used is that of Wang et al. (1998) applied to hourly observations at meteorological stations located as shown in the figure. Also shown are variance ellipses during the cruise based on estimates of the principal axes of the wind velocity variance.

Over the NEGOM region the mean winds for the cruise period were generally light and directed toward the west at 2-3 $m \cdot s^{-1}$ over the west Florida shelf. They were slightly stronger at 3-4 $m \cdot s^{-1}$ over the DeSoto Canyon and Mississippi-Alabama Shelf, and in the western portion of the region were to the southwest. Variability ellipses were oriented with the major axis mostly perpendicular to the direction of mean flow. The semi-major axis magnitude varies from about 25 $m^2 \cdot s^{-2}$ over the Mississippi-Alabama Shelf to about 5-15 $m^2 \cdot s^{-2}$ over the west Florida shelf. At least twice during the N4 cruise (15-17 November and 20-21 November), the winds reversed from their mean directions, turning north and northeastward (e.g., Figure D.1.1-2). The climatological winds over the NEGOM region for November have considerable variability owing to frequent frontal passages, but are generally directed to the west and southwest. Both wind reversals during N4 were associated with the passage of cold fronts as seen in the NOAA *Daily Weather Maps*. Offshore and south of the continental shelves of the northeastern Gulf of Mexico the climatological winds are directed to the southwest.

D.1.2 River Discharge

Daily discharge rates for the Mississippi River exceeded the 70-yr record-length mean during the months of October and November 1998 (Figure 3.1.2-2). Other major rivers discharging into the northeastern Gulf of Mexico (Alabama, Apalachicola, and Tombigbee Rivers) were generally below their mean rates for November. The Suwannee River was at or slightly above it's mean November rate. All rivers in this region and east of the Mississippi River showed a dramatic peak in discharge of 1- to 2-day duration on September 30 through October 1, which exceeded the mean rates by 2-4 times the standard deviation. This pulse of relatively lower salinity water into the region is believed to be associated with the passage of Hurricane Georges as it brought torrential rain to the coastal regions of the northeastern Gulf. In the Big Bend area, the discharge of the Suwannee River more than doubled it's mean rate with a peak discharge of about 50×10^6 $m^3 \cdot d^{-1}$.

The effects of the river discharge on the near-surface (~3 m) salinity distribution was seen most clearly in the western part of the study region (Figure D.1.2-1). Here, a strong salinity gradient was confined to the Mississippi River plume near Pass a Loutre.

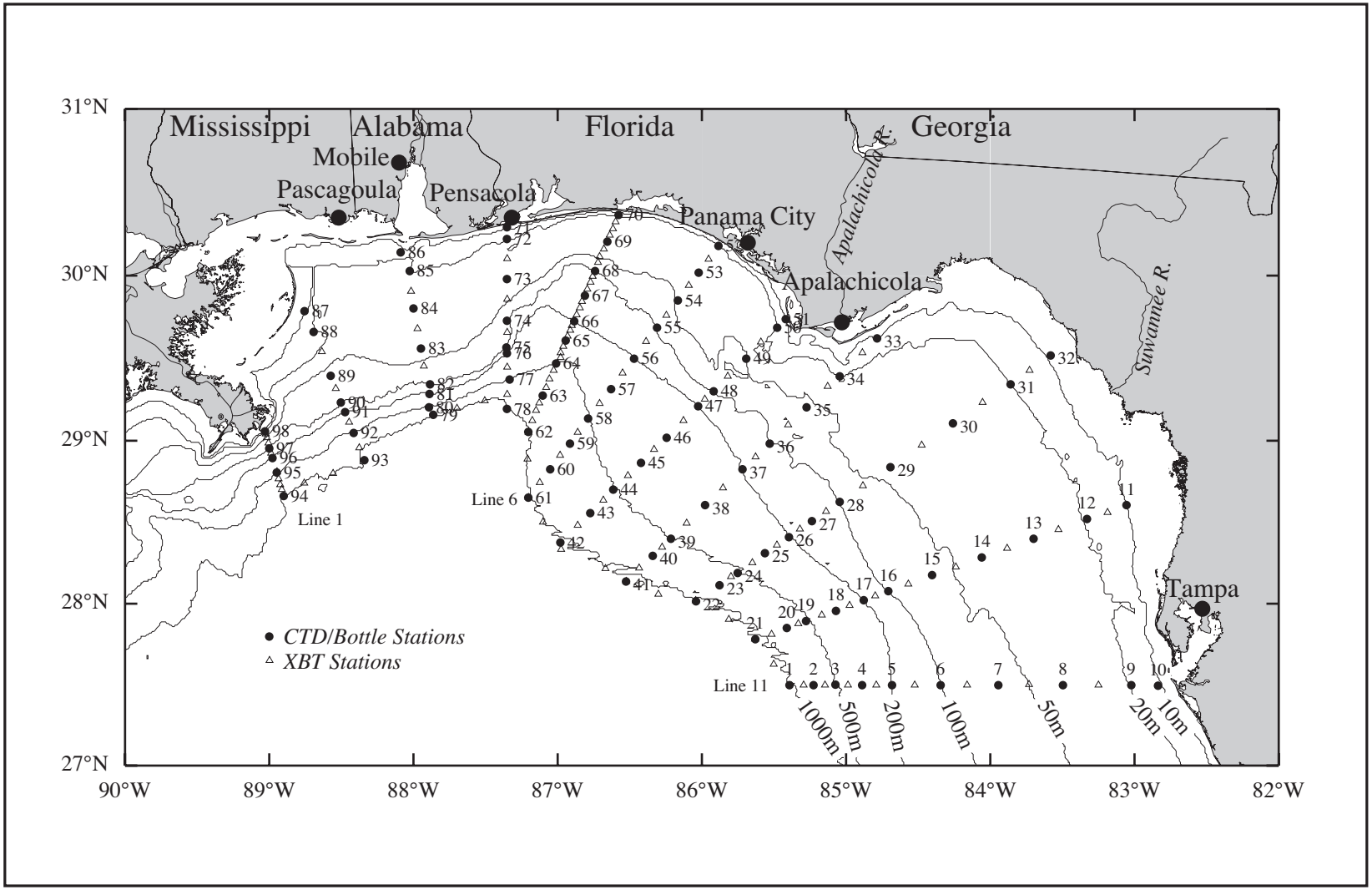

Figure D-1. Station locations for cruise N4 conducted on 13-24 November 1998. CTD stations (solid circles) are numbered; XBT stations (open triangles) are not.

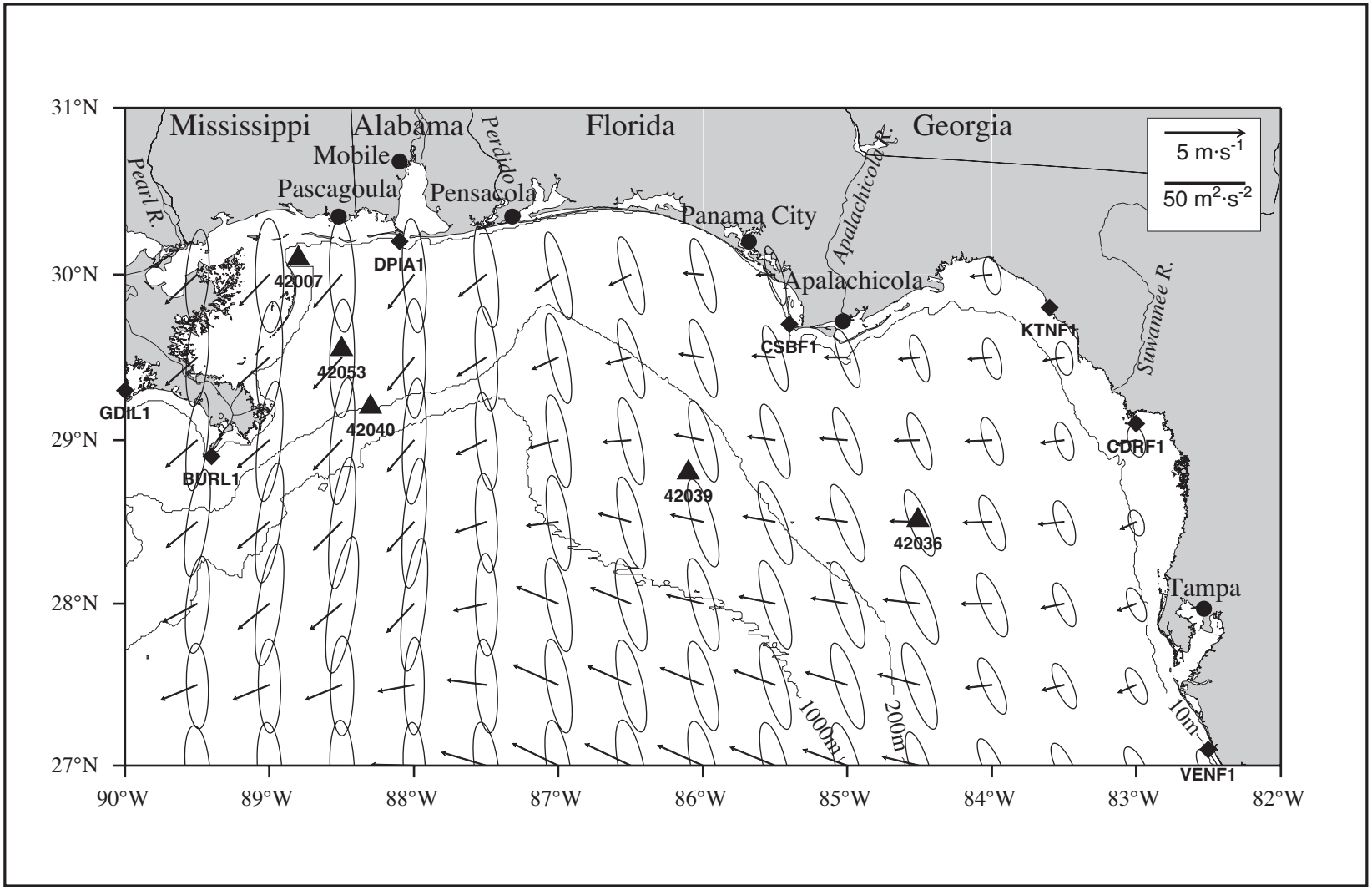

Figure D.1.1-1. Vector mean winds and variance ellipses for cruise N4 in November 1998.

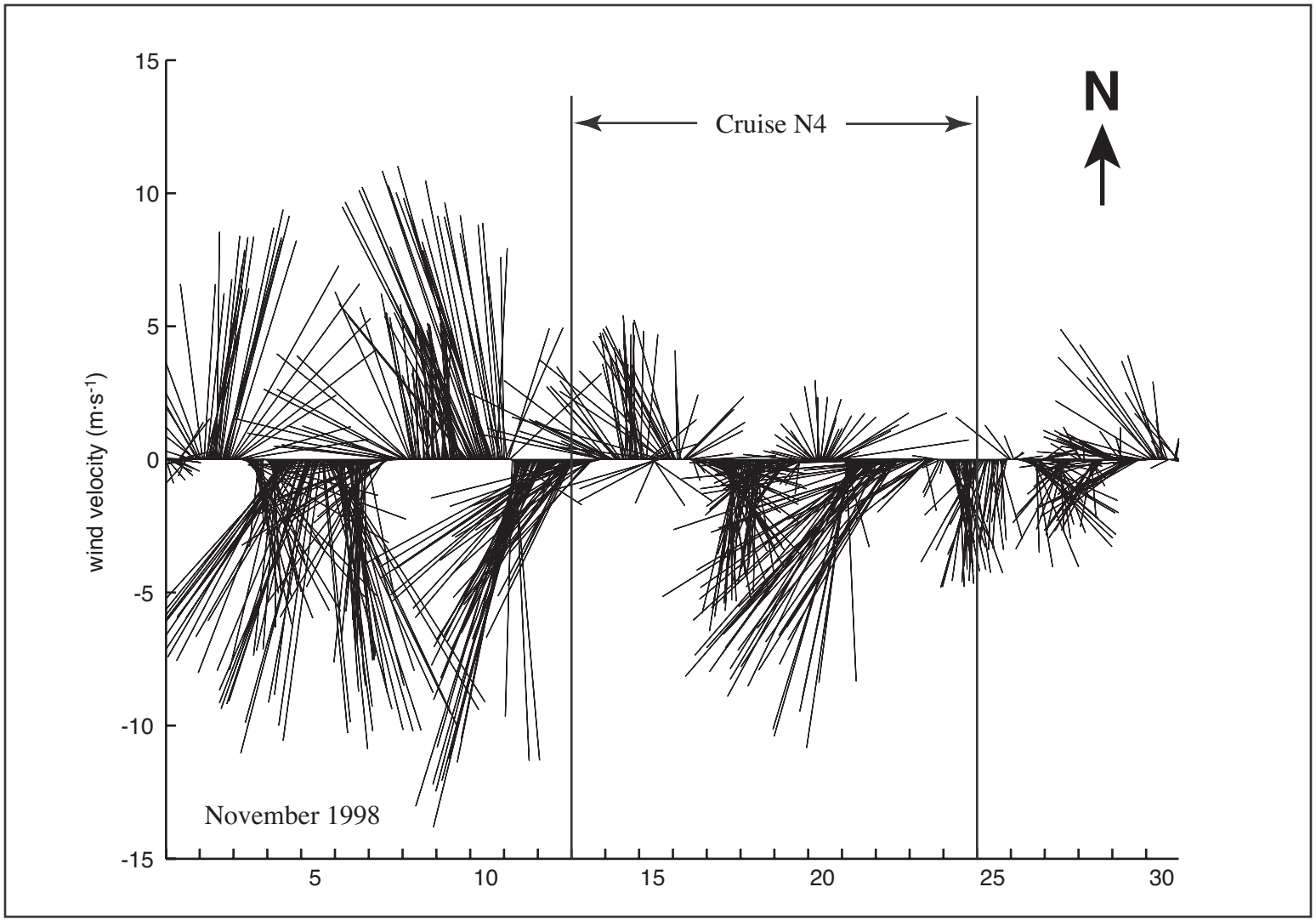

Figure D.1.1-2. Vector stick plot of wind at meteorological buoy 42040 for November 1998. Gauge height is 10 m.

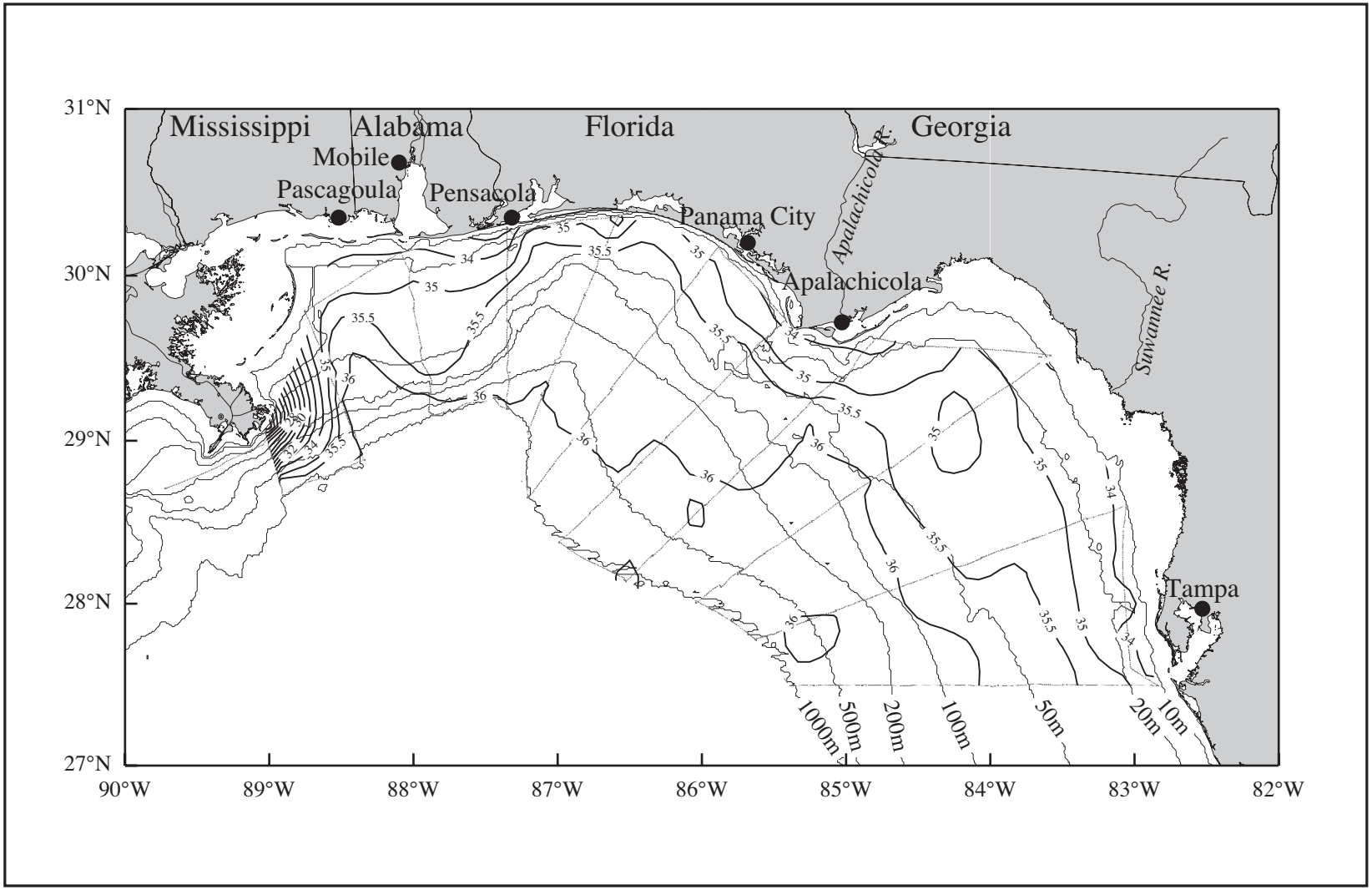

Figure D.1.2-1. Salinity at ~3 m from thermosalinograph observations on cruise N4 in November 1998.

Elsewhere relatively low salinity is confined to the inner shelf. The offshore salinity gradient is weak east of the Mississippi River from Pascagoula to Tampa with inshore values of 33.5 and offshore values on the order of 36 and higher. Between Pensacola and Panama City coastal salinity values were slightly increased to 34.5-35 as isohalines followed the bathymetry of the DeSoto Canyon and brought more saline water closer to shore.

The effects of the distribution of relatively low salinity water can also be seen in the patterns of near-surface chlorophyll *a* (Figure D.1.2-2) calculated from the underway, flow-through fluorescence and percent transmission (Figure D.1.2-3). High chlorophyll *a* (> 1.5 $\mu g \cdot L^{-1}$) and low percent transmission (< 20%) values coincide with the lowest salinity values in the Mississippi River plume. High chlorophyll *a* is also seen at the mouths of the Perdido River (> 2.0 $\mu g \cdot L^{-1}$) (near station 71) and Apalachicola Bay (> 1.5 $\mu g \cdot L^{-1}$) as well as a small patch of high chlorophyll *a* (> 2.0 $\mu g \cdot L^{-1}$) north of Tampa.

D.1.3 SSH Fields Adjacent to the Shelf

The time series of SSH fields for 30 September through 2 December 1998 (Figures 3.2.3-14, 3.2.3-15, 3.2.3-16) show the development of a weak, stationary, peanut-shaped anticyclone over the DeSoto Slope and the base of DeSoto Canyon extending eastward as far as 86.5°W and as far south as 28°N. A maximum SSH of ~20 cm occurred around 28 October and rarely exceeded 10 cm during the N4 cruise. There were no named Loop Current eddies in the vicinity of the study region; the Loop Current was well to the south, penetrating northward only to 26°N. A large circular cyclone (SSH about -20 cm) was present between the slope anticyclone and the Loop Current and centered at 26.2°N and 88.1°W. SSH for 18 November 1998 (Figure D.1.3-1) shows the weak slope anticyclone and the northern limb of the cyclone to the south.

D.2 *In Situ* Evidence of Circulation

The MMS-sponsored NEGOM DeSoto Canyon Eddy Intrusion Study (EIS), conducted by Science Applications International Corporation (SAIC), deployed 13 current meter moorings in the DeSoto Canyon region during the time of the N4 cruise. Monthly mean current speeds and variance ellipses were constructed for the month of November 1998 at 20 m below the surface. The current measurements were made using twelve 300 kHz broadband and one 150 kHz narrowband ADCP. The moorings were placed along four cross-slope lines: A, B, C, and D, with A being the most westward line and D the most eastward. Mooring numbers were assigned with increasing total water depth, where mooring A1 was the shallowest mooring on line A and A3 was the deepest. Line E consisted of a single mooring placed at 28.6°N, 86.2°W. Figure D.2-1 shows mean currents are to the east over much of the DeSoto Canyon in agreement with SSH fields during the cruise. The influence of the offshore eddy south of the DeSoto slope is to drive the currents anticyclonically toward the east. Mean speeds range from 25 to 60 $cm \cdot s^{-1}$ over the DeSoto slope (A1-3, B1-3, and C1-3), 85 $cm \cdot s^{-1}$ on the shallow shelf location (D1), and 20-30 $cm \cdot s^{-1}$ on the eastern side of the DeSoto Canyon (D2, D9, and E1). The mean vector velocity at the offshore location of A3 is directed north-northwest, indicative of the western limb of the elongated anticyclone seen in the SSH field of Figure D.1.3-1. Variance ellipses are elongated and oriented with the major axis along the bathymetry in the western locations. At eastern locations D2, D9, and E1, the ellipses are oriented across bathymetry.

Early during cruise N4, the 150 kHz broadband ADCP malfunctioned; a replacement narrowband 150 kHz ADCP was obtained late in the cruise. Thus, shipboard ADCP data are available only along Lines 1-4 (i.e., over the Mississippi-Alabama shelf). ADCP currents in a

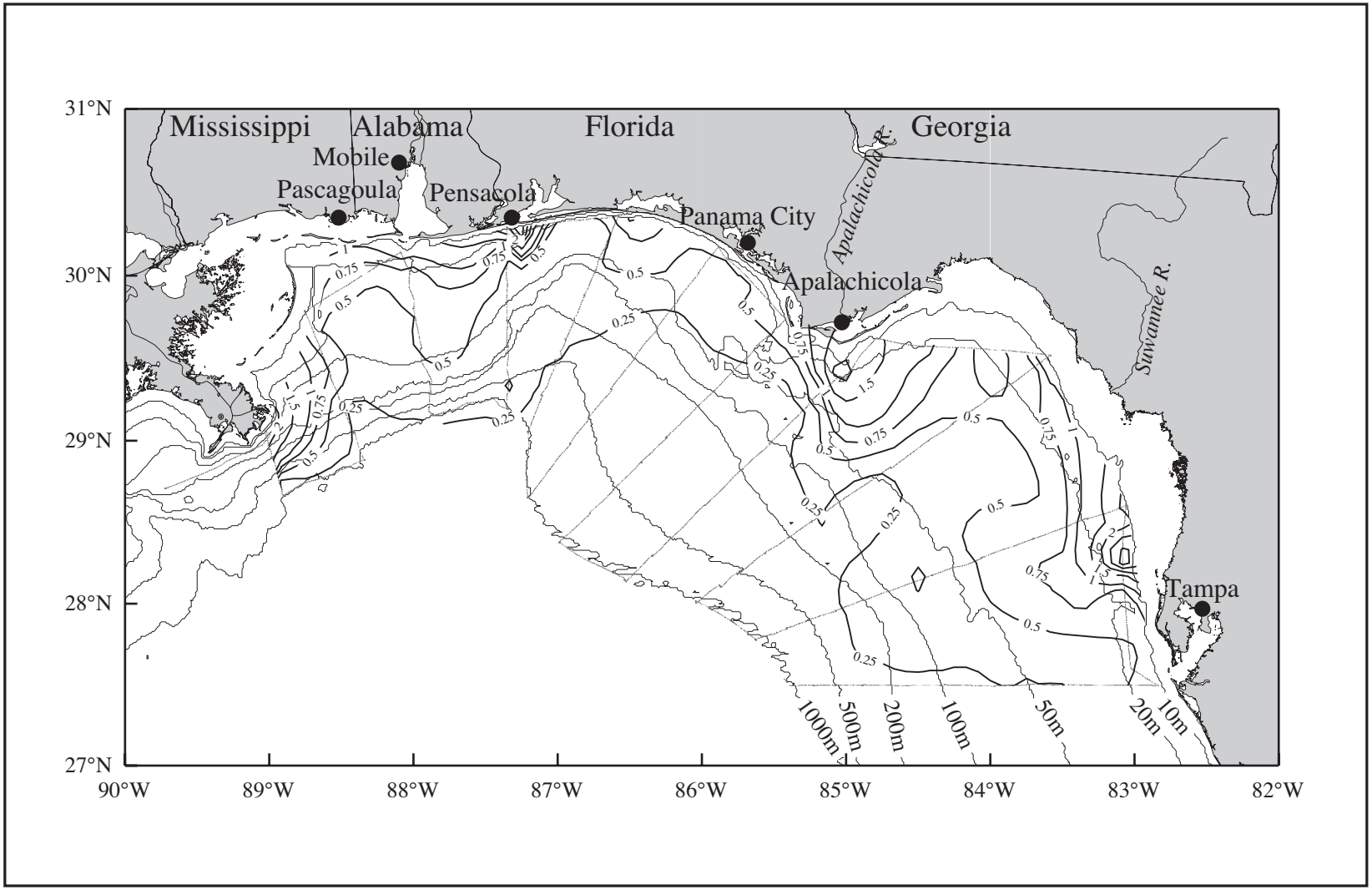

Figure D.1.2-2. Chlorophyll *a* ($\mu g \cdot L^{-1}$) at ~3 m calculated from flow-through fluorescence on cruise N4 in November 1998.

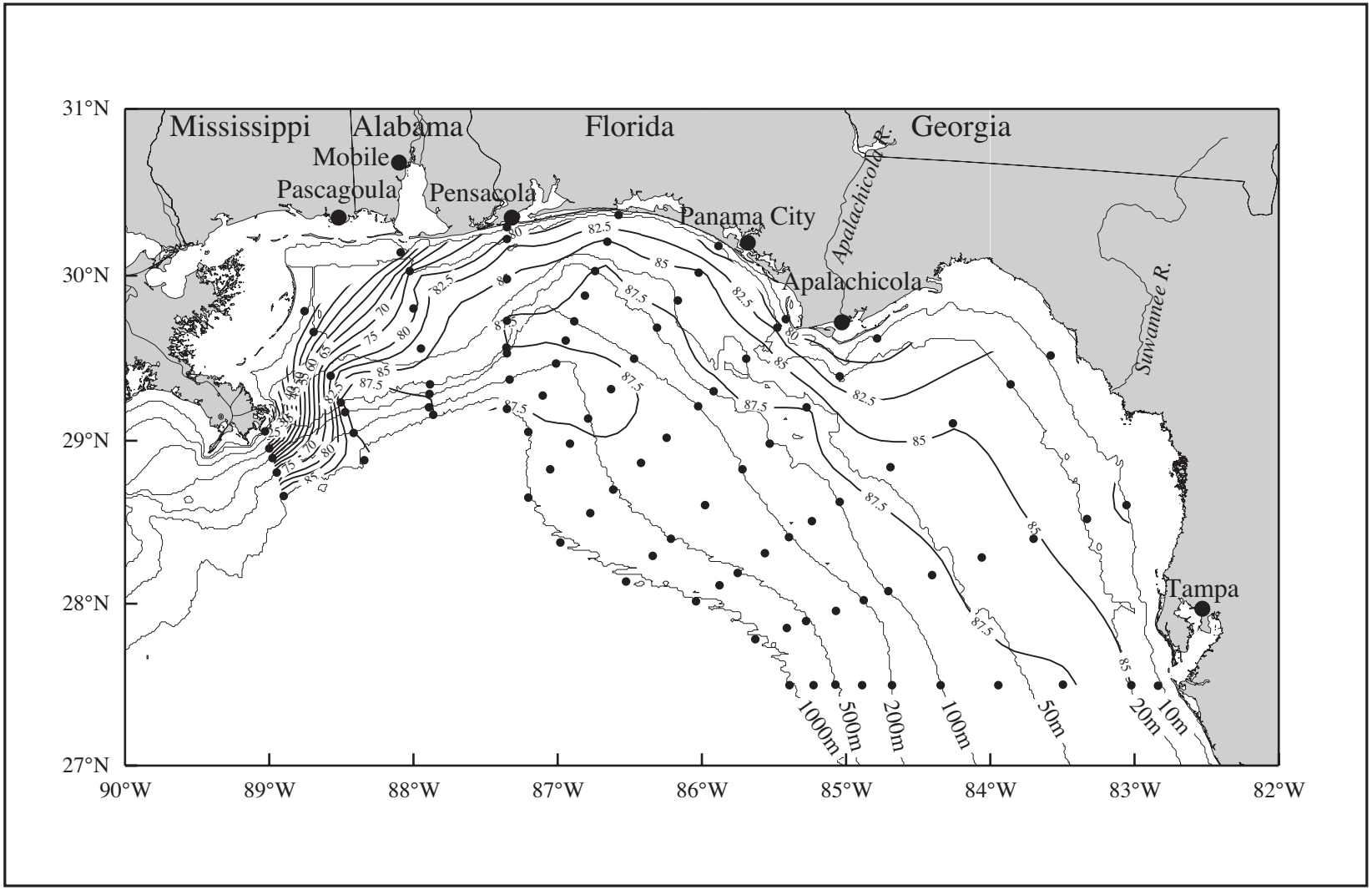

Figure D.1.2-3. Percent transmission (660 nm wave length; 25-cm path length) from the near-surface (~3.5 m) observations on cruise N4 in November 1998.

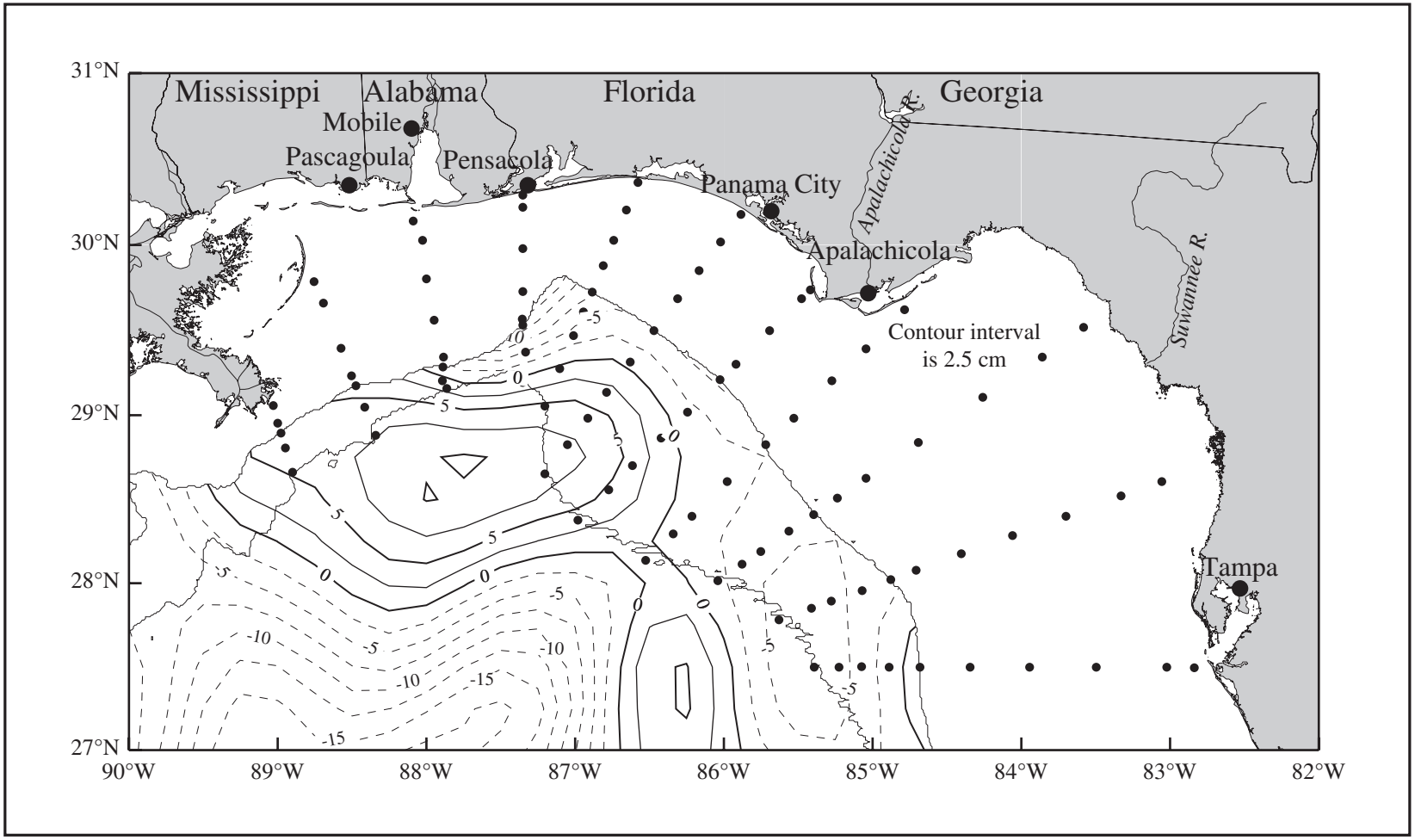

Figure D.1.3-1. Sea surface height field from satellite altimeter data for 18 November 1998 during cruise N4. The 200- and 1000-m isobath contours and CTD stations (dots) are shown. [Data provided by Robert R. Leben, University of Colorado.]

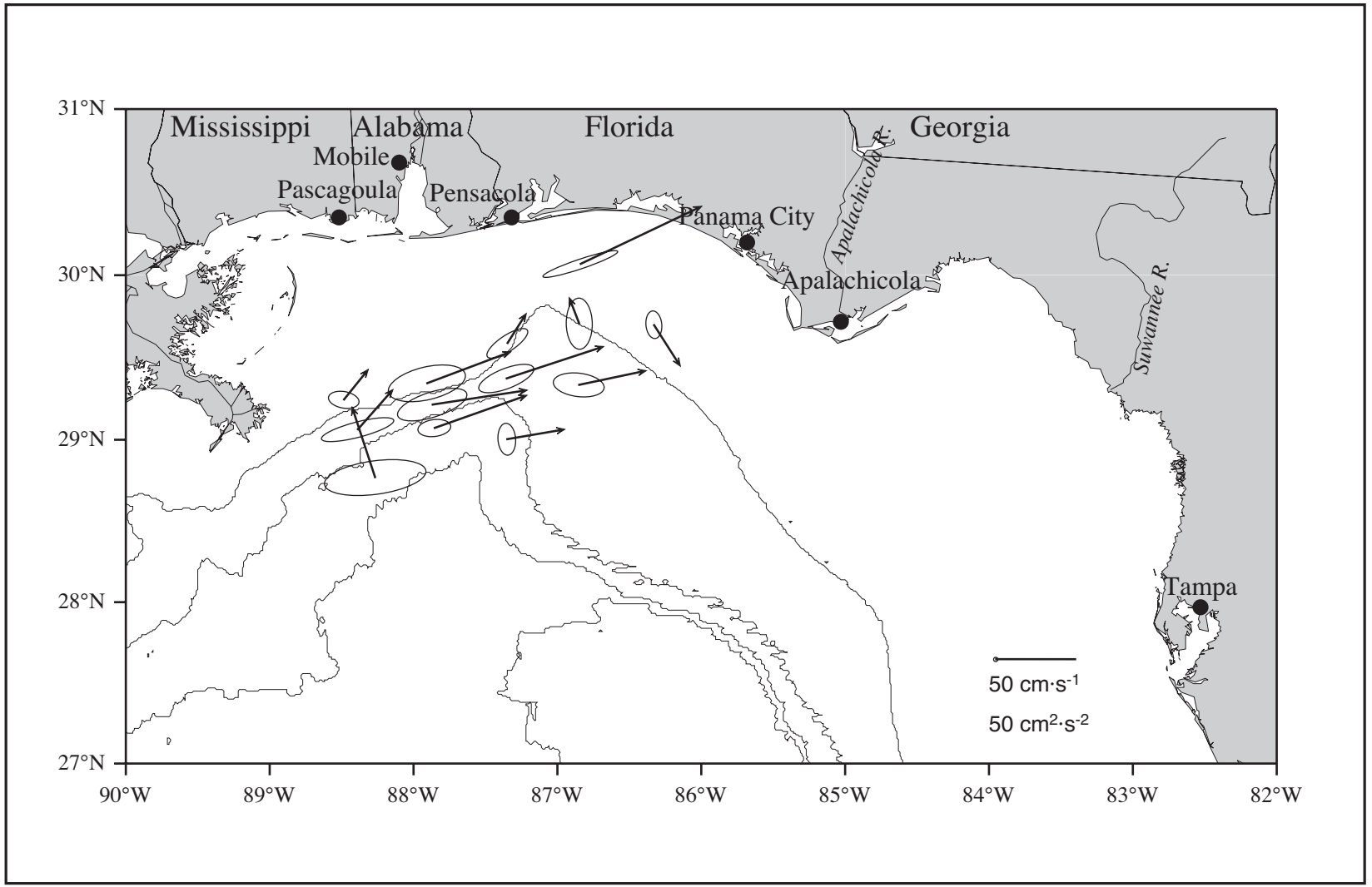

Figure D.2-1. November 1998 mean current vectors and variance ellipses for SAIC current measurements at 20-m depth. Shown are the 200-, 1000-, 2000-, and 3000-m isobaths.

4-m depth bin centered at 12-m depth are shown in Figure D.2-2. Offshore of the 100-m isobath, currents are directed upcoast to the east indicating the influence of the anticyclone hovering over the slope region (Figures D.1.3-1 and D.2-1). Inshore of the 100-m isobath, currents are directed downcoast and to the west indicating the influence of the local wind fields (Figure D.1.1-1). ADCP currents at 100-m depth (not shown) also were upcoast (eastward) and oriented along the bathymetry. The vertical structure of ADCP currents shows high coherence from the surface to the bottom, or maximum range of good ADCP data if deeper. Figure D.2-3 shows the vertical profiles of along-shelf currents from lines 1, 2, and 3 showing predominantly upcoast velocity offshore in depths greater than 50 m and downcoast currents nearshore in shallow water.

Geopotential anomaly at 3 m relative to 800 m based on cruise N4 data (Figure D.2-4) shows the edge of the offshore anticyclone in the western region, in agreement with the direct measurement by the ADCP. The indicated flow is complicated and, except for the outer shelf, is not in agreement with ADCP measurements over the Mississippi-Alabama shelf. There is much cross-isobath flow indicated. There is substantial deviation between the bottom isopycnals and isobaths (not shown), indicating the pycnobathic effect may be producing pycnobathic currents. We assign little credibility to the flow pattern indicated in Figure D.2-4.

D.3 Property Distributions

The temperature field at 3-m depth observed on N4 is shown in Figure D.3-1. There is a general cross-shelf temperature gradient with relatively cool water (<24°C) inshore and warm water (>25°C) offshore. The coastal waters between the Mississippi River delta and Apalachicola Bay are less than 22.5°C. The coastal water west of the West Florida Bight is slightly greater at 23.5°C. Offshore and southeast of the Mississippi River delta there is a strong temperature gradient from 22.5°C inshore to >25°C offshore along line 1. The temperature gradient is smaller over the west Florida shelf where temperatures are almost uniformly 25°C in water depths greater than 50 m. Steeper cross-shelf temperature gradients exist around Cape San Blas and across the Mississippi-Alabama shelf.

The presence of the Mississippi River plume is clearly seen along lines 1 and 2 in the salinity field at 3 m depth observed on N4 (Figure D.1.2-1) and coincides with cooler near-surface temperatures seen in Figure D.3-1. A tongue of saline water (>36.2) can be seen intruding onto the Mississippi-Alabama shelf between lines 2 and 3 in response to the buoyant plume to the west and on slope flow due to the high SSH south of lines 1-3 and enhanced by the dynamic low at the coastal side on line 2. Indications of this intrusion are seen as an onshore component of the current vectors along line 2 in the near-surface (12 m) plot of currents (Figure D.2-2). Near bottom temperatures (Figure D.3-2) show typical patterns of decreasing bottom temperature with increasing bottom depth. However, as stated for the fall N1 cruise (Section A.3), there is a slight indication of warm bottom temperatures in the middle inner-shelves between 10 and 50 m depth which reflects the fall cooling and mixing that reaches bottom in the nearshore regions before cooling waters deeper and further offshore.

Near bottom salinity observations, Figure D.3-3, show a narrow band of relatively high salinity greater than 36 and as large as 36.6 between 50 and 150 m depth and stretching across the entire study region. As stated previously, this indicates the intersection of the core of Subtropical Underwater with the bottom.

Examination of the vertical structure of potential temperature, salinity, and density both cross-shelf and along the 100-, 200-, 500-, and 1000-m isobaths confirms that waters are

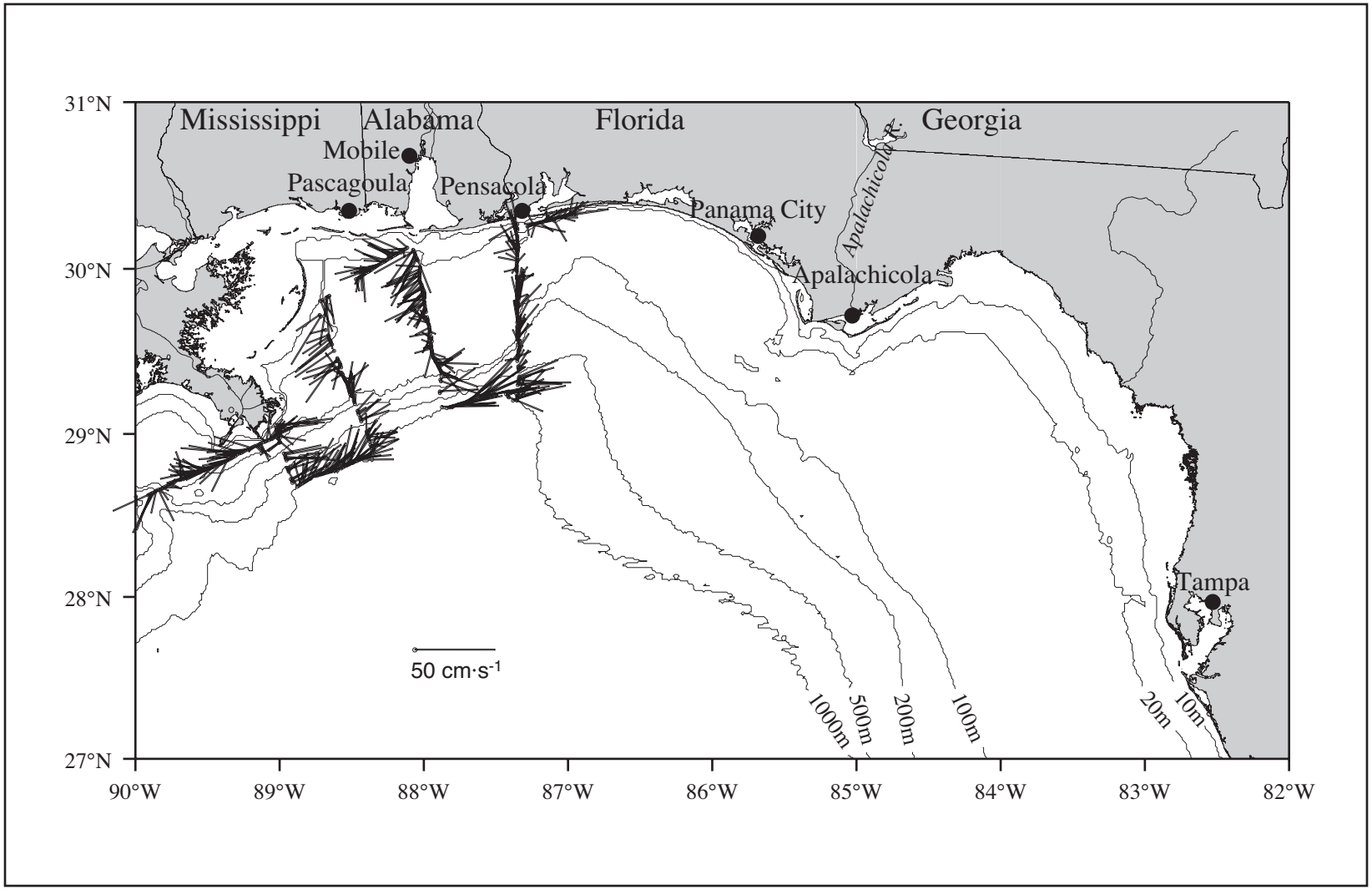

Figure D.2-2. ADCP-measured currents for the 4-m bin centered at 12 m on cruise N4 in November 1998

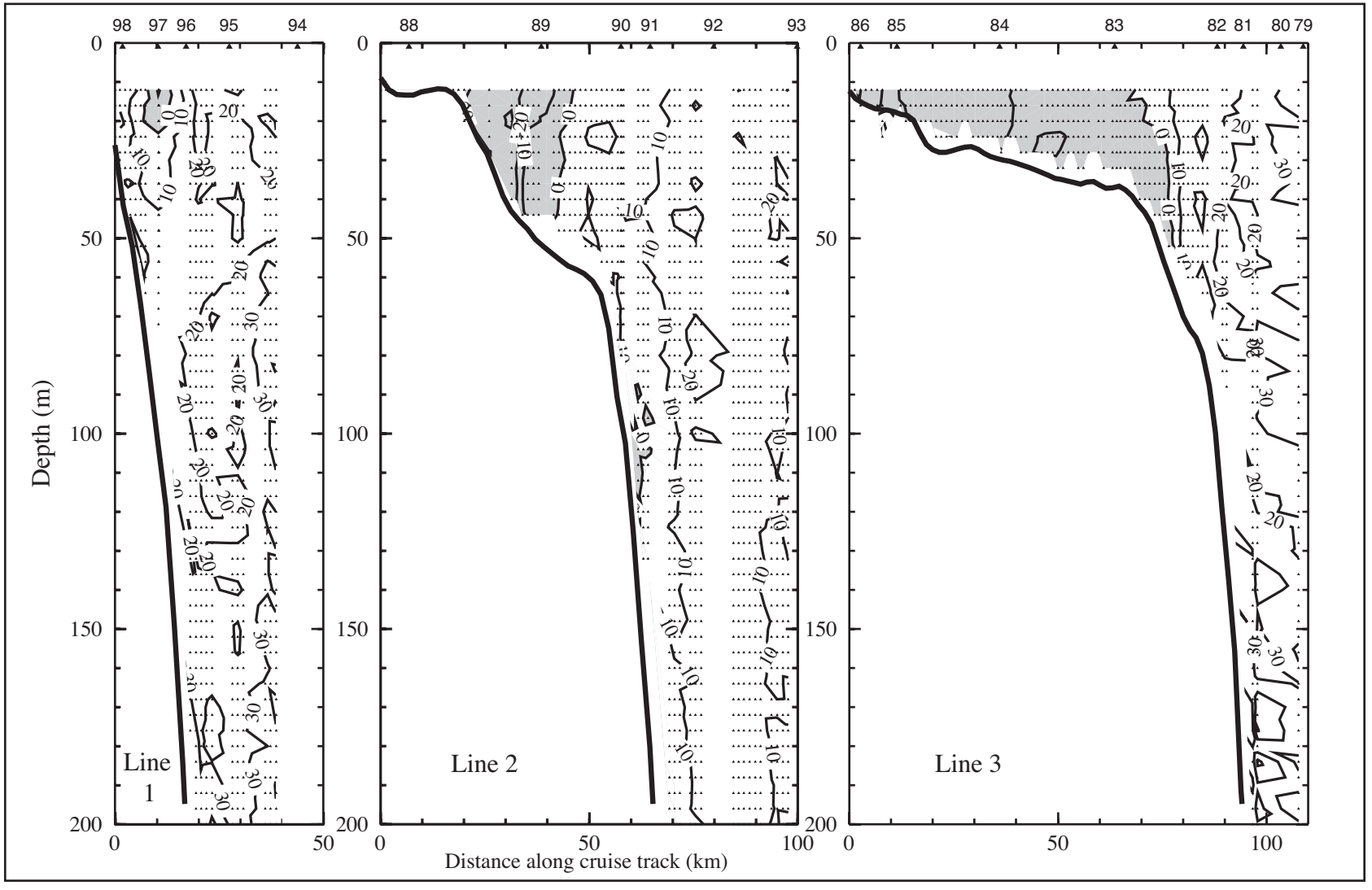

Figure D.2-3. Cross-transect velocity ($cm \cdot s^{-1}$) on lines 1, 2, and 3 on cruise N4 in November 1998. CTD station numbers are shown above each profile.

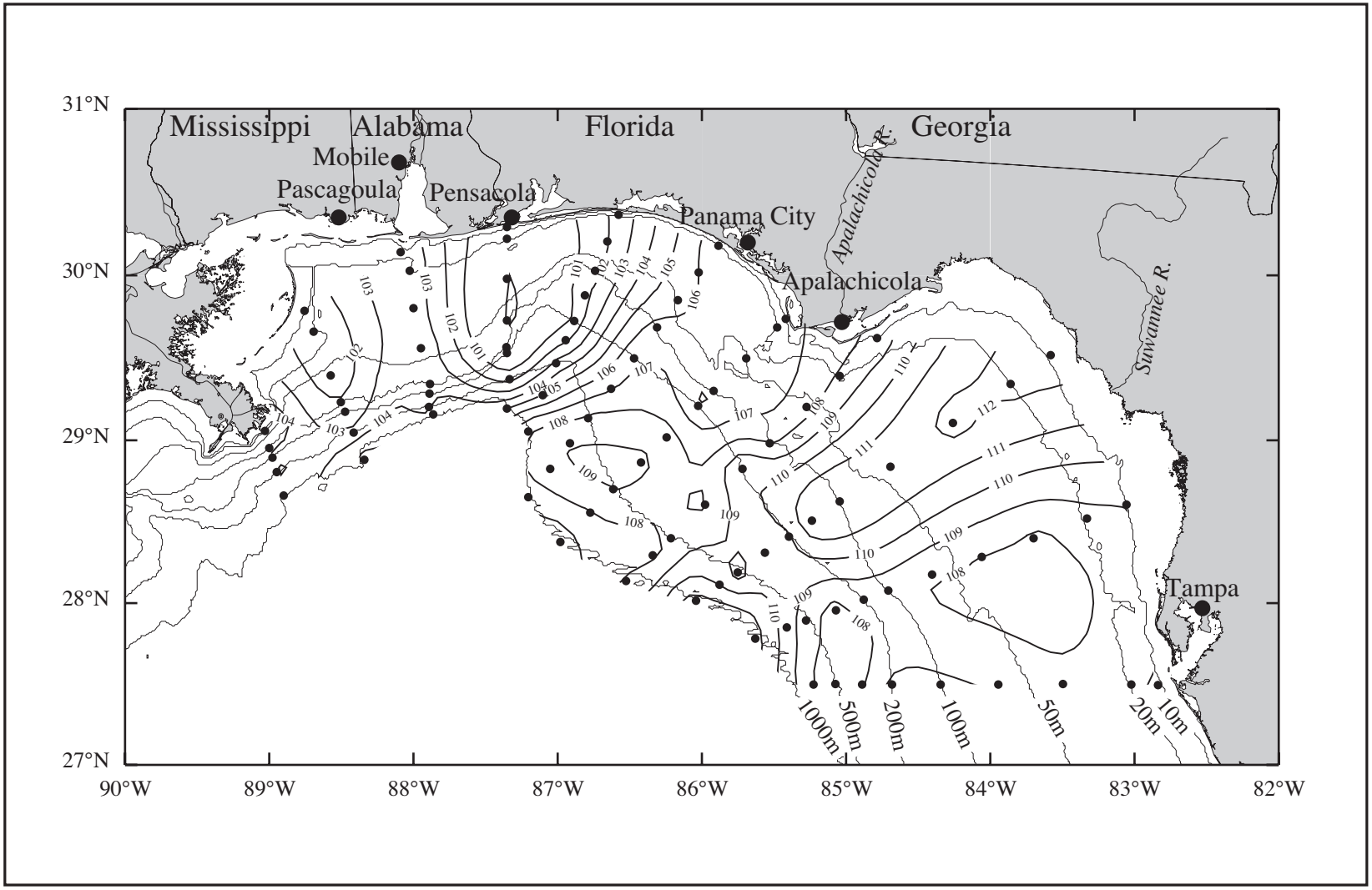

Figure D.2-4. Geopotential anomaly (dyn cm; 3 m relative to 800 m) for cruise N4 in 13-24 November 1998. CTD stations are shown.

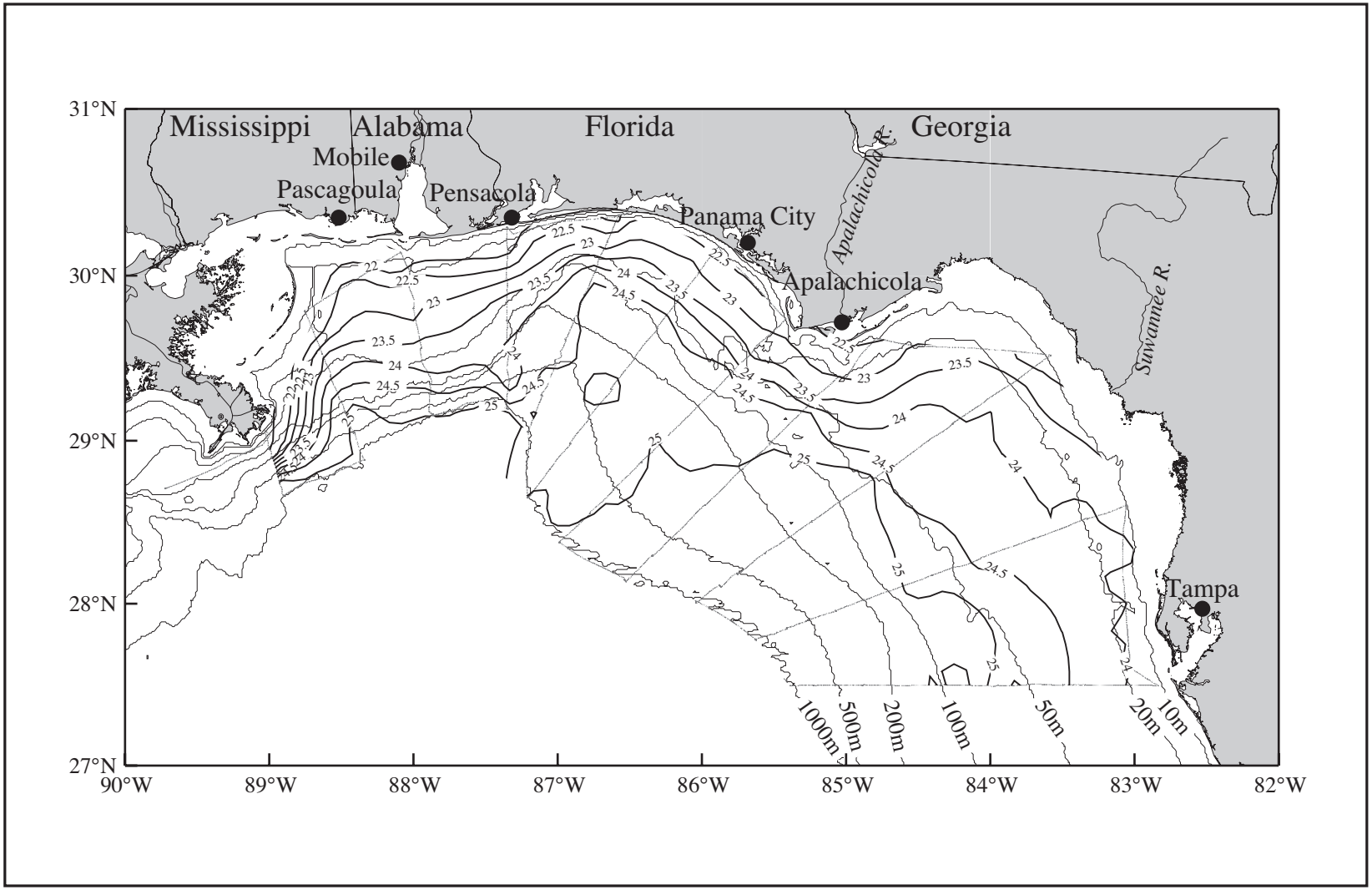

Figure D.3-1. Temperature (C) at ~3 m from thermosalinograph observations on cruise N4 in November 1998.

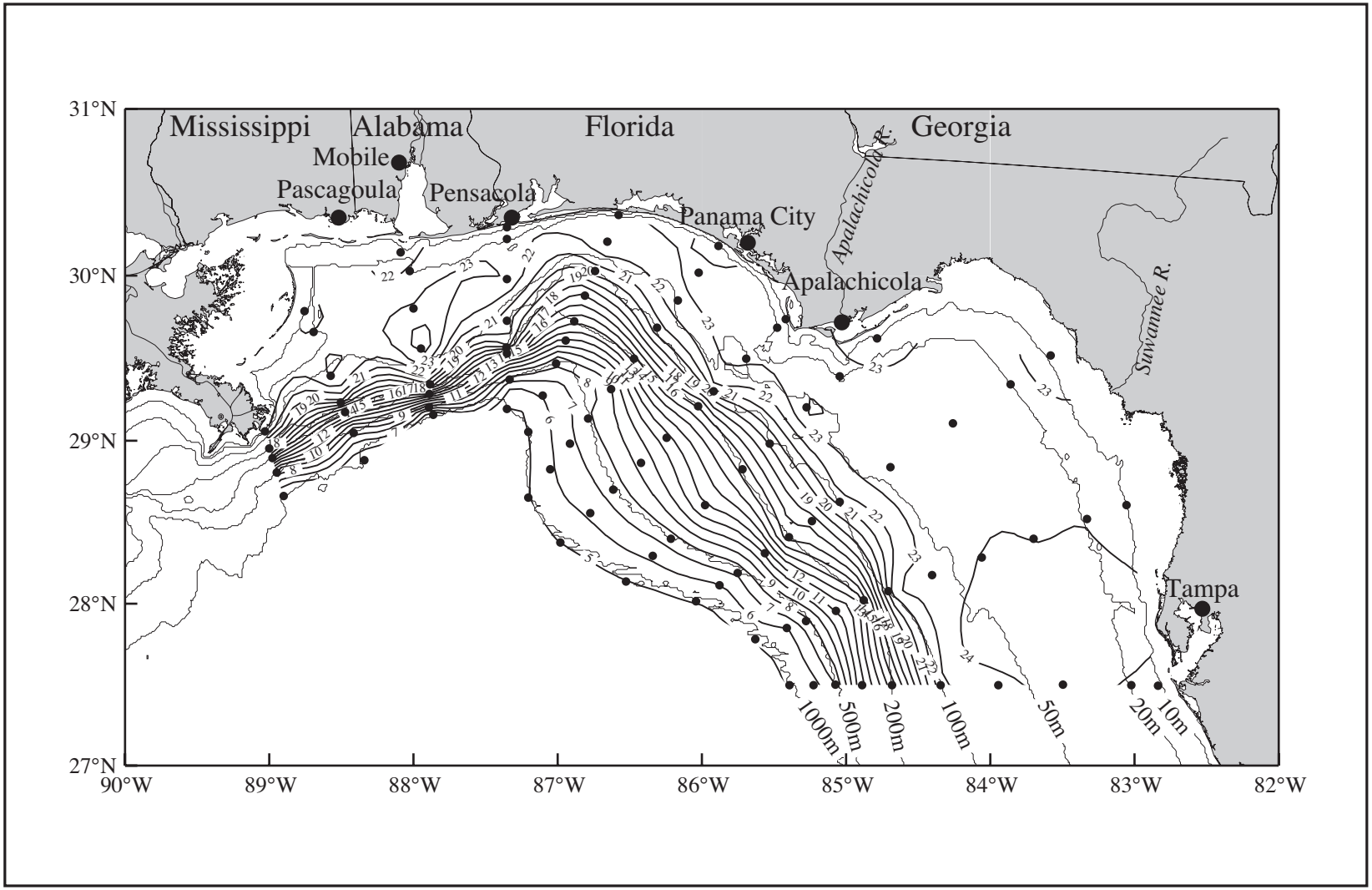

Figure D.3-2. Potential temperature (°C) from near-bottom observations on cruise N4 during 13-24 November 1998.

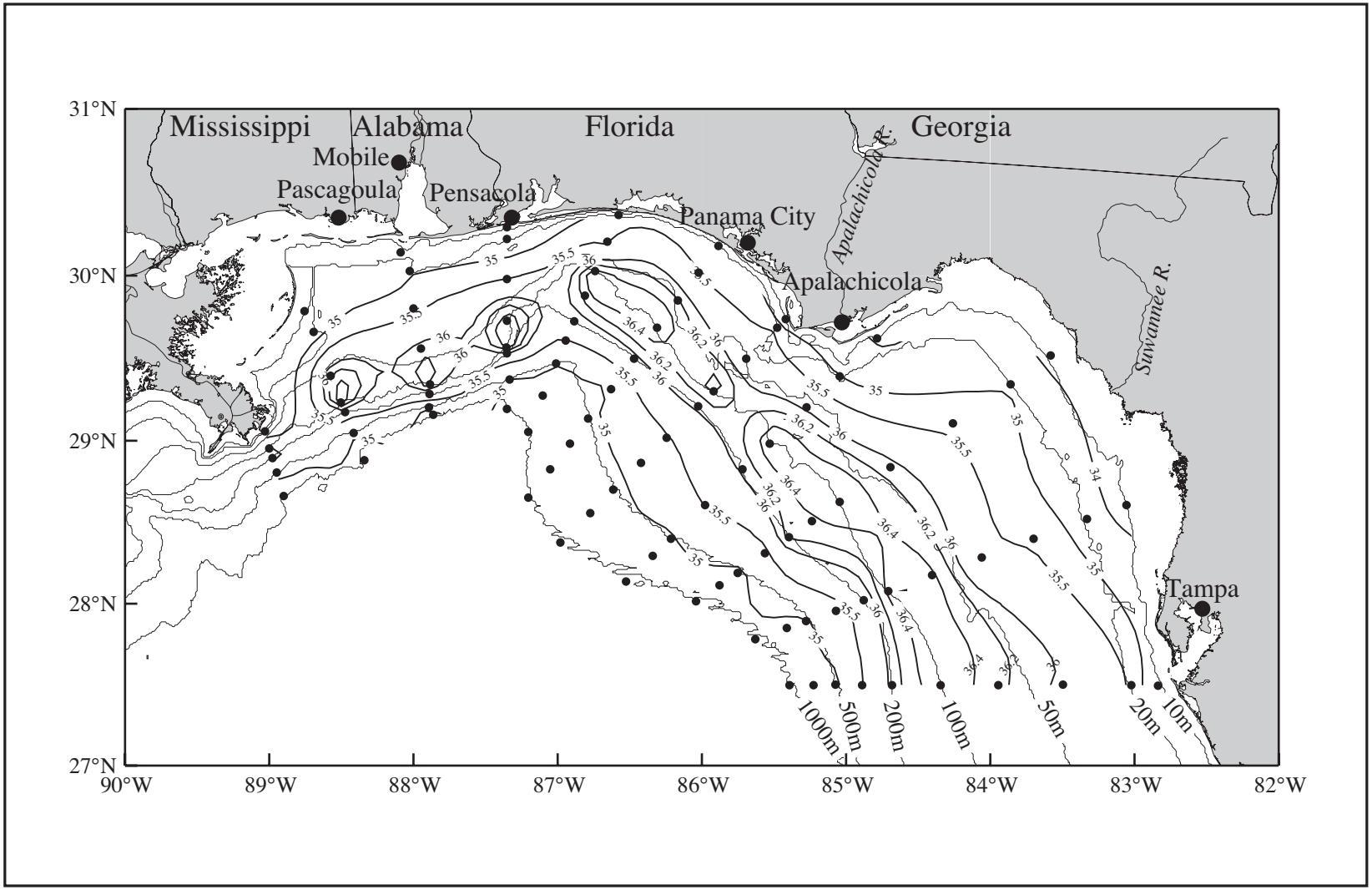

Figure D.3-3. Salinity from near-bottom observations on cruise N4 during 13-24 November 1998.

relatively well-mixed down to about 70-m depth. As with previous cruises, nutrient and oxygen concentrations confirm this basic pattern of a well-mixed upper layer of several tens of meters.

Below the mixed layer along the 1000-m isobath, nutrient concentrations increase with depth from depleted values in the mixed-layer. Phosphate and nitrate have maximum values around 650-700 m depth coinciding with the Antarctic Intermediate Water remnant.

At stations along the 500-m isobath, two prominent features are seen below water depths of 200 m in the vertical plot of density anomaly (Figure D.3-4). The 27.2 $kg \cdot m^{-3}$ isopycnal is displaced upwards about 125 m at station 77 and about 50 m at station 39. The vertical displacement is seen in salinity and temperature as well as in nutrient concentrations. By the upward doming of isolines, the vertical section of silicate concentration (Figure D.3-5) reflects the presence of two deep cyclonic features with diameters on the order of 50 km centered at stations 39 and 77. Cross-shelf vertical profiles of potential temperature along line 4 (Figure D.3-6) shows isotherms less than 11°C shoaling up the slope beginning inshore of the 1000 m station and at depths greater than 250 m. Indications of uplift also are seen along the slope at depths greater than 250 m at lines 6, 7, 8, and 9 and deeper at line 10. Line 5 shows only slight evidence of the uplift.

The dooming at station 77 on line 4 is consistent with the cyclonic flow indicated there in the SSH (Figure D.1.3-1) and in ADCP (Figure D.2-2) fields. Moreover, the SSH field indicates lowering of sea level (cyclonic tending) toward the shelf edge along lines 6-9, consonant with property distributions.

There are other areas of localized uplift on the shelf in waters less than 200 m. On line 10, high nutrient concentrations can be seen near-bottom in the vertical profiles along the 100-m and 200-m isobaths (Station 16 in Figure D.3-7 and station 17 in Figure D.3-8). The high nutrients at these stations coincide with anomalously low salinity and cooler temperatures indicative of upwelling of slope waters onto the shelf.

The near-surface (~3.5 m) silicate concentration (Figure D.3-9) shows an area of high concentrations (> 8 μM) exiting the Choctawhatchee Bay near 86.7°W and 30.3°N. Other nutrient (nitrate, phosphate) concentrations do not show increases in this region. The vertical profile of silicate concentration along line 5 (Figure D.3-10) shows an increase of near-bottom silicate concentration at 100-200 m depth. The near-bottom increase is not seen on lines 4 and 6 to the east and west or in the nitrate or phosphate concentrations on line 5. For these reasons, we believe this is not an upwelling event but sediment resuspension by currents in the DeSoto Canyon or perhaps a turbid flow originating from the Choctawhatchee Bay. This is confirmed by reduced transmission values near-bottom at station 67 and 68 (not shown).

The depth and eastward extent of the Mississippi River plume is indicated in the 100-m and 200-m isobath vertical sections of silicate concentrations seen in Figures D.3-7 and D.3-8. At the 100-m stations (Figure D.3-7), high silicate concentration associated with the Mississippi River can be seen in the west, extending to 50 m depth but is most concentrated in the upper 10 m. Offshore at the 200-m isobath, the vertical extent of the plume is confined to the upper 100 m. Both figures indicate that the eastward penetration is less than 70 km. Stations at the 500- and 1000-m isobaths show little or no indication of increased nutrient concentrations associated with the plume (Figure D.3-5). These general patterns associated with the plume are repeated in plots of nitrate, phosphate, density, and transmission.

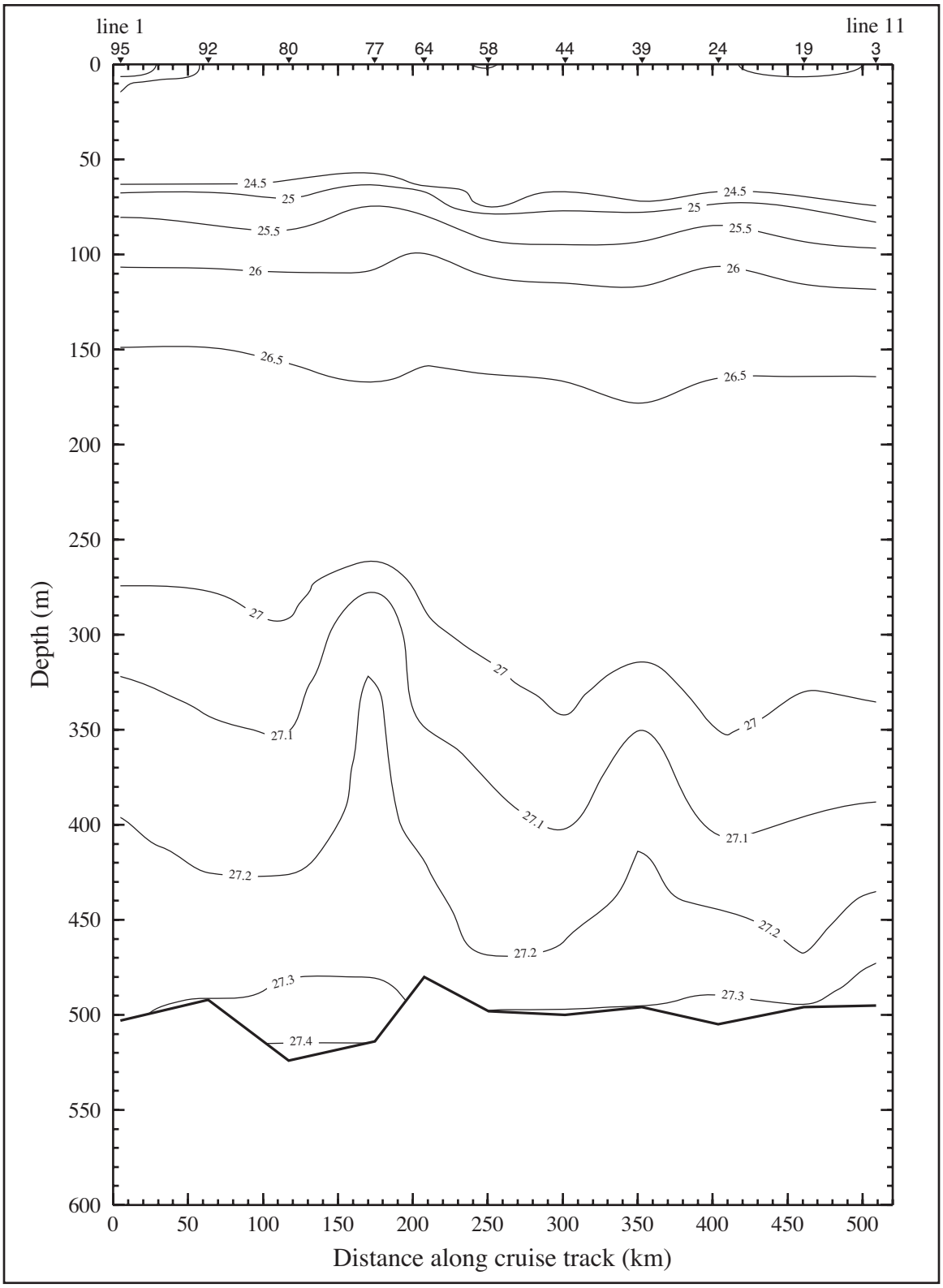

Figure D.3-4. Density anomaly (σ_θ in kg·m^{-3}) along the 500-m isobath of cruise N4 in November 1998. Stations are shown on the top axis.

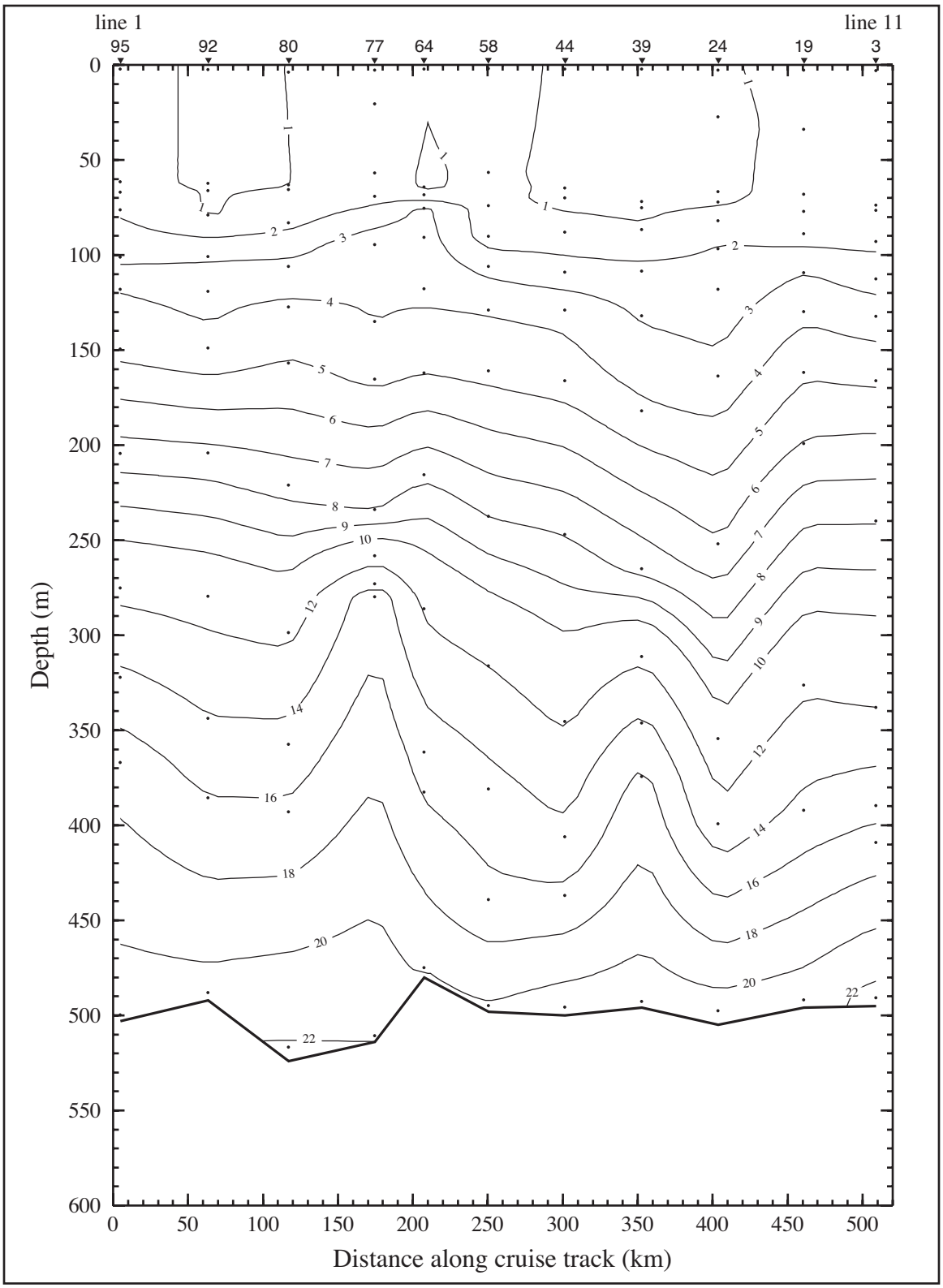

Figure D.3-5. Silicate (μM) along the 500-m isobath of cruise N4 in November 1998. Stations are shown on top axis.

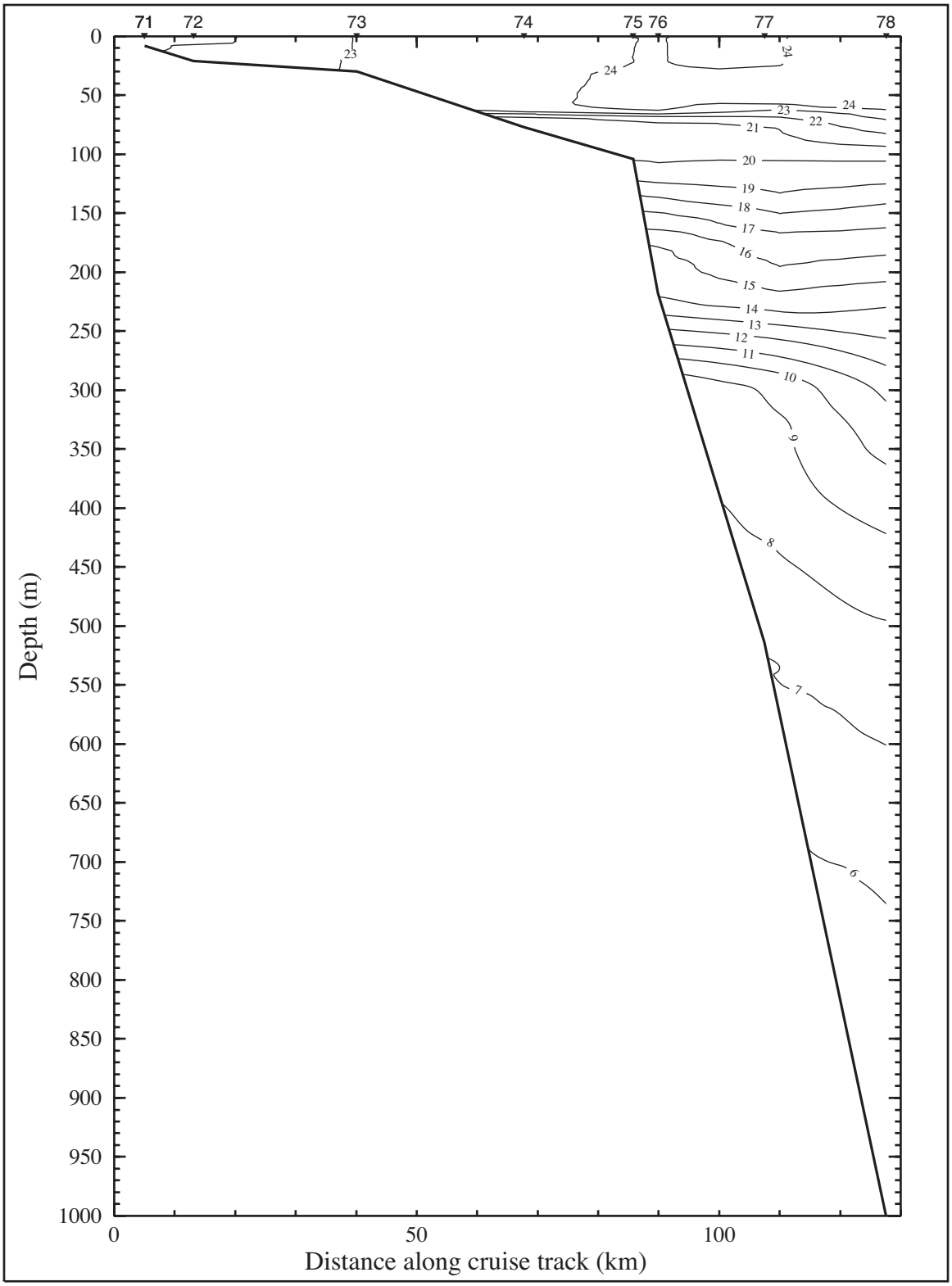

Figure D.3-6. Potential temperature (°C) along line 4 on cruise N4 in November 1998. Stations are shown on top axis. Line 1 is at the left station; line 11 at the right.

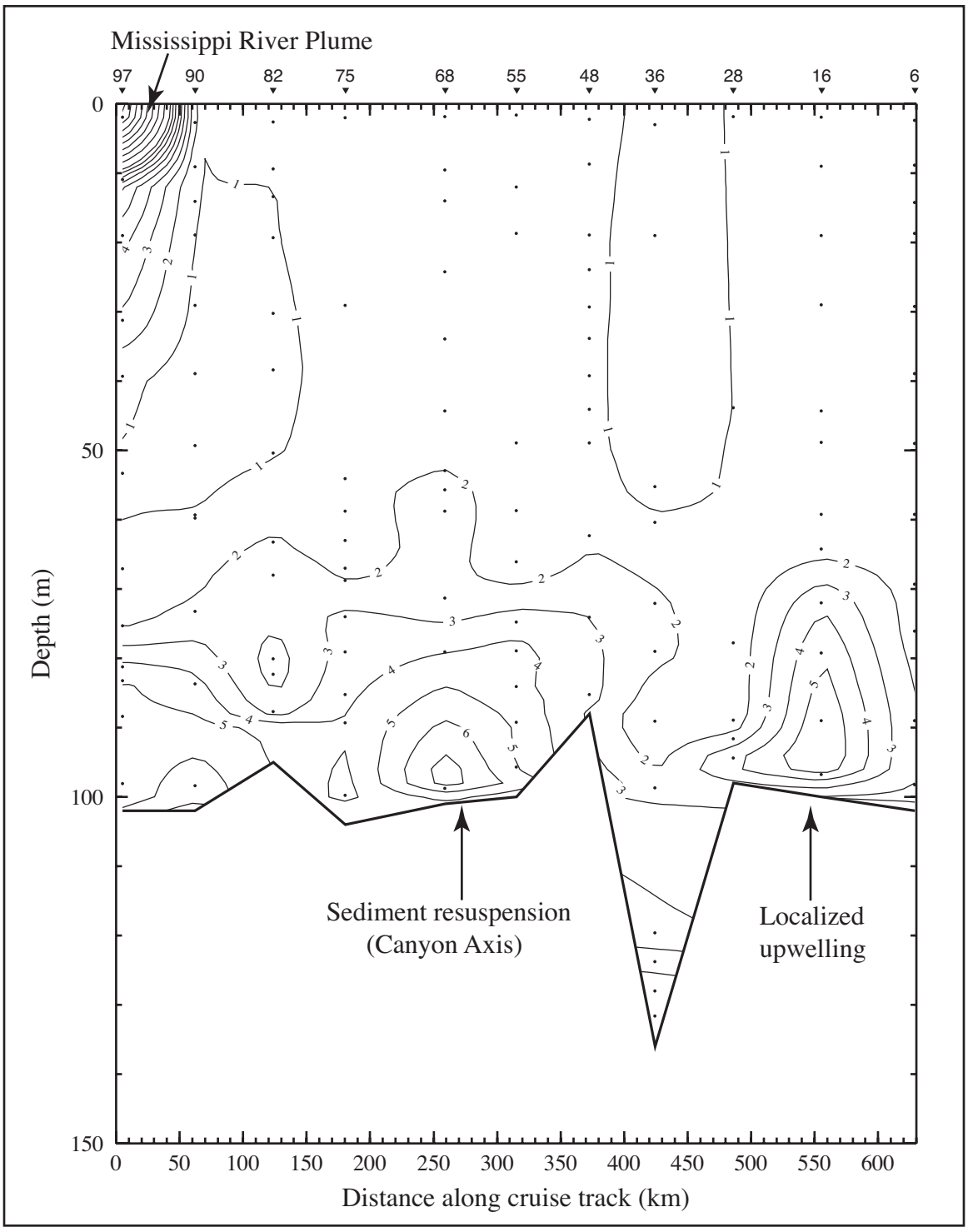

Figure 7.3-7. Silicate (μM) along the 100-m isobath on cruise N4 in November 1998. Stations are shown on the top axis. Line 1 is at the left station; line 11 at the right.

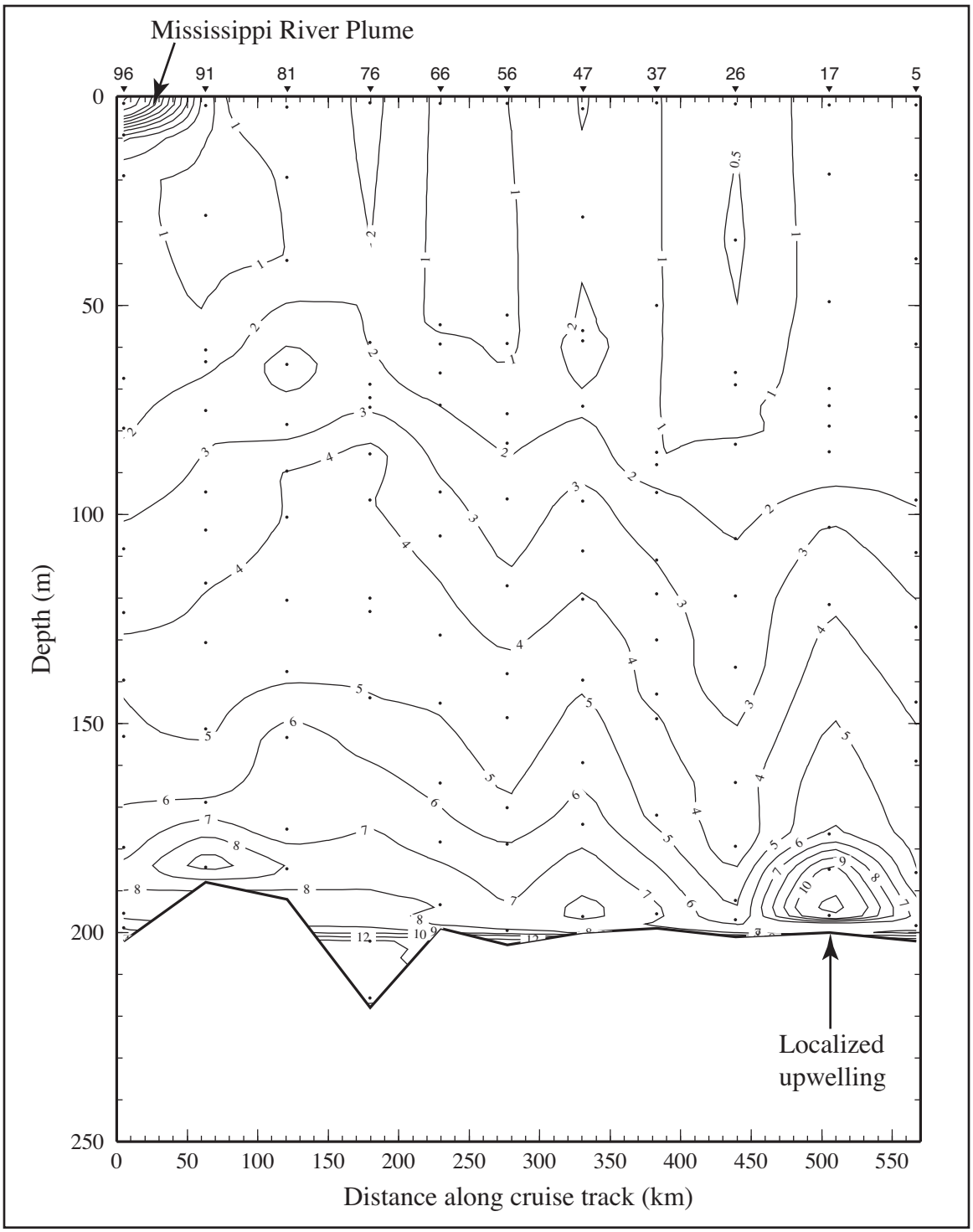

Figure 7.3-8. Silicate (μM) along the 200-m isobath on cruise N4 in November 1998. Stations are shown on the top axis. Line 1 is at the left station; line 11 at the right.

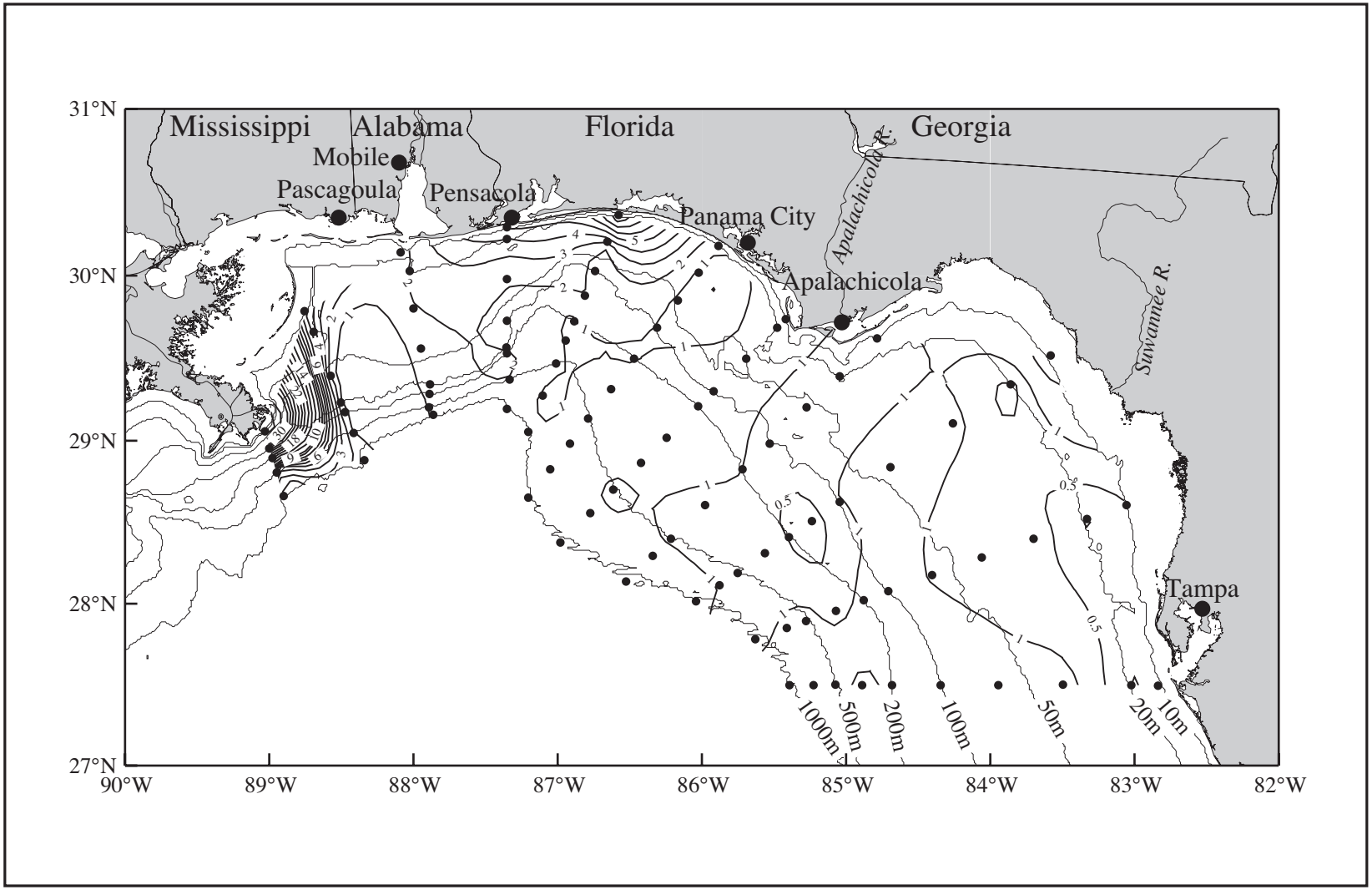

Figure D.3-9. Silicate (μM) from near-surface (~3.5 m) observations on cruise N4 in November 1998.

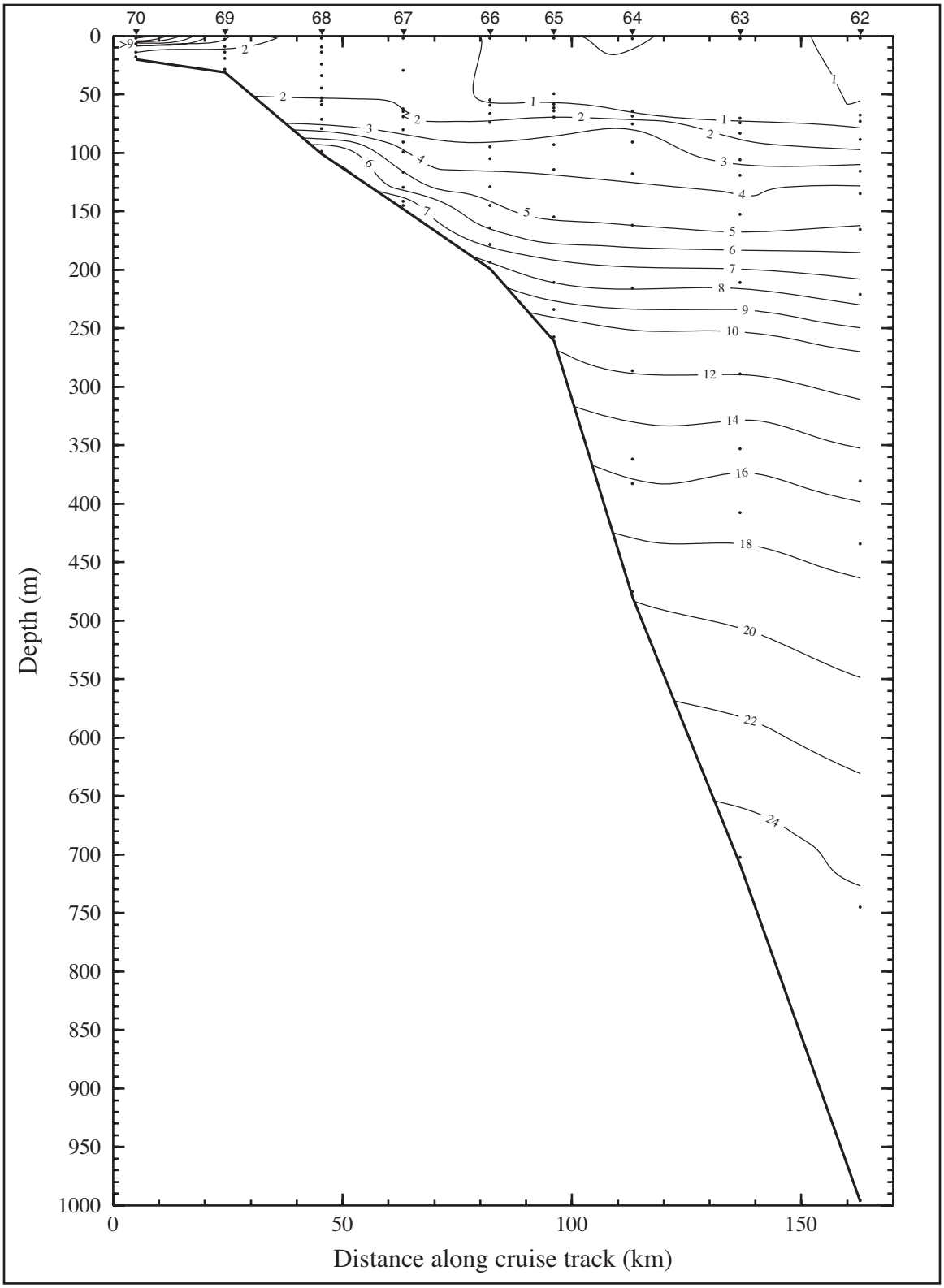

Figure D.3-10. Silicate (μM) along line 5 on cruise N4 in November 1998. Stations are shown on top axis.

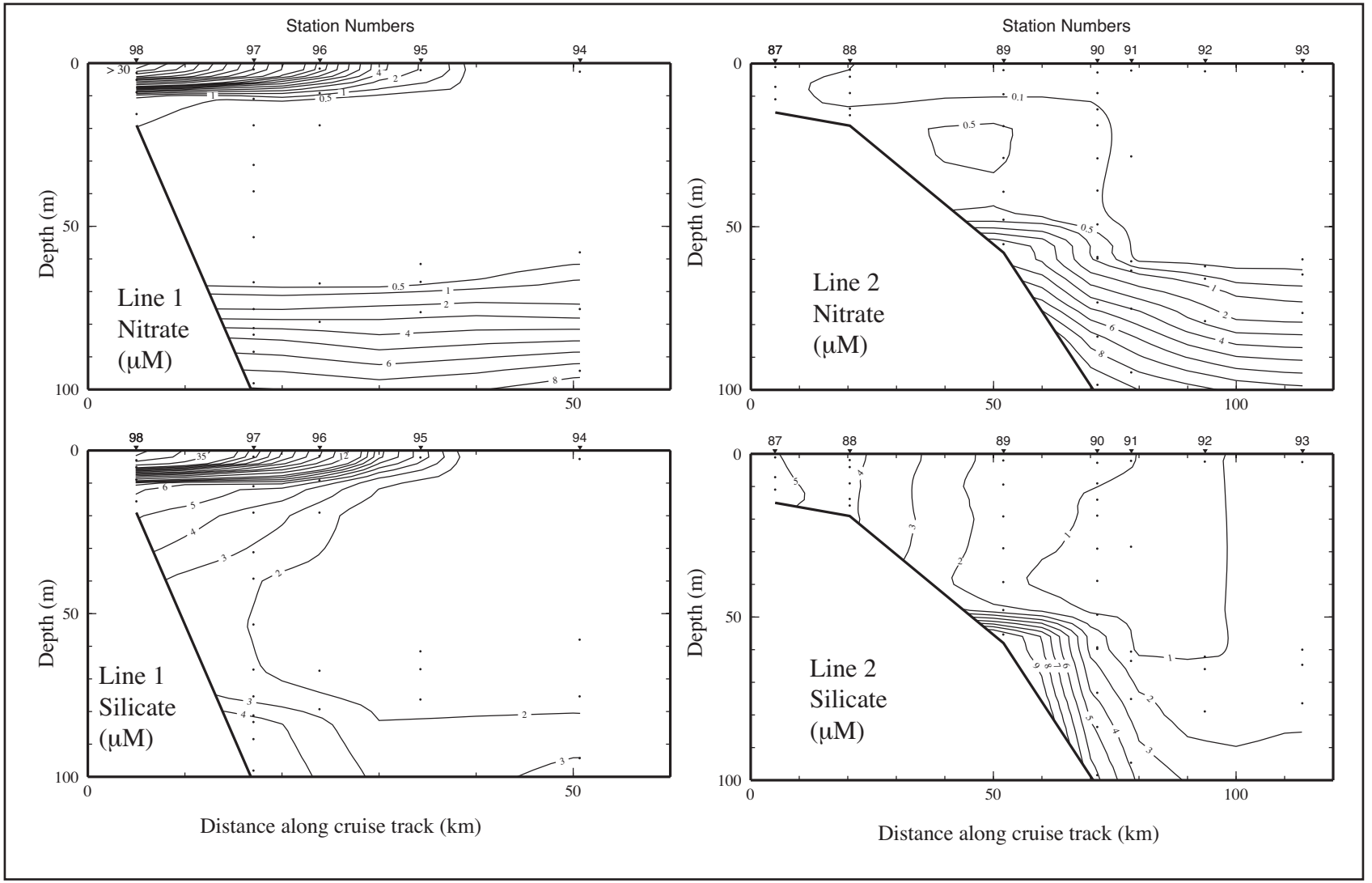

Figure D.3-11. Nitrate and silicate along lines 1 and 2 on cruise N4 in November 1998.

The vertical sections in Figure D.3-11 show nitrate and silicate concentration along lines 1 and 2. The signature of high concentration associated with the Mississippi River plume is clearly seen in the near-surface waters of line 1, but is not present on line 2. There is high silicate concentration near-bottom that may be due to sediment resuspension associated with the upcoast currents as measured by the shipboard ADCP (Figure D.2-2) or to the settling of sediment advected from a silicate-rich turbid region nearshore. The profiles of line 2 also indicate uplift of isopleths between 50- and 100-m depth that is most likely associated with the dynamic low seen at this line and indicated by the ADCP flow pattern of Figure D.2-2.

APPENDIX E
SUMMARY OF CONDITIONS DURING CRUISE N5

Cruise N5 was a spring cruise conducted 15-28 May 1999. The cruise began with a test station at the base of DeSoto Canyon in 750 m water depth. The first complete hydrographic station was the seaward-most station of line 4 followed by a station in the middle of line 4, then seaward repeating the first station. The cruise track continued upcoast along the 1000-m isobath to the seaward end of line 11. The cruise then continued in sequence along each line working back towards the west. Figure E-1 shows the station locations and gives the CTD numbers, which are sequential by sampling order. This was the second of three spring cruises carried out as part of NEGOM.

E.1 Forcing Functions

E.1.1 Winds

The mean wind field with variability ellipses for the period of cruise N5 (15-28 May 1999) is shown in Figure E.1.1-1. The methodology used is that of Wang et al. (1998) applied to hourly observations at meteorological stations located as shown in the figure. The mean wind field over the NEGOM region is characterized by large variances relative to very small speeds. The mean winds over the west Florida shelf are only of order 1 $m \cdot s^{-1}$ and generally oriented to the east and southeast. The variance ellipses are elongated slightly north-northwest-south-southeast over the entire region. The semi-major axes of the variance ellipses on the east side of the study region have magnitudes of 10-15 $m^2 \cdot s^2$. Over the Mississippi-Alabama shelf the mean wind vectors are 1-3 $m \cdot s^{-1}$ and oriented to the north. There, the variance ellipses have semi-major axes magnitudes of about 20 $m^2 \cdot s^2$. Mean winds over the DeSoto Canyon were nearly zero with variance ellipses on the order of those over the Mississippi-Alabama shelf. Coastal winds were upwelling favorable east of Pensacola.

The relatively large variability of the wind field during this cruise is due to the passage of several fronts and, therefore, a number of wind reversals (e.g., Figure E.1.1-2). Frontal passages occurred on May 19 and 24. Based on wind climatology using COADS Enhanced wind fields (1960-1997), the month of May historically represents a transition state between mean westward wintertime winds and mean northward summer winds.

E.1.2 River Discharge

The daily discharge rates of the Mississippi River during spring 1999 were marked by a series of freshwater pulses during February, March, and May, which exceeded the 70-yr record-length rates by about one standard deviation (Figure 3.1.2-2). Other major and minor rivers of the region were significantly under the 70-yr mean rates, except for the Tombigbee River which peaked to a value one standard deviation above the mean during the beginning of May and fell well below the mean during the rest of the month.

The effects of the Mississippi River discharge are seen in the near surface (~3 m) salinity field (Figure E.1.2-1). Low salinity values (<34) dominate the Mississippi-Alabama shelf and DeSoto Canyon regions and coastal regions from the Mississippi River Delta to Cape San Blas. Particularly low salinity water (salinity ~26) can be seen northeast of the delta on line 2. The effects of the relatively low salinity water can be seen in the chlorophyll *a* concentrations shown in Figure E.1.2-2. Here, the highest chlorophyll *a* concentrations coincide with the low salinity values. In section E.3, we will see that these correspond with

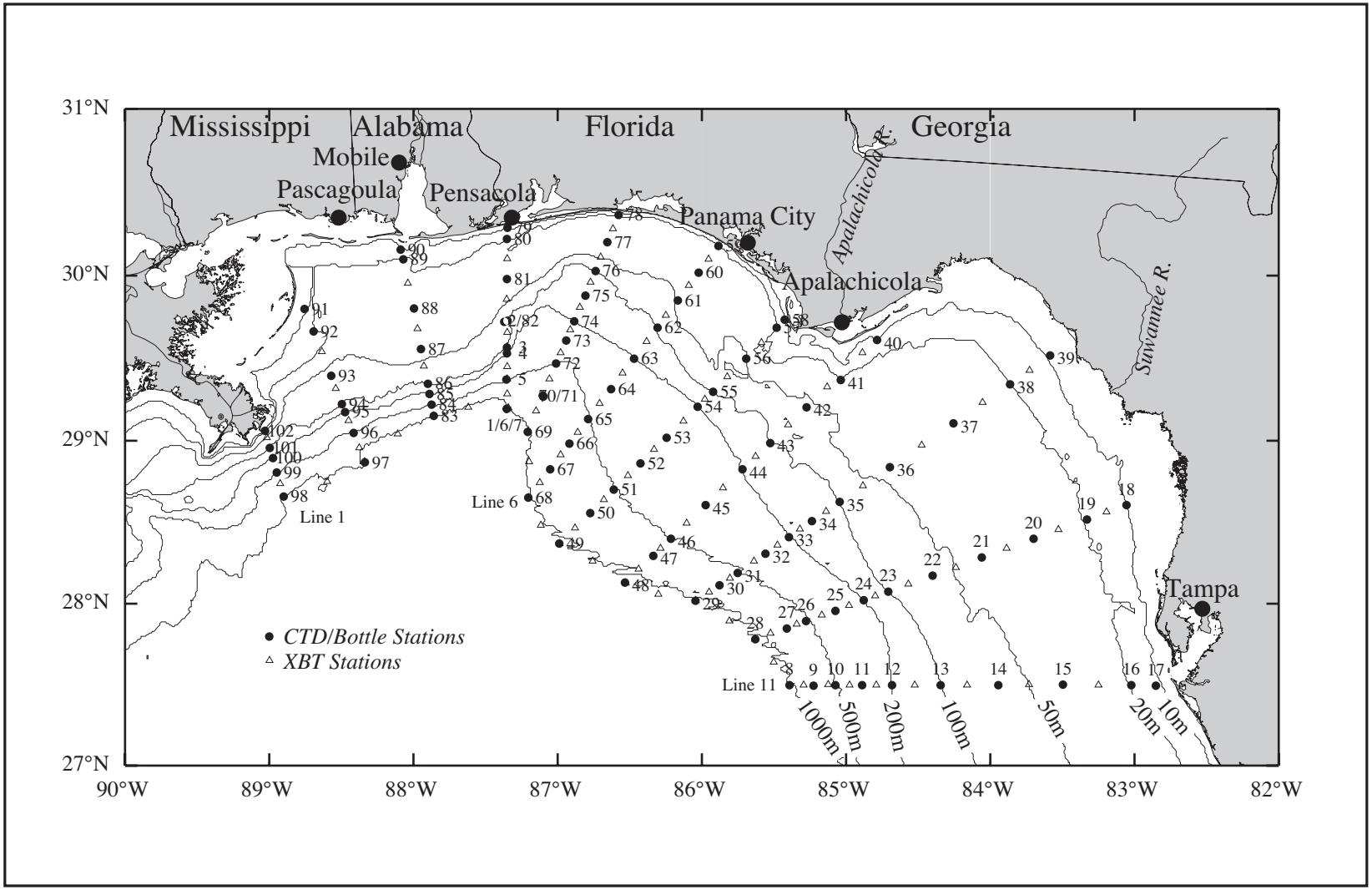

Figure E-1. Station locations for cruise N5 conducted on 15-28 May 1999. CTD stations (solid circles) are numbered; XBT stations (open triangles) are not.

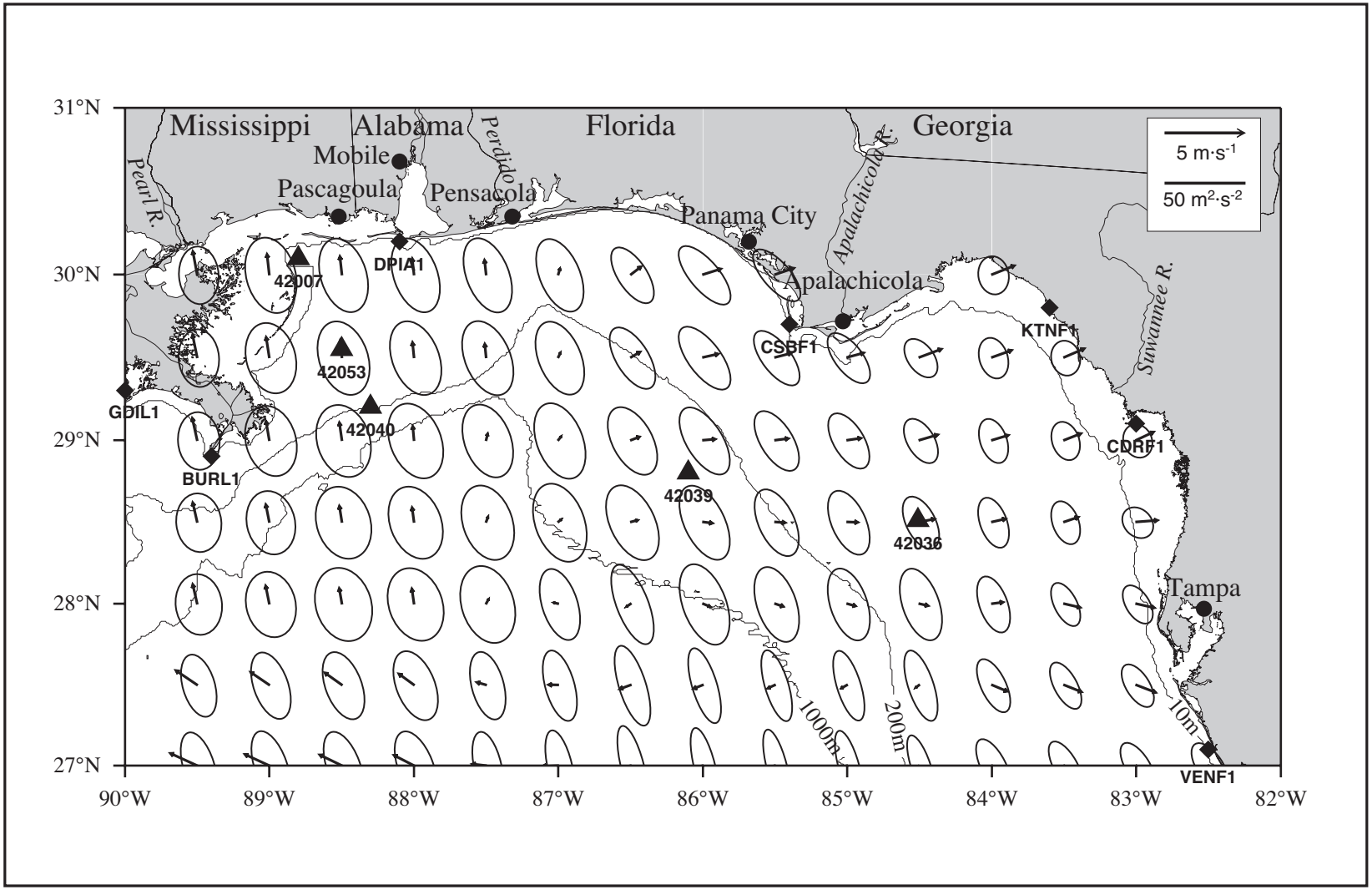

Figure E.1.1-1. Vector mean winds and variance ellipses for the period of cruise N5, 15-28 May 1999.

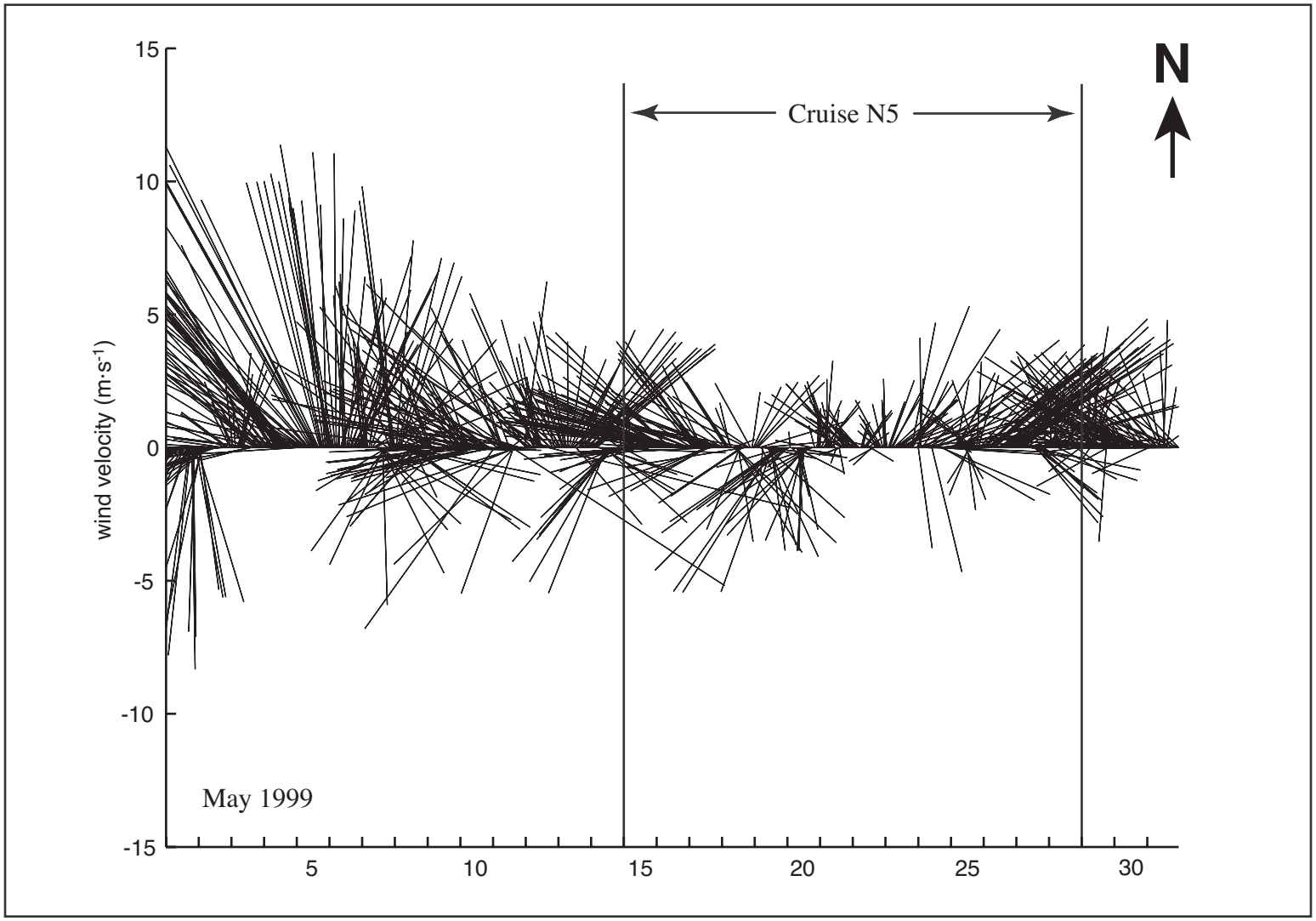

Figure E.1.1-2. Vector stick plot of wind at meteorological buoy 42040 for May1999. Gauge height is 10 m.

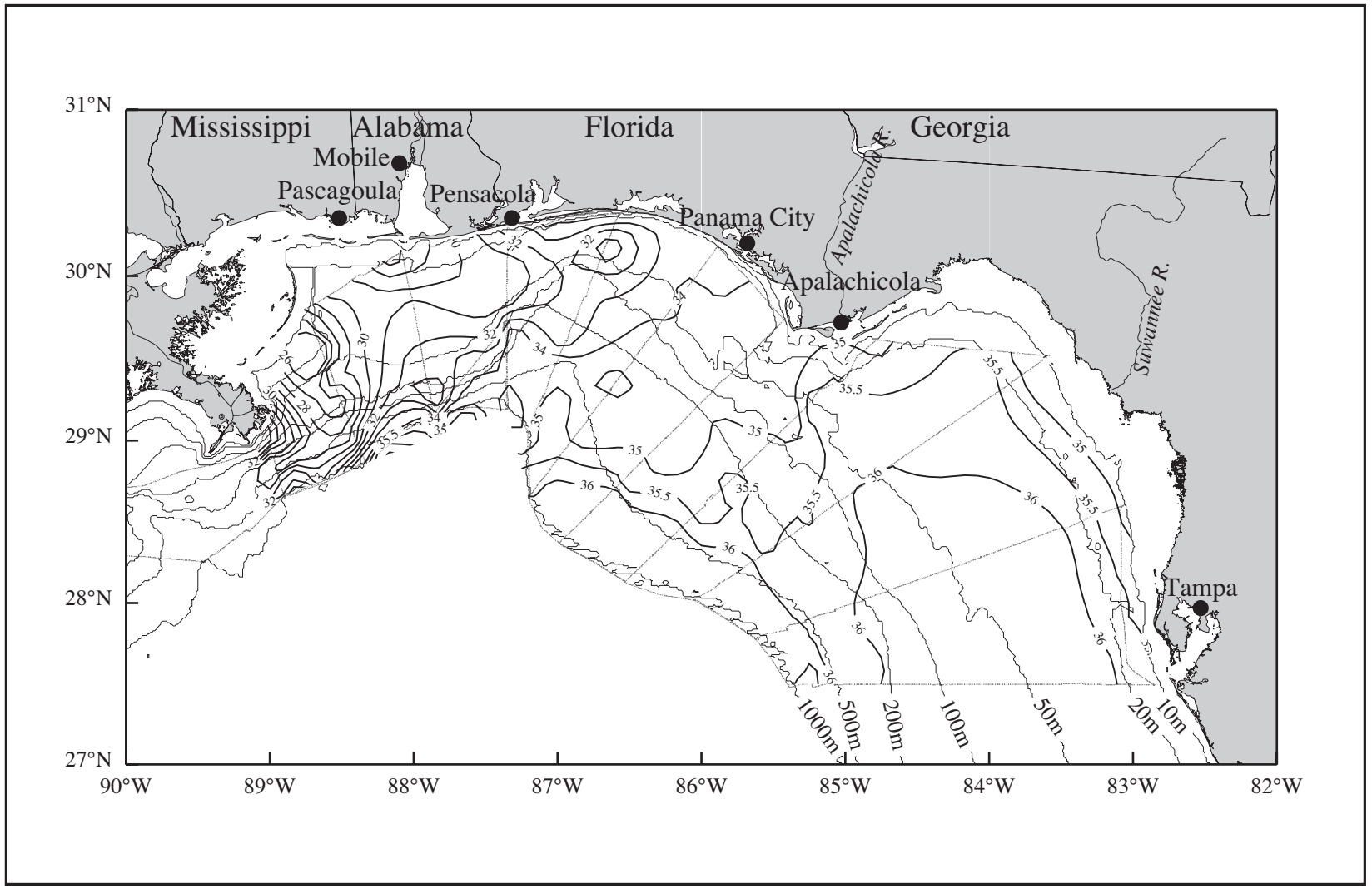

Figure E.1.2-1. Salinity at ~3 m from thermosalinograph observations on cruise N5 in May 1999.

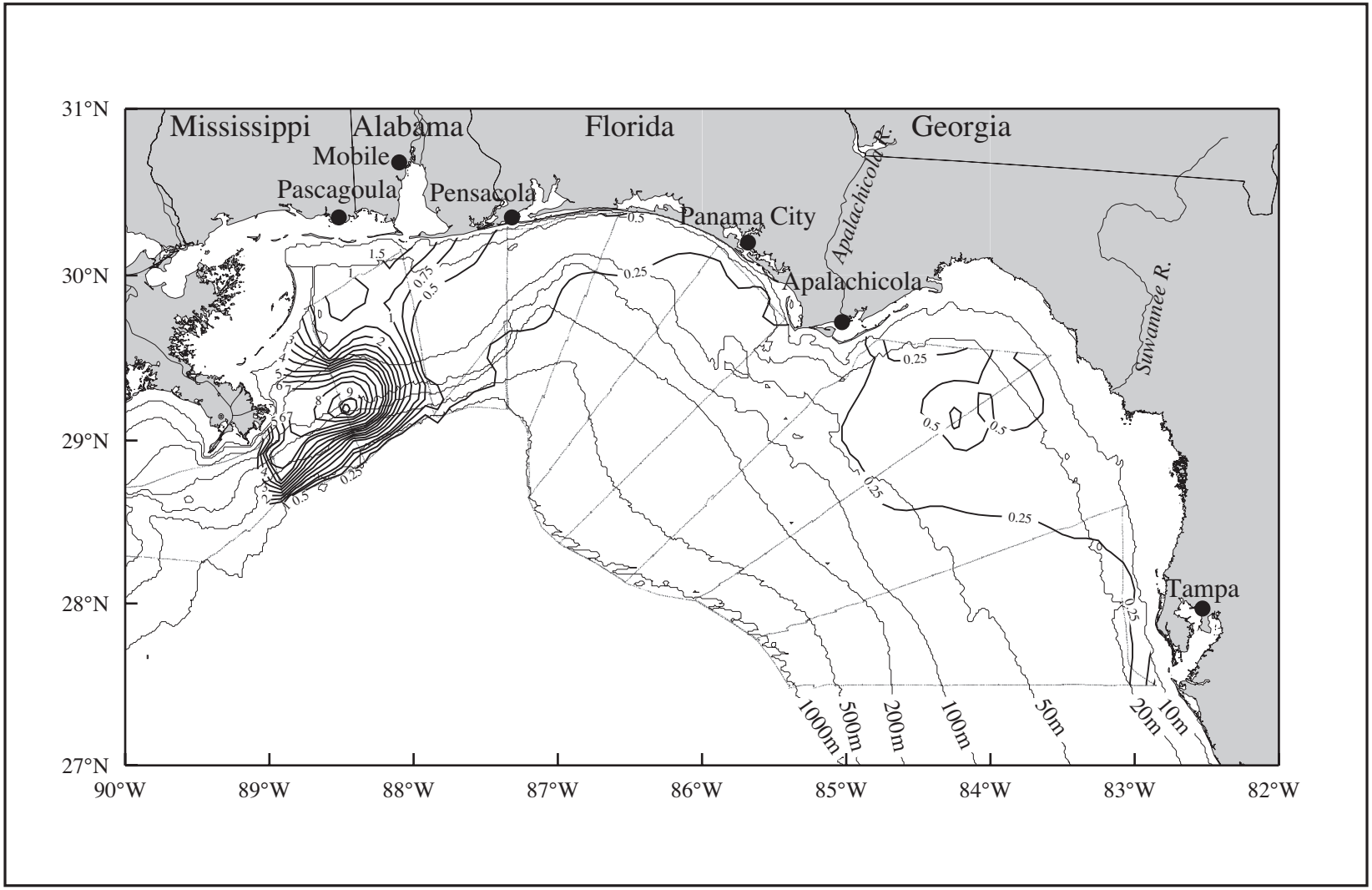

Figure E.1.2-2. Chlorophyll *a* (μg·L^{-1}) at ~3 m calculated from flow-through fluorescence on cruise N5 in May 1999.

enriched oxygen, and nutrient concentrations. The high chlorophyll *a* concentrations cover much of the Mississippi-Alabama shelf and the inner-shelf between Pensacola and Cape San Blas. The coastal chlorophyll *a* concentrations diminish with distance from the Mississippi River Delta to lowest values on the west Florida shelf.

The salinity in the coastal regime of the west Florida shelf was typically on the order of 34-35 and showed no significant evidence of river input. A relatively low salinity tongue extended southeast from the DeSoto Canyon along the shelf edge. This water had been mixed with saline oceanic water being advected anticyclonically around a high in geopotential anomaly located west of the seaward ends of lines 9 and 10 (see Section E.2).

E.1.3 SSH Fields Adjacent to the Shelf

The Loop Current penetrated northward only to about 27°N during May 1999 (Figure 3.2.3-22). However, a small bulge on the northeastern limb of the Loop Current can be seen extending onto the slope near 27.5°N and 85.5°W on 2 June 1999 and affecting the circulation and water properties of the study region. It is believed that this intrusion was dynamic during the N5 cruise and may have briefly intruded into the study region during the cruise. However, SSH fields show that an elongated cyclone centered near 87.5°W, 28°N dominated the offshore circulation on the slope and offshore limits of the study region. Figure E.1.3-1 shows the SSH for 20 May 1999.

E.2 *In Situ* Evidence of Circulation

Shipboard ADCP data were available only for measurements made in water depths of less than 100 m. Figure E.2-1 shows the near-surface (~14 m) current vectors measured with the shipboard ADCP along the N5 cruise track and in water depths less than 100 m. On the Mississippi-Alabama shelf, coastal currents are predominantly upcoast and coherent from the Chandeleur Islands to Cape San Blas. Around the apex of DeSoto Canyon, the currents appear to follow the bathymetry. At Cape San Blas, currents are directed offshore as westward flow from the west Florida shelf converges with upcoast flow from the west. On lines 10 and 11 the currents are more complex, particularly at line 11 where speeds are small and have considerable directional variability.

Geopotential anomaly (3 m relative to 800 m) based on N5 data (Figure E.2-2) shows a pattern of one major high and several relatively weak features. Most prevalent is the high at the seaward edge of lines 9 and 10 which is most likely associated with a tongue protruding from the Loop Current and intruding onto the slope (Section E.3 gives a description of water properties associated with this tongue). A weak high is seen over the apex of DeSoto Canyon close to shore and between Pensacola and Panama City; another is centered at the 200-m isobath on line 2. Lows in geopotential anomaly are present off the Mississippi River delta on line 1, offshore at the base of the DeSoto Canyon on lines 5 and 6, and inshore of the 500-m isobath on line 11. Because good ADCP data were limited to shallow water, these features in geopotential anomaly cannot be confirmed with direct measurements.

E.3 Property Distributions

The temperature field at 3.5-m depth is shown in Figure E.3-1. Warm surface temperatures (> 27°C) can be seen offshore at lines 7 through 10 as warm offshelf oceanic waters are advected onto the slope around the high in geopotential anomaly (Figure E.2-2). Warm surface temperatures (>28°C) can be seen at the inner shelf regions of line 2 and roughly

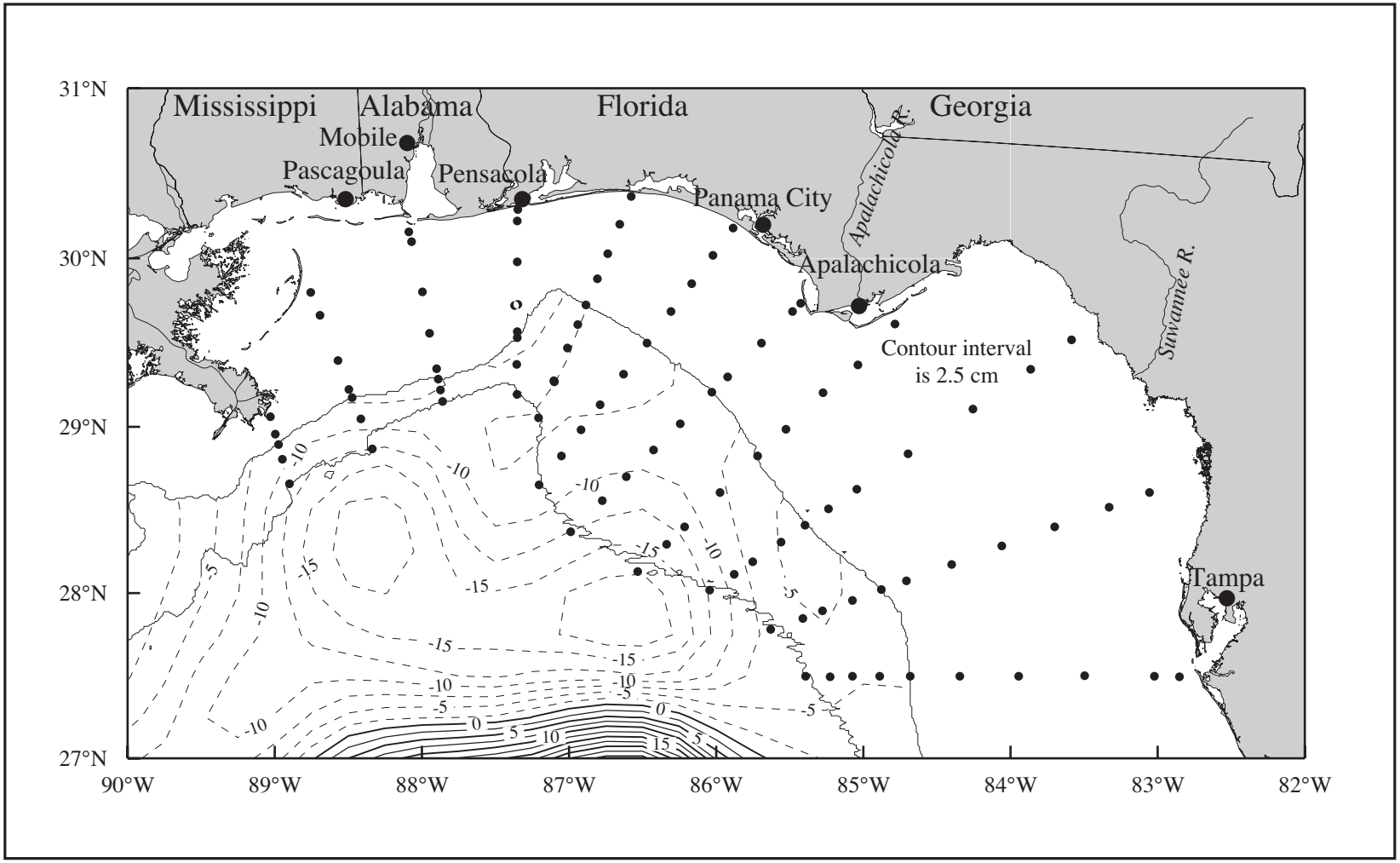

Figure E.1.3-1. Sea surface height field from satellite altimeter data for 20 May 1999 during cruise N5. The 200- and 1000-m isobath contours and CTD stations (dots) are shown. [Data provided by Robert R. Leben, University of Colorado.]

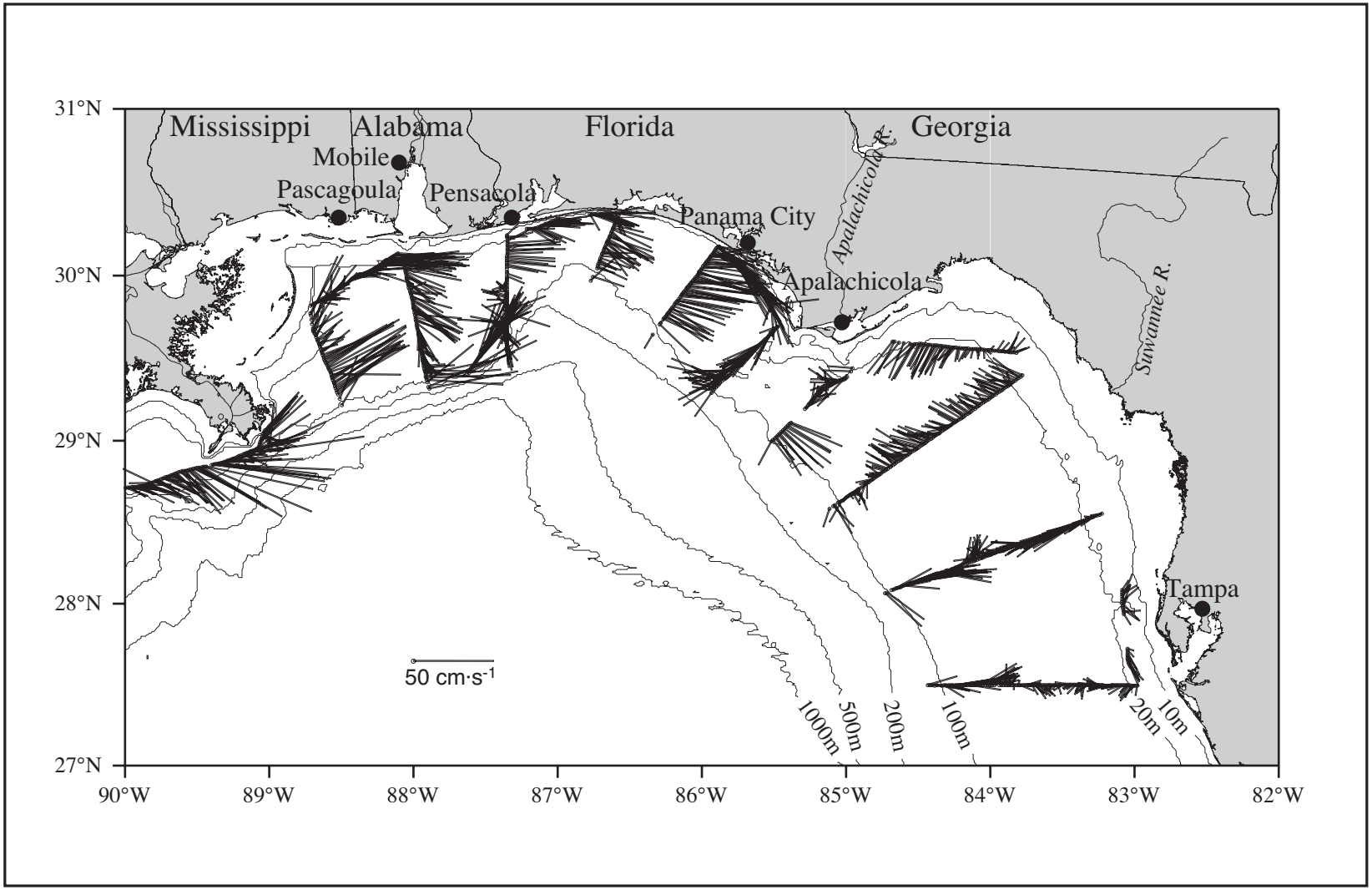

Figure E.2-1. ADCP-measured currents for the 4-m bin centered at 14 m on cruise N5 in May 1999.

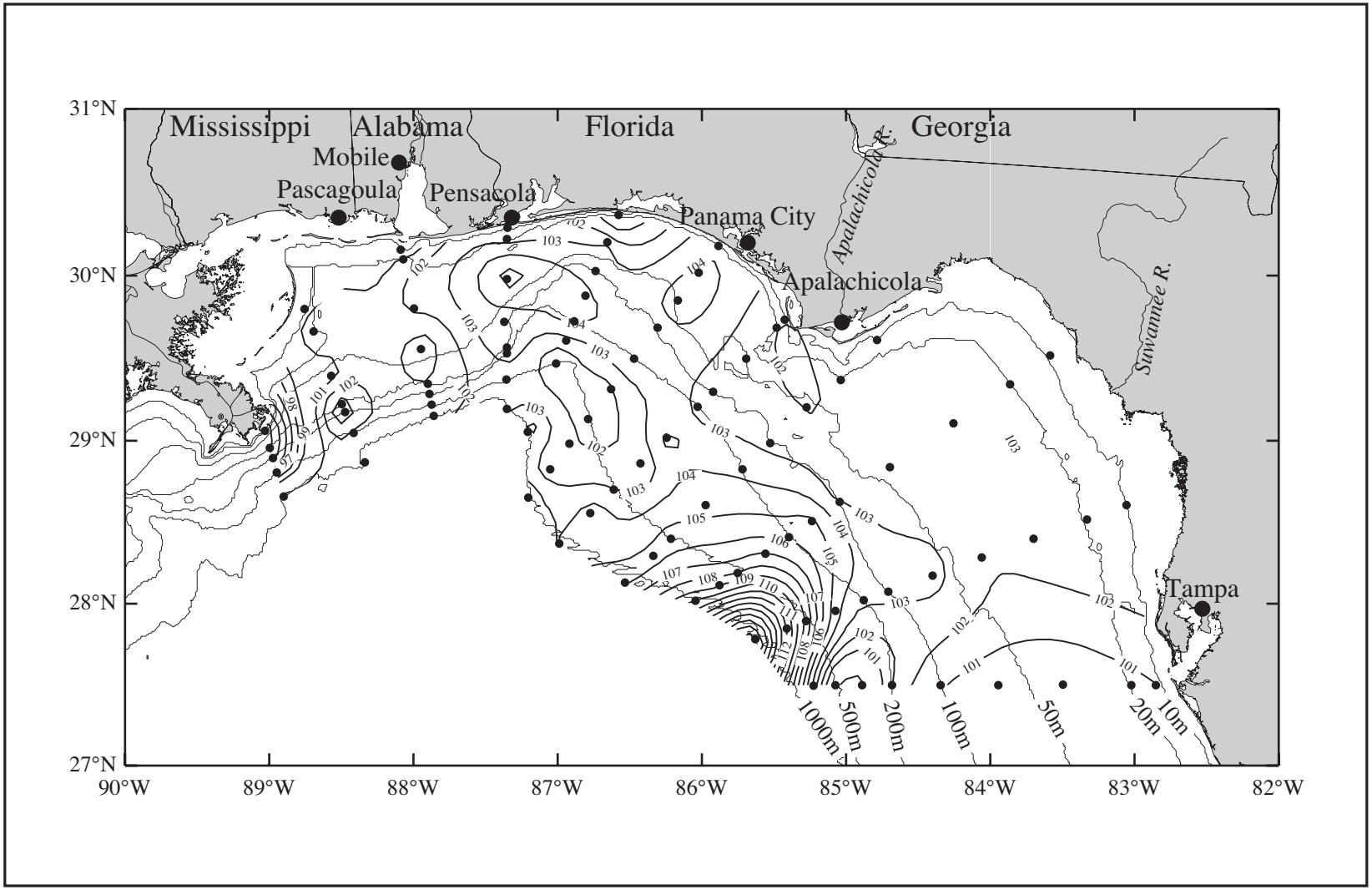

Figure E.2-2. Geopotential anomaly (dyn cm; 3 m relative to 800 m) for cruise N5 conducted 15-28 May 1999. CTD station locations are shown.

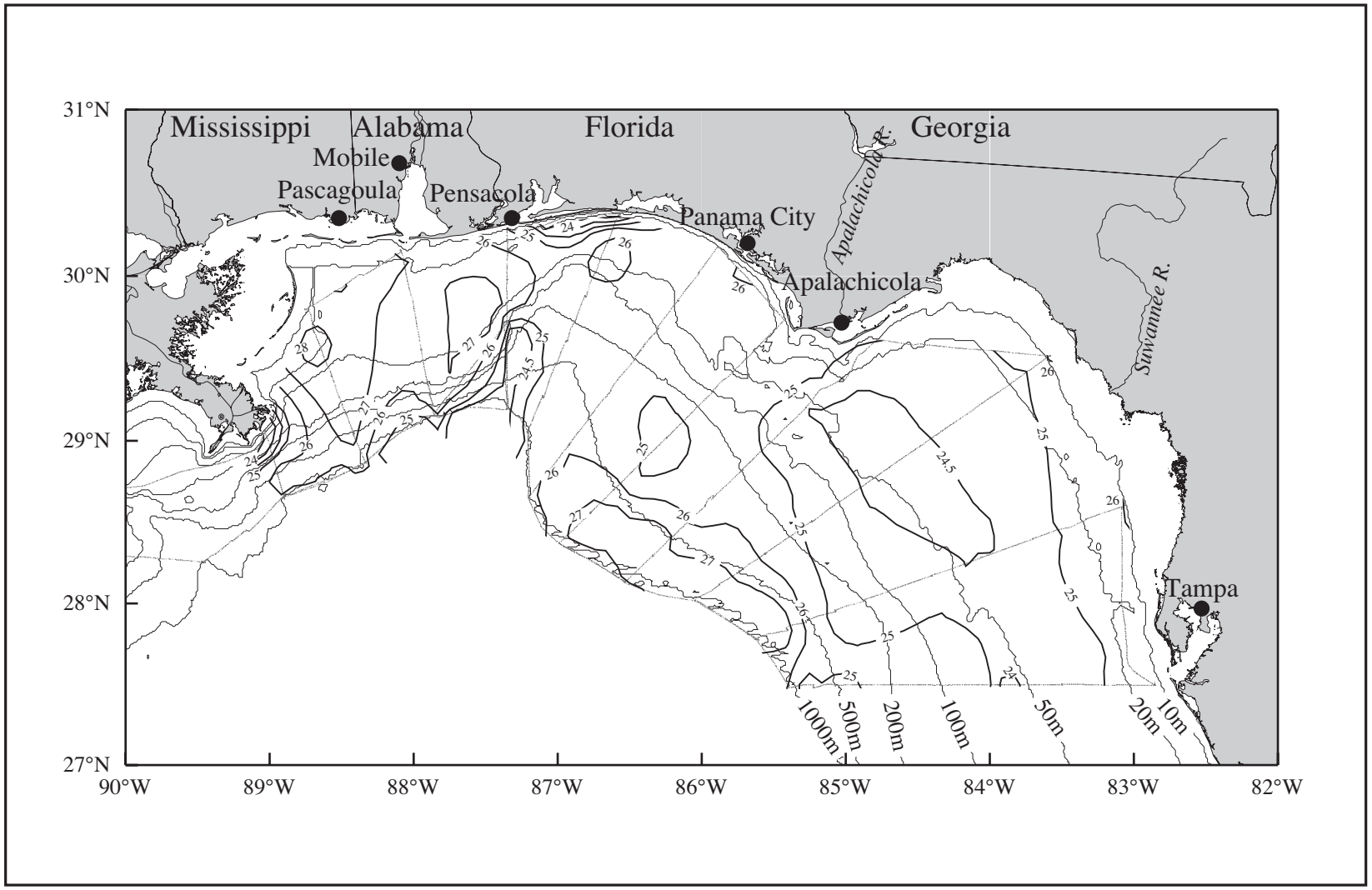

Figure E.3-1. Temperature (°C) at ~3 m from thermosalinograph observations on cruise N5 in May 1999.

correspond to the low salinity and high productivity areas resulting from river waters seen in Figures E.1.2-1 and E.1.2-2.

Figures E.3-2 and E.3-3 show the temperature and salinity profiles along the 1000-m isobath. The water column is thermally stratified and shows no evidence of a well-defined surface mixed layer. This result is generally seen across the region. At station 7 (line 4), the cold core corresponding to the region of low geopotential anomaly is seen as the center of cool/low salinity shelf water advected off the shelf between lines 2 and 7 (stations 97, 83, 7, 69, 68, and 49). This affects only the upper 150-m of the water column at the 1000-m isobath, since its source is at the shelf. Between stations 49 and 8 warmer and more saline surface waters are present due to transport by the anticyclone over the slope. The deep (to ~700 m) anticyclonic core is clearly seen depressing the isotherms at stations 29 and 28 (Figure E.3-2). Relatively low salinity water in the upper 50 m is seen in the western regions of Figure E.3-3. The Mississippi River plume is evident in the upper 10 m at station 98. Further evidence of the dynamic high off lines 9 and 10 is seen in the nitrate concentration profiles shown in Figure E.3-4, where the deep nitrate isopleths (> 10 μM) at stations 28 and 29 are displaced downwards relative to those in the west. The large nutrient loading of the Mississippi River can be seen near surface at stations 97 and 98.

At the 100-m isobath a combination of offshelf and nearshore processes are seen. Figure E.3-5 shows the density anomaly at the 100-m isobath during N5. The Mississippi River plume is clearly seen in the upper 20-m in the western regions (stations 101, 94, and 86) and perhaps further east to station 55. Deeper than 50 m, the oscillations in the isopycnals can be matched to the major features seen in geopotential anomaly (Figure E.2-2) on the Mississippi-Alabama shelf. Specifically, the highs in geopotential anomaly at lines 2 and 4 can be seen in Figure E.3-5 as negative (downward) displacement of the isopycnals at stations 94 and 3. However, the lows in geopotential anomaly at lines 1, 3, and 5 are seen as positive (upward) displacement of the isopycnals at stations 94, 3, and 76. Below the nutrient-poor, near-surface layer, nutrient concentrations are in general alternately enriched and depleted at the regions of low and high geopotential anomaly, respectively.

Figure E.3-6 shows vertical profiles of nitrate concentration along lines 10 and 11. At the seaward end of line 10 (Figure E.3-6, left panel), the Loop Current intrusion has pushed shoreward resulting in the sloping of nutrient isopleths below 150 m upwards. At line 11 (Figure E.3-6, right panel), the isopleths slope upwards at stations 8 and 9. However, the dynamic low present at stations 10, 11, and 12 domes the isopleths and slopes them downward shoreward of station 11.

Nutrient loading was high on the Mississippi-Alabama shelf during N5 due to the combined effects of Mississippi River discharge, upwelling due to favorable wind conditions, and intrusion of nutrient rich oceanic water onto the shelf between lines 1 and 2. Figures E.3-7 and E.3-8 show nitrate and silicate concentrations from the upper 100 m along lines 1, 2, and 3. Seen is a Mississippi River plume confined mostly to the upper 10 m at lines 1 and 2 with concentrations decreasing with distance from the delta. The nutrient maxima are located offshore indicating that the plume may have become detached from the delta by local wind forcing. Recall line 2 showed a maximum in chlorophyll *a* concentration (Figure E.1.2-2) and was the region of largest productivity. On line 3, nutrient concentrations near surface are diminished (bottom panels in Figures E.3-7 and E.3-8) as the bloom is transported east and subsides. Below the Mississippi River plume and near-bottom, nutrient concentrations remain high, particularly at the inshore stations. Silicate (nitrate) concentrations exceed 16 (6) μM at lines 2 and 3.

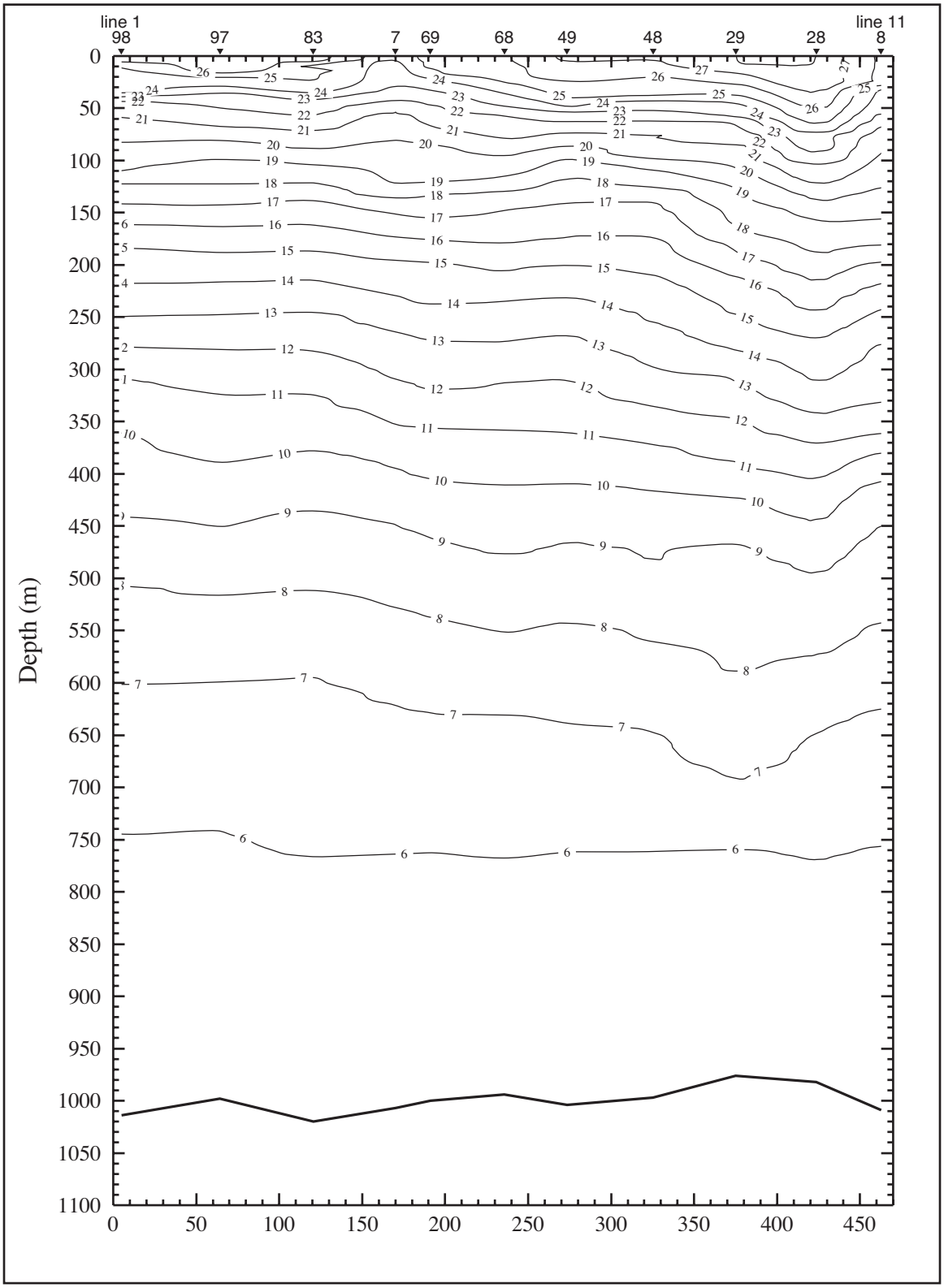

Figure E.3-2. Potential temperature (°C) along the 1000m isobath on cruise N5 in May 1999. Stations are shown on the top axis.

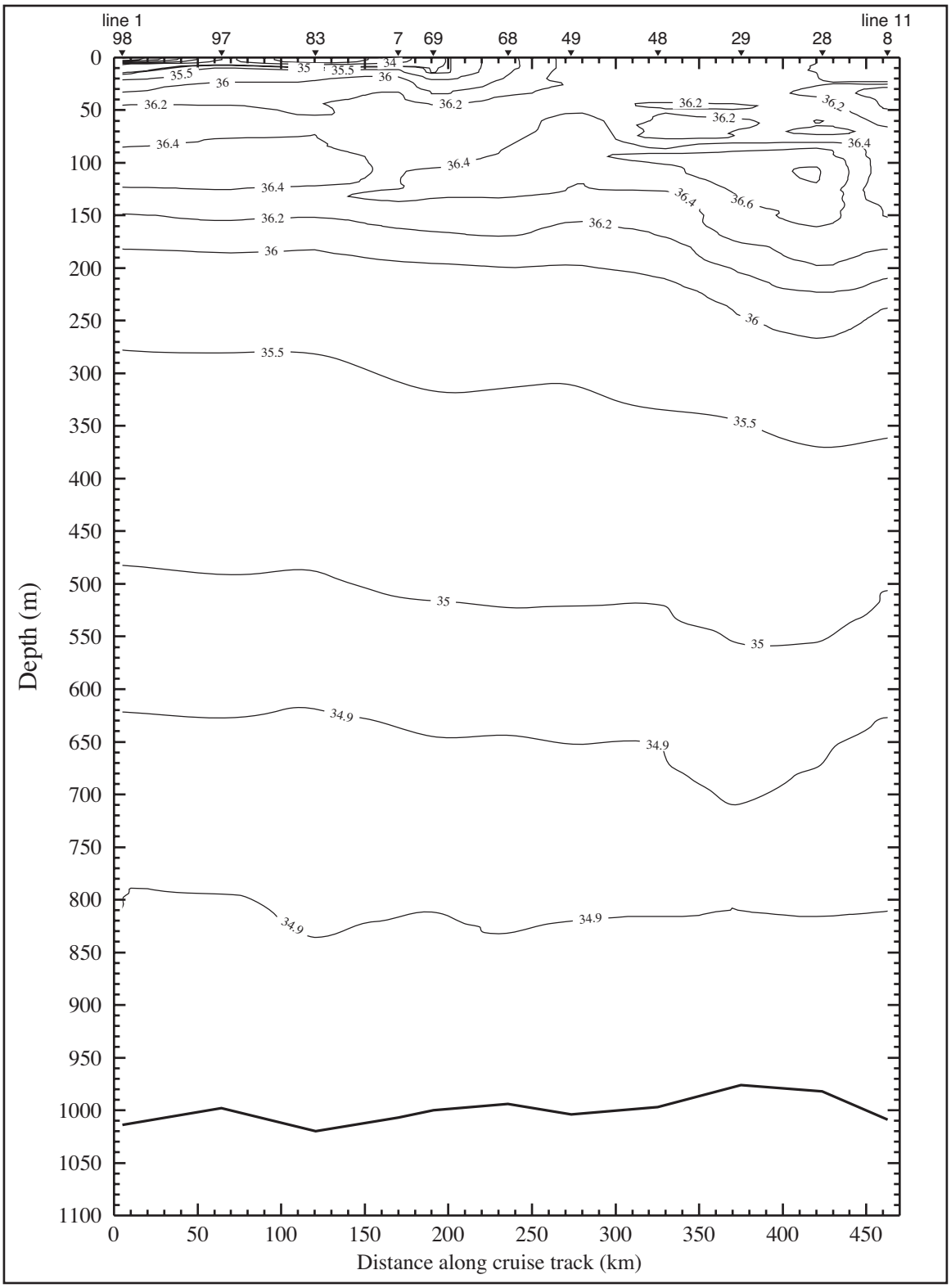

Figure E.3-3. Salinity along the 1000-m isobath on cruise N5 in May 1999. Stations are shown on the top axis.

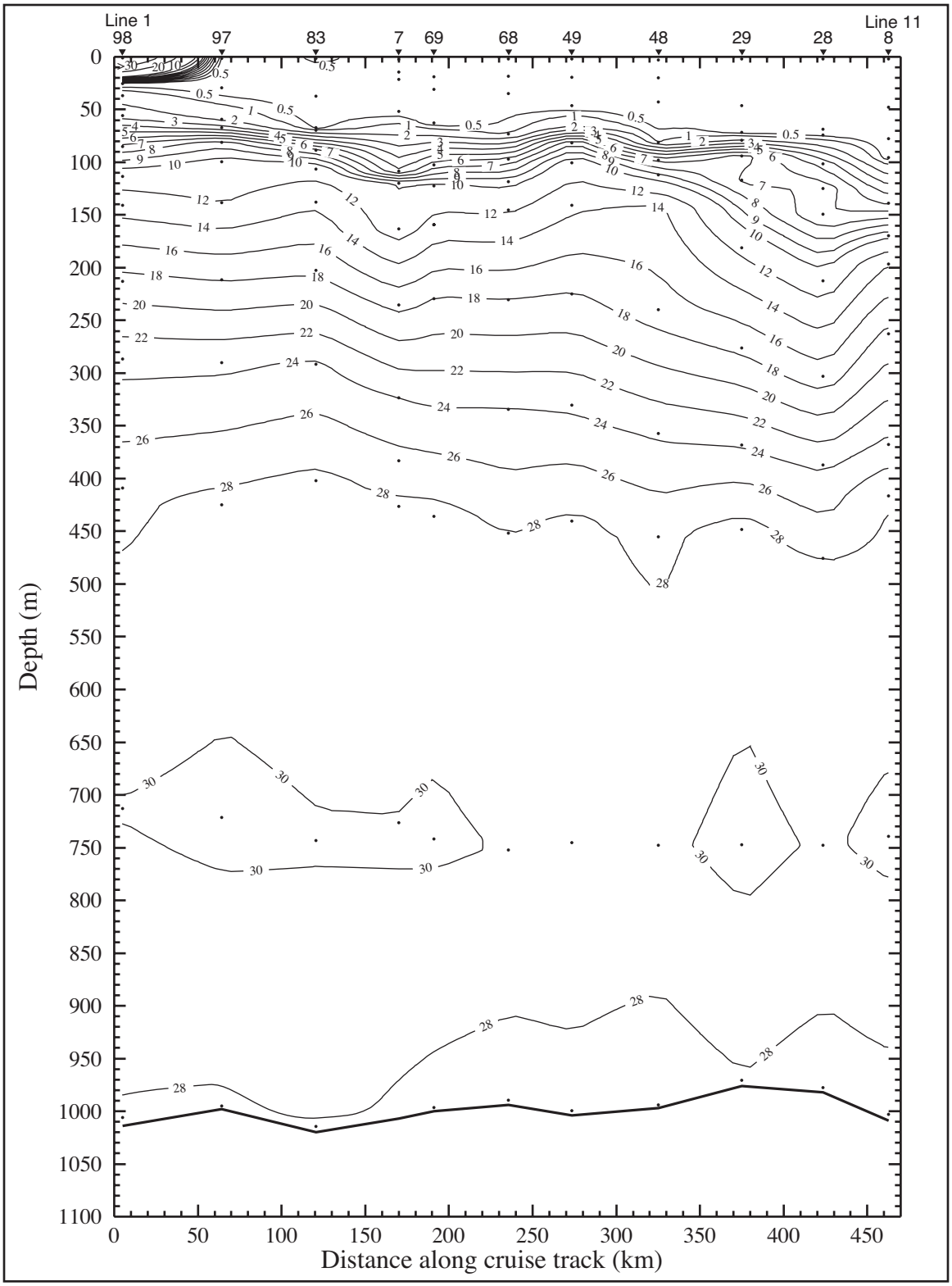

Figure E.3-4. Nitrate (μM) along the 1000-m isobath on cruise N5 in May 1999. Stations are shown on the top axis.

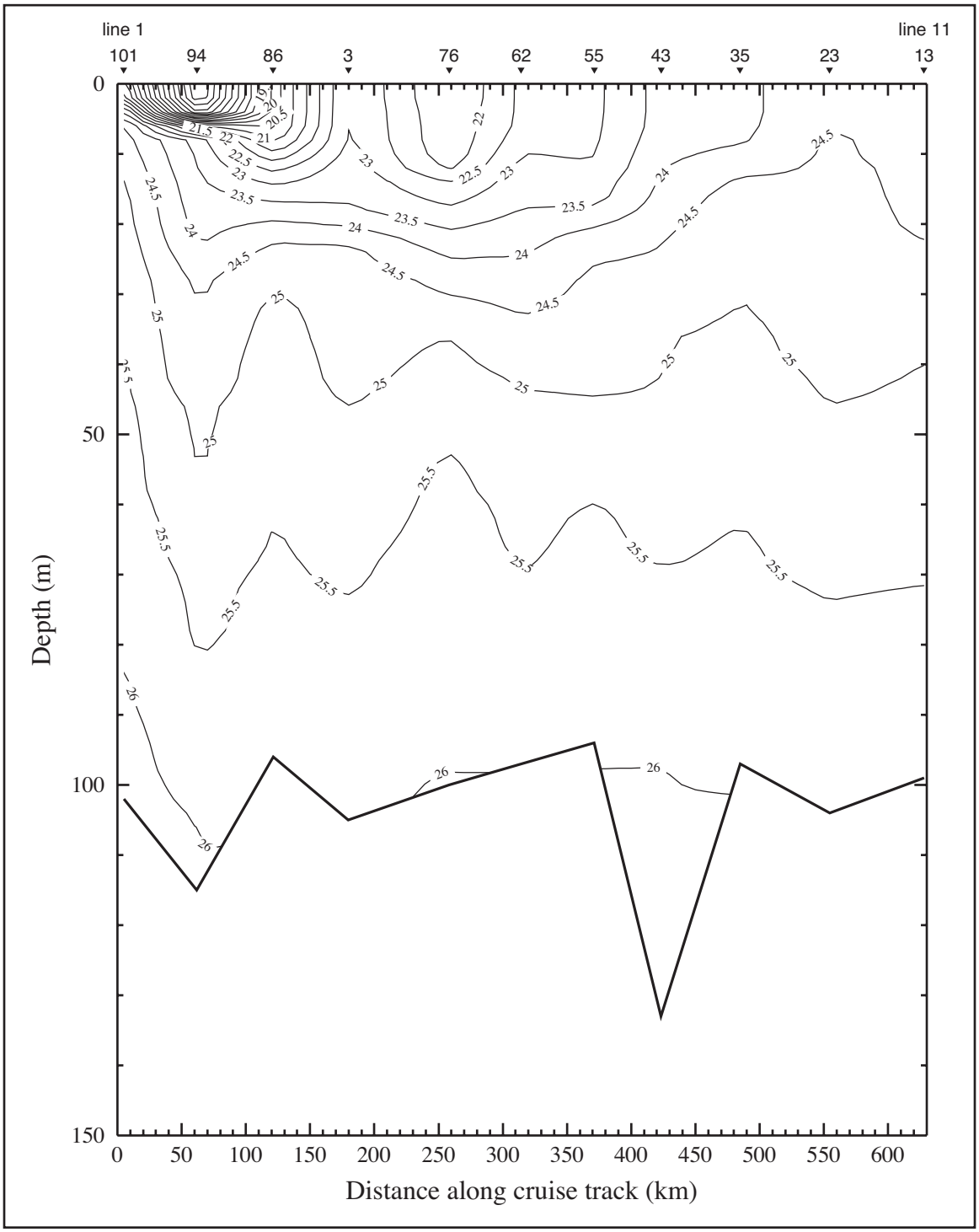

Figure E.3-5. Density anomaly (σ_θ in kg·m^{-3}) along the 100-m isobath on cruise N5 in May 1999. Stations are shown on the top axis.

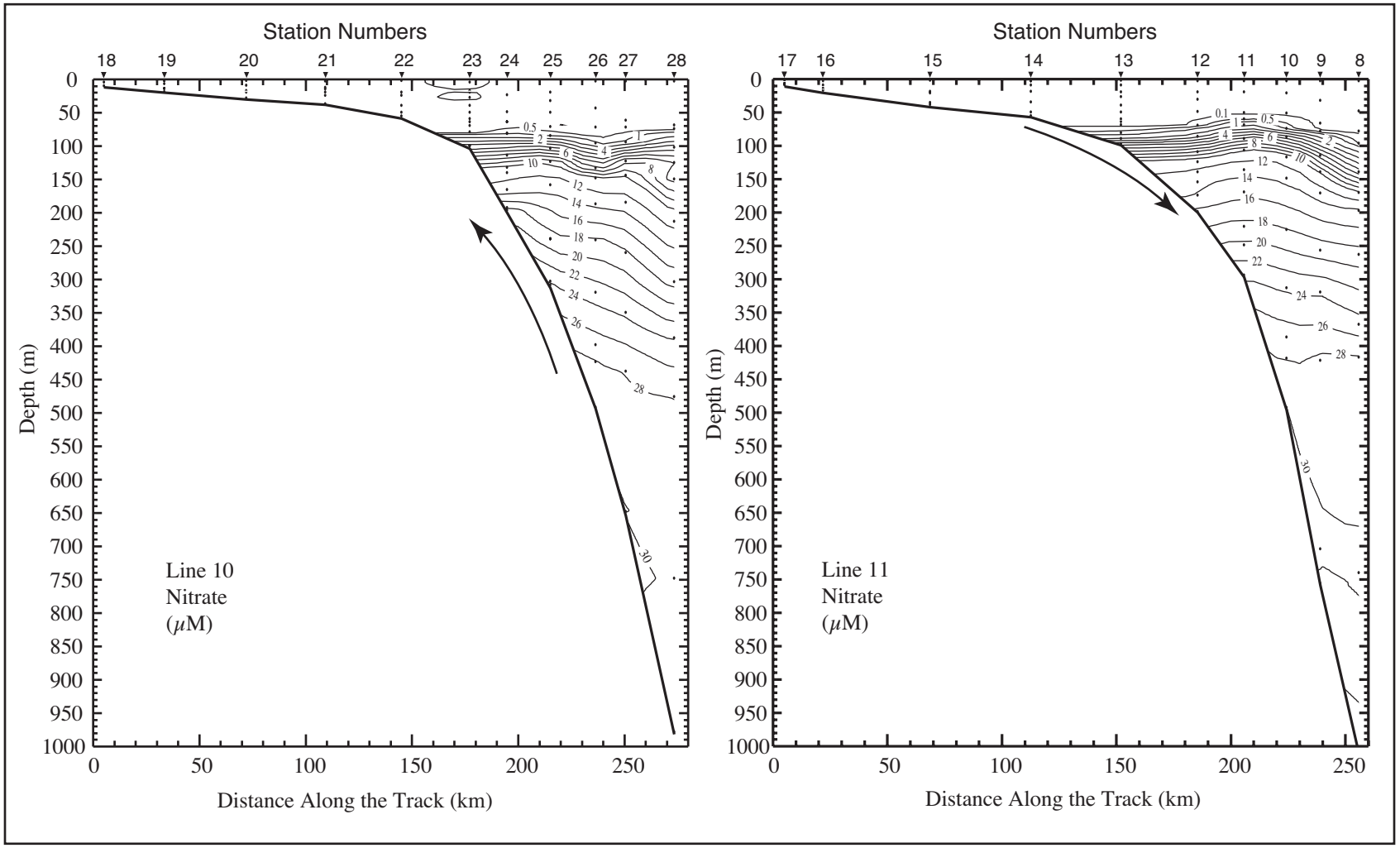

Figure E.3-6. Nitrate along lines 10 and 11 on cruise N5 in May 1999. Arrows indicate sloping of near-bottom isopleths.

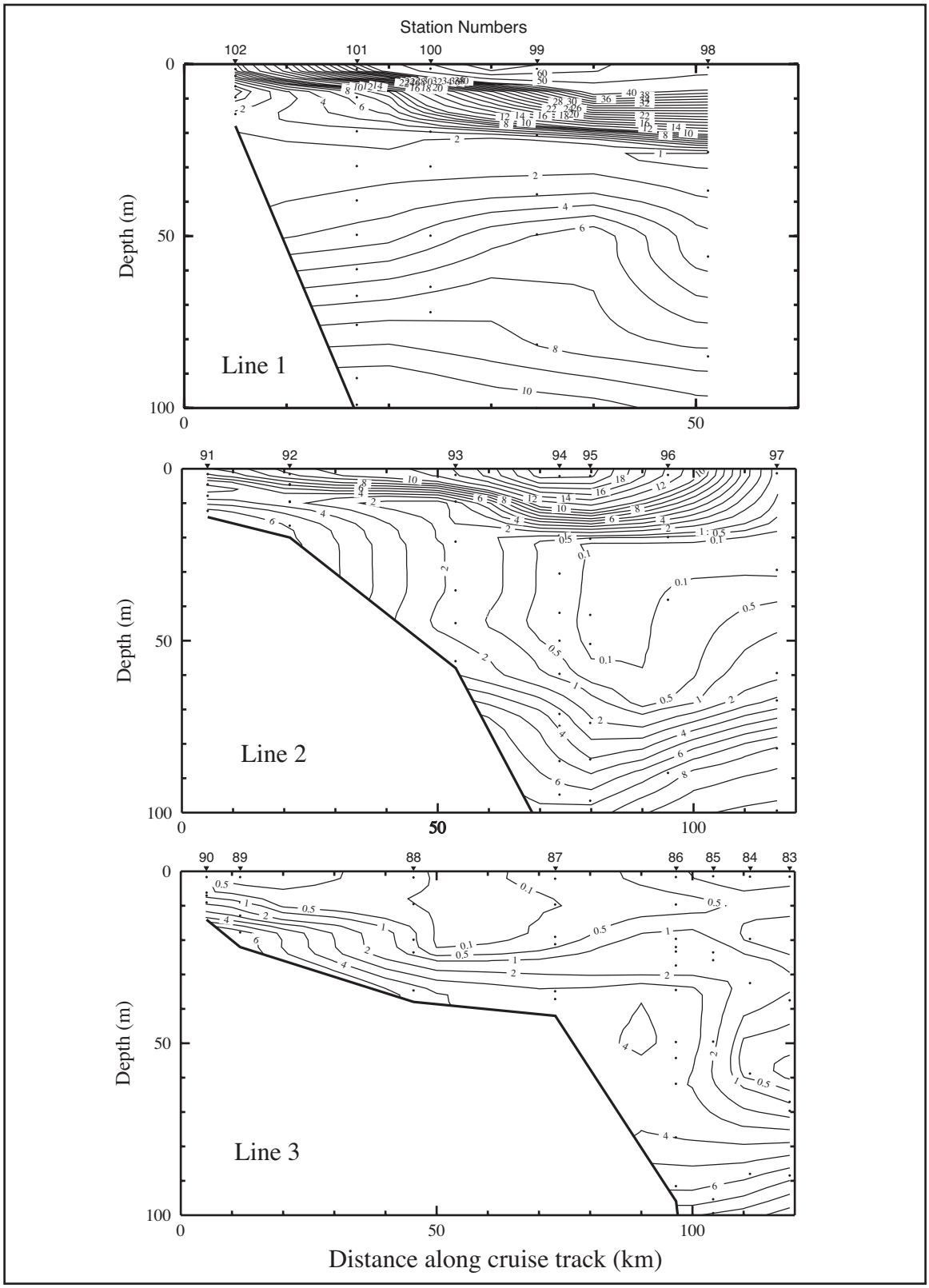

Figure E.3-7. Nitrate (μM) on lines 1, 2, and 3 on cruise N5 in May 1999.

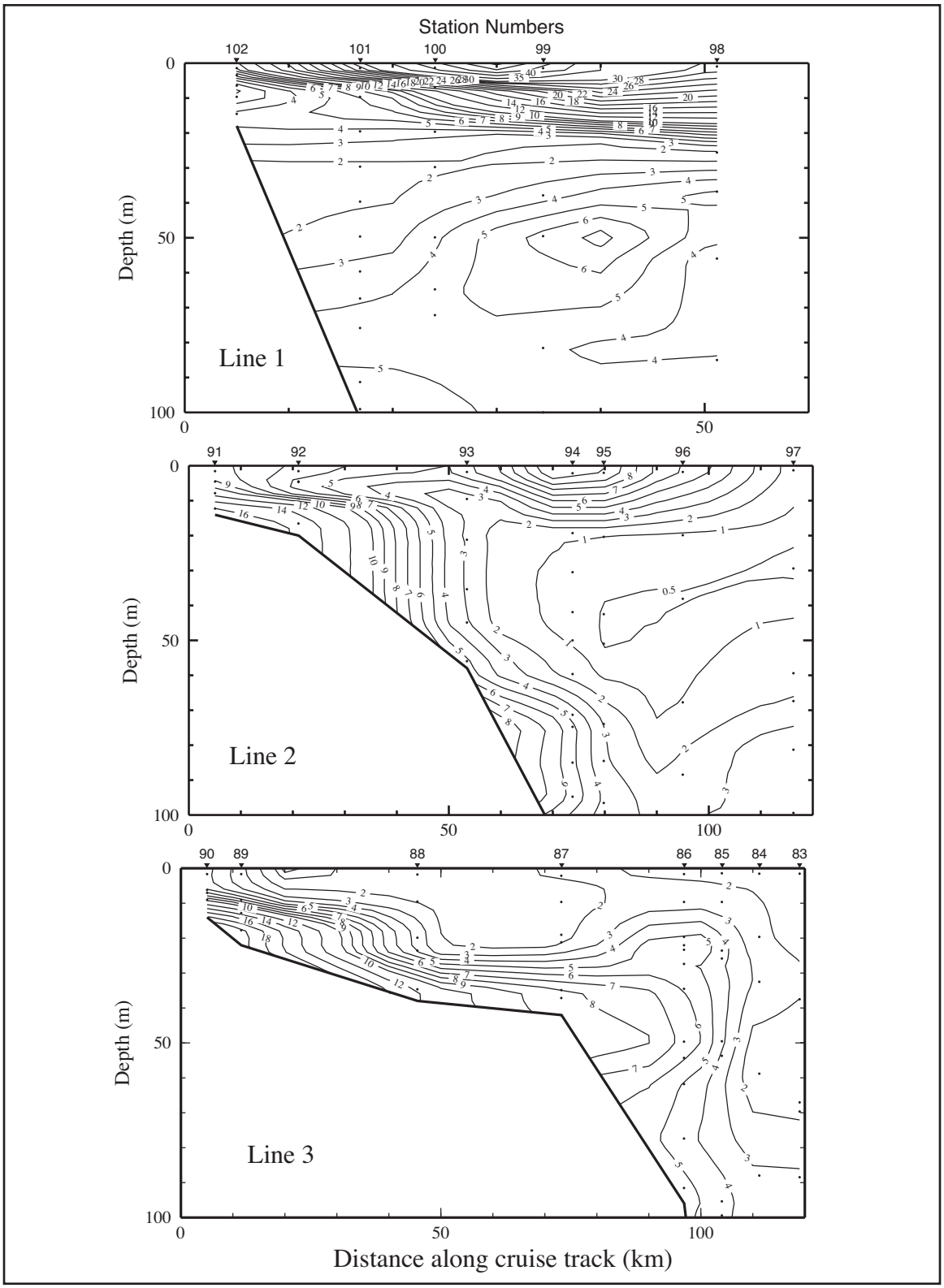

Figure E.3-8. Silicate (μM) on lines 1, 2, and 3 on cruise N5 in May 1999.

Figure E.3-9 shows dissolved oxygen concentration, salinity, and percent transmission along line 2 during N5. The high productivity evidenced by the high chlorophyll *a* near surface and the strong stratification due to the presence of the low salinity water plume (Figure E.3-9, middle panel) along this line leads to near-hypoxic conditions in the bottom waters at station 91, where the dissolved oxygen concentration was 1.495 $mL \cdot L^{-1}$. Here, nutrients near surface are consumed leading to high productivity. Organic matter then descends through the water column and decays, but the stratification prevents the oxygen deprived bottom waters from mixing with the oxygen rich surface. Light transmission in this region is below 60%.

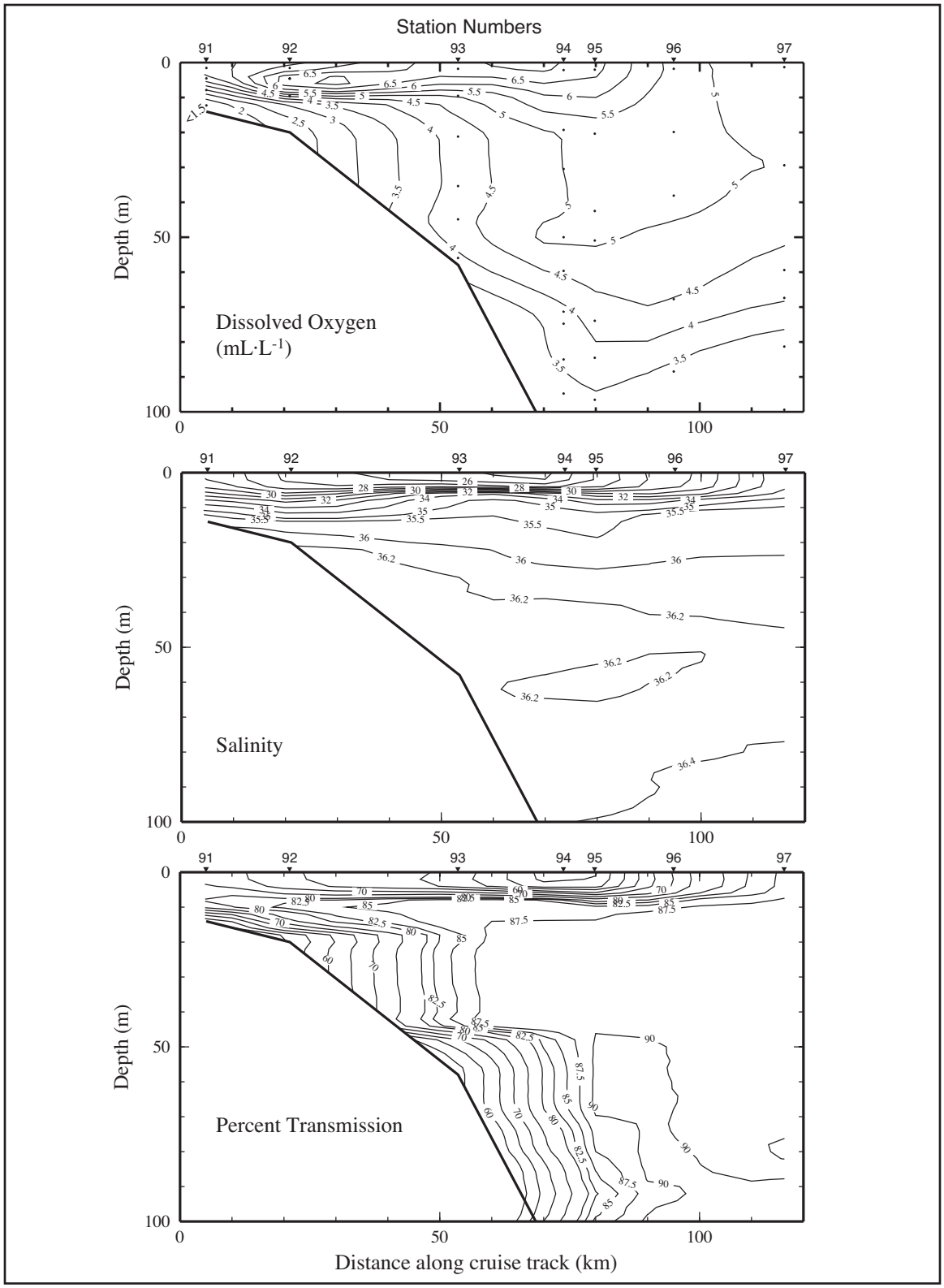

Figure E.3-9. Dissolved oxygen, salinity, and percent transmission along line 2 on cruise N5 in May 1999.

APPENDIX F
SUMMARY OF CONDITIONS DURING CRUISE N6

Cruise N6 was a summer cruise conducted 15-28 August 1999. Stations began with the most seaward station on line 1. The track ran along lines 1 through 4, then lines 11 through 8, and finally lines 5 through 7. Stations ended with the most inshore station on line 7. Figure F-1 shows the station locations and gives the CTD station numbers, which are sequential by sampling order.

F.1 Forcing Functions

F.1.1 Winds

Mean winds over the NEGOM study area during cruise N6 were weak (< 2.5 $m \cdot s^{-1}$), as expected for summer, and directed to the northeast over the Mississippi-Alabama shelf and northward over the west Florida shelf (Figure F.1.1-1; see Section A.1.1 and Wang et al. 1998 on gridding methods). Instantaneous speeds during the cruise generally were less than 7 $m \cdot s^{-1}$ and, although there predominantly was a northward component, directions were variable (e.g., Figure F.1.1-2). Variability in direction was mainly in response to the presence of atmospheric highs and low over the continent and ocean. Hurricane Bret was in the far western Gulf during 22-24 August, and Hurricane Dennis was to the southeast of Florida during 26-28 August. Neither hurricane had major effects over the NEGOM region. There were no frontal passages during the cruise, although a low, which generated cyclonic winds centered about 25°N 87°W, was present over the study area on 15 August.

F.1.2 River Discharge

The Mississippi River discharge exceeded the 70-yr record-length mean in May, was about average in June, exceeded the mean in July, and was nearly one standard deviation below the mean in August (Figure 3.1.2-2). Except for the rivers emptying into Mobile Bay, other rivers discharged at or below their record-length means during spring and summer 1999. The Tombigbee and Alabama rivers, which discharge into Mobile Bay, had pulses of higher than average discharge in July. The Tombigbee had a high discharge pulse in May. Otherwise, their discharge rates were at or below their record-length means during spring and summer 1999. The major riverine influence on the salinity in the NEGOM region was from the Mississippi River (Figure F.1.2-1). Its influence extended over the outer shelf and slope to 87°W. Except near the Mississippi Delta, the result was fresher water offshore than over the adjacent inner shelf.

F.1.3 SSH Fields Adjacent to the Shelf

In June 1999, the SSH field off the Mississippi-Alabama shelf consisted mainly of low sea surface heights, while that off the west Florida shelf was influenced by a small anticyclone that pinched off Loop Current as a Loop Current eddy was developing (Figure 3.2.3-23). This LCE is estimated to have separated from the Loop Current in August 1999 (Sturges and Leben, 2000); however, it was located south of 27°N and did not directly influence the shelf edge circulation in the study area. The small anticyclone split from the larger during July 1999 (Figure 3.2.3-24). In early July, it elongated northwestward from its center at ~27.5°N 86°W. It then contracted to a circular shape centered about 28°N 87°W. In August, it reattached to the LCE, which was beginning to move westward out of the eastern Gulf (Figure 3.2.3-25).

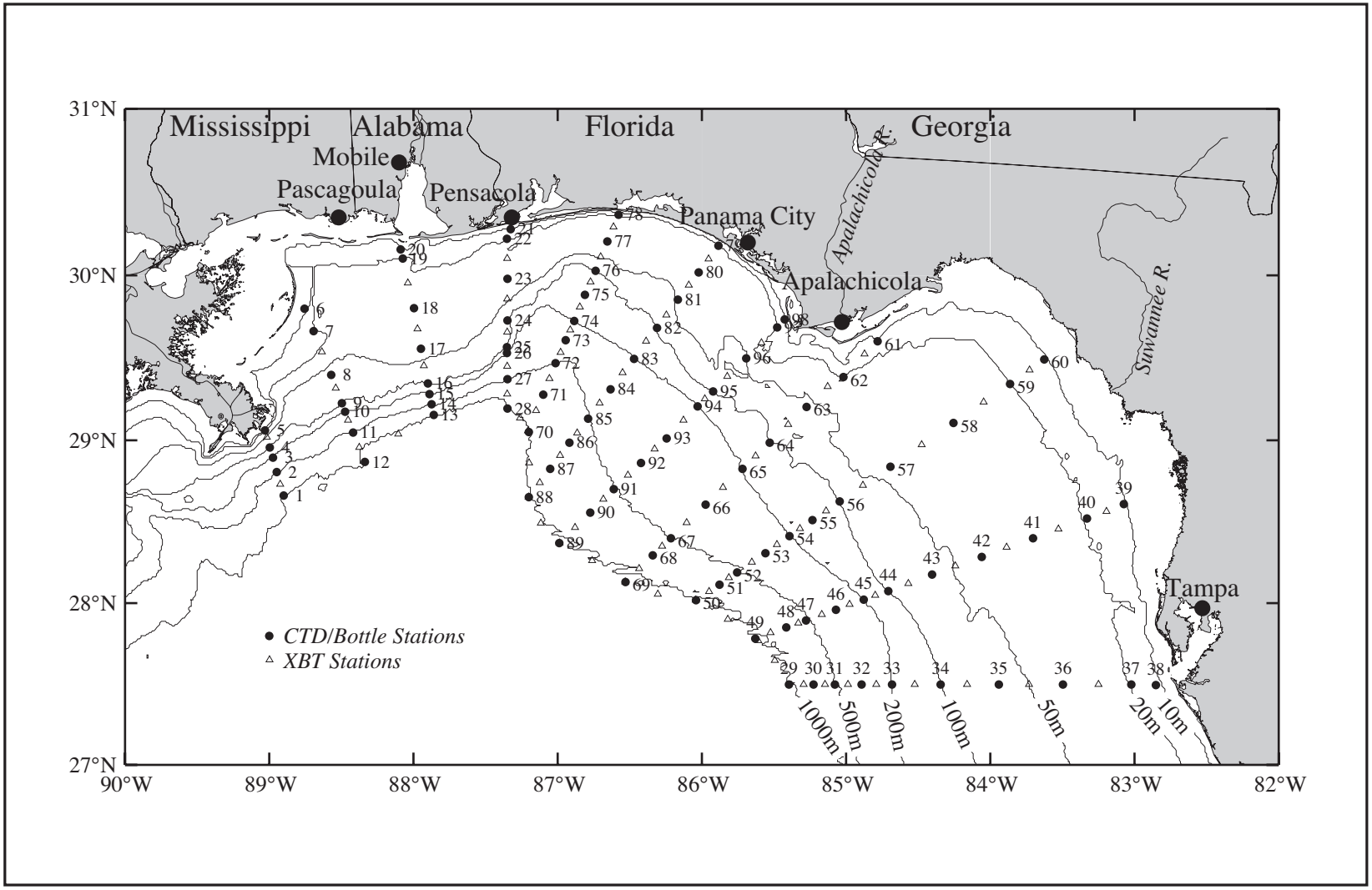

Figure F-1. Station locations for cruise N6 conducted 15-28 August 1999. CTD stations (solid circles) are numbered; XBT stations (open triangles) are not.

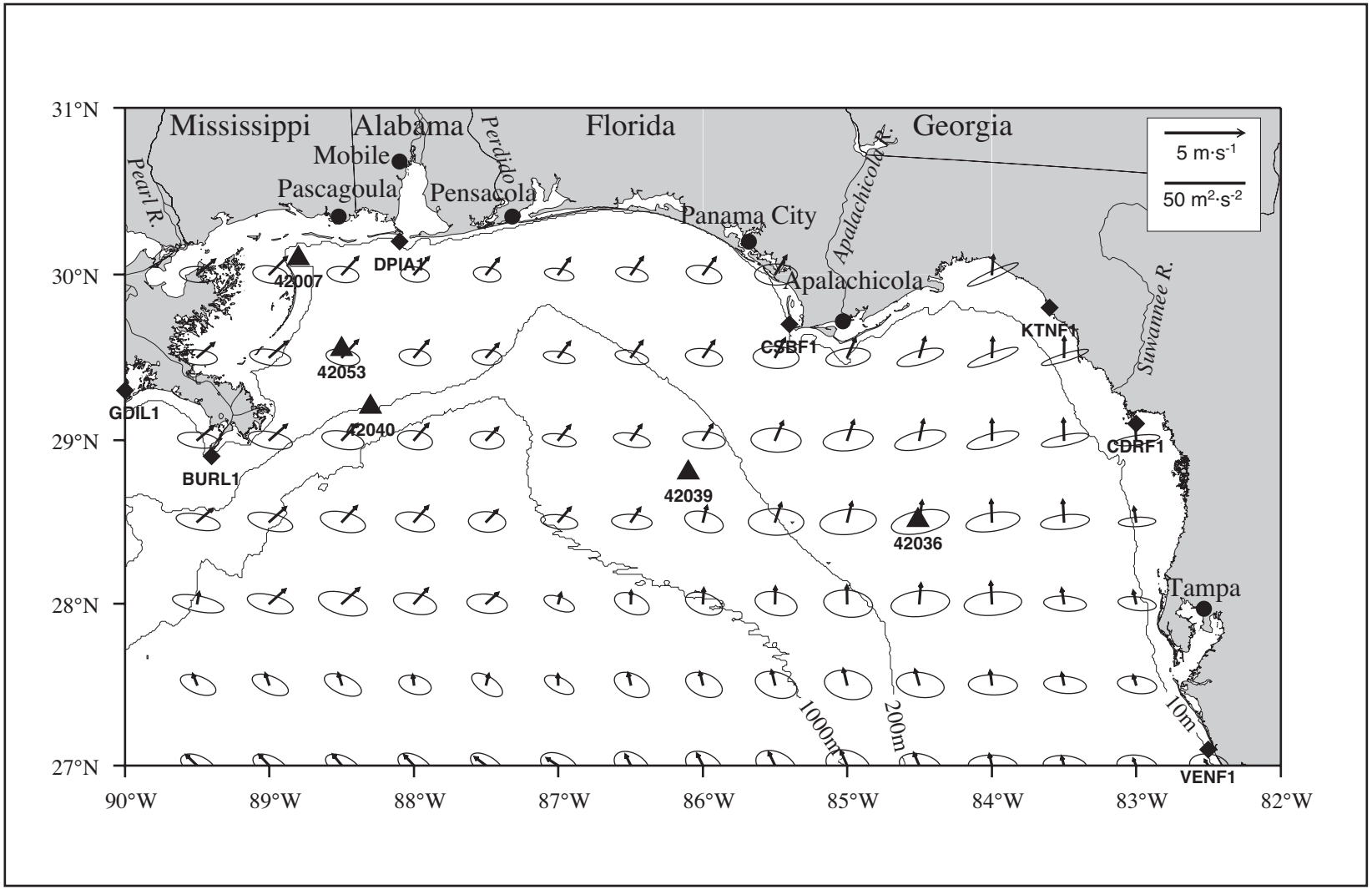

Figure F.1.1-1. Vector mean winds and variance ellipses for cruise N6 for 15-28 August 1999.

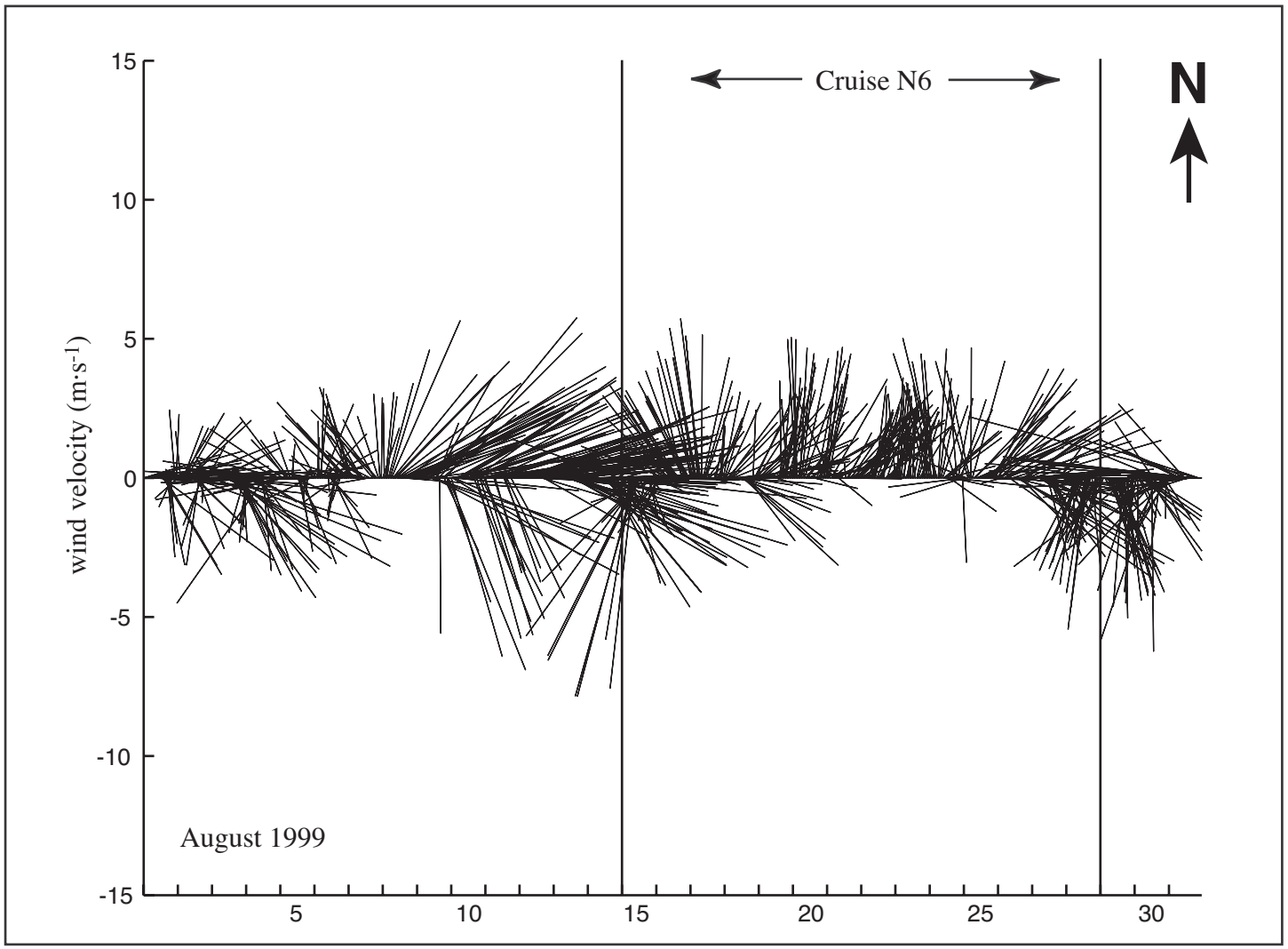

Figure F.1.1-2. Vector stick plot of wind at meteorological buoy 42040 for August 1999. Gauge height is 10 m.

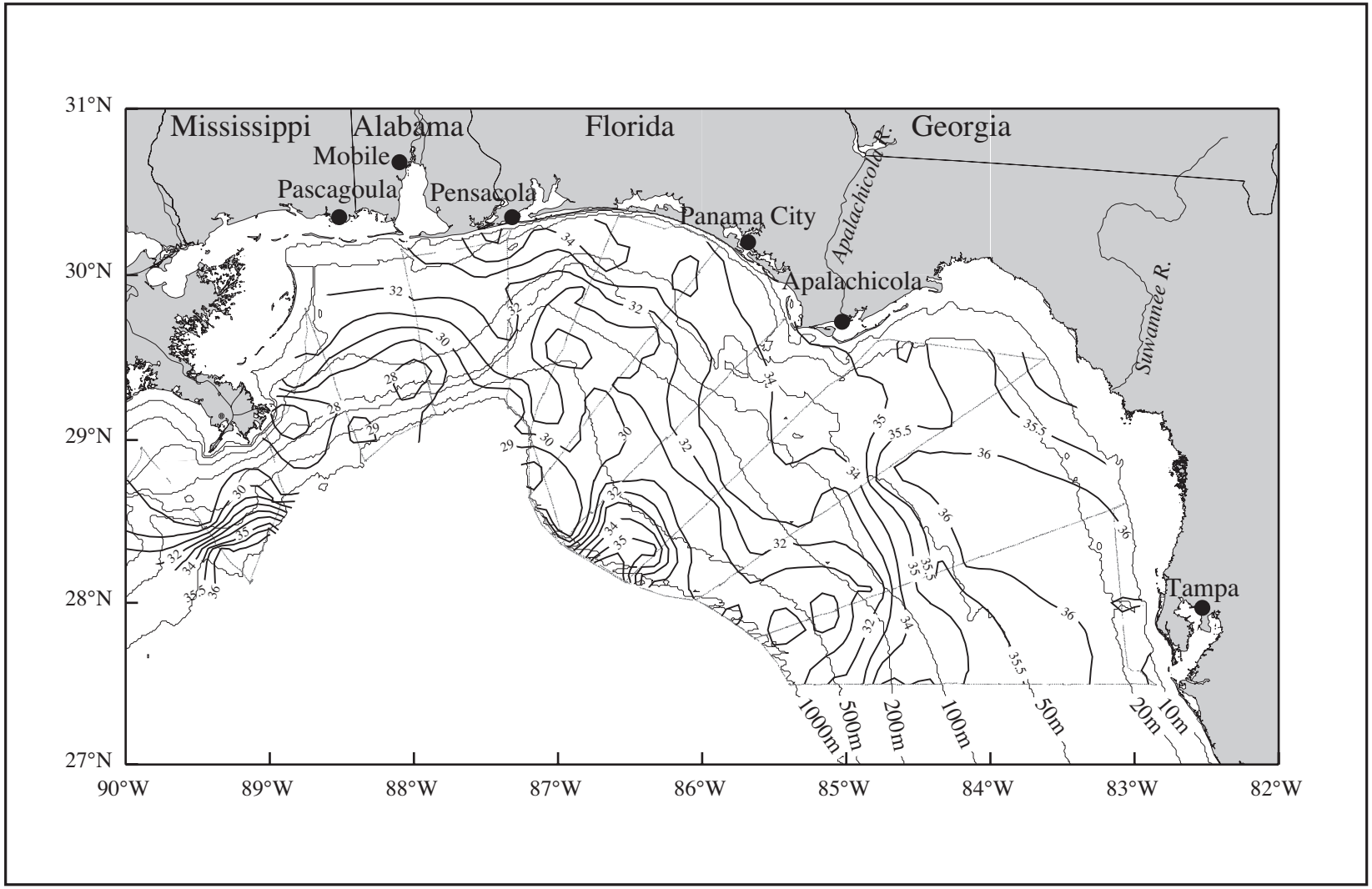

Figure F.1.2-1. Salinity at ~3 m from thermosalinograph observations on cruise N6 in August 1999.

The SSH field for 20 August, which is representative of offshelf conditions during N6, is shown in Figure F.1.3-1. The shelf break and slope of the western half of the NEGOM study area was dominated by two lows in sea surface height, one over lines 1 and 2 and the other over lines 4-6. The shelf break and slope of the eastern half shows impingement of the small anticyclone at the 1000-m isobath west of Tampa with a small negative sea surface height shoreward of that isobath.

F.2 *In Situ* Evidence of Circulation

West of Cape San Blas, the distribution of geopotential anomaly (3 m relative to 800 m) shows (Figure F.2-1) the dynamic topography increasing from the inshore to offshore over the Mississippi-Alabama shelf and a relative high over the shelf break off Panama City. The pattern along the shelf edge between lines 3 and 6, with the turning inshore of the isolines along 87°W (line 5), matches well the pattern seen in Figure F.1.3-1 of low SSH, which also turns shoreward along 87°W. It does not match the cyclonic feature over lines 1 and 2 in the SSH field. East of Cape San Blas, the dynamic topography increases from the shelf break seaward with a relative high at the seaward end of line 7. This relative high matches well the region of the impingement of the anticyclone seen in the SSH field (Figure F.1.3-1). Inshore on the west Florida shelf the dynamic topography is a broad low having a range only of 2 dynamic cm centered about the 50-m isobath.

ADCP vectors generally corroborate the patterns seen in the SSH and geopotential anomaly fields. The currents for the 4-m bin centered on the 14 m depth show the cyclonic flow over the slope and outer shelf indicated by the SSH field over lines 1 and 2 (Figure F.2-2). Near the 100-m isobath on these lines is a jet of eastward current with flows of ~50 $cm \cdot s^{-1}$. This jet turns southeast at line 3 and then on lines 4-6 follows the eastward-northward-southeastward turning pattern around the cyclone, centered near the apex of DeSoto Canyon, seen in the SSH and geopotential anomaly fields. The jet broadens and flows offshore of the 200-m isobath on lines 7-11. Magnitudes are generally 50 $cm \cdot s^{-1}$ or less. Currents along the 1000-m isobath adjacent to the impinging anticyclone are southeastward, as expected by the SSH field, and exceed 50 $cm \cdot s^{-1}$. Inshore of the shelf break over the west Florida shelf currents are smaller than elsewhere. Flow near the 100-m isobath is northwestward on lines 8-11, with currents turning into the southeastward flowing jet near the 200-m isobath on line 8. This is suggestive of possible cyclonic circulation over the mid to outer west Florida shelf, centered near line 9 between the 100- and 200-m isobaths. Currents over the inner Mississippi-Alabama shelf also mixed in directions, with both westward and eastward flows indicated. The currents from other ADCP depth bins to 102 m follow the basic patterns of direction and relative magnitudes as seen in the 14-m data; 50-m current are shown in Figure F.2-3.

F.3 Property Distributions

The near-surface salinity map shows a region of saline water intruding onto the slope between lines 7 and 8 into the relatively low salinity water located over the rest of the slope and outer shelf (Figure F.1.2-1). The SSH field indicates this is associated with the impingement of an anticyclone on the slope in that area (Figure F.1.3-1). The influence on property distributions in the vertical of the anticyclonic feature is seen in the downward dipping isolines of potential temperature, salinity, and sigma-θ along the 1000-m isobath at stations 88, 89, and 69, which respectively are the seaward ends of lines 7, 8, and 9 (Figures F.3-1, F.3-2, and F.3-3). Notable is that between approximately 200 and 400 m, the isopleths dome upward, suggesting a reversal of shear with depth (Figure F.3-1). This may be in response to the offshelf movement of water between lines 8 and 9 on the 1000-m isobath in

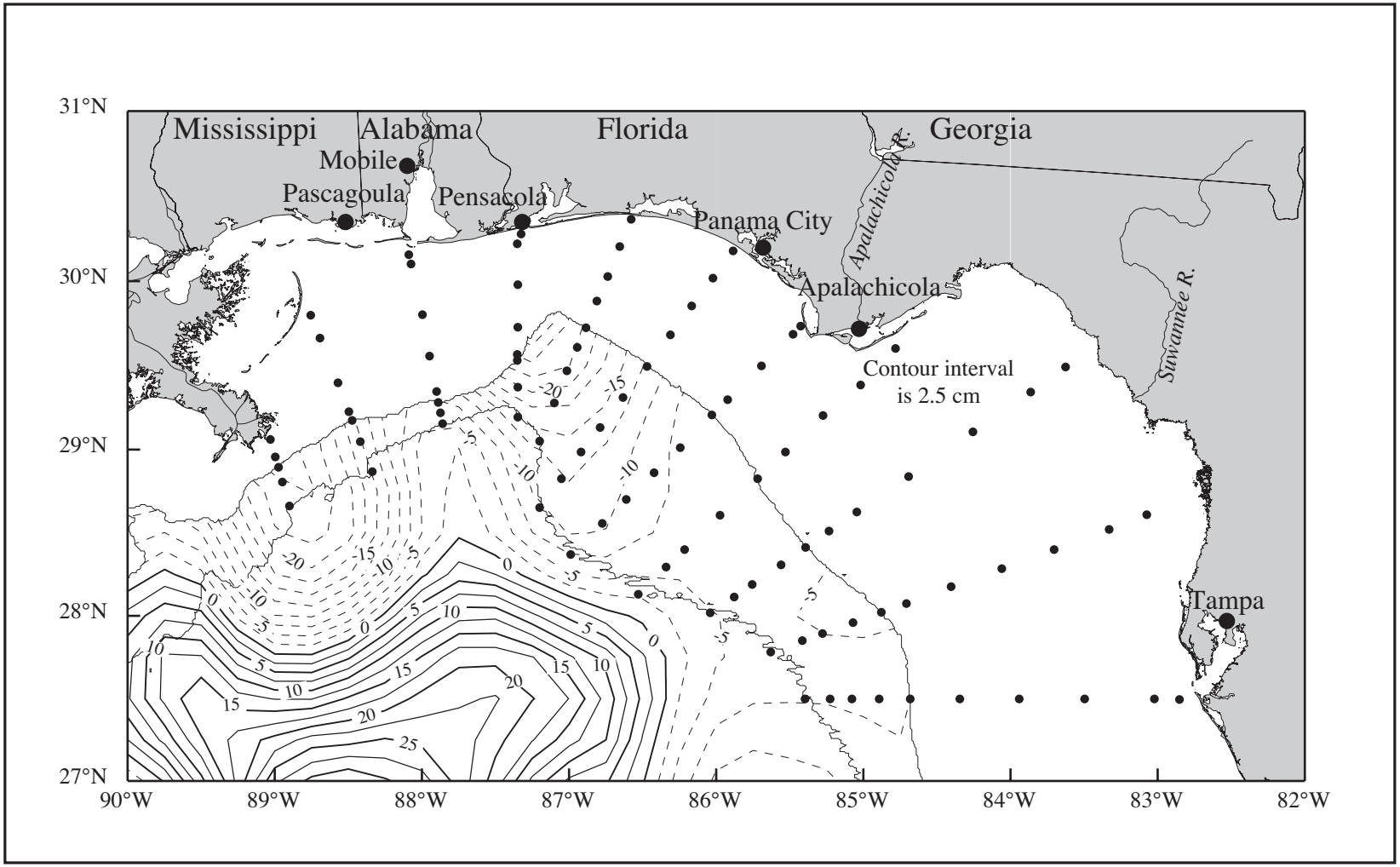

Figure F.1.3-1. Sea surface height field from satellite altimeter data for 20 August 1999 during Cruise N6. The 200- and 1000-m iosbath contours and CTD stations (dots) are shown. [Data provided by Robert R. Leben, University of Colorado.]

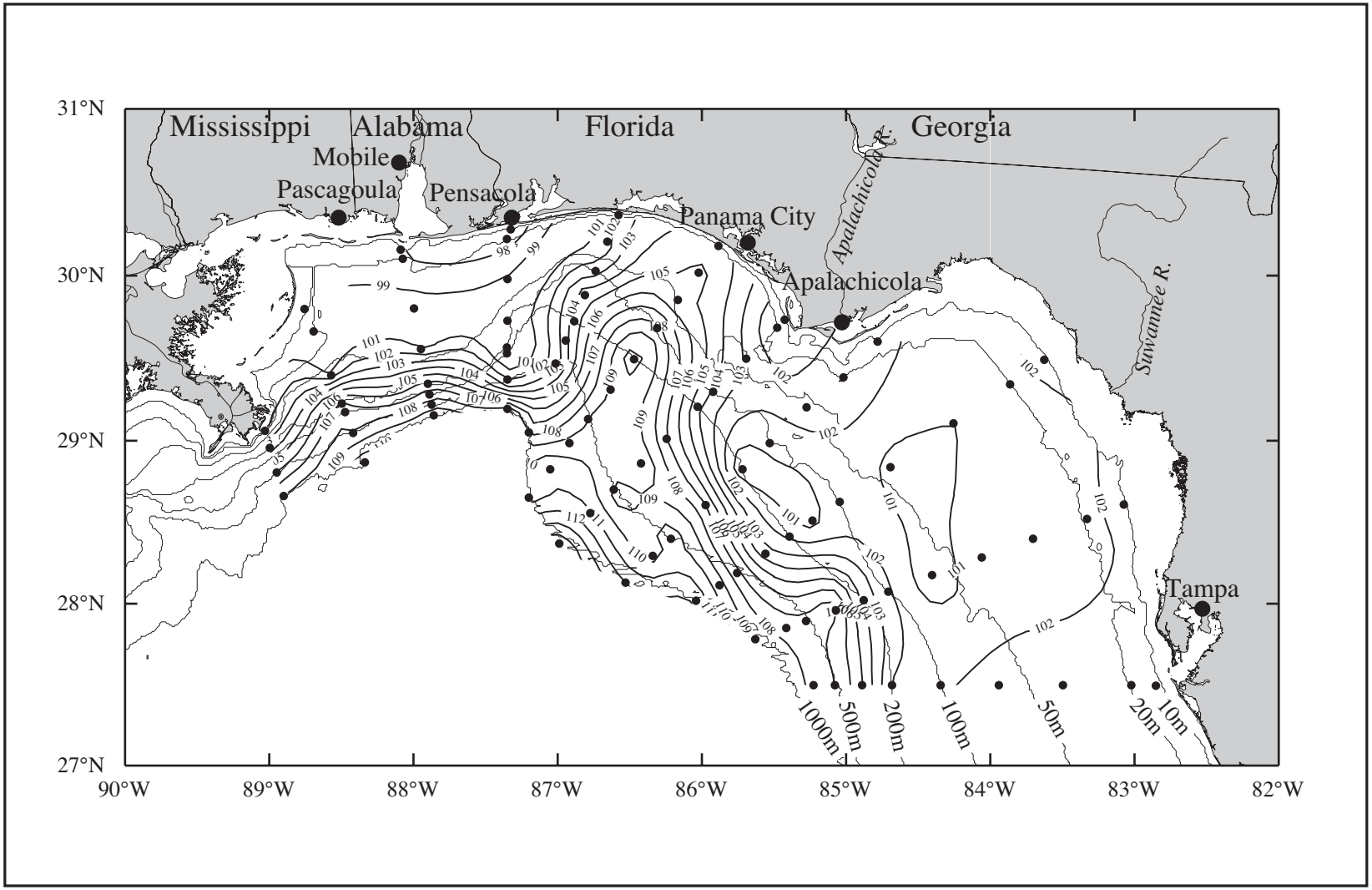

Figure F.2-1. Geopotential anomaly (dyn cm; 3 m relative to 800 m) for cruise N6 conducted 15-28 August 1999. CTD station locations are shown.

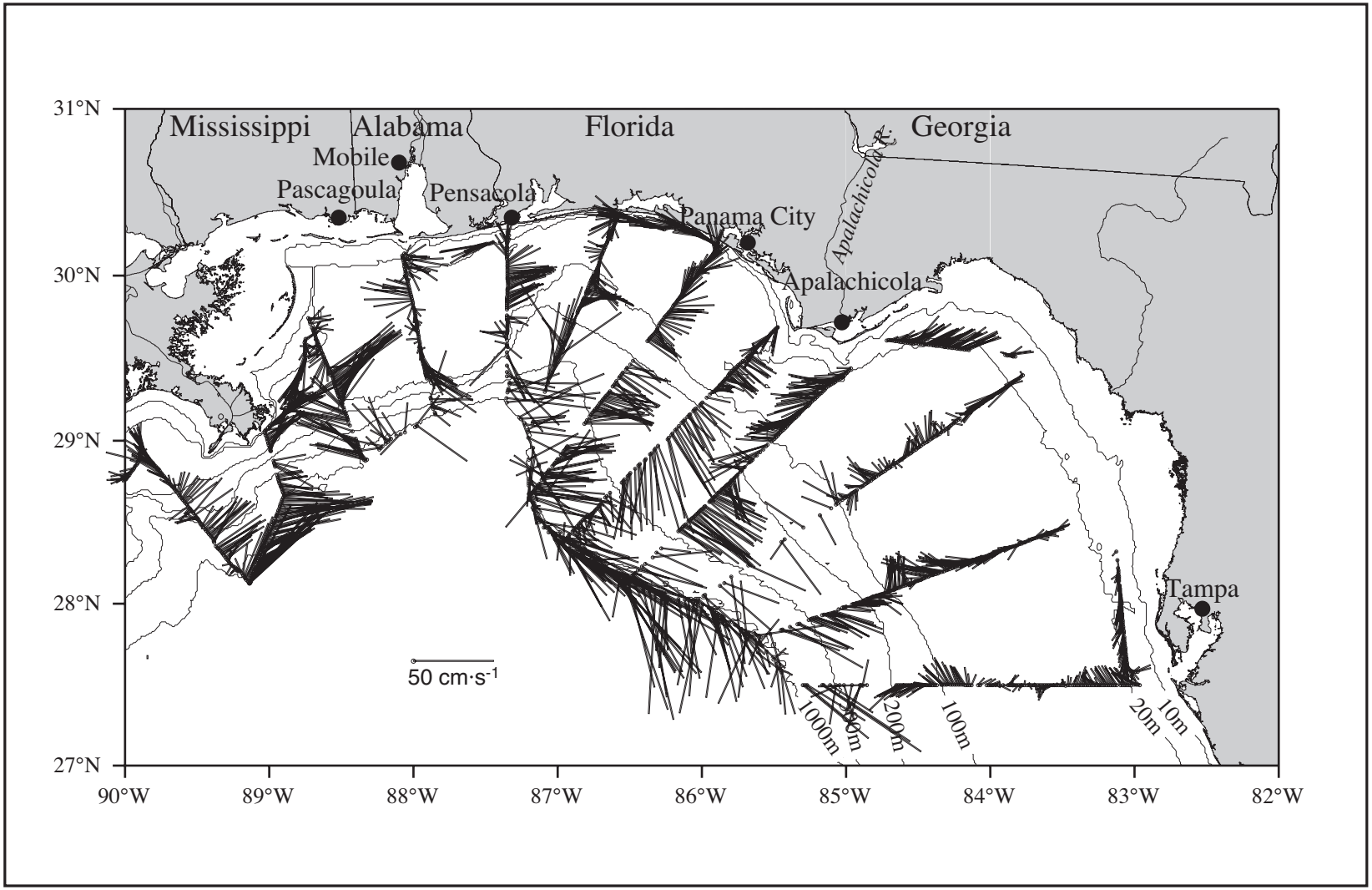

Figure F.2-2. ADCP-measured currents for the 4-m bin centered at 14 m on cruise N6 in August 1999.

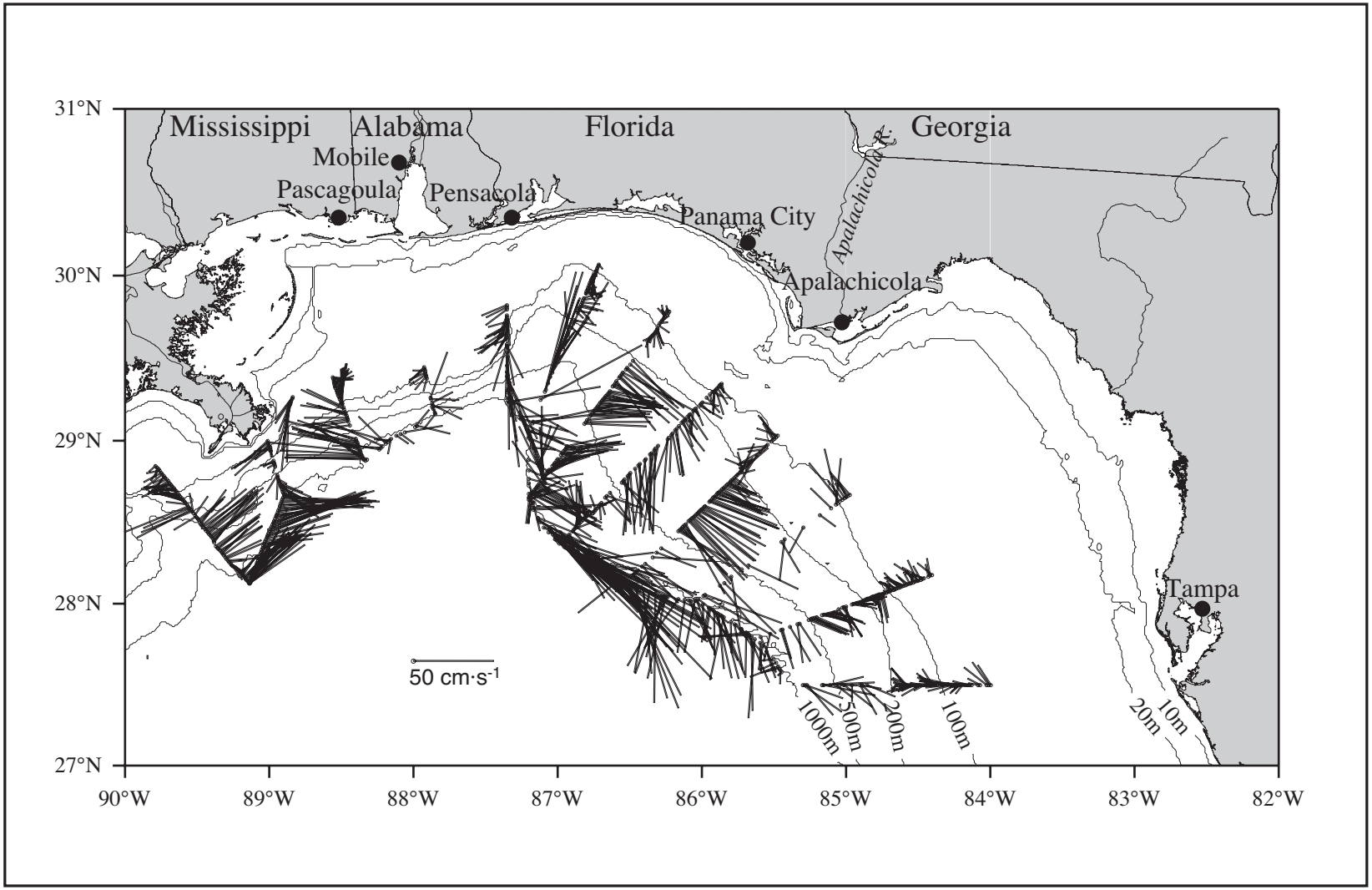

Figure F.2-3. ADCP-measured currents for the 4-m bin centered at 50 m on cruise N6 in August 1999.

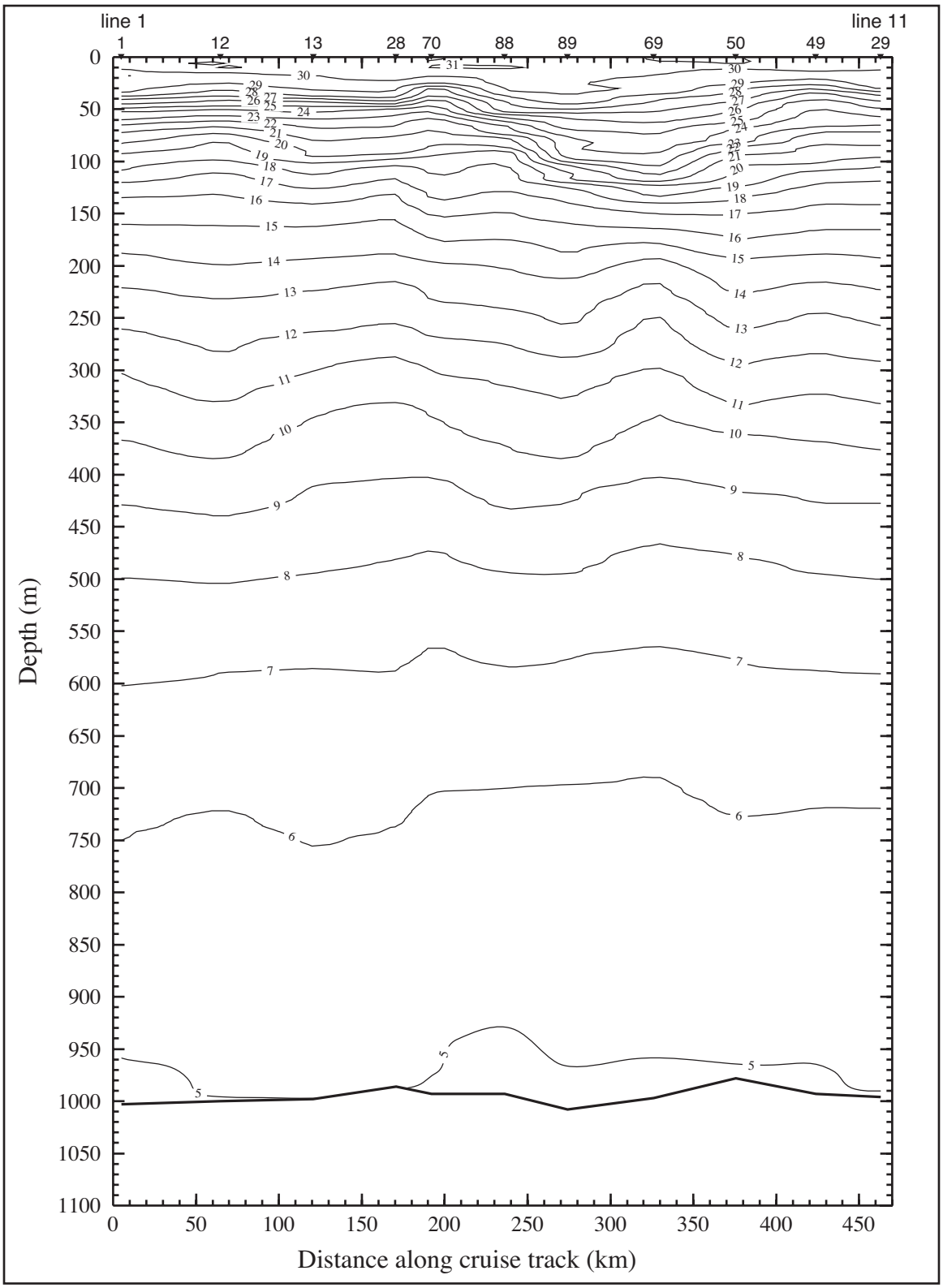

Figure F.3-1. Potential temperature (°C) along the 1000-m isobath on cruise N6 in August 1999. Stations are shown on the top axis.

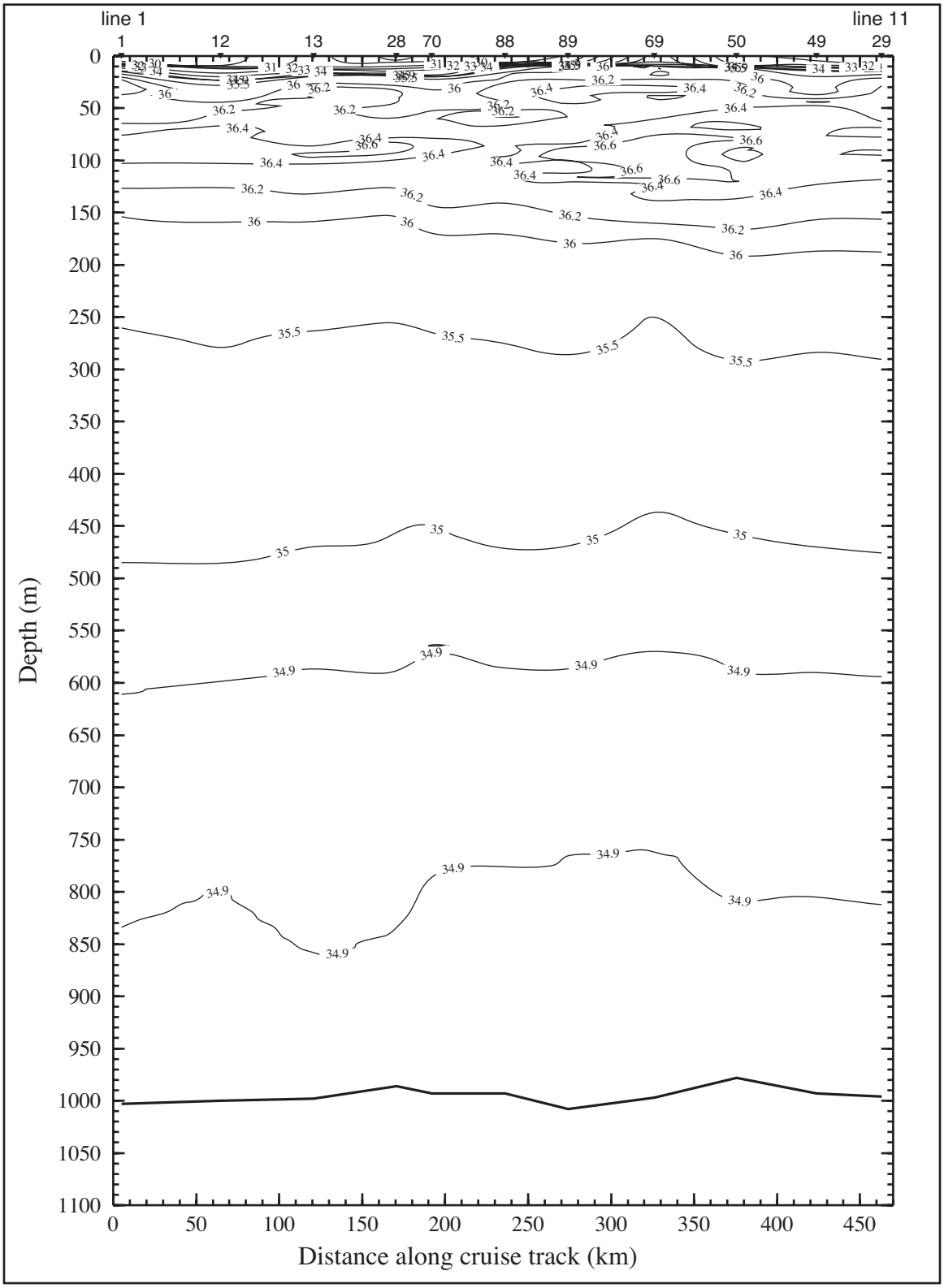

Figure F.3-2. Salinity along the 1000-m isobath on cruise N6 in August 1999. Stations are shown on top axis.

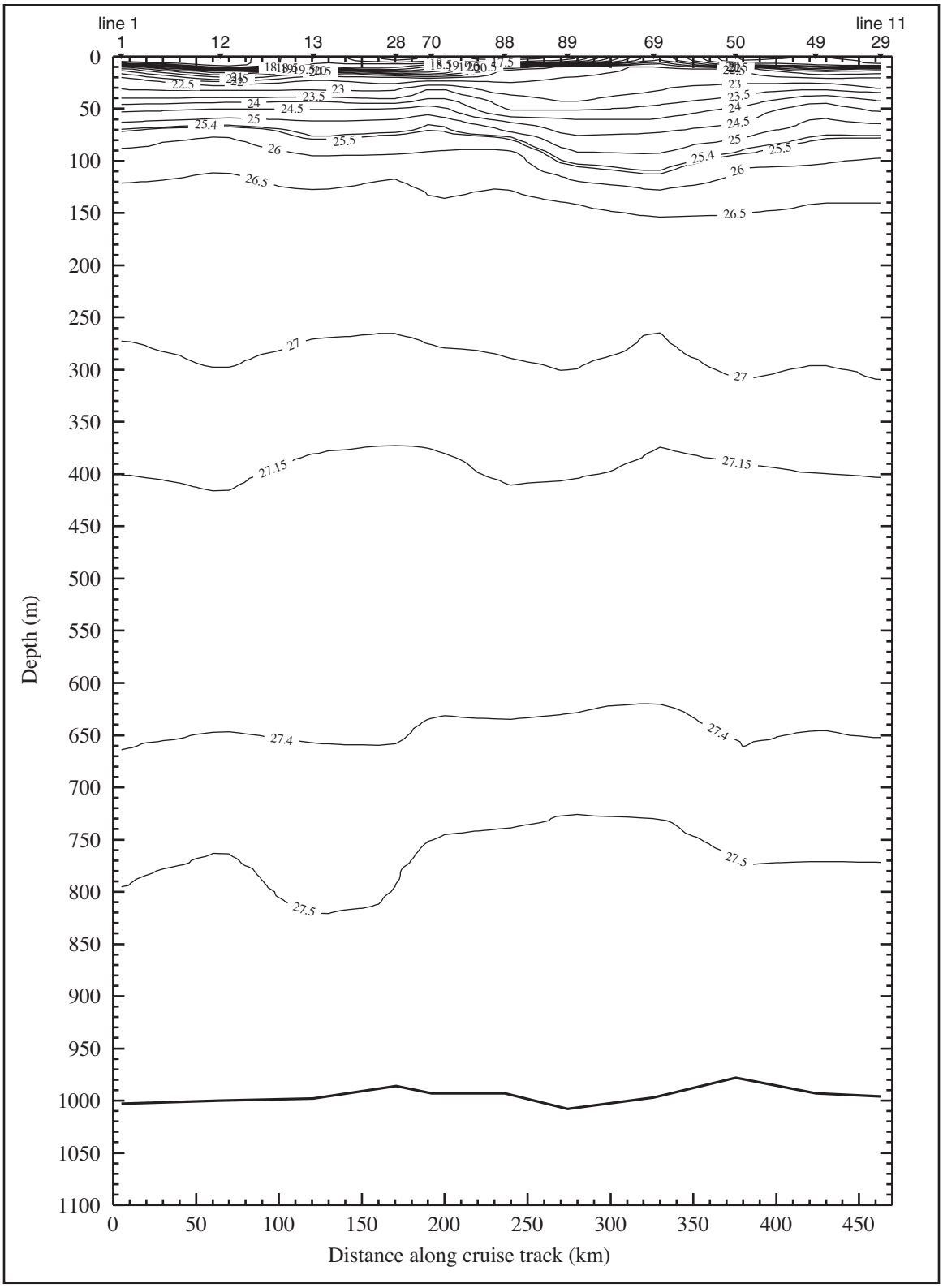

Figure 9.3-3. Density anomaly (σ_θ in kg·m^{-3}) along the 1000-m isobath on cruise N6 in August 1999. Stations are shown on the top axis.

at least the upper 100 m for which ADCP data are available (Figures F.2-2 and F.2-3). The salinity maximum at about 100-m water depth, which is associated with the impinging anticyclone, exceeds 36.6, indicating a Loop Current origin of the anticyclone. This high salinity water reaches inshore to the 300-m isobath on line 8 (station 66, Figure F.3-4, middle panel). The oxygen minimum water associated with the Tropical Atlantic Central Water is evidenced by the 2.5 $mL \cdot L^{-1}$ oxygen concentrations near bottom at the shelf break on lines 7 and 8 (Figure F.3-5). Water movement up-slope near the bottom in conjunction with the off-shelf anticyclone is evidenced by the up-slope tilt of the isotherms and isopycnals centered near station 65 on line 8 in Figure F.3-4 (upper and lower panels). There is a low centered about 200-m depth on line 8 (Figure F.2-1) and this is clearly seen in F.3-4.

Stratification in the upper 100 m was strong over the entire study area during cruise N6. This is indicated by the sigma-theta map along the 1000-m isobath (Figure F.3-3). The stratification is caused by the summertime heating, which creates a strong thermocline in the upper waters (Figure F.3-1). It also is caused by the layer of relatively low salinity water that is present in the upper 20 m over the outer shelf and slope (Figure F.3-2). One possible result of this strong stratification is the low bottom oxygen concentration of ~2.5 $mL \cdot L^{-1}$ on the inner stations of lines 1, 2, and 3. The stratification likely prevents replenishment of oxygen to the bottom while oxidation of detritus consumes the oxygen that is present.

The relatively low salinity signature of the near-surface waters over the slope and outer shelf is extensive, reaching from 50 to 100-m isobath to the 1000-m isobath across most of the study area not affected by the impingement of the anticyclonic feature (Figure F.1.2-1). The cyclone seen in the SSH field (Figure F.1.3-1) off the Mississippi River is drawing relatively low salinity water offshelf and then eastward along the outer shelf and slope. The 32 salinity line shows that the cyclone located in the DeSoto Canyon region is drawing saltier water from the inner shelf to the outer shelf and slope off Pensacola. The general pattern is of a salinity decrease going offshore. The vertical distribution of salinity in the upper waters is shown by examination of lines 1, 4, and 10 in Figure F.3-6 and line 8 in Figure F.3-4 (middle). Near the Mississippi River on line 1, the salinity nearshore is < 23, while the salinity offshore is < 29 (Figure F.3-6, top). Along line 4, on the west side of DeSoto Canyon, the relatively low salinity water is broken into patches (Figure F.3-6, middle), which reflects the drawing of the higher salinity, nearshore water across the shelf by the cyclone in the DeSoto Canyon region. The least saline water on line 4 (< 29) is located at the most seaward station over the slope. In the region of the impingement of the anticyclone on line 8, relatively low salinity water is pooled about the 300-m isobath between the high salinity water from the anticyclone intrudes from the deep Gulf and relatively high salinity waters on the inner shelf (Figure F.3-4, middle). Along line 10, a pattern of fresher water offshore is present, with waters < 30 (Figure F.3-6, lower). Although the vertical thickness varies, waters with salinity of ≤ 32 extend approximately over the upper 10-20 m, depending on proximity to cyclones and anticyclonic features.

Nitrate concentrations are low in the upper 50 m except nearshore on line 1 where the nutrient loading of the Mississippi River had not been depleted by biological production (Figure F.3-7). Bottom concentrations are high, with the highest isolines reaching farther inshore over the west Florida shelf than over the Mississippi-Alabama shelf (Figure F.3-8). Highest values are on the slope on the east side of DeSoto Canyon. Along lines 7-9, there is doming of nitrates associated with the up-slope movement of deep waters in that region and downward dipping isolines farther offshore associated with the anticyclonic feature impinging on the 1000-m isobath (Figure F.3-9, top). Phosphate and silicate patterns are similar to nitrate patterns, except silicate concentrations are not fully used up in the photic zone (e.g., Figure F.3-9, middle). Additionally, there are regions near bottom about the 50 to

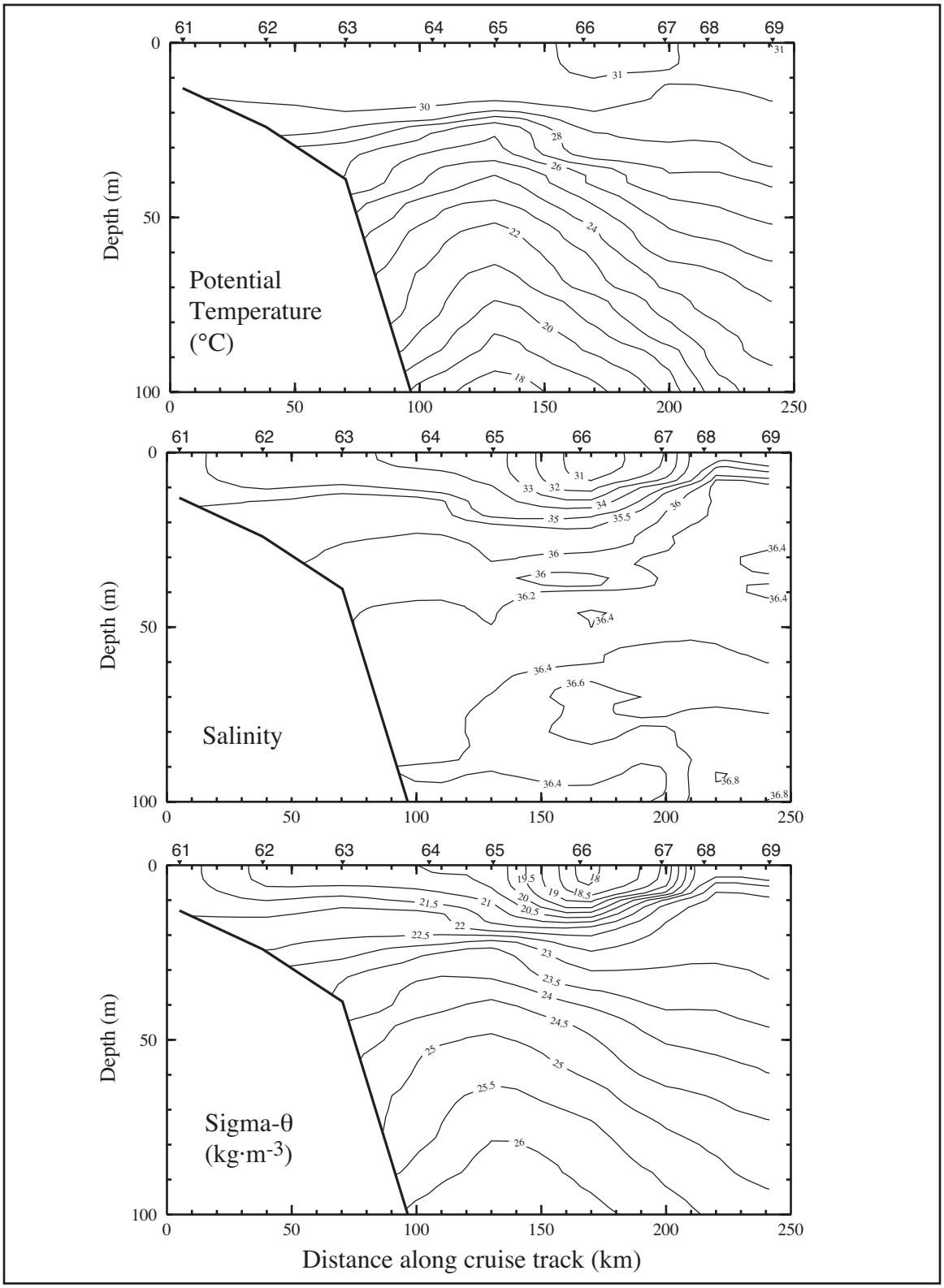

Figure F.3-4. Potential temperature, salinity, and density anomaly on line 8 of cruise N6 in August 1999. Stations are shown on top axes.

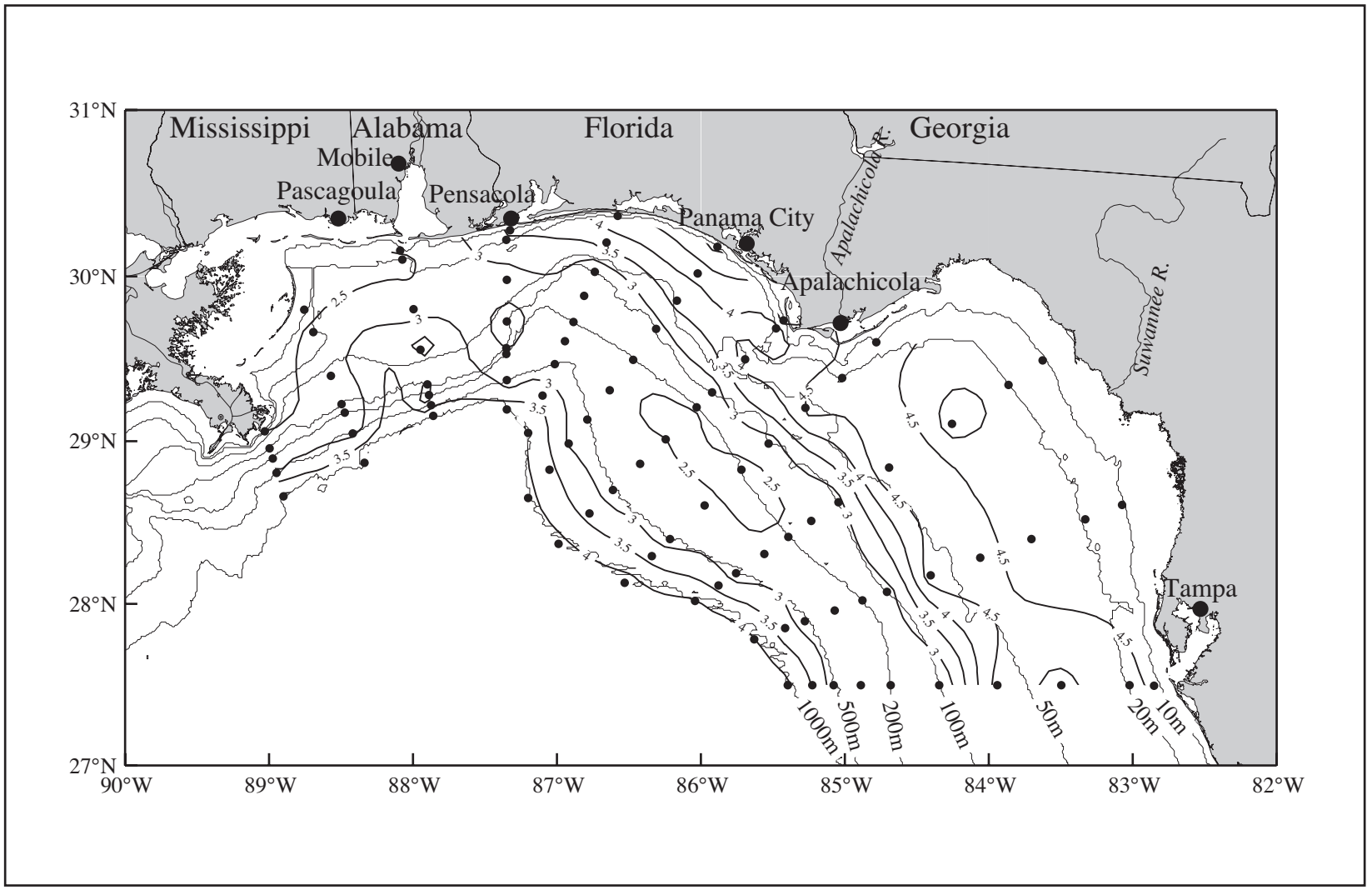

Figure F.3-5. Dissolved oxygen ($mL \cdot L^{-1}$) from the near-bottom observations on cruise N6 in August 1999.

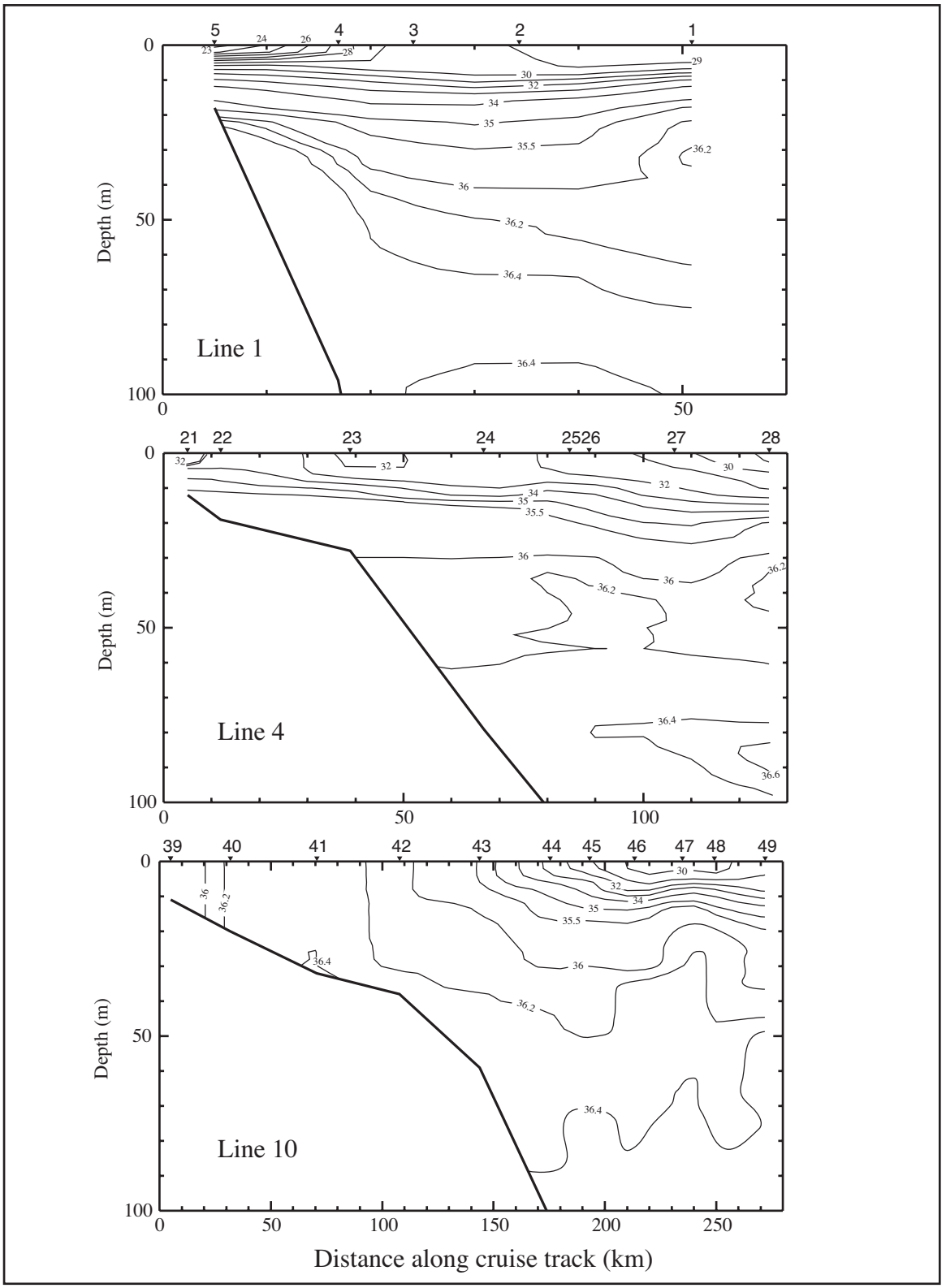

Figure F.3-6. Salinity along lines 1, 4, and 10 on cruise N6 in August 1999. Stations are shown on top axes.

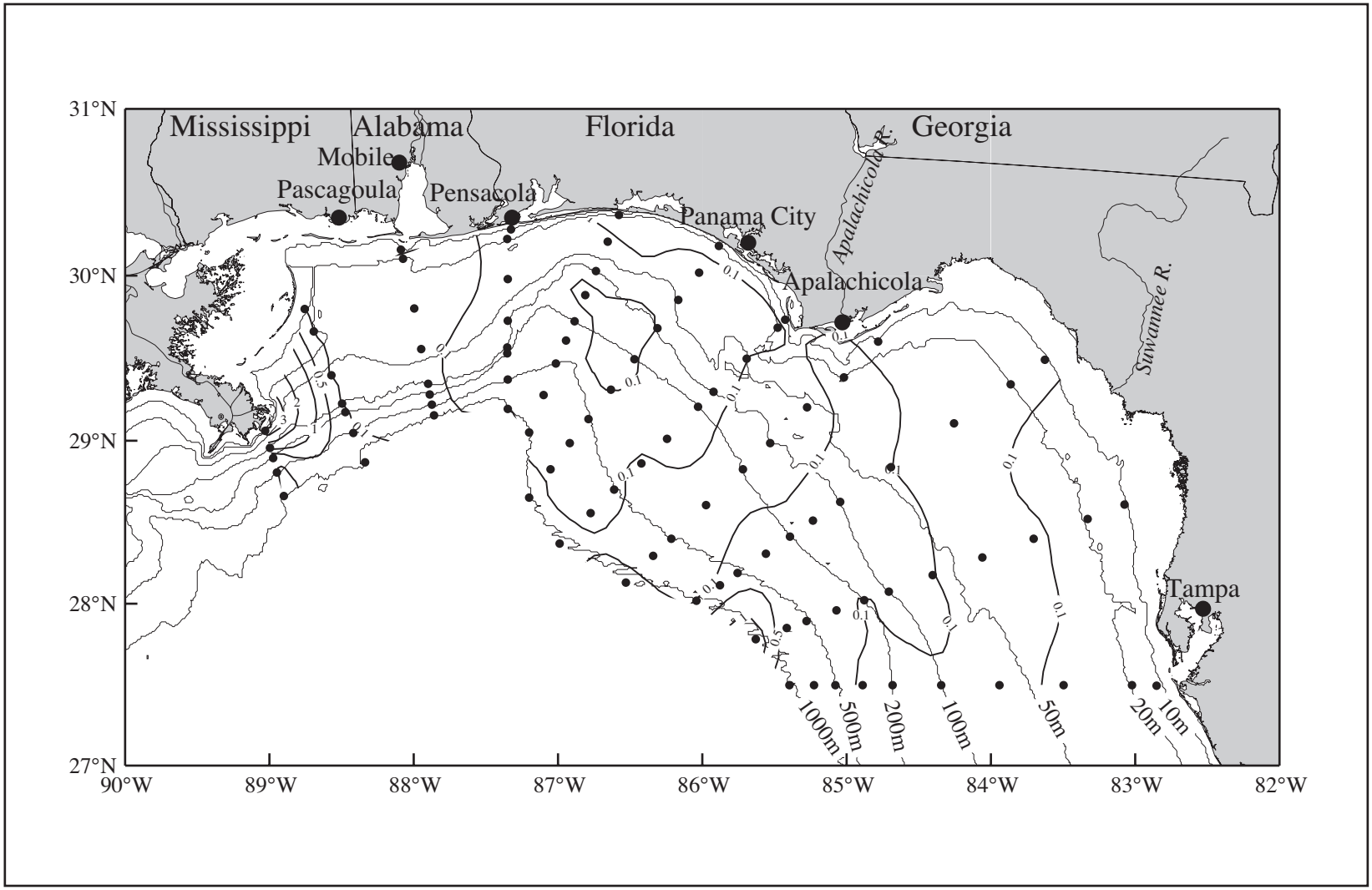

Figure F.3-7. Nitrate (μM) from the near-surface (~3.5 m) observations on cruise N6 in August 1999.

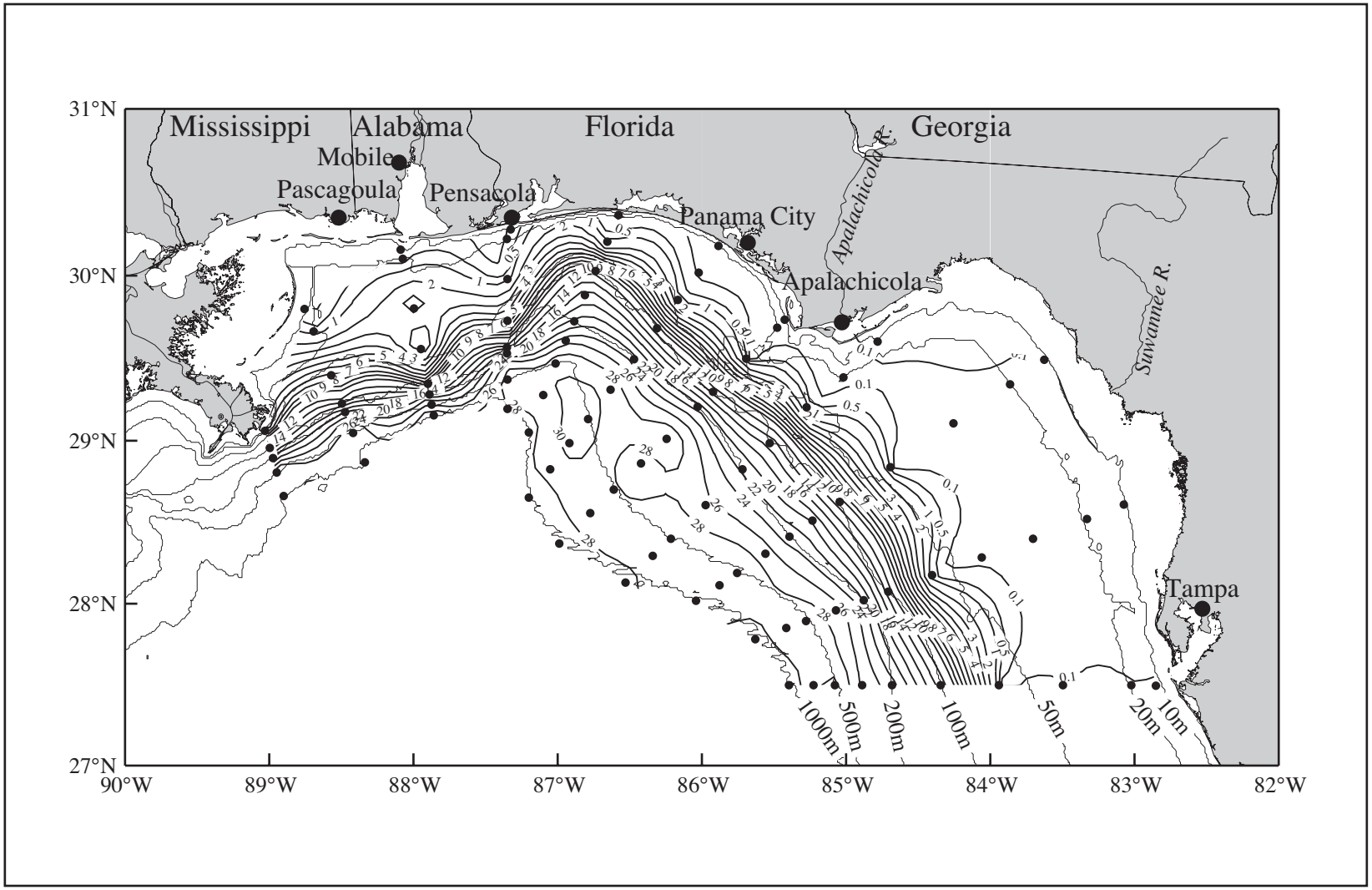

Figure F.3-8. Nitrate (μM) from the near-bottom observations on cruise N6 in August 1999.

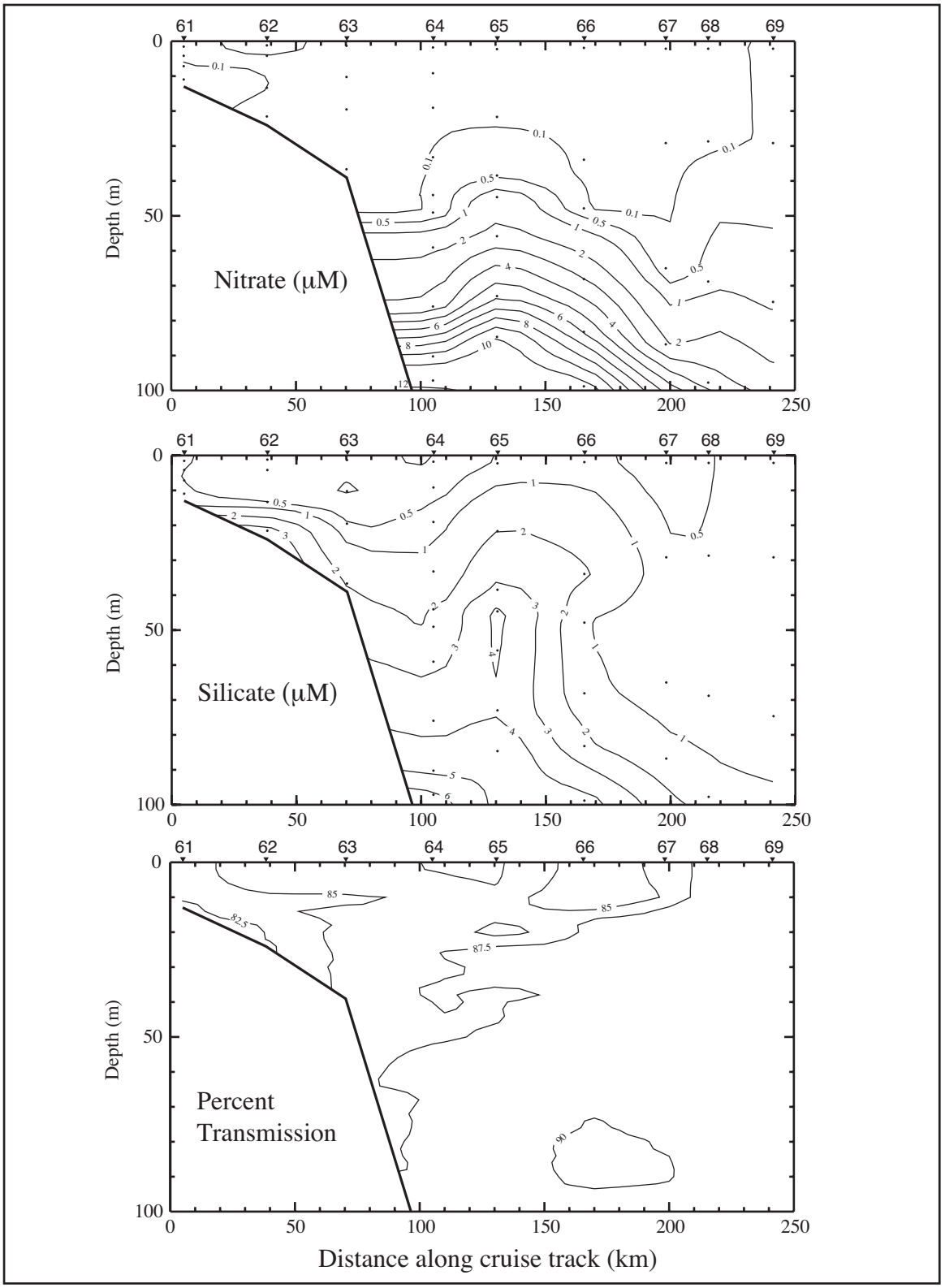

Figure F.3-9. Nitrate, silicate, and percent transmission along line 8 on cruise N6 in August 1999. Stations are shown on top axes.

100-m isobaths, mainly associated with DeSoto Canyon, with resuspension of particles, as evidenced by lower percent transmission, that enhances silicate concentrations (compare middle and bottom panels of Figure F.3-10 and Figure F.3-9).

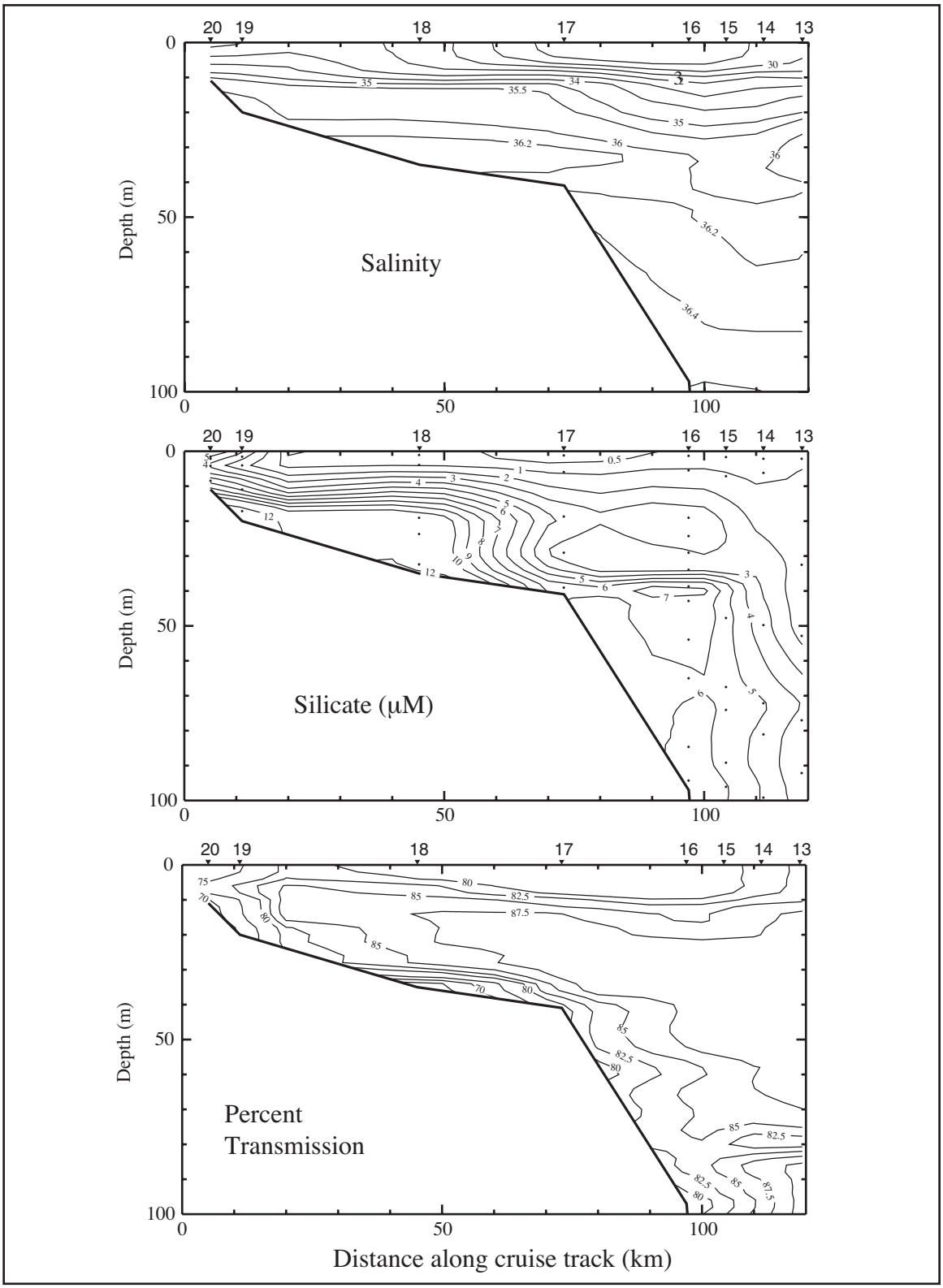

Figure F.3-10. Salinity, silicate, and percent transmission along line 3 on cruise N6 in August 1999. Stations are shown on top axes.

APPENDIX G
SUMMARY OF CONDITIONS DURING CRUISE N7

Cruise N7 was a fall cruise conducted 13-25 November 1999. The cruise began with a station on the seaward end of line 1, southeast of the Mississippi delta, and continued in sequence along each line. The cruise ended with the inshore station of line 11 near Tampa Bay. Figure G-1 shows the station locations and gives the CTD numbers, which are sequential by sampling order. This cruise was the third Fall cruise of the program.

G.1 Forcing Functions

G.1.1 Winds

The mean wind field and variability ellipses for cruise N7, 13-25 November 1999, are shown in Figure G.1.1-1. The methodology used is that of Wang et al. (1998) applied to hourly observations at meteorological stations located as shown in the figure. Over the NEGOM region mean winds were light to moderate and uniformly directed toward the southwest. Mean wind speeds were 3-6 $m \cdot s^{-1}$, with slightly stronger winds farther offshore. Variability ellipses were similar to the two prior fall cruises, oriented with the major axes mainly perpendicular to the direction of mean wind. The magnitude of the semi-major axis varied from ~10 $m^2 \cdot s^2$ over the west Florida shelf to 20-30 $m^2 \cdot s^2$ over the Mississippi-Alabama shelf. Instantaneous wind fields indicated no major reversals of the alongshore winds occurred during cruise N7. However, on 15-16 November the wind field uniformly turned to the southeast in advance of a cold front which pushed south to 25°N (e.g., Figure G.1.1-2). During 19-21 November, winds over the Mississippi-Alabama shelf turned toward the northwest and north in advance of a weak high pressure cell over land.

G.1.2 River Discharge

Daily river discharge rates for the Mississippi River during the months of September through December were less than the 70-yr record-length mean by nearly one standard deviation (Figure 3.1.2-2). This was also true for all major rivers of the northeastern Gulf of Mexico during the fall 1999; discharge rates only occasionally peaked to the 70-yr mean values.

As a result of the low Mississippi River discharge rates, lack of major offshelf anticyclones, and predominant southwestward winds, there was no development of the Mississippi River plume eastward from the delta into the study region. Figure G.1.2-1 shows the near-surface (~3 m) salinity field from the ship continuous flow-through thermosalinograph system. A slight salinity gradient exists in the extreme western part of the study area close to the Mississippi River delta with inshore salinity values of approximately 34 and offshore values greater than 36. The high salinity values at the shelf edge in the west are due to onshore flow caused by the presence of a cyclonic feature positioned south of Mississippi Canyon (see Section G.1.3). In general the near-surface salinity field is nearly uniform over the region with values greater than 35.5. Exceptions are seen in the areas close to bays associated with the other major rivers of the region, i.e., Apalachicola Bay, Mobile Bay, and Choctawhatchee Bay. A thin band of relatively high salinity water (> 36) can be seen along-shore to the west of Tampa, between 20 and 30 m depth, extending north into the West Florida Bight. The effects of the distribution of the low salinity water are also evident in the patterns of near-surface chlorophyll *a* (Figure G.1.2-2) as high concentrations can be seen at major river discharge sites along the coast.

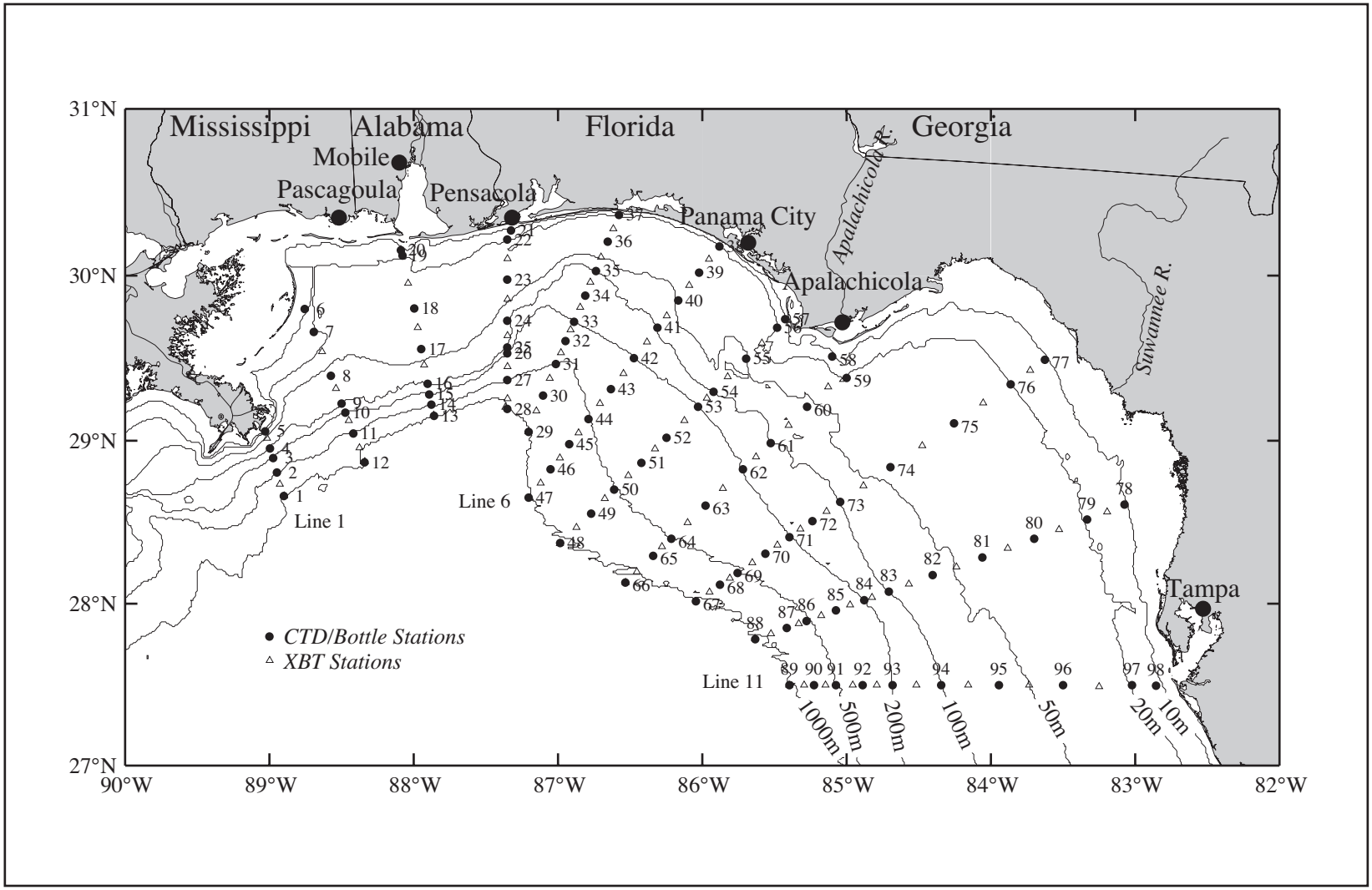

Figure G-1. Station locations for cruise N7 conducted on 13-25 November 1999. CTD stations (solid circles) are numbered; XBT stations (open triangles) are not.

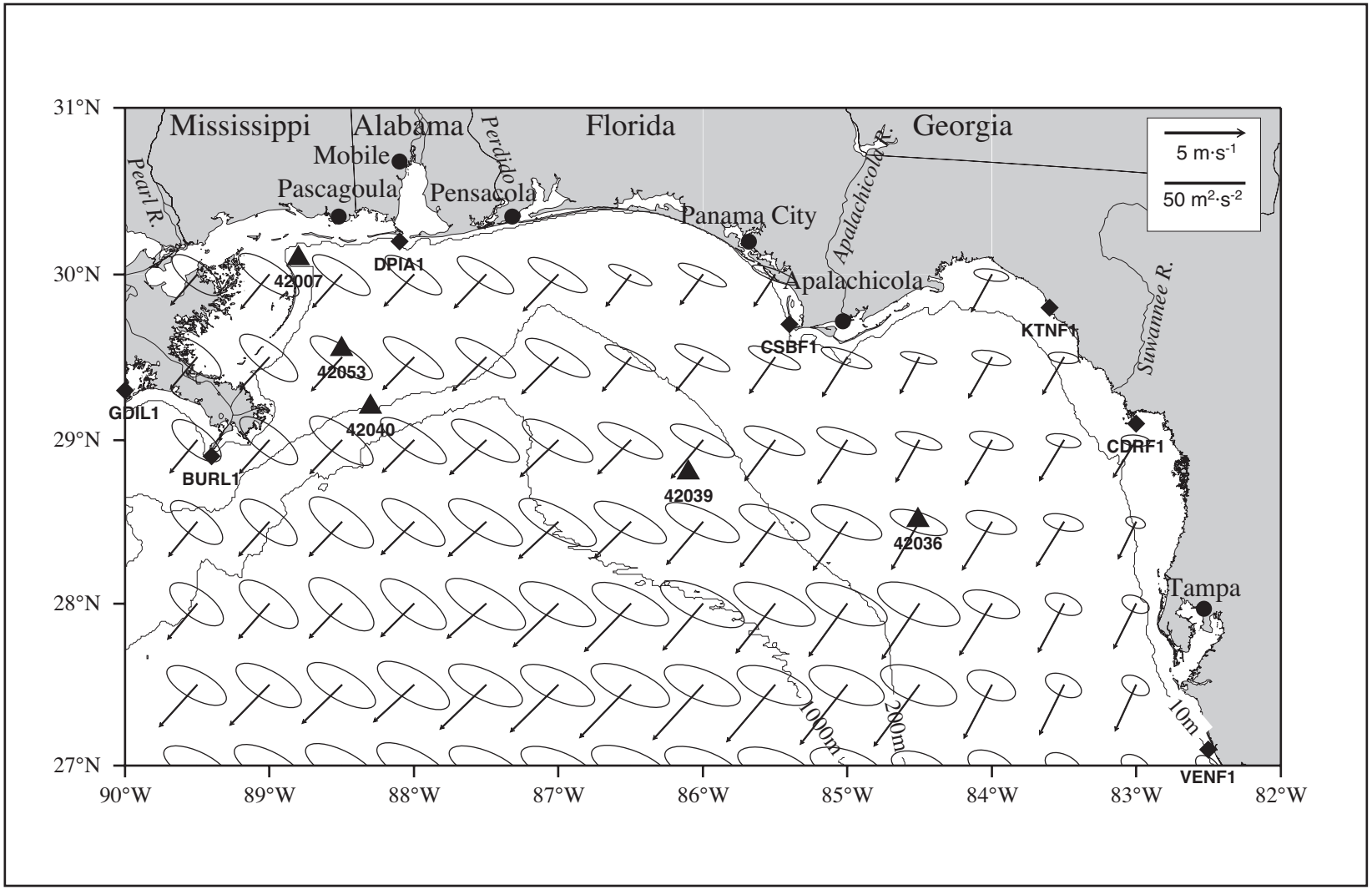

Figure G.1.1-1. Vector mean winds and variance ellipses for cruise N7 during 13-25 November 1999.

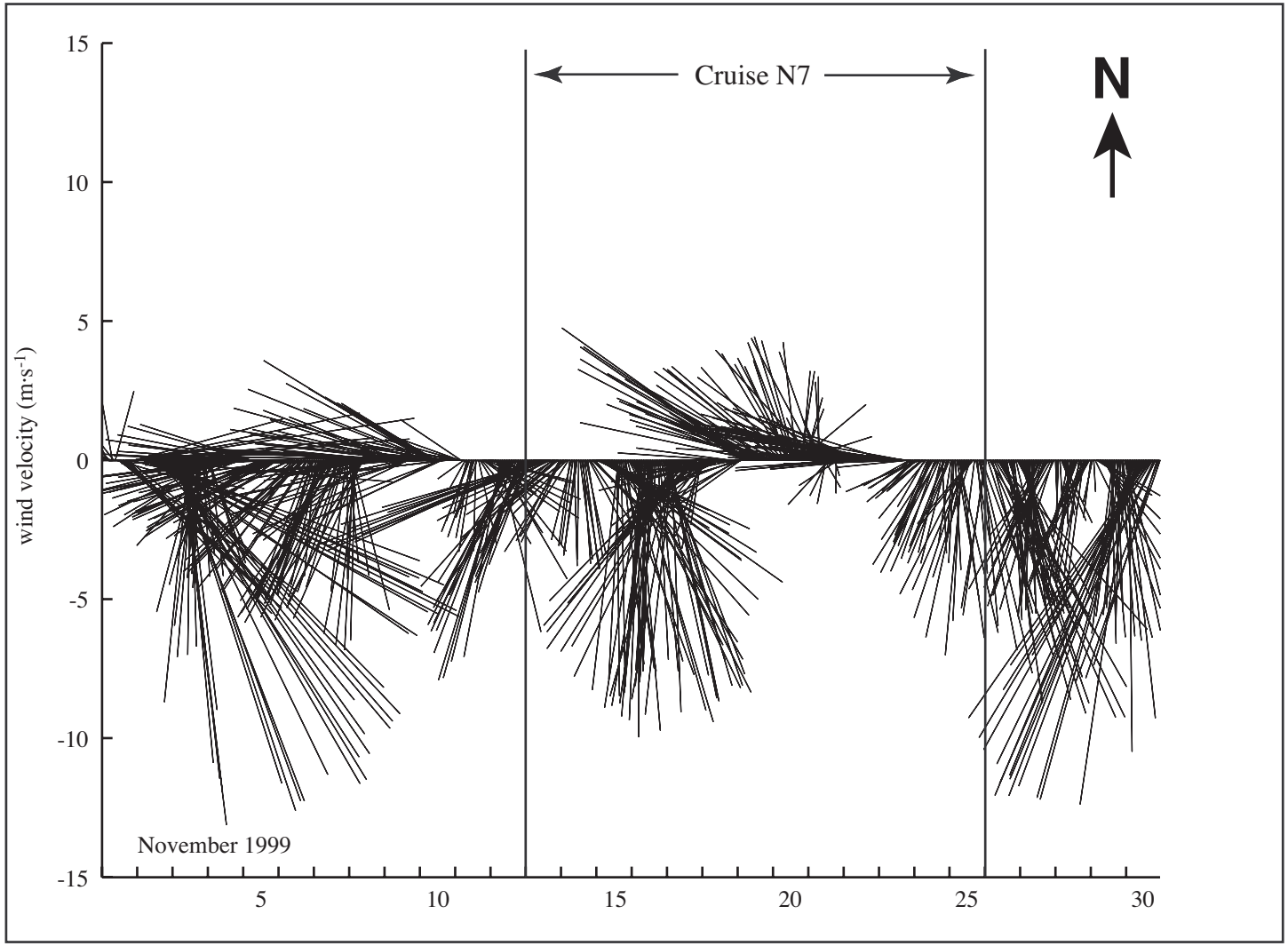

Figure G.1.1-2. Vector stick plot of wind at meteorological buoy 42040 for November 1999. Gauge height is 10 m.

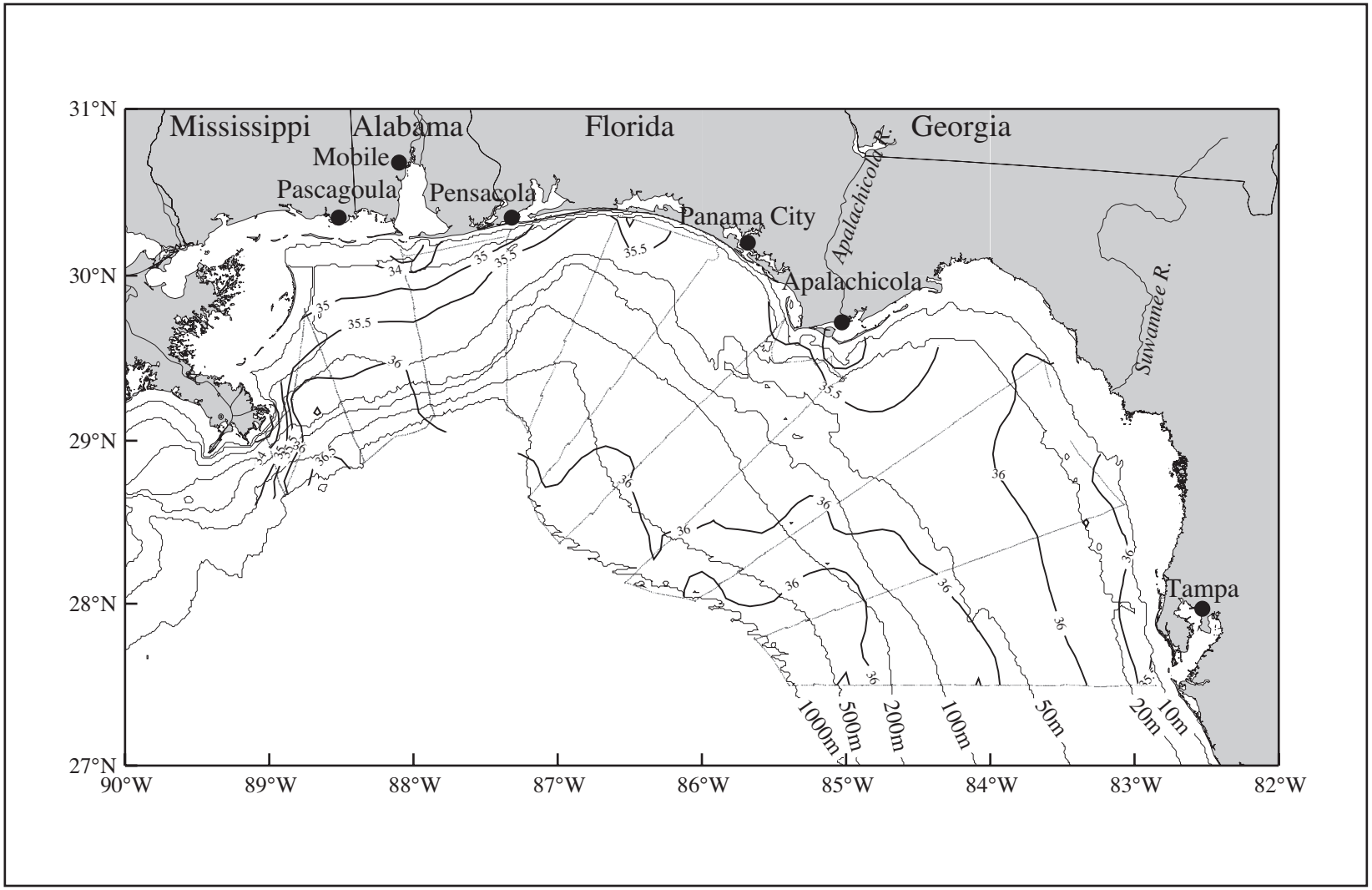

Figure G.1.2-1. Salinity at ~3 m from thermosalinograph observations on cruise N7 in November 1999.

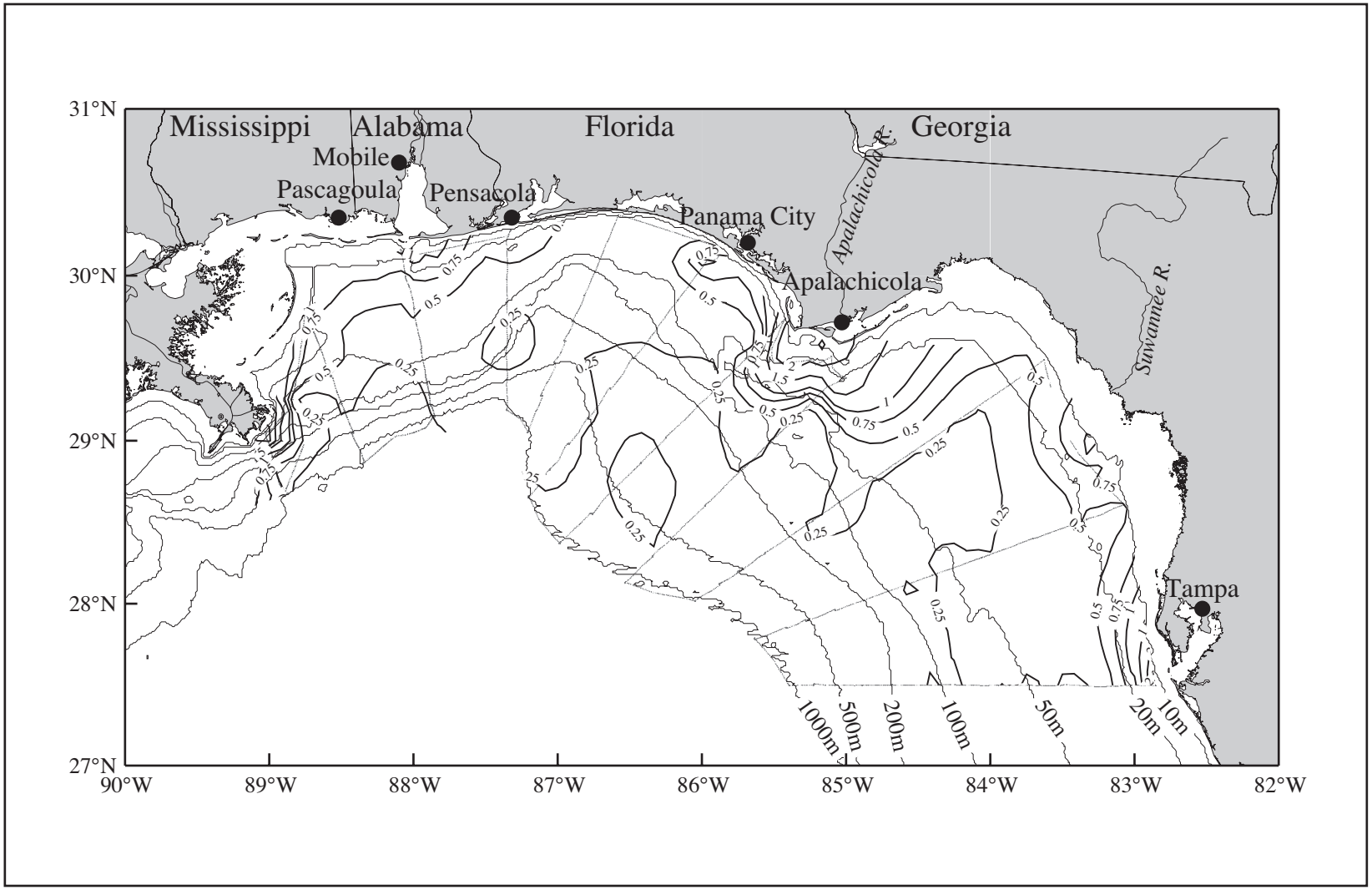

Figure G.1.2-2. Chlorophyll a ($\mu g \cdot l^{-1}$) at ~3 m calculated from flow-through fluorescence on cruise N7 in November 1999.

G.1.3 SSH Fields Adjacent to the Shelf

A major Loop Current eddy, Juggernaut, detached from the Loop Current in October 1999. This eddy was among the most powerful and largest observed in the Gulf of Mexico. The center of circulation of this eddy remained south of 27°N and west of 88°W (Figures 3.2.3-27 through 3.2.3-29) and therefore did not directly influence the study region during the November cruise. However, a tongue of positive SSH from Juggernaut can be seen near the 1000-m isobath near 28°N, 86.75°W. The SSH during N7 (Figure G.1.3-1) shows 2 lows: one centered at 90°W south of the Mississippi Canyon; the other at 27°N, 85.8°W. Both lows peripherally affected the shelf circulation: the western low moved ocean waters to the slope and shelf and the eastern moved water off the slope and shelf.

G.2 *In Situ* Evidence of Circulation

ADCP data were available only for measurements made in water depths of less than 100 m. Near-surface (~13 m) currents (Figure G.2-1) are generally 10-20 $cm \cdot s^{-1}$ and variable on the Mississippi-Alabama and west Florida shelves. A moderately strong (25 $cm \cdot s^{-1}$) coastal current is seen flowing upcoast, west of Pensacola to Cape San Blas. On the east side of Cape San Blas, flow is downcoast, creating a convergence at the Cape with flow directed offshore.

Geopotential anomaly (3 m relative to 800 m) based on N7 data (Figure G.2-2) shows a complex pattern of weak highs and lows over the study region. A high is positioned over the west Florida shelf and centered near 28.5°N, 85°W. However, the strong cross-shelf flow apparently associated with this feature and the low to the northwest are contradictory to the flow in the vicinity of Cape San Blas indicated by the ADCP measurements. A high also exists at the seaward edges of lines 6, 7, and 8 and corresponds to the tongue of high SSH extending onto the slope associated with Eddy Juggernaut (Figure G.1.3-1). Likewise the low geopotential anomaly at the seaward edges of lines 9, 10, and 11 corresponds to the western limb of the cyclone seen in Figure G.1.3-1. The region west of line 7 consists of a series of alternating highs and lows in geopotential anomaly oriented cross-shelf: highs occur at lines 1, 3, and 7, while lows are at lines 2 and 6. Little of the pattern of geostrophic shear over the shelf indicated in Figure G.2-2 is confirmed by the ADCP measurements. Therefore, the dynamic topography over the shelf should be viewed with suspicion.

G.3 Property Distributions

The temperature field at 3-m depth observed on N7 is shown in Figure G.3-1. Cool water (~22°C) is seen in the western region associated with lower salinities seen in Figure G.1.2-1. The general temperature gradient is for cool temperatures near the coast of the order of 21°C and warmer temperatures over the outer shelf and slope. The 23.5°C isotherm tends to follow the 50-m isobath. There is further evidence of the warm tongue of LCE water at the seaward end of line 7 (compare with Figure G.1.3-1). The near-surface salinity field (Figure G.1.2-1) shows salinity is greater than 36.2 at the seaward end of line 7; this is further evidence of the LCE intrusion.

As seen on previous cruises, observations of near-bottom salinity (Figure G.3-2) show a maximum between 50 and 100 m indicating the presence of Subtropical Underwater. However, values of greater than 36.4 were seen in shallow water of the West Florida Bight at line 10 indicating a possible intrusion of this water mass onto the inner shelf. The influence of the Mississippi River can also be seen as low inshore near-bottom salinity values from the delta to Pensacola. The examination of near-bottom temperature (not shown) shows an

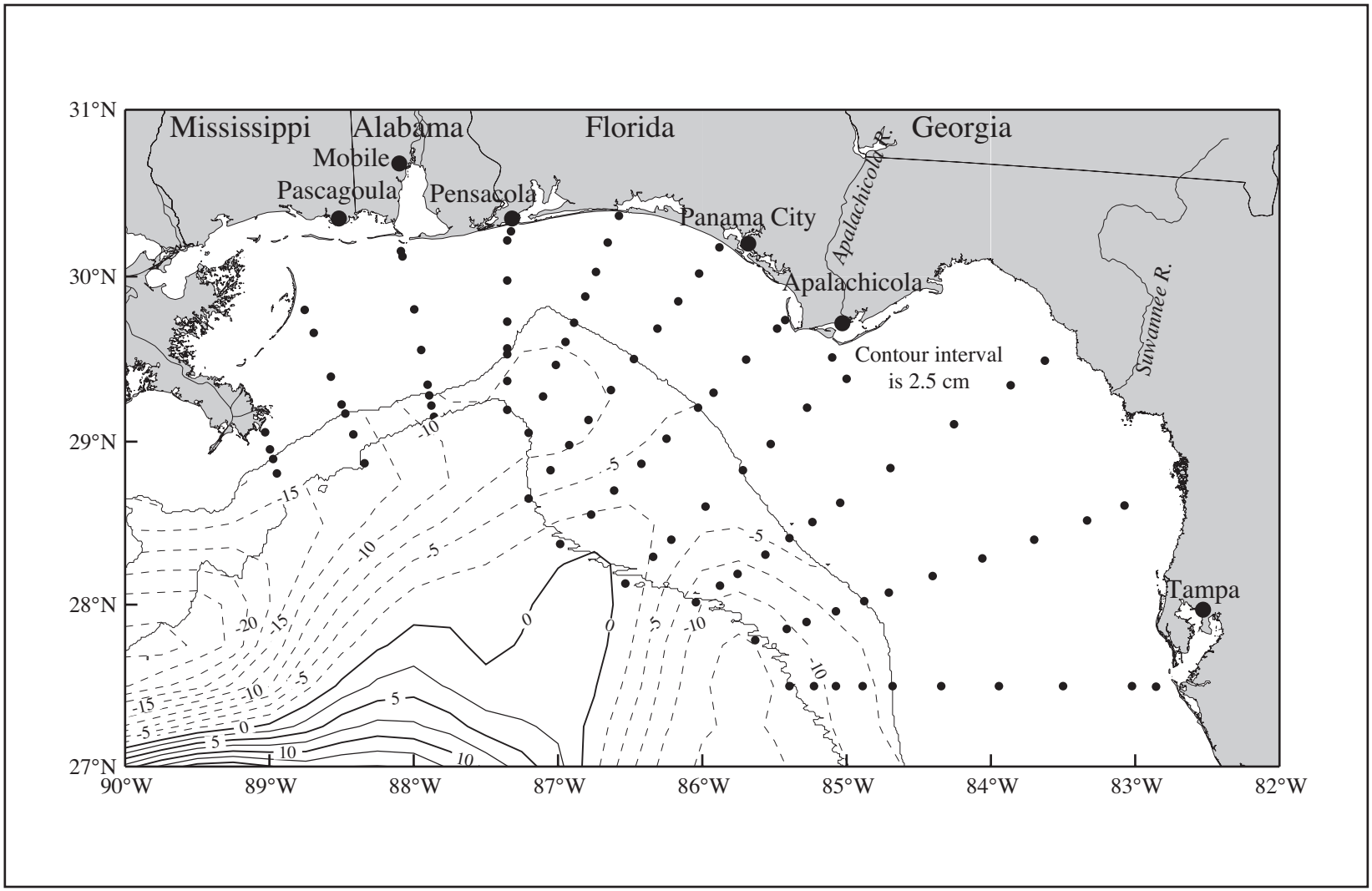

Figure G.1.3-1. Sea surface height field from satellite altimeter data for 18 November 1999 during cruise N7 . The 200- and 1000-m isobath contours and CTD station locations (dots) are shown. [Data provided by Robert R. Leben, University of Colorado]

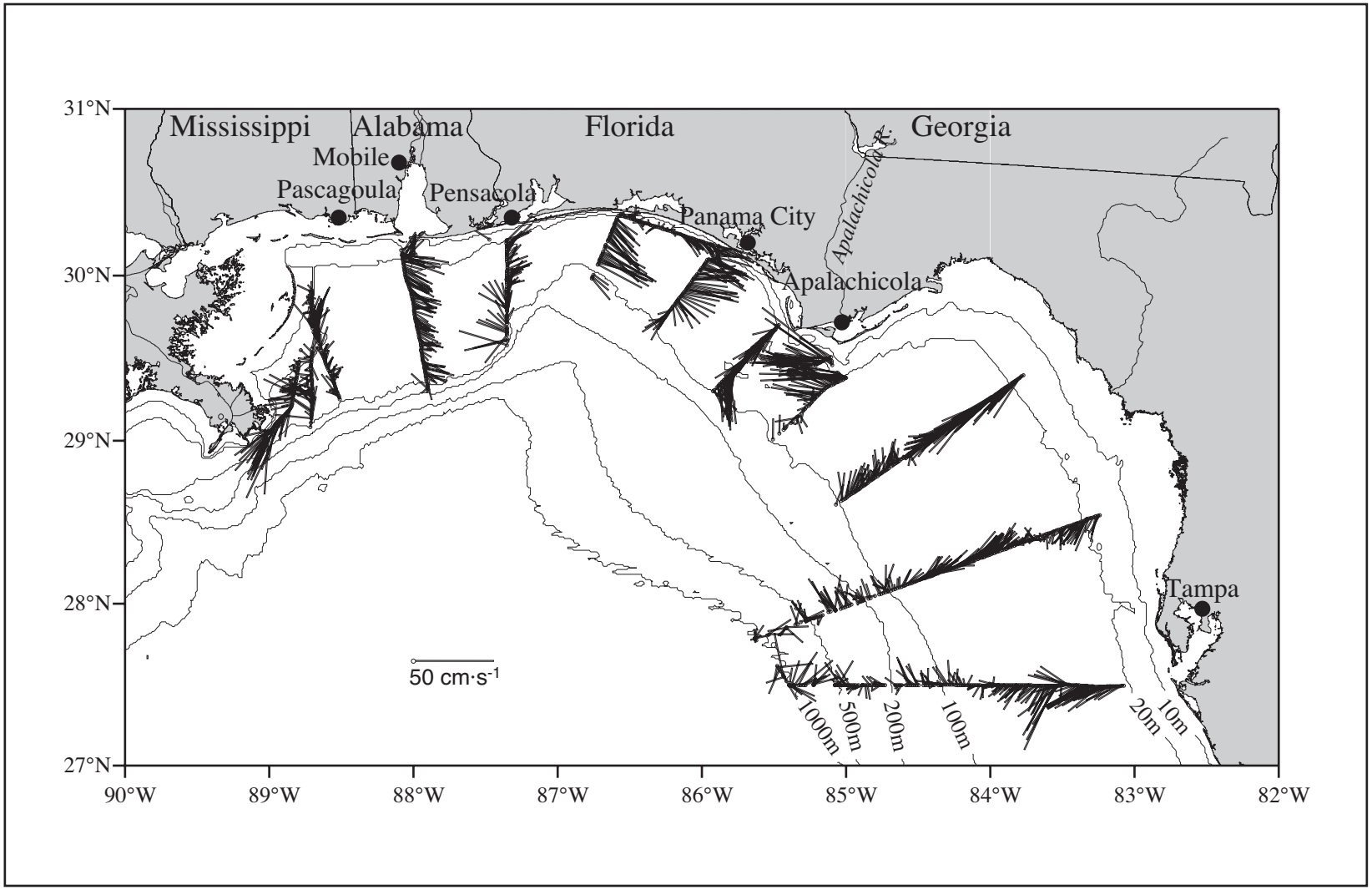

Figure G.2-1. ADCP-measured currents for the 4-m bin centered at 12 m or 14 m on cruise N7 in November 1999.

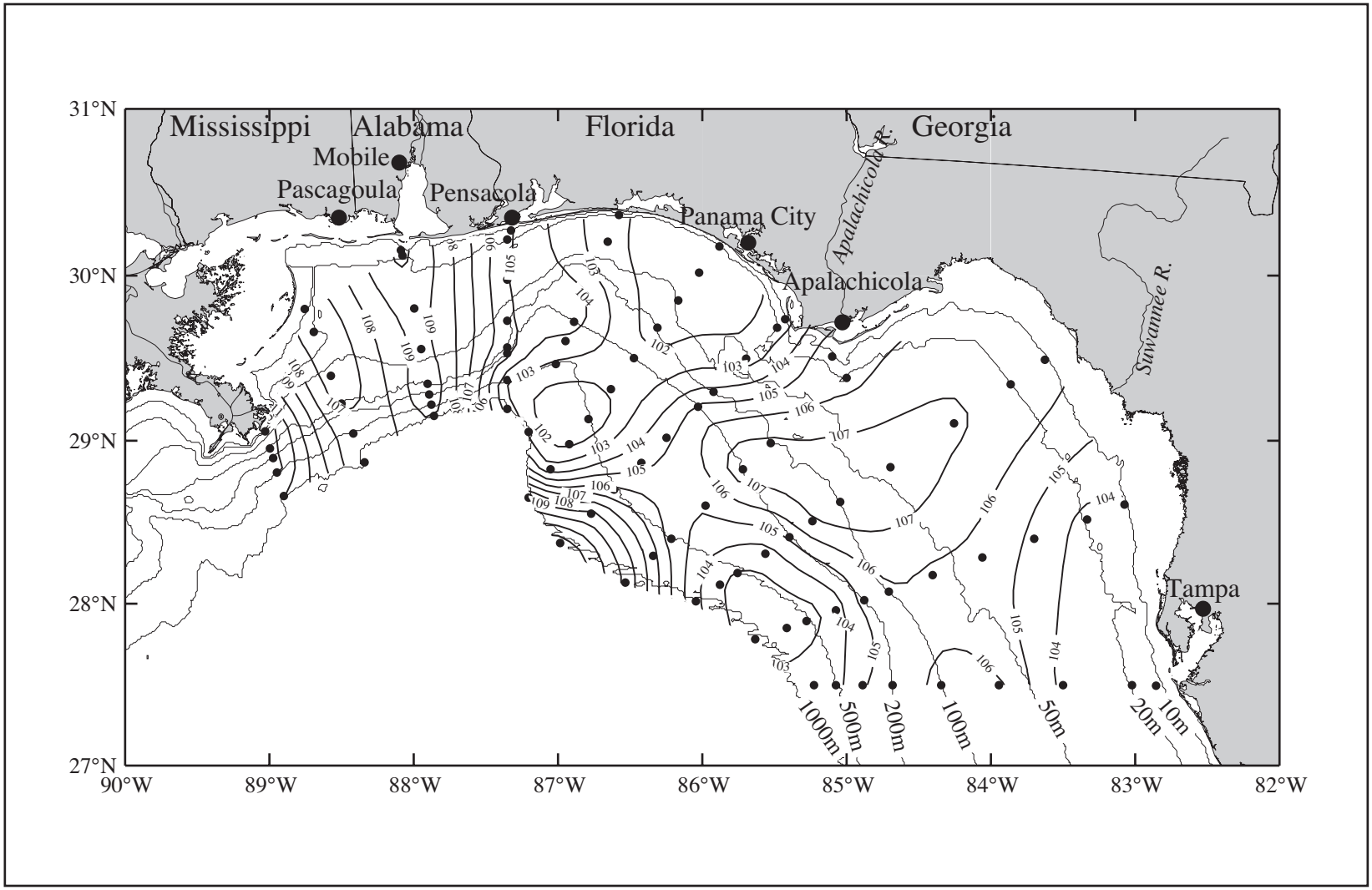

Figure G.2-2. Geopotential anomaly (dyn cm; 3 m relative to 800 m) for cruise N7 conducted 13-25 November 1999. CTD station locations are shown.

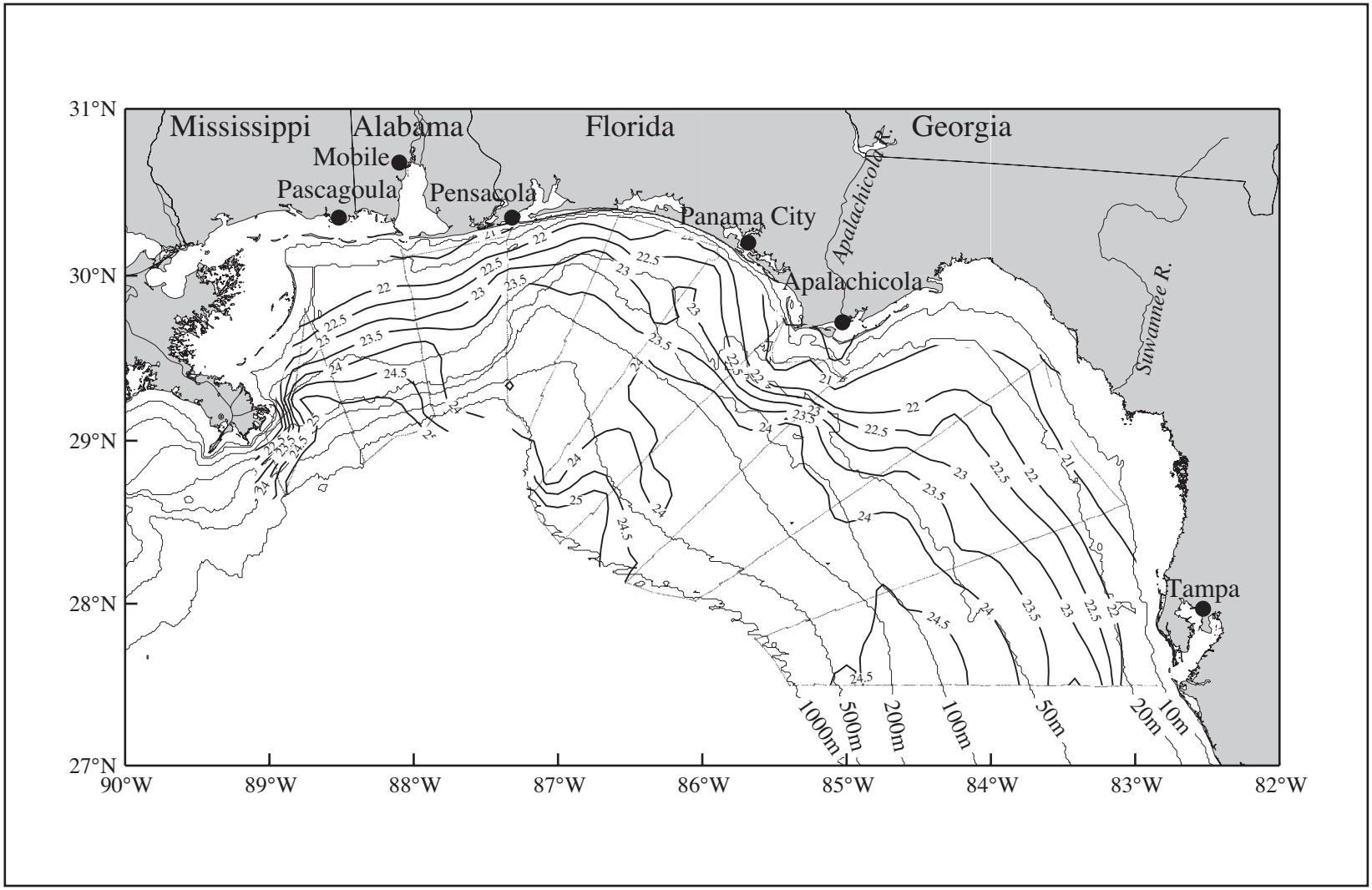

Figure G.3-1. Temperature (°C) at ~3 m from thermosalinograph observations on cruise N7 in November 1999.

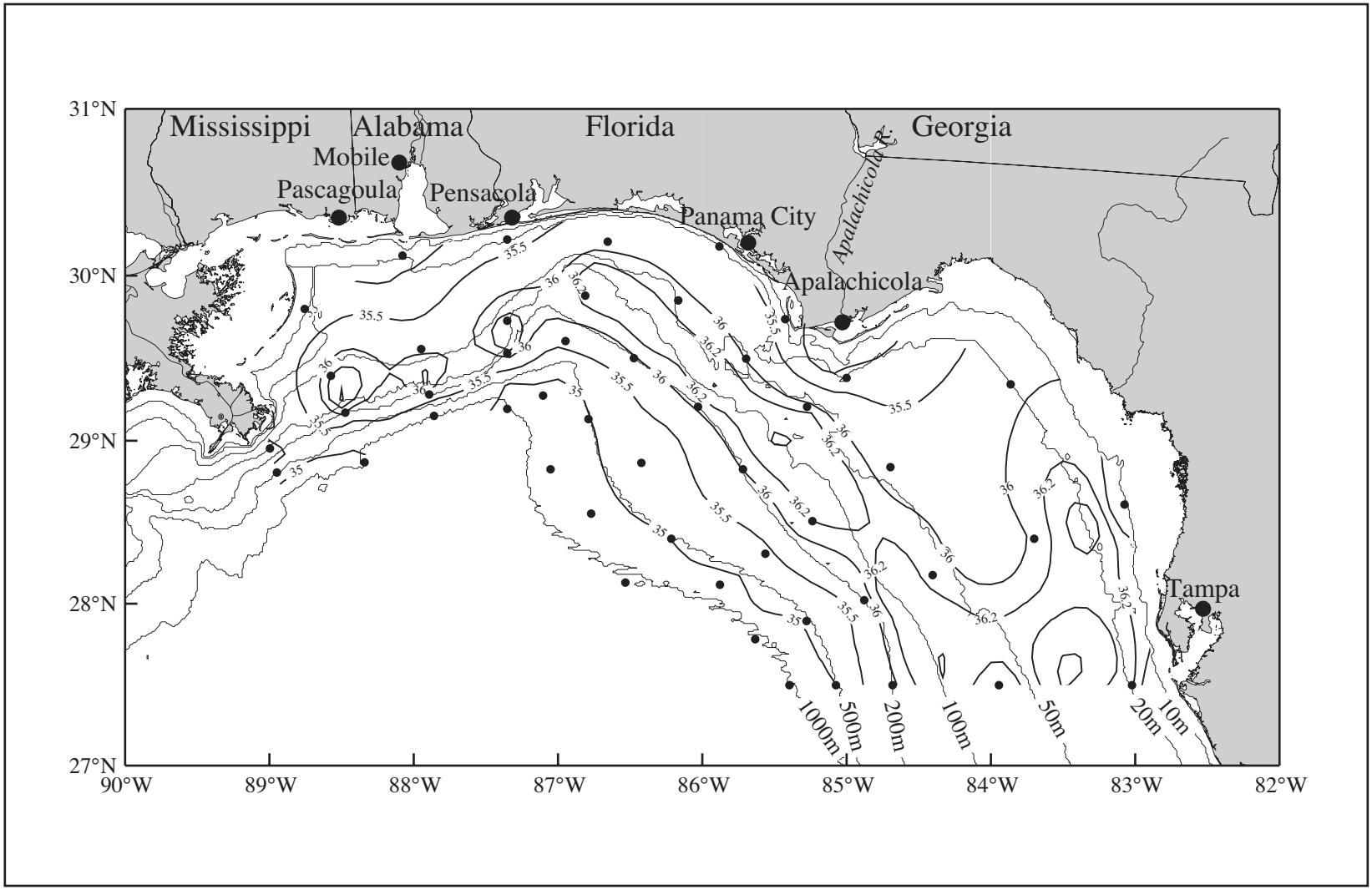

Figure G.3-2. Salinity from near-bottom observations on cruise N7 in November 1999.

indication of relatively warm bottom temperatures in the middle inner-shelves between 10 and 50 m depth which reflects the typical pattern of fall cooling and mixing.

Examination of vertical sections of potential temperature, salinity, density, nutrient, and oxygen concentrations, both cross-shelf and along the 100-, 200-, 500-, and 1000-m isobaths confirms that the upper 60 to 80 m of the water column was well-mixed.

Figure G.3-3 shows the vertical structure of potential temperature at stations along the 1000-m isobath. This illustrates the deep surface mixed layer. An oscillation in isotherms below the mixed layer is also seen with positive (upward) displacements at lines 2, 5, and 9 at 300 m depth. In the west (lines 7-9), this oscillation is due to the influence of the warm tongue of LCE water impinging upon the slope at the ends of lines 7 and 8. This is seen as a depression of the isotherms below the mixed layer and a relatively warm mixed layer as warm oceanic water is advected onto the cooler slope (at stations 47 and 48). In the west, the offshore cyclone south of Mississippi Canyon also serves to bring oceanic waters onto the slope. However, the cyclone serves to lift the isotherms below the mixed-layer at line 2 (station 12 in Figure G.3-3), while at the surface the mixed-layer temperatures are relatively warm. In DeSoto Canyon, the doming of the isotherms near the ends of lines 4, 5, and 6 (stations 28, 29, and 47) is due to the presence of a small diameter (~50 km) cyclone centered at 87°W, 29°N (Figure G.2-2).

The presence of these same features also is seen in the nutrient concentrations below the depleted mixed-layer depth as seen in the 28 μM isopleth of nitrate concentration (Figure G.3-4). These features can be traced with diminished effect to the 500-m isobath, particularly the small (50 km) cyclone over the base of DeSoto Canyon at lines 5 and 6. The cooler temperatures of the mixed layer at a given water depth across the DeSoto Canyon can be traced to the coast near Panama City and suggest the canyon as a region with enhanced cross-shelf exchange.

Figure G.3-5 shows nitrate and silicate concentration profiles along lines 1 and 2. Peak surface concentrations are at line 1 and are greater than 9 μM (silicate) and 1 μM (nitrate). These values are much smaller than the 23 μM (silicate) and 20 μM (nitrate) measured at line 1 during the November 1998 cruise (N4) and are indicative of much less Mississippi River plume penetration to the east. As in the prior November cruise, there is almost no expression of the plume at line 2.

Figure G.3-6 shows the nitrate concentration (left panel) and temperature (right panel) profiles along the 100-m isobath during cruise N7. Of note is the increased nitrate concentration between 50 m and the bottom in the region corresponding to DeSoto Canyon (stations 25, 35, 41, 54). This coincides with a decrease in near-bottom temperatures and indicates the upwelling of nutrient rich cool water from the DeSoto Canyon. This region was also characterized by a broad region of dynamic low (Figure G.2-2) which extends across the DeSoto Canyon from the coast near Panama City and out across the shelf and slope into deep water. The strong uplift onto the shelf appears to be near bottom on lines 1-4 and associated with the cyclone seen in Figure G.1.3-1.

The uplift is further characterized by the cross-shelf vertical profile of nitrate and temperature at line 6 in Figure G.3-7. Here, the nutrient isopleths and isotherms can be seen rising toward shore inshore of station 41. The opposite case exists on the west Florida shelf, where a high in geopotential anomaly dominates (Figure G.2-2) much of the shelf and shelf-edge along lines 8, 9, and 10. Below the mixed layer, the nutrient isopleths and isotherms are depressed at stations 61, 73, and 83 (Figure G.3-6). The cross-shelf sections on line 9 of

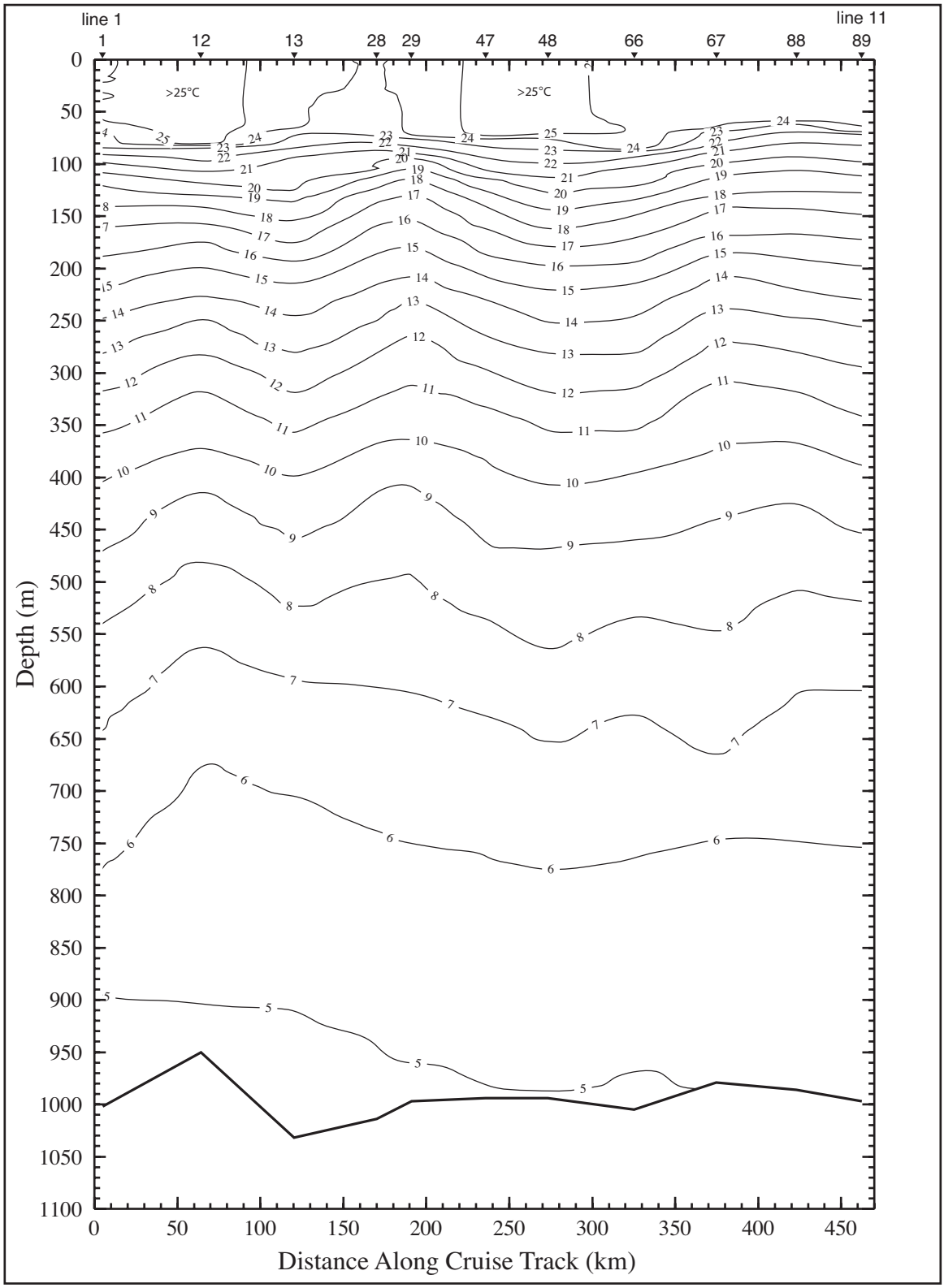

Figure G.3-3. Potential temperature (°C) along the 1000-m isobath on cruise N7 in November 1999. Stations are shown on the top axis.

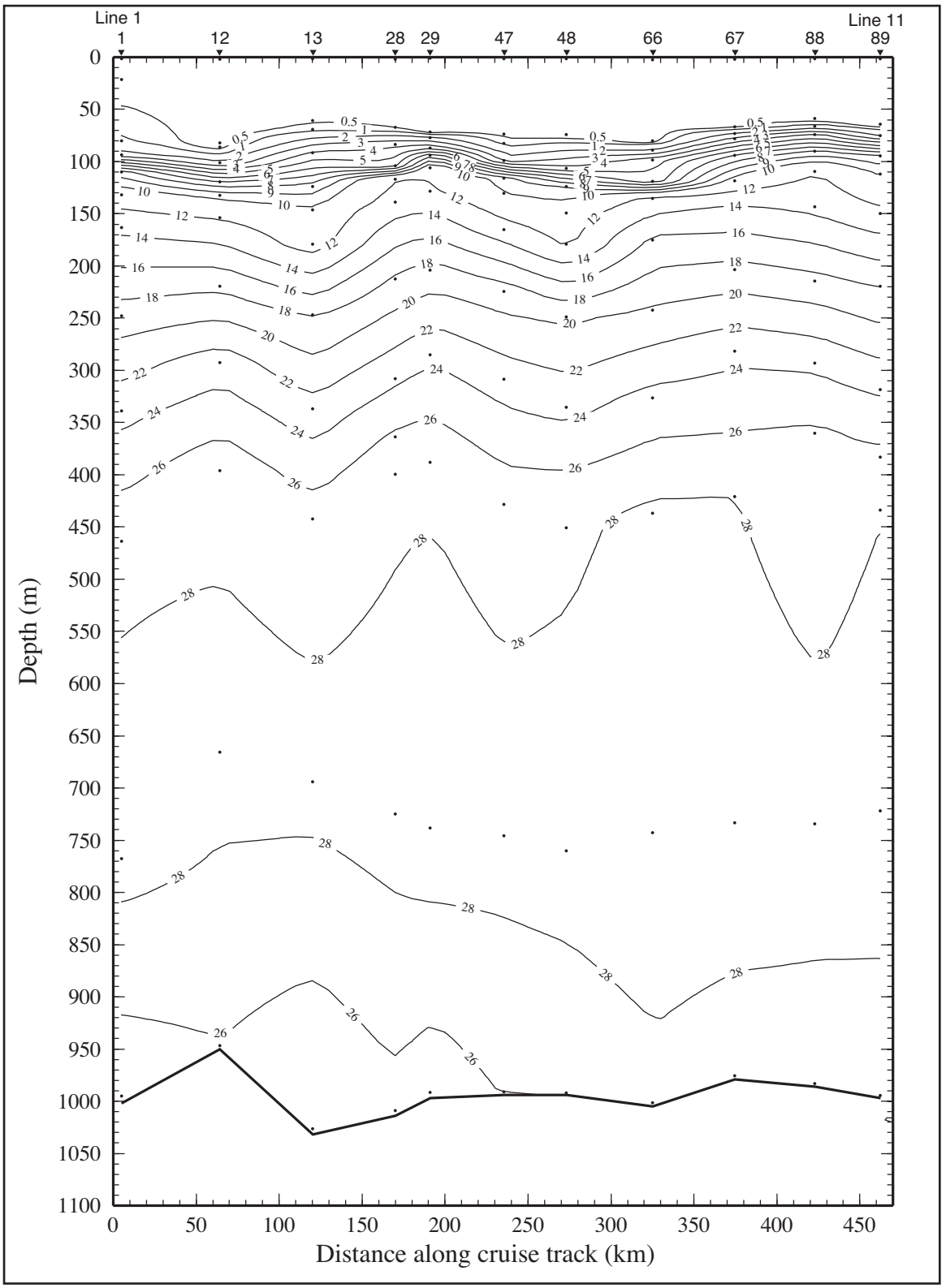

Figure G.3-4. Nitrate (μM) along the 1000-m isobath on cruise N7 in November 1999. Stations are shown along the top axis.

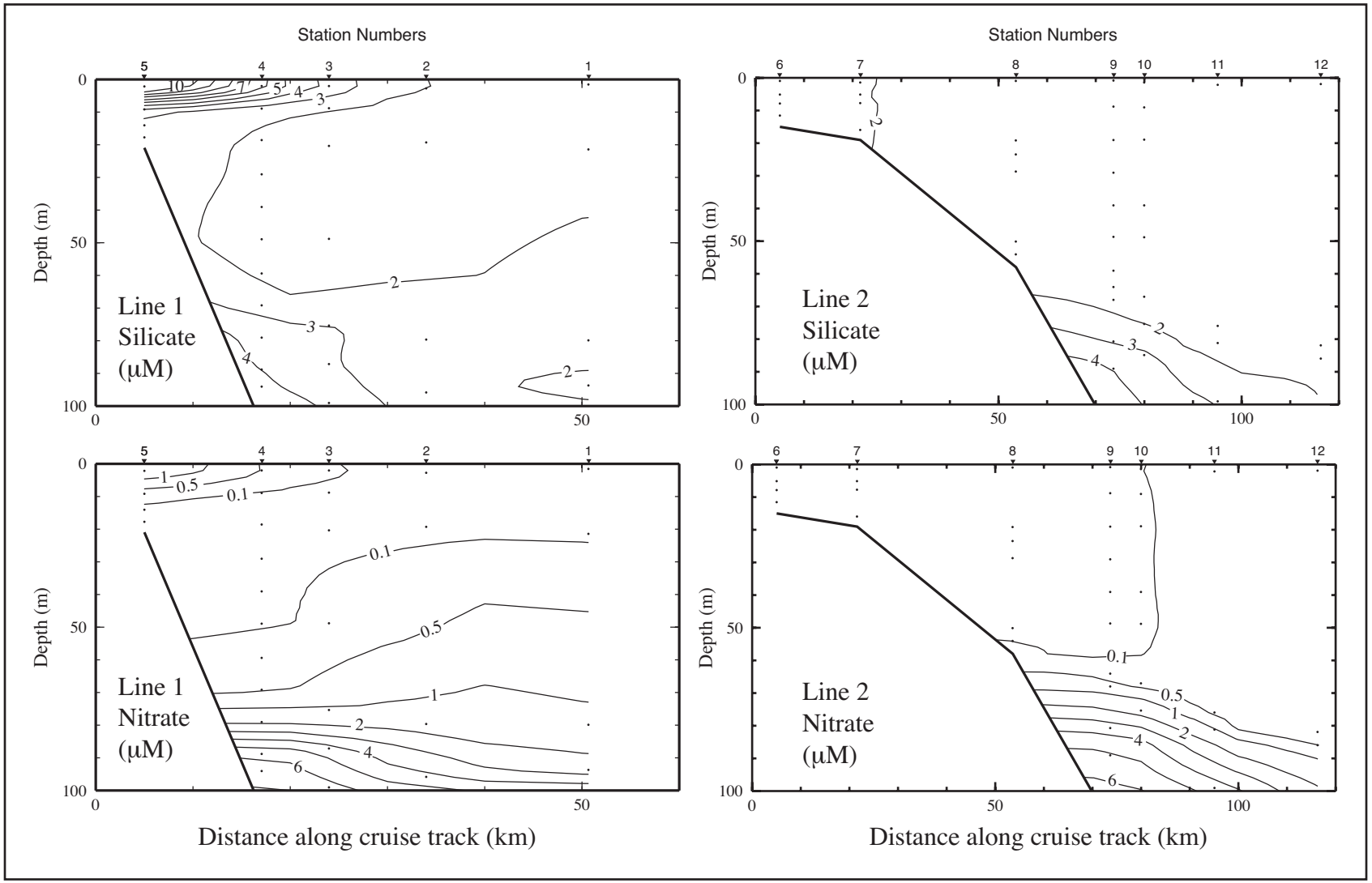

Figure G.3-5. Silicate and nitrate on lines 1 and 2 on cruise N7 in November 1999.

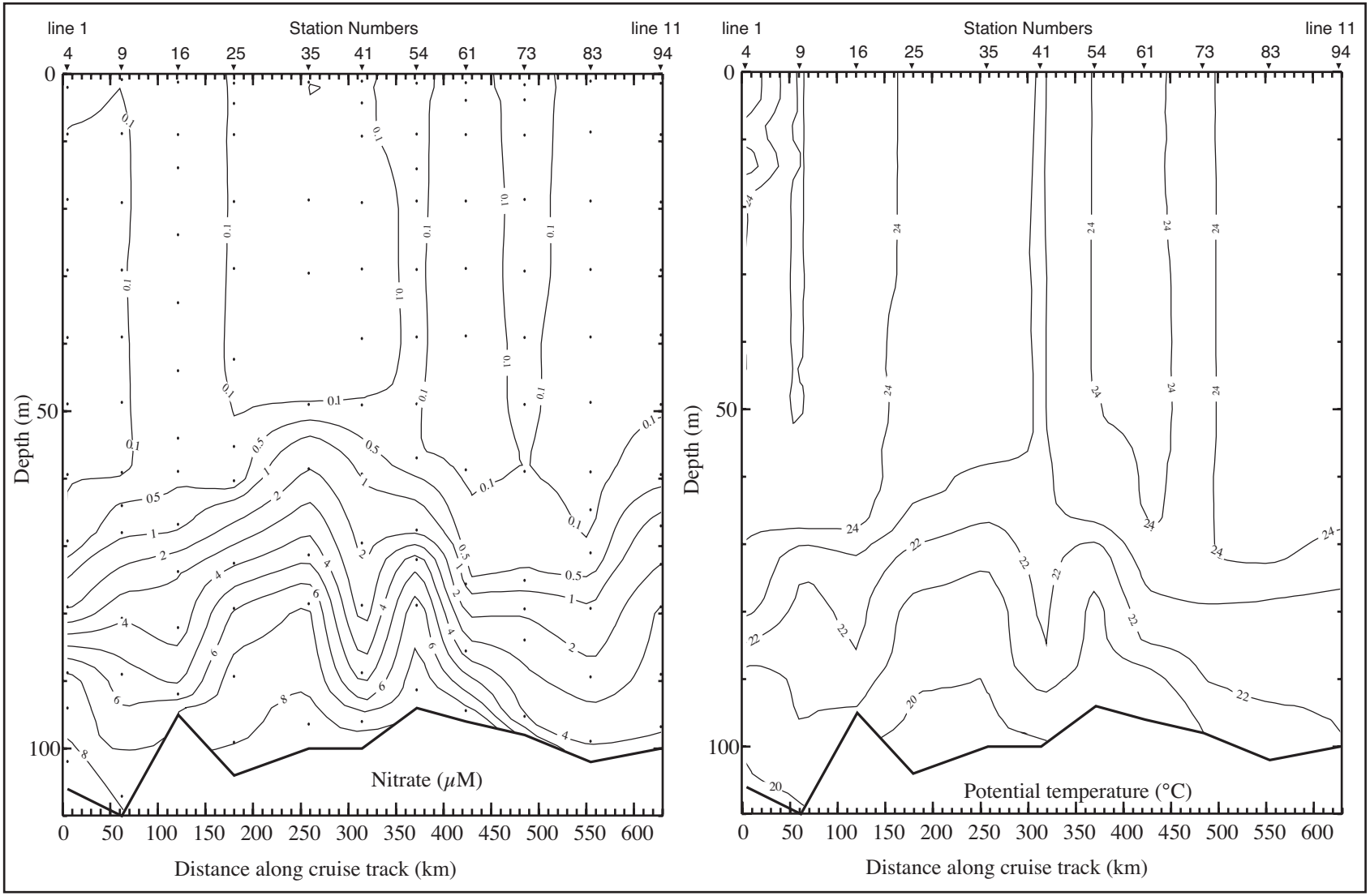

Figure G.3-6. Nitrate and potential temperature along the 100-m isobath on cruise N7 in November 1999.

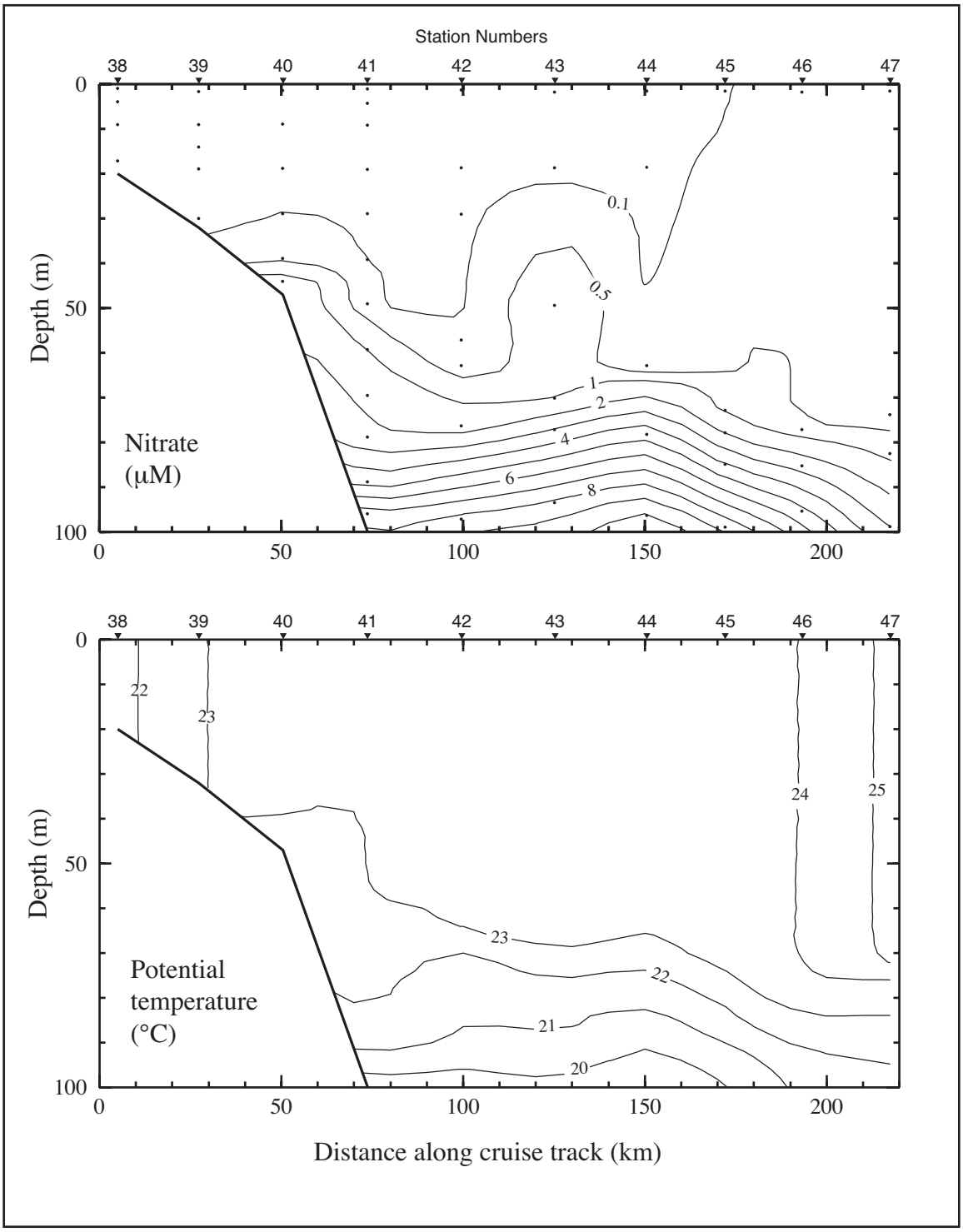

Figure G.3-7. Nitrate and potential temperature along line 6 on cruise N7 in November 1999.

nitrate concentration and temperature (Figure G.3-8) further illustrates the downwelling, as the isopleths and isotherms slope downward toward shore beneath the mixed layer and offshore of station 74.

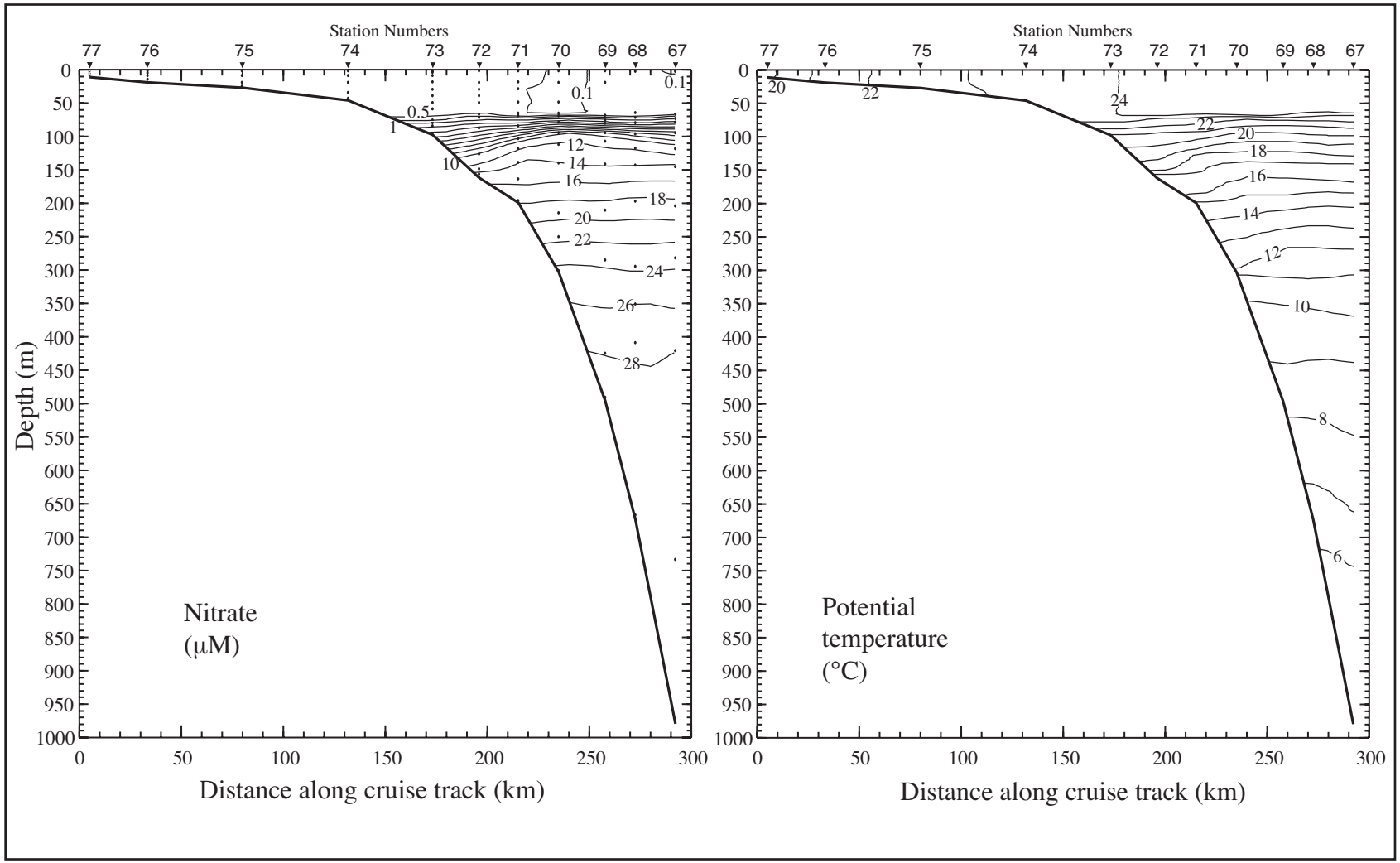

Figure G.3-8. Nitrate and potential temperature along line 9 on cruise N7 in November 1999.

APPENDIX H
SUMMARY OF CONDITIONS DURING CRUISE N8

Cruise N8 was a spring cruise conducted 15-26 April 2000. The cruise began with a hydrographic station taken on the inshore side of line 11 near Tampa. Stations then continued in sequence along each line working to the west. Line 2 was extended into deeper water to better resolve an area of low SSH present during this cruise. Figure H-1 shows the station locations and gives the CTD station numbers, which are sequential by sampling order.

H.1 Forcing Functions

H.1.1 Winds

The mean wind field and variance ellipses during cruise N8 are shown in Figure H.1.1-1. The methodology used is that of Wang et al. (1998) applied to hourly observations at meteorological stations located as shown in the figure. Mean winds during cruise N8 were to the east and east-southeast over the NEGOM region and highly variable. Three cold fronts passed through the region during this cruise. All three fronts produced winds in excess of 10 $m \cdot s^{-1}$ over much of the region (e.g., Figure H.1.1-2). Mean winds speed were light over the Mississippi-Alabama shelf and on the order of 1 $m \cdot s^{-1}$. Over the west Florida shelf, mean winds were stronger at 3-4 $m \cdot s^{-1}$. Variance ellipses were large and elliptical over the Mississippi-Alabama shelf with semi-major axes oriented northwest-southeast and with amplitudes of about 30-40 $m^2 \cdot s^{-2}$. Variance ellipses over the west Florida shelf were smaller, being 20-30 $m^2 \cdot s^{-2}$, and more circular.

H.1.2 River Discharge

The year 2000 was generally a low year for discharge of river water into the NEGOM region. Daily Mississippi River discharge rates were less than the 70-yr record-length mean for January through April 2000. Rivers west of line 4 exceeded their mean daily discharge values during early April. Those associated with Mobile Bay also had one to two short pulses of discharge exceeding the mean. Rivers discharging to the Mississippi-Alabama shelf were well below their mean values during January through April 2000. For January through April 2000, rivers east of line 4 were generally well under (order of one standard deviation) their daily mean discharge for the same period.

The effects of the river discharge on the near-surface (~3 m) salinity distribution is most clearly seen in the western areas of the study region and somewhat evident in the vicinity of Cape San Blas and Apalachicola Bay (Figure H.1.2-1). In the west, a triangle of relatively low salinity (< 35.5) water is seen extending from the Mississippi River delta to east of Pensacola. This low salinity region is mostly due to the influx of relatively fresh water from Mobile Bay and the estuarine areas south of Pascagoula and east of the Chandeleur Islands. The flow over the slope south of the delta was westward transporting Mississippi River water to the west.

The river water effects also can be seen in the distribution of chlorophyll *a* (Figure H.1.2-2). High concentrations are seen near the coast with highest concentrations near the mouth of Mobile Bay and Apalachicola Bay.

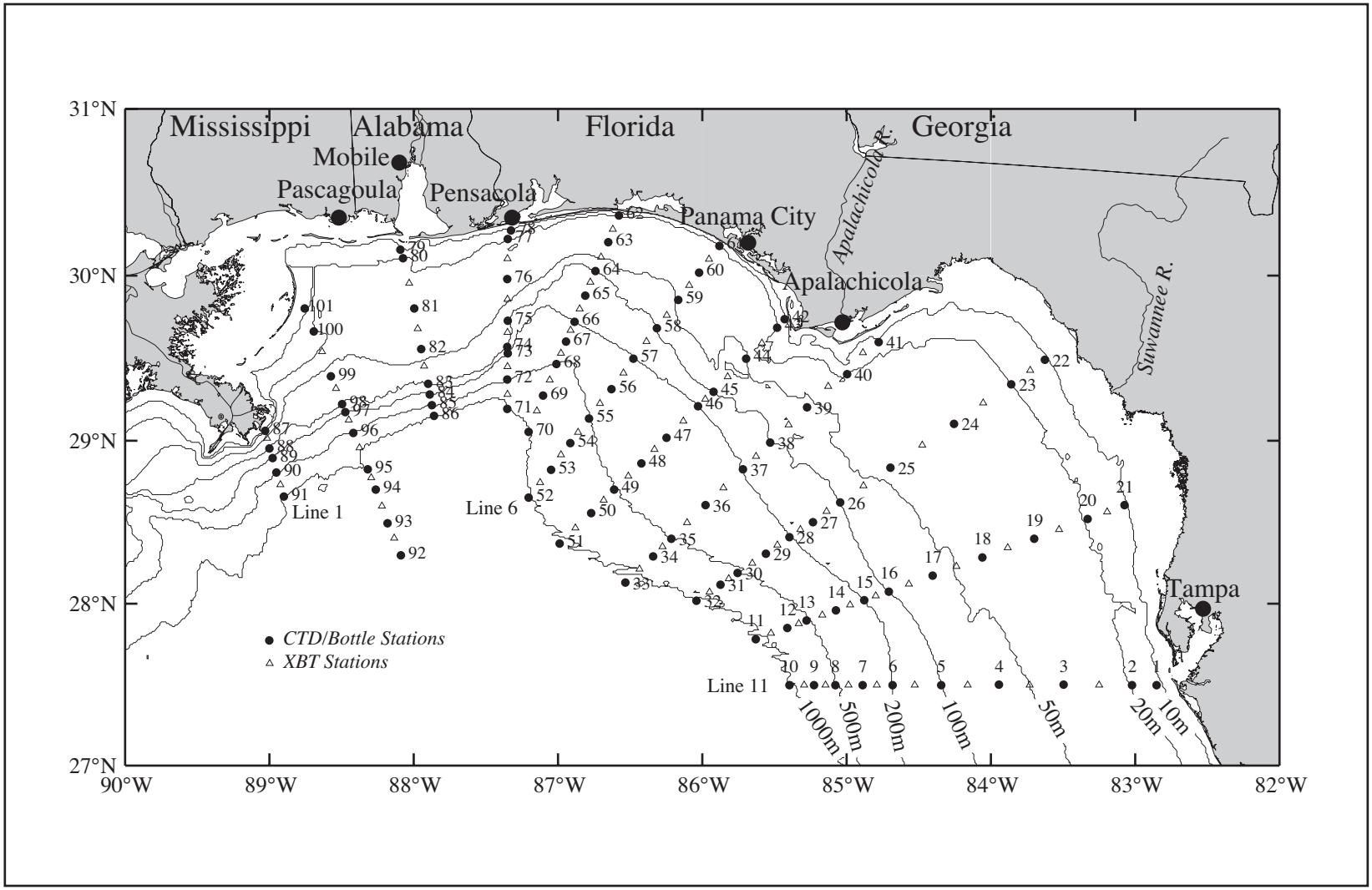

Figure H-1. Station locations for cruise N8 conducted 15-26 April 2000. CTD stations (solid circles) are numbered; XBT stations (open triangles) are not.

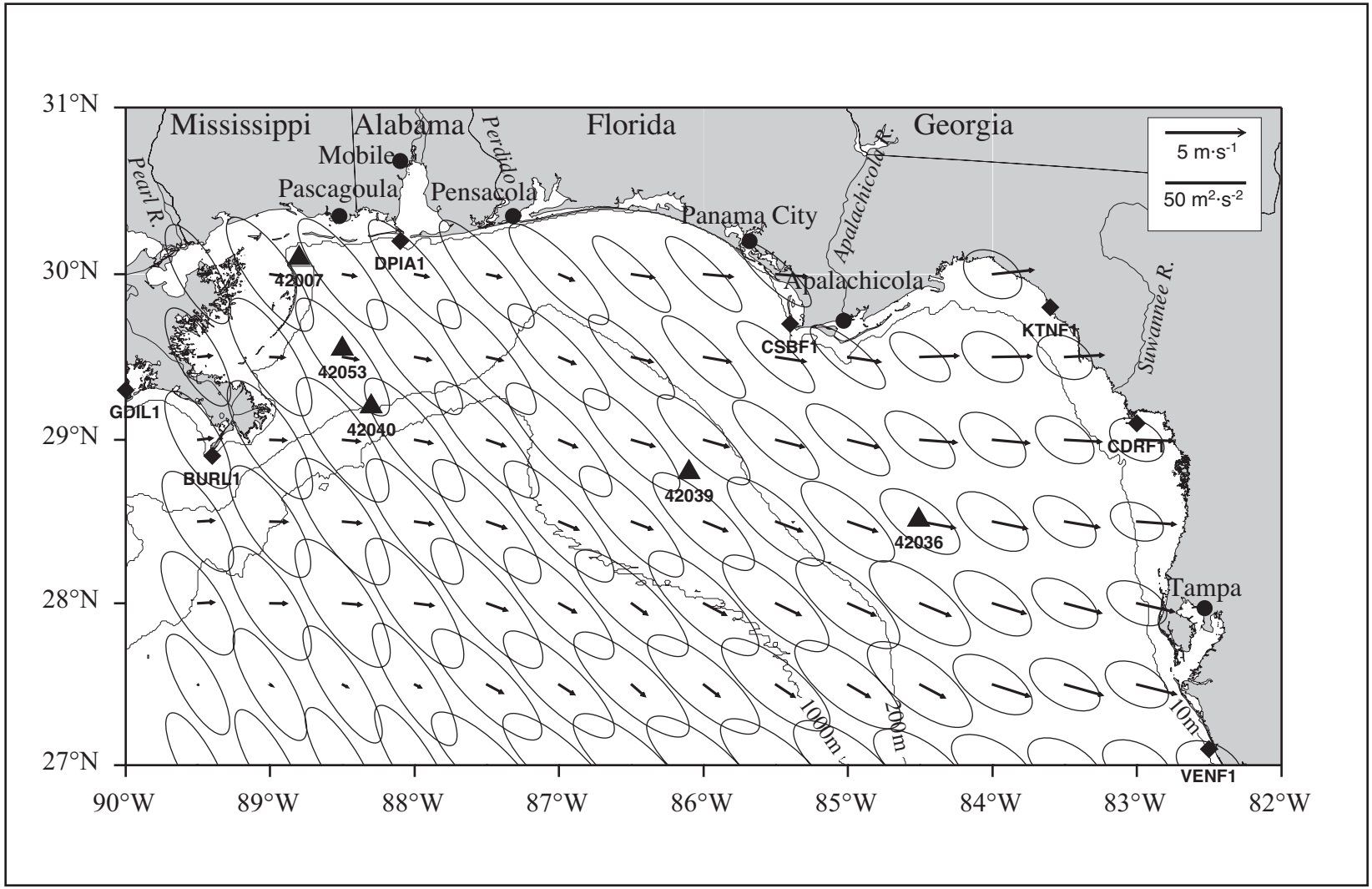

Figure H.1.1-1. Vector mean winds and variance ellipses for cruise N8 during 15-26 April 2000.

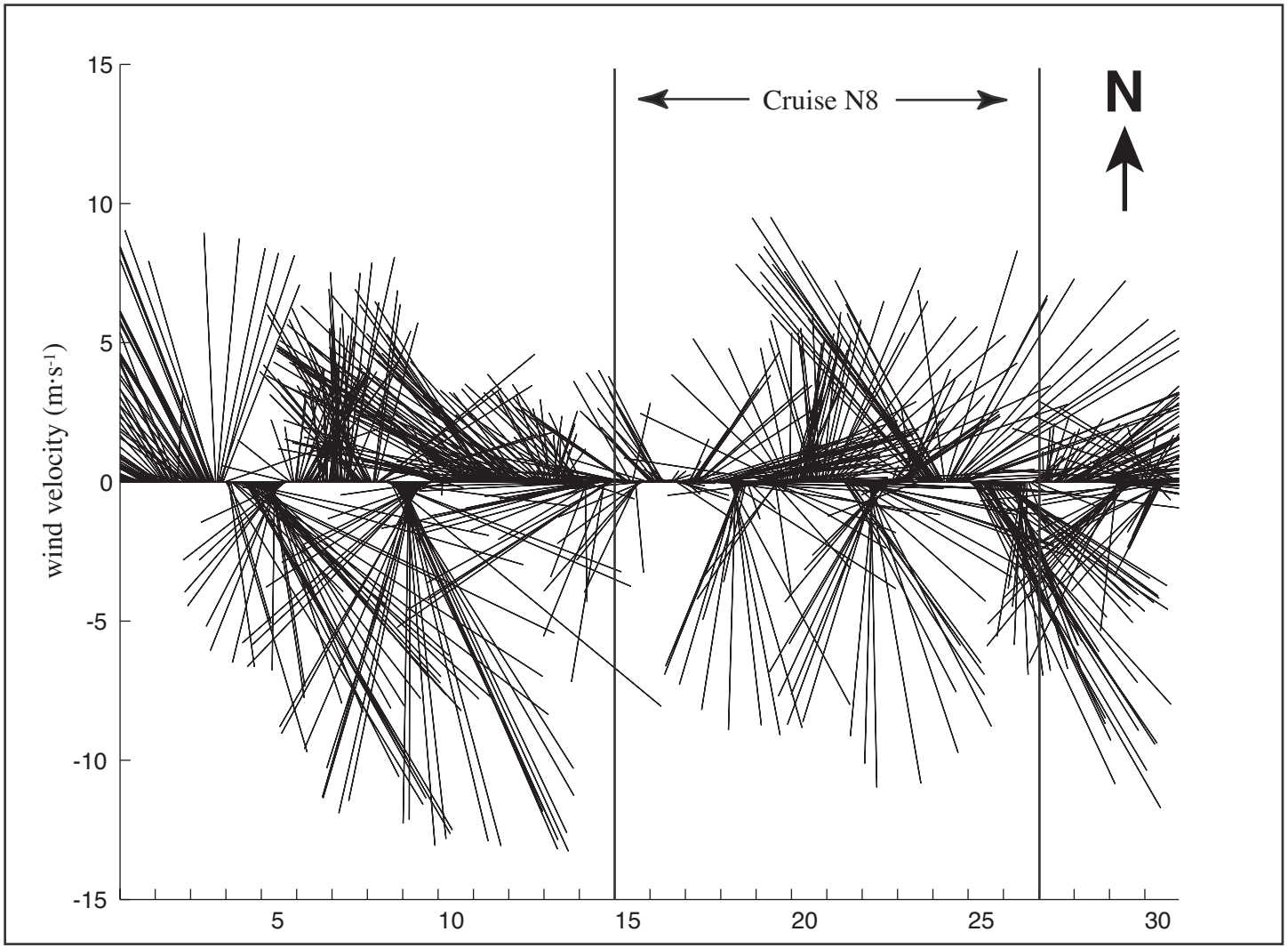

Figure H.1.1-2. Vector stick plot of wind at meteorological buoy 42040 for April 2000. Gauge height is 10 m.

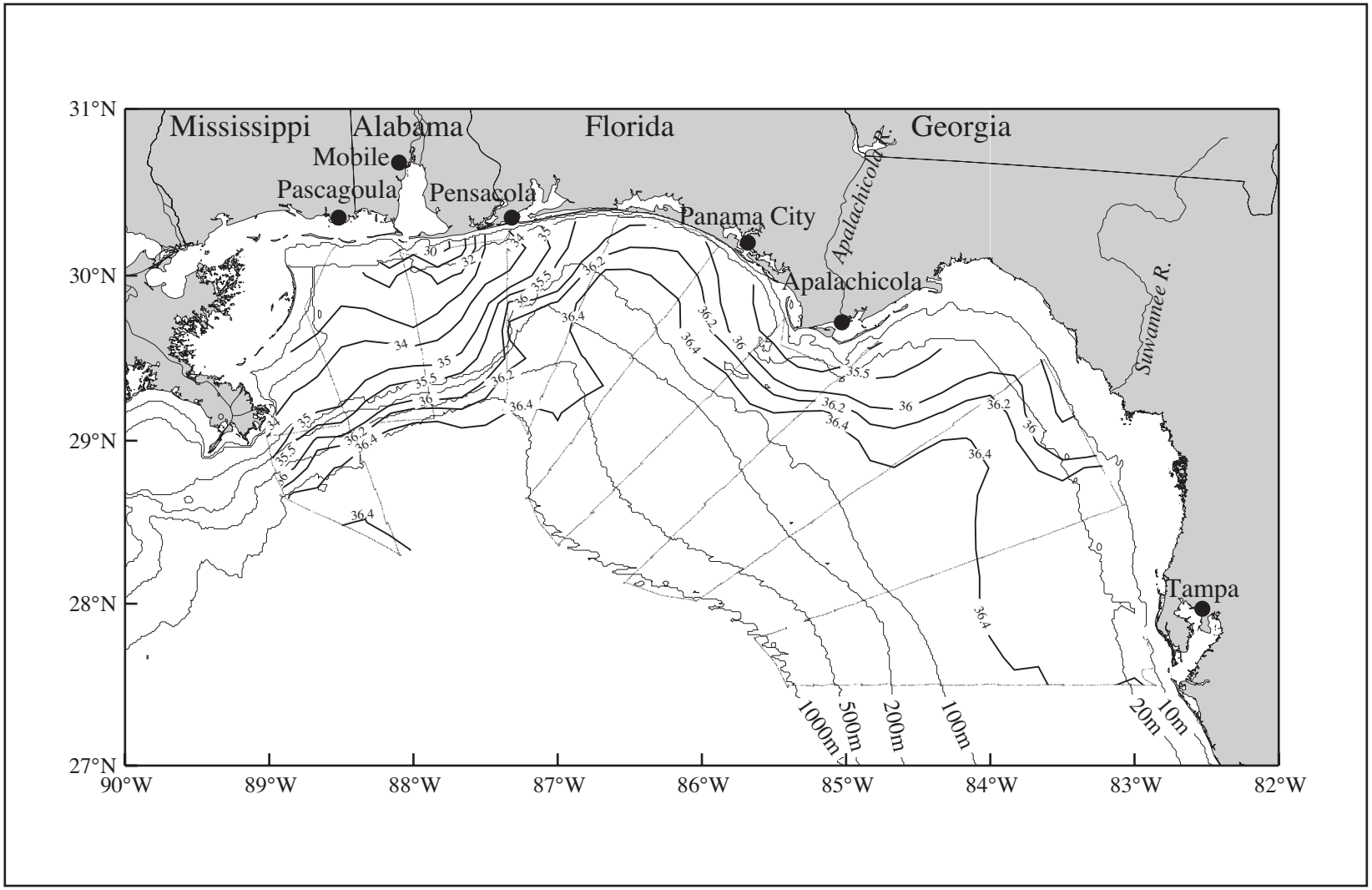

Figure H.1.2-1. Salinity at ~3 m from thermosalinograph observations on cruise N8 in April 2000.

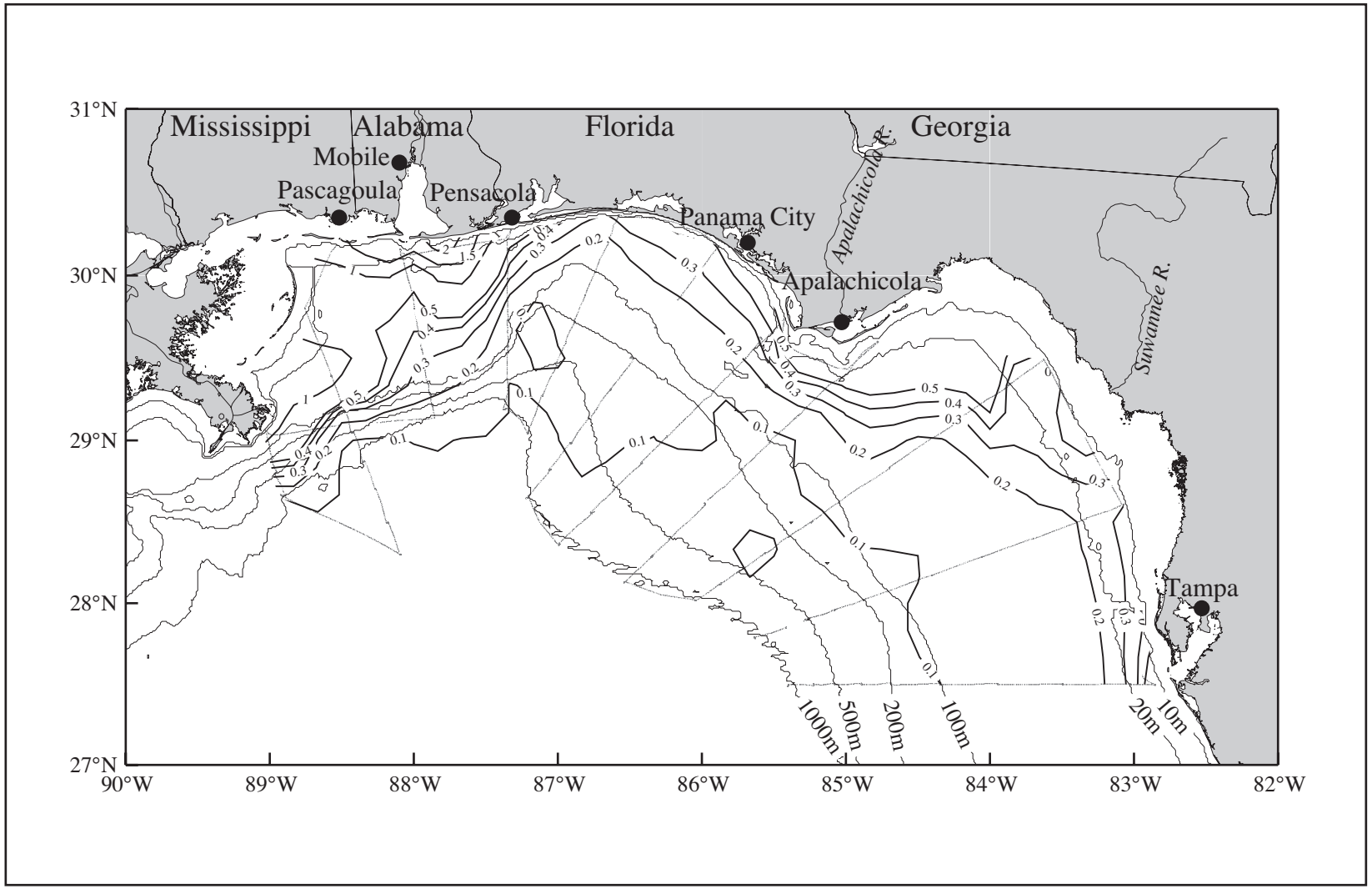

Figure H.1.2-2. Chlorophyll *a* ($\mu g \cdot L^{-1}$) at ~3 m calculated from flow-through fluorescence on cruise N8 in April 2000.

H.1.3 SSH Fields Adjacent to the Shelf

The time series of SSH fields for 15 March through 2 May 2000 is shown in Figures 3.2.3-22 and 3.2.3-23. The Loop current remained south of 27°N during March and April 2000. A region of high SSH developed southeast of the Mississippi River delta in late February and persisted through March and most of April. The high then dissipated in late April and May. A peanut shaped low oriented east-west north of the Loop Current dominated the offshore circulation during April 2000 (Figure H.1.3-1). A third lobe developed on the southeast side of the peanut (around 85°W, 27°N) , which ultimately advected anticyclonically around the Loop Current.

H.2 *In Situ* Evidence of Circulation

Figure H.2-1 shows current vectors at 12-m depth along the track of cruise N8. The currents were measured using a ship mounted 150 kHz broadband ADCP. A strong coastal current with speeds of 20-40 $cm \cdot s^{-1}$ is seen between Pensacola and Apalachicola. On the west Florida shelf, this current diminishes in magnitude after reaching line 9. This current is likely driven by the strong eastward winds seen during this cruise. The currents inshore of the 100-m isobath on the west Florida shelf were less coherent, weak, and directionally variable. Offshore currents are generally driven by mesoscale circulation features interacting with the slope. A cyclone is seen centered at 86°W, 28.3°N with a radius of roughly 50 km and speeds of 20-30 $cm \cdot s^{-1}$. This cyclone can be seen in currents measured at 100-m depth with slightly diminished speeds (Figure H.2-2). A 100-km diameter anticyclone can be seen east of the Mississippi River delta with the south limb over the slope and the rest residing over the Mississippi-Alabama shelf at lines 1 and 2. The strong westward currents offshore of lines 1 through 4 indicate the response to the northern limb of the large cyclone in that region. These westward currents are also present in the measurements at 100-m (Figure H.2-2) and 150-m (not shown). The surface (12-m) currents along the 200-m isobath and east of DeSoto canyon show considerable vertical shear (Figure H.2-1). The 100-m depth currents show consistent coherent downcoast along isobath flow while the surface currents are more variable and appear to have upcoast flow at several locations along the 200-m isobath.

Geopotential anomaly (3 m relative to 800 m) based on N8 data is shown in Figure H.2-3. Over the shelf edge and slope a series of high and low areas of geopotential anomaly are present. The high geopotential anomalies are seen on lines 2, 7, and 10; the lows are on lines 1, 6, and 9. When comparing the geopotential anomaly (Figure H.2-3) with the 12-m ADCP currents (Figure H.2-1), good agreement between the highs and lows is seen at the outer shelf. In particular, the high on line 2 and the low on line 9 are readily identified in the ADCP current vectors, as are the slightly more complex patterns over the DeSoto Canyon. Over the inner shelf, however, as seen on previous cruises, there is much less agreement. For example, there is no evidence of the coastal current seen in the ADCP currents between Choctawhatchee Bay and Apalachicola Bay. Further, many of the geopotential anomaly isopleths on the inner shelf terminate into the shore leading to unrealistic cross-shelf flow across the region.

H.3 Property Distributions

The temperature field at ~3-m depth as observed on N8 is shown in Figure H.3-1. As seen on previous cruises, there is a general increase in surface temperature with distance from shore. A tongue of cool (< 22°C) water extends across the 1000-m isobath at lines 4 and 5 as cool water is transported seaward from the coast. Some indication of this also can be seen in the salinity distribution shown in Figure H.1.2-1 (see the 36.4 isohaline).

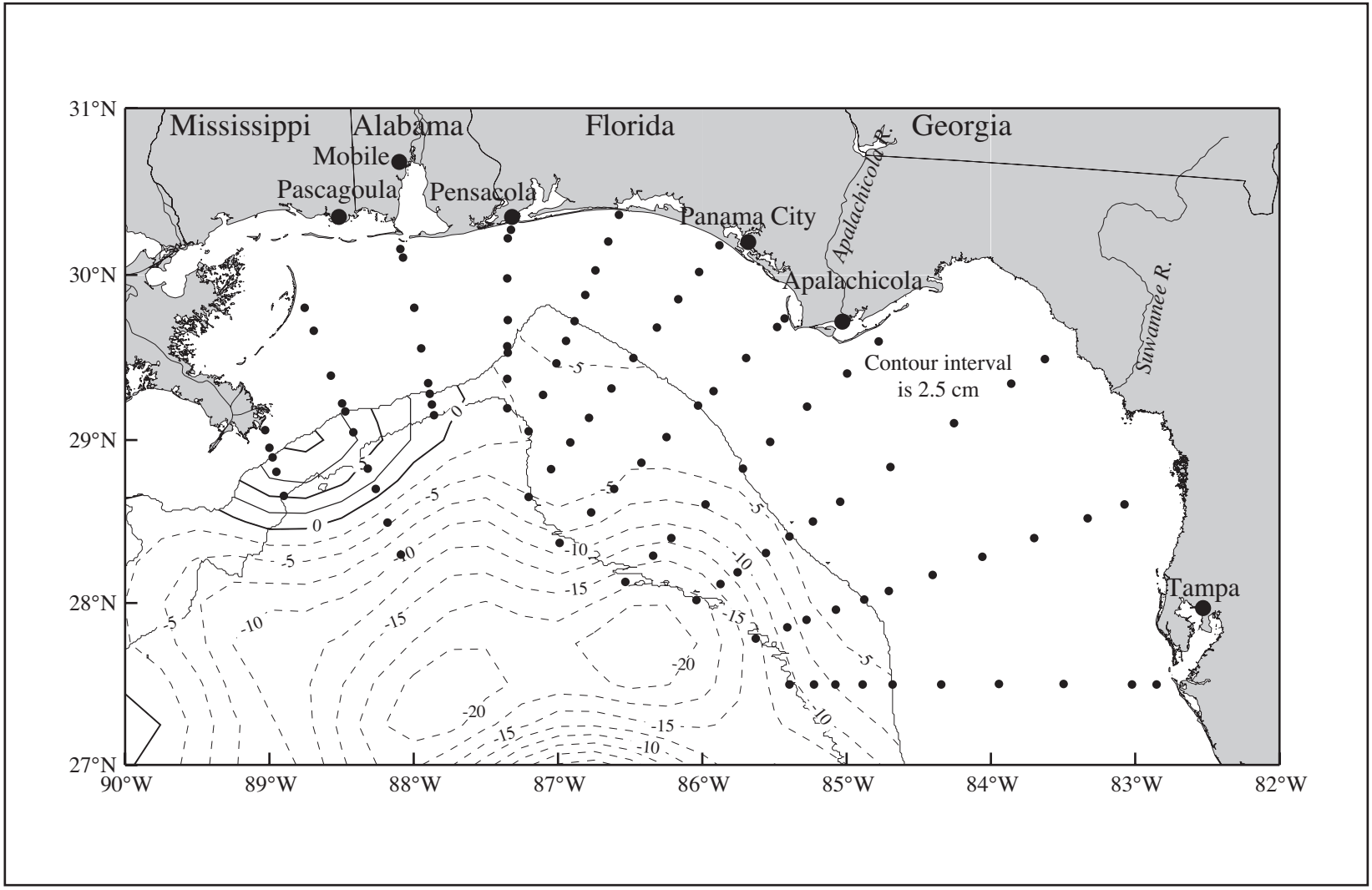

Figure H.1.3-1. Sea surface height field from satellite altimeter data for 20 April 2000 during cruise N8. The 200- and 1000-m isobath contours and CTD stations (dots) are shown. [Data provided by Robert R. Leben, University of Colorado]

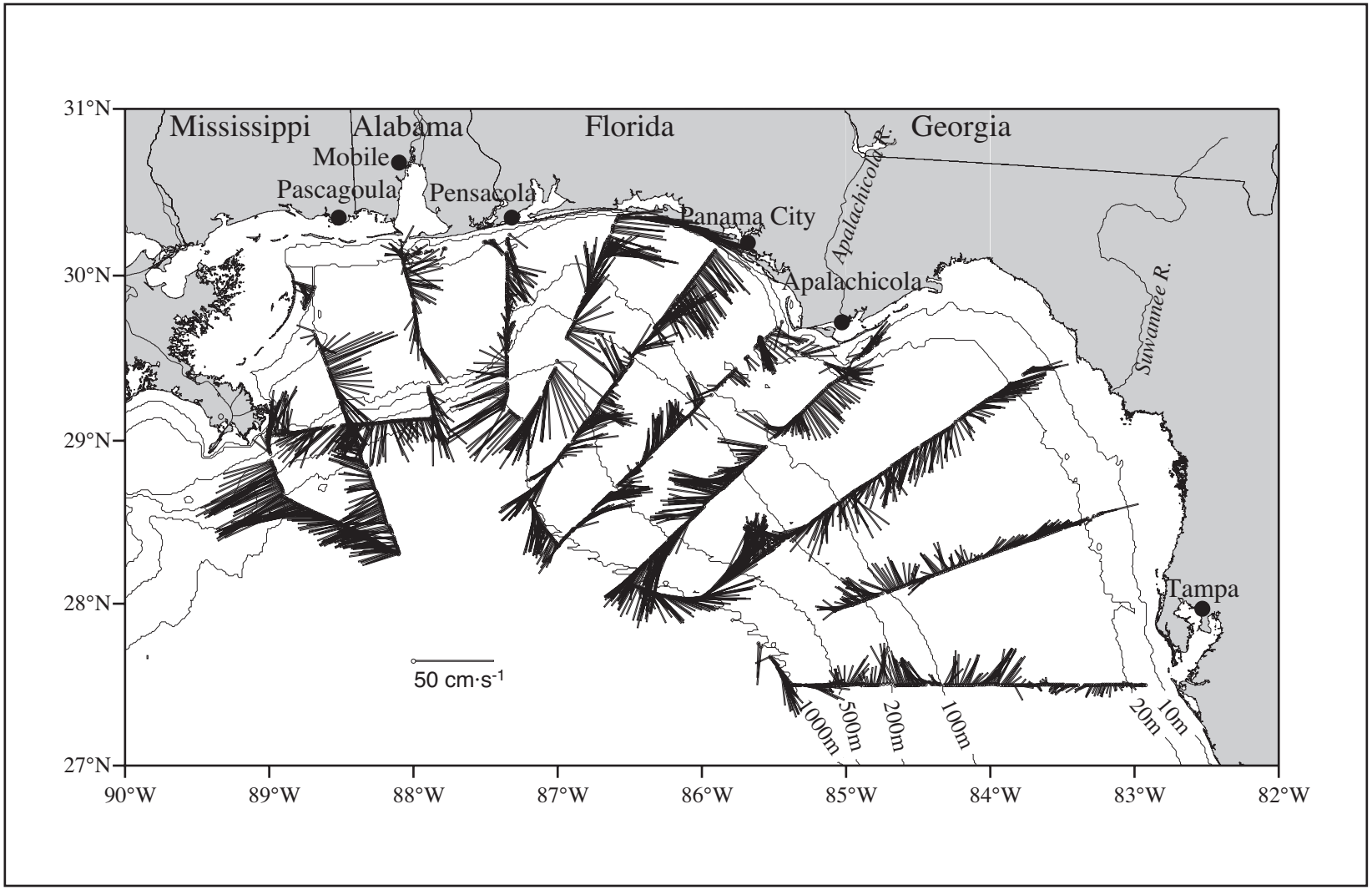

Figure H.2-1. ADCP-measured currents for the 4-m bin centered at 12 m on cruise N8 in April 2000.

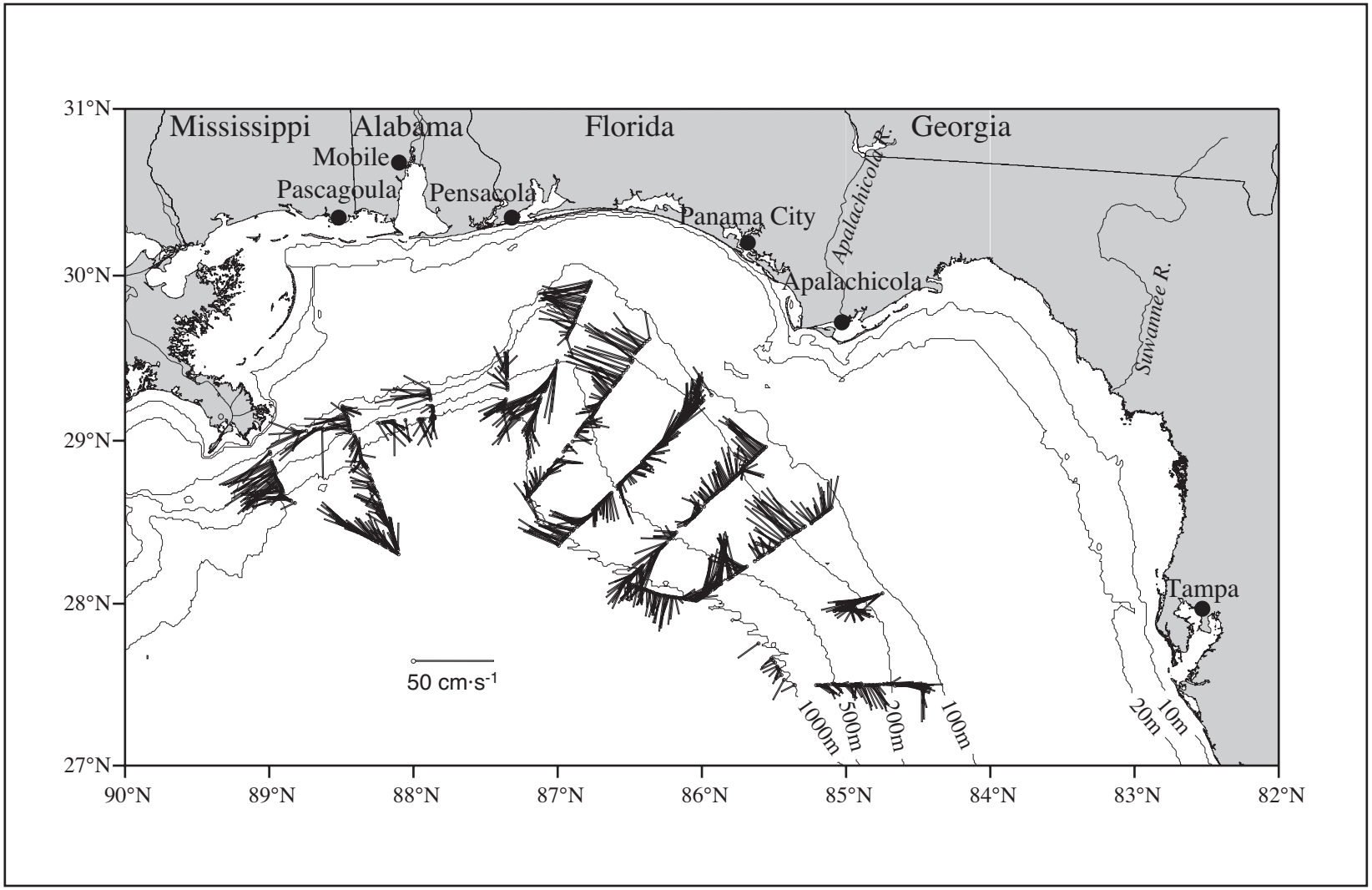

Figure H.2-2. ADCP-measured currents for the 4-m bin centered at 100 m on cruise N8 in April 2000.

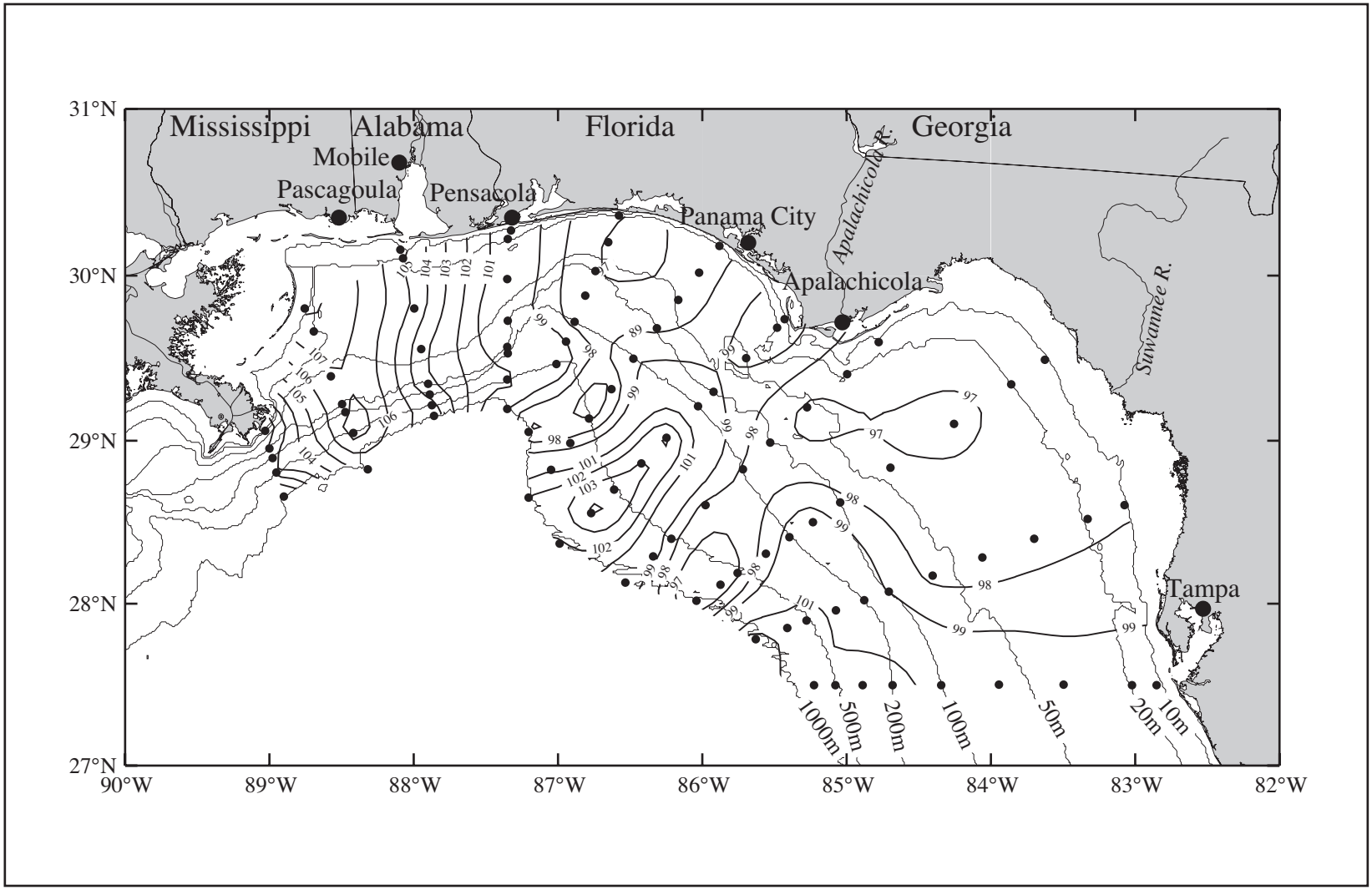

Figure H.2-3. Geopotential anomaly (dyn cm; 3 m relative to 800 m) for cruise N8 conducted 15-26 April 2000. CTD station locations are shown.

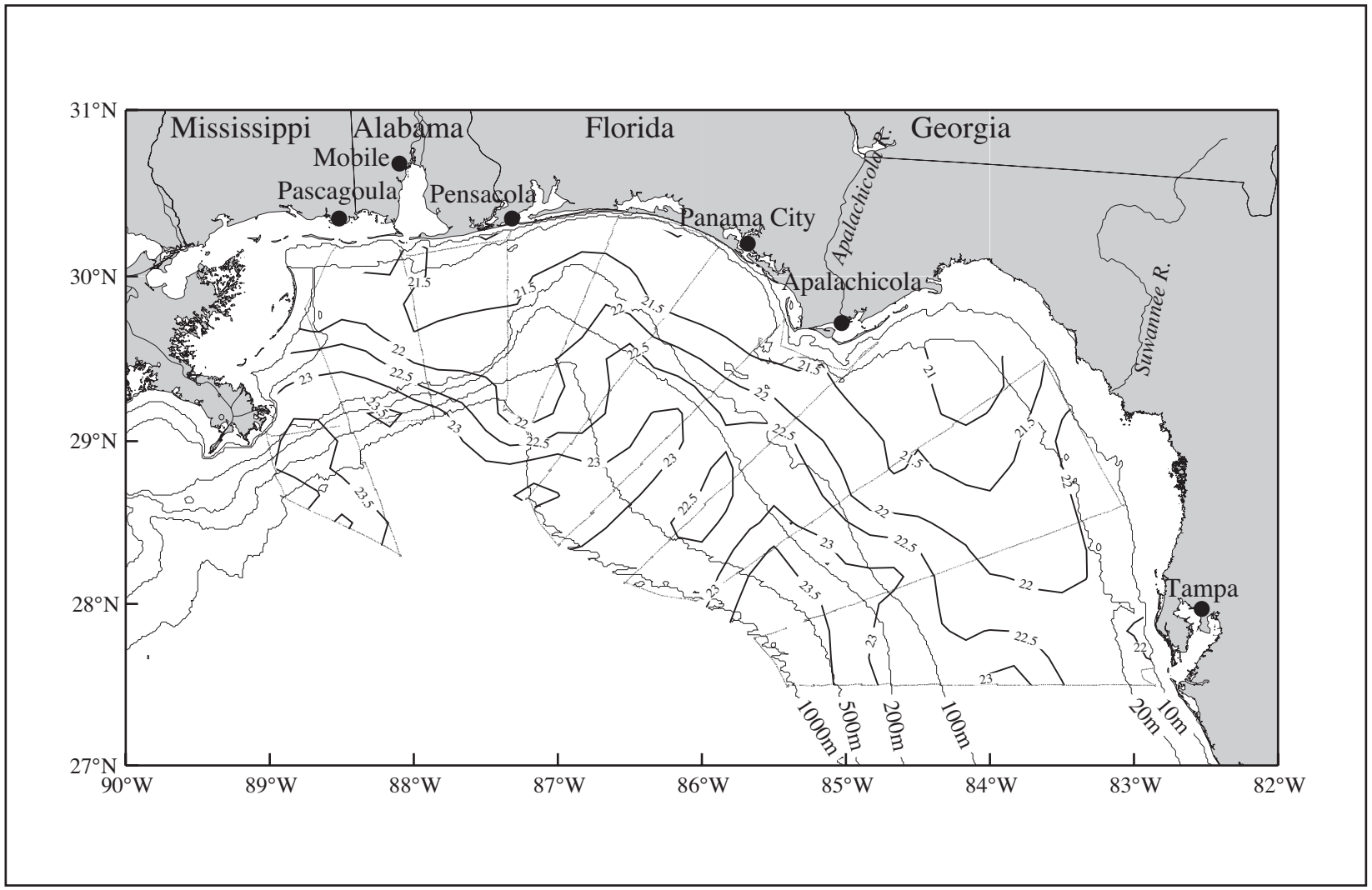

Figure H.3-1. Temperature (°C) at ~3 m from thermosalinograph observations on cruise N8 in April 2000.

Two regions of warm oceanic water being advected onto the slope and shelf are seen. The first region, in the west is strongest at lines 2 and 7. Between lines 1 and 2, warmer offshore water is being advected shoreward by the dynamic high centered over line 2. On line 7, the warm surface water is seen almost to the 200-m isobath and is associated with the dynamic high centered on line 7. The warm water on lines 9, 10, and 11 is advected between the low on line 9 and the high on lines 10 and 11.

Dissolved oxygen concentrations near-surface (not shown) were nearly uniform and greater than 5 $mL \cdot L^{-1}$ during N8.

As on previous cruises, the presence of the highs and lows along the slope leads to changes in property distributions, uplift, and downlift in the regions that they affect. The effects of the highs and lows on the temperature structure at the stations at the 1000-m isobath can be seen in Figure H.3-2. Isotherms below 80 m are displaced upwards at stations 70 and 72 corresponding to the low in geopotential anomaly at lines 5 and 6 and at stations 32 and 33 corresponding to the cyclone present on the slope at lines 8 and 9. Isotherms are displaced downwards at stations 95, 52, and 11 and correspond to regions of dynamic highs. Above 50-m depth, the cross slope transport of warm oceanic water and cool shelf water can be seen. At station 71, cool shelf water is present with temperatures less than 22°C; similarly, station 33 is located in a region where shelf water is being entrained around the low geopotential anomaly cyclone and being advected into deeper water. At station 52 and station 95 west of line 4, warm oceanic water is being transported onto the slope in association with the two areas of dynamic highs.

The effect of the offshore circulation features is also present in the nutrient fluxes into the region. Figure H.3-3 shows the nitrate concentration at stations along the 1000-m isobath. Nutrients in the upper 50 m are depleted. Beneath this layer is a strong nitracline. Thus nitrate can be made available to the photic level by uplift due to circulation features. Below 50-m the effects of such features are seen and distributions are similar to those seen in the potential temperature profile of Figure H.3-2. Nutrient isopleths are displaced upwards or downwards depending on the circulation feature associated with it.

At stations along the 100-m isobath, the vertical structure of nitrate concentration (Figure H.3-4) shows evidence of the Mississippi River plume (stations 88 and 98), nutrient loading below 50 m depth from localized uplift (stations 83 and 88), and a slight indication of enhanced nutrients around Cape San Blas and Apalachicola Bay (stations 58, 45, and 38).

Figures H.3-5 and H.3-6 show nitrate and silicate concentrations in the upper 400 m along lines 1 through 3. The Mississippi River plume can be seen along lines 1 at stations 87, 88, and 89 extending down about 10 m from the surface. At line 2, the plume is detached from the coast, has considerably smaller concentration, and is centered over the 50-m isobath. The plume has probably been blown offshore by the eastward winds during this cruise. The ADCP velocities at 12 m also indicate an eastward current jet at line 2 between the 20- and 50-m isobath. At line 3, there is no surface expression of the Mississippi River plume, which is consistent with ADCP current observations along line 3, where the mid-shelf currents are flowing south, effectively cutting off the plume from moving further west. On line 2 below 100 m, nitrate and silicate isopleths are displaced downward about 70 m at station 96 from their offshore values at station 92. This is likely related to the presence of the dynamic high located near the shelf break on line 2. This downwelling is not seen at similar depths on lines 1 and 3.

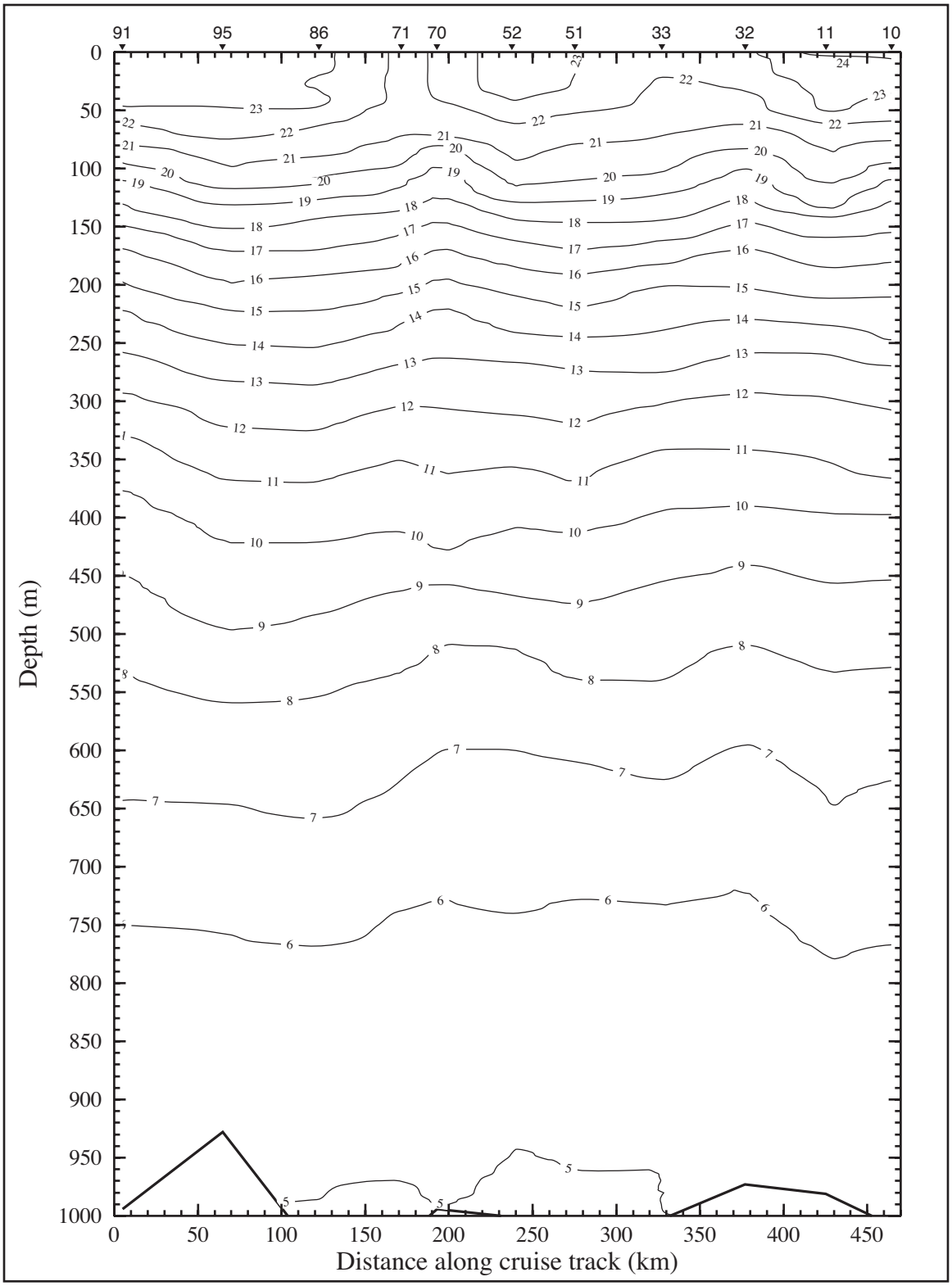

Figure H.3-2. Potential temperature (°C) along the 100-m isobath on cruise N8 in April 2000. Stations are shown on top axis. Line 1 is at the left station; line 11 at the right.

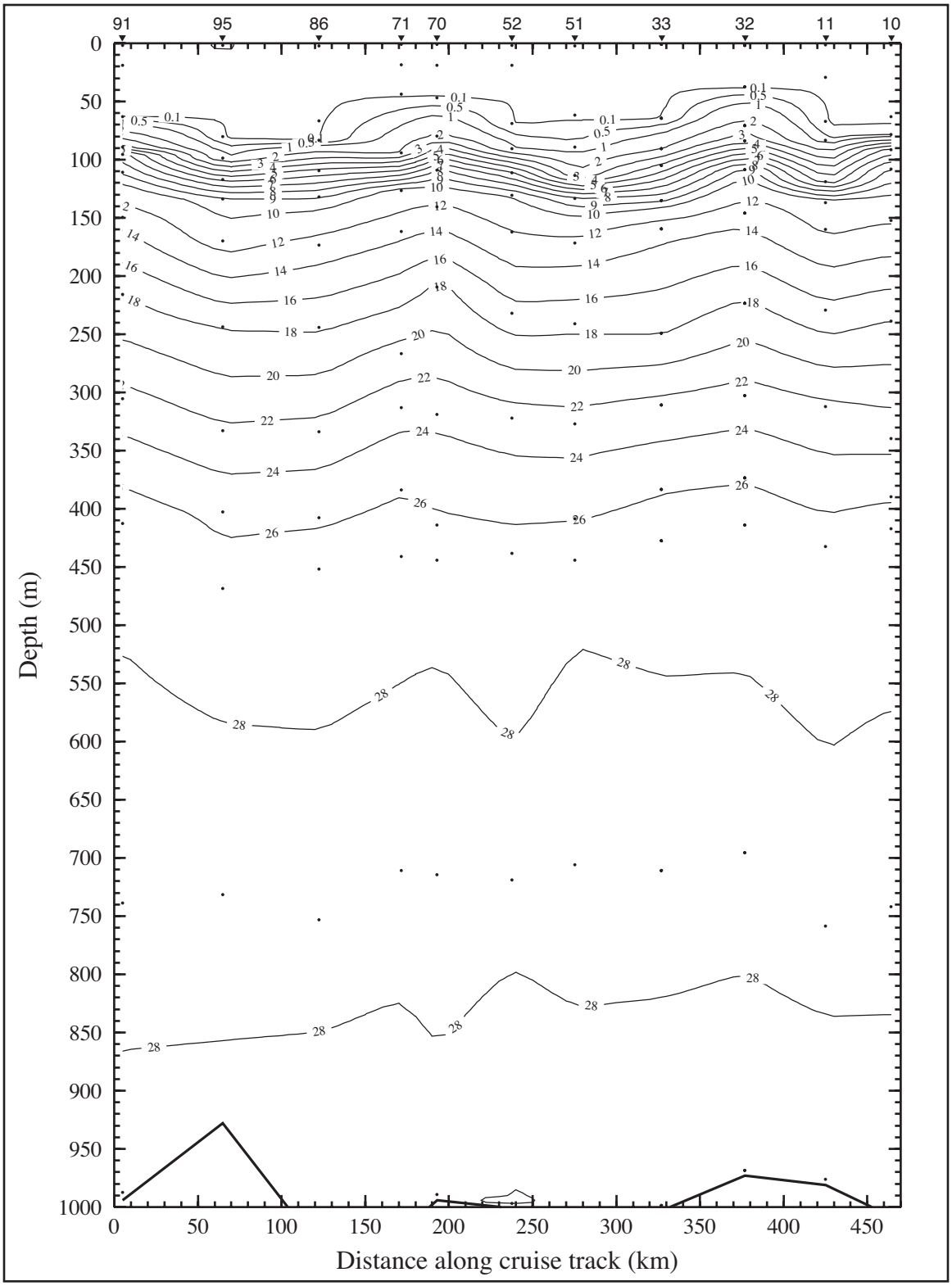

Figure H.3-3. Nitrate (μM) along the 1000-m isobath on cruise N8 in April 2000. Stations are shown on top axis. Line 1 is at the left station; line 11 at the right.

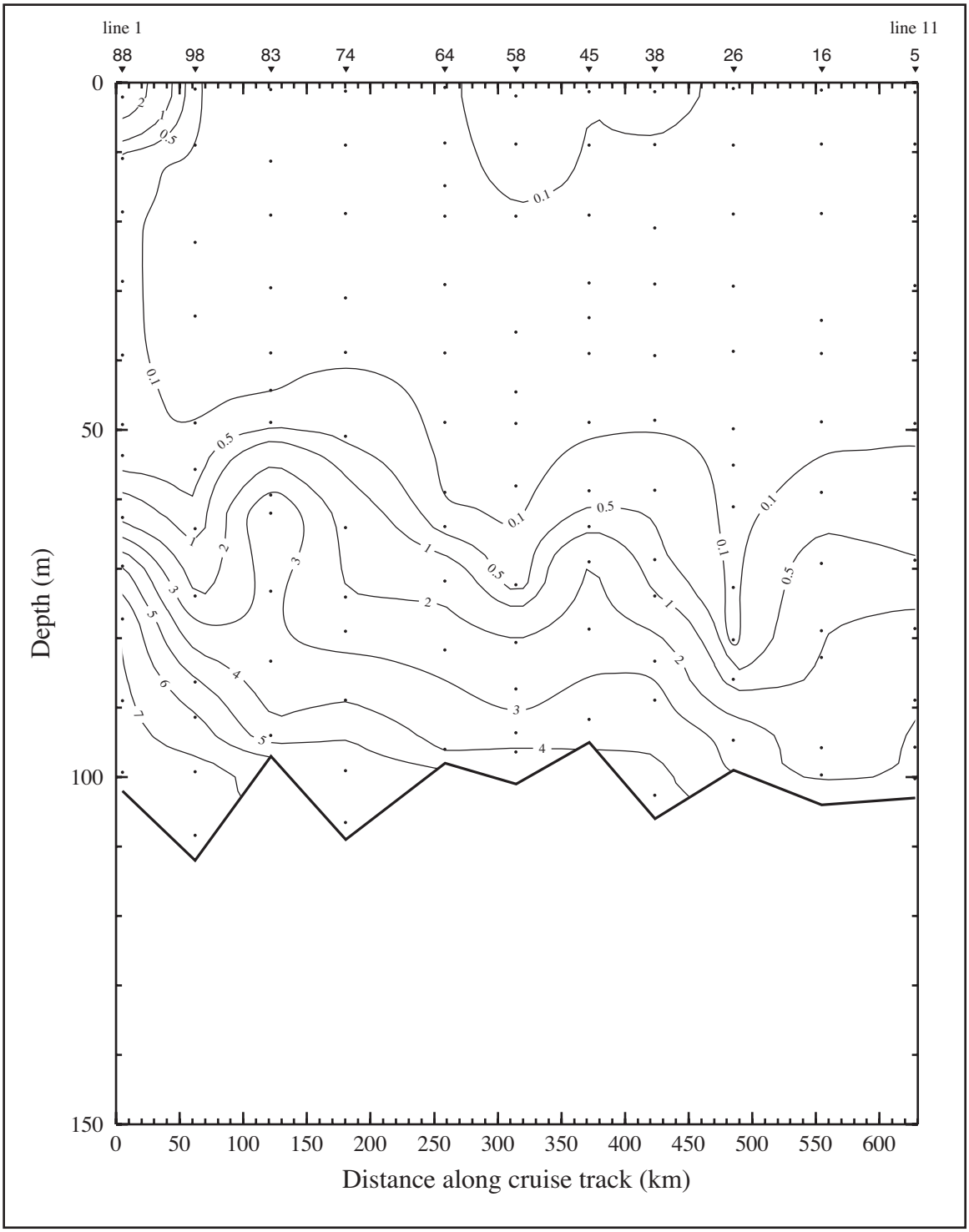

Figure H.3-4. Nitrate (μM) along the 100-m isobath on cruise N8 in April 2000. Stations are shown on the top axis.

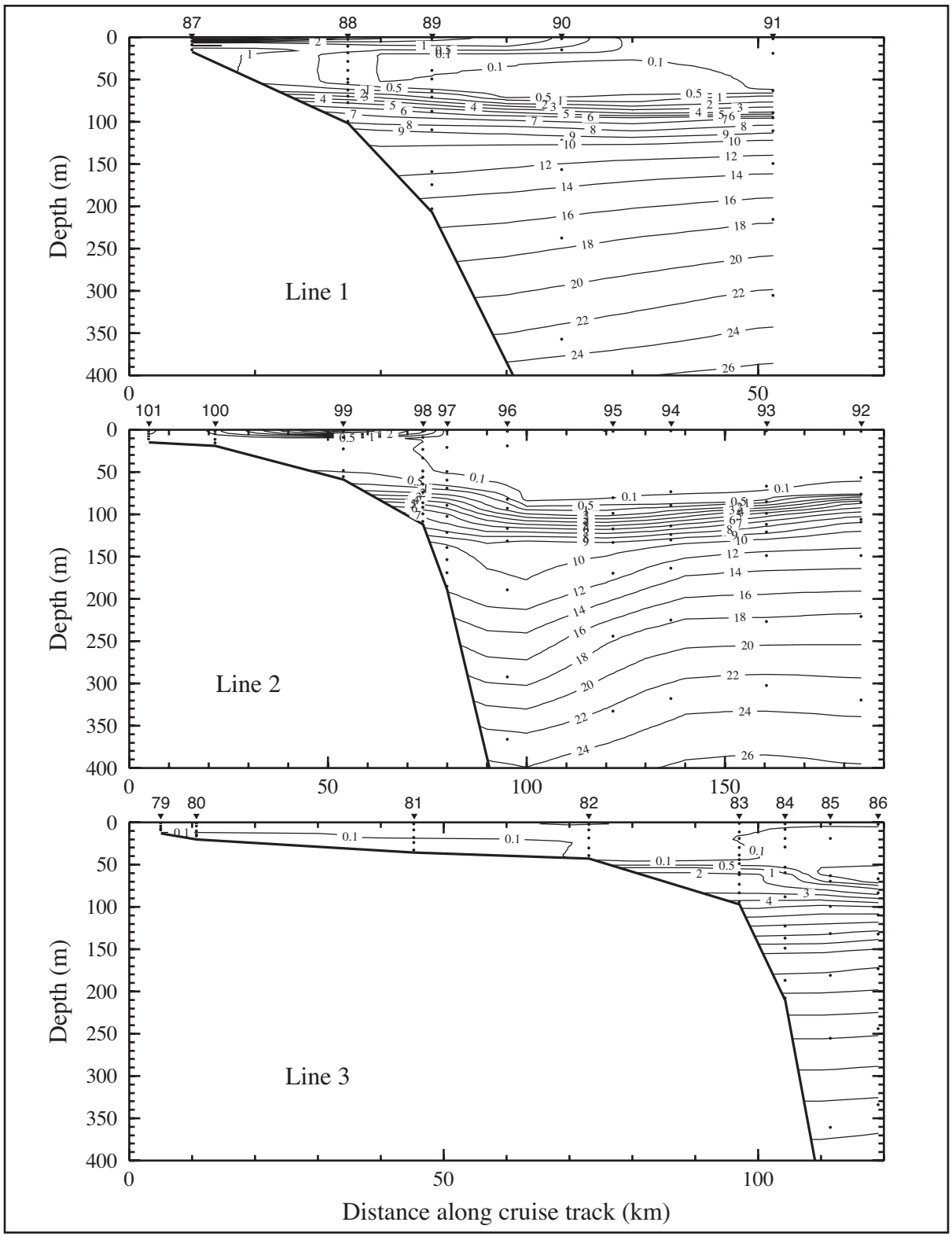

Figure H.3-5. Nitrate (μM) on lines 1, 2, and 3 of cruise N8 in April 2000. Stations are shown on top axes.

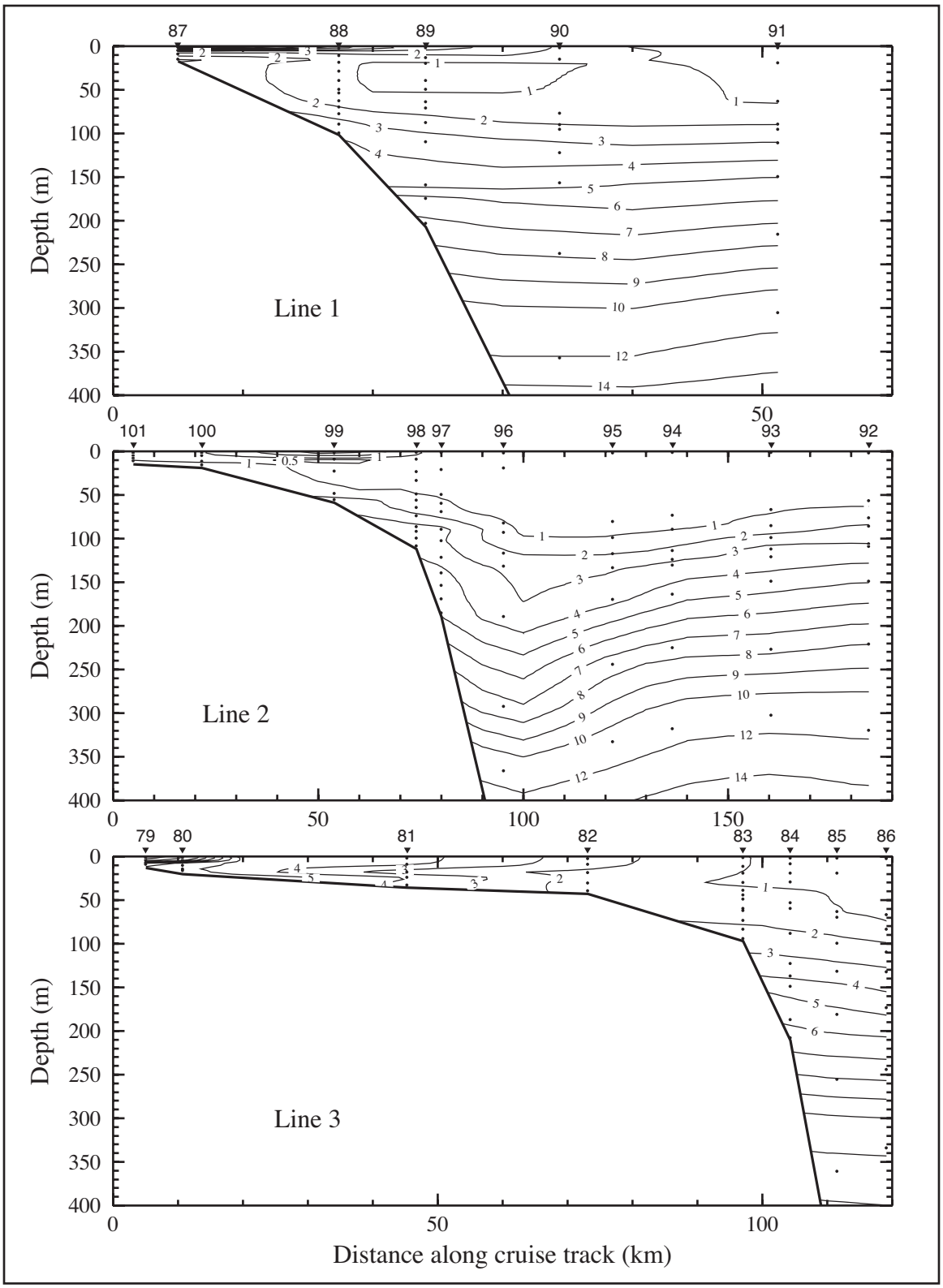

Figure H.3-6. Silicate (μM) on lines 1, 2, and 3 of cruise N8 in April 2000. Stations are shown on top axis.

Figure H.3-7 shows potential temperature and nitrate and silicate concentrations along line 9 over the west Florida shelf. There is slight indication of some uplift in the temperature section where isotherms are displaced upwards close to shore. Silicate and nitrate concentrations are well-mixed in the upper 100 m. Below 100 m, temperature and nutrient values all show evidence of downwelling with downward sloping isopleths toward shore particularly at stations 26 through 28, which are at approximately 100-200 m water depth.

This region also had current observations around 100-m depth (Figure H.2-2) which formed a near-continuous subsurface jet flowing downcoast from line 9 to line 5. This jet is coincident with the downwelling of nutrient observations in Figure H.3-7 and other potential temperature and nutrient structures observed at lines 5 through 8. The downwelling may at least in part be caused by the frictional interaction of the subsurface jet with the bottom topography.

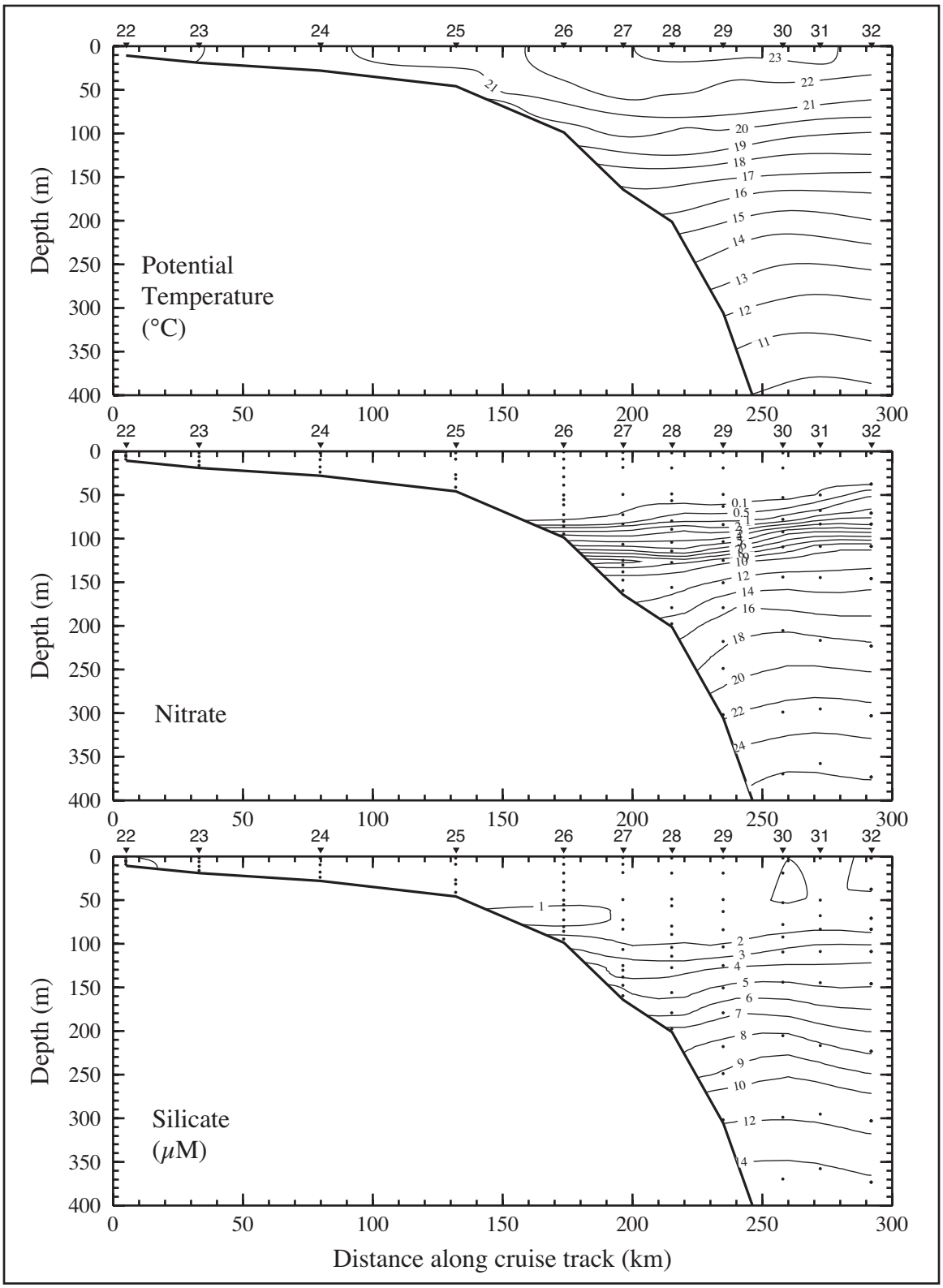

Figure H.3-7. Potential temperature, nitrate, and silicate along line 9 on cruise N8 in April 2000. Stations are shown on top axes.

APPENDIX I
SUMMARY OF CONDITIONS DURING CRUISE N9

Cruise N9 was a summer cruise conducted 28 July - 8 August 2000. Stations began with the innermost station on line 1 and ended on the most seaward station on line 11. Figure I-1 shows the station locations and gives the CTD station numbers, which are sequential by sampling order. Station 6 was the test station and is not included on the map or in the analysis.

I.1 Forcing Functions

I.1.1 Winds

The mean wind field and variance ellipses for the period of cruise N9 were computed using the methodology of Wang et al. (1998). The mean winds were < 5 $m \cdot s^{-1}$ over the study area and directed northward, with a slight, upwelling-favorable, eastward component over the Mississippi-Alabama shelf and a slight westward component over the west Florida shelf (Figure I.1.1-1). The variance was aligned mainly east-west with magnitude of ≤ 25 $m^2 \cdot s^2$. Strongest winds during the cruise were generally < 10 $m \cdot s^{-1}$ with a northward component of flow (e.g., Figure I.1.1-2). There were no frontal passages or tropical cyclones during the cruise.

I.1.2 River Discharge

During the first 8 months of 2000, river discharge onto the NEGOM study area was low. Except for a pulse in the first half of July, the Mississippi River discharge was well-below its 70-yr record-length mean (Figure 3.1.2-2). In May, it was at or below one standard deviation less. Rivers at or west of Mobile Bay generally had one or more pulses of discharge that exceeded their record-length means in May and/or April, but otherwise discharged near one standard deviation below the mean (see Section 3.1.2). Rivers east of Mobile Bay discharged below their record-length means, with much of the discharge near one standard deviation below the mean (see Section 3.1.2).

The ~3-m salinity map indicates the extent of the influence of river discharge in the near-surface waters of the NEGOM study area (Figure I.1.2-1). The influence of the Mississippi River, as indicated by the 32 salinity contour, extended eastward and southeastward from Pass a Loutre past DeSoto Canyon to line 7, even reaching line 8 over the slope. The influence of the Mississippi River discharge is also apparent in the ~3-m chlorophyll map (Figure I.1.2-2), which shows higher chlorophyll concentrations approximately co-located with the region influenced by the Mississippi River discharge (e.g., compare the 0.75 $\mu g \cdot L^{-1}$ chlorophyll contour with the 32 salinity contour in Figure I.1.2-1).

Except near the mouth of the Mississippi River, relatively low salinity water is located seaward of the shelf break. As with other summers, the saltiest waters are inshore and the freshest are offshore. In general the near-surface waters over the Mississippi-Alabama shelf are fresher by 2 or more salinity units than those over the west Florida shelf.

I.1.3 SSH Fields Adjacent to the Shelf

During June and July 2000, an anticyclonic feature was located offshelf adjacent to the Mississippi-Alabama shelf (Figures 3.2.3-36 and 3.2.3-37). It was present throughout cruise

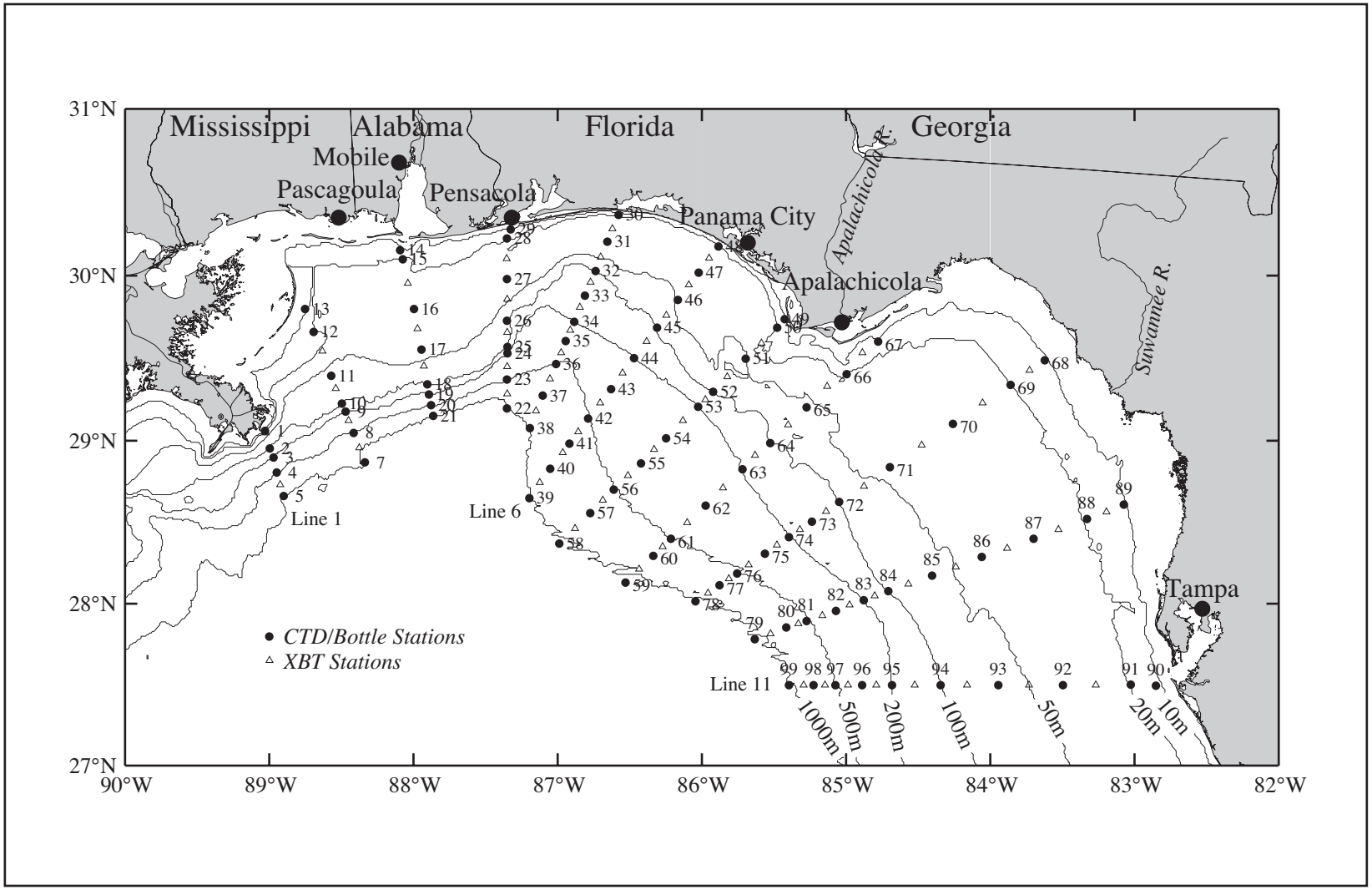

Figure I-1. Station locations for cruise N9 conducted 28 July - 8 August 2000. CTD station (solid circles) are numbered; XBT stations (open triangles) are not.

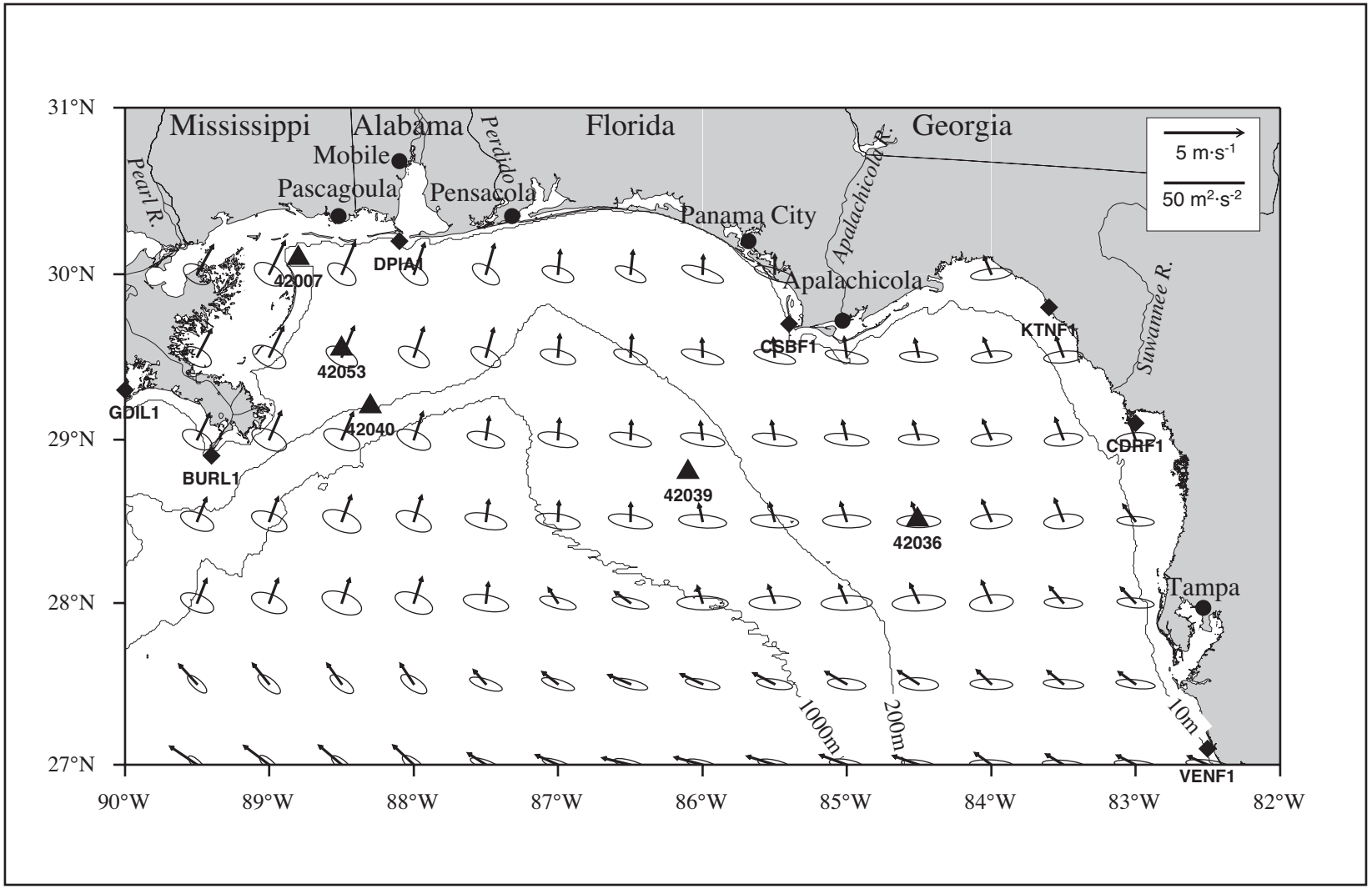

Figure I.1.1-1. Vector mean winds and variance ellipses for cruise N9 in July/August 2000.

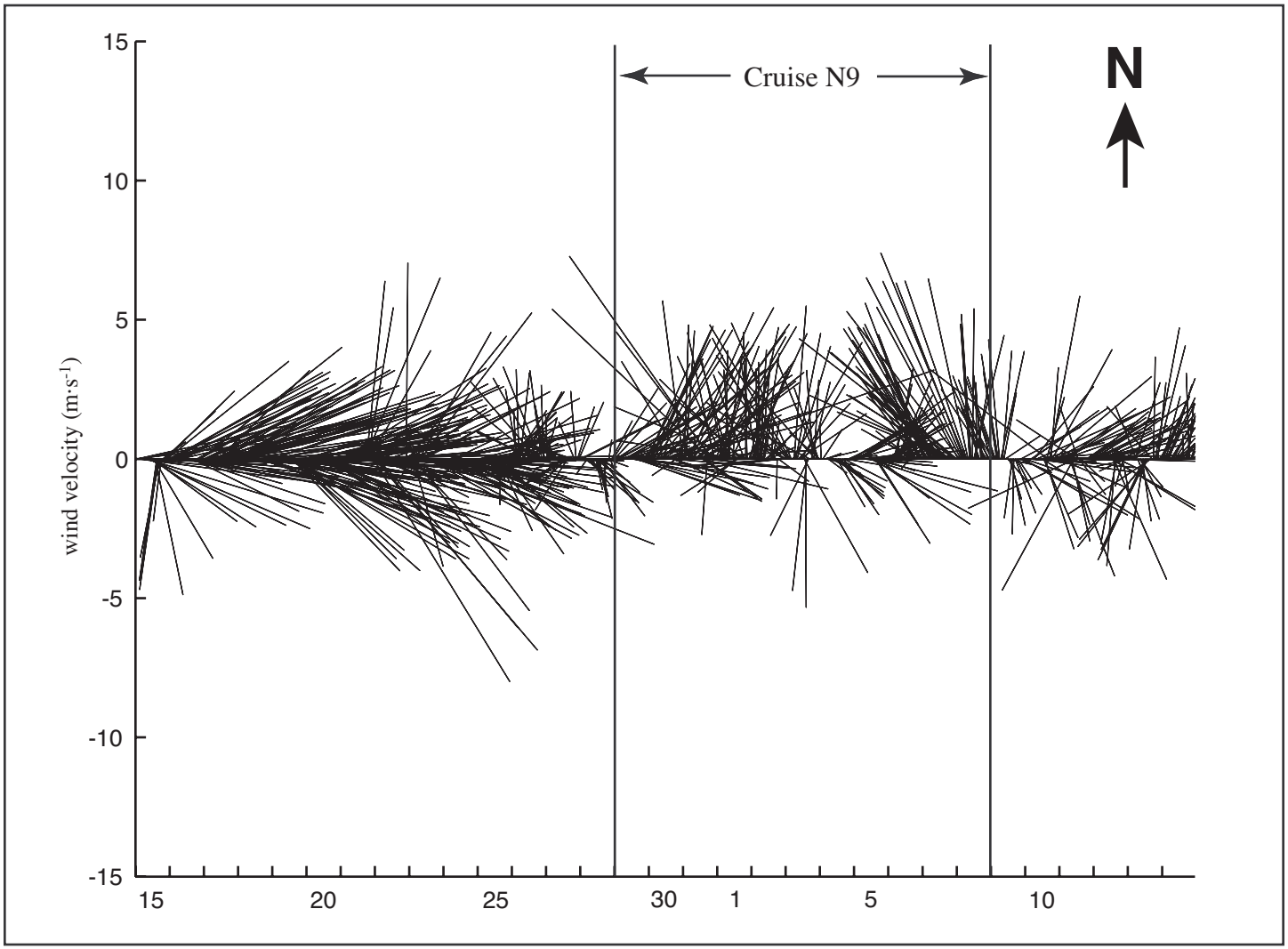

Figure I.1.1-2. Vector stick plot of wind at meteorological buoy 42040 for 15 July - 14 August 2000. Gauge height is 10 m.

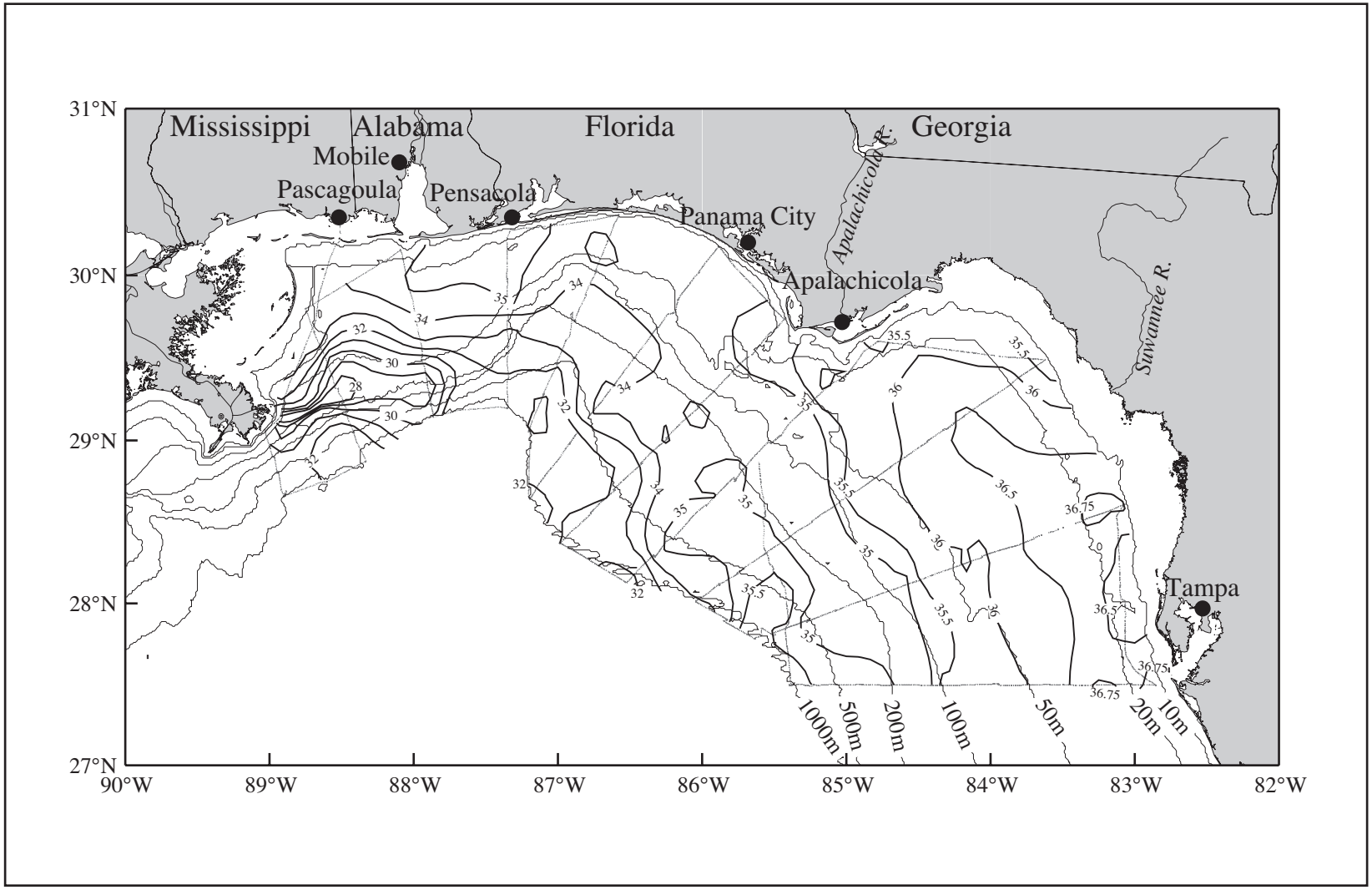

Figure I.1.2-1. Salinity at ~3 m from thermosalinograph observations on NEGOM cruise N9 in July/August 2000. Dots show sample locations and give thre track lines.

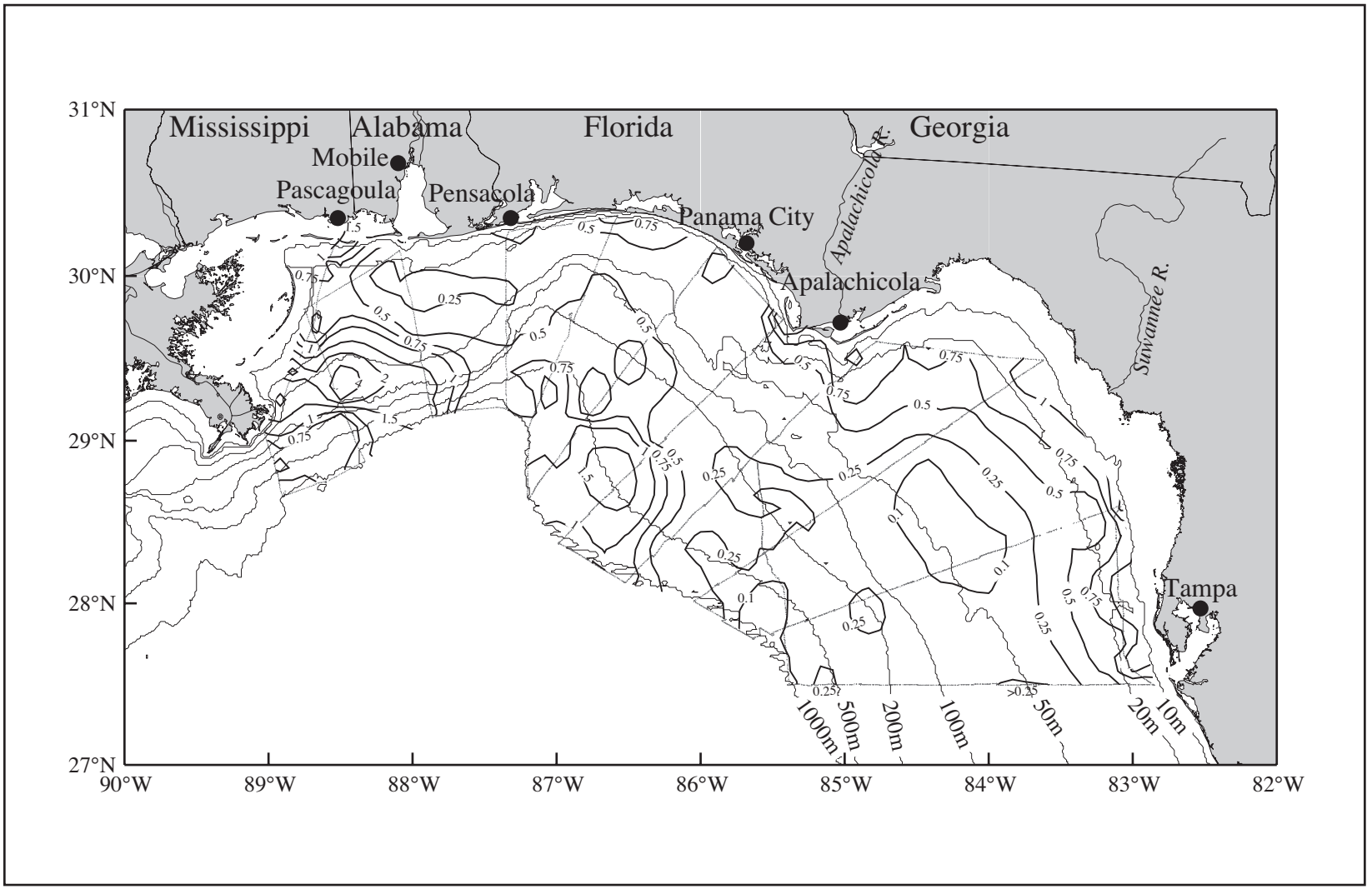

Figure I.1.2-2. Cholorophyll *a* ($\mu g \cdot L^{-1}$) at ~3 m calculated from flow-through fluorescence on cruise N9 in July/August 2000. Dots show sample locations and give the track lines.

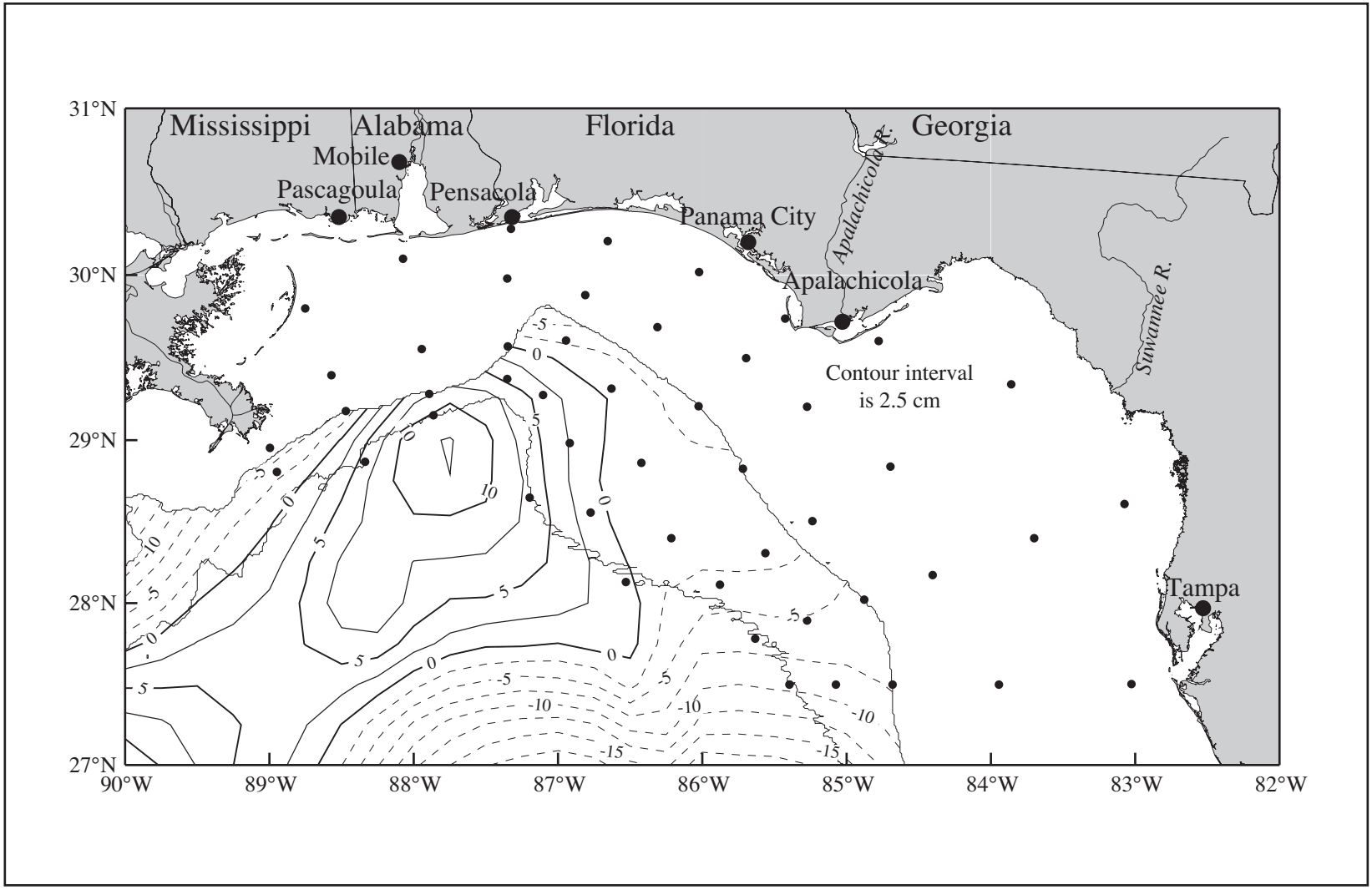

Figure I.1.3-1. Sea surface height field from satellite altimeter data for 2 August 2000 during cruise N9. The 200- and 1000-m isobath contours and CTD stations (dots) are shown. [Data provided by Robert R. Leben, University of Colorado]

N9 (Figures 3.2.3-37 and 3.2.3-38), but was not intense, as indicated by its weak gradient (Figure I.1.3-1). Adjacent to the west Florida shelf before and during cruise N9, there was an intense cyclonic feature, which was north of the Loop Current, that impinged on the shelf at and south of lines 9-11. North of these lines adjacent to the west Florida shelf, the SSH was weakly positive (maximum of 5 cm) prior to the cruise and weakly negative (about -5 cm) during the cruise.

I.2 *In Situ* Evidence of Circulation

ADCP current vectors for the 4-m bin centered at 12 m are shown in Figure I.2-1. The influence of the anticyclonic feature seen adjacent to the Mississippi-Alabama shelf in the SSH field is apparent in the anticyclonically turning vectors over the outer shelf and slope between lines 1 and 3. Magnitudes are generally < 50 $cm \cdot s^{-1}$. The strongest eastward currents are between the 100- and 500-m isobaths. This eastward flow is indicated in the geopotential anomaly (3 m relative to 800 m) field, which also shows a high in dynamic topography over the slope in this region (Figure I.2-2). However, the eastern edge of the anticyclone seen in the SSH field is not seen at that location in the ADCP currents or the geopotential anomaly field (compare area near lines 4 and 5 on Figure I.1.3-1 to that on Figures I.2-1 and I.2-2). To the east of the anticyclonic feature is a cyclonic feature in the ADCP currents located over the outer shelf and slope of the axis of DeSoto Canyon between lines 3 and 6 (Figure I.2-1). Current magnitudes in this feature exceed 50 $cm \cdot s^{-1}$ in the jet between the anticyclone and cyclone and also in the northeast flow between lines 5 and 6. The cyclone is clearly present through the water column to the 152-m depth measured by the ADCP (Figures I.2-3, I.2-4, and I.2-5). The anticyclone is not as clear at depth, which is consistent with its weak signature in the SSH field. The cyclone is apparent in the geopotential anomaly field as the southward-eastward-northward contours between lines 3 and 5 (Figure I.2-2). Note that, except in the near-shore region of the Big Bend, the geopotential anomaly and ADCP fields show about the best agreement of any of the NEGOM cruises.

Slope currents over the eastern portion of the study area are weaker than those over the western region (Figure I.2-1). This is consistent with the SSH field which shows a broad region with elevation differences of < 10 cm between lines 7 and 9. The apparent high in dynamic topography over the slope southwest of Cape San Blas and its broad gradient suggest weak currents over the slope between lines 7 and 8, with currents near line 7 being generally onshore and currents near line 8 being offshore. This is pattern of weak outer shelf and slope currents with an anticyclonic character is present in the ADCP currents (compare the region associated with lines 7 and 8 in Figure I.2-2 with that in Figure I.2-1). There is no clear indication of currents forced by the cyclone which, in the SSH field, is impinging over the slope at the southeastern part of the study area.

Along line 5 the currents in the upper 50 m of the water column are directed up-canyon to the north-northeast. At the 100-m depth ADCP bin, flow along line 5 has shifted and is to the northwest (compare Figures I.2-3 and I.2-4). In the upper water column, the up-canyon flow extends to about the 100-m isobath where it then turns to the southeast forming a current jet that moves between the 100 and 200-m isobaths and out the line 11 boundary of the study area (Figure I.2-1). This jet seems to extend through the water column (Figures I.2-3 and I.2-4). Off Cape San Blas inshore of the 100-m isobath, the general pattern is of currents moving westward until line 4, where they turn south and then east to join the up-canyon flow on line 5. The near-shore currents west of Cape San Blas are in the opposite direction (westward) to the eastward direction expected based on the wind field (Figure I.1.1-1). This suggests the winds were too weak to induce the coastal current. Near the 50-m isobath over the west Florida shelf, currents move northeastward until line 8 where they turn cyclonically to join

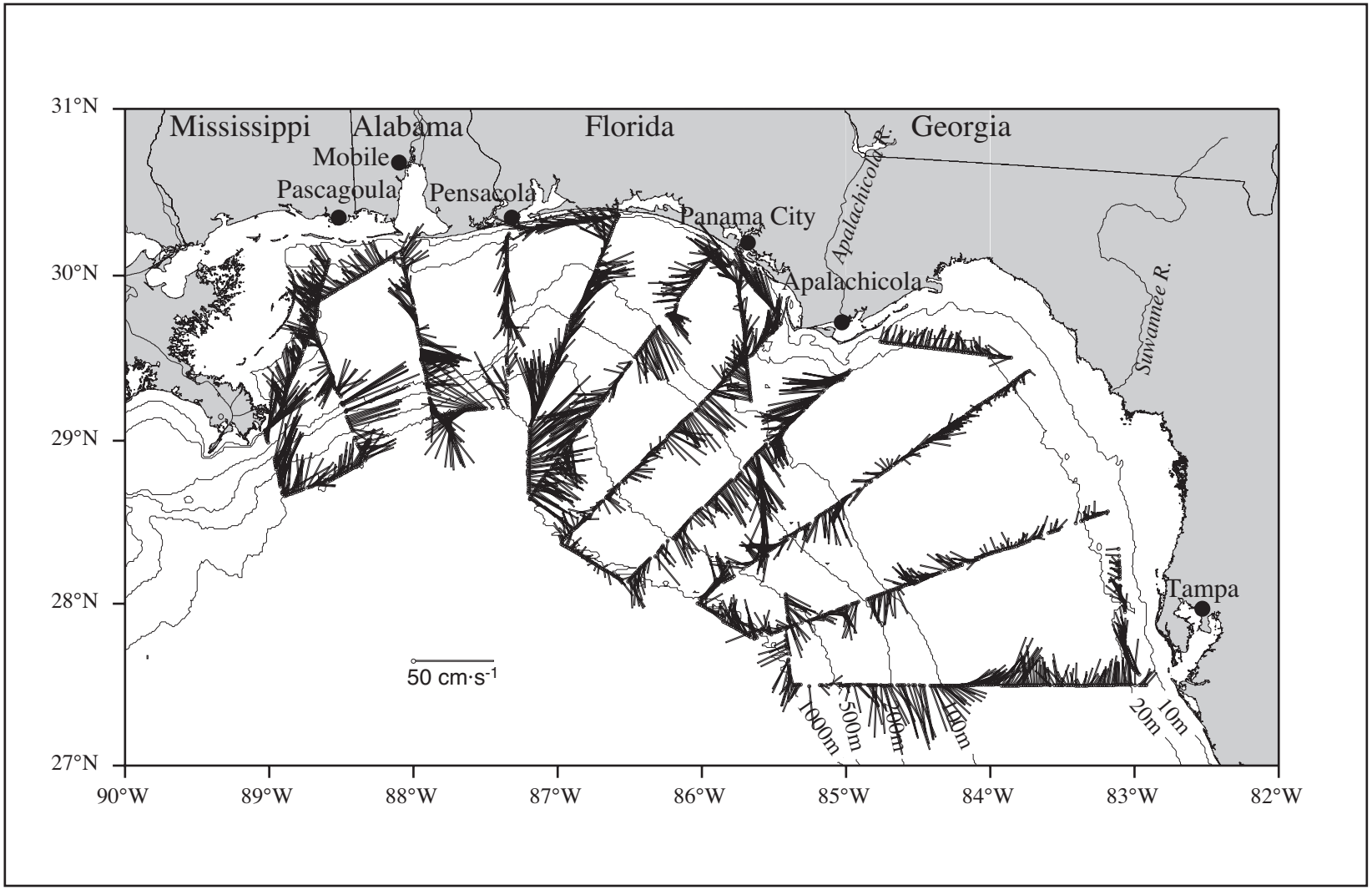

Figure I.2-1. ADCP-measured currents for the 4-m bin centered at 12 m on cruise N9 in July/August 2000.

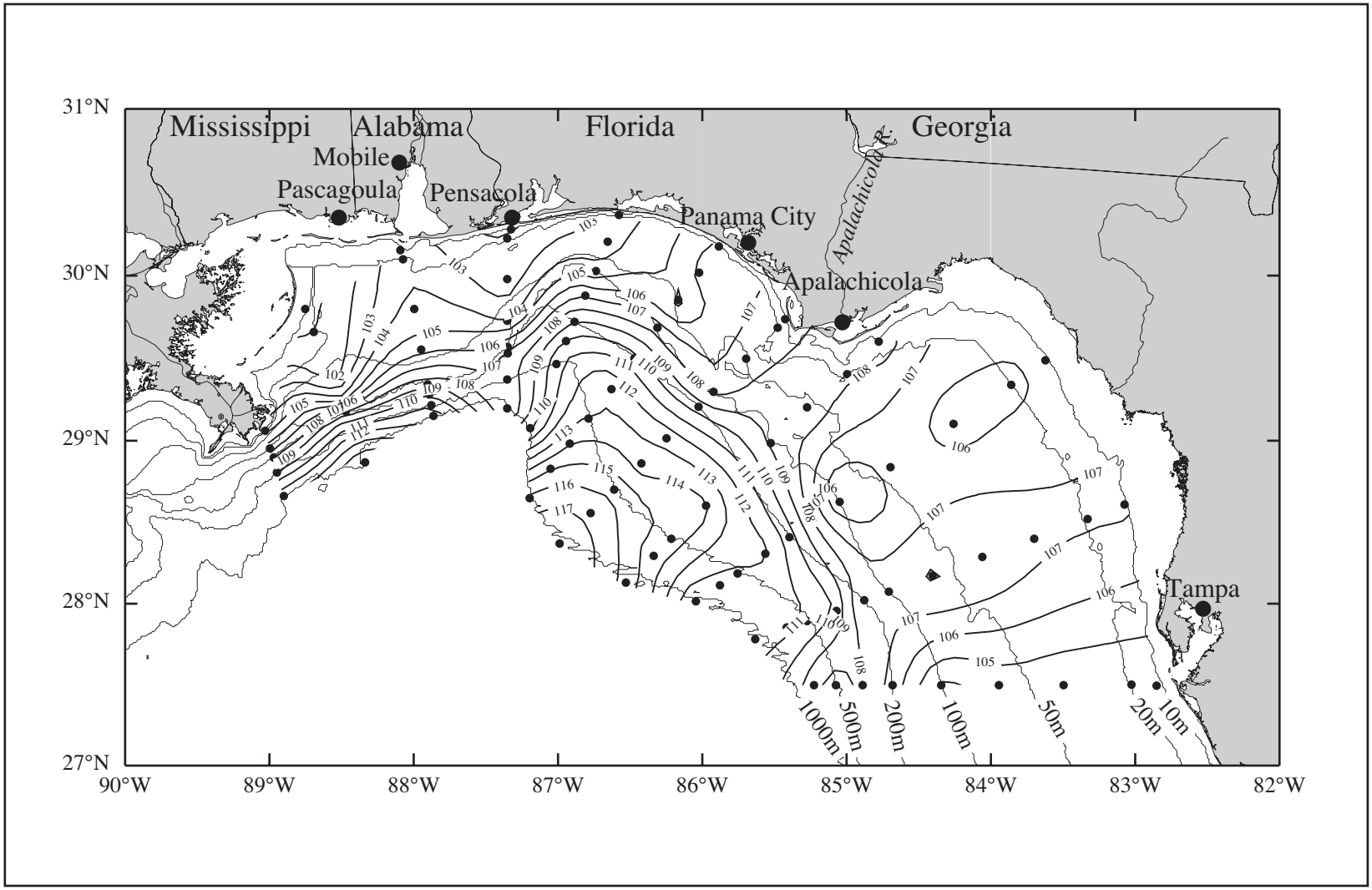

Figure I.2-2. Geopotential anomaly (dyn cm; 3 m relative to 800 m) for cruise N9 conducted July/August 2000. CTD stations are shown.

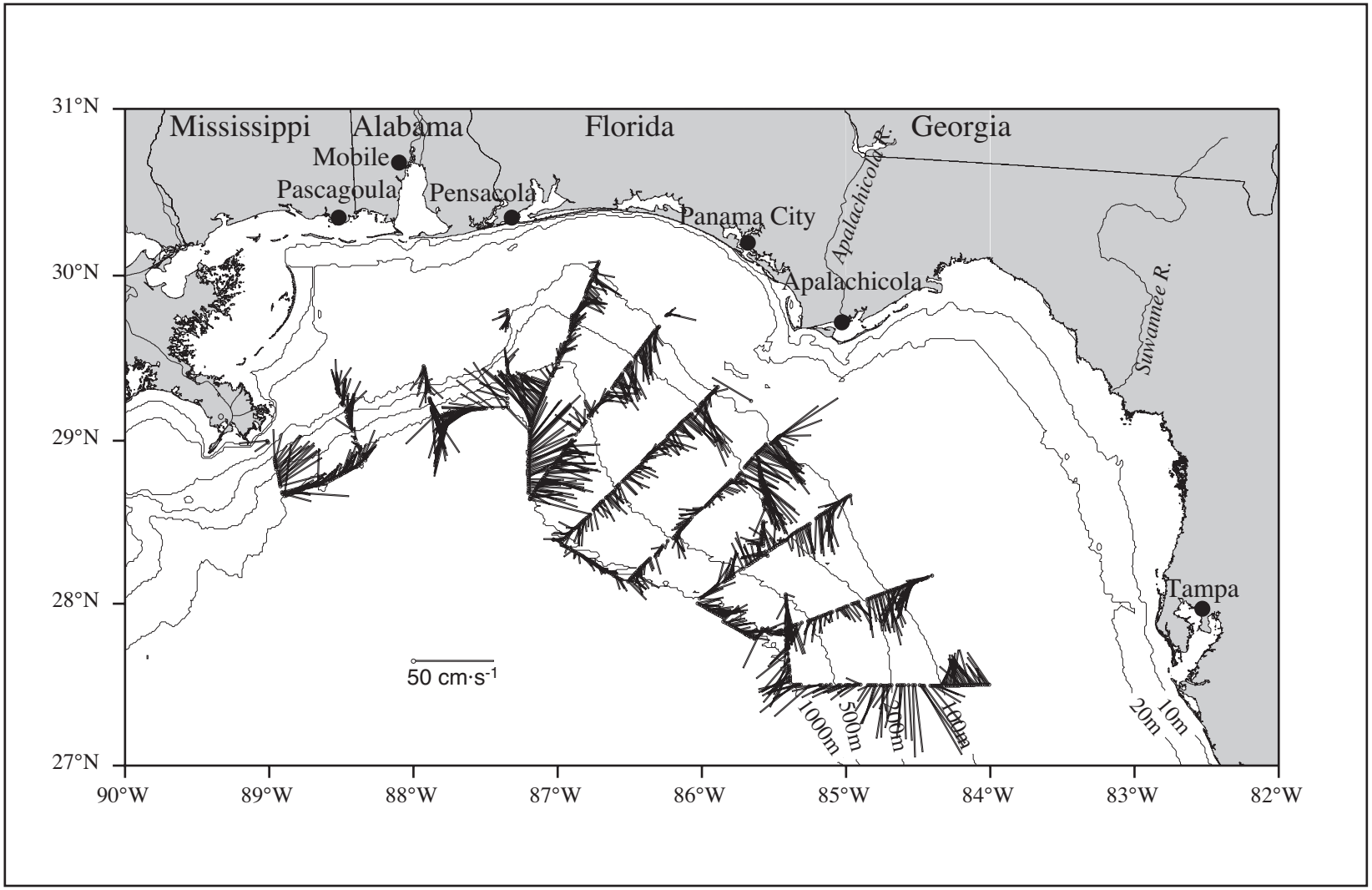

Figure I.2-3. ADCP-measured currents for the 4-m bin centered at 52 m on cruise N9 in July/August 2000.

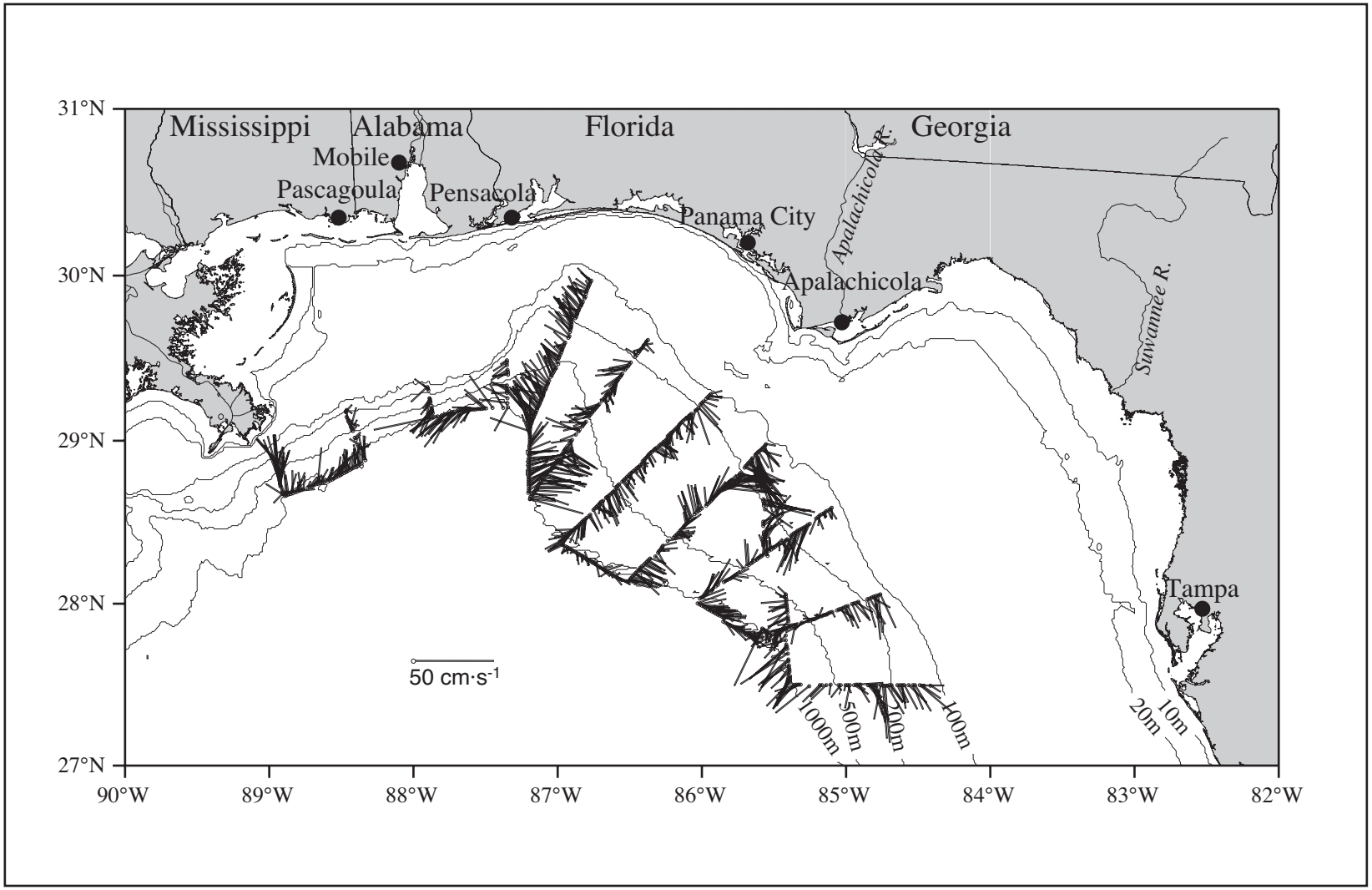

Figure I.2-4. ADCP-measured currents for the 4-m bin centered at 100 m on cruise N9 in July/August 2000.

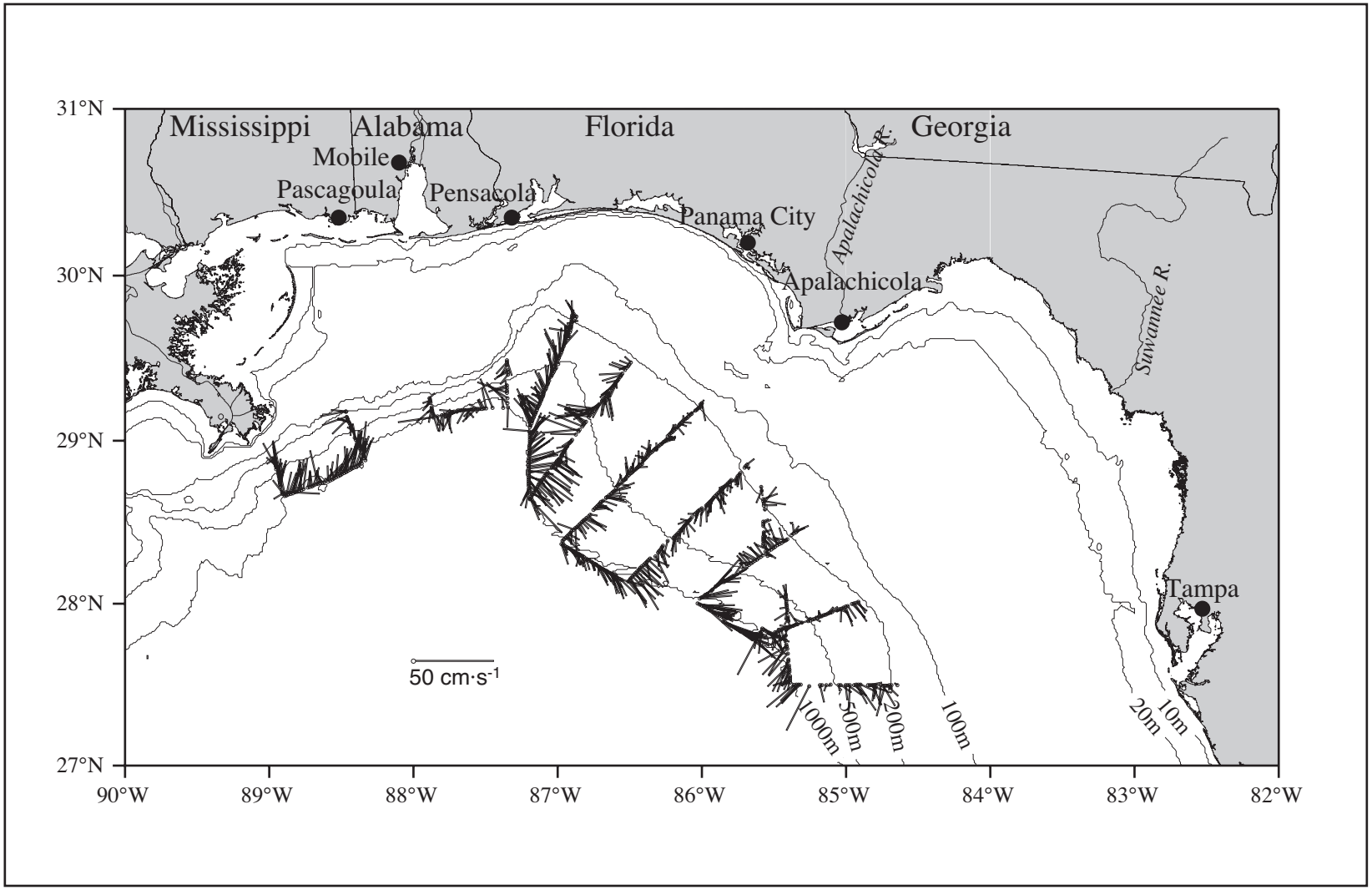

Figure I.2-5. ADCP-measured currents for the 4-m bin centered at 152 m on cruise N9 in July/August 2000.

the southeastward flow between the 100- and 200-m isobaths. Upon reaching line 11, currents inshore of the 100-m isobath turn cyclonically and then join the northeastward currents near the 50-m isobath. This indicates there is cyclonic circulation centered between lines 9 and 10 at the 100-m isobath. Currents over the inner Mississippi-Alabama shelf are generally directed to the northwest.

I.3 Property Distributions

Potential temperature, salinity, and sigma-theta distributions at the 1000-m isobath boundary of the study area show doming of isolines in the DeSoto Canyon region (stations 21, 22, and 38) that is indicative of the cyclone located there (Figures I.3-1, I.3-2, and I.3-3, respectively). This doming also occurred in the nutrient distributions (not shown). The anticyclonic feature located to the west of the cyclone and adjacent to the Mississippi-Alabama shelf is suggested by the dipping isotherms and isopycnals associated with line 2 (station 7).

At the 1000-m isobath, a small region of relatively high salinity water (> 36.6) occurred over the west Florida shelf on lines 10 and 11 (stations 79 and 99) at approximately the 100-m depth (Figure I.3-2). This high salinity water also is present at the 500-m isobath (Figure I.3-4, lower panel). At the 200-m isobath, the region of high salinity still is present at lines 10 and 11 (stations 83 and 95), but is higher in the water column at about the 75-m depth (Figure I.3-4, upper panel). The distribution of this high salinity water along line 10 is more patchy and less extensive than that along 11 (Figure I.3-5). The pattern of high salinity water indicates the water was derived from the Loop Current, most likely through transport by the cyclone that was located adjacent to the study area prior to the cruise. Because the ADCP currents in the region of the high salinity water are not directed onto the study area, the process that introduced the high salinity water into the study area likely was no longer active at the time of the cruise. The patchiness of the high salinity water indicates that mixing had eroded the high salinity maximum signal.

Another region of high salinity water (>36.6) is present in the study area. This region also is located along lines 10 and 11, but over the inner shelf (Figure I.3-5). Salinity on line 11 was just over 36.84 throughout the water column at the innermost station; that on line 10 was >36.76 at the innermost station and nearly 36.8 throughout the water column at the next station. Over the inner west Florida shelf, the near-surface distribution of salinity indicates that a tongue of relatively high salinity water extended from the southeast corner of the study area to the northwest (Figure I.1.2-1). The currents at the southeast corner suggest the very high salinity water was being transported into the study area from the south (Figure I.2-1).

In the upper 20-30 m, there is a strong pycnocline (e.g., Figure I.3-3). This is associated mainly with the strong thermocline caused by summertime heating (e.g., Figure I.3-1) and strong halocline caused by the transport of riverine water to the slope of the study area (e.g., Figure I.3-2). Although the lowest dissolved oxygen concentration is 2.068 $mL \cdot L^{-1}$, it is located in the water column at approximately 500-m on line 7 next to the most seaward station. Distribution of the near-bottom dissolved oxygen concentration over the shelf shows no indication of hypoxic conditions (Figure I.3-6).

The riverine influence over the outer shelf and slope along lines 1-3, seen in Figure I.1.2-1, included enhanced silicate concentrations and reduced light transmission. Representative of this are properties along line 3 (Figure I.3-7). The salinity distribution shows relatively low salinity water with values < 26 over the outer shelf and slope centered at the 100- to 200-m isobaths (stations 18 and 19). Associated with this relatively low salinity water are high near-

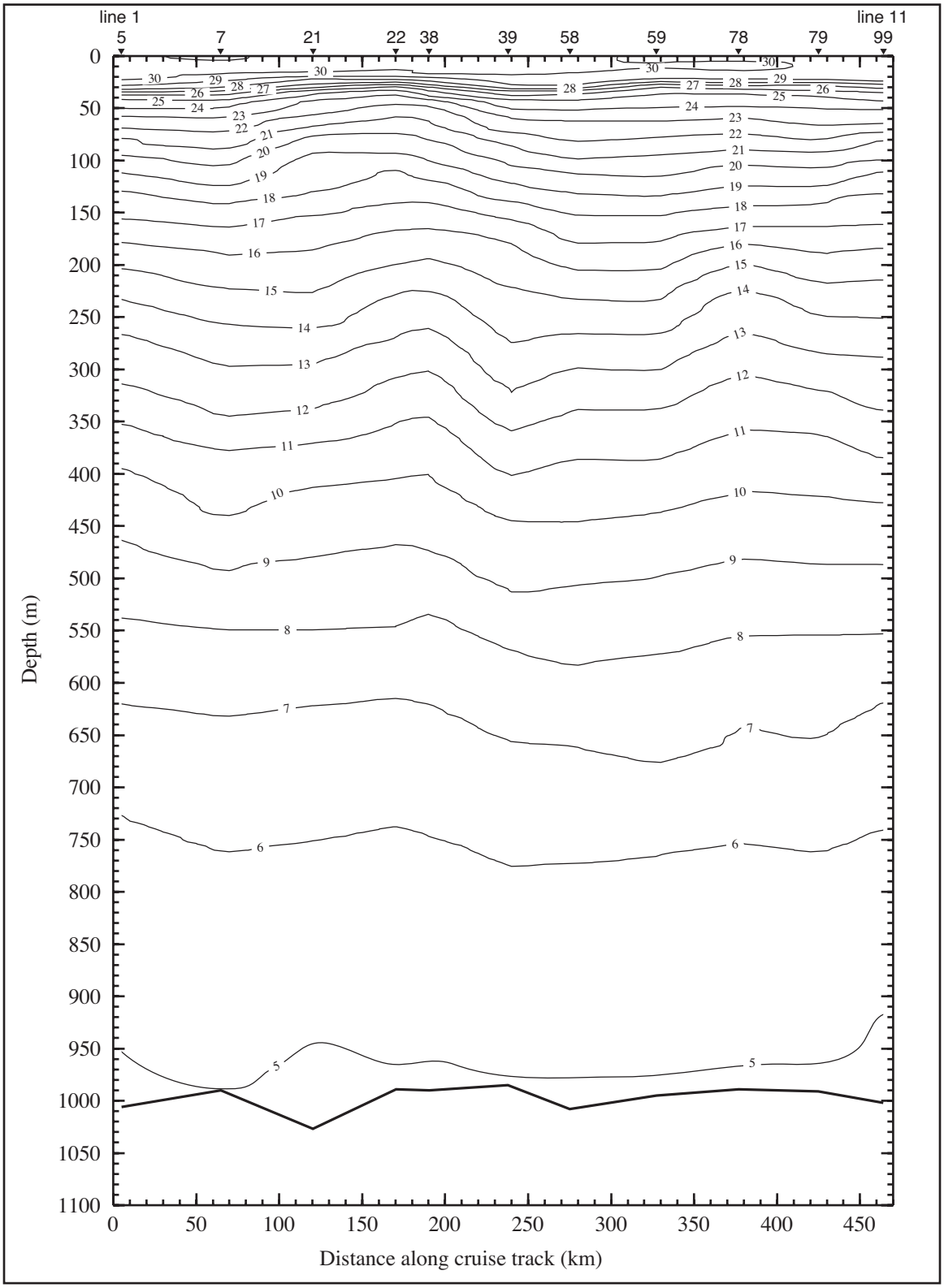

Figure I.3-1. Potential temperature (°C) along the 1000-m isobath on cruise N9 in July/August 2000. Stations are shown on the top axis.

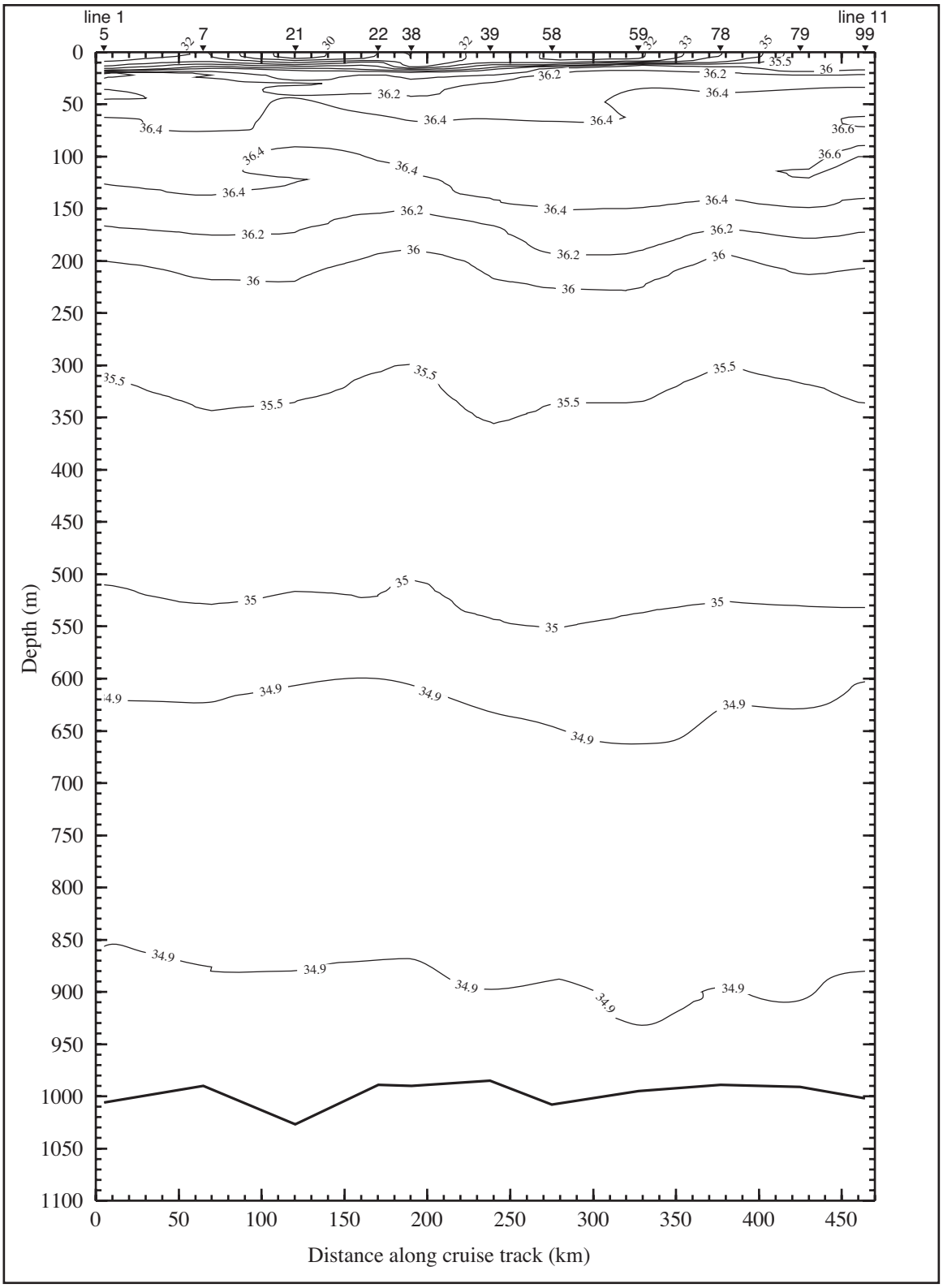

Figure I.3-2. Salinity along the 100-m isobath on cruise N9 in July/August 2000. Stations are shown on the top axis.

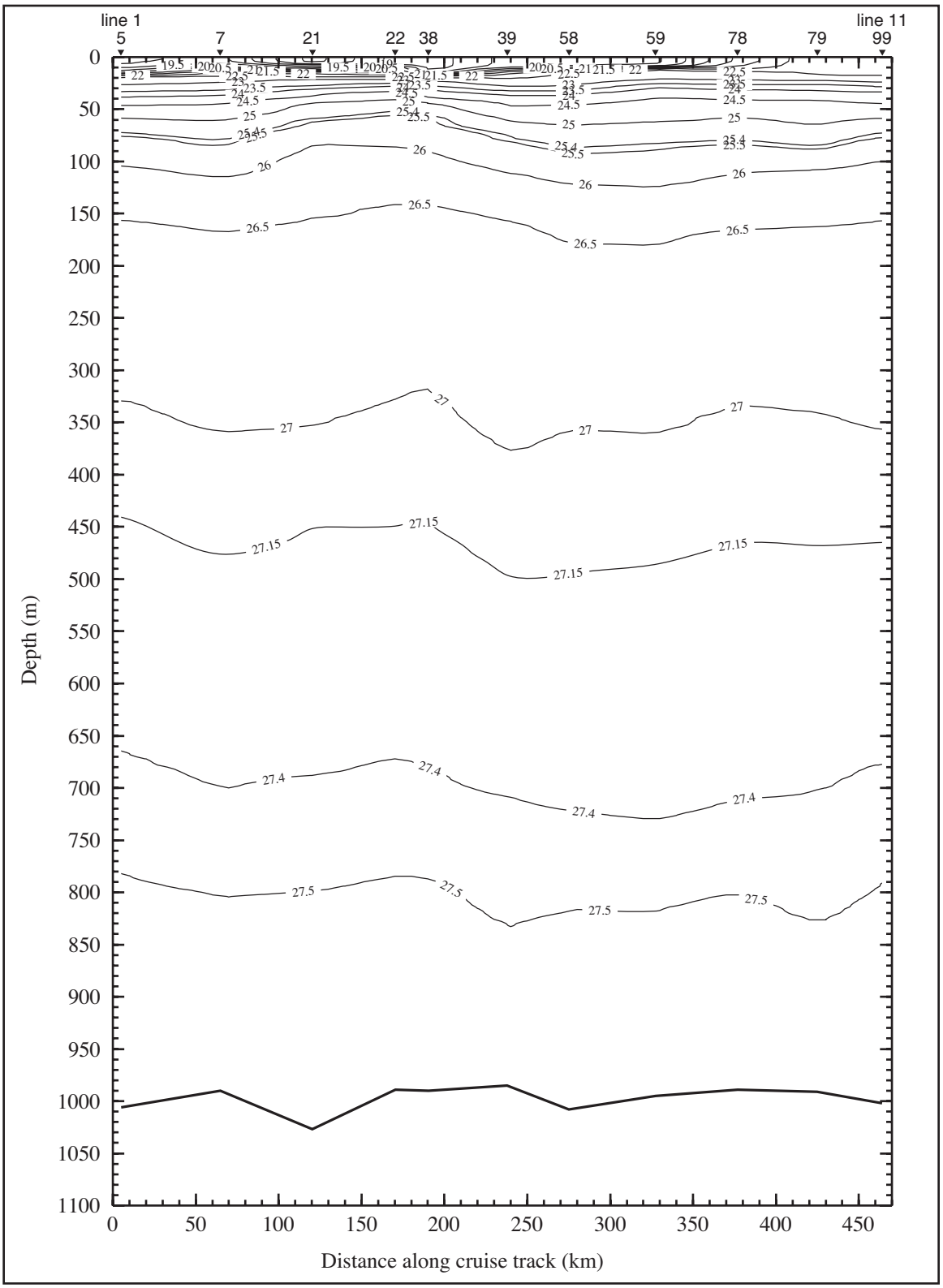

Figure I.3-3. Density anomaly (σ_θ in kg·m^{-3}) along the 1000-m isobath on cruise N9 in July/August 2000. Stations are shown on the top axis.

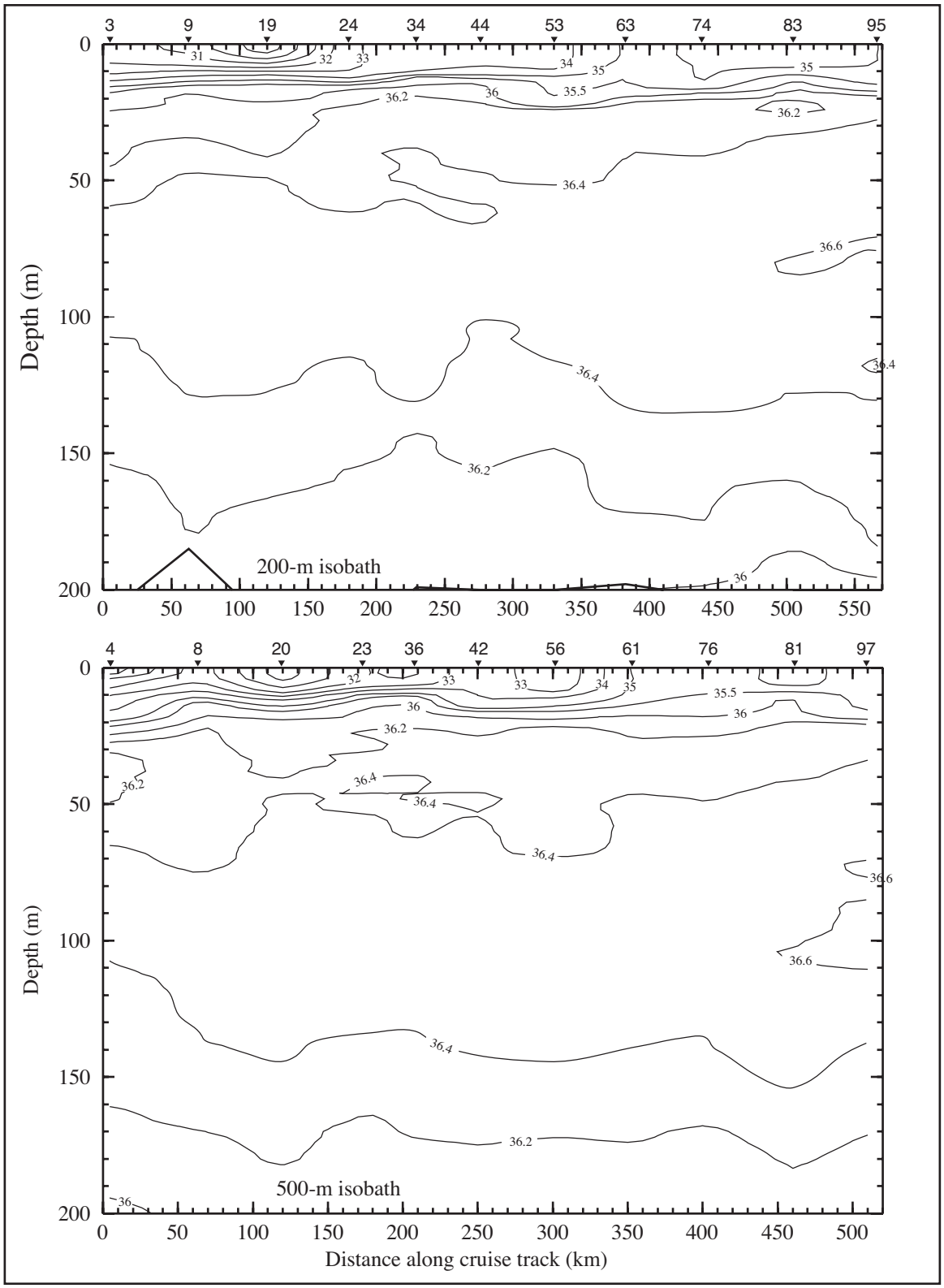

Figure I.3-4. Salinity along the 200- and 500-m isobaths on cruise N9 in July/August 2000. Stations are shown on top axes. Line 1 is at the left station; line 11 at the right.

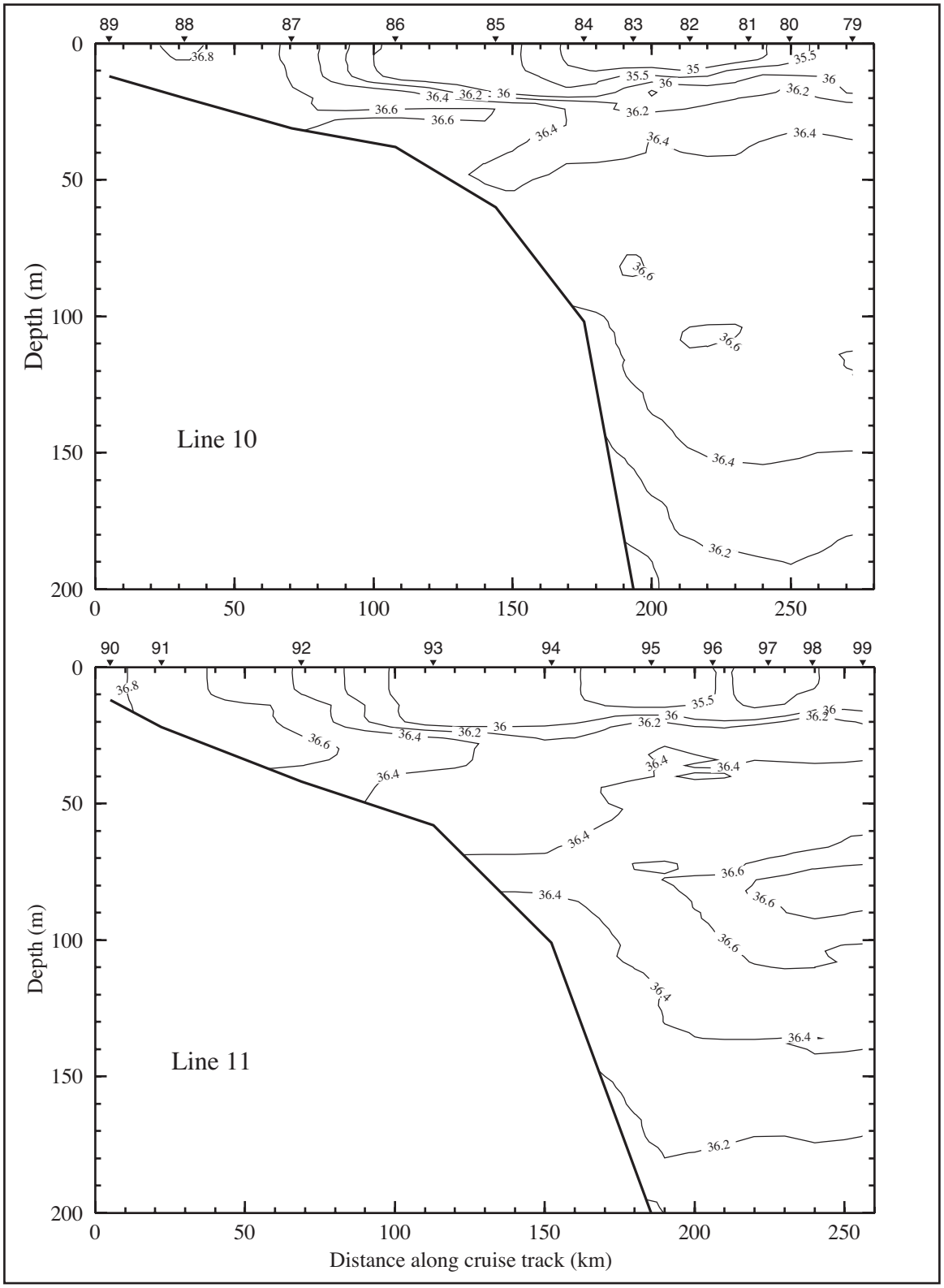

Figure I.3-5. Salinity along lines 10 and 11 on cruise N9 in July/August 2000. Stations are shown on top axes.

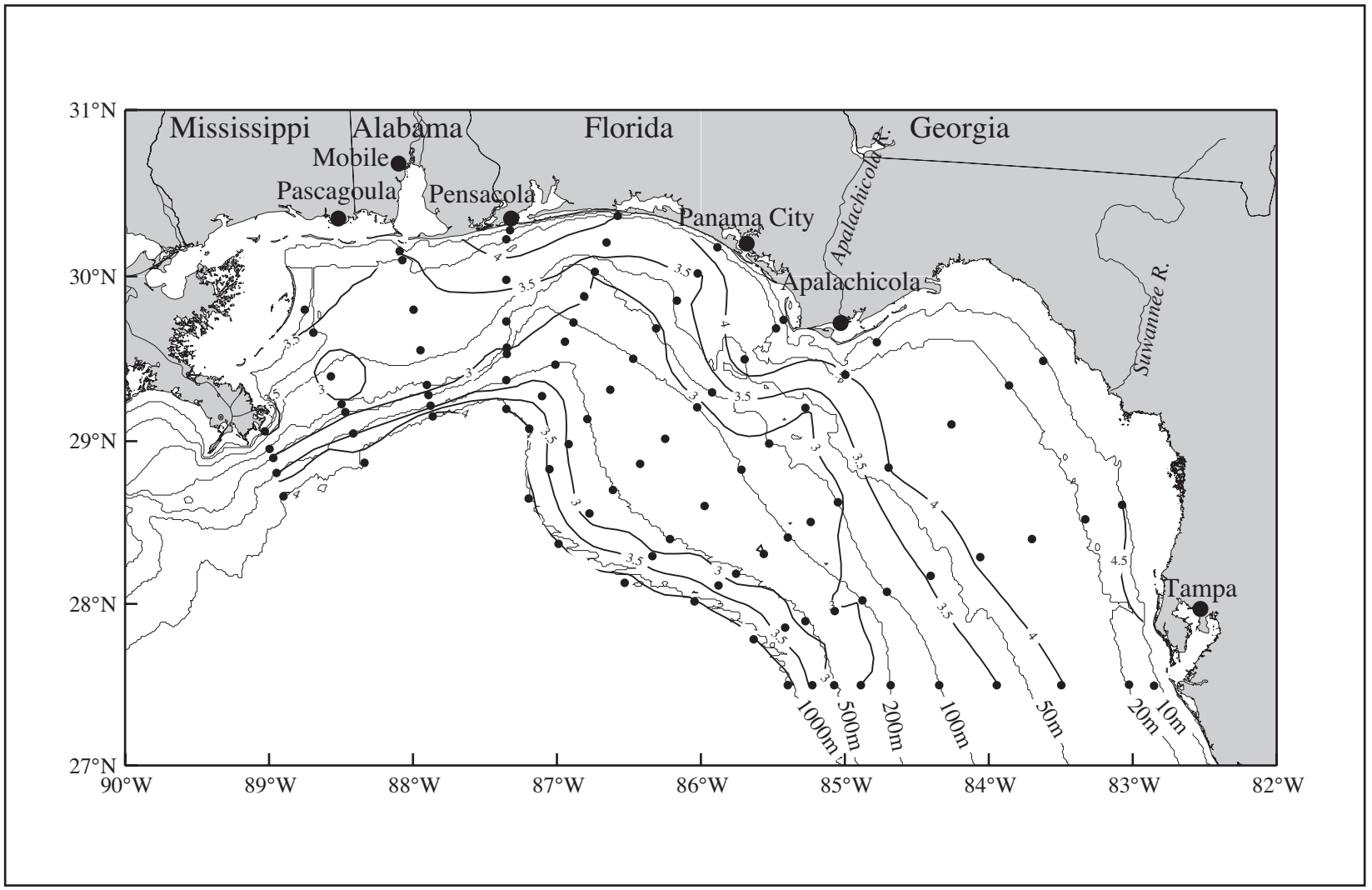

Figure I.3-6. Dissolved oxygen ($mL \cdot L^{-1}$) from near-bottom observations on cruise N9 in July/August 2000.

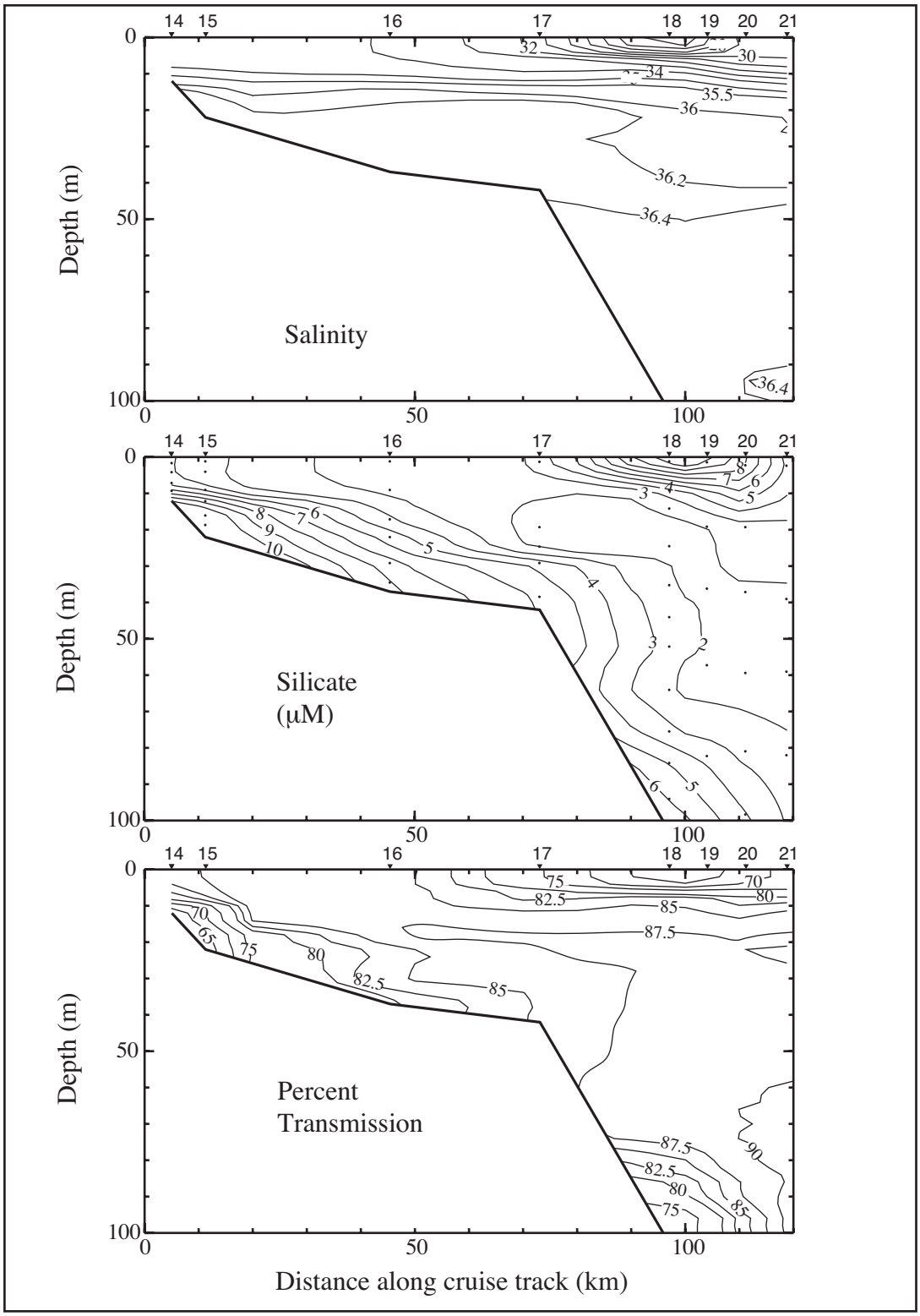

Figure I.3-7. Salinity, silicate, and percent transmission along line 3 on cruise N9 in July/August 2000. Stations are shown on top axes.

surface silicate concentrations and low percent light transmission values. The nitrate concentration was slightly elevated in the region of the freshest water relative to the remainder of the study area (Figure I.3-8).

Along line 3 are two areas with high silicate concentration and low percent light transmission associated with the sea floor (Figure I.3-7). The first is located generally between the 20- and 50-m isobaths. This pattern seems limited to line 3 and may be associated with the currents, which are directed mainly northward cross-shelf toward the coast (Figure I.2-1). Note that the elevated silicates and low percent transmission trend offshore. The second area occurs off-shore of the 50-m isobath generally near the shelf break (station 18 in Figure I.3-7). This pattern occurs mainly along the west side of DeSoto Canyon on lines 2-4. There, the low percent light transmission indicates a nepheloid layer at mid-depth (Figure I.3-9); silicates are elevated there as well (Figure I.3-10). This pattern likely results from offshelf transports associated with the cyclonic feature seen in the vicinity of DeSoto Canyon.

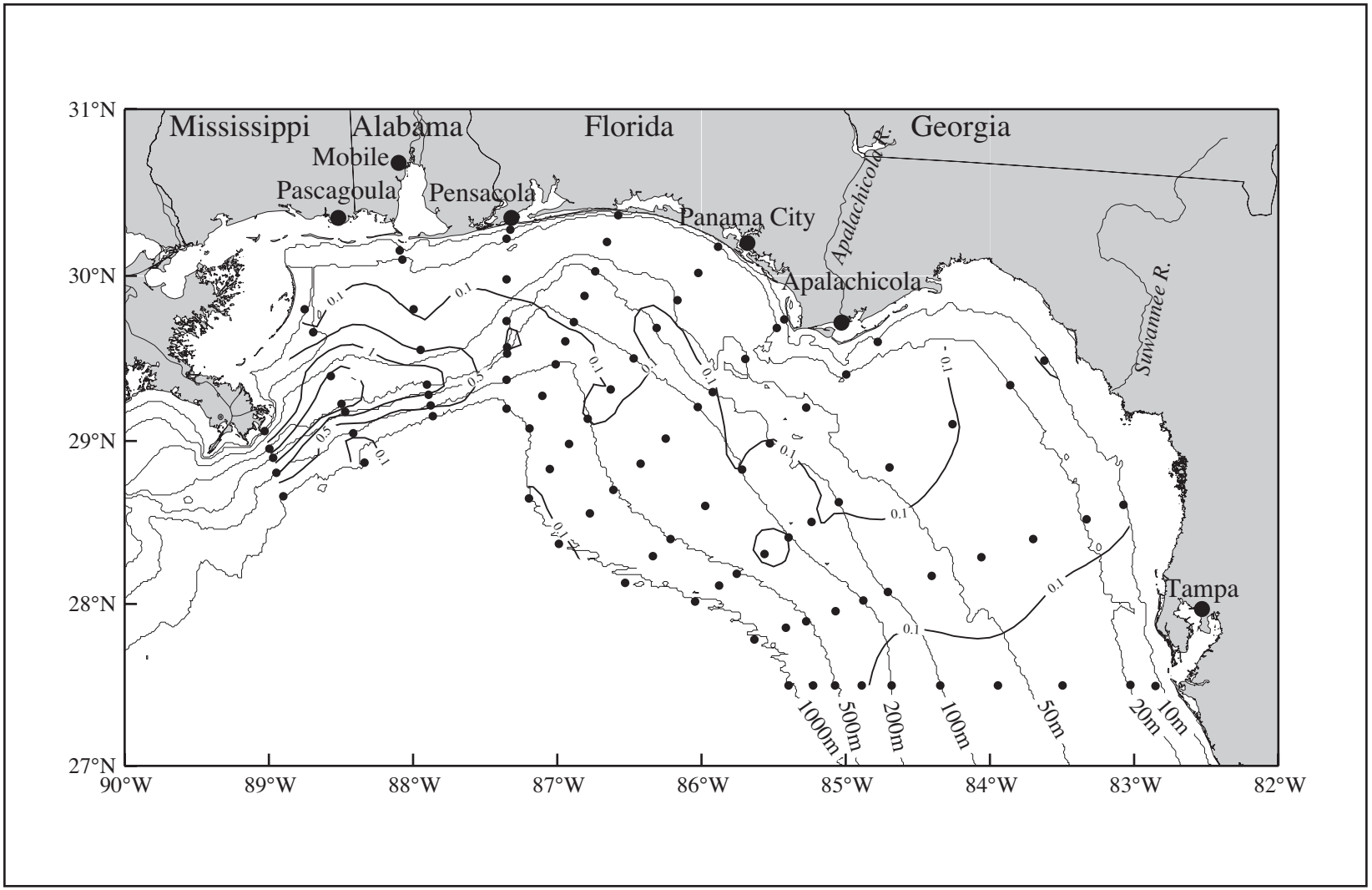

Figure I.3-8. Nitrate (μM) from the near-surface (~3.5 m) observations on cruise N9 in July/August 2000.

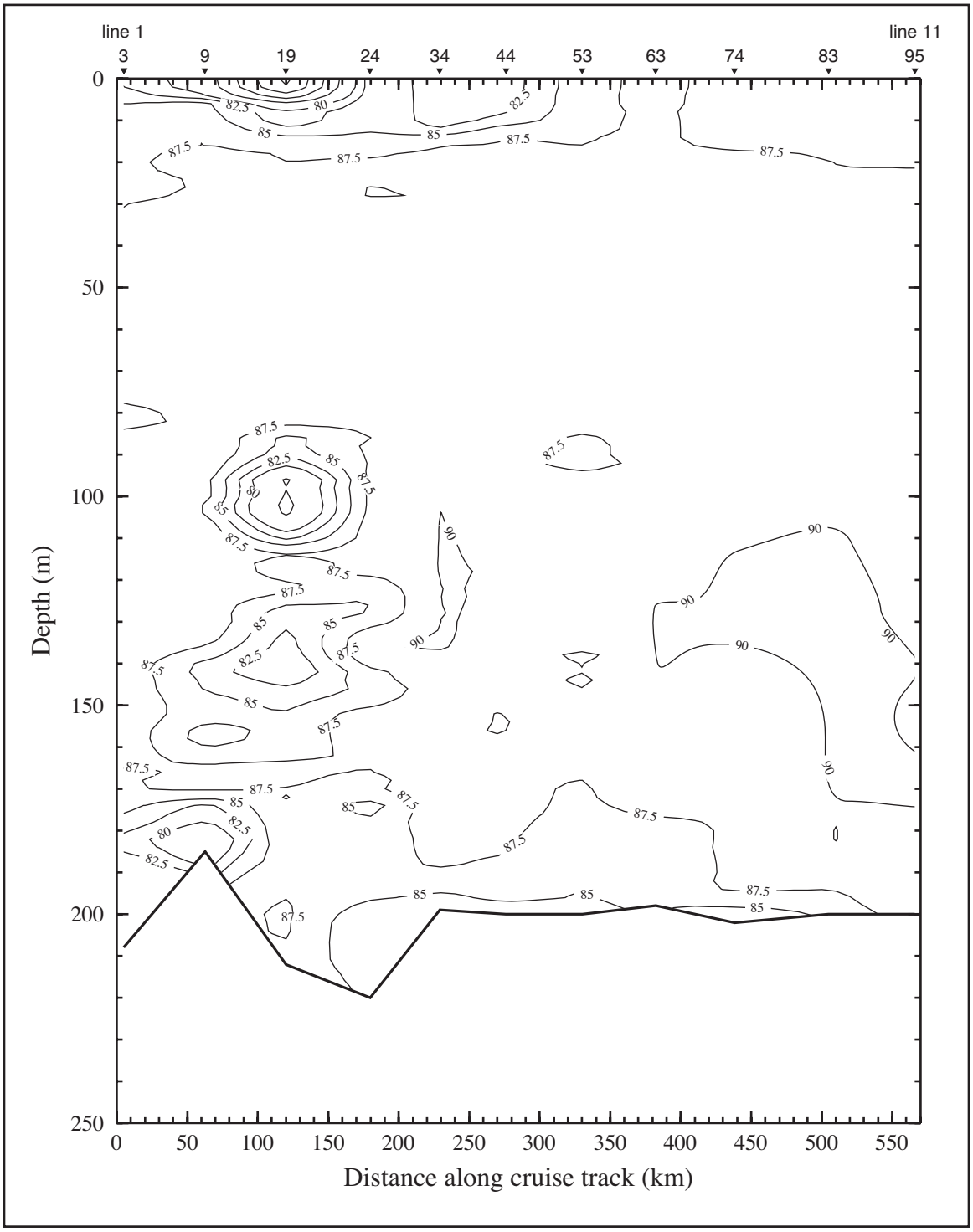

Figure I.3-9. Percent transmission (660 nm wave length; 25-cm path length) along the 200-m isobath on cruise N9 in July/August 2000. Stations are shown on the top axis.

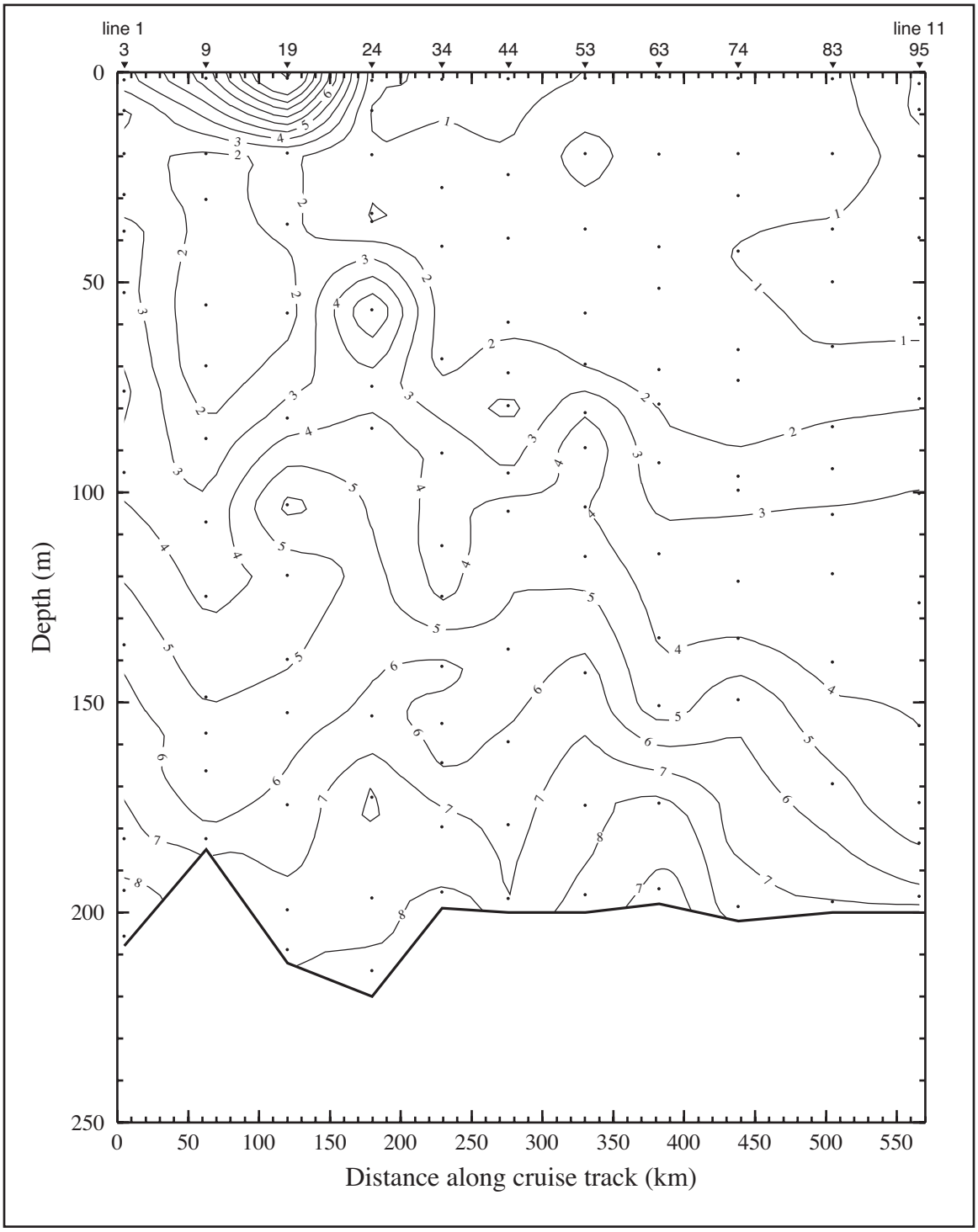

Figure I.3-10. Silicate (μM) along the 200-m isobath on cruise N9 in July/August 2000. Stations are shown on the top axis.

The Department of the Interior Mission

As the Nation's principal conservation agency, the Department of the Interior has responsibility for most of our nationally owned public lands and natural resources. This includes fostering sound use of our land and water resources; protecting our fish, wildlife, and biological diversity; preserving the environmental and cultural values of our national parks and historical places; and providing for the enjoyment of life through outdoor recreation. The Department assesses our energy and mineral resources and works to ensure that their development is in the best interests of all our people by encouraging stewardship and citizen participation in their care. The Department also has a major responsibility for American Indian reservation communities and for people who live in island territories under U.S. administration.

The Minerals Management Service Mission

As a bureau of the Department of the Interior, the Minerals Management Service's (MMS) primary responsibilities are to manage the mineral resources located on the Nation's Outer Continental Shelf (OCS), collect revenue from the Federal OCS and onshore Federal and Indian lands, and distribute those revenues.

Moreover, in working to meet its responsibilities, the **Offshore Minerals Management Program** administers the OCS competitive leasing program and oversees the safe and environmentally sound exploration and production of our Nation's offshore natural gas, oil and other mineral resources. The MMS **Minerals Revenue Management** meets its responsibilities by ensuring the efficient, timely and accurate collection and disbursement of revenue from mineral leasing and production due to Indian tribes and allottees, States and the U.S. Treasury.

The MMS strives to fulfill its responsibilities through the general guiding principles of: (1) being responsive to the public's concerns and interests by maintaining a dialogue with all potentially affected parties and (2) carrying out its programs with an emphasis on working to enhance the quality of life for all Americans by lending MMS assistance and expertise to economic development and environmental protection.